

THE JOURNAL OF PHYSICAL CHEMISTRY

Volume 71, Number 7 June 1967

Electron-Hole Trapping in X-Irradiated Calcium Carbonate and Sodium Nitrate	Joseph Cunningham	1967
Energy Transfer in the Liquid-Phase Radiolysis of Binary Alkane Systems: Cyclopentane-2,2,4-Trimethylpentane, <i>n</i> -Hexane-2,2,4-Trimethylpentane, and <i>n</i> -Hexane-Cyclopentane	T. Kudo and S. Shida	1971
Vapor Phase Charge-Transfer Complexes. I. Diethyl Sulfide-Iodine	Milton Tamres and John M. Goodenow	1982
Programmed Stresses in Homogeneous Chemical Kinetics. I. Aperiodic Stress Functions	Richard E. Cover	1990
Estimation of the Heats of Formation of Chlorofluorocarbons	Alan S. Rodgers	1996
The Second Virial Coefficient of Polyelectrolytes	Akira Takahashi, Tadayo Kato, and Mitsuru Nagasawa	2001
Dilution Effects on Dimethylsiloxane Ring-Chain Equilibria	Jack B. Carmichael, David J. Gordon, and Frank J. Isackson	2011
Thermodynamic Aspects of the Potassium Hexacyanoferrate(III)-(II) System. I. Ion Association	William A. Eaton, Philip George, and George I. H. Hanania	2016
Thermodynamic Aspects of the Potassium Hexacyanoferrate(III)-(II) System. II. Reduction Potential	George I. H. Hanania, Dennis H. Irvine, William A. Eaton, and Philip George	2 22
Displacement of Electron Energy Levels in Semiconductors as a Result of Interactions	W. W. Harvey	2031
The Kinetics and Mechanism of Fluorination of Copper Oxide. II. The Reaction of Fluorine with Copper(I) Oxide	Robert L. Ritter and Hilton A. Smith	2036
The Kinetics and Mechanism of the Thermal Decomposition of Dimethylmercury	C. E. Waring and Remo Pellin	2044
Solvent Proticity <i>via</i> Erythrosin Internal Conversion	J. Q. Umberger	2054
The Reaction of H with O ₂ . The Dissociative Lifetime of HO ₂ *	R. L. Wadlinger and B. deB. Darwent	2057
Solutions of Hydrochloric Acid in Formamide. I. Thermodynamic Properties from Electromotive Force Measurements	R. K. Agarwal and B. Nayak	2062
Conformation of Adsorbed Polystyrene Measured by Attenuated Total Reflection in the Ultraviolet Region	Paul Peyser and Robert R. Stromberg	2066
Surface Properties of Perfluoro Acids as Affected by Terminal Branching and Chlorine Substitution	Marianne K. Bernett and W. A. Zisman	2075
Reactivity of 1-Bromoalkanes with Thiocyanate	T. P. Wallace and C. H. Stauffer	2083
Electron Spin Resonance of X-Ray Irradiated Polycrystalline and Single-Crystal Sodium Hexafluoroantimonate	F. G. Herring, J. H. Hwang, and W. C. Lin	2086
Chlorophyll-Poly(vinylpyridine) Complexes. I. Conditions for Formation and Stability	G. R. Seely	2091
The Effect of Temperature on the Absorption Spectrum of the Hydrated Electron and on Its Bimolecular Recombination Reaction	W. Carl Gottschall and Edwin J. Hart	2102
The Photochemical Decomposition of Nitronium Perchlorate	J. N. Maycock, V. R. Pai Verneker, and L. Witten	2107
Ion-Solvent Interactions. VII. Apparent and Partial Molal Volumes of Some Symmetrical Tetraalkylammonium Halides in Anhydrous Methanol Solutions	J. Padova and I. Abrahamer	2112

4982 Boron trimethyl, cylinders of approx. 100g, \$2.00/1g, inc. cyl.
5373 Boron triiodide, cryst. \$15.00/10g, \$90.00/100g.

RARE & FINE CHEMICALS

**RARE
CHEMICALS
FINE**

CATALOG NUMBER **6**

SEND FOR CATALOG #6

TELEPHONE: AREA CODE 516 GENERAL 3-6262

TWX 516-433-8184
TELEX: 126464
CABLE: KALABOR PLAINVIEWNEWYORK

LABORATORIES, INC.
121 EXPRESS STREET, ENGINEERS HILL, PLAINVIEW, NEW YORK

Ion-Molecule Reactions in the Gas Phase

ADVANCES IN CHEMISTRY NO. 58

Interactions between ions and molecules are more common than had been suspected, as shown by new tools and techniques, such as tandem mass spectrometers and pulsed radiolysis. They are the cause of many chemical transformations in such energetic systems as:

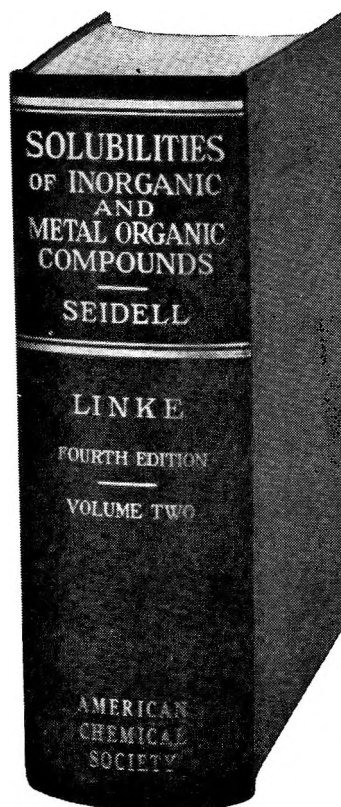
- flames
- electrical discharges
- high energy radiation
- light

Eighteen papers survey the methods and results of studies on such systems.

336 pages with index cloth bound (1966) \$8.50 postpaid in U.S., plus 20 cents in PUAS and foreign.

Set of L.C. cards free with library orders.

Order from: **Dept. M**
Special Issues Sales
American Chemical Society
1155 Sixteenth St., N.W.
Washington, D. C. 20036



NOW AVAILABLE FROM THE AMERICAN CHEMICAL SOCIETY

A new edition of an essential chemical reference . . .

Volume II of the Fourth Edition of Seidell's SOLUBILITIES OF INORGANIC AND METAL ORGANIC COMPOUNDS

Volume II has 1,914 pages of critically evaluated data, tabulated, covering a wide variety of temperature ranges, solvents, and mixtures of substances, and including melting point references. Volume II (1966) covers the elements (and compounds of them) with symbols from K through Z, and complements Volume I, which appeared in 1959.

Dr. William F. Linke, American Cyanamid Company, has

completed the careful revision of this widely used compendium started by the late Dr. Atherton Seidell.

Seidell-Linke, "Solubilities of Inorganic and Metal Organic Compounds," Fourth Edition, Vol. II, iii 1,941 pages. Cloth bound. (1966) . . . \$32.50

Order from:

Special Issues Sales, Dept. M
American Chemical Society
1155 Sixteenth Street, N. W.
Washington, D. C. 20036

Ultraviolet Photolysis of X-Irradiated Methanol at 77°K	Stephen B. Milliken and Russell H. Johnsen	2116
The Kinetics of Reaction between Oxygen Atoms and Sulfur Dioxide: an Investigation by Electron Spin Resonance Spectrometry	M. F. R. Mulcahy, J. R. Steven, and J. C. Ward	2124
1,1-Dimethylhydrazine-Water Solid-Liquid System	J. A. McMillan and S. C. Los	2132
An Examination of Some Methods for Obtaining Approximate Solutions to the Expanding-Sphere Boundary Value Problem in Direct Current Polarography	Joseph R. Delmastro and Donald E. Smith	2138
Heat of Dilution of Some Aqueous Tetraalkylammonium Fluorides	R. H. Wood, H. L. Anderson, J. D. Beck, J. R. France, W. E. de Vry, and L. J. Soltzberg	2149
Vaporization of Some Amine-Type Perchlorates	J. L. Mack and G. B. Wilmot	2155
Carbon-13 Chemical Shifts of the Carbonyl Group. V. Observation of a Deuterium Isotope Effect Using Carbon-13 Field-Frequency Lock	Gary E. Maciel, Paul D. Ellis, and Donald C. Hofer	2160
Studies of Electrolytic Conductance in Alcohol-Water Mixtures. I. Hydrochloric Acid, Sodium Chloride, and Sodium Acetate at 0, 25, and 35° in Ethanol-Water Mixtures.	H. Olin Spivey and Theodore Shedlovsky	2165
Studies of Electrolytic Conductance in Alcohol-Water Mixtures. II. The Ionization Constant of Acetic Acid in Ethanol-Water Mixtures at 0, 25, and 35°	H. Olin Spivey and Theodore Shedlovsky	2171
Studies of Electrolytic Conductance in Alcohol-Water Mixtures. III. Sodium Chloride in 1-Propanol-Water Mixtures at 15, 25, and 35°	Mario Goffredi and Theodore Shedlovsky	2176
Studies of Electrolytic Conductance in Alcohol-Water Mixtures. IV. Hydrochloric Acid in 1-Propanol-Water Mixtures at 15, 25, and 35°	Mario Goffredi and Theodore Shedlovsky	2182
Thermochemistry of Cyanocarbons. II. The Heats of Combustion of Pyridinium Dicyanomethylide, Malononitrile, and Fumaronitrile	Richard H. Boyd, K. Ranjan Guha, and Richard Wuthrich	2187
A Study of the Surface Structure of Decationized Y Zeolite by Quantitative Infrared Spectroscopy	Thomas R. Hughes and Harry M. White	2192
Gas-Liquid Interface and Solid Support Effects of Polar Solute-Nonpolar Solvent Systems in Gas Chromatography	Robert L. Pecsok and Barry H. Gump	2202
The Influence of the Alkali Halides on the Structure of Water	J. Greyson	2210
Thermodynamic Quantities in the Exchange of Zinc with Sodium Ions in Variously Cross-Linked Polystyrene Sulfonate Cation Exchangers at 25°	G. E. Boyd, F. Vaslow, and S. Lindenbaum	2214
Radiolysis of Liquid Hexafluoroethane	A. Sokolowska and Larry Kevan	2220
Electron Spin Resonance Spectra of 9-Phenylanthracene and 9,10-Diphenylanthracene Anion Radicals	L. O. Wheeler, K. S. V. Santhanam, and Allen J. Bard	2223
Nuclear Magnetic Resonance Spectra of Alkylenebisamides and Alkylenebiscarbamates	Robert H. Barker, Sidney L. Vail, and Gordon J. Boudreaux	2228
Melting of Polymer-Diluent Mixtures under Pressure. I. Polyethylene- α -Chloronaphthalene	F. E. Karasz and L. D. Jones	2234
Electronic Structure of Nitrogen Dioxide, Its Ions, and Its Dimer	L. Burnelle, P. Beaudouin, and L. J. Schaad	2240
Inhibited Autoxidation of Squalane	James C. W. Chien	2247
The Significant Structure and Properties of Liquid Hydrazine and Liquid Diborane	Mu Shik Jhon, Joe Grosh, and Henry Eyring	2253
Pressure Effects on the Thermal Decomposition of β -Cholestanyl S-Methyl Xanthate	Lin-sen Pan, Terrell N. Andersen, and Henry Eyring	2258
Pyrrole: Chemical Thermodynamic Properties	D. W. Scott, W. T. Berg, I. A. Hossenlopp, W. N. Hubbard, J. F. Messerly, S. S. Todd, D. R. Douslin, J. P. McCullough, and G. Waddington	2263
Low-Frequency Raman Spectra and Molecular Association in Liquid Formic and Acetic Acids	Peter Waldstein and L. A. Blatz	2271
Electron Affinities of Polynuclear Acceptors. Dinitro- and Trinitrophenanthrenequinones	Tapan K. Mukherjee	2277
The Hydration of Amines in Organic Solvents	M. Duane Gregory, Sherril D. Christian, and Harold E. Affsprung	2283

Do oxidation processes, products, and mechanisms interest you? "Selective Oxidation Processes" **ADVANCES IN CHEMISTRY SERIES No. 51** surveys a number of processes and details research on improving the range, selectivity, and mechanisms of such processes.

The book includes discussions of hydroxylating selected aromatics and olefins, pyrolysis of isobutylene—all of these by vapor phase processes. Among liquid phase processes are three general methods for oxidizing aromatics, sulfur dioxide as oxidant for a number of products, use of nitrogen dioxide catalyzed by selenium dioxide, and ozone as a selective oxidant. The last chapter is a broad survey of carbanion oxidation. The book is based on a symposium sponsored by the ACS Division of Petroleum Chemistry.

177 pages with index Cloth bound (1965) \$6.50

Other books in **ADVANCES IN CHEMISTRY SERIES** on topics of Industrial interest include:

No. 48 Plasticization and Plasticizer Processes. Seventeen papers survey recent studies on plasticizer action, properties, and production. Includes chapters on glass transition, plasticizer mobility, processes for phthalates and other plasticizers, and antiplasticizers.
200 pages with index Cloth bound (1965) \$7.00

No. 46 Patents for Chemical Inventions. What to do about your patentable idea before you call the attorney.
117 pages with index Cloth bound (1964) \$4.00

No. 38 Saline Water Conversion—II. Fourteen papers from two symposia; includes recovery of minerals from sea water, minimizing scale formation, wiped thin-film distillation, diffusion still, solar flash evaporation, osmosis, electro dialysis (3 papers), research in Israel, hydrate process.
199 pages Paper bound (1963) \$6.00

No. 34 Polymerization and Polycondensation Processes. An I&EC Division symposium with emphasis on unit processes. Twenty-one papers on addition polymerization, polycondensation reactions, commercial polymerization processes, and equipment design.
260 pages Paper bound (1962) \$8.00

No. 27 Saline Water Conversion. A Water and Waste Chemistry Division symposium; includes thermodynamics of desalting, solvent extraction, freezing, cen-

trifugal phase barrier recompression distillation, multi-stage flash evaporation, ion exchange, osmosis, and electrochemical demineralization.

246 pages Paper bound (1960) \$5.85

No. 24 Chemical Marketing in the Competitive Sixties. Twenty articles survey the challenge in marketing drugs, agricultural chemicals, industrial organics, inorganic and heavy chemicals, and plastics; the role of advertising; sales; delivering goods to the customer; monitoring sales performance; market research; technical service, and application research.

147 pages Paper bound (1959) \$3.50

No. 21 Ozone Chemistry and Technology. Sixty papers from the International Ozone Conference; includes ozone chemistry, high concentration ozone, ozone analysis and technology, formation in electrical discharge, toxicity, sterilization and water purification.

465 pages Cloth bound (1959) \$7.00

No. 19 Handling and Uses of Alkali Metals. Nineteen articles on the chemistry, manufacture, and use of the alkali metals; five are devoted solely or partly to lithium, two to potassium, the remainder to sodium.

177 pages Paper bound (1957) \$4.75

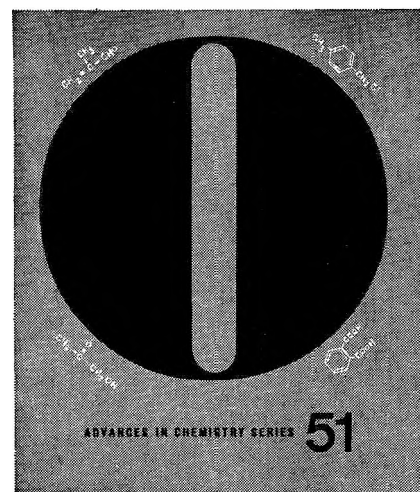
No. 10 Literature Resources for Chemical Process Industries. Information sources on market research (13 papers), resins and plastics (7 papers), textile chemistry (6 papers), food industry (10 papers), petroleum (10 papers), literature searching and language problems (13 papers).

582 pages with index Paper bound (1954) \$7.50

No. 5 Progress in Petroleum Technology. Survey of 25 years of progress at the ACS Diamond Jubilee. Thirty-two papers on all aspects of petroleum processing and products.

392 pages Cloth bound (1951) \$6.50

Order from **Special Issues Sales, Dept. M
American Chemical Society
1155 Sixteenth St., N.W.
Washington, D. C. 20036**



Substituent Effects on the Properties of Stable Aromatic Free Radicals. Oxidation-Reduction Potentials of Triarylamine-Triarylammonium Ion Systems	Lily Hagopian, Günter Kohler, and Robert I. Walter	2290
The Absorption Spectra of Simple Amides and Peptides	Eigil B. Nielsen and John A. Schellman	2297
Equations for the Calculation of Activity Coefficients of Solutions from the Intensity of Brillouin Scattering	George A. Miller	2305
Nuclear Magnetic Resonance Fluorine-Fluorine Coupling Constants in Fluorotitanate Complexes	Daniel S. Dyer and Ronald O. Ragsdale	2309
Hexamethylenetetramine Aqueous Solutions. Isopiestic Data at 25° and Density and Viscosity Data in the Range 3-34°	V. Crescenzi, F. Quadrifoglio, and V. Vitagliano	2313
Barriers to Internal Rotation in Thioamides. Experimental Results and Molecular Orbital Calculations	Jan Sandström	2318
The Kinetics of the Thermal Decomposition of 3,3-Dimethyloxetane	George F. Cohoe and W. D. Walters	2326
Relaxation Mechanisms in Polymeric Sulfur	A. Eisenberg and L. A. Teter	2332
Solubilization of Polycyclic Aromatic Hydrocarbons in Poly(methacrylic acid) Aqueous Solutions	G. Barone, V. Crescenzi, A. M. Liquori, and F. Quadrifoglio	2341

NOTES

The Photochemical Decomposition of Hydrogen Sulfide. The Reactions of Hydrogen Atoms and HS Radicals	B. deB. Darwent, R. L. Wadlinger, and Sr. Mary John Allard	2346
Ion-Solvent Interactions in Aqueous Lanthanide Solutions	J. Padova	2347
The Relative Dissociation Constants of Hydrochloric, Hydrobromic, Hydriodic, Nitric, and Perchloric Acid in Pyridine. A Hydrogen Electrode Study	L. M. Mukherjee and John J. Kelly	2348
Adiabatic Heating of Hydrazine by Flash Photolysis. Nitrogen Formation with Integrity of the N-N Bond	L. J. Stief and V. J. DeCarlo	2350
Tautomerism of N-o-Hydroxybenzylidene Anils in Nonacidic Solvents	John W. Ledbetter, Jr.	2351
Correlation of Spectra of the Monosubstituted Benzenes and Their Hydroxy Radical Adducts	B. Cercek	2354
Photolysis of Propene at 1470 Å	E. Tschuikow-Roux	2355
Conductance Studies of Ammonium and Phosphonitrilium Salts in Acetonitrile at 25°	Ismail Y. Ahmed and C. D. Schmulbach	2358
The Formation of Lead(II) Chloride Bromide (PbClBr) in the Vapor Phase	H. Bloom and J. W. Hastie	2360
Pressure and Viscosity Effects on the Recombination of <i>t</i> -Butoxy Radicals from Di- <i>t</i> -butyl Peroxide	Cheves Walling and Harold P. Waits	2361

COMMUNICATIONS TO THE EDITOR

On the Radiation Chemistry of Aqueous Nitrous Oxide Solutions	Conrad H. Cheek	2363
Circular Dichroism of Some Polypeptides in Solvent Mixtures Containing Strong Organic Acids	Franco Quadrifoglio and Dan W. Urry	2364
On the Sealed-Particle Theory of Dilute Aqueous Solutions	Robert A. Pierotti	2366
Electron Spin Resonance Spectra of Radicals Produced by the Acetaldehyde-Hydrogen Peroxide-Titanous System	J. R. Steven and J. C. Ward	2367
Comments on the Nuclear Magnetic Resonance Spectrum of Diethyldipyridylnickel	S. Castellano and H. Günther	2368
The Nuclear Magnetic Resonance Interpretation of Diethylnickel Complexes of Substituted Dipyridyl	T. Saito, M. Araki, Y. Uchida, and A. Misono	2370
Abstraction of Halogen Atoms by Methyl Radicals	K. D. King and E. S. Swinbourne	2371
Comment on "Electron Spin Resonance of O ¹⁶ -O ¹⁷ , O ¹⁷ -O ¹⁸ , and O ¹⁸ -O ¹⁶ " by L. K. Keys	A. Carrington, D. H. Levy, and T. A. Miller	2372
Reply to "Comment on Electron Spin Resonance of O ¹⁶ -O ¹⁷ , O ¹⁷ -O ¹⁸ , and O ¹⁸ -O ¹⁶ " by Carrington, Levy, and Miller	L. K. Keys	2373

A Comment on the Steric Factor Approach to Translational-Vibrational Energy Transfer	J. Daniel Kelley and Max Wolfsberg	2373
On the Structure of Pyrazole	Alan D. Mighell and Curt W. Reimann	2375
Infrared Spectra of Carbon Monoxide Adsorbed on Palladium	J. K. A. Clarke, G. Farren, and H. E. Rubalcava	2376
Calorimetric Measurements of Transition Enthalpies in the Polynucleotide System Poly A-Poly U	Eberhard Neumann and Theodor Ackermann	2377
Hybridization, Conjugation, and Bond Lengths. An Experimental Test	Richard Alden, J. Kraut, and T. G. Traylor	2379

AUTHOR INDEX

Abrahamer, I., 2112	Delmastro, J. R., 2138	Jhon, M. S., 2253	Nayak, B., 2062	Stief, L. J., 2350
Ackermann, T., 2377	de Vry, W. E., 2149	Johnsen, R. H., 2116	Neumann, E., 2377	Stromberg, R. R., 2066
Affsprung, H. E., 2283	Doulin, D. R., 2263	Jones, L. D., 2234	Nielsen, E. B., 2297	Swinbourne, E. S., 2371
Agarwal, R. K., 2062	Dyer, D. S., 2309	Karasz, F. E., 2234	Padova, J., 2112, 2347	Takahashi, A., 2001
Ahmed, I. Y., 2358	Eaton, W. A., 2016, 2022	Kato, T., 2001	Pan, L., 2258	Tamres, M., 1982
Alden, R., 2379	Eisenberg, A., 2332	Kelley, J. D., 2373	Pecsok, R. L., 2202	Teter, L. A., 2332
Allard, M. J., 2346	Ellis, P. D., 2160	Kelly, J. J., 2348	Pellin, R., 2044	Todd, S. S., 2263
Andersen, T. N., 2258	Eyring, H., 2253, 2258	Kevan, L., 2220	Peyser, P., 2066	Traylor, T. G., 2379
Anderson, H. L., 2149	Farren, G., 2376	Keys, L. K., 2373	Pierotti, R. A., 2366	Tschuikow-Roux, E., 2355
Araki, M., 2370	France, J. R., 2149	King, K. D., 2371	Quadrifoglio, F., 2313, 2341, 2364	Uchida, Y., 2370
Bard, A. J., 2223	George, P., 2016, 2022	Kohler, G., 2290	Ragsdale, R. O., 2309	Umberger, J. Q., 2054
Barker, R. H., 2228	Goffredi, M., 2176, 2182	Kraut, J., 2379	Reimann, C. W., 2375	Urry, D. W., 2364
Barone, G., 2341	Goodenow, J. M., 1982	Kudo, T., 1971	Ritter, R. L., 2036	Vail, S. L., 2228
Beaudouin, P., 2240	Gordon, D. J., 2011	Ledbetter, J. W., Jr., 2351	Rodgers, A. S., 1996	Vaslow, F., 2214
Beck, J. D., 2149	Gottschall, W. C., 2102	Levy, D. H., 2372	Rubalcava, H. E., 2376	Verneker, V. R. P., 2107
Berg, W. T., 2263	Gregory, M. D., 2283	Lin, W. C., 2086	Saito, T., 2370	Vitagliano, V., 2313
Bernett, M. K., 2075	Greyson, J., 2210	Lindenbaum, S., 2214	Sandström, J., 2318	Waddington, G., 2263
Blatz, L. A., 2271	Grosh, J., 2253	Liquori, A. M., 2341	Santhanam, K. S. V., 2223	Wadlinger, R. L., 2057, 2346
Bloom, H., 2360	Guha, K. R., 2187	Los, S. C., 2132	Schaad, L. J., 2240	Waits, H. P., 2361
Boudreaux, G. J., 2228	Gump, B. H., 2202	Maciel, G. E., 2160	Schellman, J. A., 2297	Waldstein, P., 2271
Boyd, G. E., 2214	Günther, H., 2368	Mack, J. L., 2155	Schmulbach, C. D., 2358	Wallace, T. P., 2083
Boyd, R. H., 2187	Hagopian, L., 2290	Maycock, J. N., 2107	Scott, D. W., 2263	Walling, C., 2361
Burnelle, L., 2240	Hanania, G. I. H., 2016, 2022	McCullough, J. P., 2263	Seely, G. R., 2091	Walter, R. I., 2290
Carmichael, J. B., 2011	Hart, E. J., 2102	McMillan, J. A., 2132	Shedlovsky, T., 2165, 2171, 2176, 2182	Walters, W. D., 2326
Carrington, A., 2372	Harvey, W. W., 2031	Messerly, J. F., 2263	Shida, S., 1971	Ward, J. C., 2124, 2367
Castellano, S., 2368	Hastie, J. W., 2360	Mighell, A. D., 2375	Smith, D. E., 2138	Waring, C. E., 2044
Cercek, B., 2354	Herring, F. G., 2086	Miller, G. A., 2305	Smith, H. A., 2036	Wheeler, L. O., 2223
Cheek, C. H., 2363	Hofer, D. C., 2160	Miller, T. A., 2372	Sokolowska, A., 2220	White, H. M., 2192
Chien, J. C. W., 2247	Hossenlopp, I. A., 2263	Milliken, S. B., 2116	Soltzberg, L. J., 2149	Wilmot, G. B., 2155
Christian, S. D., 2283	Hubbard, W. N., 2263	Misono, A., 2370	Spivey, H. O., 2165, 2171	Witten, L., 2107
Clarke, J. K. A., 2376	Hughes, T. R., 2192	Mukherjee, L. M., 2277, 2348	Stauffer, C. H., 2083	Wolfsberg, M., 2373
Cohoe, G. F., 2326	Hwang, J. H., 2086	Mukherjee, T. K., 2277	Steven, J. R., 2124, 2367	Wood, R. H., 2149
Cover, R. E., 1990	Irvine, D. H., 2022	Mulcahy, M. F. R., 2124	Zisman, W. A., 2075	Wuthrich, R., 2187
Crescenzi, V., 2313, 2341	Isackson, F. J., 2011	Nagasawa, M., 2001		
Cunningham, J., 1967				
Darwent, B. deB., 2057, 2346				
DeCarlo, V. J., 2350				

THE JOURNAL OF PHYSICAL CHEMISTRY

Registered in U. S. Patent Office © Copyright, 1967, by the American Chemical Society

VOLUME 71, NUMBER 7 JUNE 15, 1967

Electron-Hole Trapping in X-Irradiated Calcium

Carbonate and Sodium Nitrate

by Joseph Cunningham¹

Division of Molecular Science, National Physical Laboratory, Teddington, England

Accepted and Transmitted by The Faraday Society (December 21, 1966)

High efficiencies of formation of NO_3^{2-} in NaNO_3 crystals of CO_3^- and CO_3^{3-} in CaCO_3 crystals by X-irradiation at 77°K are compatible with their production by secondary electrons of initial energies <100 ev. The esr signal intensities from these radicals vary with thermal annealing or optical bleaching in the manner expected for trapped electrons and holes coexisting after irradiation. Neither the narrow and invariant line widths observed from radicals trapped in CaCO_3 nor the absence of satellite lines in these spectra would be expected if the spatial distribution of trapped electrons and holes was similar to that reported for energy-loss events involving secondary electrons.

Published interpretations of esr spectra observed in CaCO_3^2 and NaNO_3^{3-5} X-irradiated at 77°K identify CO_3^{3-} or CO_3^- radicals on carbonate ion sites and NO_3^{2-} or NO_3 radicals on nitrate ion sites. Such pairs of radicals are complementary in the sense that ($\text{CO}_3^- + \text{CO}_3^{3-}$) or ($\text{NO}_3^{2-} + \text{NO}_3$) result when an electron is taken from one anion and localized on another. To examine whether such electron-hole pairs were produced in close proximity by X-irradiation at 77°K, we studied the line shapes of esr spectra in single-crystal CaCO_3 . Dipolar interaction between closely spaced radicals has been reported in other irradiated systems.⁶⁻⁸ Calcite, however, represents an ideal matrix in which to study such interactions because of the almost total absence of nuclei with nonzero spins.

We wished, first, to investigate whether the species produced by X-irradiation of calcite at 77°K, and

tentatively identified by Marshall and Serway with CO_3^- or CO_3^{3-} radicals,² had properties consistent with coexistence of trapped electrons and holes. Efficiencies of formation, thermal stabilities, and response to optical bleaching were therefore studied, as follows, for electron-excess CO_3^{3-} - CaCO_3 and NO_3^{2-} - NaNO_3 and for electron-deficient CO_3^- - CaCO_3 and NO_3 - NaNO_3 .

(1) Department of Chemistry, University College, Belfield, Dublin 4, Ireland.

(2) (a) R. A. Serway, Doctoral dissertation submitted to the Illinois Institute of Technology, 1966; (b) R. A. Serway and S. Marshall, *J. Chem. Phys.*, in press.

(3) R. Addé, *Compt. Rend.*, **260**, 2781 (1965).

(4) R. Addé, *ibid.*, **261**, 685 (1965).

(5) K. Geshi and Y. Kazumata, J.A.E.R.I. (Japan) Report No. 2054 (1965).

(6) R. C. Smith and S. J. Wyard, *Nature*, **191**, 897 (1961).

(7) S. J. Wyard, *Proc. Phys. Soc. (London)*, **86**, 587 (1965).

(8) Y. Kurita and M. Kashiwagi, *J. Chem. Phys.*, **44**, 1727 (1966).

Table I: Properties of Radicals Produced in Single Crystals of CaCO₃ or NaNO₃ by 150-kv X-Rays at 77°K

	Electron-excess radicals			Electron-deficient radicals		
	CO ₃ ³⁻ -CaCO ₃	NO ₃ ²⁻ -NaNO ₃	CO ₃ ⁻ -CaCO ₃	NO ₃ (A)-NaNO ₃	NO ₃ (C)-NaNO ₃	NO ₂ -NaNO ₃ ^b
No. formed/100 ev	4	3	4	10	3	0.5
For Hc axis:						
<i>g</i> (±0.0005)	2.0012 ^{a,2}	2.0019 ^a	2.0045 ^{a,2}	2.0022	2.0024	2.0062
Δ <i>H</i> _{1/2} (<i>g</i>)	0.11 ^{a,2}	33 ^{a,c}	0.11 ^{a,2}	1.5	5	8.0
Hfs to ¹³ C or ¹³ N,(<i>g</i>)	171.2 ²	64.4 ^a	13.1 ²	4.1	0.5	50.3
For H_⊥c axis:						
<i>g</i> (±0.0005)	2.0030 ^{a,2}	2.0067 ^a	2.0148 ^{a,2}	2.0217	2.0085	1.9976 ^{a,5}
Δ <i>H</i> _{1/2} (<i>g</i>)	0.11 ^{a,2}	44 ^{a,c}	0.11 ^{a,2}	1.5	5	1.5
Hfs to ¹³ C or ¹⁴ N,(<i>g</i>)	111.3 ²	33.8 ^a	9.4 ²	3.5	0.5	62.5
<i>t</i> _{1/2} , 77°K	5 hr ^{a,2}	Stable	5 hr ^{a,2}	3-5 min	Stable ^{a,5}	Stable
Effect of 6328-Å bleach	×0.4	None	×0.5	...	None	None
Effect of 3500-7500-Å bleach	×0.02	×0.05	×0.01	...	×0.2	×0.01
References	<i>a</i> , 2a, 2b	<i>a</i> , 5	<i>a</i> , 2a, 2b	4	<i>a</i>	<i>a</i> , 5

^a Superscripts denote, (*a*) this work; (*a*,2) etc., that value measured here resembles those reported in indicated reference. ^b NO₂ rotating around an axis perpendicular to its plane, and parallel to crystal *c* axis. ^c Envelope of ten partially resolved shfs components from interaction with three Na⁺.

Efficiency of Formation. The esr spectra taken on calcite shortly after irradiation at 77°K showed only two intense signals. These had the parameters assigned to CO₃⁻ and CO₃³⁻ (see Table I). Radical concentrations were not accurately measured because of their narrow line widths but exceeded 5 × 10¹⁸ radicals cm⁻³ for megarad doses. Approximately 4 CO₃⁻ radicals and 4 CO₃³⁻ radicals must therefore be produced per 100 ev absorbed. Only secondary electrons of initial energies <100 ev are produced by low LET radiations in sufficient numbers to account for such high radical yields⁹ (*i.e.*, >1 radical/100 ev).

Similar irradiation of NaNO₃ which is isomorphous with calcite could be expected to produce NO₃ and NO₃²⁻ radicals which were isoelectronic with CO₃⁻ and CO₃³⁻. Radicals having magnetic parameters identical with those assigned in the literature to NO₃²⁻ were indeed produced with efficiency only slightly lower than that measured for CO₃³⁻-CaCO₃ (see Table I). None of the other esr features present in NaNO₃ 30 min after irradiation had *g* factors or hfs values expected for NO₃ radicals which were isoelectronic with planar triangular CO₃⁻. Addé reported such a radical in NaNO₃ after irradiation with 1.5-Mev electrons at 77°K⁴ and denoted it by NO₃(A). The efficiency of production, orientation, and magnetic parameters he reported (*cf.* Table I) were consistent with formation of planar NO₃ by hole capture on NO₃⁻. This radical was not observed in our experiments, probably because its half-life is reported to be only 3-5 min at 77°K. Thus the electron-deficient radicals we observed in

NaNO₃ may arise by dissociation or rearrangement of NO₃(A). Indeed, the magnetic parameters of the triplet signal are very similar to those assigned in the literature⁵ to rotating NO₂. The identity of the species giving the intense singlet has not been established. It may arise from one of the known isomeric forms¹⁰ of NO₃, denoted by NO₃(C) in Table I.

Thermal Stabilities. Calcite crystals observed under liquid N₂ after X-irradiation emitted an intense blue luminescence. This indication that electron-hole recombination was proceeding slowly in calcite at 77°K was supported by the observation that the intensities of both singlet esr signals decreased in similar fashion to the luminescence (*i.e.*, a rapid initial decrease having *t*_{1/2} ~ 1 hr succeeded by a slower decrease with *t*_{1/2} ~ 5 hr). Similar studies commenced on NaNO₃ *an hour after irradiation* failed to detect comparable luminescence or decay of esr signal intensities. Marshall and Serway deduced that the low-temperature decay of esr signal intensities in calcite had its origin in low mobility of CO₃⁻ after irradiation. Addé's observation that NO₃(A) decayed at 77°K within minutes of the end of an irradiation would account for the absence of luminescence in NaNO₃ 60 min after irradiation.

Optical Absorption and Bleaching. Radiation-induced optical absorption was compared for calcite and NaNO₃ crystals at 77°K after identical X-irradiations.

(9) A. Mozumder and J. L. Magee, *Radiation Res.*, **28**, 203 (1966).

(10) W. A. Guillory and H. S. Johnston, *J. Chem. Phys.*, **42**, 2457 (1965).

Calcite exhibited a deep blue-black coloration with λ_{max} for the radiation-induced optical absorption at 6500 Å. Irradiated NaNO_3 showed only faint yellow coloration and no "red" absorption band. Results of previous work suggested that the "red" absorption bands should be observed for the planar triangular form of CO_3^- or NO_3^- . Detection of the red absorption band in calcite but not in NaNO_3 1 hr after irradiation appeared consistent with the esr results which showed CO_3^- but no NO_3^- (A). The question was further examined by passing the 6328-Å output of a 35-mw gas laser directly into the microwave cavity containing an irradiated crystal immersed in liquid nitrogen. This bleaching reduced the intensities of both esr signals in calcite to one-third that of an unbleached control sample. Release of trapped CO_3^- and subsequent electron-hole recombination can explain this result and the simultaneous reduction observed in the red absorption in calcite. Similar bleaching exposure did not significantly decrease the intensities of esr signals in NaNO_3 .

The optical absorption by electron-excess radicals in both NaNO_3 ¹¹ and CaCO_3 ^{2b} have been identified, respectively, with bands having maxima at 3350 and 4850 Å. Xenon arc light filtered by Pyrex ($\lambda \sim 3500$ to 7500 Å) should therefore be absorbed by NO_3^{2-} and CO_3^{3-} centers, with promotion of electrons into the conduction band. It was experimentally observed that the esr signals of both CO_3^{3-} and CO_3^- were reduced 100-fold by 15-min exposure to this light. The esr signals of NO_3^{2-} and NO_2 in NaNO_3 were reduced beyond detection and the intensity of the esr signal designated as NO_3 (C) was reduced to one-fifth by this bleach. The bleaching effects can all be understood as electron-hole recombinations resulting from optical release of electrons and holes.

Since these results appeared consistent with formation of electrons and holes by the X-irradiation, line-width studies were made to determine whether dipolar interactions could be observed between radicals generated in the same energy-loss event. According to the treatment recently developed by Mozumder and Magee,⁹ dipolar interactions appear most probable for radicals produced in "spurs," less probable for those in "blobs," and least likely for those generated by high-energy δ -rays. This follows from their estimates of the distance separating a radiation-produced electron from its sibling positive hole: namely, separations of ca. 30 Å for the electrons of energy <100 eV which give rise to spurs; separations <120 Å for electrons of 100–500 eV energy which give rise to "blobs"; separations 100–500 Å for electrons of 500–5000 eV energy which give rise to short tracks; and separations >500 Å for δ -ray electrons of >5000 eV energies. Line

widths of the CO_3^{3-} and CO_3^- radicals were measured at 77°K within minutes of the end of irradiation, and at intervals while the signal intensities decayed thermally to one quarter of their initial values by electron-hole recombination. The line widths given in Table I for calcite were measured at 5×10^{-6} w microwave power and with 100 mGauss modulation. Line-width measurements at lower incident powers and smaller modulation depths indicated that line widths measured at the stated conditions would be free of line broadening from power-saturation or modulation-depth effects.

Dipolar interactions between adjacent radicals have been reported to give rise to satellite peaks⁸ or to general line broadening.^{6,7} Small satellite peaks symmetrically displaced about the intense CO_3^- or CO_3^{3-} esr signals would have resulted if dipolar interactions occurred between electrons of radicals separated from each other in calcite by small fixed lattice distances (5–50 Å). Because of the very small (0.110 Gauss) line half-widths in calcite, any such satellite peaks would have been detected even if the dipolar interaction had caused additional splitting of only 0.3 Mc/sec at any orientation. The absence of satellite peaks indicates that pairs or larger groups of CO_3^- and CO_3^{3-} radicals, separated by small fixed crystal distances, were not present in calcite after X-irradiation at 77°K.

On the other hand, if line widths measured for CO_3^- and CO_3^{3-} arose from dipolar interactions between radicals having a range of inter-radical separation, the measured line widths should change with post-irradiation treatment. This conclusion follows from the reasonable expectation that holes (or electrons) released from trapping sites by thermal activation or optical bleaching would exhibit rates of electron-hole recombination inversely dependent upon separations from their sibling electrons (or holes). Pairs with smallest separation, as formed in spurs, should thus recombine first, in the same manner as reported for the recombination of irradiation produced vacancy-interstitial pairs in alkali halides.¹² Electron-hole recombination occurring in calcite in this fashion would require that esr line half-widths decrease as the number of radicals decreased. Measured line widths in calcite were *not* observed to decrease while the signal intensities decayed to one-quarter of their post-irradiation values. Neither was any decrease noted when the recombination of electrons and holes ($\equiv \text{CO}_3^{3-}$ and CO_3^-) was accelerated by bleaching calcite crystal

(11) J. Cunningham, *J. Chem. Phys.*, **41**, 3522 (1964).

(12) N. Itoh, B. S. H. Royce, and R. Smoluchowski, *Phys. Rev.*, **137**, A1010 (1965).

in situ within the microwave cavity with laser light at 6328 Å. Thus, despite the very favorable condition in calcite, we were unable to obtain evidence that trapped CO_3^{3-} and CO_3^- radicals were interacting in the manner expected if their spatial distribution was that predicted by recent electron energy-loss models.⁹ On the contrary, the calcite line widths seem to require that electrons and holes be independently trapped at well-separated anion sites.

Comparable information could not be obtained from line-width studies on NaNO_3 because the principal mechanism contributed to line widths of NO_3^{2-} was interaction with three near-neighbor cations which gave large line widths and partially resolved super-hyperfine splitting. Our results on this solid and on calcite are consistent with prior suggestions that NO_3 and CO_3^- are labile or unstable at 77°K after irradiation.^{2b,4,5} A related hypothesis—that the ease, position, and permanence of hole and electron trapping in a perfect lattice of polyatomic ions depend on distortion of the latter by collision with sub-excitation electrons¹³—appears capable of explaining our results. Thus greater intramolecular configuration change is required¹⁴

to convert an anion to electron-excess NO_3^{2-} or CO_3^{3-} than to electron-deficient CO_3^- or $\text{NO}_3(\text{A})$. Less energy is therefore required to propagate the latter species through the lattice at 77°K. Collision with sub-excitation electrons and consequent distortion of polyatomic anions into configurations appropriate to the electron-excess or electron deficient radical could occur at distances >50 Å from sites of energy deposition. Electron-hole trapping at distorted-anion sites could therefore occur at such distances from sites of energy deposition.

Acknowledgments. The author is deeply grateful to S. Marshall for kindly providing calcite samples and preprints of his work with R. Serway, and to R. Cook for helpful discussions and experimental assistance. The author is also indebted to the Division of Molecular Science, NPL, for a fellowship and for permission to publish these results.

(13) J. Cunningham in "Radical Ions," E. Kaiser and L. Kevan, Ed., John Wiley and Sons, Inc., New York, N. Y., 1967, Chapter 10.

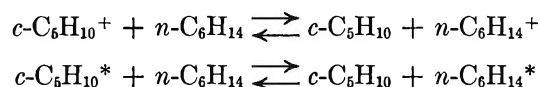
(14) M. C. R. Symons in "Free Radicals in Inorganic Chemistry," Advances in Chemistry Series, No. 37, American Chemical Society, Washington, D. C., 1962, Chapter 7.

Energy Transfer in the Liquid-Phase Radiolysis of Binary Alkane Systems: Cyclopentane-2,2,4-Trimethylpentane, *n*-Hexane-2,2,4-Trimethylpentane, and *n*-Hexane-Cyclopentane^{1a}

by T. Kudo^{1b} and S. Shida

Laboratory of Physical Chemistry, Tokyo Institute of Technology, Ookayama, Meguro-ku, Tokyo, Japan
(Received May 16, 1966)

The products from cyclopentane-2,2,4-trimethylpentane binary mixtures were analyzed after irradiation at room temperature. In the mixtures, the yield of hydrogen was reduced from that expected according to the law of averages. On the other hand, the yields of methane, isobutane, and isobutene were enhanced. These results are all consistent with an energy-transfer mechanism, the transfer occurring from cyclopentane to 2,2,4-trimethylpentane. However, the enhancement of the yields of two C₄ products, compared to the enhancement of the methane yield, was about twice as great as would be expected based on the ratio $G(\text{C}_4):G(\text{CH}_4)$ for pure 2,2,4-trimethylpentane. Consequently, it is concluded that the compendium of states of precursors for the C₄ products appears to differ depending upon whether they are produced originally or after energy transfer. From runs using methyl methacrylate as a scavenging additive, the "scavenged fractions" for the C₄ products in the mixtures which were found varied appreciably from those in pure 2,2,4-trimethylpentane. This means that, in addition to the spectrum of decomposition paths arising from the pure materials, there is superimposed another pattern of carbon-carbon bond rupture arising from the excited and/or ionized state formed on energy transfer. Similar results were obtained for the *n*-hexane-2,2,4-trimethylpentane system. However, for the cyclopentane-*n*-hexane system, although the ionization potentials of the components apparently differ, the results obtained appear to imply ideal behavior of ionic or excited molecular species produced radiolytically in the system and the following mechanism was suggested to occur, with forward and reverse rates balanced in equilibrium



Introduction

From the radiolysis of several binary saturated hydrocarbon mixtures in the liquid phase, it has been shown that the yields of hydrogen deviate from the expected values based on the electron fraction of the components. The effect has been attributed, in the majority, to a charge transfer occurring from the one component with a higher ionization potential to the other component with a lower potential.² If this mechanism is appropriate, yields of radiolysis products

other than hydrogen but having the same ionic precursor will also show similar deviation from the proportionality in electron fraction.

In this work, cyclopentane and 2,2,4-trimethylpentane were selected as binary components, because both of the materials are simple with respect to carbon-

(1) (a) This work comprises part of the Ph.D. dissertation of T. Kudo; (b) The Government Chemical Industrial Research Institute, Tokyo, Hon-machi 1, Shibuya-ku, Tokyo, Japan.

(2) T. J. Hardwick, *J. Phys. Chem.*, **66**, 2132 (1962).

carbon bond rupture reactions, the former giving lower yields of products in the C_1 to C_4 range and the latter higher ones of C_1 and C_4 products. Systems were also studied that consist of cyclopentane or 2,2,4-trimethylpentane and *n*-hexane, which has an intermediate photoionization potential with respect to the other two compounds.

Experimental Section

Materials. 2,2,4-Trimethylpentane, *n*-hexane, and cyclopentane, all Phillips, labeled 99.97 and 99.99 mole % and 99 mole % minimum, respectively, were passed through silica gel before use. Gas chromatography showed the former two compounds purified in this manner to be as pure as the materials as received, both having no impurity peak, and it also showed the silica gel treated cyclopentane to contain a 0.2–0.3 mM amount of impurities, which were detected in one peak and tentatively identified from the retention time as one or more pentenes. As received the cyclopentane contained impurities to a larger extent. On purification, no change of G value (the number of molecules produced per 100 ev of energy absorbed) of hydrogen was found for 2,2,4-trimethylpentane and *n*-hexane but for cyclopentane the hydrogen yield was enhanced by 5%. Methyl methacrylate monomer (MMA), commercially supplied from the Tokyo Chemical Industry Co., Ltd., labeled Extra Pure, and stabilized by hydroquinone, was used as received as were the other authentic hydrocarbon samples of adequate purity for identification of radiolysis products.

γ -Ray Irradiations. Five-milliliter samples of a two-component system were, in a manner described previously,³ degassed and sealed into glass cells and then irradiated in a ^{60}Co source at room temperature at an absorbed dose rate of 1.61×10^{17} ev g^{-1} min^{-1} to a total dose of 2.32×10^{20} ev g^{-1} for pure 2,2,4-trimethylpentane. For the mixtures and pure alkanes, corrected dose values were calculated based on the assumption that energy absorption is proportional to the electron density of each irradiated sample. The dose rate was determined by the FeSO_4 dosimeter [$G(\text{Fe}^{3+}) = 15.5$].

Analysis of Products. Hydrogen and methane were analyzed by PVT measurements conventional in this laboratory. The other products were analyzed by gas chromatography in a manner similar to that described previously.³

Results

Cyclopentane–2,2,4-Trimethylpentane System.

Hydrogen and Methane. Hydrogen yields in G values vs. the electron fractions of 2,2,4-trimethylpentane in the binary mixtures are shown in Figure 1,

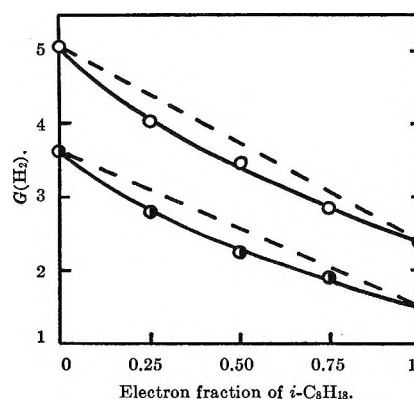


Figure 1. Hydrogen yields from the liquid system cyclopentane–2,2,4-trimethylpentane, for nonscavenger-added (○) and 0.1 *M* MMA-added (●) runs.

where dashed oblique lines indicate (as shown similarly hereafter) yields predicted from the law of averages based on electron fraction of each component. A common trend is seen between the yields from the mixtures without additives and those with 0.1 *M* added methyl methacrylate (MMA): the yields from the mixtures were always lower than predicted. The shapes of both experimental curves appear in qualitatively good agreement with those presented by Hardwick² for binary saturated hydrocarbon systems, e.g., cyclopentane–2,3-dimethylbutane.

Methane yields vs. the electron fractions for non-added and 0.1 *M* MMA-added systems have been plotted in Figure 2. Mixture law deviations are shown for the two systems, where the yields are higher than predicted. The methane yield from pure cyclopentane is essentially equal to zero as compared to that from 2,2,4-trimethylpentane.

Isobutane and Isobutene. Isobutane and isobutene are both typical products resulting from carbon–carbon bond rupture reactions in the radiolysis of 2,2,4-trimethylpentane.^{3–5} The largest portion of these products may originate in C_4 fragments initially produced, since it has been concluded that the combination of two fragments of carbon content less than the parent branched hydrocarbon, 2,2,4-trimethylpentane, is of minor significance.^{3,5}

In Figure 3, curves for production of both isobutane and isobutene from the binary nonscavenger-added system show a greater enhancement of yield than that obtained for the methane yield (Figure 2) while, for the system with 0.1 *M* added MMA, the degree of

(3) T. Kudo and S. Shida, *J. Phys. Chem.*, **67**, 2871 (1963).

(4) J. A. Knight, R. L. McDaniel, R. C. Palmer, and F. Sicilio, *ibid.*, **65**, 2109 (1961).

(5) J. A. Knight and C. T. Lewis, *Radiation Res.*, **23**, 319 (1964).

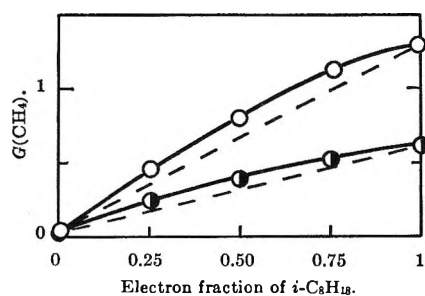


Figure 2. Methane yields from the liquid system cyclopentane-2,2,4-trimethylpentane, for nonadded (○) and 0.1 *M* MMA-added (●) runs.

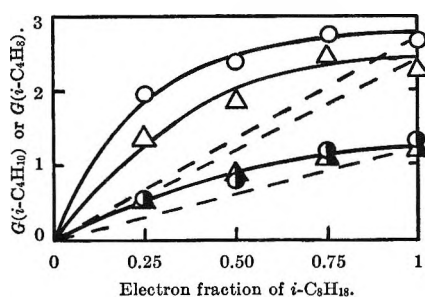


Figure 3. Isobutane [for nonadded (○) and 0.1 *M* MMA-added (●) runs] and isobutene [for nonadded (Δ) and 0.1 *M* MMA-added (▲) runs], yields from the liquid system cyclopentane-2,2,4-trimethylpentane.

change from the dashed line appears similar to the case of methane (Figure 2).

Ethylene. In Figure 4 the ethylene yields are plotted against the electron fraction of 2,2,4-trimethylpentane. All experimental values are found to appear on the same predicted dashed line within experimental error. This product results almost exclusively from cyclopentane, and its formation processes are not affected by mixing its parent hydrocarbon with 2,2,4-trimethylpentane or 0.1 *M* MMA.

Propylene. In Figure 5 the propylene yield is presented against the electron fraction of 2,2,4-trimethylpentane. For the result without additives an upward deviation of the yield from the predicted value appears in the yields from the mixtures, but this is not the case for the result with 0.1 *M* added MMA.

Scavenged Fraction with 0.1 *M* Added MMA. In Table I are tabulated the "scavenged fractions" with 0.1 *M* added MMA for each electron fraction. Here the "scavenged fraction" is defined as the ratio of the yield from the 0.1 *M* MMA-added system to the yield from the nonadded one.

Discussion

One might expect that the results of the present work would support either the view that energy is

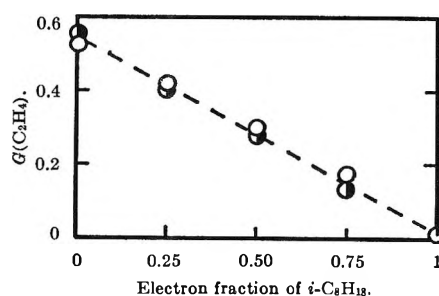


Figure 4. Ethylene yields from the liquid system cyclopentane-2,2,4-trimethylpentane, for nonadded (○) and 0.1 *M* MMA-added (●) runs.

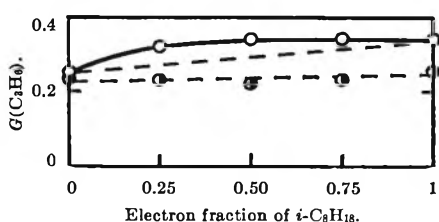


Figure 5. Propylene yields from the liquid system cyclopentane-2,2,4-trimethylpentane, for nonadded (○) and 0.1 *M* MMA-added (●) runs.

Table I: Scavenged Fraction with 0.1 *M* Added MMA for the Products from the Cyclopentane-2,2,4-Trimethylpentane Mixtures

Product	Electron fraction of 2,2,4-trimethylpentane				
	0	0.25	0.50	0.75	1.00
H ₂	0.28	0.31	0.35	0.34	0.37
CH ₄	0.2	0.45	0.51	0.53	0.52
C ₄ H ₁₀	...	0.71	0.66	0.56	0.50
C ₄ H ₈	...	0.61	0.52	0.56	0.48

absorbed in proportion to the electron fraction of the components or that energy transfer occurs between the components.

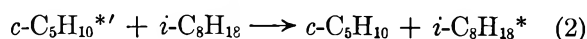
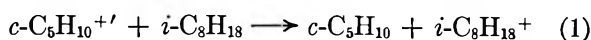
Even if there is no decisive evidence to support simple proportionality between energy absorbed and electron fraction, deviation of the actual energy absorption by each component from the ideal law should be, at worst, in the same extent as the deviation of the yields of hydrogen (Figure 1) or methane (Figure 2). For a given cyclopentane-2,2,4-trimethylpentane mixture the yield of hydrogen is decreased (Figure 1), while at the same time the yield of methane is enhanced (Figure 2). It should be noted that this effect can be explained as being due to changes in the law of absorption in proportion to electron fraction, the changes corresponding to more absorption of energy in 2,2,4-trimethylpentane. Such an explanation, how-

ever, will come to a self-contradiction with the fact of the yields of ethylene being linear (Figure 4). On the other hand, the evidence of the greatly enhanced yields of C_4 products (Figure 3) compared with the case of methane (Figure 2) seems to show an apparent existence of energy-transfer phenomena in the mixture. A similar discussion has been presented by Barzynski, *et al.*,⁶ for the results from the benzene-nickel tetracarbonyl mixtures.

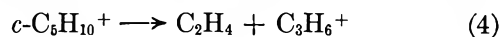
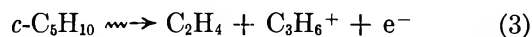
It seems to be reasonable to conclude from the work by Hardwick that there is no actual problem in using the electron fraction theory for alkane-cycloalkane systems since the results of the systems *n*-hexane-2,3-dimethylbutane and cyclopentane-2,3-dimethylbutane show good consistency with the entirety of the results of other binary systems of the saturated hydrocarbons which have been studied.² In the following discussion we have assumed, as has Hardwick, that energy is absorbed in proportion to the relative electron density of the components.

Lassetre, *et al.*,^{7,8} have shown in a series of papers on electron spectroscopy in gases for electrons with initial energies around 400 eV that "curiously, the spectra from saturated hydrocarbons are very similar to one another among energy loss spectra for helium, hydrogen, methane, ethane, propane, cyclohexane, ethylene, water, nitrogen, carbon monoxide, and oxygen." This appears to support qualitatively, though not conclusively, the preceding assumption, insofar as the components are saturated hydrocarbons.

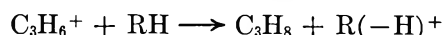
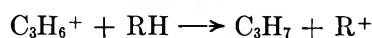
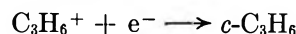
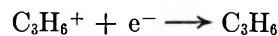
Energy-Transfer Mechanisms in the Binary System. For the deviation of hydrogen yield from the predicted value, a charge-transfer mechanism has been proposed for binary saturated hydrocarbon mixtures.² The mechanism well explains the results for methane and isobutane and isobutene, respectively, shown in Figures 2 and 3 as well as the result for hydrogen in Figure 1, based on the first adiabatic ionization potentials of cyclopentane and 2,2,4-trimethylpentane (isooctane): 10.51 and 9.84 eV, respectively.⁹ On the other hand, if excited neutral species $c-C_5H_{10}^{*}$ were produced by radiolysis transfer energy to $i-C_8H_{18}$, it would be found that such an excitation transfer mechanism also satisfies the results shown in Figures 1-3. So, although values are not known for the excitation energies involved, in the binary mixtures two types of reactions may generally be considered to proceed as immediate consequences of ionization and excitation



where the prime is used as a symbol of states of ions and excited molecules initially produced. So the products which have $C_5H_{10}^{+'}$ or $C_5H_{10}^{*}'$ as their precursor are transformed into other (or the same) products which have $i-C_8H_{18}^{+}$ or $i-C_8H_{18}^{*}$ as their precursor. It is indicated that the transformation occurred in greater ratio in the case of C_4 products (Figure 3) than in the case of hydrogen (Figure 1) or methane (Figure 2). As for ethylene formation, it is negligibly small. This indicates that either or both of the following rapid decompositions may have occurred



where $C_3H_6^{+}$ appears with the largest intensity in the 70-v mass spectra¹⁰ and thereby reaction 4 has been suggested by Hughes and Hanrahan to occur fairly efficiently in the liquid-phase radiolysis of cyclopentane.¹¹ Although they did not formulate the successive reaction of $C_3H_6^{+}$ to avoid speculation, there should be considered the following four consecutive reactions of (3) or (4)



The first and the second of these are neutralization without decomposition. Part of C_3H_7 produced in the third reaction may give C_3H_5 by H atom abstraction. The third and the fourth have recently been shown by Doepker and Ausloos to occur in the gas-phase radiolysis of cyclopentane on the basis of the isotopic analysis of the propanes formed in the mixtures of $c-C_5D_{10}$ plus various saturated and unsaturated hydrocarbons.¹² There seems to be no evident reason to exclude the possibility of these four reactions occurring in condensed phases.

(6) H. F. Barzynski, R. R. Hentz, and M. Burton, *J. Phys. Chem.*, **69**, 2034 (1965).

(7) E. N. Lassetre and S. A. Francis, *J. Chem. Phys.*, **40**, 1208 (1964), etc.⁸

(8) Reference 75 cited by H. A. Schwarz, *Ann. Rev. Phys. Chem.*, **16**, 347 (1965).

(9) F. I. Vilesov, *Soviet Phys. Usp.*, **6**, 888 (1964); see Table XVIII.

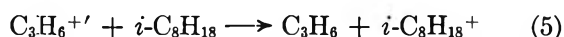
(10) American Petroleum Institute Research Project No. 44, "Catalog of Mass Spectral Data," National Bureau of Standards, Washington, D. C.

(11) M. Hughes and R. J. Hanrahan, *J. Phys. Chem.*, **69**, 2707 (1965).

(12) R. D. Doepker and P. Ausloos, *J. Chem. Phys.*, **44**, 1951 (1966).

Although we did not identify *c*-C₃H₆, a gas chromatogram peak which has approximately 1.5 times the peak area of C₃H₈ was detected at a retention time between those of C₃H₆ and butene-1, a trace of which was also detected from the run on pure cyclopentane. We obtained $G(\text{C}_2\text{H}_4) = 0.53$, $G(\text{C}_3\text{H}_6) = 0.26$, and $G(\text{C}_3\text{H}_8) = 0.07$. In addition to these values, if the $G(\text{c-C}_3\text{H}_6) = 0.10$ value presented by Hughes and Hanrahan¹¹ is taken into account as it stands in spite of lack of complete agreement between their G values and those obtained in the present work, the material balance for reaction 3 or 4 may be found satisfactory within 80%: $G(\text{C}_2\text{H}_4) = 0.53$, $G(\text{C}_3$ for (3) or (4)) = 0.43.

Part of the enhancement shown with propylene formation from the binary system (Figure 5) may possibly be accounted for by a charge transfer



followed by



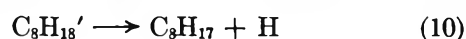
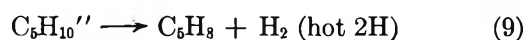
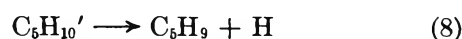
where part of C₃H₇ may disproportionate to produce C₃H₆. The charge-transfer mechanism in (5) is not explained unambiguously from the data of the ionization potentials obtained for the gas phase since most ionization potential values as yet reported for propylene are not more than the value of 9.84 eV found by Honig,¹³ which is accidentally equal to the ionization potential (IP) of *i*-C₈H₁₈. The first adiabatic IP of C₃H₆ is given to be 9.73 eV,⁹ which is lower than the IP of *i*-C₈H₁₈. However, charge transfer could occur if there were an ordering of ionization potential holding the IP of C₃H₆ higher than the ground-state IP of *i*-C₈H₁₈ in the radiolytic liquid environment. If we consider, on the other hand, excited states of C₃H₆⁺ and *i*-C₈H₁₈⁺, reaction 5 would be more probable than in the case of a ground state of C₃H₆⁺ since, in the liquid, the energy levels may be broadened to facilitate a resonant energy transfer between C₃H₆⁺ and *i*-C₈H₁₈. Of course, the increase in C₃H₆ is explicable only by reactions 1 and 2 followed by reaction 7, which involves *i*-C₈H₁₈^{*}, the product of excitation transfer reaction 2, as well as *i*-C₈H₁₈⁺, the product of charge-transfer reaction 1



where *i*-C₈H₁₈⁺ and *i*-C₈H₁₈^{*} may be surmised to be species of molecular ions in their ground states and electronically excited neutral molecules of states only slightly higher than, and/or equal to, the lowest state. If the C₃ product of reaction 7 is mainly C₃H₇, a linear

plot then may be obtained in the system with radical scavengers as shown in Figure 5.

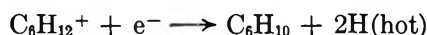
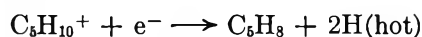
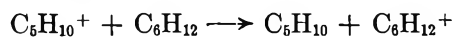
Different States of Precursors from the Same Component. For hydrogen, methane, isobutane, and isobutene the results obtained experimentally without additives and those with 0.1 *M* added MMA (Figures 1-3) are generally similar in appearance, being either convex or concave for a given product under both conditions. From Table I, it may be found that the "scavenged fraction" for hydrogen varies nearly continuously from that of pure cyclopentane to that of pure isooctane; *i.e.*, there might appear to be no evidence in this case that the behavior of precursors initially formed differs from the behavior of precursors formed after energy transfer. However, a careful consideration of Figure 1 will reveal that such a conclusion is wrong. The lower curve in Figure 1 indicates only the non-scavengable portion of the hydrogen yield. It is depressed below the ideal curve, indicating energy transfer from cyclopentane to isooctane. The difference between the two curves represents the "thermal" portion of the hydrogen yield and it must vary linearly with electron fraction, as can be shown by subtracting the two curves point by point and plotting the difference. Stated another way, the curvature evident in the total hydrogen yield (top curve) is due completely to curvature in the curve for non-scavengable processes (bottom curve). For an interpretation of the evidence, if we assume that the precursors of hydrogen are different depending on whether they yield H or H₂ (and/or hot 2H), the following five processes are considered



where single and double primes are used simply to distinguish the molecular states from each other. Thermal H atoms produced in reactions 8 and 10 are presumed to be scavenged by 0.1 *M* MMA, the concentration of the additive being nearly sufficient for complete scavenging of the atoms. If we require that only processes 9 and 11 producing "molecular" hydrogen (possibly involving hot hydrogen atoms) are affected by energy transfer (reaction 12) and recognize that this is not the case for processes 8 and 10, then the results given in Figure 1 would be well explained.

(13) R. E. Honig, *J. Chem. Phys.*, **16**, 105 (1948).

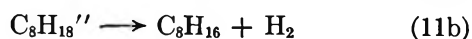
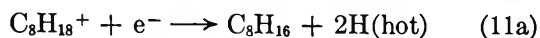
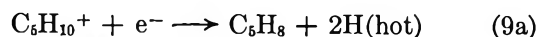
Muccini and Schuler¹⁴ have obtained linear variations of $G(c\text{-C}_5\text{H}_9\text{I})$ and $G(c\text{-C}_6\text{H}_{11}\text{I})$ in liquid mixtures of these two cycloalkanes with added iodine and have concluded that energy transfer between the cycloalkanes does not occur. Since the two cycloalkyl iodides are produced with the accompanying H atoms, this directly corresponds to the linearity of the thermal H atom scavenging in (8) and (10) (that is, behavior according to the mixture laws) in the present work. Toma and Hamill¹⁵ have proposed the following reaction scheme in the radiolysis of cyclopentane-cyclohexane mixtures



According to this mechanism the total number of hot H atoms produced by the two neutralization processes is always constant and is independent of the concentrations of the respective hydrocarbons even if charge transfer from $c\text{-C}_5\text{H}_{10}^+$ to $c\text{-C}_6\text{H}_{12}$ has occurred. Consequently, "the yield of free radicals from reactions of hot H atoms should be linear in the concentrations of the respective hydrocarbons."¹⁶ They have cited as the results of the crucial experiment the linear variations of $G(c\text{-C}_5\text{H}_9\text{I})$ and $G(c\text{-C}_6\text{H}_{11}\text{I})$ obtained by Muccini and Schuler.¹⁴ However, it should be noticed that the $c\text{-C}_5\text{H}_9$ and $c\text{-C}_6\text{H}_{11}$ radicals could also be produced as the accompanying products of thermal H atoms and by abstraction reactions of these thermal H atoms. The formation of thermal H atoms has been shown from the results depicted in Figure 1 to be independent of energy transfer.

From the results obtained in Muccini and Schuler's work¹⁴ and in this study and the proposition by Toma and Hamill,¹⁵ all described heretofore in this paper, we postulate the following mechanism for the results obtained for the hydrogen formation as shown in Figure 1.

Reactions 9 and 11 may be divided into two types of reaction, respectively



The precursors in (8) and (10) would be $\text{C}_5\text{H}_{10}^+$ and $\text{C}_8\text{H}_{18}^+$, respectively, which participate in a charge transfer such as $\text{C}_5\text{H}_{10}^+ + \text{C}_8\text{H}_{18} \rightarrow \text{C}_5\text{H}_{10} + \text{C}_8\text{H}_{18}^+$ as do the precursors in (9a) and (11a), the charge trans-

fer having no effect on the change in the number of hydrogen atoms formed after it has occurred. The precursors in (9b) and (11b) may be excited neutral species which could be produced by neutralization of the molecular ions or directly by radiolysis. Reaction 12 indicates excitation transfer concerning these species, with the double primes used in terms of the postulated mechanism, and is contained in reaction 2. According to this postulated mechanism, the energy transfer from cyclopentane to isooctane occurs by both charge and excitation transfers.

Reactions 9b and 11b correspond to "molecular" hydrogen formation which is concluded to be a small fraction (10–20%) of the total yield of hydrogen in the case of light cyclohexane C_6H_{12} by Dyne and Jenkinson.¹⁶ It is likely that the extent of the decrease shown in Figure 1 is found to be in quantitatively good agreement with that expected from the fraction. Now, let the fraction be 20%, *i.e.*, 0.2 commonly for cyclopentane and isooctane, and assume that all $\text{C}_5\text{H}_{10}''$ transfer energy to C_8H_{18} . Using G values for pure cyclopentane and isooctane, *i.e.*, 5.0 and 2.4, respectively (Figure 1), we can simply calculate the decreased yield of hydrogen for the electron fraction, *e.g.*, 0.5. That is, the total yield of "molecular" hydrogen is the sum of $5.0 \times 0.2 \times 0.5 = 0.5$ and $2.4 \times 0.2 \times 0.5 = 0.24$, *i.e.*, 0.74 in G value, if the excitation transfer (12) did not occur; after the energy transfer, 0.5 of the "molecular" hydrogen formed from $\text{C}_5\text{H}_{10}''$ will be lost and concurrently 0.24 from $\text{C}_8\text{H}_{18}''$ will be newly produced; after all net decrease of "molecular" hydrogen, the yield is given to be $0.74 - (0.24 + 0.24) = 0.26$. This value well corresponds to the extent of the decreased yield at the electron fraction 0.50 in Figure 1. However, if 10% "molecular" hydrogen were assumed as the fraction for the estimation of it, only a qualitative agreement would be found. Clearly a new experimental approach to the problem is required to obtain an unassailable conclusion.

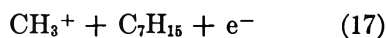
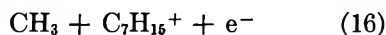
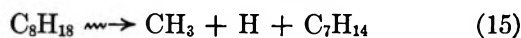
In the case of methane, a tendency for an increase of the scavenged fraction within the region of higher electron fraction of isooctane seems to exist from the quantities in the row of methane in Table I, although the situation may be almost the same within experimental error as in the case of hydrogen. This suggests, with-

(14) G. A. Muccini and R. H. Schuler, *J. Phys. Chem.*, **64**, 1436 (1960).

(15) S. Z. Toma and W. H. Hamill, *J. Am. Chem. Soc.*, **86**, 4761 (1964).

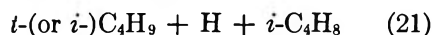
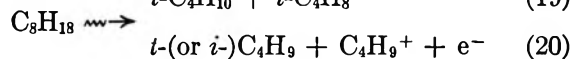
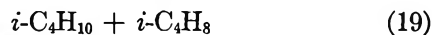
(16) P. J. Dyne and W. M. Jenkinson, *Can. J. Chem.*, **38**, 539 (1960).

out sufficient precision, that the higher the region of electron fraction, the more the radical processes contained in the following reactions occur after the energy transfer.



On the other hand, isobutane and isobutene from the mixture always have apparently higher "scavenged fractions" than from pure isooctane. This means that those C₄ products produced after the energy transfer differ from the C₄ products initially produced in their precursors.

In the previous note,³ where iodine was used as a scavenger, four types of reactions to produce the C₄ products have been discussed



where (19) and (21) were neglected. Recently, another result has been obtained where these two types of reactions should not necessarily be neglected if the experimental results were to be interpreted by the data obtained using MMA in place of I₂ as a scavenging reagent to measure the scavenged ratio of *i*-C₄H₈ formation.¹⁷ C₄H₉⁺ was assumed to give *i*-C₄H₁₀ through an ion-molecule reaction in both cases.

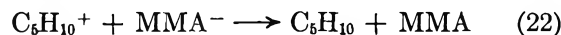
It may be stated that the radiolytic decomposition reactions of isooctane have a structure which will be defined to be composed of (i) the several modes of bond-rupture reaction, as shown in (18)–(21), producing the same product or the same pair of products and (ii) the ratio among the modes of reactions which occur. As a measure of the ratio, the *G* value of reaction used in the previous paper³ will be suitable. This ratio is the number of molecules to decompose per 100 ev of energy absorbed. Reactions (13)–(17), in which all modes of bond-rupture lead to the formation of methane and C₇ products, may correspond to another structure of reaction if *G* values of the reactions are given or taken into account.¹⁷

Using the definition of the structure, the appreciable variation of the "scavenged fractions" for the C₄ products in the mixtures compared with those in pure

isooctane (Table I) is interpreted as the result that, in addition to a structure of reaction occurring from the precursors *i*-C₈H₁₈⁺ and *i*-C₈H₁₈^{*'} produced initially by the radiolysis of *i*-C₈H₁₈, there is superimposed another structure of reaction occurring from the precursors *i*-C₈H₁₈⁺ and *i*-C₈H₁₈^{*} produced indirectly by the energy transfer. The *i*-C₈H₁₈⁺ and/or *i*-C₈H₁₈^{*} will decompose more *via* reaction paths such as (18), producing C₄ free-radical species, than by those such as (19), producing C₄ molecular products or fragments not scavenged by additives (Figure 3 and Table I).

Transformations from the products, *e.g.*, hydrogen, formed from cyclopentane, to the products, *e.g.*, isobutane, formed from isooctane, are shown in Figures 1–3. It is concluded that the transformations did not occur proportionally to the *G* values obtained from the radiolysis of pure isooctane since they are *G*(H₂) = 2.4, *G*(CH₄) = 1.3, *G*(*i*-C₄H₁₀) = 2.7, and *G*(*i*-C₄H₈) = 2.3. The increases from the expected yield of two C₄ products are about two times greater than expected from, for example, the increase of methane in the ratio *G*(C₄):*G*(CH₄). This suggests, within the range of the products analyzed, that the over-all transformation occurs *via* different ionization or electronic excitation states of precursors to give different products or reaction structures.

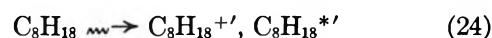
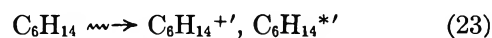
To account for the results of this study, it may still be necessary to consider the influence of competitive radical recombinations and disproportionations with major radicals such as C₅H₉[·] and C₆H₁₇[·], as have been discussed for C₅H₉[·] and C₆H₁₁[·] in the cyclopentane-cyclohexane mixtures,¹⁴ and to inspect experimentally to what extent reaction 22 competes with reactions 1, 4, 7, 9a, 11a, etc.



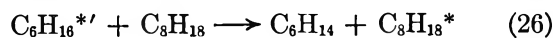
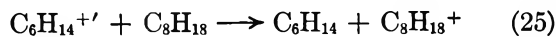
Results and Discussion

n-Hexane-2,2,4-Trimethylpentane System

General Aspects. The results obtained for this system are shown in Figures 6–12. Deviation of experimental values from the yields expected in terms of the law of mixtures, which is explicable on the basis of energy transfer from *n*-hexane to 2,2,4-trimethylpentane, is seen in all cases of H₂, CH₄, C₂H₆, C₃H₈, and *i*-C₄H₁₀. Applying the discussion for the *c*-pentane-2,2,4-trimethylpentane system as it is, the following energy-transfer mechanism may be considered in the present system



(17) T. Kudo, submitted for publication.



As the photoionization potentials of *n*-hexane and 2,2,4-trimethylpentane are 10.17 and 9.84 eV, respectively,⁹ a mechanism such as (25) could well be considered.

Several Precursors from Alkanes. In Table II, *G* values calculated by the law of averages are compared with ΔG , the deviation of the observed values from the calculated values, *i.e.*, $G_{\text{obsd}} - G_{\text{calcd}}$, for the electron fraction 0.50 of 2,2,4-trimethylpentane. If we simply assume that $|\Delta G|/G_{\text{calcd}}$ can be a measure of energy transfer, there is a striking regularity. In the first

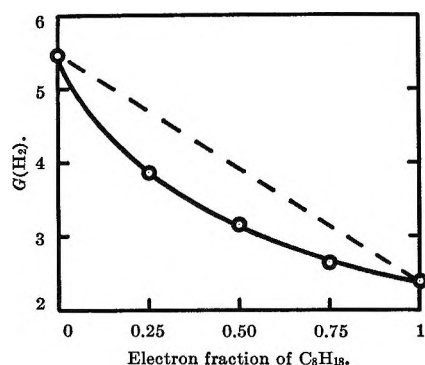


Figure 6. Hydrogen yields from the liquid system *n*-hexane-2,2,4-trimethylpentane.

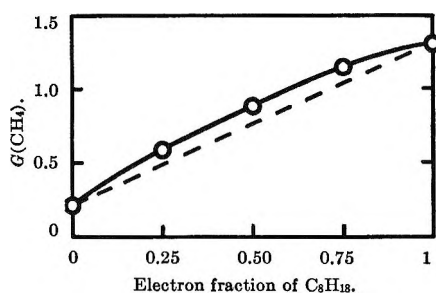


Figure 7. Methane yields from the liquid system *n*-hexane-2,2,4-trimethylpentane.

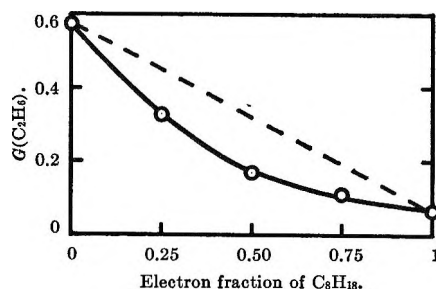


Figure 8. Ethane yields from the liquid system *n*-hexane-2,2,4-trimethylpentane.

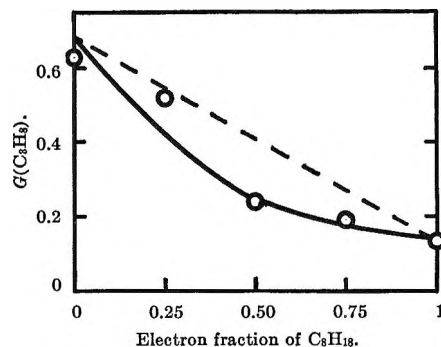


Figure 9. Propane yields from the liquid system *n*-hexane-2,2,4-trimethylpentane.

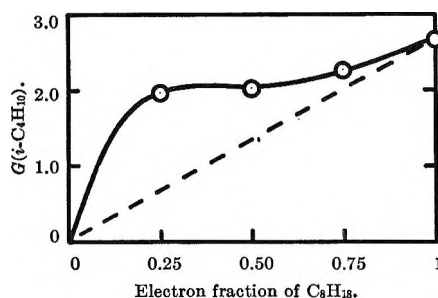


Figure 10. Isobutane yields from the liquid system *n*-hexane-2,2,4-trimethylpentane.

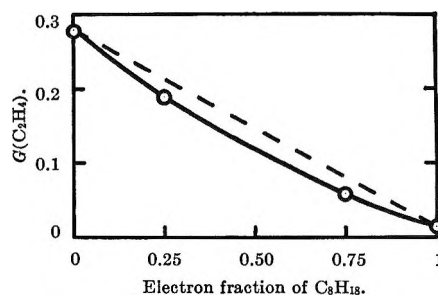


Figure 11. Ethylene yields from the liquid system *n*-hexane-2,2,4-trimethylpentane.

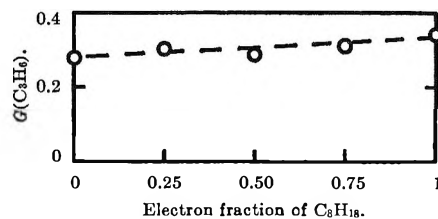


Figure 12. Propylene yields from the liquid system *n*-hexane-2,2,4-trimethylpentane.

group, hydrogen and methane are seen to be affected to the same extent by energy transfer in their processes of formation: $|\Delta G|/G_{\text{calcd}} = 0.20$ and 0.16 , respectively. On the other hand, in the second group,

ethane, propane, and isobutane, most of which are considered to be produced not by recombination of two radicals but as products finally formed containing the same carbon atoms as fragments directly formed by C-C bond scission, are found to be more remarkably influenced: $|\Delta G|/G_{\text{calcd}} = 0.47, 0.43, \text{ and } 0.50$, respectively. The G values for the latter group are 2 to 3 times greater than those for the former one. This may indicate that the hydrogen or methane and the products, except methane formed by C-C bond rupture, differ in respect to their precursors. Otherwise, $|\Delta G|/G_{\text{calcd}}$ may be of the same order for the two groups, but this is not seen in Table II. Since the ethane and propane are mainly produced from n -hexane, precursors of several kinds for these products will be ascribable to n -hexane. Probably, at least, three species of them are (i) positive molecular ions for charge transfer, (ii) excited neutral molecular species for excitation transfer, and (iii) any molecular species not affected, actually or seemingly, by energy transfer.

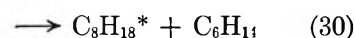
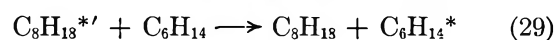
Since the same fact has also been stated previously for 2,2,4-trimethylpentane and cyclopentane, respectively, it may be generally concluded that several different precursors result from irradiated alkanes, corresponding to the differences among the products and the decomposition paths, respectively. This conclusion of precursors is, however, almost made from the apparent results experimentally observed and awaits completion of more detailed studies of the precursors of products formed from alkanes. Then, it seems to be probable that one molecular species of the precursors discussed here will have several decomposition paths.

Table II: Comparison of G Values Calculated by the Law of Averages with $\Delta G = G_{\text{obsd}} - G_{\text{calcd}}$, for the Electron Fraction 0.50 of 2,2,4-Trimethylpentane

	H ₂	CH ₄	C ₂ H ₆	C ₃ H ₈	<i>i</i> -C ₄ H ₁₀
$ \Delta G /G_{\text{calcd}}$	0.20	0.16	0.47	0.43	0.50

On the Formation of Products. The curve shown for isobutane in Figure 10, which seems to have one point of inflection, is difficult to explain. The complicated curve might indicate participation of some special quenching processes which are sensitive to concentration of component molecules surrounding the excited, neutral, or ionic species. Although confirmative conclusion cannot be arrived at because only one run for each electron fraction was accomplished, the situation appears to be the same for the case of propane

in Figure 9 in which one can depict another curve having a point of inflection, if desired. However, the results of the two products are well found commonly to indicate the existence of the over-all reactions 25 and 26. The points of inflection might correspond partly to the following sensitive excitation or charge-transfer mechanism, or quenching mechanism in a broad sense



where $\text{C}_3\text{H}_{18}^{+'}$ or $\text{C}_3\text{H}_{18}^{*'}$ implies a compendium of species directly formed by irradiation and should be taken as indicating a definite number of species, specific to reactions 27–30, of all precursors. Dyne, Denhartog, and Smith have presented a simultaneous equilibrium among intermediates of hydrogen in the light and heavy cyclohexane mixture.¹⁸ Reactions 25–30 in this work may be able to show another simultaneous equilibration.

In Figure 11, the deviation of the yield of ethylene from the predicted value is shown to be relatively small. This seems to indicate that a major part of ethylene formed almost completely from n -hexane results directly from fast, molecular processes without the influence of any energy transfer and, perhaps, of radical scavengers, and only a small fraction results indirectly from ethyl radicals.

As for propylene in Figure 12, the apparent result of linearity may be ascribable to the separate G values of the two components drawing very near.

The results for n -C₄H₁₀, neo-C₅H₁₂, *i*-C₄H₈, and C₄H₈-1 could not be shown owing to the gas chromatographs used in this work being unsuitable for the purpose of dividing the products. If we were to perform a complete analysis of them additionally using mass spectrometric techniques, resulting facts would accord with the energy-transfer mechanism from n -hexane to 2,2,4-trimethylpentane without exception. It is of interest whether the curve for *i*-C₄H₈ will be depicted as having a point of inflection.

Cyclopentane- n -Hexane System

Results of Nonapparent Energy Transfer. All results obtained for this system are shown in Figures 13–20. *c*-C₃H₆ was tentatively identified in the same manner as in the case of the cyclopentane-2,2,4-tri-

(18) P. J. Dyne, J. Denhartog, and D. R. Smith, *Discussions Faraday Soc.*, **36**, 135 (1963).

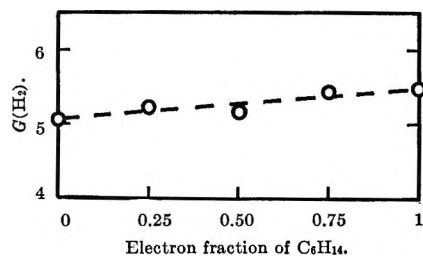


Figure 13. Hydrogen yields from the liquid system cyclopentane-*n*-hexane.

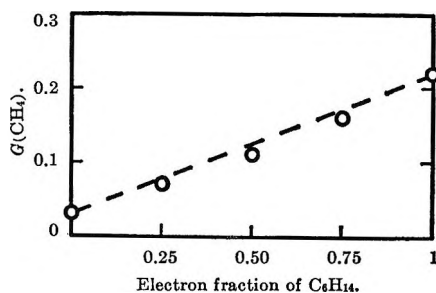


Figure 14. Methane yields from the liquid system cyclopentane-*n*-hexane.

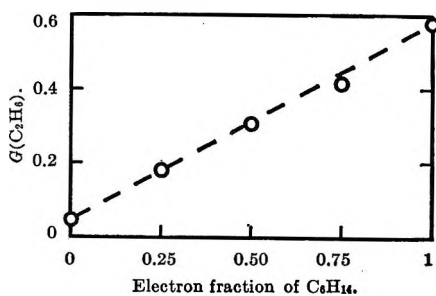


Figure 15. Ethane yields from the liquid system cyclopentane-*n*-hexane.

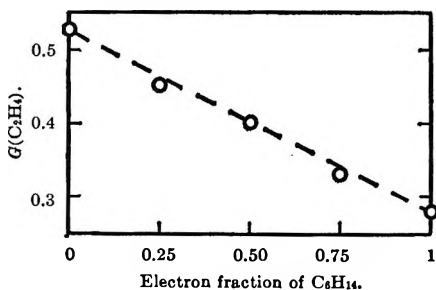


Figure 16. Ethylene yields from the liquid system cyclopentane-*n*-hexane.

methylpentane system. C₃ (trace) was a product or products detected immediately after and partly overlapped with the *c*-C₃H₆ on gas chromatograms. *n*-C₄H₁₀ and C₄H₈-1 were analyzed in one gas chroma-

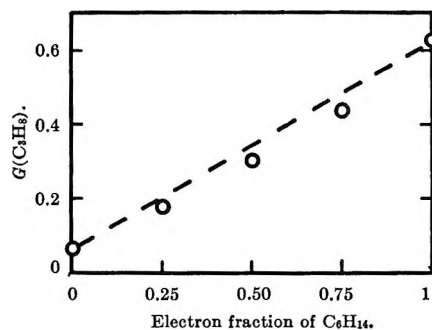


Figure 17. Propane yields from the liquid system cyclopentane-*n*-hexane.

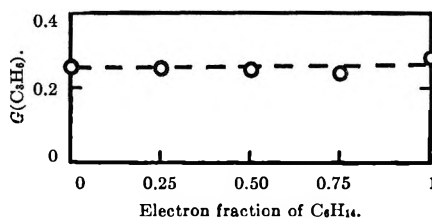


Figure 18. Propylene yields from the liquid system cyclopentane-*n*-hexane.

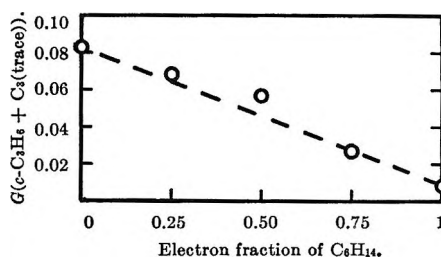


Figure 19. Cyclopropane plus C₃ (trace) yields from the liquid system cyclopentane-*n*-hexane.

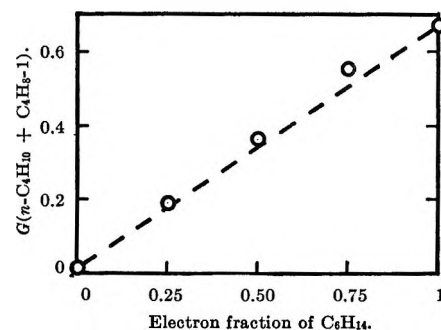


Figure 20. *n*-Butane plus butene-1 yields from the liquid system cyclopentane-*n*-hexane.

togram peak. Although energy transfer from *c*-pentane to *n*-hexane is expected on the basis of the photoionization potentials of 10.51 and 10.17 eV, respectively,⁹ no evidence indicating such results is

shown in these figures. In Figure 17 for C_3H_8 , one will see a result of slight energy transfer even inversely occurred rather than expected from the order of photoionization potentials. However, comparing the result of ethane in Figure 15 with that in Figure 8, it may be concluded that energy-transfer phenomena in the present system are negligible.

For hydrogen formation, the order of photoionization potential has been found to correlate validly with the direction of energy transfer such as, *e.g.*, from cyclopentane to 2,3-dimethylbutane.² In the present work, where hydrogen and the other products were studied, however, it was shown that the orders and the directions do not necessarily correspond with each other, even if the latter were not inversed.

Energy Transfer Inverse to That Expected from the Order of Photoionization Potentials. A similar result has been obtained by Manion and Burton¹⁹ in the cyclohexene-benzene system. They estimated the ionization potentials of these components to be approximately equal without citing photoionization data, but according to the data⁹ they are 8.95 and 9.24 eV, respectively, and the result is that the system has contained energy transfer, or excitation transfer, as they suggested, from the component lower in photoionization potential to the one higher in it. However, if

one would accept that "in a mixture of two components, irrespective of the component primarily ionized, the ionization is quickly transferred to the species of lower ionization potential"²⁰ the result of Manion and Burton may not necessarily be explained by excitation transfer alone. Concerning the results for the cyclopentane-*n*-hexane system in this work (Figures 13-20), it seems to be reasonable to conclude that they were obtained in a special situation where charge and excitation transfers from each component to the other components accidentally balanced rather than that energy transfer occurred to a negligible extent.

In both of the systems cyclopentane-2,2,4-trimethylpentane and *n*-hexane-2,2,4-trimethylpentane this effect would have been covered by the predominantly larger part of the energy transfers occurring from the one component of higher ionization potential to the other of lower potential. However, this effect is presented only as a speculation in the present work. Much more definitive work which will be carried out to examine in separate detail the intermediate steps of charge transfer and excitation transfer is awaited with interest.

(19) J. P. Manion and M. Burton, *J. Phys. Chem.*, **56**, 560 (1952).

(20) H. D. Smyth, *Rev. Mod. Phys.*, **3**, 347 (1931).

Vapor Phase Charge-Transfer Complexes. I. Diethyl Sulfide-Iodine¹

by Milton Tamres and John M. Goodenow

Chemistry Department, University of Michigan, Ann Arbor, Michigan (Received May 23, 1966)

The diethyl sulfide-iodine complex has been studied in the vapor phase by a spectrophotometric method in the temperature range 94–127°. Several of the thermodynamic and spectral properties of the complex in the vapor phase differ significantly from those previously found in *n*-heptane solution. However, the differences for this case, which is among the stronger charge-transfer complexes with iodine, are not as pronounced as those recently reported for the weaker complexes of iodine with benzene and with diethyl ether. These general trends are consistent with hypotheses on solvent influence.

Introduction

Spectral properties of charge-transfer (CT) or donor-acceptor complexes and their theoretical interpretations have received wide attention in the past 15 years.² The vast amount of spectral and thermodynamic data which has been accumulated is the result of studies made almost entirely on complexes *in solution*. The theory, on the other hand, uses properties which apply to the isolated species, a condition which is approached only in the *vapor state* at low pressures.

That spectral and thermodynamic properties are affected by the solvent, even those commonly regarded as "inert," is apparent even in an early experimental report on the subject.³ More detailed analyses of solvent effects confirm how large the influence of solvent can be.⁴

Very recently, several studies of CT complexes in the vapor phase have been reported: iodine complexes with benzene and with diethyl ether,⁵ carbonyl cyanide complexes with ethers and with aromatic hydrocarbons,⁶ and the tetracyanoethylene complex with *p*-xylene.⁷ These, generally, can be classified among the weaker CT complexes. The results make clear that important differences exist with regard to band position, equilibrium constant, and extinction coefficient. According to theory,^{8,9} these differences should be smaller for the stronger CT complexes. The strongest complex studied to date, diethyl sulfide-iodine, was mentioned in a preliminary report.¹⁰ A more detailed account is given in this paper.

Experimental Section

Reagents. The source and purification of iodine,¹¹

of *n*-heptane,¹¹ and of diethyl sulfide¹² have been given elsewhere. Vapor phase chromatography showed the absence of impurities in the diethyl sulfide and in the *n*-heptane. The iodine and the diethyl sulfide were kept in separate storage bulbs in a Pyrex vacuum line and prior to use the vapors of both were dried over phosphorus pentoxide.

Apparatus and Procedure. The metering out and transfer of reagents into a cylindrical quartz cell were made using the Pyrex vacuum line. Teflon-threaded

(1) Taken in part from the Ph. D. Thesis of J. M. Goodenow, University of Michigan, Dec 1965. This work was supported by a grant from the National Science Foundation, NSF GP-3691 Research, and also by a grant from the Horace H. Rackham School of Graduate Studies at the University of Michigan.

(2) (a) G. Briegleb, "Elektronen-Donator-Acceptor-Komplexe," Springer-Verlag, Berlin, 1961; (b) R. S. Mulliken and W. B. Person, *Ann. Rev. Phys. Chem.*, **13**, 107 (1962); (c) L. J. Andrews and R. M. Keefer, "Molecular Complexes in Organic Chemistry," Holden-Day, San Francisco, Calif., 1964.

(3) H. A. Benesi and J. H. Hildebrand, *J. Am. Chem. Soc.*, **71**, 2703 (1949).

(4) C. C. Thompson, Jr., and P. A. D. deMaine, *J. Phys. Chem.*, **69**, 2766 (1965).

(5) (a) F. T. Lang and R. L. Strong, *J. Am. Chem. Soc.*, **87**, 2345 (1965); (b) F. T. Lang, Ph. D. Dissertation, Rensselaer Polytechnic Institute, Troy, N. Y., 1964.

(6) (a) J. Prochorow, *J. Chem. Phys.*, **43**, 3394 (1965); (b) J. Prochorow and A. Tramer, *ibid.*, **44**, 4545 (1966).

(7) M. Kroll and M. L. Ginter, *J. Phys. Chem.*, **69**, 3671 (1965).

(8) N. S. Bayliss and E. G. McRae, *ibid.*, **58**, 1002 (1954).

(9) S. Carter, J. N. Murrell, and E. J. Rosch, *J. Chem. Soc.*, 2048 (1965).

(10) J. M. Goodenow and M. Tamres, *J. Chem. Phys.*, **43**, 3393 (1965).

(11) M. Brandon, M. Tamres, and S. Searles, *J. Am. Chem. Soc.*, **82**, 212c (1960).

(12) M. Tamres and S. Searles, *J. Phys. Chem.*, **66**, 1099 (1962).

valves (Fischer-Porter Co.) were used to avoid working with stopcock grease which adsorbs the reagents. The techniques for obtaining known concentrations of diethyl sulfide in the 10-cm absorption cell (2-cm i.d.) were similar to those used by Lang and Strong,⁵ *i.e.*, (1) determining the pressure and temperature of a known volume of vapor and (2) measuring out at a fixed temperature a known height of liquid diethyl sulfide from calibrated capillary tubing. A check of one method against the other gave very good agreement (within $\sim 1\%$). A further check was made by measuring out into the absorption cell a known amount of diethyl sulfide by the capillary method, adding a known volume of *n*-heptane, and determining the sulfide concentration from the known spectrum of diethyl sulfide in *n*-heptane solution. Again, agreement was good.

The concentration of iodine was measured *approximately* by allowing the iodine to sublime at room temperature into a bulb of known volume. The iodine was condensed in the absorption cell together with the sulfide at liquid nitrogen temperature and the cell was sealed off from the vacuum line. After the vapor phase data had been taken, a more precise determination of the iodine concentration was made. This was done by "cracking" open the cell and adding a known volume of *n*-heptane. Since thermodynamic values for the diethyl sulfide-iodine complex in *n*-heptane were known from earlier work,¹² the solution data were used to calculate the initial concentration of iodine in the vapor phase.

The diethyl sulfide-iodine adduct is not very volatile and requires elevated temperatures to get appreciable concentrations in the vapor phase. This was accomplished by designing a twin aluminum jacket which held the cell with complex in one compartment and a reference cell in the other. For complete insulation, aluminum covers were placed over the side arms of the cells and quartz covers were inserted in grooves cut in each end of the thermo-jacket to protect the cell windows. The thermo-jacket was wrapped with electrical heating tape and the temperature was controlled by powerstats. Temperature equilibrium could be established in about 20 min. Absorbancy readings over the wavelength range were made in about 0.5 hr, during which time the maximum temperature fluctuation was of the order of 1° . Temperatures were measured with a thermocouple which could be inserted into the side arm of the reference cell and moved to various positions within the cell.

A special aluminum and Bakelite housing was constructed for the cells and thermo-jacket assembly. To minimize reflection of stray light, the thermo-jacket

and aluminum parts of the housing were anodized and dyed black. Thermospacers were inserted next to the body of the spectrophotometer (Beckman DU) and next to the phototube housing for cooling.

The concentration of diethyl sulfide varied from 2.8×10^{-3} to 1.6×10^{-2} *M* and that of iodine from 1.4×10^{-5} to 5.8×10^{-5} *M*. Spectra were recorded at 250–500 $m\mu$ over a temperature range of 94 – 127° , with the absorbancy readings at λ_{\max} (290 $m\mu$) ranging from a high of nearly 0.7 to a low of nearly 0.1. At the end of a run, return was made to the initial temperature, and readings at λ_{\max} were taken as a check on the reproducibility of the data.

Calculations. The spectrophotometric equation which applies to this study is¹³

$$\frac{C_B b C_Z}{A - A_0} = \frac{C_B + C_Z}{\epsilon_c - \epsilon_{I_2}} + \frac{1}{K_c(\epsilon_c - \epsilon_{I_2})} - \frac{A - A_0}{b(\epsilon_c - \epsilon_{I_2})^2} \quad (1)$$

where C_B and C_Z are the initial concentrations of sulfide and of iodine, respectively, b is the cell length, ϵ_c and ϵ_{I_2} are the extinction coefficients of the complex and of free iodine, respectively, A is the absorbancy, A_0 is $\epsilon_{I_2} b C_Z$, and K_c is the association constant. At λ_{\max} (290 $m\mu$), ϵ_{I_2} is quite small, so that the A_0 correction is very small. Calculations of K_c and ϵ_c were programmed for the IBM 7090 computer. The error limits of K_c were determined using the method of Fieller.¹⁴ For work in *solution* at room temperature, reducing eq 1 from quadratic to linear form by dropping the last term produced noticeable error in K_c ,¹² but in the present work at elevated temperature, at which condition K_c is smaller, dropping the last term made very little difference, in accordance with expectation.¹³

Results

There are shown in Figure 1, for typical concentrations used in studying the *ultraviolet* region, the spectra of free diethyl sulfide and free iodine, together with the spectrum which results when the components are mixed. There is evident the intense CT band with a maximum at 290 $m\mu$, a region which is relatively optically clear with respect to the components.

The absorption of diethyl sulfide vapor becomes appreciable only at wavelengths less than 270 $m\mu$ for the concentrations used in this study and no correction for free sulfide is necessary in reading the absorbancy at λ_{\max} of the complex. The sulfide vapor showed a small increase in absorbancy with increase in temperature over the range 63 – 118° in the limited wavelength region

(13) M. Tamres, *J. Phys. Chem.*, **65**, 654 (1961).

(14) E. C. Fieller, *Appendix Suppl. J. Roy. Stat. Soc.*, **7**, 1 (1940).

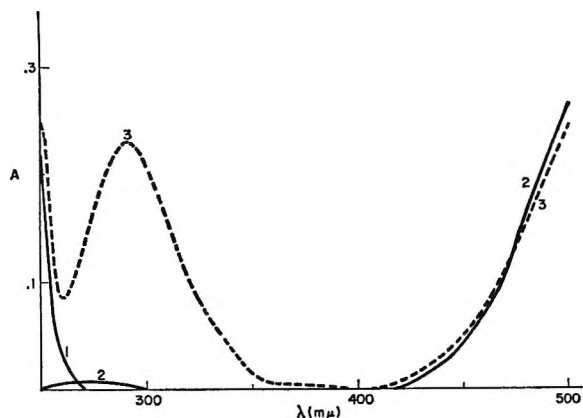


Figure 1. Spectra in the vapor phase at 100° in a 10-cm cell of 1, diethyl sulfide = $2.78 \times 10^{-3} M$; 2, iodine = $4.52 \times 10^{-6} M$; and 3, diethyl sulfide + iodine (1 + 2).

investigated (270–250 $m\mu$) where the sulfide begins to absorb. This is indicative of temperature broadening.

In the region where the CT complex is found, there is a small absorption by free iodine, which results in a very small correction in determining the absorbancy of the complex alone at λ_{\max} . As shown in Figure 1, the iodine has a weak absorption band with a maximum below 290 $m\mu$. This band has been reported not to obey Beer's law and has been attributed¹⁵ to the equilibrium



At 290 $m\mu$, the main contribution of the iodine absorption is due to the species I_2 rather than I_4 . The extinction coefficient of the former^{15,16} at 290 $m\mu$ is 10.2 l. mole⁻¹ cm⁻¹, the value used for ϵ_{I_2} in eq 1. For the concentrations of iodine used in this work, A_0 in eq 1 did not exceed 0.005 and averaged closer to 0.002.

Data for seven donor-acceptor concentrations are plotted in Figure 2 using a modified Benesi-Hildebrand-Scott equation, obtained by dropping the last term in eq 1. The best lines through the points were determined by the method of least squares. Good straight lines also were found using the Benesi-Hildebrand equation.³ The points in the vapor plot show slightly more scatter than those obtained for this complex in *n*-heptane solution.¹² A contributing reason for the greater scatter in the vapor study is due to the indirect method of determining the iodine concentration separately at the end of each vapor run by using the spectrophotometric method after the complex was dissolved in solution. This is less precise than the method used in solution work where the iodine concentration is determined directly by dilution of a common stock solution of known concentration.

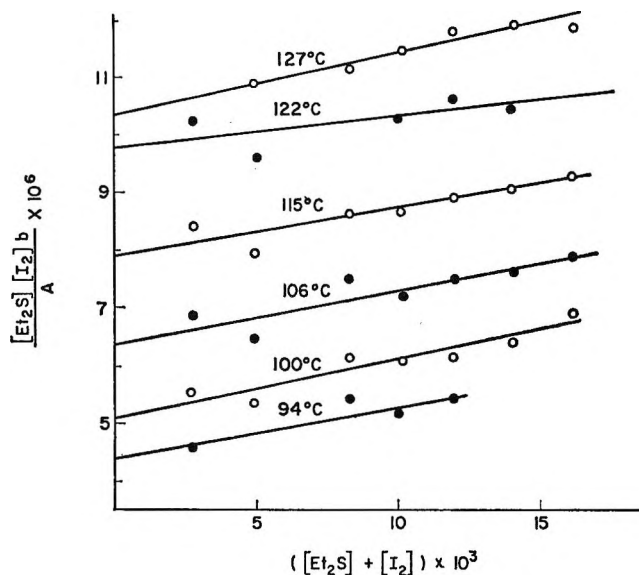


Figure 2. Modified Benesi-Hildebrand-Scott plot of vapor phase data for the diethyl sulfide-iodine complex in the vapor phase.

The values of K_c and ϵ_c determined from the absorbancy data at λ_{\max} are given in Table I. These results are based on a calculation of the initial iodine vapor concentration assuming that in *n*-heptane solution¹² at 25° $K_c = 180$ l. mole⁻¹ and $\epsilon_c = 27,600$ l. mole⁻¹ cm⁻¹, these values being in a range similar to those reported by several investigators.¹⁷ The solution data,¹² however, in one case had led to values at 25° of $K_c = 200$ l. mole⁻¹ and $\epsilon_c = 24,800$ l. mole⁻¹ cm⁻¹ which, of course, would alter the vapor phase results somewhat. To determine the magnitude of the effect, a second set of calculations based on the latter values was made and is given in parentheses in Table I. It is seen that a 10% change in K_c and ϵ_c in the solution data produces a larger percentage change in the vapor phase results, but the general order of magnitude remains similar.

Calculations involving eq 1 to evaluate K_c and ϵ_c are based on the assumption that only a 1:1 complex exists. In the present study, this assumption is supported qualitatively by the narrow (half-width ~ 5700 cm⁻¹) and nearly symmetrical shape of the diethyl sulfide-iodine CT band, published previously.¹⁰ But this feature alone is not conclusive. Even the fact that the

(15) G. Kortüm and G. Friedheim, *Z. Naturforsch.*, **2a**, 20 (1947).

(16) M. Tamres and J. M. Goodenow, unpublished work.

(17) (a) H. Tsubomura and R. P. Lang, *J. Am. Chem. Soc.*, **83**, 2085 (1961); (b) M. Good, A. Major, J. Nag-Chaudhuri, and S. P. McGlynn, *ibid.*, **83**, 4329 (1961). Calculations here were based on the Benesi-Hildebrand equation, which for this strong interaction would result in small error.¹³

Table I: K_c and ϵ_c for Diethyl Sulfide-Iodine in the Vapor Phase

Temp, °C	At λ_{\max} 290 m μ		Liptay analysis	
	$K_c^{a,b}$ l. mole ⁻¹	$\epsilon_c^{a,b}$ l. mole ⁻¹ cm ⁻¹	K_c l. mole ⁻¹	ϵ_c at 290 m μ , l. mole ⁻¹ cm ⁻¹
94	17.8 ± 6.0 (22.9 ± 6.7)	12,500 ± 4,000 (9,480 ± 3,100)	17.6 ± 6.5 (22.9 ± 7.2)	12,600 (9,440)
100	19.4 ± 2.5 (24.0 ± 2.6)	10,000 ± 1,000 (7,910 ± 830)	19.5 ± 2.7 (24.0 ± 2.7)	10,000 (7,930)
105	13.7 ± 2.5 (17.8 ± 2.6)	11,300 ± 1,600 (8,460 ± 1,200)	c c	c c
115	10.2 ± 1.8 (14.1 ± 1.8)	12,300 ± 2,200 (8,640 ± 1,100)	9.6 ± 1.8 (13.3 ± 1.7)	13,000 (9,080)
122	4.7 ± 2.8 (8.8 ± 2.8)	21,200 ± 12,600 (11,200 ± 3,200)	c c	c c
127	9.9 ± 1.2 (13.3 ± 1.3)	9,600 ± 760 (6,930 ± 430)	9.3 ± 1.3 (12.2 ± 1.7)	10,300 (7,500)
		Av 11,200 ^d ± 1,900 (8,770 ± 1,640)		Av 11,480 ± 1,330 (8,490 ± 770)

^a Error limits are for the 50% confidence interval. ^b The values not in parentheses were obtained by basing the calculation of initial iodine concentration on the solution values in *n*-heptane at 25° of $K_c = 180$ l. mole⁻¹ and $\epsilon_c = 27,600$ l. mole⁻¹ cm⁻¹; those in parentheses are based on the solution values of $K_c = 200$ l. mole⁻¹ and $\epsilon_c = 24,800$ l. mole⁻¹ cm⁻¹. ^c Readings taken at λ_{\max} only. ^d Average does not include results at 122°.

Benesi-Hildebrand and Benesi-Hildebrand-Scott type of plots at the single wavelength λ_{\max} showed good linearity, whereas plots based on 2:1 complex only and on 1:2 complex only (less likely for the concentrations used) did not, does not eliminate completely the possibility of having a second complex of 2:1 ratio present in smaller concentration.^{18,19} The second complex would produce a systematic variation in equilibrium constant with wavelength and it has been suggested that this be used as a criterion to determine its presence.¹⁸ To test this possibility, a Liptay²⁰ analysis of the data at eight wavelengths over the range 280–310 m μ was made. The constancy in the columns of the D_{mk} matrix indicates the dominant presence of the 1:1 complex and only small, random variation in K_c was obtained over the wavelength range. The Liptay average value for K_c and the value for ϵ_c are given in Table I and are seen to fall within the error limits for the values obtained at λ_{\max} . No Liptay analysis was made at 105 and 122° because data for these two temperatures were recorded only at λ_{\max} . Other work which shows the predominant formation of a strong 1:1 CT complex with iodine is that of Klaboe, *et al.*,²¹ who used the Job method of continuous variations to study the interaction with triphenylarsine in carbon tetrachloride.

It is well known that the product $K_c\epsilon_c$ can be de-

termined more precisely than either term alone, any error in one producing a comparable error in the other. The wide variation in ϵ_c , which appears to be random with temperature, results in a nonsystematic temperature dependence of K_c . For such cases it is best to assume that ϵ_c is independent of temperature and to plot $\log K_c\epsilon_c$ vs. $1/T$ to calculate the heat of reaction. An equivalent procedure²² is to plot $[\log K_c\epsilon_c - \log \epsilon_{cav}]$ vs. $1/T$. Such a plot is shown in Figure 3, where the term in brackets has been abbreviated as $\log K_{cav}$. The calculated thermodynamic values are given in Table II together with the spectral characteristics, and comparison is made to the results found in *n*-heptane solution. The values in parentheses are based on the set of data given in parentheses in Table I. It is apparent that any uncertainty in the selection of solution values for K_c and ϵ_c to calculate iodine vapor con-

(18) G. D. Johnson and R. E. Bowen, *J. Am. Chem. Soc.*, **87**, 1655 (1965).

(19) C. C. Thompson, Jr., Abstracts, 151st National Meeting of the American Chemical Society, Pittsburgh, Pa., March 1966, paper 112N.

(20) W. Liptay, *Z. Elektrochem.*, **65**, 375 (1961); also Chapter 12 of ref 2a.

(21) E. Augdahl, J. Grundnes, and P. Klaboe, *Inorg. Chem.*, **4**, 1475 (1965).

(22) M. Tamres, *J. Phys. Chem.*, **68**, 2621 (1964).

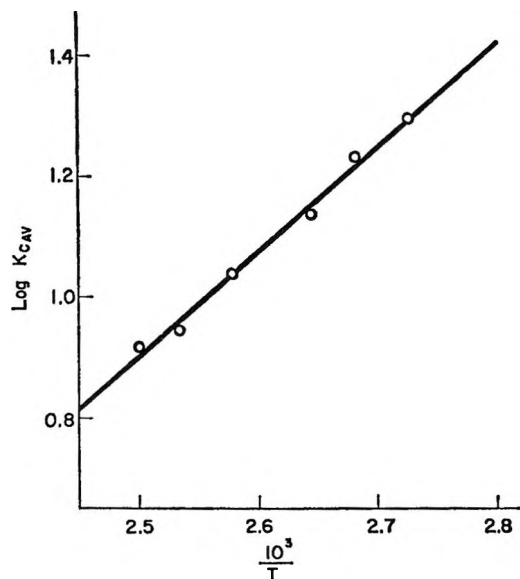


Figure 3. $\log K_{cav} - \log \epsilon_{cav}$ ($= \log K_{cav}$) vs. $1/T$ for the diethyl sulfide-iodine complex in the vapor phase.

centration, while affecting ΔG° slightly, does not affect the other thermodynamic quantities.

Discussion

The CT complex in its ground (N) and excited (V) states can be described approximately by the wave functions.

$$\Psi_N = a\Psi_0 + b\Psi_1 \quad (3)$$

and

$$\Psi_V = a^*\Psi_1 - b^*\Psi_0 \quad (4)$$

where Ψ_0 and Ψ_1 are the "no-bond" and "dative bond" wave functions, respectively.²³

The transition energy $h\nu_{CT}$ for the process $\Psi_N \rightarrow \Psi_V$ in the case of weak complexes has been approximated as^{2b,24}

$$h\nu_{CT} = I_D^v - C_1 + \frac{C_2}{I_D^v - C_1} \quad (5)$$

and, for strong complexes, as^{2b,25}

$$h\nu_{CT} = \frac{\Delta}{1 - S_{01}^2} \left[1 + \frac{4\beta_0\beta_1}{\Delta^2} \right]^{1/2} \quad (6)$$

Here

$$C_1 = E_A^v - E_c + W_0 \quad (7)$$

$$C_2 = \beta_0^2 + \beta_1^2 \quad (8)$$

$$\Delta = W_1 - W_0 \quad (9)$$

where I_D^v is the vertical ionization potential of the

Table II: Vapor and Solution Spectral and Thermodynamic Properties of Diethyl Sulfide-Iodine

	Vapor ^b	n-Heptane solution ^c
λ_{max} , m μ	290	303
ϵ_{cav} at λ_{max} , l. mole ⁻¹ cm ⁻¹	11,200 (8770)	26,400
\bar{K}_{CT} , l. mole ⁻¹	16.5 ^d (20.7)	9.38; ^e 12.5 ^f
\bar{K}_{CT} , l. mole ⁻¹	226 ^g (285) ^g	200; 180 ^g
$-\Delta G^\circ_{373}$, kcal mole ⁻¹	2.82 (2.98)	1.66; 1.75 ^f
$-\Delta G^\circ_{298}$, kcal mole ⁻¹	3.75 ^e (3.89) ^e	3.14; 3.08 ^g
$-\Delta S^\circ$, eu	15.0 \pm 1.1 ^h (14.8 \pm 1.0) ^h	19.4 \pm 2.0 ^h 17.6 \pm 0.5 ^{g,h}
$-\Delta H^\circ$, kcal mole ⁻¹	8.4 \pm 0.4 ^h (8.4 \pm 0.4) ^h	8.9 \pm 0.6 ^h 8.3 \pm 0.2 ^{g,h}
$-\Delta E^\circ$, kcal mole ⁻¹	7.7 \pm 0.4 ^h (7.7 \pm 0.4) ^h	8.9 \pm 0.6 ^h 8.3 \pm 0.2 ^{g,h}

^a Relative to a standard state where the concentrations of donor, acceptor, and complex are 1 M. ^b Where two values are given, one without and one with parentheses, that without parentheses was obtained by basing the calculation of initial iodine concentration on the solution values in n-heptane at 25° of $K_c = 180$ l. mole⁻¹ and $\epsilon_c = 27,600$ l. mole⁻¹ cm⁻¹ and that with parentheses is based on the solution values of $K_c = 200$ l. mole⁻¹ and $\epsilon_c = 24,800$ l. mole⁻¹ cm⁻¹ (see Table I). ^c Reference 12. ^d Read from the line in Figure 3, as determined by the method of least squares. ^e Extrapolated from ultraviolet data assuming constant ΔE° . ^f Extrapolated from study of blue-shifted iodine band in visible region. ^g From data in visible region. ^h Standard error.

donor; E_A^v is the vertical electron affinity of the acceptor; E_c , the coulombic energy, is equal to $-e^2/r$ where e is the electrostatic charge and r is the intermolecular distance; S_{01} is the overlap integral; W_1 and W_0 are the energies associated with Ψ_1 and Ψ_0 , respectively; and β_0 and β_1 are terms which contain overlap and exchange integrals.²⁶

An approximation which has been utilized to estimate the polarity of weak CT complexes is²⁷

(23) R. S. Mulliken, *J. Am. Chem. Soc.*, **74**, 811 (1952).

(24) S. H. Hastings, J. L. Franklin, J. C. Schiller, and F. A. Matsen, *ibid.*, **75**, 2900 (1953).

(25) H. Yada, J. Tanaka, and S. Nagakura, *Bull. Chem. Soc. Japan*, **33**, 1660 (1960).

(26) R. S. Mulliken, *J. Am. Chem. Soc.*, **74**, 811 (1952).

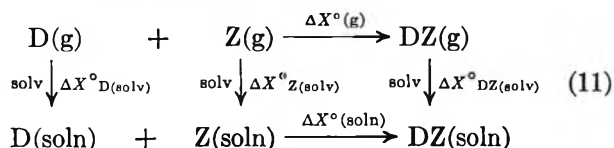
(27) J. A. A. Ketelaar, *J. Phys. Radium*, **15**, 197 (1954).

$$\frac{b^2}{a^2 + b^2} \approx \frac{b^2}{a^2} \approx -\frac{\Delta H^\circ}{h\nu_{\max}} \quad (10)$$

where ΔH° is the heat of reaction for complex formation, ν_{\max} is the frequency at the CT band maximum, and a and b are the coefficients in eq 3.

The parameters in eq 5 have been determined for iodine complexes with a wide variety of weak donors^{2a,b} and in eq 6 for iodine complexes with amines.^{2b,25} Reasonable results for the polarities have been obtained using eq 10 for iodine complexes with aromatic hydrocarbons²⁷ and with ethers.²⁸ In all instances these equations have been applied to studies in *solution* in which a *similar* of type solvents (predominantly *n*-heptane) was used, where it might be expected that solvation factors would parallel other trends in the donor-acceptor properties. It is evident that the properties of the donor, acceptor, and complex will be modified by solvent interaction, thereby influencing the individual terms in eq 5-10. Thus, the parameters in eq 5 and 6 and also the polarities of the complexes will be different in the vapor than in solution and, in fact, will be different for each solvent.

Vapor and solution thermodynamic and spectral values are related by the Born-Haber-Fajans cycle. When donor (D) and acceptor (Z) form a complex (DZ), any thermodynamic function (ΔX°) will differ in the two phases as shown



from which

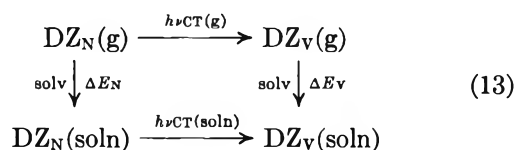
$$\Delta X^\circ(\text{g}) = \Delta X^\circ(\text{soln}) - [\Delta X^\circ_{\text{DZ(soln)}} - \Delta X^\circ_{\text{D(soln)}} - \Delta X^\circ_{\text{Z(soln)}}] \quad (12)$$

If the thermodynamic function is to be the same in both phases, the term in brackets would have to be zero; but in general, the sum of the changes due to solvation in donor and acceptor separately does not cancel that of the change in the complex. This undoubtedly is the case for ΔG° where the recent vapor phase studies of various donors (aromatic hydrocarbons and ethers) with several acceptors (iodine, tetracyanoethylene, and carbonyl cyanide), as well as the present study on diethyl sulfide-iodine, consistently give equilibrium association constants which at comparable temperatures are appreciably higher in the vapor phase, even by as much as a factor of 30.²⁹

In the present study and in the case of diethyl ether-iodine,⁵ ΔH° in the vapor phase and in *n*-heptane solu-

tion are comparable. Some difference has been reported for benzene-iodine⁵ and quite a large difference has been found for *p*-xylene-tetracyanoethylene.^{7,30} Any comparison of ΔH° should take into account the fact that solution and vapor work have been carried out in different temperature ranges and there may be a small temperature dependence of ΔH° over this temperature range. For the donor and acceptor separately, $\Delta H^\circ(\text{soln})$ can be determined from the heat of solution and the heat of vaporization (or heat of sublimation in the case of iodine). The sum of these energies is quite large, being several times that of the heat of reaction. The heat of solvation of the vapor CT complex must also be large and, although not determinable directly, especially for weak complexes, can be calculated if all other terms in eq 12 are known. Thus, the heat of solvation of benzene-iodine vapor in carbon tetrachloride is of the order of -15 kcal/mole.³¹

The Born-Haber-Fajans cycle for the charge-transfer energy is



which gives

$$h\nu_{\text{CT}}(\text{g}) = h\nu_{\text{CT}}(\text{soln}) - [\Delta E_V - \Delta E_N] \quad (14)$$

In all of the cases where spectral data on CT complexes have been obtained in both phases, there has been observed a red shift in going from vapor to solution. Bayliss³² has discussed the effect of solvent in producing a polarization red shift. This effect is related to the polarizability of the solvent and, indeed, a correlation has been noted of CT band position of aromatic hydrocarbon-TCNE complexes with the refractive index of the solvent.³³ Further, for these complexes, it has recently been shown for similar-

(28) M. Tamres and M. Brandon, *J. Am. Chem. Soc.*, **82**, 2134 (1960).

(29) There is always a problem in determining a precise K_c because of the dependence on evaluation first of ϵ_c . Where the scatter of data is greater in a Benesi-Hildebrand plot, as is the case for some of the vapor phase work compared with that in solution, it is even more difficult to evaluate K_c . Nevertheless, the difference between vapor and solution K_c values seems quite definite.

(30) Large differences also exist for other polymethyl-substituted benzene-TCNE complexes; M. Kroll, private communication.

(31) Calculation is based on ref 5; F. R. Bichowsky and F. D. Rossini "Thermochemistry of Chemical Substances," Reinhold Publishing Corp., New York, N. Y., 1936; K. Hartley and H. A. Skinner, *Trans. Faraday Soc.*, **46**, 621 (1950); M. Tamres, *J. Am. Chem. Soc.*, **74**, 3375 (1952).

(32) N. S. Bayliss, *J. Chem. Phys.*, **18**, 292 (1950).

(33) H. M. Rosenberg and D. Hale, *J. Phys. Chem.*, **69**, 2490 (1965).

type solvents that there is a linear correlation of the CT energy with the refractive index function $(n^2 - 1)/(2n^2 + 1)$, the extrapolation of which to $n = 0$ corresponds to the CT energy found in the vapor phase.³⁴

The interaction of solvent is different for the ground and excited states of solutes and depends on the relative polarities of these states.⁸ When the dipole moment of the excited state is larger than that of the ground state, there will be greater solvent stabilization of the former relative to the latter, which should lead to a larger spectral red shift in going from vapor phase to solution. Since the difference in dipole moment between the excited and ground states is larger for weak CT complexes than for strong, there should be a decreasing shift $\Delta\bar{\nu}$ or, better, a decreasing relative shift $\Delta\bar{\nu}/\bar{\nu}$ in going from weak to strong complexes. For the available data on iodine complexes presented in Table III this seems to be the case,³⁵ but the data are much too few to allow generalization. Apparently this does not hold for carbonyl cyanide complexes.⁶

When the polarities of the ground and excited states are nearly alike, then $\Delta E_N \simeq \Delta E_V$ and there would be little shift in $h\nu_{CT}$ between vapor and solution. Further, the potential energy curves of the ground and excited states would have comparable shapes and minima, thereby giving CT band shapes which are nearly symmetrical. Comparison of the *relative* shapes

metrical than that with diethyl sulfide, also decreases more slowly in slope on the low-energy side. A similar finding for triphenylarsine-iodine in carbon tetrachloride has been noted.³⁶ These are among the $n \rightarrow \sigma^*$ complexes. From accumulated data in solution for predominantly $\pi \rightarrow \pi^*$ complexes, Briegleb and Czekalla³⁷ note that the CT band is asymmetric with the slope decreasing more slowly on the high-energy side.

The *absolute* intensity of the CT band in the vapor and in solution is considerably different. In all cases, ϵ_c is smaller in the vapor phase,⁵⁻⁷ differing from the solution value by a factor of between 2 and 3 for diethyl sulfide-iodine, diethyl ether-iodine,⁵ and *p*-xylene-tetracyanoethylene,⁷ and by a factor of about 10 for benzene-iodine⁵ and $\text{CO}(\text{CN})_2$ with diethyl ether and with benzene.⁶ Since K_c is found to be larger in the vapor phase, the product $K_c\epsilon_c$ is closer in proportion in the two phases than is either term separately.²⁹

Lang and Strong⁵ have pointed out that these differences in the two phases can be accounted for in two ways. First, they say there is the possibility that the large extinction coefficient in solution is mainly due to contact charge transfer, especially for benzene-iodine. In a solvent, a "cage effect" is responsible for the large concentration of contact charge transfer and this effect is negligible at reasonably low pressures in the vapor phase. Second, as proposed recently by Murrell, *et al.*,⁹ in solution the solvation process competes with that of complexation. Omission of solvation leads to ϵ_c values which are too high and K_c values which are too low. Application of solvent corrections to solution data for benzene-iodine leads to ϵ_c and K_c results which are in qualitative agreement with those found in the vapor phase.

The effect either of contact charge transfer or of solvation should be smaller for the stronger complexes. First, since contacts are random, the weaker complexes may have several different configurations for which contact charge transfer can occur. Stronger complexes favor a single configuration and, hence, there would be a smaller contribution from contact charge transfer. If for diethyl sulfide-iodine, it is assumed that there is very little contact charge transfer in the vapor phase and also very little in solution, it seems reasonable that the ϵ_c values in the two phases

Table III: Comparison of $\bar{\nu}_{\max}$ for Iodine Complexes in the Vapor Phase and in Solution

Donor	$\bar{\nu}_g$, cm ⁻¹	$\bar{\nu}_{\text{soln}}$, cm ⁻¹	$\Delta\bar{\nu}$, cm ⁻¹	$\Delta\bar{\nu}/\bar{\nu}_g$
Benzene	37,300 ^a	33,600 ^b	3700	0.097
		34,800 ^c	2500	0.067
Diethyl ether	42,800 ^a	39,700 ^d	3100	0.074
		40,300 ^e	2500	0.057
Diethyl sulfide	34,500	33,000 ^f	1500	0.044

^a Reference 5. ^b In *n*-heptane, ref 3. ^c In benzene, ref 24. ^d In *n*-heptane, ref 28. ^e In diethyl ether, ref 15. ^f In *n*-heptane, ref 12.

of the diethyl sulfide-iodine CT band in the vapor phase and in *n*-heptane solution¹⁰ shows them to be practically superimposable except for the shift in band maximum. They are only slightly asymmetrical, with the slope on the low-energy side decreasing a little more slowly than on the high-energy side. The vapor phase CT band for iodine with diethyl ether,⁵ still more asym-

(34) E. M. Voigt, *J. Phys. Chem.*, **70**, 598 (1966).

(35) Possibly, this may not hold for iodine complexes with olefins; ref 39.

(36) E. Augdahl, J. Grundnes, and P. Klæboe, *Inorg. Chem.*, **4**, 1475 (1965).

(37) G. Briegleb and J. Czekalla, *Z. Physik. Chem. (Frankfurt)*, **24**, 37 (1960).

for this complex would be in closer agreement than, say, for the benzene-iodine case.

Second, Murrell's equations⁹ for K_c and ϵ_c when there is solvation show that the solvent should not have as much effect on strong complexes as it does on weak ones. Thus, there should be closer correlation of K_c and ϵ_c , in agreement with experiment.

Another possibility for the difference of ϵ_c in the two phases has been proposed by Prochorow and Tramer as being^{6b} due to the internal pressure of the solvent which would decrease the intermolecular distance between donor and acceptor in the complex, thereby increasing the overlap integral and, hence, ϵ_c . It might be supposed that compression by solvent would raise the energy of the complex from its potential energy minimum, thereby decreasing ΔH° . Perhaps this is more pronounced for the π - π^* complexes, such as *p*-xylene-tetracyanoethylene, which may be more compressible than the n - σ^* complexes, but the absence of any difference in ΔH° between vapor and solution for the latter type of complexes makes it doubtful that compressibility is the dominant factor.

An increase in overlap due to compression of the complex should increase C_2 (eq 8) and, as seen in eq 5 for weak complexes, should produce a blue shift. Since this is opposite to what is observed in going from vapor to solution, there must be a change in some of the other terms as well. A red shift would occur if the sum $-C_1 + C_2/(I_D^\nu - C_1)$ becomes more negative (assuming I_D^ν is unaffected in the two phases). This decrease could occur by increasing C_1 ³⁸ which, according to eq 7, could arise from compression by decreasing the coulombic energy term E_c , but it is likely that the solvent affects the other terms in eq 5-10, as mentioned earlier, and the net shift is a composite of all these changes.

The *visible* band of diethyl sulfide-iodine in *n*-heptane has been reported by others¹⁷ and was investigated in our laboratory as well.¹ There is found a pronounced *blue shift* with a maximum at about 437 $m\mu$ and is attributed to the perturbed molecular iodine which results from complexation.

Effort was made to study the visible band in the vapor phase. As seen in Figure 4, no shifted maximum in the visible region was observed. For the con-

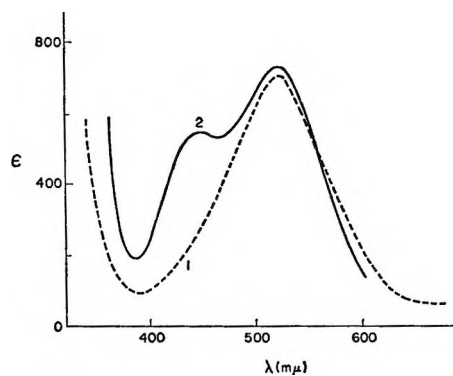


Figure 4. Apparent extinction coefficient of iodine ($\epsilon = A/b[I_2]_0$) when the iodine is 28% complexed: 1, in the vapor phase at 127°; 2, in *n*-heptane solution at 25°.

centrations used, according to the data in Table I, the iodine should have been complexed to the extent of 28% at 127°. An equal extent of complexation in *n*-heptane solution at 25° definitely shows the shifted band. Similar observations have been made by Lang and Strong⁵ on iodine complexes with benzene and with diethyl ether and by Van Tongerloo and Back³⁹ on iodine complexes with olefins.

It is not likely that the absence of a shift is due to experimental difficulty. Diethyl sulfide, unlike benzene and diethyl ether, does not undergo secondary reaction with iodine at elevated temperatures, as evidenced by the study of the complex in the ultraviolet region. Being the strongest donor of the three, it is the most favorable for studying the visible shift. Even if the reported value of K_c in the vapor phase were too large by a factor of 2,⁴⁰ there should be sufficient iodine complexed to show the effect, if vapor and solution were similar in behavior. Perhaps, as attributed by Bayliss and co-workers,^{8,41} the presence of a solvent cage is responsible for the blue shift, which would be absent in the vapor. This is a point which requires further study.

(38) A minimum occurs in eq 5 when $I_D^\nu - C_1 = \sqrt{C_2}$ and, for weak complexes, $C_1 < I_D^\nu$.

(39) A. Van Tongerloo and M. H. Back, private communication.

(40) This is not very likely, since this would result in ϵ_c being about the same in the vapor and in solution.

(41) N. S. Bayliss and A. L. G. Rees, *J. Chem. Phys.*, **8**, 377 (1940).

Programmed Stresses in Homogeneous Chemical Kinetics. I.

Aperiodic Stress Functions

by Richard E. Cover

Department of Chemistry, St. John's University, Jamaica, New York (Received August 1, 1966)

A new, general approach is proposed for the study of homogeneous kinetic systems. The technique involves adding reagents to the system under study in a time-functional manner where this time dependence is determined by constraints imposed on the mathematical model. When the constraints are obeyed by the system, the rate constants can be evaluated from the parameters of the stressing function. This results in changing the mathematical problem from one of solving differential equations into a purely algebraic one.

In 1954, Pearson and Piette¹ suggested a new technique for the study of single-step, first-order, irreversible reactions in solution. This consisted of the constant-current electrolytic generation of a reactant in the solution. Rate constants for the hydrolyses of nitroethane and ethyl acetate were calculated from the steady-state solutions of the rate equations. The technique was independently discovered by Farrington and Sawyer² and applied by them to hydrolytic and hydrogenation reactions. Since then, the coulometric addition of reagent method has been applied to more complex kinetics of bromination reactions³⁻⁵ and osmium reactions.⁶

Volumetric constant-rate addition of reagents was first considered by Cover and Meites⁷ and applied to titration curve theory and some typical inorganic kinetic mechanisms. Carr and Meites⁸ have applied this method to a uranium system.

Homogeneous kinetic studies in which there is no exit of material from the reactor may then be classified in this way: (a) the classical method in which no reactants or products are added to the reactor after time zero and (b) the constant rate of addition technique in which a reactant, or conceivably a product, is added throughout the experiment. Viewing the addition of a reagent as the imposition of a stress on the system, the classical method involves no stress while the second procedure involves a constant applied stress.

This paper proposes a more general approach to the problem. With modern equipment such as electronic function generators and analog computational com-

ponents, it is possible to generate an almost infinite variety of electrical signals. These signals can be used to apply analogous chemical stresses to a system. One can, for example, use a variable-speed, tachometer-feedback-controlled motor as a hypodermic syringe drive. An analog dc voltage signal can be used as the reference voltage for the motor, and the time-functional syringe output will follow and be proportional to the analog signal. Similarly, time-functional currents can be generated for the electrolytic application of stresses to systems.

We propose, then, the consideration of *programmed stresses*. For any kinetic system, it is possible in principle to place constraints on the mathematical model, *e.g.*, that the concentration of component A be a linear function of time, and, from the constraints and the rate equations, determine the time-functional form of the stresses necessary to satisfy the constraints. The required stresses may be zero, constant, or time dependent, this being determined by the natures of

(1) R. G. Pearson and L. H. Piette, *J. Am. Chem. Soc.*, **76**, 3087 (1954).

(2) P. S. Farrington and D. T. Sawyer, *ibid.*, **78**, 5536 (1956).

(3) J. E. Dubois, *Z. Elektrochem.*, **64**, 143 (1960).

(4) G. O'Dom and Q. Fernando, *Anal. Chem.*, **37**, 893 (1965); **38**, 844 (1966).

(5) J. Janata and O. Schmidt, *J. Electroanal. Chem.*, **11**, 224 (1966).

(6) J. G. Connery, M.S. Thesis, St John's University, 1966.

(7) R. E. Cover and L. Meites, *J. Phys. Chem.*, **67**, 1528, 2311 (1963).

(8) P. W. Carr and L. Meites, *J. Electroanal. Chem.*, **12**, 373 (1966).

the system and the constraints. The term *programmed stress* is proposed since the form of the stress is determined *a priori* by the nature of the system and the behavior sought.

The stress functions are here given the symbol ρ_x , which is the rate of addition of component X to the system. When X is added in solution form

$$\rho_x = \left(\frac{M_x V'_x}{v} \right) \quad (1)$$

where M_x is the molarity of the solution of X which is added, V'_x is the rate of volume addition in liters per second of the solution of X, and v is the volume in liters of the solution in the reactor.

When electrolytic generation of reactant is used

$$\rho_x = \frac{i}{n_x F v} \quad (2)$$

where i is the generation current in amperes, n_x is the number of faradays per mole of X used in its generation, and F is the faraday (96,491.2 coulombs/equiv). ρ_x has units of moles liter⁻¹ second⁻¹ in either case.

When the parameters in the ρ functions are properly selected, the system will obey the constraints imposed on the model. When system conformance is observed, the rate constants and other chemical system parameters are related to the parameters of the ρ -function generator by algebraic equations. The determination of rate constants can thus be changed from one where complicated nonlinear differential equations must be treated to one of simply solving algebraic problems.

The programmed stress approach thus offers the possibility of reducing mathematical difficulties considerably. In addition, since for any given system an almost infinite number of constraints is possible, it offers the opportunity for a much more stringent and searching examination of a proposed mechanism. Because this technique involves the addition of reactants to the system, there is a greater possibility for dissecting relatively fast reactions than with the classical $\rho = 0$ method. This advantage is demonstrated in the computer simulations in Figures 1 and 2 and has already been much used by various workers with the constant ρ technique.^{1,3,4}

The purpose of this work should be made clear. The solution of hypothetical kinetic problems is not intended. Instead, a new and general approach to obtaining kinetic data is proposed. Much prior experimental work is subsumed in this approach. For example, both the classical $\rho = 0$ treatment for an irreversible first-order reaction as well as Pearson and

Piette's¹ constant ρ work are special cases of the $\rho(t)$ approach where the system constraint is such that a plot of the logarithm of the concentration of the reactant vs. time is linear. The accuracy and utility of both these treatments have been long accepted.

The work of Carr and Meites⁸ represents a special case of the programmed stress approach to the disproportionation mechanism discussed below. Their work on the disproportionation of uranium(V) yielded values of rate constants in acceptable agreement with those obtained by other techniques (see Table III).

The essential difference between this and prior work is one of viewpoint. Previously, kinetic systems were studied under zero or constant stresses partly because no other forms of stress were available. In that type of experiment as well as in other areas of research, such as ac polarography, programmed-temperature and programmed-flow gas chromatography, and chronopotentiometry with programmed current, the choice of the nature of the stressing function or programmed variable has been dictated by (a) the ease of generation of the function and (b) the somewhat arbitrary decision to apply the function to the experiment.

The programmed stress approach breaks with this tradition. It provides a different criterion for the choice of the stressing function; that is, the function is so chosen as to simplify the interpretation of experimental data and the determination of rate constants. This clearly has implications not just for homogeneous kinetics but also for the other techniques employing time-dependent inputs.

The study of physical or chemical systems employing experimental inputs where differential equations are involved in the model is always severely limited. For any given functional form of the input, analytical solutions for the model will only be available for a few cases. The programmed stress technique circumvents this difficulty by using only stressing functions which permit algebraic calculations.

The nature of this technique is such that some prior knowledge of the system is required since the nature of the model conditions the choice of the stressing function. Almost any experimental information will limit the possible values of the rate constants to certain levels and thus aid in selecting the parameters in ρ . The amount of trial and error involved in the experimentation is thus already limited at the start of the work. Duplication in experimentation is further decreased since generally, for any set of parameters in the ρ function, many combinations of experimental data can occur which satisfy the system constraints. This can be seen especially clearly from the discussion of system II below.

The value of the technique lies in examining systems where some but insufficient information is available. When the system is so complex that the simple mathematical and graphical techniques of the classical $\rho = 0$ method fail, the $\rho(t)$ approach may well be used.

Frequently, kinetic data do not permit an unambiguous decision between several possible mechanisms. Since most such homeomorphism arises from simplifying assumptions about equilibria or steady states, various stressing functions may so distort system behavior as to make invalid these assumptions. The $\rho(t)$ approach thus opens the possibility of the detection and identification of mechanisms which escape conventional experimentations.

Deviations from postulated behavior manifest themselves similarly in both the classical and programmed stress experiments. In the classical method, incorrect assumptions about the system give rise to incorrect or inconstant values of the rate constants as well as to lack of conformance to model behavior. In the $\rho(t)$ experiment, incorrect assumptions about the system cause incorrect or inconstant values of the rate constants or lack of conformance to model constraints.

The above concepts are applied here to several systems. Other work is in progress in this laboratory on periodic ρ functions and experimental applications. All calculations and systems discussed have been checked and simulated on an E.A.I. TR-20 analog computer.

Two assumptions are generally made here: (a) instantaneous mixing exists and (b) dilution effects are negligible. Dilution is, of course, zero when electrolytic generation is used. When the stress is imposed by the volumetric addition of X to the system, a dilution correction of this form should be made to each rate equation

$$\frac{dC_A}{dt} = \dots - \left(\frac{\rho_X}{M_X} \right) C_A \quad (3)$$

The addition of more than one stress, *e.g.*, ρ_X and ρ_Y , changes the correction to

$$\frac{dC_A}{dt} = \dots - \left(\frac{\rho_X}{M_X} + \frac{\rho_Y}{M_Y} \right) C_A \quad (4)$$

The need for dilution corrections can be minimized and frequently obviated by using concentrated titrants and large reactor volumes.

Data on accuracy and precision in the determination of various rate constants are listed in Table I. These estimates were obtained by simulation of the mathematical model as well as the ρ function on an analog computer. The rate constants were then esti-

mated from the computed concentration-time data and the ρ -function parameters in the same manner that they would be calculated from experimental data.

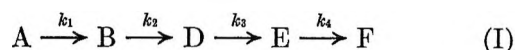
Table I: Rate Constants Determined by Computer Simulation^a

System	Constraints	Rate constants, $M^{-1} \text{ sec}^{-1}$	
		Known	Determined
IIIa	C_A linear	$k_1 = 10.0 \times 10^2$ $k_{-1} = 10.0 \times 10^2$	9.9×10^2 $9.93 \pm 0.02 \times 10^2$
IIIb	C_A linear	$k_1 = 50.0 \times 10^2$ $k_{-1} = 10.0 \times 10^2$	49.5×10^2 $9.8 \pm 0.2 \times 10^2$
IVa	C_T, C_T linear	$k_A = 1.00 \times 10^4$ $k_1 = 1.00 \times 10^4$	$1.02 \pm 0.02 \times 10^4$ $0.93 \pm 0.02 \times 10^4$
IVb	C_A, C_T linear	$k_A = 1.00 \times 10^2$	$1.05 \pm 0.02 \times 10^2$

^a $C_A^0 = 10^{-5} M$ in all cases.

Computer simulation was chosen for evaluation in preference to actual experimentation because the results of the laboratory work would reflect not only the limitations of the proposed technique but also the poverty of our understanding of the actual chemical system used. Poor interlaboratory reproducibility of kinetic data is well known. (Nevertheless, the experimental data in Table III indicate that the $\rho(t)$ technique provides satisfactory accuracy in rate-constant determination.) The rate constants obtained by simulation reflect, then, essentially the computational limitations of this physico-mathematical technique.

As an example of the viewpoint and technique proposed here and its contrast with the older constant ρ approach, consider the case of four irreversible consecutive first-order reactions. Such a system (I) might be exemplified by the stepwise formation of very stable complex ions of a tetracoordinate cation where the monodentate ligand is present in large excess.

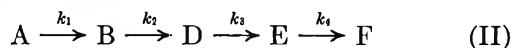


all ρ_X 's are zero except ρ_A which is constant

Pearson and Piette¹ considered a one-step reaction of this type. In line with their solution, we find that the solutions for the rate equations for A, B, D, and E all contain exponential terms which become negligible as time increases. Each of these four components reach limiting concentrations, C_{XL} , from which the rate constants can be calculated.

$$\rho_A = k_1 C_{AL} = k_2 C_{BL} = k_3 C_{DL} = k_4 C_{EL} \quad (5)$$

A typical programmed stress approach to this same system would be system II. Here a constraint is im-



all ρ_X 's are zero except ρ_A

posed on the system to define ρ_A ; namely, let ρ_A be such that the concentration of A is a linear function of time in the interval $t \geq 0$. Then

$$C_A = C_A^0 + K_A t \quad (6)$$

where $C_A^0 = C_A(0)$ and K_A is a constant. The rate equation for C_A is

$$\frac{dC_A}{dt} = -k_1 C_A + \rho_A \quad (7)$$

which on substitution from (6) becomes

$$K_A = -k_1(C_A^0 + K_A t) + \rho_A \quad (8)$$

or

$$\rho_A = (K_A + k_1 C_A^0) + k_1 K_A t \quad (9)$$

Thus, to satisfy the constraint on the system, ρ_A must be a linear function of time

$$\rho_A = Q + R t \quad (10)$$

$$Q = K_A + k_1 C_A^0 \quad (11)$$

$$R = k_1 K_A$$

It must be made perfectly clear that the parameters C_A^0 , K_A , and k_1 are properties of the chemical system studied. The parameters Q and R are properties of the ρ function, the rate of addition of species A to the system. However, when linearity is observed throughout the entire experiment, this means that Q and R have been estimated properly so that they are related to the system parameters by eq 11.

It should be pointed out that for any given system of this type, linearity in C_A can be observed for an infinite number of pairs of Q and R since, from (11)

$$Q = K_A + \frac{R C_A^0}{K_A} \quad (12)$$

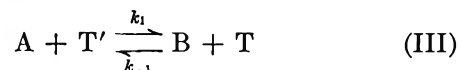
Solving the rate equations for this system when the constraint is satisfied, one finds that the solutions for C_B , C_D , and C_E all contain exponential terms which become negligible with time. When this occurs C_B , C_D , and C_E become linear functions of time. The slopes of the linear portions of the curves, K_X , are simply related to system parameters, and the rate constants can be determined using the following relationships.

$$R = k_1 K_A = k_2 K_B = k_3 K_D = k_4 K_E \quad (13)$$

As pointed out by Pearson and Piette,¹ the constant ρ technique permits the determination of rate constants of the order of 10^2 – 10^3 sec⁻¹ for such a system. This is true for this linearly constrained case as well.

For such first-order systems, of course, neither of these $\rho \neq 0$ cases presents a significant mathematical improvement over the classical $\rho = 0$ method. The mathematical advantages of the $\rho(t)$ technique become both more apparent and more real with nonlinear systems.

The single-step, reversible, second-order reaction demonstrates some of these advantages. With this system, the classical $\rho = 0$ technique presents a nonlinear rate equation which has a complicated analytical solution. Using the $\rho(t)$ approach, the problem becomes a simple algebraic one (system III)



$$C_A(0) = C_A^0 \neq 0, C_{T'}(0) = C_{T'}^0, C_B(0) = C_T(0) = 0$$

where the rate equations are

$$\frac{dC_A}{dt} = -k_1 C_A C_{T'} + k_{-1} C_B C_T$$

$$\frac{dC_{T'}}{dt} = \rho_{T'} - k_1 C_A C_{T'} + k_{-1} C_B C_T$$

and the system and $\rho_{T'}$ are to be constrained so that C_A is a linear function of time. When the constraint is satisfied

$$C_A = I_A + K_A t \quad (14)$$

where I_A and K_A are the intercept and slope, respectively, of the linear portion of the C_A vs. time curve.

The general $\rho_{T'}$ calculated from mass-balance and constraint considerations is

$$\rho_{T'} = \left(\frac{K_A}{k_1} \right) \left(\frac{K_A - (k_{-1} C_A^0)^2}{(I_A + K_A t)^2} + k_{-1} - k_1 \right) \quad (15)$$

which can be valid for all time.

If $C_{T'}^0 = 0$, however, then from the rate equation, at $t = 0$, $dC_A/dt = 0$. In this case, eq 15 cannot be applicable to $t = 0$. If $C_{T'}^0 \neq 0$, then at $t = 0$

$$\frac{dC_A}{dt} = -k_1 C_A^0 C_{T'}^0 \quad (16)$$

and substituting for K_A from (16) into (15) gives

$$\rho_{T'} = C_{T'}^0 \left(\frac{k_1 C_{T'}^0 + k_{-1} C_A^0}{(1 - k_1 C_{T'}^0 t)^2} + C_A^0 (k_1 - k_{-1}) \right) \quad (17)$$

which is valid for the interval $t \geq 0$.

Table II: Data for System IV

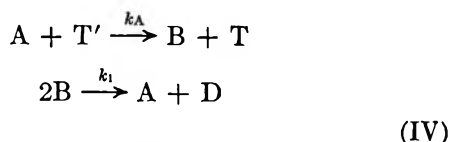
System	Linear time dependence in Constraints	Determinable	Diagnostics	$\rho_{T'}$
I	C_A, C_B^a	k_1	Constraints	$\frac{-M_{T'}[K_A + K_B + k_1(I_B + K_B t)^2]}{I_A + I_B + (K_A + K_B)t}$
II	$C_B, C_{T'}^a$	k_1	Constraints	$\frac{M_{T'}[K_B + K_T + 2k_1(I_B + K_B t)^2]}{M_T - (I_B + K_B t + I_{T'} + K_{T'}t)}$
III	$C_A, C_{T'}^a$	k_A	Constraints	$K_{T'} \left(\frac{M_{T'}}{M_{T'} - K_{T'}t} + k_A C_A^0 t \right)$
IV	$C_A, C_{T'}^b$	k_A	Constraints	$K_{T'} + k_A(I_A + K_A t)(I_{T'} + K_{T'}t)$
V	$C_A, C_{T'}^b$	k_A, k_1	Constraints ^o	$\frac{k_A K_{T'}(I_A + K_A t)^2 - K_A K_T}{k_A(I_A + K_A t)^2}$
VI	$C_B, C_{T'}^b$	k_1	Constraints ^d	$K_B + K_{T'} + 2k_1(I_B + K_B t)^2$
VII	$C_{T'}, C_{T'}^b$	k_1, k_A	Constraints ^e	$K_{T'} + K_T$

^a Dilution correction large: used in specifying $\rho_{T'}$. ^b Dilution negligible. ^c $C_B \rightarrow \sqrt{K_T/2k_1}$ as time increases. ^d C_D becomes a linear function of t^2 with increasing time; slope = $(k_1 K_B^2/3)$. ^e Constraints III are valid for $t \geq 0$. All other constraints and ρ 's are valid for $0 < t < t_1$.

In this case, the C_A vs. time curve can be forced to be linear over an interval corresponding to about 80% consumption of C_A^0 even when $k_1 = k_{-1} = 10^3 M^{-1} \text{sec}^{-1}$, and the rate constants can be calculated from the $\rho_{T'}$ causing this behavior.

The final system to be discussed involves a disproportionation reaction. Such reactions frequently occur in inorganic systems⁸⁻¹⁴ and present formidable problems in mathematical analysis. Analytical solutions for the system discussed here have been obtained for constant $\rho_{T'}$ ⁷ and constant ρ_A ⁸ where $k_A \gg k_1$.

The system demonstrates well the point made before, namely, that many possible constraints and ρ functions can be applied to a given system thereby permitting a more incisive examination of a proposed mechanism. In this case, only linearity constraints and the addition of one component have been considered. Yet from these conditions, seven different ρ functions arise by means of which conformance to the proposed mechanism can be tested and rate constants determined.



$$C_A(0) = C_A^0 \neq 0$$

$$C_B(0) = C_D(0) = C_{T'}(0) = C_T(0) = 0$$

that is, A is the only species present at $t = 0$. All ρ_x are zero except $\rho_{T'}$. Thus, species A reacts with T' to

give B and T, but the intermediate B then disproportionates to give A again and the final product D. The rate equations are

$$\begin{aligned}
 dC_A/dt &= k_1 C_B^2 - k_A C_A C_{T'} \\
 dC_B/dt &= k_A C_A C_{T'} - 2k_1 C_B^2 \\
 dC_D/dt &= k_1 C_B^2 \\
 dC_{T'}/dt &= \rho_{T'} - k_A C_A C_{T'} \\
 dC_T/dt &= k_A C_A C_{T'}
 \end{aligned}$$

Dilution effects have been assumed negligible in writing these rate equations. Corrections for dilution can be made as discussed above. Since the ρ function enters explicitly into the dilution correction, one can intentionally make the dilution effect large and use it in satisfying system constraints and specifying the required ρ function. Three such dilution ρ functions are given here. Table II summarizes the various data.

All the above ρ 's are polynomial functions of time where the coefficients are functions of experimental data. The generation of such polynomials presents no special problem with modern analog computational

(9) G. R. Hall and T. L. Markin, *J. Inorg. Nucl. Chem.*, **4**, 296 (1957).

(10) G. Gordon and H. Taube, *ibid.*, **16**, 272 (1961).

(11) E. H. Appleman and J. C. Sullivan, *J. Phys. Chem.*, **66**, 442 (1962).

(12) J. S. Coleman, *Inorg. Chem.*, **2**, 53 (1963).

(13) A. A. Bergh and G. P. Haight, *ibid.*, **1**, 688 (1962).

(14) W. C. E. Higginson and A. G. Sykes, *J. Chem. Soc.*, 2841 (1962)

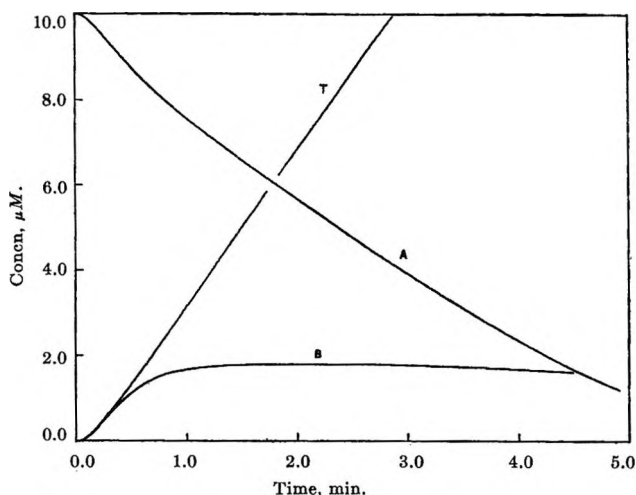


Figure 1. Variation of concentrations of species A, B, and T in system IV: $C_T^0 = 0$, $k_A = k_1 = 10^4$ l. mole $^{-1}$ sec $^{-1}$, $\rho_T' = 6.6 \times 10^{-1}$ mole l. $^{-1}$ sec $^{-1}$.

components requiring in essence a few operational amplifiers and diode circuits.

The one exception to this is the nondilution case where linearity constraints are imposed on C_T and C_T . The ρ_T' in this case is constant. Although previous work⁷ has shown that k_1 could be determined for this system with constant ρ_T' when $k_A \gg k_1$, reconsideration of the problem from the $\rho(t)$ viewpoint reveals that both k_A and k_1 are determinable. Indeed, when the experiment is performed at 10^{-5} M concentrations, both k_A and k_1 can be determined at the 10^4 M $^{-1}$ sec $^{-1}$ levels (see Table I). An analog simulation of this experiment is shown in Figure 1. k_1 can be calculated either from the limiting value of C_B where

$$C_{BL} = \sqrt{\frac{\rho_T' - K_T}{2k_1}} \quad (18)$$

or from the intercept of the linear portion of the C_A vs. time curve where

$$I_A = C_A^0 - \frac{1}{2} \sqrt{\frac{K_T}{2k_1}} \quad (19)$$

k_A can be calculated if data on C_A are available from the fact that when C_T is a linear function of time

$$k_A = \frac{K_T}{C_A C_T'} = \frac{K_T}{C_A(\rho_T' t - C_T)} \quad (20)$$

Figure 2 shows an analog simulation of the same system as in Figure 1. In this second case, however,

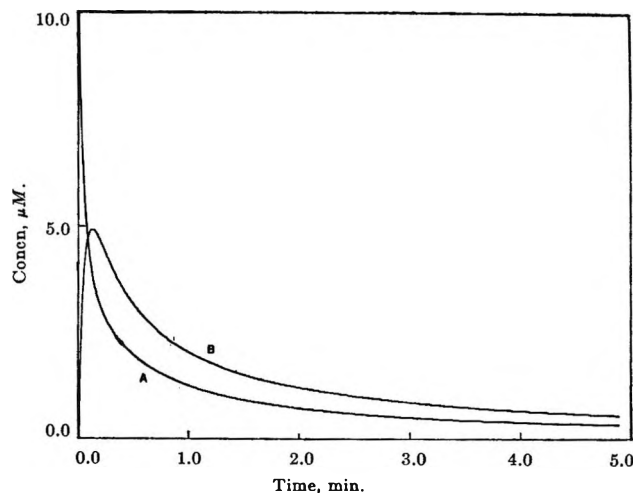


Figure 2. Variation of concentrations of species A and B. System similar to system IV except that $\rho_T' = 0$, $C_A^0 = 10.0$ μ M, and $C_T^0 = 20.0$ μ M.

the experiment was done by the classical $\rho = 0$ technique. As can be seen, the concentration of species A decreases to about 10% of C_A^0 after 60 sec despite the extreme dilution of the reactants. Under these conditions, the disproportionation reaction could easily go undetected.

As was mentioned above, the work of Carr and Meites⁸ on the disproportionation of uranium(V) represents a special case of this mechanism. Their constant ρ_T' approach satisfies constraint set VII in Table II. Some of their results are compared with data obtained by other techniques in Table III. The various data are clearly in satisfactory agreement.

Table III: Experimental Data on the Uranium(V) System

Ionic strength	(k_1/a_{H^+}) , M $^{-1}$ sec $^{-1}$	(k_1/C_{H^+}) , M $^{-2}$ sec $^{-1}$	Ref
0.4	129 \pm 2	...	a
0.4	130 \pm 4	...	b
0.93	...	121	a
1.00	...	113 \pm 14	c

^a Reference 8. ^b D. M. H. Kern and E. F. Orlemann, *J. Am. Chem. Soc.*, **71**, 2102 (1949). ^c B. McDuffie and C. N. Reilly, *Anal. Chem.*, **38**, 1881 (1966).

Acknowledgment. The writer wishes to acknowledge the summer research support from St. John's University which made this work possible.

Estimation of the Heats of Formation of Chlorofluorocarbons

by Alan S. Rodgers¹

Contract Research Laboratory, Minnesota Mining and Manufacturing Company, Saint Paul, Minnesota
(Received August 10, 1966)

The nearest neighbor interaction scheme suggested initially by Zahn has been used to correlate the available heat of formation data on $C_nF_{(2n+2)-x}Cl_x$ compounds with good results. The correlation so obtained may then be used to estimate the heats of formation of appropriate compounds of this class, which, combined with known reaction heats, have led to an estimation of the heats of formation of several olefins of the class $C_nF_{2n-x}Cl_x$ and of the strain energy of cyclic $C_4F_{8-x}Cl_x$ compounds.

Introduction

The failure of simple additivity rules in fluorocarbons was first noted by Lacher and co-workers^{2,3} in their studies on heats of reaction of fluoroolefins. Similar observations have been made by Patrick,⁴ Cox,⁵ and Skinner.⁶

As early as 1934, Zahn⁷ pointed out that the simple additivity rules of Fajans⁸ could be improved by including, in addition to a bond-energy term for each bond, an interaction term for each pair of adjacent bonds (adjacent in the sense that the bonds have a common polyvalent atom). Laidler⁹ has presented an additivity relationship based on the subclassification of bonds, and Benson and Buss^{10a} have developed one based on the additivity of groups. Both approaches take better account of nearest neighbor interactions than does the paired-term treatment of Zahn.^{10b} However, the simpler approach of Zahn will be taken here for two reasons. First, the Zahn scheme requires only six parameters for the correlation of the compounds $C_nF_{(2n+2)-x}Cl_x$ while the others require ten, and second, this scheme includes the methanes ($CF_{4-x}Cl_x$) within its scope. This latter advantage is quite important when one realizes that the five substituted methanes comprise nearly half of the reliable data for the compounds under consideration.

Before proceeding, it is of some interest to ascertain whether or not these approaches are equivalent from a practical point of view. To this end, the heats of formation of 31 hydrocarbons from C_4H_{10} to C_9H_{20} were taken from the American Petroleum Institute tables¹¹ and fitted by a least-squares procedure to the three effective Zahn parameters and the four Benson

and Buss groups.¹² The results, which are summarized in Table I, adequately demonstrate the practical equivalence of the two approaches.

Table I: Statistical Comparison of the Three-Parameter Zahn Scheme and the Four-Parameter Group Scheme for 31 Hydrocarbons from C_4H_{10} to C_9H_{20} (kcal/mole)

	Zahn scheme	Group scheme
Standard deviation	0.55	0.54
Maximum deviation ^a	-2.1	-2.0
Fraction of compounds with deviation > 1 kcal/mole	5/31	4/31

^a For hexamethylethane in both cases.

(1) Department of Thermochemistry and Chemical Kinetics, Stanford Research Institute, Menlo Park, Calif.

(2) (a) J. R. Lacher, J. M. McKinley, C. M. Snow, L. Michel, G. Nelson, and J. D. Park, *J. Am. Chem. Soc.*, **71**, 1330 (1949); (b) J. R. Lacher, J. J. McKinley, C. Walden, K. Lea, and J. D. Park, *ibid.*, **71**, 1334 (1949).

(3) J. R. Lacher, A. Kianpour, and J. D. Park, *J. Phys. Chem.*, **61**, 584 (1957).

(4) C. R. Patrick, *Advan. Fluorine Chem.*, **2**, 1 (1961).

(5) J. D. Cox, *Tetrahedron*, **18**, 1337 (1962).

(6) H. A. Skinner, *Ann. Rev. Phys. Chem.*, **15**, 449 (1964).

(7) C. T. Zahn, *J. Chem. Phys.*, **2**, 671 (1934).

(8) K. Fajans, *Chem. Ber.*, **B53**, 643 (1920).

(9) K. J. Laidler, *Can. J. Chem.*, **34**, 626 (1956).

(10) (a) S. W. Benson and J. H. Buss, *J. Chem. Phys.*, **29**, 546 (1958); (b) see also T. L. Allen, *ibid.*, **31**, 1039 (1959).

(11) American Petroleum Institute, Research Project 44, Carnegie Press, 1953.

(12) No steric repulsion parameter was included.

Table II: Heats of Formation and Heats of Atomization^a (kcal/mole)

Compound	$-\Delta H_f$	Q_a	Q_a , by eq 4	Ref
C	-170.9			13
Cl	-29.0			13
F	-18.9			13
CF ₄	222.9	468.5	468.5	13
CF ₃ Cl	166.0	422.6	422.8	13
CF ₂ Cl ₂	115.0	381.7	381.5	13
CFCl ₃	68.0	344.8	344.8	13
CCl ₄	25.5	312.4	312.5	13
CCl ₃ CCl ₃	35.3	551.1	551.1	b
CF ₂ CF ₂ < $\frac{CF_2CF_2}{CF_2CF_2}$ >CF ₂	687.3	2148.2	2147.6	c
CF ₃ CF ₂ CF< $\frac{CF_2CF_2}{CF_2CF_2}$ >CF ₂	783.5	2453.1	2453.7	c
n-C ₇ F ₁₆	801.9	2300.6	2300.5	c
CF ₂ ClCF ₂ Cl	212.6	688.0	688.0	d
(CF ₂ CF ₂) _n	(192 ± 4)/n	609.4/n	612.2/n	e

^a The uncertainty in the heats of formation will be taken as ±2 kcal/mole although in some cases the heat of combustion data are considerably better. The standard state is that of an ideal gas at 1 atm and 25°. ^b $\Delta H_f(\text{solid})$ from L. Smith, L. Bjellerup, S. Krook, and H. Westermark, *Acta Chem. Scand.*, **7**, 65 (1953); ΔH_{sub} from K. J. Ivin and F. S. Dainton, *Trans. Faraday Soc.*, **43**, 32 (1947). ^c $\Delta H_o(\text{gas})$ from W. D. Good, D. R. Douslin, D. W. Scott, A. George, J. L. Lacina, J. P. Dawson, and G. Waddington, *J. Phys. Chem.*, **63**, 1133 (1959); ΔH_f recalculated from data in ref 13. ^d $\Delta H_f(\text{CF}_2=\text{CF}_2)$ from ref 13, heat of chlorination from ref 2 corrected to 25° with ΔC_p estimated from ref 10. ^e $\Delta H_o(\text{solid})$ from W. D. Good, D. W. Scott, and G. Waddington, *J. Phys. Chem.*, **60**, 1080 (1956); $\Delta H_f(\text{solid})$ recalculated from data in ref 13; estimated ΔH_{sub} from ref 4.

Discussion

The heats of formation of relevant atoms and compounds have been taken from the JANAF tables¹³ and refer to 25°. Data taken from other literature sources have been recalculated so that the heats of formation are consistent with the JANAF tables. The heats of formation so obtained for the compounds C_nF_(2n+2-x)Cl_x are given in Table II. The heats of atomization, Q_a , are calculated at 298.2°K by the relation

$$Q_a(\text{C}_n\text{F}_{(2n+2-x)}\text{Cl}_x) = n\Delta H_f\text{C}(\text{g}) + [(2n+2) - x]\Delta H_f\text{F}(\text{g}) + x\Delta H_f\text{Cl}(\text{g}) - \Delta H_f\text{C}_n\text{F}_{(2n+2-x)}\text{Cl}_x(\text{g})$$

The heat of atomization is to be related to a sum of bond-energy terms plus bond-bond interaction terms. For this class of compounds there are three bond-energy terms, $E(\text{CC})$, $E(\text{CF})$, and $E(\text{CCl})$ and six bond-bond interaction terms corresponding to the bond pairs: I_{FCF} for C< $\frac{\text{F}}{\text{F}}$, I_{CCC} for C< $\frac{\text{C}}{\text{C}}$, I_{ClCCl} for C< $\frac{\text{Cl}}{\text{Cl}}$, I_{FCCl} for C< $\frac{\text{F}}{\text{Cl}}$, I_{FCC} for C< $\frac{\text{F}}{\text{C}}$, and I_{ClCC} for C< $\frac{\text{Cl}}{\text{C}}$.

However, these nine variables are not independent of one another and may be further reduced to six independent variables or effective bond terms.^{7,14,15} These are

$$B(\text{CF}) = E(\text{CF}) + \frac{3}{2}I_{\text{FCF}}$$

$$B(\text{CCl}) = E(\text{CCl}) + \frac{3}{2}I_{\text{ClCCl}}$$

$$B(\text{CC}) = E(\text{CC}) + 3I_{\text{CCC}}$$

$$\Gamma_{\text{FCCl}} = I_{\text{FCCl}} - \frac{1}{2}(I_{\text{FCF}} + I_{\text{ClCCl}}) \quad (1)$$

$$\Gamma_{\text{FCC}} = I_{\text{FCC}} - \frac{1}{2}(I_{\text{FCF}} + I_{\text{CCC}})$$

$$\Gamma_{\text{ClCC}} = I_{\text{ClCC}} - \frac{1}{2}(I_{\text{ClCC}} + I_{\text{CCC}})$$

The terms in eq 1 have been labeled so as to permit the heat of atomization of a compound to be given by these simple rules: (1) a $B(\text{C-X})$ term for each C-X bond and (2) a Γ_{XCY} term for each C< $\frac{\text{X}}{\text{Y}}$ interaction, in which X is different from Y, but either may be a carbon atom. The utility of these rules may be illustrated with CF₂ClCF₂Cl which consists of four C-F bonds, two C-Cl bonds, and one C-C bond, with four C< $\frac{\text{Cl}}{\text{F}}$, four C< $\frac{\text{F}}{\text{C}}$, two C< $\frac{\text{F}}{\text{F}}$, and two C< $\frac{\text{Cl}}{\text{C}}$ interactions. Therefore

(13) "JANAF Thermochemical Tables," The Dow Chemical Co., Midland, Mich., 1961, and supplements to present date.

(14) H. A. Skinner and G. Pilcher, *Quart. Rev. (London)*, **17**, 264 (1963).

(15) H. Bernstein, *J. Phys. Chem.*, **69**, 1550 (1965).

$$Q_a(\text{CF}_2\text{ClCF}_2\text{Cl}) = 4E(\text{CF}) + 2E(\text{CCl}) + E(\text{CC}) + 4I_{\text{ClCF}} + 4I_{\text{FCC}} + 2I_{\text{ClCC}} + 2I_{\text{FCF}} \quad (2)$$

Direct count for the effective bond terms results in

$$Q_a(\text{CF}_2\text{ClCF}_2\text{Cl}) = \epsilon B(\text{CF}) + 2B(\text{CCl}) + B(\text{CC}) + 4\Gamma_{\text{ClCF}} + 4\Gamma_{\text{FCC}} + 2\Gamma_{\text{ClCC}} \quad (3)$$

Substitution of eq 1 into eq 2 will confirm this result in eq 3.

The six effective bond terms have been obtained by a least-squares fit of the data in Table II. They are

$$\begin{aligned} B(\text{CC}) &= 81.28 \text{ kcal/mole} \\ B(\text{CF}) &= 117.12 \text{ kcal/mole} \\ B(\text{CCl}) &= 78.11 \text{ kcal/mole} \\ \Gamma_{\text{FCC}} &= -2.35 \text{ kcal/mole} \\ \Gamma_{\text{ClCC}} &= +0.19 \text{ kcal/mole} \\ \Gamma_{\text{FCCl}} &= -2.23 \text{ kcal/mole} \end{aligned} \quad (4)$$

These six parameters have been used to calculate the heats of atomization of the compounds in Table II and are given in the fourth column. The agreement between these and the experimental values is excellent. The values of the bond terms and bond interaction terms obtained in this work compare favorably with those obtained from a consideration of substituted methanes only by Bernstein,¹⁵ who arrived at $B(\text{CF}) = 116.6$, $B(\text{CCl}) = 78.0$, and $\Gamma_{\text{FCCl}} = -1.63$ kcal/mole (values standardized to the thermodynamic data of the JANAF tables). Unfortunately, a direct comparison of $B(\text{CC})$ and Γ_{XCC} with Bernstein's results is not possible as the methyl group was treated as a pseudo-atom. However, one can obtain a value for $B(\text{CC})$ from the heats of formation of hydrocarbons using the Zahn scheme.⁷ By fitting the data on 31 hydrocarbon compounds of four to nine carbons, the results are

$$\begin{aligned} B'(\text{CC}) &= 83.49 \text{ kcal/mole} \\ B'(\text{CH}) &= 99.21 \text{ kcal/mole} \\ \Gamma'_{\text{HCC}} &= -0.51 \text{ kcal/mole} \end{aligned}$$

A primed notation is adopted to indicate values for hydrocarbons. The values for the heats of atomization are based on $\Delta H_f^\circ(\text{C}(\text{g})) = 170.9$ kcal/mole and $\Delta H_f^\circ(\text{H}(\text{g})) = 52.1$ kcal/mole.

The value of $B(\text{CC})$ is about 2 kcal/mole lower than that for $B'(\text{CC})$ and suggests that a set of transferable bond-energy terms cannot be obtained by considering only nearest neighbor interactions. While inclusion of nearest neighbor interactions has certainly

resulted in a considerable improvement over the usual bond-energy scheme in the accuracy of prediction, other interactions must also contribute to the heats of formation. Several different types of interaction terms have been applied to the heats of formation of hydrocarbons in an effort to improve the correlation and these have been covered in two recent reviews on the subject.^{14,16} However, no attempt will be made to include such additional interaction terms in the present scheme as these require not only additional thermochemical data but also data of greater precision than are presently available.

In light of the above comments, it is of interest to consider the reliability of the present scheme in predicting heats of formation of chlorofluoroaliphatic compounds based upon the data for the hydrocarbons. It can be shown that the bond-term values derived from methane and the linear and simply branched (*i.e.*, only one side chain) hydrocarbons can be used to predict the heats of formation of other linear and simply branched hydrocarbons with a maximum deviation of 0.3 kcal/mole. However, these bond terms give predicted values for the multiply branched compounds which deviate from the observed by several kilocalories per mole. Since the present scheme for chlorofluorocarbons is based upon data for linear and simply branched compounds, one can reasonably expect accurate predictions within this group with the definite possibility of serious deviations (greater than 2 kcal/mole) for other more branched compounds.

Applications

Heats of formation calculated by the present scheme may be used in conjunction with the heat of chlorination data of Lacher, Park, *et al.*,^{2,3} to arrive at heats of formation for several chlorofluoroalkenes. Lacher and co-workers obtained their data at 90 and 128° and these have been corrected to 25° using estimated ΔC_p values.¹⁰ The relevant data are summarized in Table III. The heat of formation of $\text{CF}_2=\text{CFCl}$, which has been determined several times by combustion with alkali metal, has been recalculated based upon JANAF data,¹³ giving -117.7 ± 2 ,¹⁷ -127.5 ± 2 ,¹⁸ and -132.7 ± 1.3 ¹⁹ kcal/mole. The value of -117 kcal/mole is preferred here. From the study of the saturated compounds it has been shown that a pair of adjacent C-F

(16) G. R. Somayajulu, A. P. Kudchadker, and B. J. Zwolinski, *Ann. Rev. Phys. Chem.*, **16**, 213 (1965).

(17) H. von Wartenberg and J. Schiefer, *Z. Anorg. Allgem. Chem.*, **278**, 326 (1955).

(18) F. W. Kirkbride and F. G. Davidson, *Nature*, **174**, 79 (1954).

(19) V. P. Kolesov, I. D. Zenkov, and S. M. Skuratov, *Zh. Fiz. Khim.*, **37**, 224 (1963).

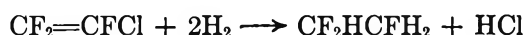
Table III: Heats of Formation of Some Chlorofluoroolefins at 25°

Compounds	$-\Delta H$ (chlorination), 25°, kcal/mole	$-\Delta H_f$ (adduct), kcal/mole	$-\Delta H_f$ (olefin), kcal/mole	$-\Delta H_f$, calcd from eq 4 and 5
CF ₂ =CF ₂	57.1 ± 0.2 ^a	212.6 ± 2	155.5 ± 2'	155.4
CF ₂ =CFCl	48.6 ± 0.5 ^b	166.1 ± 2	117.5 ± 2	117.4
CF ₂ =CCl ₂	40.9 ± 0.6 ^b	123.9 ± 2	83.0 ± 2	79.4
CCl ₂ =CCl ₂	31.7 ± 2 ^c	35.3 ± 1	3.6 ± 2 ^c	3.6
CF ₃ CF=CF ₂	47.0 ± 0.1 ^b	314.8 ± 2	267.8 ± 2	268.5
CF ₂ CF ₂ CF=CF ₂	44.7 ± 0.3 ^d	412.2 ± 2	367.5 ± 2	365.9
CF ₃ CF ₂ CF ₂ CF=CF ₂	45.3 ± 0.4 ^d	509.7 ± 2	464.4 ± 2	463.3
(CF ₃) ₂ C=CF ₂	41.9 ± 0.5 ^d	421.7 ± 2	379.8 ± 2	381.7

^a See ref 2a. ^b See ref 2b. ^c F. W. Kirkbride, *J. Appl. Chem.*, **6**, 11 (1956); J. Puyo, D. Balesdent, M. Neclause, and M. Dzierzynski, *Compt. Rend.*, **256**, 3471 (1963). ^d See ref 3. ^e $\Delta H_f(C_2Cl_4(l))$ from L. Smith, L. Bjellerup, S. Krook, and H. Westermarck, *Acta Chem. Scand.*, **7**, 65 (1953), and ΔH_{vap} from D. R. Stull, *Ind. Eng. Chem.*, **39**, 517 (1947) give $\Delta H_f(C_2Cl_4(g)) = -3.7$ kcal/mole. ^f See ref 13.

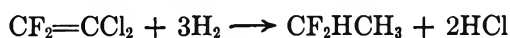
and C-Cl bonds are antibonding by about 2 kcal/mole; that the same pair should be bonding by 13 kcal/mole in the olefins seems unreasonable. In addition, it will be shown that strain energy considerations strongly favor a value of -117 kcal/mole.

The values obtained for the heats of formation of CF₂=CFCl and CF₂=CCl₂ can be combined with heat of hydrogenation data²⁰ corrected to 25° and the heat of formation¹³ of HCl to give



$$\Delta H_r^{298} = -64.0 \pm 1 \text{ kcal/mole}$$

$$\Delta H_f(CF_2HCFH_2) = -159.5 \pm 2.5 \text{ kcal/mole}$$



$$\Delta H_r^{298} = -81.9 \pm 2 \text{ kcal/mole}$$

$$\Delta H_f(CF_2HCH_3) = -120.9 \pm 3 \text{ kcal/mole}$$

The data of Table III may be used to estimate other chlorofluoroolefins, if one treats the alkyl substituents by eq 4 and assumes additivity of the vinyl bonds.^{10a} A vinyl bond will be designated by V-X and will be one of the four bonds associated with the nucleus $>C=C<$. On this basis

$$E_A(V-F) = 143.2$$

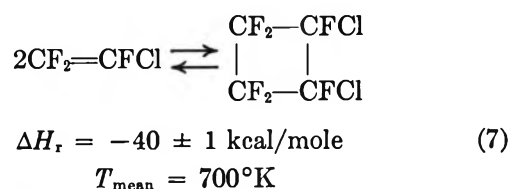
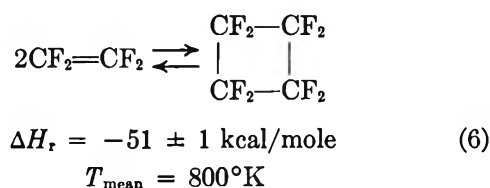
$$E_A(V-Cl) = 115.3 \quad (5)$$

$$E_A(V-C) = 120.8$$

The agreement between the observed and calculated values is given in the last column of Table III. The results appear satisfactory (however, eq 5 should be used with considerable caution) and are to be regarded as preliminary values until more direct experimental data become available.

Ring strain energies for perfluoro compounds may

also be estimated in conjunction with the present empirical scheme. The good agreement between calculated and observed heats of formation of the two perfluorocyclohexanes suggests a negligible strain, just as for hydrocarbons.¹⁴ The strain energy for the fluorinated cyclobutane ring can be estimated from the data of Atkinson and Trentworth²¹ and Butler²² for reaction 6 and Atkinson and Stedman²³ for reaction 7.



Using $\Delta C_p \cong -2 \pm 2$ cal/deg mole²⁴ to correct from 300°K to T_{mean} , one obtains $\Delta H_r(25^\circ) = -50.0 \pm 1$ kcal/mole and $\Delta H_r(25^\circ) = -39.0 \pm 1$ kcal/mole for reactions 6 and 7, respectively. These values may be combined with the heats of formation of C₂F₄ and C₂F-

(20) J. R. Lacher, A. Kianpour, F. Oetting, and J. D. Park, *Trans. Faraday Soc.*, **52**, 1500 (1956).

(21) B. Atkinson and A. B. Trentworth, *J. Chem. Soc.*, 2082 (1953).

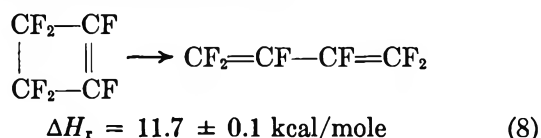
(22) J. N. Butler, *J. Am. Chem. Soc.*, **84**, 1393 (1962).

(23) B. Atkinson and M. Stedman, *J. Chem. Soc.*, 512 (1962).

(24) At 25°. ΔC_p (eq 6) = -8 cal/deg mole and ΔC_p (eq 7) = -7 cal/deg mole; if all vibrational modes are active then $\Delta C_p = +6.93$ cal/deg mole for both reactions. At 700-800°K, the value should be close to this classical limit; therefore $\Delta C_p \cong -2 \pm 2$ cal/deg mole.

F_3Cl to yield $\Delta H_f(c-C_4F_8) = -361.0 \pm 2$ and $\Delta H_f(c-C_2F_6Cl_2) = -274.0 \pm 2$ kcal/mole at 25° . The strain-free heats of formation for $c-C_4F_8$ and $c-C_4F_6Cl_2$ may be calculated by means of eq 4. These values are $\Delta H_f - S_R(c-C_4F_8) = -389.6 \pm 2$ and $\Delta H_f - S_R(c-C_4F_6Cl_2) = -297.2 \pm 2$ kcal/mole, resulting in $S_R(c-C_4F_8) = 28 \pm 3$ and $S_R(c-C_4F_6Cl_2) = 23 \pm 3$ kcal/mole. These values are essentially the same as the 26 kcal/mole strain energy calculated for cyclobutane.¹⁴ The good agreement obtained for the strain energies of the cyclobutanes adds further support to $\Delta H_f(CF_2=CFCl) = -117.5$, while the more stable value of -130 ± 2 kcal/mole would result in a negative strain energy for 1,2-dichloroperfluorocyclobutane.

Lacher and co-workers^{2b} have determined the heat of chlorination of perfluorocyclobutene to be -37.1 ± 1 kcal/mole, as corrected to 25° in the usual manner. This results in $\Delta H_f(c-C_4F_6) = -237.5 \pm 2.5$ kcal/mole. Finally, one can combine this result with the heat of isomerization of perfluorocyclobutene (reaction 8) measured by Schlag and Peatman²⁵



to yield $\Delta H_f(CF_2=CF-CF=CF_2) = -225.8 \pm 2.5$ kcal/mole at 25° , neglecting the small correction for ΔC_p . These additional heats of formation and strain energies are summarized in Table IV for convenience.

Table IV: Heats of Formation of Chlorofluorocarbons and Derived Strain Energies for Ring Compounds (kcal/mole at 25°)

Compound	$-\Delta H_f$	Strain energy
$CF_2CF \begin{array}{c} <CF_2CF_2> \\ CF_2CF_2 \end{array} CF_2$	687.2 ± 2	0 ± 2
CF_2-CF_2	361.0 ± 2	28 ± 3
CF_2-CFCl	274.0 ± 3	23 ± 3
CF_2-CF	237.5 ± 3	...
$CF_2=CF-CF=CF_2$	225.8 ± 2.5	...

(25) E. W. Schlag and W. B. Peatman, *J. Am. Chem. Soc.*, **86**, 1676 (1964).

The Second Virial Coefficient of Polyelectrolytes

by Akira Takahashi, Tadayo Kato, and Mitsuru Nagasawa

*Departments of Applied and Synthetic Chemistry, Nagoya University, Furo-cho, Chikusa-ku, Nagoya, Japan
(Received August 26, 1966)*

The second virial coefficient of linear polyelectrolytes is extremely nonideal because of the electrostatic interaction between charges of ions as well as because of the polymeric character of polyions. In this paper, the second virial coefficients of sodium polystyrenesulfonate of various molecular weights were determined by light-scattering technique in solutions of different ionic strengths. From the experimental results, the correction factors for the two kinds of nonideality were separately calculated. Then it was concluded that most of the nonideal behavior of linear polyelectrolytes arises from the strong electrostatic interaction between charges, but the contribution of the polymeric character of polyions also cannot be neglected. The correction factor for the nonideality due to the polymeric character of polyions was compared with the theories on the second virial coefficient of linear polymers. It was found that most theories, particularly the theory of Casassa and Markovitz and others, can explain the results well. The correction factor for the electrostatic interaction was also found to be as expected previously.

Introduction

It is clear from their chemical structures that polyelectrolytes must show the features of both electrolytes and linear polymers when they are dissolved in water. Because of the combination of both features, polyelectrolytes show a characteristic thermodynamic behavior which looks quite different from that of either nonionic polymers or simple electrolytes. Therefore, the second virial coefficient of polyelectrolytes is sometimes discussed as an extension of the theory of the second virial coefficient for nonionic linear polymers and sometimes discussed by applying the theory for colloidal electrolyte solutions.¹

It is assumed that the solution under consideration contains a polyelectrolyte of concentration C_p (g/100 ml) and a neutral salt of 1:1 valence type of concentration C_s (moles/l.) and also that the polyelectrolyte and the neutral salt have one ion in common, which is called the counterion. Now, suppose that the macroion is a point particle having $-Z_p$ charges and the solution is thermodynamically ideal; that is, all the particles are distributed uniformly in the solution. Then the second virial coefficient of the ideal solution can be expressed by the following equation which can be derived from the theory of Donnan and Guggenheim² without ambiguity

$$A_2^0 = 10^3 Z_p^2 / 4M^2 C_s^0 \quad (1)$$

where M is the molecular weight of macroion, and C_s^0 is the concentration of the neutral salt in an external solution which is supposed to be in equilibrium with the polyelectrolyte-neutral salt solution. Equation 1 was also derived by Hill,³ who applied the McMillan-Mayer theory⁴ to spherical colloidal solutions with ionic atmosphere of the Debye-Hückel type. The first application of eq 1 to linear polyelectrolyte solutions was reported by Pals and Hermans.⁵ The most important features of eq 1 are that A_2^0 is independent of the molecular weight and proportional to $1/C_s^0$.

However, the linear polyelectrolyte solution is not an ideal solution but extremely nonideal, first, because there is electrostatic interaction between the charges

(1) S. A. Rice and M. Nagasawa, "Polyelectrolyte Solutions," Academic Press Inc., New York, N. Y., 1961.

(2) F. G. Donnan and E. A. Guggenheim, *Z. Physik. Chem.*, **162**, 346 (1932); F. G. Donnan, *ibid.*, **168**, 369 (1934).

(3) T. L. Hill, *Discussions Faraday Soc.*, **21**, 31 (1956); *J. Phys. Chem.*, **61**, 548 (1957); T. L. Hill, "Introduction to Statistical Thermodynamics," Addison-Wesley Publishing Co., Reading, Mass., 1960, Chapter 19.

(4) W. G. McMillan and J. E. Mayer, *J. Chem. Phys.*, **13**, 276 (1945).

(5) D. T. F. Pals and J. J. Hermans, *Rec. Trav. Chim.*, **71**, 469 (1952).

of ions, and secondly, because the macroion is not a point but a chain molecule. The improvement of the theory of the second virial coefficient by taking into account the electrostatic interaction between ions was reported by many workers.^{2,5-14} The correction factor for the electrostatic interaction is usually given as a constant which is nearly independent of the molecular weight and the ionic strength, such as

$$A_2 = A_2^0 \Gamma_1 \quad (2)$$

Therefore, A_2 is still independent of the molecular weight and proportional to $1/C_s^0$. The improvement of A_2 theory by taking into account the chain character of the macroion was reported by Orofino and Flory.¹⁵ As shown later, the characteristic of their theory is that A_2 becomes a function of the expansion factor α , such as

$$A_2 = A_2^0 \Gamma_2(\alpha) \quad (3)$$

Therefore, A_2 must depend on molecular weight and may deviate from the linearity against $1/C_s^0$. Thus, if we may assume the independence of two correction factors, the second virial coefficient of linear polyelectrolytes can be expressed by

$$A_2 = A_2^0 \Gamma_1 \Gamma_2(\alpha) \quad (4)$$

The purpose of this paper is to calculate separately the contributions of Γ_1 and $\Gamma_2(\alpha)$ using the experimental data to compare them to each other. The method of calculation will be explained later.

Experimental Section

Samples. Sodium poly(styrene-*p*-sulfonate) (NaPSS) used in this investigation was the same as the sample used previously.¹⁶ It was provided by Dr. Vanderkooi and Dr. Mock of the Dow Chemical Co. One hundred grams of the dried sample, which was precipitated three times from aqueous solution with isopropyl alcohol, was dissolved in 5 l. of aqueous 0.6 *N* NaOH solution and was fractionated into eight fractions by stepwise reduction of the solution temperature from 40 to 20°. The lowest molecular weight fraction was again fractionated into two fractions.

The sodium hydroxide included in each fraction was removed by reprecipitation with isopropyl alcohol three times. The pH of the final aqueous solution was from 7 to 8 and, therefore, adjusted from 6 to 7 by adding a small amount of HCl. The amount of NaCl thus produced was so small that the effect of the salt can be neglected in the further experiments. Each fraction thus purified was dissolved in deionized distilled water and freeze-dried, followed by drying at 50° under vacuum for 2 weeks.

The fractionated sample was dissolved in NaCl aqueous solutions of given concentrations in volumetric flasks and stored at 25° as original solutions. Because the solution used in the present investigation is always a multicomponent system, the sample solutions must reach the Donnan membrane equilibrium with solvents before the scattering intensity and the refractive index increment are determined, as proposed by Casassa and Eisenberg.¹⁷ Therefore, the original solution was dialyzed against a solvent, and solutions of different polymer concentrations were made by dilution with the same solvent. This dilution method was used for all measurements of scattering intensity, refractive index increment, and intrinsic viscosity in this work. This approximate dilution method, which was originally proposed by Eisenberg, *et al.*,^{18,19} is effective if the concentration of added salt is not very low.

Light-Scattering Measurements. The light-scattering apparatus and Debye-type differential refractometer used in the present measurements were manufactured by Shimadzu Seisakusho Ltd. A cylindrical cell with a ground-glass back was used and its optical alignment was checked by using a fluorescein aqueous solution. Unpolarized light of 436 μ m from a mercury lamp was used. The calibration of the apparatus was carried out by using benzene, whose absolute scattering power was assumed to be the value reported by Kratochvil, *et al.*²⁰ ($R_{90} = 46.5 \times 10^{-6}$ at 20°). As the secondary standard, the molecular weights of NBS polystyrene 705 and 706²¹ were determined. The molecular weights

(6) G. Scatchard, *J. Am. Chem. Soc.*, **68**, 2315 (1946).

(7) J. T. Edsall, H. Edelhoeh, R. Lontie, and P. R. Morrison, *ibid.*, **72**, 4641 (1950).

(8) D. Stigter and T. L. Hill, *J. Phys. Chem.*, **63**, 551 (1959).

(9) M. Nagasawa, A. Takahashi, M. Izumi, and I. Kagawa, *J. Polymer Sci.*, **38**, 213 (1959).

(10) Z. Alexandrowicz, *ibid.*, **43**, 325, 337 (1960).

(11) N. Ise, *J. Chem. Phys.*, **35**, 1145 (1961); **36**, 3248 (1962); *J. Phys. Chem.*, **67**, 382 (1963).

(12) Z. Alexandrowicz and A. Katchalsky, *J. Polymer Sci.*, **A1**, 3231 (1963).

(13) A. Katchalsky, Z. Alexandrowicz, and O. Kedem, "Transactions of the Symposium on Electrolyte Solutions," Toronto, May 1964.

(14) G. S. Manning and B. H. Zimm, *J. Chem. Phys.*, **43**, 4250 (1965); G. S. Manning, *ibid.*, **43**, 4260 (1965).

(15) T. A. Orofino and P. J. Flory, *J. Phys. Chem.*, **63**, 283 (1959).

(16) L. Kotin and M. Nagasawa, *J. Am. Chem. Soc.*, **83**, 1026 (1961); M. Nagasawa and H. Fujita, *ibid.*, **86**, 3005 (1964).

(17) E. F. Casassa and H. Eisenberg, *J. Phys. Chem.*, **64**, 753 (1960).

(18) H. Eisenberg and E. F. Casassa, *J. Polymer Sci.*, **47**, 29 (1960).

(19) H. Eisenberg and D. Woodside, *J. Chem. Phys.*, **36**, 1844 (1962).

(20) J. P. Kratochvil, G. Deželić, M. Kerker, and E. Matijević, *J. Polymer Sci.*, **57**, 59 (1962).

(21) G. M. Kline, *Mod. Plastics*, **41**, No. 5, 188 (1964).

obtained agreed with the values reported by NBS within 5%. Measurements were made at angles from 40 to 140°. The Cabannes factor calculated from depolarization measurements was not smaller than 0.99, and hence, the factor was assumed to be unity for all the measurements in the present work.²² Temperature was maintained at $25 \pm 0.1^\circ$ by circulating thermostated water in the cell base. The room was also air-conditioned at $25 \pm 1^\circ$. The cleaning of the original solutions was carried out by centrifugation at 20,000*g* for 1 hr. The centrifugation tube was made of Delrin to avoid contamination with metal ions. The solvents used for dilution were filtered directly into the cell through an ultrafine membrane filter. The solution concentrations used in measurements were five different concentrations from 0.3 to 0.05 g/100 ml. The calibration of the differential refractometer was carried out by using KCl solutions as the standard. The value of refractive index increment experimentally observed is independent of both molecular weight and ionic strength of added salt if the NaCl concentration is between 0.5 and 0.005 *M*. The measurements of the refractive indices of the solvents were made by an Abbé refractometer with an unpolarized light at 25°.

Viscosity Measurements. The intrinsic viscosities of the various polymer fractions in sodium chloride solutions were measured with a capillary viscometer of modified Ubbelohde type with four bulbs to give variable rates of shear at $25.0 \pm 0.01^\circ$. The rate of shear correction was necessary when the salt concentration was low and the molecular weight high. The correction for kinetic energy was negligible (less than 0.3%).

At lower salt concentrations, the polymer chains were greatly expanded and interpenetrated each other; therefore, the viscosity measurements were carried out at less than 0.1 g/100 ml to obtain reliable values.

Determination of the Θ Point by Precipitation Measurements. The procedure of Mandelkern and Flory²³ modified by Takahashi, *et al.*²⁴ (in which the precipitation temperatures T_p observed in different polymer concentrations, C_p , were extrapolated both to $C_p = 0$ and to $M = \infty$), was used for the determination of the critical consolute mixture or the Θ point. The difference between the precipitation temperatures in cooling and in heating was usually within $\pm 0.5^\circ$.

Results

Determination of Θ Points. The Θ points determined from precipitation measurements in various solvent mixtures were plotted against ionic strength; one example is shown in Figure 1. The ionic strength at $\Theta = 25^\circ$ was determined from the figure as 3.1 *M* for KCl. It was found that NaCl solution of 4.17 *M* is

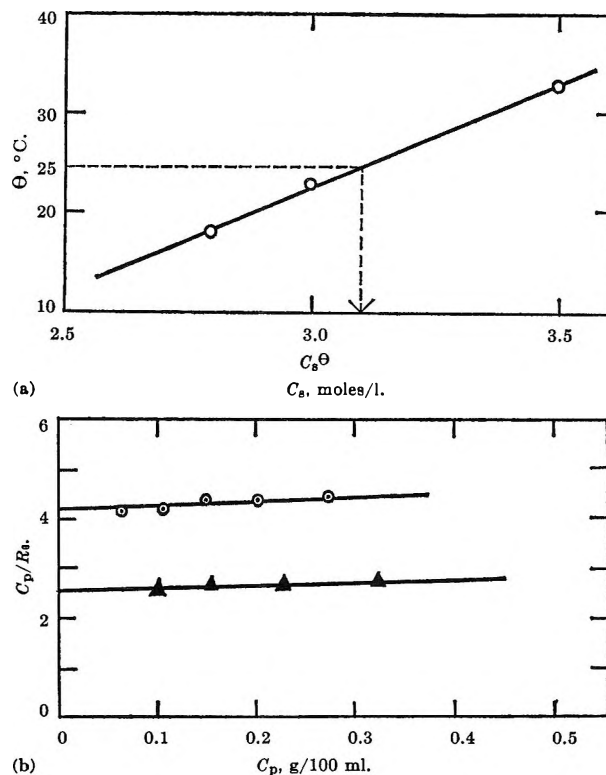


Figure 1. (a) Θ points as a function of ionic strength. The Θ solvent at 25° is indicated by the broken lines. (b) Plots of C_p/R_θ vs. C_p in 3.1 *M* KCl solutions: \blacktriangle , sample no. 4; \circ , sample no. 7.

also a Θ solvent at 25° . The concentration of added salt thus determined is described as C_s^Θ . The measurement of light scattering in the Θ system was performed only in a KCl-KPSS system, because it was very difficult to carry out experiments in such concentrated solutions as 4.17 *M* NaCl. The plot of C_p/R_θ vs. C_p in the 3.1 *M* KCl solution is given in Figure 1. The second virial coefficient observed in Figure 1 appears slightly positive, but its increase is of the same order as the value due to the scattering of added electrolyte which was pointed out by Eisenberg.²⁵ In order to confirm that these solutions are Θ solvents at 25° , the intrinsic viscosities were measured in both 4.17 *M* NaCl and 3.1 *M* KCl solutions. The relationships between $[\eta]$ and M obtained are shown in Figure 2. It is clear that $[\eta]_\Theta = KM^{0.5}$ holds satisfactorily for both systems.

(22) C. Tanford, "Physical Chemistry of Macromolecules," John Wiley and Sons, Inc., New York, N. Y., 1961, Chapter 5.

(23) L. Mandelkern and P. J. Flory, *J. Am. Chem. Soc.*, **74**, 2517 (1952).

(24) A. Takahashi and I. Kagawa, *Kogyo Kagaku Zasshi*, **64**, 1637 (1961).

(25) H. Eisenberg, *J. Chem. Phys.*, **36**, 1837 (1962).

Thus, it may be concluded that these salt solutions (C_s^\ominus) are Θ solvents at 25° .

Viscosity. In Figure 2 are shown the logarithmic plots of intrinsic viscosity $[\eta]$ in salt solutions of different ionic strength as a function of molecular weight which is determined by light-scattering measurements. In Table I are summarized the coefficients in the viscosity equation, $[\eta] = KM^\nu$, determined by the least-squares method. It appears that the value of ν is 0.5 at the Θ point in accordance with the theoretical value and increases gradually to 0.93 at 0.005 M NaCl solution.

Table I: Calculated Values of K and ν at 25° from the Equation $[\eta] = KM^\nu$

C_s^\ominus , moles/l.	$K \times 10^4$	ν
4.17	2.04	0.50
0.5	1.86	0.64
0.1	1.78	0.68
0.05	1.39	0.72
0.02	1.01	0.78
0.01	0.28	0.89
0.005	0.23	0.93

Second Virial Coefficient and Molecular Weight by Light-Scattering Measurements. Because of the high expansion of the polyion, it is often observed that KC_p/R_Θ vs. C_p plots for polyelectrolytes are not simple straight lines or simple upward-tending curves if the ionic strength is low. Since the effective diameter of the polymer molecule is much larger than the root-mean-square end-to-end distance of the nonionized chain, the third and higher terms in the virial expansion could make important contributions, resulting in upward curvature of KC_p/R_Θ vs. C_p plots even in low polymer concentrations. Moreover, a strong electrostatic repulsion occurs between segments of different molecules so that there may be a tendency of ordering of molecules or segments in solutions if the polymer concentration is high and the ionic strength is low. Such intermolecular interference causes the diminution of scattering per molecule and the reduction of the dissymmetry at high concentrations as was pointed out by Doty and Steiner.^{26,27} Therefore, the extrapolation to $C_p = 0$ in Zimm's plot must be made from the measurements of solutions of low enough polymer concentration to avoid these ambiguities. Nevertheless, the values of the second virial coefficient obtained may not be highly reliable at lower ionic strength. However, if the ionic strength is high enough, this unusual shape of KC_p/R_Θ vs. C_p plot does not appear.

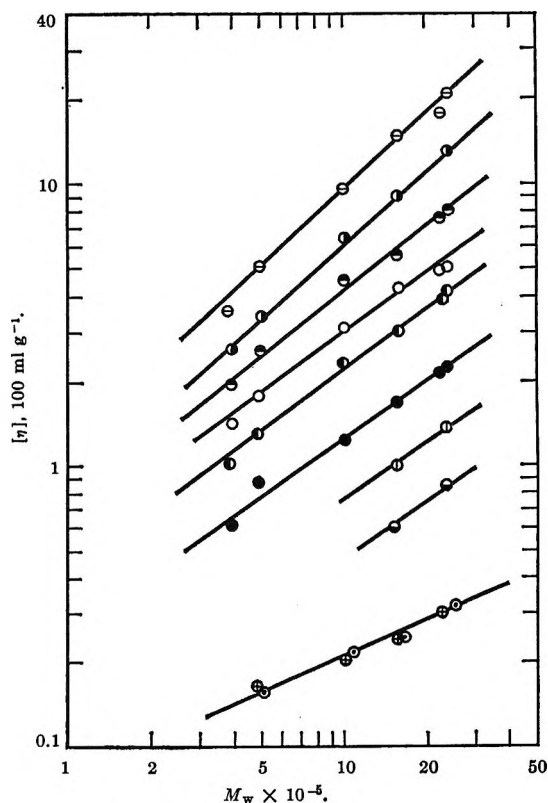


Figure 2. Relationships between intrinsic viscosities and molecular weights; ionic strength of NaCl, C_s^\ominus : \circ , 4.17 (C_s^\ominus); \bullet , 2; \circ , 1; \bullet , 0.5; \circ , 0.1; \circ , 0.05; \circ , 0.02; \circ , 0.01; \circ , 0.005 M; and \circ , 3.1 M KCl (C_s^\ominus).

The weight-average molecular weights of the fractionated samples obtained are shown in Table II. The same molecular weight was obtained for each fraction over a wide range of different ionic strengths. The average values listed in the last line of Table II are used as the molecular weights of the samples in further calculations. In Figure 3, plots of C_p/R_Θ vs. C_p at various ionic strengths are shown, and in Table III, the second virial coefficient determined from the graphs are given. The dependence of A_2 on the molecular weight is shown in Figure 4. There seems to be no molecular weight dependence in low ionic strength. In high ionic strength, however, a slight dependence of A_2 on M is observed.

In Figure 5 are shown the plots of A_2 vs. $1/C_s^\ominus$. At high ionic strength the linear relationship becomes unsatisfactory and the curvature shows a downward tendency. The same data are plotted in Figure 6 as A_2 vs. $1/\sqrt{C_s^\ominus}$ plots. The linear relationship between A_2 and $1/\sqrt{C_s^\ominus}$ appears satisfactory at high ionic

(26) P. Doty and R. F. Steiner, *J. Chem. Phys.*, **17**, 743 (1949).

(27) P. Doty and R. F. Steiner, *J. Polymer Sci.*, **5**, 383 (1950).

Table II: Molecular Weights of Samples Used for Light Scattering

C_s^0 , moles/l.	Molecular weights, $M_w \times 10^{-5}$, for sample no.					
	2	3	5	7	8	9
2.0	22.3	...	15.4
1.0	21.7	...	15.5
0.5	...	23.0	15.3	9.3	4.85	...
0.1	24.2	23.0	15.3	10.4	5.2	4.03
0.05	...	23.0	15.4	9.6	5.0	...
0.02	...	23.0	16.0	10.5	4.6	...
0.01	25.6	...	15.4	10.5	...	3.84
0.005	...	22.0	15.4	9.6
Mean \pm std dev	23.4 ± 1.0	22.8 ± 0.5	15.5 ± 0.5	10.0 ± 0.5	4.9 ± 0.3	3.9 ± 0.1

Table III^c

C_s^0 , moles/l.	Sample no.	$A_2(\text{obsd})$ $\times 10^4$	A_2^0 $\times 10^4$	A_2/A_2^0 $\times 10^2$	$\Gamma_1(\alpha)$	Γ_1 $\times 10^3$	γ_s^0 ^b	γ_0^0
2	2	0.56	2.95	2.0	0.65	3.1	0.668	0.14
	5	0.44		1.4	0.66	2.1		0.12
1	2	1.16	5.90	2.0	0.38	5.3	0.657	0.19
	5	1.12		1.9	0.41	4.5		0.17
0.5	3	3.0	11.8	2.5	0.32	8.0	0.681	0.23
	5	2.8		2.4	0.24	10.0		0.26
	7	3.1		2.6	0.26	10.2		0.26
	8	3.3		2.8	(0.11)	(25.0)		(0.41)
0.1	2	4.8	58.9	0.81	0.16	5.2	0.778	0.20
	3	4.8		0.81	0.18	4.5		0.19
	5	5.2		0.88	0.16	5.6		0.21
	7	5.7		0.98	0.14	7.1		0.21
	8	5.4		0.92	(0.12)	(7.9)		(0.25)
0.05	3	8.1	118	0.69	0.18	3.8	0.822	0.18
	5	8.2		0.70	0.13	4.7		0.20
	7	8.9		0.76	0.13	5.6		0.22
	8	5.7		0.48	(0.057)	(8.5)		(0.26)
0.02	3	15.1	295	0.51	0.16	3.3	0.872	0.17
	5	15.3		0.52	0.16	3.4		0.17
	7	15.1		0.51	0.15	3.4		0.17
	8	14.8		0.50	(0.059)	(8.5)		(0.27)
0.01	2	18.7	589	0.32	0.10	3.2	0.903	0.17
	5	20.5		0.35	0.15	2.4		0.15
	7	22.4		0.38	0.15	2.5		0.15
0.005	3	42.3	1180	0.36	0.23	1.6	0.928	0.12
	5	46.4		0.39	0.17	2.3		0.15
	7	41.2		0.35	0.19	1.9		0.13

^a The values in parentheses indicate that the molecular dimensions observed for sample no. 8 were always abnormal. ^b γ_s^0 , R. Parsons, "Handbook of Electrochemical Constants," Butterworth and Co. (Publishers) Ltd., London, 1959.

strength, while a deviation is observed at low ionic strength. In the middle range of ionic strength, therefore, the logarithmic plot of A_2 vs. $1/C_s^0$ appears to show a different slope from either unity or 0.5, as

reported by Trap and Hermans.²⁸ However, it seems to us that the slope value is unimportant.

(28) H. J. L. Trap and J. J. Hermans, *J. Phys. Chem.*, **58**, 757 (1954).

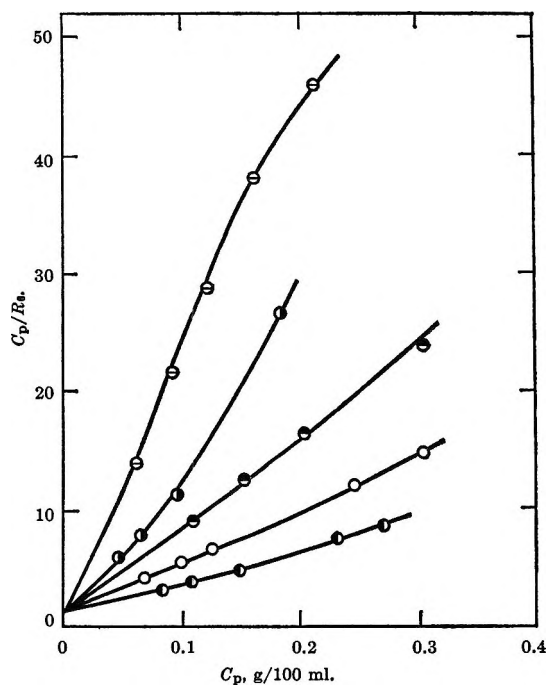


Figure 3. An example of C_p/R_θ vs. C_p plots in NaCl solutions: sample no. 5; NaCl concentrations are the same as in Figure 2.

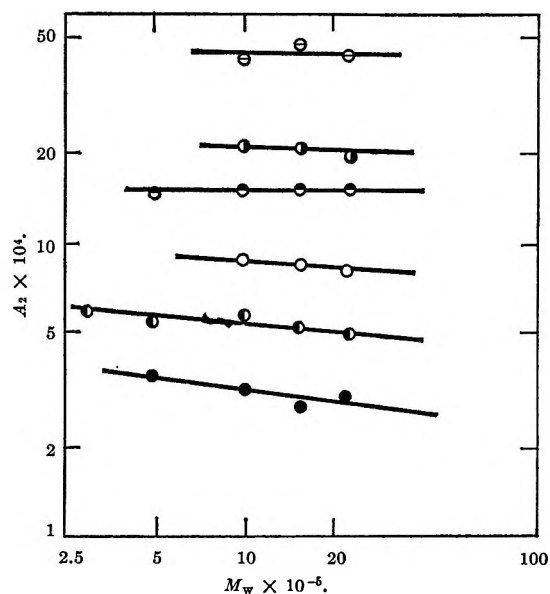


Figure 4. The dependence of A_2 on the molecular weight. NaCl concentrations are the same as in Figure 2.

Molecular Dimensions. An example of $(C_p/R_\theta)_{C_p \rightarrow 0}$ vs. $\sin^2(\theta/2)$ plots is shown in Figure 7. Radii of gyration obtained in NaCl solutions are listed in Table IV together with the unperturbed radii of gyration determined in 3.1 M KCl. The reliability of the radius of gyration obtained may not be very high because it

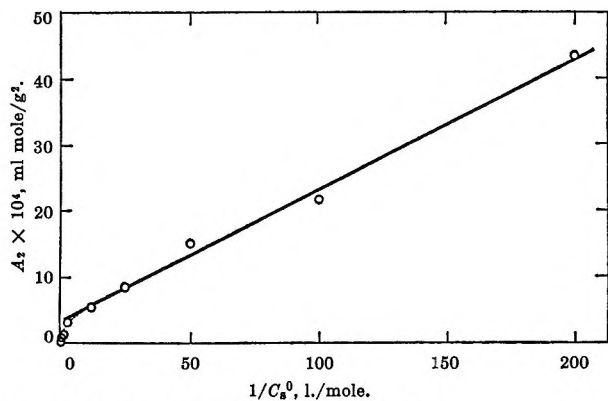


Figure 5. Plots of A_2 (obsd) against $1/C_s^0$.

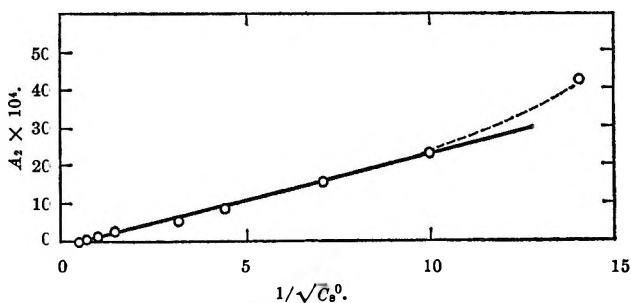


Figure 6. The second virial coefficients as a function of the reciprocal square root of the ionic strength.

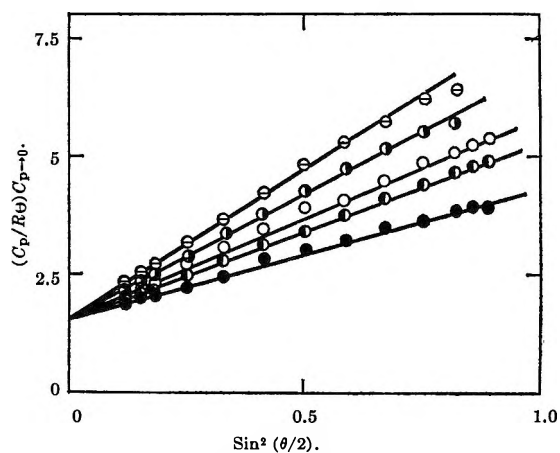


Figure 7. An example of $(C_p/R_\theta)_{C_p \rightarrow 0}$ vs. $\sin^2(\theta/2)$ plots in NaCl solutions: sample no. 5; NaCl concentrations are the same as in Figure 2.

is difficult to obtain a linear extrapolation to $C_p = 0$ due to the high expansion of polymer chains, but is enough for the purpose of this paper. The well-known Flory constant Φ' can be calculated using the relationship²⁸ in eq 5.

(29) P. J. Flory, "Principles of Polymer Chemistry," Cornell University Press, Ithaca, N. Y., 1953; P. J. Flory and T. G. Fox, Jr., *J. Am. Chem. Soc.*, **73**, 1904 (1951); *J. Polymer Sci.*, **5**, 745 (1950).

$$[\eta] = \Phi' \langle S^2 \rangle^{1/2} / M \quad (5)$$

$$[\eta] / [\eta]_0 = \alpha_\eta^3 \quad (6)$$

where $\langle S^2 \rangle$ is the square of the radius of gyration. The values of Φ' so calculated are plotted as a function of the expansion factor α_η in Figure 8. It is observed that

Table IV: Molecular Dimensions

C_s^0 , moles/l.	Molecules dimensions $\langle S^2 \rangle_s \times 10^{10}$ for samples						
	2	3	4	5	7	8	9
2.0	0.212	0.111
1.0	0.342	0.188
0.5	...	0.504	...	0.348	0.222	0.157	...
0.1	0.778	0.709	...	0.513	0.349	0.170	0.091
0.05	...	0.897	...	0.639	0.406	0.238	...
0.02	...	1.177	...	0.696	0.434	0.357	...
0.01	1.505	0.745	0.479	...	0.122
0.005	...	1.218	...	0.893	0.499
In KCl Solution at θ Point							
3.1	0.054	...	0.036

the value of Φ' at $\alpha_\eta = 1$ (i.e., Φ'_0) is close to 4.21×10^{22} ($\Phi_0 = 2.87 \times 10^{21}$ for the mean-square end-to-end distance) which is reasonable compared with the values obtained for nonionic polymers, but the value of Φ' decreases markedly with α_η . If we take an average value of Φ' over a range of concentration which is usually used for the study of polyelectrolyte solutions, the value is much lower than 3.1×10^{22} (2.1×10^{21} for the mean-square end-to-end distance). This result is in accord with the results previously reported,^{15,19,30} in which very low values, from 2.2×10^{22} to 1.3×10^{22} , were reported for Φ' of polyelectrolytes.

The theory of light scattering based on the radial distribution function of polymers in multicomponent systems has not been sufficiently developed; therefore, the present calculation is based on the assumption that molecular dimensions in three-component systems can be obtained by the same procedure as in two-component systems.³¹ Despite this lack of theoretical background for the determination of the radius of gyration, it is to be noted that values of Φ' first decrease with α_η , and then increase with further increase of α_η ,³²⁻³⁴ Theoretical predictions give only a monotonic decreasing curve for Φ' with α_η .³⁵⁻³⁷

Discussion

According to Orofino and Flory,¹⁵ the second virial coefficient of polyelectrolytes is given by

$$A_2 \simeq (16\pi N_A / 3^{1/2}) [\langle S^2 \rangle^{1/2} / M^2] \times \ln [1 + (\pi^{1/2} / 2)(\alpha^2 - 1)] \quad (7)$$

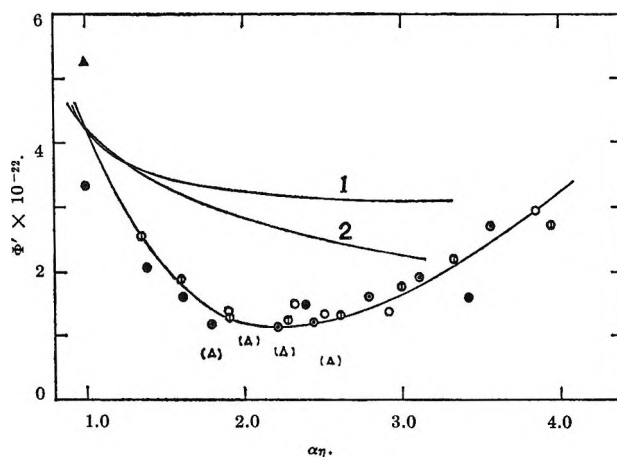


Figure 8. The Flory constant Φ' of NaPSS, temperature 25°; salt concentrations, 3.1 M KCl and from 2 to 0.005 M NaCl: sample no.; ●, 2; ○, 3; ▲, 4; ⊙, 5; ○, 7; △, 8: curve 1, Eizner and Ptitsyn;³⁵ curve 2, Kurata and Yamakawa.³⁶

where the expansion factor α is given from^{38,39}

$$\alpha^5 - \alpha^3 = 10^3 (3^{3/2} / 2^3 \pi^{1/2}) (1 / N_A V_1) \times (M V_u / M_u)^2 \langle S_0^2 \rangle^{-1/2} [1/2 - X_1 + V_1 i^2 / 4 V_u^2 C_s^0] + \dots \quad (8)$$

where V_1 and V_u are the molar volumes of solvent and segments, respectively, M_u is the molecular weight of the repeating unit of the polymer, and i is the degree of ionization of the fixed charges on the chain ($Z_p^2 = (iM/M_u)^2$). Neglecting the nonionic term in comparison with the ionic term in eq 8 and using the relationship

$$\langle S^2 \rangle^{1/2} = \langle S_0^2 \rangle^{1/2} \alpha^3 \quad (9)$$

eq 7 can be transformed into

$$A_2 = (10^3 Z_p^2 / 4 M^2 C_s^0) (4 / \pi^{1/2}) \times (1/2)(\alpha^2 - 1) \ln [1 + (\pi^{1/2} / 2)(\alpha^2 - 1)] \quad (10)$$

(30) A. Takahashi and I. Kagawa, *Nippon Kagaku Zasshi*, **83**, 11 (1962).

(31) B. H. Zimm, *J. Chem. Phys.*, **16**, 1093 (1948).

(32) W. R. Krigbaum and D. K. Carpenter, *J. Phys. Chem.*, **59**, 1166 (1955).

(33) G. V. Schulz and R. Kirste, *Z. Physik. Chem. (Frankfurt)*, **30**, 171 (1961).

(34) M. Kurata and W. H. Stockmayer, *Fortsch. Hochpolymer. Forsch.*, **3**, 196 (1963).

(35) H. Yamakawa and M. Kurata, *J. Phys. Soc. Japan*, **13**, 94 (1958); M. Kurata and H. Yamakawa, *J. Chem. Phys.*, **29**, 311 (1958).

(36) O. B. Ptitsyn and Yu. E. Eizner, *Zh. Tekh. Fiz.*, **29**, 1117 (1959); Yu. E. Eizner and O. B. Ptitsyn, *Vysokomol. Soed.*, **6**, 777 (1964).

(37) N. W. Tschoegl, *J. Chem. Phys.*, **40**, 473 (1964).

(38) P. J. Flory, *ibid.*, **21**, 162 (1953).

(39) P. J. Flory and J. E. Osterheld, *J. Phys. Chem.*, **58**, 653 (1954).

where the term $(10^3 Z_p^2 / 4M^2 C_s^0)$ is the ideal Donnan term A_2^0 . Thus, we know that $\Gamma_2(\alpha)$ is expressed by

$$\Gamma_2(\alpha) = (2/\pi^{1/2}(\alpha^2 - 1)) \ln [1 + (\pi^{1/2}/2)(\alpha^2 - 1)] \quad (11)$$

and that the theories on Γ_1 and $\Gamma_2(\alpha)$ are complementary.

In general, all theories on the second virial coefficient of linear polymers are written in the form^{34,40,41}

$$A_2 = \frac{N_A \beta n^2}{2M^2} h(\bar{z}) \quad (12)$$

where \bar{z} is defined by $\bar{z} = z/\alpha^3$ and

$$z = \left(\frac{3}{2\pi}\right)^{1/2} \left(\frac{\beta}{a^3}\right) n^{1/2} \quad (13)$$

Moreover, n is the number of segments in a molecule, a is the effective bond length, and β is the binary cluster integral. From a simple comparison between eq 10 and 12, it is clear that A_2^0 of eq 10 corresponds to the general term of eq 12 and $\Gamma_2(\alpha)$ is identical with $h(\bar{z})$. Thus, $\Gamma_2(\alpha)$ can be calculated from the following equation using the experimental data

$$\Gamma_2(\alpha) (= h(\bar{z})) = \frac{1}{4N_A \pi^{1/2}} \frac{1}{\bar{z}} \frac{A_2 M^2}{\langle S^2 \rangle^{1/2}} \quad (14)$$

To obtain $\Gamma_2(\alpha)$ avoiding the Γ_1 correction, therefore, it is necessary to determine experimentally not only A_2 , $\langle S^2 \rangle^{1/2}$, and M , but also \bar{z} . The best method of experimentally determining \bar{z} , known up to date, may be to determine the constants in z from the temperature dependence of A_2 .⁴² However, the method may not be so advisable if the solvent used is as good as in this work. In this work, therefore, \bar{z} is calculated from the following eq 15', using the experimental data of $\alpha_\eta^3 = [\eta]/[\eta]_0$.

$$\alpha_\eta^5 - \alpha_\eta^3 = 2.60z \quad (15)^{43}$$

$$\bar{z} = z/\alpha_\eta^3 = 2.60(\alpha_\eta^2 - 1) \quad (15')$$

The values of $\Gamma_2(\alpha)$ thus calculated and also the values of Γ_1 calculated from the total nonideality $(A_2(\text{obsd})/A_2^0 = \Gamma_1 \Gamma_2(\alpha))$ using these values of $\Gamma_2(\alpha)$ are both listed in Table III. From the table it can be concluded that most of the nonideal behavior of linear polyelectrolyte solutions arises from the strong electrostatic interaction between charges, but the contribution of nonideality due to the polymeric character of polyions cannot be neglected. Moreover, it is clear that Γ_1 is nearly constant, independent of the molecular weight and the ionic strength, while $\Gamma_2(\alpha)$ is changed with them.

The values of $\Gamma_2(\alpha)$ obtained are plotted against $(\alpha_\eta^2 - 1)$ in Figure 9. It is observed that $\Gamma_2(\alpha)$ de-

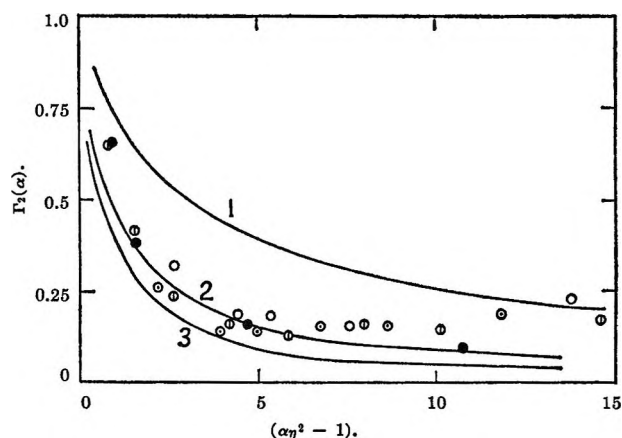


Figure 9. Comparison between the experimental $\Gamma_2(\alpha)$ and the theories. Samples are the same as in Figure 8; curve 1, Flory-Krigbaum-Orofino (original);¹⁵ curve 2, Stockmayer;⁴⁰ curve 3, Casassa-Markovitz;⁴⁴ the theory of Kurata, *et al.*,⁴¹ gives almost the same results as that of Casassa-Markovitz, though it was suggested in their paper that \bar{z} should be calculated from eq 16.

creases rapidly with increase of $(\alpha_\eta^2 - 1)$, *i.e.*, with decrease of C_s^0 to be constant. At low ionic strength, therefore, both molecular weight and ionic strength dependences of the observed A_2 are mainly determined by $A_2^0 \Gamma_1$; that is, the observed A_2 becomes almost independent of molecular weight and proportional to $1/C_s^0$. However, A_2 becomes dependent on the molecular weight and deviates from the proportionality to $1/C_s^0$ at high ionic strength since $\Gamma_2(\alpha)$ is not constant there. It can be confirmed that the linearity of A_2 to $1/\sqrt{C_s^0}$, as shown in Figure 6, arises because $\Gamma_2(\alpha)$ is roughly proportional to $\sqrt{C_s^0}$, though it is purely empirical.

In Figure 9, the values of $h(\bar{z})$ (*i.e.*, $\Gamma_2(\alpha)$) calculated from the theories of Orofino and Flory,¹⁵ Stockmayer,⁴⁰ Casassa and Markovitz,⁴⁴ and also Kurata, Fukatsu, Sotobayashi, and Yamakawa,⁴¹ are shown for comparison with the experimental results. It is interesting to see that all theories, particularly the theories of Casassa and Markovitz and Stockmayer, show good agreement with the experimental results of polyelectrolyte at high expansion.

As is well known, however, the applicability of eq 15

(40) W. H. Stockmayer, *Makromol. Chem.*, **35**, 54 (1960).

(41) M. Kurata, M. Fukatsu, H. Sotobayashi, and H. Yamakawa, *J. Chem. Phys.*, **41**, 139 (1964).

(42) G. C. Berry, *ibid.*, **44**, 4550 (1966).

(43) Recently, an improved equation of eq 15 was presented by P. J. Flory and S. Fisk, (*J. Chem. Phys.*, **44**, 2243 (1966)), but the difference is very small in our experimental range.

(44) E. F. Casassa and H. Markovitz, *ibid.*, **29**, 493 (1958).

was critically discussed by many authors.^{34,45-47} In particular, Stockmayer, Fixman, and Kurata^{34,48} presented the following equation to relate the expansion factor to \bar{z} .

$$\alpha_n^3 - 1 = 1.55z \quad (16)$$

It was often reported that eq 16 shows much better agreement with the intrinsic viscosity data of polyion than eq 15.^{19,49,50} In this study, however, if \bar{z} is calculated from eq 16 instead of eq 15, \bar{z} and hence $h(\bar{z})$ becomes almost constant over the whole experimental range, whereas $A_2M^2/\langle S^2 \rangle^{3/2}$ experimentally determined changes with the molecular weight and ionic strength markedly. It is clear that eq 16 is not applicable to polyions at high expansion. Here, however, it is to be noted that the opposite conclusions obtained for the intrinsic viscosity and the second virial coefficient should not necessarily be considered to be a contradiction since eq 16 can be favorably compared with the intrinsic viscosity data only at the limit of low molecular weight, but it shows a clear disagreement with the experiment if the molecular weight is as high as in the present work. Recently, Eisenberg⁵¹ showed by his precise experiment that the $h(\bar{z})$ function of Casassa and Markovitz⁴³ and Kurata, *et al.*,⁴¹ can well express the experimental results near the Θ point, *i.e.*, at low expansion of polyions when \bar{z} is estimated from eq 16. In this paper, however, the experimental results at much higher expansion are compared with the theories.

Strictly speaking, the expansion factor determined from the radius of gyration, that is, $\alpha_s^2 = \langle S^2 \rangle / \langle S_0^2 \rangle$ should be used instead of α_n^2 for estimating \bar{z} . Considering the ambiguity in $\langle S_0^2 \rangle$ obtained, however, we use α_n rather than α_s in this paper. If α_s is used in eq 15, the values of $\Gamma_2(\alpha)$ obtained may be a little smaller than the values shown in Table III, so that the contribution of the polymeric character of polyion to the low second virial coefficient of the polyelectrolyte may become comparable to the contribution of the electrostatic interaction between ions. However, no other change seems to be necessary in our conclusion.

The most fundamental theory on Γ_1 presently may be the theory of Scatchard⁶ which was presented for membrane equilibrium systems. The theory of Edsall, *et al.*,⁷ on the light scattering of colloidal electrolyte solutions gives completely the same result as Scatchard, since they made use of Scatchard's theory for the fluctuation of components in multicomponent systems. However, since quantitative comparison between Scatchard's theory and experimental results was found difficult because of the extreme nonideality of linear polyelectrolytes, Nagasawa, Takahashi, Izumi,

and Kagawa⁹ and Alexandrowicz¹⁰ proposed the following equation for Γ_1

$$A_2 = A_2^0(\gamma_c^0)^2/\gamma_s^0 \quad (17)$$

where γ_s^0 is the activity coefficient of added salt without polyelectrolyte and γ_c^0 is the activity coefficient of counterions in the salt-free polyelectrolyte solution averaged over the same polymer concentration. The values of γ_c^0 obtained by applying eq 17 to Γ_1 are also listed in Table III. It is observed that γ_c^0 is as small as 0.2, which can be reasonably accepted for the value of linear polyelectrolytes, and also that γ_c^0 is independent of both molecular weight and ionic strength, as was expected previously.^{9,14,52}

In Table V is shown an example of the comparisons between the experimental results and the theoretical values of Orofino and Flory calculated by their original

Table V: Comparison between Orofino and Flory's Theory¹⁵ and Experimental Second Virial Coefficients of No. 5

C_s^0 , moles/l.	A_2 (calcd) $\times 10^4$ (using α calcd from eq 8)	A_2 (obsd) $\times 10^4$	P	A_2 (calcd) $\times 10^4$ (using α obtained from (η))
2.0	3.1	0.44	0.14	0.5
1.0	6.8	1.12	0.16	1.71
0.5	15.9	2.8	0.18	6.0
0.1	37.4	5.2	0.11	13.9
0.05	56.6	8.2	0.10	22.6
0.02	74.9	15.3	0.10	29.3
0.01	92.4	20.5	0.09	35.8
0.005	130.7	46.4	0.12	54.2

method¹⁵ in which the observed values are inserted into $\langle S^2 \rangle^{3/2}$ of eq 7, whereas the values calculated from eq 8 are used for α . As usual, there is a great discrepancy between them.^{15,13,53} The discrepancy was interpreted by the introduction of the parameter P . When the nonionic term is negligible compared with the ionic

(45) M. Kurata, W. H. Stockmayer, and A. Roig, *J. Chem. Phys.*, **33**, 151 (1960).

(46) M. Fixman, *ibid.*, **23**, 1656 (1955); **36**, 3123 (1962).

(47) O. P. Ptitsyn, *Vysokomol. Soed.*, **3**, 1673 (1963).

(48) W. H. Stockmayer and M. Fixman, *J. Polymer Sci.*, **C1**, 137 (1963).

(49) A. Takahashi and M. Nagasawa, *J. Am. Chem. Soc.*, **86**, 543 (1964).

(50) S. Lapanje and S. Kovac, Preprint of IUPAC Symposium on Macromolecular Chemistry, Prague, 1965.

(51) H. Eisenberg, *J. Chem. Phys.*, **44**, 137 (1966).

(52) M. Nagasawa and I. Kagawa, *J. Polymer Sci.*, **25**, 61 (1957).

(53) W. Brown and D. Henley, *Makromol. Chem.*, **79**, 68 (1964).

term in eq 8, the introduction of the P parameter has the same meaning as the use of the effective charge density, that is, the introduction of the activity coefficient of eq 17. The slight disagreement between γ_s^0 in Table III and P in Table V arises from the disagreement of Orofino and Flory's theory, eq 11, with the experimental values of $\Gamma_2(\alpha)$ as seen in Figure 9. If the values of α_η calculated from $[\eta]$ using eq 5 and 6 are inserted into eq 7, much better agreement is found between calculated values and observed ones of A_2 as seen in Table V, since Γ_1 is taken into account by the use of experimental values of α_η .

Our present discussion is based on the assumption of the independence of Γ_1 and $\Gamma_2(\alpha)$ which is obviously open to criticism. It is highly desirable that we have a theory which takes into account both the polymeric character of polyions and the electrostatic interaction between charges. Most theories so far published are not satisfactory from this standpoint.

Finally, the results of the ionic strength dependence of the second virial coefficient experimentally determined seem different with different methods of measurement; that is, the second virial coefficient determined by the Donnan osmotic pressure measurement was usually found to be proportional to $1/C_s^0$,⁵⁴⁻⁵⁶

whereas the results obtained by light scattering are now found to be proportional to $1/\sqrt{C_s^0}$ at high ionic strength. The difference between the two results may come from the difference between the polymer concentrations used in those measurements. The Donnan osmotic pressure measurements are usually carried out in more than 0.3 g/100 ml of polymer concentration, which is much more concentrated than that used in light-scattering measurements. Because of such a high concentration and the high expansion of polyion, the segments belonging to different polymer molecules are not fully separated from each other. Therefore, it is doubtful that the results observed by osmotic pressure measurements correctly show the features of the intermolecular interactions.

Acknowledgment. We wish to thank Dr. Mock and Dr. Vanderkooi of the Dow Chemical Co. for supplying us the sample, and also Dr. I. Noda for his helpful discussion.

(54) D. T. F. Pals and J. J. Hermans, *Rec. Trav. Chim.*, **71**, 456 (1952).

(55) M. Nagasawa, H. Nakoji, and I. Kagawa, *Kogyo Kagaku Zasshi*, **57**, 9 (1954).

(56) H. Inagaki and M. Hiram, *Z. Elektrochem.*, **63**, 419 (1959).

Dilution Effects on Dimethylsiloxane Ring-Chain Equilibria

by Jack B. Carmichael,¹ David J. Gordon, and Frank J. Isackson²

Dow Corning Corporation, Midland, Michigan 48640 (Received September 22, 1966)

Experimental data showing the variation in the position of siloxane ring-chain equilibrium in the presence of solvents have been obtained. Amounts of individual cyclics, D_4 through D_{25} ($D = (\text{CH}_3)_2\text{SiO}$), were obtained by gas-liquid partition chromatography and the total amounts of cyclics were obtained by gel permeation chromatography. These data and the data of earlier workers are compared to calculations based on a model which assumes the solvent is a noninteracting fluid. Per cent differences between experimental weight per cents of D_4 , D_5 , and D_6 at 0.28 volume fraction of xylene and the ideal model are 4.3, 1.5, and 1.7%, respectively. Positive deviations of the experimental data from the model increase with increasing volume fraction solvent and reach 32.0, 26.4, and 33.2% at 0.76 volume fraction of xylene for D_4 , D_5 , and D_6 , respectively. The relative equilibrium amounts of cyclics D_4 to D_{20} obtained from polymerization in four different solvents were found to be the same, indicating that the Flory-Huggins polymer-solvent interaction parameter for a cyclic is independent of size over this range.

Introduction

Research carried out in the past few years has given much insight into the experimental and theoretical aspects of ring-chain equilibria of siloxanes. Work from this laboratory has described the ring distribution in high molecular weight dimethylsiloxane linear polymers,³ the dependence of the amounts of cyclic molecules on molecular weight of the linear portion,⁴ and the shift in position of siloxane ring-chain equilibrium when the side groups are trifluoropropyl and methyl.⁵

Scott's study by distillation of carbon tetrachloride and bulk-equilibrated mixtures of low molecular weight siloxanes was the first work on siloxane ring-chain equilibria.⁶ Hartung and Camiolo first quantitatively studied the effect of solvent polymerization medium in shifting the position of ring-chain equilibrium.⁷ Hartung reported the amounts of D_4 and D_5 (where $D \equiv (\text{CH}_3)_2\text{SiO}$) and the total D_3 to D_9 present in seven polymers prepared in 25-75 wt % xylene and heated for 16 hr at 135°. Morton and Bostick⁸ determined equilibrium conversion of D_4 to polymer, using tetrahydrofuran (THF) as a polymerization medium, as part of a detailed kinetic study of anionic polymerization of D_4 . Brown and Slusarczuk^{9,10} have studied the equilibrium distribution of cyclic and linear dimethylsiloxanes in toluene. Their equilibrium constants for

cyclics D_3 through D_9 agreed well with the earlier data obtained by Hartung and Camiolo.⁷ However, both sets of equilibrium constants^{7,9,10} differ markedly from those obtained in bulk equilibration.^{3,4,11}

In the most recently published theoretical discussion of ring-chain equilibrium, Flory and Semlyen¹² calculated macrocyclic siloxane equilibrium constants which were in excellent agreement with Brown's data.⁹ Equilibrium cyclization constants from both solvent^{7,9} and bulk³ polymerizations are shown in Figure

(1) Department of Chemistry, University of Oregon, Eugene, Ore. 97403.

(2) Summer research assistant from Saginaw Valley College.

(3) J. B. Carmichael and R. Winger, *J. Polymer Sci.*, **A3**, 971 (1965).

(4) J. B. Carmichael and J. Heffel, *J. Phys. Chem.*, **69**, 2218 (1965).

(5) E. D. Brown and J. B. Carmichael, *J. Polymer Sci.*, **B3**, 473 (1965).

(6) D. W. Scott, *J. Am. Chem. Soc.*, **68**, 2294 (1946).

(7) H. A. Hartung and S. M. Camiolo, Papers presented to the Division of Polymer Chemistry, 141st National Meeting of the American Chemical Society, Washington, D. C., March 1962.

(8) M. Morton and E. E. Bostick, *J. Polymer Sci.*, **A2**, 523 (1964).

(9) J. F. Brown, Jr., and G. M. J. Slusarczuk, *J. Am. Chem. Soc.*, **87**, 931 (1965).

(10) J. F. Brown, Jr., private communication.

(11) J. B. Carmichael, *J. Macromol. Chem.*, **1**, 207 (1966).

(12) P. J. Flory and J. A. Semlyen, *J. Am. Chem. Soc.*, **88**, 3209 (1966).

2 of ref 12. For the small rings, differences between solvent and bulk cyclization constants for a given sized ring are obvious. However, these differences are less than the variation in cyclization constant with ring size. Possibly owing to less dramatic experimental differences, the nature of solvent effects influencing ring-chain equilibrium has not been discussed in the literature.

In this paper we have repeated Hartung's polymerization experiments in xylene. Polymerization results in other solvents are also discussed. The experimental results along with those of other workers are compared with an idealized model in which no solvent-polymer interactions are assumed to occur.

Experimental Section

A. Solvent Polymerization Experiments. 1. Xylene. All polymerizations were carried out in Fisher Neutral Histological grade xylene. The starting material was octamethylcyclotetrasiloxane (>99.9% pure by glpc), hereafter referred to as D_4 . The potassium salt of a hydroxy end-blocked dimethylsiloxane polymer (equivalent weights of 1360 and 1563) was used as a catalyst at a concentration of 0.04 equiv of potassium/kg of siloxane.

Six polymers were prepared at siloxane volume per cents of 72.09, 57.83, 48.46, 38.84, 29.20, and 24.27. These samples are referred to as polymers 1-6, respectively.

The proper amounts of D_4 , catalyst, and xylene necessary to give a total sample volume of 50 ml were placed in glass ampoules, purged with helium, and then frozen at -100° in a 2-propanol-Dry Ice slurry. The ampoules were flushed again and sealed. After the ampoules had warmed to ambient temperature, they were placed in a constant-temperature bath of Dow Corning 200 Fluid at $135 \pm 2^\circ$. Several samples were prepared at each volume per cent of xylene and checked for attainment of equilibrium by glpc (gas-liquid partition chromatography). Equilibrium was assumed to be reached when no change in relative concentration of cyclics was observed.

The time required to attain equilibrium varied from 24 hr for a sample with 25 vol. % xylene to 328 hr for a sample with 75 vol. % xylene. After equilibrium had been reached, the samples were allowed to cool and a stoichiometric amount of acetic acid was added to precipitate potassium acetate.

The salt was then filtered out using a Gelman pressure filter to avoid evaporation of low molecular species. A filter aid (Super-Cel) was used to aid complete removal of the salt. Analyses of various filtered solutions showed that the residual $[K^+]$ was <1 ppm.

High-viscosity samples were diluted with gpc (gel permeation chromatography) grade toluene to aid salt precipitation, filtration, and glpc and gpc analyses.

2. Toluene. One sample of 40 vol. % D_4 and 60 vol. % toluene was prepared using the previously described procedure and treated with catalyst at 100° (polymer 7). Equilibrium was reached after 71 hr.

B. Analysis of Cyclics by Gas Chromatography. The F & M Model 810 linear temperature programmed gas-liquid partition chromatograph was used for analyses. A 0-1-mv Brown recorder equipped with Disc integrator was attached to the recorder. The column sets used were 2 ft \times 0.2 in. stainless steel, packed with 9% diphenylsiloxane-dimethylsiloxane copolymer gum prepared at Dow Corning on 60-80 mesh Chromasorb W, nonacid washed. Column temperatures were programmed as follows: 3 min isothermally at 50° , then $15^\circ/\text{min}$ to 400° . Other chromatography conditions were as follows: detector temperature, 360° ; injection port temperature, $350-360^\circ$; bridge current, 140 ma; column and reference He flow rates, 60 ml/min.

Response factors were determined from a mixture of D_3 through D_6 using MD_3M as a marker. Response factors for higher cyclics were extrapolated by least-squares analysis.¹³ A typical tabulation of response factors can be found in ref 4.

Integrated areas for each cyclic were converted to weight per cent utilizing response factors.

Amounts of cyclics containing up to 25 siloxane units are shown in Table I.

C. Analysis of Cyclics by Gel Permeation Chromatography. The total cyclic concentration was determined using the Waters gel permeation chromatograph. Four columns were $3/8$ in. \times 4 ft stainless steel packed with specially treated polystyrene gel with the following permeabilities: 10^6 , 10^5 , 10^4 , and 10^3 A. Toluene was used as a solvent. Column temperature was 50° .

Response factors were determined using D_6 and a sharp fraction of a high molecular weight dimethylsiloxane polymer (mol wt, 5×10^5) prepared by double fractional precipitation. Three samples of D_5 and high polymer were used to obtain calibration factors. Weight per cents of D_5 in the three samples were 10, 30, and 60, respectively. Areas of the cyclic and high polymer portions were determined using a compensating polar planimeter. A plot of response factor vs. area per cent of cyclics is given in Figure 1.

Analyses of total weight per cent of cyclics using

(13) J. B. Carmichael, D. J. Gordon, and C. E. Ferguson, *J. Gas Chromatog.*, **4**, 347 (1966).

Table I: Analysis of Cyclics in Solvent-Equilibrated Polydimethylsiloxanes

Poly- mer no.	Time, hr	Vol. (135°) % D ₄	Wt % of [(CH ₃) ₂ SiO] _x based on the siloxane portion Gpc analysis for cyclics with x = 3-25																									
			3	4	5	6	7	8	9	10	11	12	13	14	15	16	17	18	19	20	21	22	23	24	25	Total		
a	...	100	0.21	6.6	4.8	1.7	0.44	0.19	0.11	0.07	0.09	0.12	0.15	0.16	0.20	0.19	0.17	0.18	0.14	0.12	0.10	0.08	0.06	14.12	21.63	Gpc	Gpc	
1	24	72.09	9.58	6.57	2.32	0.67	0.26	0.16	0.14	0.15	0.18	0.21	0.22	0.29	0.29	0.22	0.27	0.28	0.26	0.23	0.22	0.16	0.14	0.13	31.64	23.00		
2	42	57.88	13.87	9.21	3.18	1.18	0.48	0.26	0.21	0.18	0.20	0.22	0.26	0.31	0.31	0.29	0.28	0.25	0.23	0.20	0.18	0.14	0.15	0.15	38.90	37.30		
3	40	48.46	17.74	11.66	3.92	1.13	0.45	0.29	0.23	0.20	0.21	0.25	0.28	0.40	0.44	0.38	0.35	0.31	0.27	0.24	0.20	0.24	0.25	0.25	45.28			
4	48	38.84	20.23	13.46	4.77	1.25	0.57	0.34	0.27	0.22	0.21	0.25	0.28	0.43	0.51	0.55	0.41	0.43	0.39	0.33	0.31	0.20	0.14	0.14	71.16	70.00		
5	135	29.20	32.94	21.76	7.09	2.11	0.85	0.51	0.40	0.34	0.33	0.39	0.43	0.51	0.55	0.56	0.41	0.43	0.39	0.33	0.31	0.20	0.14	0.16	91.87			
6	328	24.27	40.39	27.18	10.56	4.35	1.87	0.94	0.54	0.42	0.40	0.39	0.41	0.53	0.56	0.57	0.53	0.52	0.43	0.39	0.32	0.24	0.18	0.18	46.09	49.1		
7 ^b	71	40	40	22.4	14.64	4.79	1.48	0.62	0.30	0.29	0.19	0.20	0.22	0.27	0.30													

^a Average cyclic distribution for the bulk polymer prepared at 150°. See ref 11. ^b Polymer prepared at 60 vol. % toluene for 71 hr at 100° using D₅ as the starting cyclic.

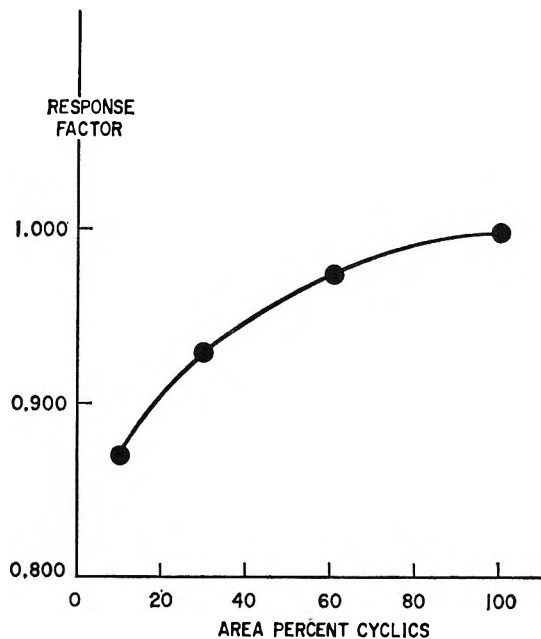


Figure 1. Experimental response factors for converting area per cent to weight per cent of total cyclics obtained from gel permeation chromatography.

gpc were obtained on polymers 1, 2, 3, 5, and 7. Areas of the cyclic and high-polymer portions were obtained using a compensating polar planimeter. The area per cents of the cyclic portions were converted to weight per cents using gpc response factors as

$$\left(\frac{P_1}{P_1 + P_2} \right) 100 = Q(F) = \text{wt } \%$$

where P_1 = area of cyclic portion, P_2 = area of high-polymer portion, Q = area per cent of cyclics, F = response factor (Figure 1). Total weight per cent of cyclics of polymers 1, 2, 3, 5, and 7 obtained from the gpc are included in Table I.

In all cases the molecular weight of linear polymer was several orders of magnitude greater than the cyclic material and the cyclic and linear portions were well separated on the chromatogram.

Discussion

A. *Model.* The simplest view of ring-chain equilibria in solvent is to consider the solvent as a non-interacting fluid; *i.e.*, it merely occupies space within the polymerization vessel. Elementary principles of chemical equilibria dictate that under such conditions the equilibrium cyclization constant, K , must be independent of the amount of solvent present. In the experiments discussed here, the molecular weight of the linear polymer is sufficiently high that $K = [R_x]$.³ The brackets refer to concentration in moles of siloxane

units/l. of solution. It then follows that $[R_x]_{0 < V_1 < 1} / [R_x]_{V_1=0} = 1$, where V_1 is the volume fraction of solvent.

The experimental data are most conveniently compared with the model using the amounts of cyclics in units of weight fraction. The relationship between weight fraction of cyclics and volume fraction of solvent for the ideal model is given by $W_x = B_x / (1 - V_1)$, where W_x = equilibrium weight fraction in solvent of a cyclic of size x (based on the amount of siloxane in the equilibrate), B_x = equilibrium weight fraction in the bulk of a cyclic of size x , V_1 = volume fraction of solvent.

Thus a plot of $\log W_x$ vs. $\log [1/(1 - V_1)]$ yields a straight line with a slope of 1. The only data necessary to construct the plot are B_x . The values of B_4 , B_5 , and B_6 were taken from ref 11. The total weight fraction of cyclics in the bulk was taken to be 0.17. This figure is admittedly somewhat arbitrary and was arrived at by the sum of cyclics D_3 - D_{10} , which equals 14.1 wt % for the equilibrium bulk polymer at 150°, and Brown's statement that "the macrocyclic population, arbitrarily defined as the cyclics above D_{12} , was found to constitute 2-3% of the total polymer in commercial methylsilicone oils, gums, and rubbers."⁷

B. Comparison of Experimental Results with the Model. The experimental variations of W_x with V_1 are compared with the model for total cyclics and $x = 4, 5, \text{ and } 6$ in Figures 2, 3, and 4. The plot of total cyclics in Figure 2 includes data from the works of Hartung and Camiolo⁷ and Morton and Bostick.⁸ Hartung and Camiolo⁷ obtained the sum of cyclics D_3 - D_9 , which should be expected to lie below our data owing to the cutoff at D_9 . We have converted the units of the abscissa in Figure 1 of their paper to volume fraction of solvent. Morton and Bostick⁸ carefully point out that equilibrium conversion of D_4 was obtained by measuring the equilibrium conversion to polymer (defined by them as $\overline{DP} > 4$) by precipitation of the polymer from dilute THF solution and by vacuum drying. Since their data fit more nearly the expected result for total cyclics than for D_4 , these are included in Figure 2. Hartung and Camiolo⁷ also reported amounts of individual cyclics D_4 and D_5 which are compared with our results in Figures 3 and 4, respectively.

In Figure 2 considerable scatter is seen between the experimental data on total cyclics from various sources. Data from the present work show a systematically increasing deviation from the model with increasing volume fractions of solvents. The Hartung and Camiolo data for D_4 and D_5 shown in Figures 3 and 4 agree well with our data. Amounts of D_4 , D_5 , and D_6

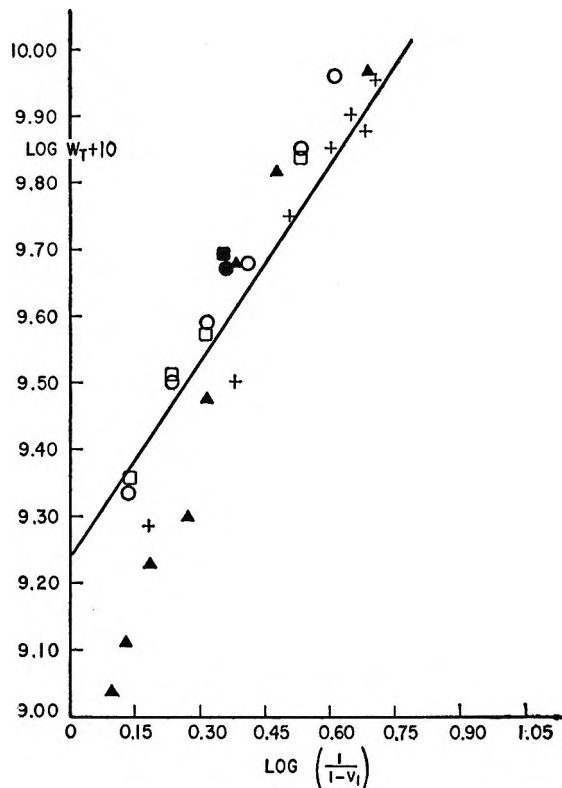


Figure 2. Experimental and calculated variation of weight fraction of total cyclics with volume fraction of solvent: W_T , equilibrium weight fraction of total cyclics in the system; V_1 , volume fraction of solvent; straight line calculated from ideal model; O, this work, glpc analysis (xylene); □, this work, gpc analysis (xylene); ●, this work, glpc analysis (toluene); ■, this work, gpc analysis (toluene); +, data of Hartung and Camiolo⁷ (xylene); ▲, data of Morton and Bostick⁸ (THF).

show the expected dilution effect over a limited dilution range but deviate markedly from the calculated straight line at large dilutions. Experimental and calculated amounts of cyclics at $V_1 = 0.28$ and 0.76 are compared in Table II.

The approach taken by the Flory-Huggins model of

Table II: Comparison of Experimental and Calculated Weight Fractions of Cyclodimethylsiloxanes at 0.28 and 0.76 Volume Fraction of Xylene^a

	$V_1 = 0.28$			$V_1 = 0.76$		
	Exptl ^a	Calcd	% dif	Exptl ^a	Calcd	% dif
D_4	0.0958	0.0917	+4.3	0.404	0.275	+32.0
D_5	0.0657	0.0667	-1.5	0.272	0.200	+26.4
D_6	0.0232	0.0236	-1.7	0.106	0.0708	+33.2
D_{total}^b	0.216	0.236	-9.3	0.92	0.708	+23.7

^a Glpc data. ^b From gpc data, $D_{total} = 0.230$ at $V_1 = 0.28$.

concentrated polymer solutions¹⁴ should provide a logical method for quantitatively predicting the experimentally observed amounts of cyclics present in solvent equilibrates with $V_1 > 0.3$. However, the arguments used in this model are based on linear polymer and the inclusion of cyclic molecules appears to pose a difficult problem in combinatorial analysis.

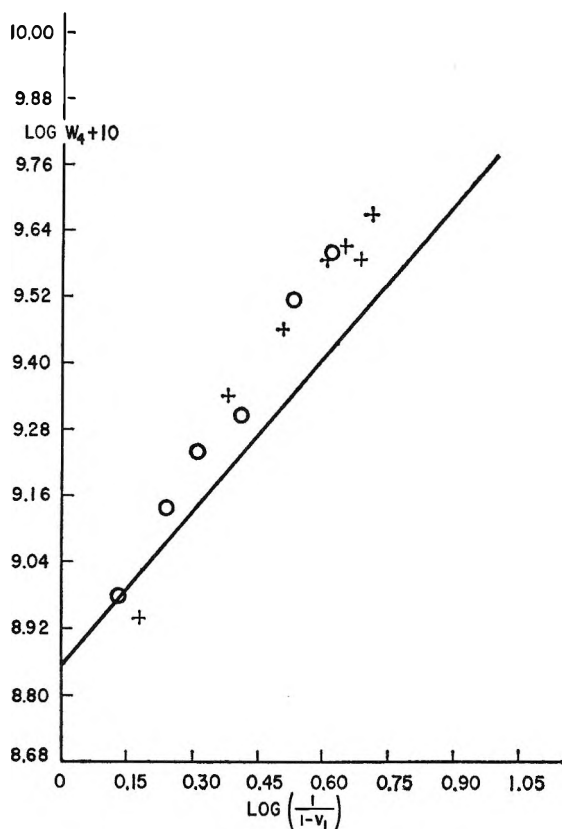


Figure 3. Experimental and calculated variation of weight fraction of D_4 with volume fraction of xylene: W_4 , equilibrium weight fraction in solvent of octamethylcyclotetrasiloxane; V_1 , volume fraction of solvent; straight line calculated from ideal model; O, this work, glpc analysis; +, data of Hartung and Camiolo.⁷

The relative amounts of cyclics D_4 - D_{20} were also determined from equilibrium polymerizations in isooctane and chlorobenzene at 100° using 50 vol. % siloxane. These relative amounts of cyclics were found to agree within experimental error with the relative amounts of cyclics obtained at equilibrium in xylene and toluene polymerizations. The results indicate that within this size range the Flory-Huggins polymer-solvent interaction parameter (where polymer refers to a cyclic oligomer in this discussion) is independent of cyclic size.

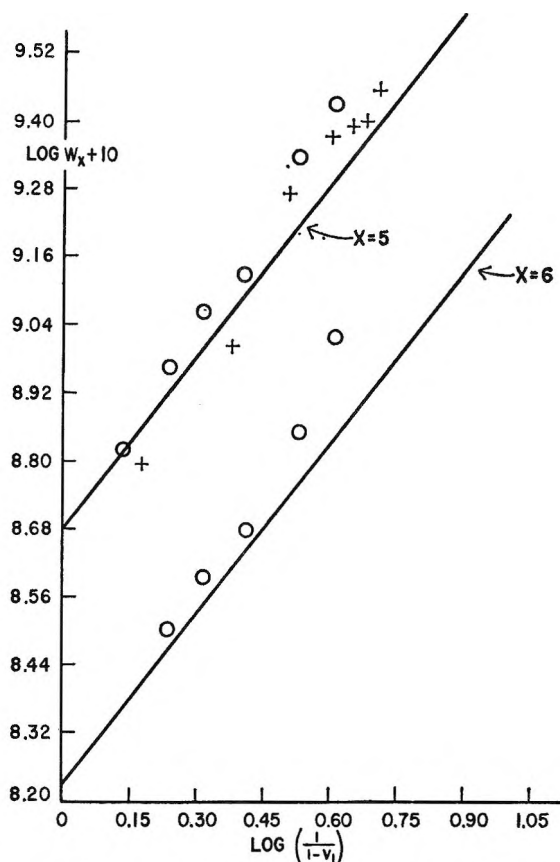


Figure 4. Experimental and calculated variation of weight fraction of D_5 and D_6 with volume fraction of xylene: W_x , equilibrium weight fraction in solvent of a cyclic of size x ; V_1 , volume fraction of solvent; straight line calculated from ideal model; O, this work, glpc analysis; +, Data of Hartung and Camiolo.⁷

Glossary of Terms

glpc	Gas-liquid partition chromatography
gpc	Gel permeation chromatography
W_x	Equilibrium weight fraction of a dimethylsiloxane cyclic with x units in a solvent polymerization
B_x	Equilibrium weight fraction of a dimethyl cyclic with x units in a bulk polymerization
D	A dimethylsiloxane unit, $(\text{CH}_3)_2\text{SiO}$
D_4	Octamethylcyclotetrasiloxane, $[(\text{CH}_3)_2\text{SiO}]_4$
V_1	Volume fraction of solvent
\overline{DP}	Number-average degree of polymerization of rings plus chains
K	Equilibrium cyclization constant
R	The glpc response factor
F	The gpc response factor
THF	Tetrahydrofuran

Acknowledgments. The authors are grateful to Dr. Adiel Litan and Professor Terrell Hill for reading the manuscript. Mr. Roger Chaffee performed the experiments in isooctane and chlorobenzene.

(14) See P. J. Flory, "Principles of Polymer Chemistry," Cornell University Press, Ithaca, N. Y., 1953, p 513.

Thermodynamic Aspects of the Potassium Hexacyanoferrate(III)-(II)

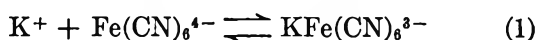
System. I. Ion Association¹

by William A. Eaton,² Philip George, and George I. H. Hanania

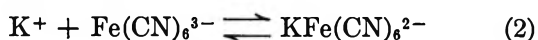
Department of Chemistry and Graduate Group on Molecular Biology, University of Pennsylvania, Philadelphia, Pennsylvania 19104 (Received October 4, 1966)

A thermodynamic study has been made of the ion-association equilibria involving K^+ and the anions $Fe(CN)_6^{4-}$ and $Fe(CN)_6^{3-}$. Conditions were determined under which a cation-sensitive glass electrode could be used in this investigation. Using this electrode to measure K^+ activity in aqueous solutions of $K_4Fe(CN)_6$ and $K_3Fe(CN)_6$, the free-energy and enthalpy changes were obtained potentiometrically. The enthalpy changes were also determined in a precision solution calorimeter. The results show that ion binding is significant in both cases, and that the reactions are due to favorable entropy changes.

It has long been recognized that salts like the potassium hexacyanoferrates are incompletely ionized in aqueous solution. In fact, the classical work of Noyes and Johnston³ had shown that the "degree of ionization" as determined from conductivity measurements was different from that derived from colligative properties of the solutions. It was discrepancies of this type which led to the development of the concept of activities of ions. Nevertheless, in later work on electrolytic conductance, one interpretation of experimental conductances being less than those calculated by the Onsager-Fuoss limiting equation was to attribute this to incomplete dissociation of the salts, and on this basis to calculate ion-association constants for the chemical equilibria involved. Thus using conductivity data,⁴ Davies⁵ calculated an association constant for the equilibrium



and James and Monk⁶ using a similar method obtained an association constant for the corresponding equilibrium



From changes in the ultraviolet absorption spectra of hexacyanoferrate(II) salts with various cations, Cohen and Plane⁷ obtained values for the association constant of eq 1 and for analogous equilibria with Ba^{2+} and Mg^{2+} .

The recent introduction of reliable cation-sensitive glass electrodes has made possible the direct potentiometric determination of cation activity in salt solutions over a very wide range of conditions. Using this method, we have redetermined the ion-association constants and obtained thermodynamic parameters for the above equilibria. In part II,⁸ we show that specific salt effects have a profound influence on the reduction potential of the hexacyanoferrate (III)-(II) couple.

A preliminary account of this investigation has been presented elsewhere.⁹

Experimental Section

Materials. $K_3Fe(CN)_6$, $K_4Fe(CN)_6 \cdot 3H_2O$, KCl , and $Mg(NO_3)_2 \cdot 6H_2O$ were of AnalaR or Baker Analyzed

(1) This work was supported by Grants AM-03187 and AM 04764 from the National Institutes of Health.

(2) Scholar of the Pennsylvania Plan to Develop Scientists in Medical Research.

(3) A. A. Noyes and J. Johnston, *J. Am. Chem. Soc.*, **31**, 991 (1909).

(4) G. Jones and F. C. Jelen, *ibid.*, **58**, 2561 (1936).

(5) C. W. Davies, *ibid.*, **59**, 1760 (1937).

(6) J. C. James and C. B. Monk, *Trans. Faraday Soc.*, **46**, 1041 (1950).

(7) S. R. Cohen and R. A. Plane, *J. Phys. Chem.*, **61**, 1096 (1957).

(8) G. I. H. Hanania, D. H. Irvine, W. A. Eaton, and P. George, *ibid.*, **71**, 2022 (1967).

(9) G. I. H. Hanania, W. A. Eaton, and P. George, Abstracts, 151st National Meeting of the American Chemical Society, Pittsburgh, Pa., March 1966, p 45N.

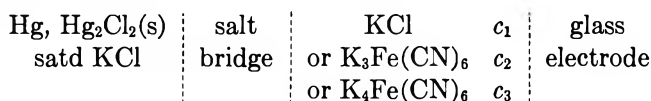
grade, and were used from freshly opened bottles without further purification. Tetrapropylammonium bromide, Pr_4NBr , was purchased from Eastman Organic Chemicals and was used without further purification. Solutions were always made just before every measurement using distilled deionized water.

Potentiometric Apparatus. The potentiometric cell employed consisted of a Beckman 39137 cation-sensitive glass electrode and a reference which was either a saturated calomel electrode with an agar-saturated KCl bridge or an Ag, AgCl electrode. The cell was kept in a black-box Faraday cage and was thermostated by circulating water from a bath, temperature control being to $\pm 0.05^\circ$ or better. The emf measurements were made on a Radiometer PHM 4 meter to 0.1 mv.

Behavior of Glass Electrode. The properties of cation-sensitive glass electrodes have been extensively investigated (see, for instance, Eisenman¹⁰). In the present work, we have found that the Beckman electrode is capable of precision to 0.1 mv, provided that the electrode is maintained free from thermal, mechanical, and electrical shocks, and is always kept in a solution of a potassium salt, in the dark.

We have investigated the response of this electrode to potassium ion in a cell without liquid junction using Ag, AgCl as the reference electrode. Since the glass electrode has no standard potential, emf measurements on this type of cell can only yield ratios of mean molar ionic activity coefficients for KCl, γ_{KCl} . We have shown that in the ionic strength range 0.001 to 0.1 M, with or without added $\text{Mg}(\text{NO}_3)_2$, neither electrode responding to magnesium or nitrate ions, the calculated γ_{KCl} ratios¹¹ are in excellent agreement with the published literature values.^{12,13} These results show that the cell is thermodynamically reversible and hence that the cation-sensitive electrode responds to K^+ activity.

Determination of Ion Association Constants. In order to determine the association constants for equilibria 1 and 2, it is necessary to measure the free (*i.e.*, unbound) K^+ activity, and hence the concentration, in a solution of known total salt concentration. For this purpose, we employed the cell



In this cell, the glass electrode is immersed in 100 ml of a solution of KCl or $\text{K}_3\text{Fe}(\text{CN})_6$ or $\text{K}_4\text{Fe}(\text{CN})_6$; an agar-saturated KCl bridge makes connection with a saturated calomel electrode. It is readily shown that the concentration of free K^+ is given by

$$\log [\text{K}^+]_x = \frac{(E_x - E_s) - (E_{xj} - E_{sj})}{2.303RT/F} + \log \frac{\gamma_s}{\gamma_x} + \log [\text{K}^+]_s \quad (3)$$

where $[\text{K}^+]_x$ is the molar concentration of free K^+ in the (unknown) hexacyanoferrate solutions, c_2 or c_3 ; $[\text{K}^+]_s$ is the molar concentration of free K^+ in a (standard) KCl solution, c_1 , assuming complete dissociation of the ions; and E_x and E_s are the emf's for the unknown and standard solutions, respectively. E_{xj} and E_{sj} are the corresponding liquid junction potentials. γ_x and γ_s are the corresponding K^+ single molar ion activity coefficients obtained on the following two assumptions: (1) $\gamma_s = \gamma_{\text{KCl}}$, the mean molar ionic activity coefficient in the standard KCl solution; and (2) $\gamma_x = \gamma'_{\text{KCl}}$, the mean molar ionic activity coefficient at the calculated total molar ionic strength of the unknown hexacyanoferrate solution, taking ion association into account. Furthermore, the dilution of the solutions and the small temperature range employed about 25° were such that no practical distinction could be made between molal and molar activity coefficients. Values of the appropriate activity coefficients at the various temperatures were obtained from the data listed in ref 12 and 13.

The difference in liquid junction potentials, $E_{xj} - E_{sj}$, was evaluated for every pair of solutions used in the measurements employing the Henderson equation.¹⁴ In some cases, the value of this term was found to be zero and was never more than ± 0.1 mv; consequently, this term was neglected in the calculations.

An attempt was made to use cells without liquid junction for the above measurements, the glass electrode being employed against Ag, AgCl as well as the recently introduced chloride-sensitive membrane electrode (National Instruments Labs, Inc.) as reference. In both cases, however, these electrodes were also sensitive to hexacyanoferrate ions and produced erratic results.

The association (formation) constants, K , for equilibria 1 and 2 are defined in terms of the molar concentrations of all three species in each case. In dilute

(10) G. Eisenman in *Advan. Anal. Chem. Instr.*, **4**, 213 (1965).

(11) W. A. Eaton, G. I. H. Hanaia, P. George, and R. J. Witonsky, unpublished results.

(12) W. M. Latimer, "Oxidation Potentials," 2nd ed, Prentice-Hall, Inc., New York, N. Y., 1952, p 355.

(13) R. A. Robinson and R. H. Stokes, "Electrolyte Solutions," 2nd ed (revised), Butterworth and Co. (Publishers) Ltd., London, 1959, p 481.

(14) R. G. Bates, "Determination of pH," John Wiley and Sons, Inc., New York, N. Y., 1964, p 40.

solutions, where a Debye-Hückel relation may be assumed, these association constants are related to the apparent thermodynamic association constants (MacInnes single-ion activity coefficient convention), K° , by the equation

$$\log K^\circ = \log K + nI^{1/2}/(1 + 1.5I^{1/2}) \quad (4)$$

where at 25.0°, $n = 4.08$ for equilibrium 1 and 3.06 for equilibrium 2.

The enthalpy changes for these equilibria are obtained from the temperature variation of the measured association constants at an ionic strength well within the region where the Debye-Hückel relation is obeyed. On this basis, using eq 4, the difference between the enthalpy changes at the low finite ionic strengths employed and the enthalpy changes at infinite dilution would only amount to about 0.1 kcal/mole, which is well within the limits of experimental uncertainty. We have therefore adopted the measured enthalpy change, ΔH , as a satisfactory approximation to the thermodynamic quantities, ΔH° .

Calorimetric Measurements. An independent determination of the above enthalpy changes was made in a precision solution calorimeter. The apparatus and its calibration are described elsewhere.¹⁵ A typical experiment consisted of the following: (a) 4.00 ml of a concentrated solution of $K_4Fe(CN)_6$ was mixed with 950 ml of an appropriate KCl solution at 25°, and the free K^+ concentration in the mixture was determined as described above; (b) 4.00 ml of the same $K_4Fe(CN)_6$ solution was mixed with 950 ml of water, and the free K^+ concentration was again determined. In both cases the heat evolved or absorbed was measured to the nearest 100 mcal.

The difference between the observed heats of mixing, $q_a - q_b$, was found to be slightly endothermic. This difference in the heats of mixing was attributed to the difference between the degree of ion association in the two mixtures. The number of moles of K^+ bound to $Fe(CN)_6^{4-}$ in the two cases, n_a and n_b , respectively, can be calculated from the known composition of each mixture, the ionic strength, and the equilibrium constant. On this basis, the enthalpy change for the ion association equilibrium 1 is

$$\Delta H = -\frac{(q_a - q_b)}{(n_a - n_b)} \text{ kcal/mole} \quad (5)$$

the corresponding case of equilibrium 2 being determined in an analogous manner. It is to be noted that this method neglects any difference between the heats of dilution of the potassium hexacyanoferrate salts into water and dilute KCl solution which may arise from differences in ionic strength and ionic

composition. In an attempt to preserve constant ionic strength in the final mixtures, two different types of calorimetric experiments were carried out.

(1) A sample consisting of 4.000 g of KCl was dissolved in 950 ml of $2.00 \times 10^{-3} M K_3Fe(CN)_6$ and also in 950 ml of $1.00 \times 10^{-2} M KCl$. Here the ionic strength is nearly the same in the two mixtures. The heats evolved were -224.8 ± 0.4 and -224.4 ± 0.4 cal, respectively, again indicating net endothermicity for the ion-binding reaction. Although this type of experiment has the advantage of constant ionic strength, the heat being determined comes out as the small difference between two large quantities and inevitably will carry a large uncertainty.

(2) In this experiment, 4.00 ml of 0.475 $M K_3Fe(CN)_6$ was mixed with 950 ml of 0.0565 $M KCl$ and also with 950 ml of 0.0534 $M Pr_4NBr$, the ionic strength being the same in the two mixtures assuming negligible binding of the tetrapropylammonium ion to $Fe(CN)_6^{3-}$. The heats evolved were -1.94 ± 0.10 and 1.44 ± 0.13 cal, respectively. In this case, the strongly exothermic result is in sharp contrast with the above observations, and suggests that Pr_4N^+ ions exert strong specific salt effects on the solvent and/or solute ions. Quaternary ammonium salts were therefore not used for the adjustment of ionic strength in the present work. All calorimetric experiments referred to above were performed in triplicate.

Spectrophotometric Studies. Another independent check on the effect of Pr_4NBr on these solutions was made by examining the ultraviolet absorption spectra of hexacyanoferrate(II) and (III) ions in the presence of excess Pr_4NBr as well as KCl. The spectra quantitatively confirmed previous observations⁷ that K^+ has no perceptible effect on the $Fe(CN)_6^{3-}$ spectrum but has an appreciable effect on the $Fe(CN)_6^{4-}$ spectrum. Furthermore, Pr_4NBr was found to have no appreciable effect on the absorption spectrum of either $Fe(CN)_6^{3-}$ or $Fe(CN)_6^{4-}$.

All spectra were taken following the usual precautions, including careful blanking, using either a Cary 14 recording spectrophotometer or a Zeiss PMQ II spectrophotometer.

Results

The potentiometric method described above has been applied in determining the ion-association constants for equilibria 1 and 2 over a range of ionic strength and temperature. The results are summarized in the following tables (where in all cases concentra-

(15) C. Wu, R. J. Witonsky, P. George, and R. J. Rutman, *J. Am. Chem. Soc.*, in press.

tions are in moles per liter and the association constants in liters per mole).

Tables I and II give the results at 25.0°. Table III gives the values of the equilibrium constants at various temperatures between 9.9 and 45.0° at constant total salt concentration (the corresponding ionic strengths over this temperature range vary by about 1% or less). It is apparent from the data that the enthalpy change is small for both reactions and that there is some scatter in the isochore plots. Moreover, K values as determined in the present work have an average uncertainty of $\pm 5\%$. Only a mean ΔH value for the temperature range can therefore be obtained, and this comes out as 0.6 ± 0.4 and 0.5 ± 0.4 kcal/mole for ion association equilibria 1 and 2, values which we take as equal to the thermodynamic quantities, ΔH° (see Experimental Section). The corresponding calorimetric data are given in Table IV. Here the ΔH values, as determined at 25°, are 1.0 ± 0.3 and 0.5 ± 0.5 kcal/mole for equilibria 1 and 2, respectively, and as the measurements were made on dilute solutions,

Table III: Variation of Ion Association Constants K for Equilibria 1 and 2 with Temperature

Temperature, °C	9.9	15.0	25.0	35.0	40.0	45.0
Equilibrium 1 ($1.00 \times 10^{-3} M$ $K_4Fe(CN)_6$)	88.9	94.0	101	...	102	103
Equilibrium 2 ($1.25 \times 10^{-3} M$ $K_3Fe(CN)_6$)	16.1	18.2	17.6	18.6	...	18.9

these values are taken to be ΔH° . The means between the potentiometric and calorimetric values are therefore 0.8 ± 0.4 and 0.5 ± 0.5 kcal/mole, respectively. The corresponding thermodynamic entropy changes are obtained from the relation $\Delta S^\circ = (\Delta H^\circ - \Delta G^\circ)/T$ yielding at 25.0°: 13 ± 2 eu and 8 ± 2 eu for equilibria 1 and 2.

Table IV: Calorimetric Determination of ΔH at 25°

	q_a , ^a cal	q_b , ^b cal	$(n_a - n_b)$, mmole	ΔH , kcal/mole
Equilibrium 1	-5.84 ± 0.10	-5.15 ± 0.10	0.65	1.0 ± 0.3
Equilibrium 2	-1.94 ± 0.10	-1.68 ± 0.15	0.49	0.5 ± 0.5

^a q_a is the heat evolved when 4.00 ml of 0.727 M $K_4Fe(CN)_6$ or 0.475 M $K_3Fe(CN)_6$, is mixed with 950 ml of 0.0565 M KCl.
^b q_b is the heat evolved when 4.00 ml of the above solutions is mixed with 950 ml of water.

The above type of measurement was also extended to more concentrated solutions, about 0.01 M and above. The data indicate that a second K^+ binds to the hexacyanoferrate(II) ion. However, the uncertainties about assumptions concerning activity coefficients in these solutions preclude the calculation of reliable association constants.

Discussion

In the present work, an attempt has been made to obtain reliable thermodynamic quantities for the ion association equilibria involving K^+ and the hexacyanoferrate anions. Previous workers have deduced the existence of these chemical equilibria from independent lines of evidence.

From conductivity measurements, deviations from the limiting slopes predicted by Onsager's equation have been interpreted as due to the formation of ion pairs. Although this method has been successfully and extensively used in studying ion association equi-

Table I: Variation of Ion Association Constant K for Equilibrium 1 with Ionic Strength at 25.0°^a

$[K_4Fe(CN)_6]$ $\times 10^{-3}$	$[Free K^+]$ $\times 10^{-3}$	K	Ionic strength $\times 10^{-3}$	$\log K^\circ$ (eq 4)
0.350	1.35	126	3.30	2.32
0.400	1.53	136	3.72	2.36
0.500	1.91	132	4.62	2.34
0.700	2.65	108	6.38	2.32
0.800	3.01	104	7.24	2.33
1.00	3.73	101	8.92	2.34
2.00	7.28	77.2	17.1	2.33
3.00	10.6	83.8	24.4	2.44
4.00	14.2	59.6	32.7	2.35
			Mean	2.35 ± 0.02

^a See eq 4 and related text for definition of K° .

Table II: Variation of Ion Association Constant K for Equilibrium 2 with Ionic Strength at 25.0°^a

$[K_3Fe(CN)_6]$ $\times 10^{-3}$	$[Free K^+]$ $\times 10^{-3}$	K	Ionic strength $\times 10^{-3}$	$\log K^\circ$ (eq 4)
1.00	2.95	19.4	5.84	1.50
1.25	3.67	17.6	7.27	1.48
2.00	5.84	14.6	11.5	1.45
2.50	7.27	14.3	14.3	1.46
5.00	14.3	10.8	28.0	1.44
			Mean	1.46 ± 0.02

^a See eq 4 and related text for definition of K° .

libria,^{16,17} the reported thermodynamic constants for the hexacyanoferrate equilibria^{5,6} appear to carry a large uncertainty.

The observed small changes in the ultraviolet absorption spectra resulting from the addition of KCl to dilute $K_4Fe(CN)_6$ solutions have been attributed to the existence of the chemical species $KFe(CN)_6^{3-}$ and enabled the calculation⁷ of a more precise association constant. In this connection, we have observed that the addition of excess Pr_4NBr to dilute $K_4Fe(CN)_6$ solutions has no perceptible effect on the absorption spectrum. The Pr_4N^+ cation is known to have a small affinity for hexacyanoferrate anions¹⁸ and is believed to have a large structure-promoting effect on the water solvent.¹⁹ These considerations suggest that the spectral change with K^+ is not due to a medium effect but to the formation of an ion pair. However, this type of argument is not conclusive.

In a study of the specific effects of cations on the rate of electron exchange between hexacyanoferrate(II) and (III) ions,²⁰ ion pairs were invoked as reaction intermediates in order to account for the observed kinetics. However, no quantitative conclusions were made regarding the extent of ion association.

In our work, a different approach was employed. Using a cation-sensitive glass electrode, K^+ activity was measured, and consequently, association constants under a variety of conditions were determined. This method depends upon certain necessary assumptions concerning activity coefficients and liquid-junction potentials (see Experimental Section). The validity of these assumptions as well as the existence of ion pairs is borne out by the internal consistency of the results over the concentration range of our experiments (Tables I and II). Furthermore, the enthalpy changes for the equilibria obtained calorimetrically at 25° agree well with the mean enthalpy changes obtained from the temperature variation of the equilibrium constants (Table V). Perhaps the strongest evidence for the existence of ion association equilibria in hexacyanoferrate solutions is the agreement between thermodynamic constants determined by three independent methods: conductivity, spectrophotometry, and potentiometry (Table V).

The present work confirms previous results which showed that ion association is appreciable in $K_3Fe(CN)_6$ solutions and considerably more so in $K_4Fe(CN)_6$ solutions. Thus in $5.00 \times 10^{-3} M$ $K_3Fe(CN)_6$, 13% of the anions are complexed, and in $4.00 \times 10^{-3} M$ $K_4Fe(CN)_6$ the extent of the association is 46%. In more concentrated solutions, the extent of binding will of course be greater, and at least in the case of $Fe(CN)_6^{4-}$, the binding of a second K^+ also occurs.

Table V: Summary of Thermodynamic Data at 25.0°

	Equilibrium 1	Equilibrium 2
Log K°	2.35 ± 0.02	1.46 ± 0.02
ΔH°_{pot} , kcal/mole ^a	0.6 ± 0.4	0.5 ± 0.4
ΔH°_{cal} , kcal/mole ^b	1.0 ± 0.3	0.5 ± 0.5
ΔS° , eu	13 ± 2	8 ± 2
Log K° (ref 5)	2.3	...
Log K° (ref 6)	...	1.2
Log K° (ref 7)	2.37	...

^a ΔH°_{pot} from potentiometric measurements. ^b ΔH°_{cal} from calorimetric measurements.

Quantitative knowledge of these equilibria is important in determining the ionic composition, computing ionic strengths, and elucidating other specific salt effects in hexacyanoferrate solutions. An example is the role of ion association in interpreting oxidation-reduction potential data for the hexacyanoferrate(III)-(II) couple. This aspect will be discussed in detail in part II.⁸

The enthalpy changes for both ion association equilibria are slightly endothermic. Unless extensive desolvation is involved, this suggests that the chemical bonding is weak in both ion pairs. In fact, the reactions are driven entirely by the favorable entropy changes (Table V).

Assuming the simple electrostatic picture of ion-pair formation to hold in these systems, one can calculate the distance of closest approach of the centers of the associating ions from the Bjerrum equation.²¹ Using our association constants, we have calculated $4.3 \pm 0.1 \text{ \AA}$ for $KFe(CN)_6^{3-}$ and $6.6 \pm 0.2 \text{ \AA}$ for $KFe(CN)_6^{2-}$. Although this type of calculation can be criticized, the difference between the two cases nevertheless appears to be significant. On this basis, it may be concluded that the structures of the two ion pairs are significantly different.

In this connection, it is interesting to note that although $Fe(CN)_6^{4-}$ forms two conjugate acids, $HFe(CN)_6^{3-}$ and $H_2Fe(CN)_6^{2-}$, acidimetric titration of

(16) G. H. Nancollas, *Quart. Rev.* (London), **14**, No. 4, 402 (1960).

(17) C. W. Davies, "Ion Association," Butterworth and Co. (Publishers) Ltd., London, 1962.

(18) D. W. Larsen and A. C. Wahl, *Inorg. Chem.*, **4**, 1281 (1965).

(19) H. S. Frank, *J. Phys. Chem.*, **67**, 1554 (1963).

(20) R. J. Campion, Ph.D. dissertation, Washington University, St. Louis, Mo., 1963.

(21) H. S. Harned and B. B. Owen, "Physical Chemistry of Electrolytic Solutions," 3rd ed, Reinhold Publishing Corp., New York, N. Y., 1958, Chapter 5.

$\text{Fe}(\text{CN})_6^{3-}$ shows no evidence for the formation of conjugate acids above pH 1.²² Furthermore, whereas the ultraviolet absorption spectrum of $\text{Fe}(\text{CN})_6^{4-}$ undergoes changes on the addition of various metal cations, no spectral changes are detected on the addition of various metal cations to $\text{Fe}(\text{CN})_6^{3-}$, although ion association is known to occur. A possible explanation for the above observations is that there is a greater penetration of the hydration shell in the $\text{KFe}(\text{CN})_6^{3-}$ ion pair than in the $\text{KFe}(\text{CN})_6^{2-}$ ion pair. A similar conclusion has been reported in the case of the $\text{LaFe}(\text{CN})_6$ ion pair.^{16,23}

Acknowledgment. We wish to thank Dr. R. J.

Witonsky for much help and useful discussion of this work.

(22) J. Jordan and G. I. Ewing, *Inorg. Chem.*, **1**, 587 (1962).

(23) NOTE ADDED IN PROOF. Since submitting this paper, the work of R. W. Chlebek and M. W. Lister [*Can. J. Chem.*, **44**, 437 (1966)] has come to our attention. In studying the kinetics of electron transfer between $\text{K}_4\text{Fe}(\text{CN})_6$ and $\text{K}_2\text{S}_2\text{O}_8$ they found that the rate constants varied according to the Brønsted equation, provided ion association by both reacting species was taken into account. They investigated the ion association equilibria using a cation-sensitive glass electrode with solutions containing the tetramethylammonium ion. The apparent disagreement between their thermodynamic data and those quoted above for solutions containing only the KCl cation may be due in part to their use of higher concentrations, and in part to the additional specific salt effects which we have observed when tetraalkylammonium salts are employed (see Experimental Section and part II⁸).

Thermodynamic Aspects of the Potassium Hexacyanoferrate(III)-(II)

System. II. Reduction Potential^{1,2}

by George I. H. Hanania, Dennis H. Irvine, William A. Eaton,³ and Philip George

Department of Chemistry and Graduate Group on Molecular Biology, University of Pennsylvania, Philadelphia, Pennsylvania 19104 (Received October 3, 1966)

The reduction potential for the hexacyanoferrate(III)-(II) couple has been measured potentiometrically over a range of temperature, pH, ionic strength, and in the presence of various 1:1 salts. The following thermodynamic quantities were obtained at 25.0° and $I = 0$: $E^\circ = 0.355 \pm 0.001$ v, $\Delta H^\circ = -26.7 \pm 0.3$ kcal/mole, and $\Delta S^\circ = -62.1 \pm 1.0$ eu. The data on the variation of reduction potential with concentration are shown to be consistent with the assumption of cation binding to both oxidant and reductant anions (thermodynamic parameters for these ion association equilibria are presented in part I). The strong salting-out effect of tetraalkylammonium salts on the reduction potential suggests that these ions exert an additional specific salt effect. The data on the variation of reduction potential with pH in solutions of pH < 6 are shown to be consistent with the assumption that the reductant anion forms two successive conjugate acids. Potentiometric and calorimetric measurements lead to thermodynamic parameters for the protonation equilibria. Oxidation-reduction data for a number of complex ions are compared, and some factors which influence reduction potentials and entropies in these systems are discussed.

Introduction

A number of workers have investigated the hexacyanoferrate(III)-(II) oxidation-reduction system, most studies having been made on the potassium salts $K_3Fe(CN)_6$ and $K_4Fe(CN)_6$. Values for the standard reduction potential have been reported by Kolthoff and Tomsicek,⁴ Lin and Breck,⁵ and Rock;⁶ values for the enthalpy change for the cell reaction have been reported by Hepler, *et al.*,⁷ and Lin and Breck.⁵ The protonation of the hexacyanoferrate(II) ion has been studied by Jordan and Ewing.⁸ Unfortunately, the reported standard reduction potentials are not in good agreement. A major source of uncertainty is probably the substantial specific salt effects. The need has therefore remained for a more complete thermodynamic study of this system.

The hexacyanoferrate system is of particular interest in the comparative study of octahedral iron complexes in aqueous solution. Thus, in an earlier publication,⁹ we showed that the difference in entropy between oxidant and reductant ions is small in the case of the tris-

dipyridyl and tris-*o*-phenanthroline complexes of iron, and that partial replacement of the organic ligand by cyanide ions increases this entropy difference. In the hexacyanoferrate complex, complete replacement of the organic ligand has occurred. A knowledge of the thermodynamic parameters for this system enables one to test the above trend in ionic entropy differences

(1) Part I: W. A. Eaton, P. George, and G. I. H. Hanania, *J. Phys. Chem.*, **71**, 2016 (1967).

(2) Work supported by Grants AM 03187 and AM 04764 from the National Institutes of Health, and an Arts and Sciences grant from the American University of Beirut.

(3) Scholar of the Pennsylvania Plan to Develop Scientists in Medical Research.

(4) I. M. Kolthoff and W. J. Tomsicek, *J. Phys. Chem.*, **39**, 945 (1935).

(5) J. Lin and W. G. Breck, *Can. J. Chem.*, **43**, 766 (1965).

(6) P. A. Rock, *J. Phys. Chem.*, **70**, 576 (1966).

(7) L. G. Hepler, J. R. Sweet, and R. A. Jessor, *J. Am. Chem. Soc.*, **82**, 304 (1960).

(8) J. Jordan and G. J. Ewing, *Inorg. Chem.*, **1**, 587 (1962).

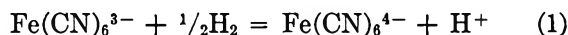
(9) P. George, G. I. H. Hanania, and D. H. Irvine, *J. Chem. Soc.*, 2548 (1959).

between pairs of oxidant and reductant ions. In the case of the tetracyanodipyridyliron(III)-(II) couple, we showed that the ionic entropies of the oxidant and its protonated reductant are quite different although the ions carry equal charge. Since the hexacyanoferrate(II) ion is known to form a series of conjugate acids,⁸ a further test can be made of the apparently anomalous entropies of protonated complex ions. Furthermore, from the thermodynamic parameters for ion association,¹ it is possible to compare the entropies of the protonated hexacyanoferrate complexes with the K^+ ion pairs.

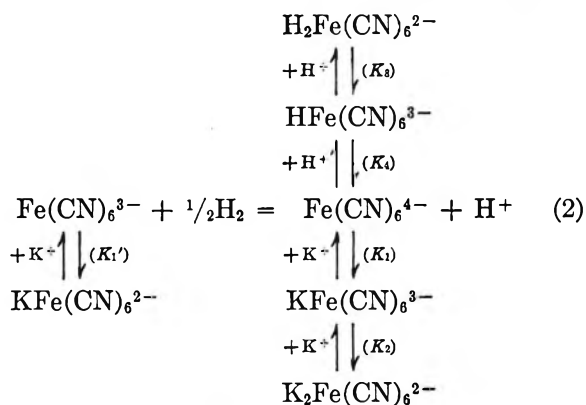
In this paper, we record the results of a detailed potentiometric study of the cell reaction over a wide range of conditions, taking into account the relevant ion-association equilibria. Preliminary reports have already been presented.^{10,11}

Theory

The parent cell reaction for the hexacyanoferrate(III)-(II) couple is



In aqueous solutions of the potassium salts it is necessary to consider the binding of K^+ as well as H^+ to both oxidant and reductant anions. Under the experimental conditions of the present study, only a few of the possible equilibria are detectable; these equilibria, which affect the measured free-energy change, are indicated in the following reaction scheme



Following general practice, all acid-base equilibria are considered as dissociation, so that $K_4 = h \times [\text{Fe}(\text{CN})_6^{4-}]/[\text{HFe}(\text{CN})_6^{3-}]$, etc., whereas the cation-binding equilibria are considered as association, *viz.* $K_1 = [\text{KFe}(\text{CN})_6^{3-}]/[\text{Fe}(\text{CN})_6^{3-}] \times k$, etc. Furthermore, all equilibria are defined in terms of the molar concentration of K^+ and the activity of H^+ (using the symbols k and h , respectively), and of the molar concentrations of all other species. The effect of the above ionic equilibria on the measured reduction potential,

E , which is defined for equal total molar concentrations of oxidant and reductant, may be considered with reference to the parent cell reaction (eq 1). Since

$$[\text{oxidant}] = [\text{Fe}(\text{CN})_6^{3-}](1 + kK_1') \quad (3)$$

[reductant] =

$$[\text{Fe}(\text{CN})_6^{4-}] \left(1 + \frac{h}{K_4} + \frac{h^2}{K_3K_4} + kK_1 + k^2K_1K_2 \right) \quad (4)$$

it can be shown that

$$E = E^\circ + \frac{RT}{F} \times \ln \frac{1 + \frac{h}{K_4} + \frac{h^2}{K_3K_4} + kK_1 + k^2K_1K_2}{1 + kK_1'} + \frac{RT}{F} \ln \frac{y_O}{y_R} \quad (5)$$

where E° is the standard reduction potential of the couple in equation 1 relative to s.h.e., y_O and y_R are the molar activity coefficients of free oxidant and reductant anions, with the other terms as defined above. At a given finite ionic strength, I , the reduction potential for the parent couple, E_i , is defined as

$$E_i = E^\circ + \frac{RT}{F} \ln \frac{y_O}{y_R} \quad (6)$$

Hence, in the limit of very dilute solutions at 25.0°

$$E_i = E^\circ + 0.209I^{1/2} \quad (7)$$

In sufficiently dilute solutions where the binding of ions to $\text{KFe}(\text{CN})_6^{3-}$ can be neglected, it follows from eq 5 that

$$E_i = E - \frac{RT}{F} \ln \frac{1 + \frac{h}{K_4} + \frac{h^2}{K_3K_4} + kK_1}{1 + kK_1'} \quad (8)$$

i.e., E_i is the reduction potential independent of H^+ and K^+ binding. At $\text{pH} > 6$, where the measured reduction potential is independent of pH , and in sufficiently dilute solutions where multiple K^+ binding is negligible, eq 8 reduces to

$$E_i = E - \frac{RT}{F} \ln \frac{1 + kK_1}{1 + kK_1'} \quad (9)$$

Experimental Section

The two salts, $\text{K}_3\text{Fe}(\text{CN})_6$ and $\text{K}_4\text{Fe}(\text{CN})_6 \cdot 3\text{H}_2\text{O}$, were of AnalaR or Baker Analyzed grade and were

(10) Delaware Valley Regional Meeting of the American Chemical Society, Philadelphia, Pa., Feb 1958, Abstract 14, p 71.

(11) G. I. H. Hanania, W. A. Eaton, and P. George, Abstracts, 151st National Meeting of the American Chemical Society, Pittsburgh, Pa., March 1966, p 45N.

used from freshly opened bottles without further purification. Tetraalkylammonium salts were purchased from Eastman Organic Chemicals and were not further purified. Tetrapropylammonium hexacyanoferrates were prepared on Dowex cation-exchange resin following conversion of the resin to the tetrapropylammonium form with subsequent washing to neutral pH. Solutions were freshly made for every set of measurements and were always kept in the dark. The most dilute solutions were deoxygenated with prepurified nitrogen. All solutions were prepared with deionized distilled water. No spurious effects were observed.

Potentiometric measurements were carried out in a jacketed glass vessel using two or three bright platinum electrodes cleaned with boiling acetone and hot concentrated nitric acid. A preequilibrated saturated calomel electrode with an agar-saturated KCl bridge was used as a reference electrode. The calomel electrodes employed were selected from a group of commercial calomel electrodes which agreed to within 0.0002 v at several temperatures. The fiber junction calomel electrodes from Beckman Instruments Co. (39970) were guaranteed to have a potential *vs.* a standard hydrogen electrode of 0.2445 ± 0.0005 v at 25° (including liquid-junction potential) and those from the Arthur H. Thomas Co. (4857-F10) were guaranteed to have a potential of 0.244 ± 0.002 v at 25°. These values were confirmed by measurements against Ag, AgCl electrodes, prepared according to the method of Brown and MacInnes,¹² in KCl solutions of various concentrations. Taking 0.2224 v as the standard potential of the Ag, AgCl electrode at 25.0°¹³ and using the activity coefficient data for KCl from Latimer,¹⁴ the standard potential of the calomel electrodes (including liquid junction potential) was found to be 0.245 ± 0.002 v over a 100-fold range of KCl concentrations. Liquid junction potentials for the hexacyanoferrate solutions, as estimated from the Henderson equation,¹⁵ were found to vary between the narrow limits of 2 to 5 mv. It was therefore assumed that liquid junction makes a relatively constant or an insignificantly small contribution to the measured potentials in very dilute solutions, and no corrections to the emf data were applied. The uncertainty produced on this account in the derived thermodynamic quantities will be commented upon later in the Discussion.

The apparatus was kept in a black-box Faraday cage, and the measurements were recorded only when the emf's were constant with time and the platinum electrodes agreed to better than 0.0002 v. Temperature was controlled to within $\pm 0.05^\circ$ by circulating water from a thermostat. The emf was read to the nearest 0.0001 v on a Radiometer pHM4 meter. The mea-

sured reduction potential, E , refers to the emf against a standard hydrogen electrode, calculated from the data of Bates¹⁶ on the saturated calomel electrode. The pH measurements were made with the same apparatus using glass and calomel electrodes, following the recommendations of Bates for standardization.¹⁷

The heat of the reaction $\text{H}^+ + \text{Fe}(\text{CN})_6^{4-} \rightleftharpoons \text{HFe}(\text{CN})_6^{3-}$ was measured in a precision solution calorimeter using the following procedure: 4.00 ml of 0.727 *M* $\text{K}_4\text{Fe}(\text{CN})_6$ was mixed with 950 ml of approximately 0.006 *M* HClO_4 and, as a control, 4.00 ml of 0.727 *M* $\text{K}_4\text{Fe}(\text{CN})_6$ was mixed with 950 ml of H_2O . The pH of the final mixtures was measured and hence the enthalpy change for the above reaction could be calculated according to the method already described.¹ Appropriate corrections were applied to the observed heat to take into account contributions from the dissociation of $\text{KFe}(\text{CN})_6^{3-}$, the formation of a small fraction of $\text{H}_2\text{Fe}(\text{CN})_6^{2-}$, as well as the possible formation of $\text{HKFe}(\text{CN})_6^{2-}$ for which the heat of binding has been assumed equal to that for $\text{KFe}(\text{CN})_6^{3-}$. The value for $\text{H}_2\text{Fe}(\text{CN})_6^{2-}$ was obtained from a similar experiment at a higher acidity.

Results

Effect of Ionic Strength and Ion Association; Determination of E° . The potential of equimolar mixtures of $\text{K}_3\text{Fe}(\text{CN})_6$ and $\text{K}_4\text{Fe}(\text{CN})_6$ was measured over a wide range of concentrations. The results agreed to within 0.001 v with the data of Kolthoff and Tomsicek.⁴

Figure 1 shows our data for the low ionic strength region at 25.0°. It can be seen that the measured reduction potential, E , deviates from the limiting theoretical Debye-Hückel slope even in the most dilute solutions, the apparent limiting slope being 0.260 v/ $M^{1/2}$. On the other hand, taking ion association into account, the resulting E_i values fit the limiting theoretical Debye-Hückel slope of 0.209 v/ $M^{1/2}$ up to an ionic strength of 0.003 *M* and show the expected type of deviation at the higher ionic strengths.

Values of E_i were calculated from eq 9 by the following procedure: (1) for each mixture, the free K^+ concentration, k , was measured following the method already described;¹ (2) for all these mixtures,

(12) A. S. Brown and D. A. MacInnes, *J. Am. Chem. Soc.*, **57**, 1356 (1935).

(13) D. J. G. Ives and G. J. Janz, "Reference Electrodes," Academic Press Inc., New York, N. Y., 1961, p 189.

(14) W. M. Latimer, "Oxidation Potentials," 2nd ed, Prentice-Hall, Inc., New York, N. Y., 1952, p 355.

(15) R. G. Bates, "Determination of pH," John Wiley and Sons, Inc., New York, N. Y., 1964, p 40.

(16) R. G. Bates, ref 15, p 278.

(17) R. G. Bates, ref 15, Chapter 4.

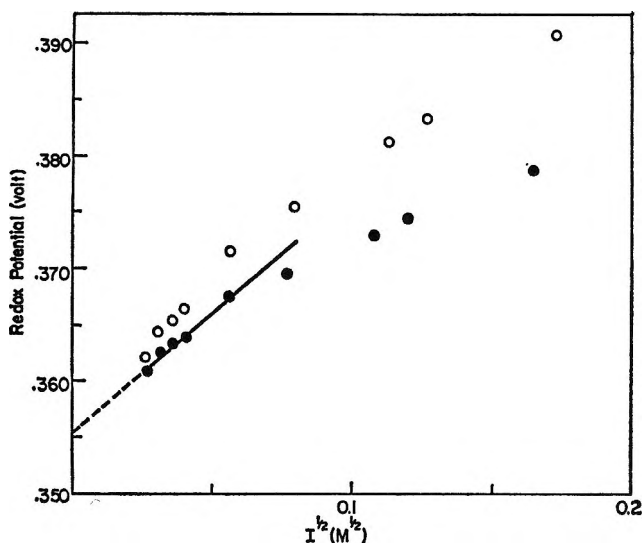


Figure 1. Variation of reduction potential with ionic strength at 25.0° for equimolar concentrations of $K_3Fe(CN)_6$ and $K_4Fe(CN)_6$: O, measured reduction potential, E , the total molar ionic strength being computed on the basis of complete dissociation of both salts; ●, E_i , the cation-independent reduction potential for equilibrium 1, calculated from eq 9. Ionic strength is computed taking ion-association equilibria into account. Linear extrapolation along theoretical Debye-Hückel slope of $0.209 \text{ v } M^{-1/2}$ yields $E^\circ = 0.355 \pm 0.001 \text{ v}$.

pH > 6 and consequently the terms h/K_4 and h^2/K_4K_3 made no significant contribution to E_i ; (3) in each case, the total molar ionic strength was calculated by successive approximations taking the presence of ion pairs into account; (4) the appropriate values of the cation association constants K_1 and K_1' at the ionic strengths of the mixtures were used;¹ (5) assuming K_2 to be of the order of magnitude of K_1' , the term $k^2-K_1K_2$ was found to be insignificant except in the two most concentrated mixtures.

The extrapolation of E_i to zero ionic strength gives the standard reduction potential at 25.0° for the couple in eq 1: $E^\circ = 0.355 \pm 0.001 \text{ v}$.

Other Salt Effects. The reduction potential was also measured in the presence of varying concentrations of added electrolytes. Figure 2 shows the effect of added 1:1 salts. The reduction potential rises progressively in all cases except where the added electrolyte is a tetraalkylammonium halide (R_4NX). There is a gradation of salting-out effects with R_4NX salts, reaching what appears to be a limit in the case of Pr_4NBr and Bu_4NBr . The same sharp salting-out effect is observed by varying the concentration of an equimolar mixture of tetrapropylammonium hexacyanoferrates. The extent of these specific salt effects can be seen for instance at 0.5 M added salt where the reduction potential measured in the presence of Pr_4-

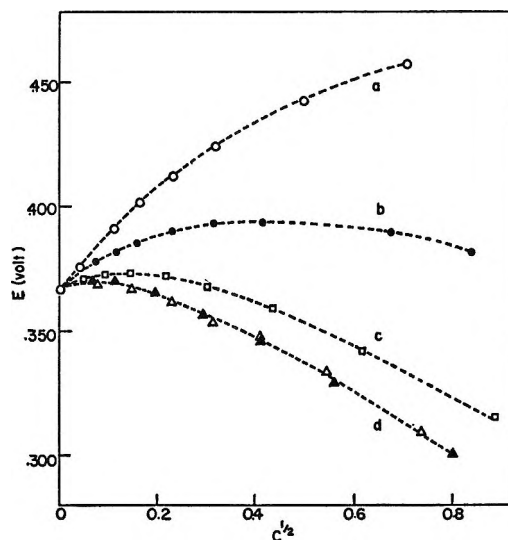


Figure 2. Variation of measured reduction potential, E , with the concentration of added 1:1 salts; $1.00 \times 10^{-4} \text{ M}$ each $K_3Fe(CN)_6$ and $K_4Fe(CN)_6$; $T = 25.0^\circ$; (a) KBr (and similar salts⁴); (b) Me_4NBr ; (c) Et_4NBr ; (d) $n-Pr_4NBr$ (\blacktriangle), and $n-Bu_4NBr$ (\triangle).

NBr is about 0.15 v lower than it is in the presence of the "neutral salts" like KBr, NaCl, NH_4Cl , etc. Furthermore, when one of these salts is added to a hexacyanoferrate(III)-(II) mixture containing excess R_4NX , an immediate dramatic rise in the reduction potential is observed.

Effect of Temperature. The reduction potential was measured at four temperatures between 15 and 30° at $I = 0.064 \text{ M}$. At each temperature, E_i was calculated as described above. The mean value of dE_i/dT was $-(2.69 \pm 0.04) \times 10^{-3} \text{ v deg}^{-1}$, which was taken as a first approximation to be the value of dE°/dT . Thus, for the parent cell reaction in eq 1: $\Delta H^\circ = -26.7 \pm 0.3 \text{ kcal/mole}$ and $\Delta S^\circ = -62.1 \pm 1.0 \text{ eu}$.

Effect of pH. The measured reduction potential is constant above pH 6 whereas in more acidic solutions its value increases progressively. From simultaneous measurements of E and pH in a solution containing equimolar concentrations of $K_3Fe(CN)_6$ and $K_4Fe(CN)_6$ titrated with $HClO_4$, the ionization constants K_4 and K_3 were calculated from eq 8 in the following manner. At pH > 6, the free K^+ concentration, k , is measured and the ionic strength is calculated.¹ E_i is then obtained from eq 9 using the appropriate ion association constants K_1 and K_1' . In the more acidic solutions, the ionization constants K_4 and K_3 are calculated from eq 8 by successive approximations. In this calculation, the small changes in ionic strength and k are taken into account. The value of h , the activity

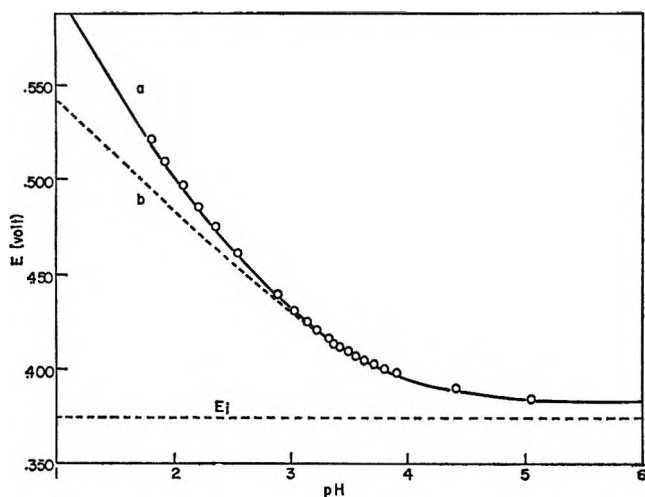


Figure 3. Variation of measured reduction potential, E , with pH at 25.0 and at $I = 0.014\text{--}0.023\text{ M}$. Curve a gives the theoretical variation in accordance with eq 8, while curve b gives the corresponding relation on the basis of only one conjugate acid for the hexacyanoferrate(II) ion, *i.e.*, ignoring the term h^2/K_3K_4 in eq 8.

of hydrogen ions, is obtained from the measured pH assuming that $\text{pH} = -\log h$. The mean value of K_4 is obtained from about 15 measurements in the range of pH 2.6 to 1.7. Figure 3 shows the variation of E with pH at 25°. Two theoretical curves have been drawn, one assuming the participation of only one conjugate acid of the hexacyanoferrate(II) ion, and the other taking into account two overlapping ionizations. The experimental points are best fitted by the curve corresponding to two successive ionizations. It can also be seen that the limiting difference, $E - E_i$, in neutral solution is 9.5 mv. This represents the effect of ion association in this experiment with $1.0 \times 10^{-3}\text{ M K}_4\text{Fe(CN)}_6$ and $1.0 \times 10^{-3}\text{ M K}_3\text{Fe(CN)}_6$.

The above method of calculation was also applied to the data at other ionic strengths. However, there is a limitation on the range of ionic strengths which can be covered in these measurements. For, at the extreme of dilute solutions, the ionic strength will vary appreciably as the pH is changed during an experiment, and at the other extreme of $I > 0.05\text{ M}$, uncertainties about the various ionic equilibria which are involved preclude the precise determination of the parameters required in the calculations. We have therefore confined our measurements to the range shown in Table I. Here the results at 25.0° are given together with the calculated thermodynamic ionization constant using the relation $\text{p}K_4^0 = \text{p}K_4 + 3.56I^{1/2}/(1 + 1.5I^{1/2})$. Thus the mean value of $\text{p}K_4^0$ is 4.28 ± 0.02 .

Table I: Variation of $\text{p}K_4$ with Ionic Strength at 25.0°^a

Concn each, M	2.50×10^{-3}	1.00×10^{-3}	5.00×10^{-4}
I, M	0.036	0.015	0.0075
$\text{p}K_4$	3.76	3.92	4.02
$\text{p}K_4^0$	4.28	4.28	4.29

^a $\text{p}K_4$ values were obtained from simultaneous measurements of E and pH in equimolar mixtures of $\text{K}_4\text{Fe(CN)}_6$ and $\text{K}_3\text{Fe(CN)}_6$ titrated with HClO_4 . Calculation involves successive approximation using eq 8, as described in the text. $\text{p}K_4^0 = \text{p}K_4 + 3.56I^{1/2}/(1 + 1.5I^{1/2})$. Mean deviations are ± 0.02 .

The above treatment of the data also yielded a value for the third ionization constant: $\text{p}K_3 = 1.96 \pm 0.03$ at 25.0° and $I = 0.020\text{--}0.025\text{ M}$. Beyond this range, in either direction, uncertainties are involved which preclude any precise calculation. We have therefore taken the thermodynamic constant on the basis of the single determination, using the corresponding relation $\text{p}K_3^0 = \text{p}K_3 + 2.55I^{1/2}/(1 + 1.5I^{1/2})$, and hence $\text{p}K_3^0 = 2.3 \pm 0.1$ at 25.0°, showing the maximum limits of uncertainty.

Jordan and Ewing⁸ have determined K_4 and K_3 from acidimetric titrations of $\text{K}_4\text{Fe(CN)}_6$ solutions. Their results are $\text{p}K_4^0 = 4.17 \pm 0.02$ and $\text{p}K_3^0 = 2.25 \pm 0.15$ at 25.0°. When our $\text{p}K_4$ data are treated taking no account of K^+ binding, the results become almost identical with those of Jordan and Ewing. Furthermore, when our data are analyzed as an acidimetric titration, again excluding K^+ binding, the results are also in accord. The apparent discrepancy in $\text{p}K_4^0$ can thus be accounted for satisfactorily in terms of ion association. The calorimetric measurements yielded a value of $\Delta H_4 = -0.5 \pm 0.5\text{ kcal/mole}$ for the ionization of HFe(CN)_6^{3-} . The limits of uncertainty in this value represent uncertainties due to the overlap of the two ionizations as well as uncertainties in the contribution to the observed heat from various ion association equilibria. Assuming $\Delta H_4^0 = \Delta H_4$, it follows that $\Delta S_4^0 = -21 \pm 2\text{ eu}$.

The enthalpy change for the ionization of one proton from $\text{H}_2\text{Fe(CN)}_6^{2-}$ was obtained calorimetrically using the same method as for ΔH_4 . In addition to uncertainties arising from heats of ion association, there are larger uncertainties due to the instability of the hexacyanoferrate(II) ion in the more acidic solutions. ΔH_3 was found to be approximately -1 kcal/mole . This yields an approximate value of $\Delta S_3^0 = -14\text{ eu}$.

Jordan and Ewing⁸ report $\Delta H_4 = \Delta H_3 = 0.0$ from thermometric titrations of $\text{K}_4\text{Fe(CN)}_6$ with hydrochloric acid. However, the conditions of these experiments are not given in sufficient detail for comparison with our results.

Discussion

The standard reduction potential for the hexacyanoferrate(III)-(II) couple (eq 1) as determined in the present study is $E^\circ = 0.355 \pm 0.001$ v at 25.0°. This value is independent of both protonation and ion-association equilibria. E° was obtained from the measured reduction potentials, corrected for ion association, and extrapolated to zero ionic strength from the region of extremely dilute solutions. In this region, the data fit well the limiting Debye-Hückel function (see Figure 1). The same value is obtained using the extended Debye-Hückel function, $I^{1/2}/(1 + BaI^{1/2})$, the best fit being for $a \approx 6$ Å. This agreement with Debye-Hückel behavior supports the assumption that any residual junction potential in the experimental cell, in the region of very low ionic strength, is either insignificantly small or is virtually constant but indeterminate.

The above value is to be compared with the results of previous workers. Kolthoff and Tomsicek⁴ obtained 0.356 v by an empirical extrapolation from extensive measurements in extremely dilute solutions. Lin and Breck,⁵ whose measurements were made in somewhat more concentrated solutions, reported 0.3644 v. Two factors could account for this slightly higher value. In the first place, the slope of the plot of their data is considerably lower than the theoretical Debye-Hückel slope, as would be expected for the range of concentrations employed. Secondly, ion association is significant. Calculations using eq 9 show that the contribution from ion association varies from 0.006 to 0.020 v over the range of concentrations in their work. Using a cell without salt bridges in which the liquid junction potential was minimized by an appropriate choice of reference electrode, Rock⁶ arrived at a value of 0.3704 v for E° , based on measurements made on solutions of the order of 0.1 *m*. This author adopted a strong electrolyte standard state in order to take ion-association effects into account. It may be that liquid-junction potentials account for part of the difference between Rock's value and 0.355 v which was obtained in the present work by direct extrapolation of experimental data to infinite dilution. At any rate, the difference leads to an uncertainty in the entropy change associated with the cell reaction of about 1 eu; this is quite acceptable for the type of correlation between partial molal entropies of variously charged species which is presented in our discussion below.

The present study shows that in the determination of the hexacyanoferrate(III)-(II) reduction potential, three types of salt effects operate.

(1) *Ionic Equilibria, i.e., Binding of Cations, Protons, etc.* It is the magnitudes and the difference

in affinity of oxidant and reductant for the various ions which determine the magnitude of the effect of ion binding. For instance, in a 0.1 *M* mixture of potassium hexacyanoferrates the contribution is approximately 0.040 v.

(2) *Ionic Strength.* After correcting for ion association, limiting Debye-Hückel behavior for highly charged ions can only be expected in extremely dilute solutions, *e.g.*, in the present case at $I < 0.003$ *M*.

(3) *Other Specific Salt Effects.* Reference to Figure 2 shows that although the effect of various 1:1 salts on the reduction potential is similar in the limit of dilute solutions, there is very marked divergence at higher concentrations. In the case of NaCl, KBr, etc., and possibly Me_4NBr , the greater extent of binding of cation to reductant over that of oxidant accounts for the sharp rise in reduction potential with increasing concentration of added electrolyte. The larger tetraalkylammonium salts, however, cause a sharp reversal of the salt effect in an unusually low ionic strength region ($I = 0.01$ *M*). There is evidence that Pr_4N^+ , and probably also Bu_4N^+ , have a weak affinity for hexacyanoferrate ions.^{1,18} Furthermore, estimates of the extent of binding at concentrations above 0.1 *M* lead to the conclusion that ion association is quite insufficient to account for the rapid divergence of the curves for Pr_4NBr and KCl in Figure 2, which reaches 0.15 v at $I = 0.5$ *M*. These observations indicate that the tetraalkylammonium salts exert an additional specific salting-out effect of quite large magnitude. In recent years, effects of this kind have been well established for these salts and explanations are currently being sought in terms of the "structure promoting" influence of these organic cations on the solvent water¹⁹ and in terms of nonideal configurational entropies of mixing due to the large size difference between these cations and the water molecule.²⁰

The enthalpy change for the cell reaction in eq 1, as determined potentiometrically in this work, is -26.7 ± 0.3 kcal/mole. The only other values reported in the literature are -27.6 obtained potentiometrically⁵ and -26.8 ± 0.4 derived from the heat of oxidation of hexacyanoferrate(II) by bromine.⁷

Since the standard reduction potential and enthalpy change seem to be well established, the uncertainty in the entropy change for this cell reaction cannot be more than 2 eu.

Comparison of data for the hexacyanoferrate(III)-(II) oxidation-reduction couple with the corresponding

(18) D. W. Larsen and A. C. Wahl, *Inorg. Chem.*, **4**, 1281 (1965).

(19) H. S. Frank, *J. Phys. Chem.*, **67**, 1554 (1963).

(20) R. E. Conway and R. E. Verrall, *ibid.*, **70**, 1473 (1966).

Table II: Thermodynamic Data, at 25° and $I = 0$, for Some Oxidation-Reduction Couples of Complex Ions in Aqueous Solution

	Charge, O/R	E° , v	ΔH° , kcal/mole	ΔS° , eu	Reference
Fe _{aq}	3+/2+	0.771	-9.95	26.4	a, b
Fe(CN) ₆	3-/4-	0.355	-26.7	-62.1	This paper
Fe(CN) ₅ dipy	1-/2-	0.542	-27.3	-49.5	c
Fe(dipy) ₃	3+/2+	1.120	-32.7	-23.1	c
Fe(dipy(CH ₃) ₂) ₃	3+/2+	0.941	-26.8	-17.1	d
Fe(phen) ₃	3+/2+	1.141	-32.5	-20.8	c
Ru(dipy) ₃	3+/2+	1.374	-36.3	-15.4	c
Os(dipy) ₃	3+/2+	0.878	-24.7	-14.8	e
Fe(pyridine-2-aldoxime) ₃	0/1-	0.347	-21.0	-43.6	f
Fe(pyr-2,6-dialdoxime) ₂	1-/2-	0.204	-24.7	-67.1	f
Fe(4,7-dihydroxyphen) ₃	3-/4-	-0.20	-5	-32	g

^a Reference 23. ^b R. E. Connick and W. H. McVey, *J. Am. Chem. Soc.*, **73**, 1798 (1951). ^c Reference 9. ^d D. H. Irvine, *J. Chem. Soc.*, 2977 (1959). ^e G. T. Barnes, F. P. Dwyer, and E. C. Gyrfas, *Trans. Faraday Soc.*, **48**, 269 (1952). ^f G. I. H. Hanania, D. H. Irvine, M. Michaelides, and F. Shurayh, Abstracts, 9th International Conference on Coordination Chemistry, St. Moritz, Switzerland, Sept 1966. ^g G. I. H. Hanania, M. W. Makinen, P. George, and W. A. Eaton, unpublished results.

data for a number of other oxidation-reduction cell reactions allow certain generalizations to be made. The available thermodynamic data are summarized in Table II.

Thus, on comparing the dipyriddy complexes of iron, ruthenium and osmium, it is seen that the differences in their reduction potentials are reflected mainly in the enthalpy changes for their cell reactions. Presumably, for such a series of structurally similar low spin octahedral complexes of the same charge type, it is the bonding to the metal which is the major factor.

One may also compare a series of nitrogen-coordinated octahedral iron complexes which differ principally in their net charge. The tris-*o*-phenanthroline and trisdipyriddyiron(III)-(II) couples have reduction potentials of about 1.1 v, whereas the analogous tris-(4,7-dihydroxyorthophenanthroline)iron(III)-(II) couple has a reduction potential of about -0.1 v when all six hydroxyl groups are ionized. Thus the reduction potential decreases as the electrostatic charge in the neighborhood of the iron becomes more negative, spanning the exceptionally wide range of 1.34 v (*i.e.*, about 30 kcal/mole in free energy). The data show that this effect arises mainly from a decreased exothermicity of the cell reaction and to a lesser extent from the more unfavorable entropy change.

Entropy effects may be compared in terms of the standard ionic entropies of the various species involved in the cell reaction

$$\Delta S^\circ = \bar{S}^\circ_{\text{R}} - \bar{S}^\circ_{\text{O}} + \bar{S}^\circ_{\text{H}^+} - \frac{1}{2}\bar{S}^\circ_{\text{H}_2}$$

where \bar{S}°_{R} and \bar{S}°_{O} represent the partial molal entropies of the reductant and oxidant species, respectively.

Taking $\bar{S}^\circ_{\text{H}_2} = 31.2$ eu, a quantity δS° can be evaluated, where

$$\delta S^\circ = \bar{S}^\circ_{\text{R}} - \bar{S}^\circ_{\text{O}} + \bar{S}^\circ_{\text{H}^+} = \Delta S^\circ + 15.6 \text{ eu}$$

Lin and Breck⁵ concluded that the small negative values of δS° , about -6 eu, in the case of some organic ligands such as dipyriddy, lend support to Gurney's "absolute" entropy scale²¹ based on $\bar{S}^\circ_{\text{H}^+} = -5.5$ eu since it might be expected that with the charge buried in the center of the complex \bar{S}°_{R} and \bar{S}°_{O} would be almost identical.^{9,22} However, further data for this type of complex show rather greater variations, so although there may be some justification for this simple interpretation it cannot be accepted as a general rule.

Use of the absolute scale with $\bar{S}^\circ_{\text{H}^+} = -5.5$ eu makes \bar{S}° for anions more positive and \bar{S}° for cations more negative by 5.5 eu per unit charge than values based on the practical scale where $\bar{S}^\circ_{\text{H}^+}$ is arbitrarily put at zero. In comparing the magnitudes of ionic entropies, this has the important consequence that while the increments between the values for ions of the same charge remain unchanged, the increments between the values for ions of different charge are decreased by 5.5 eu per unit charge. However, in the comparisons made below, this latter consideration does not affect the conclusions, and since $\bar{S}^\circ_{\text{H}^+}$ is not yet known very precisely, all the \bar{S}° values have been calculated according to the practical scale.

(21) R. W. Gurney, "Ionic Processes in Solution," McGraw-Hill Book Co., Inc., New York, N. Y., 1953.

(22) P. George, G. I. H. Hanania, and D. H. Irvine, *J. Chem. Phys.*, **22**, 1616 (1954).

Another consideration in comparing the entropies for a series of structurally related compounds is the contribution from the symmetry number, σ , which, by decreasing the rotational partition function, lowers the entropy by an amount $R \ln \sigma$. For pairs of compounds related by a chemical reaction, *e.g.*, ionization or complex formation, it is these symmetry numbers that give rise to the more familiar "kinetic statistical factors." For the ions under discussion, the maximum symmetry numbers are 24 for $\text{Fe}(\text{CN})_6^{4-}$ and $\text{Fe}(\text{CN})_6^{3-}$, 4 for $\text{HFe}(\text{CN})_6^{3-}$ and $\text{KFe}(\text{CN})_6^{3-}$, 8 for the *trans* configuration of $\text{H}_2\text{Fe}(\text{CN})_6^{2-}$, and 2 for the *cis* configuration. Hence, if corrections for the maximum symmetry numbers were to be made so as to make the comparisons solely on the basis of the intrinsic contributions from each constituent structural group, they would range from a maximum of 6.3 eu to a minimum of 1.4 eu, and the maximum correction to the entropy change for any of the reactions would be $R \ln 6$, *i.e.*, 3.6 eu. These corrections, like the use of the absolute entropy scale, do not affect the following conclusions in any way, and so they have been left out of the calculations. The use of the unit mole fraction standard state to obtain Gurney's "unitary ionic entropies"²¹ also does not affect the conclusions since this would only shift the entropy scale by $R \ln 55.5$ eu without changing the differences between the ionic entropies for any pair of ions.

Table III lists the entropies of the various hexacyanoferrate ions, taking $\bar{S}^\circ_{\text{K}^+} = 24.5$ eu²³ and $\bar{S}^\circ_{\text{Fe}(\text{CN})_6^{3-}} = 64.8$ eu.²⁴ In looking for correlations between \bar{S}° and charge type, it is immediately apparent that while the values for the potassium complexes are broadly in accord with expectation, those for the conjugate acid species are quite anomalous. With the former, \bar{S}° increases substantially in going from $\text{Fe}(\text{CN})_6^{4-}$ to $\text{KFe}(\text{CN})_6^{3-}$ to $\text{KFe}(\text{CN})_6^{2-}$, *i.e.*, 18, 56, and 97 eu, respectively. In addition, the value for $\text{KFe}(\text{CN})_6^{3-}$ is only 9 ± 3 eu lower than that for $\text{Fe}(\text{CN})_6^{3-}$, a relatively small difference which could be attributed to lack of complete charge cancellation within the complex. On the other hand, \bar{S}° for $\text{HFe}(\text{CN})_6^{3-}$ is much more negative, by 26 ± 3 eu, than that of $\text{Fe}(\text{CN})_6^{3-}$, and the value for $\text{H}_2\text{Fe}(\text{CN})_6^{2-}$ is even more negative than the values for the 3- species $\text{Fe}(\text{CN})_6^{3-}$ and $\text{KFe}(\text{CN})_6^{3-}$ despite its more favorable charge. This same feature appears, although to a lesser extent, in the case of the tetracyanodipyridyl complexes,⁹ where the value for $\text{HFe}(\text{CN})_4\text{dipy}^-$ is 20 eu more negative than that for $\text{Fe}(\text{CN})_4\text{dipy}^-$.

These very marked differences in \bar{S}° between the Fe(III) complex and the conjugate acid species of the Fe(II) complex with the same charge suggest there is

Table III: Partial Molal Entropies of Hexacyanoferrate Ions at 25.0°, Based on: $\bar{S}^\circ_{\text{H}^+} = 0$, $\bar{S}^\circ_{\text{K}^+} = 24.5$ eu,²³ and $\bar{S}^\circ_{\text{Fe}(\text{CN})_6^{3-}} = 64.8$ eu.²⁴ $\Delta\bar{S}^\circ$ Values Obtained from Oxidation-Reduction and Protonation Equilibria (This Work) and Ion-Association Equilibria^b

Ion	Oxidation state	\bar{S}° , eu
$\text{Fe}(\text{CN})_6^{4-}$	II	18 ± 1
$\text{Fe}(\text{CN})_6^{3-}$	III	64.8
$\text{KFe}(\text{CN})_6^{3-}$	II	56 ± 3
$\text{HFe}(\text{CN})_6^{3-}$	II	39 ± 3
$\text{KFe}(\text{CN})_6^{2-}$	III	97 ± 2
$\text{H}_2\text{Fe}(\text{CN})_6^{2-}$	II	53 ± 6

^a Reference 24. ^b Reference 1.

some crucial difference in structure, charge distribution, solvent interaction, or some combination of these factors. In the case of the hexacyanoferrate system, we proposed earlier that a H_3O^+ ion could be bonded to three cyanides at the corners of an octahedral face of the complex.²⁵ However, this structural feature alone would not account for the observation that with the tetracyanodipyridyl system the corresponding entropy difference is significantly smaller.

Presumably, in the conjugate acids the hydrogen is covalently bonded, so in these complexes the ligands are of two types, CN^- and HNC . The ligand field would thus have a lower symmetry. However, although an effect of this kind might be expected to have a marked influence in determining ΔH° , it is difficult to envisage a mechanism by which it could hold the \bar{S}° values at such low levels.

This peculiar property of the conjugate acids is not, however, restricted to the cyanoferrate complexes.

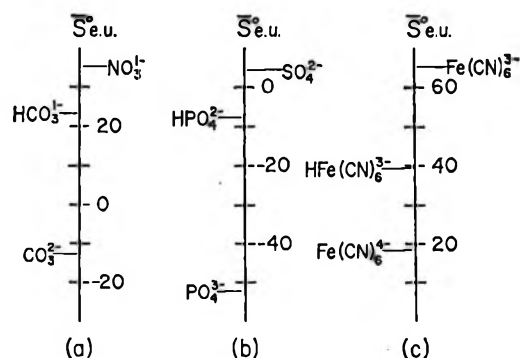


Figure 4.

(23) W. M. Latimer, "Oxidation Potentials," 2nd ed, Prentice-Hall Inc., New York, N. Y., 1952.

(24) R. H. Busey, *J. Phys. Chem.*, **69**, 3179 (1965).

(25) P. George, G. I. H. Hanania, and D. H. Irvine, *Rec. Trav. Chim.*, **75**, 759 (1956).

Latimer²³ pointed out some years ago that the entropies of conjugate acid oxyanions are smaller than those for the oxyanions having the same charge but with no hydrogen. In Figure 4, typical data for oxyanions in (a) and (b) are compared to the present data for the hexacyanoferrates in (c). $S^\circ_{\text{HCO}_3^-}$ is about 12 eu more negative than $S^\circ_{\text{NO}_3^-}$; $S^\circ_{\text{HPO}_4^{2-}}$ is about 12 eu more negative than $S^\circ_{\text{SO}_4^{2-}}$; while $S^\circ_{\text{HFe}(\text{CN})_6^{3-}}$ is about 26 eu more negative than $S^\circ_{\text{Fe}(\text{CN})_6^{3-}}$. In a consideration of the magnitude of the discrepancy in the case of the oxyanions, Connick and Powell²⁶ showed that the HO-group appears to make very little contribution to S° ; *i.e.*, to a first-approximation, species such as XO_2^- and HYO_3^- , or XO_3^{2-} and HYO_4^{2-} , etc. have the same S° . This type of comparison cannot be made in the case of the cyanoferrates because species of the type $\text{Fe}(\text{CN})_5^{3-}$ or $\text{Fe}(\text{CN})_4^{2-}$ with five and

four ligands, respectively, are unknown. Nevertheless, the discrepancy, amounting to about 26 eu, approximately twice that for the oxyanions, would be in keeping with the whole HNC- group making a relatively small contribution to S° , since HNC- has two structurally bonded atoms (in Cobble's²⁷ sense) compared to the one in HO-. In view of these similarities between the two series of ionic species, we are inclined to believe that the discrepancies originate in some common feature arising from the interaction between the conjugate acid grouping and the solvent water molecules, rather than in some special structural property of the individual conjugate acids.

(26) R. E. Connick and R. E. Powell, *J. Chem. Phys.*, **21**, 2206 (1953).

(27) J. W. Cobble, *ibid.*, **21**, 1451 (1953).

Displacement of Electron Energy Levels in Semiconductors as a Result of Interactions

by W. W. Harvey

Ledgemont Laboratory, Kennecott Copper Corporation, Lexington, Massachusetts 02173
(Received October 4, 1966)

Interactions among imperfections in semiconductors affect the occupancy of electron energy levels and lead to displacements of these levels relative to a fixed reference level. The conduction band edge and acceptor impurity levels are displaced downward and the valence band edge and donor impurity levels are displaced upward by attractive interactions. Consequently, the band gap and impurity ionization energies decrease with increasing concentration of imperfections; moreover, the rate of displacement of an ionized impurity level is considerably greater than for the neutral impurity level, so that their separation decreases rapidly. The general method for determining the contribution of interactions to the displacement of electron energy levels consists of writing a chemical equation for the occupation of the empty level by an electron or hole. This gives a relation between the electron electrochemical potential, or Fermi level, and the electrochemical potentials of the occupied and unoccupied levels. The relation is expanded in terms of concentrations and activity coefficients and compared with a corresponding expression obtained by application of Fermi-Dirac statistics to the occupancy of the given energy level. The dependence of the position of the level on the concentration-dependent activity coefficients of the chemical species constituting its occupied and unoccupied states is thereby derived.

Introduction

While it is generally recognized that the intrinsic energy gap and impurity ionization energies in semiconductors are decreased by attractive interactions between mobile charge carriers and ionized impurities, the question of the directions and relative magnitudes of the shifts of band-edge energies and impurity levels does not seem to have been treated explicitly. For example, the width of the forbidden gap would be reduced by a downward displacement of the conduction band edge \mathcal{E}_C or an upward displacement of the valence band edge \mathcal{E}_V relative to a fixed reference level of energy. It could be of value to know not only whether \mathcal{E}_C and \mathcal{E}_V are shifted to higher or lower energies, but also the concomitant displacements of impurity levels.

In a previous publication,¹ the implicit concentration dependence of \mathcal{E}_C and \mathcal{E}_V was derived by comparison of thermodynamic and Fermi-Dirac statistical expressions for the electron and hole concentrations. The expressions obtained may be written

$$\mathcal{E}_C(T, x, \psi) = \xi_C^\circ(T) - e\psi + kT \ln \gamma_n \mathfrak{N}_C / \mathfrak{N}_C^\circ \quad (1)$$

$$\mathcal{E}_V(T, x, \psi) = \xi_V^\circ(T) - e\psi - kT \ln \gamma_p \mathfrak{N}_V / \mathfrak{N}_V^\circ \quad (2)$$

where T denotes absolute temperature, ψ the (macroscopic) electrostatic potential, and x represents concentration dependence. $\gamma_n(T, x)$ and $\gamma_p(T, x)$ are the chemical activity coefficients of electrons and holes and $\mathfrak{N}_C(T, x)$ and $\mathfrak{N}_V(T, x)$ are the effective densities of states in the conduction band and valence band, respectively. $\mathcal{E}_C^\circ(T, \psi) \equiv \xi_C^\circ(T) - e\psi$ and $\mathfrak{N}_C^\circ(T)$ are the limiting values of \mathcal{E}_C and \mathfrak{N}_C at extremely low concentrations of carriers, impurities, and other imperfections and $\mathcal{E}_V^\circ(T, \psi) \equiv \xi_V^\circ(T) - e\psi$ and $\mathfrak{N}_V^\circ(T)$ are the corresponding limits of \mathcal{E}_V and \mathfrak{N}_V .

It is shown below that attractive interactions lead to a simultaneous downward displacement of \mathcal{E}_C and upward displacement of \mathcal{E}_V . Moreover, an extension of the treatment developed in the previous paper gives

(1) W. W. Harvey, *Phys. Chem. Solids*, **23**, 1545 (1962).

precise expressions for the displacements of various impurity levels in terms of the concentration-dependent activity coefficients of the chemical species constituting the occupied and unoccupied levels. Briefly, the procedure consists of writing a chemical equation to represent the occupation of the empty level by an electron or hole. This gives an equilibrium relation between the electron electrochemical potential $\zeta \equiv \zeta_n$ or Fermi level ε_F and the electrochemical potentials

$$\zeta_i \equiv \mu_i + z_i e \psi = \mu_i^\circ + kT \ln c_i \gamma_i + z_i e \psi \quad (3)$$

and hence concentrations c_i and activity coefficients γ_i of the occupied and unoccupied levels. From a comparison of the equilibrium thermodynamic relation with a corresponding expression obtained by application of Fermi-Dirac statistics to the occupancy of the impurity level, the desired functional variation of its energy can be deduced.

Interactions and Imperfections

The electrons and lattice ions of a perfect crystal interact, but the effects of their interactions are fully accounted for by particulars of the band theory.² The interactions of concern here are primarily those among imperfections, *viz.*, electrons in normally empty bands, holes in normally filled bands, impurity atoms and ions, and lattice defects. These "chemical" interactions may, especially at high concentrations, modify the interactions between imperfections and the lattice and contribute, for example, to changes in the effective masses of the carriers.³ The primary interactions, together with the modifications they induce, determine the magnitudes of the chemical activity coefficients of the imperfections; their effect on the effective densities of states is superposed upon that of an inherently nonquadratic form of the energy-wave vector relation $\varepsilon(\mathbf{k})$.

In addition to the chemical interactions, electrons and holes are subject to repulsive interactions, which may be called "quantum statistical." These are due to quantum attributes, especially indistinguishability and the Pauli exclusion principle, not common to Boltzmann and Fermi-Dirac statistics. The quantum statistical interactions determine the values of the quantities f_n and f_p in the expressions¹

$$nf_n = \mathcal{N}_C \exp[(\varepsilon_F - \varepsilon_C)/kT] \quad (4)$$

and

$$pf_p = \mathcal{N}_V \exp[(\varepsilon_V - \varepsilon_F)/kT] \quad (5)$$

Three effects contributing to displacements of electron energy levels can thus be formally identified (Table I).

Table I: Effects Contributing to Displacements of Electron Energy Levels

"Chemical" (including electrostatic) interactions	Pertain to imperfections generally, determine γ 's, contribute to $\delta\mathcal{N}_C$ and $\delta\mathcal{N}_V$, affect occupancy and position of electron energy levels generally
Quantum statistical interactions	Pertain to electrons and holes, determine f_n and f_p , affect occupancy but not position of ε_C and ε_V
Nonquadratic form of $\varepsilon(\mathbf{k})$	Pertains to electrons and holes, contributes to $\delta\mathcal{N}_C$ and $\delta\mathcal{N}_V$, affects occupancy and position of ε_C and ε_V

Chemical Activity Coefficients

Considering individual imperfections as particles of solute, each γ_i approaches unity as the *total* concentration of imperfections becomes very small. At finite concentrations the change in free energy $\Delta F_{T,V}$ for a chemical reaction involving imperfections deviates from the value it would have in the absence of chemical interactions by an amount

$$\delta\Delta F = kT \sum \nu_i \ln \gamma_i \quad (6)$$

where the ν 's are the coefficients, negative for reactants, in the chemical equation. The deviation of ΔF from its ideal value may also be written

$$\delta\Delta F = 1/2 \sum \nu_i w_i \quad (7)$$

where w_i is the energy of the resultant interaction between an imperfection of the *i*th kind and the assemblage of imperfections. The factor $1/2$ prevents counting each interaction twice.

For imperfections with a net charge $z_i e$, the interaction energies may be written

$$w_i = z_i e \psi_i' \quad (8)$$

where ψ_i' is the potential of the resultant field of all of the imperfections but one, which acts on the one. For free carriers and ionized shallow impurities in germanium⁴ and silicon,⁵ ψ_i' can be approximated by the Debye-Hückel screened coulombic potential, $-z_i e \kappa / \varepsilon(1 + \kappa a)$.⁶ In the following development, ψ_i' is as-

(2) L. Pincherle, *Proc. Intern. School Phys. "Enrico Fermi"* (Varenna, Italy), **22**, 3 (1963).

(3) V. L. Bonch-Bruевич and A. G. Mironov, *Soviet Phys. Solid State*, **3**, 2194 (1962).

(4) W. W. Harvey, *Phys. Rev.*, **123**, 1666 (1961).

(5) W. W. Harvey, *Proc. Intern. Conf. Semicond., Paris, 1964*, 839 (1964).

sumed to be opposite in sign (net attraction) and approximately proportional to the charge $z_i e$ on the imperfection. The symbol ψ' without subscript denotes the magnitude of an average interaction potential for singly charged imperfections.

Displacement of the Band Edges

In some earlier literature, the energy of exciting an electron from the level ε_V to the level ε_C (*i.e.*, the width of the forbidden gap $\Delta\varepsilon_G \equiv \varepsilon_C - \varepsilon_V$) was considered to differ from its value $\Delta\varepsilon_G^\circ$ in the absence of interactions by an amount $e\psi_n'$, defined as above. Equations 1, 2, and 6-8 reveal that an approximation is involved. Thus, if the concentration dependence of \mathfrak{N}_G and \mathfrak{N}_V can be neglected, consistent with the effective-density-of-states formulation⁷ leading to eq 4 and 5, the band-edge energies are displaced according to

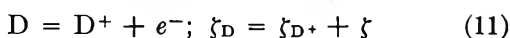
$$\varepsilon_C = \varepsilon_C^\circ + \frac{1}{2}(-e\psi_n') \approx \varepsilon_C^\circ - \frac{1}{2}e\psi' \quad (9)$$

$$\varepsilon_V = \varepsilon_V^\circ - \frac{1}{2}(+e\psi_p') \approx \varepsilon_V^\circ + \frac{1}{2}e\psi' \quad (10)$$

The variation in the width of the gap is determined only in part by the interaction of the electron with its "atmosphere" of imperfections, the remainder being determined by the interaction of the hole. In general, the displacement of an electron energy level involves both the unoccupied and occupied conditions. The important point to make now is that attractive interactions result in a simultaneous downward displacement of ε_C and upward displacement of ε_V , relative to a fixed reference level (Figure 1a).

Displacement of Impurity Levels

For the ionization of a donor impurity



the electron electrochemical potential may be formulated as

$$\zeta = \zeta_D - \zeta_{D^+} = \mu_D^\circ - \mu_{D^+}^\circ + kT \ln (c_D/c_{D^+})(\gamma_D/\gamma_{D^+}) - e\psi \quad (12)$$

with $kT \ln \gamma_D/\gamma_{D^+} = \frac{1}{2}(w_D - e\psi_{D^+}')$. The activity coefficient of the neutral donor atom is difficult to evaluate, but if the interactions are predominantly electrostatic, γ_D is probably close to unity up to reasonable concentrations of neutral donors c_D . Hence, $kT \ln \gamma_D/\gamma_{D^+}$ will be approximately equal to $+\frac{1}{2}e\psi'$.

Randomly distributed impurities will introduce impurity levels covering a range of energies. If the range is sufficiently narrow, as might be expected in the absence of association and clustering, the occupancy will approximate that of a single, N_D -fold degenerate level situated at the mean level of energy ε_D . In this cir-

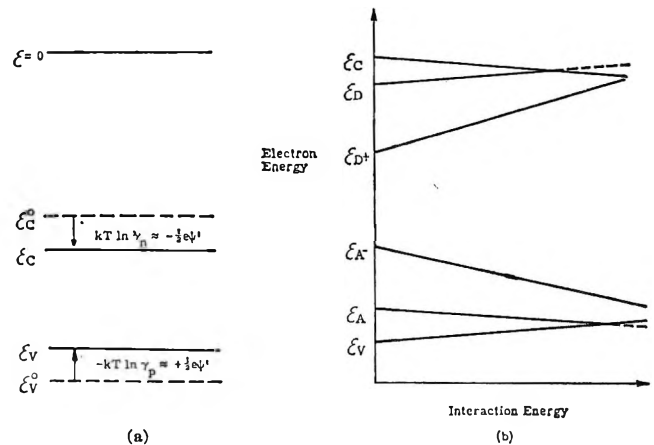


Figure 1. (a) Displacement of band-edge energies; (b) variation of electron energy levels with interaction energy.

cumstance, the concentration of occupied donor levels will be given by the usual expression

$$c_D = N_D / \{1 + (\frac{1}{2}g_D) \exp[(\varepsilon_D - \varepsilon_F)/kT]\} \quad (13)$$

where $N_D = c_D + c_{D^+}$ is the donor concentration. The preexponential factor $\frac{1}{2}$ makes allowance for the occupation of an empty donor level by an electron with either sign of spin⁸ and g_D is the statistical degeneracy of the ground-state donor level.⁹

Equation 13 can be rearranged to

$$\varepsilon_F = \varepsilon_D - kT \ln 2g_D + kT \ln c_D/c_{D^+} \quad (14)$$

where $(N_D/c_D) - 1$ has been replaced by c_{D^+}/c_D . Note that use of Boltzmann statistics not only introduces no simplification, but actually leads to an incorrect result, giving c_D/N_D rather than c_D/c_{D^+} in the logarithm.

By equating ζ and ε_F , which are identical¹⁰ if measured from the same reference level, the following functional dependence of the donor energy level is obtained

$$\begin{aligned} \varepsilon_D(T, x, \psi) &= \xi_D^\circ(T) - e\psi + kT \ln \gamma_D/\gamma_{D^+} \quad (15) \\ &= \varepsilon_D^\circ(T, \psi) + \frac{1}{2}(w_D - e\psi_{D^+}') \approx \\ &\quad \varepsilon_D^\circ + \frac{1}{2}e\psi' \quad (15a) \end{aligned}$$

Equation 15 follows from the consideration that the standard chemical potentials μ_D° and $\mu_{D^+}^\circ$ are functions of temperature only (eliminating pressure as a possible variable). The donor level is thus displaced

(6) P. Debye and E. Hückel, *Physik. Z.*, **24**, 185 (1923).

(7) R. A. Smith, "Semiconductors," Cambridge University Press, Cambridge, 1959, p 77.

(8) See ref 7, p 88.

(9) T. H. Geballe, "Semiconductors," N. B. Hannay, Ed., Reinhold Publishing Corp., New York, N. Y., 1959, pp 338, 340.

(10) N. B. Hannay, ref 9, p 26.

Table II: Displacement of Energy Levels Relative to a Fixed Reference Level

Energy level	Interactions	Displacement		
		Thermodynamic	Physical	Approx
ϵ_C	e^-	$kT \ln \gamma_n$ ($+kT \ln \mathcal{N}_C/\mathcal{N}_C^\circ$)	$-1/2e\psi_n'$	$-1/2e\psi'$
ϵ_D	D, D^+	$kT \ln \gamma_D/\gamma_{D^+}$	$1/2(w_D - e\psi_{D^+})$	$+1/2e\psi'$
ϵ_{D^+}	D^+, D^{2+}	$kT \ln \gamma_{D^+}/\gamma_{D^{2+}}$	$1/2(e\psi_{D^+}' - 2e\psi_{D^{2+}})$	$+3/2e\psi'$
ϵ_{A^-}	A^-, A^{2-}	$kT \ln \gamma_{A^{2-}}/\gamma_{A^-}$	$1/2(-2e\psi_{A^{2-}}' + e\psi_{A^-}')$	$-3/2e\psi'$
ϵ_A	A, A^-	$kT \ln \gamma_A/\gamma_{A^-}$	$-(1/2e\psi_{A^-}' + w_A)$	$-1/2e\psi'$
ϵ_V	e^+	$-kT \ln \gamma_p$ ($-kT \ln \mathcal{N}_V/\mathcal{N}_V^\circ$)	$-1/2e\psi_p'$	$+1/2e\psi'$

upward by attractive interactions involving the positively charged donor ion.

A similar treatment applies to acceptor impurities, for which

$$A = A^- + e^+; \quad \zeta_A = \zeta_{A^-} + \zeta_p \quad (16)$$

so that

$$\zeta = -\zeta_p = \mu_{A^-}^\circ - \mu_A^\circ + kT \ln (c_{A^-}/c_A)(\gamma_{A^-}/\gamma_A) - e\psi \quad (17)$$

The concentration of singly ionized acceptor levels is given by an expression of the same form as eq 15 except that the spin factor becomes 2 rather than $1/2$

$$c_{A^-} = N_A / \{1 + (2/g_A) \exp[(\epsilon_A - \epsilon_F)/kT]\} \quad (18)$$

or

$$\epsilon_F = \epsilon_A - kT \ln (g_A/2) + kT \ln c_{A^-}/c_A \quad (19)$$

Thus, the energy of an acceptor level varies as

$$\begin{aligned} \epsilon_A(T, x, \psi) &= \epsilon_A^\circ(T) - e\psi + kT \ln \gamma_{A^-}/\gamma_A \quad (20) \\ &= \epsilon_A^\circ(T, \psi) - 1/2(e\psi_{A^-}' + w_A) \approx \\ &\quad \epsilon_A^\circ - 1/2e\psi' \quad (20a) \end{aligned}$$

corresponding to a downward shift of the acceptor level.

Displacements of impurity levels and band-edge energies with increasing energy of interaction are shown schematically in Figure 1b and catalogued in Table II. All of these levels vary as $-e\psi$ and may also exhibit an inherent variation with temperature. It is interesting that donor and acceptor levels move apart, their separation being governed by

$$\begin{aligned} \epsilon_D - \epsilon_A &= kT \ln (4g_D/g_A) + \\ &\quad kT \ln (c_{D^+}/c_D)(c_{A^-}/c_A) \quad (21) \end{aligned}$$

Extension of this treatment to multiple ionization of impurities will merely be indicated. Successive stages of ionization should be formulated separately as, for example, selenium in germanium, $Se = Se^+ +$

e^- and $Se^+ = Se^{2+} + e^-$, consistent with a separation of the levels for the neutral and the singly ionized impurity. However, the displacement of the level of the singly ionized impurity as a result of interactions will be greater than for the level of the neutral impurity, owing to the greater charge of the unoccupied level. Where the interaction potentials are of the Debye-Hückel screened variety, the factor is 3 (Table II). Consequently, the separation of neutral and ionized impurity levels should decrease rapidly with concentration (Figure 1b).

Discussion

The treatment given above may not apply quantitatively to certain problems of technological importance, notably semiconductors at temperatures giving high intrinsic concentrations of carriers (*i.e.*, low-gap materials at ordinary temperatures and higher gap materials at elevated temperatures¹¹) and heavily doped semiconductors, such as are employed in lasers and tunnel diodes. The basic assumptions become untenable for very high-impurity contents; for example, the treatment ignores the spreading of the impurity ground-state energies and the tailing of the band edges, the existence of excited states, limitations in the applicability of Fermi-Dirac statistics, and non-parabolicity of the energy bands.

A random spacial distribution would result in a spread of impurity states giving, in effect, an impurity band. The proper density-of-states function would then have to be formulated in order to calculate occupancies. The neglect of excited impurity states lying between the ground state and the conduction and valence band edges could be serious; the band edges themselves undoubtedly become smeared at high doping levels. Fermi-Dirac statistics should still apply, provided that the electron energy levels in the distribution undergo identical displacements as a result of the interactions.

(11) F. J. Morin and J. P. Maita, *Phys. Rev.*, **94**, 1525 (1954).

On the other hand, for distinctly nonparabolic energy bands, the quantum statistical and the chemical contributions to the activity coefficients are not separable as is implied in eq 4 and 5.

In view of the indicated deficiencies of the treatment, only qualitative significance can be attached to the extrapolation of calculated energy level displacements to points of crossover, as in Figure 1b. (In the case of electrically active impurities, crossover corresponds to complete ionization; in the case of free carriers, to transition from semiconducting to metallic behavior.) However, solid-state physicists are making great strides in formulating and estimating the effects mentioned, and the treatment provides a framework for transposing their results into a thermodynamic formulation.

The principal conclusion drawn from this work should be broadly valid: attractive interactions displace the relevant electron energy levels in the directions indicated, leading to an increase in the degree of ionization of impurities and, eventually, to overlapping of impurity levels and band edges.

The approach to metallic behavior is a consequence of a net attractive interaction experienced by the free carriers. While statistical degeneracy may set in at high concentrations of imperfections, it is not a causative factor. On the contrary, the exclusion principle operates in opposition to attractive interactions among the carriers and other imperfections.

Appendix

Proof That the Displacements of ϵ_C and ϵ_V Are Opposed. It can be shown that of three possible sets of displacements which diminish the intrinsic gap by

approximately $e\psi'$, only that can occur whereby ϵ_C is decreased by $ye\psi'$ and ϵ_V is increased by $(1-y)e\psi'$, with $y \approx 1/2$. Thus, if the edge of the conduction band is shifted to the higher energy $\epsilon_V^\circ + \alpha$ and the edge of the valence band is shifted simultaneously to the higher energy $\epsilon_V^\circ + (\alpha + e\psi')$, the sum $\epsilon_C + \epsilon_V$ will be increased by $2\alpha + e\psi'$. If the shifts are to the lower energies $\epsilon_C^\circ - (\beta + e\psi')$ and $\epsilon_V^\circ - \beta$, the sum will be decreased by $2\beta + e\psi'$.

However, comparison of the expression

$$2\epsilon_F = \epsilon_C + \epsilon_V + kT \ln (n/p)(f_n/f_p) - kT \ln \mathcal{N}_C/\mathcal{N}_V \quad (22)$$

obtained by combining eq 4 and 5, with its thermodynamic equivalent

$$2\zeta = \mu_n^\circ + \mu_p^\circ - 2e\psi + kT + \ln (n/p)(f_n/f_p) + kT \ln \gamma_n/\gamma_p \quad (23)$$

reveals that $\epsilon_C + \epsilon_V$ varies as $kT \ln \gamma_n/\gamma_p$. Equation 23 is obtained by applying the equilibrium condition $\zeta_n = -\zeta_p$ to eq 3 for electrons and holes. For predominantly electrostatic interactions, the activity coefficients of singly charged species would be comparable in magnitude, so that the ratio γ_n/γ_p will be close to unity. (Actually, as shown in ref 12, γ_p includes the activity of the semiconductor; this latter will be given closely enough by the mole fraction for most cases of interest.) Accordingly, the permissible change of $\epsilon_C + \epsilon_V$ is not $2\alpha + e\psi'$ or $-2\beta - e\psi'$, but $1/2(-e\psi_n') - 1/2e\psi_p' \approx 0$.

(12) W. W. Harvey, *Phys. Chem. Solids*, **24**, 701 (1963).

The Kinetics and Mechanism of Fluorination of Copper Oxide. II.

The Reaction of Fluorine with Copper(I) Oxide¹

by Robert L. Ritter

Technical Division, Oak Ridge Gaseous Diffusion Plant, Union Carbide Corporation, Oak Ridge, Tennessee

and Hilton A. Smith

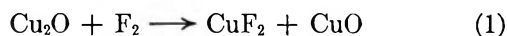
Department of Chemistry, The University of Tennessee, Knoxville, Tennessee (Received October 5, 1966)

The kinetics and mechanism of the reaction of fluorine with Cu₂O powders have been investigated at temperatures between 152.0 and 207.4° and at fluorine pressures between 50 and 800 mm. The Cu₂O powders were relatively uniform and had specific surface areas ranging from 6.5 to 29.3 m²/g. The reaction occurred by means of a two-step mechanism given by the reactions Cu₂O + F₂ → CuF₂ + CuO and CuO + F₂ → CuF₂ + 1/2O₂. The first of these two reactions was shown to obey the linear kinetic law. Possible mechanisms to explain the observed pressure and temperature dependence are advanced.

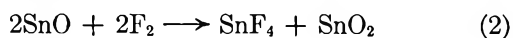
Introduction

The kinetics and mechanism of the reaction of fluorine with CuO powders have been previously investigated and the results were presented in part I of this paper.^{2a} As a continuation of this work, the kinetics and mechanism of the fluorination of Cu₂O powders have been investigated.

The reaction of fluorine with Cu₂O has been qualitatively studied by Haendler, *et al.*^{2b} Copper(I) oxide powder, presumably of a relatively low specific surface area, was found to react with fluorine at temperatures between 150 and 300° with the formation of CuO and CuF₂, according to the reaction



At temperatures above 300°, the CuO reacted to form additional CuF₂. Haendler, *et al.*,³⁻⁶ have also investigated qualitatively the reaction of fluorine with a series of metals and their oxides, including CdO, ZnO, NiO, TiO₂, ZrO₂, V₂O₅, SnO, and SnO₂. It is interesting to note that they report the reaction of fluorine with SnO to be similar to that between fluorine and Cu₂O. At temperatures between 200 and 300°, the reaction products were identified as SnF₄ and SnO₂, presumably formed by the reaction



Above 300°, the SnO₂ underwent further reaction to yield additional SnF₄.

Experimental Section

Copper(I) Oxide Preparation. The method employed for preparation of Cu₂O powders was a modification of a method suggested by the work of James⁷ in which he investigated the influence of aging on the reactivity of certain precipitates. He precipitated Cu(OH)₂ by mixing solutions of CuCl₂ and NaOH and then, after various aging periods, added hydroxylamine to the slurry and measured the rate of reduction by the rate of color change of the precipitate. In one run, the hydroxylamine was added to the NaOH solution prior to mixing with the CuCl₂ solution and in this case an immediate yellow precipitate of Cu₂O was obtained

(1) This document is based on work performed at the Oak Ridge Gaseous Diffusion Plant operated by Union Carbide Corp. for the U. S. Atomic Energy Commission.

(2) (a) R. L. Ritter and H. A. Smith, *J. Phys. Chem.*, **70**, 805 (1966); (b) H. M. Haendler, L. H. Tawle, E. F. Bennett, and W. L. Patterson, Jr., *J. Am. Chem. Soc.*, **76**, 2178 (1954).

(3) H. M. Haendler and W. J. Bernard, *ibid.*, **73**, 5218 (1951).

(4) H. M. Haendler, *et al.*, *ibid.*, **74**, 3167 (1952).

(5) H. M. Haendler, *et al.*, *ibid.*, **76**, 2177 (1954).

(6) H. M. Haendler, *et al.*, *ibid.*, **76**, 2179 (1954).

(7) T. H. James, *J. Phys. Chem.*, **46**, 1068 (1942).

when the solutions were mixed. Attempts were made during the present investigation to reproduce these results, but in every case an initial black precipitate of CuO was obtained which was then rapidly reduced to Cu_2O .

To prevent the intermediate formation of CuO , the technique was modified as follows. A solution of hydroxylamine hydrochloride and CuCl_2 with a molar ratio of 6.1:1, respectively, was prepared. Concentrated NaOH was added to a pH of 6.2. During this addition, the solution at first turned dark blue, characteristic of the tetraamminecopper(II) complex ion, $\text{Cu}(\text{NH}_3)_4^{2+}$. Evidently the analogous complex with hydroxylamine, $\text{Cu}(\text{NH}_2\text{OH})_4^{2+}$, was formed. Further NaOH addition caused this blue color to fade, the final solution being colorless and evidently containing the hydroxylaminecopper(I) complex ion analogous to the colorless tetraamminecopper(I) complex ion, $\text{Cu}(\text{NH}_3)_4^+$. This colorless solution was then rapidly mixed with an equal volume of dilute NaOH , resulting in the formation of an immediate yellow precipitate of Cu_2O . This precipitate was recovered by filtering, drying at 110° under vacuum, and pulverizing with a mortar and pestle.

Early in the investigation it was found that exposure of small particle size Cu_2O powder to air resulted in the oxidation of the particle surfaces to CuO . Accordingly, the above described precipitation and processing of the Cu_2O powders were performed under a nitrogen atmosphere in a Lucite glove box.

Control of the particle size of the precipitated Cu_2O was achieved by varying the concentration of the dilute NaOH solution and/or the digestion time between precipitation and final processing of the slurry. The particle size was increased by employment of more dilute NaOH and by utilization of longer digestion periods.

Each Cu_2O powder sample was sintered under vacuum at 300° for 1 hr prior to being employed in any of the kinetic investigations. During this sintering treatment, a thin layer of CuO of between 5 and 10 Å thickness was formed on the surface of the Cu_2O particles. Since the fluorine pretreatment to which the powders were subjected, as described in a later section, was more than sufficient to convert this thin film of CuO to CuF_2 , it appears that the presence of this CuO film on the Cu_2O particles was not deleterious to the results of the kinetic investigations.

Using the above described techniques, a series of five Cu_2O powders was prepared. The experimental conditions employed and the specific surface areas of the resulting powders, as determined by the nitrogen BET method, are summarized in Table I; the particles were

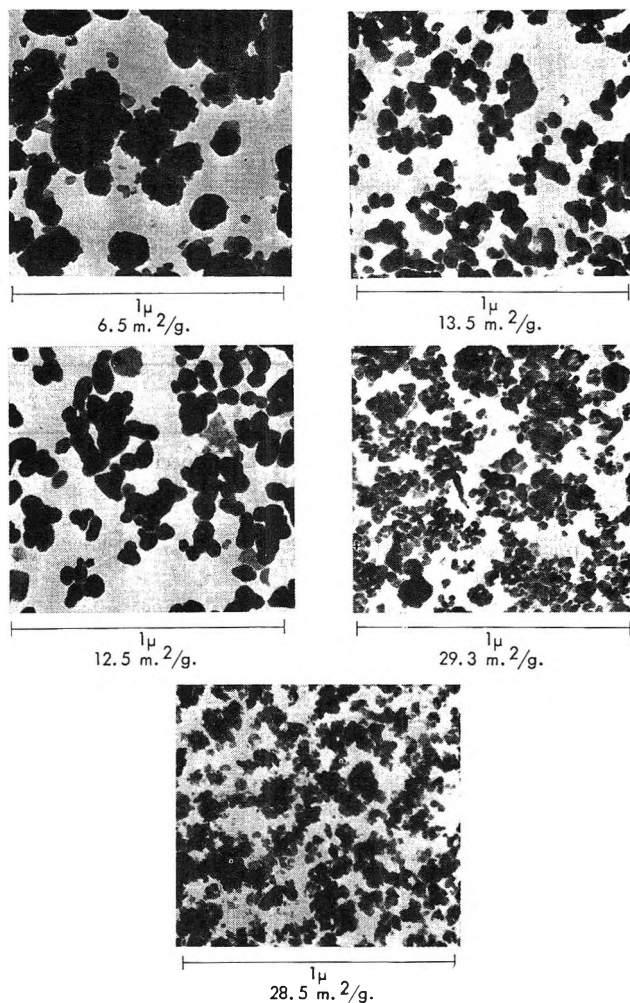


Figure 1. Cu_2O powder samples.

relatively uniform in size and approximated a spherical geometry. Electron micrographs of the five samples are presented in Figure 1.

Determination of Initial Particle Radii. During the drying and fluorine pretreatment procedures described below, the powder samples exhibited a decrease in specific surface area. If the drying treatment was rapid, the surface area change occurred during the drying with little further change during fluorine pretreatment. If the drying treatment was very slow, no surface area change was observed; however, the surface area then decreased during the fluorine pretreatment, even when this pretreatment was performed very slowly over a 4-day period. The total change in surface area was the same in each case. This surface area decrease was probably partially caused by agglomeration of the particles by a sintering mechanism, but it is believed that most of the change was the result of a smoothing of the particle surface. It was noted earlier

Table I: Conditions Employed for Preparation of Copper(I) Oxide Powders

CuCl ₂	Concn after mixing, <i>M</i>		Digestion time before processing	Specific surface area, m ² /g	Sintering temp, °C	Specific surface area after sintering, m ² /g
	NH ₂ OH	NaOH				
0.050	0.305	0.050	4 days	6.61	310	6.5
0.050	0.305	0.050	1 day	15.6	300	13.5
0.050	0.305	0.075	6 hr	...	280	29.3
0.050	0.305	0.050	1 day	14.7	300	12.5
0.050	0.305	0.090	8 hr	...	300	28.5

Table II: Comparison of Initial and Final Specific Surface Area

Specific surface area of initial powder sample, m ² /g	Fractional conversion to CuF ₂	Final specific surface area, m ² /g	Final average particle radius, Å	Calculated initial average particle radius, Å	Calculated initial specific surface area, m ² /g
6.5	0.980	5.8	1061	882	5.67
6.5	0.956	5.5	1113	928	5.39
6.5	0.959	5.9	1038	865	5.78
				Av 892	5.61
12.5	0.673	9.9	580	506	9.88
12.5	0.890	11.1	543	457	10.94
13.5	0.936	11.1	549	459	10.89
13.5	0.985	11.8	522	434	11.52
13.5	0.948	12.3	497	415	12.05
				Av 454	11.06
28.5	0.981	22.0	280	233	21.46
29.3	0.988	22.9	269	223	22.42
29.3	0.962	22.2	276	230	21.74
29.3	0.952	22.8	268	224	22.32
				Av 228	21.99

that the Cu₂O particles were coated with a thin film of CuO formed during the sintering procedure. A sample of pure Cu₂O, with a specific surface area of 21.9 m²/g, was exposed to air for 4 days during which the powder slowly turned black, indicating formation of CuO. The surface area of the oxidized sample had increased to 31.7 m²/g. Evidently, oxidation of the surface of the Cu₂O particles to CuO produced an increase in the surface roughness of the particles. Thus, the decrease in surface area during drying and fluorine pretreatment was probably caused by smoothing of the particle surfaces.

After this initial decrease in surface area during pretreatment, no significant surface area changes were observed during further reaction. The particles apparently underwent further reaction with the formation of an intact, nonporous fluoride film. This permitted the calculation of the initial particle size, *i.e.*, the particle size following pretreatment, from the mea-

sured final specific surface area, employing the equation

$$r_g = r_i(1 + cF)^{1/3} \quad (3)$$

relating the total particle radius, r_g , to the initial radius, r_i , and the fractional completion of reaction, F . The constant c is related to the coefficient of expansion of the reaction as defined in the Discussion. The results of this calculation are summarized in Table II. The calculated initial particle radii in Table II are the radii employed below to correlate the kinetic data with particle size.

Fluorine. The fluorine employed was a commercial high-purity product and was 99.3 mole % pure by analysis.

Apparatus. The kinetic data were obtained using a totally enclosed recording thermobalance. This apparatus has been outlined in the previous paper.^{2a}

Procedure. The Cu₂O powder sample, of between 0.6 and 0.7 g, was placed in the thermobalance reactor

and dried at 150° under vacuum. After cooling to room temperature, nitrogen was admitted to the reactor to a pressure of 200 mm. A few mm of fluorine was then added with the total pressure held constant at 200 mm. The fluorine diffused to the Cu₂O sample and initiated a relatively slow reaction. When the reaction rate began to decrease, additional fluorine was added. This procedure was continued until the sample was finally exposed to a flowing stream of pure fluorine.

The reactor was then evacuated and refilled to the desired pressure with pure fluorine. The temperature was then increased to the desired level and data collection was begun. When the run was completed, the reactor was evacuated, cooled, and filled with nitrogen. The resulting powder was sampled and stored in a nitrogen-filled desiccator.

Results and Discussion

Reaction Mechanism. The equations for analyzing a set of kinetic data for the reaction of a gas with solid spherical particles for obedience to linear or parabolic kinetic laws were presented in part I of this series^{2a} and are given by

$$f_L(F) = [1 - (1 - F)^{1/3}] = \frac{k_L M_O P^n}{d_O r_i} t \quad (4)$$

and

$$f_P(F) = [(c + 1) - c(1 - F)^{2/3} - (1 + cF)^{2/3}] = \frac{2k_P M_O c P^n}{d_O r_i^2} t \quad (5)$$

respectively, where F is the fractional completion of reaction, k_L and k_P are the linear and parabolic rate constants, respectively, M_O and d_O are the molecular weights and density, respectively, of the solid oxide, r_i is the initial particle radius, P is the fluorine pressure, t is the time, and c and n are constants.

The fractional completion of reaction, F , can be calculated using the equation

$$F = \frac{\Delta W}{\Delta W_{100}} \quad (6)$$

where ΔW is the observed weight change and ΔW_{100} is the theoretical weight change for complete reaction. For the reaction



eq 6 becomes

$$F = \frac{\Delta W}{0.4191 W_i} \quad (8)$$

where W_i is the initial weight of Cu₂O. The constant c is given by the equation

$$c = \beta - 1 \quad (9)$$

where β is the coefficient of expansion for the reaction given by $2M_F d_O / M_O d_F$, in which M_F and M_O are the molecular weights and d_F and d_O are the densities of the fluoride and oxide, respectively. For reaction 7, the value of c is 0.756.

When attempts were made to analyze the data using eq 4 and 5 and assuming reaction 7 as a mechanism, linear plots were not obtained. Rather, the data indicated the reaction rate to be increasing with time. A typical set of data is presented in Figure 2. Plots of the fractional completion of reaction, F , and the linear kinetic function, $f_L(F)$, are included; a plot of the parabolic kinetic function, $f_P(F)$, departed even further from linearity.

These results indicated that either an autocatalytic effect was occurring or else the proposed single-reaction mechanism was incorrect. The latter of these two choices is most feasible, especially in light of the results of Haendler, *et al.*,^{2b} given above, in which the fluorination of Cu₂O was found to involve the intermediate formation of CuO. In addition, X-ray dif-

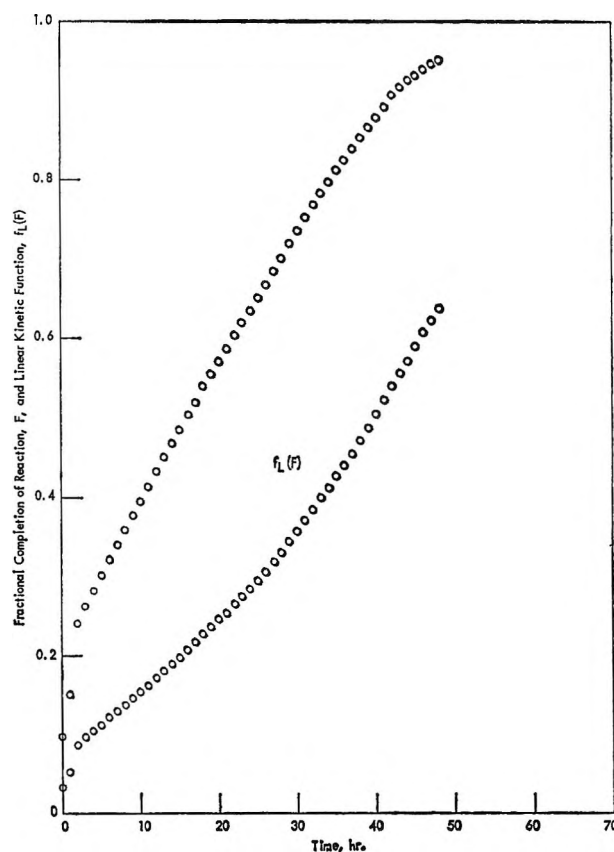


Figure 2. Fluorination rate of Cu₂O. Initial surface area, 29.3 m²/g; temperature, 171.6°; fluorine pressure, 200.0 mm.

fraction analysis of the products from the kinetic investigations indicated the presence of CuO, thus confirming the intermediate formation of this oxide.

It was not possible to derive the required analytical equations for such a two-step mechanism because of the uncertainty of the initial particle size of the CuO. Also, since fresh CuO is continually formed during the course of the reaction, the CuO particles present in the mixture will present an entire spectrum of fractional completions of reaction. Accordingly, a graphical method of data analysis was employed. For reaction 1, the fractional completion of reaction is given by

$$F_1 = \frac{\Delta W_i}{0.257W_i} \quad (10)$$

and the constant c is 0.399. Otherwise, the equations for $f_L(F)$ and $f_P(F)$ given above are unchanged. Plots of $f_L(F_1)$ and $f_P(F_1)$ were prepared, and the resulting curves were again nonlinear because of the added contribution to the observed weight change produced by the second step of the proposed mechanism. However, in the early stages of reaction before the contribution of the second step of the mechanism had become significant, the reaction rate was largely attributable to the first reaction only. Thus, by graphically constructing the initial tangent to the curve, it was possible to determine the reaction rate of the first step in the reaction mechanism.

Decision between Parabolic or Linear Kinetic Laws. The rate of reaction of fluorine with Cu₂O, as given by the first reaction in the two-step mechanism proposed above, can be obtained by a graphical analysis of the kinetic data as has been described in detail in an earlier section. The decision as to whether the reaction obeyed the linear or the parabolic kinetic law was made as follows. Plots of the linear and parabolic functions, $f_L(F_1)$ and $f_P(F_1)$, were made and the initial tangents to the resulting curves were graphically constructed. The two tangents then represented the functions $f_L(F_1)$ and $f_P(F_1)$ for the first reaction in the proposed mechanism. It was found that the premise that the reaction exhibited parabolic kinetics led to impossibilities in the late stages of reaction. As an example, consider the data given in Table III, taken from a run on the 6.5-m²/g sample. The values for the linear and parabolic functions, $f_L(F_1)$ and $f_P(F_1)$, were read from the two tangents drawn as described above. Knowing these functions, it was possible to calculate the fractional completion of the first reaction in the two-step mechanism and the corresponding weight change, ΔW_1 , attributable to this reaction. Then by subtracting ΔW_1 from the total observed weight change,

the weight change attributable to the second reaction step, ΔW_2 , was calculated. Finally, the fractional completion of the second reaction was computed. In Table III, the assumption that the first reaction obeyed the parabolic kinetic law led to the impossible conclusion that the second reaction was more than 100% complete after 80 hr. On the other hand, the assumption that the first reaction obeyed the linear kinetic law led to reasonable conclusions regarding the fractional completion of the second reaction. Results similar to those of Table III were obtained in every fluorination run. On the basis of these results, it was concluded that the initial reaction in the proposed mechanism for the fluorination of Cu₂O probably obeyed the linear kinetic law.

Temperature Dependence of the Reaction Rate. The effect of temperature on the reaction rates of the five Cu₂O samples was determined at temperatures between 152.0 and 207.4° and a fluorine pressure of 200.0 mm. A typical set of data is presented in Figure 3, in which the linear function $f_L(F_1)$ has been plotted against time and the initial tangent to the curve has been taken as

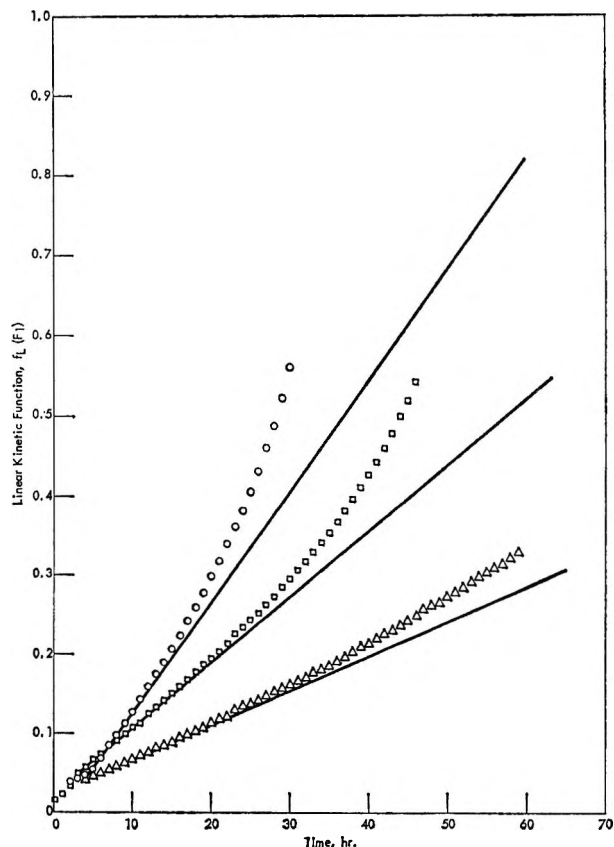


Figure 3. Effect of temperature on the fluorination rate of Cu₂O. Initial surface area, 6.5 m²/g; fluorine pressure, 200.0 mm; O, 207.4°; □, 196.0°; Δ, 183.3°.

Table III: Comparison between Linear and Parabolic Data for the 6.5-m²/g Sample

Time, hr	Observed weight gain, g	$f_L(F_1)$	Linear ΔW_1 , ^a g	Linear ΔW_2 , ^b g	Linear F_2	$f_P(F_1)$	Parabolic ΔW_1 , g	Parabolic ΔW_2 , g	Parabolic F_2
40	0.1467	0.3546	0.1275	0.0192	0.1833	0.0245	0.1024	0.0443	0.4231
50	0.1741	0.4374	0.1487	0.0254	0.2426	0.0308	0.1121	0.0620	0.5922
60	0.1987	0.5201	0.1608	0.0379	0.3620	0.0370	0.1203	0.0784	0.7488
70	0.2221	0.6029	0.1695	0.0526	0.5024	0.0433	0.1279	0.0942	0.8997
80	0.2409	0.6856	0.1753	0.0656	0.6266	0.0495	0.1348	0.1061	1.0134
90	0.2564	0.7684	0.1787	0.0777	0.7421	0.0558	0.1411	0.1153	1.1012
100	0.2689	0.8511	0.1804	0.0885	0.8453	0.0620	0.1465	0.1224	1.1691

^a ΔW_1 for total reaction = 0.1809 g. ^b ΔW_2 for total reaction = 0.1047 g.

the true linear kinetic curve for the first of the two reactions in the mechanism.

An Arrhenius plot of the logarithm of k''/r_i , where $k'' = k_L M_O P^n / d_O$, is presented in Figure 4. Also included in Figure 4 are the data, reported below, obtained during runs to investigate the effect of the fluorine pressure on the reaction rate. In these Arrhenius plots, the data on the 12.5- and 13.5-m²/g samples have been combined, as have the data on the 28.5- and 29.3-m²/g samples. These two pairs of samples were essentially identical in their properties as can be seen by reference to their descriptions above. An average activation energy of 19.74 kcal/mole was obtained at a fluorine pressure of 200.0 mm.

By using the curves of Figure 4 to calculate the values of k''/r_i at a temperature and employing the average values of r_i calculated in Table II, the data were tested for compliance to the linear kinetic law. This law states that the rate of reaction should be inversely proportional to the initial particle radius. The results are presented in Table IV. It is seen that the agreement between k'' for the three powders is not as good as might be expected and certainly not good enough to constitute a proof of obedience to the linear kinetic law.

There are two possible reasons for this poor agreement between the values of k'' for the three powders. First, the inherent inaccuracy involved in the graphical method employed introduces a relatively large uncertainty in the values of k''/r_i . This is especially true for the powders of smaller average particle radii, in which case the plot of the function $f_L(F)$ exhibits curvature after a relatively short time. As a result, only a few points near the beginning of the reaction are available from which to determine the position of the initial tangent. The early occurrence of this curvature in the data would tend to increase the slope of the apparent tangent. It is thus suggested that the

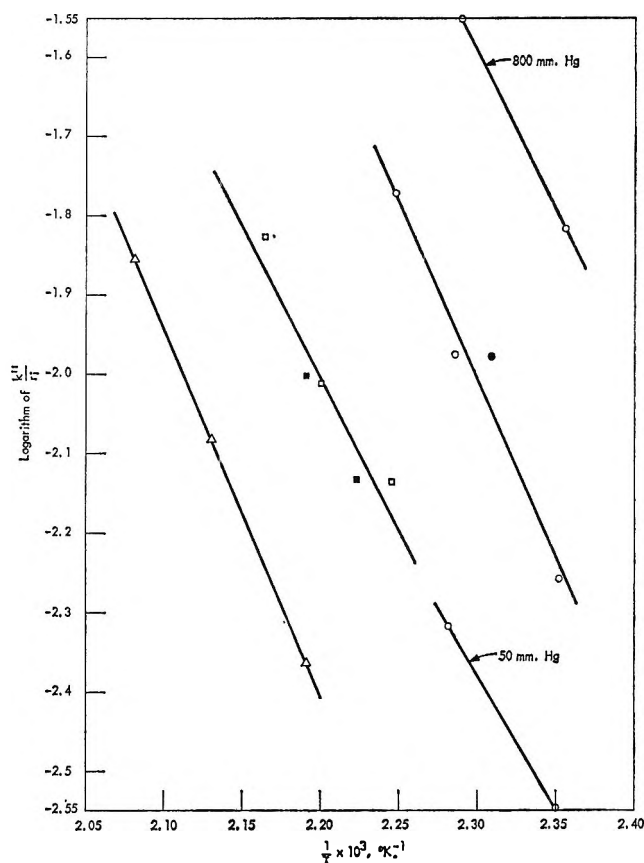


Figure 4. Arrhenius plot for the fluorination of Cu₂O. Fluorine pressure, 200.0 mm except where otherwise indicated; ○, 29.3 m²/g; ●, 28.5 m²/g; □, 13.5 m²/g; ■, 12.5 m²/g; △, 6.5 m²/g.

values of k''/r_i measured for the powders of smaller average radii may be biased high, which would account for at least part of the poor agreement in the values of k'' presented in Table IV.

A second possible source of error in the value of k'' is the initial particle radius employed in the calcula-

Table IV: Variation of Reaction Rate With Initial Particle Radius

Initial average particle radius, A	$k''/r_i, \text{hr}^{-1}$			$k'', \text{A hr}^{-1}$		
	170°	180°	190°	170°	180°	190°
892	2.153×10^{-3}	3.664×10^{-3}	6.107×10^{-3}	1.92	3.27	5.45
454	5.960×10^{-3}	9.296×10^{-3}	1.425×10^{-2}	2.71	4.22	6.47
228	1.544×10^{-2}	2.578×10^{-2}	4.219×10^{-2}	3.52	5.88	9.62

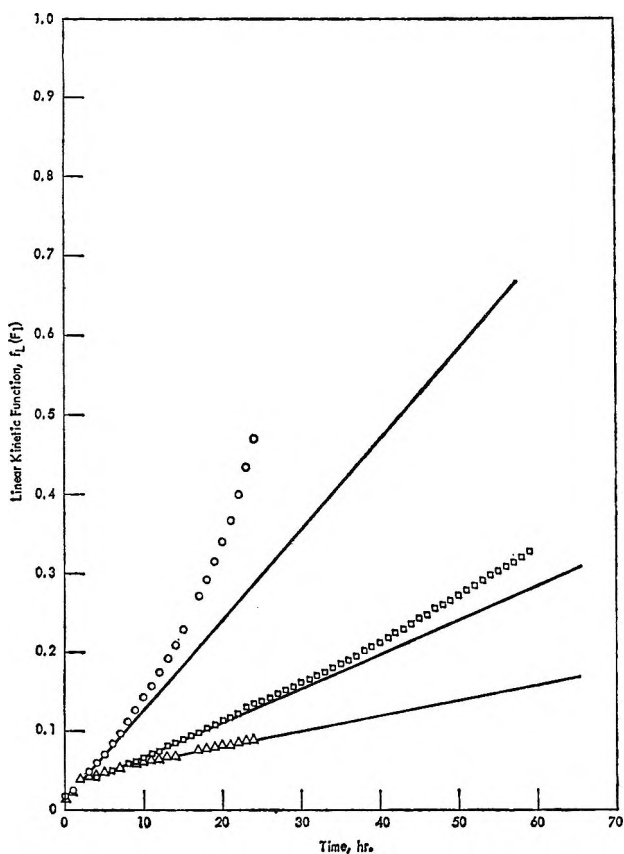


Figure 5. Effect of fluorine pressure on the fluorination rate of Cu_2O : temperature, 181.9° ; \circ , 800 mm; \square , 200 mm; \triangle , 50 mm.

tion. These initial radii were calculated from the specific surface areas of the product CuF_2 powders. The particle radius calculated from the specific surface area is biased toward the larger particles, especially when the powder exhibits as broad a particle size distribution as did these Cu_2O powders after drying and pretreatment. The extent of this error is not certain, but it could possibly explain a large amount of the disagreement in the calculated values of k'' .

Pressure Dependence of the Reaction Rate. The effect of fluorine pressure on the reaction rates of the

Cu_2O samples was studied at pressures of 50, 200, and 800 mm and temperatures of 151.9 , 164.4 , and 181.9° . A typical set of data, obtained on the $6.5\text{-m}^2/\text{g}$ sample, is presented in Figure 5. A plot of $\log k''/r_i$ vs. the log of the fluorine pressure is presented in Figure 6. Linear least-squares analysis of these data yielded an average slope for the curves of Figure 6 of 0.63. It should be noted, however, that the reaction rates measured at a fluorine pressure of 800 mm are probably biased high. This is a result of the extreme curvature of the data

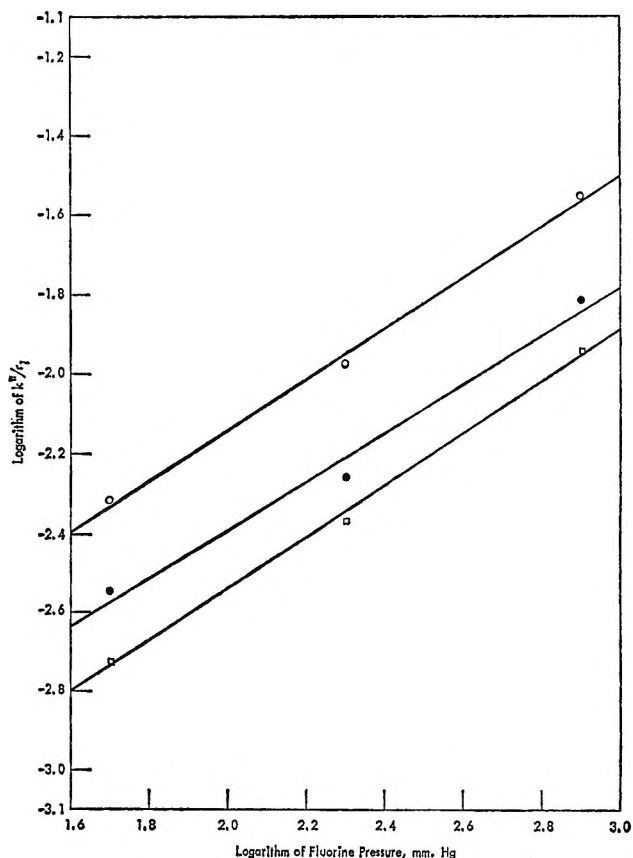
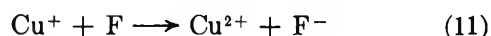


Figure 6. Variation of the fluorination rate of Cu_2O with fluorine pressure: \circ , $29.3 \text{ m}^2/\text{g}$, temperature, 164.4° ; \bullet , $29.3 \text{ m}^2/\text{g}$, temperature, 151.9° ; \square , $6.5 \text{ m}^2/\text{g}$, temperature, 181.9° .

at the higher pressure, as can be seen in Figure 5. This extreme curvature made it difficult to ascertain the proper slope of the required tangent and tended to cause the measured reaction rate to be high. It is thus suggested that the true slopes of the curves of Figure 6 are appreciably less than the measured value of 0.63 and in fact may be close to 0.5.

It was brought out in an earlier section that following the initial fluorine pretreatment, further reaction occurred with the formation of an intact, nonporous fluoride film. If such is the case and the reaction at the same time exhibits linear kinetic dependence, the rate-controlling process must be a surface reaction of some kind. The nature of this rate-controlling surface reaction can only be surmised. One of the most logical suggestions is the electron-transfer reaction which must occur, *i.e.*



in which an electron is transferred from a copper(I) ion to a fluorine atom.

A further indication that this electron-transfer reaction may be the rate-controlling step in the reaction mechanism is found in the pressure dependence of the reaction. The rate of the transfer of electrons from copper(I) ions to fluorine atoms, as given by the above reaction, would be expected to be proportional to the concentration of fluorine atoms. If the dissociation of fluorine molecules involves the equilibrium reaction



it follows directly that the concentration of fluorine atoms is proportional to the square root of the fluorine

pressure. It would then be found that the rate of reaction of fluorine with Cu_2O was proportional to the square root of the fluorine pressure, as suggested above.

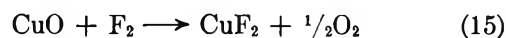
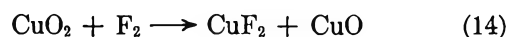
Over-all Reaction Rate Constant. Using the values of ΔH and n given above and the measured values of $k''/\tau_i = k_L M_O P^n / d_O r_i$, the final equation for the linear reaction rate constant, k_L , was

$$k_L = (2.378 \pm 0.277) \times 10^{-17} e^{-19,740/RT} \quad (13)$$

where the units of k_L are moles $\text{A}^{-2} \text{hr}^{-1} (\text{mm})^{-0.63}$.

Conclusions

The reaction between fluorine and Cu_2O powder has been shown to take place by means of a two-step mechanism given by the reactions



This two-step mechanism necessitated the employment of a graphical method of data analysis. Using this graphical method, the first reaction in the proposed mechanism was shown to obey the linear kinetic law. This was done by demonstrating that the assumption that the reaction exhibited parabolic kinetic dependence led to an impossible situation near the completion of reaction.

The reaction rate of the first reaction in the two-step mechanism was found to be proportional to the 0.63 power of the fluorine pressure. However, it is believed that this value is probably too high, and arguments have been advanced in support of a square root pressure dependence of the reaction rate.

The Kinetics and Mechanism of the Thermal Decomposition of Dimethylmercury

by C. E. Waring and Remo Pellin

Department of Chemistry, University of Connecticut, Storrs, Connecticut 06268 (Received October 20, 1966)

The kinetics of the pyrolysis of dimethylmercury have been investigated over a pressure range from 2.0 to 90.3 mm between 312 and 401.1°. The reaction is homogeneous and first order in a conditioned reaction flask. The predominant gaseous products of the decomposition are methane and ethane. Nitric oxide produces inhibition with the result that the rate of disappearance of DMM is reduced and the ethane concentration falls almost to zero. Propylene also inhibits the pyrolysis but hydrogen catalyzes it. A reaction mechanism is postulated which is in accord with the experimental results.

Introduction

A recent paper by Kallend and Purnell¹ has pointed out the lack of agreement in the experimental results obtained by various investigators² on the pyrolysis and photolysis of dimethylmercury (DMM). Here, again, the results and interpretations of these authors are not wholly in agreement with the previous papers in certain important areas.

Our study of the thermal decomposition of DMM was actually undertaken with the aim of determining the role of nitric oxide in the presence of methyl radicals. This compound was chosen because it appeared to be a simple and uncomplicated source of methyl radicals. In order to better understand the reactions of NO, propylene, and other foreign gases, it was, of course, first necessary to investigate thoroughly the kinetics and mechanism of the decomposition of DMM. The data presented here extend the work of Kallend and Purnell. In some instances our results are in agreement with theirs; in others, there appears to be no ready explanation for the wide disparity in the experimental observations.

Although many of the data presented here were obtained prior to the report of Kallend and Purnell, a number of experiments have been subsequently repeated and extended. It was thought worthwhile, therefore, to present our results in the hopes that the similarities and differences between these data and those of others may eventually lead to a complete un-

derstanding of this reaction and the effects of foreign gases on it.

Experimental Section

A. Apparatus. The rate studies were made using a static manometric system. The reaction chambers were cylindrical Pyrex tubes of 150-ml capacity. Before using, each was uniformly coated inside by a layer of carbon. The reaction flask was placed in a copper tube which in turn fitted into the well of an electric furnace. The temperature of the furnace was controlled by an electronic regulator to within $\pm 0.2^\circ$ as measured by a calibrated nitrogen-filled mercury thermometer. The temperature inside the copper tube was found to be constant to within $\pm 0.05^\circ$ over its middle 12 in. The maximum temperature variation of the furnace over a 24-hr period was $\pm 0.5^\circ$.

Because of the corrosive action of dimethylmercury on stopcock lubricants, mercury cutoff valves were employed. To prevent condensation, the vacuum

(1) A. S. Kallend and J. H. Purnell, *Trans. Faraday Soc.*, **60**, 93, 103 (1964).

(2) H. W. Thompson and M. Meissner, *Nature*, **139**, 1018 (1937); J. P. Cunningham and H. S. Taylor, *J. Chem. Phys.*, **6**, 359 (1938); J. H. Raley, F. F. Rust, and W. E. Vaughan, *J. Am. Chem. Soc.*, **70**, 88 (1948); F. P. Lossing and A. W. Tickner, *J. Chem. Phys.*, **20**, 907 (1952); K. U. Ingold and F. P. Lossing, *ibid.*, **21**, 368, 1135 (1953); L. M. Yeddapanalli, R. Srinivasan, and B. Paul, *J. Sci. Ind. Res. (India)*, **B12**, 232 (1954); C. M. Laurie and L. H. Long, *Trans. Faraday Soc.*, **51**, 665 (1955); J. Cattanaach and L. H. Long, *ibid.*, **56**, 1286 (1960).

line was wrapped in Nichrome ribbon and heated electrically to a controlled 75°.

The reaction system was evacuated by the usual techniques and before each run the reaction system was evacuated until the pressure was 10^{-5} mm or less as measured by a McLeod gage. This, together with the flaming out of the vacuum line before each run, eliminated the possibility of oxygen contamination. The gaseous reaction products were removed for analysis by means of a Toepler pump which was attached directly into the line. The analyses were made by a modified Bone-Wheeler technique, a vapor phase chromatograph, and by a mass spectrometer.

B. Material. Dimethylmercury was prepared by the method of Marvel and Gould.³ The physical constants for this preparation were bp (cor) 94.8°, N_d (22.2°) = 1.5325, and density (22.2°) = 2.9542. These values were in good agreement with those in the literature⁴ of 95°, 1.5327, and 2.95412, respectively.

Nitric oxide was prepared by the method of Johnston and Giaque.⁵ The hydrogen, nitrogen, helium, and propylene employed were Matheson Co. CP grade. The hydrogen was passed over copper oxide at 400° and through a Dry Ice trap before use. Before the propylene was introduced into the reaction chamber, it was first bubbled through dibutyl phthalate. The other gases were used without further purification.

Results

1. Nature of the Decomposition. DMM was found to decompose at a conveniently measurable rate at temperatures between 312.0 and 401.0° and at initial pressures from 2.0 to 90.3 mm to give predominantly methane and ethane.

The over-all profile of the decomposition as observed by pressure-time readings is unusual, as is seen in Figure 1. The graph shows that the pressure first increases to a maximum value, p_m , which is nearly twice that of the initial pressure, p_i . The pressure then decreases to a final pressure, p_f , which is about 40% greater than the p_i . At this point, no further decrease in pressure with time occurs. This phenomenon was observed at all eight temperatures investigated and was readily reproducible.

The formation and disappearance of this maximum is undoubtedly due to two concurrent effects. It was observed that finely dispersed mercury droplets condensed on the walls of the tubing extending from the furnace during the phase of the decomposition when the pressure was decreasing from the maximum. The other effect was a yellow translucent film which also deposited on the exit tube outside the reaction flask when the gaseous products were being evacuated.

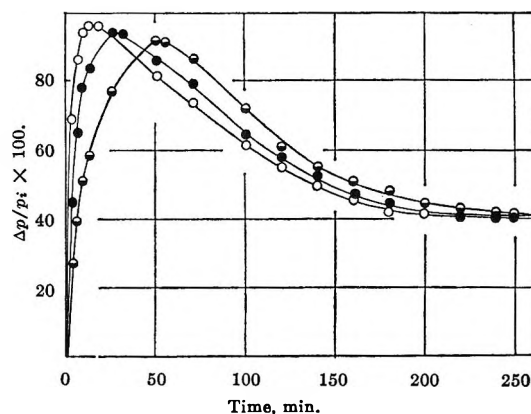


Figure 1. Pressure change with time for dimethylmercury ($p_i = 36.0$ mm) at ●, 370.0°; ●, 384.8°; and ○, 401.0°.

It seems evident, therefore, that the decomposition of DMM is complicated by the simultaneous occurrence of a condensation and polymerization process.

It should be noted in Figure 1 that at 401°, P_m is reached at approximately 20 min reaction time. Table I presents the variation of the methane and ethane concentration with time at 401°.

Table I: Partial Pressures and Mole Per Cents of CH_4 and C_2H_6 from the Decomposition of 30 mm of DMM at 401.0°

Time, sec	p_{CH_4} , mm	$p_{\text{C}_2\text{H}_6}$, mm	% CH_4	% C_2H_6
0	0	0	0	0
40	5.0	4.0	55.6	44.4
60	7.4	5.7	56.5	43.5
120	10.6	7.6	58.3	41.7
240	14.4	10.4	58.1	41.9
600	16.7	12.2	57.8	42.2
840	17.6	13.0	57.5	42.5
3,300	18.0	13.2	57.7	42.3
15,000	18.4	13.0	58.6	41.4

These data clearly show that the decomposition of DMM is essentially complete at the pressure maximum. Consequently, insofar as the formation of methane and ethane are concerned, p_m may be taken to be equivalent to the final pressure of this reaction. The subsequent decrease in pressure, then, refers to the condensation and polymerization processes which

(3) C. S. Marvel and V. L. Gould, *J. Am. Chem. Soc.*, **44**, 153 (1922).

(4) "International Critical Tables," McGraw-Hill Book Co., Inc., New York, N. Y., 1933.

(5) H. L. Johnston and W. F. Giaque, *J. Am. Chem. Soc.*, **51**, 1394 (1929).

become predominant after the decomposition is complete.

Figure 2 shows that the ratios of p_m/p_i and p_f/p_i are invariant with temperature and with initial pressures between 20 and 90.3 mm. This constancy lends additional support to the contention that the decomposition of DMM proceeds independently of the subsequent processes. The slight increase in these ratios at the lower initial pressures is probably due to the decomposition of condensation products which were found to occur at the higher pressures.

2. *Order of Reaction.* Table II presents typical data for the change of pressure with time for various initial pressures.

Table II: Change in Pressure (mm) with Time for Various Initial Pressures of DMM at 401°

<i>t</i> , sec	<i>p_i</i> , mm						
	6.0	14.5	23.5	34.7	48.0	70.2	90.3
0	0	0	0	0	0	0	0
3	0.12	0.30	0.54	0.72	0.96	1.54	1.89
5	0.20	0.49	0.84	1.21	1.63	2.38	2.97
8	0.32	0.79	1.33	1.97	2.64	3.86	4.87
10	0.40	1.00	1.66	2.39	3.26	4.70	6.05
20	0.85	2.10	3.33	4.85	6.62	9.68	12.37
30	1.27	3.10	5.02	7.14	9.69	15.16	18.96
60	2.05	4.98	8.34	12.11	16.80	24.99	31.51
90	2.62	6.38	10.78	15.92	21.88	31.66	41.17
120	3.18	7.64	12.64	18.21	25.92	38.04	48.40
150	3.50	8.48	13.81	20.29	28.32	41.41	52.82
180	3.90	9.39	15.32	22.52	31.58	45.77	58.33
210	4.14	10.03	16.45	24.46	33.84	49.14	62.93
240	4.42	10.68	17.39	25.67	35.61	51.94	66.46
270	4.56	11.23	18.35	27.10	37.44	54.47	69.71
300	4.86	11.81	19.17	28.28	39.31	57.07	73.14
360	5.14	12.60	20.18	29.84	41.71	60.23	77.38
420	5.36	13.19	21.05	30.88	43.68	62.47	80.36
480	5.58	13.70	21.85	31.92	44.88	64.58	83.25
540	5.76	13.99	22.32	32.79	45.60	65.28	84.43
600	5.88	14.28	27.70	33.13	45.88	65.98	84.88

These data were programmed on an IBM 1620 computer to solve for k_i , the initial rate constant, and n , the order of reaction, in the equation

$$\log (dp/dt)_0 = \log k_i + n \log p_i \quad (1)$$

A value of $n = 1.01$ was obtained, indicating that the order of the decomposition is unquestionably first. The linearity of the curve was further checked by computing the second-order term, which proved to be negligible. Visual evidence for the first-order kinetics of this reaction is given in Figure 3.

Table III presents typical data for the variation of

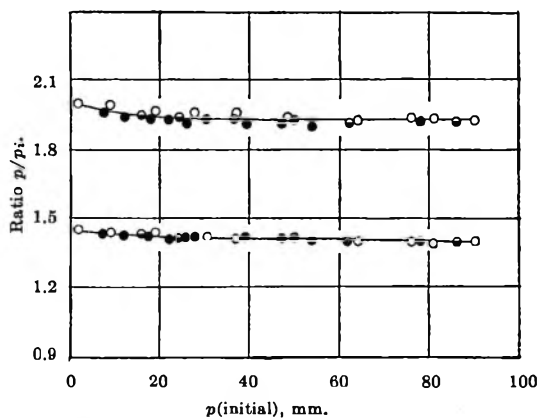


Figure 2. Ratio of the maximum pressures (upper curve) and final pressures (lower curve) to various initial pressures of DMM at 401.0° (○), 384.8° (◐), and 370.0° (●).

partial pressures of methane and ethane for various initial pressures of DMM at 401°.

These data were also programmed on the IBM 1620 computer to solve for the initial rate constant, k_i , and n , the order of reaction for both methane and ethane in eq 1. Values of $n = 0.990$ and 1.00 were obtained for methane and ethane, respectively, again indicating first-order kinetics.

3. *Energy of Activation.* A plot of the logarithms of the initial rate constants, k_i , vs. the reciprocals of the absolute temperature at eight different temperatures gave an excellent straight line, as seen in Figure 4. The activation energy was calculated by the method of least squares, and the rate constant for the thermal decomposition of DMM, expressed in terms of the Arrhenius equation, is

$$k_i = 9.04 \times 10^9 e^{-37,300/RT} \text{ sec}^{-1} \quad (2)$$

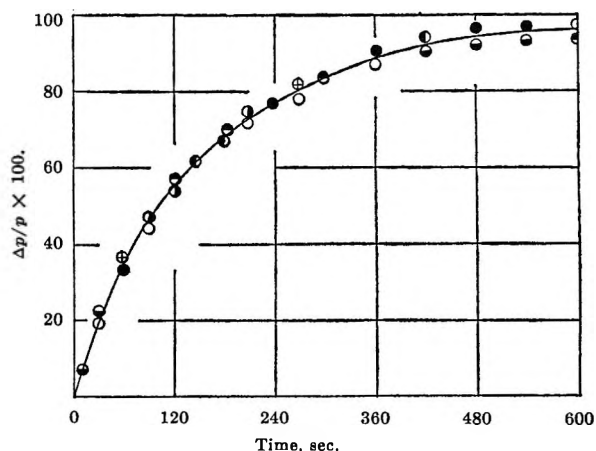
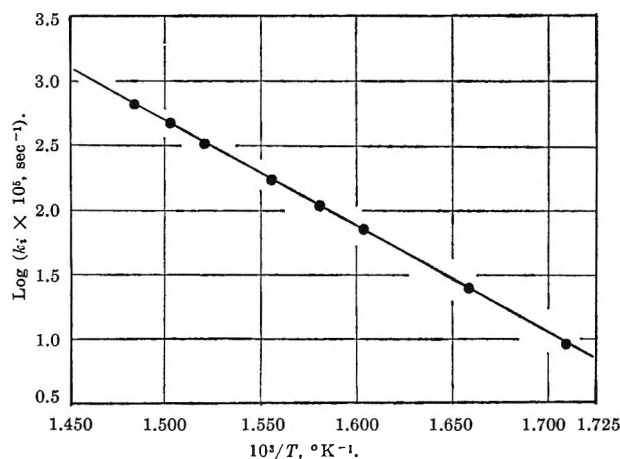


Figure 3. Pressure change with time for dimethyl mercury at 401° at initial pressures: ○, 6.0 mm; ●, 14.0 mm; ◐, 23.5 mm; ◑, 34.7 mm; ◒, 48.0 mm; ◓, 70.2 mm; ◔, 90.3 mm.

Table III: Variation of Partial Pressures of CH₄ and C₂H₆ with Time for Different Initial Pressures of DMM at 401°

<i>t</i> , sec	<i>p</i> _i , mm									
	14.5		23.5		30.0		48.0		70.2	
	CH ₄	C ₂ H ₆	CH ₄	C ₂ H ₆	CH ₄	C ₂ H ₆	CH ₄	C ₂ H ₆	CH ₄	C ₂ H ₆
0	0	0	0	0	0	0	0	0	0	0
30	1.9	1.4	3.2	2.3	4.1	2.9	6.6	4.6	9.6	8.2
60	3.5	2.4	5.7	4.1	7.4	5.7	11.8	8.3	17.8	13.3
120	5.6	3.8	8.9	6.5	10.6	7.6	18.4	12.8	26.8	19.1
180	6.5	4.5	10.5	7.6	13.4	9.4	21.4	15.0	31.3	22.3
240	7.0	5.0	11.3	8.1	14.4	10.4	23.1	16.7	33.6	24.2
360	7.5	5.5	12.2	8.9	15.6	11.4	24.9	18.3	36.4	26.6
480	7.8	5.8	12.6	9.4	16.1	12.0	25.8	19.2	38.0	27.9
600	8.1	5.9	13.1	9.9	16.7	12.2	26.7	19.5	39.2	28.5

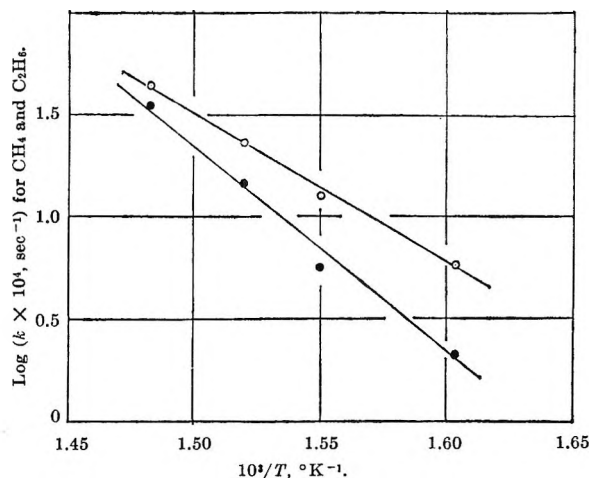
**Figure 4.** Determination of the activation energy for the thermal decomposition of dimethylmercury.

The activation energies for the decomposition of DMM as measured by the initial rate of formation of methane and ethane were also obtained. In these cases, the rate constants, k_{CH_4} and $k_{\text{C}_2\text{H}_6}$, were found by dividing the number of moles of each gas at various times, t , by the time and by the original number of moles of reactant.

Table IV gives the rate constants obtained at four different temperatures and Figure 5 presents the plots of the logarithms of these rate constants against the reciprocals of the absolute temperatures.

Table IV: Variation of the Rate Constants of CH₄ and C₂H₆ with Temperature

<i>T</i> °	$k_{\text{CH}_4} \times 10^3$ sec ⁻¹	$k_{\text{C}_2\text{H}_6} \times 10^4$ sec ⁻¹
350.5	0.621	0.215
370.0	1.22	0.538
384.8	2.36	1.45
401.0	4.30	3.36

**Figure 5.** Determination of the activation energies for the formation of methane (O) and ethane (●) during the decomposition of 30 mm of DMM.

Again, the activation energies for the formation of these two products were obtained by the method of least squares, and the rate equations are

$$k_{\text{CH}_4} = 6.84 \times 10^9 e^{-32,200/RT} \text{ sec}^{-1} \quad (3)$$

$$k_{\text{C}_2\text{H}_6} = 1.93 \times 10^{12} e^{-45,100/RT} \text{ sec}^{-1} \quad (4)$$

If these energies are weighted according to the number of moles of CH₄ and C₂H₆ present at the various temperatures, a value for the over-all activation energy is obtained that is in close agreement with that calculated from the initial rate constants, k_i .

4. *Surface Effects.* A reaction flask, identical in dimensions and volume with an unpacked bulb, was packed with 700 pieces of 3.0-mm Pyrex tubing 1.0-cm long. The surface-to-volume ratio of the unpacked bulb was 1.36/cm and that of the packed bulb was 16.7/cm. The packed flask was conditioned with a carbon coating similar to that of the unpacked flask before using. Reproducibility of results was excellent

in both flasks at all temperatures. Table V summarizes the results of runs conducted in packed and unpacked vessels at 401°. The data indicate that the thermal decomposition of DMM is homogeneous in nature.

5. *Products of Reaction.* The reaction products analyzed were methane, ethane, propane, hydrogen, ethylene, and other unsaturated hydrocarbons. Repeated analyses, employing chemical, mass spectrographic, and vapor phase chromatographic techniques, showed that the only gaseous products present to any appreciable extent were methane and ethane. Higher hydrocarbons and olefins were found to be present only to the extent of 1-2%.

Table V^a

S/V	p(DMM), mm	1/t _{12.5%}	1/t _{25%}	1/t _{50%}	p _m /p _i	p _f /p _i
1.36/cm	42.0	0.0520	0.0251	0.0092	1.95	1.42
16.7/cm	43.2	0.0528	0.0256	0.0091	1.84	1.41

^a 1/t_{x%} = reciprocal of the time for a given percentage increase over the initial pressure.

Table VI presents the gaseous products from the thermal decomposition of DMM at various time intervals. These time intervals were chosen so that the analyses were made at times corresponding to pressure increases of 25, 50, and 75% of the initial pressure. Analyses were also performed at time intervals corresponding to the pressure maximum, p_m, to a decrease in pressure to 70% above the initial pressure, and to the final pressure. By so doing, representative analyses were obtained over the curve shown in Figure 1.

It is readily apparent from the table that the agreement between the chemical and mass spectrographic analyses is good. The data further indicate that, at a

Table VI: Mole Per Cent Gaseous Products from the Decomposition of 30 mm DMM at 401.0°

Time, sec	Δp/p _i	% CH ₄	% C ₂ H ₆	% C ₃ H ₈	% C ₄ H ₁₀	% C ₄ H ₈
Chemical Analysis						
38	0.25	56.4	43.2
108	0.50	58.1	41.7
270	0.75	57.8	42.0
840	0.97	57.4	42.3
3,300	0.70	58.4	41.3
15,000	0.41	59.6	40.0
Mass Spectrograph						
108	0.50	57.8	42.0	Trace
840	0.97	58.2	41.0	1.0	2.0	2.0
15,000	0.41	59.1	40.0	1.0	1.5	1.8

given temperature, the CH₄/C₂H₆ ratio is fairly constant over the entire pressure range. There is, however, a slight increase in [CH₄] as the reaction proceeds.

The decomposition of DMM also produced two solid products. Both were evident in the glass tubing leading out of the reaction furnace. One was finely dispersed mercury droplets that appeared during the phase of the decomposition when the pressure was decreasing from the maximum. The other was a yellow, translucent film which collected on the exit tube from the reaction flask outside the furnace when the gaseous products were being pumped out. A qualitative analysis of this material showed only carbon, hydrogen, and mercury to be present. It was not established as to whether the mercury was chemically bound or merely occluded. However, in view of the fact that the substance was highly colored, the assumption that the material was an unsaturated hydrocarbon polymer seems not unwarranted. A similar polymeric substance has been reported by Laurie and Long² and Cattanach and Long² but not found under the experimental conditions employed by Kallend and Purnell.¹

6. *Effect of Nitric Oxide.* Previous investigators^{1,2} have reported that nitric oxide has little or no effect on the rate of decomposition of DMM. Contrary to their observations, we find that nitric oxide produces several marked effects on this reaction.

While nitric oxide does not change the general profile of the time-pressure curve in Figure 1, the pressure maxima, p_m, and the final pressures, p_f, were much higher in the fully inhibited reaction. For example, with 20 mm NO in the presence of 30 mm DMM at 401.0°, p_m/p_i = 2.48 and p_f/p_i = 1.70, as compared to 1.96 and 1.41, respectively, for the uninhibited reaction at the same temperature. For a given concentration of NO (30 mm) the p_m/p_i ratio decreases with increasing initial pressure of DMM above 20 mm p_i. This behavior argues that NO is not merely acting as an inhibitor but, in addition, is involved in some sort of chemical process.

In Figure 6 the ratio of the inhibited to the uninhibited rate constants is plotted as a function of the partial pressure of NO for three different initial pressures of DMM at 401.0°. It is seen that at all initial pressures of DMM, the limiting rate is attained at p_{NO} = 15 mm and that the limiting value is unchanged out to approximately 85 mm partial pressure NO. Although the extent of the maximum inhibition is only 10%, this value is constant and reproducible at all temperatures investigated.

Since inhibition curves based upon rates of pressure change are not indicative as to the mechanistic effect of

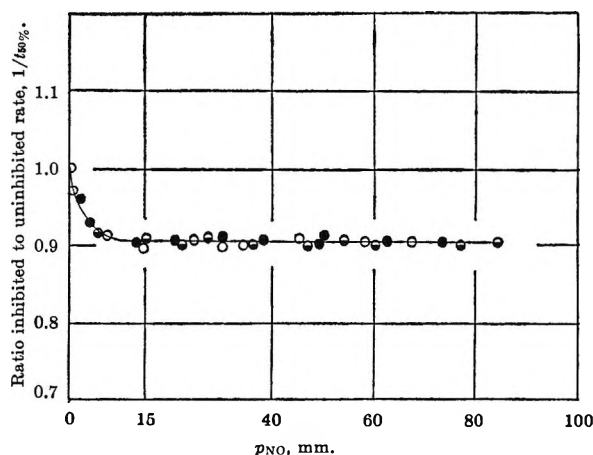


Figure 6. Retardation of decomposition rate, $1/t_{50}\%$, by nitric oxide at 401.0° for: \bullet , 15 mm; \bullet , 30 mm; \circ , 60 mm of dimethylmercury.

the inhibitor, the absolute amounts of methane and ethane were determined as a function of time for the NO-inhibited reaction. These data are presented in Table VII.

Table VII: Partial Pressures and Mole Per Cents of CH_4 and C_2H_6 from the Decomposition of 30 mm DMM in the Presence of 30 mm NO at 401.0°

Time, sec	p_{CH_4} , mm	$p_{\text{C}_2\text{H}_6}$, mm	% CH_4	% C_2H_6
0	0	0	0	0
40	4.8	0	100	0
60	7.3	0	100	0
120	10.4	0.1	99.5	0.5
240	14.4	0.4	97.3	2.7
600	17.3	0.7	96.2	3.8
1,200	20.1	0.2	99.0	1.0
1,800	20.8	1.3	94.2	5.8
3,300	21.3	1.1	95.1	4.9
7,500	21.2	1.0	95.6	4.4
12,000	21.8	0.7	97.0	3.0

A comparison of these data with those in Table I shows that nitric oxide produces two rather startling effects upon the reaction mechanism. First, it is seen that, within the limits of experimental error, the concentration of methane at any given time interval is essentially the same in both the uninhibited and inhibited reactions. This clearly indicates that the reaction producing methane is unaffected by NO. Second, in the inhibited process, the ethane concentration is reduced to zero initially and only small amounts are generated in the latter stages of the decomposition. This argues strongly for the fact that NO is effective in

completely quenching the principal ethane-producing step.

The course of the NO-inhibited reaction was also followed by making careful analyses of all the products of reaction at various time intervals from the beginning to the end of the decomposition by both chemical and mass spectrographic methods of analysis. The results are presented in Table VIII.

Table VIII: Mole Per Cent of All Gaseous Products from the Decomposition of 30 mm DMM in the Presence of 30 mm NO at 401.0°

Time, min	% NO	% CH_4	% C_2H_6	% HCN	% CO	% N_2
0.66	93.7	6.0
2.0	75.0	24.3	0.2
4.0	62.4	33.8	1.0	2.6
10	41.0	50.2	1.4	6.0	1.0	0.2
20	32.4	53.5	0.6	8.1	4.1	0.4
30	23.4	54.0	3.5	6.6	9.3	2.8
55	23.3	51.5	2.9	7.0	11.6	3.6
66.6	22.5	51.8	0.9	8.2	13.1	3.6
110	17.3	55.5	2.4	7.7	10.8	6.0
125	18.7	55.2	2.8	6.7	11.5	5.3
200	18.8	56.2	1.8	3.6	12.2	6.5
300	17.8	58.4	0.7	2.8	13.6	6.8

Water was also identified as one of the reaction products, but since a quantitative analysis for water was not possible, it was not included in the table.

A total of five mass spectrograms were made on the nitric oxide inhibited decompositions over five different time intervals from 2 to 110 min reaction time. In the early stages of the decomposition a fairly large peak was observed at mass number 45. At longer time intervals it rapidly diminished and was not observed after 20 min. From the nature of the reaction involved, it seems that the only compound that reasonably could correspond to a molecular weight of 45 would be formaldoxime, CH_2NOH , or one of its tautomers.

7. *Effect of Propylene.* Propylene was found to have a pronounced inhibiting effect on the decomposition of DMM as measured by the rate of pressure increase. This is shown in Figure 7 where the ratios of the inhibited to the uninhibited rate constants are plotted as a function of the partial pressure of propylene. In contrast to the inhibiting effect of NO, it is seen that the extent of propylene inhibition is dependent upon the partial pressure of DMM.

The p_m/p_i and p_i/p_i ratios for propylene were 1.86 and 1.28, respectively. Thus, these values differ

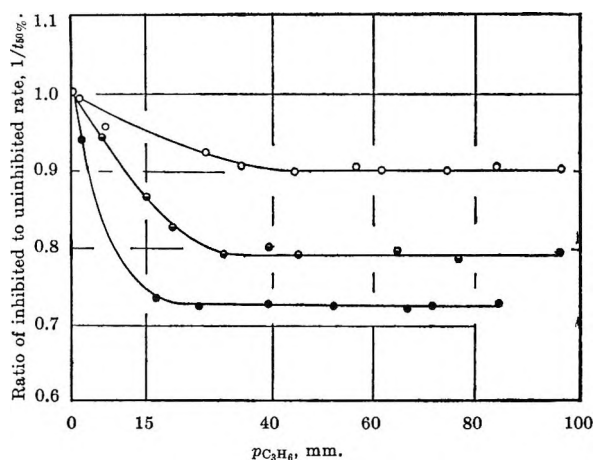


Figure 7. Retardation of decomposition rate, $1/t_{50}\%$, by propylene for 15 (●), 30 (◐), and 60 (○) mm of dimethylmercury at 401.0° .

appreciably from both the NO inhibited and uninhibited reactions.

Table IX presents the effect of propylene on the reaction products from the decomposition. These data indicate that the main effect of propylene is to reduce the concentration of ethane below that found in the uninhibited decomposition (Table I). They also suggest that the concentration of methane has been increased. Since it is known that propylene reacts with methyl radicals to form methane and allyl radicals, the true effect of propylene on the reaction's methane-producing step cannot be evaluated. The data in Table IX also emphasize the fact that propylene is a much less efficient inhibitor of the ethane-producing step than NO.

Table IX: Mole Per Cents of CH_4 and C_2H_6 from the Decomposition of 30 mm DMM in the Presence of 30 mm Propylene at 401.0°

Time, sec	Chemical analysis		Vpc		Mass spectroscopy	
	% CH_4	% C_2H_6	% CH_4	% C_2H_6	% CH_4	% C_2H_6
60	73.9	26.1	73.5	26.5
180	74.7	25.3	74.6	25.4
300	74.9	25.1	74.4	25.6	77.8	22.2
600	76.5	23.5	75.2	24.8
1200	76.9	23.1

8. *Effect of Other Foreign Gases.* In addition to nitric oxide and propylene, the effects of hydrogen, nitrogen, and helium on the decomposition of DMM were also studied. Table X compares the effect of the foreign gases on the CH_4 - C_2H_6 production, cal-

culated on the basis of the gaseous products being 100% hydrocarbons.

Table X: Effect of Foreign Gases on the Decomposition of 30 mm of DMM at 401°

Foreign gas, 30 mm	% CH_4	% C_2H_6	$\text{CH}_4/\text{C}_2\text{H}_6$
None	59.4	40.1	1.49
NO (at p_m)	98.8	1.2	82.2
C_2H_6 (at p_m)	75.2	24.8	3.04
H_2	86.8	13.2	6.57
N_2	67.6	32.4	2.08
He	77.7	22.3	3.48

These data show that while propylene, hydrogen, helium, and nitrogen cause a decrease in the amount of ethane formed, they do not reduce its concentration in the dramatic fashion of nitric oxide.

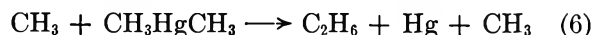
Discussion

The experimental evidence presented here indicates that DMM thermally decomposes to give essentially only methane and ethane. These results are in agreement with those of a number of investigators² who have studied this reaction both thermally and photochemically. The only other products found in the uninhibited decomposition were 1-2% of butane and butene. Attempts to find all of the products reported by Kallend and Purnell¹ were, under our experimental conditions, unsuccessful by three independent analytical techniques.

Although a number of mechanisms have been proposed for the thermal decomposition of DMM, none successfully account for all of the experimental kinetic and analytical data. Taylor and Cunningham,² for example, postulate that the ethane formed in this reaction is the result of



or possibly to

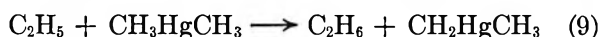
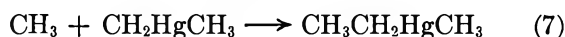


Reaction 5 cannot be defended on two important counts. First, it can be seen in Table I that the concentration of ethane in the initial stages of the decomposition is high, being nearly equal to that of methane. Since the concentration of DMM in the early stages of the reaction would be extremely high in comparison to the relatively small steady-state concentration of methyl radicals, it is difficult to understand how reaction 5 alone could account for the observed amount of

ethane, even though the activation energy for this process is zero or nearly so. The formation of ethane by reaction 6 avoids this criticism.

Second, neither reactions 5 nor 6 can account for the observed inhibition effect of nitric oxide. Table VII shows that NO reduces the ethane concentration virtually to zero while the methane concentration is essentially the same as in the uninhibited decomposition. It is obvious, therefore, that NO is not removing methyl radicals and that most of the ethane formed, at least, must be produced by a mechanism other than reactions 5 or 6.

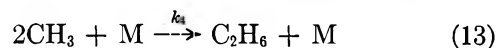
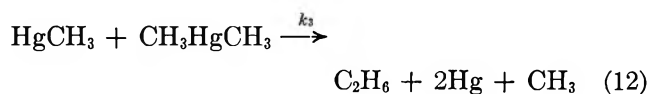
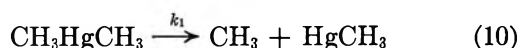
Kallend and Purnell,¹ on the other hand, have proposed that ethane is formed according to



While this mechanism can successfully account for the effect of NO on the formation of ethane, it also fails to account adequately for the observed quantity of ethane found initially. Certainly in the early stages of the reaction the chance of a CH_2HgCH_3 radical colliding with a methyl radical could be no greater than that of a methyl-methyl collision. Like the methyl radical, the chance of CH_2HgCH_3 initially colliding with anything other than a DMM molecule would be negligible. Further, if ethyl radicals are indeed formed as indicated by reactions 7-9, one would expect to find detectable quantities of methyl ethyl mercury, C_3H_8 , and C_4H_{10} in the reaction products. The authors report only the presence of C_3H_8 .

It is evident, therefore, that any mechanism proposed for the thermal decomposition of DMM must be able to account for the following salient experimental facts: (a) the rate of decomposition of DMM is of the first order, (b) the gaseous reaction products are essentially only methane and ethane, (c) the amounts of methane and ethane produced initially in the uninhibited decomposition are approximately equal, (d) the rates of formation of methane and ethane also follow first-order kinetics, and (e) in the nitric oxide inhibited reaction, the concentration of ethane is reduced virtually to zero while the concentration of methane remains essentially the same as in the uninhibited decomposition.

A mechanism which successfully satisfies these criteria is postulated as



There is general agreement among investigators as to step 1. Step 2 is undoubtedly the only methane-forming reaction since the probability of a methyl radical colliding with any other particle than DMM in the initial stages of the decomposition is extremely remote. It also accounts for the observed presence of the yellow translucent solid, probably $(\text{CH}_2\text{Hg})_x$. Step 3 is postulated as being the principal ethane-producing reaction. The postulation of a three-body process for the formation of ethane in step 4 is not unreasonable, especially at lower pressures. Since the data in Table V indicate the absence of any surface effects, the assumption is made that the third body, M, is a DMM molecule. In the event that objection might be raised against step 4 at higher pressures, it will be seen that this step may be written as two successive bimolecular processes which give the same over-all third-order kinetics.

Among the arguments strongly supporting this mechanism are the kinetic and energy relationships. If one makes the usual steady-state assumptions it can be shown that

$$\begin{aligned} d[\text{CH}_3]/dt &= k_1[\text{DMM}] + \\ &k_3[\text{HgCH}_3][\text{DMM}] - 2k_4[\text{CH}_3]^2[\text{M}] = 0 \quad (14) \end{aligned}$$

and

$$\begin{aligned} d[\text{HgCH}_3]/dt &= k_1[\text{DMM}] - \\ &k_3[\text{HgCH}_3][\text{DMM}] = 0 \quad (15) \end{aligned}$$

Adding eq 14 and 15 and remembering that $[\text{M}] = [\text{DMM}]$

$$[\text{CH}_3] = (k_1/k_4)^{1/2} \quad (16)$$

and

$$[\text{HgCH}_3] = k_1/k_3 \quad (17)$$

The rate of disappearance of DMM is then found to be

$$\begin{aligned} -d[\text{DMM}]/dt &= \\ &[2k_1 + k_2(k_1/k_4)^{1/2}][\text{DMM}] = dp/dt \quad (18) \end{aligned}$$

Thus, the rate of decomposition of [DMM] is seen to be first order in agreement with that observed experimentally.

In like manner, the rates of formation of methane and ethane can also be shown to be first order, again in agreement with experiment.

$$k_{\text{CH}_4} = k_2[\text{CH}_3][\text{DMM}] = k_2(k_1/k_4)^{1/2}[\text{DMM}] \quad (19)$$

and

$$k_{\text{C}_2\text{H}_6} = k_3[\text{HgCH}_3][\text{DMM}] + k_4[\text{CH}_3]^2[\text{M}] = 2k_1[\text{DMM}] \quad (20)$$

It can further be demonstrated that the rates of formation of methane, k_{CH_4} , and ethane, $k_{\text{C}_2\text{H}_6}$, can be equated to expressions 3 and 4, respectively

$$k_{\text{CH}_4} = k_2(k_1/k_4)^{1/2} = 6.84 \times 10^9 e^{-32,200/RT} \text{ sec}^{-1} \quad (21)$$

and

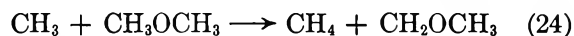
$$k_{\text{C}_2\text{H}_6} = 2k_1 = 1.93 \times 10^{12} e^{-45,100/RT} \text{ sec}^{-1} \quad (22)$$

from which

$$k_1 = 0.97 \times 10^{12} e^{-45,100/RT} \text{ sec}^{-1} \quad (23)$$

Since the strength of the C-Hg bond in DMM is given as 51.0 kcal/mole,⁶ an activation energy somewhat less than this for k_1 is not unreasonable. From eq 21 and 23 and the fact that the activation energy for step 4 is zero, the activation energy for k_2 is calculated to be 9.6 kcal/mole. This value is in excellent agreement with other hydrogen abstraction reactions by methyl radicals.

A further check on the validity of the experimental data can be made by calculating the preexponential factor for k_4 . The activation energy for the reaction

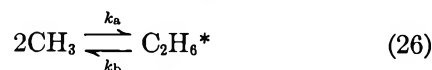


is given as 9.5 kcal/mole⁷ and 3.2×10^8 l./mole sec for the frequency factor. From eq 21

$$k_4 = \frac{0.97 \times 10^{12} e^{-45,100/RT} (3.2 \times 10^8 e^{-9500/RT})^2}{(6.84 \times 10^9 e^{-32,200/RT})^2} = 2.1 \times 10^9 \text{ l.}^2/\text{mole}^2 \text{ sec} \quad (25)$$

This value also agrees well with that of 1.1×10^9 l.²/mole² sec given⁸ for the collision frequency of a three-body process.

It has been pointed out⁹ that the mechanism for methyl radical combination in step 4 may be written as two successive bimolecular processes.



k_a is given⁸ as 2.2×10^{10} l./mole sec and k_c is of the order of the bimolecular collision frequency, or about 2×10^{11} l./mole sec. Thus, k_b can be calculated from

$$k_4 = k_a k_c / k_b = 2.1 \times 10^9 \text{ l.}^2/\text{mole}^2 \text{ sec} \quad (28)$$

to be about $2 \times 10^{12} \text{ sec}^{-1}$, which is a reasonable value

for the unimolecular collision frequency. For the reaction to be third order it is necessary, of course, for $k_b \gg k_c[\text{M}]$. Since $[\text{M}]$ is less than 10^{-2} mole/l., this is indeed the case.

The mechanism given in steps 10-13 does suggest that slightly more ethane than methane should be formed. The fact that somewhat less ethane is actually found is explainable on the basis that some of the HgCH_3 formed in step 1 decomposes into CH_3 and Hg before it can react with DMM. The contribution of step 4 to the total ethane concentration is very small, though measurable, as will be shown later.

Another argument in favor of this mechanism is that it can adequately explain the inhibition effect of NO. As previously mentioned, in view of the essentially unchanged methane concentration, NO cannot be removing methyl radicals directly. If, instead, NO removes the large radical, HgCH_3 , then step 3 would be eliminated and the only ethane formed would be by step 4. Table VII indicates that a small amount of ethane is, indeed, formed in the latter stages of the decomposition. The net effect of the elimination of step 3 is to give a steady-state concentration of methyl radicals of

$$[\text{CH}_3] = (k_1/2k_4)^{1/2} \quad (29)$$

The rate of formation of methane in the inhibited reaction then becomes

$$k_{\text{CH}_4} = k_2(k_1/2k_4)^{1/2}[\text{DMM}] \quad (30)$$

If one compares eq 30 with eq 19 it is immediately apparent that the rate of formation of methane should be virtually the same in the uninhibited and inhibited reactions. This conclusion is supported by the data in Tables I and VII.

It can be further argued that if NO reacted with methyl radicals to any appreciable extent, it would be expected that the equilibrium



would be shifted strongly to the left at these temperatures. Under these conditions, the steady-state concentration of methyl radicals and the concentration of NO would be essentially unchanged. On the other hand, if NO reacts according to

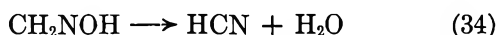


(6) T. L. Cottrell, "The Strength of Chemical Bonds," Academic Press, London, 1958, p 210.

(7) S. W. Benson, "The Foundations of Chemical Kinetics," McGraw-Hill Book Co., Inc., New York, N. Y., 1960, p 391.

(8) See ref 7, p 157.

(9) We are grateful to a referee for this suggestion.



then NO should disappear as the reaction proceeds. Table VIII shows that this is the case experimentally. It is also of interest to note that the pressure maximum in the NO-inhibited reaction corresponds to the maximum concentration of HCN. Additional support for the fact that NO reacts preferentially with large radi-

cals rather than methyls is found in the studies of Hobbs¹⁰ and Smith and Hinshelwood¹¹ on the pyrolysis of diethyl ether.

One final argument can be offered in support of the mechanism proposed in reactions 10–13. It was postulated here that most of the ethane was produced by reaction 12 rather than 13. For this assumption to be valid, after the initiating step DMM should disappear primarily through two independent mechanisms: one involving CH_3 , the other involving HgCH_3 . If NO removes the radical responsible for producing ethane, namely HgCH_3 , but does not interfere with the methane-producing step by attacking methyl radicals, then the disappearance of DMM is due primarily only to reaction 11. Since the rate of this reaction has been shown by eq 19 and 30 to be the same in both the uninhibited and inhibited processes, one would then expect the rate of disappearance of DMM to be slower in the inhibited reaction. Figure 8 shows this to be the case.

Acknowledgment. The authors gratefully acknowledge the support of this work in part by the U. S. Naval Ordnance Test Station, China Lake, Calif., under Contract No. N123s-60530s(5150a). They also wish to thank Drs. S. R. Smith and C. W. David of this department for their help in the interpretation of the mass spectrographic analyses and for their valuable suggestions regarding mechanisms.

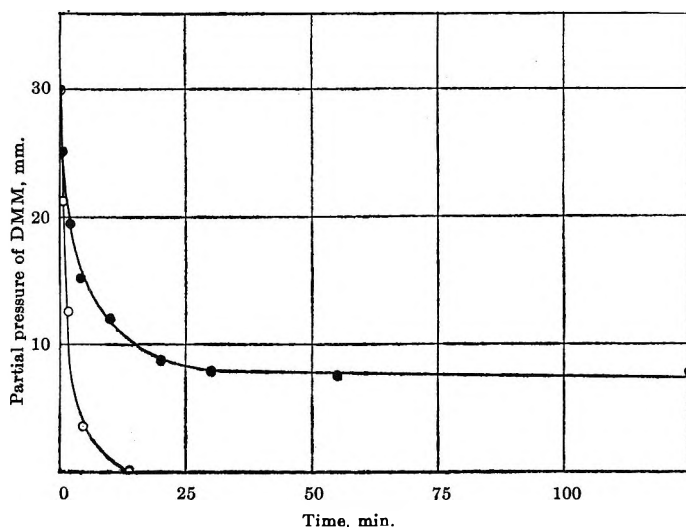


Figure 8. Rate of disappearance of 30 mm of DMM at 401°C: uninhibited, O; inhibited (30 mm NO), ●.

(10) J. E. Hobbs, *Proc. Roy. Soc. (London)*, **A167**, 456 (1938).

(11) J. R. E. Smith and C. N. Hinshelwood, *ibid.*, **A180**, 468 (1942).

Solvent Proticity *via* Erythrosin Internal Conversion

by J. Q. Umberger

*E. I. du Pont de Nemours and Co., Inc., Photo Products Department,
Parlin, New Jersey (Received October 24, 1966)*

Systematic solvent variations show erythrosin fluorescence is quenched in accordance with solvent H bond donor strength. Unlike solvatochromism, the quenching appears insensitive to solvent polarity; thus, common organic solvents—from alcohols through halogenated hydrocarbons like chloroform—are listed according to protic strength. The quenching involves nonadiabatic transition from excited state to "hot" ground state. Apparently the high energy of the "hot" ground state of symmetrical dyes results from resonance inhibition, *e.g.*, by proton transfer from solvent to erythrosin, by *intramolecular* proton transfer in ultraviolet screeners, by rotation out of coplanarity in carbocyanines, and by skeletal folding in symmetrical anthracenes.

Past work^{1,2} indicates that diminution of fluorescence accompanying iodine substitution in fluorescein is due not only to intersystem crossing but also to internal conversion from S_1 to S_0 . I have measured erythrosin fluorescence in a wide variety of solvents and conclude internal conversion is encouraged by solvent proticity,³ *i.e.*, H-bond-donor strength. Aside from fundamental energy conversion implications, these measurements arrange solvents according to proticity and correlate structures with activities.

Trifluoroethanol and water, Table I, are quite protic, are active quenchers, and yield a short fluorescence lifetime and low fluorescence; they also dissolve gelatin—further indication of protic strength.^{4a} Ethylene glycol and glycerol are surprisingly protic; intramolecular H bonding of one H apparently activates the second H. The first H is weakened by chelation, as in glycol monoethers. Tertiary alcohols are less protic than secondary which are less protic than primary.^{4b} With inductive activation, chloroform is more protic than *n*-butylamine and almost as protic as *t*-butyl alcohol. Quenching appears independent of polarity, as shown by large τ for polar aprotic solvents.

Experimental Section

Spectrophotometer curves showed a plateau in the absorption of erythrosin at ~ 500 m μ . This spectral region, from a filtered incandescent projector, excited the fluorescence. Emission was measured at 90°

from excitation *via* an S13 photocathode, Dumont 7664 photomultiplier.

Lifetimes confirmed the above intensity measurements. τ was measured *via* a sub-nsec phase fluorometer⁵ of P. C. Hoell, DuPont Central Research Department. A precision check gave 10^{-7} M aqueous uranine $\tau = 4.2$ nsec, 4.3 published;⁶ 10^{-4} M aqueous erythrosin $\tau = 0.1$ nsec, 0.08 published.⁶ A stock solution was prepared as follows: 236 mg of Erythrosin B, Fisher E513, CI 45430 (93% dye) in 50 ml of dimethylformamide (Fisher Certified D119); 2 ml of stock + 98 ml of test solvent (Fisher Certified) formed 10^{-4} M. Measurements in 100% Matheson Spectroquality solvents yielded the same τ . The Ca_4SO desiccant (5 g/100 ml of solution) increased $\tau \sim 0.1$ nsec for aprotic solvents, *e.g.*, acetone. Erythrosin, Na^+ was relatively insoluble in nonpolar solvents; replacing Na^+ by $(\text{C}_4\text{H}_9)_4\text{N}^+$ increased lipophilicity. The τ values of Rose bengal (CI 45440) were 1.41 times those of erythrosin.

(1) A. H. Adelman and G. Oster, *J. Am. Chem. Soc.*, **78**, 3977 (1956).

(2) L. S. Forster and D. Dudley, *J. Phys. Chem.*, **66**, 838 (1962).

(3) A. J. Parker, *Quart. Rev. (London)*, **16**, 163 (1962); *Intern. Sci. Technol.*, No. 44, 28 (1965).

(4) (a) J. Q. Umberger, *Phot. Sci. Eng.*, in press; gelatin dissolves in strongly protic solvents and gels in polyprotic solvents; (b) A. K. Chandra and A. B. Sannigrahi, *J. Phys. Chem.*, **69**, 2494 (1965).

(5) P. Pringsheim, "Fluorescence and Phosphorescence," Interscience Publishers, Inc., New York, N. Y., 1949, p 10.

(6) See ref 5, p 373.

Table I: Solvent Proticity from Quenching of Erythrosin Fluorescence (24°)

Solvent	Fluorescence lifetime, τ , $\times 10^9$ sec	Relative fluorescence yield	Dissolves gelatin
Trifluoroethanol	~ 0.1	2	Yes
Water	0.1	3	Yes
Glycerol	0.7	8	Yes
Ethylene glycol		8-10	Yes
Formamide ^a	~ 0.8	14-15	Yes
Methanol	~ 0.8	14-15	No
Primary alcohols	1.0	15-16	No
Secondary alcohols	1.3	18-20	No
Glycol monomethyl ether		22	No
<i>t</i> -Butyl alcohol	1.7	23	No
Trichloroethylene, chloroform	~ 2.0	~ 24	No
Methylene dichloride, methylchloroform, <i>n</i> -butylamine	~ 2.5	~ 30	No
Acetonitrile	2.8	} ~ 45	No
Dimethylformamide	2.9		
Acetone	3.5		

^a Formamide, though no more protic than methanol, dissolved gelatin on long stirring at 200°F. This is ascribed to formamide chelation with gelatin backbone, converted to *cis*-amide. *Trans*-amides, *e.g.*, *N*-methylacetamide, are gelatin precipitants; *cis*-amides, *e.g.*, acetamide and 2-pyrrolidinone, are compatible with gelatin.⁴ That formamide is no more protic than methanol suggests that resonance is secondary to induction in proticity activation.

Discussion

The interpretation of the decreased fluorescence yield in protic solvents as due to increased $S_1 \rightarrow S_0$ internal conversion is strengthened by the work of Kuchta,⁷ who found decreased erythrosin triplet yield in protic solvents such as water, and Gollnick and Schenck,⁸ who found that the quantum yield of triplet-state formation for erythrosin in methanol is as high as 0.6. It thus seems improbable that increased intersystem crossing is the cause of the greatly reduced fluorescence when the solvent is changed to water. H-bond activated fluorescence in aromatic aldehydes, with close-lying η, π^* , and π, π^* states,⁹ confirm Table I. But in view of the long wavelength $\pi \rightarrow \pi^*$ absorption of erythrosin, a close-lying $\eta \rightarrow \pi^*$ absorption appears improbable. Indeed, both the peak (546 $m\mu$ in CCl_3 , 526 $m\mu$ in H_2O) and the plateau (512 $m\mu$ in CCl_3 , 495 $m\mu$ in H_2O) in the absorption of erythrosin and also its fluorescence emission show hypsochromic shift with increase in solvent polarity. Unlike the above aldehydes, erythrosin is a symmetrical dye;

the present data, combined with recent work on carbocyanines¹⁰ and Moffitt's theory of formamidinium ion,¹¹ suggest that the internal conversion be rationalized in terms of destruction of symmetry.

Judging from the carbocyanines,¹⁰ hypsochromic absorption shift with increase in solvent polarity is typical of symmetrical ionic dyes. From this and the essentially unchanged shape and height of the optical density curve in the various solvents, it is assumed that the dianion is the predominant species of erythrosin in the ground state. Internal conversion apparently is encouraged by transfer of a proton from solvent to dianionic erythrosin, after its excitation, to form an asymmetric or monoanionic transient which is non-fluorescent. In protic solvents, the proton transfer apparently is so rapid as to compete with fluorescence and cause quenching in $\sim 10^{-9}$ sec. This time allows proton transfer in phenols but is too fast for rearrangement of the nuclear skeleton in pseudo-acids.¹² Thus, proticity or "isoskeletal" acidity is determining. H bridging must exist prior to excitation for quick protonation. Consistent with this view, it was observed that rigid glycerol at Dry Ice temperature did not lessen fluorescence quenching relative to glycerol at room temperature. Apparently, viscous glycerol does not hamper protonation as it, with Franck-Condon factors, might hamper other quenching mechanisms involving greater molecular rearrangement, *e.g.*, carbon-iodine bond rupture or gross bending or twisting of the molecular frame. For completeness, it is desirable to rationalize differences in erythrosin and uranin; the fluorescence yield of uranin is relatively high and independent of solvent proticity. In erythrosin, iodine might increase proton affinity *via* electron donation to the adjacent oxygen. Iodine also brings S_1 and S_0 states closer, as evinced in its bathochromic absorption shift, and thus might encourage $S_1 \rightarrow S_0$ internal conversion on protonation.¹³

- (7) A. D. Kuchta, private communication.
- (8) K. Gollnick and G. O. Schenck, *Pure Appl. Chem.*, **9**, 507 (1964).
- (9) K. Brederick, *et al.*, "International Conference on Luminescence," New York University, 1961, John Wiley and Sons, Inc., New York, N. Y., 1962, p 161.
- (10) J. Q. Umberger, *Phot. Sci. Eng.*, in press.
- (11) W. E. Moffitt, *Proc. Phys. Soc.*, **A63**, 700 (1950).
- (12) M. Eigen, *Angew. Chem. Intern. Ed. Engl.*, **3**, 1 (1964), OH⁻ reacts with phenols, $k \sim 1.4 \times 10^{10}$, and with pseudo-acid acetylacetone, $k \sim 4 \times 10^4$. Also see S. H. Maron and V. K. La Mer, *Ann. N. Y. Acad. Sci.*, **39**, 355 (1940); J. Hine, *J. Org. Chem.*, **31**, 1236 (1966).
- (13) It is conceivable that symmetry-destroying processes, *e.g.*, single protonation, also encourage very rapid $S_1 \rightarrow T_1$ intersystem crossing followed by very rapid $T_1 \rightarrow S_0$ nonadiabatic transition to asymmetric ground state. Invention of 0.01- μ sec flash photolysis apparatus would permit detection of such short-lived triplets if they exist.

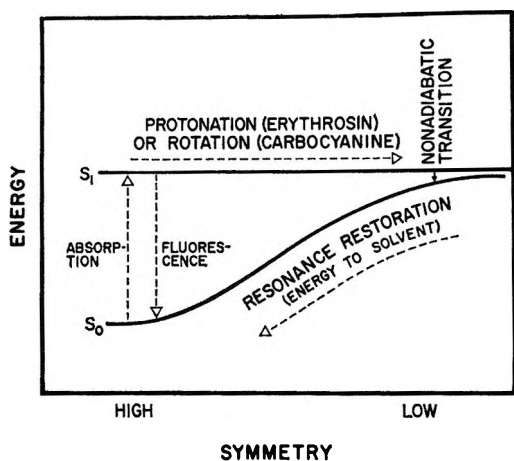


Figure 1. Internal conversion in symmetrical molecules. If skeletal folding is added to protonation and internal rotation as a symmetry-lessening process, the viscosity-dependent internal fluorescence quenching observed in symmetrical or vibrationally deficient anthracenes (E. J. Bowen and J. Sahu, *J. Phys. Chem.*, **63**, 4 (1959); *Advan. Photochem.*, **1**, 34 (1963)) also might be rationalized by Figure 1. Though recent work (R. G. Bennett and P. J. McCartin, *J. Chem. Phys.*, **44**, 1969 (1966)) indicates that both T_1 and T_2 states contribute to anthracene internal fluorescence quenching, fluorescence enhancement by viscous solvent still suggests some skeletal deformation process. For example, Bennett and McCartin found 9,10-dichloroanthracene yields 80% fluorescence in solid poly(methyl methacrylate) but only 52% in liquid ethanol at 25°. A folded triplet state could undergo nonadiabatic transition to a similarly folded S_0 state of energy close to said triplet. Indeed, skeletal deformation processes are not uncommon in excited electronic states: ethylene, coplanar in S_0 , rotates 90° out of plane in the excited state; formaldehyde, with sp^2 coplanarity in S_0 , becomes tetrahedral after excitation; and acetylene, colinear in S_0 , relaxes to *trans*- structure after excitation (N. J. Turro, private communication). Anthracene has symmetrical, out-of-plane, skeletal deformation modes of vibration (S. Califano, *J. Chem. Phys.*, **36**, 903 (1962)) which, on excitation by light absorption or heat absorption (2–4 kcal/mole), might encourage molecular folding along an axis through the 9- and 10-positions. Thus, planarity and resonance in the outer rings would be preserved in the folded molecule as in 9,10-dihydroanthracene (J. D. Roberts and M. C. Caserio, "Basic Principles of Organic Chemistry," W. A. Benjamin Inc., New York, N. Y., 1964, p 817). An alternate view of the effect of viscosity on fluorescence in symmetrical anthracenes is that the rigid media "freeze out" a skeletal deformation mode of vibration which, in the fluid media, promotes intersystem crossing.

In Figure 1, S_0 absorbs protons to form S_1 ; then protonation of one oxygen lessens erythrosin symmetry and resonance, increases S_0 energy, and encourages nonadiabatic transition to S_0 . The high energy of "hot" S_0 thus formed resides in electron localization^{14a} and/or in atomic vibration. Deprotonation restores S_0 symmetry as energy goes to sol-

vent. Broad applicability to symmetrical molecules is suggested by ultraviolet stabilizers^{14b} and carbocyanines¹⁰ where intramolecular proton transfer and rotation out of coplanarity, respectively, destroy symmetry. That rotation brings S_1 and S_0 together is evinced by bathochromic absorption shift in sterically crowded symmetrical dyes.¹⁵ Figure 1 is inapplicable to the asymmetric aldehydes. Protonation—destructive of erythrosin symmetry—increases aldehyde symmetry, *i.e.*, equalizes resonance-form energies $Ar-CH=OH \leftrightarrow Ar-CH=O^+$. Proton transfer from solvent to oxygen *after* excitation apparently stabilizes the fluorescent π, π^* states in aldehydes.⁹

Resonance differs in S_0 and S_1 states of symmetrical dyes. S_0 stabilization is strong; symmetry-destroying processes, *e.g.*, rotation or bond formation, are resisted by energy increase, Figure 1. Delocalization is encouraged by stepwise electron migration¹⁶ into adjoining unfilled orbitals or "positive holes" $Q=CH-\bar{Q} \leftrightarrow \bar{Q}-CH=Q$. Thus, an analogy exists between liquids where flow results from holes and light absorbers where chromophores, oxidation, etc., provide unfilled orbitals. Such a "hole theory"¹⁰ integrates light absorption in dyes, radicals, metals, etc.

S_1 stabilization is lessened by exclusion¹¹ of the middle resonance form $\bar{Q}-CH-\bar{Q}$; rotation and localization of electrophilicity and nucleophilicity, at opposite ends of the molecule, resemble classic nonresonating structures. In the absence of $\bar{Q}-CH-\bar{Q}$, charge migration or delocalization along the total conjugation path becomes improbable, occurring only *via* synchronized electron motion $Q=CH-\bar{Q} \rightarrow \bar{Q}-CH=Q$.

Thus, nonemissive S_0 appears associated with stepwise (incoherent) electron migration analogous to diffusion and emissive S_1 with synchronized (coherent) electron migration analogous to antenna oscillation. Though synchronized motion of the π electrons might readily be *induced* in S_1 as in laser emission, the *spontaneous* process should be relatively slow due to the general improbability of synchronized events. Thus, fluorescence should occur by correspondence with

(14) (a) W. Kauzmann, "Quantum Chemistry," Academic Press, New York, N. Y., 1957, pp 536–541; (b) J. R. Merrill and R. G. Bennett, *J. Chem. Phys.*, **43**, 1410 (1965). Also see A. A. Lamola and L. J. Sharp, *J. Phys. Chem.*, **70**, 2634 (1966). These workers suggest that in the molecules possessing the internal H bond, very fast radiationless decay (perhaps from the singlet state precluding intersystem crossing) in the form of a tautomerism takes place.

(15) M. J. Dewar in "Steric Effects in Conjugated Systems," Academic Press, New York, N. Y., 1958, p 46.

(16) L. Pauling, *Proc. Natl. Acad. Sci. U. S.*, **25**, 579 (1939).

linear radio antennae only when the conjugated π electrons finally happen to move coherently or synchronously, apparently after a gestation period of $\sim 10^{-8}$ sec.

Stark effect data¹⁷ suggest that symmetrical dyes have no permanent dipole in the S_0 and S_1 states and that S_1 is more polarizable than S_0 . This is quite consistent with the present view that electron delocalization and resonance stabilization are less in S_1 than in S_0 . In S_1 , electrons and positive hole apparently can be localized at opposite ends of a molecule under the influence of an electric field. But S_0 is relatively resistant to polarization by an external field, because

such polarization would localize the electrons and reduce resonance stabilization. The high polarizability of S_1 states might contribute to "photochemical forces,"¹⁸ e.g., the relatively high binding energy in "excimers" such as an excited helium atom associated with a normal helium atom.¹⁹

(17) J. Kumamoto, J. C. Powers, Jr., and W. R. Heller, *J. Chem. Phys.*, **36**, 2893 (1962), and *Chem. Eng. News*, **41**, 89 (1962); also see J. R. Platt, *J. Chem. Phys.*, **34**, 862 (1961).

(18) J. Q. Umberger, *Can. Chem. Process Ind.*, **29**, 108 (1945).

(19) J. O. Hirschfelder, C. F. Curtiss, and R. B. Bird, "Molecular Theory of Gases and Liquids," John Wiley and Sons, Inc., New York, N. Y., 1954, p 1098.

The Reaction of H with O₂. The Dissociative Lifetime of HO₂¹

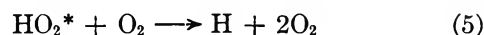
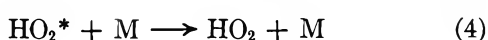
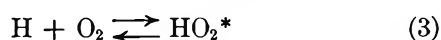
by R. L. Wadlinger and B. deB. Darwent

The Maloney Chemistry Laboratory, The Catholic University of America, Washington, D. C. 20017
(Received October 24, 1966)

The reactions of H with H₂S and O₂, the dissociative life of HO₂^{*}, and the deactivation of HO₂^{*} by CO₂, CF₄, and SF₆ have been investigated by measuring the effect of the concentration of inert gas on the rate of formation of H₂ in the photolysis of H₂S mixed with O₂. The photochemically produced H has been shown to be hot, but the technique used in these measurements is sound provided that the concentrations of H₂S and O₂ are much less than that of the inert gas. The efficiencies of CO₂, CF₄, and SF₆ in deactivating HO₂^{*} are identical. The rate constant for the dissociation of chemically activated HO₂ is approximately $2 \times 10^{10} \text{ sec}^{-1}$. The reaction of H with H₂S requires $E = 2.7 \text{ kcal mole}^{-1}$, if H + O₂ requires zero activation energy.

I. Introduction

The photolysis of H₂S has been used as a source of H atoms for investigations of the kinetics of their reactions with a variety of hydrocarbons^{2a} and with oxygen.^{2b} The mechanism



was suggested^{2b} for the reactions of H with O₂. Reaction 5 is unusual in that it represents the collision-induced decomposition of a vibrationally excited

(1) This work was supported by Project SQUID, which is supported by the U. S. Office of Naval Research, Department of the Navy, under Contract N6 ori-105-Task 3.

(2) (a) B. deB. Darwent and R. Roberts, *Discussions Faraday Soc.*, **14**, 55 (1953); (b) B. deB. Darwent and V. J. Krasnansky, *Symp. Combust.*, 7th, London, 1958, 3 (1958).

species and was rationalized as proceeding through the intermediate formation of O_4 .

The experimental basis on which reaction 5 was suggested was as follows: the simple mechanism, reactions 1-4 inclusive, leads to the relationship

$$\gamma \equiv \phi/(1 - \phi) = (k_1 p_1/k_2 p_2)(1 + k_3/k_4 m) \quad (I)$$

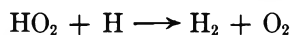
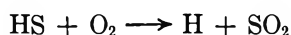
where, ϕ is the quantum yield of H_2 , p_1 and p_2 the concentrations of H_2S and O_2 , respectively, and m that of all third bodies in reaction 4. Although eq I was obeyed when $m = H_2S + O_2$ (two-component system) and when $m = H_2S + O_2 + CO_2$ (three-component system), the intercepts of the linear plots of γ vs. $1/m$ at constant p_1/p_2 were much smaller in the three- than in the two-component data. The complete mechanism yields

$$\gamma = (k_1 p_1/k_2 p_2) \{1 + (k_3 + k_5 p_2)/k_4 m\} \quad (II)$$

which was found to be in agreement with experiment.

We have recently shown³ that the photochemically produced H atom is "hot" and this suggests that reaction 5 may be unnecessary and that the difference between the two- and three-component data may have been due to the reactions of the hot H in the former case.

The reaction has been investigated over a wider range of conditions to test the hot H hypothesis and also to seek more definite information on whether HS or HO_2 radicals complicated the kinetics by reactions such as



which had been discarded previously^{2b} on the basis of reasonable argument.

II. Experimental Section

The apparatus and experimental procedure were essentially the same as those described previously.^{2b} The reaction vessel was a quartz cylinder, 5 cm diameter and 10 cm long, of approximately 200 cm³, connected to a unidirectional circulating pump, traps, etc. The rate of circulation was approximately 1 l. min⁻¹. The total volume of the reaction system was approximately 2500 cm³. The full light of a medium-pressure mercury arc was collimated by a quartz lens and filled the reaction cell.

The CF_4 was purified by circulation through a tube containing copper needles heated to 350-400°. The purity of all the inert gases was demonstrated by the fact that their presence in large excess (170/1) did not

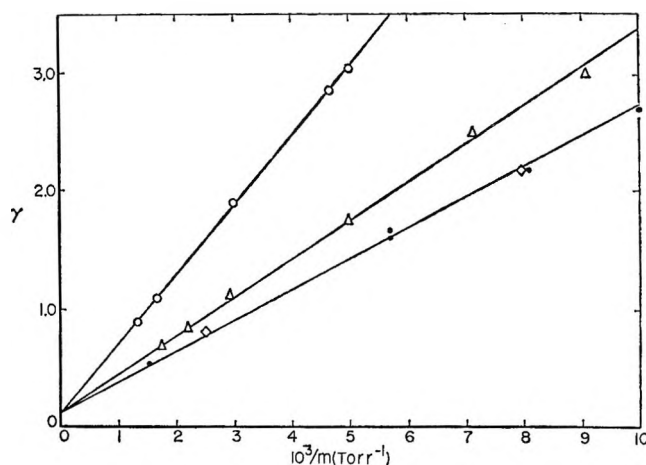


Figure 1. The effect of concentration of H_2S on the quantum yield of H_2 in the photolysis of $H_2S-O_2-CO_2$ mixtures at 50° at constant $p_1/p_2 = 1.0$: \circ , 100; Δ , 20; \bullet , 4.0; \diamond , 1.0.

alter the rate of formation of H_2 in the photolysis of H_2S .

The conversion in most experiments was kept to less than 1% and in no case exceeded 3%.

III. Results

The effect of varying p_2 but keeping p_1/p_2 constant on the relationship between γ and $1/m$ is shown in Figure 1. The relationship is shown to be linear, the slopes decrease with decreasing p_2 , and the intercepts appear to be independent of p_2 . This is not in disagreement with eq II but is also as expected if the decrease in slope with decreasing p_2 were due to the decreasing importance of reactions involving hot H atoms. An important result is that conditions can be and were attained, at 4.0 and 1.0 mm of H_2S , such that the relationship becomes effectively independent of p_2 . Under those "limiting" conditions eq I is obeyed and the kinetics are not complicated by "hot" H atom reactions or by reaction 5.

The effect of temperature on the intercepts of the two- and three-component systems suggested that hot H atoms and not reaction 5 were responsible for the difference observed. Thus, in the two-component system with $p_1/p_2 = 0.10$ the intercepts were 0.19 at 150° and 0.12 at 50° , the ratio being 1.58. In the three-component system, with $p_1 = p_2 = 4$ torr, the ratio of intercepts was $0.51/0.17 = 3.0$ at the same temperatures. The values of k_1/k_2 at 50° are 1.2 for the two-component and 0.17 for the three-component system. The much larger value for the two-component data is consistent with the suggestion that "hot" H reactions, e.g., with H_2S , are important. The smaller tempera-

(3) B. deB. Darwent, R. L. Wadlinger, and M. J. Allard, in press.

ture coefficient is also suggestive of "hot" H in the two-component system.

The photolysis of CH₃SH has been shown⁴ to produce CH₃S and H so that it should be possible to use CH₃SH instead of H₂S and there should then be no HS radicals to complicate the kinetics. The results obtained from two- and three-component systems with CH₃SH at $p_1/p_2 = 0.40$ for the two- and 4/10 for the three-component system at 50° are shown in Figure 2. Again, the relationships between γ and $1/m$ are linear, as expected from eq I and II, and the intercept for the two-component is considerably greater than for the three-component data, although the ratio p_1/p_2 was the same in both cases. Thus, it is very unlikely that any reaction involving HS was responsible for the difference observed with H₂S.

The essential independence of γ on intensity and surface:volume ratio in both the two- and three-component systems and at 50° is shown in Table I. The subsequent experiments were done with the three-component system under "limiting" conditions.

Table I: The Effects of Intensity and Surface on the Photolysis, Temperature 50°

I_a , quanta cm ⁻² sec ⁻¹	S/V , cm ⁻¹ ($p_1 = 51.5$ torr)	γ ($p_2 = 100$ torr)
(a) Two-Component System		
22.95×10^{14}	1.07	2.10
1.41×10^{14}	1.07	2.07
21.0×10^{14}	19.20	2.03
	($p_1 = 4.0$ torr)	($p_2 = 4.0$ torr $p_3 = 167$ torr)
(b) Three-Component System		
10.50×10^{14}	1.07	1.61; 1.66
0.91×10^{14}	1.07	1.60
7.06×10^{14}	19.20	1.68

Information about the effect of the nature of the inert gas was obtained by substituting CF₄ and SF₆ for CO₂. The results of those experiments (Figure 3) suggest that there is no significant difference among the three gases.

The effect of temperature on the relationship between γ and $1/m$ is shown in Figure 4. It is evident that both the intercepts and the slopes increase significantly with temperature. Those data were obtained with the three-component system under limiting conditions so that they may be examined on the basis of eq I. The unbroken lines were drawn by the method of least squares and the intercepts (and accordingly k_1/k_2) are given in Table II. Taking the in-

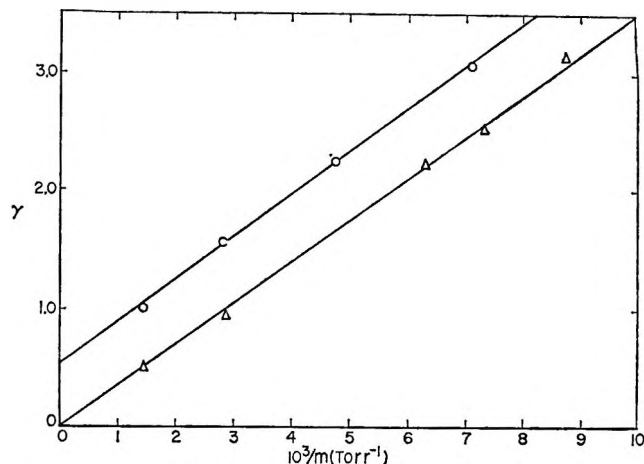


Figure 2. The effect of inert gas on the photolysis of CH₃SH in the presence of O₂, $p_1/p_2 = 0.40$, temperature = 50°: O, no CO₂ present; Δ, $p_1 = 4.0$; $p_2 = 10.0$ torr; CO₂ variable.

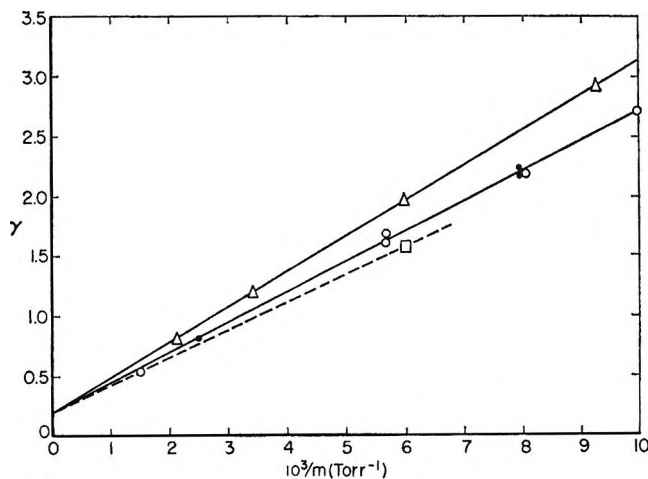


Figure 3. The effect of the nature of the inert gas on the relationship between γ and $1/m$ at 50° ($p_1 = p_2 = 4$ torr): O, CO₂; ●, $p_1 = p_2 = 1.0$ torr; Δ, CF₄; □, SF₆.

tercepts in pairs, we find values of $E_1 - E_2$ of 3.37 and 2.03 kcal mole⁻¹ for 50 and 100° and for 50 and 150°, respectively. Taking the average of these (2.70 kcal mole⁻¹) and assuming the data at 50° to be correct, since they were more numerous and self-consistent than those at 100 or 150°, we have obtained "corrected" values of the intercepts and slopes which are given parenthetically in Table II. The broken lines in Figure 4 are drawn on the basis of the "corrected" values; it is obvious that those values are well within the experimental accuracy of the measurements.

(4) T. Inaba and B. deB. Darwent, *J. Phys. Chem.*, **64**, 1431 (1960).

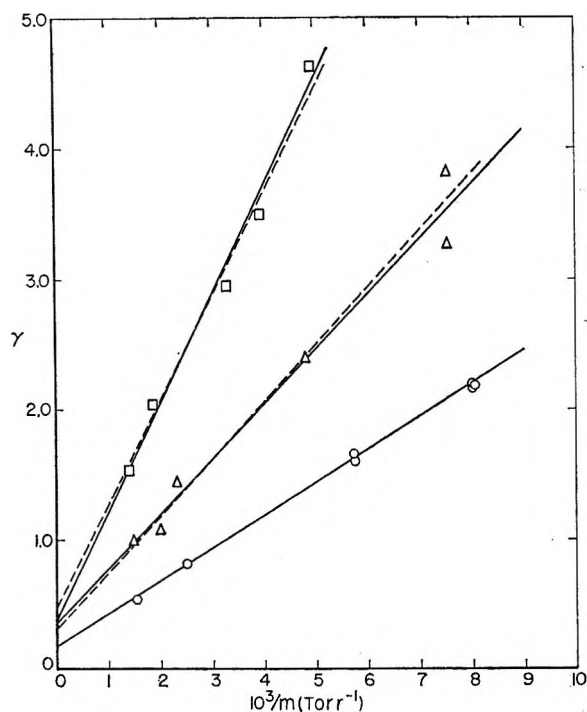


Figure 4. The effect of T on the relationship between γ and $1/m$ under "limiting" conditions: \circ , 50° ; Δ , 100° ; \square , 150° ; —, least squares; ---, "corrected" relationship.

Table II: Effect of Temperature on Rate Constants

T , $^\circ\text{K}$	k_1/k_2^a	$k_1k_3/k_2k_4^a$, torr	k_3/k_4^a , torr
323	0.181 (0.181)	254 (254)	1411 (1411)
373	0.365 (0.31)	422 (439)	1156 (1416)
423	0.381 (0.49)	835 (807)	2190 (1754)

^a "Corrected" values in parenthesis.

IV. Discussion

(a) *The Mechanism of the Reaction.* The difference in temperature coefficients of the intercepts of the γ as $1/m$ plots for the two- and three-component systems supports the claim that hot H atoms are produced in the initial photochemical act. In the two-component system the photochemical H collides only with H_2S or O_2 and, if it is sufficiently energetic, will react rapidly. Thus the intercept, which includes k_1/k_2 , will not be markedly dependent on temperature. In the three-component system, under limiting conditions, essentially all the hot H will collide with CO_2 and so is deactivated. The intercept in that case reflects k_1/k_2 for thermal H and so should be more dependent on temperature.

The results obtained when CH_3SH was substituted for H_2S as a source of H atoms indicate very strongly

that reactions of HS with, for example, O_2 or HO_2 were not responsible for the difference between the two- and three-component systems results, since the same type of difference was found with CH_3SH as with H_2S and previous work⁴ has shown that HS radicals are not produced in the photolysis of CH_3SH . Moreover, Zeelenberg⁵ has produced evidence that HS disappears rapidly by reaction with O_2 to form SO and OH which would not influence the rate of formation of H_2 . It is very likely that any OH so produced will react with H_2S to form H_2O and SH as suggested also by Zeelenberg. The reaction $\text{HS} + \text{OH} \rightarrow \text{H}_2 + \text{SO}$, also suggested by Zeelenberg, should be of little or no importance in the present experiments since the stationary concentration of HS is always very much lower than that of H_2S and the reaction of OH with H_2S is fast. This conclusion is supported by the fact that the quantum yield is not a function of intensity. The fact that the quantum yield was independent of intensity and of surface:volume ratio demonstrates also that the data were not subject to other unforeseen complications.

Accordingly, we consider that the rate of formation of H_2 in the photolysis of H_2S in the presence of O_2 and inert gas is determined by a simple mechanism, provided that the concentration of inert gas is sufficiently large relative to those of H_2S and O_2 and that the process is adequately described by eq I. When the concentration of inert gas is not sufficiently greater than those of the reactants, complications due to hot H atom reactions become increasingly important and are reflected by increasing slopes of the γ as $1/m$ plots. The slopes contain the terms (k_1k_3/k_2k_4) and when hot H is important it is likely that both k_1 and k_3 will increase and k_2 and k_4 will either be unaffected or decrease. Consequently, the slopes are expected to increase, on the basis of eq I, under non-limiting conditions. The agreement with eq I under limiting conditions and the departure from eq I under nonlimiting conditions are both strong indications of the adequacy of that equation under proper experimental conditions.

(b) *The Reaction of H with H_2S .* The effect of temperature on the γ vs. $1/m$ plots is shown in Figure 4, in which the full lines were drawn by the method of least squares. The intercepts of those lines give the values of k_1/k_2 and the slopes the values of k_1k_3/k_2k_4 which are listed together with their "corrected" values in Table II.

The values of k_1/k_2 obtained here are larger than those reported previously^{2b} by a factor of approximately

(5) A. P. Zeelenberg, *Symp. Combust.*, 7th, London, 1953, 68 (1958).

3 at the same temperature. The reason for this discrepancy is not immediately obvious; theory requires that the intercepts for the three-component system data should not be influenced by hot H atom reactions and this is supported by our data (Figure 1). However, the intercepts are very small and the discrepancy may well be only an indication of the inherent inaccuracy of the value of k_1/k_2 obtained by this technique.

Since reaction 2 involves only the pairing of electron spins, we assume that E_2 is zero. Accordingly, we find $E_1 = 2.7$ kcal mole⁻¹ which is consistent with the value of 2.8 kcal mole⁻¹ found for the similar⁶ reaction of CH₃ with H₂S and with that found³ by competing reaction 1 with the reactions of H with I₂ and Br₂. The previous observation^{2a} that the activation energies for the reactions of D with D₂S and with H₂ were equal and about 5.5 kcal mole⁻¹ was certainly wrong and appears to have been due to the excess energy of the photochemically produced D atom.

From the "corrected" values of k_1/k_2 (Table II) and $\sigma_{O_2} = 3.62$ Å and $\sigma_{H_2S} = 6.92$ Å, we find $P_1/P_2 = 8$, which leads to $P_2 = 0.1$ if P_1 is assumed to be unity.

(c) *The Deactivation of HO₂**. The relative efficiencies of CO₂, CF₄, and SF₆ in deactivating HO₂* are illustrated in Figure 3. Assuming kinetic theory diameters of 4.98, 4.63, and 4.70 for HO₂*, CO₂, and CF₄, respectively, we find the ratios of collision frequencies for CO₂ and CF₄ with HO₂* to be $Z_{CO_2}/Z_{CF_4} = 1.1$. The data in Figure 3 give $(k_3/k_4)_{CF_4}/(k_3/k_4)_{CO_2} = k_{4(CO_2)}/k_{4(CF_4)} = 1.14$. Accordingly, the efficiencies of CO₂ and CF₄ in deactivating HO₂* are essentially identical. This suggests that they both deactivate HO₂* on every collision, for it is unlikely that both CO₂ and CF₄ would be so nearly of the same inefficiency. The one point for SF₆ in Figure 3 also suggests that SF₆ is as efficient as CO₂ or CF₄ in reaction 4. The above conclusion is essentially in agreement with the findings of Dickens and Linnett,⁷ that deactiva-

tions involving the transfer of small quanta of vibrational energy occur efficiently. Timmons⁸ has recently shown that, in the deactivation of NOCl*, the deactivating efficiencies of inert gases were in the order He \ll N₂ < CF₄, He being about five to six times less efficient than CF₄. This suggests that most molecules of three or more atoms, which possess a weak bending vibration, are efficient in removing the small quanta of energy in excess of the bond dissociation energy and so stabilizing the excited species.

(d) *The Decomposition of HO₂**. The data obtained in the present experiments (Table III) suggest that k_3 is about 2×10^{10} sec⁻¹ and is approximately independent of temperature. That value was obtained from the slopes (k_1k_3/k_2k_4) and the intercepts (k_1/k_2) of the γ vs. $1/m$ plots. The slopes appear to be reasonably well defined, to within about $\pm 10\%$, but the intercepts are subject to a much greater uncertainty and probably are not known more precisely than within a factor of about 2. Thus, the values of k_3 are probably accurate to within a factor of about 2, subject to the validity of the assumption that reaction 4 occurs on every collision.

Table III: Effect of Temperature on k_3 and k_4 ^a

	Temperature, °K		
	323	373	423
k_3/k_4 , mole cm ⁻²	4.23×10^{10}	3.62×10^{10}	4.00×10^{10}
k_4 , mole ⁻¹ cm ² sec ⁻¹	4.32×10^{-10}	4.86×10^{-10}	5.14×10^{-10}
k_3 , sec ⁻¹	1.83×10^{10}	1.76×10^{10}	2.06×10^{10}

^a Assumed collision diameters $\sigma_{CO_2} = 4.63$ Å; $\sigma_{HO_2^*} = \sigma_H + \sigma_{O_2} = 4.96$ Å.

(6) N. Imai and O. Toyama, *Bull. Chem. Soc. Japan*, **33**, 652 (1960).

(7) P. G. Dickens and J. W. Linnett, *Mol. Phys.*, **2**, 259 (1959).

(8) R. B. Timmons, Ph.D. Dissertation, The Catholic University of America, 1963.

Solutions of Hydrochloric Acid in Formamide. I. Thermodynamic

Properties from Electromotive Force Measurements

by R. K. Agarwal and B. Nayak

*Department of Applied Chemistry, Indian Institute of Technology, Kharagpur, India
(Received October 25, 1966)*

The emf of the cell Pt, H₂; HCl(*m*); AgCl-Ag in formamide has been measured at 5° intervals over the temperature range 25–55°. The standard potential of Ag-AgCl electrode ranges from 0.1986 v at 25° to 0.1715 v at 55°. The mean molal activity coefficient of HCl at various rounded molalities and the standard thermodynamic values ΔG° , ΔH° , and ΔS° for the cell reaction have been determined from the emf data.

Introduction

In a previous communication, we reported the standard reduction potential of the Ag-AgCl electrode ($E^\circ_{\text{Ag-AgCl}}$) in formamide together with the mean molal activity coefficient of HCl solution in this solvent at 25°. The results were obtained from the study of the cell Pt, H₂; HCl(*m*); AgCl-Ag in formamide at 25°. Variation of the mean molal activity coefficient was found to follow the expected theoretical trend based on interionic attraction theory.

In the present investigation, we have extended the studies to higher temperature and now report the results over the temperature range 25–55°. From the values of $E^\circ_{\text{Ag-AgCl}}$ and its temperature coefficient, various thermodynamic quantities for the cell reaction $\frac{1}{2}\text{H}_2(\text{g}) + \text{AgCl}(\text{s}) \rightleftharpoons \text{Ag}(\text{s}) + \text{HCl}(\text{solvated})$ have also been calculated.

Experimental Section

The preparation of the electrodes has been described earlier.¹ The emf cell was an all-glass type of the design recommended by Daniels and others.² Electromotive force measurements were made with a type K-2 Leeds and Northrup potentiometer. A dc galvanometer supplied by Leeds and Northrup Co. was used in conjunction with the potentiometer. A Weston normal cell supplied by Cambridge Instrument Co. Ltd., England, was used as reference.

The purification of materials needed for the emf measurements and preparation of various solutions was done as described in our earlier article.¹

After preparing the cell and placing it in position, a hydrogen flow of about 1 bubble/sec was continued for 30–45 min before emf readings were taken. Successive readings, which were taken at intervals of ~30 min, were found to vary slowly with time, the variation being more pronounced at higher temperature and high acid concentration. This was probably due to the slow decomposition of the solvent under the experimental condition. The true emf of the cell corresponding to the undecomposed solution was therefore found out by extrapolating the observed emf values to zero time. Such extrapolation created no difficulty as the emf readings showed almost a linear variation with time up to a period of at least 2.5 hr in all cases except for some cells at 50 and 55° where slight departure from linearity was noticed beyond a period of 2 hr. All emf measurements were reduced to 760 mm pressure. The vapor pressure of formamide was estimated to be less than 10 mm below 60° from the data available in the literature.³ The correction for barometric pressure in most cases was found to be negligible.

Results and Discussion

A summary of emf data at 45° is given in Table I as a function of HCl molality. Similar experimental values were obtained at each of the 5° temperature intervals throughout the range. As usual values of

(1) R. K. Agarwal and B. Nayak, *J. Phys. Chem.*, **70**, 2568 (1966).

(2) F. Daniels, J. H. Mathews, J. W. Williams, P. Bender, and R. A. Alberty, "Experimental Physical Chemistry," McGraw-Hill Book Co., Inc., New York, N. Y., 1956, p 179.

(3) D. R. Stull, *Ind. Eng. Chem.*, **39**, 517 (1947).

E' were calculated with the help of eq 1 and the standard potential of silver-silver chloride electrode E° was found by using Hitchcock's method⁴ of extrapolating the auxiliary function, E' , given by⁵

$$E' = E + \frac{2(2.3026)RT}{F} \log m - \frac{2(2.3026)RT}{F} \alpha \sqrt{m} = E^\circ - \frac{2(2.3026)RT}{F} \beta m \quad (1)$$

to $m = 0$, the symbols in eq 1 having their usual significance.

Table I: Summary of Emf Data for HCl in Formamide at 45°

HCl, m	E , v ^a
1.97×10^{-2}	0.3990
2.50×10^{-2}	0.3875
5.04×10^{-2}	0.3510
5.20×10^{-2}	0.3490
9.90×10^{-2}	0.3178
14.00×10^{-2}	0.2935
16.22×10^{-2}	0.2910
17.30×10^{-2}	0.2831
28.17×10^{-2}	0.2555

^a Extrapolated values, corrected to 1 atm.

A plot of E' vs. m at each temperature should yield a straight line with slope = $[2(2.303)RT/F]\beta$ and intercept E° . Extrapolation of E' to zero molality was done by the method of least squares. Values of $E^\circ_{\text{AgCl-Ag}}$ in formamide together with similar data in water and N-methylacetamide (NMA) (dielectric constant 165.5 at 40°) for the sake of comparison are shown in Table II.

The probable errors in E° values have been estimated to be within the range ± 0.2 – 0.5 mv. Mandel and Decroly⁶ have also published a set of E° values for the

Table II: Values of E° for the Cell Reaction $\frac{1}{2}\text{H}_2 + \text{AgCl} = \text{Ag} + \text{HCl}$ in Formamide, NMA, and Water

Temp, °C	E° in formamide		E° in NMA	E° in H ₂ O
	a	b		
25	0.1986	0.204	...	0.22239
30	0.1937	0.198	...	0.21912
35	0.1888	0.191	0.21187	0.21563
40	0.1853	0.181	0.20573	0.21200
45	0.1801	0.172	0.20091	0.20821
50	0.1753	...	0.19456	0.20437
55	0.1715	...	0.19972	0.20035

^a Values obtained by us. ^b Values reported by Mandel and Decroly.

Ag-AgCl electrode in formamide at several temperatures. Although their values are not as accurate as ours and full experimental details of their work are lacking, for the sake of comparison, we have included these data in column b of Table II. E° values found in the present investigation are in fair agreement with those of Mandel and Decroly except at 45° where the difference is as large as 8 mv. The E° values are found to be less in formamide than in NMA or water, the relative order being $E^\circ_{\text{formamide}} < E^\circ_{\text{NMA}} < E^\circ_{\text{water}}$.

The mean molal activity coefficients (γ_{\pm}) were calculated as described earlier.¹ The results have been presented in Table III and the typical variations of $\log \gamma_{\pm}$ with the square root of m have been illustrated in Figures 1–3 at three selected temperatures. The theoretical and experimental limiting slopes are given

Table III: Summary of Activity Coefficients for HCl in Formamide

HCl, m	25°	30°	35°	40°	45°	50°	55°
0.005	0.957	0.950	0.957	0.957	0.955	0.954	0.952
0.01	0.944	0.934	0.943	0.943	0.940	0.939	0.934
0.02	0.926	0.908	0.928	0.928	0.904	0.919	0.911
0.03	0.916	0.904	0.920	0.919	0.909	0.906	0.894
0.04	0.909	0.896	0.914	0.913	0.900	0.896	0.881
0.05	0.904	0.889	0.911	0.909	0.893	0.889	0.873
0.06	0.899	0.884	0.909	0.908	0.888	0.883	0.863
0.07	0.895	0.880	0.908	0.907	0.884	0.878	0.852
0.08	0.895	0.897	0.908	0.907	0.881	0.874	0.845
0.09	0.894	0.875	0.908	0.906	0.877	0.870	0.837
0.1	0.893	0.874	0.911	0.909	0.877	0.868	0.835

Table IV: Values of Theoretical and Experimental Limiting Slopes

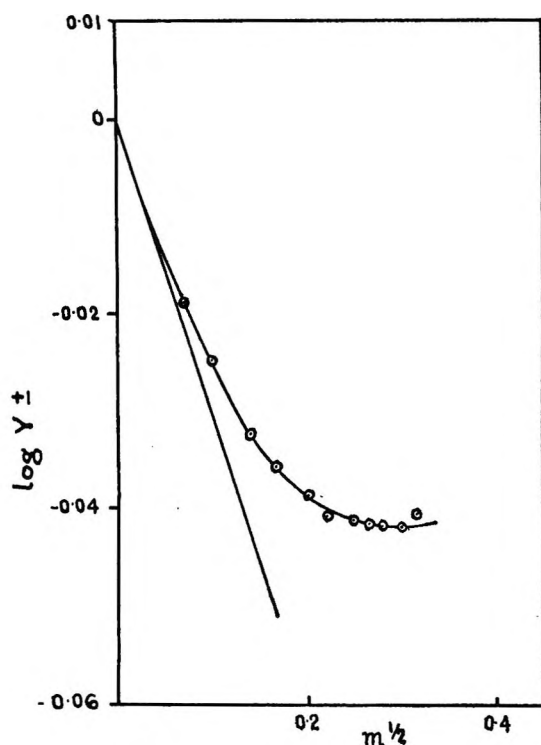
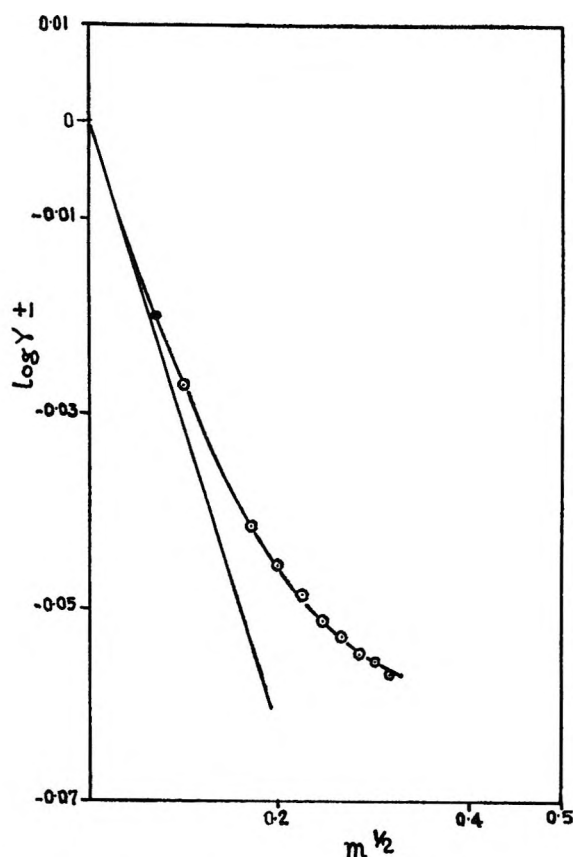
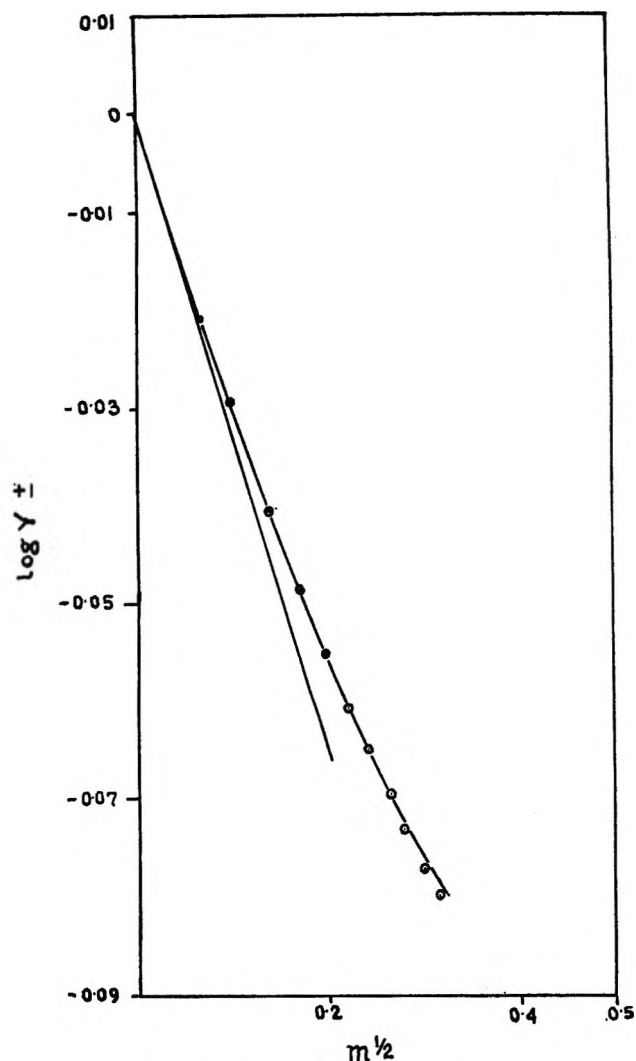
Temp, °C	Experimental values	Theoretical values
25	–0.300	–0.307 ^a
30	–0.307	–0.308
35	–0.291	–0.309
40	–0.308	–0.310
45	–0.310	–0.311
50	–0.313	–0.312
55	–0.321	–0.314

^a A value of –0.309 was quoted for this temperature in our previous article.¹ This was based on a slightly lower value of the dielectric constant reported by G. P. Johari and P. H. Tewari, *J. Phys. Chem.*, **69**, 697 (1965).

(4) D. Hitchcock, *J. Am. Chem. Soc.*, **50**, 2076 (1928).

(5) In eq 1 $\log \gamma_{\pm}$ is assumed to be equal to $-\alpha\sqrt{m} + \beta m$.

(6) M. Mandel and P. Decroly, *Trans. Faraday Soc.*, **56**, 29 (1960).

Figure 1. Variation of $\log \gamma_{\pm}$ vs. $m^{1/2}$ at 35° .Figure 2. Variation of $\log \gamma_{\pm}$ vs. $m^{1/2}$ at 45° .Figure 3. Variation of $\log \gamma_{\pm}$ vs. $m^{1/2}$ at 55° .

in Table IV. For the calculation of limiting slopes the values of the dielectric constant for formamide as found by Mandel and Decroly⁶ were used.

The mean molal activity coefficients show the usual trend, *i.e.*, decrease with concentration at all temperatures. Plots of $\log \gamma_{\pm}$ vs. concentration yield smooth curves of the expected shape at all temperatures and limiting slopes are in very good agreement with the theoretical slopes predicted by the Debye-Hückel limiting law. Because of the higher dielectric constant of formamide these slopes are expected to be less negative in the case of this solvent than in the case of water and consequently the mean molal activity coefficient of HCl in formamide decreases much less with increasing molality than it does in aqueous solution. Again for the same reason, but the sequence now being the opposite, the decrease of γ_{\pm} HCl in formamide with molality is found to be more than in N-methylaceta-

mide. For the sake of comparison, the values of activity coefficients of HCl at some selected molalities in these three solvents are shown in Table V.

Table V: Mean Molal Activity Coefficients in Different Solvents

m	γ_{\pm} in water ^a at 40°	γ_{\pm} in formamide at 40°	γ_{\pm} in NMA ^b at 40°
0.01	0.901	0.943	0.971
0.05	0.825	0.909	0.952
0.1	0.789	0.909	0.950

^a H. S. Harned and B. B. Owen, "The Physical Chemistry of Electrolytic Solutions," Reinhold Publishing Corp., New York, N. Y., 1950, p 547. ^b L. R. Dawson, W. H. Zuber, Jr., and H. C. Eckstrom, *J. Phys. Chem.*, **69**, 1335 (1965).

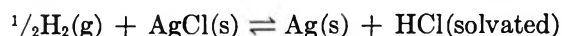
From the E° values at different temperatures, the thermodynamic quantities ΔG° , ΔH° , and ΔS° for the cell reaction were calculated at these temperatures. A summary of these values is given in Table VI.

At each temperature the standard reduction potential of the Ag-AgCl electrode in formamide is less than it is in water or NMA. For example, at 35° $E^{\circ}_{\text{Ag-AgCl}}(\text{formamide}) = 0.1888$ v, $E^{\circ}_{\text{Ag-AgCl}}(\text{water}) = 0.21563$ v,⁷ and $E^{\circ}_{\text{Ag-AgCl}}(\text{NMA}) = 0.21187$ v.⁸ This would place the ΔG° values of the cell reaction in these solvents in the order $\Delta G^{\circ}_{\text{formamide}} > \Delta G^{\circ}_{\text{NMA}} > \Delta G^{\circ}_{\text{water}}$. The standard free energy change does not appear to be a simple function of the dielectric constant as the dielectric constants of the solvents occur in the order

Table VI: Standard Thermodynamic Changes for the Cell Reaction

Temp, °C	E° , v	$\Delta G^{\circ} \times 10^{-3}$, joules	$\Delta H^{\circ} \times 10^{-3}$, joules	ΔS° , joules/deg
25	0.1986	-19.16	-46.13	-90.50
30	0.1937	-18.69	-45.76	-89.35
35	0.1888	-18.22	-45.38	-88.29
40	0.1853	-17.88	-45.12	-87.03
45	0.1801	-17.38	-44.69	-85.87
50	0.1753	-16.92	-44.28	-84.72
55	0.1715	-16.55	-43.92	-83.46

$D_{\text{H}_2\text{O}} < D_{\text{formamide}} < D_{\text{NMA}}$ at all temperatures. The change in standard electrode potential may be ultimately related to the change in ΔG° value for the cell reaction in different solvents. For a reaction like



any change taking place in ΔG° will be largely due to the variation of free energy of solvation of the solute. Again for HCl, this would be largely due to the differences in the solvation energy of the proton in these solvents. One could therefore expect at least a qualitative correlation between the E° (or ΔG°) values and the basicity of the solvents. This is indeed observed in the case of these three solvents. Water is likely to be the most basic of all the three solvents, followed by NMA and then formamide. The E° and $-\Delta G^{\circ}$ values appear in the same order as the basicity.

(7) See Table V, footnote a, p 330.

(8) See Table V, footnote b.

Conformation of Adsorbed Polystyrene Measured by Attenuated Total Reflection in the Ultraviolet Region¹

by Paul Peyser² and Robert R. Stromberg

*Institute for Materials Research, National Bureau of Standards, Washington, D. C. 20234
(Received October 27, 1966)*

A method using the technique of internal reflection spectroscopy is described for the measurement of the extension and concentration of a film on a transparent surface. In this method, attenuated total reflection (ATR) in the ultraviolet region was applied to polystyrene adsorbed on a quartz surface from cyclohexane solution at the θ temperature. The ATR prism, which allowed 15–16 reflections, was constructed from synthetic crystalline quartz. It was designed to be placed in a spectrophotometer without the need of additional optical components. The measured adsorbed polymer "extension" agreed reasonably well with similar ellipsometric measurements on nearly the same system. The study reported here was restricted to the use of an adsorbed layer that could be treated as a homogeneous film. The possible use of the method to determine the concentration distribution of adsorbed segments normal to the surface is discussed. Measurements in the ultraviolet region of the refractive indexes of the polymer solutions and of the benzene–methanol and toluene–methanol solutions that were used to test the method are also described.

Introduction

Measurement of the conformation of adsorbed molecules is required for an understanding of the adsorption of polymers on surfaces. Ellipsometry³ and viscosity⁴ measurements have previously been made to measure an average thickness of the adsorbed polymer layer in contact with the polymer solution. However, neither of these techniques permits a measurement of the distribution of segments in the layer as a function of distance normal to the surface. In this paper we describe a method for the simultaneous measurement of the thickness normal to a transparent surface and the concentration of polymer in a film. The method, employing attenuated total reflection (the technique is known as internal reflection spectroscopy), is well suited for the study of adsorbed polymer films where contact with the polymer solution is required to prevent changes in the conformation of the adsorbed molecule. We have applied the method to polystyrene adsorption on a quartz surface.

In this application of attenuated total reflection

(ATR), polymer is adsorbed on a prism in contact with the polymer solution. Light transmitted through the prism will be totally reflected at the boundary between the prism and the solution if the angle of incidence is greater than the critical angle. Under these circumstances it is well known that the reflected ray penetrates into the solution for distances of the order of one wavelength before reentering the prism. If the adsorbed layer absorbs light, some of the incident light will be absorbed by the layer and the process is described as attenuated total reflection. Measurement of this attenuation is related to the thickness

(1) This work was supported in part by the Army Research Office, Durham. It was presented at the 152nd National Meeting of the American Chemical Society, New York, N. Y., Sept 1966.

(2) National Academy of Sciences, National Research Council Postdoctoral Resident Research Associate at the National Bureau of Standards, 1963–1966.

(3) R. R. Stromberg, D. J. Tutas, and E. Passaglia, *J. Phys. Chem.*, **69**, 3955 (1965);

(4) F. W. Rowland and F. R. Eirich, *J. Polymer Sci.*, **A4**, 2033 (1966); **4**, 2401 (1966).

of the adsorbed film if the entire film is penetrated. As will be discussed later, it is desirable to confine this penetration to the order of the thickness of the film.

The ATR process described here provides a method in addition to ellipsometry and viscosity for the measurement of the thickness (a measure of the extension of the adsorbed polymer molecule normal to the surface) and concentration of an adsorbed polymer film. In many respects it is similar to the technique of ellipsometry. Using ATR the absolute values of the two reflection coefficients are measured, whereas in ellipsometry a ratio of reflection coefficients and a phase shift of the light are measured. Both techniques usually allow a simultaneous determination of thickness and concentration of polymer in the film. (However, if the light is totally reflected in ellipsometric measurements, both of these parameters cannot always be measured.⁵) The sensitivity and utility of ellipsometry and ATR are dependent on the differences in refractive index among film, substrate, and surrounding medium. In the work described in this paper, we have used the difference in absorption (related to the imaginary component of the refractive index) between polymer film and solution as well as the real refractive index difference between polymer film and substrate.

The most significant information that could result from ATR studies of polymer adsorption would be the segment distribution. This would require ray penetration depths of the order of the extension of the adsorbed polymer molecule normal to the surface. For sufficient sensitivity it would also be necessary to have large extinction coefficients. The ultraviolet region most closely meets these requirements, since the depth of penetration^{6,7} decreases with decreasing wavelength and many polymers have large extinction coefficients in this region. Synthetic quartz was chosen for the prism because of its transparency and relatively high and well-established refractive index in the ultraviolet range and the availability of crystals that are homogeneous. However, the birefringent nature of crystalline quartz somewhat complicated the calculations.

Here we describe the use of ATR to a measurement of the thickness and concentration of an adsorbed film of polystyrene, mol wt 76,000, and compare the results with measurements by other techniques. The method was also tested on two simpler model systems, toluene-methanol and benzene-methanol solutions, where any adsorbed film would not significantly affect the results. Toluene and benzene both absorb in the wavelength range used here for the polystyrene solutions. The methanol solutions of these two ma-

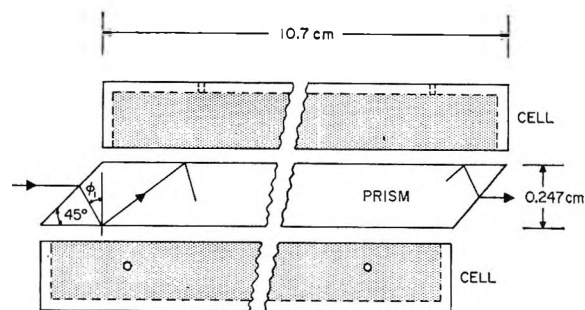


Figure 1. Schematic representation of a single crystal quartz prism and fused quartz cell. The angle of incidence, ϕ , varied with wavelength. The direction of the optic axis of the prism was normal to its base.

terials provided systems for which calculated reflectance values could be compared with experiment, thereby testing the experimental design and method of analysis. We also discuss the possible application of the technique to the measurement of the segment distribution for adsorbed polymer films of greater thickness.

Prism and Cell Design

The prism and the cell used to contain the liquid media are shown in Figure 1. The attenuated total reflection prism was constructed from a synthetic quartz crystal and was designed to be used in a spectrophotometer without the need of additional optical components. Incident and emergent beams of light were both in the same plane and parallel to the base of the prism. The direction of the optic axis of the prism was normal (measured to within 0.1°) to the base of the prism. The four optical faces were optically polished flat to within one-fourth of a fringe of the green line of mercury.

The cell was constructed from fused quartz. A rectangular cavity was formed in both the bottom and top portions by ultrasonic cavitation and the surfaces in contact with the ATR prism were polished optically flat. Holes for the addition of liquids and removal of air were drilled into the side of the bottom portion and the top of the upper portion of the cell. Each hole was fitted with a polytetrafluoroethylene insert penetrated by a stainless steel hypodermic needle. The assembly was clamped together in a holder; the liquid was retained by the close contact afforded by the opti-

(5) E. Passaglia and R. R. Stromberg, *J. Res. Natl. Bur. Std.*, **A68**, 601 (1964).

(6) J. Fahrenfort, *Spectrochim. Acta*, **17**, 698 (1961); **18**, 1103 (1962).

(7) N. J. Harrick, *Ann. N. Y. Acad. Sci.*, **101**, 3, 928 (1963); *J. Phys. Chem.*, **64**, 1110 (1960).

cal finishes on the prism and cell surfaces. The holder was constructed to fit the sample compartment of the spectrophotometer in a reproducible manner.

Experimental Procedure

The liquids toluene, methanol, benzene, and cyclohexane were of reagent grade and were purified by fractional distillation and stored above molecular sieves. The toluene-methanol and the benzene-methanol mixtures were prepared in a 1:6 and a 1:4 volume ratio (before mixing), respectively.

The polystyrene was supplied by Dr. H. W. McCormick of the Dow Chemical Co. (Dow's sample No. S 102) and was the same fractionated anionically polymerized sample that has been described previously.⁸ The molecular weight of the fractionated sample, determined by intrinsic viscosity, was 76,000 and the value of \bar{M}_w/\bar{M}_n was less than 1.05. The concentration of the polystyrene-cyclohexane solution used for the ATR measurements was 7.9 mg/ml.

Prior to each experiment the components of the ATR prism and cell were cleaned overnight with benzene in a Soxhlet extractor. In addition, immediately before use the prism and cell were heated to 500° in a muffle furnace and held at this temperature for 1 hr. The pieces were removed to a vacuum desiccator and allowed to cool for approximately 30 min. The two cell halves and the prism were then assembled using flamed platinum-tipped tongs, clamped, and the cells filled with liquid. Measurements were first carried out on the "solvent," *i.e.*, methanol or cyclohexane. The cells were then emptied, dried, and filled with the appropriate solution.

The measurements were carried out in a recording ultraviolet spectrophotometer with a Glan-Thompson prism in the beam. Measurements were made at two polarizations of the light. Air temperature of the sample compartment was maintained at $35 \pm 0.1^\circ$. The wavelength range was scanned manually in one direction. Measurements were repeated for the wavelength range until the absorbance remained constant with time at each wavelength measured.

The difference in absorbance between the solution and the solvent represented the absorbance due to the solute or to the absorbing polymer film. A slight shift in the base line measured at the nonabsorbing wavelengths of 300, 290, and 280 nm was observed between solvent and solution. This shift was identical at each wavelength for the benzene and toluene solutions and the absorbance was adjusted accordingly. However, for the polystyrene solutions the shift was not identical for all three wavelengths, but increased with decreasing wavelength. In these cases, a linearly extrapolated

correction factor was used. Because of this extrapolation we selected 260 nm as the lower limit for our measurements.

Calculations

The reflection coefficients for light polarized with its electric vector parallel and perpendicular to the plane of incidence are r_{qs}^p and r_{qs}^s , respectively. These can be accurately calculated from the Fresnel equations, which for our arrangement can be expressed as

$$r_{qs}^p = \frac{N_s \cos \varphi_1 - n_q \cos \varphi_2}{N_s \cos \varphi_1 + n_q \cos \varphi_2} \quad (1)$$

$$r_{qs}^s = \frac{n_q \cos \varphi_1 - N_s \cos \varphi_2}{n_q \cos \varphi_1 + N_s \cos \varphi_2}$$

The subscripts q and s refer to the quartz prism and solution of solvent, respectively, n_q is the refractive index of the quartz prism, and N_s is the complex refractive index of the solution or solvent. The angle of incidence is φ_1 and the angle of refraction is φ_2 .

For the case of a homogeneous film between the quartz prism and the liquid medium, the total reflection coefficients for the system are given by the exact Drude equations⁹

$$R^p = \frac{r_{qt}^p + r_{ts}^p \exp D}{1 + r_{qt}^p r_{ts}^p \exp D} \quad (2)$$

where

$$D = -4\pi i N_t \cos \varphi_t (d_t/\lambda) \quad (3)$$

and an identical expression for R^s , where r^s is substituted for r^p . The subscript f refers to the film, φ_t is the angle of refraction in the film, d_t is the film thickness, λ is the wavelength of light under vacuum, and r is the reflection coefficient at a single boundary indicated by the subscripts, as given in eq 1.

The complex refractive index N of the solution or of the film measured by ATR can be expressed as

$$N = n(1 - ik) \quad (4)$$

where n is the real part of the refractive index, and k can be directly related to the absorbance A obtained from a transmission spectrum. From the Beer-Lambert relationship, for no interaction among absorbing molecules

$$A = \alpha c_T l / 2.3 \quad (5)$$

(8) R. R. Stromberg, E. Passaglia, and D. J. Tutas, *J. Res. Natl. Bur. Std.*, **A67**, 431 (1963).

(9) P. Drude, *Ann. Physik.*, **272**, 532 (1889); **272**, 865 (1889); **275**, 481 (1890).

Table I: Refractive Indexes and Angles of Incidence for ATR Quartz Prism

$\lambda, \text{Å}$	n_o^a	$\varphi_o, ^\circ \text{ deg}$	n_e^c	n_{EN}^d	n_{ER}^e	Average of n_{EN}, n_{ER}	$\varphi_{EN}, ^\circ \text{ deg}$	$\varphi_{ER}, ^\circ \text{ deg}$	Average of $\varphi_{EN}, \varphi_{ER}, ^\circ \text{ deg}$
2500	1.60064	71.22	1.61166	1.61048	1.61047	1.61047	71.04	70.80	70.92
2550	1.59823	71.27	1.60855	1.60739	1.60739	1.60739	71.10	70.86	70.98
2600	1.59487	71.32	1.60567	1.60453	1.60452	1.60452	71.15	70.91	71.03
2670	1.59128	71.38	1.60196	1.60083	1.60083	1.60083	71.21	70.98	71.10
2680	1.59080	71.39	1.60146	1.60034	1.60033	1.60033	71.22	70.99	71.10
2690	1.59032	71.40	1.60096	1.59984	1.59984	1.59984	71.23	71.00	71.11

^a n_o , ordinary refractive index. ^b φ_o , ordinary ray angle of incidence. ^c n_e , extraordinary refractive index. ^d n_{EN} , normal-extraordinary refractive index. ^e n_{ER} , ray-extraordinary refractive index. ^f φ_{EN} , angle of refraction for normal-extraordinary ray. ^g φ_{ER} , angle of refraction for ray-extraordinary ray.

where the absorbance is obtained from a transmission spectrum for a solution of concentration c_T and a path length l and α is a constant independent of concentration. The value of k for the solution or film measured by the ATR process is related to α by

$$\alpha c_{ATR} = \frac{4\pi n k}{\lambda} \tag{6}$$

where c_{ATR} is the measured concentration of the solution or polymer film obtained by ATR. Then the value of k is given by

$$k = \frac{2.3A}{l} \left(\frac{c_{ATR}}{c_T} \right) \frac{\lambda}{4\pi n} \tag{7}$$

The ordinary and extraordinary refractive indexes were calculated for the birefringent quartz prism by equations given by Radhakrishnan.¹⁰ The ordinary ray, as the name implies, presents no difficulties in determining the refractive index and angle of incidence. The extraordinary ray, however, gives rise to two refractive indexes (and correspondingly, two angles of incidence) known as the ray index and the wave front normal index. The refractive indexes can be calculated geometrically by application of Huygens' principle to doubly refracting crystals.¹¹ Figure 2 shows the Huygens' construction applied to our case and the results for the refractive indexes are given in Table I. The values of n_q and φ used in eq 2 for the extraordinary ray were obtained by averaging the values obtained for the ray and the normal refractive indexes.

Because of its height, a portion of the light beam is reflected 15 times in our prism and a portion 16 times. The average number of reflections was calculated geometrically for each wavelength and the value of A per reflection was obtained. The determination of the refractive indexes of polymer-solvent, benzene-methanol, and toluene-methanol mixtures at the wavelengths used in this study is discussed in the Appendix.

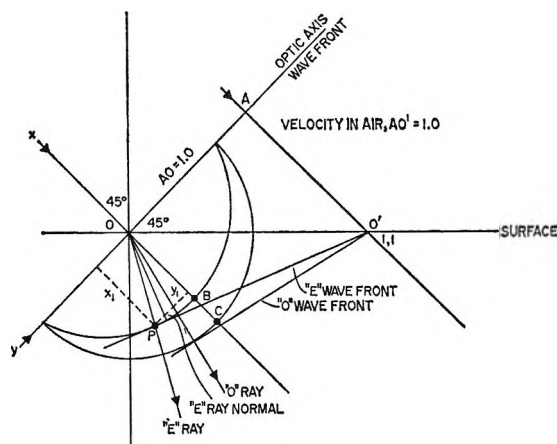


Figure 2. Huygens' construction for light incident as shown in Figure 1 for the uniaxial negative quartz crystal. This construction was modified for our system from that given in ref 11.

For measurements on benzene or toluene solutions, the measured experimental reflectance values obtained from ATR were compared with those calculated from eq 1 and 4-7. The values of n were measured directly as described in the Appendix.

For calculations involving an adsorbed polymer layer the Drude equations are used. The adsorbed polymer layer is treated as a homogeneous film. (The effect of a nonhomogeneous film is discussed later.) All of the parameters in the Drude equations are known, independently measured, or calculated, except for d_f , the film thickness, and N_f , the complex refractive index of the film (which depends on the film concentration). For each wavelength and polarization of the light,

(10) T. Radhakrishnan, *Proc. Indian Acad. Sci.*, **A25**, 260 (1947).
 (11) A description of the application of Huygens' principle to doubly refracting prisms is given by E. E. Wahlstrom, "Optical Crystallography," 3rd ed, John Wiley and Sons, Inc., New York, N. Y., 1960, p 100.

reflectance values were calculated from eq 2 for a series of given film thicknesses at various given film concentrations. (The value of n for a given film concentration was obtained from dn/dc_p , which was determined as described in the Appendix, and the value of k was obtained using eq 4-7.) The measured experimental reflectance value, obtained directly from ATR, was then compared with the series of calculated reflectance values for each given concentration in order to determine the value of film thickness corresponding to the experimental reflectance value. In this manner one value of film thickness was obtained at each concentration for each of the two polarizations at each wavelength. Curves of film thickness *vs.* film concentration were constructed for each of the two polarizations, as shown in Figure 3. The point of intersection of these curves was taken to represent the experimental value for film thickness and concentration, as determined at that wavelength.

The solutions of the Fresnel and Drude equations were carried out using a computer program¹² that had previously been written for ellipsometry measurements.

Results and Discussion

A typical ATR spectrum in the ultraviolet region is shown in Figure 4 for a solution of benzene in methanol. Also given is a transmission spectrum of a more dilute benzene solution. The ATR spectrum qualitatively was quite similar to the transmission spectrum, offering a technique for obtaining ultraviolet spectra in a region close to a surface.

For our purposes, a quantitative analysis of the attenuation at a reflection was required. To check the technique and the apparatus, especially the alignment of the quartz prism, measurements were made on a simple system for which the reflectance values could be calculated and independently compared with experiment. The experimentally measured absorbance values for benzene and toluene solutions are compared in Table II with absorbances calculated from the Fresnel equations. Comparisons are made at a number of wavelengths and for the two polarizations of light. The refractive indexes used for calculating the values of the absorbance at the wavelengths given in Table II were extrapolated from the measured range shown in Table VI. Nevertheless, as shown in Table II, there was reasonable agreement between the experimental and calculated values of the absorbance, demonstrating for a simple model system the validity of the experimental design and method of analysis.

The thickness and concentration (relative to solution concentration) of the polystyrene layer adsorbed on the quartz prism as determined by the ATR mea-

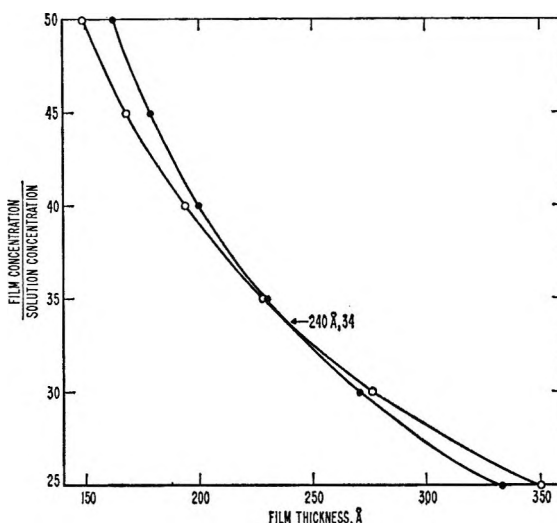


Figure 3. Concentration of the adsorbed polystyrene layer as a function of thickness for each of the two polarizations of light of wavelength 2670 Å: O, light polarized with its electric vector perpendicular to the plane of incidence; ●, light polarized with its electric vector parallel to the plane of incidence.

Table II: Comparison of Calculated and Experimental ATR Absorbance for Toluene and for Benzene Solutions

λ , Å	Toluene solution			Benzene solution		
	Calcd	Exptl	Difference	Calcd	Exptl	Difference
Ordinary Ray						
Polarization with Electric Vector Perpendicular to Plane of Incidence						
2690	0.067	0.091	0.024
2680	0.075	0.096	0.021
2670	0.077	0.091	0.014
2600	0.105	0.110	0.005	0.67	0.077	0.010
2550	0.094	0.090	0.004	0.087	0.102	0.015
2500	0.069	0.072	0.003	0.100	0.087	0.013
Extraordinary Ray						
Polarization with Electric Vector Parallel to Plane of Incidence						
2690	0.080	0.088	0.008
2680	0.089	0.093	0.004
2670	0.092	0.103	0.010
2600	0.125	0.132	0.007	0.070	0.088	0.018
2550	0.110	0.118	0.008	0.101	0.126	0.025
2500	0.081	0.097	0.016	0.116	0.118	0.002

surement are shown in Table III. These values were determined at several wavelengths by the intersection of the curves obtained for the two polarizations of the light, as described in the section on calculations and

(12) F. L. McCrackin and J. Colson, National Bureau of Standards Technical Note 242, 1964.

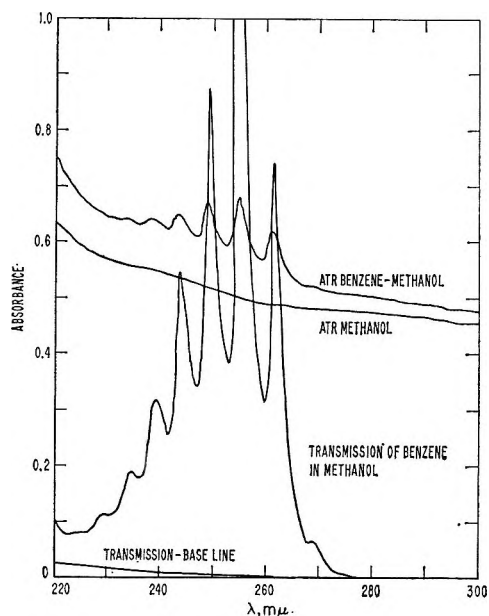


Figure 4. Ultraviolet spectra of benzene-methanol solution. ATR spectra were obtained *vs.* air. No ATR cell was in the reference beam. Composition of benzene-methanol solution, 1:4 (by volume). Transmission spectra were obtained *vs.* methanol. Composition of benzene-methanol solution, 1:16 (by volume); path length 0.1 mm.

as shown in Figure 3 for one wavelength. For the larger concentration found for this film, the critical angle would not be exceeded at the quartz-film interface, but rather at the film-solution interface. Nevertheless, the Drude equations are applicable to this situation and correctly account for the absorption of light in its multiple reflections through the film.

The values given in Table III, however, represent "average" values of the segment distribution; the relations between these averages and various segment distributions have not yet been determined. The ATR value of the extension, 240 Å, is in good agreement with the value obtained by ellipsometry and cal-

culated for a homogeneous adsorbed layer.¹³ This ellipsometric value, 225 Å, was for the same sample adsorbed on a metallic surface from cyclohexane at 34° (approximately the Flory θ point). The value of 35 for the concentration of the adsorbed layer as measured by ATR appears to be high when compared with the ellipsometric results obtained at lower equilibrium concentrations at 24 and 34°. However, a similar value for this solution concentration was obtained by ellipsometry for this polystyrene sample adsorbed at 24° from a similar solution concentration.⁸ The value for the extension can also be compared with that measured by viscometry. With this technique a value of 196 Å was obtained⁴ for a 110,000 mol wt sample of polystyrene adsorbed from cyclohexane on glass at the θ point.

Although these measurements were carried out on different surfaces, *i.e.*, silica, metal, and glass, all three surfaces were oxides and the surface energies should be of the same order of magnitude. It appears, then, that there is good agreement among the three different measurement techniques.

The changes in the properties of the attenuated reflecting light beam that occur as a result of penetration beyond the boundary are accurately treated by the Fresnel and Drude equations. As described earlier, our calculations were carried out in this manner. However, in order to give a physical picture of the penetration and to emphasize its relation to dimensions of the adsorbed polymer layer, the following approximate treatment can be considered. If the absorption of the film is neglected, *i.e.*, k is put equal to zero in eq 4, the intensity, I (square of the amplitude of the electric vector), of the light beam penetrating into the rarer medium decreases exponentially¹⁴ as

$$I = I_0 \exp(-\beta 4\pi t/\lambda_q) \quad (8)$$

where I_0 is the intensity of the light before penetration, t is the penetration distance normal to the boundary, λ_q is the wavelength of light in the quartz and

(13) In the reference cited in ref 3, the value obtained by ellipsometry was 225 Å, calculated for a homogeneous film model. For an exponential distribution, this value can be related to a root-mean-square average molecular extension of 170 Å, which is the value given in that reference.

(14) The light is also translated (Goos-Hänchen shift) in the rarer medium parallel to the boundary by a distance d_{\perp} for the perpendicular component of the light, where $d_{\perp} = (1/\pi)(\sin \varphi \cos^2 \varphi / \cos^2 \varphi + \beta^2)(\lambda_q/\beta)$, and by a distance d_{\parallel} for the parallel component of the light which is given by a similar expression.¹⁵ We have found, for example, that for the toluene solution the exact value of the reflectance as calculated by the Fresnel equations was approximately the same as that calculated for a model in which the light penetrated, with decreasing intensity, into the rarer medium, returned to the vicinity of the boundary, and then translated a distance d before reentering the quartz.

(15) R. H. Renard, *J. Opt. Soc. Am.*, **54**, 1190 (1964).

Table III: Thickness and Concentration of Polystyrene Layer Adsorbed on Quartz

Wavelength, Å	Film thickness, Å	Film concn/ solution concn ^a
2690	230	39
2680	260	32
2670	240	34
2600	240	34
	\bar{A}_v 240	35

^a Solution concentration = 7.9 mg/ml.

$$\beta = [\sin^2 \varphi - (n/n_q)^2]^{1/2} \quad (9)$$

where φ is the angle of incidence, n is the refractive index of the rarer medium (solution, solvent, or film), and n_q is the refractive index of the quartz. Since the films and solutions studied here are weakly absorbing, eq 8 is a reasonably good approximation. For our discussion here, the term "penetration depth," $t_{1/2}$, is defined as the value of t where the value of I is $I_0/2$, *i.e.*

$$t_{1/2} = \frac{\lambda_q \ln 2}{\beta 4\pi} \quad (10)$$

The "penetration depth" of the light beam is dependent on the angle of incidence and the ratio of the refractive indexes and is most sensitive to small changes in these quantities near the critical angle. If the polymer concentration in the film, and consequently its refractive index, becomes sufficiently large, the angle of incidence at the quartz-adsorbed polymer film interface no longer exceeds the critical angle and total reflection occurs within the film or at the "film-solution" interface. The ratio of film concentration-solution concentration for which total reflection no longer occurs at the quartz-film interface is defined here as the "critical ratio."

In principle the segment distribution normal to the surface for an adsorbed polymer layer can be determined by ATR. For the work reported here a homogeneous film was assumed and only a thickness and film concentration representing average values of the actual distribution were determined. This assumption was reasonable, as shown in Table IV for the ordinary ray for polystyrene adsorbed on quartz. These penetration depths were calculated for the polymer solution, assuming the critical angle to be exceeded at the quartz-solution interface (no adsorbed film). In our case, however, the concentration of polymer in the adsorbed film was such that the critical ratio was exceeded and reflection occurred at the film-solution interface. The actual penetration of light beyond the quartz boundary was, therefore, greater than the $t_{1/2}$ values given in Table IV as well as the thickness values given in Table III. Thus, for the experimental conditions used here the entire film certainly was penetrated. Moreover, as shown in Table IV, little variation occurred in either the penetration depth or the critical ratio for the wavelength region of interest. Hence, the agreement among the measured film thicknesses and concentrations shown in Table III for the four wavelengths is to be expected.

However, if the penetration depth is of the order of the extension of the polymer molecule and the concen-

Table IV: Penetration Depth and Critical Ratio for the Ordinary Ray

λ , A	n_{PS}^a	$t_{1/2}^b$, A	Critical concn ratio ^c
2500	1.48058	427	14.3
2550	1.47704	425	15.5
2600	1.47378	431	16.2
2670	1.46961	438	17.5
2680	1.46905	436	17.6
2690	1.46850	437	17.8

^a n_{PS} is the refractive index of polystyrene-cyclohexane solution. ^b $t_{1/2}$ is the "penetration depth," eq 10. ^c The critical concentration ratio is the ratio of a concentration of polymer film-solution for which a critical angle at the quartz-film boundary is no longer exceeded.

tration of the adsorbed film is less than or not much greater than the critical ratio, the calculated average film thickness and concentration will be altered if the penetration or the critical ratio is varied over a significant range. It should be possible to relate such results to the segment distribution.

Acknowledgment. The authors wish to express their appreciation to I. H. Malitson for his advice and the use of his equipment for the refractive index measurements and M. J. Dodge for her technical assistance in those measurements. They also wish to thank Dr. F. McCrackin for many helpful conversations.

Appendix

Refractive Index Measurements. Refractive indexes of the solvents and solutions used for the ATR studies were measured for wavelengths ranging from 5460 Å into the ultraviolet. The determinations were carried out on a modified Gaertner spectrometer by the method of minimum deviation, using a water-jacketed hollow prism to contain the liquids. The method and instrumentation have been previously described¹⁶ and we will describe here only certain modifications and details relevant to our measurements.

The prism was almost identical with that used by Tilton and Taylor¹⁷ in their classical determination of the refractive index of water, except that the plane parallel windows were constructed of high-quality fused quartz cemented to the stainless steel body. The temperature in the prism was maintained at $35 \pm 0.05^\circ$. In order to prevent a temperature gradient

(16) W. S. Rodney and R. J. Spindler, *J. Res. Natl. Bur. Std.*, **53**, 185 (1954).

(17) L. W. Tilton and J. K. Taylor, *ibid.*, **20**, 419 (1938).

near the cell windows, as evidenced by a broadening of the spectral lines, it was necessary to maintain the room at a temperature near that of the cell.

The light source was a mercury lamp and a photomultiplier tube was used as a detector. The angle of minimum deviation cannot be independently obtained on the modified instrument used here because the position of the undeviated beam cannot be directly measured. However, the scale position of the undeviated beam differs from the minimum deviation angle by a constant amount.¹⁸ This difference was determined from an average of measurements¹⁷ on distilled water at 26° at several wavelengths in the visible region. The wavelengths in the ultraviolet region were identified from a knowledge of the emission spectrum of the mercury source, with the aid of the dispersion equation

$$(n^2 - x)^{-1} = (a - b/\lambda^2) - (c/\lambda^4) \quad (11)$$

This is a slightly modified form of the equation used by Lauer²⁰ and found by him to be applicable to cyclohexane, toluene, and methanol. His equation contains the term $(n^2 - 1)^{-1}$ and has no fourth power term in λ .

Typical results at a few values of λ are given in Table V for each of the solutions and solvents studied. n_{exptl} represents the refractive index obtained directly from the experimental data and n_{calcd} represents the value obtained by fitting eq 11 by least squares, using $1/\lambda^2$ as the independent variable and $(n^2 - x)^{-1}$ as the dependent variable.

The value of x used for each of the systems, the constants a , b , and c , which were calculated from a fit of the data to eq 11, and the standard deviation, σ_n , are given in Table VI.

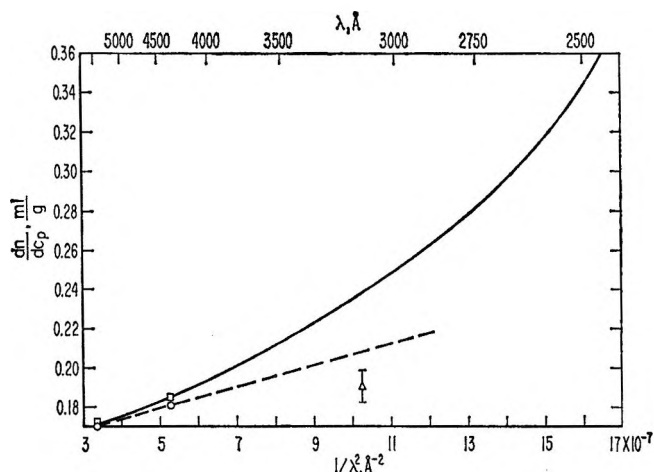


Figure 5. Dependence of dn/dc_p on $1/\lambda^2$ for polystyrene in cyclohexane at 35°: —, from eq 12; ---, linear extrapolation of two lowest points; O, values obtained from ref 22; □, values obtained from ref 23; Δ, value obtained from ref 24 ($T = 30^\circ$).

Table V: Refractive Indexes

Material	λ , Å	n_{exptl}	n_{calcd}
Cyclohexane	5461	1.41968	1.41973
	3650	1.43645	1.43640
	3126	1.44856	1.44855
	2576	1.47277	1.47272
	2378	1.48768	1.48762
PS 1 (0.95 mg/ml)	5461	1.41985	1.41990
	3650	1.43663	1.43660
	3126	1.44880	1.44879
	2753	1.46321	1.46324
	2378	1.48803	1.48801
PS 2 (2.12 mg/ml)	5461	1.42004	1.42010
	3650	1.43688	1.43683
	2760	1.46322	1.46325
	2378	1.48853	1.48851
PS 3 (5.61 mg/ml)	5461	1.42065	1.42067
	3650	1.43759	1.43758
	2753	1.46450	1.46449
Benzene-methanol (1:4 v/v)	5461	1.35718	1.35742
	2756	1.40485	1.40458
Toluene-methanol (1:6 v/v)	5461	1.35248	1.35261
	2803	1.39485	1.39461

A value of dn/dc_p was calculated using the three polystyrene solutions. These calculations were carried out in 50-Å increments for the wavelength range 5500–2300 Å for values of n obtained from eq 11 for cyclohexane and the polymer solutions. The average value of dn/dc_p at each wavelength was fitted to an equation of the form²¹

$$dn/dc_p = a + (b/\lambda^2) + (c/\lambda^4) \quad (12)$$

The values of a , b , and c and the standard deviation are given in Table VI. In Figure 5, dn/dc_p is given as a function of $1/\lambda^2$ (eq 12).

Also shown are two literature values^{22,23} of dn/dc_p

(18) It has been found¹⁹ that the scale position of the undeviated beam is constant for prisms having nearly identical refracting angles, provided the scale of the instrument has not been moved between change of prisms. Under such experimental conditions, refractive indexes have been determined with fifth decimal place accuracy. We have considered the exchange of liquids in the hollow prism to be the equivalent of this exchange.

(19) I. H. Malitson, private communication.

(20) J. L. Lauer, *J. Chem. Phys.*, **16**, 612 (1948).

(21) The form of eq 12 with $c = 0$ was used by Spencer for a number of polystyrene-solvent systems as reported by R. F. Boyer and R. Simha in "Styrene, Its Polymers, Copolymers, and Derivatives," R. H. Boundy and R. F. Boyer, Ed., Reinhold Publishing Corp., New York, N. Y., 1952, p 374.

(22) J. H. O'Mara and D. McIntyre, *J. Phys. Chem.*, **63**, 1435 (1959).

(23) H. J. Cantow, *Z. Physik. Chem. (Frankfurt)*, **7**, 58 (1956).

Table VI: Constants and Standard Deviations for Dispersion Equation

Material	Wavelength range, Å	No. of wave-lengths measured	a	b	c	x	σ_n^a
Cyclohexane	5461-2378	17	1.0188	1.001×10^6	5.6×10^{11}	1	4.6×10^{-5}
PS 1 (0.95 mg/ml)	5461-2378	16	1.0183	1.002×10^6	5.7×10^{11}	1	5.2×10^{-5}
PS 2 (2.12 mg/ml)	5461-2378	13	1.0178	1.001×10^6	5.8×10^{11}	1	4.0×10^{-5}
PS 3 (5.61 mg/ml)	5461-2753	13	1.0166	1.014×10^6	5.3×10^{11}	1	1.8×10^{-5}
Benzene-methanol (1:4 v/v)	5461-2756	11	0.6394	0.31×10^6	11×10^{11}	0.25	31.4×10^{-5}
Toluene-methanol (1:6 v/v)	5461-2803	10	0.8555	0.55×10^6	15×10^{11}	0.63265	16.0×10^{-5}
							$\sigma_{dn/dc}^b$
dn/dc_p			1.545×10^{-4}	3.0×10^2	4.98×10^9	7.7×10^{-7}	

^a σ_n was obtained by first computing the standard deviation of the residuals of the fit in terms of $(n^2 - x)^{-1}$, converting it to σ_n at the extremes of the range, and averaging. ^b The standard deviation of dn/dc_p does not reflect experimental errors in the usual manner, but rather the closeness of the fit of eq 12 to smoothed values of dn/dc_p .

for 35° at 546 nm and one value²⁴ for 30° in the ultra-violet region at 313 nm. The values in the visible region are in reasonably good agreement with the curve. However, the value at 313 nm is low both with respect

to the curve and with respect to a linear extrapolation of the other literature values at 546 and 436 nm.

(24) W. R. Krigbaum, P. Smith, and F. G. Mark, *J. Appl. Phys.*, **34**, 3218 (1963).

Surface Properties of Perfluoro Acids as Affected by Terminal Branching and Chlorine Substitution

by Marianne K. Bernett and W. A. Zisman

Naval Research Laboratory, Washington, D. C. 20390 (Received November 4, 1966)

When an otherwise fully fluorinated carboxylic acid molecule was altered by terminal branching and terminal chlorine atom substitution, significant increases resulted in the wettability of its adsorbed monolayer. Two new homologous series of acids, $(\text{CF}_3)_2\text{CF}(\text{CF}_2)_n\text{COOH}$ and $\text{CF}_2\text{Cl}(\text{CF}_3)\text{CF}(\text{CF}_2)_n\text{COOH}$, where n ranged from 11 to 1 and 9 to 1, respectively, were adsorbed as condensed monolayers on highly polished clean disks of chromium and platinum. The critical surface tension of wetting (γ_c) of each resulting surface was determined by contact angle measurements on homologous series of n -alkanes, open-chain polydimethylsiloxanes, and miscellaneous other liquids. In every case γ_c was increased by branching or by terminal chlorine substitution. Thus, in the series $(\text{CF}_3)_2\text{CF}(\text{CF}_2)_n\text{COOH}$, γ_c ranged from 13.3 (when $n = 11$) to a maximum of 15.2 dynes/cm (when $n = 1$). In the series $\text{CF}_2\text{Cl}(\text{CF}_3)\text{CF}(\text{CF}_2)_n\text{COOH}$, γ_c ranged from 17.2 (when $n = 9$) to around 20 dynes/cm (when $n = 1$). These results are excellent examples of the effect on γ_c on substituting one terminal chlorine atom in the surface for a fluorine atom. For a given acid monolayer, the same critical surface tensions were obtained on each of the two metals except when the acid was a lower homolog in each series. The results and causes are discussed in terms of adsorption site spacing, molecular packing, and chain adlineation of the adsorbed compound.

Introduction

The influence of chemical constitution on the wetting properties of solid surfaces has been investigated extensively by our laboratory.¹ A surface rich in covalent fluorine atoms had a critical surface tension of wetting (γ_c) which was lower than that containing any other chemical substituent. The lowest critical surface tensions ever reported were for smooth solid surfaces coated with a condensed monolayer of fully fluorinated fatty acids (or derivatives), oriented so as to present an outermost array of close-packed trifluoromethyl groups. As the molecular weight of the adsorbed compound increased, closer packing resulted through increased lateral cohesion and adlineation between neighboring fluorocarbon chains. The high members of the family of fully fluorinated n -alkanoic acids² were the compounds best fulfilling the requirements for vertical orientation, close packing, and molecular adlineation; the lowest value of γ_c yet reported (6 dynes/cm at 20°) was obtained with a condensed monolayer of perfluoro-

dodecanoic acid. Partially fluorinated long-chain fatty acids, where the completely fluorinated portion is attached to an unfluorinated alkyl chain terminated by the carboxylic acid group,³ adsorbed as monolayers whose values of γ_c were slightly higher.⁴ Complete adlineation of adjacent adsorbed molecules of these partially fluorinated acids was not possible because of the smaller cross-sectional diameter of the hydrocarbon segment compared to the fluorocarbon segment.

Since such small departures from complete adlineation of the adsorbed aliphatic molecules caused observable changes in the critical surface tension of the coated solid, any other change in molecular structure affecting molecular packing in the monolayer would

(1) W. A. Zisman, *Advan. Chem.*, **43**, 1 (1964).

(2) E. F. Hare, E. G. Shafrin, and W. A. Zisman, *J. Phys. Chem.*, **58**, 236 (1954).

(3) N. O. Brace, *J. Org. Chem.*, **27**, 4491 (1962).

(4) E. G. Shafrin and W. A. Zisman, *J. Phys. Chem.*, **66**, 740 (1962).

also be expected to measurably alter γ_c . This report is concerned with the effect on γ_c of (a) introducing terminal branching in the fully fluorinated acid molecule and (b) replacing with chlorine a fluorine atom attached to the ω (or terminal) carbon atom. The influence of the metal substrate on the packing density, wettability of the adsorbed monolayer, and value of γ_c was also investigated.

Experimental Materials and Methods Used

Compounds investigated were members of two new homologous series of acids with the general formulas $(CF_3)_2CF(CF_2)C_nOOH$ and $CF_2Cl(CF_3)CF(CF_2)_nCOOH$, where n ranges from 1 to 11 and 1 to 9, respectively. Table I gives the boiling points and melting points of these compounds as prepared by Hauptschein and co-workers.⁵ These carefully distilled compounds were used without further purification.

Table I: Melting Points and Boiling Points of Branched Fluorinated Acids $CF_2X(CF_3)CF(CF_2)_nCOOH^a$

n	X = F		X = Cl	
	Mp, °C	Bp, °C (mm)	Mp, °C	Bp, °C (mm)
1	...	141 (760)	...	100 (50)
3	...	130 (150)	...	115 (28)
5	33-36	115 (20)	...	134 (24)
7	61-64	125 (10)	44-50	141 (8)
9	88-89	117 (0.5)	71-74.5	117 (0.3)
11	100-107	...		

^a See ref 5.

Each compound was adsorbed on plane polished disks of chromium and platinum, whose purity was reported as 99.99% by weight or better. A mirror finish to each metal was imparted by standard metallographic procedures which included rubbing on 3M 600-grit silicon carbide paper under water, followed by 4/0 emery paper and then polishing on a metallographic cloth impregnated with an aqueous dispersion of 0.3- μ Al_2O_3 (Linde "Fine Abrasive" A-5175). The last step consisted of gentle rubbing on a grease-free wet cloth followed by copious rinsing with freshly distilled grease-free water to remove any adhering abrasive. The completely water-wetted and therefore "clean" metal specimen in the sense of being free from organic contamination was dried in a clean, grease-free oven for 10 min at 120°, cooled in an acid-cleaned covered glass container, and used as soon as possible in the adsorption experiments.

A condensed monolayer of each acid was adsorbed on the clean, dry metal specimen by the melt retraction method⁶ which depends on the autophobic property of the molten acid. (When a nonspreading drop of pure acid is rolled over the solid surface, it leaves an adsorbed monolayer behind.) If the acid was solid at room temperature, the metal specimen was first heated to a few degrees above the melting point of the compound. After a 10-min contact of liquid acid and metal surface, the residual sessile drop of surplus liquid was carefully rolled off and removed with the help of a loop of clean platinum wire. The monolayer-coated specimen was stored briefly at 25° in a clean covered container until used for the measurements of contact angles.

After each set of measurements, the adsorbed acid monolayer was completely removed from the metal surface to allow adsorption by another acid. The platinum disk could be readily freed of the adsorbed monolayer by brief flaming to a dull red heat; hence the polishing procedure had to be repeated only for the last few steps. Chromium, however, held the monolayers of the adsorbed carboxylic acids so tenaciously that even immersion in a 50/50 hot nitric acid-sulfuric acid bath for 3 hr or ultrasonic agitation in Freon 113 solvent for 15 min could not remove them. Therefore, prior to each adsorption experiment on chromium, the complete procedure, starting with the polishing on 3M 600-grit silicon carbide paper, had to be repeated.

The wettability of each adsorbed monolayer was determined by measuring, with a previously described goniometer telescope,⁷ the slowly advancing contact angle of each of the various pure liquids listed in Tables II and III. Any traces of polar impurities in each liquid were removed just prior to use by slowly percolating the liquid through an adsorbent column packed with Florisil and activated alumina. Each contact angle reported in Tables II and III was the average of at least three measurements on different sessile drops using several independently prepared surfaces. Unless stated otherwise, all observations reported were made in room air at 25° and 50% relative humidity.

Wettability of $(CF_3)_2CF(CF_2)_nCOOH$ Monolayers

Table II lists the contact angle θ and surface tension γ_{LV} of most of the liquids used for wettability measurements on chromium or platinum coated with an

(5) M. Hauptschein and M. E. Miville, Canadian Patent 735,493 (1966).

(6) R. L. Cottingham, E. G. Shafrin, and W. A. Zisman, *J. Phys. Chem.*, **62**, 513 (1958).

(7) H. W. Fox and W. A. Zisman, *J. Colloid Sci.*, **5**, 514 (1950).

Table II: Contact Angles of Liquids on Monolayers of $(CF_3)_2CF(CF_2)_nCOOH$ Series Adsorbed on Chromium and Platinum (25°)

Liquids	γ_{LV} , dynes/cm	Contact angles, deg											
		$n = 11$		$n = 9$		$n = 7$		$n = 5$		$n = 3$		$n = 1$	
		Cr	Pt	Cr	Pt	Cr	Pt	Cr	Pt	Cr	Pt	Cr	Pt
<i>n</i> -Alkanes													
Hexadecane	27.6	73	72	72	71	70	69	69	69	68	68	65	57
Tetradecane	26.7	69	69	68	69	66	66	65	65	65	65	63	52
Tridecane	25.9	68	65	66	66	64	65	63	63	62	63	61	49
Dodecane	25.4	66	64	65	65	63	62	60	61	60	59	59	47
Undecane	24.7	64	60	62	63	60	60	59	59	58	52	55	41
Decane	23.9	62	58	60	60	57	58	58	55	56	50	54	40
Octane	21.8	53	52	51	52	49	49	51	52	48	44	47	30
Heptane	20.3	49	48	48	44	42	44	46	45	42	35	41	22
Critical surface tension, ^a dynes/cm	...	13.3	13.3	14.0	13.9	14.5	14.5	14.8	14.8	15.0	17.2	15.2	19.0
Miscellaneous liquids													
Water	72.8	116	111	116	106	110	90	110	90	103	70	103	85
Formamide	58.2	104		104						80			
Methylene iodide	50.8	98	98	98	97	97	98	97	98	96	95	94	85
Ethylene glycol	47.7	97	Unstable	92	Unstable					75	Unstable		
Trichlorobiphenyl	45.3	94	91										
α -Bromonaphthalene	44.6	87	84	85	84					82	55		
Tricresyl phosphate	40.9	84	81		81								
α -Methylnaphthalene	38.7	83	80										
Hexachloropropylene	38.1	79	79										
Dicyclohexyl	33.0	78	74		73								

^a Obtained from plot of $\cos \theta$ vs. γ_{LV} by extrapolation to $\cos \theta = 1$ of data points for the *n*-alkanes.

Table III: Contact Angles of Liquids on Monolayers of $CF_2Cl(CF_3)CF(CF_2)_nCOOH$ Series Adsorbed on Chromium and Platinum (25°)

Liquids	γ_{LV} , dynes/cm	Contact angles, deg									
		$n = 9$		$n = 7$		$n = 5$		$n = 3$		$n = 1$	
		Cr	Pt	Cr	Pt	Cr	Pt	Cr	Pt	Cr	Pt
<i>n</i> -Alkanes											
Hexadecane	27.6	56	54	56	55	54	51	52	48	50	26
Tetradecane	26.7	53	51	54	51	52	48	41	46	48	15
Tridecane	25.9	51	49	52	49	48	46	49	43	45	<10
Dodecane	25.4	49	47	50	48	47	43	47	38	40	<i>b</i>
Decane	23.9	43	40	43	41	42	39	42	34	36	<i>b</i>
Octane	21.8	35	31	35	32	36	29	34	22	≈ 20	<i>b</i>
Heptane	20.3	29	27	29	24	30	22	27	<i>b</i>	<i>b</i>	
Critical surface tension, ^a dynes/cm		17.2	17.8	17.5	18.3	18.0	18.7	18.4	20.2	19.6	26.6
Miscellaneous liquids											
Water	72.8	108	96	110	84	103	74	94	75	93	58
Formamide	58.2	102	Unstable	91			Spr	75			
Methylene iodide	50.8	91	92	92	87	90	87	91	Unstable	84	74
Ethylene glycol	47.7	95	Unstable					65			
Trichlorobiphenyl	45.3			79			72				
α -Bromonaphthalene	44.6	75	68	75			64	72			
Tricresyl phosphate	40.9			73			72				
α -Methylnaphthalene	38.7			72			69				
Hexachloropropylene	38.1			61			≈ 48				
Dicyclohexyl	33.0			63			60		56		

^a Obtained from plot of $\cos \theta$ vs. γ_{LV} by extrapolation to $\cos \theta = 1$ of data points for the *n*-alkanes. ^b Not reproducible.

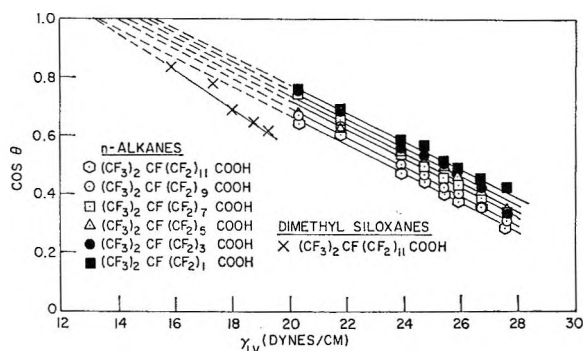


Figure 1. Wettability of $(\text{CF}_3)_2\text{CF}(\text{CF}_2)_n\text{COOH}$ monolayers adsorbed on chromium (25°).

oriented and condensed monolayer of any one of the series of $(\text{CF}_3)_2\text{CF}(\text{CF}_2)_n\text{COOH}$ acids. In Figure 1 are examples to show the consistency and rectilinearity of the data when $\cos \theta$ is plotted against γ_{LV} of the n -alkanes and the dimethylsiloxanes on chromium. The resulting intercepts on the $\cos \theta = 1$ line are the values of γ_c given in the middle of Table II. Although γ_c for the monolayer having $n = 1$ or $n = 3$ was larger for platinum than for chromium, values for $n > 3$ were nearly equal for the two metals.

A comparison of the contact angles of various liquids on the $(\text{CF}_3)_2\text{CF}(\text{CF}_2)_{11}\text{COOH}$ monolayer adsorbed on chromium with those on platinum reveals that they were nearly the same when the liquids were the n -alkanes or polydimethylsiloxanes; however, other hydrocarbons or halogen-containing liquids generally exhibited somewhat higher contact angles on the former metal substrate. The possibility that solvent action of the liquid drop had removed the monolayer resting beneath was eliminated when saturation of any of these liquids, such as ethylene glycol, with $(\text{CF}_3)_2\text{CF}(\text{CF}_2)_{11}\text{COOH}$ resulted in sessile drops with unaltered contact angles. Apparently the packing of the adsorbed acid molecules was not the same on each metal and there resulted an appreciable difference in the penetration of such small molecules as water, ethylene glycol, and formamide. This difference in packing will be discussed in a later section.

Effect on γ_c of Replacing a Terminal Fluorine Atom by Chlorine

The contact angles of each of a variety of liquids on an adsorbed condensed monolayer on chromium and platinum of the $\text{CF}_2\text{Cl}(\text{CF}_3)\text{CF}(\text{CF}_2)_n\text{COOH}$ series of acids were measured as before; the resulting plots of $\cos \theta$ vs. γ_{LV} for the n -alkane liquids were good rectilinear plots like those of Figure 1; from these were obtained the values of γ_c given in the middle of Table III. It should be noted that γ_c for each metal sub-

strate was about the same for the high homologs, but they became noticeably different for those acids having $n < 3$. Only when $n = 1$ was there poor reproducibility of the n -alkane contact angles.

Previous investigations⁷⁻¹⁰ had demonstrated that γ_c was lowered when a hydrogen atom in the surface of a solid was replaced with fluorine, whereas γ_c was raised on replacing it with a chlorine atom. Present data here confirm this conclusion. A difference in γ_c of 3.2 ± 0.2 dynes/cm was obtained for all comparable pairs of monolayers, where one chlorine atom was substituted for a fluorine on the terminal carbon, adsorbed on chromium as n varied from 9 to 3 (Tables II and III). With platinum as the substrate, the difference in γ_c was 3.9 ± 0.1 dynes/cm for all values of n from 9 to 5, but it increased when n was lower. The rise in γ_c by 3.2 and 3.9 dynes/cm, depending on the metal substrate, is comparable to the reported rise in γ_c of from 2.5 to 4 dynes/cm when the fluorine atoms were replaced progressively by chlorine atoms in the series of halogenated polyethylene surfaces.¹⁰ The rise in γ_c following substitution of a chlorine for a fluorine atom was thus of the same magnitude whether the surface was a closely packed adsorbed monolayer of carboxylic acid or was a polymer whose covalent chlorine and fluorine atoms are distributed statistically in the surface.

Figure 2 compares γ_c for adsorbed condensed monolayers of the two series of terminally branched fluorinated acids with that of the straight-chain fluorinated acid series $\text{F}(\text{CF}_2)_N\text{COOH}$ on the basis of equal values of N , where N is the number of fluorinated carbon atoms in the principal n -alkyl chain. The similarity between the straight chain and branched acids adsorbed on chromium and between those adsorbed on platinum is readily seen, as well as the displacement toward higher γ_c with the successive change in molecular structure from straight chain to terminally branched to chlorine atom substitution.

Influence of Metal Substrate on Packing of Adsorbed Molecules

The difference in γ_c between monolayers of the same low homolog adsorbed on chromium and platinum reveals a difference in the surface density of adsorption sites on these metals. In a recent investigation of stearic acid monolayers adsorbed on various metals, Timmons and Zisman¹¹ observed similar variations in γ_c and ex-

(8) A. H. Ellison and W. A. Zisman, *J. Phys. Chem.*, **58**, 260 (1954).

(9) E. G. Shafrin and W. A. Zisman, *ibid.*, **64**, 519 (1960).

(10) H. W. Fox and W. A. Zisman, *J. Colloid Sci.*, **7**, 109 (1952).

(11) C. O. Timmons and W. A. Zisman, *J. Phys. Chem.*, **69**, 984 (1965).

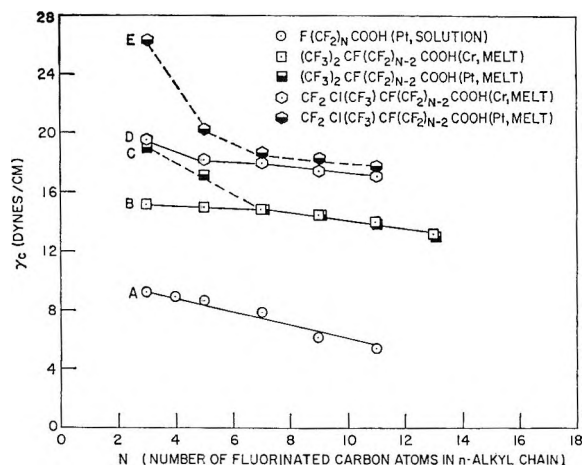


Figure 2. Effect of molecular structure on γ_c .

plained them in terms of the differences in metal lattice parameters and atomic radii. The carboxylic acids, because of their large cross-sectional areas, could not adsorb over each adsorption site when the cross-sectional radius of the acid was less than twice the atomic radius of the substrate metal. This misfit in packing was shown to become more pronounced as the acids decreased in chain length because the decreased lateral attraction between the principal chains of the adsorbed molecules promoted looser molecular packing and also increased tilting and vibration away from the vertical. Similar conclusions resulted from the present study of the fully fluorinated branched acids. When $\cos \theta$ of each n -alkane liquid was plotted against N (the number of fluorinated carbon atoms in the principal n -alkyl chain of the adsorbed fluorinated acid), values of $\cos \theta$ for chromium (Figure 3a) and platinum (Figure 3b) were nearly identical when N ranged from 13 to 7. However, when $N = 5$, $\cos \theta$ values for the platinum substrate increased somewhat over those for chromium (*i.e.*, θ became smaller); when $N = 3$ this difference became markedly larger.

Analogous behavior was observed with films of the terminally monochloro-substituted acids adsorbed on these two metals. When N ranged from 11 to 7, the contact angles of a given n -alkane on the monolayers adsorbed on chromium (Figure 4a) were nearly the same as on those adsorbed on platinum (Figure 4b). When $N < 7$, the contact angles varied widely between metal substrates; for instance, where $N = 3$ sessile drops of alkanes lower than tetradecane had very small and irreproducible contact angles on the coated platinum, whereas they were larger and reproducible on coated chromium. The comparative behavior of these coated metals followed the same pattern as those coated with the fully fluorinated acids except that detectable

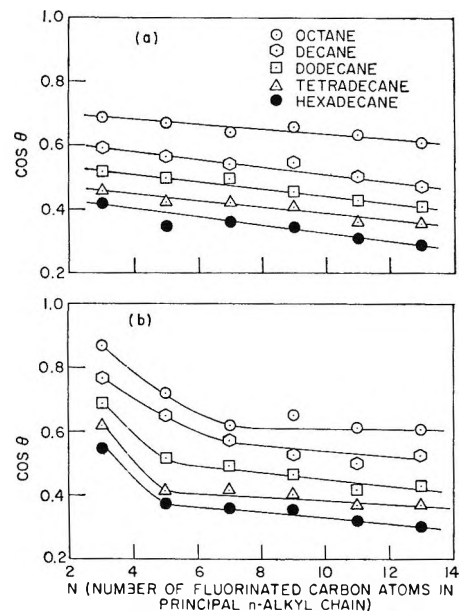


Figure 3. Influence of metal substrate on packing of adsorbed monolayers of $(\text{CF}_3)_2\text{CF}(\text{CF}_2)_{N-7}\text{COOH}$ determined by n -alkanes on (a) chromium and (b) platinum.

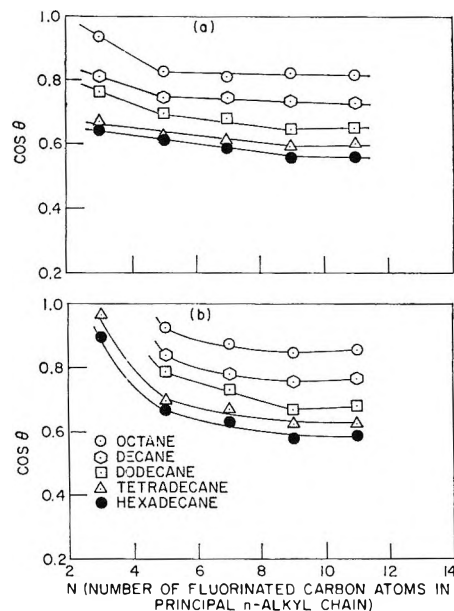


Figure 4. Influence of metal substrate on packing of adsorbed monolayers of $\text{CF}_2\text{Cl}(\text{CF}_3)\text{CF}(\text{CF}_2)_{N-2}\text{COOH}$ determined by n -alkanes on (a) chromium and (b) platinum.

variations began with higher members of acids and became even more noticeable with lower ones.

The smaller contact angles exhibited by the lower n -alkanes might be attributed to the ability of a drop of such a liquid to dissolve the adsorbed monolayer beneath. However, drops of each n -alkane saturated with the appropriate fluorinated acid exhibited the

same contact angles as those observed with the pure *n*-alkane. The possibility of such solvent action was also investigated in another way by allowing a large drop of the *n*-alkane liquid to remain on the adsorbed acid monolayer for increasingly longer times. The drop was then removed with a filter paper and a fresh drop of the *n*-alkane placed on the identical spot. Since in each case the contact angle values were the same, no significant fraction of the adsorbed monolayer could have been removed by the solvent action of the *n*-alkane. The sharp decrease in contact angles exhibited on monolayer coatings of the short-chain acids ($N = 3$ and 5) could have resulted from evaporation of the adsorbed monolayers. Therefore, contact angles of freshly deposited drops of an alkane were measured immediately after coating the metal with the monolayer and again 20 hr later to detect any decrease with time. As no difference was observed in the contact angles, the possibility of monolayer evaporation was ruled out.

Since smaller contact angles exhibited by the lower *n*-alkanes were not artifacts produced by either solution or evaporation of the adsorbed acid monolayer, the cause must lie in a difference in packing of the adsorbed film of the lower acids. The high molecular homologs of each series pack in a manner which results in the same value of γ_c regardless of the difference in the lattice parameters of the two metals. This does not appear possible unless there is a difference in axial tilting of the molecules adsorbed on these metals. Curves B and C in Figure 2 show clearly that γ_c is the same when $N = 7$. Decreased intermolecular cohesion between the adsorbed molecules when $N < 7$ results in increased axial vibration and tilting. This would explain the smaller contact angles and the divergence in curves B and C (and D and E) from that point on. Possibly, if curves D and E were extrapolated to high values of N , they also might eventually merge to indicate again that with adequate molecular chain length the intermolecular attraction becomes sufficient to make the nature of the substrate surface inconsequential.

The cross-sectional radius of the normal (or stretched-out) configuration of a $(CF_3)_2CF(CF_2)_nCOOH$ molecule is 3.9 Å (as measured by Stuart-Briegleb molecular models) which corresponds to a cross-sectional area of 48.2 Å². This large area was obtained when each branched perfluoroisopropyl group $(CF_3)_2CF-$ located at the terminal of the acid molecule was oriented identically, as shown in Figure 5a. When alternate adsorbed molecules in each horizontal row were given a 90° rotation around the principal axis and those in the next row were shifted by one molecule, the resulting

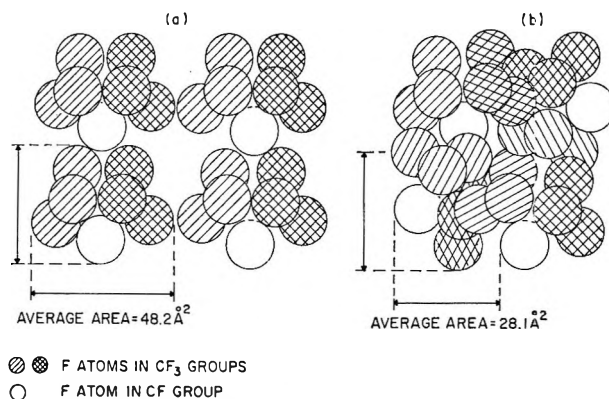


Figure 5. End view of $(CF_3)_2CF(CF_2)_nCOOH$ molecules in different packing arrangements.

planar arrangement, shown in Figure 5b, was more closely packed. The resulting average area per molecule of this arrangement was only 28.1 Å² and the corresponding cross-sectional radius was 2.9 Å. Assuming that the acid molecules will adsorb directly over one of the metal atoms which are arranged in a hexagonal close-packed array, they will be able to pack closer on substrates of smaller radius. The atomic radius of chromium atoms in the surface of the metal is smaller than that of platinum;¹² hence there will be closer packing of the adsorbed acid molecules on chromium and γ_c should be lower on chromium than on platinum. Evidence of lower values of γ_c is found in the adsorbed short-chain acids where, as discussed earlier, the decreased lateral attraction between the adsorbed molecules of short chain length permits looser molecular packing. This difference in packing becomes more obvious when the cross-sectional radius of the acid is less than twice the atomic radius of the substrate metal.

The much lower melting point of each terminally branched acid than that of the straight-chain acid having the same number of carbon atoms in the *n*-alkyl chain suggests a somewhat less well-adapted crystal structure of the branched compound. Figure 6 compares the melting points of the perfluoro *n*-alkanoic acids (curve A) with those of the terminally branched acids (curves B and C) on the basis of the same principal chain length. Melting points of these fluorinated acids are also compared with those of the analogous unfluorinated acids, as shown in curves D and E.¹³ The melting point difference between curves A and B for equal chain length is about 20° in each case,

(12) R. T. Sanderson, "Chemical Periodicity," Reinhold Publishing Corp., New York, N. Y., 1960, pp 26-28.

(13) K. E. Arosenius, G. Stallberg, E. Stenhagen, and B. Tägtstrom-Eketop, *Arkiv Kemi Mineral. Geol.*, A26(19), 20 (1948).

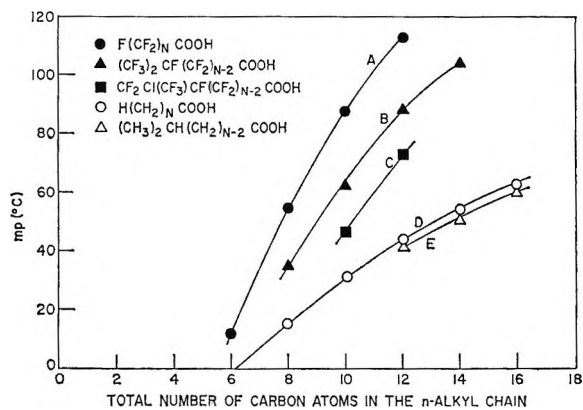


Figure 6. Melting points of aliphatic and fluorinated aliphatic acids.

whereas for the unfluorinated acids the difference between curves D and E is only about 2 or 3°. Thus, branching on the carbon atom next to the terminal carbon has a much larger disrupting influence on the crystalline structure of the fluorinated than of the hydrocarbon fatty acids since the bulky perfluoroisopropyl group presents a larger steric hindrance than the much smaller isopropyl group. Hence, close packing as illustrated in Figure 5b may occur only for the long-chain acids.

As expected, molecules of $\text{CF}_2\text{Cl}(\text{CF}_3)\text{CF}(\text{CF}_2)_n\text{COOH}$ cause greater disruption and disorientation in the crystal structure because of the presence of the large chlorine atom; this effect is evidenced by the even lower melting points (Figure 6) and the higher values of γ_c of their adsorbed monolayers.

Maximum Pore Size in Adsorbed Monolayer

Timmons and Zisman¹⁴ have shown that penetration of adsorbed monolayers by the molecules of liquid occurs when the cross-sectional dimensions of the pores in the monolayer are as large (or larger) than the cross-sectional dimensions of the molecules in the sessile drop. In the investigation reported here, similar results were obtained. Thus, drops of the n -alkanes showed no significant contact angle hysteresis (difference between the advancing and receding contact angles) on any of the monolayers adsorbed on either metal. However, hysteresis was observed with liquids of such small molecular volumes (and cross-sectional areas) as water, methylene iodide, ethylene glycol, glycerol, and formamide. Of these liquids, only glycerol was completely free of contact angle hysteresis on monolayers of any of the high homologs of the $(\text{CF}_3)_2\text{CF}(\text{CF}_2)_n\text{COOH}$ series adsorbed on chromium. The molar volumes of these liquids at 25° expressed in cc/mole are 18.0 for water, 39.8

for formamide, 55.8 for ethylene glycol, 73.0 for glycerol, 80.5 for methylene iodide, 139.0 for α -bromonaphthalene, and 163.0 for n -octane.

From these data and the contact angle hysteresis observed, we can postulate that the pores between the molecules of a $(\text{CF}_3)_2\text{CF}(\text{CF}_2)_n\text{COOH}$ monolayer adsorbed on chromium must be small enough to prevent penetration of an α -bromonaphthalene molecule, but large enough to permit penetration of a methylene iodide molecule. Drops of glycerol showed no significant hysteresis and ethylene glycol with a hysteresis of 4° was a borderline case; however, these compounds can readily associate to form a dimer, corresponding to molar volumes of at least 146.0 and 112.0 cc/mole in the liquid state, respectively. Since liquids of larger molar volume than ethylene glycol did not exhibit hysteresis, its molar volume can be indicative of the limiting size capable of penetrating the monolayer. If the molecules are assumed to be of spherical shape, the average cross-sectional area of the intermolecular pores can be calculated to be approximately 39 Å². By using the same reasoning, the approximate maximum pore sizes of the other adsorbed monolayers were calculated for all members of the two acid series on both metals. The pore sizes of monolayers on chromium varied from 39 to 48 Å² for the fully fluorinated acids ranging from $n = 9$ to $n = 3$ and from 45 to 50 Å² for the chlorine-substituted acids in the same range of values of n . Comparable pore sizes of the monolayers on platinum ranged from 45 to 50 Å² for the branched perfluoro acids. No maximum pore size could be obtained with the chlorinated acids when $n < 5$; however, when $n > 5$, the pore size was about 48 Å².

Since liquids of small molar volumes can penetrate monolayers of the short-chain homologs, the molecular packing of these acid molecules must be less tight than that of the higher homologs. In addition, the more ready penetration by such liquids through monolayers adsorbed on platinum than on chromium is an indication of the more condensed molecular packing of each monolayer adsorbed on chromium.

Calculation of γ_c from Surface Composition

Since the large chlorine atom prevents free rotation of the CF_2Cl - group around the C-C bond, there exist three possible surface chemical positions of the chlorine atom in the molecule, as shown in Figure 7 as both top view and schematic. Assuming that all three arrangements are equally probable, the actual surface composition of an adsorbed monolayer of $\text{CF}_2\text{Cl}(\text{CF}_3)\text{CF}$ -

(14) C. O. Timmons and W. A. Zisman, *J. Colloid Interfacial Sci.*, **22**, 165 (1966).

$(\text{CF}_2)_n\text{COOH}$ molecules will consist of equal proportions of acid as indicated in Figure 7a, b, and c. The lowest value of γ_c obtained for any of the adsorbed monolayers of $\text{CF}_2\text{Cl}(\text{CF}_3)\text{CF}(\text{CF}_2)_n\text{COOH}$ molecules was 17.2 dynes/cm. Molecular ball models show that of the three types of molecules with $\text{CF}_3\text{-CF}_2\text{Cl}$, $\text{CF}_3\text{-CF}_2\text{-}$, and $\text{CF}_3\text{-CF}_2$ terminals, the chlorine atom

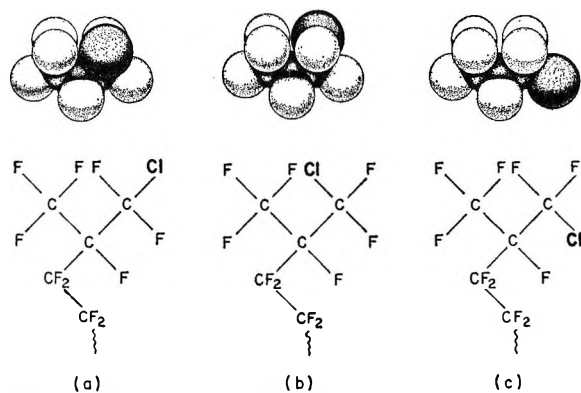


Figure 7. Three possible positions of the chlorine atom in the surface.

in two molecules is either completely below the surface (Figure 7c) or only partially present in it (Figure 7b). Surfaces whose constitution is comprised solely of a single molecular species in close packing have the following γ_c values: 6 dynes/cm for a $\text{CF}_3\text{-}$ surface,² 18 dynes/cm for a $\text{-CF}_2\text{-}$ surface,⁷ and 31 dynes/cm for a $\text{-CF}_2\text{Cl}$ surface.¹⁰ If the appropriate contributions determining the value of γ_c of the mixed system

are assigned according to their frequency of occurrence in the surface, γ_c can be computed for the surface.

$$\gamma_c = \frac{3\gamma_c(\text{CF}_3) + 2\gamma_c(\text{CF}_2) + \gamma_c(\text{CF}_2\text{Cl})}{6}$$

The resulting calculated value of $\gamma_c = 14$ is valid only if the acid molecules are packed as closely as the well-adlinedated, close-packed, perfluoro n -alkanoic acids for which γ_c is 6 dynes/cm. However, if to a first approximation the packing of the branched acids terminated by $\text{CF}_2\text{Cl-}$ groups is of the same surface density as that of the analogous terminally branched perfluoro acids, the value of γ_c for such a spacing should be 13.3 dynes/cm, which is the lowest value of γ_c obtained for these close-packed acids (see Table II). If γ_c is now computed in the same manner as above, but the value of 13.3 dynes/cm is substituted for that of 6 dynes/cm as the contribution from the $\text{CF}_3\text{-}$ groups, a value of γ_c of 17.6 dynes/cm is calculated. This is in excellent agreement with the experimental value of 17.2 dynes/cm.

The above computation suggests the possibility of predicting γ_c for any surface whose molecular constitution, atomic arrangement, and surface density (packing) are known.

Acknowledgment. Through the cooperation of Dr. Murray Hauptschein and the Pennsalt Chemicals Corp., the two new homologous series of branched halogenated carboxylic acids investigated here were generously donated to this laboratory for research in surface chemistry.

Reactivity of 1-Bromoalkanes with Thiocyanate

by T. P. Wallace and C. H. Stauffer

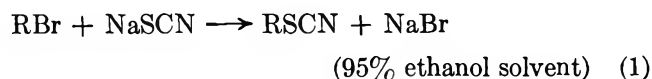
*Department of Chemistry, State University of New York at Potsdam, Potsdam, New York
(Received November 8, 1966)*

This investigation was concerned with the evaluation of the average rate constants, E_a , and ΔS^\ddagger for the S_N2 reaction of 1-bromoalkanes with the nucleophilic thiocyanate ion in a 95% ethanol medium. The 1-bromoalkanes studied contained the two-, four-, six-, and eight-membered carbon chains. The values of E_a for the reactions involving the four compounds showed no deviation within the experimental error. The values of ΔS^\ddagger showed no deviation within the experimental error for the four-, six-, and eight-membered carbon chains. However, the value of ΔS^\ddagger for 1-bromoethane was substantially larger. The results indicate that the two-carbon chain is the most reactive of the four compounds studied owing to a difference in the entropy of activation.

Introduction

Numerous reports in the literature indicate that the reactivity of straight-chain alkyl halides undergoing displacement reactions decreases from ethyl through butyl, but then increases as the length of the chain increases.¹

In 1953, Crowell² used the nucleophilic thiocyanate ion to determine the rate constants for the S_N2 reaction of various alkyl bromides with alcoholic sodium thiocyanate at 25°. The homogeneous reaction may be expressed by



The rate of reaction can be followed by determining the amount of thiocyanate ion present at different time intervals. Crowell² used Lang's iodine-cyanide method³ for the quantitative determination of the thiocyanate ion, but it was found that the Andrews method⁴ gave more reproducible results.

Crowell's² investigation was concerned only with the reaction of alkyl bromides with sodium thiocyanate at 25° in a solvent of 95% ethanol. Therefore, it was not possible to calculate the activation energies or the entropies of activation from the data. It was the purpose of this investigation to determine the activation energy as well as the entropy and enthalpy of activation for certain alkyl bromides as shown in eq 1. In order to do this, similar data were obtained at 0,

40, 60, and 70° for 1-bromoethane, 1-bromobutane, 1-bromohexane, and 1-bromooctane, thereby making available five rate constants over a 70° temperature differential. From these data, the activation energy and the entropy of activation for each alkyl bromide reacting with thiocyanate were calculated.

Experimental Section

A. Materials. Commercially available 1-bromoalkanes were shaken with cold concentrated sulfuric acid, washed with cold water, and then shaken with solid sodium bicarbonate. After being washed again with cold water, the alkyl bromides were dried for 24 hr over anhydrous potassium carbonate before being fractionated through a 60-cm vacuum-jacketed column packed with beryl saddles. The 1-bromohexane and 1-bromooctane were distilled at reduced pressures because of their higher boiling points.

Fisher Certified Reagent sodium thiocyanate was dried at 130° for 24 hr and then used to prepare an approximate 0.40 *M* solution, using 95 vol % ethanol as the solvent.

A standard solution of approximately 0.3 *N* potas-

(1) (a) J. B. Conant and R. E. Hussey, *J. Am. Chem. Soc.*, **47**, 488 (1925); (b) J. Semb and S. M. McElvain, *ibid.*, **53**, 690 (1931); (c) P. D. Bartlett and L. J. Rosen, *ibid.*, **64**, 543 (1942).

(2) T. I. Crowell, *ibid.*, **75**, 6046 (1953).

(3) R. Lang, *Z. Anorg. Allgem. Chem.*, **122**, 332 (1922); **142**, 239, 280 (1925); **144**, 75 (1925).

(4) L. W. Andrews, *J. Am. Chem. Soc.*, **25**, 756 (1903).

Table I: Reaction of SCN^- and 1-Bromoethane at 40°a

Reaction time, sec	$x, {}^b M$	$a^c - x, M$	$b^c - x, M$	$\log \frac{b(a-x)}{a(b-x)}$	$k \times 10^6, \text{l. mole}^{-1} \text{sec}^{-1}$
0	0	0.19663	0.13403		
7,740	0.01580	0.18083	0.11823	0.01809	8.60
16,440	0.03060	0.16603	0.10343	0.03909	8.75
25,340	0.04363	0.15300	0.09040	0.06107	8.53
42,660	0.06046	0.13617	0.07357	0.09743	8.40
79,380	0.08517	0.11460	0.04886	0.19172	8.88
90,660	0.08958	0.10705	0.04445	0.21427	8.73
104,160	0.09568	0.10095	0.03835	0.2538	8.97
					Av 8.68 \pm 0.18

^a Significant figures are considered in last column only (*i.e.*, values of k). ^b x represents the number of moles per liter which reacts in time t . ^c a and b represent the initial molar concentrations of SCN^- and RBr.

sium iodate was prepared after drying Fisher Certified Reagent potassium iodate at 120° for 2 hr.

For the quantitative analysis of thiocyanate, a concentrated stock solution of iodine monochloride was prepared⁵ and stored in the dark. This stock solution was prepared by adding 38.64 g of potassium iodate, 60 g of potassium iodide, and 450 ml of H_2O to 450 ml of concentrated hydrochloric acid. After the stock solution was prepared, 20 ml of carbon tetrachloride was added and the solution titrated with potassium iodate until the carbon tetrachloride layer was slightly pink. This provided a solution of iodine monochloride containing only a slight amount of iodine. This excess iodine was later removed by the addition of a drop of two of potassium iodate in the preparation of the solution for use in the quantitative determination of sodium thiocyanate.

B. Procedure. A quantity of alkyl bromide necessary to give a concentration of about 0.1 M was added to a 100-ml volumetric flask containing about 25 ml of 95% ethanol (solvent). All solutions and the flask were at the reaction temperature in a constant-temperature bath. After adding 50 ml of standard 0.4 M sodium thiocyanate, the solution was diluted to the 100-ml mark with solvent at the reaction temperature. At different time intervals, 5-ml samples were withdrawn from the reaction flask and added to an iodine monochloride solution prepared⁶ by adding 25 ml of the ICl stock solution to 50 ml of water, 5 ml of carbon tetrachloride (indicator), and 75 ml of concentrated hydrochloric acid. A separatory funnel was used to contain the above iodine monochloride mixture, as the two-phase system needed frequent shaking. Potassium iodate solution was added dropwise until the carbon tetrachloride layer was colorless. The sample from the reaction flask was then added to the separa-

tory funnel. The displacement reaction was quenched by rapid reaction of the thiocyanate with iodine monochloride. After the initial shaking, the sample was titrated with standard potassium iodate with frequent additional shaking until the carbon tetrachloride layer again just became colorless. The amount of thiocyanate present was calculated from the volume of standard potassium iodate added.

Calculations

Average rate constants, activation energies, and the precision of each were obtained in the usual manner⁷ by a linear least-squares analysis. The entropies of activation were then calculated using the appropriate quantities listed above. The computations were carried out by an IBM 1620 computer and appropriate Fortran programs.

Discussion

Table I indicates the variation in the rate constants with time. The standard deviation of the rate constants was between 2 and 3%.

The average rate constants in Table II follow the trend that has previously been reported for straight-chain alkyl halides.¹ The differences between the values for 1-bromohexane and 1-bromooctane are admittedly very close to the experimental error. However, repeated trials indicated that the 1-bromooctane was definitely the more reactive of the two compounds.

Table III shows the calculated values of the entropies of activation at various temperatures studied.

(5) I. M. Kolthoff and R. Belcher, "Volumetric Analysis, Titration Methods: Oxidation-Reduction Reactions," Vol. III, Interscience Publishers, Inc., New York, N. Y., 1957, p 456.

(6) See ref 5, pp 456, 457.

(7) S. Benson, "The Foundations of Chemical Kinetics," McGraw-Hill Book Co., Inc., New York, N. Y., 1960.

Table II: Average Rate Constants at Various Temperatures (Eq 1) (l. mole⁻¹ sec⁻¹)

Alkyl bromide	Temperature, °C				
	0	25 ^a	40	60	70
1-Bromoethane	6.74×10^{-7}	1.67×10^{-6}	8.68×10^{-6}	5.10×10^{-4}	12.8×10^{-4}
1-Bromobutane	5.60×10^{-7}	1.14×10^{-6}	5.99×10^{-6}	3.93×10^{-4}	9.50×10^{-4}
1-Bromohexane	6.20×10^{-7}	1.22×10^{-6}	6.46×10^{-6}	4.38×10^{-4}	9.98×10^{-4}
1-Bromooctane	6.41×10^{-7}	1.27×10^{-6}	6.88×10^{-6}	4.54×10^{-4}	10.2×10^{-4}

Table III: Entropy of Activation at Various Temperatures (cal deg⁻¹ mole⁻¹) (Reaction 1)

Compound	Temperature, °K				
	273.2	298.2	313.2	333.2	343.2
1-Bromoethane	-15.56	-15.31	-15.57	-15.57	-15.50
1-Bromobutane	-16.63	-16.71	-16.60	-16.66	-16.65
1-Bromohexane	-16.66	-16.79	-16.65	-16.64	-16.74
1-Bromooctane	-16.65	-16.76	-16.58	-16.62	-16.74

It is observed that the deviations with temperature are extremely small.

Table IV contains the thermodynamic quantities and the appropriate precision of each value. It is observed that the values of activation energy are the same within the experimental error as are the entropy of activation values, except for the entropy of activation of 1-bromoethane. 1-Bromoethane has the highest activation energy, yet it is the most reactive of the four compounds. The greater reactivity of 1-bromoethane compared to the longer chain homologs is due to a difference in the entropy of activation.

Table IV: Thermodynamic Quantities (eq 1)

Alkyl bromide	E_a , kcal mole ⁻¹	ΔS^\ddagger , cal mole ⁻¹ deg ⁻¹
1-Bromoethane	20.02 ± 0.22	-15.4 ± 0.1
1-Bromobutane	19.83 ± 0.07	-16.6 ± 0.1
1-Bromohexane	19.76 ± 0.10	-16.7 ± 0.1
1-Bromooctane	19.75 ± 0.12	-16.7 ± 0.1

Similar reactions have been observed where a decrease in reactivity caused by a decrease in entropy of activation has been accompanied by a decrease in activation energy. Crowell and Hammett⁸ investigated the reaction of ethyl and *n*-propyl bromides with thiosulfate ion. In this reaction, they observed a rate decrease in progressing from 1-bromoethane to the higher homologs, despite the fact that the acti-

vation energy became less. They attributed this situation to a decrease in the entropy of activation, as has been found for the thiocyanate reaction reported in this paper. They also pointed out that this effect was observed in ester hydrolysis⁹ and in the formation of semicarbazones.¹⁰ The decrease in the relative reactivity of the 1-bromoalkanes on progressing from the ethane member to higher homologs may possibly be attributed to an increase in the interference with the rotation about the C_α-C_β bond in the transition state due to the size of the β substituent.

It has been suggested¹¹ that the differences in the entropy of activation among 1-bromo-2-chloroethane, 1-bromo-2-fluoroethane, and 1,2-dibromoethane reacting with thiophenolate may be due to differences in the size of the β substituents. It is believed that the same situation exists in comparing the reactivity of 1-bromoethane with the higher homologs.

Therefore, the reactivity of 1-bromoethane relative to the other three homologs reacting with thiocyanate in a 95% ethanol medium results from a difference in the entropy of activation rather than any difference in the activation energy. It is believed that this difference in the entropy of activation is due to differences in the interference with the rotation about the C_α-C_β bond.

(8) T. Crowell and L. Hammett, *J. Am. Chem. Soc.*, **70**, 3444 (1948).

(9) H. Smith and J. Steel, *ibid.*, **63**, 3466 (1941).

(10) F. Price and L. Hammett, *ibid.*, **63**, 2387 (1941).

(11) J. Hine, "Physical Organic Chemistry," McGraw-Hill Book Co., Inc., New York, N. Y., 1962, pp 172-175.

Electron Spin Resonance of X-Ray Irradiated Polycrystalline and Single-Crystal Sodium Hexafluoroantimonate

by F. G. Herring, J. H. Hwang, and W. C. Lin

*Department of Chemistry, The University of British Columbia, Vancouver 8, British Columbia, Canada
(Received November 16, 1966)*

The esr spectra of X-ray irradiated polycrystalline and single-crystal NaSbF₆ were studied. The hyperfine structure was shown to be due to Sb¹²¹ with $I = 5/2$ and Sb¹²³ with $I = 7/2$. The coupling tensor A for Sb¹²¹ was found to be axially symmetric with $A_{\parallel} = 74.6$ gauss and $A_{\perp} = 60.8$ gauss and the g tensor was also found to be axially symmetric with $g_{\parallel} = 2.018$ and $g_{\perp} = 2.011$. The ratio of the coupling-tensor components of Sb¹²¹ to that of Sb¹²³ was found to agree with the ratio calculated from the accepted values of the nuclear magnetic moments. No hyperfine splittings due to the fluorine atoms were observed. The species was suggested to be either SbF₅⁻ or SbF₆²⁻.

Introduction

Morton reported¹ an esr study of irradiated NH₄PF₆ crystals and concluded that the radical formed was PF₄. The esr spectra showed large hyperfine interactions due to both the phosphorus and the fluorine nuclei. Moreover, the radical was found to rotate freely in the lattice for the spectra of an irradiated single crystal were found to be the same for all orientations and also the same as the spectrum of irradiated powder. We have found that when NaSbF₆ was irradiated with X-rays, a paramagnetic species was formed which was of quite a different type from the corresponding phosphorus complex. Most significant was the fact that the fluorine splitting was found to be absent. In addition, the radical was found not to be rotating but rather held rigidly in a fixed orientation compatible with the symmetry of the host crystal. In what follows, we shall present the experimental results and shall try to interpret the spectra as being due to either SbF₅⁻ or SbF₆²⁻. Both radical species represent antimony complexes with a formal valency of four. The former species could be formed from the SbF₆⁻ ion by the loss of one fluorine atom while the latter could be formed by the capture of an electron. At present, it is quite difficult to decide which assignment is the correct one but, as will be shown later, qualitative considerations seem to favor slightly the former choice.

Experimental Section

The powder sample of sodium hexafluoroantimonate, NaSbF₆, was from Alfa Inorganics, Inc., Beverly, Mass., without further purification. The single crystals were prepared by recrystallization from solutions containing hexafluoroantimonic acid, the latter being also obtained from Alfa Inorganics. Cubic crystals of approximately 1.5 mm to the edge were obtained. There were some minor contradictions in the description of the crystal structure in the literature.^{2,3} Unfortunately our esr work did not help to decide which is the more correct since, in general, the orientation of the radical formed does not necessarily have to be exactly the same as that of the parent molecule. In our work, we arbitrarily called three perpendicular edges of the cube the a , b , and c axes and obtained esr spectra with the external magnetic field lying, in turn, in the ab , bc , and ca planes. The irradiation technique and the esr spectrometer used in this work were the same as those described previously.⁴ The measurements were carried out at room temperature.

Results

None of the spectra showed any splittings due to the

- (1) J. R. Morton, *Can. J. Phys.*, **41**, 706d (1963).
- (2) N. Schrewelius, *Z. Anorg. Allgem. Chem.*, **238**, 245 (1938).
- (3) G. Tenfer, *Acta Cryst.*, **9**, 539 (1956).
- (4) W. C. Lin and C. A. McDowell, *Mol. Phys.*, **7**, 223 (1964).

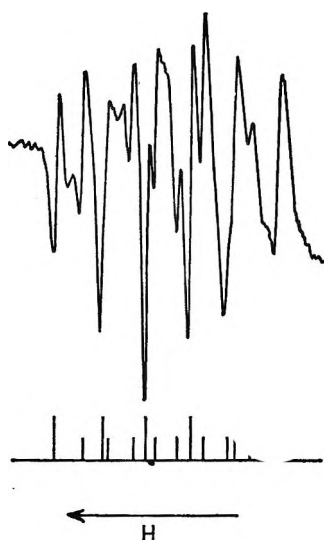


Figure 1. ESR spectrum of an X-ray irradiated single crystal of NaSbF_6 with $\mathbf{H} \parallel a$.

fluorine nuclei. For the special orientations with the external field \mathbf{H} parallel to the crystal axes, a , b , and c , all molecular sites were equivalent. Figure 1 shows the spectrum corresponding to \mathbf{H} parallel to a . The six major lines are attributed to the hyperfine interaction due to the isotope Sb^{121} with spin $I = 5/2$. The eight minor lines are due to isotope Sb^{123} with spin $I = 7/2$. The natural abundances of Sb^{121} and Sb^{123} are, respectively, 57.25 and 42.75%. Therefore the theoretical intensity ratio should be 1.78:1. For more general orientations, *i.e.*, with \mathbf{H} in the crystallographic planes ab , bc , and ca , there were two inequivalent sites; hence, there were 12 major lines. Figure 2 shows the spectrum for \mathbf{H} in the ab plane with direction cosines $1/\sqrt{2}$, $1/\sqrt{2}$, 0. Not all of the minor lines due to the species Sb^{123} could be seen. In fact, most of them were lost in the predominant structure of the major lines. Hence, for these orientations, only the splittings due to Sb^{121} could be measured. The observed splittings (hfs) were taken to be the differences between the first and the last lines, divided by the appropriate number of spacings, five for Sb^{121} and seven for Sb^{123} . The observed g values were deduced from the centers of the spectra. The components of the hyperfine coupling tensors were calculated from eq 1 written for Sb^{121} and the g -tensor components were calculated from eq 2, both by the method of least squares.

$$\text{hfs} = \frac{1}{2} \left[\left\{ \sum_{ijk} (A_{ik} - G\delta_{ik})(A_{kj} - G\delta_{kj})l_i l_j \right\}^{1/2} + \left\{ \sum_{ijk} (A_{ik} + G\delta_{ik})(A_{kj} + G\delta_{kj})l_i l_j \right\}^{1/2} \right] \quad (1)$$

$$g = \left[\sum_{ijk} g_{ik} g_{kj} l_i l_j \right]^{1/2} \quad (2)$$

Here, the subscripts $i, j, k = a, b, c$, δ_{ij} is the Kronecker delta, A_{ij} and g_{ij} are components of the A and g tensors, respectively, l_i are the direction cosines of \mathbf{H} , and $G = 2g_n \beta_n H_0 / g_e \beta_e$ with H_0 being the field corresponding to the center of the spectrum (this approximation is justified when $G \ll A_{ij}$). Equations 1 and 2 were deduced from first-order perturbation calculation using the spin Hamiltonian

$$\mathcal{H} = \beta_e \mathbf{H} \cdot \mathbf{g} \cdot \mathbf{S} + \mathbf{S} \cdot \mathbf{A} \cdot \mathbf{I} - g_n \beta_n \mathbf{H} \cdot \mathbf{I} \quad (3)$$

with the first term as the zero-order term and the last two terms as the first-order term and with \mathbf{S} being quantized in the direction of $\mathbf{H} \cdot \mathbf{g}$ and \mathbf{I} being quantized in the direction of the resultant field $(\mathbf{S} \cdot \mathbf{A} - g_n \beta_n \mathbf{H})$. Although the second-order perturbation is on the order of 1 gauss, it was not taken into account, for the observed hyperfine splitting was taken to be the average across the entire spectrum and the second-order effect increases the splitting on one end of the spectrum and decreases it on the other end. The second-order effect on the g shift was calculated to be 0.001 and was within the experimental error.

The \mathbf{A} and the \mathbf{g} tensors thus calculated are given below: for Sb^{121}

$$\mathbf{A} = \begin{bmatrix} 65.34 & 4.74 & 4.52 \\ 4.74 & 65.41 & 4.59 \\ 4.52 & 4.59 & 65.39 \end{bmatrix} \pm 0.5 \text{ gauss}$$

$$\mathbf{g} = \begin{bmatrix} 2.0134 & 0.0024 & 0.0025 \\ 0.0024 & 2.0133 & 0.0024 \\ 0.0025 & 0.0024 & 2.0127 \end{bmatrix} \pm 0.0015$$

for Sb^{123}

$$\mathbf{A} = \begin{bmatrix} 36.33 & \dots & \dots \\ \dots & 36.19 & \dots \\ \dots & \dots & 36.45 \end{bmatrix} \pm 0.5 \text{ gauss}$$

$$\mathbf{g} = \begin{bmatrix} 2.0113 & \dots & \dots \\ \dots & 2.0105 & \dots \\ \dots & \dots & 2.0085 \end{bmatrix} \pm 0.0015$$

For reasons previously mentioned, the \mathbf{A} and the \mathbf{g} tensors for Sb^{123} could not be completely determined. Thus, only the diagonal elements are given in order to compare with the corresponding elements for Sb^{121} . For the same reasons, the principal values of \mathbf{A} and \mathbf{g} could only be calculated for the isotope species Sb^{121} . These results are given in Table I. Note: Only one set of the relative signs of the direction cosines is given corresponding to one molecular site. The respective direction cosines corresponding to the re-

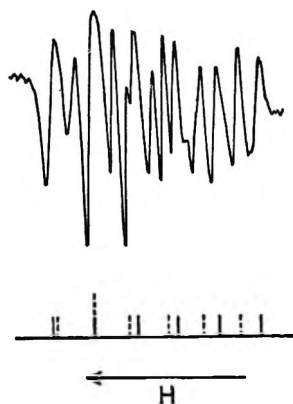


Figure 2. ESR spectrum of an X-ray irradiated single crystal of NaSbF_6 with \mathbf{H} having direction cosines $1/\sqrt{2}, 1/\sqrt{2}, 0$.

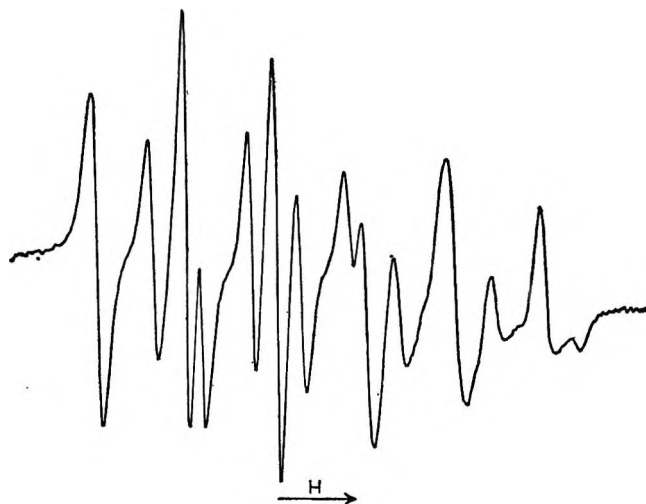


Figure 3. ESR spectrum of X-ray irradiated polycrystalline NaSbF_6 .

Table I

	Principal values of \mathbf{A} tensor, gauss	Principal axes with reference to crystal axes		
		a	b	c
A_{\parallel}	74.6 ± 0.5	0.577	0.583	0.573
A_{\perp}	60.9 ± 0.5	0.458	0.350	-0.817
	60.6 ± 0.5	-0.677	0.733	-0.065
Principal values of \mathbf{g} tensor				
g_{\parallel}	2.0180 ± 0.0015	0.600	0.584	0.546
g_{\perp}	2.0104 ± 0.0015	0.429	0.341	-0.836
	2.0110 ± 0.0015	-0.674	0.736	-0.046

maining three sites can be obtained by changing the signs of two direction cosines at a time.

From Table I it can be seen that the \mathbf{A} and the \mathbf{g} tensors are axially symmetric. Hence, the direction cosines of the two A_{\perp} (or g_{\parallel}) axes are entirely arbitrary and have no special significance. The unique principal axis A_{\parallel} (or g_{\parallel}) was found to make approximately equal angles with crystal axes a , b , and c ; *i.e.*, it is roughly parallel to the (1,1,1) direction of the cubic crystal.

In addition to the single-crystal work, the esr spectra of irradiated NaSbF_6 powder were also recorded and measured. A sample spectrum is shown in Figure 3. It shows six major lines due to Sb^{121} and eight minor lines due to Sb^{123} , both corresponding to the orientations with H perpendicular to the unique principal axis. In the spectrum, the fifth Sb^{121} line and the seventh Sb^{123} line are seen to be unresolved. The very weak line just outside the last Sb^{121} line is thought to be due to Sb^{121} but corresponding to H parallel to the unique principal axis. There should also be a very weak first Sb^{121} line for this orientation outside the low-field end of the spectrum. It was however not observed.

From the spectrum, the following results were obtained: for Sb^{121}

$$A_{\perp} = 59.4 \pm 1.0 \text{ gauss}$$

$$g_{\perp} = 2.018 \pm 0.002$$

for Sb^{123}

$$A_{\perp} = 32.6 \pm 1.0 \text{ gauss}$$

$$g_{\perp} = 2.018 \pm 0.002$$

That the assignment for the powder spectrum is correct can be seen from the fact that A_{\perp} for Sb^{121} calculated from single-crystal data was 60.7 ± 0.5 gauss comparable with the above figure of 59.4 ± 1.0 gauss. The g_{\perp} agreement was, however, not too satisfactory.

Finally, it is instructive to compare here the ratio of hyperfine splittings for the two isotopes with the theoretically expected value. The nuclear magnetic moments for Sb^{121} and Sb^{123} are, respectively, 3.3417 and 2.5335,⁵ in units of nuclear magnetons. The comparison is shown in Table II.

Table II: Ratio of $A(\text{Sb}^{121}):A(\text{Sb}^{123})$

Theoretical	Single crystal			Poly-crystalline A_{\perp}
	A_{aa}	A_{bb}	A_{cc}	
1.85	1.80	1.81	1.80	1.82

(5) Varian Associates, Inc., "NMR Table," 5th ed, Palo Alto, Calif., 1965.

Discussion

Unlike the case of NH_4PF_6 , the radical formed in NaSbF_6 was found not to be rotating at the temperature of the experiments. Fragments like SbF_4 or smaller ones are therefore not likely to be the species formed. Moreover, while it is more likely for phosphorus to be stable with a coordination number of four, it is less likely that antimony would have this coordination number. This leaves the most likely choice to be either SbF_5^- or SbF_6^{2-} , the former being formed by the loss of an F atom and the latter by the capture of an electron. The loss of an electron by SbF_6^- to form the neutral SbF_6 is also highly unlikely since it requires Sb to have a formal valency of six. For both SbF_5^- and SbF_6^{2-} , the formal valency of Sb is four, similar to that of phosphorus in PF_4 .

The structure of the normal ion SbF_5^{2-} has been investigated⁶ and was found to be that of a square pyramid with the Sb atom slightly below the plane of the square, the Sb-F bond length being 2.02 Å for the basal F atoms and 2.08 Å for the apex F atom. It has been discussed by Cotton and Wilkinson⁷ that for compounds of nontransitional elements, the AB_5 -type compounds with 10 valence electrons, *e.g.*, SbF_5 , have trigonal-bipyramid structure but those with 12 valence electrons, *e.g.*, SbF_6^{2-} , have square-pyramidal structure. Our radical is quadrivalent and has 11 valence electrons and hence does not fall in either category. We have, however, assumed that the radical SbF_5^- has essentially the same structure as SbF_5^{2-} . It thus belongs to the point group C_{4v} and the Sb atom can use hybrid orbitals of the type $\text{sp}^3\text{d}_{x^2-y^2}$ ⁷ to form bonds with fluorine atoms. This would leave the unpaired electron in a predominantly nonbonding d_{z^2} orbital. In C_{4v} symmetry, this last orbital belongs to the irreducible representation A_1 as are the s and the p_z orbitals. The inclusion of the p_z orbital makes it easier to explain the not too small anisotropy in the hyperfine coupling. Although d_{z^2} also contributes to the anisotropy, the magnitude has been shown to be very small for As⁸ and would be expected to be small for Sb also. The slight positive shift of the g value could also be explained if one assumes that there are nearby occupied orbitals of the E symmetry (p_x , p_y and d_{xz} , d_{yz}) such that, through spin-orbit coupling, mixing from states in which an electron is excited from a doubly occupied orbital to the singly occupied orbital becomes important. A virtual excitation of an electron from a doubly occupied orbital to a singly occupied orbital is equivalent to a hole resonance which is generally associated with a negative spin-orbit coupling parameter λ and a positive g shift while that from a singly occupied orbital

to an empty orbital is an electron resonance and is associated with a positive λ and a negative g shift (see, *e.g.*, ref 9).

Unfortunately, SbF_5^- seems not to be the only possibility which would satisfy most of the experimental results. By the capture of an electron, SbF_6^- could form the radical SbF_6^{2-} and one could expect a distortion of the octahedron along the trigonal axis. This would also put the extra electron in one of the nonbonding metal orbitals belonging originally to the T_{2g} representation, $[\text{d}_0, (\text{d}_2, \text{d}_{-1}), (\text{d}_{-2}, \text{d}_1)]^{10}$ of the O_h group. If the distortion is a flattening, the odd electron could go to a d_{z^2} orbital belonging to the A_{1g} representation of D_{3d} . In this case, however, the p_z orbital of the metal atom could not mix in and it would be more difficult to account for the not too small anisotropy observed for the A tensor. It would also be more difficult to explain the positive shift of the g value for there would be very closely located empty nonbonding orbitals of the E_g type (d_{xz} , d_{yz}) which would mix with the d_{z^2} orbital, and excitation from the singly occupied orbital to the empty orbital would be favored, resulting in a negative g shift. It would seem, therefore, that SbF_5^- is the better choice of the two but this is in no way conclusive. Perhaps it should be mentioned here that the trigonal axes of the parent SbF_6^- octahedron were, according to one worker,³ exactly parallel to the (1,1,1) axis of the cube while, according to the other,² nearly so. This is of course in close agreement with the fact that the unique principal axis of the A tensor was also found to be parallel to the (1,1,1) axis.

A semiempirical MO calculation of the electronic structure of SbF_5^- was carried out somewhat along the line described in a previous paper.⁸ Because of the lack of atomic data, simple ionization potentials of the neutral Sb atom were used instead of the valence-state ionization potentials. Also, no iteration to charge consistency was carried out such as was generally done. The problem was treated as a 41-electron, 33-orbital problem, and the calculation showed that the odd electron was in an A_1 orbital of the form

(6) A. Byström and K. A. Wilhelmi, *Arkiv Kemi*, **3**, 461 (1951).

(7) F. A. Cotton and G. Wilkinson, "Advanced Inorganic Chemistry," Interscience Publishers, Inc., New York, N. Y., 1962, pp 70, 307-312, 373.

(8) H. Hampton, F. G. Herring, W. C. Lin, and C. A. McDowell, *Mol. Phys.*, **10**, 565 (1966).

(9) C. P. Slichter, "Principles of Magnetic Resonance," Harper and Row, New York, N. Y., 1963, p 184.

(10) B. Bleaney and K. W. H. Stevens, *Rept. Progr. Phys.*, **16**, 131 (1953).

$$\begin{aligned}
&0.592(5s) - 0.758(5p_z) + 0.222(5d_{z^2}) - \\
&0.004(6s) - 0.095(2s^{(1)} + 2s^{(2)} + 2s^{(3)} + \\
&2s^{(4)}) + 0.014(2s^{(5)}) + 0.105(2p_z^{(1)} + \\
&2p_z^{(2)} + 2p_z^{(3)} + 2p_z^{(4)}) - 0.039(2p_z^{(5)} - \\
&0.122(2p_z^{(1)} + 2p_y^{(2)} - 2p_z^{(3)} - 2p_y^{(4)})
\end{aligned}$$

The above function shows that the orbital is predominantly a metal orbital with large 5s and 5p_z characters. If the unpaired electron is in a strictly nonbonding orbital, the hyperfine structure due to the fluorine atoms would, of course, be very small if not absolutely zero, owing to the presence of the dipolar interaction. However, one cannot expect the particular molecular orbital (MO) to be a pure metal orbital in this case. From the line widths, it was estimated that the maximum value for each fluorine hyperfine splitting was of the order of 5 gauss. This corresponds to a spin density of 0.0003 in the fluorine 2s orbital ($A_0 = 47,910$ Mcps¹¹) and implies a coefficient of the order of 0.02 for the

fluorine 2s orbital in the MO. This agrees with only one of the coefficients in the above calculated MO but one, of course, must remember that the empirical calculation was very crude and the result should not be taken too seriously.

No similar calculation was carried out for the molecular species SbF_6^{2-} mainly because of the geometrical complexity. A qualitative argument would put the unpaired electron in a predominantly metal A_{1g} orbital of the D_{3d} point group consisting largely of 5s and 5d_{z²} orbitals of Sb.

Acknowledgments. The authors wish to thank Professor C. A. McDowell for discussions and constant interest in the work and to the National Research Council of Canada for a generous grant in support of the research. The authors also wish to thank the referees for making many useful suggestions.

(11) J. R. Morton, *Chem. Rev.*, **64**, 456 (1964).

Chlorophyll-Poly(vinylpyridine) Complexes.

I. Conditions for Formation and Stability

by G. R. Seely

Contribution No. 268 from the Charles F. Kettering Research Laboratory, Yellow Springs, Ohio
(Received November 21, 1966)

Chlorophyll and some of its derivatives form complexes with poly(4-vinylpyridine) in nitromethane by binding of the metal of the pigment to the pyridine nitrogen of the polymer. The binding of chlorophyll to the polymer is followed by observing small changes in the position and width of the main red band of the absorption spectrum. Chlorophyll-polymer aggregates result which may have as few as five to ten pyridine groups per molecule of chlorophyll. The extent of binding at low polymer concentration and the spectrum of the complex are affected by the presence of water or other impurities in the nitromethane. In pure, dry nitromethane, chlorophyll forms aggregates which are probably dimers of the same sort as those that are supposed to exist in hydrocarbon or chlorocarbon solvents; they are broken up on addition of polymer. In dense aggregates of chlorophyll on polymer, fluorescence is largely quenched; on further addition of polymer, the fluorescence is restored, and the degree of polarization of fluorescence excited by polarized light is increased. The dependences of quenching and of depolarization of fluorescence on polymer concentration suggest that there is energy transfer between pigment molecules attached to the same polymer molecule. An energy of 1 kcal/mole was calculated, using an Ising model, for adjacent chlorophyll molecules attached to the same polymer. A polymer-catalyzed allomerization of chlorophyll by O₂ was noted. Magnesium phthalocyanine also forms aggregates with poly(vinylpyridine) which have properties very similar to those of chlorophyll.

Introduction

There is substantial evidence that the chlorophyll molecules in the chloroplast are grouped into aggregates, the so-called photosynthetic units, the functions of which are to absorb light, transfer the excitation energy to a reaction center which probably consists of one or more chlorophyll molecules in a special environment, and there to convert it into chemical energy.¹

In efforts to gain a better understanding of these processes, there has naturally been much interest in the study of the physical and chemical properties of artificial aggregates of chlorophyll. Previous investigations of this sort have employed chlorophyll and its derivatives in suspensions,^{2,3} emulsions,⁴⁻⁶ adsorbates,^{7,8} and monolayers.⁹ Most of these have been macroscopically heterogeneous systems, the investigation

of which has been complicated by light scattering, and sometimes by instability. We now report properties of a new kind of aggregate of chlorophyll and related

(1) R. K. Clayton in "The Chlorophylls," L. P. Vernon and G. R. Seely, Ed., Academic Press, Inc., New York, N. Y., 1966, Chapter 19, p 609.

(2) L. P. Vernon, *Acta Chem. Scand.*, **15**, 1639, 1651 (1961).

(3) B. B. Love, *Biochim. Biophys. Acta*, **64**, 318 (1962).

(4) L. P. Vernon and E. R. Shaw, *Biochemistry*, **4**, 132 (1965).

(5) M. Hertogs and J. S. C. Wessels, *Biochim. Biophys. Acta*, **109**, 610 (1965).

(6) A. I. Oparin, K. B. Serebrovskaya, and G. I. Lozovaya, *Dokl. Akad. Nauk SSSR*, **162**, 1418 (1965).

(7) R. A. Cellarius and D. Mauzerall, *Biochim. Biophys. Acta*, **112**, 235 (1966).

(8) G. G. Komissarov, V. A. Gavrilova, L. I. Nekrasov, N. I. Kobozev, and V. B. Evstigneev, *Dokl. Akad. Nauk SSSR*, **150**, 174 (1963).

(9) W. D. Bellamy, G. L. Gaines, Jr., and A. G. Tweet, *J. Chem. Phys.*, **39**, 2528 (1963).

compounds, prepared by reversible attachment of the pigment to a high molecular weight polymer in dilute solution. The systems are homogeneous and may be studied by ordinary spectroscopic techniques. The size of the aggregates and the number of pigment molecules in each of them can be varied within wide limits, making them promising subjects for studying the effect of pigment density on energy transfer, fluorescence quenching, and photochemical activity.

Chlorophyll and other metal-containing pigments can be attached to poly(4-vinylpyridine), by taking advantage of their ability to form complexes with basic substances such as water, alcohol, pyridine, and the pyridine side groups of the polymer.¹⁰ The choice of solvent was critical; nitromethane was selected because it dissolves both the polymer and chlorophyll, but does not compete with the polymer as a complexing agent for chlorophyll even in dilute polymer solution. Although no survey of solvents was made, it is unlikely that many would be as suitable as nitromethane. In early attempts to form chlorophyll-poly(vinylpyridine) complexes in ethanol,¹¹ we found that to achieve appreciable complexing, the polymer concentration had to be so high (*ca.* 1%) that "aggregates of chlorophyll" could hardly be said to exist.

In the present article, the conditions for formation and stability of chlorophyll-poly(vinylpyridine) aggregates are discussed; later articles will be devoted to detailed examination of particular photophysical and photochemical properties.

Experimental Section

Materials. *Poly(vinylpyridine).* Freshly distilled 4-vinylpyridine (Reilly Tar and Chemical) was diluted with an equal volume of ethanol and polymerized at 70–80° under N₂ for 2–3 hr with 2,2'-azobisisobutyronitrile as the initiator. The polymer was precipitated out of ethanol with ethyl acetate or ether at least four times and dried. Most work was done with two samples, of intrinsic viscosities 1.95 and 3.5 dl/g in ethanol. Their weight-average molecular weights, determined from light scattering in ethanol, were 425,000 and 1,210,000—somewhat less than those calculated from their intrinsic viscosities by the equation of Berkowitz, *et al.*,¹² 530,000 and 1,245,000.

Nitromethane is a poor solvent for poly(4-vinylpyridine), and dilute (~1%) solutions become turbid on refrigeration. The intrinsic viscosity was about half that in ethanol—0.90 dl/g for the first polymer sample. In attempts to determine the molecular parameters of poly(vinylpyridine) by measuring light scattering in nitromethane, we encountered persistent anomalies in the dissymmetry of scattered light,

which may have been of the same origin as those which Utiyama and Kurata have ascribed to optical anisotropy.¹³ We have not pursued this matter further.

Pigments. Chlorophylls a and b were prepared by the methods of Zscheile and Comar¹⁴ and of Anderson and Calvin;¹⁵ ethyl chlorophyllide a was prepared by the method of Holt and Jacobs.¹⁶ Magnesium phthalocyanine (Du Pont) was recrystallized from pyridine-methanol to remove a yellow impurity.

Pyrochlorophyll a was prepared by a variation of the Anderson-Calvin procedure. The thawed and drained contents of a 10-oz package of frozen spinach (Birdseye) were extracted with 500 ml of acetone in a Waring blender, diluted with water to 70% acetone, and chromatographed on polyethylene. The chlorophyll a fraction was evaporated to dryness in a rotary evaporator, dissolved in 10 ml of pyridine, and pyrolyzed by refluxing for 24 hr under N₂. The pyridine was removed by evaporation, and the residue was chromatographed on sugar with isooctane + 0.2% propanol, and on polyethylene with acetone. Pyrochlorophyll a was precipitated from a 1:1 acetone-water mixture, dissolved from the filter with purified acetone, and evaporated to dryness. The spectrum in acetone was very similar to that of chlorophyll a. The HCl number was 23–24.

The preparation of zinc pyropheophytins a and b started as an attempt to prepare the pyrochlorophylls directly by Soxhlet extraction of fresh spinach with pyridine. However, during pyrolysis the pigments were entirely converted to pyropheophytins, probably by the action of acids present in the spinach. Thirty minutes of warming with zinc acetate converted them to the zinc derivatives. The pigments were then transferred to isooctane solution, extracted ten times with 80% methanol in water and four times with water, and chromatographed on powdered sugar with propanol as eluent. Zinc pyropheophytin a was eluted with 0.25% propanol; zinc pyropheophytin b was eluted with 1% propanol. The former was recovered by precipitation from a 1:1 acetone-water mixture, the latter by ex-

(10) S. Freed and K. M. Sancier, *J. Am. Chem. Soc.*, **76**, 198 (1954).

(11) Performed in collaboration with Dr. R. G. Jensen. We also attempted to force aggregation by diluting the solutions with water, but the aggregates were unstable with respect to colloidal chlorophyll. For details, see R. G. Jensen, Ph.D. Dissertation, Brigham Young University, Provo, Utah, 1965.

(12) J. B. Berkowitz, M. Yamin, and R. M. Fuoss, *J. Polymer Sci.*, **28**, 69 (1958).

(13) H. Utiyama and M. Kurata, *Bull. Inst. Chem. Res. Kyoto Univ.*, **42**, 28 (1964).

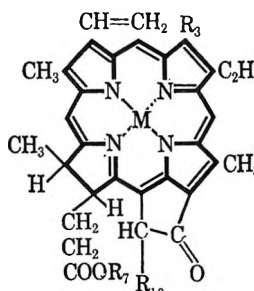
(14) F. P. Zscheile and C. L. Comar, *Botan. Gaz.*, **102**, 463 (1941).

(15) A. F. H. Anderson and M. Calvin, *Nature*, **194**, 285 (1962).

(16) A. S. Holt and E. E. Jacobs, *Am. J. Botany*, **41**, 710 (1954).

traction into purified pentane and evaporation. The ease with which these pigments dissolved in hydrocarbons was evidence that the phytol group had been retained. Structures of the chlorophyll derivatives are illustrated in Table I.

Table I: Chlorophyll Derivatives Mentioned in Text



	M	R ₃	R ₇	R ₁₀
Chlorophyll a	Mg	CH ₃	Phytyl	COOCH ₃
Ethyl chlorophyllide a	Mg	CH ₃	C ₂ H ₅	COOCH ₃
Pyrochlorophyll a	Mg	CH ₃	Phytyl	H
Zinc pyropheophytin a	Zn	CH ₃	Phytyl	H
Pyropheophytin a	2H	CH ₃	Phytyl	H
Chlorophyll b	Mg	CHO	Phytyl	COOCH ₃
Zinc pyropheophytin b	Zn	CHO	Phytyl	H

(Phytyl = C₂₀H₃₉-)

Nitromethane. The better commercially available grades contain nitroethane, 2-nitropropane, and water as major impurities, and at least three minor impurities which we could detect by gas chromatography, but could not identify. The first two are probably innocuous, but water and perhaps some of the minor impurities interfere with the attachment of chlorophyll to polymer. The nitromethane samples used in the present experiments were purified by various combinations of distillation, fractional distillation at 10:1 reflux ratio, and fractional crystallization. They were dried with CaSO₄ or by azeotropic distillation with benzene or toluene. Nitromethane deteriorates on storage and repurification was occasionally necessary.

Water in nitromethane was estimated from the ratio of the optical density (ρ_{1901}) of a band at 1.901 μ in the near-infrared, relative to that (ρ_{1932}) of a band at 1.932 μ due to nitromethane alone, by the formula

$$\%(\text{v}) \text{ water} = \frac{\rho_{1901}/\rho_{1932} - 0.740}{3.335} \quad (1)$$

Methods. The progress of attachment of chlorophyll to the polymer was followed by observing changes in the position (λ) of the peak of the principal red band,

and its half-width (δ) and optical density (ρ). This band is so sharp that λ and δ can be measured to ± 1 A by scanning at 2.5 A/sec on a Cary Model 14 spectrophotometer. The influence of various solvents on these parameters has been reported in earlier articles;^{17,18} equations were derived there for their expected values when two or more complexed forms of chlorophyll coexist.¹⁷ In the present work, however, the variations in these parameters are used mainly as qualitative indicators of the progress of complexing; they cannot be used for quantitative calculation without restrictive assumptions about the number, location, and shape of the bands present.

The half-width of the band at half-maximum absorbancy (δ) was measured on the red side of the absorption band to avoid overlap with vibrational satellites. As most aggregated forms of chlorophyll absorb to the red of the normal band in solution, δ is a rather sensitive measure of aggregation.

The variation in ρ is generally just opposite to that of δ , and therefore conveys little additional information. The reported values of ρ have been adjusted to correct for concentration changes during an experiment. Because the corrected values are subject to errors in volume determination, ρ may be less dependable than δ as evidence of change in the state of the chlorophyll.

Relative fluorescence intensity was measured with a Brice-Phoenix photometer (excitation at 4358 A), or with an RCA 7102 photomultiplier (excitation by a projector lamp through Corning blue filter No. 5562, fluorescence from the front surface observed through red filter No. 2434). The numbers assigned to the intensities are not meant to be compared from figure to figure. No corrections for concentration change, reabsorption, and band shift were made. Fluorescence polarization was measured on an Aminco-Bowman spectrofluorometer, with excitation at 650 nm. Scattered exciting light did not interfere with measurements at the fluorescence maximum.

The interaction of chlorophyll with the polymer was studied by adding aliquots of a solution of the polymer to a solution of chlorophyll. The reverse mode of addition was not attempted because of the instability of concentrated solutions of chlorophyll in nitromethane and the desirability of maintaining an approximately constant pigment concentration for spectral measurements. There is no problem of irreversibility in the attachment of chlorophyll to the polymer in the absence of allomerization.

The cell had an optical path of 0.5 cm, and the volume

(17) G. R. Seely, *Spectrochim. Acta*, **21**, 1847 (1965).

(18) G. R. Seely and R. G. Jensen, *ibid.*, **21**, 1835 (1965).

of chlorophyll solution initially was 2.5 ml; addition of polymer solution increased the volume to a maximum of 3.5 ml. Chlorophyll solutions were flushed with N_2 to prevent allomerization; this precaution was unnecessary with pyrochlorophyll. All measurements were made at $\sim 25^\circ$. The proximity of the θ point of the polymer in nitromethane to room temperature made measurements at lower temperatures inadvisable.

The solution of chlorophyll was prepared by evaporating an aliquot of stock solution of the pigment in acetone and dissolving the film in nitromethane. It was found that films of chlorophyll a and of certain other pigments would not entirely redissolve in the more highly purified samples of nitromethane, nor would the film go entirely into solution when polymer was added. It became evident that nitromethane would dissolve some pigments, especially chlorophyll b, only to the extent that it contained basic impurities. To obviate this difficulty of solubility, 0.025 ml of α -methylnaphthalene was added before evaporation of the acetone to keep the pigment in solution. At this concentration ($\sim 1\%$), the presence of α -methylnaphthalene did not interfere with attachment of the pigment to the polymer.

The chlorophyll concentration was calculated from the optical density and the extinction coefficient (ϵ); the latter was calculated from the half-width (in the presence of a large excess of polymer) by the relation

$$\epsilon\delta = 7.34 \times 10^6 M^{-1} \text{ cm}^{-1} \text{ \AA} \quad (2)$$

established earlier for chlorophyll in pure solvents.¹⁸ In this way, the concentration can be determined even if the pigment does not dissolve entirely in the nitromethane. The spectra of ethyl chlorophyllide a, pyrochlorophyll a, and even of zinc pyropheophytin a are so much like the spectrum of chlorophyll a that it was felt justifiable to apply eq 2 to these also.¹⁹ Concentrations thus derived are probably correct within 5%.

Results

Figure 1 correlates the spectral changes that ensue on adding increments of poly(vinylpyridine) to a solution of chlorophyll a. The band first moves to the red by about 30 Å, stops rather abruptly, and then returns slightly to the blue. The half-width (δ) passes through a maximum and returns shortly to a value not much different from its original value. The optical density (ρ) at first varies oppositely to δ ; the decrease in ρ at high polymer concentration noticeable in this run is unusual, and the reason for it is not apparent. The

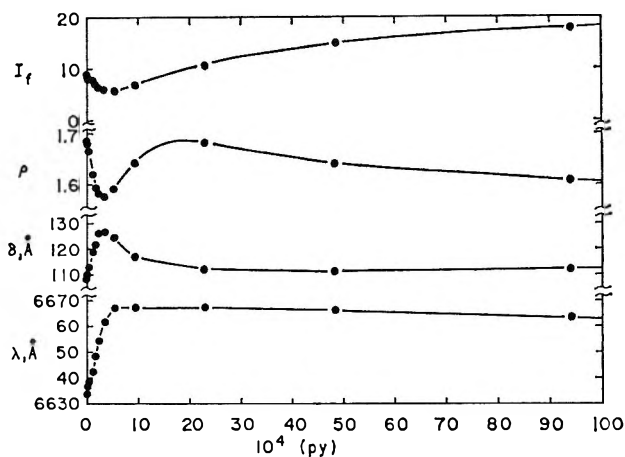


Figure 1. Correlation of changes in red band position (λ), half-width (δ), and optical density (ρ) corrected for concentration changes, and relative fluorescence intensity (I_f), as a solution of poly(vinylpyridine) ($M_w = 425,000$) is added to a solution of chlorophyll a in dried, distilled nitromethane. Polymer concentration expressed as equivalents of pyridine per liter, (py); chlorophyll $5.2 \times 10^{-5} M$ initially.

relative fluorescence intensity decreases at first, then gradually increases to at least twice its original value in pure nitromethane. The minimum in the fluorescence coincides with the turning point in λ , but the maximum in δ occurs somewhat earlier.

The initial red shift of λ and decrease of fluorescence intensity (I_f) indicate the progressive attachment of chlorophyll to polymer. The abruptness with which the red shift stops indicates that beyond this point the chlorophyll must be nearly all attached to the polymer. What is perhaps surprising is the polymer concentration at which this occurs. In most experiments it occurred when the concentration of pyridine units was only about ten times the pigment concentration. As the diameter of a chlorophyll molecule is approximately equal to the length of polymer chain containing six pyridine units, the polymer must be quite heavily loaded with pigment at this stage. Any further changes in the spectrum as more polymer is added must be due to redistribution of pigment molecules among the increasingly numerous pyridine units, and the consequent thinning out of pigment along the polymer chain.

It is convenient to characterize a pigment-polymer system by the pyridine-to-pigment ratio, $(py)/(C)$, which for values greater than about 10 can be in-

(19) F. C. Pennington, H. H. Strain, W. A. Svec, and J. J. Katz, *J. Am. Chem. Soc.*, **86**, 1418 (1964), report values of 86,300, 83,000, and 80,000 $M^{-1} \text{ cm}^{-1}$ for the extinction coefficients of the red bands of chlorophyll a, methyl chlorophyllide a, and pyrochlorophyll a in ether.

terpreted simply as the average separation of pigment molecules along the polymer chain in terms of monomer units.

If polymer addition is continued beyond the point at which fluorescence is restored, fluorescence excited with polarized light becomes increasingly polarized (Figure 2). Although the maximum degree of polarization (p) is not as large as it would be in a viscous solution, *i.e.*, about 0.4,²⁰ it indicates a definite restriction of rotation of the bound chlorophyll. Its value, $p \cong 0.1$, is close to that found for chemically bound chlorophyll in a different polymeric system.²¹

That the attachment of chlorophyll to polymer is reversible is implied by the spectral and fluorescence changes of Figures 1 and 2. Reversibility was also demonstrated in another way. An excess of poly(vinylpyridine) ((py)/(C) = 165) was added to a solution of chlorophyll, whereupon λ moved from 6635 to 6668 Å, characteristic of fully complexed pigment. On addition of 4-ethylpyridine in 45-fold excess over polymer, the band moved back to 6645 Å. At the same concentration of ethylpyridine, but without polymer, the band was at 6646 Å.¹⁷ The near identity of these values proves the displacement of chlorophyll from the polymer by ethylpyridine. After this, the solution was evaporated nearly to dryness and extracted with ether. The green extract contained chlorophyll, as shown by the spectrum, and the polymer was left as a colorless, undissolved film.

Chlorophyll and similar pigments form complexes not only with one mole of basic solvent but also with two, and the binary complexes with pyridine and 4-ethylpyridine have a characteristic spectrum with vibrational satellite bands at 620 and 640 nm.^{18,22} If a binary complex formed with the polymer, chlorophyll would act as a cross-linking agent. However, although the spectrum continues to move to the red at higher polymer concentration (to 6672 Å in 3.4% polymer and to 6683 Å in 32% polymer), there was no sign of the bands characteristic of the binary complex. Furthermore, five molecules of chlorophyll per molecule of polymer did not cause any change in the solution viscosity attributable to cross-linking. Probably the hindrance of the polymer prevents the binary complex from forming.

Effect of Solvent Purity. The results of Figure 1 were obtained with nitromethane that had merely been dried over CaSO₄ and distilled. It soon became apparent that the details of the spectral changes depended on the nature and concentration of impurities in the solvent. We examined the effect of successive steps of purification of one sample of nitromethane on the spectral changes of pyrochlorophyll (used instead of chloro-

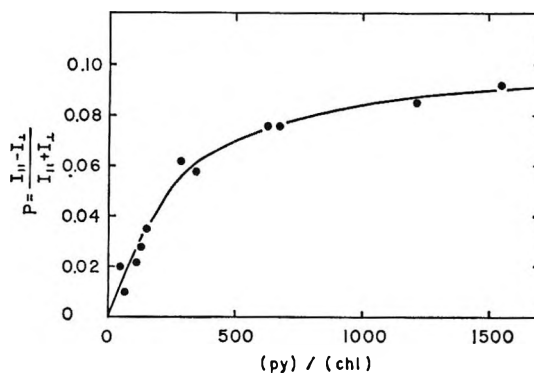


Figure 2. Degree of polarization of fluorescence (p) of chlorophyll as function of polymer pyridine to chlorophyll ratio, (py)/(C), calculated from spectrophotofluorometer tracings of fluorescence spectra, excited at 650 nm. A fresh solution was prepared for each point because chlorophyll was slightly unstable to intense illumination in nitromethane, even under N₂; polymer and nitromethane as in Figure 1.

phyll to avoid the complication of allomerization, see below).

The spectral changes became more pronounced with increased purity of the nitromethane; the greatest differences were in the low-polymer region, before the pyrochlorophyll was entirely bound (Figure 3). In commercial nitromethane, before the addition of polymer, the value of δ was within the normal range (<110 Å) for monomolecularly dispersed solutions.¹⁸ The increase in δ with increasing solvent purity suggested that an increasing fraction of pyrochlorophyll was in an aggregated state, even before addition of polymer. The aggregated form clearly predominated in nitromethane of highest purity, and addition of polymer caused a steady decrease in half-width as these aggregates were broken up by complex formation with the polymer.

The spectral changes accompanying addition of polymer to pyrochlorophyll in the purest nitromethane are shown in Figure 4. Before polymer is added, the red band can be resolved into two components, one near the normal solution position, and the other much to the red. On the addition of polymer, the far-red component is lost, and absorption increases most in the region around 675 nm. The spectrum at (py)/(C) = 9.2 in Figure 4, which is approximately that of an aggregate in which the polymer is densely coated with pyrochlorophyll, can also be analyzed into two bands at 666 and 675 nm, of half-width 103 Å. This resolu-

(20) M. Gouterman and L. Stryer, *J. Chem. Phys.*, **37**, 2260 (1962).

(21) R. G. Jensen, G. R. Seely, and L. P. Vernon, *J. Phys. Chem.*, **70**, 3307 (1966).

(22) P. J. McCartin, *ibid.*, **67**, 513 (1963).

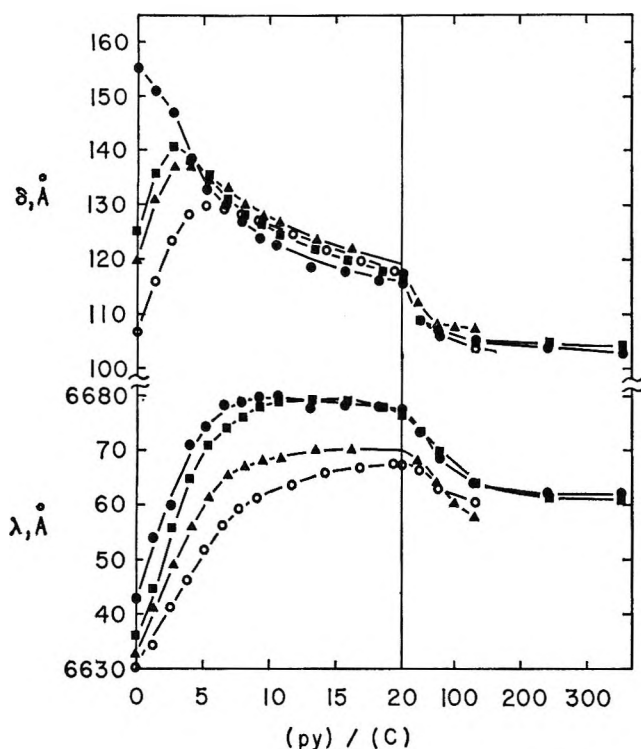


Figure 3. Effect of purification of nitromethane on spectral changes of pyrochlorophyll. Initial pyrochlorophyll concentration $2.5 \times 10^{-5} M$; polymer $M_w = 1,210,000$. Commercial nitromethane (O), dried *via* benzene azeotrope and distilled (▲), then frozen nine times with discard of small supernatants (■), then azeotroped again and fractionated at a 10:1 reflux ratio (●). Note change of abscissa scale at $(py)/(C) = 20$.

tion is not, of course, the only possible one, but it is suggested by the absorption increase around 675 nm. Further addition of polymer converts this spectrum to one with a single band at 666 nm, characteristic of an aggregate in which the pigment is sparsely distributed and which is indistinguishable from a normal solution band. The existence of dimers of chlorophyll and of some of its derivatives, in which the Mg of one molecule is bound to the carbonyl of the other, is well established in pure, dry hydrocarbon and chlorocarbon solvents.²³⁻²⁵ The similarity in the shape of the red band of pyrochlorophyll in the purest nitromethane to that of chlorophyll in nonpolar solvents,^{23,26,27} and the sensitivity to disaggregation by small amounts of impurities, suggest that the same sort of dimers are present here also. Dimers have not previously been reported for dilute nonaqueous solutions in so polar a solvent as nitromethane, and it is interesting that nonpolarity is not a requirement for their existence, as might heretofore have been inferred.

The two-component nature of the red band in dense

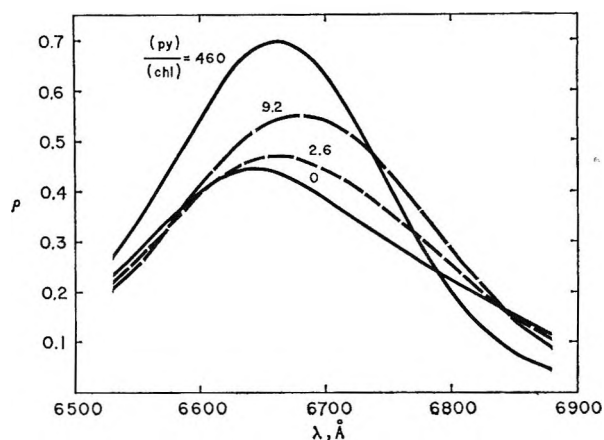


Figure 4. Changes in the red band of pyrochlorophyll during the experiment with purest nitromethane of Figure 3. Traces recorded at $(py)/(C)$ ratios indicated. Optical density corrected for dilution in the course of the experiment.

aggregates is confirmed by difference spectral analysis at low polymer concentration. For example, the first aggregate formed when polymer is added to zinc pyropheophytin a has a red band which appears resolvable into two components near 662 and 670 nm, though a detailed analysis was not made. However, it is not known whether the two components arise by splitting of a band belonging to one molecular species, or whether they belong to molecules in two different environments. There is no isosbestic point in the transition from uncomplexed pigment to dense aggregate; the more heavily loaded aggregates absorb further to the red, even when the pigment is not extensively dimerized to start with, as in Figure 1. It is probable that pigment attached to polymer exists in a variety of environments, differing in the degree of crowding between adjacent molecules. The more crowded environments disappear as more polymer is added.

It will be noticed in Figure 3 that the position of the red band is sensitive to solvent purity, even when the pyrochlorophyll is entirely complexed by the polymer. The half-width is much less affected. These differences are probably traceable to complexing of the Mg by impurities on the side of the chlorophyll ring opposite the pyridine of the polymer.

(23) A. F. H. Anderson and M. Calvin, *Arch. Biochem. Biophys.*, **107**, 251 (1964).

(24) J. J. Katz, G. L. Closs, F. C. Pennington, M. R. Thomas, and H. H. Strain, *J. Am. Chem. Soc.*, **85**, 3801 (1963).

(25) G. L. Closs, J. J. Katz, F. C. Pennington, M. R. Thomas, and H. H. Strain, *ibid.*, **85**, 3809 (1963).

(26) K. Sauer, *Proc. Natl. Acad. Sci. U. S. A.*, **53**, 716 (1965).

(27) R. Livingston, W. F. Watson, and J. McArdle, *J. Am. Chem. Soc.*, **71**, 1542 (1949).

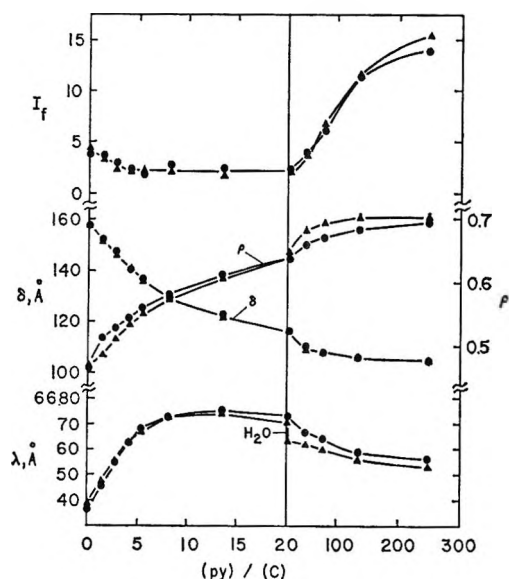


Figure 5. Effect of addition of 0.016% water at $(py)/(C) = 20$ on spectral changes of pyrochlorophyll with poly(vinylpyridine) ($M_w = 1,210,000$) in the purest nitromethane of Figure 3.

There is direct evidence for such an effect with water. The two experiments in Figure 5 were run with the same materials and by the same procedure up to $(py)/(C) = 20$, when 0.016% water was added to the second. The 7-A blue shift observed on addition of water is well beyond the error of measurement. Addition of this amount of water does not appear to have dissociated pyrochlorophyll from the polymer, because the half-width and the relative fluorescence intensity remained unchanged, and the blue shift continued on further addition of polymer. However, too much water dissociates the pigment from the polymer, and we have not been able to prepare aggregates very successfully when the water content was much in excess of one part per thousand.

These experiments also show the extent to which reproducibility is possible when the solvent is in a constant state of purity. They also confirm the reciprocal relationship between half-width and optical density, and show the extent to which fluorescence is quenched in dry nitromethane and in dense aggregates.

Other Pigments. The relative extent of complexing of pyrochlorophyll a, chlorophyll a, and ethyl chlorophyllide a by poly(vinylpyridine) agrees with what one might expect from their structures (Figure 6). Possession of the phytol group and absence of the 10-carboxymethyl group enhance the concentration of dimers in pure nitromethane and reduce the concentration of polymer at which all the pigment is bound.²⁸ Once the chlorophyll derivatives are completely bound to the polymer, however, their spectra are very similar.

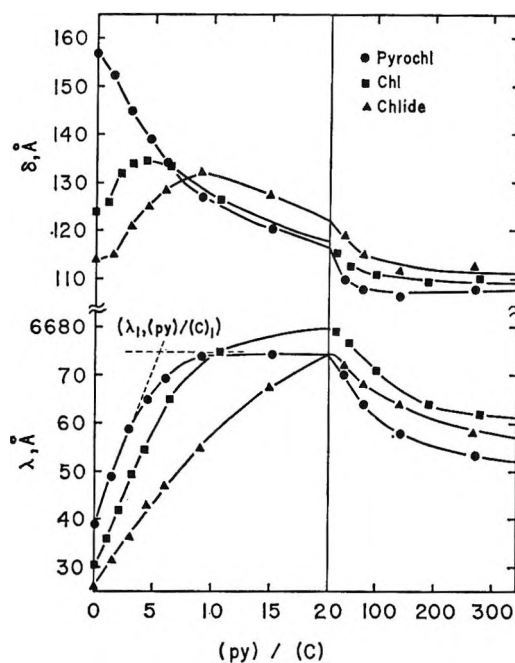


Figure 6. Interaction of pyrochlorophyll (●), chlorophyll (■), and ethyl chlorophyllide (▲), with poly(vinylpyridine) compared. Polymer and solvent are as for Figure 5, pigment concentration in Table II. Intersection of dashed lines is $(\lambda_1, (py)/(C)_1)$ for pyrochlorophyll in Table II.

The spectral and fluorescence changes observed with zinc pyropheophytin a are similar to those of the chlorophylls, but the initial red shift is greater, about 70 Å. The half-width (108 Å) and the relatively strong fluorescence suggest that it is largely monomeric in pure nitromethane. Nevertheless, it is bound by the polymer as readily as is pyrochlorophyll.

Magnesium chlorin *e*₆-butylamide phytol methyl ester, the product of aminolysis of chlorophyll a with *n*-butylamine,^{21,29} is also bound by the polymer, but more gradually than the other chlorophyll derivatives.

Pyropheophytin a, lacking a metal through which to complex with poly(vinylpyridine), exhibits no spectral changes up to $(py)/(C) = 165$.

Chlorophyll b did not completely dissolve in nitromethane even with the aid of α -methyl-naphthalene. Although the red and the Soret bands in the purest nitromethane were at the normal positions for non-associated chlorophyll b, 646.5 and 454.5 nm (*cf.* 645 and 455 nm in acetone), the Soret band had a shoulder on the red side near 475 nm, suggesting the presence of some associated species. On the addition of polymer,

(28) The greater extent of aggregation of pyrochlorophyll than of chlorophyll in nonpolar solvents has been deduced from infrared spectra by Pennington, *et al.*¹⁹

(29) A. Weller and R. Livingston, *J. Am. Chem. Soc.*, **76**, 1575 (1954).

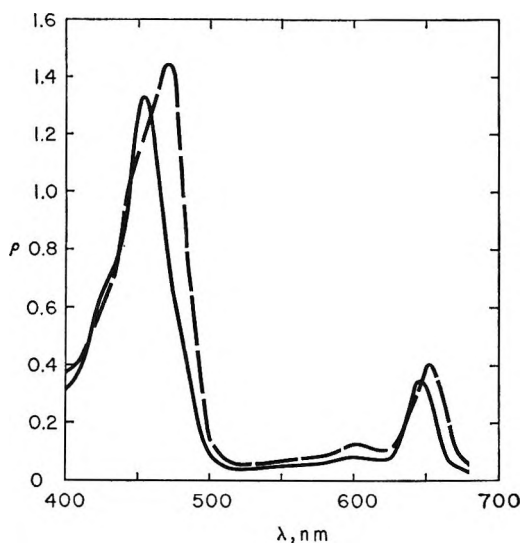


Figure 7. Spectrum of chlorophyll b in purified nitromethane alone (—) and in the presence of large excess of polymer (---), $(py)/(C) = 774$.

the red band moved about 80 Å to longer wavelengths, and the Soret bands were replaced by a single band at 4725 Å. The spectrum of chlorophyll b in the presence of a large excess of polymer is shown in Figure 7. The red shifts of 8 and 18 nm for the red and Soret bands, respectively, are much larger than with chlorophyll a. However, in less highly purified nitromethane chlorophyll b did not show such large displacements, and it may be that the presence of impurities in the solvent is a more critical matter here than with chlorophyll a.

Zinc pyropheophytin b, in nitromethane not of the highest purity, showed spectral changes similar to those of zinc pyropheophytin a, but there is some question as to the state of esterification of the sample used.

As an aid in interpreting the spectral changes associated with complexing of chlorophyll derivatives by poly(vinylpyridine), we examined the complexing of magnesium phthalocyanine, a compound having spectral and solution properties somewhat similar to those of chlorophyll, but of a basically simpler structure. Having no carbonyl group through which to dimerize, magnesium phthalocyanine is monomeric in nitromethane.

The spectral changes on adding polymer to magnesium phthalocyanine in two samples of nitromethane are shown in Figure 8. One was the pure, dry sample of solvent used in the experiments of Figures 6 and 7; the other was freshly distilled but wetter (0.033% water). The results are similar to those with chlorophyll, including the effect of water; however, the

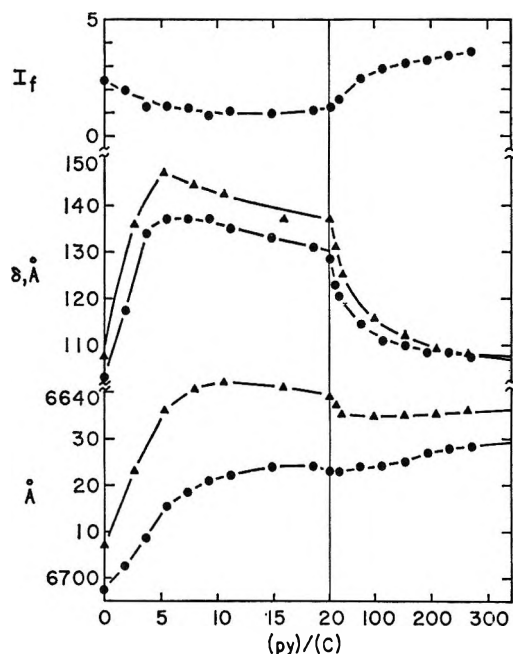


Figure 8. Spectral changes of magnesium phthalocyanine with addition of poly(vinylpyridine) in dry nitromethane (▲) and nitromethane containing 0.033% water (●). Initial pigment concentrations 1.28×10^{-5} and $1.97 \times 10^{-5} M$.

transition from dense aggregates to sparse ones is marked less by a change in the position of the red band than by its narrowing, and by restoration of fluorescence. The fluorescence of dense aggregates seems to be less strongly quenched than with chlorophyll derivatives.

The alteration of the red band in the wetter sample of nitromethane is shown in Figure 9. As there was no dimerization in pure solvent, the broadening of the red band toward the red in dense aggregates is more evident than with pyrochlorophyll (Figure 4). The lack of a clearly defined isobestic point in the transition from uncomplexed pigment to dense aggregates implies a gradation in the strength of interaction of neighboring pigment molecules. An isobestic point does appear at 6841 Å in the transition from dense to sparse aggregates.

Allomerization. In early experiments with chlorophyll a, we noted that the red shift upon addition of a small amount of polymer was followed by a more or less rapid blue shift, which continued even without further addition of polymer, until the band was located considerably to the blue of its original position. The rate of the blue shift varied inversely with the amount of polymer added, and the shift was quenched by polymer well in excess of that needed to bind all the chlorophyll. The rate was unaffected by light. The blue

shift was accompanied by a decrease in the optical density of the red band and an increase in the ratio of the Soret to the red band absorbancies nearly to 2.

The change was identified as allomerization by its requirement for oxygen and by the identity of the spectrum of the final product with that of magnesium "unstable" chlorin, a known primary allomerization product.³⁰ The oxygen requirement is illustrated in Figure 10, which shows that the spectral changes followed exposure to air. In these and other experiments, there was an induction period, which rather strangely increased with the length of time the solution of chlorophyll and polymer had stood in the absence of oxygen.

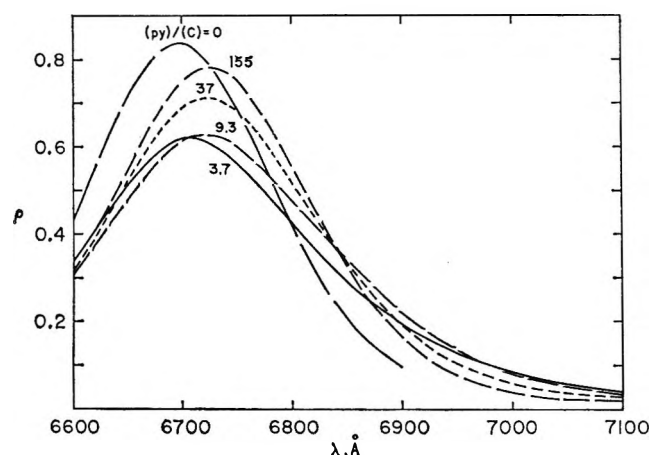


Figure 9. The red band of magnesium phthalocyanine in the wetter nitromethane sample of Figure 8, at various poly(vinylpyridine) concentrations. Optical density corrected for dilution in the course of the experiment.

Allomerized chlorophyll was still complexed by the polymer, because in the presence of excess polymer the fluorescence retained polarization. Freshly allomerized chlorophyll could be extracted from a dried polymer film with tetrahydrofuran, but after 2 or 3 days, some of the pigment became fixed to the polymer, probably by peroxide-catalyzed grafting, and could no longer be extracted.

In subsequent, more carefully purified samples of nitromethane, allomerization proceeded much more slowly, if at all. It would appear, then, that an impurity in the nitromethane, possibly a metallic ion (Fe^{3+}), was responsible.³¹ Perhaps the polymer binds both the chlorophyll and the metallic catalyst, thus increasing the chance of a bimolecular reaction between them. To prevent allomerization, experiments with chlorophyll were conducted under nitrogen, and pyrochlorophyll was used when the possibility of allomerization had to be avoided altogether.

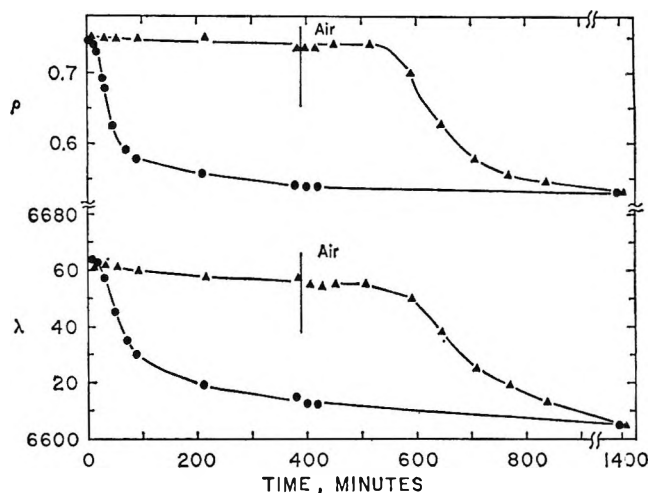


Figure 10. Demonstration of oxygen requirement for poly(vinylpyridine)-catalyzed allomerization of chlorophyll. Changes in position and optical density of red band in the presence of air (●), and under N_2 (▲) until admission of air at the time indicated; chlorophyll concentration $1.2 \times 10^{-6} M$; $(\text{py})/(\text{C}) = 134$.

Discussion

Spectral data for pigment-poly(vinylpyridine) complexes are summarized in Table II. The coordinates $(\text{py})/(\text{C})_1$ and λ_1 characterizing the densest aggregates are those of the intersection of a linear approximation of the initial red shift of λ when pigment is in excess with the extrapolated curve of λ vs. polymer concentration when polymer is in excess. If the polymer molecule offered a certain fixed number of binding sites which are all occupied when pigment is in excess, and if all of the pigment is bound when polymer is in excess, these coordinates would characterize the number of pyridine units per binding site and the position of the red band when the polymer is saturated. However, the intrinsic solubility of the pigment in nitromethane and complexing by impurities assure that the polymer is not saturated when pigment is in excess, the number of binding sites is probably somewhat variable at high loading, and the assumption that λ varies linearly with the concentrations of pigment species is only an approximation. Nevertheless, we would expect some kind of relationship between $(\text{py})/(\text{C})_1$ and the maximum possible loading of the polymer under the given condition of solvent purity and pigment concentration.

Values of $(\text{py})/(\text{C})_1$ range from 4 to 14, and are fairly reproducible for a given pigment. They do not de-

(30) A. S. Holt, *Can. J. Biochem. Physiol.*, **36**, 439 (1958).

(31) The oxidation of chlorophyll by Fe^{3+} , leading to its destruction, has been known for some time (E. Rabinowitch and J. Weiss, *Nature*, **138**, 1098 (1936)).

Table II: Typical Values of Spectral Parameters of Pigments of Poly(vinylpyridine) in Pure Nitromethane

Pigment	$10^5 \times$ initial concn, M	λ_0^a	δ_0	λ_1	$(py)/(C)_1$	λ_2	δ_2
Chlorophyll a	3.21	6630	124	6682	9.0	6661	109
Pyrochlorophyll a	2.40	6639	157	6675	5.5	6650	108
Ethyl chlorophyllide a	2.44	6626	114	6678	14.0	6658	110
Zinc pyropheophytin a	2.44	6556	108	6630	4.2	6613	102
Chlorophyll b	1.53	6465	109	6548	9.8	(6535) ^b	(115)
Magnesium chlorin <i>e</i> - 6-butylamide phytyl methyl ester	3.30	6404	118	6440	14.0	6432	102
Magnesium phthalocyanine	1.29	6707	108	6745	5.9	6733	107

^a λ_0 and δ_0 , in Å, are initial wavelength and half-width of red band in nitromethane. $\delta_0 > 110$ Å indicates some degree of association. λ_1 and $(py)/(C)_1$ are extrapolated values for densest aggregate obtained as in Figure 6. λ_2 and δ_2 are final values measured in the presence of excess polymer. ^b These estimates are obscured by a gradual change in the spectrum of sparse aggregates of chlorophyll b, which may have been due to pickup of an impurity or to a slow chemical reaction.

pend much on solvent purity. For example, in four experiments with Zn pyropheophytin a ranging in concentration from 1.05 to 2.96×10^{-5} M, $(py)/(C)_1$ ranged from 3.9 to 4.9; in seven experiments with chlorophyll a in nitromethane samples of different purity, at concentrations ranging from 1.04 to 5.61×10^{-5} M, $(py)/(C)_1$ ranged from 6.0 to 10.2. Because the porphyrin ring system of a bound chlorophyll molecule would physically cover three pyridine units of a syndiotactic polymer, the least possible value of $(py)/(C)_1$ would be 3. If a bound chlorophyll molecule would also prevent binding of other chlorophyll molecules to nearby pyridine groups directed at an angle to the one to which the chlorophyll is bound, the minimum value of $(py)/(C)_1$ would be 5 or 7. Actual values approach this estimate, suggesting that chlorophyll molecules are lined up edge to edge in the saturated polymer, with little overlap of their porphyrin planes.

The idea that there is little overlap and therefore little electronic interaction between adjacent chlorophyll molecules even in the densest chlorophyll-polymer aggregates is supported by the position of the red absorption band, which lies at 668 nm and is distinguishable from a normal solution band only by its greater width.¹⁸ In contrast, the bulk of chlorophyll in chloroplasts and quantasomes has maximum absorption at 678 nm, analyzable into two bands at 668 or 673 nm and at 683 nm corresponding to distinct aggregated varieties.^{32,33} In monolayers where there is random rotational orientation, the band is at 680 nm;⁹ in crystals where electronic interaction is strongest it is near 735 nm.³⁴ However, the form of pyrochlorophyll responsible for the band near 675 nm (Figure 4) may have a degree of pigment-pigment interaction approximating that in the plant.

In spite of the lack of strong electronic interaction, fluorescence in dense aggregates is largely quenched. The quantum yield is no more than one-tenth of that of the isolated pigment molecules in sparse aggregates, or about 3% if the latter have the usual dilute-solution value of about 30%, and would probably be less if proper correction were made for the normal fluorescence of the few isolated molecules. The yield for green plants is about 2% at low light intensities, though this is averaged over the various aggregated forms of chlorophyll present.¹ The fluorescence curves in Figure 5 are typical for the chlorophyll derivatives; the fluorescence of magnesium phthalocyanine is comparatively less strongly quenched in dense aggregates.

In contrast, the fluorescence of undiluted monolayers of chlorophyll⁹ and of dense adsorbates of pheophytin⁷ is only about $1/1000$ of the normal solution fluorescence. In this respect, our dense aggregates resemble the state of chlorophyll in the plant more closely than do pigments in condensed phases or undiluted monolayers.

Concentration quenching of fluorescence is often associated with the presence of nonfluorescent dimers or low polymers of the emitter. There should then be a relationship between the spectral changes accompanying the transition from dense to sparse aggregates and the fluorescence yield. The fluorescence of chloro-

(32) W. L. Butler in "The Chlorophylls," L. P. Vernon and G. R. Seely, Ed., Academic Press, Inc., New York, N. Y., 1966, pp 348-354.

(33) C. N. Cederstrand, E. Rabinowitch, and Govindjee, *Biochim. Biophys. Acta*, **126**, 1 (1966).

(34) E. E. Jacobs, A. E. Vatter, and A. S. Holt, *Arch. Biochem. Biophys.*, **53**, 228 (1954).

phyll derivatives characteristically attains half its maximum value at about $3/2$ of the (py)/(C) ratio at which the transition from the spectrum of the densest aggregate (λ_1) to the spectrum of the isolated but bound pigment (λ_2) is half complete. (Values of (py)/(C) for spectral and fluorescence half-way marks were 95 and 120 for chlorophyll a, 80 and 125 for ethyl chlorophyllide a, 80 and 130 for pyrochlorophyll a, 50 and 80 for zinc pyropheophytin a, and 37 and 80 for magnesium phthalocyanine.)

The lag in restoration of fluorescence suggests the existence of "quenching centers," to which energy is transferred from the original site of excitation, because otherwise the fluorescence yield would be at least approximately proportional to the displacement of the wavelength. Probably, these quenching centers are merely chlorophyll molecules which happen to be next to each other on the polymer chain; the spectral evidence does not support the presumption of a strong interaction between them. It is possible, though it seems rather unlikely, that a quenching center is simply a single chlorophyll molecule at a place of unusual conformation of the polymer chain.

The polarization of fluorescence of chlorophyll b, pyrochlorophyll a, and zinc pyropheophytin a depends on (py)/(C) in much the same way as does that of chlorophyll a (Figure 2). The degree of polarization for magnesium phthalocyanine is expected to be much less because the first transition is degenerate, and the maximum value at high (py)/(C) was indeed found to be only 0.02. The depolarization of fluorescence provides good evidence for the occurrence of energy transfer at rather high (py)/(C) ratios.

The interaction energy between adjacent chlorophyll molecules on poly(vinylpyridine) can be estimated by treating the system according to a one-dimensional Ising model. We start with the formulation of Reiss,³⁵ which Cellarius and Mauzerall have applied to pheophytin adsorbed onto polystyrene particles.⁷

If N molecules are distributed over a very long linear array of M sites in m clusters, m_j or j molecules each (a cluster being simply a set of j adjacent molecules), and if a pair of adjacent molecules have an energy of interaction ϵ , then the total fraction of molecules in clusters of $j > 1$ is given by the expressions in eq 3, in which Λ is an activity function, $n = N/M$, $\phi_1 = m_1/M$, and $\mu = e^{\epsilon/kT}$.

$$1 - \phi_1/n = 1 - \Lambda\mu \left(\frac{1}{n} - 2 + \Lambda \right)$$

$$1 - \Lambda = \frac{-\mu + \sqrt{\mu^2 + 4\mu(1 - \mu)n(1 - n)}}{2n(1 - \mu)} \quad (3)$$

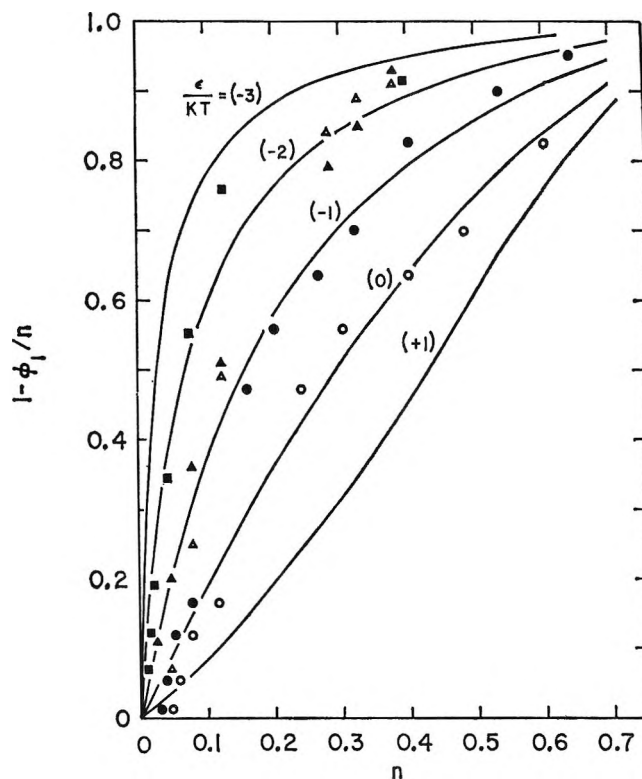


Figure 11. Determination of interaction energies from Ising model. Curves are plots of eq 3 for various values of the energy ratio (ϵ/kT). Points are for the optical density variation of magnesium phthalocyanine at 6720 Å, with $S = 9$ (○) and $S = 6$ (●), for the optical density variations of pyrochlorophyll at 6660 Å (▲) and 6820 Å (△), and for the wavelength variation of pyrochlorophyll (■).

These equations express the extent of aggregation in terms of the fraction of sites occupied and the energy parameter μ . They are plotted for a few values of ϵ/kT in Figure 11.

To apply these equations to our data, we require two things: the number (S) of pyridine units that compose a "site" for the purpose of analysis, and an observable function of the extent of aggregation of the pigment. For the latter, $1 - \phi_1/n$, we may use the wavelength function $(\lambda - \lambda_2)/(\lambda_1 - \lambda_2)$ or the corresponding function of optical density at a particular wavelength $(\rho - \rho_2)/(\rho_1 - \rho_2)$. In either case, the spectral change is small, and the terminal values are subject to uncertainty. The values of (py)/(C)₁ in Table II suggest that there are 5–10 pyridines per site. We used magnesium phthalocyanine to test (3) and obtain an estimate of S . As magnesium phthalocyanine has no substituents, and the central part of the chromophore is somewhat shielded by the outer ben-

(35) H. Reiss, *J. Chem. Phys.*, **40**, 1783 (1964).

zene rings, lateral interaction between adjacent molecules should be small. The change in optical density at 6720 Å vs. $n = S(C)/(py)$ fits about equally well to $S = 9$, $\epsilon/kT = 0$, and to $S = 6$, $\epsilon/kT = -1$ (Figure 11). As the diameter of magnesium phthalocyanine is about 15 Å and the monomer unit length is about 2.5 Å, the second choice appears physically more reasonable.

Points for pyrochlorophyll are also plotted in Figure 11 for $S = 6$, using the wavelength variation from the experiment of Figure 6 and the optical density variations at 6660 and 6820 Å from the experiment of Figure 4. All three sets of data fall between the curves for $\epsilon/kT = -3$ and -1 and are best represented by $\epsilon/kT = -2$. Plots of wavelengths variation for chlorophyll a, ethyl chlorophyllide a, and zinc pyro-

pheophytin also fell close to the curve for $\epsilon/kT = -2$, indicating an attractive energy of a little over 1 kcal/mole for all these compounds.

The smallness of the interaction energy so estimated is in keeping with the picture of the chlorophyll-poly(vinylpyridine) aggregate as a string of randomly located pigment molecules, which though rather tightly bound to the polymer, interact only weakly among themselves. Nevertheless, the latter interaction is sufficient to achieve quenching of at least 90% of the fluorescence in dense aggregates.

Acknowledgments. This work was in part supported by National Science Foundation Grants No. GB-2089 and GB-5098. The technical assistance of Mr. Donald Stoltz and Mr. Thomas Meyer is appreciated.

The Effect of Temperature on the Absorption Spectrum of the

Hydrated Electron and on Its Bimolecular Recombination Reaction¹

by W. Carl Gottschall and Edwin J. Hart

Chemistry Division, Argonne National Laboratory, Argonne, Illinois 60439 (Received November 23, 1966)

An investigation of the effect of temperature on the absorption spectrum of the hydrated electron e_{aq}^- and on the bimolecular reaction $e_{aq}^- + e_{aq}^- = H_2 + 2OH^-$ (1) has been carried out in the temperature range 10–96°. The band maximum shifts to longer wavelengths with increasing temperature with an energy shift $dE_{\lambda_{max}}/dT$ of -2.9×10^{-3} eV/deg. The rate constant of reaction 1 is $(6.3 \pm 1) \times 10^9$ at 22° and it proceeds with an activation energy of 5.2 ± 0.3 kcal/mole.

Introduction

The discovery of the absorption spectrum of the hydrated electron^{2,3} has prompted further investigations concerning the nature of this unique species.^{4–6} The shift of absorption maximum with change in temperature has been shown to be an informative factor in the interpretation of charge-transfer-to-solvent spectra.⁷ Jortner,⁸ utilizing a self-consistent field version of the dielectric model, theoretically had predicted a

value of -2.2 to -3.3×10^{-3} eV/deg for $dE_{\lambda_{max}}/dT$, which implies a cavity radius for e_{aq}^- of approxi-

(1) Based on work performed under the auspices of the U. S. Atomic Energy Commission.

(2) E. J. Hart and J. W. Boag, *J. Am. Chem. Soc.*, **84**, 4030 (1962).

(3) J. P. Keene, *Nature*, **197**, 147 (1963).

(4) S. Gordon, E. J. Hart, M. S. Matheson, J. Rabani, and J. K. Thomas, *J. Am. Chem. Soc.*, **85**, 1375 (1963).

(5) G. Czapski and A. O. Allen, *J. Phys. Chem.*, **66**, 262 (1962).

mately zero. ($E_{\lambda_{\max}}$ is the energy at the absorption spectrum maximum.) The mean or effective radius was accordingly deduced to be 2.6 Å and this study was undertaken chiefly to permit calculation of the effective radius to use in *a priori* calculations of the rate constants utilizing the Debye equation.

Experimental Section

The absorption spectrum of the hydrated electron at several temperatures was determined from measurements on the steady-state transient produced by Co^{60} γ irradiation of H_2 -saturated 0.01 *N* NaOH.⁹ Triply distilled water was degassed in a 500-ml evacuation chamber to remove most of the O_2 and CO_2 before adding sufficient 1 *N* NaOH to make the solution 0.01 *N*. The carbonate content in the 1 *N* NaOH was 2×10^{-6} *M* and hence roughly 20 n*M* carbonate was introduced into the matrix solution. The solution was then saturated with H_2 , degassed, resaturated, and degassed again. Finally the solution was saturated with H_2 and forced into the previously H_2 -purged irradiation cell by H_2 pressure.

The water-jacketed quartz irradiation cell is represented in Figure 1. Access to the 30-cm long cylindrical cell of 3-cm diameter was via 5/20 $\frac{1}{8}$ joints at the top and bottom as illustrated. The quartz cell and its jacket were fitted with high-purity silica end windows which did not discolor under the irradiation conditions. End-window thermostating was found to be absolutely necessary in order to prevent optical distortion by temperature gradients. Slightly acidic distilled water was used in the constant-temperature bath and circulated through the jacket of the irradiation cell in order to prevent interfering transient absorption in the optical path outside the dimensions of the cell. The temperature of the circulating water was constant to $\pm 0.2^\circ$.

The schematic drawing of the experimental setup is shown in Figure 2. The light source, lenses, irradiation cell, and mirrors are mounted on an optical bench. Two spherical mirrors are adjusted to pass the monitoring light beam from a quartz tungsten-iodine lamp through the 30-cm cell three times. The monitoring beam then went out of the cave to the detection equipment, through a 0.5-in. diameter tube penetrating the 4-ft thick magnetite walls. The beam passed through selected filters and a Bausch and Lomb F 3.5 monochromator before the wavelength of interest reached a photomultiplier (P.M. tube) whose output was amplified and recorded.

A 15,000-curie Co^{60} γ source was employed. It consisted of two cylinders, 30 cm long, 25 cm diameter, mounted on a movable rack with a chain drive. Rapid

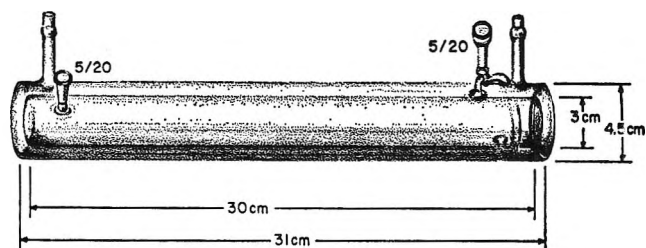


Figure 1. End-window thermostated irradiation cell.

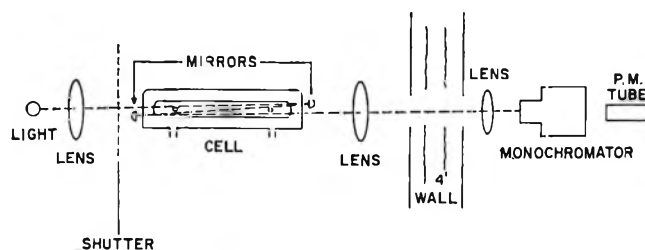


Figure 2. Schematic drawing of experimental setup.

position changing was possible from a near position of about 3 cm to a far position of 1 m. In the maximum dose position, the dose rate was 6.25×10^{19} ev/l. sec as determined with the Fricke dosimeter. Figure 3 illustrates typical traces. The first broad absorption peak corresponding to an o.d. of ≈ 0.02 illustrates the signal obtained upon leaving the source in the near position for ≈ 1 min. Later, sharp peaks were obtained by continuously cycling the source between far and near positions.

The effect of temperature on the absorption spectrum of e_{aq}^- is presented in Figure 4. The absorption maximum shifts from 7000 Å at 10° to 8000 Å at 96° . The shift in $E_{\lambda_{\max}}$ with temperature yields a value of -2.9×10^{-3} ev/deg in good agreement with theory. At higher temperatures the maximum optical density decreases and at 96° is only 30% of the value at 10° . In contrast, electron pulse experiments on a linear accelerator indicate that the initial e_{aq}^- absorption at λ_{\max} is independent of temperature in the range $5-90^\circ$.¹⁰ On the assumption that the molar extinction coefficient of e_{aq}^- is independent of temperature, this decrease enables one to calculate the activation energy for the chief electron-consuming reaction under these conditions, *i.e.*, reaction 1. Calculations on an



(6) J. P. Keene, *Radiation Res.*, 27, 1 (1964).

(7) I. Burak and A. Treinin, *Trans. Faraday Soc.*, 59, 1490 (1963).

(8) J. Jortner, *Radiation Res. Suppl.*, 4, 24 (1964).

(9) S. Gordon and E. J. Hart, *J. Am. Chem. Soc.*, 86, 5343 (1964).

(10) E. M. Fielden, W. C. Gottschall, and E. J. Hart, unpublished results.

Table I: Effect of Temperature on the Absorption Spectrum of the Hydrated Electron

	Temperature, °C							
	10	22	24	43	52	66	72	96
λ_{\max} , ev	1.76	1.72	1.71	1.65	1.63	1.58	1.56	1.51
O.d. at λ_{\max}	0.034	0.029	0.025	0.022	0.016	0.015	0.013	0.010
$[e_{\text{aq}}^-]_{\text{ss}} \times 10^9$	24.35	20.64	18.50	15.38	11.85	10.97	9.63	7.42
$k^a \times 10^{-9}$	4.50	6.26	6.40	11.1	15.5	21.7	23.0	38.4
$\ln k - 20.7$	1.50	1.83	1.86	2.41	2.74	3.08	3.14	3.65
$1/T(^{\circ}\text{K}) \times 10^3$	3.53	3.39	3.36	3.16	3.08	2.95	2.90	2.71

^a k obtained from $-d[e_{\text{aq}}^-]/dt = d[e_{\text{aq}}^-]/dt$. $2k[e_{\text{aq}}^-] = [(6.25 \times 10^{19})(5.7)/(6.02 \times 10^{26})][d/1.024]$, where d is the density of the water at temperature t .

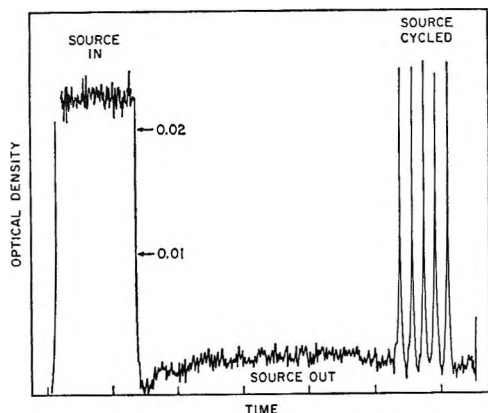
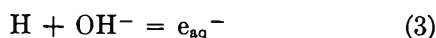
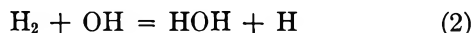


Figure 3. Measurement of e_{aq}^- concentration by steady-state methods: solution, 0.01 *N* NaOH, 0.0007 *M* H_2 ; path length, 90 cm; dose rate, 6.25×10^{19} ev/l. sec obtained with a 15,000-curie Co^{60} γ -ray source; $(e_{\text{aq}}^-)_{\text{ss}} = 1.6 \times 10^{-8}$ *M*; abscissa, time in minutes; ordinate, optical density.

IBM 1620 computer indicated that in pH 12, hydrogen-saturated (~ 0.7 mM) water, 96% of the electrons disappear *via* this reaction. Although higher pH values would make this reaction even more dominant, consideration of impurities likely to be found in more alkaline solutions led to this pH as a practical workable optimum. The yield of primary products and the extinction coefficient ($15,800 \text{ M}^{-1} \text{ cm}^{-1}$)¹¹ of the hydrated electron have been assumed to remain constant over the temperature range considered. The yields used for e_{aq}^- , OH, and H were 2.6, 2.6, and 0.5 radicals/100 ev, respectively. Under the experimental conditions employed, OH and H are converted to e_{aq}^- *via* the reactions



Values of the rate constant, k_1 , were then calculated from the steady-state equation $d(e_{\text{aq}}^-)/dt = -d(e_{\text{aq}}^-)/dt$. Substituting the appropriate quantities,

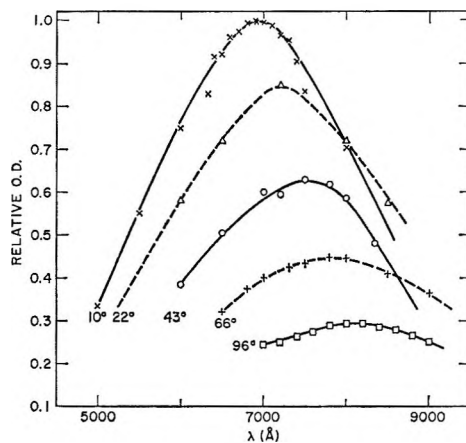


Figure 4. Effect of temperature on e_{aq}^- spectrum.

one obtains: dose rate $\times \Sigma G$ producing $e_{\text{aq}}^- \times$ density correction/ $6.02 \times 10^{26} = 2k_1(e_{\text{aq}}^-)^2$. The various constants and data at different temperatures are assembled in Table I. Reaction 2 would be expected to have the largest activation energy, but an increase in this reaction rate simply makes the experimental conditions more ideal, as would a rate increase in reaction 3.

Discussion

In 1954, Platzman and Franck¹² drew attention to the theoretical similarity of the charge-transfer-to-solvent spectrum for halide ions and that for an electron in the same solvent. Several papers have subsequently reported investigations of the effect of other ions^{13,14} and various solvents^{7,14} on the absorption spectrum of iodide ions. Recently,¹⁵ the effects of

(11) M. S. Matheson, *Advances in Chemistry Series*, No. 50, American Chemical Society, Washington, D. C., 1965, p 45.

(12) R. L. Platzman and J. Franck, *Z. Physik*, **138**, 411 (1954).

(13) G. Stein and A. Treinin, *Trans. Faraday Soc.*, **56**, 1393 (1960).

(14) M. Smith and M. C. R. Symons, *ibid.*, **54**, 338, 346 (1958).

(15) M. Anbar and E. J. Hart, *J. Phys. Chem.*, **69**, 1244 (1965).

solvent on $E_{\lambda_{\max}}$ for the solvated electron spectrum were compared with the $E_{\lambda_{\max}}$ for iodide ions.

The charge transfer to solvent spectrum of an anion X^- is given by the expression^{16,16}

$$E_{\lambda_{\max}} = E_X + E_g - L_X - B$$

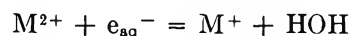
where E_X is the electron affinity of the X radical, L_X the heat of hydration of the X radical and E_g the energy involved in removing the ion from its cavity in the solvent, both without disturbing the persistent polarization of the medium, and B the binding energy of the electron to the polarized medium in its excited state. In the case of e_{aq}^- , $E_{\lambda_{\max}}$ has been shown to be only slightly less than its energy of hydration¹⁷ which means $E_{\lambda_{\max}} \approx E_g$ (B is small at any rate). Changes in $E_{\lambda_{\max}}$ are thus due principally to changes in E_g

$$E_g = e^2/r_0[(1/2) + (1/2D_{\text{op}}) - (1/D_s)]$$

where $D_{\text{op}} = n^2$; n is the index of refraction, and D_s is the static dielectric constant. Calculating the temperature effect utilizing the known variation of the dielectric constant of water with temperature indicates that the hydrated electron radius, r_0 , must increase with increasing temperature, a plausible concept. Since $E_{\lambda_{\max}}$ is inversely proportional to the radius and the observed E for the electron in water is larger than in liquid ammonia, the mean or effective radius in water is concluded to be less than the value of 5.9 Å in ammonia and our calculations indicate a value of 2.9 Å.

The value of $k = (6.3 \pm 1) \times 10^9$ determined in this investigation by our steady-state method falls well within the range of previous pulse radiolysis values. Matheson and Rabani¹⁸ report $(5.5 \pm 0.75) \times 10^9$ and Dorfman and Taub¹⁹ report $<6.5 \times 10^9$, but after normalization to a common value of the molar extinction coefficient of e_{aq}^- the latter value becomes $<7.0 \times 10^9$. At low-pulse intensities a higher k was observed¹⁸ which was attributed to impurities and hence if the difference is considered significant it may reflect an impurity effect thereby making all values of this rate constant as upper limits. The transient e_{aq}^- signal was obtained immediately upon irradiation in our studies, however, which implies a very low concentration or absence of reducible impurities. Other studies^{20,21} have shown that O_2 and H_2O_2 present under these conditions are reduced to unreactive water and the e_{aq}^- transient signal increases with irradiation time. Organic impurities would be reduced to saturated compounds with low reactivity and the known carbonate or bicarbonate and Na^+ concentrations multiplied by their rate constants show that they should not interfere. If a metallic ion is present which will be reduced by the electron and reoxidized by water, this cycle

could continue indefinitely, but the resultant k determined would be unchanged since the electron consumed by

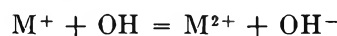


will be replaced *via*



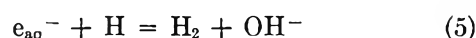
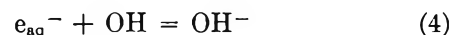
followed by regeneration of e_{aq}^- *via* reaction 3.

If the reduced ion is oxidized only by OH, however

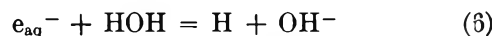


a cycle may be established which would make the observed k too high. An impurity of this kind, if reacting at a diffusion-controlled rate, would need only be present in $10^{-7} M$ concentration to compete with reaction 2.

The activation energy obtained from the Arrhenius plot of Figure 5 is 5.2 ± 0.3 kcal/mole. Because of the possible effect of impurities and because of the intervention of unknown reactions, this value must be regarded as an upper limit. Activation energies for other simultaneously occurring reactions are unknown, but they should not have a pronounced effect on this result. Diffusion-controlled reactions 4 and 5 should contribute less than 5% of the e_{aq}^- consumption at room temperature.



Besides they should have very small activation energies. Also unimportant at room temperature under our reaction conditions is the reaction



since the H atom so formed is readily converted into e_{aq}^- *via* reaction 3.

Although the detailed mechanism of the reaction of two hydrated electrons is in the realm of pure speculation, our activation energy of 5.2 kcal/mole provides proof of its diffusion-controlled nature. Wang²² reports an activation energy of self-diffusion of water of approximately 6.4 kcal/mole at 0° and an

(16) G. Stein and A. Treinin, *Trans. Faraday Soc.*, **55**, 1086 (1959).

(17) J. H. Baxendale, *Radiation Res. Suppl.*, **4**, 139 (1964).

(18) M. S. Matheson and J. Rabani, *J. Phys. Chem.*, **69**, 1324 (1965).

(19) L. M. Dorfman and I. A. Taub, *J. Am. Chem. Soc.*, **85**, 2370 (1963).

(20) W. C. Gottschall, unpublished observation.

(21) E. J. Hart and E. M. Fielden, *Advances in Chemistry Series*, No. 50, American Chemical Society, Washington, D. C., 1965.

(22) J. H. Wang, *J. Am. Chem. Soc.*, **73**, 510 (1951).

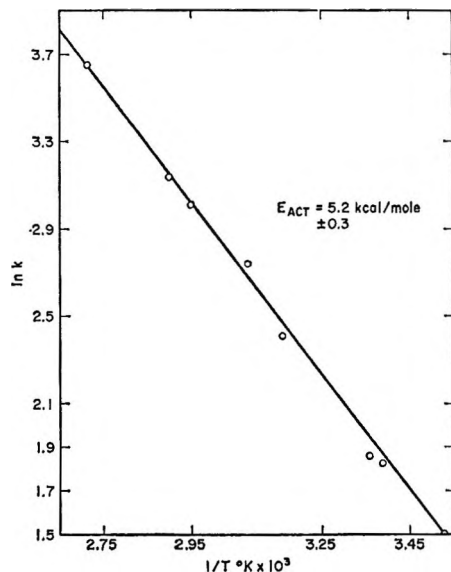


Figure 5. Arrhenius plot for $e_{\text{aq}}^- + e_{\text{aq}}^- = \text{H}_2 + 2\text{OH}^-$: abscissa, $1/T(^{\circ}\text{K}) \times 10^3$; ordinate, $\ln k - 20.7$.

average of 4.58 kcal/mole for the temperature range 10–50°. Apparently, the hydrated electron diffuses by a mechanism similar to the diffusion of water molecules. In contrast to the diffusion phenomena in water where the activation energy progressively decreases with rising temperature, our curve is linear within experimental error. We suspect that the steady-state concentration of e_{aq}^- may be lowered by side or

thermal reactions unimportant at lower temperatures. If this is the case, the actual activation energy curve would be concave downward just as the self-diffusion curve of water. Careful work using a pulse radiolysis method could resolve this question. In previous studies²³ it was pointed out that the activation energy of e_{aq}^- reactions is substantially equal to that of diffusion of the species in water. The activation energy of $e_{\text{aq}}^- + \text{H}^+$ reaction is nearly identical with that of the neutralization reaction $\text{OH}^- + \text{H}^+$ (3.2 and 3.5 kcal/mole, respectively).^{11,23,24} The reported value of 4.55 kcal/mole for reaction 6 is probably for the reaction of e_{aq}^- with hydrogen peroxide, the principal impurity introduced by their large $1 \times 10^{-6} M$ e_{aq}^- electron pulse.²³ Later work²⁵ demonstrated the need of using $<1 \times 10^{-8} M$ e_{aq}^- pulses and of keeping the hydrogen peroxide concentration at $5 \times 10^{-9} M$ or less in order to measure $k_{e_{\text{aq}}^- + \text{H}_2\text{O}}$ reliably.

Acknowledgment. We wish to acknowledge the technical assistance of Howard Harvey and Joseph Hoh of the Chemistry Division, Argonne National Laboratory.

(23) J. K. Thomas, S. Gordon, and E. J. Hart, *J. Phys. Chem.*, **68**, 1524 (1964).

(24) G. Ertl and H. Gerischer, *Z. Elektrochem.*, **66**, 560 (1962).

(25) E. J. Hart, S. Gordon, and E. M. Fielden, *J. Phys. Chem.*, **70**, 150 (1966).

The Photochemical Decomposition of Nitronium Perchlorate¹

by J. N. Maycock, V. R. Pai Verneker, and L. Witten

Research Institute for Advanced Studies, Baltimore, Maryland 21227 (Received November 28, 1966)

The kinetics of gas evolution from nitronium perchlorate irradiated with ultraviolet light from a high-pressure mercury arc has been investigated as a function of intensity, temperature, and time of irradiation. Different gaseous products of decomposition have been identified mass spectrometrically, the predominant species being O₂ and NO. The data indicate that two primary mechanisms for photolysis are operating simultaneously. The first mechanism starts out rapidly, builds up to a large rate of photolytic decomposition, and then dies off with time. The second slower mechanism then takes over and is responsible for the long-time photolytic behavior. An absorption spectrum of a single crystal of nitronium perchlorate has also been measured. The results agree with the threshold energies for photodecomposition.

Introduction

Photolysis of metastable materials in the solid state can provide very illuminating information about their stability and electronic structure. Evidence for this statement is found in the wealth of information resulting from photolytic studies of the azides,² many of which are highly explosive. So far, no photochemical decomposition studies have been made on the perchlorates although the thermal decomposition of these materials, particularly of ammonium perchlorate,³ has been thoroughly investigated.

One perchlorate which has received relatively little attention, either thermally or photochemically, is nitronium perchlorate. The thermal decomposition of nitronium perchlorate has been studied over a temperature range of 70 to 112° by conventional techniques⁴ and has been found to be probably dependent on an electron-transfer mechanism. Further work to elucidate this proposed mechanism has been performed in our laboratory.⁵ To complement these thermal decomposition studies, we have investigated the photolytic behavior of pure nitronium perchlorate powder under ultraviolet irradiation. In the next sections, we describe the experimental results of the photolytic study and outline a possible physical mechanism that yields the observed results.

Experimental Section

It is very well known that nitronium perchlorate is extremely hygroscopic, nitric acid and perchloric acid

being formed immediately upon contact with water. For this reason, the transference of the Callery Chemical Co. nitronium perchlorate powder from the stock batch to any sample container was always performed in a drybox having a stream of pure, dry nitrogen gas passing through it. However, by differential thermal analysis and mass spectrographic analysis, it was found that all samples invariably absorbed a certain amount of water. Using mass spectroscopy as a guideline, it was found that complete removal of water and hydrolysis products was attained by pumping on each individual sample for a period of 18 hr in a vacuum line maintained at 10⁻⁴ torr.

The perchlorate was contained in a Pyrex cell fitted with a flat quartz window and connected to the vacuum line. This consisted in sequence of an outlet to the mass spectrometer, a cold trap, a Pirani gauge, an ionization gauge, a thermocouple gauge, a McLeod gauge, a cold trap, a three-stage silicone oil diffusion pump, and a mechanical backing pump. A roughing line was also installed from the mechanical pump to the ir-

(1) Supported by the U. S. Army Missile Command, Contract No. DA-01-021-AMC-12596(Z).

(2) B. L. Evans, A. D. Yoffe, and P. Gray, *Chem. Rev.*, **59**, 515 (1959).

(3) A. K. Galway and P. W. M. Jacobs, *J. Chem. Soc.*, **974**, 5031 (1960).

(4) H. F. Cordes, *J. Phys. Chem.*, **67**, 1693 (1963).

(5) J. N. Maycock, C. S. Gorzynski, and D. E. Grabenstein, unpublished results.

radiation cell so that the cell could be quickly dismantled while keeping the main line at 10^{-4} torr and then pumped out when reassembled without having to break the high vacuum. The mass spectrometer, a Consolidated Electrodynamics 21-613 residual gas analyzer, was connected to the main high-vacuum line through a Varian 951-5100 adjustable leak valve having a minimum leak rate of 10^{-9} torr l./sec. The working volume was determined by calibration with nitrogen using the McLeod gauge for pressure measurement. The thermocouple and Pirani gauges were also calibrated against the McLeod gauge. All ground-glass joints and stopcocks were lubricated with Kel-F grease which does not interact with nitronium perchlorate. Unfortunately, the vapor pressure of the Kel-F grease prevented experimentation at pressures much below 10^{-4} torr.

A typical sample size weighed about 500 mg; the area of irradiation was about 3 cm². The sample was photolytically decomposed into a working volume of 1.3 l. For typical decomposition runs (approximately 1 hr long), there was no visible change in the sample size. Weighing before and after a photolytic decomposition run was impracticable due to the unstable properties of nitronium perchlorate.

The irradiation source was a water-cooled General Electric AH-6 high-pressure mercury arc whose radiant intensity was varied by placing neutral density filters between the sample cell and the Hg lamp. The transmittance of these filters was calibrated by replacing the cell with a thermopile; intensities are recorded in terms of the thermopile emf since the spectral output of the lamp is more nearly a continuum than a line spectrum due to the high-pressure broadening of the spectral lines. Thus the number of photons received by the perchlorate is unknown; all intensities are relative to the unfiltered lamp. It was found necessary to monitor the light output due to occasional voltage fluctuations.

The low-temperature baths were ice and water for 0°. For -20 and -40°, CaCl₂·6H₂O plus ice were used in different proportions. In each case efficient stirring of the baths was achieved by bubbling helium through the solutions; in this way, the baths maintained constant temperature. All temperature measurements were made with a copper-constantan thermocouple.

Results

Absorption spectra studies of nitronium perchlorate crystals grown from a nitric acid solution were made prior to the photochemical decomposition studies. After being grown, the crystals were cleaved, polished

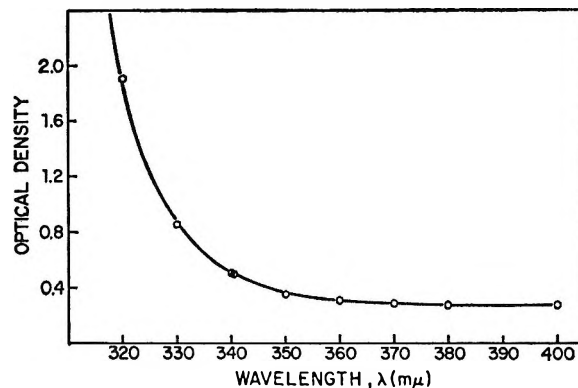


Figure 1. Absorption spectrum of a nitronium perchlorate crystal at 25°. This crystal had been grown from a nitric acid solution of nitronium perchlorate.

in nitric acid, dried *in vacuo*, and then used for the absorption spectra studies. The room temperature absorption spectrum, Figure 1, was obtained by using a Cary Model 14 spectrophotometer. The main features of the absorption spectrum are that nitronium perchlorate is transparent in the visible region and has its absorption edge at about 340 mμ.

Prior to the irradiation experiments, possible decomposition products were considered to be oxygen, nitrogen oxides, and chlorine oxides. For this reason, methanol and solid CO₂ were used for the cold traps, since this cold-trap mixture would trap out all possible species except O₂ and NO.

The rate of evolution of O₂ and NO from the irradiation of nitronium perchlorate with the high-pressure lamp as a function of time is shown in Figure 2. It is apparent that this rate, after the initial periods of acceleration and deceleration, is constant with time. Long irradiations of the order of 8 hr have been performed with no change in rate, which appears to imply that the rate will remain essentially constant until all of the salt is completely transformed. It is also apparent upon careful investigation of the pressure *vs.* time curve, Figure 3, that there is, in every case, a small but definite induction period of the order of 2 min. When a shutter is placed between the light source and the sample, photolysis immediately ceases and there is absolutely no evidence of any "dark rate" even at 25°. Upon reirradiation of the same sample, the same constant first rate is achieved after an initial induction period consisting of only an acceleratory period to this constant rate; no deceleratory period exists. We have also allowed an irradiated sample to stand under the gaseous product atmosphere for 18 hr, after which we pumped the atmosphere out and reirradiated the sample. This again produced no effect

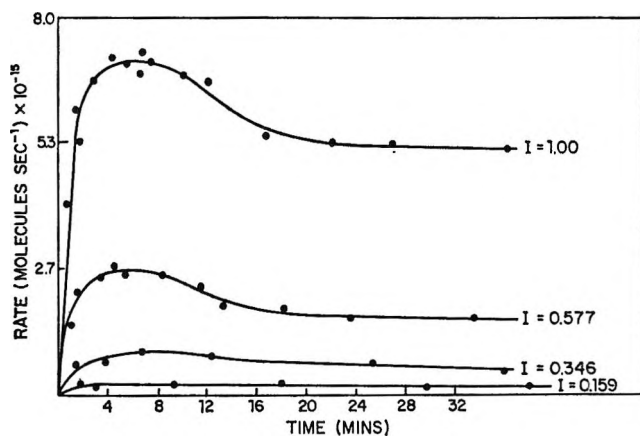


Figure 2. Rate of gas (O₂ with a relatively small admixture of NO) evolution as a function of time from nitronium perchlorate being irradiated with a high-pressure Hg lamp at 25°. The different intensities of irradiation were obtained by using neutral density filters; I indicates relative intensity.

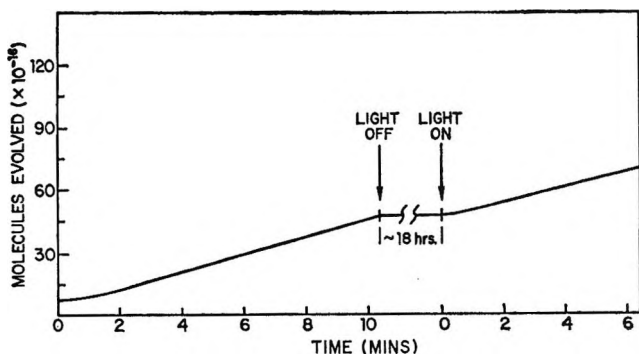


Figure 3. "Stop-start" experiment showing the reproducibility of the pressure-time curve for photolytic decomposition at 25°. The two slopes between 2 and 6 min are equal within the limits of reproducibility of the data.

on the pressure curve, which reproduced the original data quite closely, implying that the gaseous products do not catalyze the decomposition processes (Figure 3).

The rate of product formation both at long times and in the early stages of photolysis is proportional to the square of the intensity of the light. This dependence is valid over the temperature range 25 to -40° which has been investigated. A typical intensity dependence plot for 25° is shown in Figure 4, where the intensity is measured in thermopile emf output.

The activation energies of the photochemical decomposition reactions were determined at various times and are displayed in Table I. As is evident from Figure 5, the temperature dependence of the rate of gas evolution obeys an Arrhenius type of plot quite accurately over the complete temperature range covered.

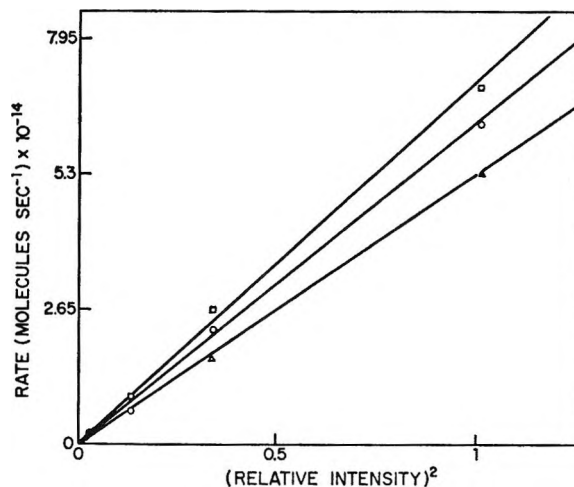


Figure 4. Rate of gas (O₂ + NO) evolution as a function of I^2 : ○, after 2 min, *i.e.* in the initial acceleratory period; □, after 6 min, *i.e.*, at the maximum of the rate *vs.* time curves; △, after 20 min where the rate is constant until complete disappearance of the salt.

Table I: The Values of the Activation Energy, E , for the Photochemical Decomposition of Nitronium Perchlorate

Time of irradiation, min	2	6	30
Activation energy, kcal mole ⁻¹	10.5	10.5	8.25

By a mass spectral analysis of the decomposition products not trapped out, it is clear that during a normal 30-min run the only observed species present are O₂ and NO, whereas in a long run, 8 hr duration, the data showed that chlorine is also formed. However, a mass spectral analysis of an untrapped decomposition shows O₂, NO, NO₂, ClO₂, OCl, and Cl₂. Of the species observed, oxygen is by far the most abundant species, followed by nitric oxide and chlorine. The oxides of chlorine were only observed as very minor constituents. In all probability, the observed OCl is due to the cracking of ClO₂ in the mass spectrometer. We have concluded that NO is a primary product and not formed only by cracking of NO₂ since the experimentally observed ratios of these two peaks do not agree at all with the known cracking pattern of NO₂.

Due to the low scanning speed of the mass spectrometer, the mass spectra in different portions of the decomposition rate-time curve was not determined.

In an attempt to determine the threshold wavelength necessary for photolysis, we found that the intensity of the output from a Hilger-Watts Model D246/7 spectrometer was not sufficient to produce measurable photolysis. By filtering the output of the high-pres-

sure lamp using optical absorption filters, we were able to establish qualitatively the threshold wavelength necessary for photolysis. The detection of photolysis was achieved by mass spectrometrically gating on the oxygen, O_2 , peak. Table II shows that photolysis is considerable at wavelengths less than approximately $370\text{ m}\mu$. This is in very good agreement with the absorption spectrum found for the crystalline nitronium perchlorate.

Table II: Analysis of the Threshold Wavelength ($\text{m}\mu$) Necessary for the Photolysis of Nitronium Perchlorate

Corning filter	Wavelength cutoff, $\text{m}\mu$	Photolysis
3-67	~ 544	None
3-71	~ 460	None
3-73	~ 416	None
3-75	~ 370 (transmission at $365\text{ m}\mu$ is $<0.5\%$)	Very slight
7-37	$\sim 315\text{--}390$ (transmission band)	Considerable

Discussion

The results of the present investigation indicate there are two photolytic processes taking place when nitronium perchlorate is irradiated with ultraviolet light. By an analysis of the results for the rate of gas production with respect to time (Figure 2), temperature (Figure 5), and wavelength (Table II) of the ultraviolet source, we may conclude that fresh, pure nitronium perchlorate is decomposed by light of wavelength less than $340\text{ m}\mu$, at a rate which (i) initially increases to a maximum and then falls to a constant value, (ii) depends in each region on the square of the intensity of the light (I^2), and (iii) is associated with an activation energy of about 9 kcal mole^{-1} .

One possible explanation of the pressure increase during the initial stages of photolysis above the final steady-state rate is that it is associated with outgassing or desorption phenomena. Outgassing is very unlikely due to the long (18 hr) pumping treatment the sample has undergone. A desorption process is unlikely due to the fact that the initial acceleration in the rate-time curve is reproduced if a photolyzed salt is pumped down and the photolytic process is started again; moreover the rate is proportional to I^2 in this region. A further argument against a desorption mechanism is that, in our thermal decomposition study⁵ using a time-of-flight mass spectrometer, we did not observe any foreign species at any time during the decomposition. This is contrary to the

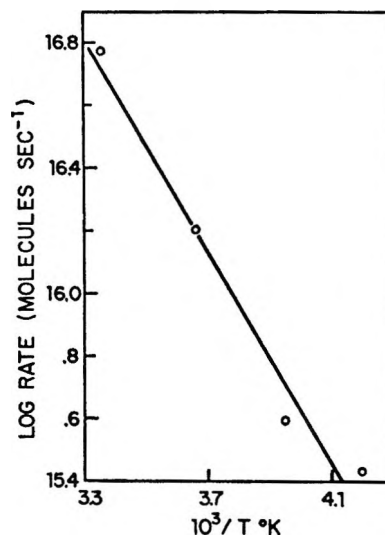
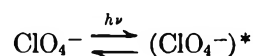


Figure 5. Log of the rate of gas ($O_2 + NO$) evolution vs. $10^3/T$ ($^\circ\text{K}$) for the photochemical decomposition of pure nitronium perchlorate 6 min after onset of irradiation.

work of Cordes.⁴ Our experimental technique differed from that of Cordes in that he condensed the gases and then analyzed, whereas we analyzed by performing the decomposition directly in the analyzing mass spectrometer. The observed decreasing rate of photolysis at about 10 min indicates that the photochemical reaction proceeds at centers or traps which are being consumed. A similar phenomenon has been observed in the azides,^{6,7} in which case the traps have been postulated to be impurity ions or point defects.

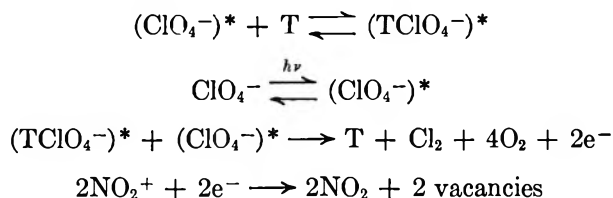
The data can be qualitatively understood by postulating that two processes or mechanisms, releasing O_2 and NO , are taking place simultaneously, each mechanism being dependent on I^2 . The first mechanism occurs quite rapidly and is responsible for the initial fast reaction rate. However, this mechanism depends on the existence of impurity or trapping centers which are consumed in carrying out their part of the reaction mechanism. Hence, this mechanism causes a rapid initial increase of the reaction rate and then dies out, at which time a second reaction process takes over. This second reaction process does not depend on impurity trapping centers and continues presumably until the crystal itself is consumed.

The first mechanism proposed is



(6) P. W. M. Jacobs, F. C. Tompkins, and D. A. Young, *Discussions Faraday Soc.*, 28, 234 (1959).

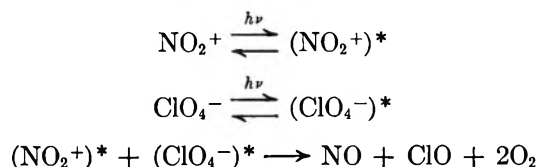
(7) P. W. M. Jacobs, F. C. Tompkins, and V. R. P. Verneker, *J. Phys. Chem.*, 66, 1113 (1962).



A perchlorate ion is excited by an incoming photon. Ordinarily, it will decay after some time into its ground state; however, in the vicinity of a trap (electron acceptor), it may form a complex with the trap in which the electron is partially or completely transferred to the trap. The perchlorate-trap complex then reacts with another excited perchlorate ion to give the reaction products indicated above; the free electrons are now absorbed in some fashion. The amount of oxygen evolved is proportional to I^2 . The trap which participated in the above mechanism is now associated with two anion vacancies and the crystal assumes different properties in the neighborhood of the trap.⁷ In this new neighborhood, the trap can no longer participate in the mechanism outlined, the number of active traps decreases as time goes by, and the photolytic rate due to this mechanism decreases. The rise and decline of this mechanism may account for the initial acceleratory and deceleratory parts of the rate-time curve. The observed activation energy of about 9 kcal mole⁻¹ is in reasonable agreement with the values reported for the breakup of similar trap complexes

in silver azide.⁸ The two electrons placed into the conduction band by this process are eventually captured by other traps or more probably by nitronium ions, NO_2^+ . The resultant NO_2 may be photolyzed directly by the incident radiation, may evolve as a gas, or remain as an impurity in the crystal lattice.

During this whole period of time, a second process has been acting slower than the mechanism described but with no self-consuming features. This process can be represented in the following way



Again, the amount of oxygen plus NO evolved is proportional to I^2 ; the process proceeds until the nitronium perchlorate crystal itself is consumed. Evidence for the existence of two such complementary mechanisms was observed experimentally since a second photolysis of an already photolyzed sample exhibited no deceleratory period. The absence of any dark rate or gas evolution on warmup leads us to deduce that we are not invoking any free-radical photolytic mechanisms in the temperature range studied.

(8) F. P. Boden and A. D. Yoffe, "Fast Reactions in Solids," Butterworth and Co. Ltd., London, 1958, p 96.

Ion-Solvent Interactions. VII. Apparent and Partial Molal Volumes of Some Symmetrical Tetraalkylammonium Halides in Anhydrous Methanol Solutions¹

by J. Padova and I. Abrahamer

Radiochemistry Department, Soreq Nuclear Research Centre, Israel Atomic Energy Commission, Yavne, Israel (Received November 28, 1966)

The densities of NH_4Br , $(\text{C}_2\text{H}_5)_4\text{NBr}$, $(n\text{-C}_3\text{H}_7)_4\text{NBr}$, $(n\text{-C}_4\text{H}_9)_4\text{NBr}$, $(\text{CH}_3)_4\text{NCl}$, and $(\text{C}_2\text{H}_5)_4\text{NCl}$ were determined at 25° in anhydrous methanol. All of the salts are shown to follow Root's equation over the investigated concentration range. The apparent and partial molal volumes were calculated and were found to increase with concentration. The results obtained are discussed and interpreted in terms of ion-solvent interaction and compared with data obtained in aqueous solutions.

Introduction

The partial molal volumes \bar{V}_2 of tetraalkylammonium halides in aqueous solutions have been found to be anomalous,²⁻⁴ in that the decrease of volume with concentration for both chlorides⁴ and bromides^{2,3} becomes greater with cation size. Moreover, it has been shown that at very low concentrations of bromides³ and chlorides⁴ the slopes of \bar{V}_2 vs. $c^{1/2}$ are positive and reasonably close to the Debye-Hückel limiting slope.⁵

In this paper we report the molar volume behavior of ammonium bromide, tetraethylammonium bromide, tetra-*n*-propylammonium bromide, tetra-*n*-butylammonium bromide, tetramethylammonium chloride, and tetraethylammonium chloride in anhydrous methanol at 25° with regard to ascertaining the influence of the cation size on ion-solvent interaction as compared with the situation in aqueous solutions.

Experimental Section

Fluka methyl alcohol, purissimum (AR) and acetone free, was twice distilled over Drierite, the middle part only being redistilled as recommended by Weissberger⁶ and its purity checked by density and refractive index measurements.

The compounds tetramethylammonium chloride, tetraethylammonium chloride, tetraethylammonium bromide, tetra-*n*-propylammonium bromide, tetra-*n*-butylammonium bromide, purum grade, were ob-

tained from Fluka A.G. and purified by several recrystallizations from methanol, except for $(\text{C}_2\text{H}_5)_4\text{NCl}$ which was twice recrystallized from chloroform⁷ by the addition of ether and dried under vacuum at 80° and $(n\text{-C}_4\text{H}_9)_4\text{NBr}$ which was twice recrystallized from benzene and dried under vacuum for about 1 week.⁸ Ammonium bromide, AnalaR, was twice recrystallized from anhydrous methanol and dried under vacuum.

All solutions were prepared by weight and vacuum corrected. Owing to the hygroscopic nature of the salts, all transfers were carried out in a drybox.

The density measurements were carried out in bi-capillary pycnometers⁹ of a 50-ml approximate capacity, which were calibrated with mercury and checked with

(1) Presented in part at the 35th Meeting of the Israel Chemical Society, Haifa, Israel, Feb 1966.

(2) W. Y. Wen and S. Saito, *J. Phys. Chem.*, **68**, 2639 (1964).

(3) F. Franks and H. T. Smith, XVI C.I.T.C.E. Meeting, Budapest, Hungary, Sept 1965.

(4) (a) B. E. Conway and R. E. Verrall, *J. Chem. Phys.*, **40**, 1473 (1966); (b) B. E. Conway, R. E. Verrall, and J. E. Desnoyers, *Trans. Faraday Soc.*, **62**, 2738 (1966).

(5) O. Redlich and D. M. Meyer, *Chem. Rev.*, **64**, 221 (1964).

(6) A. Weissberger and E. S. Proskauer, "Organic Solvents," 2nd ed, Interscience Publishers, Inc., New York, N. Y., 1955, p 335.

(7) A. K. R. Unni, L. Elias, and H. I. Schiff, *J. Phys. Chem.*, **67**, 1216 (1963).

(8) E. A. S. Cavell, *Trans. Faraday Soc.*, **61**, 1678 (1965).

double-distilled water at 25°, the density of which was taken to be 0.997074 g/ml. The changes in volume were followed through a cathetometer readable to 0.01 mm. The temperature in the thermostat was kept constant to within $\pm 0.002^\circ$. Weissberger's procedure⁹ was followed and the duplicate measurements carried out for each solution are believed to be precise within 10^{-5} giving a precision of ± 0.05 ml for the apparent molal volume ϕ_v . Density measurements for each salt were carried out over a concentration of 0.05 *m* to near saturation excluding $(n\text{-C}_4\text{H}_9)_4\text{NBr}$ which was found to be very soluble.

Results

In all cases the density increased with the concentration of the salt and was found to be represented by Root's¹⁰ equation

$$d = d_0 + Ac - Bc^{1/2} \quad (1)$$

A and *B* being constants specific to the salt considered.

The apparent molal volumes ϕ_v were calculated from the density data by the equation

$$\phi_v = \frac{1}{m} \left(\frac{1000 + mM_2}{d} - \frac{1000}{d_0} \right) \quad (2)$$

where d_0 is the density of pure methanol, M_2 the molecular weight of the salt, d the density of the solution, and m its molality.

In all cases ϕ_v was found to vary linearly with \sqrt{c} over the concentration range investigated, following Masson's¹¹ equation

$$\phi = \phi_v^0 + S_v \sqrt{c} \quad (3)$$

as may be expected from eq 1 since

$$\phi_v^0 = \frac{M_2 - 1000A}{d_0} \quad (4)$$

$$S_v = 1000B/d_0 \quad (5)$$

ϕ_v^0 is ϕ_v at infinite dilution and S_v the limiting slope. Values of ϕ_v^0 and S_v obtained from eq 3 are given in Table I. However, the experimental data are much better represented by eq 3 than by expression b of the Redlich and Meyer method.⁵

The partial molal volumes \bar{V}_2 of the tetraalkylammonium halides were computed from ϕ_v from the equation¹²

$$\bar{V}_2 = \phi_v + \frac{1000 - c\phi_v}{2000 + c^{3/2} \frac{d\phi_v}{dc^{1/2}}} c^{1/2} \frac{d\phi_v}{dc^{1/2}} \quad (6)$$

where $d\phi_v/dc^{1/2}$ may be replaced by S_v .

The values of \bar{V}_2 thus obtained are tabulated at

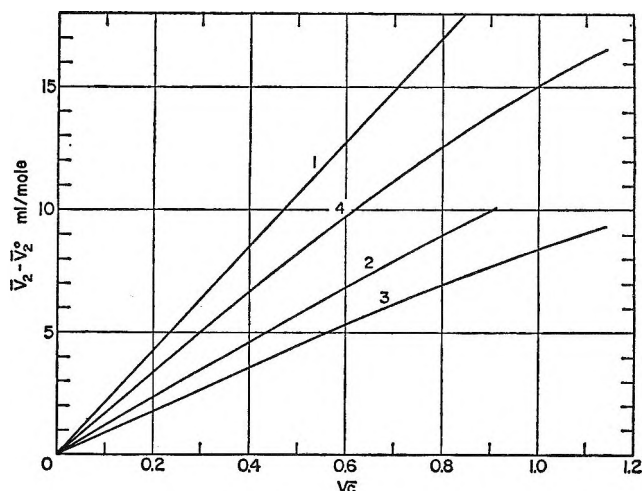


Figure 1. Partial molal volumes of tetraalkylammonium bromides: 1, NH_4Br ; 2, $(\text{C}_2\text{H}_5)_4\text{NBr}$; 3, $(n\text{-C}_3\text{H}_7)_4\text{NBr}$; 4, $(n\text{-C}_4\text{H}_9)_4\text{NBr}$.

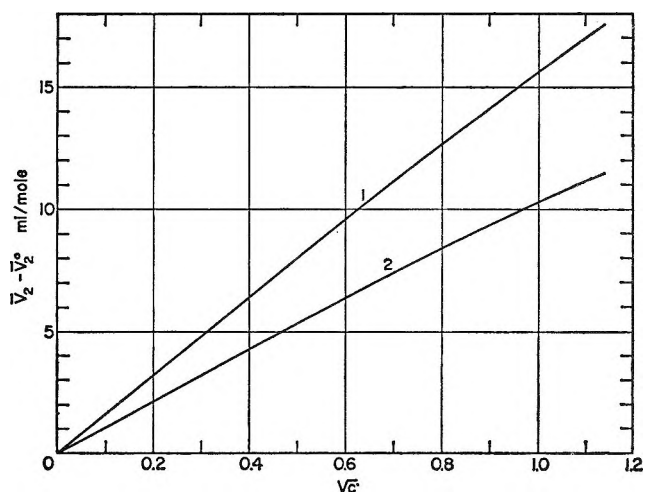


Figure 2. Partial molal volumes of tetramethylammonium and tetraethylammonium chlorides: 1, $(\text{CH}_3)_4\text{NCl}$; 2, $(\text{C}_2\text{H}_5)_4\text{NCl}$.

various molal concentrations, m , in Table II. These values are plotted against \sqrt{c} in Figures 1 and 2. The experimental values of S_v do not agree exactly in general with that predicted by Debye-Hückel theory,⁵ which for methanol is 15.77 as calculated from expression¹³

$$S_v = kw^{3/2} \quad (7)$$

(9) A. Weissberger, "Physical Methods of Organic Chemistry," Vol. I, 2nd ed, Interscience Publishers, Inc., New York, N. Y., 1949, Part I.

(10) W. C. Root, *J. Am. Chem. Soc.*, **55**, 850 (1933).

(11) D. O. Masson, *Phil. Mag.*, (7) **8**, 219 (1929).

(12) H. S. Harned and B. B. Owen, "The Physical Chemistry of Electrolytic Solutions," 3rd ed, Reinhold Publishing Corp., New York, N. Y., 1958, p 329.

(13) O. Redlich, *J. Phys. Chem.*, **67**, 496 (1963).

Table I: Apparent Molal Volumes at Infinite Dilution and the Limiting Slopes for the Tetraalkylammonium Halides at 25° (ml/mole)

	NH ₄ Br	(C ₂ H ₅) ₄ NBr	(C ₃ H ₇) ₄ NBr	(C ₄ H ₉) ₄ NBr	(CH ₃) ₄ NCl	(C ₂ H ₅) ₄ NCl
ϕ_v^0	20.10	149.6	222.1	285.9	83.7	142.30 ^a
	20.75	148.0	220.0	286.2	83.0	140.7 ^b
S_v	14.32	7.73	6.06	11.19	10.8	7.21

^a From eq 3. ^b Limiting value of $\phi_v - 15.77\sqrt{c}$ vs. c .⁵

Table II: Apparent and Partial Molal Volumes of Tetraalkylammonium Halides in Methanol Solutions at 25° (ml/mole)

Concn., <i>m</i>	NH ₄ Br		(C ₂ H ₅) ₄ NBr		(C ₃ H ₇) ₄ NBr		(C ₄ H ₉) ₄ NBr		(CH ₃) ₄ NCl		(C ₂ H ₅) ₄ NCl	
	ϕ_v	\bar{V}_2	ϕ_v	\bar{V}_2	ϕ_v	\bar{V}_2	ϕ_v	\bar{V}_2	ϕ_v	\bar{V}_2	ϕ_v	\bar{V}_2
0.1	24.08	20.27	151.8	152.9	213.8	224.7	289.0	290.5	86.8	88.4	151.8	152.9
0.2	25.75	22.77	152.6	154.1	224.5	225.6	290.2	292.3	88.1	90.2	152.6	154.1
0.3	27.02	24.66	153.3	155.1	225.0	226.4	291.3	293.6	89.0	91.6	153.3	155.1
0.4	28.10	26.27	153.8	155.9	225.4	226.9	291.9	294.7	89.7	92.6	153.8	155.9
0.5	29.02	27.63	154.3	156.5	225.8	227.4	292.5	295.5	90.4	93.6	154.2	156.5
0.6	29.86	28.87	154.7	157.1	226.1	227.9	293.1	296.3	90.9	94.4	154.7	157.1
0.7	30.65	30.03	155.1	157.6	226.3	228.2	293.6	296.9	91.5	95.1	155.1	157.6
0.8	31.38	31.10	155.5	158.1	226.6	228.6	294.1	297.5	92.0	95.9	155.5	158.1
0.9	32.06	32.09	155.8	158.6	226.9	228.9	294.5	298.0	92.5	96.5	155.8	158.6
1.0			156.1	159.0	227.1	229.2	294.9	298.5	92.9	97.2	156.1	159.0
1.1			156.3	159.3	227.3	229.4	295.2	298.9	93.4	97.8	156.3	159.3
1.2					227.4	229.6	295.5	299.3	93.8	98.3		
1.4					227.8	230.0	296.1	299.9	94.5	99.0		
1.6					228.1	230.4	296.6	300.5	95.2	99.9		
1.8					228.4	230.7						
2.0					228.6	231.0						

where

$$w = (1/2) \sum v_i Z_i^2$$

$$k = 2N^2 e^3 (2\pi/1000RT)^{1/2} \epsilon^{-1/2} \left(\frac{d \ln \epsilon}{dp} - \beta/3 \right)$$

and N is Avogadro's number, ϵ and β are the dielectric constant and the compressibility of the solvent, respectively, and the other terms have their usual meaning. The derivative $d \ln \epsilon / dp$ was calculated from Owen's expression¹⁴

$$\frac{d \ln \epsilon}{dp} = \frac{A}{B + p} \quad (8)$$

the constants A and B being calculated from the measurements of Hartman, *et al.*,¹⁵ and extrapolated to 25°.

The sign and order of magnitude are similar to the latest results found for aqueous solutions.^{2,3,4b} This tends to point out that in methanol, tetraalkylammonium halides seem to behave like small electrolytes in water, as confirmed by studies of conductance¹⁶ and viscosity.¹⁷

From Table I, the difference in ϕ_v^0 between (C₂H₅)₄NCl and (C₂H₅)₄NBr, which is 7.3 ml/mole, in good agreement with the difference between KCl and KBr,¹⁸ gives for the partial molal volume of (CH₃)₄NBr at infinite dilution $\bar{V}_2^0 = 91.0$.

In the series from NH₄Br to (n-C₄H₉)₄NBr the increase in volume per methylene group is 17.5 ml/mole in going from NH₄⁺ to (CH₃)₄N⁺, 14.5 ml/mole in going from (CH₃)₄N⁺ to (C₂H₅)₄N⁺, 18.5 ml/mole in going from (C₂H₅)₄N⁺ to (n-C₃H₇)₄N⁺, and 18.3 ml/mole in going from (n-C₃H₇)₄N⁺ to (n-C₄H₉)₄NBr. This is close to the difference of 15 ml/mole in \bar{V}_2^0 of methane^{19,20} and propane²¹ in methanol and 16 ml/mole in water,²² except for NH₄⁺ and (CH₃)₄N⁺ as expected

(14) See ref 12, p 162.

(15) H. Hartman, A. Neuman, and G. Rinck, *Z. Physik. Chem. (Frankfurt)*, **44**, 218 (1965).

(16) R. L. Kay, C. Zawoyski, and D. F. Evans, *J. Phys. Chem.*, **69**, 4208 (1965).

(17) R. L. Kay, T. Vituccio, C. Zawoyski, and D. F. Evans, *ibid.*, **70**, 2336 (1966).

(18) G. Jones and H. J. Fornwalt, *J. Am. Chem. Soc.*, **57**, 2041 (1935).

Table III: Apparent Molar Volumes of Tetraalkylammonium and Ammonium Cations in Methanol at 25° (ml/mole)

	NH ₄ ⁺	(CH ₃) ₄ N ⁺	(C ₂ H ₅) ₄ N ⁺	(<i>n</i> -C ₃ H ₇) ₄ N ⁺	(<i>n</i> -C ₄ H ₉) ₄ N ⁺
Methanol	14.1	85.0	143.6	216.1	279.9
Water ²	17.40	89.1	149.6	215.1	277.3
Water ^{4b}		88.5	148.6	213.9	275.4

since these are smaller ions for which the influence of the charge is noticeable. It should be kept in mind, however, that the partial molal volume \bar{V}_2^0 shows only part of the ion-solvent interaction since it is given²³ by

$$\bar{V}_2^0 = V_{in} + \Delta V \quad (9)$$

where V_{in} and ΔV are the intrinsic volume of the ion and electrostriction of the solvent, respectively. Furthermore, it has been shown²⁴ that the B coefficients of the Jones-Dole equation may be written as

$$B = k\phi_s^0 \quad (10)$$

where k is a shape factor (2.5 for spheres) and ϕ_s^0 is the volume occupied by 1 mole of solvated electrolyte. Assuming the tetraalkylammonium ions as well as the bromide ion to possess spherical symmetry, the values of ϕ_s^0 may be calculated from eq 10 and literature data of the viscosities,¹⁷ since²⁵

$$\phi_s^0 = \phi_v^0 + n^0V^0 \quad (11)$$

where n^0 is the solvation number at infinite dilution and $V^0 = 41$ ml is the molar volume of methanol. The results obtained for n^0 ($1.2 > n^0 > 1.0$) tend to show a specific interaction between the Br⁻ ion and the methanol ($n^0 = 1$) since they do not depend upon the cation considered, within the experimental results for B . This points out that the tetraalkylammonium ions are not solvated in methanol either, as has been assumed in water.²⁶ A value for the solvated ionic volume for the Br⁻ may be estimated from the best value of λ_0^- for Br⁻ in methanol¹⁶ ($\lambda_0 = 56.45$) which gives for the solvated volume of Br⁻

$$\phi_s^0(\text{Br}^-) = 47.0 \text{ ml/mole}$$

from which the apparent molar volume of the bromide ion is obtained through eq 11

$$\phi_v^0 = \phi_s^0 - n^0V^0 = 47.0 - 41.0 = 6 \text{ ml/mole}$$

The cationic apparent molar volumes obtained are compared in Table III with their respective values in water.^{2,4b} These values seem to be rather close.

From the continuum theory applied to methanol solutions²⁷ it was possible to calculate the intrinsic radii r_s^0 ²³ which are given in Table IV together with the

radii r_a calculated for various solvents and r_b obtained by applying to methanol²⁸ the procedure used by Robinson and Stokes,²⁹ to estimate the radii r_c of the tetraalkylammonium ions in water. The agreement is as good as can be expected, with the (CH₃)₄N⁺ showing the largest deviation as usual.

Table IV: Intrinsic Radii of Ions in Methanol at 25° (Å)

	r_e	r_a^a	r_b^b	r_c^c
NH ₄ ⁺	2.31			
(CH ₃) ₄ N ⁺	3.33	3.18	3.74	3.47
(C ₂ H ₅) ₄ N ⁺	3.91	3.84	3.97	4.00
(<i>n</i> -C ₃ H ₇) ₄ N ⁺	4.46	4.34	4.54	4.52
(<i>n</i> -C ₄ H ₉) ₄ N ⁺	4.84	4.81	4.99	4.94
Cl ⁻	2.09			
Br ⁻	2.20			

^a D. F. Tuan and R. M. Fuoss, *J. Phys. Chem.*, **67**, 1343 (1963).

^b Reference 28. ^c Reference 29.

All these results tend to show that the positive structural effects shown by the alkyl groups in water solutions³⁰ (to be differentiated from hydration) are quite weak in methanol. This is confirmed by measurements of nmr relaxation time measurements³¹ which show that the tendency to structure formation decreases from

(19) J. H. Hildebrand and R. L. Scott, "The Solubility of Non-electrolytes," 3rd ed, Reinhold Publishing Corp., New York, N. Y., 1955, p 247.

(20) A. Lanning and J. C. Fjaldeick, *Acta Chem. Scand.*, **14**, 1124 (1960).

(21) Extrapolated from ref 19 and 20.

(22) L. Masterton, *J. Chem. Phys.*, **22**, 1830 (1954).

(23) J. Padova, *ibid.*, **39**, 1552 (1963).

(24) J. Padova, *ibid.*, **38**, 2538 (1963).

(25) J. Padova, *ibid.*, **39**, 2599 (1963).

(26) *Cf.*, e.g., R. Gopal and A. K. Rastogi, *J. Indian Chem. Soc.*, **43**, 269 (1966).

(27) J. Padova, to be published.

(28) L. G. Longworth, *J. Phys. Chem.*, **67**, 689 (1963).

(29) R. A. Robinson and R. M. Stokes, "Electrolyte Solutions," 2nd ed, Butterworth and Co. Ltd., London, 1959, p 125.

(30) *Cf.*, e.g., M. J. Blandamer, M. J. Foster, N. J. Hidden, and M. C. R. Symons, *Chem. Commun.*, 62 (1966).

(31) M. G. Hertz and M. D. Zeidler, *Ber. Bunsenges. Physik. Chem.*, **68**, 821 (1964).

water to methanol, ethanol, and acetone and does not exist in the latter.

From Table I it is seen that the slope of S_v of n -Bu₄NBr is higher than those of the other alkylammonium salts.³² It seems that the large size of the ion is responsible for the steeper increase of ϕ_v^0 with concentration. This might possibly be due to a stronger alcoholphobic effect if it may be said so, since no evidence could be found for the formation of micelles

in methanol as tested through light-scattering measurements.

Acknowledgments. The authors wish to thank Dr. G. Cohen for the light-scattering measurements and Miss E. Halperin for technical help.

(32) Measurements carried out on dilute solutions of (CH₃)₄NBr seem to indicate that the slope S_v for this salt is higher than that for (C₂H₅)₄NBr.

Ultraviolet Photolysis of X-Irradiated Methanol at 77°K¹

by Stephen B. Milliken and Russell H. Johnsen

Department of Chemistry, Florida State University, Tallahassee, Florida 32306 (Received November 29, 1966)

X-Irradiated methanol was photolyzed at 77°K in the epr cavity and in bulk samples with selected wavelengths. Wavelengths shorter than 3100 Å lead to a continuing production of ·CHO and a steady-state concentration of ·CH₃ in the matrix; hence the production of CH₄ and CO from the thawed material is proportional to the duration of photolysis time. Wavelengths between 3300 and 4000 Å yield an amount of ·CHO trapped in the matrix equal to the original concentration of spins produced by X-irradiation. A study of the hydrogen and methane yields was made in both the glassy and the polycrystalline solids.

Introduction

A useful feature of the radiolysis of solid organic materials at low temperatures is that intermediates, reactive at room temperature, can often be trapped and studied at leisure. Radical intermediates can be identified by electron paramagnetic resonance and correlated with the yields from the thawed material. When relating such intermediates to radiolysis mechanisms it is necessary to know whether these trapped species are produced by decomposition of excited molecules, by ion molecule reactions, or by radical precursors which are still able to react with the substrate at the low temperature. For this reason reactions of radicals in the matrix at low temperatures relate directly to radiation chemistry. In the irradiated aliphatic alcohols such radical reactions may be initiated by the photolysis of the irradiated material by

visible and ultraviolet light. It is possible to photolyze the alcohol samples in an epr cavity and directly observe the radical reactions during and after the photolysis. Investigations of this type have been made,²⁻⁵ but the question of radical reactivity at 77°K has not been answered fully and study is continuing. This particular work is concerned with methanol.

Previously it has been shown²⁻⁴ that ·CH₂OH and e⁻ are the paramagnetic entities trapped in irradiated

(1) This material was abstracted in part from the thesis of S. B. Milliken and was supported in part by U. S. Atomic Energy Commission Contract AT-(40-1)-2001. This is AEC Document ORO-2001-3.

(2) R. S. Alger, T. H. Anderson, and L. A. Webb, *J. Chem. Phys.*, **30**, 685 (1959).

(3) C. Chachaty and E. Hayon, *Nature*, **200**, 59 (1965).

(4) E. Hayon and C. Chachaty, *J. Chim. Phys.*, **61**, 1115 (1965).

(5) D. R. Smith and J. J. Pieroni, *Can. J. Chem.*, **43**, 876 (1965).

methanol at -196° . Ultraviolet light transforms the $\cdot\text{CH}_2\text{OH}$ radical into $\cdot\text{CHO}$. This $\cdot\text{CHO}$ radical is further decomposed by visible light into CO and H \cdot . Visible light also removes the trapped electron and simultaneously produces $\cdot\text{CH}_2\text{OH}$. Chemical analyses⁶ of the products of the photolyzed radicals have indicated that the transformation of the $\cdot\text{CH}_2\text{OH}$ by ultraviolet followed by visible light gives a yield of CO equal to the original yield of radicals. This chemical analysis corroborated the results of Anderson, Alger, and Webb,² who found that each $\cdot\text{CH}_2\text{OH}$ photolyzed produced a $\cdot\text{CHO}$ radical. It was in disagreement with the results of Tepley and Dainton,⁷ who observed that a steady-state concentration of $\cdot\text{CH}_2\text{OH}$ was produced by a "cyclic" process propagated by the ultraviolet light.

In the present study both the photolysis experiments and the chemical analyses were repeated, using optical filters to control the wavelength of the photolyzing light. In the course of the investigation a dependence of the yields upon the nature of the solid was found.

Experimental Section

The methanol was Baker Analyzed reagent grade used without further purification, since it was found that ordinary chemical means produced no measurable improvement. Samples were handled in sealed containers or in a drybox to control their water content. The amount of water added regulated the phase of the solid. It was found that with less than 2 mole % of water the methanol froze in a white, opaque, polycrystalline solid. Greater than 2% water content produced a clear, glassy solid. When observing the effect of the state (glassy or polycrystalline) on the radiolysis yields it was noted that no change appeared until sufficient water had been added to produce the glassy solid. Additional water caused no further change in yields. After it had been shown that it is the type of solid and not the water which changes the yields, a concentration of 5 mole % was used in the glassy samples to make the samples insensitive to the method of freezing.

Degassing was effected by the technique of repeated freezing and thawing with pumping. Samples to be examined in the epr apparatus were prepared either in thin-walled Thermosil tubes 3 mm in diameter or by freezing drops in liquid nitrogen. The drops were frozen by injecting a 20- μl aliquot of degassed methanol under the surface of liquid nitrogen by means of a Hamilton syringe. This minimized the oxygen content. Methanol containing water formed glassy spheres which could be transferred to the dewar in the epr cavity after irradiation and held in position with

a quartz fork. The polycrystalline material was fragile and required the use of the Thermosil tubes to contain it. Irradiation of these tubes generated some epr signal which, however, was small compared with the signal from the irradiated alcohol and could easily be subtracted from the spectrum of the alcohol radicals. Irradiations were carried out with the Florida State University Van de Graaff accelerator using 3-Mv peak X-rays. The epr spectrometer was a Varian Model V-4502. Ultraviolet photolyses were carried out with a General Electric A-H6 lamp. The total dose varied from 10^{19} to 10^{20} ev/g. In general, 10^{20} ev/g were required for accurate determinations of molecular products; however, 10^{19} ev/g produced a more than sufficient radical concentration for epr spectra to be taken. The effects of photolysis of the radicals were not dependent on total dose and the lower concentration permitted a more nearly complete photolysis of $\cdot\text{CH}_2\text{OH}$ radicals in a given period of time. Except for a lower $G(\text{radicals})$ in the polycrystalline material at the higher dose which is discussed later, none of the yields of radicals or products appeared to be dose dependent. Dosimetry was by the Fricke method,⁸ using a $G(\text{Fe}^{3+}) = 15.5$.

Gas yields were determined by gas chromatography using a 1-m charcoal column at room temperature and a thermal conductivity detector.

Corning Glass filters and Baird Atomic interference filters were used to study the effect of different wavelengths. The Corning Glass filters, with broader band pass and greater transparencies than the interference filters, were used for the study of the concentration as a function of time during photolysis. The Baird Atomic interference filters were used to help fix the wavelength region between that which produced a net increase in radical concentration and that which did not. The filters were inserted into the path of light collimated and focused from the AH-6 source by two quartz lenses. By using a combination of filters, fairly narrow wavelength regions could be investigated at the expense of decreased intensity. Transmission regions of the optical filters are defined arbitrarily as the region where the transmittance is greater than 10% of the peak transmittance. (Thus, Corning Glass filter No. 5860 transmits approximately 25% of the light at 3600 A. It transmits 2.5% of the light at 3300 and 3825 A. Its transmittance region is then defined as being approximately 3300-3800 A.) The

(6) R. H. Johnsen, *J. Phys. Chem.*, **65**, 2144 (1961).

(7) F. S. Dainton, G. A. Salmon, and J. Tepley, *Proc. Roy. Soc. (London)*, **A286**, 27 (1965).

(8) A. Weiss and H. Swarc, *Proc. Intern. Conf. Peaceful Uses At. Energy, Geneva, 1955*, **14**, 179 (1956).

respective upper and lower wavelength limits for the visible and ultraviolet light which photolyzes radicals were determined approximately by the combination of Corning Glass filters No. 9863 and No. 3850. Light in this region of transmission, approximately 3650–4050, affected neither the $\cdot\text{CHO}$ nor the $\cdot\text{CH}_2\text{CH}$ radical. Relative concentrations reported in the tables were determined by numerical integrations of the esr spectrograms and in the graphs from the product of peak height and line width. These methods were used only in those cases when spectra did not show appreciable overlap or when only total concentration of spins was of interest. Ultraviolet photolysis of an unirradiated sample generated a small concentration of radicals when the light source was intense and included short wavelengths. The concentration of these radicals after several hours of photolysis did not exceed 10% of the radicals generated by X-irradiation, indicating that the effects seen are due to the photolysis of the radicals and not the bulk material.

Results

It was found that the effects of photolysis depend on the wavelengths employed. Ultraviolet light in the approximate range 3300–3600 Å transforms the $\cdot\text{CH}_2\text{OH}$ radical into $\cdot\text{CHO}$ with no change in the total radical concentration as reported earlier² (Figures 1 and 2). Photolysis with light that includes ultraviolet of shorter wavelengths (3100 Å) but excludes visible light produces a net increase in the radical concentra-

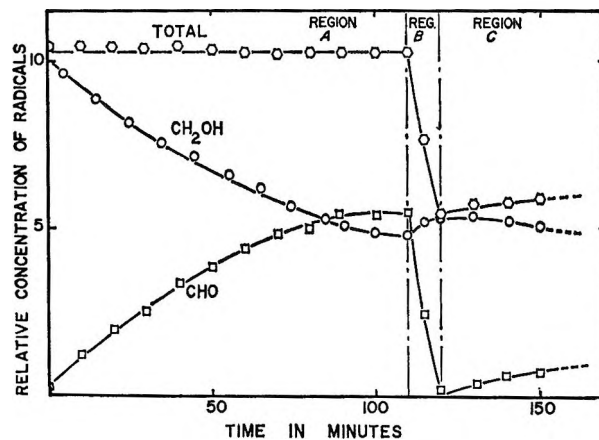


Figure 2. Relative concentration of $\cdot\text{CH}_2\text{OH}$ and $\cdot\text{CHO}$ during ultraviolet photolysis. Regions A, B, and C refer to the band pass of filters during a given period of photolysis: region A, 3300–3800 Å; region B, 4500–7000 Å; region C, 3000–3900 Å. Slight increase in $\cdot\text{CH}_2\text{OH}$ concentration in region B also occurs in the dark and is not related to photolysis by visible light.

tion, as found by Dainton.⁷ This can be seen from an examination of experiments 1 and 2 in Table I. When a filter transparent over a broad region is used the intensity of light is sufficient to establish a steady-state concentration of $\cdot\text{CH}_2\text{OH}$ radicals in 20–30 min. This is the case in experiment 1 in Table I; the last column represents the approximate steady-state concentration of $\cdot\text{CH}_2\text{OH}$ relative to the original concentration. Light filtered through narrow band-pass filter combinations took somewhat longer to establish the steady-state concentration. However, as long as light with wavelengths shorter than 3100 Å is present a net increase in radicals is actually seen. The results in Table I are supported by the chemical analysis of bulk samples which showed a continuing production of CO and CH_4 with photolysis by light below 3100 Å. This effect is shown in Figure 3. On the other hand, an ultimate yield of CO equal to the original concentration of $\cdot\text{CH}_2\text{OH}$ was found previously by Johnsén,⁶ using thin-walled Pyrex ampoules which were appreciably transparent only above 3300 Å.

In this work an attempt was made to duplicate the effects of the thin-walled Pyrex tubes by using an optical filter system, but the intensity limitations precluded the complete destruction of the $\cdot\text{CH}_2\text{OH}$ within practicable time limits. The results are shown in Table II. It can be observed that methane has reached a limit and the rate of production of carbon monoxide and hydrogen has slowed after 6 hr of photolysis with the filter systems No. 5850 and 0160 (3100–4800 Å). Photolysis with filter No. 5860, which is less trans-

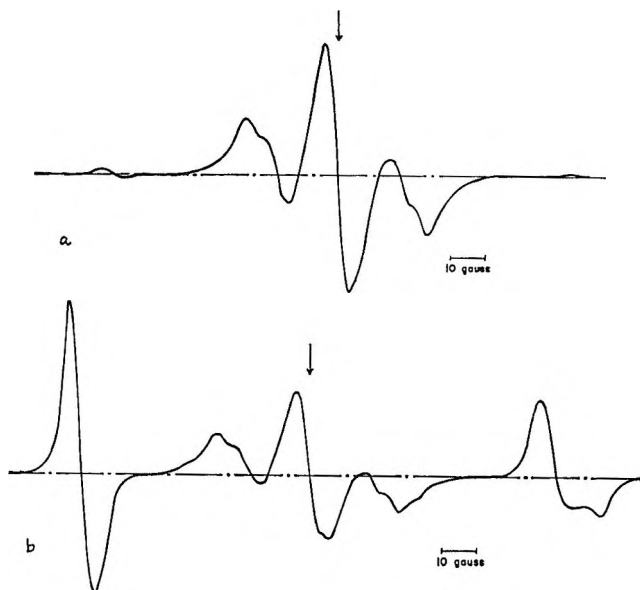
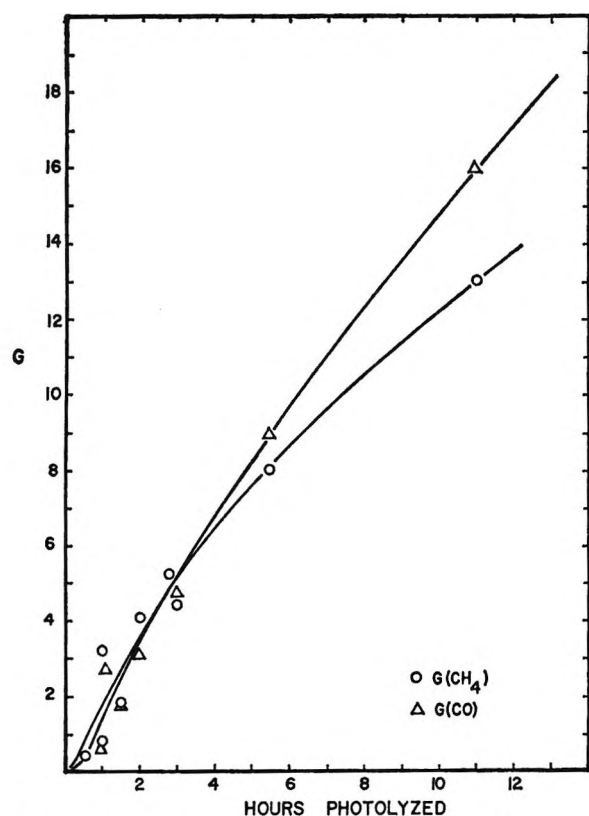


Figure 1. ESR spectra: a, X-irradiated methanol; b, X-irradiated methanol after 35-min ultraviolet photolysis (λ 3300–3800 Å). Arrow indicates g of free electron.

Table I: Effect of Ultraviolet Photolysis on Radical Concentration

Expt no.	Filter ^a	Transparent region, A	Relative transparency	Relative yields of radicals (total dose 10 ¹⁸ ev/g)									
				Initial			5-min photolysis			Limiting values			
				·CH ₂ OH	·CHO	·CH ₃	·CH ₂ OH	·CHO	·CH ₃	·CH ₂ OH	·CHO	·CH ₃	Total
1	9863	2400-4000	1.0	1.0	0	0	0.70	0.22	0.22	0.45	0.67	0.16	1.30
2	9863 + 7740	2900-4000	0.98	1.0	0	0	0.95	0.05	0	0.75	0.30	0.05	1.10
3	9863 + Pyrex	3400-4000	Unknown	1.0	0	0	1.0	0	0
4	5860	3300-3800	0.36	1.0	0	0	0.92	0.08	0	0.8	0.20	0	1.00

^a Corning stock number.

Figure 3. Product yield from ultraviolet photolyzed X-irradiated methanol; λ 2400-4000 A; dose 10²⁰ ev/g.

parent, has not appreciably used up the $\cdot\text{CH}_2\text{OH}$ ($G = \approx 6$) even after 6 hr.

The long-wavelength limit of light of sufficient energy to bring about a net increase in radicals during photolysis lies somewhere between 3100 and 3300 A. It cannot be fixed more exactly because of the band width of the filters necessary to transmit sufficient light to cause an observable change. It was noted that a Baird Atomic interference filter centered on 3130 A permits the passage of light which generates

Table II: Product Yields Resulting from Ultraviolet Photolysis

Filter	Hours photolyzed					
	3		6		3	
	No. of molecules/100 ev (total dose 10 ²⁰ ev/g)					
	H ₂		CO		CH ₄	
5850 + 0160 ^a (3100-4800 A)	8.8	10.0	2.4	3.7	1.3	1.3
5860 ^a (3300-3800 A)	4.0	6.3	1.0	1.8	0.4	0.8
Reference 6	23.0 ^b		6.6 ^b		11.0 ^b	

^a Corning stock number. ^b Limiting value.

an increase in radical concentration, while a similar filter centered on 3300 A does not. Both have a one-tenth band width of about 300 A.

Other observations follow which are indicative of a more complex system than has been suggested previously.

1. Whenever there is a net production of radicals the presence of $\cdot\text{CH}_3$ is observed (Figures 4 and 5). When short-wavelength light is excluded there is no evidence of methyl radicals (Figure 1b). With light of wavelength less than 3100 A the concentration of $\cdot\text{CH}_2\text{OH}$ drops rapidly, with the initial production of $\cdot\text{CH}_3$, then reaches a steady-state concentration. The concentration of methyl radicals passes through a maximum, then ultimately also approaches a steady state. The production of $\cdot\text{CHO}$ continues indefinitely. This behavior is shown in Figure 6.

2. The $\cdot\text{CH}_3$ disappears in the dark by a process which is approximately first order at least in the initial stage (Figure 7) and which is accompanied by a net production of $\cdot\text{CH}_2\text{OH}$. Double integration of the four-line spectrum was not conclusive, but it appears that at least three $\cdot\text{CH}_2\text{OH}$ radicals are produced by every four $\cdot\text{CH}_3$ radicals that disappear.

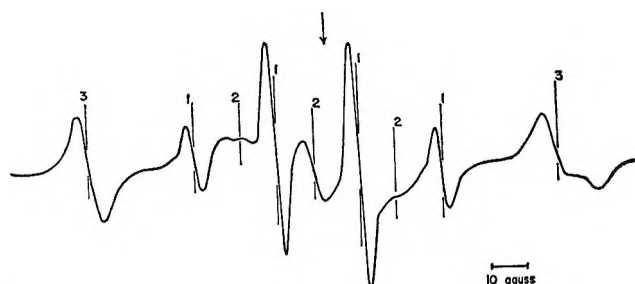


Figure 4. Dry methanol photolyzed 5 min with ultraviolet light (2300–4000 Å): 1, methyl quartet; 2, $\cdot\text{CH}_2\text{OH}$ triplet; 3, $\cdot\text{CHO}$ doublet. Arrow indicates g of free electron.

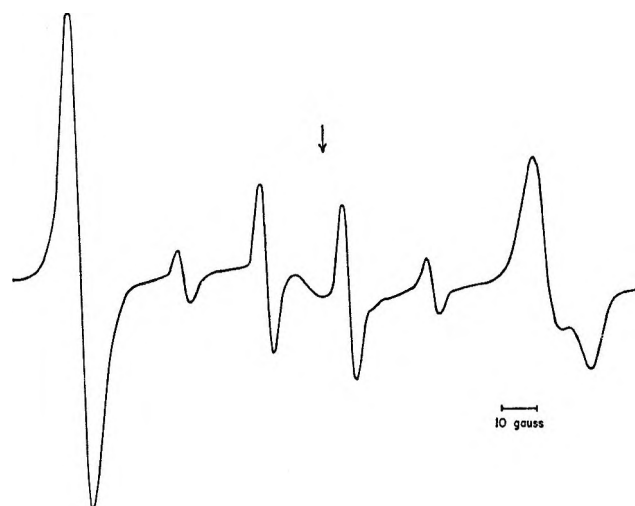


Figure 5. Same sample as Figure 4 after 35 min of photolysis.

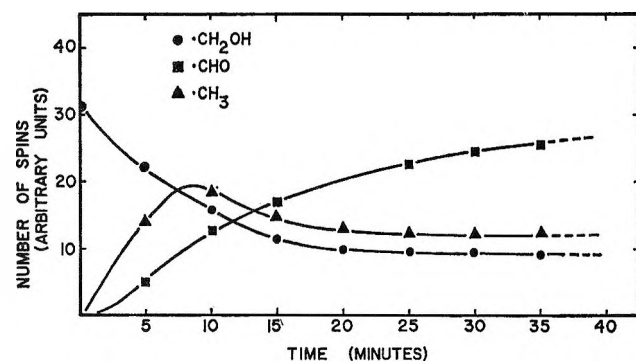


Figure 6. Changes in radical concentration with photolysis below 3100 Å.

3. Under intense ultraviolet light in the 2400–4000-Å region the central peak of the $\cdot\text{CH}_2\text{OH}$ triplet does not exhibit the monotonic decay of the side peaks but passes through a maximum during the first 5 min of photolysis. This is shown in Figure 8.

4. Formyl radicals do not appear to be destroyed by ultraviolet light. Most of the $\cdot\text{CH}_2\text{OH}$ can be transformed into $\cdot\text{CHO}$ by photolysis with ultraviolet

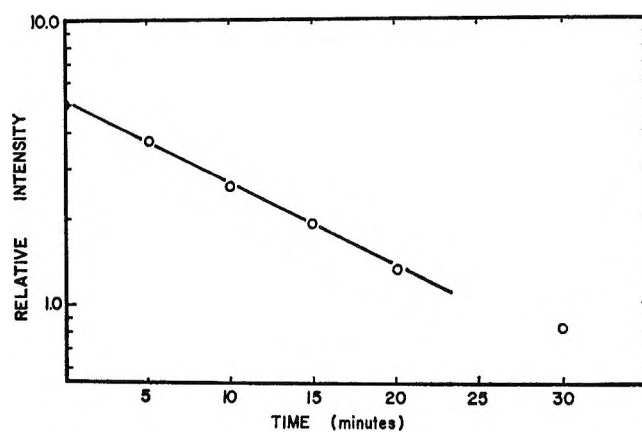


Figure 7. Decay of the methyl radical in the dark.

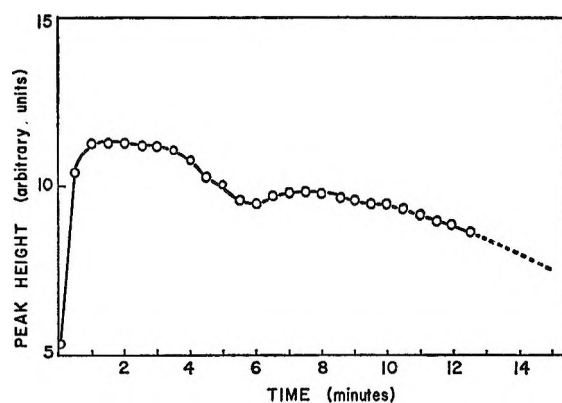


Figure 8. Behavior of the central ESR peak of the $\cdot\text{CH}_2\text{OH}$ spectrum during ultraviolet photolysis with 2400–4000-Å light.

light above 3300 Å over an extended period of time. When most of the $\cdot\text{CH}_2\text{OH}$ is gone, continued photolysis by ultraviolet light from 2400–4000 Å does not materially affect the concentration of $\cdot\text{CHO}$. These results appear to be in contradiction with the observation made by Dainton.⁷ A steady-state concentration of $\cdot\text{CH}_2\text{OH}$ unrelated to the $\cdot\text{CHO}$ concentration can be established at any concentration of $\cdot\text{CHO}$ by preceding the short-wavelength photolysis with photolysis by light above 3300 Å.

While the complications cited above seemed primarily related to the choice of wavelength of the photolyzing light, other organic systems have shown yields which varied as a function of phase.⁹ Thus, solids which are not homogeneous can exhibit varying yields.¹⁰ Since the radiolysis yields from solid methanol previously reported⁸ were not as reproducible as those found for liquid methanol, an investigation of the effect of phase seemed relevant.

(9) R. M. A. Hahne and J. E. Willard, *J. Phys. Chem.*, **68**, 2582 (1964).

(10) H. Swarc, *J. Chim. Phys.*, **59**, 1067 (1962).

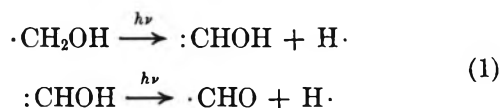
As mentioned above, the type of solid obtained by freezing is a function of the water content. The independence of product yields and water content has been reported by Tepley, *et al.*¹¹ The yields obtained from the two different solids are shown in Table III. They are as reproducible as the yields from liquid methanol providing the solid is homogeneous. The yield of hydrogen is greater in the glass than in the crystal while the yield of methane is lower. The initial yields of $\cdot\text{CH}_2\text{OH}$ are apparently the same in both solids, but after a dose of 10^{19} ev/g is exceeded more spins seem to be trapped in the glass. The photolysis of the $\cdot\text{CH}_2\text{OH}$ is unaffected by the nature of the solid.

Table III: Effect of Phase at -196°

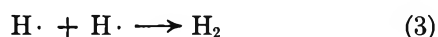
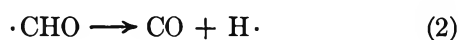
Phase	No. of molecules/100 ev		
	H ₂	CO	CH ₄
Glassy	3.4	0.06	0.50
Crystal	2.8	0.08	1.60
Reference 6 (possibly a mixture)	3.6	0.45	0.57

Discussion

The effect of ultraviolet light with wavelengths greater than 3300 Å is to transform the $\cdot\text{CH}_2\text{OH}$ into $\cdot\text{CHO}$. This may be a two-photon process

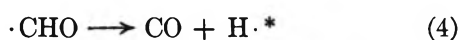


That the first step is probably reversible is suggested by a slight increase in the $\cdot\text{CH}_2\text{OH}$ concentration after ultraviolet photolysis is stopped (region B of Figure 2), Figure 6. If ultraviolet photolysis is followed by exposure to visible light

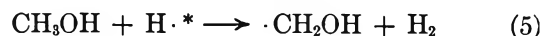


takes place.

The photolysis of $\cdot\text{CHO}$ with visible light does not result in the continuing formation of radicals. Photolysis with light in the ultraviolet region has no effect on the $\cdot\text{CHO}$ radical concentration. It would thus seem that the $\text{H}\cdot$ atom so produced is of thermal energy. This is in contrast with the proposal of Tepley and Dainton,⁷ who suggested that $\cdot\text{CHO}$ was destroyed by ultraviolet light with the production of a hot hydrogen atom

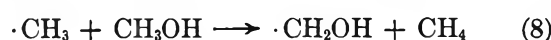
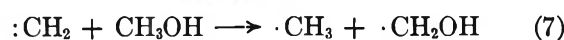
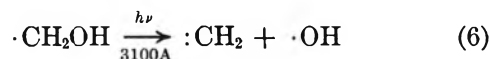


According to these workers, this hot $\text{H}\cdot$ atom could then abstract to produce $\cdot\text{CH}_2\text{OH}$



However, the effect of ultraviolet light in the absence of visible light was evidently never investigated. Moreover, the postulated cyclic process involving the regeneration of $\cdot\text{CH}_2\text{OH}$ through the photolysis of $\cdot\text{CHO}$ should determine a value for the relative concentration of $\cdot\text{CH}_2\text{OH}$ and $\cdot\text{CHO}$. However, we have observed that the steady-state concentration of $\cdot\text{CH}_2\text{OH}$ is independent of the concentration of $\cdot\text{CHO}$. This is further evidence that no process involving hot $\text{H}\cdot$ atoms from the photolysis of $\cdot\text{CHO}$ is involved with wavelengths between 3300 and 4000 Å. Light above 4000 Å simply removes the $\cdot\text{CHO}$ without the generation of more radicals in agreement with the results obtained by Johnsen⁶ and those of Anderson, Alger, and Webb.²

The effect of light with wavelengths shorter than 3100 Å cannot be explained in a simple manner. The lowering of the $\cdot\text{CH}_2\text{OH}$ concentration by light in this region is always accompanied by the appearance of the $\cdot\text{CH}_3$ radical, implicating the $\cdot\text{CH}_2\text{OH}$ as the source of the methyl radicals, perhaps in the fashion indicated by eq 6–8.



The abstraction of a hydrogen atom by $\text{CH}_3\cdot$ (eq 8) in the cage to produce $\cdot\text{CH}_2\text{OH}$ would result in the net increase in the radical concentration, such as is observed. This increase continues after the light source is removed and the sample allowed to remain in the dark, with the concomitant disappearance of the methyl radicals by what would be interpreted as a process first order in that radical. The half-life for this disappearance is of the order of 600 sec. This is much faster than one would predict on the basis of the extrapolation of rate constants measured in the gas or liquid phase.^{12–14}

An alternate source for the methyl radicals would involve the breakage of a carbon–oxygen bond in a

(11) J. Tepley, A. Habersbergerova, and K. Vacek, *Collection Czech. Chem. Commun.*, **30**, 793 (1965).

(12) T. W. Shannon and A. G. Harrison, *Can. J. Chem.*, **41**, 2455 (1963).

(13) R. Shaw and J. C. J. Thyne, *Trans. Faraday Soc.*, **62**, 104 (1966).

(14) M. Cher, *J. Phys. Chem.*, **67**, 605 (1963).

neighboring methanol owing to a sensitization by the $\cdot\text{CH}_2\text{OH}$ radical. This is not as an attractive hypothesis because of the immediate decrease in the alcohol radical concentration during the early stage of the photolysis.

The abstraction reaction involving methylene radicals is made plausible by the fact that such reactions have recently been observed in isobutane¹⁵ and by the observed behavior of the central peak shown in Figure 7. This temporary increase of the signal intensity in the center of the spectrum can be explained by the transient presence of a singlet. The methoxy radical spectrum is such a singlet; the indiscriminate abstraction by $\cdot\text{CH}_2$ would be expected to produce some methoxy radicals.

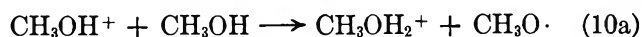
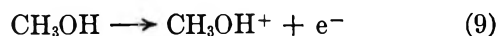
It is here, where the interpretation of the epr spectra becomes conjectural, that the implications for the radiolysis mechanism become most important. It is uncertain whether the $\cdot\text{CH}_2\text{OH}$ is the initial radical in the radiolysis process or is preceded by $\text{CH}_3\text{O}\cdot$.¹⁶ The proposed abstraction in the dark of hydrogen atoms by $\cdot\text{CH}_3$ suggests that $\text{CH}_3\text{O}\cdot$, which has similar reactivity, might also participate in an abstraction reaction at 77°K. The behavior of the central peak, if it is indeed due to $\cdot\text{CH}_3\text{O}$, indicates that this species does abstract. Since there is evidence for alkoxy radicals in the liquid and gas phase radiolysis of ethanol and methanol^{17,18} it seems probable that they are also present in the solid. The implication is, then, that the radical $\cdot\text{CH}_2\text{OH}$ does have a radical precursor at least in some cases.

The hydroxyl radical is not observed in the methanol matrix under any of the experimental conditions. It seems likely that it is not trapped, but diffuses through the matrix and reacts by the more rapid radical-radical process as does the hydrogen atom.

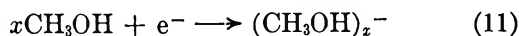
The change in the nature of the solid (glassy or microcrystalline), while having no apparent effect on the photolysis of $\cdot\text{CH}_2\text{OH}$ or $\cdot\text{CHO}$, gave the interesting change in radiolysis yields shown in Table III. No peak attributable to electrons is seen in the epr spectrum of the polycrystalline material. While the yield of $\cdot\text{CH}_2\text{OH}$ is the same in both glass and crystalline material at low doses, after a total dose of about 10^{19} ev/g the concentration of the $\cdot\text{CH}_2\text{OH}$ in the polycrystalline material is less than in the glass. Upon warming, the polycrystalline material gives a greater yield of CH_4 and a lower yield of H_2 than the glass.

Changes in radiolysis yields with phase, both molecular and radical, have been observed in other organic systems but no general explanation has been offered.¹⁰ Here the absence of electrons in the polycrystalline material and the increase of CH_4 yield are regarded

as related. The sequence of events in the glass may be considered to be similar to that in the liquid,¹⁹ which has been proposed



and the electron is solvated



Ultimately neutralization occurs between the protonated species and the electron to produce hydrogen.

Reaction 10a has been observed to occur in the gas phase on the first collision; it might also be expected to occur rapidly in the solid. Whether the radical produced is $\text{CH}_3\text{O}\cdot$ or $\cdot\text{CH}_2\text{OH}$ cannot be settled conclusively with the available evidence; both, in fact, may be produced. From the epr evidence it is clear that the net effect is the production of $\cdot\text{CH}_2\text{OH}$. The plausibility of an abstraction reaction by $\text{CH}_3\text{O}\cdot$ has been discussed above.

Reaction 11 is postulated to occur exclusively in the glass. Evidence from saturation studies⁴ indicates that solvation takes place at an average distance of 40 Å from the parent positive ion. This close proximity of the electron to a positive ion indicates that neutralization would be the favored reaction once the electron was released from the trap by thawing or exposure to visible light.

In crystalline methanol the pattern of hydrogen bonds extends in one dimension,²⁰ linking molecules into endless chains between which van der Waals forces alone are operative. These chains are arranged laterally in an approximately close-packed arrangement with each chain symmetrically surrounded by six neighbors. In the glass, with added water, while the hydrogen bonding can be assumed to persist, one would expect a disordered three-dimensional system of shortened chains. This difference probably accounts for the observation that neither color nor the esr spectra of the trapped electron is seen in crystalline material. Solvation of the electron necessary for trapping is prohibited

(15) M. L. Halberstadt and J. R. McNesby, *J. Chem. Phys.*, **45**, 1666 (1966).

(16) R. A. Basson, *Nature*, **211**, 630 (1966).

(17) J. J. J. Myron and G. R. Freeman, *Can. J. Chem.*, **43**, 1484 (1965).

(18) K. R. Ryan, L. W. Sieck, and H. J. Futrell, *J. Chem. Phys.*, **41**, 111 (1964).

(19) L. M. Theard and M. Burton, *J. Phys. Chem.*, **67**, 59 (1963).

(20) R. C. Evans, "An Introduction to Crystal Chemistry," Cambridge University Press, London, 1964, p 363.

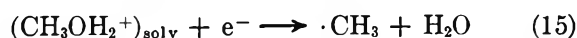
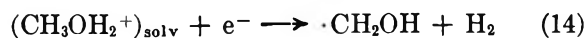
in the one-dimensional array of hydrogen bonds. Similarly one would not expect the counterion $\text{CH}_3\text{-OH}_2^+$ to be as extensively solvated in the crystalline material as in the glass.

In the polycrystalline material one would expect a competition between reactions 12 and 13 in which unsolvated electrons react with unsolvated ions almost immediately following their respective formation.



These reactions would be expected to be rapid and have relatively small activation energies. It would not be unreasonable to expect them to occur with approximately equal probability. Experimentally one finds that $G(e^-)$ is ~ 3 and that the yield of CH_4 is ~ 1.5 , which is consistent with this formulation.

On the other hand, in glassy methanol the reactions of the electrons take place only upon untrapping by bleaching and would thus be expected to occur with a highly solvated species.



Reactions such as these might be expected to have appreciable energies and entropies of activation and, furthermore, differ significantly in this regard. If this is true then one might expect reaction 14 to be favored under these circumstances, leading to dimin-

ished yields of methane in the case of glassy material. Furthermore, a yield of water has been noted in solid radiolysis but not in dry liquid in which solvated electrons have been observed.²¹

Conclusions

The photolysis of trapped $\cdot\text{CH}_2\text{OH}$ shows a wavelength dependence indicating more than one mode of decomposition of $\cdot\text{CH}_2\text{OH}$. The subsequent reactions do not involve a hot hydrogen but may involve a methylene biradical. Thermal atoms that are free to move do not abstract at 77°K, but trapped radicals such as $\cdot\text{CH}_3$ apparently do abstract, at a rate somewhat faster than predicted by extrapolation of the rate in fluid media at higher temperatures. The reactivity of $\cdot\text{CH}_3$ suggests that $\cdot\text{CH}_2\text{OH}$ may be preceded by another radical, most probably $\text{CH}_3\text{O}\cdot$. A change of yields is observed with a change in the nature of the solid. Explanation remains speculative, but the coincidence of the lack of electron trapping with the changed yield suggests that a change in the neutralization step may account for the observations.

Acknowledgments. Appreciation is expressed to the Atomic Energy Commission for its support of this work, to Mr. D. Pritchett for help with the irradiations, and to Mr. K. Morgan for assistance with the analyses.

(21) A. H. Samuel and J. L. Magee, *J. Chem. Phys.*, **21**, 1080 (1953).

The Kinetics of Reaction between Oxygen Atoms and Sulfur Dioxide: an Investigation by Electron Spin Resonance Spectrometry

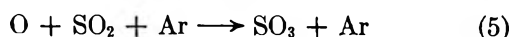
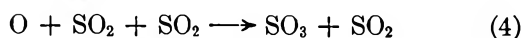
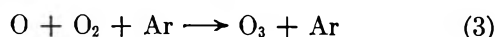
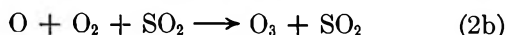
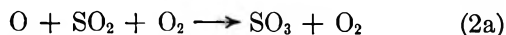
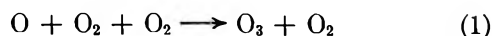
by M. F. R. Mulcahy, J. R. Steven, and J. C. Ward

CSIRO Division of Coal Research, Chatswood, N.S.W., Australia (Received November 29, 1966)

The kinetics of disappearance of oxygen atoms in the presence of sulfur dioxide at $299 \pm 2^\circ\text{K}$ and total pressure 0.7–3 torr have been determined using esr spectrometry to measure the concentration of atoms. The most direct interpretation of the data leads to the mean values $k_{2a} = (2.7 \pm 0.5) \times 10^{15} \text{ cm}^6 \text{ mole}^{-2} \text{ sec}^{-1}$, $k_5 = (2.4 \pm 0.15) \times 10^{15} \text{ cm}^6 \text{ mole}^{-2} \text{ sec}^{-1}$, and $k_4 = (10 \pm 4) \times 10^{15} \text{ cm}^6 \text{ mole}^{-2} \text{ sec}^{-1}$ for the rate constants of the reactions $\text{O} + \text{SO}_2 + \text{O}_2 \xrightarrow{k_{2a}} \text{SO}_3 + \text{O}_2$, $\text{O} + \text{SO}_2 + \text{Ar} \xrightarrow{k_5} \text{SO}_3 + \text{Ar}$, and $\text{O} + \text{SO}_2 + \text{SO}_2 \xrightarrow{k_4} \text{SO}_3 + \text{SO}_2$.

Introduction

The view is now widely held that much of the sulfur trioxide in the combustion products of sulfur-containing fuels derives from reaction between sulfur dioxide and oxygen atoms in the gaseous phase.^{1,2} Oxygen atoms can be transiently present in "above-equilibrium" concentration during combustion and the rate of formation of sulfur trioxide has been correlated with the magnitude of this concentration.^{3,4} This paper reports the first phase of investigations undertaken to obtain quantitative information on the rate of reaction between oxygen atoms and sulfur dioxide. The kinetics have been studied at room temperature and total pressures between 0.7 and 3 torr. Oxygen atoms generated in excess molecular oxygen or argon by a microwave discharge were mixed with sulfur dioxide in a stirred-flow reactor and the rate of reaction was determined by monitoring the inlet and outlet concentrations of the atoms by esr spectrometry. It is shown that the kinetics can be interpreted in terms of the reactions



Previous direct investigation of the reaction between SO_2 and atomic O has not been extensive. Geib and Harteck⁵ found that reaction occurs at liquid air temperature and deduced that if it depends on three-body collisions, its activation energy is $>1 \text{ kcal mole}^{-1}$. Kaufman⁶ made a brief study of the decay of O atoms in the presence of SO_2 in a flow tube and arrived at the approximate value $3 \times 10^{16} \text{ cm}^6 \text{ mole}^{-2} \text{ sec}^{-1}$ for k_2 at room temperature. Thrush and Halstead⁷ reported a similar value, namely about $5 \times 10^{16} \text{ cm}^6 \text{ mole}^{-2} \text{ sec}^{-1}$.⁸ The value of k_2 obtained in the present work is notably smaller than these values.

(1) R. E. Barrett, J. D. Hummell, and W. T. Reid, *J. Eng. Power*, **88**, 165 (1966).

(2) K. S. Pankhurst and M. C. Styles, *B.C.U.R.A. Mon. Bull.*, **27**, 497 (1963).

(3) G. Whittingham, *Trans. Faraday Soc.*, **44**, 141 (1948).

(4) A. Levy and E. L. Merryman, *Combust. Flame*, **9**, 299 (1965).

(5) K. H. Geib and P. Harteck, *Chem. Ber.*, **66**, 1815 (1933).

(6) F. Kaufman, *Proc. Roy. Soc. (London)*, **A247**, 123 (1958).

(7) B. A. Thrush and C. J. Halstead, "10th Symposium (International) on Combustion," The Combustion Institute, Pittsburgh, Pa., 1965, p 470.

(8) NOTE ADDED IN PROOF. After this paper had been accepted for publication, the revised value ($k_2 = (4.7 \pm 0.8) \times 10^{15} \text{ cm}^6 \text{ mole}^{-2} \text{ sec}^{-1}$) obtained by C. J. Halstead and B. A. Thrush, *Proc. Roy. Soc. (London)*, **A295**, 363 (1966), became available to the authors, and their attention was drawn to the unpublished work of J. W. Powers and R. D. Cadle (quoted by E. A. Allen and R. D. Cadle, *Photochem. Photobiol.*, **4**, 979 (1965)), who obtained $k_2 = 4.9 \times 10^{15} \text{ cm}^6 \text{ mole}^{-2} \text{ sec}^{-1}$. It is not clear to what extent these values include a contribution from k_4 .

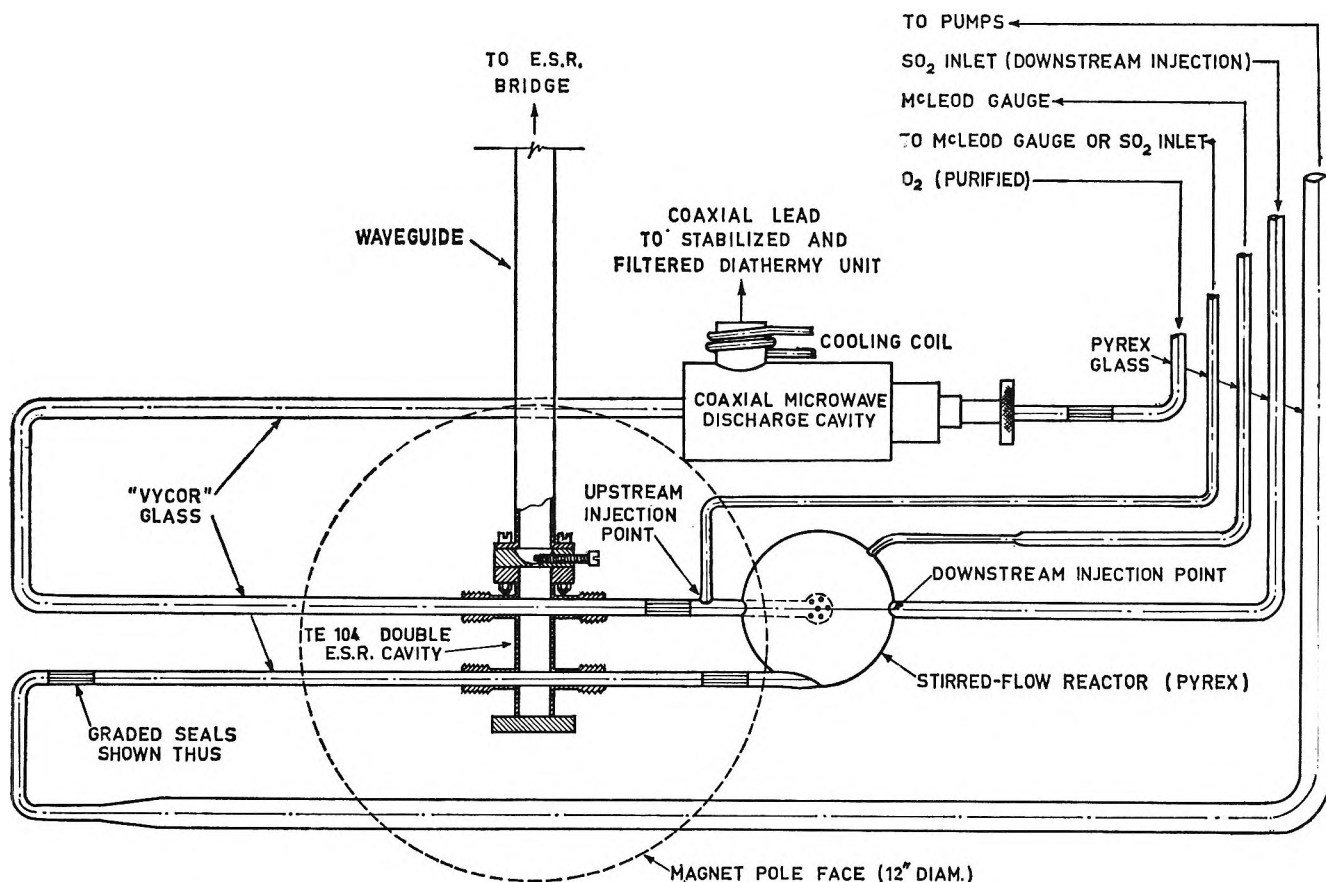


Figure 1. Flow system with esr double cavity for measuring oxygen atom concentrations at inlet and outlet of stirred-flow reactor.

Experimental Section

Apparatus and General Procedure. Assuming perfect mixing in the stirred-flow reactor, the steady state is given by

$$v_{in}[O]_{in} = V k_{pfo}[O]_{out} + v_{out}[O]_{out} \quad (Ia)$$

where v_{in} and v_{out} refer, respectively, to the total volumetric rates of flow of gas entering and leaving the reactor measured at the appropriate pressure; $[O]_{in}$ and $[O]_{out}$ are the corresponding concentrations in the gas stream, $[O]_{out}$ being identical with the stationary concentration in the reactor (which has the volume V). The term k_{pfo} is a pseudo-first-order rate constant covering all reactions in which oxygen atoms are destroyed. In principle, k_{pfo} is a function of the stationary concentrations $[SO_2]$, $[O_2]$, $[O]$, etc., in the reactor. The procedure was to determine k_{pfo} via eq Ia, that is, from the relation

$$k_{pfo} = \frac{v_{in}[O]_{in} - v_{out}[O]_{out}}{V[O]_{out}} \quad (Ib)$$

and to establish its dependence on the concentrations of SO_2 and other species present.

The essential parts of the apparatus are shown in Figure 1. The discharge cavity⁹ was energized with about 20 w of stabilized microwave power. Before entering the Pyrex spherical stirred-flow reactor¹⁰ ($V = 285$ ml), the gas from the discharge passed through 88 cm of silica tubing to the first section of the rectangular TE_{104} X-band dual esr cavity inserted between the poles of the 12-in. magnet of a Varian V4501 esr spectrometer. After reaction with SO_2 , the stream passed to the second section of the cavity and thence to the pumps. The two sections of the microwave cavity were independently modulated at 400 cps, and a switch enabled the esr signals to be recorded alternately on a chart recorder, thus giving, in principle, a quasi-continuous record of quantities proportional to $[O]_{in}$ and $[O]_{out}$. Since k_{pfo} was found not to depend on $[O]$, absolute atom concentrations were not required. However, some approximate determinations¹¹ were made to define the reaction condi-

(9) H. E. Radford, *Phys. Rev.*, **126**, 1035 (1962).

(10) M. F. R. Mulcahy and D. J. Williams, *Australian J. Chem.*, **14**, 534 (1961).

(11) A. A. Westenberg and N. de Haas, *J. Chem. Phys.*, **40**, 3087 (1964).

tions. Negligible proportions of SO₂ and O₂ were consumed by the reaction.

Reagents. Oxygen and Ar-O₂ mixtures were freed from hydrogenous impurities by passing them at 1.2 atm pressure through a silica tube packed with silica wool at 1100°. This was provided with a platinized asbestos plug at the downstream end, which led to 1 m of Linde 5A molecular sieve at room temperature. After entering the flow system, the gas traversed a tube 70 cm long and 1 cm in diameter packed with glass wool and glass beads at 77°K before entering the discharge. Sulfur dioxide from a cylinder was degassed by repeated freezing and pumping.

Corrections. Four factors, other than different atom concentrations, could influence the relative signal strengths from the two sections of the cavity: (i) different sensitivities of the two sections, (ii) differential line broadening due to the pressure drops along the column of flowing gas, (iii) further broadening in the downstream section due to the presence of SO₂, and (iv) generation of signal from one section by the modulation coil of the other.

The effects of factors i and ii were determined together by comparing peak heights and first moments of the "E-line"¹¹ of the spectrum given at various pressures by a stream of molecular oxygen passing through both sections; the resulting correction, applied to the "in" signal from O atoms, amounted to a few per cent. No specific effect of SO₂ (factor iii) could be detected. Factor iv was eliminated by counterbalancing the stray field in the unused section of the cavity with a small modulation current taken from the "live" coil through a resistor. The correction was usually less than 10%, but could amount to as much as 40% of the "out" signal at the lowest values of the latter. After allowance for these effects, the concentrations of atoms were taken as proportional to the peak heights h_{in} and h_{out} .

These concentrations differed from the [O]_{in} and [O]_{out} values to be substituted in eq Ib because of the reaction in the tubing between the esr cavity and the reactor. Assuming plug-flow conditions in the tubes, the following equations apply

$$[O]_{in} = \alpha [O]_{in}' \equiv [O]_{in}' \exp(-k_H V_H / v_{in}) \quad (\text{IIa})$$

$$[O]_{out} = \beta [O]_{out}' \equiv [O]_{out}' \exp(k_T V_T / v_{out}) \quad (\text{IIb})$$

where $[O]_{in}' \propto h_{in}$, $[O]_{out}' \propto h_{out}$, k_H is the pseudo-first-order rate constant for the disappearance of O atoms in the inlet tube, and k_T is the like constant for the reactions occurring in the outlet tube. V_H (8.5 cm³) and V_T (10 cm³) are the corresponding volumes of the tubes between the esr cavity and the reactor. Equation Ib then becomes

$$k_{pto} = \left(\frac{v_{in} \alpha h_{in} - v_{out} \beta h_{out}}{V \beta h_{out}} \right) \quad (\text{III})$$

In the absence of SO₂

$$k_{pto} = k_w + k_1' [O_2]^2 \quad (\text{IV})$$

and

$$k_H \simeq k_T \simeq R k_w + k_1' [O_2]^2 \quad (\text{V})$$

where k_w refers to the wall reaction in the reactor, k_1' is an empirical constant relating to the kinetics of reaction 1 (to be discussed later), and R (=6) is the ratio of the surface to volume ratios for tubing and reactor, which were assumed to possess the same specific efficiency for atom recombination. With the knowledge of k_1' , k_w was evaluated approximately from eq III and IV by setting $\alpha = \beta = 1$; the values of k_{pto} , k_w , α , and β were then improved by iteration. When SO₂ was added (at the downstream point, see Figure 1), the final value for k_H obtained above was used for the α factor, and an analogous iteration gave β and k_{pto} . When this procedure was continued until successive values of k_{pto} differed by less than 0.01, the final value was up to 35% less than that obtained with $\alpha = \beta = 1$.

Conditioning the Reactor. As observed by Kaufman,⁶ the SO₃ produced in the reaction increased the catalytic action of the walls on the recombination of O atoms. The effect was time dependent and difficult to control. However, on alternately carrying out the reaction and admitting atmospheric air, an oily layer was deposited on the walls of the reactor and connecting tubing. In the presence of this layer, reproducible values of [O]_{out} and [O]_{in} and the maximum survival of atomic O in the absence of SO₂ could be obtained (50–80%). The values of k_{pto} obtained in the presence of SO₂ could then be reproduced to within about $\pm 10\%$ in the same series of measurements. This was achieved only after several weeks of operation.

"Perfectly-Stirred" Flow in the Reactor. This was checked in two ways. (a) Under the conditions of the kinetics experiments, the glow produced by adding a little N₂ to the O₂ before the discharge appeared as a perfectly uniform sphere except for an insignificant volume at the base of the central inlet tube.¹² (b) The esr signal at the outlet was recorded continuously while equal flows of SO₂ were admitted alternately at the upstream and downstream points, each adjustment taking a few seconds. No significant difference in the signals was detected. Since the two modes of entry were geometrically and aerodynamically very

(12) When gross amounts of SO₂ were admitted (greater than the flow of oxygen), a dark region appeared near the SO₂ entrance and gradually filled the reactor as the flow of SO₂ was further increased.

Table I: Data Obtained from Typical Experiments

Esr signal strength, cor arbitrary units		Flow velocities, cm ³ sec ⁻¹		Reactor pressure, torr	k_{pfo} , uncor	Pseudo-first-order constant, sec ⁻¹ k_{pfo} , cor ^a	Stationary concn, mole cm ⁻³		
h_{in}	h_{out}	v_{in}	v_{out}				[SO ₂] × 10 ³	[O ₂] × 10 ³	[Ar] × 10 ³
Experiment No. 18. Pure Oxygen ($k_{pfo} = 0.16$ sec ⁻¹ (mean value))									
99.7	60.9	257	269	0.75	0.51	0.44	2.03	3.90	
105.2	46.2	253	280	0.76	1.01	0.87	4.19	3.75	
103.6	34.5	248	293	0.77	1.54	1.36	6.60	3.58	
104.5	28.6	244	304	0.79	2.00	1.76	8.80	3.45	
103.8	18.6	237	326	0.81	3.39	2.94	11.96	3.22	
104.9	12.0	230	352	0.84	5.60	4.70	15.50	2.98	
105.6	58.8	255	272	0.75	0.64	0.55	2.50	3.86	
106.6	63.4	256	270	0.75	0.55	0.47	2.19	3.88	
Experiment No. 31. 2.2% Oxygen in Argon ($k_{pfo} = 0.47$ sec ⁻¹ (mean value))									
106.1	19.0	296	349	1.50	4.44	3.34	12.04	0.149	6.63
105.0	23.0	296	337	1.50	3.46	2.61	9.53	0.154	6.87
103.0	32.8	300	321	1.49	2.11	1.57	5.18	0.162	7.20
102.2	21.8	300	340	1.49	3.63	2.74	9.28	0.153	6.80
98.2	56.2	302	305	1.47	0.76	0.52	0.54	0.171	7.59
96.3	41.0	304	315	1.47	1.35	1.01	2.77	0.165	7.33
94.5	34.8	302	321	1.47	1.71	1.25	4.46	0.162	7.21
95.2	12.1	292	357	1.53	6.59	4.87	14.70	0.146	6.48

^a That is, corrected for the extent of reaction occurring in the inlet and outlet tubes (volumes 8.5 and 10 cm³, respectively).

different, it was concluded that perfect stirring occurred with both. Downstream admission was used in all the kinetics experiments.

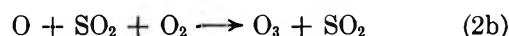
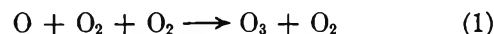
Results

The effect of SO₂ on the magnitude of k_{pfo} was determined in 17 sets of measurements covering a range of reactant concentrations and total pressures. Such a set of measurements will be called an "experiment." In each experiment a constant flow of O₂, or O₂-Ar mixture, containing a steady concentration of O atoms was passed into the reactor and readings of the esr signals and reactor pressure were taken at a number of measured flows of SO₂. The values of k_{pfo} , [SO₂], [O₂], and, if appropriate, [Ar], were determined at each point, the small dilution of the O₂ or Ar concentration by the sulfur dioxide being taken into account.¹³ Data obtained from two typical experiments are given in Table I.

Reaction in Pure Oxygen. If, in the presence of sulfur dioxide, the oxygen atoms were consumed by reaction 2a only



k_{pfo} would be related linearly to the product of the sulfur dioxide and oxygen concentrations. Figure 2 shows that this is not the case. Neither the presence of reaction 1 nor of reaction 2b



can account for the upward curvature of the plot; the former makes too small a contribution to k_{pfo} and the latter is indistinguishable kinetically from reaction 2a. Reaction 4



provides the most obvious source of a higher order dependence of k_{pfo} on [SO₂] and therefore on [SO₂][O₂], ([O₂] being relatively constant).

We shall now show that the formal kinetics can be explained by reactions 1, 2, 4, and W, the last named being the (first-order) recombination of oxygen atoms at the wall. If, in fact, these reactions alone are involved in the disappearance of oxygen atoms, it follows that

$$k_{pfo} = k_w + k_1'[O_2]^2 + k_2[O_2][SO_2] + k_4[SO_2]^2 \quad (VI)$$

where, for reasons given subsequently, k_1' is to be regarded as an apparent rather than the true rate constant for reaction 1, and $k_2 = (k_{2a} + k_{2b})$. Equation VI can be rearranged to give

$$\frac{k_{pfo} - (k_w + k_1'[O_2]^2)}{[O_2][SO_2]} = k_2 + k_4 \frac{[SO_2]}{[O_2]} \quad (VII)$$

(13) These and subsequent calculations, including the various corrections, were programmed for a Control Data 3200 digital computer.

OR

$$Y = k_2 + k_4 X$$

A plot of Y against X should therefore be linear.

The sum of the terms k_w and $k_1'[\text{O}_2]^2$ is small and is equal to the value of k_{pfo} in the absence of sulfur dioxide (${}^\circ k_{pfo}$). This is of the same order of magnitude as the intercept of the curve in Figure 2 on the ordinate but is not in general equal to it because of variation in $[\text{O}_2]$. However, k_w and $k_1'[\text{O}_2]^2$ can be separated if k_1' is known. Experiments carried out in the absence of sulfur dioxide showed ${}^\circ k_{pfo}$ to be approximately linear with $[\text{O}_2]^2$, with a slope (k_1') of about $0.02 \times 10^{15} \text{ mole}^2 \text{ cm}^{-6} \text{ sec}^{-1}$. Although k_w remained almost constant during an experiment, it varied from one experiment to another (between 0.06 and 0.97 sec^{-1}). The value for each experiment was determined by subtracting $0.02 \times 10^{15} [\text{O}_2]^2$ from the mean of values of ${}^\circ k_{pfo}$ determined at intervals during the experiment. Using this value for k_w and the above value for k_1' , Y can be plotted against X . Figure 3 shows the plot derived from the data given in Table I and Figure 2. Satisfactory agreement with the form of eq VII is obtained. Eleven other experiments each gave the same result. Hence, we identify the intercept of the regression line (calculated on the assumption that X is more accurately known than Y) on the ordinate with k_2 and the slope with k_4 . The values so obtained are given in Table II. The values of ${}^\circ[\text{O}]$ listed in column 3 refer to the atom concentration which obtained in the reactor in the absence of sulfur dioxide.

The arithmetical mean of all values of k_2 is $k_2 = (2.7 \pm 0.5) \times 10^{15} \text{ cm}^6 \text{ mole}^{-2} \text{ sec}^{-1}$ at $299 \pm 2^\circ \text{K}$. The error is the standard deviation (as also are subsequent errors quoted). Within the extreme values

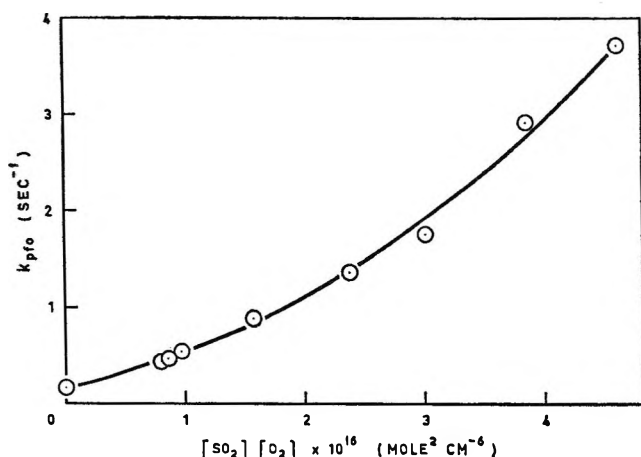


Figure 2. Typical plot of pseudo-first-order rate constant against $[\text{SO}_2][\text{O}_2]$.

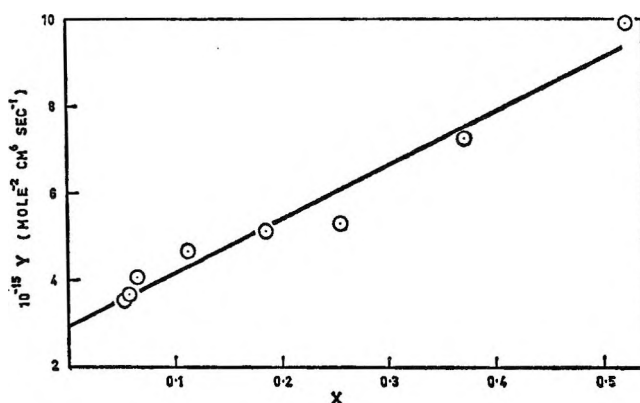


Figure 3. Typical Y - X plot (based on the same data as Figure 2). (Y and X are defined by eq VII in the text.)

Table II: Results of Experiments with SO_2 in Pure O_2 and O_2 -Ar Mixtures

Expt no.	Pressure, torr	Approx ^a ${}^\circ[\text{O}] \times 10^{10}$, mole cm^{-3}	$k_2 \times 10^{-16}$, $\text{cm}^6 \text{ mole}^{-2} \text{ sec}^{-1}$	$k_4 \times 10^{-16}$, $\text{cm}^6 \text{ mole}^{-2} \text{ sec}^{-1}$
Pure O_2				
7	1.14	2.4	2.95 ± 0.40^b	6.9 ± 1.6^b
14	1.69	7.0	2.99 ± 0.34	4.8 ± 2.1
15	1.68	2.6	3.04 ± 0.34	5.0 ± 2.8
15, 17	1.68	2.6	2.59 ± 0.20	7.8 ± 2.2
16	1.69	5.1	2.12 ± 0.13	11.4 ± 0.9
18	0.74	2.2	2.95 ± 0.25	12.3 ± 1.0
19	0.73	3.0	3.57 ± 0.22	11.3 ± 0.8
20	0.74	3.6	3.06 ± 0.36	16.9 ± 1.3
21	0.74	2.5	2.84 ± 0.21	14.3 ± 0.8
22	2.94	4.5	2.18 ± 0.15	15.1 ± 2.6
23	2.95	3.8	1.66 ± 0.11	12.5 ± 1.4
24	2.93	3.0	2.12 ± 0.10	12.2 ± 1.4
$k_3 \times 10^{-15}$				
2.2% O_2 in Air				
31	1.50	3.3	2.13 ± 0.18	9.3 ± 1.4
10.6% O_2 in Ar				
41	1.44		2.32 ± 0.17	9.1 ± 1.4
42	2.17		2.47 ± 0.14	8.7 ± 1.3
44	1.03	1.1	2.44 ± 0.13	6.7 ± 0.6
45	0.70	0.7	2.46 ± 0.11	5.8 ± 0.4

^a Average values of $[\text{O}]_{\text{out}}$ in absence of SO_2 . ^b Standard deviations.

($10^{-15}k_2 = 1.7, 3.6$) there is a tendency toward an inverse dependence of k_2 on oxygen pressure. The effect is probably genuine but has been ignored in taking the mean value. No effect of atom concentration on k_2 can be detected. The mean value of k_4 is $k_4 = (11 \pm 4) \times 10^{15} \text{ cm}^6 \text{ mole}^{-2} \text{ sec}^{-1}$ at $299 \pm 2^\circ \text{K}$.

No effect of oxygen pressure on k_4 can be discovered within the scatter of the individual values. The first four experiments (Table II) gave distinctly lower values for k_4 and somewhat lower correlation coefficients than those given by subsequent experiments. The reason for this is not known. If the corresponding values are omitted in taking the mean, k_4 becomes $13 \pm 2 \times 10^{15} \text{ cm}^6 \text{ mole}^{-2} \text{ sec}^{-1}$, but the value of k_2 is not significantly changed.

Reaction in Argon-Oxygen Mixtures. The general behavior (Tables I and II) is similar to that found with pure oxygen. The analogous relation to eq VII, ignoring the term $k_1'[\text{O}_2]^2$ which is now negligible, is

$$\frac{k_{pfo} - (k_w + k_3'[\text{O}_2][\text{Ar}] + k_2[\text{O}_2][\text{SO}_2])}{[\text{Ar}][\text{SO}_2]} = k_5 + k_4 \frac{[\text{SO}_2]}{[\text{Ar}]} \quad (\text{VIII})$$

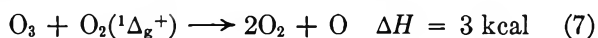
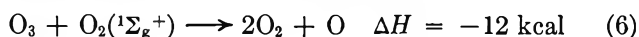
that is

$$Y' = k_5 + k_4 X'$$

k_3' , the apparent rate constant for the reaction $\text{O} + \text{O}_2 + \text{Ar} \rightarrow \text{O}_3 + \text{Ar}$, was found experimentally to be 0.07×10^{15} and $0.9 \times 10^{15} \text{ cm}^6 \text{ mole}^{-2} \text{ sec}^{-1}$ for 10 and 2% oxygen in argon, respectively.

Plots of Y' (as shown in Figure 4) were in agreement with eq VIII. The derived values of k_5 and k_4 are given in Table II. The mean value of k_5 is $(2.4 \pm 0.15) \times 10^{15} \text{ cm}^6 \text{ mole}^{-2} \text{ sec}^{-1}$. The difference from k_2 is in the direction to be expected from the relative third-body efficiencies of argon and oxygen in other reactions but may not be significant. The mean value of k_4 is $(8 \pm 1.5) \times 10^{15} \text{ cm}^6 \text{ mole}^{-2} \text{ sec}^{-1}$, in fair agreement with the value obtained with pure oxygen.

k_1' and k_3' . Some comment should be made on the significance of these constants. Oxygen atoms consumed by reactions 1 and 3 are known to be partly regenerated from ozone by reactions of excited molecular species carried out of the discharge^{14,15}



Values of $^{\circ}k_{pfo}$ obtained with discharged oxygen are therefore lower than those to be expected purely on the basis of reaction 1 or 3. However, it is an interesting fact that $^{\circ}k_{pfo}$ remains approximately proportional to $[\text{O}_2]^2$ or $[\text{O}_2][\text{Ar}]$ over the relevant pressure range; k_1' and k_3' are the respective proportionality constants and for present purposes are to be regarded simply as empirical correction factors. In fact, the effects of the terms $k_1'[\text{O}_2]^2$ and $k_3'[\text{O}_2][\text{Ar}]$ on the values obtained for k_2 and k_4 are small.

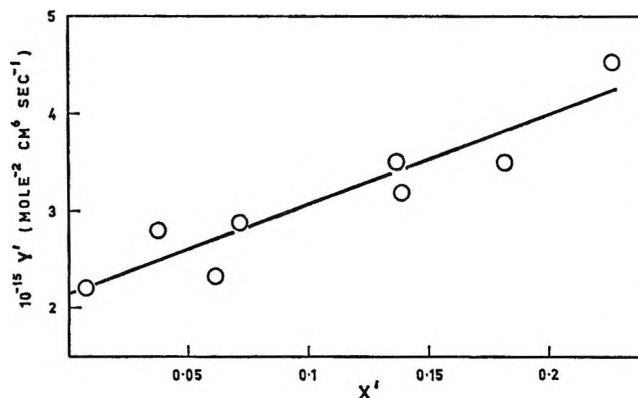


Figure 4. Typical Y' - X' plot. (Y' and X' are defined by eq VIII in the text.)

Discussion

The value of k_2 , $2.7 \times 10^{15} \text{ cm}^6 \text{ mole}^{-2} \text{ sec}^{-1}$, is only about one-tenth as large as the value obtained by Kaufman.⁶ Kaufman mixed SO_2 containing 4% NO with O atoms from a microwave discharge and followed the disappearance of the atoms along a flow tube by measuring the decay of the air afterglow. In the absence of details of the kinetic analysis carried out by this investigator, it is not easy to attribute the discrepancy to any particular difference in the experimental techniques. The condition of the surface, which was troublesome to stabilize in both Kaufman's and the present work, is a possible source of error. In the present work, the surface recombination was measured and allowed for in each experiment. It may be, however, that the discrepancy arises in some indirect way from the difference in flow techniques, but whether this is the case and, if so, how it comes about, need further investigation. The present mean value of k_4 ($10 \pm 4 \times 10^{15} \text{ cm}^6 \text{ mole}^{-2} \text{ sec}^{-1}$) is close to the value $k = 14 \times 10^{15} \text{ cm}^6 \text{ mole}^{-2} \text{ sec}^{-1}$ for the reaction $\text{O} + \text{SO}_2 + \text{M} \rightarrow \text{SO}_3 + \text{M}$ (where $\text{M} = \text{SO}_2$ or NO_2) obtained by Jaffe and Klein¹⁶ from photolytic experiments. The agreement is remarkable considering the great difference between the experimental techniques.

To extract the value of k_{2a} from k_2 , the value of k_{2b} is required. This is not known directly. However, since $k_2 \approx k_5$, and k_5 includes no term corresponding to k_{2b} , it is concluded that $k_{2b} \ll k_{2a}$. Were it not for reactions 6 and 7, k_{2b} could be estimated from the value¹⁴ of k_1 and the relative third-body efficiencies of O_2 , O_3 , and CO_2 (1:2.3:2.4) as determined from the

(14) F. Kaufman and J. R. Kelso, *Discussions Faraday Soc.*, **37**, 26 (1964).

(15) F. S. Larkin and B. A. Thrush, *ibid.*, **37**, 112 (1964).

(16) S. Jaffe and F. S. Klein, *Trans. Faraday Soc.*, **62**, 2150 (1966).

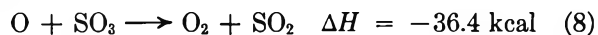
Table III: Data for Comparison of Reaction 2a with Reactions 1, 11, and 12

No.	Reaction	Termolecular rate constant, $10^{-14}k_T$, $\text{cm}^6 \text{mole}^{-2} \text{sec}^{-1}$	$-\Delta H$, kcal mole^{-1}	Q_{2a}/Q_i			Ref to column 3
				For $s_{2a} = 4$; $s_i = 2$	For $s_{2a} = 4$; $s_i = 3$	For $s_{2a} = 3$; $s_i = 2$	
1	$\text{O}_2 + \text{O} + \text{O}_2$	0.27	24	5×10^{-3}	4×10^{-3}	1×10^{-1}	14
11	$\text{NO} + \text{O} + \text{O}_2$	24	72	2×10^{-4}	5×10^{-3}	3×10^{-3}	20
12	$\text{SO} + \text{O} + \text{O}_2$	$\sim 500^a$	130	1×10^{-5}	7×10^{-4}	3×10^{-4}	21
2a	$\text{SO}_2 + \text{O} + \text{O}_2$	2.7	82	This work

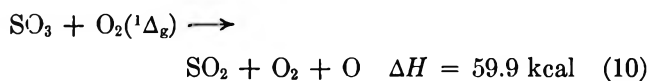
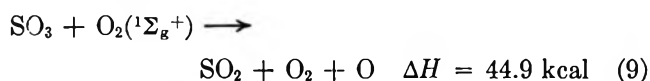
^a Assumes relative third-body efficiencies of O_2 and Ar to be 1.7:1, i.e., similar to those for reaction 1.²²

kinetics of decomposition of ozone.¹⁷ However, reaction 2b is undoubtedly partly counteracted by reactions 6 and 7 and the effective value of k_{2b} is probably best obtained from k_1' . Hence, assuming the third-body efficiency of SO_2 to be similar to those of O_3 and CO_2 , $k_{2b} \approx 2.4k_1' = 0.05 \times 10^{15}$. Thus $k_{2a} \approx k_2 = 2.7 \times 10^{15} \text{ cm}^6 \text{ mole}^{-2} \text{ sec}^{-1}$.

Two possible complications have been ignored in the kinetic analysis. (a) If reaction 8¹⁸ were to occur in the gaseous phase



with $k_8 > \sim 10^9 \text{ cm}^3 \text{ mole}^{-1} \text{ sec}^{-1}$, the above values of k_{2a} , k_4 , and k_5 would be too high; a value of $k_8 > \sim 5 \times 10^{10}$ would require them to be divided by 2. (b) Since reactions of SO_3 analogous to (6) and (7) are strongly endothermic



they cannot influence the kinetics. If, however, the SO_3 is formed in an excited electronic state, this may be no longer the case.

Comparison of Reaction 2a with Similar Reactions: Possible Formation of Triplet SO_3 . The addition of a ground-state O atom to SO_2 to form ground-state (singlet) SO_3 violates the spin conservation rule and may therefore be expected to be improbable. Webster and Walsh¹⁹ have inferred that the SO_3 is formed in an excited (spin-allowed) triplet state from the fact that the rate constant for the removal of O atoms by SO_2 (derived from inhibition of the $\text{H}_2\text{-O}_2$ reaction by SO_2) appears to be of similar magnitude to the rate constants of certain other termolecular atomic reactions which are spin-allowed. It seems, however, that more detailed comparisons are required to justify this conclusion. Likewise, the similar third-body efficiencies of Ar and O_2 do not necessarily rule out a spin-forbidden

step in the over-all termolecular process. Rate constants of the spin-allowed reactions 1, 11, and 12 are given together with k_{2a} in Table III.²⁰⁻²²



The rates of addition of O to the diatomic species increase with increasing exothermicity of the reaction,²³ a result in qualitative accord with classical RRRK theory²⁴ which states that the rate constant should be approximately proportional to $Q(\Delta H/sRT)^{s-1}$. Q is a "steric" factor related to the inherent probability of reaction and s the number of effective oscillators in the product molecule. The rate should also increase with increasing s , that is, with increasing molecular complexity. This, however, is not verified when reaction 11 is compared with reaction 2a: for the latter both molecular complexity and $-\Delta H$ are the greater, but the rate constant is the smaller. The discrepancy is revealed more clearly by the values of Q_{2a}/Q_1 , Q_{2a}/Q_{11} , and Q_{2a}/Q_{12} (shown as Q_{2a}/Q_i in Table III). These were calculated from the experimental rate constants and values of ΔH using the above formula and assuming that $E_{2a} = 0$. The alternative assignments (s_{2a} , s_i) are based empirically on known behavior of analogous molecules²⁵⁻²⁷

(17) S. W. Benson and A. E. Axworthy, *J. Chem. Phys.*, **26**, 1718 (1957).

(18) C. P. Fenimore and G. W. Jones, *J. Phys. Chem.*, **69**, 3593 (1965).

(19) P. Webster and A. D. Walsh, ref 7, p 463.

(20) F. Kaufman, *Progr. Reaction Kinetics*, **1**, 26 (1961).

(21) C. J. Halstead and B. A. Thrush, quoted in ref 23.

(22) E. Castellano and H. J. Schumacher, *Z. Physik. Chem. (Frankfurt)*, **34**, 198 (1962).

(23) M. A. A. Clyne, D. J. McKenny, and B. A. Thrush, *Trans. Faraday Soc.*, **61**, 2701 (1965).

(24) S. W. Benson, "The Foundations of Chemical Kinetics," McGraw-Hill Book Co., Inc., New York, N. Y., 1960.

(25) H. J. Schumacher, "Chemische Gasreaktionen," Steinkopff, Dresden, 1938.

(26) E. K. Gill and K. J. Laidler, *Proc. Roy. Soc. (London)*, **A250**, 121 (1959).

and the value of k_{-2a} (calculated from k_{2a} and the equilibrium constant²⁸) which leads to $s_{2a} = 3$ to 4. The values of Q_{2a}/Q_i are all less than 1, most of them considerably so. They cannot be taken literally because of the limitations of the theory, but considered together they suggest that if reaction 2a proceeds directly to ground-state SO_3 (i.e., $\Delta H = -82$ kcal), it is intrinsically slower than reactions 1, 11, and 12. Nevertheless, it is doubtful whether the effect can be imputed to spin-prohibition. If the (bimolecular) formation of the excited complex SO_3^* is spin-forbidden, the same is true of the reverse dissociation. This means that spin prohibition will have little effect on the over-all rate unless it reduces the dissociation rate below that of the collisional deactivation. However, if the transmission coefficient arising from the spin reversal were such (10^{-3} for $s_{2a} = 4$, 10^{-4} for $s_{2a} = 3$) as to cause Q_{2a} to be less than about $1/20$ of its "normal" value (Q_i), the kinetics would be indistinguishable from second order in the pressure range used in this work.²⁹ On the other hand, the observed third-order kinetics can be explained if the onus for the apparently low rate is put upon ΔH_{2a} rather than Q_{2a} . The calculated values of Q_{2a} can be increased by reducing $-\Delta H_{2a}$, that is, by assuming that SO_3 is formed in an excited electronic state, presumably a triplet.

Thus we return to the view of Webster and Walsh¹⁹ but base it on different grounds. Obviously, these are such that independent confirmation is desirable. If triplet molecules are indeed formed, some reinterpretation of the kinetics may be necessary: the reaction could be reversible or the kinetics influenced by excited species from the discharge, or both. However, pending further work, the values of the rate constants k_{2a} , k_4 , and k_5 given above can be provisionally accepted as providing the simplest quantitative interpretation of the experimental results.

Acknowledgments. The authors are indebted to Mr. H. R. Brown (Chief of the Division of Coal Research) for his constant support and encouragement, to Mr. D. J. Williams for valuable discussions, to Mr. J. McLay for technical services, to Mr. F. G. Boland for constructing the esr cavity, and to Mr. B. R. Carruthers for constructing the glass work.

(27) P. G. Ashmore and M. G. Burnett, *Trans. Faraday Soc.*, **58**, 1801 (1962).

(28) Calculated from data in National Bureau of Standards Circular No. 500, U. S. Government Printing Office, Washington, D. C.

(29) Similar reasoning has been used in reverse to explain the observed second-order kinetics of the spin-forbidden reaction $\text{O} + \text{CO} \rightarrow \text{CO}_2$. See B. H. Mahan and R. B. Solo, *J. Chem. Phys.*, **37**, 2669 (1962).

1,1-Dimethylhydrazine–Water Solid–Liquid System¹

by J. A. McMillan and S. C. Los

Solid State Science Division, Argonne National Laboratory, Argonne, Illinois (Received December 1, 1966)

The 1,1-dimethylhydrazine–water solid–liquid system has been studied by thermal analysis covering the equilibrium phase diagram and the irreversible transformations that take place during warm-up of the supercooled liquid. The monohydrate, melting at 242.5°K, has been identified. It forms a eutectic with 1,1-dimethylhydrazine (*u*-DMH) of 0.125 water molar fraction, melting at 208.5°K. A region around 20 mole % *u*-DMH could not be resolved owing to very slow rates of crystallization. Introduction of the temperature range of spontaneous inverse crystallization of supercooled mixtures shows that crystallization in this region cannot occur within the time scale of the experiments. Measurements of the activation barriers for this process indicate that crystallization occurs, when it does, by nucleation, since the values of entropy of the activated complex are very large and positive. A comparative study of the glass-transformation range and the viscosity of these mixtures shows a maximum in their free energies of activation at 20 mole % *u*-DMH. These results, together with a eutectic-type plateau detected in the water-rich part of the equilibrium diagram, occurring at 238°K, suggest the existence of a reaction involving a higher order hydrate, probably *u*-DMH·4H₂O.

Introduction

The 1,1-dimethylhydrazine–water system has been studied during the course of a systematic investigation of irreversible transformations that occur during warm-up of supercooled, hydrogen-bonded compounds^{2,3} and their binary mixtures.^{4,5} The basic idea behind the approach used is that studies of the irreversible transformations and the phase-equilibria diagram⁴ should be complementary and illuminate each other. Viscosity measurements play an analogous role and have been performed to gain additional information.

Experimental Methods

Two techniques have been used to deal with the problem, namely differential thermal analysis (DTA) and viscometry. They are briefly described in the following sections.

Differential Thermal Analysis. DTA was used to determine the transformation temperatures and adapted to measure process durations. The samples were prepared by weighing distilled water and CP grade *u*-DMH distilled over calcium hydride at reduced pressure.⁶ Approximately 7.5 ml of the sample was sealed in a test tube provided with an inner, thin-

walled capillary that hosted a copper–constantan thermocouple. This capillary was filled with benzene to ensure good thermal contact. A duplicate tube contained an equal amount of benzene as reference substance. Both tubes were placed in a copper block 20 cm in height and 5 cm in diameter, having two cylindrical, symmetrical cavities to hold them. The entire unit was cooled down to 77°K by immersion in liquid nitrogen and warmed up at rates determined by the thickness of insulating material around the copper block, always below 1 deg/min. It was considered unnecessary to introduce a programming device to achieve constant rates, for the transformations studied start and proceed to completion within narrow temperature ranges, the linear approximation to the Newtonian heating curve being therefore appropriate enough. The thermocouple array permitted the recording of the

(1) Based on work performed under the auspices of the U. S. Atomic Energy Commission.

(2) J. A. McMillan, *J. Chem. Phys.*, **42**, 3497 (1965).

(3) J. A. McMillan and S. C. Los, *Nature*, **206**, 806 (1965).

(4) J. A. McMillan and S. C. Los, *J. Chem. Phys.*, **42**, 829 (1965).

(5) J. A. McMillan, *ibid.*, **46**, 622 (1967).

(6) J. B. Class, J. G. Aston, and T. S. Oakwood, *J. Am. Chem. Soc.*, **75**, 2937 (1953).

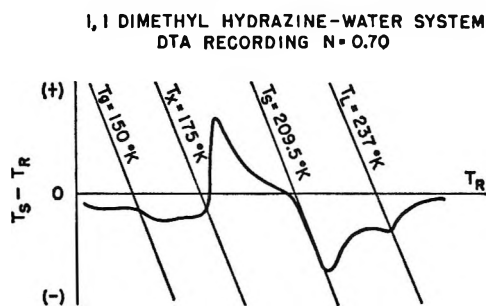


Figure 1. Typical warm-up DTA recording showing the glass transformation at T_g , spontaneous crystallization at T_x , solidus point at T_s , and liquidus point at T_L .

temperature difference between sample and reference, $T_s - T_r$, as a function of the reference temperature, T_r , or of the sample temperature, T_s . An X-Y recorder having sensitivities of 25 and 5 cm/mv in the Y ($T_s - T_r$) and X (T_r or T_s) axes, respectively, was used. Figure 1 shows a typical warm-up curve including glass transformation, crystallization, solidus, and liquidus temperatures.

Viscometry. An eight-speed Brookfield Synchronic viscometer, Model LV, was used with a Brookfield adapter to cover down to the 0–10-cp range. The container was immersed in an ice thermostat for the determinations at 0°. In the other cases, it was tightly placed inside a copper block. The latter was cooled by cold nitrogen circulating through a copper-tubing coil. The block was in turn placed inside a styrofoam block to minimize thermal leaks. A copper-constantan thermocouple located near the bottom, in thermal contact with the container, permitted measurement of the temperature of the sample. The temperature was set by a stream of cold nitrogen obtained by boiling liquid nitrogen at a controlled rate. The whole unit was installed in a drybox filled with nitrogen gas. The viscometer was calibrated at low temperatures with aqueous solutions of glycerol whose room-temperature viscosities were calibrated against appropriate Brookfield standards. The viscosities of these solutions at lower temperatures were then taken from tables.⁷ The calibration at low temperatures was necessary since the torsion suspension of the spindle changed its elastic characteristics upon cooling.

Experimental Results

Thirty-five samples of composition ranging from pure water to pure *u*-DMH were observed for thermal behavior. They were cooled by immersion in liquid nitrogen and then warmed up at different rates, always below 1 deg/min. Some of them were also used for viscosity measurements.

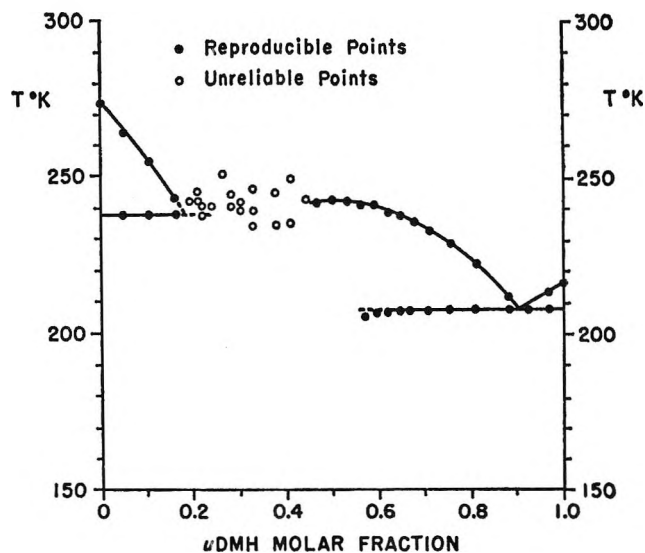


Figure 2. Phase diagram of the *u*-DMH-H₂O system.

Phase-Equilibria Diagram. Figure 2 illustrates the phase diagram constructed with data displayed in Table I. The 0.15–0.40 molar fraction range could not be resolved. Solutions of these compositions give metastable, supercooled phases in which crystallization does not occur for all practical purposes. To a much lesser extent, such a situation takes place in the hydrazine-water system,⁸ but in this case cycling of the samples about the melting range finally induces crystallization. Cycling of the *u*-DMH-water solutions failed to induce crystallization in this region; nor was it possible to observe any consistent crystallization after storing the samples for several days at a temperature just below the interpolated melting range. Whenever samples in this composition range were analyzed for thermal behavior, it was found that very small fractions of the samples crystallized during warm-up, melting at irreproducible temperatures (unreliable points in Figure 2). This behavior is characteristic of composition inhomogeneities, most likely favored by the large viscosities observed in this region. For *u*-DMH molar fraction lower than $N = 0.15$, however, there appears a solidus transformation at 238°K that suggests the existence of a eutectic or peritectic with a higher order hydrate. Interpretation of the rest of the phase diagram is straightforward. Formation of the monohydrate is unambiguous, with a melting point of 242.5°K. It forms in turn a eutectic with *u*-DMH, at an over-all water molar fraction of 0.125, melting at 208.5°K. The slight departure of the solidus

(7) C. S. Miner and N. N. Dalton, "Glycerol," Reinhold Publishing Corp., New York, N. Y., 1953, p 283.

(8) J. A. McMillan and S. C. Los, *J. Chem. Phys.*, **42**, 160 (1965).

points toward $N = 0.50$ from the eutectic straight line may be attributed to unidentified impurities in the u -DMH. A preliminary chromatographic analysis of the u -DMH used in these experiments showed, in fact, a faint, unidentified peak. The very narrow solid-solution ranges of the pure components are undetectable and appear in the phase diagram as vertical lines.

Table I: Solidus and Liquidus Points of the u -DMH-H₂O System

N	T_L , °K	T_S , °K
0.00	273	273
0.05	264	238
0.10	255	238
0.15	243	238
...
0.46	241.5	...
0.49	242.5	...
0.53	242	...
0.55	241	207.0
0.59	241	207.5
0.62	238	207.5
0.66	237	208.0
0.68	235	208.0
0.71	233	208.0
0.75	228	208.5
0.81	221	208.5
0.88	210	208.5
0.92	...	208.5
0.96	212	208.5
1.00	217	217

Irreversible Transformations. If a liquid may be supercooled to sufficiently low temperatures it undergoes the so-called glass transformation, below which some degrees of freedom are frozen in. Such a transformation may be termed irreversible in that one of the ends, the vitreous phase, generally is not in internal thermodynamic equilibrium. Such a transformation, being characterized by an over-all activation barrier, may be repeatedly effected without a significant change in its main features, provided the conditions of the experiment be reproduced. It is then possible to evaluate the free energy, enthalpy, and entropy of activation.^{2,9} In addition, a supercooled liquid will eventually crystallize during warm-up if the rate of warm-up is appropriately low. The study of the two processes in the case of binary mixtures shows in general a correlation with the solid-liquid equilibria that provides some information on the microstructure of the supercooled phases.^{4,5} Figure 3 illustrates the results of this approach in the case of the u -DMH-water system, results that are separately discussed in the following sections.

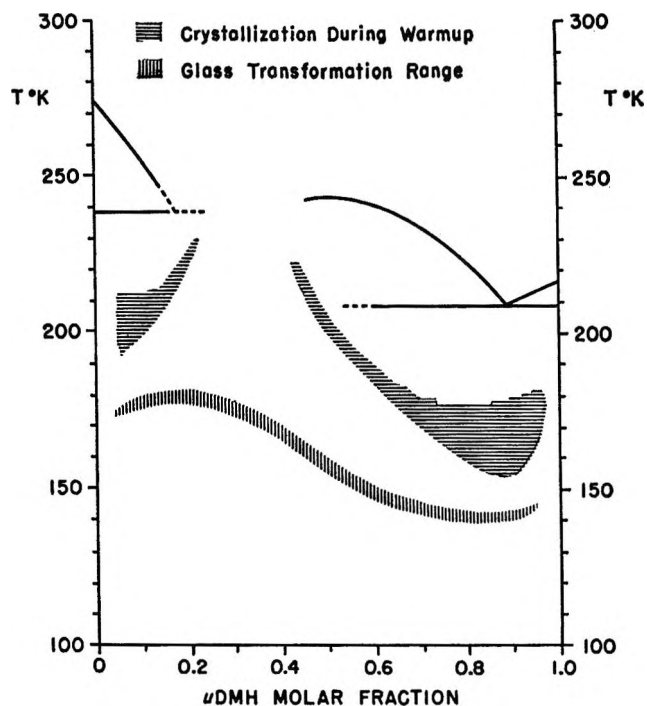


Figure 3. Diagram of irreversible phase transformations of the u -DMH-H₂O system.

Glass Transformation. The range of glass transformation is defined by the time scale of the experiment. In conventional DTA, the change in specific heat characterizing the glass transformation becomes visible when the glass relaxation occurs with a relaxation time of several minutes.¹⁰ The temperature at which it occurs is then proportional to the activation free energy, since the relaxation time is given by

$$\tau = (h/kT) \exp(\Delta G_g^\ddagger/RT) \quad (1)$$

where ΔG_g^\ddagger is the activation free energy and the rest of the symbols have the conventional meanings. The range within which the glass transformation takes place in the system u -DMH-water varies smoothly with composition, exhibiting a maximum value near $N = 0.20$ and a minimum value near the composition of the eutectic, as may be seen in Figure 4. The smoothness of the curve would seem to indicate that the composition of the vitreous phase follows the over-all composition of the sample, in contrast to the hydrazine-water system. In the latter, the vitreous phase has the composition of each of the eutectic, crystals of the excess component being present in different amounts.^{4,5} A homogeneous vitreous phase

(9) B. Wunderlich, D. M. Bodily, and M. H. Kaplan, *J. Appl. Phys.*, **35**, 95 (1964).

(10) W. Kauzmann, *Chem. Rev.*, **43**, 219 (1948).

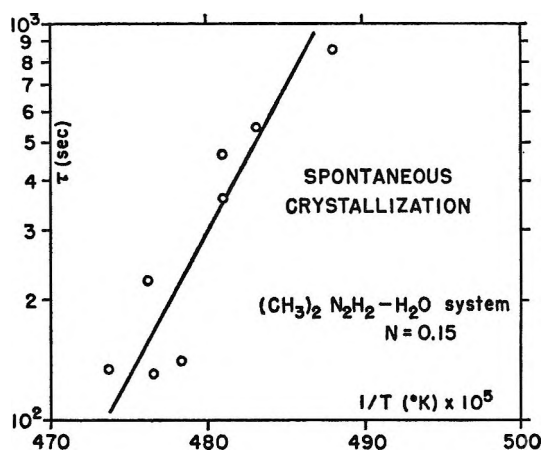


Figure 4. Activation curve of irreversible crystallization at $N = 0.20$.

in the *u*-DMH-water system is consistent with the assumption that nucleation is the rate-controlling factor, as is seen in the next section. The well-defined maximum between $N = 0.15$ and 0.25 suggests the existence of strong association in the liquid, perhaps with formation of a higher order hydrate, independently supported by the maximum in the viscosity and the results on the phase diagram.

Spontaneous Crystallization. Figure 3 also shows a shaded area where crystallization during warm-up occurs. The approach developed in a previous publication⁵ fails to yield accurate estimates of the activation enthalpy of the process owing to its remarkably high value. In fact, the basic feature of crystallization over all the composition range is its high rate. Experiments at different warm-up rates lead to results that exhibit a rather large dispersion about the best fit straight line, as illustrated in Figure 5. Nevertheless, it is possible to infer that the process occurs with a large, positive entropy of activation in view of the large value of the activation enthalpy and the normal value of the activation free energy, at least in the regions where crystallization may be observed. Typical values of the activation barrier are, in the case of $N = 0.15$, for example

$$\Delta G_x^\ddagger = 12.6 \text{ kcal/mole}$$

$$\Delta H_x^\ddagger = 29.6 \text{ kcal/mole}$$

$$\Delta S_x^\ddagger = 81 \text{ eu}$$

Such large values of ΔS_x^\ddagger point toward a cooperative effect of a large number of molecules, the breaking of whose intermolecular bonds necessitates commensurately large activation enthalpies. These characteristics indicate that crystallization is nucleation con-

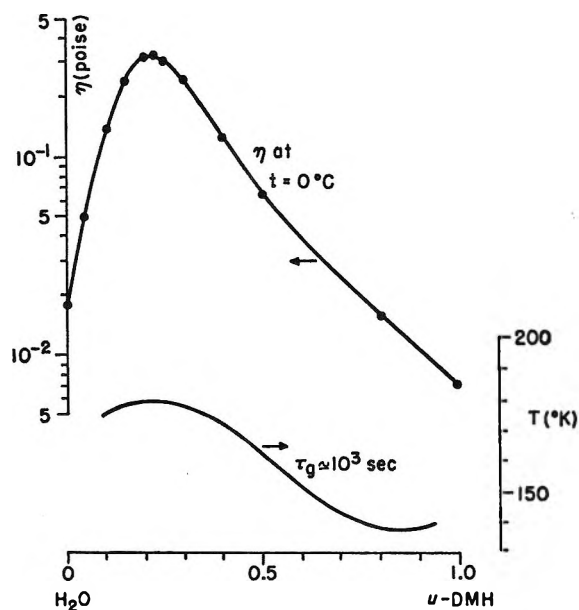


Figure 5. Viscosity and glass-transition curve of the *u*-DMH- H_2O system.

trolled over the entire composition range, contrary to what had been observed in the hydrazine-water system.^{4,5} The values of ΔG_x^\ddagger characterizing the process of crystallization in this system should then include the actual free energy of activation for nucleation and the corresponding value for growth of the nucleus. This state of affairs also applies to the enthalpy and entropy of activation. The problem is to decide whether nucleation is homogeneous or heterogeneous. Usually, unless special falling-drop experiments were performed, one should expect nucleation to be heterogeneous. Heterogeneous nucleation would explain, in addition, the rather large dispersion of results. The possibility of doing any further elaborations following Turnbull's ideas¹¹ seems therefore too speculative, with the exception that the very large value of the activation entropy seems strongly to support a process of nucleation of either kind.

These conclusions are in essential agreement with those drawn from the study of the glass transformation, as was anticipated in the preceding section.

Perhaps the most interesting feature of the crystallization pattern is the rise of the activation free energy toward the region of permanent supercooling. If one extrapolates the temperatures of crystallization into the region where crystallization does not occur, one finds that they intercept the interpolated phase-equilibrium curves. Under such circumstances, it is

(11) D. Turnbull, *Trans. AIME*, 221, 422 (1961).

clear that crystallization must be an extremely slow process, to the extent of being unobservable. Existence of enhanced association could account for this behavior.

Viscosity measurements. The viscosity of samples of various compositions was measured at several temperatures with the device described above. In all cases a maximum was observed near 20 mole % *u*-DMH. Figure 5 illustrates the results obtained at 0°, displayed in Table II. It is seen that no indication of formation of the monohydrate may be obtained from the plot. However, the existence of the monohydrate is hardly questionable in view of the phase diagram. A possible explanation is that its liquidus curve intercepts the liquidus curve of a higher order hydrate close to the monohydrate composition, resembling the situation commonly found in alkyl alcohol-hydrazine systems.¹² At the same time, the unusually large value of the viscosity in this region makes crystallization a very slow process, as confirmed by the study of the temperature range of inverse crystallization, so that the higher order hydrate cannot be crystallized in experiments having the conventional time scale. It is interesting to compare the viscosity values with the temperatures at which the glass transformation pro-

Table II: Viscosity at 0° of the *u*-DMH-H₂O System

<i>N</i>	η , cp	<i>N</i>	η , cp
0.000	1.74	0.300	24.9
0.050	4.93	0.400	12.6
0.100	13.8	0.500	6.51
0.150	23.9	0.550	4.80
0.200	34.0	0.600	1.58
0.225	34.1	0.800	1.05
0.250	31.0	1.000	0.70

ceeds with a relaxation time of the order of 10³ sec. Since the glass relaxation time is related to the activation barrier by eq 1, a plot of the temperatures at which τ has the same value for different compositions is clearly proportional to $\Delta G_{\ddagger}^{\ddagger}$, if one neglects the much smaller variation of the (h/kT) term. On the other hand, the values of $\log \eta$ are in turn proportional to the free energy of activation for flow, so that comparison between these two quantities is physically meaningful. Figure 5 shows in this respect that the glass-transformation free energy of activation also exhibits a maximum in the same region, suggesting that the association in the liquid is maximum at this composition, close to the tetrahydrate. Further handling of the viscosity data displayed in Table III permits the

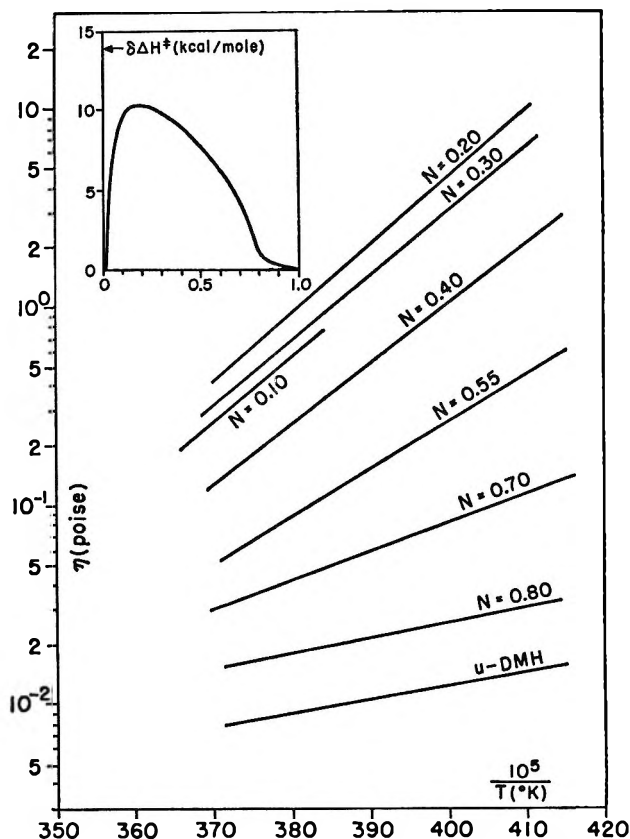


Figure 6. Activation curves of flow of the *u*-DMH-H₂O system. The excess enthalpy of activation for flow as a function of the molar fraction is shown in the upper-left corner.

evaluation of the mean enthalpies of activation for flow at -20°, as proportional to the slopes of the best fit straight lines shown in Figure 6. If one defines an ideal activation enthalpy as

$$\Delta H_i^{\ddagger} = N\Delta H_d^{\ddagger} + (1 - N)\Delta H_w^{\ddagger}$$

where ΔH_d^{\ddagger} and ΔH_w^{\ddagger} are the activation enthalpies of *u*-DMH and water, respectively, and *N* is the *u*-DMH molar fraction, one may introduce the excess enthalpy of activation $\delta\Delta H_{\eta}^{\ddagger}$ as

$$\delta\Delta H_{\eta}^{\ddagger} = \Delta H_{\text{obsd}}^{\ddagger} - \Delta H_i^{\ddagger}$$

where $\Delta H_{\text{obsd}}^{\ddagger}$ is the observed value. Table IV displays the experimental results. The plot $\delta\Delta H_{\eta}^{\ddagger}$ vs. *N* is shown in the upper-left corner of Figure 6. The value of ΔH_w^{\ddagger} in the interval around -20° has been extrapolated from available data at higher temperatures.¹³ Again, a well-defined maximum is found for

(12) N. N. Ogimachi, J. N. Corcoran, and H. W. Kruse, *J. Chem. Eng. Data*, **6**, 238 (1961).

(13) S. Glasstone, K. J. Laidler, and H. Eyring, "The Theory of Rate Processes," McGraw-Hill Book Co., Inc., New York, N. Y., 1941, p 505.

Table III: Viscosity of the *u*-DMH-H₂O System at Several Compositions and Temperatures^a

<i>t</i> , °C	<i>u</i> -DMH molar fraction							
	0.10	0.20	0.30	0.40	0.55	0.70	0.80	1.00
-30		11.1 ^b	7.20 ^b	2.52 ^b	0.430 ^b	0.183	0.0333	0.0156
-25		6.00 ^b	3.81 ^b	1.42 ^b	0.298	0.087	0.0285	0.0134
-20		3.29	1.99	0.70	0.199	0.079	0.0243	0.0118
-15		1.81	1.21	0.440	0.131	0.0537	0.0212	0.0101
-10	0.69	0.98	0.73	0.265	0.092	0.0441	0.0183	0.0088
-5	0.357	0.544	0.423	0.178	0.065	0.0331	0.0164	0.0078
0	0.239	0.327	0.249	0.126	0.048	0.0261	0.0158	0.0070
10	0.049	0.153	0.114	0.061	0.032	0.018	0.0112	0.0058

^a The values of the viscosity are in poise. ^b Supercooled liquid.

$N \cong 0.20$. A remarkable feature of the plot is that $\delta\Delta H_{\eta}^{\ddagger}$ is practically zero between $N = 0.80$ and pure *u*-DMH, where the eutectic between *u*-DMH and its monohydrate appears. Since, despite the constancy of $\Delta H_{\text{obsd}}^{\ddagger}$, the free energy increases with decreasing concentration of *u*-DMH, one must conclude that the entropy of the activated complex of eutectic composition is lower than that of pure *u*-DMH. A possible explanation is that the long-range order of the liquid of eutectic composition resembles that of the corresponding solid phase, thus reducing the configurational entropy. Further work is under progress to clarify this point, since analogous results have been recently observed by the authors in the hydrazine-water system.

Conclusions

From the consideration of the experiments described in this paper the following are concluded.

1. There is formation of the *u*-DMH·H₂O hydrate melting at 242.5°K.
2. The monohydrate and pure *u*-DMH form a eutectic of 12.5 mole % water, melting at 208.5°K.
3. The solutions are easily supercooled, leading to vitreous phases of the over-all composition of the sample, with the exception of the regions with small concentration of each pure component.
4. The supercooled samples crystallize by nuclea-

Table IV: Activation Enthalpy for Flow of the *u*-DMH-H₂O System at -20°^a

$\Delta H_{\text{obsd}}^{\ddagger}$	<i>N</i>								
	0.00	0.10	0.20	0.30	0.40	0.55	0.70	0.80	1.00
$\Delta H_{\text{obsd}}^{\ddagger}$	6.0 ^b	15.8	15.8	14.8	13.9	11.8	6.4	3.4	3.4

^a The enthalpy values are given in kilocalories per mole.

^b Extrapolated from data from ref 13, p 505.

tion during warm-up, if at all, indicating the absence of crystalline nuclei.

5. There is a strong association in the region of 20 mole % *u*-DMH reflected in a well-defined maximum of the free energy and enthalpy of activation for flow and for glass relaxation and an impossibility of inducing crystallization within the time scale of conventional experiments.

6. There is a eutectic or peritectic reaction involving a higher order hydrate, melting at 238°K, observed between $N = 0+$ and $N \cong 0.15$, most likely extending into the region of permanent supercooling (noncrystallizable region).

The problem that remains to be solved is the phase-equilibria diagram between 15 and 45 mole % *u*-DMH, a region in which crystallization does not proceed under ordinary conditions.

An Examination of Some Methods for Obtaining Approximate Solutions to the Expanding-Sphere Boundary Value Problem in Direct Current Polarography¹

by Joseph R. Delmastro^{2a} and Donald E. Smith^{2b}

Department of Chemistry, Northwestern University, Evanston, Illinois 60201 (Received December 5, 1966)

The present work considers whether two approximate theoretical methods, representing extensions of the Lingane–Loveridge approach, can satisfy the need for reasonably accurate assessment of the combined effects of drop growth and curvature in dc polarography while avoiding the disadvantage of extreme complexity often associated with the rigorous approach. The approximate methods are subject to detailed evaluation by comparing polarographic waves predicted by these methods with those given by rigorous solutions to the expanding-sphere problem. Mechanistic schemes considered are the reversible case, the quasi-reversible case, and systems with catalytic and preceding coupled chemical reactions. Both approximate methods are found to have considerable merit. Equations of competitive accuracy and greater simplicity relative to rigorously derived expressions are obtained. Of particular interest is a relatively simple expression for the quasi-reversible dc polarographic wave which reproduces the predictions of the highly cumbersome rigorous theory to within 1%. Evidence is obtained indicating that the assumption of mathematical separability of drop-growth and curvature effects represents an approximation of general applicability and reasonable accuracy.

Introduction

Since Ilkovič first derived the well-known equation for the diffusion-controlled limiting current in dc polarography on the basis of the expanding-plane electrode model,³ a number of workers have undertaken modification of the Ilkovič equation to take into account the curvature of the mercury drop.^{4–14} One of the first attempts to account theoretically for both the curvature and expansion of the electrode surface was made by Lingane and Loveridge.⁴ They assumed that since the Ilkovič theory showed that the expansion of the electrode surface into the solution can be accounted for by multiplying the equation for diffusion to a stationary plane electrode by $(7/3)^{1/2}$, an equation accounting for curvature and expansion of the electrode surface should be obtained by an analogous operation on the diffusion-current expression for the stationary-sphere electrode. Their intuitive arguments led to the equation for the polarographic limiting current (see Appendix for notation definitions)

$$i_{LL} = nFAC_0 * D_0 \left(\sqrt{\frac{7}{3\pi D_0 t}} + \frac{1}{r_0} \right) \quad (1)$$

Upon rearrangement and substitution of the appropriate expression for r_0 , they obtained

$$i_{LL} = \sqrt{\frac{7}{3\pi t}} nFAC_0 * D_0^{1/2} (1 + 44.6 D_0^{1/2} t^{1/6} m^{-1/3}) \quad (2)$$

While they clearly outlined the mathematical

(1) This work was supported by National Science Foundation Grants GP-2670 and GP-5778.

(2) (a) Present work taken in part from Ph.D. Thesis of J. R. Delmastro, Northwestern University, 1967. (b) To whom reprint inquiries should be addressed.

(3) D. Ilkovič, *Collection Czech. Chem. Commun.*, **6**, 498 (1934).

(4) J. J. Lingane and B. A. Loveridge, *J. Am. Chem. Soc.*, **72**, 438 (1950).

(5) H. Strehlow and M. von Stackelberg, *Z. Elektrochem.*, **54**, 51 (1950).

(6) T. Kambara, M. Suzuki, and I. Tachi, *Bull. Chem. Soc. Japan*, **23**, 219 (1950).

(7) T. Kambara and I. Tachi, *ibid.*, **23**, 225 (1950).

steps leading to eq 1 and 2, Lingane and Loveridge were not explicit in stating the basic assumption underlying their derivation. Normally, one would expect this to be of little consequence as the assumption should be apparent from the method of derivation. However, careful study indicates that an ambiguity exists in the case of the Lingane-Loveridge method in that two alternative assumptions appear consistent with their result. One may interpret the Lingane-Loveridge derivation as equivalent to assuming that the contribution of spherical diffusion can be simply represented as an alteration of the effective diffusion coefficient which is calculable with the aid of stationary-sphere theory. On this basis Laitinen, Kivalo, and Oldham¹⁵ presented an equation for the diffusion-controlled (reversible) dc polarographic wave which allegedly accounted for drop growth and curvature. Their equation was derived from the expression based on the expanding plane diffusion model by multiplying $D_0^{1/2}$ and $D_R^{1/2}$ by the factors $(1 + 44.6D_0^{1/2}t^{1/6}m^{-1/3})$ and $(1 \pm 44.6D_R^{1/2}t^{1/6}m^{-1/3})$, respectively. The sign in the spherical correction factor for D_R is dependent on whether the reduced form is soluble in solution (+ sign) or in the electrode phase (- sign). Their expression for the entire reversible dc polarographic wave may be written

$$i_{es1} = \sqrt{\frac{7}{3\pi t}} \left[\frac{nFAC_0^*D_0^{1/2}(1 + 44.6D_0^{1/2}t^{1/6}m^{-1/3}) \times (1 \pm 44.6D_R^{1/2}t^{1/6}m^{-1/3})}{(1 \pm 44.6D_R^{1/2}t^{1/6}m^{-1/3}) + (1 + 44.6D_0^{1/2}t^{1/6}m^{-1/3})e^j} \right] \quad (3)$$

where

$$j = \frac{nF}{RT}(E_{dc} - E_{r_{1/2}}) \quad (4)$$

$$E_{r_{1/2}} = E^0 - \frac{RT}{nF} \ln \left(\frac{f_R}{f_0} \right) \left(\frac{D_0}{D_R} \right)^{1/2} \quad (5)$$

Equation 3 reduces to the Lingane-Loveridge equation for the limiting current (eq 2) when the electrode potential becomes sufficiently cathodic ($e^j \rightarrow 0$).

An alternative interpretation of the basic assumption underlying the Lingane-Loveridge derivation is that coupling of the perturbations on the mass transfer process associated with electrode growth and curvature may be neglected; *i.e.*, the contributions of drop growth and curvature may be considered separable or additive. A more explicit statement of this principle can be given in terms of a mathematical relationship as follows. Let i_p denote the current flowing at a stationary plane electrode after an electrolysis

time t , i_s the corresponding current at a stationary sphere electrode, and i_{ep} the current for an expanding-plane electrode. The assumption that drop growth and curvature perturbations do not couple then permits one to represent $(i_s - i_p)$ as the correction for drop curvature and $(i_{ep} - i_p)$ as the correction for drop growth. The same assumption suggests that addition of these corrections to i_p should yield an expression for the current at an expanding sphere electrode, i_{es2} . That is, one may write

$$i_{es2} = i_p + (i_{ep} - i_p) + (i_s - i_p) \quad (6)$$

or

$$i_{es2} = i_{ep} + i_s - i_p \quad (7)$$

Recalling the relevant expressions for the limiting current^{3,16,17}

$$i_p = \frac{nFAC_0^*D_0^{1/2}}{(\pi t)^{1/2}} \quad (8)$$

$$i_{ep} = \sqrt{\frac{7}{3}} \frac{nFAC_0^*D_0^{1/2}}{(\pi t)^{1/2}} \quad (9)$$

$$i_s = nFAC_0^*D_0^{1/2} \left[\frac{1}{(\pi t)^{1/2}} + \frac{D_0^{1/2}}{r_0} \right] \quad (10)$$

and substituting them in eq 6 yields eq 1, so it is clear that the Lingane-Loveridge method is consistent with the principle of separability of drop-growth and curvature effects.

The intuitive method underlying the Lingane-Loveridge equation obviously represents a rather uncertain theoretical base. Fortunately, an assessment of the accuracy of eq 2 was forthcoming in the form of more rigorous theoretical formulations of the expanding-sphere boundary value problem. Kambara and Tachi showed that eq 2 is an approximate solution to the MacGillavry-Rideal equation for diffusion to an

(8) T. Kambara and I. Tachi, "Proceedings of the First International Polarographic Congress, Prague, 1951," Vol. 1, Pírodovědecké Vydavatelství, Prague, 1951, p 126.

(9) T. Kambara and I. Tachi, *Bull. Chem. Soc. Japan*, **25**, 285 (1952).

(10) H. Matsuda, *ibid.*, **26**, 342 (1953).

(11) J. Koutecký, *Czech. J. Phys.*, **2**, 50 (1953).

(12) V. G. Levich, "Physicochemical Hydrodynamics," Prentice-Hall, Englewood Cliffs, N. J., 1962, Chapter 10.

(13) R. Subrahmanya, *Can. J. Chem.*, **40**, 289 (1962).

(14) A. Kimla and F. Štráfelda, *Collection Czech. Chem. Commun.*, **28**, 3206 (1963).

(15) K. B. Oldham, P. Kivalo, and H. A. Laitinen, *J. Am. Chem. Soc.*, **75**, 5712 (1953).

(16) F. G. Cottrell, *Z. Physik. Chem.*, **42**, 385 (1902).

(17) P. Delahay, "New Instrumental Methods in Electrochemistry," Interscience Publishers Inc., New York, N. Y., 1954, pp 61-63.

expanding sphere electrode. Rigorous treatments of the diffusion-controlled limiting current at an expanding-sphere electrode have been presented by Koutecký,¹¹ Levich,¹² and Matsuda.¹⁰ Their solutions can be expressed in the form of an infinite series

$$i_{es} = nFAC_0^* \sqrt{\frac{7D_0}{3\pi t}} \left[1 + \sum_{i=1}^{\infty} a_i \left(\frac{D_0^{1/2} t^{1/6}}{m^{1/3}} \right)^i \right] \quad (11)$$

In the Koutecký and Levich treatments, only the a_1 term contributes significantly to the instantaneous current under normal experimental conditions. A value of 39.6 is found for a_1 in both cases, compared to the value of 44.6 associated with the corresponding term in the Lingane-Loveridge equation (eq 2). Matsuda's treatment yielded a slightly different result with a significant a_2 term compensating for a slightly smaller a_1 term ($a_1 = 36.3$), so that his theory yields essentially the same results as the Koutecký-Levich expression. The magnitude of the a_1 term, which represents the spherical diffusion contribution for a dropping mercury electrode (dme), differs significantly ($\sim 13\%$) in the rigorous solution and the approximate equation of Lingane and Loveridge. However, since this term represents a small (10–15%) contribution to the total diffusion current, the approximate Lingane-Loveridge equation comes surprisingly close to predicting the same diffusion current magnitudes as the rigorous solution. The diffusion currents predicted by eq 2 are slightly larger ($\sim 2\%$) than those predicted by the more exact expressions. The direction of the error is as expected since the Lingane-Loveridge method is equivalent to assuming that the effects of drop growth and curvature do not couple, while in fact the movement of the electrode surface should tend to decrease the contribution of spherical diffusion. A mathematical basis for this statement has been provided by Koutecký and von Stackelberg¹⁸ who, by appropriate manipulation of the MacGillavry-Rideal equation, identified a term manifesting coupling of the drop-growth and curvature perturbations. Nevertheless, the rather small difference between eq 2 and the rigorous expression provides evidence that the assumptions inherent in the Lingane-Loveridge equation are reasonably accurate as far as the polarographic limiting current is concerned.

Koutecký and Čížek have extended the method for rigorously solving the MacGillavry-Rideal equation to several more complex electrode reaction mechanisms in which chemical reactions or charge transfer compete with diffusion for rate control.^{19,20} These studies indicate that rigorous solution of the MacGillavry-Rideal equation for most mechanistic schemes will

prove extremely tedious and, unlike the diffusion-controlled case, the final results will often assume rather complex forms involving series solutions whose coefficients are defined by cumbersome recurrence relations.¹⁹ These facts apparently have discouraged most workers from applying the rigorous theory to the analysis of experimental results as attested by the almost exclusive use of the expanding plane theory. In many applications it would be advantageous to be able to estimate the magnitude of the spherical diffusion contribution with the aid of a conveniently implemented approximate theory which is accurate to within a few per cent in estimating the current magnitude (the corresponding error in the expanding plane theory is 10–20%^{11,18,21}).

The success of the Lingane-Loveridge equation in predicting the diffusion-controlled limiting current with reasonable accuracy led us to consider whether a similar correction for the effects of drop growth and curvature can be obtained for the entire dc polarographic wave with various electrode reaction mechanisms by applying either of the assumptions leading to equation 2. The present work evaluates the following two approximate methods originating in the assumptions which are consistent with the Lingane-Loveridge equation: (1) correcting the theory based on the expanding-plane electrode model for spherical diffusion by modifying the diffusion coefficients by "spherical correction factors" of the type used by Oldham, Kivalo, and Laitinen;¹⁵ (2) assuming that the effects of drop growth and curvature do not couple so that eq 7 is applicable over the entire dc polarographic wave.

Either of these approximate methods would be quite useful if proven sufficiently accurate. Method 1 is simplest in both implementation and final result. However, the literature abounds in the essential theoretical equations for i_s , i_p , and i_{ep} so that application of method 2 also will be quite convenient with most mechanisms, although the final results will prove somewhat more cumbersome than those of method 1.

Theory

The present work evaluates approximate methods 1

(18) J. Koutecký and M. von Stackelberg in "Progress in Polarography," P. Zuman, Ed., with the collaboration of I. M. Kolthoff, Vol. I, Interscience Publishers Inc., New York, N. Y., 1962, Chapter 2.

(19) J. Koutecký and J. Čížek, *Collection Czech. Chem. Commun.*, **21**, 836 (1956).

(20) J. Koutecký and J. Čížek, *ibid.*, **21**, 1063 (1956).

(21) J. Kůta and I. Smoler in "Progress in Polarography," P. Zuman, Ed., with collaboration of I. M. Kolthoff, Vol. I, Interscience Publishers Inc., New York, N. Y., 1962, Chapter 3.

and 2 by comparing dc polarographic waves calculated on the basis of these methods with those calculated from exact solutions of the MacGillavry-Rideal equation provided by Koutecký and co-workers.^{11,18-20} This is done for dc polarographic waves in which: (a) diffusion is the sole rate-determining step (the reversible case); (b) charge transfer and diffusion are the rate-determining steps (the quasi-reversible case); (c) chemical reactions coupled to the charge-transfer step and diffusion are the rate-determining steps. To aid in comparison of accuracy and complexity of mathematical expressions associated with the various theoretical electrode models, both equations and results of calculations are given for all relevant theoretical models, including equations based on the stationary plane and sphere electrode models, suitably adapted for applicability to polarography. In all cases the expression for the electrode area appropriate to the dme [$A = 8.515 \times 10^{-3}(mt)^{2/3}$] is employed in calculations. Through this operation on the electrode area term, the theoretical expressions for the potentiostatic response of stationary plane and sphere electrodes are transformed to approximate theoretical models for the polarographic experiment with the dme. Calculations based on the resulting equations are then performed in the context of the polarographic experiment; *i.e.*, parameters of importance in stationary electrode experiments such as initial (rest) potential have no relevance, while neglect of depletion effects and other assumptions inherent in most theoretical polarographic work are employed (*cf.* ref 18). Such utilization of the stationary-plane theory represents one of the earliest approaches to obtaining a quantitative theory for the polarographic wave,^{15,17} which yields an expression in which effects of drop growth and curvature are neglected. The stationary-sphere theory applied in this manner represents an approximation to the dme which ignores contributions of drop growth.

I. Diffusion-Controlled Processes. For the case of a simple electrode process, $O + ne \rightleftharpoons R$, in which charge transfer does not exert rate control, two basic cases will be considered: (A) both forms of the electroactive oxidation-reduction couple soluble in solution, and (B) the reduced form soluble in the electrode, as in amalgam formation. The equations for the stationary- and expanding-plane diffusion models are independent of the mode of diffusion of the reduced form, due to the symmetry of the diffusion process.¹⁸ Equations presented for the amalgam case will neglect the finite volume effect.^{11,22,23} It has been shown that this effect does not become important for normal polarographic conditions.²² When the equations differ

between cases A and B, the upper sign will refer to case A (as in eq 3).

An expression for the polarographic current with a reversible electrode process which is based on the stationary plane model (i_p) may be written¹⁵

$$i_p = \frac{nFAC_0^*D_0^{1/2}}{(\pi t)^{1/2}(1 + e^j)} \quad (12)$$

where j is given by eq 4. The corresponding expression for diffusion to an expanding plane has the form²⁴

$$i_{ep} = \sqrt{\frac{7}{3}} \frac{nFAC_0^*D_0^{1/2}}{(\pi t)^{1/2}(1 + e^j)} \quad (13)$$

For the stationary spherical electrode model, it has been shown that^{23,25-27}

$$i_s = \frac{nFAC_0^*D_0^{1/2}}{(1 + e^j)} \left\{ \frac{1}{(\pi t)^{1/2}} \pm \frac{D_0^{1/2}D_R^{1/2}r_0^{-1}(1 + e^j)}{e^jD_0^{1/2} \pm D_R^{1/2}} + \frac{e^j(D_0^{1/2} \mp D_R^{1/2})^2r_0^{-1}}{(1 + e^j)(e^jD_0^{1/2} \pm D_R^{1/2})} \exp(a_{\pm}t) \operatorname{erfc}(a_{\pm}t^{1/2}) \right\} \quad (14)$$

where

$$a_{\pm} = \frac{e^jD_0^{1/2} \pm D_R^{1/2}}{r_0(1 + e^j)} \quad (15)$$

For all potentials encompassed by the polarographic wave, Koutecký's rigorous solution of the expanding-sphere problem assumes the form^{11,18}

$$i_{es} = \sqrt{\frac{7}{3}} \frac{nFAC_0^*D_0^{1/2}}{(\pi t)^{1/2}(1 + e^j)} \times \left\{ 1 + \frac{39.6D_0^{1/2}t^{1/4} \left[1 \pm \left(\frac{D_R}{D_0} \right)^{1/2} e^j \right]}{m^{1/4}(1 + e^j)} \right\} \quad (16)$$

As stated before, eq 3 is the appropriate expression for the expanding-sphere model on the basis of approximate method 1. Method 2 yields (substituting eq 12, 13, and 14 in eq 7)

$$i_{es2} = \sqrt{\frac{7}{3\pi t}} \frac{nFAC_0^*D_0^{1/2}}{(1 + e^j)} \left\{ 1 + \frac{\sqrt{\frac{3\pi t}{7}}}{e^jD_0^{1/2} \pm D_R^{1/2}} \times \left[\pm D_0^{1/2}D_R^{1/2}(1 + e^j) + \frac{e^j(D_0^{1/2} \mp D_R^{1/2})^2}{1 + e^j} \right] \exp(a_{\pm}t) \operatorname{erfc}(a_{\pm}t^{1/2}) \right\} \quad (17)$$

(22) W. H. Reinmuth, *Anal. Chem.*, **33**, 185 (1961).

(23) I. Shain and K. J. Martin, *J. Phys. Chem.*, **65**, 254 (1961).

(24) J. Heyrovský and D. Ilkovič, *Collection Czech. Chem. Commun.*, **7**, 198 (1935).

II. *Electrode Processes Kinetically Controlled by Charge Transfer and Diffusion.* As in the reversible case, one must consider whether the reduced form is soluble in the solution (case A) or electrode phase (case B) in deriving theory for diffusion to a stationary- or expanding-spherical electrode. The same sign convention will be employed as with the reversible case.

Theory for diffusion to a stationary planar electrode yields for this case²⁸⁻³⁰

$$i_p = nFAC_0^* \left(\frac{D_0}{D}\right)^{1/2} k_h e^{-\alpha j} \exp(\lambda^2 t) \operatorname{erfc}(\lambda t^{1/2}) \quad (18)$$

where

$$\lambda = \frac{k_h}{D^{1/2}} (e^{-\alpha j} + e^{\beta j}) \quad (19)$$

$$\beta = 1 - \alpha \quad (20a)$$

$$D = D_0^\beta D_R^\alpha \quad (20b)$$

The expanding-plane electrode model produces the expression^{31,32}

$$i_{ep} = \sqrt{\frac{7}{3}} \frac{nFAC_0^* D_0^{1/2}}{(\pi t)^{1/2} (1 + e^j)} F(\chi) \quad (21)$$

where

$$\chi = \sqrt{\frac{12}{7}} \lambda t^{1/2} \quad (22)$$

and $F(\chi)$ is defined and tabulated by Koutecký and co-workers.^{31,33} Recently, the appropriate relations for the stationary-sphere model were presented for both cases A and B. It was found that^{27,34}

$$i_a = nFAC_0^* \left(\frac{D_0}{D}\right)^{1/2} k_h e^{-\alpha j} \left\{ \frac{1}{(a_\pm - b_\pm)} \times \left[a_\pm - r_0^{-1}(D_0^{1/2} \pm D_R^{1/2}) \pm \frac{r_0^{-2} D_0^{1/2} D_R^{1/2}}{a_\pm} \right] \times \exp(a_\pm^2 t) \operatorname{erfc}(a_\pm t^{1/2}) - \frac{1}{(a_\pm - b_\pm)} \times \left[b_\pm - r_0^{-1}(D_0^{1/2} \pm D_R^{1/2}) \pm \frac{r_0^{-2} D_0^{1/2} D_R^{1/2}}{b_\pm} \right] \times \exp(b_\pm^2 t) \operatorname{erfc}(b_\pm t^{1/2}) \pm \frac{r_0^{-2} D_0^{1/2} D_R^{1/2}}{a_\pm b_\pm} \right\} \quad (23)$$

where

$$2a_\pm = r_0^{-1}(D_0^{1/2} \pm D_R^{1/2}) + \lambda - \left\{ [r_0^{-1}(D_0^{1/2} \pm D_R^{1/2}) + \lambda]^2 \mp 4 \left[r_0^{-2} D_0^{1/2} D_R^{1/2} + \frac{k_h r_0^{-1}}{D^{1/2}} (D_R^{1/2} e^{-\alpha j} \pm D_0^{1/2} e^{\beta j}) \right] \right\}^{1/2} \quad (24)$$

$$2b_\pm = r_0^{-1}(D_0^{1/2} \pm D_R^{1/2}) + \lambda +$$

$$\left\{ [r_0^{-1}(D_0^{1/2} \pm D_R^{1/2}) + \lambda]^2 \mp 4 \left[r_0^{-2} D_0^{1/2} D_R^{1/2} + \frac{k_h r_0^{-1}}{D^{1/2}} (D_R^{1/2} e^{-\alpha j} \pm D_0^{1/2} e^{\beta j}) \right] \right\}^{1/2} \quad (25)$$

The rigorous solution of the expanding-sphere boundary value problem for the quasi-reversible case has been provided by Koutecký and Čížek.¹⁹ They showed that

$$i_{es} = \sqrt{\frac{7}{3}} \frac{nFAC_0^* D_0^{1/2}}{(\pi t)^{1/2} (1 + e^j)} \times \left\{ 1 + \frac{39.6 D_0^{1/2} t^{1/6} \left[1 \pm \left(\frac{D_R}{D_0}\right)^{1/2} e^j \right]}{m^{1/2} (1 + e^j)} \right\} \times \left\{ F(\chi) - \frac{39.6 D_0^{1/2} t^{1/6} \left[1 \pm \left(\frac{D_R}{D_0}\right)^{1/2} e^j \right]}{m^{1/2} (1 + e^j)} F(\chi) + \varepsilon_0 G_\pm(\chi) \right\} \quad (26)$$

ε_0 , $G_\pm(\chi)$, and $F(\chi)$ are defined in Koutecký and Čížek's article, where $G_+(\chi)$ and $G_-(\chi)$ are represented as $G_A(\chi)$ and $G_B(\chi)$, respectively, in the Koutecký-Čížek paper.¹⁹ χ is given by eq 22.

Approximate method 1 gives the relationship

$$i_{es1} = \sqrt{\frac{7}{3}} \left\{ \frac{nFAC_0^* D_0^{1/2} (1 + 44.6 D_0^{1/2} t^{1/6} m^{-1/2}) \times (1 \pm 44.6 D_R^{1/2} t^{1/6} m^{-1/2})}{(\pi t)^{1/2} [(1 \pm 44.6 D_R^{1/2} t^{1/6} m^{-1/2}) + e^j (1 + 44.6 D_0^{1/2} t^{1/6} m^{-1/2})]} \right\} \times F(\chi^+) \quad (27)$$

where

$$\chi^+ = \sqrt{\frac{12}{7}} \lambda + t^{1/2} \quad (28)$$

(25) I. Shain and D. S. Polcyn, *J. Phys. Chem.*, **65**, 1649 (1961).

(26) W. G. Stevens and I. Shain, *Anal. Chem.*, **38**, 865 (1966).

(27) J. R. Delmastro and D. E. Smith, *ibid.*, **38**, 169 (1966).

(28) M. Smutek, *Collection Czech. Chem. Commun.*, **18**, 171 (1953).

(29) T. Kambara and I. Tachi, *Bull. Chem. Soc. Japan*, **25**, 135 (1952).

(30) P. Delahay, *J. Am. Chem. Soc.*, **75**, 1430 (1953).

(31) J. Koutecký, *Collection Czech. Chem. Commun.*, **18**, 597 (1953).

(32) H. Matsuda and Y. Ayabe, *Bull. Chem. Soc. Japan*, **28**, 422 (1955).

(33) J. Weber and J. Koutecký, *Collection Czech. Chem. Commun.*, **20**, 980 (1955).

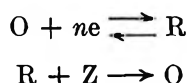
$$\lambda^+ = \frac{k_h}{D^{1/2}} \left\{ \frac{e^{-\alpha j}}{(1 + 44.6D_0^{1/2}t^{1/2}m^{-1/2})} + \frac{e^{\beta j}}{(1 \pm 44.6D_R^{1/2}t^{1/2}m^{-1/2})} \right\} \quad (29)$$

This is obtained by replacing $D_0^{1/2}$ by $D_0^{1/2}(1 + 44.6D_0^{1/2}t^{1/2}m^{-1/2})$ and $D_R^{1/2}$ by $D_R^{1/2}(1 \pm 44.6D_R^{1/2}t^{1/2}m^{-1/2})$ in eq 21.

Method 2 yields (substituting eq 18, 21, and 23 in eq 7)

$$i_{\text{ca}2} = nFAC_0^*D_0^{1/2} \left\{ \sqrt{\frac{7}{3}} \frac{F(x)}{(\pi t)^{1/2}(1 + e^j)} + \frac{k_h e^{-\alpha j}}{D^{1/2}} \times \left[\frac{1}{a_{\pm} - b_{\pm}} \left(a_{\pm} - r_0^{-1}(D_0^{1/2} \pm D_R^{1/2}) \pm \frac{r_0^{-2}D_0^{1/2}D_R^{1/2}}{a_{\pm}} \right) \exp(a_{\pm}t) \operatorname{erfc}(a_{\pm}t^{1/2}) - \frac{1}{a_{\pm} - b_{\pm}} \left(b_{\pm} - r_0^{-1}(D_0^{1/2} \pm D_R^{1/2}) \pm \frac{r_0^{-2}D_0^{1/2}D_R^{1/2}}{b_{\pm}} \right) \exp(b_{\pm}t) \operatorname{erfc}(b_{\pm}t^{1/2}) \pm \frac{r_0^{-2}D_0^{1/2}D_R^{1/2}}{a_{\pm}b_{\pm}} - \exp(\lambda^2 t) \operatorname{erfc}(\lambda t^{1/2}) \right] \right\} \quad (30)$$

III. *Electrode Processes Controlled by Diffusion and Chemical Reaction. 1. The Simple Catalytic Mechanism with Nernstian Conditions.* The approximate methods of obtaining theory for dc polarography applicable at the dme will be examined for the simple catalytic mechanism³⁵ represented by



where the oxidizing agent Z is electroinactive in the potential range of the O-R oxidation-reduction couple and is present in sufficient excess to produce pseudo-first-order conditions. Theory presented for this mechanism assumes $D_0 = D_R$.

The appropriate theory for the catalytic mechanism with diffusion to a stationary planar electrode has been presented by a number of workers.³⁶⁻³⁸ They found that

$$i_p = \frac{nFAC_0^*D_0^{1/2}}{(1 + e^j)} \left\{ \frac{e^{-k_0 t}}{(\pi t)^{1/2}} + k_0^{1/2} \operatorname{erf}[(k_0 t)^{1/2}] \right\} \quad (31)$$

Koutecký derived the following expression for the polarographic current with diffusion to an expanding plane electrode³⁹

$$i_{\text{ep}} = \sqrt{\frac{7}{3\pi t}} \frac{nFAC_0^*D_0^{1/2}}{1 + e^j} \psi(k_0 t) \quad (32)$$

$\psi(k_0 t)$ is defined and tabulated in Koutecký's article.³⁹ For $k_0 t > 9$, eq 31 and 32 reduce to³⁶⁻³⁹

$$i_p = i_{\text{ep}} = \frac{nFAC_0^*D_0^{1/2}k_0^{1/2}}{1 + e^j} \quad (33)$$

To our knowledge, an expression for the current with diffusion to a stationary-sphere electrode and the simple catalytic mechanism has not been presented. However, the following expression is readily obtained by application of the method of the Laplace transformation⁴⁰

$$i_s = \frac{nFAC_0^*D_0^{1/2}}{1 + e^j} \left\{ \frac{e^{-k_0 t}}{(\pi t)^{1/2}} + k_0^{1/2} \operatorname{erf}[(k_0 t)^{1/2}] + \frac{D_0^{1/2}}{r_0} \right\} \quad (34)$$

Koutecký and Čížek solved the boundary value problem for the simple catalytic mechanism with diffusion to an expanding sphere.²⁰ They obtained

$$i_{\text{ca}} = \sqrt{\frac{7}{3\pi t}} \frac{nFAC_0^*D_0^{1/2}}{1 + e^j} [1 + 39.6D_0^{1/2}t^{1/2}m^{-1/2}] \times \{ \psi(k_0 t) + 50.31D_0^{1/2}t^{1/2}m^{-1/2} [\theta(k_0 t) - 0.7868\psi(k_0 t)] \} \quad (35)$$

$\theta(k_0 t)$ is defined in the original manuscript.²⁰

Method 1 yields the expression

$$i_{\text{ca}1} = \sqrt{\frac{7}{3\pi t}} \frac{nFAC_0^*D_0^{1/2}(1 + 44.6D_0^{1/2}t^{1/2}m^{-1/2})}{(1 + e^j)} \psi(k_0 t) \quad (36)$$

For $k_0 t > 9$, eq 36 simplifies to

$$i_{\text{ca}1} = \frac{nFAC_0^*D_0^{1/2}(1 + 44.6D_0^{1/2}t^{1/2}m^{-1/2})k_0^{1/2}}{1 + e^j} \quad (37)$$

The expression for the simple catalytic mechanism given by method 2, obtained by substituting eq 31, 32, and 34 in eq 7, takes the form

$$i_{\text{ca}2} = \sqrt{\frac{7}{3\pi t}} \frac{nFAC_0^*D_0^{1/2}}{1 + e^j} \times [\psi(k_0 t) + 44.57D_0^{1/2}t^{1/2}m^{-1/2}] \quad (38)$$

For $k_0 t > 9$

$$i_{\text{ca}2} = \frac{nFAC_0^*D_0^{1/2}}{1 + e^j} (k_0^{1/2} + D_0^{1/2}r_0^{-1}) \quad (39)$$

(34) I. Shain, K. J. Martin, and J. W. Ross, *J. Phys. Chem.*, **65**, 259 (1961).

(35) P. Delahay, "New Instrumental Methods in Electrochemistry," Interscience Publishers Inc., New York, N. Y., 1954, pp 100-104.

(36) P. Delahay and G. Stiehl, *J. Am. Chem. Soc.*, **74**, 3500 (1952).

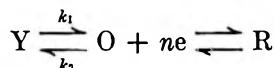
(37) S. Miller, *ibid.*, **74**, 4130 (1952).

(38) J. Koutecký, *Collection Czech. Chem. Commun.*, **18**, 183 (1953).

(39) J. Koutecký, *ibid.*, **18**, 311 (1953).

(40) J. R. Delmastrc and D. E. Smith, unpublished work.

2. *Limiting Current in a System Involving a Preceding Chemical Reaction.* Methods 1 and 2 will be evaluated for the electrode reaction mechanism



where first-order or pseudo-first-order conditions prevail with respect to the preceding chemical reaction. Theory presented will be restricted to expressions for the limiting current under conditions where a steady state is achieved; *i.e.*, $(k_1 + k_2)t > 10$.⁴¹ This is done since the rigorous calculation for the expanding-sphere electrode applies only under these conditions.¹⁹ For the sake of simplicity, equality of diffusion coefficients ($D_0 = D_Y = D_R$) is also assumed.

For the conditions listed above, the expression based on the stationary-plane electrode model takes the form⁴²⁻⁴³

$$i_p = nFAC_0^*D_0^{1/2}(1 + K)k^{1/2} \times \exp(K^2kt) \operatorname{erfc}(Kk^{1/2}t^{1/2}) \quad (40)$$

where

$$k = k_1 + k_2 \quad (41)$$

$$K = k_1/k_2 \quad (42)$$

The expression for the limiting current based on the expanding-plane model also was presented by Koutecký who showed³¹

$$i_{op} = \sqrt{\frac{7}{3\pi t}} nFAC_0^*D_0^{1/2} \left(\frac{1 + K}{K} \right) F(\chi_k) \quad (43)$$

where

$$\chi_k = \sqrt{\frac{12}{7}} Kk^{1/2}t^{1/2} \quad (44)$$

$F(\chi_k)$ is defined in the original article.³¹

The corresponding equation for diffusion to a stationary-sphere electrode may be obtained by routine application of the method of the Laplace transformation.⁴⁰ The more exact steady-state approximation was employed *i.e.*, neglecting only the $\partial/\partial t$ term, but retaining the $(2/r)\partial/\partial r$ term⁴⁴ in Fick's second law for diffusion to a stationary-sphere electrode. The result may be expressed

$$i_s = \frac{nFAC_0^*D_0^{1/2}(1 + K)(k^{1/2} + D_0^{1/2}r_0^{-1})}{K(k^{1/2} + D_0^{1/2}r_0^{-1}) + D_0^{1/2}r_0^{-1}} \times [K(k^{1/2} + D_0^{1/2}r_0^{-1}) \exp(a^2t) \operatorname{erfc}(at^{1/2}) + D_0^{1/2}r_0^{-1}] \quad (45)$$

where a is defined in eq 46.

$$a = K(k^{1/2} + D_0^{1/2}r_0^{-1}) + D_0^{1/2}r_0^{-1} \quad (46)$$

Koutecký and Čížek's equation for diffusion to an expanding sphere has the form¹⁹

$$i_{es} = \sqrt{\frac{7}{3\pi t}} nFAC_0^*D_0^{1/2} \left(\frac{1 + K}{K} \right) \times (1 + 39.6D_0^{1/2}t^{1/2}m^{-1/2}) \times [F(\chi_k) - \varepsilon_0 H_c(\chi_k)] \quad (47)$$

where χ_k is given by eq 44. $F(\chi_k)$ and $H_c(\chi_k)$ are defined in the original article.¹⁹

Approximate method 1 leads to the expression

$$i_{es1} = \sqrt{\frac{7}{3\pi t}} nFAC_0^*D_0^{1/2} \left(\frac{1 + K}{K} \right) \times (1 + 44.6D_0^{1/2}t^{1/2}m^{-1/2}) F(\chi_k) \quad (48)$$

while method 2 (substituting eq 40, 43, and 45 in eq 7) gives

$$i_{es2} = nFAC_0^*D_0^{1/2} \left(\frac{1 + K}{K} \right) \left\{ \sqrt{\frac{7}{3\pi t}} F(\chi_k) + \frac{K(k^{1/2} + D_0^{1/2}r_0^{-1})}{K(k^{1/2} + D_0^{1/2}r_0^{-1}) + D_0^{1/2}r_0^{-1}} \times [K(k^{1/2} + D_0^{1/2}r_0^{-1}) \exp(a^2t) \operatorname{erfc}(at^{1/2}) + D_0^{1/2}r_0^{-1}] - k^{1/2}K \exp(K^2kt) \operatorname{erfc}(Kk^{1/2}t^{1/2}) \right\} \quad (49)$$

Results and Discussion

To evaluate approximate methods 1 and 2, numerous dc polarographic waves predicted by these methods have been calculated and compared with waves calculated on the basis of exact solutions for the expanding-sphere model. A CDC 3400 digital computer was utilized to facilitate this work. Some typical results are depicted in Figures 1-5. For reference purposes, these figures include polarographic waves predicted by the stationary-plane, stationary-sphere, and expanding-plane models, along with those based on method 1, method 2, and the exact solution. The stationary-electrode equations were converted to expressions relevant to the polarographic experiment as indicated at the beginning of the theoretical section. The difference in polarographic waves calculated on the basis of the stationary- and expanding-plane models indicates the magnitude of the drop-growth contribution. The magnitude of the spherical-diffusion effect can be ascertained either from differences in polaro-

(41) R. Brdička, V. Hanus, and J. Koutecký in "Progress in Polarography," P. Zuman, Ed., with collaboration of I. M. Kolthoff, Vol. I, Interscience Publishers Inc., New York, N. Y., 1962, Chapter 7.

(42) R. P. Buck, *J. Electroanal. Chem.*, **5**, 295 (1963).

(43) J. Koutecký and R. Brdička, *Collection Czech. Chem. Commun.*, **12**, 337 (1947).

(44) J. Čížek and J. Koutecký, *ibid.*, **28**, 2808 (1963).

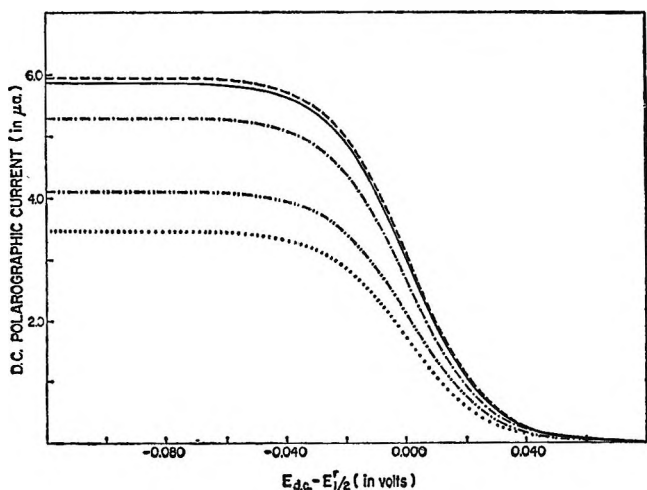


Figure 1. Calculated dc polarograms for a reversible system with both oxidation-reduction forms soluble in solution. Plots show instantaneous currents at end of drop life for $C_0^* = 1.00 \times 10^{-3} M$; $D_0 = D_R = 5.00 \times 10^{-6} \text{ cm}^2 \text{ sec}^{-1}$; $D_R = 1.00 \times 10^{-5} \text{ cm}^2 \text{ sec}^{-1}$; drop life = 6.00 sec; $T = 25.0^\circ$; $n = 2$; $r_0 = 0.0528 \text{ cm}^2$ (at $t = 6 \text{ sec}$); $m = 1.39 \text{ mg sec}^{-1}$: —, calculated from rigorous expanding-sphere theory; ---, calculated from methods 1 and 2; - · - ·, calculated from expanding-plane electrode model; - · · - ·, calculated from stationary-sphere electrode model; · · · ·, calculated from stationary-plane electrode model.

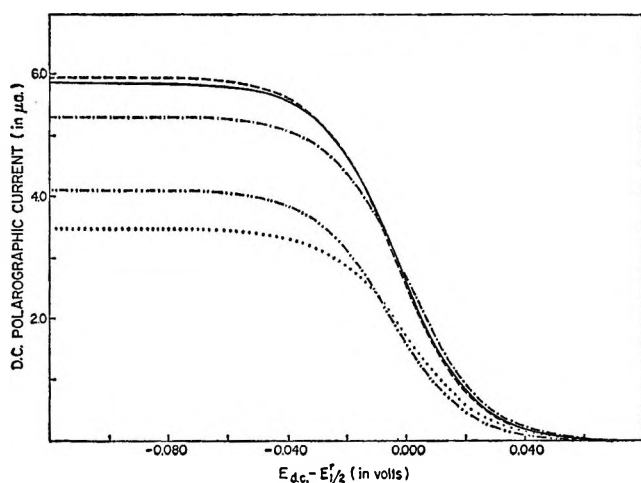


Figure 2. Calculated dc polarograms for a reversible system with the reduced form soluble in the electrode. Plots show instantaneous currents at end of drop life. Conditions and notation same as Figure 1.

graphic waves predicted by the stationary-plane and stationary-sphere models or from differences in the expanding-plane and expanding-sphere predictions. The latter differences are of particular interest in light of the fact that the expanding-plane theory is most frequently applied to the analysis of dc polarographic

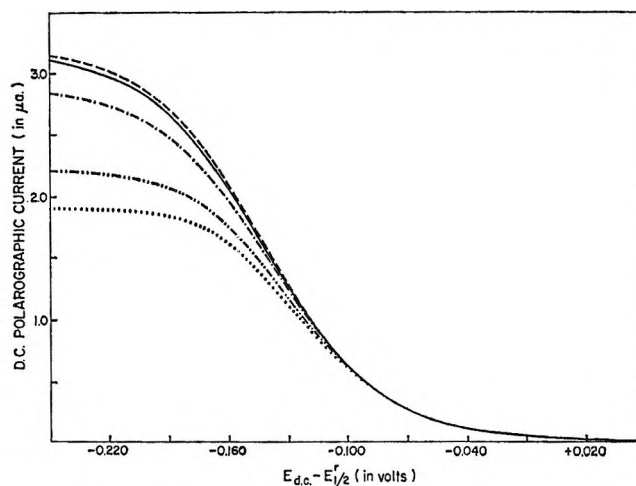


Figure 3. Calculated dc polarograms for irreversible system. Plots show instantaneous currents at end of drop life for $C_0^* = 1.00 \times 10^{-3} M$; $D_0 = D_R = 5.00 \times 10^{-6} \text{ cm}^2 \text{ sec}^{-1}$; drop life = 5.00 sec; $T = 25.0^\circ$; $n = 1$; $r_0 = 0.0528 \text{ cm}^2$ (at $t = 5 \text{ sec}$); $m = 1.67 \text{ mg sec}^{-1}$; $k_b = 1.00 \times 10^{-6} \text{ cm sec}^{-1}$; $\alpha = 0.800$. Notation same as Figure 1.

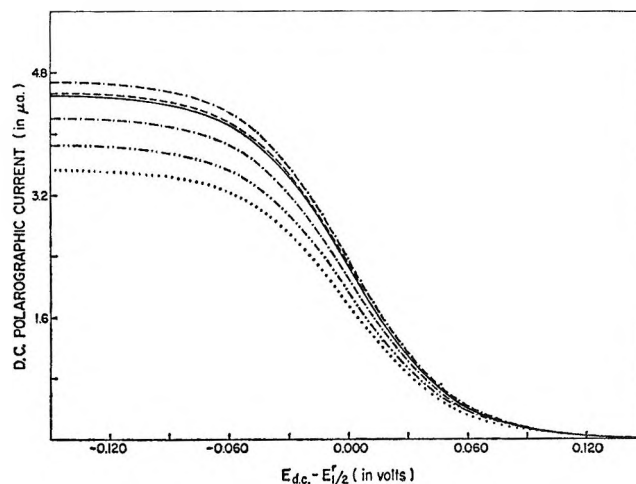


Figure 4. Calculated dc polarograms for catalytic system with Nernstian conditions. Plots show instantaneous currents at end of drop life for $C_0^* = 1.00 \times 10^{-3} M$; $D_0 = D_R = 5.00 \times 10^{-6} \text{ cm}^2 \text{ sec}^{-1}$; drop life = 5.00 sec; $T = 25.0^\circ$; $n = 1$; $r_0 = 0.0528 \text{ cm}^2$ (at $t = 5 \text{ sec}$); $m = 1.67 \text{ mg sec}^{-1}$; $k_c = 0.20 \text{ sec}^{-1}$: —, calculated from rigorous expanding-sphere theory; ---, calculated from method 2; - · - ·, calculated from method 1; - · · - ·, calculated from expanding-plane model; - · · - ·, calculated from stationary-sphere model; · · · ·, calculated from stationary-plane model.

data. In Figures 1-3, the waves predicted by methods 1 and 2 are represented by a single curve. In these cases, differences between the predictions of these two methods are so small ($<0.5\%$) that graphical

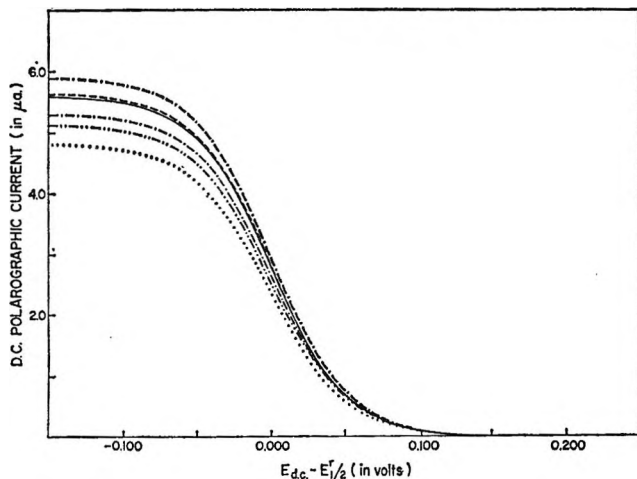


Figure 5. Calculated dc polarograms for catalytic system with Nernstian conditions. Conditions and notation same as Figure 4 except $k_0 = 0.40 \text{ sec}^{-1}$.

illustration is discouraged. In addition, these small deviations are of no practical significance as they lie within the normal range of experimental uncertainty.

Results depicted in Figures 1 and 2 are representative of those obtained in calculations for systems in which diffusion is the sole rate-determining step. Figure 1 illustrates typical results for both oxidation-reduction forms soluble in solution, while Figure 2 shows results with the same parameter values for the case where the reduced form is soluble in the electrode phase. For both forms soluble in solution, methods 1 and 2 predict current magnitudes which are slightly larger ($\sim 2\%$) over the entire wave than those calculated from Koutecký's exact solution. For the reduced form soluble in the electrode, the differences between the exact solution and the results predicted by both approximate methods are again quite small. In the limiting-current region, the error in the current magnitudes predicted by methods 1 and 2 is the same as in case A, but at the foot of the polarographic wave they predict current magnitudes which are 2–3% smaller than given by the exact solution. All these deviations between predictions of methods 1 and 2 and the exact solution represent overcorrection for the effects of spherical diffusion by the approximate methods. Thus, methods 1 and 2 predict slightly larger currents than the exact solution where spherical diffusion tends to increase the current magnitude (over the entire wave in case A and at potentials cathodic to $E^r_{1/2}$ in case B¹⁸) and slightly smaller currents where spherical diffusion decreases the current (at potentials anodic to $E^r_{1/2}$ in case B¹⁸).

Figure 3 depicts some typical calculated polarograms for systems in which diffusion and charge

transfer are the rate-controlling processes. Rate parameters used in Figure 3 correspond to an irreversible process,⁴⁵ which represents the greatest departure from the pure diffusion-controlled case. If effects of charge-transfer kinetics magnify errors incorporated in methods 1 and 2, this should be most readily apparent with irreversible systems. Figure 3 indicates that the accuracy of equations based on methods 1 and 2 is not degraded by charge-transfer kinetic contributions. If anything, these approximate methods fare better than with pure diffusion control. Differences between current magnitudes predicted by methods 1 and 2 and the exact solution of Koutecký and Čížek (eq 26) are no larger than 2% over the entire wave. On the rising portion of the dc wave, current magnitudes predicted by methods 1 and 2 are typically 0.5–1.5% larger than those calculated from the exact solution. In contrast, the frequently employed expanding plane approximation (eq 21) predicts current magnitudes which are approximately 10–15% lower than those calculated from eq 26.

In Figures 4 and 5 are depicted typical theoretical dc polarographic waves for the simple catalytic mechanism.^{35–39} The values of the chemical rate constant (k_c) employed in calculating the results shown in Figures 4 and 5, 0.2 and 0.4 sec^{-1} , are sufficiently small that drop growth and geometry still contribute significantly to the current magnitude. (These effects become insignificant for $kt > 10$).²⁰ It can be seen that in this case method 1 does not provide a reasonably accurate assessment of the contribution of spherical diffusion because introduction of "spherical correction factors" of the form $(1 + 44.6D^{1/2}t^{1/2}m^{-1/3})$ fails to consider that the chemical reaction reduces the contribution of spherical diffusion, because of an associated reduction in the thickness of the diffusion layer. Method 2 yields significantly better results because the influence of the chemical reaction on drop growth and geometry effects is explicitly incorporated in the expressions for i_{ep} and i_s which are employed in the application of this approximate method.

For the case of homogeneous chemical reactions preceding charge transfer, calculations were restricted to the limiting-current region for reasons stated above. For convenience, the results are depicted in a plot of i_k/i_d vs. $\log K\sqrt{(k_1 + k_2)t}$, where i_k is the kinetic limiting current predicted by a particular diffusion model (eq 40, 43, 45, 47, 48, or 49), and i_d is the diffusion-controlled limiting current for the same diffusion model (eq 3, 12, 13, 14, 16, or 17 with $e^j = 0$). Calcu-

(45) P. Delahay, "New Instrumental Methods in Electrochemistry," Interscience Publishers Inc., New York, N. Y., 1954, Chapter 4.

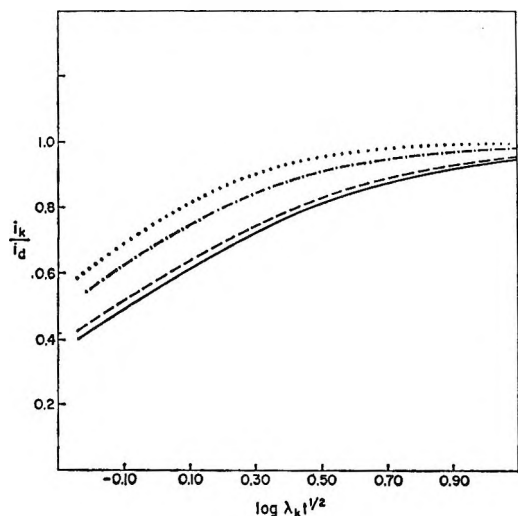


Figure 6. Calculated ratio of kinetic limiting current with preceding coupled chemical reaction (i_k) and diffusion-controlled limiting current (i_d) vs. $\log K(k_1 + k_2)^{1/2} t^{1/2}$.

Plots show ratios of instantaneous currents at end of drop life for $C_0^* + C_Y^* = 1.00 \times 10^{-3} M$; $D_0 = D_Y = D_R = 5.00 \times 10^{-6} \text{ cm}^2 \text{ sec}^{-1}$; drop life = 6.00 sec; $T = 25.0^\circ$; $n = 1$; $r_0 = 0.0528 \text{ cm}$ (at $t = 6 \text{ sec}$); $m = 1.39 \text{ mg sec}^{-1}$; —, calculated from rigorous expanding-sphere theory and method 2; ---, calculated from method 1 and expanding-plane model; - · -, calculated from stationary-sphere model; ·····, calculated from stationary-plane model.

Calculations were restricted to values of the rate parameters where the steady-state approximation is valid, *i.e.*, for $(k_1 + k_2)t \geq 10$. The results are shown in Figure 6. The predictions of method 1 are found to superimpose on those for the expanding-plane model. Values of i_k/i_d given by method 2 are in excellent agreement (<1% error) with those predicted by the rigorous expanding-sphere solution. Errors in the absolute current magnitudes are slightly larger (0.5–3% for method 2), because of an over-rating of the contribution of spherical diffusion. The relative error is reduced substantially upon taking the ratio i_k/i_d because the overemphasis of the effects of spherical diffusion incorporated in expressions for i_k and i_d tends to cancel. This fact is well known and frequently exploited in applications of expanding plane theory to analysis of polarographic data.^{46,47}

When the chemical reaction exerts appreciable rate control ($i_k/i_d < 0.9$), the current magnitudes predicted by method 1 are significantly larger (~9%) than those predicted by the rigorous solution, while method 2 yields appreciably better results as indicated above. The rationale for the failure of method 1 and the relative success of method 2 in this case is essentially the same as given above for similar observations with

the catalytic mechanism. Clearly, method 1 cannot be expected to yield reasonably accurate predictions for mechanisms involving rate control by chemical reactions coupled to the charge-transfer step.

It is of interest to recognize that the spherical correction factors ($1 \pm 44.6D^{1/2}t^{1/6}m^{-1/3}$) originated in the approximate Lingane–Loveridge equation. Oldham, *et al.*, had no other basis on which to assess the magnitude of these factors when they utilized them in their work,¹⁵ since Koutecký's rigorous solution had not been published. Their application in the present study was based on the desire to determine the accuracy of direct, unmodified extensions of the Oldham–Kivalo–Laitinen method. As seen above, method 1 invariably overcorrects for spherical diffusion. This is not surprising since this property is shared by the origin of the "spherical correction factors"—the Lingane–Loveridge equation. One can argue that a more accurate assessment of the appropriate spherical correction factors should be based on Koutecký's rigorous expanding-sphere solution for the polarographic limiting current (eq 16). On this basis, the spherical correction factors would have the form ($1 \pm 39.6D^{1/2}t^{1/6}m^{-1/3}$). We have carried out calculations on this basis. The results show considerable improvement in the predictions of method 1. For reversible or quasi-reversible systems, method 1 with the "improved spherical correction factors" predicts polarographic waves which are almost identical with those given by the rigorous expanding-sphere solutions (errors normally <1.5% in current magnitudes). An improvement in the predictions of method 1 is also obtained for systems with catalytic or preceding chemical reactions, although the results for these cases remain significantly less satisfactory than those produced by method 2.

The foregoing observations indicate that both approximate methods suggested may have considerable merit in appropriate circumstances. The fact that methods 1 and 2 reproduce with good accuracy the predictions of the rigorous theory for diffusion-controlled (reversible) processes is of significance only because it serves as evidence for the tenability of the basic assumptions inherent in the approximate methods. Application of method 1 or 2 to reversible systems appears to have no practical advantage as the available rigorous solution is simple in form and conveniently applicable to experimental data. However, the success of methods 1 or 2 with the more complex mech-

(46) R. Brdička in "Advances in Polarography," Vol. II, I. S. Longmuir, Ed., Pergamon Press, Oxford, England, 1960, pp 655–671.

(47) R. Brdička, *Collection Czech. Chem. Commun. Suppl. II*, 19, 41 (1954).

anistic schemes is quite significant. The fact that method 1 with "improved spherical correction factors" reproduces the predictions of the Koutecký-Čížek rigorous expanding-sphere theory for the quasi-reversible system indicates that the relatively simple relationship

$$i_{es1} = \sqrt{\frac{7}{3\pi t}} \left\{ \frac{nFAC_0^*D_0^{1/2}(1 + 39.6D_0^{1/2}t^{1/6}m^{-1/3}) \times (1 \pm 39.6D_R^{1/2}t^{1/6}m^{-1/3})}{(1 \pm 39.6D_R^{1/2}t^{1/6}m^{-1/3}) + e^j(1 + 39.6D_0^{1/2}t^{1/6}m^{-1/3})} \right\} \times F(\chi^*) \quad (50)$$

where

$$\chi^* = \sqrt{\frac{12}{7}} \lambda^* t^{1/2} \quad (51)$$

$$\lambda^* = \frac{k_b}{D^{1/2}} \left[\frac{e^{-\alpha j}}{(1 + 39.6D_0^{1/2}t^{1/6}m^{-1/3})} + \frac{e^{\beta j}}{(1 \pm 39.6D_R^{1/2}t^{1/6}m^{-1/3})} \right] \quad (52)$$

can be used in place of the very cumbersome expressions associated with the rigorous solution.¹⁹ The error introduced will seldom exceed 1.5%. A further simplification and slight improvement in accuracy (error < 1%) is still possible by recognizing that all terms preceding $F(\chi^*)$ in eq 50 represent the polarographic wave expression for the reversible process within the framework of method 1. These terms may be replaced by the corresponding terms from the rigorous solution (eq 16) to yield the expression

$$i_{es3} = \sqrt{\frac{7}{3\pi t}} \frac{nFAC_0^*D_0^{1/2}}{(1 + e^j)} \times \left\{ \frac{1 \pm \left(\frac{D_R}{D_0}\right)^{1/2} e^j}{1 + e^j} \right\} F(\chi^*) \quad (53)$$

which represents a hybrid of the rigorous solution and method 2 (χ^* is defined by eq 51 and 52).

Results of calculations for mechanisms involving catalytic or preceding coupled chemical reactions indicate that only method 2 can be applied with good accuracy to systems with coupled chemical reactions. Although method 2 produces more cumbersome expressions than method 1, its application normally will provide a much simpler approach to correcting for spherical diffusion than that provided by the rigorous method when coupled chemical reactions are important. The application of method 2 to such systems

normally will provide expressions of significantly better accuracy than the normally applied expanding-plane theory. Use of method 2 in place of the rigorous expanding sphere solution will introduce an error not exceeding 3% (approximately) in most cases for absolute current magnitudes. Substantially better accuracy will be realized in estimating ratios such as i_k/i_d .

The success of method 2 in all cases considered indicates that neglecting coupling of the effects of drop growth and curvature is an approximation of general applicability and reasonable accuracy. On the other hand, the foregoing results show that representing effects of spherical diffusion as corrections on diffusion coefficients of the magnitude $(1 + 39.6D^{1/2}t^{1/6}m^{-1/3})$ (method 1) must be considered reasonably accurate only when the mass transfer process is kinetically unperturbed by coupled chemical reactions. This fact does not preclude the possibility of the existence of a different type of "spherical correction factor" which can be applied as in method 1 and which will effectively account for influences of coupled chemical reactions on the spherical diffusion contribution.

Appendix

Notations and Definitions

A	Electrode area
D_i	Diffusion coefficient of species i
C_i	Concentration of species i
C_i^*	Initial concentration of species i
E°	Standard oxidation-reduction potential in European convention
E_{do}	Applied dc potential
$E'_{1/2}$	Reversible polarographic half-wave potential based on planar diffusion model
F	Faraday constant
R	Ideal gas constant
T	Absolute temperature
n	Number of electrons transferred in the heterogeneous charge-transfer step
t	Time in seconds
r_0	Spherical electrode radius in centimeters
k_b	Apparent heterogeneous rate constant for charge transfer at E°
k_c	Chemical rate constant in catalytic process
k_1, k_2	Forward and reverse chemical rate constants for preceding chemical reaction
K	Equilibrium constant for preceding chemical reaction
m	Mercury flow rate in milligrams per second
α	Charge-transfer coefficient
f_i	Activity coefficient of species i
i_p	The dc polarographic current based on stationary-plane electrode model
i_{ep}	The dc polarographic current based on expanding-plane electrode model
i_s	The dc polarographic current based on stationary-sphere electrode model

i_{es}	The dc polarographic current based on rigorous expanding-sphere solution		solution obtained by combination of method 1 and rigorous solution
i_{es1}	The dc polarographic current based on expanding-sphere solution of approximate method 1	i_{LL}	The dc polarographic limiting current expression of Lingane and Loveridge
i_{es2}	The dc polarographic current based on expanding-sphere solution of approximate method 2	exp	Exponential function
i_{es3}	The dc polarographic current based on expanding-sphere	erf	Error function
		erfc	Error function complement

Heat of Dilution of Some Aqueous Tetraalkylammonium Fluorides¹

by R. H. Wood, H. L. Anderson, J. D. Beck, J. R. France,
W. E. de Vry, and L. J. Soltzberg

University of Delaware, Newark, Delaware (Received December 5, 1966)

The heats of dilution of the compounds R_4NF where $R =$ methyl, ethyl, and n -propyl have been measured from 0.005 to 3 m at 25°. The tetrapropylammonium fluoride has the highest known ϕ_L for a 1-1 electrolyte. The results are explained by cation-cation interactions in which some of the ordered water around the cation is displaced by the neighboring cation.

Aqueous solutions of the tetraalkylammonium halides show many unusual properties²⁻⁷ and these properties can be explained on the basis of an increase in the amount of hydrogen bonding in the water surrounding the cation.⁸⁻¹⁰

For the chloride and bromide salts, Lindenbaum⁶ has found that the heat and entropy effects of this hydrogen bonding are much larger than the free energy effect and, in fact, the heats of dilution are the largest ever measured for a 1-1 electrolyte. It seems to be generally true that this kind of structural effect contributes to the heats and entropies much more than to the free energy.^{11,12}

The purpose of the present work is to extend the measurements of Lindenbaum to include the fluorides. This extension is particularly interesting because the activity coefficients of the fluorides are the highest series known and are quite different from the other halides.

Experimental Section

Preparation of the Tetraalkylammonium Fluorides. The tetraalkylammonium fluorides were prepared

from the corresponding bromides¹³ which were recrystallized and then converted to the hydroxides by passing them through an ion-exchange column. Pre-

(1) This study was aided by a grant from the Office of Saline Water U. S. Department of the Interior.

(2) For a review of earlier evidence, see W. Y. Wen and S. Saito, *J. Phys. Chem.*, **68**, 2639 (1964).

(3) H. G. Hertz and M. D. Zeidler, *Ber. Bunsenges. Physik. Chem.*, **68**, 821 (1964).

(4) (a) R. L. Kay and D. F. Evans, *J. Phys. Chem.*, **69**, 4216 (1965); **70**, 2325 (1966); (b) D. F. Evans and R. L. Kay, *ibid.*, **70**, 366 (1966); (c) R. L. Kay, T. Vituccio, C. Zawoyski, and D. F. Evans, *ibid.*, **70**, 2336 (1966); (d) D. F. Evans, G. P. Cunningham, and R. L. Kay, *ibid.*, **70**, 2974 (1966).

(5) S. Lindenbaum, *ibid.*, **70**, 814 (1966).

(6) W. Y. Wen, S. Saito, and C. Lee, *ibid.*, **70**, 1244 (1966).

(7) W. Y. Wen and S. Saito, *ibid.*, **69**, 3569 (1965).

(8) H. S. Frank and M. W. Evans, *J. Chem. Phys.*, **13**, 307 (1945).

(9) H. S. Frank and W. Y. Wen, *Discussions Faraday Soc.*, **24**, 133 (1957).

(10) H. S. Frank, *Z. Physik. Chem. (Leipzig)*, **228**, 367 (1965).

(11) Y. C. Wu and H. L. Friedman, *J. Phys. Chem.*, **70**, 166 (1966).

(12) H. S. Frank and A. L. Robinson, *J. Chem. Phys.*, **8**, 933 (1940).

(13) Supplied by Distillation Products Industries, Rochester 3, N. Y.

liminary results showed that regenerating the column with 30 equiv of 2 M NaOH for each equivalent of resin would give a product of about 98% purity. However, if regeneration by reverse flow was used, 15 equiv of 2 M NaOH per equivalent of resin gave a product of better than 99.9% purity providing that only 0.5 equiv of salts per equivalent of resin was used. Both Amberlite IRA400¹⁴ and Dowex 2-X4¹⁵ were used successfully in this way. The column should be rinsed with HCl to remove carbonate before using and carbonate-free sodium hydroxide should be used as the regenerant. The hydroxide solution was neutralized with 50% HF to prepare the fluoride solutions.

Analysis. The final solutions were analyzed for R_3NHF and HCO_3^- by titration of 1 M solutions from pH 11 to 8. Comparison with blank runs showed that the total impurities were approximately 0.1, 0.9, and 0.1% for the methyl, ethyl, and *n*-propyl salts, respectively. Titration of the original solution of tetramethylammonium fluoride in the pH 7–8 region showed considerable SiF_6^{2-} which buffers in this region. This impurity was traced to the inadvertent use of glass containers while the pH was below 8. A recrystallization from water reduced the impurity to less than 0.1%. The other solutions were kept in polyethylene containers whenever the pH was below 8. A flame spectrophotometer check on sodium ion impurity showed the tetramethylammonium fluoride contained less than 0.01% Na^+ .

The salts were analyzed for total cation by precipitation and weighing as the tetraphenylborate following the directions of the alkaline procedure of Flaschka and Barnard¹⁶ using four times as much sample and reagents. The results of triplicate determinations agreed to within 0.1% and an analysis of both tetramethylammonium and tetrapropylammonium chloride solutions by this method agreed with the chloride analysis to 0.1%. In this procedure, it was sometimes necessary to refilter the precipitate several times.

The initial stock solutions contained up to 2% excess HF since diluted aliquots liberated this amount of acid. However, the pH of the concentrated solutions (1–3 M) was 9–11. This indicates that there is an interaction between the HF_2^- ion and the tetraalkylammonium ion. In some of the experiments excess tetraalkylammonium hydroxide was added to ensure that the initial solution was above pH 8 so that the solution holder would not be attacked. In addition, the preliminary results with the dewar calorimeter show a large error owing to attack by the acidic final solution. This was corrected by adding additional tetraalkylammonium hydroxide to the initial solution. An alternate procedure using dilute base in-

stead of water in the calorimeter gave comparable results after correcting for the neutralization of the liberated HF. In a few of the very dilute solutions sodium hydroxide was used instead of the corresponding tetraalkylammonium hydroxide to neutralize the acid. Because of the small heat effects in these solutions the error introduced is negligible.

Calorimeters. For the low-concentration runs where high sensitivity was necessary, the twin calorimeter which has been described previously¹⁷ was used. This calorimeter has very high sensitivity (2×10^{-6} deg) and requires 100 ml of solution to load the pipets. Because the sample size was limited, some of the higher concentrations were measured in a 250-ml dewar calorimeter which used samples of from 3 to 10 ml. This calorimeter used as a vessel a commercial glass dewar¹⁸ made from borosilicate glass and available in almost any hardware store. The vessel was attached to a brass collar which was cemented to a ground-glass joint. The vessel has a capacity of 250 ml when filled to within 18 mm of the top. The heat leak constant was 0.0028/min and the response time was such that 99.9% response was achieved 45 sec after heat input was stopped. This quick response was probably due to the thin walls of the dewar.

A 200-rpm stirrer was attached to a 5-mm glass tube in a close-fitting 4.5-in. aluminum bearing. The aluminum was in direct contact with the bath. Even though friction is three or four times higher than with a Teflon bearing, this bearing should allow less heat to go to the vessel because of the large increase in heat conduction to the bath.

Glass ampoules were gripped by a slotted stainless steel tube which was epoxy cemented to a solid glass rod running down inside the stirring shaft.

The heater power supply was a Heathkit Model IP-20,¹⁹ 0–50-v supply (0.01% stability). The timer²⁰ and heater were switched simultaneously with a double-pole, double-throw toggle switch. Tests showed the maximum difference in opening or closing times to be 0.01 sec. The heater consisted of 500 ohms of 0.0025-in. diameter Evanohm wire²¹ in a 5-mm Pyrex tube.

(14) Rohm and Haas Co., Philadelphia 5, Pa.

(15) The Dow Chemical Co., Midland, Mich.

(16) H. Flaschka and A. J. Barnard, Jr., *Advan. Anal. Chem. Instr.*, **1**, 24 (1960).

(17) H. S. Jongenburger and R. H. Wood, *J. Phys. Chem.*, **69**, 4231 (1965).

(18) Thermos replacement filler No. 50F, The American Thermos Bottle Co., Norwich, Conn.

(19) The Heath Co., Benton Harbor, Mich.

(20) Model S1, Standard Electric Time Co., Springfield 2, Mass.

(21) A low-temperature coefficient of resistance wire supplied through the courtesy of the Wilbur B. Driver Co., Newark, N. J.

Two Teflon-coated No. 26 AWG copper wire leads were used. The resistance of these leads was negligible (0.02%).

The temperature was measured with a 2000-ohm thermistor²² in a Wheatstone bridge. The bridge output was amplified with a Beckman Model 14 breaker amplifier and recorded. A temperature sensitivity of 2×10^{-5} deg was attainable.

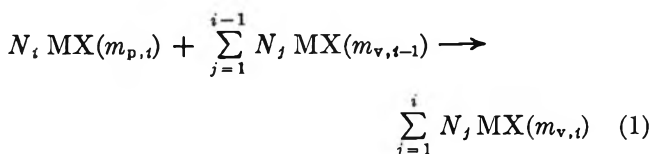
The calorimeter was checked by measuring the heat of addition of 10–15% excess of 0.5 *N* NaOH sealed in a glass ampoule to dilute (about 0.01 *N*) HCl. The results were corrected for the heat of dilution of reactants and products using the data of Vanderzee and Swanson.²³ The results of four runs were a heat of neutralization of 13.355 cal/mole and a standard deviation of a single run of 0.25%. This compares with the value 13.34 ± 0.02 cal/mole of Hale, Izatt, and Christensen²⁴ and Vanderzee and Swanson.²³

As an additional check the heat of adding tris(hydroxymethyl)aminomethane to 0.1110 *N* HCl was measured. The result of five measurements was 7117 cal/mole with a standard deviation of a single experiment of 0.25%. This compares with the value of 7107 cal/mole recommended by Gunn²⁵ and by Wadso.

Results and Discussion

The results of the measurements with the twin calorimeter are given in Table I.

The equation for the reaction upon opening the *i*th pipet



where N_i moles of the salt MX (molality $m_{p,i}$) in the *i*th pipet to be opened are mixed with the sum of the number of moles in the preceding pipets at a molality in the vessel $m_{v,i-1}$ to give a final solution of molality $m_{v,i}$. The heat of mixing for this process is

$$q_i = N_i[\phi_L(m_{p,i}) - \phi_L(m_{v,i})] + \sum_{j=1}^{i-1} N_j[\phi_L(m_{v,i-1}) - \phi_L(m_{v,i})] \quad (2)$$

If the pipets all contain solutions of the same molality (m_p), the results can be combined to give

$$\sum_{i=1}^i q_i = \sum_{j=1}^i N_j[\phi_L(m_p) - \phi_L(m_{v,i})] \quad (3)$$

These runs were combined to give heats of dilution in the low-concentration region and the results were fitted to an extended Debye-Hückel equation. The

method of combining the data and least-square fitting have been described previously.¹⁷ The results of the fit are given in Table II.

The values of $\phi_L(m_{p,i}) - \phi_L(m_{v,i})$ given in column 6 of Table I were calculated from eq 3 if the molality in the pipet was constant and from eq 2 if the molality varied. Values of $\phi_L(m_{v,i-1}) - \phi_L(m_{v,i})$ for use in eq 2 and the values of $\phi_L(m_{v,i})$ in column 7 were derived from the extrapolation or, for data outside of the range of the extrapolation, from large-scale plots of ϕ_L vs. m . The values of $\phi_L(m_{p,i})$ in columns 8 and 9 are calculated from data in columns 6 and 7.

The results of the runs with the 250-ml dewar calorimeter are given in Table III. The values of ϕ_L final were obtained from the least-squares extrapolation of the low-dilution data.

Because of the difficulty in preparing pure salts and the possibility of some corrosion of the calorimeter, the data may have errors as high as 10 cal/mole and 1% of the total heat. The low-concentration runs with the tetra-*n*-propylammonium fluoride do not connect smoothly with the high-concentration runs so that there might have been a reaction with the glass pipets during the long time necessary for temperature equilibration in this calorimeter. This would affect only the ϕ_L values below 1 *m*.

Results and Discussion

The results of the measurements are given in Table IV. A comparison of these results with the results for the other halides⁵ (Figure 1) shows that the tetraalkylammonium fluorides have higher apparent molal heat contents than any other series. Except for the tetraethylammonium bromide at low concentrations there is a regular increase in ϕ_L in going from the iodide to the fluoride and in going from tetramethylammonium to tetrapropylammonium. There is a much larger difference between the activity coefficients of the fluoride and chloride than between the chloride and bromide³ and this same behavior is observed in the values of ϕ_L . For instance, at 3 *m* the values of ϕ_L for the tetraethylammonium fluoride, chloride, and bromide are 1302, -502, and -902 cal/mole, respectively.

Frank and Robinson¹² have explained the entropies of dilution of aqueous electrolytes using the changes in the overlap of the hydration spheres of the oppositely charged ions as the salt is diluted. In the case of the

(22) No. 32A1, Victory Engineering Corp., Springfield, N. J.

(23) C. E. Vanderzee and J. A. Swanson, *ibid.*, **67**, 2608 (1963).

(24) J. D. Hale, R. M. Izatt, and J. J. Christensen, *J. Phys. Chem.*, **67**, 2605 (1963).

(25) S. R. Gunn, *ibid.*, **69**, 2902 (1965).

Table I: Calorimetric Data from Twin Calorimeter at 25°

Pipet ^a	$N_{i,i}$ mmoles	$m_{p,i}$	$m_{v,i}$	q_i cal	$\phi_L(m_{p,i}) -$ $\phi_L(m_{v,i})$, cal/mole	$\phi_L(m_{v,i})$, cal/mole	$\phi_L(m_{p,i})$, cal/mole	\bar{A}_v $\phi_L(m_{p,i})$, cal/mole
(A) $(CH_3)_4NF$								
L1	4.222	0.1968	0.00602	0.325	77.0	33.4	110.4	114
L3	4.211	0.1968	0.01167	0.267	70.2	44.7	114.9	
L2	4.225	0.1968	0.01701	0.218	64.0	52.4	116.4	
L4	4.238	0.1968	0.02207	0.128	55.5	58.1	113.5	
R3	4.225	0.1977	0.00602	0.323	76.4	33.4	109.8	112
R1	4.222	0.1977	0.01169	0.235	66.1	44.8	110.9	
R2	4.220	0.1977	0.01702	0.206	60.3	52.4	112.7	
L1	12.19	0.5925	0.01741	1.226	100.5	52.9	153.4	
L3	12.27	0.5925	0.03392	0.719	79.5	68.1	147.6	151
L2	12.25	0.5925	0.04948	0.737	73.1	77.1	150.2	
L4	12.28	0.5925	0.06424	0.624	67.5	82.8	151.3	
R4	12.26	0.5925	0.01749	1.173	95.7	53.0	148.7	
R2	12.27	0.5925	0.03401	0.891	84.1	68.2	152.3	431
R3	12.30	0.5925	0.04963	0.665	74.1	77.1	151.2	
R1	12.25	0.5925	0.06434	0.590	67.6	82.8	150.4	
L1	47.35	2.997	0.06806	16.382	346.0	84.2	430.2	
L3	33.19	1.974	0.1130	5.658	189.3	97.4	286.7	287
L2	19.91	0.995	0.1371	1.368	90.2	102.7	192.9	
R4	51.74	2.997	0.0742	17.850	345.0	86.3	431.3	
R2	36.85	1.974	0.1237	6.216	187.9	100.0	287.9	
R3	19.98	0.995	0.1475	1.346	88.0	104.8	192.8	193
(B) $(CH_3CH_2)_4NF$								
L1	1.870	0.0876	0.002666	0.125	66.9	24.3	91.2	80.7
L3	1.884	0.0876	0.005192	0.038	43.4	33.6	77.0	
L2	1.884	0.0876	0.007573	0.062	39.9	40.2	80.1	
L4	1.886	0.0876	0.009823	0.038	35.0	45.4	80.4	
R4	1.884	0.0874	0.002685	0.122	64.8	24.3	89.1	82.5
R2	1.884	0.0874	0.005211	0.047	44.9	33.6	78.5	
R3	1.881	0.0874	0.007587	0.062	40.9	40.3	81.2	
R1	1.885	0.0874	0.009833	0.058	38.4	45.5	83.9	
L1	9.504	0.4658	0.01357	1.523	160.2	52.6	212.8	213.2
L3	9.495	0.4658	0.02636	1.178	142.2	69.5	211.7	
L2	9.510	0.4658	0.03846	1.130	134.4	79.4	213.8	
L4	9.358	0.4658	0.04974	1.028	128.3	85.3	213.6	
R4	9.455	0.4669	0.01350	1.594	168.6	52.5	221.1	220.1
R2	9.239	0.4669	0.02596	1.236	151.4	69.1	220.5	
R3	9.557	0.4669	0.03815	1.157	141.1	79.2	220.3	
R1	9.494	0.4669	0.04960	1.081	134.3	85.2	219.5	
(C) $(CH_3CH_2CH_2)_4NF$								
L1	2.019	0.0948	0.002878	0.249	123.4	24.4	147.8	149
L3	2.027	0.0948	0.005598	0.239	120.6	33.8	154.4	
L2	2.025	0.0948	0.008159	0.186	111.0	40.7	151.7	
L4	2.020	0.0948	0.01057	0.117	97.4	46.4	143.8	
R4	2.020	0.0950	0.002880	0.275	136.2	24.4	160.6	158
R2	2.036	0.0950	0.005612	0.235	125.7	33.8	159.5	
R3	2.027	0.0950	0.008175	0.191	115.2	40.8	156.0	
R1	2.034	0.0950	0.01060	0.201	111.1	46.5	157.6	
L1	5.635	0.2733	0.008043	1.835	325.6	40.4	366.0	363
L3	5.637	0.2833	0.01563	1.602	304.9	56.8	361.7	
L2	5.637	0.2733	0.02279	1.501	292.0	69.5	361.5	
L4	5.627	0.2733	0.02956	1.424	282.3	80.4	362.7	

Table I (continued)

Pipet ^a	$N_{i,}$ mmoles	$m_{p,i}$	$m_{v,i}$	g_i cal	$\phi_L(m_{p,i}) -$ $\phi_L(m_{v,i}),$ cal/mole	$\phi_L(m_{v,i}),$ cal/mole	$\phi_L(m_{p,i}),$ cal/mole	Av $\phi_L(m_{p,i}),$ cal/mole
R4	5.634	0.2735	0.008041	1.843	327.1	40.4	367.5	365
R2	5.632	0.2735	0.01562	1.640	309.2	56.7	365.9	
R3	5.648	0.2735	0.02280	1.498	294.5	69.5	364.0	
R1	5.634	0.2735	0.02957	1.412	283.5	80.4	363.9	
L1	14.48	0.7757	0.02073	13.040	900.4	66.0	966.4	
L3	14.59	0.7757	0.04052	12.311	871.9	97.0	968.9	970
L2	14.64	0.7757	0.05936	11.466	842.3	124.2	966.5	
L4	14.59	0.7757	0.07720	11.094	821.8	149.7	971.5	
R4	14.57	0.7757	0.02086	13.193	905.2	66.2	971.4	
R2	14.61	0.7757	0.04067	12.335	874.7	97.2	971.9	
R3	14.66	0.7757	0.05953	11.713	849.4	124.5	973.9	
R1	14.59	0.7757	0.07737	10.591	818.5	150.0	968.5	

^a The letters indicate the left or right vessel and the numbers indicate the pipet opened. The order of opening in a vessel is from the top down.

Table II: Least-Squares Fit of Low-Concentration Data

$$\phi_L = 707 m^{1/2} [1 / (1 + Am^{1/2}) - \sigma(Am^{1/2})/3] + Bm + Cm^{3/2}$$

	A	B	C	Concn range, M
$(\text{CH}_3)_4\text{NF}$	1.0	-150.48	-495.31	0.006-0.064
$(\text{C}_2\text{H}_5)_4\text{NF}$	1.0	675.27	-3329.52	0.003-0.09
$(\text{C}_3\text{H}_7)_4\text{NF}$	1.0	-148.81	2378.51	0.003-0.10

tetraalkylammonium ions, Frank and Wen⁹ postulate large flickering clusters of hydrogen-bonded water molecules in the hydration sheaths. Lindenbaum's measurements of the heats of dilution of the tetraalkylammonium chlorides, bromides, and iodides showed that the interactions of the larger tetraalkylammonium ions are dominant since the heats of dilution and entropies of dilution are relatively independent of the anion.⁵ This result is in accord with the heat of mixing measurements of Wood and Anderson²⁶ which show that the interactions between the larger tetraalkylammonium ions give high heats of mixing.

The present results are explained by the changes in the overlap of the cage-like structures around the tetraalkylammonium ions as the salt is diluted. Then the more highly hydrogen-bonded regions around the tetraalkylammonium ions are completed because there is less overlap and thus there is more total hydrogen bonding. This increase in structure causes the observed heating of the solution. It also causes an increase in the volume of the solution because of the larger volume of the more hydrogen-bonded water.

From their partial molal volume data Wen and Saito² postulated that the water clusters join up at higher con-

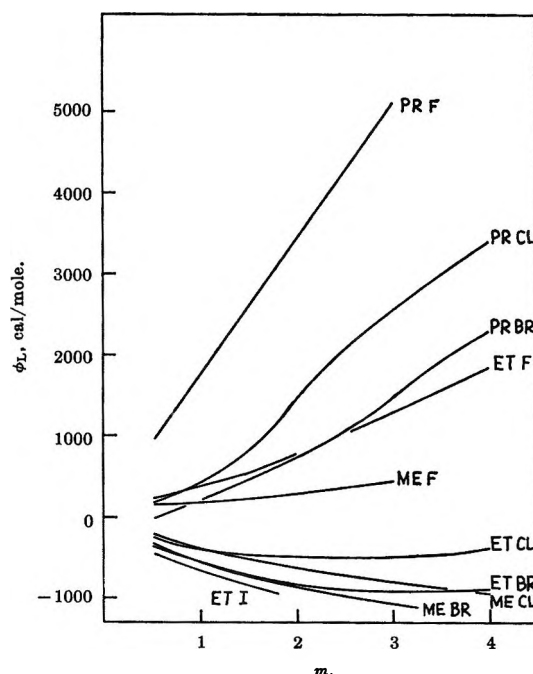


Figure 1. Relative apparent molal heat content (ϕ_L) plotted against molality for the tetraalkylammonium halides. The symbol ETCL stands for the tetraethylammonium chloride and so on.

centrations and force the large cations and anions to get inside. This is in accord with the "structural salting in" of the large cations for each other. The heat of dilution data require that as the clusters join up (overlap) there be less total hydrogen bonding.

(26) R. H. Wood and H. L. Anderson, *J. Phys. Chem.*, 71, 1817 (1967).

Table III: Results with the Dewar Calorimeter

Initial soln, <i>m</i>	Salt, mmoles	Final soln, <i>m</i>	<i>q</i> , cal	$\Delta\phi_L$, cal/mole	ϕ_L final, cal/mole	ϕ_L initial, cal/mole
A. $(C_2H_5)_4NF$						
1.000	8.883	0.0343	2.735	307.9	78.6	386.5
1.000	8.200	0.0318	2.554	311.5	76.8	388.3
1.000	7.865	0.0306	2.417	307.3	75.7	383.0
1.000	4.985	0.0196	1.569	314.7	63.8	378.5
						Av 384
2.001	10.14	0.0398	7.134	703.6	82.3	785.9
2.001	10.12	0.0397	7.159	707.1	82.3	789.4
2.001	10.25	0.0402	7.222	704.6	82.4	787.0
2.001	10.42	0.0408	7.350	705.4	82.7	788.1
						Av 788
3.000	9.18	0.0363	11.205	1220	80.0	1300
3.000	9.27	0.0720 ^a	11.097	1197	88 ^a	
3.000	9.02	0.0356	11.029	1223	79.5	1303
3.000	9.57	0.0726 ^a	11.442	1195	91 ^a	
						Av 1302
3.999	9.73	0.0386	17.436	1792	81	1873
3.999	8.71	0.0346	15.631	1794	79	1873
3.999	10.34	0.0410	18.504	1789	83	1872
						Av 1873
B. $(CH_3CH_2CH_2)_4NF$						
1.000	5.919	0.0231	10.061	1700	69	1769
1.000	4.517	0.0177	7.632	1690	60	1750
						Av 1760
2.000	8.797	0.0346	28.10	3194	87	3281
2.001	9.833	0.0386	31.28	3182	93	3275
2.001	6.405	0.0253	20.38	3182	73	3255
						Av 3270
3.075	6.215	0.0247	31.95	5140	72	5212
3.013	8.011	0.0317	41.01	5119	83	5202

^a In these experiments the bulb was broken in the solution left after the experiment directly above. ϕ_L final is calculated from the results of both experiments using eq 3 and is an independent check of the results of the low-concentration experiments.

Table IV: Values of ϕ_L (cal/mole) at Various Concentrations at 25°

<i>m</i>	$(CH_3)_4NF$	$(C_2H_5)_4NF$	$(n-C_3H_7)_4NF$
0.01	42	47	45
0.02	56	64	64
0.04	72	82	95
0.06	81	89	124
0.08		89	152
0.20	113		
0.50	142	226	
1.00	193	384	1760
2.00	290	788	3269
3.00	431	1302	5115
4.00		1874	

Frank¹⁰ postulated that the cation with a cage has a smaller volume than the cation without a cage and that as the concentration is increased the cages link

up and stabilize each other, thus increasing their half-lives and decreasing the volume. As before, the heat of dilution results require a smaller number of hydrogen bonds in the concentrated solutions so that if the half-lives of the cages are increased, there must be a decrease in the total number of water molecules involved. The decrease in volume is then naturally explained by the lower number of water molecules involved in hydrogen bonding.

The present explanation is also supported by the results of Wen and Saito,⁷ who found that the partial molal volume of the tetrakis(2-hydroxyethyl)ammonium ion is only slightly larger than the tetraethylammonium ion in aqueous solutions ($\bar{V}_2 = 151.7$ and 149.6 ml, respectively). The similarity in volumes of these two ions is explained by the high volume of the structural water around the hydrocarbon tails. This structure is destroyed by the hydroxyl ions which

fit in to the normal hydrogen-bonded structure of the water.^{9,27}

Franks and Smith²⁸ explained the increase in volume of sodium dodecyl sulfate solutions below the critical miscible concentration by the loss of structural water on forming dimers. This is in agreement with the present interpretation of the behavior of the tetraalkylammonium ions.

In the case of the fluorides, the present model predicts an additional gain in structure on dilution since the fluoride is a structure-making ion.⁸ The chloride and bromide would be expected to give structure-breaking contributions since these ions are structure breakers.⁸ On this basis, the order for ϕ_L of $F^- > Cl^- > Br^- > I^-$ is correctly predicted. Some unpublished calculations of Wu and Friedman²⁹ indicate that in the 1-3 *m* region overlap will be approximately

proportional to concentration and the ++, --, and +- overlap will all make significant contributions. The calculation explains the large contribution of the overlap of two tetraalkylammonium ions to the heat of dilution and also explains the rough linearity of ϕ_L vs. *m* plots in this concentration range for the higher members of the series where the overlap is the main contribution to the value of ϕ_L .

Acknowledgment. The authors wish to acknowledge the help of Mr. J. W. Jackson, Mr. C. J. Twardowski, Mr. J. R. Ward, and Mr. D. E. Werner in constructing the dewar calorimeter used in this work.

(27) L. A. D'Orazio and R. H. Wood, *J. Phys. Chem.*, **67**, 1435 (1963).

(28) F. Franks and J. T. Smith, *ibid.*, **68**, 3581 (1964).

(29) See ref 11, footnote 31.

Vaporization of Some Amine-Type Perchlorates¹

by J. L. Mack and G. B. Wilmot

Research and Development Department, Naval Ordnance Station, Indian Head, Maryland 20640
(Received December 6, 1966)

Ammonium perchlorate, hydroxylammonium perchlorate, methylammonium perchlorate and hydrazine perchlorate have been shown by the cold matrix isolation-infrared spectroscopic technique to vaporize by dissociation; *i.e.*, $RNH_3ClO_4 \rightarrow RNH_2(g) + HClO_4(g)$. The relative vaporization temperatures of these salts can be correlated with the *pK* values of the bases in aqueous solution. Evidence is presented that this proton transfer reaction plays an important role in the thermal decomposition of hydrazine diperchlorate and guanidinium perchlorate.

The proton-transfer mechanism has been postulated to play an important role in the thermal decomposition of ammonium perchlorate.^{2,3} While it has long been known that this mechanism is also involved in the vaporization of the ammonium halides,⁴ Galwey and Jacobs² have proposed that, since perchloric acid is an exceptionally strong acid, the sublimation of ammonium perchlorate may proceed without dissociation to give an ammonium perchlorate vapor species.

However, by the matrix isolation-infrared spectroscopic method, we were able to show that the vaporization

(1) This work was funded under the Foundational Research Program of the Director of Naval Laboratories.

(2) A. K. Galwey and P. W. M. Jacobs, *J. Chem. Soc.*, 837 (1959).

(3) R. D. Schultz and A. O. Dekker, "Sixth Symposium (International) on Combustion," Reinhold Publishing Corp., New York, N. Y., 1957, p 618.

(4) W. R. Rodebush and J. C. Michalek, *J. Am. Chem. Soc.*, **51**, 743 (1929).

zation of ammonium perchlorate proceeds *via* a proton-transfer reaction to yield ammonia and perchloric acid as vapor species.⁵ Recently, Heath and Majer⁶ have shown mass spectrometrically that sublimation proceeds *via* dissociation. Cassel and Liebman⁷ and Inami, *et al.*,⁸ have given indirect evidence for vaporization by dissociation. We describe here the further application of the matrix-isolation method to the determination of the vapor species of a variety of amine perchlorates.

The matrix-isolation method was chosen for these studies since it is a direct method whereby vapor species are trapped without further reaction in a frozen matrix of some inert gas for identification by infrared spectroscopy. This method was considered to be more promising for the detection of a weakly associated complex than mass spectrometry where complete dissociation of a complex or free base by electron impact is a possibility.

Experimental Section

Compounds. Ammonium perchlorate (AP) was taken from clear portions of single crystals grown in aqueous solution by slow isothermal evaporation at 34° from once-recrystallized reagent grade ammonium perchlorate. Hydrazine dperchlorate (HP₂) of 99% purity was used as received. Hydrazine perchlorate (HP) was synthesized *in situ* by thermal decomposition of hydrazine dperchlorate in an evacuated Pyrex effusion cell at temperatures up to 135°. Hydroxylammonium perchlorate (HAP) and guanidinium perchlorate (GP) were twice recrystallized from ethanol-chloroform solutions. Methylammonium perchlorate (MAP) was synthesized by the addition of dilute perchloric acid to an aqueous solution of methylamine. The water was pumped off and the product twice recrystallized from ethanol-chloroform solution.

Spectroscopic Method. The matrix isolation technique^{9,10} has found wide application to the spectroscopic study of reactive species. The technique has been elaborated by Weltner and Warn¹¹ and Linevsky¹² for the determination of the spectra of the high-temperature species of a wide variety of compounds and reactions. Our methods and equipment were similar to those of these latter workers. A few hundred milligrams of the salt was placed in a Pyrex cell 2.0-cm × 1.2-cm diameter. One end was closed and the other open with a 7-mm diameter orifice facing an infrared transmitting window cooled to 7–10°K. The cell was heated resistively and the temperature monitored by a copper-constantan thermocouple in contact with the external wall of the cell. The temperature required to deposit in 30 min sufficient material for spectral

observation was determined by a separate vacuum vaporization experiment. The cell was heated to this temperature and the effusing species together with a large excess of nitrogen were condensed onto the cold window. The window was cooled in a metal cryostat of the type usual for spectral studies.¹¹ Ratios of matrix gas to active species in the range 500–1500 were used. At the conclusion of the deposition, the window was rotated 90° about a vertical axis into the infrared beam. The spectrum was recorded by a double-beam grating spectrophotometer over the range 250–4000 cm⁻¹.

The matrix-isolated spectra of ammonia and perchloric acid were recorded for comparison purposes. The ammonia deposit was obtained by premixing the matrix gas and ammonia in the ratio 700:1 and depositing the mixture over a 30-min period. Anhydrous perchloric acid was prepared by the method of Smith¹³ and distilled into a calibrated capillary tube for volume determination. The capillary was opened to a tube directed toward the cold window onto which the nitrogen matrix gas simultaneously impinged. The flow rate of the perchloric acid was controlled by a thermostated bath and by the length and diameter of the connecting tube. The HClO₄/N₂ ratio was 1:600.

Results and Discussion

From a comparison of the spectra of matrix-isolated ammonia and perchloric acid with that of the matrix-isolated vapor species from AP (Figures 1 and 2), it is clear that the principal vapor species of AP at this temperature (180°) are perchloric acid and ammonia. The spectrum of the vapor species from HAP at 120° (Figure 1) clearly shows perchloric acid and the bands at 3640, 1604, 1364, 1132, and 893 cm⁻¹ agree well with the hydroxylamine gas-phase bands of Giguere and Liu¹⁴ at 3656, 1605, 1125, 1115, and 896 cm⁻¹ if small matrix shifts are permitted. It should be noted that the spectrum of perchloric acid contains impurity bands at 2855 (HCl), 2350 (CO₂), 1525 (unidentified),

(5) J. L. Mack, A. S. Tompa, and G. B. Wilmot, *Spectrochim. Acta*, **18**, 1375 (1962).

(6) G. A. Heath and J. R. Majer, *Trans. Faraday Soc.*, **60**, 1783 (1964).

(7) H. M. Cassel and I. Liebman, *J. Chem. Phys.*, **34**, 343 (1961).

(8) S. H. Inami, W. A. Rosser, and H. Wise, *J. Phys. Chem.*, **67**, 1077 (1963).

(9) E. Whittle, D. A. Dows, and G. C. Pimentel, *J. Chem. Phys.*, **22**, 1943 (1954).

(10) E. D. Becker and G. C. Pimentel, *ibid.*, **25**, 224 (1956).

(11) W. Weltner, Jr., and J. R. W. Warn, *ibid.*, **37**, 292 (1962).

(12) M. J. Linevsky, *ibid.*, **34**, 587 (1961).

(13) G. G. Smith, *J. Am. Chem. Soc.*, **75**, 184 (1953).

(14) P. A. Giguere and I. D. Liu, *Can. J. Chem.*, **30**, 948 (1952).

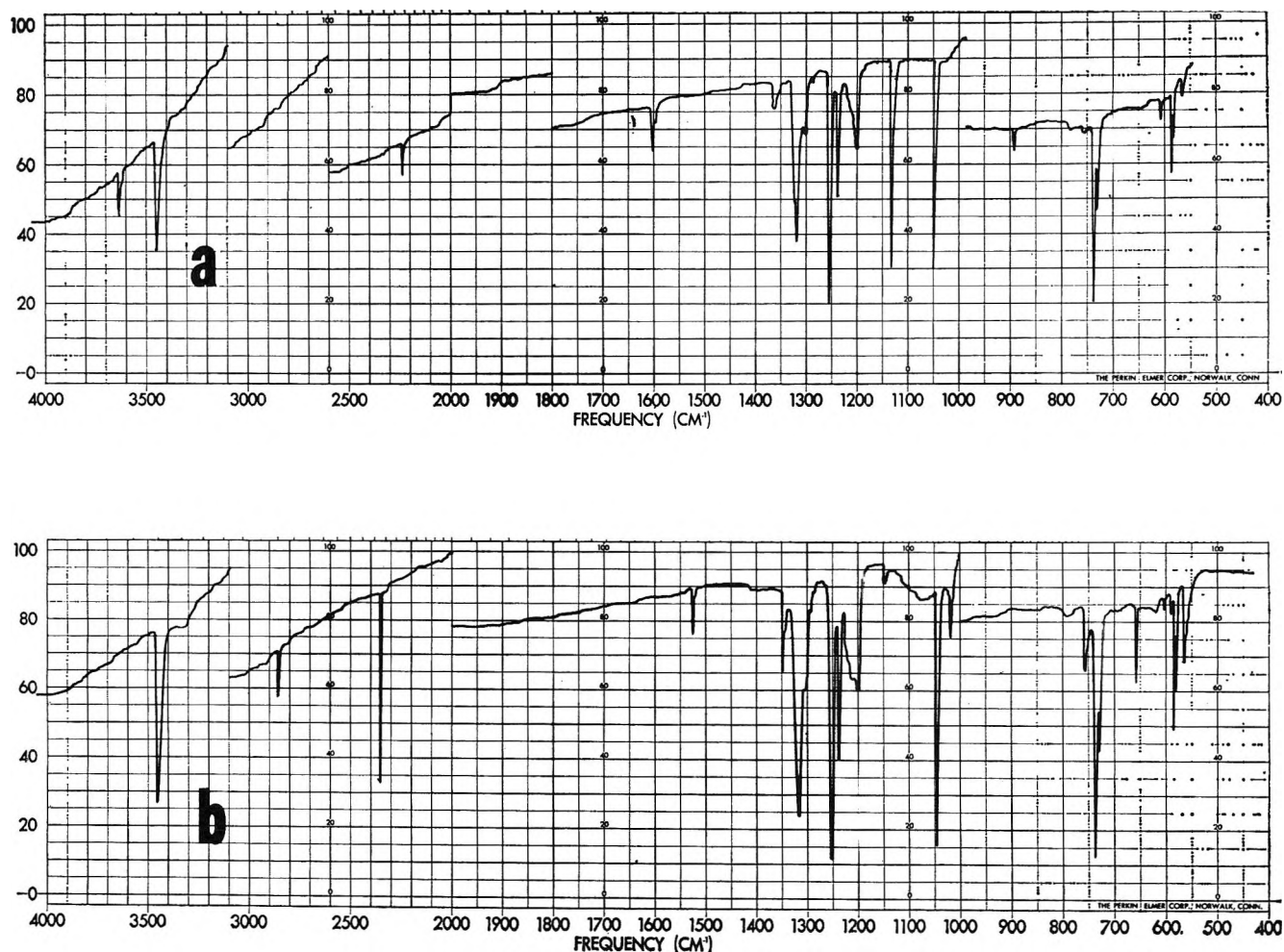


Figure 1. (a) Spectrum of matrix-isolated hydroxylammonium perchlorate vapor species; (b) spectrum of matrix-isolated perchloric acid.

and 662 cm^{-1} (CO_2). The ammonia spectrum contains impurity bands at 3727 (H_2O), 2350 (CO_2), 1600 (H_2O), 662 (CO_2), and 612 cm^{-1} (instrumental). For the AP spectrum, except for three very weak, unidentified bands in the $1100\text{--}1200\text{ cm}^{-1}$ region, the only bands found other than ammonia and perchloric acid were shown to be weak or moderate intensity bands of H_2O , N_2O , and CO_2 . CO_2 is a frequent impurity in our trapping experiments and N_2O and H_2O are well-known low-temperature decomposition products of AP.¹⁵ Besides the bands of hydroxylamine and perchloric acid, the spectrum of the HAP vapor products showed only N_2O and H_2O in relatively small amounts which can arise from the decomposition of hydroxylamine.¹⁶

Although the spectra of hydrazine perchlorate and methylammonium perchlorate showed evidence of more extensive thermal decomposition, the major species were shown to be the free bases and perchloric acid.

The free bases were identified from the matrix-isolated spectra of hydrazine¹⁷ and methylamine.¹⁸

Hydrazine diperchlorate had a relatively high vapor pressure at low temperatures ($50\text{--}100^\circ$) and the vapor species proved to be mainly perchloric acid and water. Upon prolonged heating to 135° , evolution of water and perchloric acid ceased, leaving a residue of HP. The water was an impurity in the very hygroscopic HP_2 and the salt was thus shown to decompose to give perchloric acid vapor and HP. The dissociation was catalyzed by the water since the vaporization temperature increases as the water is driven off.

Although the spectrum of the vapor products of

(15) L. L. Bircumshaw and B. H. Newman, *Proc. Roy. Soc. (London)*, **A227**, 115 (1954).

(16) K. A. Hofmann and F. Kroll, *Chem. Ber.*, **B57**, 937 (1924).

(17) E. Catalano, R. H. Sanborn, and J. W. Frazer, *J. Chem. Phys.*, **38**, 2265 (1963).

(18) J. R. Durig, private communication.

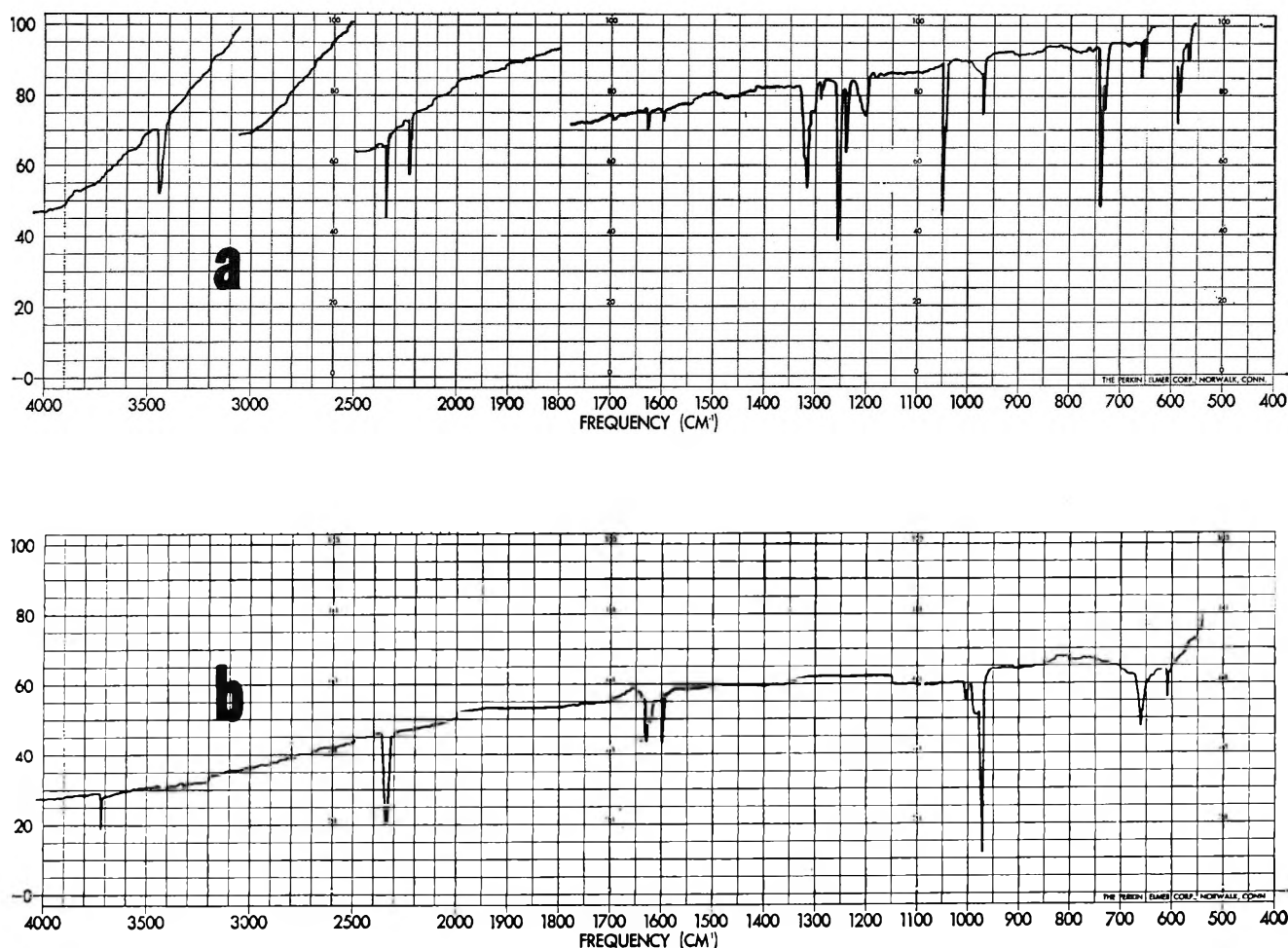
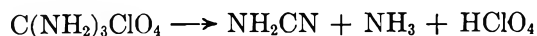


Figure 2. (a) Spectrum of matrix-isolated ammonium perchlorate vapor species; (b) spectrum of matrix-isolated ammonia.

guanidinium perchlorate showed large amounts of perchloric acid, no guanidine was detected. However, in addition to other products, ammonia in roughly a 1:1 mole ratio with perchloric acid and cyanamide was detected. There was some evidence for condensation products of cyanamide. These products support the decomposition mechanism of GP proposed by Glasner and Makovsky¹⁹



Recently we have trapped the vapor species from several guanidinium salts.²⁰ The entire series studied follows the vaporization temperature-acid strength relationship discussed below. For those salts which vaporize at the lowest temperatures, complete vaporization to guanidine and free acid was found with no evidence for decomposition. Salts vaporizing at intermediate temperatures gave both guanidine and decomposition products, while, at the highest temperature, GP gave

only guanidine decomposition products and HClO_4 . Thus, it appears that proton transfer is the initial step for both vaporization and decomposition and, at the highest temperature, the decomposition reaction predominates with the free guanidine breaking down as fast as it is formed.

By the matrix isolation-infrared spectroscopic method, direct evidence has been obtained in this study that AP, HAP, MAP, and HP vaporize by proton transfer



and that the proton-transfer reaction also is important in the decomposition of GP and HP_2 . While, in nearly all cases, weak unidentified bands were found, the intensities of these bands increased more rapidly with increasing temperature than those of the free base and

(19) A. Glasner and A. Makovsky, *J. Chem. Soc.*, 182 (1953).

(20) J. L. Mack, presented at 153rd National Meeting of the American Chemical Society, Miami Beach, Fla., April 1967.

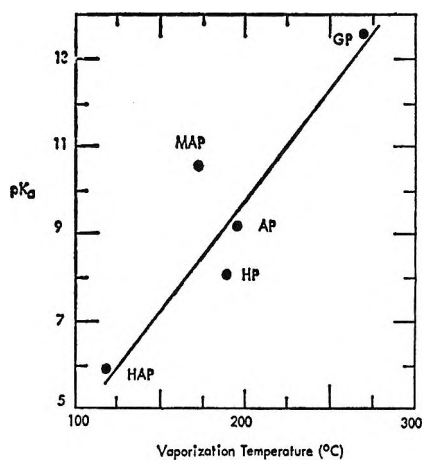


Figure 3. Vaporization temperature *vs.* pK_a (pK_a values from H. K. Hall, Jr., *J. Am. Chem. Soc.*, **79**, 5441 (1957) and N. F. Hall and M. R. Sprinkle, *ibid.*, **54**, 3469 (1932)).

perchloric acid and thus could not be assigned to a complex RNH_3-ClO_4 vapor species. Such a vapor species would have a lower heat of vaporization and hence increase less rapidly with temperature than the dissociation products.

By adjusting the temperature required to produce a given intensity of the perchloric acid spectrum in a given time, it is possible to define a "vaporization temperature" for each compound. This temperature is a temperature at which the compound has a vapor pressure of roughly 10^{-4} torr. Figure 3 shows the rela-

tionship between this temperature and the pK values of the free bases in aqueous solution for several of the perchlorates studied. Although no guanidine was found in the vapor products of GP, the vaporization temperature of GP is included in Figure 3 since proton transfer appears to be the controlling step for the decomposition of GP and no $HClO_4$ decomposition was noted.

It is evident that there is a correlation between proton-transfer equilibria in solution (pK) and those in vaporization (vapor pressure). The relative stabilities with respect to vaporization follow the order of the pK values in every case except methylammonium perchlorate which has a higher vapor pressure than this relation would predict. A similar relation between the acid strength and volatility exists. Thus, Markowitz and Boryta²¹ find sublimation temperatures of the ammonium halides to be in order $NH_4Cl < NH_4Br < NH_4I$ and we find for some guanidinium (G) salts the order $GOH < G_2CO_3 < GCl < GBr < GClO_4$.²⁰ The volatilities of the salts in both series decrease with increasing acid strength.

This relationship, while not of high accuracy, may be of value in predicting the relative volatilities of new amine salts and, where the decomposition also proceeds *via* proton transfer, in estimating the relative thermal stabilities with respect to degradation.

(21) M. M. Markowitz and D. A. Boryta, *J. Phys. Chem.*, **66**, 1477 (1962).

Carbon-13 Chemical Shifts of the Carbonyl Group. V. Observation of a Deuterium Isotope Effect Using Carbon-13 Field-Frequency Lock^{1,2}

by Gary E. Maciel, Paul D. Ellis, and Donald C. Hofer

Department of Chemistry, University of California, Davis, California (Received December 7, 1966)

An isotope effect of -0.28 ppm on the ^{13}C chemical shift of the carbonyl group in acetone- d_6 with respect to that of acetone has been observed. This result is discussed from a basic vibrational point of view and in the popular language of isotope substituent effects. A useful method for observing ^{13}C magnetic resonance spectra based on a direct ^{13}C field-frequency lock system is described.

Introduction

Secondary deuterium isotope effects have received considerable attention during the past few years, particularly from the point of view of understanding their basis and their relationship to studies of mechanisms of chemical reactions.³⁻⁶ In addition to the kinetics and equilibrium studies where they are most frequently observed and employed, such effects have been known for some time in proton and fluorine magnetic resonance spectra.⁷⁻¹⁴ In view of recent demonstrations of a rather sensitive relationship between ^{13}C chemical shifts of the carbonyl group and the structural details of the corresponding carbonyl compounds^{1,15-20} it became of interest to us to learn the influence of α -deuterium substitution on this physical parameter for a representative ketone. Carbonyl- ^{13}C shieldings have been studied in some detail both experimentally and theoretically²¹ so that a meaningful interpretation of the results could be anticipated. With the recent development in our laboratories and elsewhere of precise and sensitive ^{13}C magnetic resonance techniques a practical capability exists for the first time for determining small effects such as the expected isotope influences.

Experimental Section

Nmr Measurements. The method employed in our experiments used a standard Varian HA-100 spectrometer operating at 23.5 kgauss and 25.1 MHz and a C1024 time-averaging computer which enabled us to record the computer memory from many repetitive frequency-sweep scans. The spectrometer stability

necessary for effective time averaging was due to a field-frequency control lock signal provided by a capillary (1.2-mm i.d.) containing a ^{13}C -labeled (55%) material. The field-frequency stability resulting from this simple application of a ^{13}C lock signal from an ex-

(1) This investigation was supported by a PHS research grant (GM-11439-03) from the National Institute of General Medical Science, U. S. Public Health Service.

(2) Paper IV of this series: G. E. Maciel and D. D. Traficante, *J. Am. Chem. Soc.*, **88**, 220 (1966).

(3) E. R. Thornton, *Ann. Rev. Phys. Chem.*, **17**, 349 (1966).

(4) E. A. Halevi, *Progr. Phys. Org. Chem.*, **1**, 109 (1963).

(5) E. A. Halevi, M. Nussin, and A. Ron, *J. Chem. Soc.*, 866 (1963).

(6) E. A. Halevi and M. Nussin, *ibid.*, 876 (1963).

(7) D. D. Traficante and G. E. Maciel, *J. Am. Chem. Soc.*, **87**, 4917 (1965).

(8) G. V. D. Tiers, *ibid.*, **79**, 5585 (1957).

(9) G. V. D. Tiers, *J. Chem. Phys.*, **29**, 963 (1958).

(10) H. Kusumoto, T. Itoh, K. Horota, and J. Ueda, *Nippon Seirigaku Zasshi*, **15**, 728 (1960).

(11) T. W. Marshall, *Mol. Phys.*, **4**, 61 (1961).

(12) H. S. Gutowsky, *J. Chem. Phys.*, **31**, 1683 (1959).

(13) E. B. Whipple, W. E. Stewart, G. S. Reddy, and J. A. Goldstein, *ibid.*, **34**, 2136 (1961).

(14) M. Saunders, J. Plostnieks, P. S. Wharton, and H. H. Wasserman, *ibid.*, **32**, 317 (1960).

(15) J. B. Stothers and P. C. Lauterbur, *Can. J. Chem.*, **42**, 1563 (1964).

(16) K. S. Dhami and J. B. Stothers, *ibid.*, **43**, 498 (1965).

(17) K. S. Dhami and J. B. Stothers, *ibid.*, **43**, 479 (1965).

(18) G. E. Maciel and J. J. Natterstad, *J. Chem. Phys.*, **42**, 2752 (1965).

(19) G. E. Maciel, *ibid.*, **42**, 2746 (1965).

(20) G. E. Maciel and G. B. Savitsky, *J. Phys. Chem.*, **68**, 437 (1964).

(21) J. A. Pople, *Mol. Phys.*, **7**, 301 (1964).

ternal reference is capable of maintaining long-term (several hours) spectrometer resolution of about 1 Hz, with even better results in favorable cases. Methyl alcohol, methyl iodide, carbon disulfide, acetonitrile (methyl labeled), and probably many other simple organic substances furnish adequate lock signals. By employing control-channel modulations up to about 7 kc from an external audio oscillator and judicious combinations of upper and lower side-band control and analytical frequencies the usual range of ^{13}C chemical shifts can be covered. Thus, the observation of ^{13}C magnetic resonance spectra of natural abundance samples becomes a relatively routine application of the time-averaging technique. Field-sweep experiments with slow sweep rates are also possible, but the lock condition is more fragile.

Materials. The ^{13}C -labeled acetone (55% ^{13}C), acetone- d_6 (99% D), and deuterium oxide (99.8% D) were used as obtained from their commercial suppliers, the Isomet Corp., Diaprep Inc., and Bio-Rad Laboratories, respectively.

Results

Using the new technique described in the Experimental Section on a solution containing 5% $\text{CH}_3\text{-}^{13}\text{COCH}_3$ (55% labeled) and 95% CD_3COCD_3 with ^{13}C present in natural abundance, we obtained a composite frequency-sweep spectrum of the two resonance signals in the carbonyl region. The signal from $\text{CH}_3\text{-}^{13}\text{COCH}_3$ appeared as the expected septuplet resulting from spin-spin coupling with the six equivalent protons; the splitting was 6.0 Hz and the line width about 1 Hz. Superimposed on this pattern was a broad peak due to $\text{CD}_3\text{-}^{13}\text{COCD}_3$, centered at an effective frequency²² about 7.0 ± 0.5 Hz higher than that of the undeuterated analog. The line width of this broad peak was about 5.0 ± 0.5 Hz, presumably owing to the envelope of the unresolved 13-line multiplet resulting from splitting by the six equivalent deuterons. Our inability to resolve the individual lines is not surprising in view of the expected 0.9-Hz ^{13}C -C-D spin-spin coupling constant.²³ The spectrum of this solution is shown in Figure 1 where it is compared with the spectra obtained from acetone and acetone- d_6 separately.

With the available precision of the method and the demonstrated sensitivity of the carbonyl ^{13}C shielding to subtle environmental changes, we compared a 10% solution of ^{13}C -labeled acetone in water with an analogous solution in D_2O ; with uncertainty limits of about ± 0.2 Hz we can state that no shift is observed in this case.

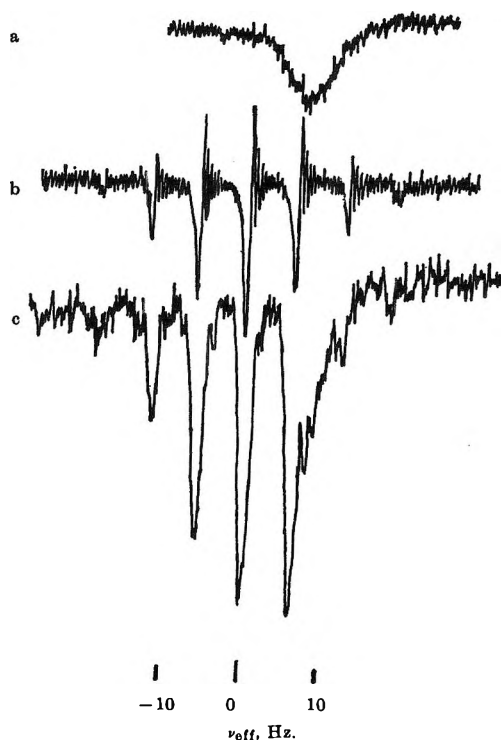


Figure 1. ^{13}C magnetic resonance spectra of acetone and acetone- d_6 on the same scale with the effective frequency ν_{eff} of the center of the acetone multiplet taken as zero. Spectra are frequency sweep and are inverted because of the use of lower side-band detection. A capillary of $^{13}\text{CH}_3\text{OH}$ provided the lock signals: a, $\text{CD}_3\text{-}^{13}\text{COCD}_3$ in natural abundance, 120 scans; b, $\text{CH}_3\text{-}^{13}\text{COCH}_3$, 55% ^{13}C label, one sweep; c, solution consisting of 95% CD_3COCD_3 (with $\text{CD}_3\text{-}^{13}\text{COCD}_3$ present in natural abundance) and 5% $\text{CH}_3\text{-}^{13}\text{COCH}_3$ (55% ^{13}C label), 421 scans.

Discussion

Several attempts have been made to understand isotope effects in terms of the vibrational zero-point energies and/or amplitudes on which they depend. Essentially two approaches have been used in this effort: (i) a direct focus of attention on the vibrational phenomena at their origin and (ii) an analysis in terms of "substituent isotope effects." Within the framework of i, interpretations have been advanced based on an apparently greater inductive electron-donating tendency of D or -C-D compared to H or -C-H and a reduced hyperconjugative ability of -C-D compared to -C-H, *i.e.*, in language appropriate to nonisotopic substituents and classified above as ii. Thus, Halevi^{4,5} and co-workers have presented justification for con-

(22) The effective frequency, ν_{eff} in Figure 1, is defined for lower side-band operation as the center-band frequency minus the modulation frequency of the analytical channel. This is the frequency at which resonance occurs in a fixed field.

(23) This is given by $(\gamma_{\text{D}}/\gamma_{\text{H}})(J_{^{13}\text{C}-\text{C}-\text{H}})$.

Table I: Related Isotope Effects

R	$\delta^{13}\text{C}(\text{R}_2)^a$	$\delta^{19}\text{F}(p\text{-RC}_6\text{H}_4\text{F})^b$	$\delta^{19}\text{F}(m\text{-RC}_6\text{H}_4\text{F})^c$	ΔpK_a^d	K_{assoc}^e
CH ₃	0	0	0	0	K
CD ₃	-0.28	-0.01	0	0.026	0.93K
C ₂ H ₅	-1.2	-0.60	0	0.114	0.72K

^a ¹³C chemical shifts of the carbonyl group with respect to that of acetone from the present work and ref 15. ^b ¹⁹F chemical shifts of *p*-alkylfluorobenzenes from ref 7. ^c ¹⁹F chemical shifts of *m*-alkylfluorobenzenes from ref 7. ^d pK_a's of carboxylic acids relative to that of acetic acid from ref 5. ^e Relative association constants for the formation of chloranil-alkylbenzene complexes from ref 6.

sidering these essentially vibronic phenomena in terms of normal substituent characteristics. Keeping the ultimate vibronic origin in mind, those authors have tried to "correlate secondary deuterium isotope effects in terms of the electrical influences that have proved valuable in interpreting the effects of nonisotopic substituents"⁵ and saw no valid objection to regarding deuterium isotope effects as due to small but real differences in the ease of hyperconjugative or inductive electron release. Thus "isotope effects on eminently electronic properties" were accounted for.⁵ In the following discussion we consider our results from both of the above points of view.

Substituent Isotope Effects. The result of this work, that a carbonyl carbon attached to two CD₃ groups is less shielded by about 0.28 ppm than the carbonyl group in acetone, bears an interesting relationship to some previous work as exhibited in Table I. One sees no correspondence between the ¹³C carbonyl shieldings and the ¹⁹F chemical shifts of the *m*-fluoroalkylbenzenes for which an "inductive isotope effect" was not found. Trends in the same direction are noted between the ¹³C carbonyl shieldings and the ¹⁹F shieldings in *p*-fluoroalkylbenzenes and might be discussed in terms of hyperconjugative effects; however, the ratio of increments corresponding to given substituent changes is not at all comparable for these two series of data. A qualitatively more attractive trend is observed between the carbonyl-¹³C shieldings and the equilibrium constants for the association of chloranil with toluene, toluene- α,α,α -d₃, and ethylbenzene, which Halevi and Nussin have interpreted primarily in terms of the hyperconjugative abilities of CH₃, CD₃, and C₂H₅. This comparison can also be made in the table. Thus, the present data could be rationalized in terms of hyperconjugative influences if one is willing to view these problems from the point of view of "substituent isotope effects." However, in that event, one must note that in the ketone series CH₃-¹³COCH₃, CD₃-¹³COCD₃, C₂H₅-¹³COC₂H₅, the effect on the ¹³C shielding of replacing CH₃ by CD₃ is roughly the same fraction of the effect of replacing CH₃ by

C₂H₅ as the corresponding ratio of ΔpK_a 's in the series of acids⁵ CH₃CO₂H, CD₃CO₂H, and C₂H₅CO₂H, which are structurally more closely related to the ketones than are the alkylbenzenes. Since the results on the carboxylic acids, shown in Table I, were assumed by Halevi to reflect a dominant role of an inductive effect, one might therefore conclude that the order of carbonyl-¹³C shieldings is due to substituent inductive and isotopic inductive effects. This would be consistent with the interpretations of Stothers and Lauterbur¹⁵ and Maciel¹⁹ that inductive withdrawal by a substituent depolarizes the carbonyl π bond, thereby increasing the shielding of the carbonyl-¹³C nucleus. This relationship has been put in quantitative terms by an application to the case of carbonyl systems¹⁹ of the independent electron molecular orbital theory for carbon-13 chemical shifts formulated by Karplus²⁴ and Pople.^{21,24} This treatment¹⁹ expresses the dominant paramagnetic term for ¹³C carbonyl shielding by eq 1, where λ has the usual meaning of π -bond po-

$$\sigma_p^{\text{AA}} = -(296 + 95.7\lambda)[1 + 0.273(1 - \lambda^2)^{1/2}] \quad (1)$$

larity.²⁵ For a range of λ between 0 and about 0.7 this expression predicts a nearly linear dependence of the carbon shielding on the bond polarity parameter and has been useful in interpreting both inductive substituent and solvent effects on ¹³C carbonyl shieldings. The present data could be interpreted in "substituent effect" language in terms of eq 1 if one assumes that the order of inductive electron-withdrawing ability is CH₃ > CD₃ > C₂H₅ as in Halevi's carboxylic acid pK_A interpretation⁵ and that λ thereby decreases in that order.

Unfortunately, the effect of conjugating or hyperconjugating substituents attached to carbonyl groups on their ¹³C chemical shifts has been obscured by the lack of an effective means of correcting for the "neighbor anisotropy effect."¹⁹ Thus, it is not possible at

(24) M. Karplus and J. A. Pople, *J. Chem. Phys.*, **38**, 2833 (1963).

(25) The definition of λ is given by the expression for a localized π -bond orbital $\psi = [(1 - \lambda)/2]^{1/2}\Phi_{\text{p}\pi\text{C}} + [(1 + \lambda)/2]^{1/2}\Phi_{\text{p}\pi\text{O}}$.

this time to predict with even qualitative certainty the hyperconjugative influence in carbonyl systems. It is of relatively little help to compare directly the influences of alkoxy or amino groups on carbonyl- ^{13}C shieldings; those substituents, while exerting electron-donating conjugation effects, simultaneously exert electron-withdrawing inductive influences on the carbonyl group and one can rationalize the resulting relatively high shieldings on the latter basis. Reference to the related ^{17}O data is somewhat more helpful. Indeed, the available ^{17}O carbonyl chemical shifts²⁶ (with respect to H_2^{17}O) for acetone (-572 ppm), 3-pentanone (-548 ppm), ethyl acetate (-356 ppm), and acetamide (-286 ppm) seem to reflect primarily the mesomeric electron-donating ability of the methoxy and amino groups compared to alkyl groups attached to the carbonyl. Neglecting the neighbor anisotropy effects of the alkyl groups on the ^{17}O shielding and assuming that an expression analogous to eq 1 applies, the position of 3-pentanone in this series would seem to indicate that either CH_3 is more inductively withdrawing (or less inductively donating) or else it is less electron donating in a hyperconjugative sense than is C_2H_5 . Since the latter alternative is contrary to the usual interpretation of hyperconjugative effects it would seem more plausible to ascribe the order to the relative inductive effects of the methyl and ethyl groups. If this is a valid indication of the influence which these substituents exert on the polarity parameter λ , then one would expect a corresponding influence in the opposite sense on the ^{13}C shielding in the carbonyl. A relationship of this type based on a mutual dependence on λ has been demonstrated previously for the case of solvent effects on the ^{13}C and ^{17}O chemical shifts of acetone in a variety of solvents in which λ varies; this correlation is shown in Figure 2. Thus, the present data can, in the language of "isotope substituent effects," be interpreted most reasonably as demonstrating the following decreasing order of inductive withdrawing ability: $\text{CH}_3 > \text{CD}_3 > \text{C}_2\text{H}_5$. However, for reasons to be discussed in the next section this general type of view (ii above) should be employed only with careful reference to the more fundamental vibrational foundation and not without caution.

Vibronic Point of View. The previously mentioned investigation of isotope effects in fluorotoluenes has been viewed by Thornton as "about as close as one can hope to get to isolating purely electronic effects from the average vibrational effects." In that case the isotope effects on the ^{19}F chemical shifts were found to be much smaller than one might have estimated by comparison of isotope and substituent effects on chemical reactivity parameters and a considera-

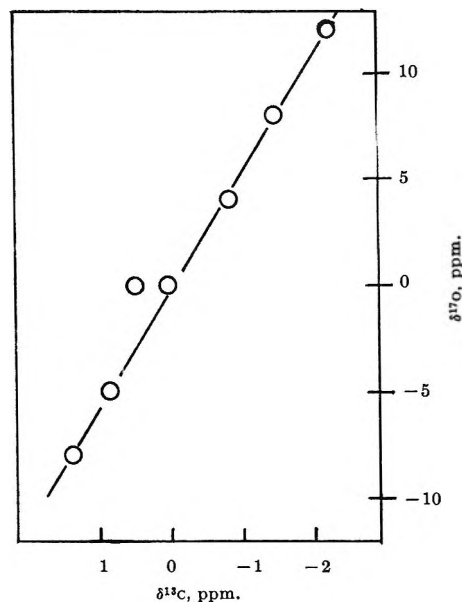


Figure 2. Plot of ^{13}C carbonyl chemical shift of acetone in solvents at 1:1 volume ratio vs. the ^{17}O chemical shift in the same solvents at the same concentration. Data from ref 27 and 28.

tion of substituent effects on ^{19}F shieldings in substituted benzenes. Now, in the present case the effects on the ^{13}C carbonyl shielding of replacing a methyl group by a perdeuteriomethyl group or an ethyl group are in roughly the same proportions as such structural changes on the cited reactivity parameters. However, this does not mean that the present results on isotopic substitution should be interpreted as representing electronic effects in the usual sense. That is, the present results do not suggest a case for which the Born-Oppenheimer approximation is invalid. Such an invalidation would require different potential energy surfaces describing the potential energy functions of nuclear motion for the isotopically related molecules. This surface, in the Born-Oppenheimer approximation, results from solving the electronic Schrödinger equation as a function of the coordinates describing internuclear separations and must be essentially identical for isotopic isomers,³ leading to identical force constants for molecular vibrations. As emphasized by Thornton this is an entirely different case from that of comparing different compounds; even for closely related homologs different potential energy surfaces and consequently different force con-

(26) H. A. Chrast, P. Diehl, H. R. Schneider, and H. Dahn, *Helv. Chim. Acta*, **44**, 865 (1961).

(27) J. J. Natterstad, M.S. Dissertation, University of California, Davis, Calif., 1965.

(28) H. A. Christ and P. Diehl, *Helv. Phys. Acta*, **36**, 170 (1963).

stants and molecular geometries apply. Thus, the effects of isotopic substitution result entirely from changes in the details of nuclear motion and, unlike the case with molecules which differ by more than just isotopic substitution, are not related to or dependent on different potential energy surfaces, *i.e.*, on different parametric solutions to different parametric electronic Schrödinger equations. Because of this fundamental difference cautious restraint should be exercised in discussing isotope effects in the language of substituent effects.

With this in mind, it appears that the most useful and proper interpretation of the present results is simply based on the fact that, although the force constants for vibrations in acetone and acetone- d_6 are essentially identical, the mass differences of H and D result in differences in vibrational amplitudes and different "effective" molecular geometries. If the molecular vibrations are anharmonic, then different vibration amplitudes will result in different mean bond distances for the isotopically related molecules. This means that one must, in principle, solve two slightly different electronic Schrödinger equations to describe the electronic properties, such as the electronic shielding constant of the molecules. In a sense this amounts to a different choice of the nuclear orientation index λ in Ramsey's original formulation of the theory of magnetic shielding of nuclei in molecules.²⁹ These same ideas have been presented in a useful form by Marshall¹¹ in a theoretical consideration of isotope shifts in the nmr spectra of H_2 , HD, and D_2 . He has expressed the "center of gravity" of a resonance line as corresponding to a value of the shielding constant σ averaged over nuclear motion

$$\sigma_{\text{obsd}} = \int_0^{\infty} \Psi^2 \sigma dR \quad (2)$$

where R is the value of the internuclear separation and $\Psi(R)$ is the wave function describing nuclear motion. Then, expressing σ as an expansion in the neighborhood of R_e , the equilibrium internuclear separation, Marshall obtains

$$\sigma(R) = \sigma(R_e) + (R - R_e)\sigma'(R_e) + \frac{1}{2}(R - R_e)^2\sigma''(R_e) \quad (3)$$

$$\sigma_{\text{obsd}} = \sigma(R_e) + \sigma'(R_e) \int \Psi^2 (R - R_e) dR + \frac{1}{2}\sigma''(R_e) \int \Psi^2 (R - R_e)^2 dR \quad (4)$$

where $\sigma(R_e)$ is the shielding corresponding to the equilibrium configuration (bottom of the potential energy

curve) and the primed symbols refer to derivatives. Analogous polydimensional expressions would apply to the ^{13}C carbonyl shielding in acetone. According to eq 4 only two distinct effects need be considered for isotopic effects (the first term on the right is the same for isotopic isomers since the potential energy curves or surfaces are essentially identical). The second term on the right is nonzero if the potential energy curve or surface has an anharmonic part so that the average internuclear configuration differs from R_e ; in this case $\int \Psi^2 (R - R_e) dR$ will depend on the isotope, owing to the differences in vibrational amplitudes. This effect has been mentioned above. The third term on the right also depends on the amplitudes of vibration, but it is nonvanishing even in the event of a purely harmonic potential function; this will also contribute to an isotope effect on shielding. Thus, the present data can, within the framework of the Born-Oppenheimer approximation, be interpreted as a demonstration of the effect of isotopic substitution on the effective geometry of the acetone molecule, resulting in slightly different effective electronic properties such as magnetic shielding; this is conceptually associated with the hypothetical solution of the electronic problem corresponding to slightly different spatial configurations of the nuclei.

There is an apparent contrast in the results with the acetones of this work and the fluoroalkylbenzenes previously reported; in the latter case isotope effects on the ^{19}F shieldings did not reflect the magnitudes observed in isotope effects on superficially analogous chemical properties, while in the former case the ^{13}C shieldings appear to be more directly related to chemical results. The reason for this is presumably that those aspects of the molecular electronic wave function of the acetone molecule in a magnetic field which determine the magnetic shielding of its carbonyl carbon are more profoundly influenced upon deuterium substitution in methyl groups by the changes in the "effective" spatial orientation of the nuclei (*i.e.*, by changes from one portion of the potential energy surface to another) than are the corresponding factors determining ^{19}F shieldings in fluoroalkylbenzenes. This is most likely related to the relative proximity of the position of deuterium substitution and the magnetic nuclei of interest in the two cases. In this regard it is of interest to note that the relatively huge isotope effect of 3 ppm has been reported for the difference between the ^{17}O chemical shifts in D_2O and H_2O .²⁵

(29) N. F. Ramsey, *Phys. Rev.*, **78**, 699 (1950).

Studies of Electrolytic Conductance in Alcohol-Water Mixtures. I.

Hydrochloric Acid, Sodium Chloride, and Sodium Acetate

at 0, 25, and 35° in Ethanol-Water Mixtures¹

by H. Olin Spivey and Theodore Shedlovsky

Rockefeller University, New York, New York (Received December 9, 1966)

Conductance data on dilute solutions of hydrochloric acid, sodium chloride, and sodium acetate in ethanol-water mixtures at 0, 25, and 35° are presented. Measurements were made in approximately 10, 20, 40, 60, and 80 wt % ethanol, but at 40% ethanol, potassium instead of sodium salts were used. These and supplementary data from the literature were examined in terms of the 1965 theoretical Fuoss-Onsager equation. It describes the experimental results within the limits of experimental accuracy and with reasonable values for the ion-size parameters. No detectable ion association was found for these electrolytes below 80 wt % ethanol. Variations in the Walden products with solvent composition and temperature are reported and discussed with respect to current theories concerning solvent structure and ion-solvent interactions.

Studies of electrolytic conductance in ethanol-water mixtures were initiated to provide experimental data on the behavior of strong and weak electrolytes in such systems. In this paper, we limit ourselves to results obtained for hydrochloric acid, sodium chloride, and sodium acetate;² results on acetic acid will be reported in a following paper.

Interest in alcohol-water mixtures stems, in part, from the similar amphiprotic properties of alcohol and water molecules, both involved in ion solvation and proton binding, but to different extents. Variations of these interactions may thus be studied by measurements over the composition range of the binary solvent system. Numerous properties of alcohol-water mixtures which are a function of solvent composition exhibit extrema which may well be reflections of increased solvent structure in this region of solvent composition.³ Appropriate conductance measurements provide useful and sensitive indications of ion-solvent interaction, proton-anion and proton-solvent association, and solvent structure. Conductance studies over the complete range of solvent composition have been previously published only for the methanol-water system at 25°,⁴ although a few measurements on

selected water-ethanol compositions are also available.⁵ As demonstrated by our present work, the variation of conductance with temperature provides further useful insights into these phenomena.

Experimental Section

The resistance measurements were made with alternating current bridges which had been carefully calibrated.^{6,7} Oil thermostats at 25 and 35° were regulated to within $\pm 0.005^\circ$, and temperatures were observed with periodically calibrated Beckmann differential thermometers. A dewar flask containing water and crushed ice served as the thermostat at 0°. A

(1) This research was supported by the National Science Foundation through Grant 21385.

(2) The potassium salts were used for the measurements in 40% ethanol.

(3) F. Franks and D. J. G. Ives, *Quart. Rev. (London)*, **20**, 1 (1956).

(4) T. Shedlovsky and R. L. Kay, *J. Phys. Chem.*, **60**, 151 (1956).

(5) (a) B. L. Murr and V. J. Shiner, *J. Am. Chem. Soc.*, **84**, 4672 (1962); (b) J. L. Hawes and R. L. Kay, *J. Phys. Chem.*, **69**, 2420 (1965); (c) I. I. Bezman and F. H. Verhoek, *J. Am. Chem. Soc.*, **67**, 1330 (1945).

(6) J. G. Janz and G. D. E. McIntyre, *J. Electrochem. Soc.*, **108**, 272 (1961).

(7) T. Shedlovsky, *J. Am. Chem. Soc.*, **52**, 1793 (1930).

quartz flask cell⁸ (cell constant 0.43184) with unplatinized electrodes and one of Pyrex (cell constant 6.4832) with lightly platinized electrodes⁹ were used for all the measurements at 25° and some of the measurements at 0 and 35°. Jena glass pipet cells¹⁰ were used for the remaining experiments. Electrode polarization errors were eliminated by taking readings at several frequencies and extrapolating to infinite frequency.¹¹ Readings at 5 and 10 kHz were usually found to be sufficient for this purpose in subsequent measurements. In contrast to flask cells, no significant current shunt errors were found with the pipet cells when used in the ice-water bath, within the frequency range employed in the measurements. Cell constants were determined to within $\pm 0.01\%$ precision at various times by calibration with aqueous potassium chloride or hydrochloric acid solutions,¹² and by means of cell intercomparisons with acetic acid solutions. Previous experience and simple calculation indicates that cell constants are not significantly altered within the temperature range of our experiments.¹³

Conductance water was obtained from a Barnstead High Purity conductivity water still which was fed through a deionizing column. The specific conductance of this water was routinely between 1 and 4×10^{-7} mho/cm. Ethanol was prepared by distillation of commercial grade absolute ethanol through a vacuum-jacketed column after refluxing 12 hr with magnesium ethoxide.¹⁴ Nitrogen gas which passed through an oxygen removing and drying train was bubbled through the boiling ethanol and the middle liter of a 1.8-l. distillate was collected in a nitrogen-filled flask and used for conductance solutions. The specific conductance of the azeotrope was about 2×10^{-8} mho/cm. The composition of ethanol-water mixtures was computed from duplicate density measurements by interpolation from known density data.¹⁵ Reagent grade sodium chloride was carefully purified by recrystallization. Sodium acetate solutions were prepared fresh by the addition of pure acetic acid¹⁶ to standardized, carbon dioxide free sodium hydroxide in ethanol. Standardizations and solution transfers were made with weight burets and approximately 1% excess acetic acid was used to suppress hydrolysis.

The general procedure for sodium chloride and sodium acetate experiments was essentially the same as had been previously described.⁸ Argon gas was used to remove atmospheric impurities from the solvents and solutions in the conductance cell. Passage of this or other inert gases through the cell for hours did not change the conductance of any of the electrolyte solutions, including hydrochloric acid. Increments of stock solutions (approximately 0.1 M in electrolyte)

were added to the conductance cell from weight burets to give various concentrations in the range of 0.001 to 0.015 M. For each electrolyte and solvent system, at least two separate series of measurements were performed at 25°. However, successive series of measurements on hydrochloric acid solutions failed to show sufficient reproducibility for the precision we were seeking. This was judged by the fact that marked negative deviations, which increased with dilution, were observed in the Λ'_{017} or Λ'_{18} plots and that these deviations were not sufficiently reproducible from experiment to experiment by amounts as large as 1%. This could be due to some loss of acid through adsorption or ion exchange¹⁹ at the walls of the cells. To reduce such possible acid losses, the following procedures were adopted. A previously cleaned and steamed cell was soaked several hours with approximately 1 M hydrochloric acid in the solvent to be used. It was then rinsed four times with fresh solvent before starting a series of measurements. This procedure did not result in significant changes in the conductances of the solvents, which varied from 2×10^{-8} in 99% to 2.5×10^{-7} mho/cm in 10% ethanol.²⁰ In addition, measurements were also made on successive portions of individual solutions of definite concentrations, prepared and stored in a Pyrex flask.^{12b} These modifications in the experimental procedure improved reproducibility in the dilute range about tenfold, namely, to within 0.1%.

To check on possible errors arising from esterifica-

(8) T. Shedlovsky, *J. Am. Chem. Soc.*, **54**, 1411 (1932).

(9) G. Jones and G. M. Bollinger, *ibid.*, **53**, 411 (1931).

(10) T. Shedlovsky in "Technique of Organic Chemistry," 3rd ed, Interscience Publishers, Inc., New York, N. Y., 1963, p 3031.

(11) R. A. Robinson and R. H. Stokes, "Electrolyte Solutions," 2nd ed, Butterworth and Co. Ltd., London, 1955, p 92.

(12) (a) J. E. Lind, J. J. Zwolenik, and R. M. Fuoss, *J. Am. Chem. Soc.*, **81**, 1557 (1959); (b) R. H. Stokes, *J. Phys. Chem.*, **65**, 1242 (1961).

(13) See ref 11, p 97.

(14) L. F. Fieser, "Experiments in Organic Chemistry," 3rd ed, D. C. Heath and Co., Boston, Mass., 1955, p 285.

(15) The d^0_{25} values were taken from A. V. Rakovski, *Chem. Abstr.*, **23**, 2624⁹ (1929); values of d^{25}_{25} are from N. S. Osborne, E. C. McKelvy, and H. W. Bearce, *Bull. Bur. Std.*, **9**, 424 (1913); and values of d^{35}_{25} are from N. S. Osborne, E. C. McKelvy, and H. W. Bearce, *J. Wash. Acad. Sci.*, **2**, 95 (1912).

(16) The glacial acetic acid was a special cut obtained from the Niacet Co. and judged to be 99.94% pure on the basis of its freezing point (see ref 4).

(17) T. Shedlovsky, *J. Am. Chem. Soc.*, **54**, 1405 (1932).

(18) R. M. Fuoss and F. Accascina, "Electrolyte Conductance," Interscience Publishers, Inc., New York, N. Y., 1959, p 197.

(19) J. E. Prue, *J. Phys. Chem.*, **67**, 1152 (1963); E. Grunwald, *et al.*, *J. Am. Chem. Soc.*, **84**, 4664 (1962); H. O. Spivey, unpublished studies.

(20) Solvent composition is always specified on a weight per cent basis.

Table I: Properties of Water-Ethanol Mixtures

	Wt % C ₂ H ₅ OH						
	0	10	20	40	60	80	100
d_0 {							
0°	0.99987	0.98477	0.97567	0.94941	0.90726	0.86035	0.80627
25°	0.99708	0.98038	0.96640	0.93151	0.88700	0.83909	0.78507
35°	0.99406	0.97685	0.96134	0.92385	0.87851	0.83209	0.77641
D {							
0°	88.03	82.32	76.80	63.72	49.87	37.92	28.3
25°	78.54	72.8	66.99	55.02	43.40	32.84	24.3
35°	74.78	69.2	63.5	52.0	41.0	31.0	22.8
$10^3\eta$ {							
0°	17.921	33.11	53.19	71.4	57.50	36.90	17.7
25°	8.949	13.28	18.08	23.74	22.32	17.38	11.01
35°	7.225	10.06	13.32	17.2	16.6	13.55	9.14

tion in hydrochloric acid solutions, conductance experiments with 60% ethanol solvent were performed using first aqueous stock solutions, then stock solutions in 60% ethanol-water solvent. The ethanol content of the cell was readjusted with ethanol after each addition of aqueous stock solution. No difference in results was obtained in these experiments. Since, in addition, the conductance remained stable with time, esterification errors of importance are unlikely.

The conductance data for 0 and 35° were obtained by comparing measurements at these temperatures with values at 25°. Resistance ratios, R_0/R_{25} and R_{35}/R_{25} , were determined, usually in pipet cells, for at least three concentrations for each electrolyte and solvent. Solvent background conductance was sufficiently small to have no disturbing effect on the resistance ratios. Rinsing and filling of the cells were made in an argon atmosphere and solution resistance was measured first at 25°, then at 0 or 35°, and again at 25°. The values were considered to be acceptable only if the resistance returned to its original value at 25° to within 0.1%. In a few instances in which the pipet cell measurements did not meet this criterion, satisfactory results were obtained by using flask cells.

Results

The densities, d ,¹⁵ dielectric constants, D , at 0°, 25°, 22 and 35°, and viscosities, η ,²³ used in the calculation of our results are from the literature and are summarized in Table I.

Our conductance data were analyzed with the Fuoss-Onsager 1965²⁴ equations: (1) for associated electrolytes, and (2) for unassociated electrolytes

$$\Lambda = \Lambda_0 - Sc^{1/2}\gamma^{1/2} + E'c\gamma \ln(6E'_1c\gamma) + Lc\gamma - K_Ac\gamma\Lambda f^2 \quad (1)$$

$$\Lambda = \Lambda_0 - Sc^{1/2} + E'c \ln(6E'_1c) + Lc \quad (2)$$

In these equations, Λ is the equivalent conductance at the concentration c (equivalents per liter of solution)

and Λ_0 is its limiting value, γ is the degree of dissociation, K_A is the association constant, and f is the activity coefficient. The constants S and E' , but not E'_1 , depend on Λ_0 , as well as on the temperature T (Kelvin), D , and η , but are not otherwise adjustable parameters. The coefficient of the linear concentration term, L , is an adjustable parameter. It is a function of the "ion size," $a^\circ(L)$, the values for which are thus obtained from the data. Numerical values for all the theoretical coefficients involved in the equations depend of course on fundamental constants such as electronic charge, Avogadro's number, etc. In our computations we had adopted the values given by Fuoss, *et al.*²⁴

Using the computer program of Skinner and Fuoss,²⁵ the data were analyzed with eq 1. However, if the value obtained for the association constant, K_A , was less than 10, recomputation with eq 2 was made. Data from separate experiments on a given electrolyte and solvent were combined for purposes of the above analysis. The values for the parameters in the equations are listed in Table II. The experimental results are thus given in implied form for reasons of compactness of presentation of the large number of measurements. The degree of agreement between experimental values and the corresponding ones given by the equations is indicated in the columns, σ , the standard deviation, while the columns, N , list the number of experimental measurements in each case. The results are given for only 25°, at which temperature the experimental accuracy was somewhat greater. This is because the conductance values at 0 and 35° were calculated from resistance ratios²⁶ relative to those at

(21) J. Wyman, Jr., *J. Am. Chem. Soc.*, **53**, 3292 (1931).

(22) G. Åkerlöf, *ibid.*, **54**, 4125 (1932).

(23) E. C. Bingham and R. F. Jackson, *Bull. Bur. Std.*, **14**, 59 (1918-1919).

(24) R. M. Fuoss, L. Onsager, and J. T. Skinner, *J. Phys. Chem.*, **69**, 2581 (1965).

(25) We are indebted to Drs. Fuoss and Skinner for making their computer program available to us.

Table II: Conductance of Hydrochloric Acid, Sodium Chloride, and Sodium Acetate in Water-Ethanol Mixtures in Terms of Fuoss-Onsager Equations

Wt % ethanol in mixture	A_s		L		$\alpha(L)$ 25°	K_A 25°	N		
	0°	35°	0°	25°			35°	0°	25°
{ HCl 0 } NaCl	246 ^a	426.75 ^b	489.8 ^c	469	3.3	—	0.17	0.3	12
	67.5 ^a	126.43 ^a	155 ^a	213	3.9		0.06	2.0	18
	46.6 ^a	90.94 ^f		187	4.3		0.05		9
{ HCl 10 } NaCl	181.9	326.7	386.7	488	3.9	0.3	0.12	0.2	3
	42.63	92.01	116.1	54	3.1	0.003	0.02	0.1	3
	29.86	66.98	85.68	49	3.6	0.02	0.06	0.015	3
{ HCl 20 } NaCl	122.88	249.4	304.8	470	<i>l</i>	0.10	0.40	0.8	3
	28.34	70.74	92.21	39	3.2	0.06	0.02	0.07	3
	19.95	51.76	68.34	32	2.8	0.02	0.13	0.03	6
{ HCl 40 } (KCl) { (KAc)	66.34	153.7	196.4	363	3.8	0.01	0.14	0.2	3
	21.74 ^h	56.70 ^g	75.52 ^h	88	2.7	0.01	0.07	0.06	3
	16.88	45.05	60.33	20					8
{ HCl 60 } NaCl	45.07	101.0	129.3	469	3.8	0.09	0.26	0.3	3
	18.31	43.51	57.24	98	2.5	0.01	0.02	0.02	3
	14.69	35.91	47.86	91	2.5	0.01	0.04	0.04	3
{ HCl 80 } NaCl	32.17	65.38	83.06	309	3.4	0.12	0.11	0.09	4
	20.29	41.18	52.53	41	2.6	0.10	0.01	0.28	3
	17.23	35.56	45.54	74	2.6	0.008	0.01	0.02	5
{ HCl 100 } NaCl	(53.34) ⁱ	84.65 ^j	(160)	441	3.4	(0.04)	0.14		(5)
		42.24 ^k		268	3.0		0.02		6

^a Reference 11, p 465. ^b Reference 12b. ^c B. B. Owen and F. H. Sweeton, *J. Am. Chem. Soc.*, **63**, 2811 (1941). ^d Reference 8. ^e H. E. Gunning and A. R. Gordon, *J. Chem. Phys.*, **10**, 126 (1942). ^f D. A. MacInnes and T. Shedlovsky, *J. Am. Chem. Soc.*, **54**, 1429 (1932). ^g Reference 28. ^h Obtained by extrapolation of conductance ratios of 0 to 25° and 35 to 25° to zero concentration. ⁱ HCl data at 4°, A. G. Ogston, *Trans. Faraday Soc.*, **32**, 1679 (1936). ^j Reference 5c. ^k Reference 26b. ^l Value was set at 0 to avoid negative convergence by computer program.

Table III: Walden Products in Water-Ethanol Mixtures at 25°^a

	Wt %						
	0	10 ^b	20	40	60	80	100
$\lambda_0\eta_0$ { K ⁺	0.658	0.72	0.753	0.676	0.509	0.373	0.259
Na ⁺	0.448	0.51	0.546		0.435	0.319	0.224
H ⁺	3.130	3.6	3.76	2.97	1.710	0.744	0.690
Cl ⁻	0.683	0.71	0.727	0.699	0.536	0.390	0.241
Ac ⁻	0.366	0.38	0.387	0.391	0.369	0.298	

^a Values of λ_0 are from ref 28. ^b Values of λ_0 in 10 wt % ethanol are estimated from data at 0, 20, 40, etc., wt % ethanol and are subject to considerable uncertainty. See text.

25°. However, except in a few cases, the $\alpha^\circ(L)$ and K_A values at 0 and 35° did not differ substantially from those at 25°.

Due to systematic errors in connection with the hydrochloric acid solution conductances and the elaborate procedure for preparing sodium acetate solutions previously discussed, such results may be less accurate than may appear from the σ values. For data at 25°, we estimate uncertainties of $\pm 0.3\%$ in Λ_0 for hydrochloric acid and sodium acetate and $\pm 0.05\%$ for sodium chloride. At 0 and 35°, the uncertainties in Λ_0 values for each electrolyte may be as great as 0.5%, due in part to the smaller number of experimental points. Adjustment of Λ_0 data to round weight per cent solvent composition involved only small corrections and involved no loss in accuracy of the data. Other parameters of the conductance equation are not significantly altered by these small changes, as can be verified by calculation.

For comparing the behavior of individual ions in the mixed solvents, we examined limiting ionic Walden products, $\lambda_0\eta_0$, which are listed in Table III. The individual ionic conductances were computed with the transference number data at 25° of Gordon, *et al.*,²⁷ in water and in pure ethanol, and those of Fratiello²⁸ at 20.10, 39.94, 60.27, and 79.37% ethanol. Because of uncertainty in the graphical interpolation between 0 and 20.1% for the value we chose for 10% ethanol, the listings in Table III for this solvent composition may be in error by as much as 10%.

Discussion

The only data available for comparison with ours were those of Murr and Shiner^{5a} for hydrochloric acid conductance in water-ethanol mixtures at 25°. From their Λ_0 values at 60, 70, and 80 volume % ethanol, we estimate a limiting conductance of 100.8 in 60 weight % ethanol. This value is in very good agreement with our experimental value of 101.0 ± 0.2 based on more than ten separate experiments in this solvent with the various experimental procedures we have used.

The ion-size parameters and association constants calculated from eq 1 or 2 and listed in Table II are reasonable and consistent with data on other electrolytes in water-ethanol solvents.^{5b} Thus, no significant ion association ($K_A < 10$) is indicated below 80% ethanol. Unfortunately, the physical interpretation of these parameters is too uncertain to draw further conclusions, a situation which is aggravated by the relatively small deviations of these data from Onsager's limiting law.²⁴ However, the fact that reasonable values for these parameters are obtained in each case is significant.

Because a different transport mechanism is involved for the proton than for normal ions, one might suppose that the concentration dependence of hydrochloric acid conductance might show differences from that of salts in the mixed dipolar solvents. However, this does not appear to be the case. The assumption that the nature of the transport mechanism is immaterial for the Onsager theory²⁹ is consistent with our results.

As shown in Figure 1, limiting equivalent conductances of each electrolyte at 25° decrease smoothly with solvent composition throughout most of the composition range, despite the large maximum in viscosity near 50% ethanol. Conductance curves at 0 and 35° are similar. In this respect, the Λ_0 profiles resemble those observed in methanol,⁴ although the viscosity maximum in water-ethanol mixtures is approximately twice as large. Obviously, ion mobilities are not predominantly controlled by the bulk viscosity. This is more clearly demonstrated by the Walden products, which are normalized to their value in water and shown in Figure 2 as a function of solvent composition. If

(26) $\Lambda_i/\Lambda_{25} = (R_{25}/R_i)(d_{25}^2/d_i^2)$.

(27) (a) G. C. Benson and A. R. Gordon, *J. Chem. Phys.*, **13**, 473 (1945); (b) J. R. Graham, G. S. Kell, and A. R. Gordon, *J. Am. Chem. Soc.*, **79**, 2352 (1957).

(28) A. Fratiello, University Microfilms, Ann Arbor, Mich., Order No. 63-1019; *Dissertation Abstr.*, **23**, 2338 (1963). Transference number data at 0 and 35° were not available.

(29) See ref 11, p 371.

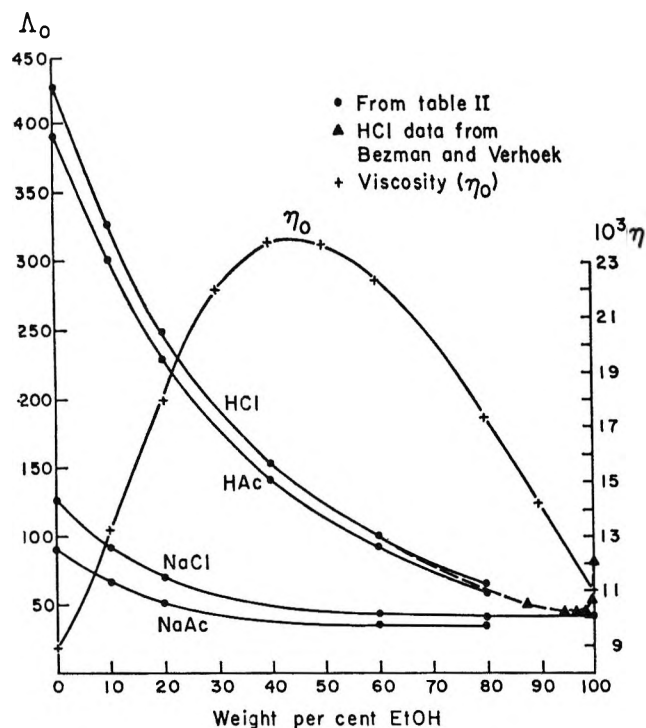


Figure 1. Variation of limiting equivalent conductances (Λ_0) and of solvent viscosity (η_0) with solvent composition at 25°.

ion mobility depended on bulk viscosity in accord with Stokes' law, the Walden products would be proportional to the reciprocal of the ion sizes.³⁰ The variations in Walden products with solvent composition (Table III and Figure 2) and temperature (Table IV) might then be explained through changes in ion

Table IV: Temperature Dependence of Walden Products, $(\Lambda_0\eta_0)_{35}/(\Lambda_0\eta_0)_{25}$

	Wt % ethanol					
	0	10	20	40	60	80
NaCl	0.930	0.8273	0.8133		0.9026	0.9461
HCl	0.741	0.6463	0.6208	0.7084	0.8271	0.9528
NaAc		0.8708	0.8568		0.9406	0.9530

^a Ratios of 25 to 0° and 35 to 25° show similar trends with solvent composition; all exhibit minima near 20 wt % ethanol, for example.

solvation alone. Such an explanation, however, requires increasing ion solvation with increasing temperature, ignores other data indicating structure-breaking effects of ions (particularly potassium and chloride ions³¹), and does not explain the behavior of the Walden product for the hydrogen ion. An al-

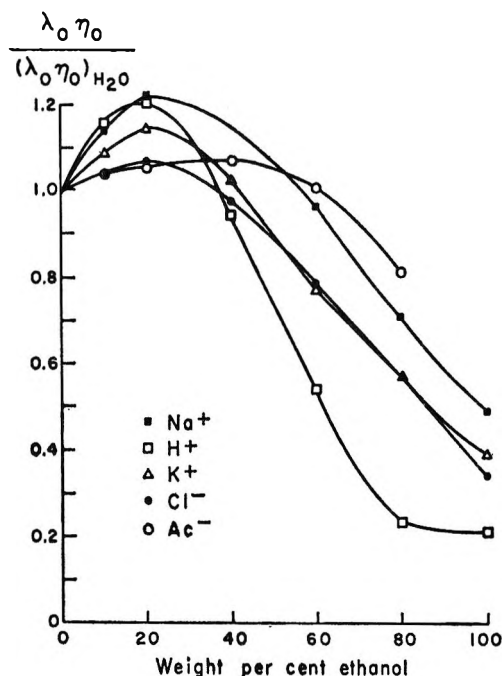


Figure 2. Variation of ionic "Walden products," normalized to water with solvent composition at 25°.

ternative and more satisfactory interpretation of the Walden products is based on the views summarized by Franks and Ives³ concerning the structure of ethanol-water mixtures and the effect of ions on this structure. A variety of thermodynamic, kinetic, ultrasonic, and transport data³ indicate that addition of simple alcohols to water initially enhances the structure of the solvent. This structure enhancement appears to reach a maximum near 20 to 30% alcohol in the case of ethanol; at higher ethanol compositions, the water structure is progressively reduced. The sharp maximum in $\lambda_0\eta_0$ for the hydrogen ion supports this conclusion since its excess mobility depends on proton transfers among associated solvent dipolar molecules. For other ions, the large Walden products in water relative to their values in pure alcohol are thought to be due to the local structure-breaking effect of these ions on water. The maxima in the Walden products near 20% ethanol may thus be a consequence of the greater disruption of water structure in the vicinity of the ions for solvent of this composition. This viewpoint also predicts that Walden products should decrease with increased temperature because of reduction in solvent structure at higher temperatures. Moreover, one might expect the temperature effect on the Walden product to be largest near 20% ethanol cor-

(30) See ref 11, p 130.

(31) R. L. Kay and D. F. Evans, *J. Phys. Chem.*, **70**, 2325 (1966).

responding to maximum structure. Both these predictions are in agreement with the ratios of Walden products as listed in Table IV.

We observe that the concentration dependence of ionic mobilities in alcohol-water mixtures is in accord with theories based largely on ionic electrostatic forces and on a continuum model for the solvents. However, mobilities themselves and their temperature dependence are predominantly affected by ion-solvent interactions which are not easily explained in terms of ionic solvation alone. The conductance behavior of the salts in

this study is consistent with their known structure-altering effects in water and current views concerning the structure of alcohol-water mixtures. Conductance and transference number measurements on other salts at different temperatures in alcohol-water solvents would be helpful in elucidating the competing ion-solvent and solvent-solvent interactions that occur.

Acknowledgment. We are indebted to Miss Lorraine Seher for her valuable technical assistance in our experimental studies.

Studies of Electrolytic Conductance in Alcohol-Water Mixtures.

II. The Ionization Constant of Acetic Acid in Ethanol-Water

Mixtures at 0, 25, and 35°¹

by H. Olin Spivey and Theodore Shedlovsky

Rockefeller University, New York, New York 10021 (Received February 3, 1967)

Measurements are reported on the electrical conductance of dilute solutions of acetic acid at 0, 25, and 35° in ethanol-water mixtures over the whole range of solvent composition. From these data and those on hydrochloric acid, sodium chloride, and sodium acetate solutions in the same solvent systems previously reported by us, values for the dissociation constants for acetic acid have been computed for these temperatures over the entire solvent composition range. The results of these studies are discussed briefly from theoretical considerations.

Introduction

Studies of electrolytic conductance of the typical weak acid, acetic acid, in alcohol-water mixtures over the entire range of solvent composition provide a convenient and accurate means for determining the ionization constant. Not only do such determinations provide useful data for the theoretical understanding of the ionization process in such systems in which two different dipoles, water and alcohol, as well as the anion compete for the proton, but they can also serve the

practical purpose of establishing pH scales in these systems.

In this paper we shall present the results of conductance measurements on dilute solutions of acetic acid in ethanol-water mixtures at 0, 25, and 35° over practically the entire range of solvent composition. The corresponding ionization constants were obtained in a

(1) This research was supported by the National Science Foundation through Grant No. 21385.

manner previously described,² using the mass action law in combination with appropriate equations for the conductance of weak electrolytes. The limiting equivalent conductances Λ_0 for acetic acid were computed from the corresponding Λ_0 values for hydrochloric acid, sodium chloride, and sodium acetate which we had reported in a previous paper.³

Experimental Section

The apparatus, chemicals, and procedure were the same as we had previously described.³ Duplicate conductance experiments on dilute acetic acid solutions in each solvent mixture were made with an average of five different concentrations for each experiment at 25°. However, as we had done previously, data at 0 and 35° were obtained as resistance ratios from 0 to 25° or 35 to 25°, although in some cases measurements were made for only a single concentration.

Calculations and Results

For the calculations of the dissociation constants at 25°, K_{25° , the equations of Shedlovsky and Kay² were employed. Retaining their symbols, the equation

$$L - L_0 = \frac{\Lambda_0 K^{1/2} c^{1/2}}{Sf} \left[1 - \frac{\Lambda^* S}{\Lambda_0} \left(1 - \frac{L_0}{L} \right) \right]^{1/2} \quad (1)$$

permits calculation of K and L_0 independent of measured solvent conductances. In this equation, L and L_0 are 1000 times the specific conductance of the solution and solvent, respectively; Λ_0 is the limiting equivalent conductance; $\Lambda^* = L/c$ where c is molar concentration of acetic acid; $\log f = -a\sqrt{cx}$ where $a = 1.825 \times 10^6 / (DT)^{1/2}$ and x is the degree of dissociation of the acetic acid; $S \equiv [(Z/2) + \sqrt{1 + (Z/2)^2}]^2$ where $Z = (\alpha\Lambda_0 + \beta)\sqrt{c\Lambda/\Lambda_0^{3/2}}$ and $\alpha = 8.203 \times 10^5 / (DT)^{1/2}$ and $\beta = 82.43/\eta(DT)^{1/2}$ are the Onsager coefficients involving the dielectric constant D , the viscosity η , and the absolute temperature T . As a first approximation, a least-squares fit of data to

$$L = L_0 = \left[\frac{\Lambda_0 K^{1/2} c^{1/2}}{Sf} \right] \left[1 - \frac{\Lambda^* S}{\Lambda_0} \right]^{1/2} \quad (2)$$

was used to obtain an initial value of L_0 which was then recycled with eq 1. These calculations were recycled again, but in no case were the calculated dissociation constants significantly changed in so doing. Values of $\Lambda_0(\text{HAc}) = \Lambda_0(\text{HCl}) - \Lambda_0(\text{NaCl}) + \Lambda_0(\text{NaAc})$ were obtained from data on the strong electrolytes reported in our previous paper.³ For the values at 94.6 and 99.7 wt % ethanol at 25°, $\Lambda_0(\text{NaCl})$ and $\Lambda_0(\text{NaAc})$ were obtained from former data^{3,5a} by interpolation and extrapolation, respectively, and for $\Lambda_0(\text{HCl})$ the data of Bezman and Verhoek^{5b} were used.

This gave Λ_0 values of 45.70, 41.90, and 35.85 for HCl, NaCl, and NaAc, respectively, at 94.64% ethanol and 55.0, 42.1, and 36.0 at 99.67%. Although graphical analysis revealed no systematic deviation of data from eq 1 within the experimental error (1% in the slope), computed values of L_0 were occasionally slightly negative. This is most likely due to the hydrogen ion losses in dilute solutions which have been noticed, particularly in hydrochloric acid-ethanol solutions.³ Fortunately, the K values calculated from eq 1 are insensitive to L_0 . Thus, either the measured or the computed L_0 for the solvent conductance gave essentially the same K value within an experimental accuracy of 2%. Measured specific conductances are given in Table I together with the $\Lambda_0(\text{HAc})$ values used and the K values obtained from each experiment with eq 1. Graphs of eq 1 using data from one experiment at each solvent composition are illustrated in Figure 1.

For calculations of K at 0 and 35°, the degree of dissociation as given by conductance

$$x = \Lambda S / \Lambda_0 \quad (3)$$

and the mass action equation

$$K = cx^2f^2 / (1 - x) \quad (4)$$

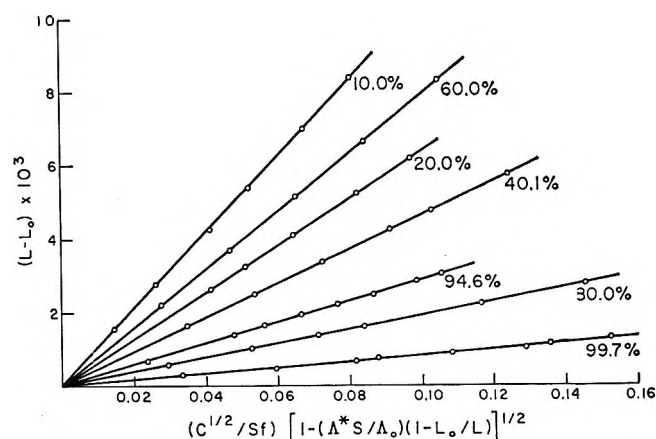


Figure 1. Equation 1 for acetic acid at various solvent compositions. For 10.0% ethanol, multiply abscissas by 2. For 10.0, 20.0, 40.1, 94.6, and 99.7% ethanol multiply the ordinates by 20, 10, 5, 0.1, and 0.05, respectively.

(2) T. Shedlovsky and R. L. Kay, *J. Phys. Chem.*, **60**, 151 (1956).

(3) H. O. Spivey and T. Shedlovsky, *ibid.*, **71**, 2165 (1967).

(4) We are grateful to Dr. Mario Goffredi for the conductance measurements on acetic acid solutions in 94.64 and 99.67% ethanol at 25°.

(5) (a) J. R. Graham, G. S. Kell, and A. R. Gordon, *J. Am. Chem. Soc.*, **79**, 2352 (1957); (b) I. I. Bezman and F. H. Verhoek, *ibid.*, **67**, 1330 (1945).

Table I: Conductances of Acetic Acid in Water-Ethanol Mixtures at 25°

10°C	10%L	10°C	10%L	10°C	10%L	10°C	10%L
9.97 Wt % EtOH, $\Lambda_0 = 302.0$				80.04 Wt % EtOH, $\Lambda_0 = 59.73$			
0.9581	30.840	1.3778	37.331	0.8725	0.58356	0.6469	1.5513
2.8638	54.855	6.8602	86.031	2.7331	1.0208	1.0369	1.9669
6.9655	84.785	13.381	121.16	4.9682	1.3731	2.3580	2.9792
10.887	107.68	22.793	159.01	6.8888	1.6154	3.2597	3.5110
17.927	139.89			13.199	2.2391	5.2434	4.4716
25.419	167.59			20.424	2.7883		
$K = 1.185 \times 10^{-5}$		$K = 1.198 \times 10^{-5}$		$K = 1.036 \times 10^{-7}$		$K = 1.042 \times 10^{-7}$	
20.03 Wt % EtOH, $\Lambda_0 = 230.3$				94.64 Wt % EtOH, ^a $\Lambda_0 = 39.65$			
1.7873	26.699	2.3953	30.987	0.56578	0.085163	0.94807	0.10827
2.6834	32.941	4.5717	43.227	2.7117	0.16702	2.2620	0.15693
4.2193	41.571	8.5503	59.506	5.5142	0.23412	3.1157	0.18150
6.7707	52.972	13.890	76.187	7.4197	0.26798	3.7265	0.19313
9.3771	62.562	19.767	91.168	9.1299	0.29508	4.3610	0.21192
$K = 6.75 \times 10^{-6}$		$K = 6.68 \times 10^{-6}$		10.934	0.32149	5.7925	0.23892
40.07 Wt % EtOH, $\Lambda_0 = 141.8$				99.67 Wt % EtOH, ^a $\Lambda_0 = 48.9$			
1.2758	8.1354	1.2122	7.9308	$K = 5.36 \times 10^{-9}$		$K = 5.25 \times 10^{-9}$	
2.9101	12.470	3.1578	13.012	99.67 Wt % EtOH, ^a $\Lambda_0 = 48.9$			
5.1949	16.798	5.4227	17.179	1.0902	0.040077	7.6869	0.062640
8.2206	21.243	7.5237	20.315	3.5169	0.049653	18.306	0.082379
10.366	23.915	10.569	24.191	6.6190	0.059327	23.101	0.090493
15.017	28.888			11.682	0.068909		
$K = 2.69 \times 10^{-6}$		$K = 2.73 \times 10^{-6}$		16.520	0.078019		
60.01 Wt % EtOH, $\Lambda_0 = 93.4$				$K = 6.51 \times 10^{-11}$		$K = 7.62 \times 10^{-11}$	
10°C	10%L	10°C	10%L	10°C	10%L		
1.1319	2.6787	0.76946	2.1915	1.013	2.505		
2.1723	3.7252	2.1615	3.6953	2.380	3.863		
4.1895	5.1878	4.1897	5.1683	3.767	4.874		
6.5322	6.4927	6.9163	6.6595	6.981	6.676		
9.9909	8.0459	10.766	8.3325	9.867	7.952		
$K = 7.92 \times 10^{-7}$		$K = 7.81 \times 10^{-7}$		$K = 7.81 \times 10^{-7}$			

^a From the measurements of Dr. Mario Goffredi.

were combined and ratios of K from 0 to 25° or 35 to 25° were calculated from the resulting expression

$$\frac{K_2}{K_1} = \frac{c_2}{c_1} \left[\frac{S_2 f_2 \Lambda_2}{S_1 f_1 \Lambda_1} \right]^2 \left[\frac{\Lambda_{0,1}(\Lambda_{0,1} - \Lambda_{0,1} S_1)}{\Lambda_{0,2}(\Lambda_{0,2} - \Lambda_{0,2} S_2)} \right] \quad (5)$$

where the subscripts 1 and 2 denote the different temperatures. In this way only ratios of $\Lambda_2/\Lambda_{25^\circ} = W$ obtained from the data as $L_2 c_{25^\circ}/L_{25^\circ} c_2$ are needed. Values for S at 0 and 35° were calculated from $\Lambda_2 = W \Lambda_{25^\circ}$ and Λ_{25° was computed from eq 3 and 4 using previously determined values for K at 25°. Thus, uncertainties in the solvent conductance at 0 and 35° should cancel out with sufficient accuracy in these calculations. Table II lists dissociation constant ratios as determined from the conductance measurements and Table III summarizes the average values of pK

at each temperature and solvent composition. We estimate K to be accurate to within $\pm 2\%$ or pK to ± 0.006 for all values reported.

Table II: Dissociation Constant Ratios for Acetic Acid in Water-Ethanol Solvents from 0 to 25° and 35 to 25°

		Wt % C ₂ H ₅ OH				
		10	20	40	60	80
K_{0°/K_{25°	}	0.9258	0.9608	0.9439	1.0074	0.8854
		0.9332	0.9602			0.8825
						0.8776
						0.8804
$K_{35^\circ}/K_{25^\circ}$	}	0.9757	0.9754	0.9636	0.9354	1.1596
		0.9794			0.9369	
					0.9373	
					0.9357	

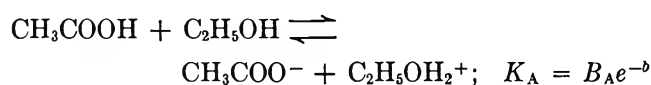
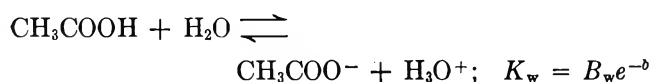
Table III: Average pK Values of Acetic Acid in Water-Ethanol Solvents at 0, 25, and 35°

Temp, °C	Wt % C ₂ H ₅ OH							
	0	9.97	20.03	40.07	60.01	80.04	94.64 ^a	99.67 ^a
0	4.780	4.956	5.191	5.592	6.101	6.926		
25	4.756	4.924	5.173	5.567	6.104	6.984	8.276	10.139 ^b
35	4.762	4.934	5.185	5.583	6.134	7.031		

^a From the measurements of Dr. Mario Goffredi. ^b This value of pK was calculated from the combined data of duplicate experiments with 99.67% ethanol.

Discussion

Our pK values at 25° are in good agreement with the data of Grunwald and Berkowitz⁶ except at 80 (and perhaps 20) wt % ethanol where the difference is greater than the estimated errors. In Figure 2, pK_{25°} appears to vary smoothly with solvent composition. On larger scale graphs, however, pK at 20 wt % is seen to be at least 0.06 pK unit above the smooth curve through the other points. In other words, Figure 2 may be represented by two intersecting smooth curves, one representing values below 20 wt % ethanol and one representing pK's above 20 wt % ethanol. If the variation in dissociation constants is due primarily to interionic coulombic forces, then, as suggested by Shedlovsky,⁷ application of the familiar Bjerrum's relationship, $K = Be^{-b}$, to both equilibria



with the further assumption that $B_w \gg B_A$, leads to equations

$$Ke^b/C = B_w X \quad (6)$$

and

$$\ln K - \ln [\text{H}_2\text{O}] + (\epsilon^2/kTa)(1/D) = \ln B_w \quad (7)$$

where $b = \epsilon^2/DkTa$, ϵ is the electronic charge, k the Boltzmann constant, and a the average ionic diameter for anion and cation; C is the sum of the solvent concentrations $[\text{H}_2\text{O}] + [\text{C}_2\text{H}_5\text{OH}]$; and X is the mole fraction of water; other terms have been previously identified. Graphs of eq 6 and 7 are shown in Figures 3 and 4. If the simplifying assumptions involved in eq 6 and 7 are valid, deviations would still be expected at high ethanol compositions. It is, nevertheless, interesting that again points below 20% ethanol deviate from the line through higher ethanol compositions.

Figure 5 shows the variation of pK with temperature in each of the solvents studied. Only three tem-

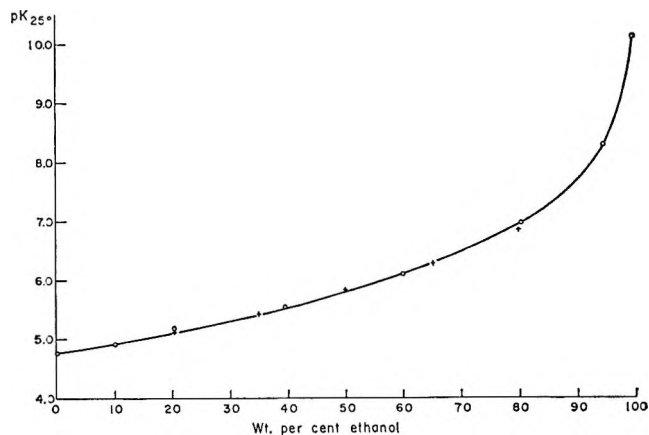


Figure 2. Variation in pK of acetic acid with solvent composition at 25°.

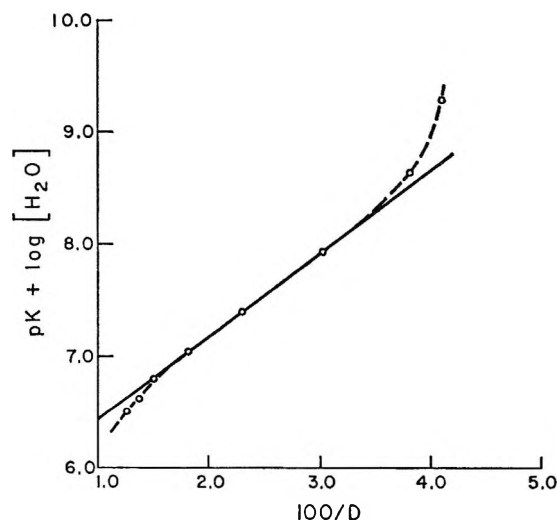


Figure 3. Equation 7 for acetic acid in water-ethanol mixtures at 25°. Solid line corresponds to $a = 3.4 \text{ \AA}$; 0, 10, and 20% ethanol gives $a = 2.3 \text{ \AA}$.

peratures are used, but they demonstrate that pK values have a minimum which progresses from near

(6) E. Grunwald and B. J. Berkowitz, *J. Am. Chem. Soc.*, **73**, 4939 (1951).

(7) T. Shedlovsky in "Electrolytes," B. Pesce, Ed., Pergamon Press, Inc., New York, N. Y., 1962, p 146.

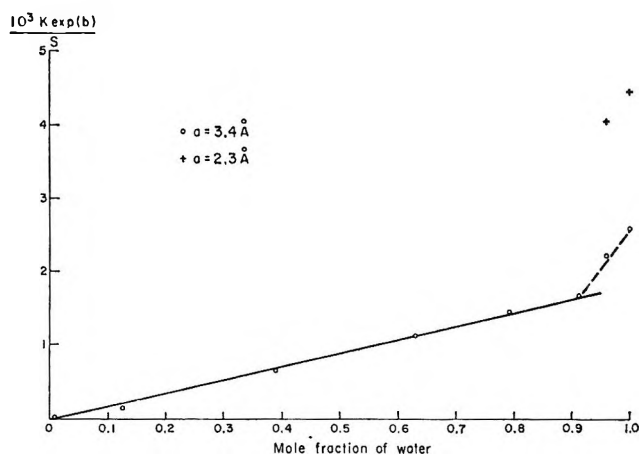


Figure 4. Equation 6 for acetic acid in water-ethanol mixtures at 25°.

room temperature in water to below 0° in 80% ethanol. These minima are similar to those of other weak acids and the shift in temperature of the minima, T_m , with solvent composition is such as would be expected on the basis of macroscopic theories discussed by Gurney.⁸ A minimum in pK requires that the enthalpy of acetic acid dissociation, ΔH° , pass from negative through zero to positive values as the temperature is decreased below room temperature. Such a variation in ΔH° would, in general, require a quadratic equation with three parameters to represent it; integration of ΔH° to obtain the free energy ΔG° would lead to four parameters. Fortunately, as pointed out by Harned and Owen,⁹ the pK 's of all the weak acids examined in aqueous solution and also in a number of binary mixtures can be described by a parabolic dependence on temperature

$$pK = pK_m + \alpha(T - T_m)^2 \quad (8)$$

where pK_m and T_m are minimum values (maximum in K) and α is a constant. On this basis, values of pK_m , T_m , and α were calculated from the three temperature points in each solvent and they are given in Table IV. The values for T_m are considered to be accurate to within $\pm 0.5^\circ$ and those for pK_m to ± 0.006 . We therefore find

Table IV: Parameters of Eq 8, $pK = pK_m + \alpha(T - T_m)^2$

Wt % ethanol	pK_m	$\alpha \times 10^6$	$T_m, ^\circ C$
0	4.756	5	22.6
9.97	4.925	5.6	22.8
20.03	5.168	5.2	19.4
40.07	5.564	7.0	20.5
60.01	6.088	6.8	10.8
80.04	6.919	7.6	-3.5

$$\Delta H^\circ = -4.606RT^2\alpha(T - T_m) \quad (9)$$

Within the temperature range of 0–35°, ΔH° , calculated from eq 9, does not exceed 1 kcal/mole in any of the solvents from 0 to 80% ethanol. Thus, as is the case in pure water, bond-energy differences for the proton are insignificant compared to the entropy factors which seem to dominate the ionization equilibria in these solvent mixtures. As pointed out by Harned and Owen,⁹ the specific heat change, ΔC_p° , is more characteristic of the type of ionization (change in net charge) than is ΔG° , ΔH° , or ΔS° . $\Delta C_p^\circ = -41$ cal/mole deg for HAc and other uncharged acids. Also, "... C_p° for the ionization of acetic acid in aqueous mixed solvents is very nearly the same as that found in pure water, although the dielectric constant varied from 78.5 to 17.7."

$$\Delta C_p^\circ = -4.606R\alpha[T + 2(T - T_m)]$$

In our studies, ΔC_p° ranged from -41 cal/mole deg (in water and T near T_m) to -86 cal/mole deg for 80% ethanol at 35°, namely, at $T - T_m = 38^\circ$.

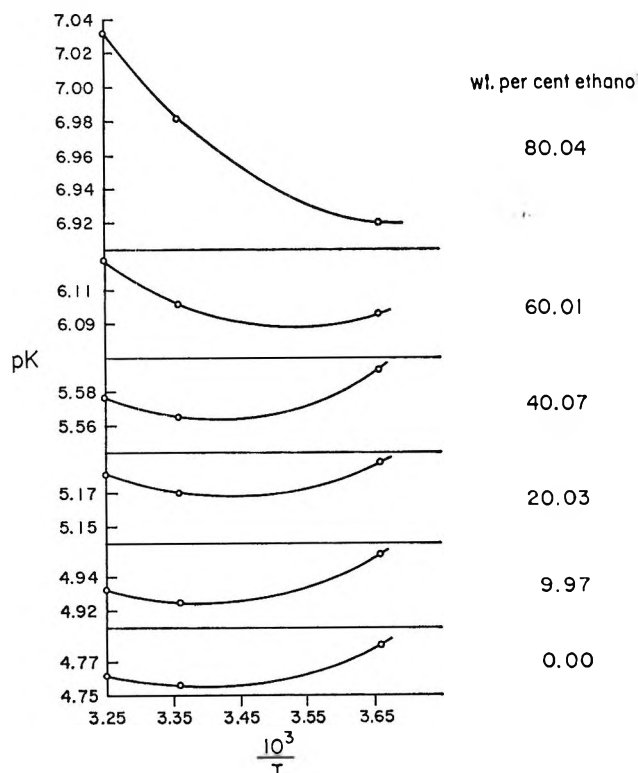


Figure 5. pK of acetic acid in ethanol-water mixtures at 0, 25, and 35°. Curves through the experimental points were calculated from eq 8 with constants from Table IV. Data on pure water are from ref 9.

(8) R. W. Gurney, "Ionic Processes in Solution," McGraw-Hill Book Co., Inc., New York, N. Y., 1953, p 128.

(9) H. S. Harned and B. B. Owen, *Chem. Rev.*, 25, 50 (1939).

Studies of Electrolytic Conductance in Alcohol-Water Mixtures. III.

Sodium Chloride in 1-Propanol-Water Mixtures at 15, 25, and 35°¹

by Mario Goffredi and Theodore Shedlovsky

Rockefeller University, New York, New York 10021 (Received January 31, 1967)

Conductance data are presented for dilute solutions of sodium chloride in 1-propanol-water mixtures at 15, 25, and 35°. Measurements were made in approximately 10, 20, 40, 60, 80, and 90 wt % 1-propanol as well as in water, but extrapolated values were obtained for pure 1-propanol because of the very low solubility of the salt in this solvent. Measurements of density, viscosity, and dielectric constant are also presented for the various solvent mixtures at the three temperatures. The conductance data were examined in terms of the 1965 theoretical Fuoss-Onsager linearized equation with the aid of a computer program. This equation describes the experimental results with very high accuracy and with reasonable values for the ion-size parameters. Evidence of ion association is found above approximately 60 wt % 1-propanol. Variations in the Walden products with solvent composition and temperature are reported and briefly discussed.

Introduction

Studies of electrolytic conductance in alcohol-water mixtures over the entire composition range of the binary solvent systems have been in progress in this laboratory. The experimental data for the behavior of strong and weak electrolytes at various temperatures are of interest not only because of the relevance to electrolyte theory but also because of the light they can throw on the structural interactions between water and alcohol, substances which have similar amphiprotic properties.

In the present paper we present data at 15, 25, and 35° on the densities, viscosities, and dielectric constants of 1-propanol-water mixtures over the entire composition range and on the electrolytic conductance of dilute sodium chloride solutions in these systems.

Experimental Section

Materials. The conductivity water used in our studies was prepared by distillation in a "High Purity" Barnstead still after passage through mixed-bed ion-exchange resins and also carbon cartridges. It was collected and stored in an all Pyrex glass closed system under purified argon. The specific conductance of this water was always under 2×10^{-7} ohm⁻¹ cm⁻¹.

Purification of 1-propanol was carried out by re-

fluxing the reagent grade over "activated" alumina for many hours under an atmosphere of dry nitrogen and collecting the middle third of a fractional distillation. The specific conductance of this material was less than 1×10^{-8} ohm⁻¹ cm⁻¹. At 25° our measurements of the density and dielectric constant were 0.7998 and 20.40, respectively, in good agreement with the corresponding values in the literature for pure 1-propanol.² Reagent grade NaCl was recrystallized three times from conductivity water and dried for several days at 200°. Its molecular weight was taken to be 58.443.

Viscosity. Viscosity measurements were made with a quartz viscometer of the Ostwald type described by Washburn and Williams³ having negligible drainage and kinetic energy correction. It was used in a range of Reynolds number less than 10 and calibrated with water at $15 \pm 0.01^\circ$, density 0.99913 g ml⁻¹, and viscosity $\eta = 0.011381$ poise based on the new values of the National Bureau of Standards.⁴

(1) This research was supported by the National Science Foundation through Grant No. GB-3062.

(2) K-Y. Chu and A. R. Thompson, *J. Chem. Eng. Data*, **7**, 358 (1962); T. A. Grover and P. A. Sears, *J. Phys. Chem.*, **60**, 330 (1956).

(3) E. W. Washburn and G. Y. Williams, *J. Am. Chem. Soc.*, **35**, 737 (1913).

Dielectric Constant. All our measurements were carried out at 1MHz using the General Radio Type 1610-AM capacitance-measuring assembly by the substitution method. The cell used for the measurements and its temperature control to $\pm 0.01^\circ$ were the same as described by Lind and Fuoss.^{5a} The cell was calibrated with acetone (D_{25° 20.70), with methanol^{5b} (D_{15° 34.68; D_{35° 30.72), and with conductivity water⁶ (D_{15° 81.95; D_{25° 78.30; D_{35° 74.82). The true cell constant at 25° was found to be 7.98 and the lead capacitance correction 3.42 pf.

Conductivity. A Pyrex and a quartz cell of the Shedlovsky type⁷ with unplatinized electrodes were used. Cell constants were determined at 25° by measuring the conductance of dilute solutions of aqueous KCl and using the equation of Lind, Zwolenik, and Fuoss.⁸ All measurements were made with the cell in a constant-temperature oil bath maintained within 0.005° with the aid of a calibrated platinum resistance thermometer and a Mueller bridge assembly. The electrical resistance measurements were made with a carefully calibrated ac bridge⁹ provided with a frequency range of 1, 5, and 10 kc which enabled polarization corrections to be made in the usual manner. These were never large but necessary to consider in work of high precision with the unplatinized electrodes we used to avoid adsorption and other possible sources of trouble with platinum black in our solvent mixtures.

The general procedure used in the present work is essentially the same as in former studies in this laboratory.^{7,10,11} All solvent mixtures and solutions were prepared by weight with appropriate vacuum corrections, of course. Stock solutions of electrolyte (about 0.1 M) were usually freshly prepared. Weight-buret technique was employed without exposure to the laboratory atmosphere by using purified argon gas in the preparation of the stock solutions and in their incremental additions to the conductance cell. Five or six such additions were made in each experiment, covering a concentration range from a fraction to several millimoles per liter in most cases.

Results and Discussion

The properties of the water-1-propanol solvent mixtures over their entire range of composition and at the three temperatures used in our studies (15° , 25° , and 35°) are listed in Table I. In this table, as elsewhere in this paper, weight per cent is the weight per cent 1-propanol in the mixture of density d_0 , viscosity $10^3\eta$ (in millipoise), and dielectric constant D . The specific conductances κ_0 are the "solvent correction" values that were subtracted from the measured specific conductances of the solutions. We made use of density

Table I: Properties of Water-1-Propanol Mixtures

Wt % $n\text{-C}_3\text{H}_7\text{OH}$	d_0	$10^3\eta$	D	$\kappa_0 \times 10^7$
15°				
0	0.99913	11.381	81.95	1.0
20	0.97201	26.90	68.39	0.8
40	0.93293	36.51	52.45	0.7
60	0.89184	38.05	38.60	0.3
80	0.85125	33.10	28.19	0.2
90	0.83051	28.81	24.50	0.1
100	0.80733	24.95	21.92	0.03
25°				
0	0.99707	8.903	78.30	1.5
20	0.9672	18.36	64.89	1.3
40	0.9263	24.97	49.70	0.9
60	0.8845	26.61	36.61	0.4
80	0.8434	23.94	26.41	0.2
90	0.8224	21.62	22.86	0.1
100	0.7998	19.38	20.40	0.05
35°				
0	0.99406	7.194	74.82	3.2
20	0.9613	13.30	62.14	2.8
40	0.9192	17.93	47.02	1.4
60	0.8766	19.40	34.49	0.7
80	0.8350	18.02	24.70	0.3
90	0.8140	16.62	21.34	0.2
100	0.7914	15.34	19.22	0.07

and viscosity values at 25° and 35° of Mikhail and Kimel¹² and the density values at 15° of the "International Critical Tables," but all the other listings in Table I are from our own measurements. Not listed in the table are our viscosity measurements at 0° since they were not essential in this paper. These were 17.865, 57.55, 75.80, 75.91, 72.08, 56.75, 47.81, and 37.05 mpoise in 0, 20, 40, 50, 60, 80, 90, and 100 wt % 1-propanol, respectively. In Figure 1 the variation in viscosity of the solvent mixtures is shown graphically as a function of mole per cent 1-propanol at the various

(4) J. F. Swindells, J. R. Coe, Jr., and T. B. Godfrey, *J. Res. Natl. Bur. Std.*, **48**, RP2279 (1952).

(5) (a) J. E. Lind and R. M. Fuoss, *J. Phys. Chem.*, **65**, 999 (1961); (b) R. G. Bates and R. A. Robinson, Institute of the Symposium of the Electrochemical Society, Toronto, May 1964.

(6) C. G. Malberg and A. A. Maryott, *J. Res. Natl. Bur. Std.*, **56**, 1 (1956).

(7) T. Shedlovsky, *J. Am. Chem. Soc.*, **54**, 1411 (1932).

(8) J. E. Lind, Jr., J. J. Zwolenik, and R. M. Fuoss, *ibid.*, **81**, 1557 (1959).

(9) J. G. Janz and G. D. E. McIntyre, *J. Electrochem. Soc.*, **108**, 272 (1961).

(10) T. Shedlovsky and R. L. Kay, *J. Phys. Chem.*, **60**, 151 (1956).

(11) H. O. Spivey and T. Shedlovsky, *ibid.*, **71**, 2165 (1967).

(12) S. Z. Mikhail and W. R. Kimel, *J. Chem. Eng. Data*, **8**, 323 (1963).

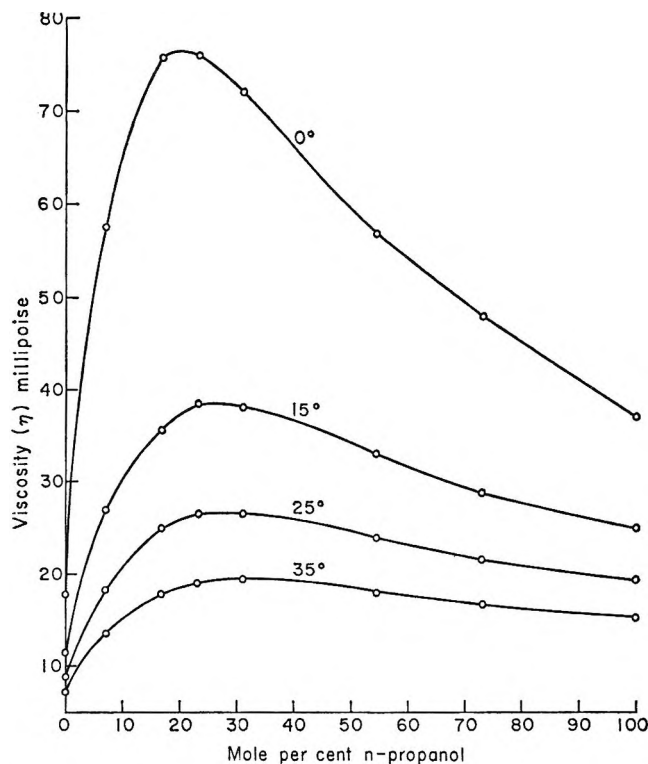


Figure 1. Viscosity of water-1-propanol mixtures.

temperatures indicated. The maxima in the curves grow flatter with increasing temperature and seem to shift gradually in position from about 20 mole % at 0° to about 30 mole % at 35°.

Measured equivalent conductances Λ at the concentrations C in equivalents per liter for dilute sodium chloride solutions are listed in Table II. The values in water at 25° are omitted because they had been previously published.⁷ Those for solvent above 90% 1-propanol were not obtained because the solubility of the salt became altogether too low for good work. The experimental values listed in the table are representative of at least two and often three experimental series that gave essentially the same results (within no more than about 0.02 or 0.03% in most cases). These are not reported for the sake of reasonable brevity.

The conductance data were analyzed with the Fuoss-Onsager¹³ 1965 three-parameter equation in the form

$$\Lambda = \Lambda_0 - SC^{1/2}\gamma^{1/2} + 2EC\gamma \ln \tau\gamma^{1/2} + LC\gamma - K_A C\gamma\Lambda f^2$$

in which γ is the degree of dissociation, K_A the association constant, f the activity coefficient, and S is the limiting Onsager slope. The coefficient L is a function of the "ion size" \bar{a} and is an adjustable parameter from the data as are the limiting equivalent conduct-

ance Λ_0 and also K_A , whereas E depends on Λ_0 but is not otherwise "adjustable." The dimensionless variable τ is the ratio of the "Bjerrum" distance to the Debye-Hückel ion atmosphere thickness.

The results of the computer analysis are summarized in the form of conductance parameters in Table III in which the symbols have already previously been defined¹³ except for the last column, σ_A , which lists the standard deviations for the various experiments. It will be noted that in no case does the standard deviation correspond to more than a few hundredths of a per cent difference between the Fuoss-Onsager equation and the actual data, as is shown by $\Delta\Lambda$ in Table II. The analysis also shows that ion pairing appears to be insignificant below 60% 1-propanol.¹⁴

In those cases where the K_A ion-pair association term, in the three-parameter equation was less than about 6, indicating relatively negligible ion pairing, the data were reprocessed without this term and with

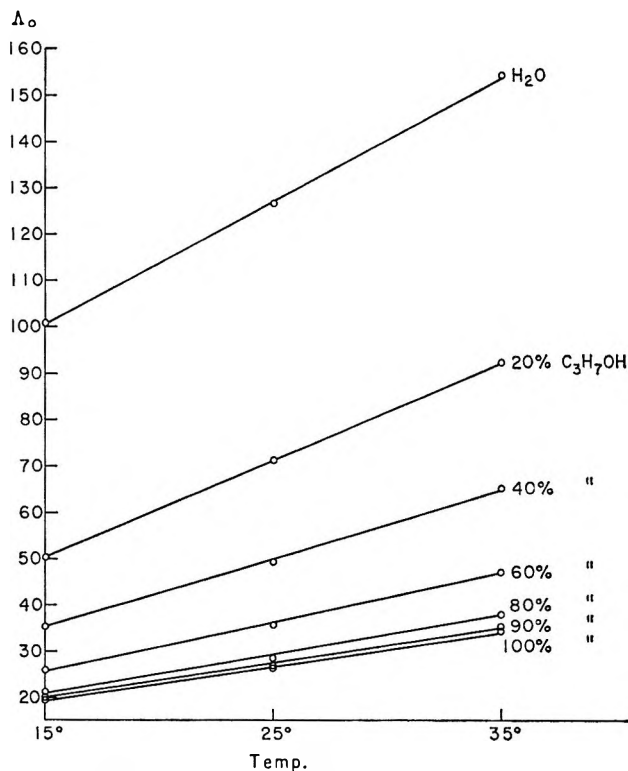


Figure 2. NaCl in water-1-propanol mixtures.

(13) R. M. Fuoss, L. Onsager, and J. T. Skinner, *J. Phys. Chem.*, **69**, 2581 (1965). We are indebted to Drs. Fuoss, Skinner, and Lind for making their Fortran computer program available to us.

(14) The values in Table III for Λ_0 , L , and \bar{a} in water (0% 1-propanol) at 25 and 35° differ a little from those previously reported from this laboratory.¹¹ It is due to the fact that different values of viscosity and dielectric constant were used in the two papers. We prefer the present values which are based on newer data.

Table II: Conductances of NaCl in Water-1-Propanol Mixtures

10°C	Λ	$\Delta\Lambda$	10°C	Λ	$\Delta\Lambda$	10°C	Λ	$\Delta\Lambda$
0.00% <i>n</i> -C ₃ H ₇ OH								
10.359	98.843	-0.006				33.496	147.755	-0.003
15.176	98.409	0.003				56.705	146.075	-0.005
19.680	98.066	0.008				77.398	144.939	0.014
24.285	97.739	-0.008				91.505	144.259	0.005
35.701	97.111	0.009				105.664	143.638	-0.011
47.425	96.554	-0.006						
20.00% <i>n</i> -C ₃ H ₇ OH								
7.688	49.447	-0.002	4.8256	68.934	-0.002	5.2965	90.633	-0.003
15.813	48.999	-0.006	7.0817	68.691	0.003	8.747	90.159	-0.003
24.233	48.667	0.004	9.6815	68.450	-0.001	12.093	89.801	0.010
30.481	48.461	0.010	15.963	67.993	0.001	17.909	89.263	0.000
38.374	48.216	0.000	19.607	67.770	-0.002	22.249	88.926	-0.003
48.374	47.949	-0.006	23.923	67.541	0.001			
40.01% <i>n</i> -C ₃ H ₇ OH								
5.1663	34.615	0.005	8.4391	47.903	0.011	3.1132	64.053	0.004
12.120	34.179	0.011	13.903	47.440	-0.008	6.7991	63.416	-0.004
23.043	33.677	-0.012	18.988	47.108	-0.002	13.021	62.669	-0.002
31.119	33.398	-0.014	25.290	46.746	-0.006	17.674	62.229	0.001
37.665	33.213	-0.002	31.168	46.458	-0.001	26.337	61.545	0.001
53.837	32.814	0.012	36.972	46.205	0.007			
60.01% <i>n</i> -C ₃ H ₇ OH								
6.9827	24.711	0.000	2.7841	34.732	-0.003	5.0869	45.337	0.002
15.131	24.115	0.000	7.2432	34.035	0.003	11.130	44.269	-0.006
21.872	23.741	-0.001	13.749	33.329	0.006	18.452	43.352	0.005
29.964	23.374	0.003	20.517	32.749	-0.008	24.239	42.759	0.000
40.449	22.970	-0.002	27.103	32.298	-0.002	33.823	41.959	0.000
48.830	22.700	0.001	32.712	31.964	0.003			
80.01% <i>n</i> -C ₃ H ₇ OH								
7.5318	19.245	0.001	6.1857	26.257	0.000	4.4477	35.081	0.004
15.123	18.375	-0.003	20.918	23.997	-0.003	10.986	33.205	-0.005
24.757	17.592	0.001	27.546	23.328	0.002	17.716	31.865	-0.006
32.409	17.104	0.001	38.771	22.423	0.001	24.607	30.812	0.004
43.719	16.518	-0.001	49.356	21.751	-0.001	34.212	29.652	0.009
						42.774	28.809	-0.007
90.00% <i>n</i> -C ₃ H ₇ OH								
2.3101	18.876	0.000	1.762	25.426	0.001	1.4379	33.229	0.002
4.3826	18.286	0.002	3.5088	24.587	-0.002	4.0318	31.433	-0.002
6.2153	17.867	0.001	5.9662	23.703	0.001	6.6842	30.150	-0.005
8.0485	17.501	-0.007	7.9047	23.136	0.000	8.6972	29.379	0.005
9.6691	17.232	0.007	8.7871	22.905	-0.001	11.524	28.465	0.005
11.752	16.900	-0.001				14.322	27.702	-0.003

$\gamma = 1$, yielding a corresponding two-parameter equation. This had negligible effect on the values of Λ_0 but did influence the values of the mean ionic diameters \bar{d} which became lowered by several tenths of an angstrom at about 40% 1-propanol. Otherwise, \bar{d} remains relatively constant at the three temperatures with the reasonable average value of about 3.3 Å. Referring to Table III again we note that from 60 to 90 wt % the K_A values increase progressively at each of the

three temperatures. Also, they become a bit higher as the temperature increases.

In Figure 2 the variations in Λ_0 for sodium chloride in the various solvent systems are shown to be reasonably linear with temperature. However, we report the temperature coefficients of conductance $(100/\Lambda_0) \cdot (\Delta\Lambda_0/\Delta T)$ with greater accuracy in Table IV in which the second column refers to the interval 15–25° and the last column to the interval 25–35°.

Table III: Conductance Parameters and Constants for NaCl in Water-1-Propanol Mixtures

Wt % ⁿ⁻ C ₃ H ₇ OH	Λ_0	d	K_A	S	E	L	σ_A
15°							
00.00	101.15 ^a ± 0.01	3.15 ± 0.05		70.04	15.77	138	0.02
00.00	101.057 ± 0.008	3.38 ± 0.06		70.02	15.75	148	0.009
20.00	50.487 ± 0.006	2.75 ± 0.06		36.82	15.26	75	0.007
40.01	35.43 ± 0.01	2.50 ± 0.07		34.02	24.99	66	0.01
60.01	25.894 ± 0.005	3.1 ± 0.1	6 ± 1	38.67	46.16	100	0.002
80.01	21.144 ± 0.008	3.19 ± 0.06	31 ± 1	51.35	96.22	114	0.003
90.00	20.19 ± 0.02	3.2 ± 0.6	76 ± 10	62.01	139.7	110	0.006
100.00	19.0 (extrapolated)						
25°							
00.00	126.52 ± 0.02	3.51 ± 0.06		89.75	20.33	191	0.04
20.00	70.124 ± 0.002	3.36 ± 0.03		53.68	22.18	132	0.002
40.01	49.428 ± 0.008	2.43 ± 0.05		49.62	36.79	86	0.008
60.01	35.79 ± 0.01	3.5 ± 0.4	8 ± 2	55.42	67.29	170	0.007
80.01	28.734 ± 0.006	3.50 ± 0.03	39 ± 1	72.57	144	184	0.002
90.00	27.093 ± 0.005	3.52 ± 0.02	117 ± 3	85.67	208	303	0.002
100.00	22.8 (extrapolated)						
35°							
00.00	153.84 ^a ± 0.03	3.61 ± 0.07		111.6	25.58	237	0.04
00.00	153.94 ± 0.02	3.34 ± 0.03		111.6	25.62	219	0.01
20.00	92.335 ± 0.007	3.50 ± 0.08		73.41	29.81	180	0.007
40.01	65.329 ± 0.003	2.56 ± 0.02		68.96	51.68	123	0.004
60.01	47.38 ± 0.01	3.2 ± 0.2	13 ± 1	76.72	96.34	332	0.006
80.01	37.96 ± 0.02	3.66 ± 0.08	45 ± 1	99.4	212	247	0.009
90.00	35.34 ± 0.01	3.68 ± 0.02	158 ± 3	115.6	305	534	0.006
100.00	27.7 (extrapolated)						

^a G. C. Benson and A. Gordon, *J. Chem. Phys.*, **13**, 473 (1945), recalculated data.

Table IV: Temperature Coefficients of Limiting Equivalent Conductance for Sodium Chloride in Water-1-Propanol Mixtures

Wt % <i>n</i> -C ₃ H ₇ OH	$\frac{100}{\Lambda_0} \left(\frac{\Delta \Lambda_0}{\Delta T} \right)_{25-20}^\circ$	$\frac{100}{\Lambda_0} \left(\frac{\Delta \Lambda_0}{\Delta T} \right)_{35-20}^\circ$
0.00	2.52	2.17
20.00	3.89	3.17
40.01	3.95	3.22
60.01	3.82	3.24
80.01	3.59	3.21
90.00	3.40	3.06
100.00	2.00	2.15

A plot of Λ_0 against the solvent composition is shown in Figure 3 for the three temperatures we had used. The extrapolations that appear as the broken lines between 90 and 100% propanol and the corresponding extrapolated values in Table III are based on similar

extrapolations of conductance data of sodium acetate solutions which we shall report in a subsequent paper dealing with the ionization constant of acetic acid. Sodium acetate has a more respectable solubility in pure 1-propanol than does sodium chloride. We had prepared plots of Λ_0 differences between these two salts and these appeared to vary quite smoothly with alcohol enrichment, making the extrapolation of $\Lambda_0(\text{NaCl})$ to 100% 1-propanol acceptable in our view. The dips in the curves between 90 and 100% parallel our experimental findings for sodium acetate in this region of solvent composition.

In Figure 4, the Walden products $\Lambda_0 \eta_0$ are shown for sodium chloride as a function of the dielectric constant D over the total range of solvent composition for the three curves corresponding to 15, 25, and 35°. These curves are not linear and cross flatly in the region between $D = 42$ and 43 with their order reversed. The crossing region corresponds to about 47% at 35°,

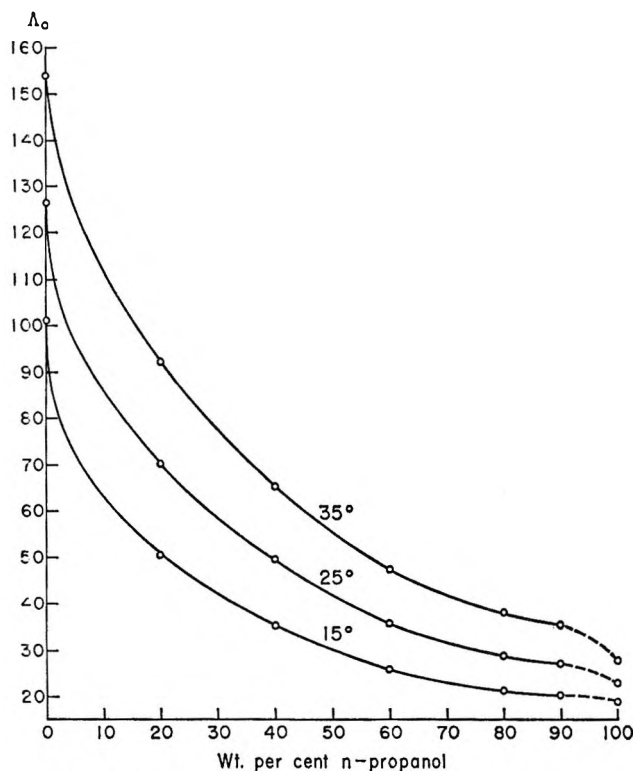


Figure 3. NaCl in water-1-propanol mixtures.

51% at 25°, and 56% at 15° solvent composition, whereas the viscosity maximum lies between 50 and 60% for all three temperatures. In the inset of Figure 4 we note that the Walden products $\Lambda_0\eta_0$ are linear with temperature for a given solvent composition, with a decreasing negative slope from 20 to 90% at which solvent composition the slope becomes zero, but it decreases again at 100% 1-propanol.

These observations, interesting though they may

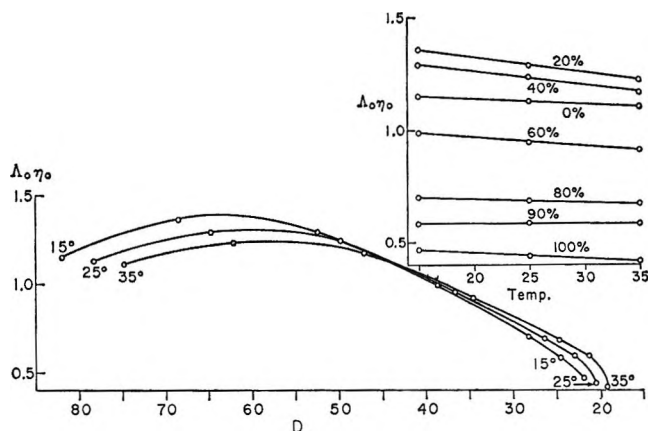


Figure 4. NaCl in water-1-propanol mixtures.

seem, do not obscure the fact that no simple generalization based on the bulk viscosity of the solvent mixtures can satisfactorily account for the variations in Λ_0 or in the corresponding $\Lambda_0\eta_0$ products found from our measurements. Although we cannot blandly accept various popular contemporary ideas about water and alcohol structures, since no really good theory for these liquids is yet at hand, it does appear that they have at least some qualitative merit.¹¹ We prefer, however, to reserve discussion of this matter for a subsequent communication that will make it possible to compare the experimental results for several electrolytes in different alcohol-water systems.

Acknowledgment. We are indebted to Mrs. Catherine Wolowodink for her valuable technical assistance throughout the course of the experimental studies and to Mrs. Marion Angell for her most skillful and gracious help in the analysis of our data with the 7090 IBM computer.

Studies of Electrolytic Conductance in Alcohol-Water Mixtures. IV.

Hydrochloric Acid in 1-Propanol-Water Mixtures at 15, 25, and 35°¹

by Mario Goffredi and Theodore Shedlovsky

Rockefeller University, New York, New York 10021 (Received January 31, 1967)

Conductance measurements on dilute solutions of hydrochloric acid in approximately 20, 40, 60, 80, 90, and 100 wt % 1-propanol-water mixtures at 15, 25, and 35° are reported. The data were analyzed with the aid of a computer programmed for the linearized 1965 theoretical Fuoss-Onsager equation which describes the data within the limits of experimental accuracy with reasonable values for the ion-size parameters. Despite the fact that the conductance process differs in detail for proton carriers from that of the "normal" ions, our results show no evidence of abnormalities in the solvent mixtures other than those which are well known in aqueous solutions such as "abnormally" high conductance and relatively low temperature coefficients of conductance as compared with "normal" ions. Evidence of ion association does not appear until approximately 80 wt % 1-propanol. Variations in the Walden products of hydrochloric acid with solvent composition and temperature are reported and compared with those of sodium chloride in the same solvent mixtures. A comparison of the Walden products for the acid in these solvents is also made with those in ethanol-water and in methanol-water systems from previous work in this laboratory.

Introduction

In our previous paper² we reported studies on the electrolytic conductance of dilute sodium chloride solutions in the binary solvent systems water-1-propanol at 15, 25, and 35° over the entire range of solvent composition. We also reported our measurements of viscosity and of dielectric constant for these solvents at these temperatures, values which are required for a theoretical analysis of the electrical conductance of solutions of electrolytes.

The present paper reports our results on the conductance of dilute hydrochloric acid solutions, again at 15, 25, and 35° in the same solvent system water-1-propanol over the entire range of composition.

Experimental Section

The hydrochloric acid used in this work was prepared from the reagent grade acid by a fractional redistillation that yielded a constant-boiling product. Its concentration was accurately determined from conductance measurements on appropriate aqueous solutions using the values of Stokes.³ All the stock solutions of

HCl that were used in the incremental additions for each experimental series of conductance measurements were prepared from such constant-boiling acid, except in the case of pure 1-propanol solvent. Here, to prevent the unavoidable addition of water to the pure alcohol from the constant-boiling acid, the stock solution was prepared with pure, dry HCl gas. Its concentration was determined analytically by careful titration against a borax standard using methyl red as an indicator.

The preparation of the conductivity water and of the 1-propanol as well as the apparatus and the general experimental procedures employed in the present work were the same as those we had formerly used and have described in our previous paper.² However, in order to avoid trace losses of acid through adsorption or ion exchange^{4a} in our flask conductance cells,^{4b} a matter

(1) This research was supported by the National Science Foundation through Grant No. GB-3062.

(2) M. Goffredi and T. Shedlovsky, *J. Phys. Chem.*, **71**, 2176 (1967).

(3) R. H. Stokes, *ibid.*, **65**, 1242 (1961).

of importance at the lower acid concentrations measured, we presoaked the cells with approximately 1 M HCl in the solvent to be used⁵ before final rinsing and the beginning of an experimental series of measurements.

Results and Discussion

Experimental values for the equivalent conductance Λ at the concentrations C (equivalents per liter) for dilute solutions of hydrochloric acid in the various water-1-propanol solvent mixtures at 15, 25, and 35° are listed in Table I. (We have omitted the values in pure water at 15 and 25° because they had been previously published.) No solvent correction was made since the specific conductances of our solvents were always quite low, usually less than 10^{-7} ohm⁻¹ cm⁻¹, which was probably due at least in part to residual CO₂. The solvent compositions given in Table I are expressed in weight per cent 1-propanol as they will be throughout this paper. The columns $\Delta\Lambda$ list the standard deviations for the corresponding Λ values from the best fitted Fuoss-Onsager equation that will be discussed presently. As was the case in our work on sodium chloride solutions² the data in Table I are representative of at least two series of measurements that were in close agreement with one another. As before, we analyzed the conductance data with the Fuoss-Onsager equations⁶

$$\Lambda = \Lambda_0 - SC^{1/2}\gamma^{1/2} + 2EC\gamma \ln \tau\gamma^{1/2} + LC\gamma - K_A C\gamma\Delta f^2 \quad (1)$$

or

$$\Lambda = \Lambda_0 - SC^{1/2} + 2EC \ln \tau + LC \quad (2)$$

in which the symbols have been previously defined,^{2,6} but to repeat in part, γ is the degree of dissociation, f the activity coefficient, S the Onsager limiting slope, K_A the association constant, E a constant depending on Λ_0 , and L a constant which is a function of the "ion size" δ . To make the numerical computations, we used the dielectric constant and viscosity values listed for the various solvent mixtures at the three temperatures in Table I of our previous paper.² In this work, eq 1 was first used and if the values of K_A , the association constant, were low enough to indicate no ion pairing of any significance, the data were recycled without the K_A term, namely, eq 2.

The results of the analyses are listed in Table II which is self-explanatory. Note that no significant ion association is evident below 80% 1-propanol, that the standard deviations σ_Λ are quite small throughout the experimental series, and that the "ion sizes," δ , are not unreasonable. The average value at each

of the three temperatures is about 4 Å and any apparent trend we believe to be within the experimental errors in our measurements. As noted in $\Delta\Lambda$ of Table I the probable errors in the conductance values Λ are within a few hundredths of a per cent, except in pure or nearly pure 1-propanol. Here it rose to slightly over 0.1% owing to the fact that the concentrations of the stock solutions, prepared from HCl gas and analyzed by titration, were less accurately known.

In footnotes *a* and *b* of Table II we have listed the values of Λ_0 , etc., for HCl in water at 15, 25, and 35° from the work of others. At 35°, where a direct comparison is made between Owen's and Sweeton's work and ours, the agreement is excellent. At 15 and 25° we made no measurements in pure water, but Stokes' value at 25° we know to be in very close agreement with work previously published by one of us.^{4b}

As we had observed for NaCl in the same solvent systems,² "ion pairings," K_A values, for HCl also increase with 1-propanol enrichment and are somewhat higher at a higher temperature. However, below 80% 1-propanol HCl behaves as a strong electrolyte.

In Table III, the temperature coefficients for Λ_0 of HCl are listed for the various solvent compositions. As can be seen from columns 2 and 3, for (15-25°) and (25-35°), respectively, they tend to decrease somewhat with increasing temperature, but what is more important, they steadily increase with 1-propanol enrichment. In comparison with the corresponding coefficients for NaCl (Table IV of our previous paper²) the coefficients for the acid remain lower than for the salt up to 80% 1-propanol. They are about the same at 90%, above which the values drop for NaCl but not for HCl.

As is shown in Figure 1, the limiting conductance Λ_0 for HCl decreases smoothly, although not linearly, with 1-propanol enrichment of the solvent at each of the three temperatures we had used. However, unlike the values for NaCl² that showed a small drop in Λ_0 between 90 and 100% 1-propanol, for HCl Λ_0 rose very sharply near pure 1-propanol, as may be seen in the inset of Figure 1. Similar behavior for HCl had been observed at alcohol ends in the water-methanol⁷ and water-ethanol^{5,8} systems. The Walden products $\Lambda_0\eta_0$ for

(4) (a) J. E. Price, *J. Phys. Chem.*, **67**, 1152 (1963); (b) T. Shedlovsky, *J. Am. Chem. Soc.*, **54**, 1411 (1932).

(5) H. O. Spivey and T. Shedlovsky, *J. Phys. Chem.*, **71**, 2165 (1967).

(6) R. M. Fuoss, L. Onsager, and J. T. Skinner, *ibid.*, **69**, 2581 (1965).

(7) T. Shedlovsky and R. L. Kay, *ibid.*, **60**, 151 (1956).

(8) I. I. Bezman and F. H. Verhoek, *J. Am. Chem. Soc.*, **67**, 1330 (1945).

Table I: Conductances of HCl in Water-1-Propanol Mixtures

15°			25°			35°		
10°C	Λ	$\Delta\Lambda$	10°C	Λ	$\Delta\Lambda$	10°C	Λ	$\Delta\Lambda$
0.00% $n\text{-C}_3\text{H}_7\text{OH}$								
						18.441	481.779	-0.020
						23.400	480.857	-0.001
						29.609	479.866	0.026
						37.888	478.694	0.015
						47.943	477.461	-0.019
20.00% $n\text{-C}_3\text{H}_7\text{OH}$								
1.3533	195.449	-0.033	5.3994	249.860	0.011	23.837	304.074	-0.027
3.8627	194.893	0.006	7.3456	249.427	-0.005	29.751	303.369	-0.004
4.6300	194.779	0.024	10.718	248.832	-0.004	37.540	302.601	0.051
6.0649	194.553	0.012	13.496	248.413	-0.010	44.583	301.923	0.018
7.7047	194.331	-0.002	16.568	248.023	0.000	51.973	301.270	-0.037
10.066	194.088	0.007	19.756	247.663	0.008			
12.602	193.860	0.006						
14.564	193.680	-0.021						
40.01% $n\text{-C}_3\text{H}_7\text{OH}$								
3.7168	121.382	-0.027	5.5080	159.615	0.006	6.7023	201.093	-0.002
4.7143	121.224	-0.010	7.4423	159.202	-0.006	12.480	199.712	-0.013
5.8768	121.064	0.008	9.9045	158.776	0.002	18.425	198.650	-0.004
7.4714	120.865	0.023	12.440	158.378	-0.010	24.939	197.741	0.042
10.154	120.559	0.020	15.198	158.028	0.010	33.969	196.591	-0.020
12.869	120.293	0.012	18.697	157.604	-0.002	44.071	195.611	-0.003
16.299	119.978	-0.027						
60.01% $n\text{-C}_3\text{H}_7\text{OH}$								
4.6686	71.648	0.002	6.5037	93.932	0.013	6.2395	120.980	0.001
7.0528	71.217	-0.005	10.545	93.103	0.001	11.977	119.442	0.014
13.765	70.326	-0.001	12.809	92.704	-0.013	14.770	118.822	0.000
15.178	70.183	0.012	17.488	92.024	-0.006	17.699	118.247	-0.005
16.385	70.045	0.000	21.077	91.568	-0.006	23.516	117.229	-0.038
17.878	69.889	-0.008	27.893	90.837	0.011	28.631	116.550	0.028
80.01% $n\text{-C}_3\text{H}_7\text{OH}$								
9.3314	36.975	0.001	8.9820	48.214	0.002	4.6996	64.897	0.004
14.441	36.292	-0.002	9.0454	48.196	-0.002	10.823	62.764	-0.006
20.788	35.625	-0.003	23.571	45.846	0.008	14.594	61.794	-0.001
26.318	35.155	0.005	25.906	45.555	-0.006	19.299	60.778	-0.002
33.769	34.609	-0.002	31.157	44.993	-0.003	25.568	59.667	0.002
			39.113	44.275	0.002	30.458	58.943	0.011
						36.284	58.174	-0.008
90.00% $n\text{-C}_3\text{H}_7\text{OH}$								
6.1697	25.264	0.004	4.6520	34.001	0.008	3.6881	44.556	0.009
12.717	24.223	-0.009	10.767	32.425	-0.009	9.3656	42.222	-0.013
16.981	23.723	-0.004	15.635	31.530	-0.006	13.627	41.002	-0.009
21.667	23.272	0.012	24.852	30.246	-0.003	21.116	39.388	0.009
29.214	22.645	-0.002	31.155	29.575	0.011	26.608	38.467	0.016
35.809	22.205	-0.003	40.889	28.724	0.010	35.482	37.260	-0.010
			49.881	28.085	-0.009			
99.48% $n\text{-C}_3\text{H}_7\text{OH}$								
8.9218	15.944	0.010	9.2832	20.691	0.001	13.388	25.088	-0.004
11.714	15.519	-0.007	17.497	19.126	-0.002	19.884	23.628	0.010
19.189	14.657	-0.013	27.162	17.888	-0.001	26.510	22.476	-0.010
31.293	13.708	0.014	35.346	17.118	0.006	33.023	21.593	-0.001
40.796	13.142	0.004	42.729	16.553	-0.002	40.770	20.740	0.001
49.278	12.734	-0.006						

Table I (Continued)

15°			25°			35°		
10°C	Λ	$\Delta\Lambda$	10°C	Λ	$\Delta\Lambda$	10°C	Λ	$\Delta\Lambda$
100.00% <i>n</i> -C ₃ H ₇ OH								
9.1226	18.213	0.006	2.5770	26.975	0.013	5.4357	33.057	0.007
15.198	17.110	-0.004	8.3811	24.233	-0.031	10.118	30.433	-0.018
23.903	15.998	-0.021	15.575	22.249	-0.023	17.279	27.826	0.016
32.180	15.273	0.030	24.168	20.665	-0.012	25.309	25.799	0.000
44.995	14.380	-0.009	30.783	19.750	-0.016	33.325	24.318	0.000
			38.370	18.901	-0.037			
			44.341	18.337	-0.070			

Table II: Conductance Parameters and Constants for HCl in Water-1-Propanol Mixtures

Wt % <i>n</i> - C ₃ H ₇ OH	Λ_0	i	K_A	S	E	L	σ_A
15°							
00.00	362.52 ^a ± 0.02	3.43 ± 0.03		129.1	74.17	417	0.03
20.00	196.40 ± 0.02			80.09	71.35	649	0.02
40.01	122.84 ± 0.02	5.5 ± 0.2		72.62	99.5	534	0.02
60.01	73.418 ± 0.008	3.55 ± 0.04		71.89	147.7	289	0.007
80.01	39.69 ± 0.02	3.7 ± 0.1	4 ± 2	72.13	198.0	241	0.005
90.00	27.52 ± 0.03	3.7 ± 0.1	15 ± 3	72.14	200	197	0.01
99.48	18.71 ± 0.05	3.4 ± 0.1	41 ± 7	71.69	173.1	129	0.01
100.00	22.0 ± 0.1	3.8 ± 0.1	118 ± 15	77.53	213	160	0.03
25°							
00.00	426.59 ^b ± 0.04	3.66 ± 0.05		158.8	89.71	525	0.07
20.00	252.43 ± 0.01	4.63 ± 0.06		109.3	96.27	553	0.009
40.01	162.113 ± 0.009	4.53 ± 0.05		100.9	138.7	559	0.008
60.01	96.82 ± 0.01	3.73 ± 0.03		99.3	205	404	0.01
80.01	52.02 ± 0.02	3.89 ± 0.09	8 ± 1	99.9	284	331	0.006
90.00	36.77 ± 0.02	3.78 ± 0.05	21 ± 2	99.8	299	235	0.01
99.48	25.02 ± 0.02	3.66 ± 0.04	88 ± 3	97.2	263	175	0.005
100.00	29.81 ± 0.07	3.90 ± 0.05	171 ± 9	106.1	329	171	0.05
35°							
00.00	489.55 ^a ± 0.09	4.0 ± 0.1		190.2	106.1	655	0.1
	489.85 ± 0.03	4.21 ± 0.06		190.2	106.2	698	0.02
20.00	310.99 ± 0.07	4.3 ± 0.1		141.1	121.4	620	0.04
40.01	204.86 ± 0.02	4.05 ± 0.04		134.5	186.6	613	0.03
60.01	124.86 ± 0.03	3.75 ± 0.05		134.8	286	511	0.03
80.01	68.69 ± 0.02	4.22 ± 0.06	12 ± 1	137.3	416	500	0.008
90.00	48.08 ± 0.03	4.3 ± 0.1	41 ± 2	135.2	437	415	0.02
99.48	32.5 ± 0.1	3.70 ± 0.09	128 ± 8	127.7	375	169	0.01
100.00	39.76 ± 0.07	3.93 ± 0.02	255 ± 7	141.4	483	176	0.02

^a B. B. Owen and F. H. Sweeton, *J. Am. Chem. Soc.*, **63**, 2811 (1941). ^b R. H. Stokes, *J. Phys. Chem.*, **65**, 1242 (1961) (both values recomputed with new η_0 and D_0 values).

HCl are shown in Figure 2, plotted against the dielectric constant D for 15, 25, and 35°. The values for D and for the solvent viscosity η_0 are from our previous paper.² We had observed for NaCl that the $\Lambda_0\eta_0$ vs. D curves for the three temperatures are not linear, exhibit maxima toward the aqueous regions of compo-

sition, and cross at a common point with their order reversed. We note the same behavior for HCl, but the maxima and common crossing point are sharper than for NaCl, although their positions relative to 1-propanol composition remain quite similar. The crossing point is at $D = 41$ for HCl and at $D = 42-43$

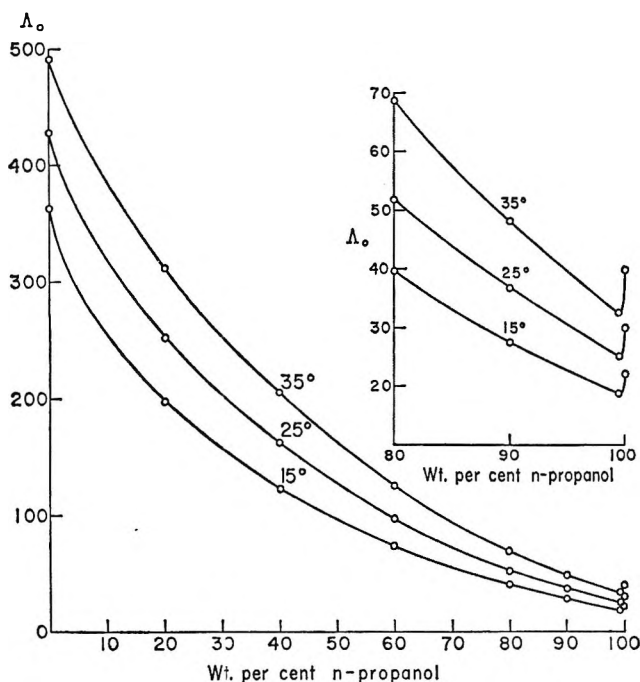
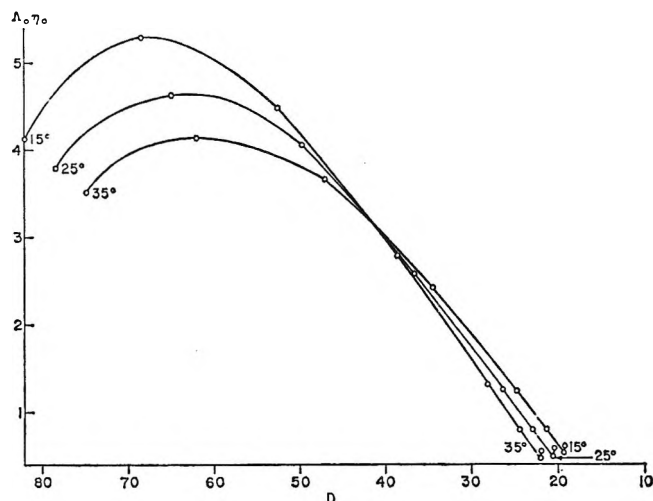
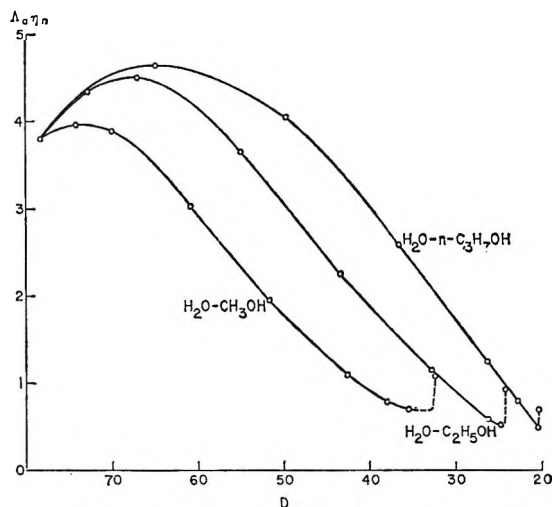


Figure 1. HCl in water-1-propanol mixtures.

Figure 2. Λ_{070} vs. D for HCl in water-1-propanol mixtures.**Table III:** Temperature Coefficients of Limiting Conductance for Hydrochloric Acid in Water-1-Propanol Mixtures

Wt % $n\text{-C}_3\text{H}_7\text{OH}$	$\frac{100(\Delta\Lambda_0)}{\Lambda_0(\Delta T)}_{15-25^\circ}$	$\frac{100(\Delta\Lambda_0)}{\Lambda_0(\Delta T)}_{25-35^\circ}$
0.00	1.77	1.48
20.00	2.85	2.32
40.01	3.20	2.64
60.01	3.19	2.90
80.01	3.11	3.20
90.00	3.36	3.08
100.00	3.55	3.36

for NaCl. It is of interest to note that the common point, Λ_{070} at $D = 41$, for HCl at the three temperatures is at the viscosity maxima of the corresponding solvent mixtures: 56, 53, and 49% 1-propanol for 15, 25, and 35°, respectively. The abrupt rise in Λ_0 close to the pure alcohol end of solvent composition has been mentioned above. This is also true of the Walden products Λ_{070} as may be seen in the dotted regions of the curves in Figure 3. These curves represent the variation of Λ_{070} with the dielectric constant D for the three different water-alcohol systems at 25°, namely, $\text{H}_2\text{O}-\text{CH}_3\text{OH}$,⁷ $\text{H}_2\text{O}-\text{C}_2\text{H}_5\text{OH}$,^{5,8} and $\text{H}_2\text{O}-\text{C}_3\text{H}_7\text{OH}$,

Figure 3. Λ_{070} vs. D for HCl in water-alcohol mixtures at 25°.

the present work. We note that the curves are similar in form but that there are marked quantitative differences between them. These differences are not obviously explainable through solvent viscosity and dielectric constant properties. For the present, we are content to present experimental data which may later help in really understanding these complicated, hydrogen bond structured systems.

Acknowledgment. We are indebted to Drs. Fuoss, Skinner, and Lind for making their FORTRAN computer program available to us, to Mrs. Catherine Wolowodiuk for her devoted technical assistance, and to Mrs. Marion Angell for her help in the analysis of our data with the 7090 IBM computer.

Thermochemistry of Cyanocarbons. II. The Heats of Combustion of

Pyridinium Dicyanomethylide, Malononitrile, and Fumaronitrile

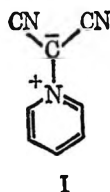
by Richard H. Boyd, K. Ranjan Guha, and Richard Wuthrich

Department of Chemistry, Utah State University, Logan, Utah 84321 (Received December 12, 1966)

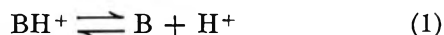
The heats of formation of solid and gaseous pyridinium dicyanomethylide, malononitrile, and fumaronitrile have been determined *via* the heats of combustion of the solids and their heats of vaporization (from vapor pressure curves). From these data, the thermochemical bond energy of the N^+-C^- bond in the ylide is calculated to be 67 kcal mole⁻¹. The data for malononitrile and fumaronitrile are used to revise and extend a discussion of the electrostatic and electronic effects of cyano group substitution. The pK_a for the dissociation in water of the conjugate acid of the ylide was determined to be -1.55 .

Introduction

Ylides are compounds in which the formal structure has a positively charged atom covalently bonded to negatively charged carbon. There are a number of examples of phosphorus ylides, whose stability may perhaps be promoted by d-orbital participation rendering the actual structure less ionic. With nitrogen, where this possibility is remote, stable ylides are rare. How-



ever, recently the compound pyridinium dicyanomethylide (I), an example of a stable nitrogen ylide, has become known,^{1,2} and its structure was confirmed by X-ray diffraction.³ In the present work we have measured the heat of combustion and heat of vaporization of I in order to provide quantitative information about the stability of this structure. Also of interest in assessing the stability of the ylide is the ease or difficulty with which it protonates, *i.e.*, the position of the equilibrium



where B represents I and BH^+ its protonated form (presumably protonated on the N carbon). Consequently, we have measured the pK_a of reaction 1.

In order to provide auxiliary data to aid in the interpretation of the stability of I we have also measured the heats of combustion and vaporization of malononitrile (dicyanomethane) for which there are no modern values. Malononitrile is an interesting compound thermochemically in its own right as it is one of the simplest compounds in which the phenomenon of electrostatic repulsion between highly polar cyano groups can manifest itself. We have previously investigated this effect in tri- and tetracyanoethylene.⁴ In order to make the study of cyano group interaction more complete we have also included fumaronitrile (*trans*-dicyanoethylene) in this study.

Experimental Section

The pyridinium dicyanomethylide furnished to us had been synthesized *via* the reaction of pyridine and tetracyanoethylene oxide.^{1,2} It was purified by three recrystallizations from acetone and then further purified by twice subliming along a temperature gradient⁵ and keeping the center fraction. It was necessary to keep

(1) W. J. Linn, O. W. Webster, and R. E. Benson, *J. Am. Chem. Soc.*, **85**, 2032 (1963).

(2) A. Rieche and P. Dietrich, *Chem. Ber.*, **96**, 3044 (1963).

(3) C. Bugg, R. Desiderato, and R. L. Sass, *J. Am. Chem. Soc.*, **86**, 3157 (1964).

(4) R. H. Boyd, *J. Chem. Phys.*, **38**, 2529 (1963); paper I of this series.

(5) G. J. Sloan in "Physics and Chemistry of the Organic Solid State," D. Fox, M. M. Labes, and A. Weissberger, Ed., Interscience Publishers, Inc., New York, N. Y., 1963, Chapter 2.

Table I: Energy of Combustion at 25°^a

<i>M</i>	<i>M_F</i>	ΔR	$\Delta R'$	<i>q</i> ₁	<i>q</i> ₂	<i>q</i> ₃	<i>q</i> ₄	$-\Delta E_c^\circ$, cal/g (air vs. stainless steel)
Malononitrile								
0.294024	0.002191	0.198924	0.197911	0.5	7.6	1.5	-0.2	5988.3
0.285834	0.002136	0.193452	0.192464	0.5	7.3	1.5	-0.2	5990.5
0.287224	0.002182	0.194601	0.193592	0.5	7.4	1.5	0.0	5995.6
0.280415	0.002247	0.189836	0.188797	0.4	7.4	1.5	0.0	5988.6
0.286695	0.002372	0.193838	0.192742	0.4	7.4	1.5	0.0	5980.5
0.287360	0.002391	0.194540	0.193435	0.4	7.4	1.5	0.0	5988.2
								5988.6 Av
								$\sigma = 4.3$
								5984.3 cal/g (vacuum)
Fumaronitrile								
0.257870	0.002122	0.190108	0.189126	0.5	6.0	1.5	0.0	6528.6
0.258884	0.002086	0.190822	0.189857	0.5	6.0	1.5	0.0	6528.3
0.256558	0.002134	0.189053	0.188066	0.5	5.8	1.5	0.0	6525.8
0.259922	0.002170	0.191256	0.190253	0.4	6.1	1.5	0.0	6515.8
0.269708	0.002148	0.198478	0.197485	0.4	6.2	1.5	0.0	6518.9
								6523.5 Av
								$\sigma = 5.2$
								6518.7 cal/g (vacuum)
Pyridinium Dicyanomethylide								
0.257673	0.002303	0.206981	0.205916	0.6	5.7	1.4	-0.4	7118.9
0.240911	0.002012	0.193557	0.192627	0.5	5.3	1.4	-0.4	7123.2
0.240165	0.002200	0.193046	0.192029	0.4	5.3	1.4	-0.3	7123.0
0.252531	0.002020	0.202727	0.201793	0.4	4.0	1.4	-0.5	7126.0
0.240709	0.002359	0.193338	0.192247	0.6	5.3	1.4	-0.4	7114.6
0.244217	0.002302	0.195997	0.194933	0.5	5.2	1.4	-0.3	7111.2
								7119.5 Av
								$\sigma = 5.2$
								7114.8 cal/g (vacuum)

^a *M* = mass of sample (g, in air vs. stainless steel). *M_F* = mass of cotton thread fuse (g, in air vs. stainless steel). ΔR = corrected temperature rise (ohms). $\Delta R' = \Delta R - M_F(0.4624)$ (ohms). *q*₁ = electrical ignition energy (cal). *q*₂ = nitric acid correction (cal). *q*₃ = correction to standard states (Washburn correction) (cal). *q*₄ = unburned carbon correction (cal). $-\Delta E_c^\circ = [\varepsilon \Delta R' - q_1 - q_2 - q_3 - q_4]/M$; the energy of combustion corrected to standard states. $\varepsilon = 8944.0$ cal ohm⁻¹.

the hot end of the sublimer at ~110° or less to avoid decomposition (dark residue) during sublimation. The final melting point was 245°, in agreement with the literature values.^{1,2}

Malononitrile was furnished to us purified by repeated zone refining.⁵ It was then sublimed through a temperature gradient from the zone-refining tube.

Fumaronitrile was purchased from Chemical Intermediates and Research Laboratories, Inc. It was purified by repeated zone refining and sublimed through a temperature gradient from the zone-refining tube.

The heats of combustion were measured by previously described techniques.⁶ The calorimeter differed from that previously described in having a dif-

ferent resistance thermometer. The technique also differed in that the electrical energy was supplied from the capacitor bank charged to 20–23 v rather than 45 v as previously described.⁷ This resulted in a smaller electrical energy correction and lessened the pitting of the contacts on the firing switch due to arcing which was noticed previously. A calibration based on 12 combustions of benzoic acid (National Bureau of Standards sample 39i) by two different operators resulted in an energy equivalent of 8944.0 ± 3.1 cal ohm⁻¹, where

(6) R. H. Boyd, R. Christensen, and R. Pua, *J. Am. Chem. Soc.*, **87**, 3554 (1965).

(7) R. H. Boyd, *Rev. Sci. Instr.*, **35**, 1086 (1964).

the uncertainty is the 95% confidence level for the sample mean.

Weights were reduced to *in vacuo* values with the following densities (g/ml) estimated from the dimensions of weighed pellets: malononitrile, 1.1; fumaronitrile, 1.15; and pyridinium dicyanomethylide, 1.27.

The results of the combustions are recorded in Table I.

The vapor pressures were determined by an effusion cell technique.⁶ The results are given in Table II.

Table II: Vapor Pressures^a

Temp, °C	Wt loss, mg	Effusion time × 10 ³ , sec	P, μ
Malononitrile			
-17.50	1.240	76.7	0.637
-12.55	1.103	24.85	1.765
-7.85	1.860	21.07	3.55
-2.35	2.933	18.80	6.33
3.15	6.477	21.58	12.31
8.15	10.550	20.53	21.26
Fumaronitrile			
8.15	19.868	19.30	39.00
2.60	10.955	19.27	21.43
-1.95	6.841	18.95	13.49
-7.70	3.796	20.19	6.95
-12.70	1.885	19.62	3.52
-17.60	1.053	20.50	1.864
-22.85	1.050	39.43	0.956
-27.75	2.000	169.17	0.420
Pyridinium Dicyanomethylide			
130.5	1.262	91.69	0.465
137.1	2.497	67.35	1.256
140.9	0.912	21.60	1.441
149.9	1.584	18.00	3.04
154.2	1.894	12.37	4.53
160.2	2.219	11.50	5.73
166.8	2.158	6.06	12.55
133.3	1.256	66.03	0.643
Log P(μ) = (A/T) + B			
		A	B
Malononitrile		-4139	16.076
Fumaronitrile		-3758	14.970
Pyridinium dicyanomethylide		-6549	15.955

^a Orifice diameter, 0.333 mm.

The constants in the equation $\log P = (A/T) + B$ were calculated by least squares, and the heat of vaporization was calculated from the relation $\Delta H_{\text{vap}} = -2.303RA$.

A summary of the derived thermochemical data is given in Table III.

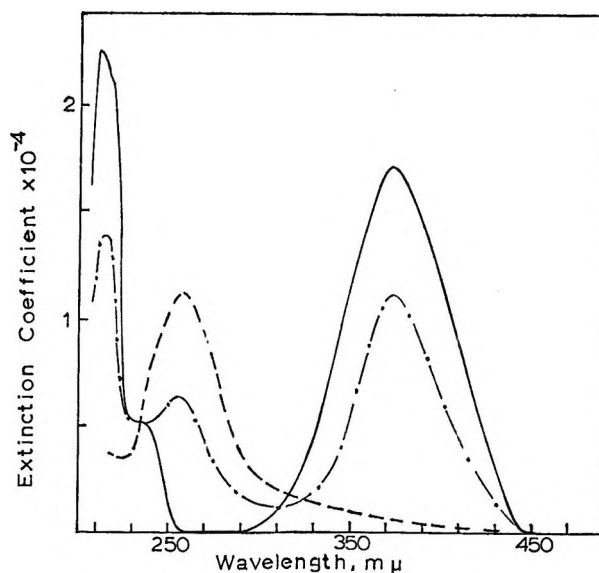


Figure 1. Absorption spectrum of pyridinium dicyanomethylide. Solid curve is neutral form in water; dashed curve is protonated form in strong aqueous hydrochloric acid; dashed-dot curve is in hydrochloric acid of intermediate strength where both protonated and neutral forms are in equilibrium.

The pK_a for the dissociation of the conjugate acid of I (eq 1) was measured spectrophotometrically in hydrochloric acid solutions. A Beckman DU spectrophotometer with the cell compartment thermostated at 25° was used for the quantitative measurements. The neutral form, B, has an absorption maximum at 374 $m\mu$ (ϵ 1.74 $\times 10^4$). This absorption decreases (reversibly) in solutions of increasing acid strength. A slight residual absorption at this wavelength due to BH^+ remains in strong acid (see Figure 1). Prolonged exposure to strong acid solution results in irreversible changes in the spectrum. The pK_a was determined⁸ from the intercept at $C_{H^+} = 0$ of a plot of

$$\log R + \log C_{H^+} = \log K - \log (f_H + f_B / f_{BH^+})$$

where $R = C_B / C_{BH^+}$, C is the molar concentration (C_{H^+} refers to hydrogen ion concentration of the aqueous hydrochloric acid solvent), and f is the molar activity coefficient, *vs.* C_{H^+} . The protonation ratio, R , was determined from

$$R = [D - D^0(BH^+)] / [D^0(B) - D]$$

where D is the optical density of a given solution (at λ_{max} 374 $m\mu$ of B), $D^0(B)$ is the optical density of a given solution of same concentration in pure water (entirely in B form), and $D^0(BH^+)$ is the optical density of

(8) M. A. Paul and F. A. Long, *Chem. Rev.*, 57, 1 (1957).

Table III: Summary of Thermochemical Data

Compound		ΔH_o° , kcal mole ⁻¹	ΔH_{vap}° , kcal mole ⁻¹	ΔH_f° , kcal mole ⁻¹
Malononitrile	(c)	-395.03 ± 0.3^b	18.9 ± 0.2	44.56 ± 0.3
	(g)	-413.9 ± 0.5^c		63.5 ± 0.5
Fumaronitrile	(c)	-508.63 ± 0.4^b	17.2 ± 0.2	64.11 ± 0.4
	(g)	-525.8 ± 0.6^c		81.3 ± 0.6
Pyridinium dicyano- methylide	(c)	-1018.3 ± 0.8^b	30.0 ± 0.3 (403–440°K)	95.1 ± 0.8
	(g)	-1048.3 ± 3.0^c		125.1 ± 3.0

^a Uncertainties are arbitrary estimates. ^b Uncertainty is $\pm \sigma \Delta H_o^\circ$, where $\sigma = (\sigma_1^2 + \sigma_2^2)^{1/2}$ and σ_1 and σ_2 are relative standard deviations of calibration and sample runs. ^c Uncertainty is summed uncertainty of *a* and *b*, plus added uncertainty for pyridinium dicyanomethylide due to experimental ΔH_{vap} range being far from 25°.

a solution of same concentration in strong acid (residual absorption due to shoulder of BH⁺ at λ_{max} for B). The log *R* values at various acid concentrations are listed in Table IV.

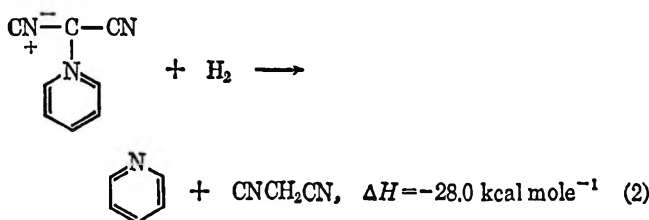
Table IV: Determination of the p*K*_a for the Dissociation of the Conjugate Acid of Pyridinium Dicyanomethylide^a

[H ⁺], <i>M</i>	Log <i>R</i> + log C _{H⁺}
1.006	1.211
1.506	1.034
2.00	0.881
2.51	0.684
3.00	0.405
3.52	0.210

^a From intercept at C_{H⁺} = 0, p*K*_a = $-(\log R + \log C_{H^+})_0 = -1.55$.

Discussion

Probably of most direct interest in discussing the stability of pyridinium dicyanomethylide would be the thermochemical average bond energy of the C⁻-N⁺ bond in this compound. We have assigned this by considering the average thermochemical C-CN bond energies to be the same as in malononitrile. Then the enthalpy of the reaction⁹



is related to thermochemical bond energies as

$$\Delta H = E(\text{C}^--\text{N}^+) + E(\text{H}-\text{H}) - 2E(\text{C}-\text{H}) \quad (3)$$

Using¹⁰ $E(\text{H}-\text{H}) = 104 \text{ kcal mole}^{-1}$ and $E(\text{C}-\text{H}) = 99.5 \text{ kcal mole}^{-1}$, we arrive at $E(\text{C}^--\text{N}^+) = 67 \text{ kcal mole}^{-1}$. This considerable stability of the formal C⁻-N⁺ bond is no doubt related to the presence of the cyano groups which stabilize the structure through delocalization of

the negative charge. The stability of the $\begin{array}{c} \text{CN} \\ | \\ \text{C}^- \\ | \\ \text{CN} \end{array}$ group

is well known and, for example, accounts in part for the strengths of cyanocarbon acids.¹¹ The stability of the structure I is further evidenced by the negative value for the p*K*_a for the dissociation of its conjugate acid (-1.55); *i.e.*, the protonated form is quite a strong acid which in turn implies considerable stability of the ylide.

The thermochemistry of cyano-substituted hydrocarbons was discussed in paper I⁴ in terms of electrostatic repulsion between cyano groups and, where appropriate, the π -electron conjugation of a cyano group with the carbon-carbon double bond. A table was presented comparing the actual heats of formation with those expected in the absence of the cyano group and conjugation interactions. We present here a revised table (Table V) with the results of the present work incorporated. The calculated heats of formation of the reference structures (column 2) are computed from Franklin's¹² group contributions and a value for the

(9) Calculated from our present data and using $\Delta H_f^\circ[\text{pyridine}(\text{g})] = 33.55 \text{ kcal mole}^{-1}$: W. N. Hubbard, F. R. Frow, and G. Waddington, *J. Phys. Chem.*, **65**, 1326 (1961).

(10) F. D. Rossini, *et al.*, "Selected Values of Chemical Thermodynamic Properties," U. S. National Bureau of Standards Circular 500, U. S. Government Printing Office, Washington, D. C., 1952. This value of the C-H thermochemical bond energy is the average bond energy in methane and is used in simple bond energy schemes for hydrocarbons. Its use here therefore assigns any differences in the C-CN bonds in malononitrile and the ylide to the C⁻-N⁺ bond in the ylide.

(11) R. H. Boyd, *J. Phys. Chem.*, **67**, 737 (1963).

(12) J. L. Franklin, *Ind. Eng. Chem.*, **41**, 1070 (1949).

Table V: Stabilization Energies of Cyanocarbons

Compound	(1) $\Delta H_f^\circ(\text{g})$, obsd	(2) $\Delta H_f^\circ(\text{g})$, calcd	(3) Stabilization ^c energy. (2) - (1)	(4) Dipole-dipole ^c energy (calcd) ^d	(5) Delocalization energy (calcd) ^d ($\beta = 4$)	(6) Sum (4) + (5)
Malononitrile	63.5	53	-10	-9	0	-9
Succinonitrile	53	48	-5	-4	0	-4
Cyanogen	73.6 ^a	58	-6	-24	1	-23
Acrylonitrile	43.7 ^b	44	0	0	2	2
Fumaronitrile	81.3	76	-5	-3	3	0
Tricyanoethylene	123.9	107	-17	-19	5	-14
Tetracyanoethylene	168.5	140.6	-28	-37	7	-30
Tetracyanoquinodimethane	184.0	205.1	21	-16	4.0 β ^e	...

^a Reference 9. ^b H. S. Davis and O. F. Weideman, *Ind. Eng. Chem.*, **37**, 482 (1945). ^c The sign of the stabilization energy is taken to be positive when the actual molecule is more stable than the reference structure. For comparison with stabilization energy, dipole-dipole energy is taken to be negative for a repulsive configuration contrary to usual usage. ^d The carbon-carbon bond resonance integral, β , is taken to be equal to 4. ^e The value $\beta = 4$ would be questionable here and the delocalization energy is reported in units of β .

group contribution of $-\text{CN}$ of 29 kcal mole⁻¹ that we have selected. The latter is based on Evans and Skinner's¹³ data for propyl cyanide, isopropyl cyanide, and phenyl cyanide and data reported in Kharasch's compilation¹⁴ for acetonitrile. In passing, it may also be noted that the older data in Kharasch's compilation for malononitrile ($\Delta H^\circ = 394.8$ kcal mole⁻¹) and succinonitrile ($\Delta H^\circ = 545.7$ kcal. mole⁻¹) (from Berthollet and Petit (1889)) are in remarkable agreement with our present results and a recent heat of combustion of succinonitrile.¹⁵

Acknowledgments. The authors are indebted to the U. S. Army Research Office (Durham) for financial sup-

port of this work. They are also very grateful to Professor R. C. Anderson of this department for furnishing the pyridinium dicyanomethylide and to Dr. G. J. Sloan of the Central Research Department, Du Pont Co., for furnishing the purified malononitrile. R. W. is grateful to the National Science Foundation for assistance from the Undergraduate Research Participation Program.

(13) R. W. Evans and H. A. Skinner, *Trans. Faraday Soc.*, **55**, 255 (1959).

(14) M. S. Kharasch, *J. Res. Natl. Bur. Std.*, **2**, 359 (1929).

(15) $\Delta H_f^\circ = -546.22 \pm 0.035$ kcal mole⁻¹; N. Rapport and E. Westrum, Jr., private communication.

A Study of the Surface Structure of Decationized Y Zeolite by Quantitative Infrared Spectroscopy

by Thomas R. Hughes and Harry M. White

Chevron Research Company, Richmond, California (Received December 15, 1966)

The intensities of infrared absorption bands of adsorbed amines and of two types of surface hydroxyl groups in decationized Y zeolite have been determined. From the intensities, the concentrations of these species were measured. Experiments with piperidine demonstrated that both OH groups are protic acids and are accessible to molecules in the large intracrystalline channels. The concentration of these sites is much smaller than the ion-exchange capacity. Results with pyridine revealed that the OH group with ϵ band at 3650 cm^{-1} is a stronger Brønsted acid than the group with a band at 3550 cm^{-1} . Experiments with *t*-butyl alcohol showed that the lower frequency OH group is strongly hydrogen bonded to other oxygen atoms of the zeolite, whereas the other OH group is not. Dehydration at elevated temperatures converts the Brønsted sites to the Lewis form. Exposure to water converts some of the Lewis sites to Brønsted sites but not necessarily to the original OH groups.

I. Introduction

Infrared spectroscopy has been widely used for the qualitative and semiquantitative investigation of surface functional groups and adsorbed species on solids. During the past 2 years a number of quantitative infrared studies have also been published.¹⁻⁴ In the present work, quantitative infrared spectroscopy was used to study the surface structure of decationized Y zeolite.

The theoretical structure of metal ion-exchanged forms of the faujasitelike X- and Y-type zeolites does not include any hydroxyl groups. However, several infrared absorption bands have been reported in the OH region of the spectrum.⁵⁻¹³ Some of these bands have been attributed to OH groups associated with the metal ion.⁷⁻¹⁰ Others have been assigned to OH groups connected with the aluminosilicate portion of the zeolite.^{5-7,10-13} The present work is concerned with the latter type of hydroxyl group.

One of these OH groups has a sharp absorption band at $3740\text{--}3750\text{ cm}^{-1}$ ^{10,12,13} which closely resembles the band of isolated surface SiOH groups in silica¹⁴ and noncrystalline silica-alumina.¹⁵ In the zeolites, the $3740\text{--}3750\text{ cm}^{-1}$ band is weak and the OH group re-

sponsible does not appear to play an important structural role.

Infrared absorption bands due to two other OH groups have been observed in the ammonium forms

- (1) D. A. Seanor and C. H. Amberg, *J. Chem. Phys.*, **42**, 2967 (1965).
- (2) H. Heyne and F. C. Tompkins, *Proc. Roy. Soc. (London)*, **A292**, 460 (1966).
- (3) J. D. Russell, *Trans. Faraday Soc.*, **61**, 2284 (1965).
- (4) M. R. Basila and T. R. Kantner, *J. Phys. Chem.*, **70**, 1681 (1966).
- (5) J. A. Rabo, P. E. Pickert, D. N. Stamiros, and J. E. Boyle, *Actes Congr. Intern. Catalyse, 2^e, Paris, 1960*, 2055 (1961).
- (6) H. A. Szymanski, D. N. Stamiros, and G. R. Lynch, *J. Opt. Soc. Am.*, **50**, 1323 (1960).
- (7) S. P. Zhdanov, A. V. Kiselev, V. I. Lygin, and T. I. Titova, *Dokl. Akad. Nauk SSSR*, **150**, 584 (1963).
- (8) L. Bertsch and H. W. Habgood, *J. Phys. Chem.*, **67**, 621 (1963).
- (9) S. P. Zhdanov, A. V. Kiselev, V. I. Lygin, and T. I. Titova, *Russ. J. Phys. Chem.*, **38**, 1299 (1964).
- (10) J. L. Carter, P. J. Lucchesi, and D. J. C. Yates, *J. Phys. Chem.*, **68**, 1385 (1964).
- (11) H. W. Habgood, *ibid.*, **69**, 1764 (1965).
- (12) J. B. Uytterhoeven, L. G. Christner, and W. K. Hall, *ibid.*, **69**, 2117 (1965).
- (13) C. L. Angell and P. C. Schaffer, *ibid.*, **69**, 3463 (1965).
- (14) R. S. McDonald, *ibid.*, **62**, 1168 (1958).
- (15) M. R. Basila, *ibid.*, **66**, 2223 (1962).

of near faujasites after heating to temperatures high enough to decompose the ammonium ions.^{5,7,12,13} These OH groups presumably are formed by the combination of oxygen atoms from the zeolite framework and the protons left behind by the decomposition of the NH_4^+ ions.⁵ One of the bands, which is fairly narrow, has been reported at 3655 cm^{-1} in deaminated NH_4X ⁷ and at 3660 ¹² and 3640 cm^{-1} ¹³ in deaminated NH_4Y . The other band, which is broader, has been reported at 3570 cm^{-1} ^{5,12} and at 3540 cm^{-1} ¹³ in deaminated NH_4Y zeolite.

In the present work the integrated absorption intensities, accessibilities, relative acidities, and hydrogen-bonding characteristics of both the 3650- and 3550-cm^{-1} OH groups were determined. The concentrations of both types of OH groups and of the Lewis sites formed by their dehydration were measured as functions of pretreatment temperature.

II. Experimental Section

A. Materials. The ammonium form of Y-type zeolite (Lot No. 12218-19-1) was supplied by the Linde Co. This sample (NH_4Y) contained 66.1% SiO_2 , 23.2% Al_2O_3 , 8.3% $(\text{NH}_4)_2\text{O}$, and 1.6% Na_2O on a dry basis. The particles smaller than *ca.* $1\ \mu$, as measured from electron micrographs, were removed by sedimentation in water in order to minimize the fraction of sites on the external faces of the crystals. The Ag^+ exchange capacity was $3860\ \mu\text{moles/g}$ of dry, ammonia-free Y zeolite.

An alumina gel was prepared in a methanol-water solution by the method of Ziese,¹⁶ washed with methanol and then with ethyl ether, and converted to the aerogel form by removal of the ether above its critical temperature.¹⁷ A silica gel was prepared by hydrolysis of ethyl orthosilicate in methanol-water solution and converted to the aerogel in the same way as the alumina.

A 25% alumina, 75% silica cracking catalyst (Aerocat AAA) with a BET N_2 surface area of $430\text{ m}^2/\text{g}$ was obtained from American Cyanamid. Nalco Chemical Co. supplied a sample of alumina which had a surface area of $328\text{ m}^2/\text{g}$ after drying under vacuum at 450° .

The pyridine used was Baker Analyzed reagent. The piperidine was Eastman Practical grade redistilled to a constant boiling range ($106.7\text{-}107.0^\circ$). A purified sample of *t*-butyl alcohol was prepared by five recrystallizations of Eastman White Label No. 820. Each of the reagents was stored over Type 5A Linde Molecular Sieve.

B. Wafer Preparation and Pretreatments. All infrared measurements were made with adsorbents in

the form of self-supporting wafers prepared by pressing 20–50 mg of fine powder in a 1-in. diameter die at 20,000 psi. Heat treatments of the wafers were performed in the infrared cell.

Wafers of NH_4Y were pretreated at 300° for at least 1 hr to decompose the ammonium ion prior to the experiments in which the band intensities of pyridinium ion (PyB) and piperidinium ion (PiB) were determined. In the experiments made to determine the effect of pretreatment temperature on the concentrations of acid sites, the wafers were successively heated for 1 hr at each pretreatment temperature studied. The dimensions and weights of the wafers were measured at the end of each experiment.

The alumina aerogel (Al-600) and Nalco alumina (Nal-600) wafers were exposed to 200 torr of O_2 at 500° for 2 hr and then degassed at 2×10^{-6} torr for 2 hr at 600° . The wafer of Aerocat AAA was pretreated by heating for 4 hr at 500° in 200 torr of O_2 and then for 16 hr at 500° and 2×10^{-6} torr (SA-500). The silica aerogel wafers were heated at 200° for 2 hr at 2×10^{-6} torr (Si-200).

C. Infrared Spectrophotometer, Sample Cell, and Vacuum System. The infrared instrument used is an altered version of the modified Beckman IR-7 ratio-recording spectrophotometer described by Keahl and Rea.¹⁸ They installed a 480-cps beam chopper and replaced the thermocouple detector with fast-response semiconductor detectors. The design of Keahl and Rea included extra optics in both sample and reference beam paths in order to accommodate long, externally heated cells. The internally heated cell described below is short enough to permit a return to the IR-7 optics with a more than fourfold improvement in signal-to-noise ratio.

The infrared cell, pictured in Figure 1, is in two parts. The Pyrex cell body is permanently mounted in the spectrometer sample compartment. The removable sample holder carries a heater of Nichrome wire wrapped around a quartz cylinder axially aligned with the infrared beam. The sample wafer is held in place in the center of this cylinder by means of quartz rings. The inside of the cylinder is lined with gold sheet in order to shield the wafer from direct radiation from the heater. The heater is sheathed from the vacuum system by the quartz envelope of the sample holder. During high-temperature operation, the heater

(16) W. Ziese, *Ber. Deut. Chem. Ges.*, **66**, 1965 (1933).

(17) S. S. Kistler, *Nature*, **127**, 741 (1931); *J. Phys. Chem.*, **36**, 52 (1932).

(18) G. T. Keahl and D. G. Rea, presented at the 12th Pittsburgh Conference on Analytical Chemistry and Applied Spectroscopy, Feb 1961.

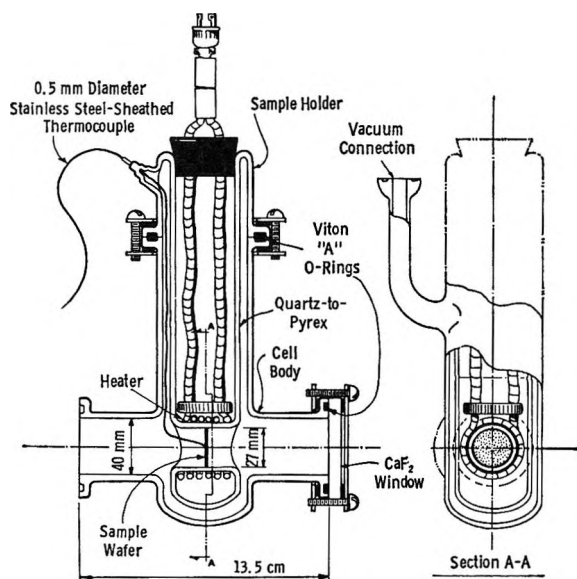


Figure 1. Infrared cell for catalyst studies.

is protected from oxidation by a stream of N_2 in the sample holder envelope.

The heater section of the sample holder is wrapped with a gold heat shield with access holes for the infrared beam and additional gold heat shields are placed just inside the windows. With this cell, spectra have been recorded from 1300 to 4000 cm^{-1} at wafer temperatures up to 760° and, with the sample holder envelope filled with coolant, down to -110°. A blank cell identical with the sample cell is placed in the reference beam and attached to the vacuum system.

D. Measurement of Band Intensities and Concentrations of Adsorbed Species. Band intensities of adsorbed species were measured by adding accurately known increments of adsorbate and recording the spectrum of the wafer 2.5–3 hr after each addition. Wafers were maintained at 150° during all of these calibrations except for Si-200, which was at 35°. Adsorbed species and the temperatures at which their spectra were measured are designated as follows: pyridinium ion at 150° (PyB-150), coordinately bonded pyridine at 150° (PyL-150), piperidinium ion at 150° (PiB-150), coordinately bonded piperidine at 150° (PiL-150), and hydrogen-bonded piperidine at 35° (PiH-35).

For experiments in which the concentration of acid sites was determined as a function of the highest pretreatment temperature, an excess of adsorbate was added to the wafer. After at least 0.5 hr, the pressure was reduced to 2×10^{-6} torr and the spectrum was recorded. For experiments in which the effect of water was studied, 15–20 torr of H_2O was allowed

to contact the wafer at 35° for 16 hr before the excess was removed by pumping to 2×10^{-6} torr, usually for 2 hr.

Band area rather than band height was used for the quantitative measurements. The former is a better measure of concentration than the latter when the half-width of an absorption band is not large compared to the spectral slit width.¹⁹ Arbitrary but consistent procedures were used to construct the backgrounds for integration of the absorption bands of adsorbed pyridine and piperidine. For the pyridine bands at 1540, 1490, and 1450 cm^{-1} , smooth curves were drawn tangent to the spectra on either side of the absorption bands (Figures 2B, 2C). A tangent background was also used for the bands of piperidine species at 1450–1460 cm^{-1} (Figures 3A, 3B, 3C). For the piperidine bands in the 1600–1650- cm^{-1} region, the spectrum of the wafer before addition of piperidine was used to construct the background (blank background).

In the OH stretching region, approximate band areas

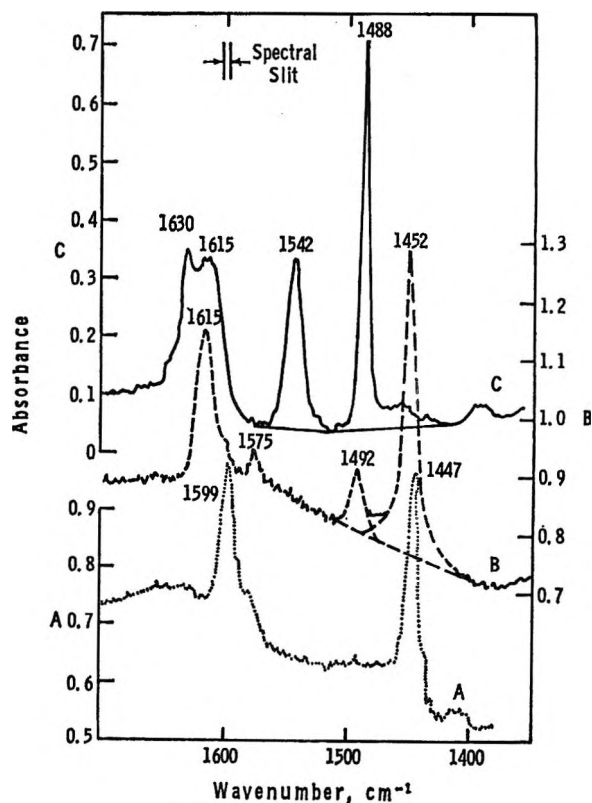


Figure 2. Spectra of adsorbed pyridine species: A, hydrogen-bonded pyridine (PyH) on Si-200; B, coordinately bonded pyridine (PyL) on Al-600; C, pyridinium ion (PyB) on NH_4Y -300.

(19) D. A. Ramsay, *J. Am. Chem. Soc.*, **74**, 72 (1952).

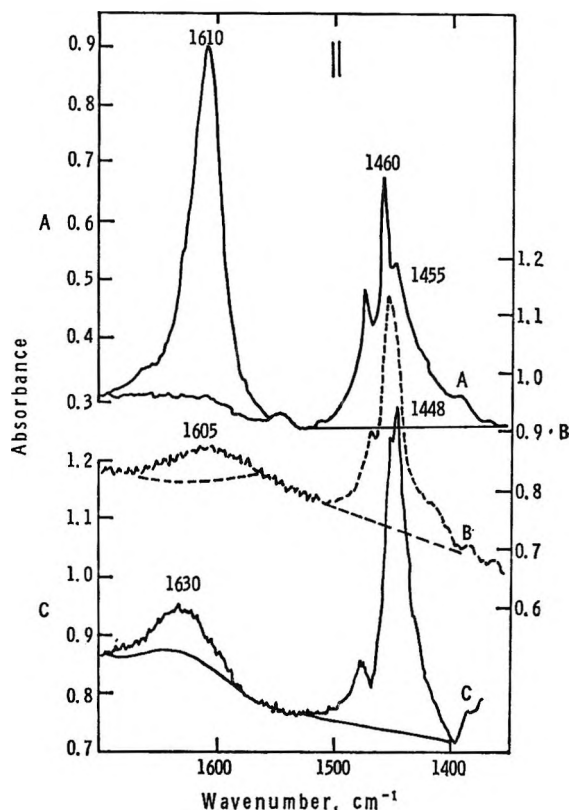


Figure 3. Spectra of adsorbed piperidine species: A, piperidinium ion (PiB) on $\text{NH}_4\text{Y-300}$; B, coordinately bonded piperidine (PiL) on NaI-600 ; C, hydrogen-bonded piperidine (PiH) on Si-200 .

were obtained by drawing a straight background line tangent to the spectrum at about 3700 and 2000 cm^{-1} . Vertical lines were drawn from the peaks of the 3650 - and 3550-cm^{-1} bands down to the background line. The high-frequency side of each band was integrated (shaded areas in Figure 4A) and the total area was taken as twice the integrated portion.

Band intensities were obtained from the slopes of plots of the integrated form of the Beer-Lambert law.

$$B = \int \log (T_0/T)_\nu d\nu = (cl) \int \epsilon_\nu^{(a)} d\nu$$

where B is the integrated absorbance in cm^{-1} , $(T_0/T)_\nu$ the ratio of reference beam to sample beam transmittance as measured with a given spectrometer set at wavenumber ν , (cl) the concentration of adsorbate expressed as micromoles per square centimeter of wafer cross section, $\epsilon_\nu^{(a)}$ the apparent molar extinction coefficient, and $\int \epsilon_\nu^{(a)} d\nu = 0.4343 \times$ apparent integrated absorption intensity, as used by Jones, *et al.*^{20,21} For brevity, $\int \epsilon_\nu^{(a)} d\nu$ will be referred to as "intensity" throughout the rest of this paper.

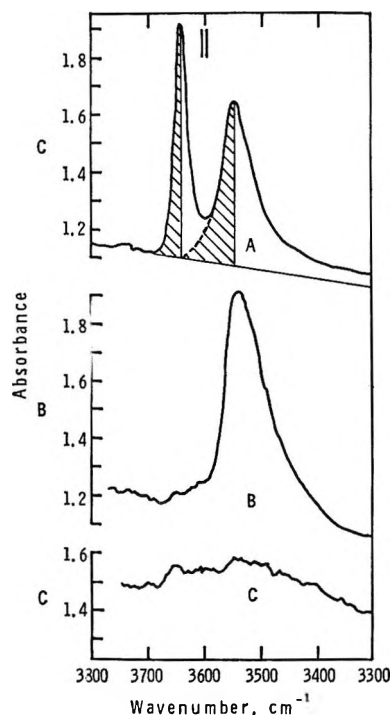


Figure 4. Spectra of the hydroxyl stretching region of $\text{NH}_4\text{Y-300}$, showing the interaction of the 3650 - and 3550-cm^{-1} OH groups with pyridine and piperidine: A, $\text{NH}_4\text{Y-300}$ at 150° ; B, $\text{NH}_4\text{Y-300}$ treated with an excess of pyridine at 35° , then degassed at 150° at 2×10^{-6} torr; C, $\text{NH}_4\text{Y-300}$ treated with an excess of piperidine at 35° and degassed at 2×10^{-6} torr. The spectra shown were obtained from three different wafers.

III. Results

A. Interaction of Pyridine with Surface Sites. The present quantitative infrared study required finding a set of adsorbents, adsorbates, and conditions such that only a single adsorbed species was present in each calibrational measurement. Some of the requirements were established by Parry.²² He found only hydrogen-bonded pyridine (PyH) on silica, PyH and PyL on alumina, and PyB, PyH, and PyL on silica-alumina. In each case, PyH was removed by degassing at 150° . Thus, the spectrum of PyH was obtained by dosing silica with pyridine at 35° (Figure 2A) and the spectrum of PyL was obtained by dosing alumina with pyridine at 150° (Figure 2B). We found that the spectrum obtained by adding small amounts of pyridine to $\text{NH}_4\text{Y-300}$ at 150° was almost entirely that of PyB (Figure 2C).

(20) R. N. Jones, D. A. Ramsay, D. S. Keir, and K. Dobriner, *J. Am. Chem. Soc.*, **74**, 80 (1952).

(21) R. N. Jones and C. Sandorfy in "Technique of Organic Chemistry," Vol. IX, A. Weissberger, Ed., Interscience Publishers, Inc., New York, N. Y., 1956, pp 271-276.

(22) E. P. Parry, *J. Catalysis*, **2**, 371 (1963).

Table I: Apparent Integrated Absorption Intensities of Infrared Bands

Species and temperature of spectrum	Wave-number, cm^{-1}	Adsorbent	Background	No. of points on linear region of plot	Strongly adsorbed amine, $\mu\text{moles/g}^a$	Apparent integrated absorption intensity, $\text{cm}/\mu\text{mole}^b$
PyB-150	1490	$\text{NH}_4\text{Y-300}$	Tangent	3.4^c
	1540	$\text{NH}_4\text{Y-300}$	Tangent	5	>475	3.03 ± 0.13
PyL-150	1450	Al-600	Tangent	4	80	3.26 ± 0.13
	1450	SA-500	Tangent	2	30	3.88^d
PiB-150	1490	Al-600	Tangent	0.56^e
	1450	$\text{NH}_4\text{Y-300}$	Tangent	5	570	8.72 ± 0.62
PiL-150	1620	$\text{NH}_4\text{Y-300}$	Blank	5	570	12.98 ± 0.76
	1450	NaI-600	Tangent	3	150	8.11 ± 1.31^f
PiH-35	1620	NaI-600	Blank	3	150	2.78 ± 0.54^g
	1450	Si-200	Tangent	3	430	8.49 ± 0.24^f
OH Group-150	1620	Si-200	Blank	3	430	3.01 ± 0.23^g
	3550	$\text{NH}_4\text{Y-300}$	<i>h</i>	19.9^i
OH Group-150	3650	$\text{NH}_4\text{Y-300}$	<i>h</i>	5	...	12.23 ± 0.89

^a Amount added at inflection point of calibration curve. Up to this point, essentially all of the added amine was adsorbed by the wafer. ^b The intensities were evaluated from the slopes of least-squares lines of plots analogous to that in Figure 3 for cases in which the number of points on the linear region is listed. In these cases, the 95% confidence interval is also given. ^c Evaluated from the intensity of the 1540-cm^{-1} band of PyB-150 on $\text{NH}_4\text{Y-300}$ and the absorbance ratio of the 1490- and 1540-cm^{-1} bands. ^d The intensity from SA-500, which is 19% higher than that from Al-600, is based on only two points from a plot with a short linear region. It is shown to indicate agreement in magnitude with the intensity of PyL-150 on alumina and was not used for calculation of concentrations. ^e Evaluated from the intensity of the 1450-cm^{-1} band of PyL-150 on alumina and the absorbance ratio of the 1490- and 1450-cm^{-1} bands. ^f From the 1450-cm^{-1} band intensities for PiL and PiH, an average was calculated by weighting each value by the inverse of its variance. The result, $8.48 \text{ cm}/\mu\text{mole}$, was used in the calculation of the coefficients in the equations for (c_{PiL}) and $[(c_{\text{PiL}} + c_{\text{PiH}})]$. ^g A weighted average of $2.98 \text{ cm}/\mu\text{mole}$ was calculated from the 1620-cm^{-1} band intensities of PiL and PiH. ^h The backgrounds of the OH bands were constructed as described in section II-D. ⁱ Evaluated from $[(\text{PiB-35}) - (\text{PyB-150})]$ for $\text{NH}_4\text{Y-300}$, wafer cross section and weight, and initial intensity of the 3550-cm^{-1} band before amine was added. The listed value is the average of the results from two wafers, 19.2 and $20.6 \text{ cm}/\mu\text{mole}$.

The intensity of the 1540-cm^{-1} band of PyB-150 on $\text{NH}_4\text{Y-300}$ was found from Figure 5. The slope of the linear plot yielded the intensity, which is listed together with those of other bands in Table I. Addition of excess pyridine at 150° to $\text{NH}_4\text{Y-300}$ produced a small band at *ca.* 1450 cm^{-1} which was not completely removed by degassing. Thus, $\text{NH}_4\text{Y-300}$ appears to contain some Lewis acid sites, but they adsorb little pyridine until the Brønsted sites are essentially saturated.

The temperature dependences of the intensities of both the 1540- and 1490-cm^{-1} bands of PyB were measured by dosing $\text{NH}_4\text{Y-300}$ with pyridine at room temperature, degassing at 200° , isolating the wafer, and measuring spectra from 200 to -110° . The results showed that both bands are essentially independent of temperature between 35 and 200° . On cooling from 35 to -110° , the 1540-cm^{-1} band intensity decreased by about 12% and the 1490-cm^{-1} band intensity increased by about 5%. In contrast, the intensities of the bands at 1610 and 1630 cm^{-1} are highly temperature dependent.

The intensity of the 1450-cm^{-1} band of PyL-150 was determined by dosing both Al-600 and SA-500 with pyridine. Both oxides showed only the spectrum of PyL.²³

B. Interaction of Piperidine with Surface Sites. In order to study Brønsted acid sites too weak to transfer a proton to pyridine, we also measured the spectra of piperidine on three different oxides. Piperidine was chosen because it is similar to pyridine in size but is a much stronger base with respect to protons.²⁴ The spectrum of piperidine adsorbed on $\text{NH}_4\text{Y-300}$ at 150° is shown in Figure 3A. The band at 1610 cm^{-1} is probably due to the same vibration as the 1597-cm^{-1} band

(23) In preliminary experiments, PyB as well as PyL was observed in SA-500. However, when the pyridine was dried in the vacuum system by means of activated Linde 5A Molecular Sieve in the dosing bulb, the spectrum of PyB was not observed.

(24) The aqueous $\text{p}K_a$ at 25° for piperidine is 11.22 ,²⁵ compared to 5.23 for pyridine at 20° .²⁶

(25) S. Searles, M. Tamres, F. Block, and L. A. Quarterman, *J. Am. Chem. Soc.*, **78**, 4917 (1956).

(26) A. Albert, R. Goldacre, and J. Phillips, *J. Chem. Soc.*, 2240 (1948).

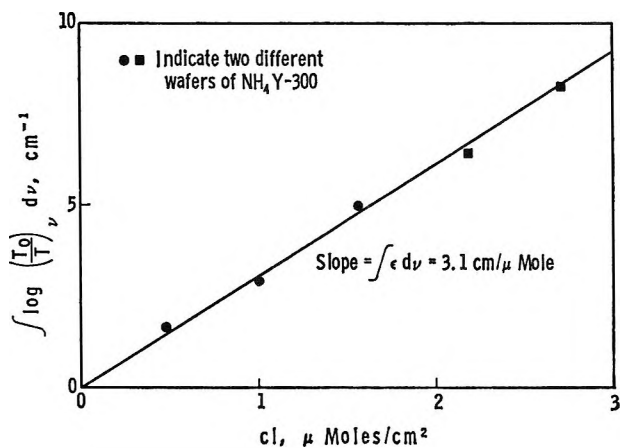


Figure 5. Integrated absorption intensity of 1540-cm⁻¹ band of PyB-150 on NH₄Y-300.

found for piperidine hydrochloride in Nujol by Heacock and Marion.²⁷ They assigned this band to the -NH₂⁺ deformation vibration of piperidinium ion. The bands centered at about 1460 cm⁻¹ are due to the methylene deformation vibrations. Because of the similarity of this spectrum to that of piperidine hydrochloride and because the spectrum of pyridine at low coverages revealed only Brønsted acid sites on NH₄Y-300, we assume that the spectrum in Figure 3A is that of piperidinium ion adsorbed at Brønsted sites (PiB). This assumption is supported by the linear dependence of the integrated absorbances of both the 1610- and 1460-cm⁻¹ bands on the amount of piperidine added. This linearity strongly suggests that all piperidine adsorbed on NH₄Y-300 at low coverage is in the same form.

The spectrum of piperidine adsorbed on alumina (Nal-600) at 150° is shown in Figure 3B. Because (1) the strong -NH₂⁺ band is practically absent from this spectrum, (2) both 1455- and 1605-cm⁻¹ band areas increased linearly with added piperidine, and (3) pyridine adsorbed on this alumina showed only the spectrum of PyL, we assume that the spectrum in Figure 3B is that of piperidine adsorbed at Lewis acid sites (PiL).

The spectrum at 35° of piperidine adsorbed on silica (Si-200) is shown in Figure 3C. A relatively weak band appears at about 1630 cm⁻¹; the strong 1610-cm⁻¹ band of PiB is not present. Because (1) PiB was absent, (2) both 1448- and 1630-cm⁻¹ band areas increased linearly with added piperidine, and (3) Si-200 dosed with pyridine showed only the spectrum of PyH, the spectrum in Figure 3C is assumed to be that of a hydrogen-bonded piperidine species (PiH) analogous to PyH.

The intensities of the 1605-1630- and 1448-1460-cm⁻¹ bands of PiB-150, PiL-150, and PiH-35 were obtained from plots like that in Figure 5. The effects of lowering the temperature from 150 to 35° on the intensities of the 1610- and 1460-cm⁻¹ bands of PiB, 4.3 and 0.7%, respectively, were small enough to permit measurement of the concentration of this species at 35° from the intensities evaluated at 150°.

The concentrations of individual adsorbed piperidine species can be measured only because of a fortunate coincidence. PiL and PiH have essentially the same intensities in both the 1450- and 1620-cm⁻¹ regions, so that the concentrations of these two species can be combined in the calculations (Table I, footnotes *f* and *g*). The resulting simplification yields the following equations for the concentrations of PiB and (PiL + PiH): $(c_{\text{PiB}})l = 0.1009B_{1620} - 0.0354B_{1450}$ and $[(c_{\text{PiL}} + c_{\text{PiH}})]l = 0.1544B_{1450} - 0.1037B_{1620}$.

C. Interactions of Surface Hydroxyl Groups with Adsorbates. Uytterhoeven, Christner, and Hall¹² showed that deamination of NH₄Y zeolite was complete by 290° and that absorption bands due to two hydroxyl groups appeared in the OH stretching region as the ammonia was removed. These OH bands in the spectrum of NH₄Y-300 are shown in Figure 4A. Uytterhoeven, *et al.*,¹² also showed that addition of ammonia to NH₄Y-290 caused both of these OH bands to disappear and the spectrum of the ammonium ion to reappear.

Figure 4B shows that at 150° pyridine abolished the 3650-cm⁻¹ OH band without affecting the 3550-cm⁻¹ band. The linear decrease in the intensity of the 3650-cm⁻¹ band with the amount of pyridine added (Figure 6) suggests that all the pyridine reacted with the 3650-cm⁻¹ OH group to form PyB (section III-A, Figure 5). From the slope of the line in Figure 6, the band intensity was estimated on the assumption that each hydroxyl group reacted with one molecule of pyridine (Table I).

The intensity of the 3550-cm⁻¹ band cannot be measured as precisely as that of the 3650-cm⁻¹ band, but the former remained constant to within about ±10% in the titration with pyridine and showed no systematic change with amount of pyridine added. This semiquantitative result confirms the qualitative evidence in Figures 4A and 4B that pyridine does not interact with the 3550-cm⁻¹ band at 150°.

Excess piperidine vapor added to NH₄Y-300 at 35° formed PiB (section III-B) and eliminated both the 3650- and 3550-cm⁻¹ OH bands (Figure 4C). Evacuation over a range of temperatures showed that the

(27) R. A. Heacock and L. Marion, *Can. J. Chem.*, **34**, 1782 (1956).

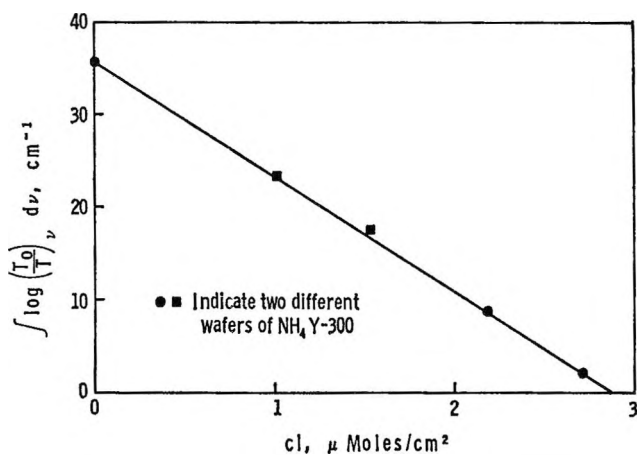


Figure 6. Effect of pyridine addition on integrated absorbance of 3650-cm⁻¹ OH band of NH₄Y-300. Slope = -12.2 cm/μmole.

PiB complex with the 3650-cm⁻¹ OH group is stronger than that with the 3550-cm⁻¹ group. Neither complex dissociated upon degassing at room temperature. The 3550-cm⁻¹ band was partly restored after 2 hr at 200°. After 1.5 hr at 300°, the 3550-cm⁻¹ band was almost completely restored, but only a very weak band appeared at 3660 cm⁻¹. Evacuation at 400° for 3 hr restored the 3550-cm⁻¹ band completely and the 3650-cm⁻¹ band almost completely.

Equilibration of a wafer of NH₄Y-300 at 35° with *t*-butyl alcohol at a partial pressure of 0.8 torr eliminated the 3650-cm⁻¹ band. The 3550-cm⁻¹ band was broadened and shifted to *ca.* 3500 cm⁻¹. After evacuation down to 2 × 10⁻⁶ torr at room temperature, the spectrum at 35° showed that the 3550-cm⁻¹ band had returned to its original width and position within 1.8 hr; but even after 19 hr the 3650-cm⁻¹ band was still not restored to its initial intensity. After evacuation at 200°, both OH bands had fully regained their initial intensities.

D. Effect of Pretreatment on Concentration of Adsorbed Amines. The concentrations of pyridine species adsorbed by Y zeolite after degassing at temperatures from 300 to 700° were calculated by means of the 1540-cm⁻¹ band intensity for PyB and the 1450-cm⁻¹ band intensity for PyL. The maximum concentration of PyB-150 in NH₄Y-300 was 520 μmoles/g (Figure 7D). From this concentration, the wafer cross section and weight, and the 3650-cm⁻¹ band area before addition of pyridine, a second estimate was made for the intensity of this band. The result, 12.1 cm/μmole, is in excellent agreement with the slope of the line in Figure 6. The concentration of PyB-150 (Figure 7D) decreased monotonically with increasing pretreatment temperature, most steeply between 500 and 600°.

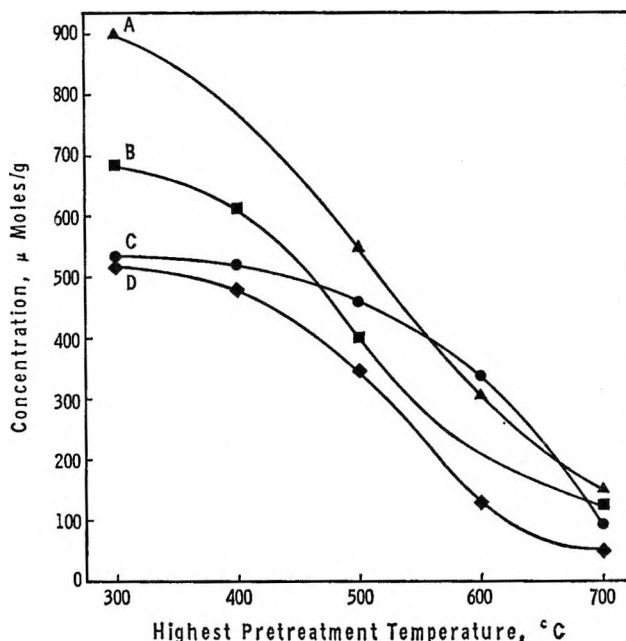


Figure 7. Effect of pretreatment temperature on concentrations of amines adsorbed at surface Brønsted acid sites in decationized Y zeolite: A (▲), PiB-35; B (■), PiB-150; C (●), PyB-150 after rehydration of zeolite; D (◆), PyB-150.

The concentration of PyL-150 (Figure 8A) was low after pretreatment at 300°,²⁸ rose to a maximum at about 600°, and then dropped sharply at 700°.

The concentrations of PiB-35 (Figure 7A) and PiB-150 (Figure 7B) decreased with pretreatment temperature in a manner similar to that of PyB-150 (Figure 7D). At each temperature, (PiB-35) > (PiB-150) > (PyB-150). These results agree with those of section III-C, which show that PiB-35 is formed at all 3650- and 3550-cm⁻¹ OH groups, PiB-150 at all 3650-cm⁻¹ groups but only some of the 3550-cm⁻¹ groups, and PyB-150 at 3650-cm⁻¹ groups only. The concentration of the 3550-cm⁻¹ OH group in NH₄Y-300 is estimated to be 479 μmoles/g from the difference between PiB-35 (Figure 7A) and PyB-150 (Figure 7D). For two wafers, this concentration, the wafer cross section and weight, and the 3550-cm⁻¹ integrated absorbance before addition of piperidine gave estimates of 19.2 and 20.6 cm/μmole for the band intensity.

Comparison of Figures 7C and 7D shows that rehydration had only small effects on NH₄Y-300 and NH₄Y-400. However, rehydration of NH₄Y-500 and NH₄Y-600 converted an appreciable fraction of the acid sites from the Lewis form into strong Brønsted

(28) The uncertainty in the concentration of PyL-150 in NH₄Y-300 and NH₄Y-400 is due to overlap of the strong 1490-cm⁻¹ band of PyB with the 1450-cm⁻¹ band of PyL.

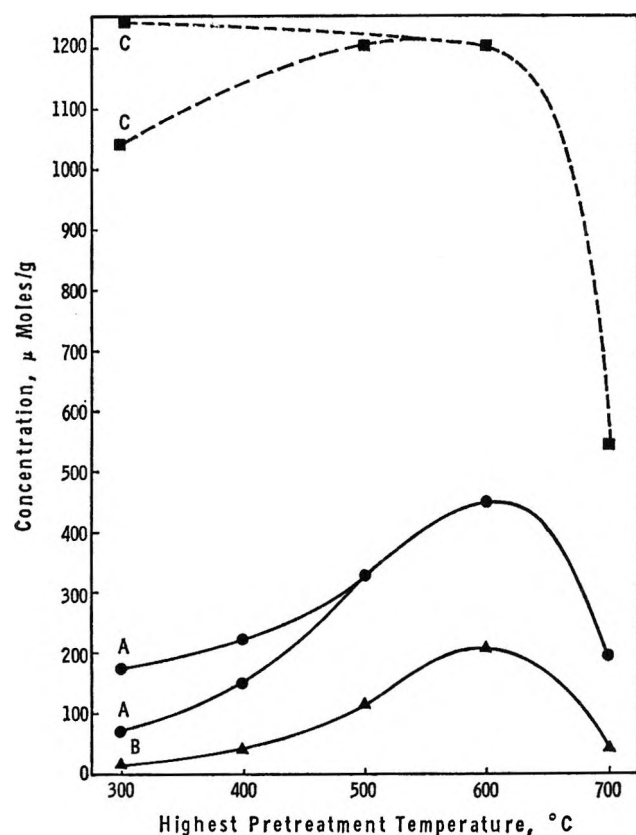


Figure 8. Effect of pretreatment temperature on concentrations, in decationized Y zeolite, of acid sites which can adsorb cyclic amines: A (●), PyL-150; B (▲), [(PyB-150 after rehydration) - (PyB-150)]; C (■), [(PiB-35) + 2(PyL-150)].

sites which retained pyridinium ion at 150°. ²⁹ Rehydration of NH₄Y-600 did not intensify the 3650-cm⁻¹ OH band despite the increase in PyB-150. The concentration of strong Brønsted sites formed by rehydration passed through a maximum after pretreatment at about 600° (Figure 8B), just as did the concentration of PyL-150 (Figure 8A).

IV. Discussion

A. Integrated Absorption Intensities. The magnitudes of the apparent integrated absorption intensities listed in Table I will first be compared with those of similar bands in previously published studies.

Basila and Kantner⁴ recently estimated that the ratio of the extinction coefficient of PyB to that of PyL at 1490 cm⁻¹

$$\frac{\epsilon_{1490}^{\text{PyB}}}{\epsilon_{1490}^{\text{PyL}}}$$

is 6.0 ± 0.9 . This value is in satisfactory agreement with our estimate of the integrated absorption intensity ratio

$$\int \epsilon_{1490}^{\text{PyB}} d\nu / \int \epsilon_{1490}^{\text{PyL}} d\nu = 3.26/0.56 = 5.8$$

for the two bands have roughly similar apparent half-widths.

Another comparison of our measured intensities can be made with those of OH stretching bands in silicate glasses. Scholze³⁰ found that the intensities of these bands increased monotonically with decrease in wave-number as expected for hydrogen-bonded OH groups.³¹ The data plotted in his Figure 8 give values of $\int \epsilon d\nu$ of about 10–18 cm/μmole at 3650 cm⁻¹ and 16–25 cm/μmole at 3550 cm⁻¹. These values are close to our results of 12.2 cm/μmole for the 3650-cm⁻¹ band and 19.9 cm/μmole for the 3550-cm⁻¹ band of NH₄Y-300.

B. Locations of OH Groups. The structure of the sodium form of X zeolite was determined by Broussard and Shoemaker.³² From their study, it was deduced that the exchanged cations in zeolite types X and Y occupy the following three types of sites.³³

Type I, in the centers of hexagonal prisms, 16 sites per unit cell.

Type II, on the unjoined hexagonal faces of truncated cube octahedra (sodalite cages), 32 sites per unit cell.

Type III, on the walls on the channels, 48 sites per unit cell.

Ions in type I sites can be approached by adsorbate molecules which can pass through a distorted ring of six oxygen atoms of about 2.2-Å free diameter. Ions in sites of types II and III are accessible to molecules which can penetrate into the large intracrystalline channels of the zeolite crystals with apertures about 8–9 Å across. Each aluminum or silicon ion in the zeolite framework is bonded to four crystallographically distinguishable oxygen ions which form bridges between adjacent framework cations. Two of these types of oxygen ions, designated O₁ and O₄,³² protrude into the large intracrystalline channels. The other two types, called O₂ and O₃, are partly shielded from the large channels.

The 3650- and 3550-cm⁻¹ OH groups in deaminated NH₄Y zeolite are presumably formed by the combination of protons, left behind by decomposition of NH₄⁺ ions, with framework oxygen ions to form SiOH or AlOH groups adjacent to three-coordinate alumi-

(29) This result is similar to that of Uytterhoeven, Christner, and Hall,¹² who demonstrated that addition of water to ammonia adsorbed on Lewis acid sites of decationized Y zeolite caused the ammonium ion to re-form.

(30) H. Scholze, *Glastech. Ber.*, **32**, 81 (1959).

(31) G. C. Pimentel and A. L. McClellan, "The Hydrogen Bond," W. H. Freeman and Co., San Francisco, Calif., 1960, pp 95, 96.

(32) L. Broussard and D. P. Shoemaker, *J. Am. Chem. Soc.*, **82**, 1041 (1960).

(33) D. W. Breck, *J. Chem. Educ.*, **41**, 678 (1964).

num^{5,6,12} or silicon⁶ ions. A hydroxyl group formed by the union of a proton with an O₁ oxygen would be expected to be the most accessible to adsorbate molecules in the large channels, and an OH group formed from an O₄ oxygen should be somewhat less accessible. The reaction of all the 3650- and 3550-cm⁻¹ OH groups with piperidine indicates that they are accessible to molecules in the large channels and are probably formed from oxygen ions of the O₁ or O₄ types.

Conclusive evidence has not yet been presented on whether SiOH or AlOH groups are responsible for the two observed OH bands. Szymanski, Stamires, and Lynch⁶ noted that either type of hydroxyl group could be formed, depending on whether an AlO or an SiO bond was broken by attack of the proton from NH₄⁺. Infrared results of Basila suggest that the surface hydroxyl groups in a noncrystalline aluminosilicate dehydrated at 500° are predominantly attached to silicon atoms.¹⁵ If AlOH groups on four-coordinate aluminum in a crystalline aluminosilicate are also easily dehydrated, the 3550- and 3650-cm⁻¹ OH bands are likely to be due to SiOH groups, for both bands remain after dehydration at 500°.¹³ The deamination of NH₄Y zeolite was considered by Uytterhoeven, Christner, and Hall¹² to form SiOH groups only.

C. Hydrogen Bonding of OH Groups. The 3650-cm⁻¹ OH group of NH₄Y-300 is not strongly bonded to other groups of the zeolite,³⁴ as is shown by the complete disappearance of its absorption band after equilibration with 0.8 torr of *t*-butyl alcohol. This behavior is in contrast to that of the 3750-cm⁻¹ isolated SiOH group of silica, part of which remains free when exposed to *t*-butyl alcohol under these conditions.³⁵ The greater strength of hydrogen bonding of *t*-butyl alcohol with the 3650-cm⁻¹ group of NH₄Y-300 than with the free silanol group of silica is probably due to the stronger acidity of the former surface OH group (see section IV-D). An increase of hydrogen-bonding strength with increasing acid strength of the proton donor has been demonstrated for homogeneous systems.³⁶

The 3550-cm⁻¹ OH group is hydrogen bonded to oxygen ions on the surface of the zeolite, for, despite its greater acidity (see section IV-D), it fails to interact with *t*-butyl alcohol as strongly as does the free SiOH group of silica.³⁵ However, this intrasurface hydrogen bond does not necessarily involve an interaction between neighboring OH groups, as suggested by Angell and Schaffer.¹³ Instead, the proton of the 3550-cm⁻¹ OH group may participate in a hydrogen bond to an adjacent bridge oxygen connecting two of the framework (Si or Al) cations. The distances between the O₄-type oxygens and their nearest neigh-

boring oxygen ions in NaX zeolite are 2.64–2.81 Å.³² These distances are fairly close to the O–H···O bond distances, 2.83–2.91 Å, estimated from the correlation of Pimentel and McClellan³⁷ for frequency shifts of 100–200 cm⁻¹ due to hydrogen bonding. When an Al–O bond is broken and an SiOH group is formed by the deamination of NH₄Y zeolite, it is likely that small increases occur in the distances between the oxygen atom of the SiOH group and the three oxygens still bonded to the adjacent aluminum ion. Thus the intrasurface hydrogen-bonded 3550-cm⁻¹ OH group is likely to be formed from the slightly shielded O₄-type oxygen, and the 3650-cm⁻¹ OH group from the highly accessible O₁-type oxygen.

D. Relative Acidities of the 3650- and 3550-Cm⁻¹ OH Groups. Both the 3650- and 3550-cm⁻¹ OH groups of NH₄Y-300 are stronger Brønsted acids than the OH groups of silica and alumina, for the zeolitic OH groups can protonate piperidine (aqueous pK_a = 11.22 at 25°^{2c}) and ammonia¹² (aqueous pK_a = 9.27 at 25°⁴⁰), whereas the OH groups of silica⁴¹ and alumina⁴² cannot. The 3650-cm⁻¹ OH group is a stronger Brønsted acid than the 3550-cm⁻¹ group. The former, but not the latter, can transfer a proton to the weak base pyridine (aqueous pK_a = 5.23 at 20°²⁶) at 150°. The weaker acidity of the 3550-cm⁻¹ OH group may be due to its intrasurface hydrogen bond, for this bond is disrupted when the proton is transferred to an adsorbed base. The enthalpy of the protonation reaction should be decreased for the 3550-cm⁻¹ group, with respect to that for the 3650-cm⁻¹ group, by the heat of the intrasurface hydrogen bond of the former. A frequency shift of 100 cm⁻¹ due to hydrogen bonding corresponds to a heat of several kilocalories per mole (about 4–5 kcal/mole for phenol-ester hydrogen bonds⁴³). If the

(34) The 3650-cm⁻¹ OH group may be weakly hydrogen bonded to other atoms of the Y zeolite, for its OH stretching band is much broader than the band of the isolated SiOH group of silica and about 100 cm⁻¹ lower in wavenumber. However, Uytterhoeven, *et al.*,¹² suggested that the shift of frequency is due to interaction between the hydroxyl oxygen and the adjacent aluminum ion.

(35) V. Ya. Davydov, A. V. Kiselev, and V. I. Lygin, *Russ. J. Phys. Chem.*, **37**, 243 (1963).

(36) See ref 31, pp 85, 92.

(37) Reference 31, pp 88, 89. This correlation is based on data of Glemser and Hartert³⁸ and of Pimentel and Sederholm³⁹ for O–H···O bonds in solids.

(38) C. Glemser and E. Hartert, *Z. Anorg. Allgem. Chem.*, **283**, 111 (1956).

(39) G. C. Pimentel and C. H. Sederholm, *J. Chem. Phys.*, **24**, 639 (1956).

(40) T. C. Bissot, R. W. Parry, and D. H. Campbell, *J. Am. Chem. Soc.*, **79**, 796 (1957).

(41) N. W. Cant and L. H. Little, *Can. J. Chem.*, **43**, 1252 (1964).

(42) J. B. Peri, *J. Phys. Chem.*, **69**, 231 (1965).

(43) See ref 31, pp 85, 86.

entropy of protonation of a base were similar for both 3650- and 3550-cm⁻¹ groups, a difference in enthalpy of 4 kcal/mole would correspond to a difference of about 3 in the pK_a of the two groups.

E. Types of Acid Sites and the Dependence of Their Concentrations on Pretreatment Temperature. From the stoichiometry suggested by Uytterhoeven, Christner, and Hall,¹² the number of Lewis acid sites formed in deaminated NH₄Y zeolite by dehydration of the Brønsted sites should be half that of the precursor Brønsted sites. The sum of the Brønsted site concentration plus twice the Lewis site concentration in deaminated, nonrehydrated NH₄Y should not change after thermal treatments which merely convert Brønsted to Lewis sites (without disrupting the crystal structure. This sum, [(PiB-35) + 2(PyL-150)], is shown in Figure 8C to remain constant, within experimental error, between 300⁴⁴ and 600°; but it decreases by more than 50% after pretreatment at 700°. These results suggest that the Lewis acid sites (PyL-150) arise from dehydration of both the strong (PyB-150) and weak [(PiB-35) - (PyB-150)] Brønsted sites. This dehydration occurred without appreciable disruption of the structure at temperatures up to 600°, but structural disruption decreased the concentration of accessible acid sites after treatment at 700°. This disruption may have been due either to the 700° heat treatment or to the exposure of the zeolite to water at 35° after the 600° heat treatment.

F. Comparison of Acid Site Concentration with Cation-Exchange Capacity. The alumina content of NH₄Y corresponds to 4950 μmoles of Al³⁺/g. The

NH₃ and Na contents of NH₄Y correspond to 3490 μmoles of NH₄⁺/g and 570 μmoles of Na⁺/g for an ion-exchange capacity of 4060 μmoles/g. The Ag⁺ exchange capacity is 3860 μmoles/g. The (Na⁺ + NH₄⁺) and Ag⁺ contents are, respectively, 18 and 22% lower than the ion-exchange capacity calculated from the Al₂O₃ content. This deficiency of exchanged cations is similar to, but somewhat larger than, the Na⁺ deficiency in NaX zeolite found by Carter, Lucchesi, and Yates.¹⁰

The total concentration of acid sites accessible to large molecules in NH₄Y-300, about 1200 μmoles/g, is much lower than would be expected from the alumina content or the ion-exchange capacity. Several factors are responsible for this discrepancy: (1) only half of the oxygen ions (types O₁ and O₄) from which OH groups can be formed by deamination are accessible to pyridine and piperidine; (2) the distribution of the Na⁺ ions between accessible (types II and III) and inaccessible (type I) exchange sites is unknown; and (3) the zeolites are sensitive to hydrothermal reactions—differences in deamination procedure affect the concentration of acid sites formed. For example, a wafer deaminated by heating under vacuum to 300° at a rate of 2.5°/min showed 3550- and 3650-cm⁻¹ band intensities about 50% greater than the more rapidly heated wafers used for the previously measured pyridine and piperidine concentrations.

(44) See ref 28 regarding uncertainty of PyL-150 concentration in NH₄Y-300.

Gas-Liquid Interface and Solid Support Effects of Polar

Solute-Nonpolar Solvent Systems in Gas Chromatography¹

by Robert L. Pecsok and Barry H. Gump²

Department of Chemistry, University of California, Los Angeles, California 90024 (Received December 15, 1966)

The measurement of activity coefficients at infinite dilution by gas chromatography is very attractive but requires validation by static measurements. Previous work concerning polar stationary phases is extended to include polar solutes in nonpolar solvents. Both gas-liquid interface and solid support effects interfere with the determination of activity coefficients. The static behavior of methanol, ethanol, acetone, and diethylamine as solutes in the solvent squalane spread on several solid supports as well as in bulk is described. For meaningful activity coefficients by gas chromatography, the systems should be restricted to small activity coefficients, nonpolar solutes and solvents, and inert solid supports carrying high liquid loads.

Martin,^{3,4} Pecsok,⁵ and Martire, Pecsok, and Purnell^{6,7} have shown that solute adsorption at the gas-liquid interface can be an important factor in determining retention volumes of nonpolar solutes on low per cent liquid loaded gas chromatographic columns when the column substrate is polar. A new equation for the retention volume has been proposed³ to take this factor into account

$$V_{Rg}^{\circ} = KV_L + k_a A_L \quad (1)$$

V_{Rg}° is the net retention volume per gram of packing; K , the bulk partition coefficient, is the concentration of the solute in the liquid phase divided by the concentration of the solute in the gas phase; k_a , the surface partition coefficient, is the concentration of the solute on the surface in excess of that in bulk divided by the concentration of the solute in the gas phase; V_L is the volume of the liquid substrate per gram of packing; and A_L is the area of the liquid surface per gram of packing. The second term in eq 1 represents the gas-liquid interface adsorption which becomes important at low per cent liquid substrate loadings where the liquid surface area is relatively large and is rapidly changing with per cent liquid.

Values of K and k_a at 25 and at 50° for various hydrocarbons in β, β' -thiodipropionitrile (TDPN) have been reported by Pecsok.⁵ To corroborate the measurements made by gas chromatography, Martin⁴ and

later Martire, Pecsok, and Purnell^{6,7} made static measurements on various polar liquid substrate-nonpolar solute systems. They explained their results in terms of the Gibbs adsorption equation, which can be written

$$\Gamma_2^{(1)} = -\frac{X_2}{RT} \left(\frac{\partial \gamma}{\partial X} \right)$$

This equation shows that a surface excess concentration of solute, $\Gamma_2^{(1)}$, is to be expected and that its magnitude is a function of the rate of change of surface tension with bulk mole fraction of solute, $(\partial \gamma / \partial X)$. The Gibbs equation is related to that of Martin by

$$\Gamma_2^{(1)} = -\frac{X_2}{RT} \left(\frac{\partial \gamma}{\partial X} \right)^{\infty} = \frac{k_a^{\infty}}{K^{\infty}} X_2 n_L \quad (2)$$

(1) Presented at the 152nd National Meeting of the American Chemical Society, New York, N. Y., Sept 1966. Contribution No. 2017 from the Department of Chemistry, UCLA.

(2) Taken in part from the dissertation presented to the Graduate Division, UCLA, in partial fulfillment of the requirement for the Ph.D.

(3) R. L. Martin, *Anal. Chem.*, **33**, 347 (1961).

(4) R. L. Martin, *ibid.*, **35**, 116 (1963).

(5) R. L. Pecsok, A. de Yllana, and A. Abdul-Karim, *ibid.*, **36**, 452 (1964).

(6) D. E. Martire, R. L. Pecsok, and J. H. Purnell, *Nature*, **203**, 1279 (1964).

(7) D. E. Martire, R. L. Pecsok, and J. H. Purnell, *Trans. Faraday Soc.*, **61**, 2496 (1965).

where $\Gamma_2^{(1)}$ is the excess concentration of solute at the surface (moles/cm²) over that in a system in which the liquid retains the bulk composition up to an infinitely sharp interface, X_2 the solute mole fraction, R the gas constant, T the temperature (°K), $(\partial\gamma/\partial X)^\infty$ the change in liquid surface tension with solute concentration at infinite dilution, and n_L , moles of liquid/cm³ of liquid, is ρ/M_L where ρ is the density of the liquid substrate and M_L is the formula weight of the liquid substrate. Values of the partition coefficients K^∞ and k^∞ obtained by the static method were in good agreement with the values obtained by gas chromatography.

For the present discussion, a polar molecule is one with a resultant dipole moment; a nonpolar molecule has a zero dipole moment. Previous work has concerned various nonpolar solute-polar solvent³⁻⁷ and polar solute-polar solvent⁸ systems. In the latter work, Martire⁸ has suggested that adsorption at gas-liquid interfaces should be negligible for all solutes nonpolar and polar alike on nonpolar liquid phases. One purpose of this work was to attempt to demonstrate that liquid surface effects can be observed in polar solute-nonpolar solvent systems. Whereas the above authors were able to use gas chromatography, as well as a static method, because of solid support-polar solute interactions which precluded the use of gas chromatography, a static method with bulk liquid substrate was used here. As a second part of this work, substrate coated Chromosorb supports were examined to determine the type and magnitude of the solid support effects. Urone and Parcher⁹ have studied systems similar to those described here; their measurements were made chromatographically whereas ours were made on static systems.

Experimental Section

Equipment. Two instrumental systems were used in this work. The first system comprised a McBain balance¹⁰ and a de Noy tensiometer enclosed within a single thermostated enclosure.^{6,7} This was used to obtain values of the surface tension of solute-bulk liquid substrate solutions. The quartz helix (Microchemical Specialties Co., Berkeley, Calif.) used for the McBain balance was calibrated at 50-mg intervals with NBS certified weights, giving a stretch constant of 0.9989 ± 0.0004 mm/mg. The quartz helix used for the tensiometer (Worden Laboratory, Houston, Texas) had a spring constant of 0.09916 ± 0.0001 mm/mg. The standard platinum-iridium ring (Fisher Scientific Co.) used with the tensiometer had a given radius, R' , of 9.557 mm with a given value of R'/r equal to 53.7937 where r is the wire radius. These dimensions were confirmed by measuring the surface tensions of

several pure solvents—benzene, ethanol, and aniline—at 30°.

The second system consisted of a Cahn electrobalance, Model RG, installed in the glass vacuum bottle supplied with the balance. The bottle was sealed for use under water and was modified for use with organic vapors. The Cahn electrobalance was used to obtain partition isotherms and f_2° values.

Materials. Several solid support materials were used. Chromosorb W 80/100 mesh and Chromosorb P 45/60 mesh regular grades obtained from Wilkens Instrument and Research, Inc., Chromosorb W (AW-DMCS) 80/100 mesh obtained from Perco Supplies, San Gabriel, Calif., and (Teflon) Tee Six 50/60 mesh obtained from Analytical Engineering Laboratories, Inc., were used without further treatment. The squalane and hexadecane substrates were supplied by Wilkens Instrument and Research, Inc. The β,β' -thiodipropionitrile, Eastman Kodak Yellow Label, was recrystallized four times from water until snow-white opaque needles, mp 28.2–28.7°, were obtained. The infrared spectra of all liquid phases were compared to the known spectra in the literature. Zone-refined benzene (99.999%) was supplied by J. Hinton, Valparaiso, Fla. All other chemicals were of spectroquality grade and were used without further purification.

Experimental Procedure Used with the McBain Balance and Tensiometer. A sample of about 100 mg of liquid substrate was weighed into the McBain balance quartz pan forming a liquid layer approximately 1 mm in thickness. Liquid substrate was also placed in the tensiometer dish to give a layer of the same thickness. The apparatus was then assembled, placed in a water bath at $30.00 \pm 0.01^\circ$ and brought to temperature, and evacuated to approximately 10^{-2} mm.

Reference positions of the balance pan and the ring were read with a cathetometer (Wild Heerbrugg Ltd., Model 1002) while the system was evacuated. The data for surface tension were obtained by raising the platform and solvent dish to the ring and then withdrawing the platform at the rate of 1 cm/min. A reference mark on the ring hook was followed with the cathetometer. At the point of release the cathetometer was read and the difference between this reading and the reference reading recorded as the stretch of the spring due to the surface tension of the liquid.

Subsequently, increments of solute vapor were ad-

(8) D. E. Martire, *Anal. Chem.*, **38**, 244 (1966).

(9) P. Urone and J. F. Parcher, *ibid.*, **38**, 271 (1966).

(10) J. W. McBain and A. M. Bakr, *J. Am. Chem. Soc.*, **48**, 630 (1926).

mitted to the vessel. Following each addition the system was allowed to come to equilibrium overnight. The vapor pressure and the weight of solute in solution in the balance pan were recorded and the tensiometer measurements made. Tensiometer readings were taken at 2.5-hr intervals. Between readings the ring rested on the surface of the liquid while equilibrium was being reestablished.

Experimental Procedure Used with the Cahn Electrobalance. Samples of 80/100 mesh Chromosorb W at approximately 0, 2, 5, and 10% liquid loadings by weight of squalane and 10% liquid loading by weight of hexadecane, of 80/100 mesh Chromosorb W (AWD-MCS) at 10% liquid loading by weight of squalane, and of 50/60 mesh Tee Six at 10% liquid loading by weight of squalane were prepared. Weighed amounts of these materials and of bulk squalane were placed in an aluminum foil bucket and suspended from the balance beam. The balance was assembled, placed in the water bath, and brought to temperature, and the system was evacuated to approximately 10^{-2} mm.

Measurements on a number of vapors in squalane and hexadecane were made as follows. The reference position of the balance pan was noted on the 1.0-mv recorder chart while the system was evacuated. Small additions of solute vapor were then admitted to the system and the uptake of this solute by the sample again recorded on the chart. Measurements were made on both the sorption and desorption of solute vapor for many of the points. The same procedure was followed for the study of bare 45/60 mesh Chromosorb P.

Data from measurements of the solute vapor pressure and the solute sorption by the various samples were used without the respective meniscus and buoy-

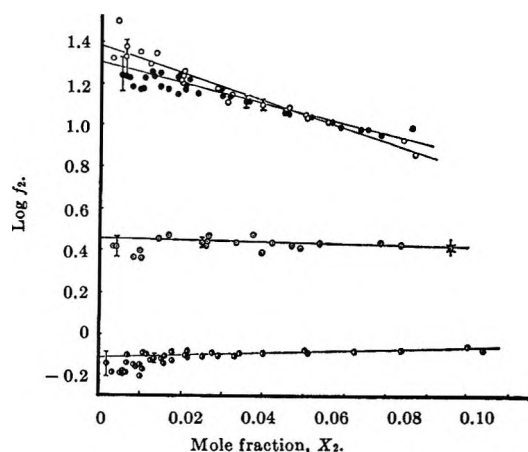


Figure 1. Activity coefficient vs. mole fraction for solute-bulk squalane systems at 30°: O, methanol; ●, ethanol; ⊙, acetone; ⊙, diethylamine.

ancy corrections. Typical measurements indicate that the meniscus correction corresponds to a possible error in the solute vapor pressure of 0 ± 0.15 mm in the systems studied. The reproducibility of successive surface tension measurements at equilibrium was found to be ± 0.04 mm of spring stretch which corresponds to an error of $\pm 0.12\%$ in the surface tension of liquid squalane solutions.

With the Cahn electrobalance the weight of solute sorbed by the sample could be determined to within ± 0.002 mg. Using acetone as an example and including the buoyancy correction this corresponds to a mole fraction of 0.087 with a possible error of $\pm 2.1\%$ or of 0.025 with a possible error of $\pm 3.5\%$. The corresponding error in the activity coefficient is thereby $\pm 4.6\%$ at a mole fraction of 0.025.

Results and Discussion

Activity Coefficients. Several authors have reported activity coefficients as determined by gas-liquid chromatography.¹¹⁻¹⁸ These have been shown to compare quite favorably with those extrapolated from traditional static measurements in bulk liquid under well-defined equilibrium conditions.^{15,16,19} Calculations of $\log f_2$ vs. X_2 for the solute-bulk substrate and solute-substrate coated solid support systems were made. Figure 1 shows the data for the solute-bulk squalane systems at 30°. The relevant constants employed in the calculations of f_2 are listed in Table I.

Surface Tension Measurements. Measurements were made with methanol, ethanol, acetone, and diethylamine as solutes in squalane at $30.00 \pm 0.01^\circ$ and with methanol and ethanol as solutes in squalane at $50.00 \pm 0.01^\circ$. The data for the ethanol-squalane system are presented in Figure 2, graphed as γ vs. X_2 with the limiting slope $(\partial\gamma/\partial X)^\infty$ drawn in. The surface tension experiences an initial sharp decrease as the mole fraction of solute is increased and then levels off without much change upon further addition of solute vapor. These limiting values of the surface tension are close

(11) A. J. Ashworth and D. H. Everett, *Trans. Faraday Soc.*, **56**, 1609 (1960).

(12) E. R. Adlard, M. A. Khan, and B. T. Whitham, *Gas Chromatog. Proc. Symp.*, *3rd*, Edinburgh, 1960, 251 (1961).

(13) P. E. Porter, C. H. Deal, and F. H. Stross, *J. Am. Chem. Soc.*, **78**, 2999 (1956).

(14) D. E. Martire, *Anal. Chem.*, **33**, 1143 (1961).

(15) D. E. Martire in *Gas Chromatog. Intern. Symp.*, *4th*, 33 (1963).

(16) D. H. Everett and C. T. H. Stoddart, *Trans. Faraday Soc.*, **57**, 746 (1961).

(17) D. H. Desty and W. T. Swanton, *J. Phys. Chem.*, **65**, 766 (1961).

(18) C. J. Hardy, *J. Chromatog.*, **2**, 490 (1959).

(19) A. Kwantes and G. W. A. Rijnders, *Gas Chromatog. Proc. Symp.*, *2nd*, Amsterdam, 1958, 125 (1958).

Table I: Physical Constants Employed in the Calculation of f_2^a

Compound	P^s , mm	$-B_{22}$, ml/mole	V^s , ml/mole
At 30°			
Acetone	282.4 (20)	1860 (21)	74.53 (20)
Ethanol	78.06 (20)	3026 (22)	59.00 (20)
Diethylamine	299 (20)	1400 (22)	105.5 (20)
Methanol	160.2 (20)	1570 (21)	40.97 (20)
At 50°			
Ethanol	220.9 (20)	25.60 (22)	60.35 (20)
Methanol	410.8 (20)	1550 (21)	41.88 (20)

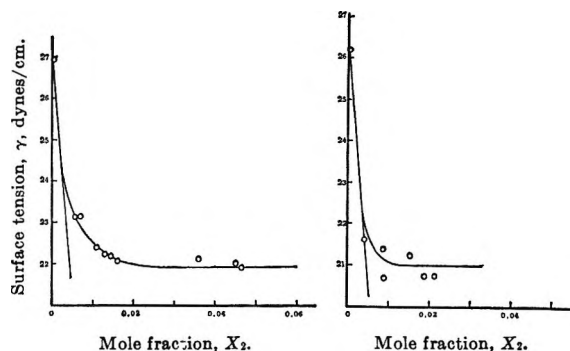
^a References in parentheses.

to those of the individual solutes. They decrease as the temperature rises to 50° as do the surface tensions of the pure solutes.

McBain²³ has classified surface tension *vs.* concentration curves into three types of which types I and III are of interest here. Type I curves are typical of non-polar materials in polar solvents, the amount of curvature being a function of the solubility of the solute in the solvent. Type III curves are typical of systems of long-chain ions at an air-water interface; they are characterized by a very great lowering of the surface tension in very dilute solution, the surface tension thereafter remaining approximately constant.

The solute-TDPN and solute-squalane systems considered here are analogous to the ones described by McBain. In the solute-TDPN systems nonpolar organic solutes were adsorbed on the surface of a polar solvent, TDPN, and the surface tension *vs.* concentration curves decrease smoothly with increase in solute concentration, the value of the limiting slope increasing roughly as does the value of the activity coefficient from one system to another. An experimental example of a type I plot is available in ref 7.

In the solute-squalane systems the various solute molecules were made up of two groups, a hydrocarbon part and a polar oxygen (in the case of methanol, ethanol, and acetone) or nitrogen (diethylamine) atom. Osipow²⁴ discusses the comparable type III case of fluorine-containing compounds as solutes on organic liquid solvents. Here the organophilic groups were generally hydrocarbon chains, while the organophobic groups were fluorocarbon chains. It was found that as little as 0.01 mole/l. of partially fluorinated carboxylic esters dissolved in organic solvents was able to reduce the surface tension by as much as 50%. Larger surface tension depressions were obtained, the higher the surface tension of the solvent.

Figure 2. Surface tension *vs.* mole fraction for ethanol-squalane system at 30 and 50°.

Liquid Surface Adsorption. The addition of a second component to a pure solvent results in a surface layer with a different composition from that of the bulk of the mixture. One component is said to be "adsorbed" at the dividing surface between the two components.²⁵ The amount of surface adsorption or the "surface excess concentration" is usually obtained from the value of the surface tension of the solution and the Gibbs adsorption equation

$$d\gamma = -\sum \Gamma_i d\mu_i = -RT \sum \Gamma_i d \ln a_i$$

where γ is the surface tension of the solution, μ_i the chemical potential of component i , a_i the activity of component i , and Γ_i the surface excess concentration of component i . For a two-component system

$$\partial\gamma = -\Gamma_1 d\mu_1 - \Gamma_2 d\mu_2$$

or substituting from the Gibbs-Duhem equation ($X_1 d\mu_1 + X_2 d\mu_2 = 0$) we obtain

$$\frac{X_2}{d\mu_1} \partial\gamma = \Gamma_2 X_1 - \Gamma_1 X_2$$

where the term $(X_2/d\mu_1)\partial\gamma$ signifies the surface excess (moles per unit area), the extent by which the surface concentration of a given component exceeds its concentration in the bulk liquid, and $\Gamma_1 + \Gamma_2$ correspond to the surface concentrations of components 1 and 2, respectively.

(20) J. Timmermans, "Physico-Chemical Constants of Pure Organic Compounds," Elsevier Publishing Co., Amsterdam, The Netherlands, 1950, pp 145, 311, 354, 521.

(21) J. S. Rowlinson, *Trans. Faraday Soc.*, **45**, 974 (1949).

(22) J. Dymond, unpublished data.

(23) J. W. McBain, "Colloid Science," D. C. Heath and Co., Boston, Mass., 1950, p 56.

(24) L. I. Osipow, "Surface Chemistry," Reinhold Publishing Corp., New York, N. Y., 1962, p 266.

(25) J. J. Kipling, "Adsorption from Solutions of Non-electrolytes," Academic Press Inc., New York, N. Y., 1965, Chapter 11.

Guggenheim and Adam²⁶ have defined several ways in which surface excess has been used. The definition most valuable for studies of dilute solutions, such as considered here, places the dividing surface between the two components such that $\Gamma_1^{(1)}$, the surface excess of the solvent, is zero. It follows that, since $\Gamma_1^{(1)}$ is zero, the surface excess is $\Gamma_2^{(1)}$ and

$$\Gamma_2^{(1)} = -\frac{\partial\gamma}{d\mu_2}$$

Recalling that $d\mu_2 = RT d \ln a_2$ and that for an ideal solution $a_2 \rightarrow X_2$ as $X_2 \rightarrow 1$, we have

$$\Gamma_2^{(1)} = -\frac{1}{RT} \left(\frac{\partial\gamma}{\partial X_2} \right) \left[\frac{1}{X_2} + \frac{\partial \ln f_2}{\partial X_2} \right]^{-1}$$

Values of f_2° and $(\partial\gamma/\partial X)^\infty$ obtained for the solute-bulk squalane systems, along with the respective values of K^∞ and $10^6 k_a^\infty$ calculated from them, are listed in Table II. For comparison the values of f_2° and $(\partial\gamma/\partial X)^\infty$ for the systems benzene and cyclohexane in TDPN obtained by Martire, *et al.*,⁷ are included at the bottom of the table. One observes that for comparable values of the activity coefficient the solute-squalane systems exhibit much larger values for the limiting slope of the surface tension *vs.* mole fraction curves.

Table II

A. Values of f_2° , $(\partial\gamma/\partial X)^\infty$, K^∞ , and $10^6 k_a^\infty$ for Solutions in Squalane

	Methanol	Ethanol	Acetone	Diethyl- amine
		30°		
f_2°	24.38	19.90	2.85	0.757
$(\partial\gamma/\partial X)^\infty$	-2464	-1249	-209.2	-248.5
K^∞	9.15	23.02	44.00	158.0
$10^6 k_a^\infty$, cm	473.0	602.8	195.2	999.5
		50°		
f_2°	17.18	12.92		
$(\partial\gamma/\partial X)^\infty$	-1903	-1092		
K^∞	5.31	13.14		
$10^6 k_a^\infty$, cm	202.1	286.9		

B. Comparison Values of f_2° and $(\partial\gamma/\partial X)^\infty$ for Solutions in β,β' -Thiodipropionitrile at 30° Taken from Martire, *et al.*⁷

	Cyclo- hexane	Benzene
f_2°	40.5	3.38
$(\partial\gamma/\partial X)^\infty$	-644	-86.4

The experimental values of $(\partial\gamma/\partial X)^\infty$ and $10^6 k_a^\infty$ decrease in the methanol- and ethanol-squalane systems as the temperature is increased from 30 to 50°. This

trend agrees with that reported by Pecsok, *et al.*,⁵ in their work with TDPN systems. Comparing the decrease in K^∞ and $10^6 k_a^\infty$ with temperature (see Table II), one may conclude with Martin³ that the effects of temperature over this range are different for the adsorption and solution processes.

Effect of the Solid Support and of Solid Support Treatment. If one is attempting to determine activity coefficients or other thermodynamic properties of solute-solvent systems *via* gas chromatography, he must answer the question, does spreading a liquid on a so-called "inert" solid support material cause the properties of the liquid to change from those of the bulk? Ormerod and Scott²⁷ and Fukuda²⁸ report that gas-liquid chromatography of strongly polar solutes using nonpolar liquid phases invariably results in poor separations and retention volumes strongly dependent on the sample size. Furthermore, Dal Nogare and Juvet²⁹ have listed several papers dealing with the alteration of liquid phase properties by the solid support.

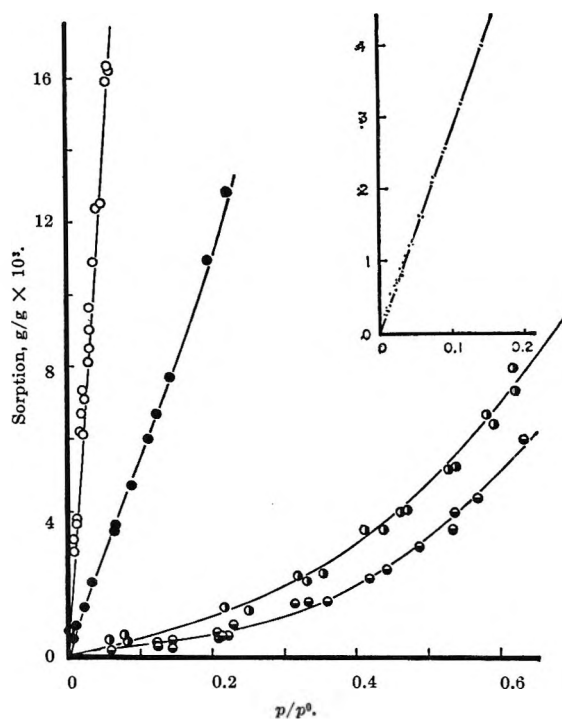


Figure 3. Partition isotherms of solute-bulk squalane systems at 30°: \ominus , methanol; \circ , ethanol; \bullet , acetone; \circ , diethylamine. Inset is expanded plot of diethylamine isotherm.

(26) E. A. Guggenheim and N. K. Adam, *Proc. Roy. Soc. (London)*, **A139**, 218 (1933).

(27) E. C. Ormerod and R. P. W. Scott, *J. Chromatog.*, **2**, 55 (1959).

(28) T. Fukuda, *Bunseki Kagaku*, **8**, 627 (1959).

(29) S. Dal Nogare and R. S. Juvet, Jr., *Anal. Chem.*, **38**, 61R (1966).

Partition isotherms for the solute-bulk squalane systems at 30° are plotted in Figure 3. With the exception of the system methanol-2% squalane 80/100 Chromosorb W which is slightly concave to the concentration axis, all the partition isotherms of the various solute-solvent coated solid support systems have this same general shape, that is, curved convex to the concentration axis. Although bare Chromosorb W and P are relatively inert as adsorbants for the compounds studied, the amount of solute adsorbed by the bare support is a substantial part of that sorbed by the various coated supports, especially in the case of the low-solubility alcohols. This is due to the low solubility of the respective solute vapors in squalane. Thus, the methanol-2% squalane curve exhibits this effect of solid support adsorption.

A Raoult's law plot shows that the systems methanol-, ethanol-, and acetone-bulk squalane exhibit positive deviations from Raoult's law, while the system diethylamine-bulk squalane exhibits a slight negative deviation (see Figure 4). This change from a positive deviation (methanol-squalane) to a negative one (diethylamine-squalane) occurs in spite of the fact that the corresponding isotherms are of the same general shape.

Spreading the liquid substrate squalane on a solid support material can have a dramatic effect upon the deviation from Raoult's law and the measured activity coefficient. This is shown in Figures 5 and 6 for the former. In Figure 7, using the ethanol-squalane system as an example, one observes that the logarithm of the measured solute activity coefficient on liquid substrate coated Chromosorb W decreases sharply as zero mole fraction is approached. This effect is more pronounced on the lower per cent liquid loadings in a given solute-solvent system and becomes less pronounced as one goes from the system methanol-solvent to that of diethylamine-solvent.

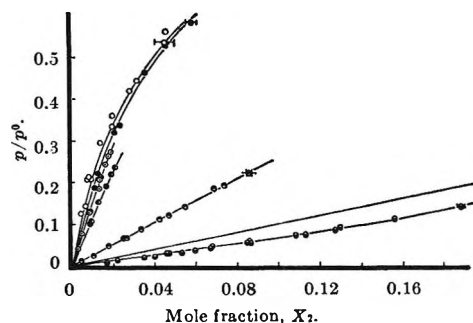


Figure 4. Deviations from Raoult's law for various solute squalane systems at 30 and 50°: ○, methanol (30°); ●, ethanol (30°); ○, methanol (50°); ●, ethanol (50°); ●, acetone (30°); ●, diethylamine.

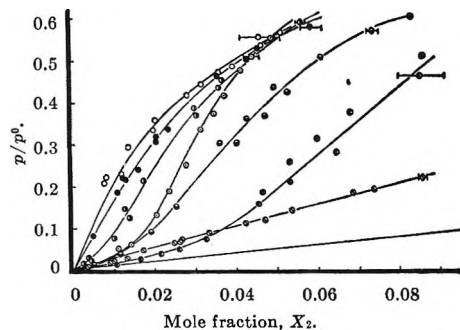


Figure 5. Deviations from Raoult's law for the systems methanol- and ethanol-squalane in bulk and coated on Chromosorb W at 30°: ○, methanol-bulk squalane; ○, methanol-10% squalane; ●, methanol-2% squalane; ●, ethanol-bulk squalane; ○, ethanol-10% squalane; ●, ethanol-5% squalane; ○, acetone-bulk squalane.

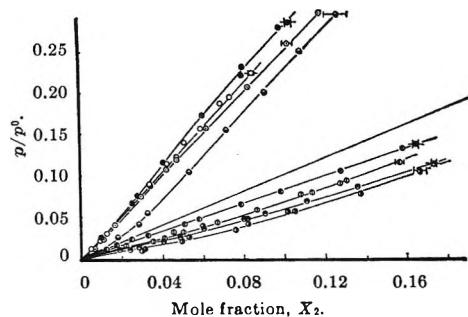


Figure 6. Deviations from Raoult's law for the systems acetone- and diethylamine-squalane in bulk and coated on Chromosorb W at 30°: ○, acetone-bulk squalane; ●, acetone-10% squalane; ○, acetone-5% squalane; ●, acetone-2% squalane; ○, diethylamine-bulk squalane; ●, diethylamine-10% squalane; ●, diethylamine-5% squalane; ●, diethylamine-2% squalane.

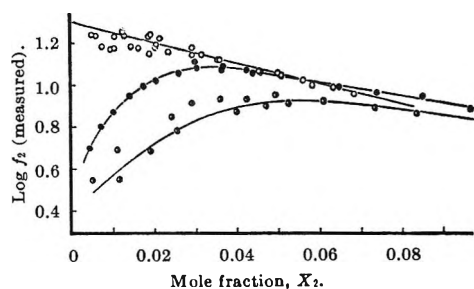


Figure 7. Activity coefficient vs. mole fraction for ethanol-squalane systems in bulk and coated on Chromosorb W at 30°: ○, bulk liquid; ●, 10% liquid; ○, 5% liquid.

To show that the decrease of $\log f_2$ vs. X_2 at low mole fraction of solute is a solid support effect, the systems benzene- and cyclohexane-10% TDPN 80/100 Chromosorb W were studied. TDPN, a rather polar liquid substrate, should cover up the active sites on the solid

support. Thus, one would expect to obtain a linear plot of $\log f_2$ vs. X_2 similar to that obtained for the solute-bulk TDPN systems. The data show (see Figure 8 for the cyclohexane-TDPN system) that this effect on the activity coefficient at low mole fraction in polar solute-nonpolar solvent systems is due to the solid support.

The data for the sorption of the various solutes in bulk squalane and on squalane coated Chromosorb W at 30° were reduced to the form of weight solute sorbed by the sample per gram of squalane in the sample vs. p/p^0 as shown in Figure 9 for the acetone-squalane system. If the bulk solution process were the only one occurring, these curves should coincide. That they do not coincide is quite evident. In all the systems studied the data show that the weight of solute sorbed per gram of solvent follows the progression 2% > 5% > 10%. This is the same progression that Pecsok, *et al.*,⁵ have shown for the surface areas of coated supports. If liquid surface adsorption were occurring, this is what one would expect; the amount of solute sorbed per gram of solvent (at a value of p/p^0 where solid support adsorption is not important, *e.g.*, $p/p^0 = 0.3$ in Figure 9) should increase as does the surface area of the coated support. While this comparison is not conclusive in showing liquid surface adsorption in these systems, it does point in that direction.

Treated Supports and Teflon Support Materials. The systems methanol- and ethanol-10% squalane 80/100 Chromosorb W (acid washed, silanized) and ethanol-9% squalane 50/60 Tee Six (a Teflon support material) have also been studied at 30°. It was of interest to determine what effect the acid washing and silanization treatment would have on the solid support adsorption of the solute and what effect the use of the above materials would have on the measured value of the activity coefficient at infinite dilution.

Figure 10 summarizes these solid support effects with regard to the activity coefficients of the ethanol-squalane system. Acid washing and silanizing the

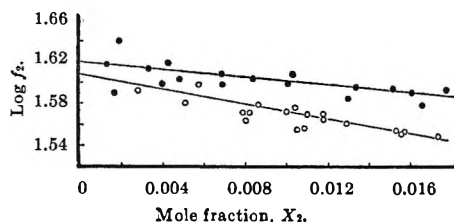


Figure 8. Activity coefficient vs. mole fraction for cyclohexane-TDPN systems in bulk and coated on Chromosorb W at 30°: O, bulk liquid; ●, 10% liquid.

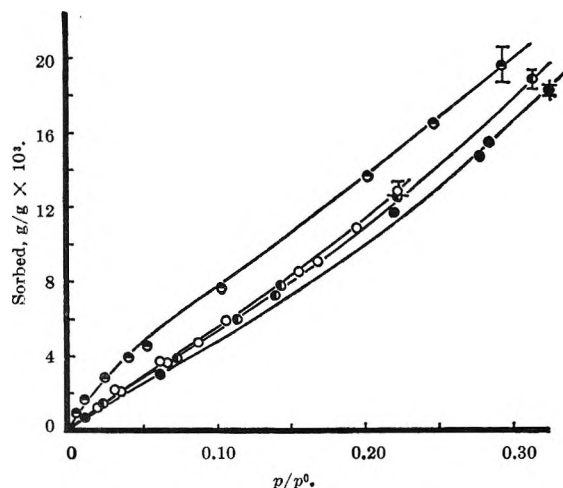


Figure 9. Partition isotherms for acetone sorbed in squalane in bulk and coated on Chromosorb W at 30°: O, bulk liquid; ●, 10% liquid; ◐, 5% liquid; ◑, 2% liquid.

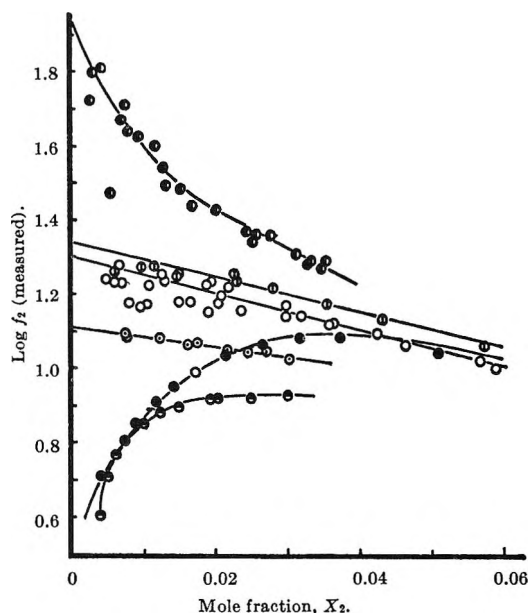


Figure 10. Activity coefficient vs. mole fraction for the ethanol-squalane system showing effects of temperature and the solid support: O, bulk squalane (30°); ●, 10% squalane on Chromosorb W (30°); ◑, 10% squalane on AWDMCS (30°); ◒, 9% squalane on T-6 (30°); ◐, bulk squalane (50°); ◑, 10% squalane on Chromosorb W (50°).

Chromosorb support causes the value of f_2^0 to be substantially higher than that obtained with the bulk liquid. In addition, at a very low mole fraction ($X_2 \leq 0.01$) $\log f_2$ tends to increase. Since one is essentially working at infinite dilution in gas chromatography, this could have a considerable effect upon the value of the activity coefficient determined with this tech-

nique. The data for the substrate coated Teflon support material are also shown in Figure 10. In this case no solid support adsorption effect on the value of the activity coefficient is observed and the value of $\log f_2^\circ$ obtained is close to but slightly higher than that obtained with the bulk liquid. The difference in the two values is due to the liquid surface adsorption. The same feature to a lesser degree is seen in Figure 8 for the cyclohexane-TDPN system. Table III summarizes the differences in the activity coefficients for the methanol- and ethanol-squalane systems.

Table III: Comparative Values of the Solute Activity Coefficients at Infinite Dilution

	Bulk squalane		10% squalane 80/100 Chromo- sorb W (AWDMCS) $T = 30^\circ$	9% squalane- 50/80 Tee Six $T = 30^\circ$
	30°	50°		
Methanol	24	17	150	..
Ethanol	20	13	75	22

If, as is concluded here, liquid surface adsorption of the solute is an important feature of polar solute-nonpolar solvent systems, then partition coefficients, activity coefficients, and other thermodynamic properties determined by gas-liquid chromatography of these systems would be incorrect unless corrected for adsorption at the gas-liquid interface. It appears that the use of Teflon-type support materials at higher temperatures (decrease of k_a with increase in T) may be the best means of avoiding solid support and liquid surface effects and yield a curve with a closer coincidence to that of the bulk squalane system. Further study of these support materials is desirable in order to critically evaluate their usefulness in determining thermodynamic properties of the polar solute-nonpolar solvent type of system. On the other hand, as Martin has shown,³ liquid surface adsorption can be used to alter elution orders of compounds. Thus, this variable adds an extra measure of selectivity to the gas chromatographic process as a separation tool.

Acknowledgment. Helpful discussions of some of the material with D. E. Martire are gratefully acknowledged.

The Influence of the Alkali Halides on the Structure of Water¹

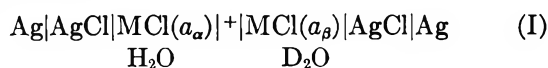
by J. Greyson

Atomics International Division of North American Aviation, Inc., Canoga Park, California
(Received December 16, 1966)

Measurements of emf of electrochemical cells containing heavy and normal water solutions of several alkali halides have been made. The cell potentials have been combined with available heat of solution data to determine the entropy of transfer of the salts between the isotopic solvents. From the values of the entropy of transfer, the order of the structure-influencing properties of alkali cations and halide anions was found to be $K^+ > Na^+ > Li^+$ and $I^- > Br^- > Cl^- > F^-$. Differences in values among the ions indicated that structure-influencing properties are more sensitive to ion size for negatively charged species than for positively charged species.

Introduction

Current interest in sea water desalination has stimulated a number of reports on the nature of the structure of water and the effect of dissolved species upon it. We,^{2,3} along with others,⁴⁻⁶ have reported experiments in which differences in properties between heavy and normal water solutions have been studied. Such differences have been attributed to the extent to which the solvents' structure is destroyed or enhanced by the dissolved species. The specific approach we have taken has entailed an investigation of electrochemical cells in which heavy and normal water ionic solutions are separated by an ion-permeable membrane. That is, measurements have been made of the emf values of cells of the type



where the symbol $|+$ represents a cation-exchange membrane and the a 's are the activities of the salts (MCl) in their respective solutions. The emf of cell I has been shown² to be related to the free-energy change for the process of transfer of 1 equiv of MCl from D_2O at activity a_β to H_2O at activity a_α . By combining the free energy with the heat of transfer or by measuring its temperature coefficient, one can obtain the entropy of transfer. Since the differences between normal and heavy water are considered to result almost entirely from differences in structure, the magnitude of the entropy of transfer can be related to the influence of the dissolved salt on structure.⁷

Type I cells have yielded entropies for the transfer of several uni-univalent chlorides between the isotopic solvents.⁸ For the alkali chlorides, the sign and magnitude of the entropies indicated that the salts were more disruptive to the structure of heavy water than to normal water and that the order of structure-breaking influence was $\text{CsCl} > \text{KCl} > \text{NaCl} > \text{LiCl}$. Since the work on type I cells was reported, several publications have appeared in which confirmation of the data interpretation has been made.⁴⁻⁶ In this paper, we report the results of some new measurements the purpose of which was to obtain data for other halide ions. Having such data, in combination with the data for the alkali chlorides, one can establish a sequence of structural-influencing properties for all the alkali halides in aqueous solution.

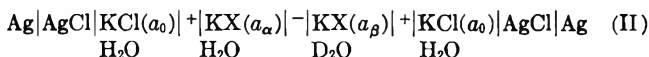
Type I cells with chloride reversible electrodes and cation-exchange membranes limit transfer measurements to families of chloride salts. For measurements of other halides in a cell configuration similar to that of type I, electrodes reversible to each of the halide ions to be studied are required. Although electrodes

- (1) This research was supported by the Research Division of the Office of Saline Water, U. S. Department of the Interior.
- (2) J. Greyson, *J. Phys. Chem.*, **66**, 2218 (1962).
- (3) J. Greyson, *ibid.*, **71**, 259 (1967).
- (4) R. E. Kerwin, Ph.D. Thesis, University of Pittsburgh, 1964.
- (5) R. L. Kay and D. F. Evans, *J. Phys. Chem.*, **69**, 4216 (1965).
- (6) Y. C. Wu and H. L. Friedman, *ibid.*, **70**, 166 (1966).
- (7) (a) G. Némethy and H. A. Scheraga, *J. Chem. Phys.*, **41**, 680 (1964); (b) H. S. Frank and M. W. Evans, *ibid.*, **13**, 507 (1945).

Table I: Emf Values for the Cell $\text{Ag}|\text{AgCl}|\text{MCl}(a_0)|\text{MX}(a_\alpha)|\text{MX}(a_\beta)|\text{MCl}(a_0)|\text{AgCl}|\text{Ag}$ at $a_\beta = a_\alpha$

Emf, mv	MX							
	KF	KCl	KBr	KI	NaCl	NaBr	NaI	LiCl
	-0.15 ± 0.3	3.8 ± 0.3	5.3 ± 0.3	6.8 ± 0.3	2.7 ± 0.3	4.3 ± 0.3	5.9 ± 0.3	1.4 ± 0.3

reversible to bromide and iodide ions with good stability and low bias potentials can be constructed,⁸ fluoride ion electrodes cannot. At least to our knowledge, no electrodes reversible to fluoride with the requisite properties (bias potentials of less than 0.2 mv) for these measurements are currently available. Therefore, instead of attempting to use type I cells, measurements of other halides were carried out in cells of the configuration shown in (II).



In type II cells, the configuration



is a cation reversible membrane electrode (here reversible to potassium ion), the symbol X refers to an anion, and the anion-exchange membrane, $|-|$, permits the diffusion of anions between the solvents. It has been shown that the emf of cell II, like cell I, is related to the free energy of transfer of 1 equiv of KX from D_2O at activity a_β to H_2O at activity a_α .³

Measurements of cell II emf values have been carried out for KF, KBr, KI, NaBr, and NaI solutions. The values at $a_\alpha = a_\beta$ have been used to obtain the transfer free energies and entropies for the transfer of these salts from D_2O to H_2O .

Experimental Section

The experimental procedure and apparatus were the same as those described in previous publications.^{2,3} All solutions were about 0.1 aquamolal and were prepared from reagent grade salts which were used without additional purification. Measurements were carried out at 25°.

Results and Discussion

The results of the measurements are shown in Table I along with values for KCl, NaCl, and LiCl taken from an earlier publication.³ Experimental reproducibility has varied from 0.2 to 0.3 mv and is shown in the table as 0.3 mv. The sign of the emf is defined such that positive values indicate a spontaneous transfer of salt from heavy to normal water. It is to be noted

that the emf values increased positively from KF to KI and from NaCl to NaI.

In an earlier paper³ it was shown that the measured emf's of these ion-exchange membrane cells contained contributions resulting from solvent transport. That is, a quasi-thermodynamic treatment of electrochemical cells composed of half-cells containing heavy and normal water solutions leads to the equation

$$\frac{Ef}{RT} = \frac{E^\circ f}{RT} - 2t_M + \ln \frac{a_{MX}^\beta}{a_{MX}^\alpha} + (t_W - t_D) \quad (1)$$

for the cell emf. E° is the standard emf for the transfer of MX between the solvents; t_M , t_W , and t_D are the mass transport numbers of cations, normal water, and heavy water, respectively; and the other symbols have their usual significance. The term $(t_W - t_D)$ expresses the contribution to the emf due to solvent transport through the junction between the half-cells. Applied to cell II³ eq 1 resulted in

$$\frac{Ef}{RT} = \frac{E^\circ f}{RT} - 2 \ln \frac{a_{MCl}^\beta}{a_{MCl}^\alpha} + (t_W - t_D)^+ - (t_W - t_D)^- \quad (2)$$

where $(t_W - t_D)^+$ and $(t_W - t_D)^-$ represent the contributions to the cell emf resulting from solvent transport in the cation- and anion-exchange membranes, respectively. Thus the emf's given in Table I must be corrected for the values $(t_W - t_D)^+$ and $(t_W - t_D)^-$ to obtain E° and hence ΔF° and ΔS° .

A method for obtaining $(t_W - t_D)^-$ from cell measurements has been described.^{3,9} The values obtained for the anion membrane used in cell II bounded by chloride, bromide, and iodide solutions were 3.2 ± 0.2 , 4.1 ± 0.2 , and 5.1 ± 0.2 mv, respectively.⁹ To obtain an estimate³ of $(t_W - t_D)^+$ for sodium and potassium ions, we have used free-energy values obtained by Kerwin⁴ from solubilities of NaCl and KCl in heavy water. Kerwin⁴ has given the values of the standard free energy of transfer of NaCl and KCl from D_2O to H_2O as -116 and -121 cal/mole, respectively (corresponding to 5.02 and 5.26 mv, respectively,

(8) D. G. Ives and G. J. Janz, "Reference Electrodes," Academic Press Inc., New York, N. Y., 1961, p 209.

(9) J. Greyson, submitted for publication.

in a cell without solvent transport). Using these values and previously reported cell I data³ for NaCl and KCl one gets 1.2 and 1.5 mv, respectively, for $(t_w - t_D)^+$ in the cell II measurements reported here. Applying these solvent corrections in eq 2 one obtains the values for E° shown in Table II for cells containing solutions of NaCl, NaBr, NaI, KCl, KBr, and KI. The data for these salts are shown with an increased uncertainty (0.5 instead of 0.3) to reflect the uncertainty in the measurement of $(t_w - t_D)^-$.

Table II: Solvent Corrected Emf (mv) Values for Alkali Halides in H₂O-D₂O Cells

	F	Cl	Br	I
Li	$[-2.5 \pm 4.0]$	1.4 ± 4.0	$[2.9 \pm 4.0]$	$[4.4 \pm 4.0]$
Na	$[-1.2 \pm 4.0]$	4.7 ± 0.5	7.2 ± 0.5	9.8 ± 0.5
K	-0.2 ± 4.0	5.5 ± 0.5	7.9 ± 0.5	10.4 ± 0.5

It is of interest to include data for lithium and fluoride salts for comparison to the other alkali halides. We have therefore attempted to obtain reasonable estimates for these salts and have included in Table II a set of bracketed emf values for several of the lithium halides and the alkali fluorides. The brackets indicate that the experimental data for these salts are incomplete and that the values have been obtained by calculation. The calculated emf's were obtained by taking advantage of the fact that the free energy of an ionic salt is equal to the sum of the free energies of the individual ions. It has been shown that the data derived from these cells are true equilibrium values.³ Therefore, one can calculate the emf's for all the alkali halides from data for the potassium halides and the alkali chlorides. For example, one can calculate the emf of a cell containing LiI from the relationship

$$E_{KI} + E_{LiCl} - E_{KCl} = E_{LiI} \quad (3)$$

and the measured emf's for KI, LiCl, and KCl. That these relationships are valid can be further verified by comparing the measured values for NaBr and NaI which are shown in Table II with values which can be calculated from the other salts. Combination of the measured emf's for LiCl and KF with those of the appropriate salts in eq 3 yielded the data shown for LiF, LiBr, LiI, and NaF.

The large uncertainty in all the values for the fluoride and lithium salts reflects lack of information about solvent transport. No data relative to solvent transport in membranes associated with solutions of these salts are available. Although the uncertainties are

larger than the emf values themselves, as will be seen later, the differences in the resulting entropies of transfer among the lithium halides are significant. The 4-mv uncertainty which has been applied to the values in Table II is approximately equal to the maximum solvent correction which was obtained from experimental data for the other alkali halides. The largest solvent correction was 3.9 mv and was applied to the measured emf for a cell containing NaI solutions. As has been discussed recently,⁹ the solvent correction is inversely proportional to the mobility of the ion in the membrane. Lithium and fluoride ions have lower aqueous mobilities than the other alkali halide ions. Thus, one would expect them to have lower membrane mobilities and higher solvent corrections. In fact, the solvent correction for each of these two may be bigger than that of iodide. But it is also to be noted from eq 2 that the total solvent correction in cell II is obtained by subtracting that of the anion membrane from the cation membrane. Thus, the resulting difference is probably never much greater than the maximum difference observed for NaI. Adding an uncertainty to the measured values for lithium and fluoride salts of ± 4.0 mv is probably conservative.

The emf values from Table II have been used to calculate the free energies of transfer between the solvents for each of the alkali halides. The values of ΔF° are shown in Table III along with the associated uncertainty resulting from the emf measurements. As in earlier discussions of these measurements,^{2,3} the integral heat of solution data of Lange and Martin¹⁰ have been assumed equal to values of ΔH° and have been used to calculate the entropies of transfer, ΔS° . Heats and entropies are also shown in Table III. Reading across the table, one notes that the entropy of transfer becomes more negative from fluoride to iodide salts. As was pointed out above, this is true even for the lithium salts where, although the large solvent-transfer uncertainty leads to some possible overlap, the differences are big enough to display a definite ordering. The negative values of the entropy indicate that the salts are more structure disrupting to D₂O than to H₂O and the order of structure-breaking influence is $I^- > Br^- > Cl^- > F^-$. Reading down the columns of Table III, one notes a similar ordering from lithium to potassium salts. Except for LiBr and LiI, entropy values become more negative in passing from lithium to potassium salts. The apparent inconsistency in the values of LiBr and LiI is probably not real since the uncertainty in the numbers

(10) H. E. Lange and W. Martin, *Z. Elektrochem.*, **42**, 662 (1936).

Table III: Free Energy, Heat,¹⁰ and Entropy of Transfer of Alkali Halides from D₂O to H₂O

	F			Cl			Br			I		
	$-\Delta F^\circ$	$-\Delta H$	$-\Delta S^\circ$	$-\Delta F^\circ$	$-\Delta H$	$-\Delta S^\circ$	$-\Delta F^\circ$	$-\Delta H$	$-\Delta S^\circ$	$-\Delta F^\circ$	$-\Delta H$	$-\Delta S^\circ$
Li	-58 ± 92	-155	-0.33 ± 0.30	32 ± 92	420	1.30 ± 0.30	67 ± 92	560	1.65 ± 0.30	100 ± 92	720	2.08 ± 0.30
Na	-28 ± 92	10	0.13 ± 0.30	110 ± 12	510	1.34 ± 0.04	170 ± 12	650	1.61 ± 0.04	230 ± 12	810	1.95 ± 0.04
K	-3 ± 92	60	0.21 ± 0.30	130 ± 12	560	1.44 ± 0.04	180 ± 12	695	1.73 ± 0.04	240 ± 12	865	2.09 ± 0.04

^a Units are calories per mole for ΔF and ΔH and calories per mole degree for ΔS .

is much larger than the differences between values passing down the columns. It would appear that there is nothing in the data which would contradict the conclusions of the earlier papers,^{2,3} that the structure-breaking sequence for these alkali cations is $K^+ > Na^+ > Li^+$.

In conclusion it should be emphasized that the differences between the entropies of transfer for the halide anions are considerably larger than the differences between values for the alkali cations. It appears that structure-breaking properties are more dependent upon ionic radii for the negatively charged species than for the positively charged species. An explanation may lie in the results and conclusions of a recent series of investigations of Raman spectra of aqueous electrolyte solutions.^{11,12} The intensity of Raman librational bands associated with ion-water interaction was observed to be more sensitive to halide ion size than to cation size. The size dependence was attributed to ion polarizability which increases with the size of the halide ions. It was suggested that the

proton of the solvated water molecule polarizes the large halide ions and leads to a water-anion bond less polar than the $OH \cdots O$ of water itself while the less polarizable cations form hydrate bonds similar in polarity to that of water. We assert that such conclusions are compatible with the results of this work. Species, otherwise hydrophilic but less polar in nature than water, are less compatible with surrounding solvent structure and tend to disrupt it. Species with bond polarity more similar to that of water are more compatible with the surrounding structure and less disruptive. Since the polarizabilities of the halide ions are strongly size dependent, the polarity of the associated ion-solvate bonds would also be strongly size dependent. A resulting size dependence would be exhibited by the ions in their structure-breaking properties.

(11) G. E. Walrafen, *J. Chem. Phys.*, **36**, 1035 (1962).

(12) G. E. Walrafen, *ibid.*, **44**, 1546 (1966).

Thermodynamic Quantities in the Exchange of Zinc with Sodium Ions in Various Cross-Linked Polystyrene Sulfonate Cation Exchangers at 25°¹

by G. E. Boyd, F. Vaslow, and S. Lindenbaum

Oak Ridge National Laboratory, Oak Ridge, Tennessee 37880 (Received December 19, 1966)

Standard free energy, ΔG° , and enthalpy, ΔH° , changes for the reaction of zinc ion in dilute aqueous solutions with sodium ion in cross-linked polystyrenesulfonic acid type cation exchangers were estimated from equilibrium ionic distribution and heat of exchange measurements at 25°. The selective uptake of Zn^{2+} ion was accompanied by the absorption of heat and by an increase in the standard entropy, ΔS° . A maximum in ΔG° with increasing exchanger cross-linking was observed with the exchanger containing approximately 8% divinylbenzene, in contrast to ΔH° and ΔS° which increased progressively with cross-linking. The difference in the entropies of hydration of zinc and sodium ions appeared to be a major factor in determining ΔS° , which in turn governed the selective uptake of the former ion.

Comparatively very little is known about the causes for the decrease in free energy which accompanies the preferential uptake of multicharged cations in their reactions with less highly charged cations in strong-acid type cation exchangers. Unquestionably the lowering of the electrostatic energy of the system is an important factor, as, generally, the more highly charged ion is favored over the less highly charged one.² However, the contribution of the entropy to the free energy change may be significant because of (a) increases or decreases in ion hydration during the ion-exchange reaction and (b) changes in configurational entropy when unequal numbers of ions replace one another.

Information on the enthalpy changes in reactions between unequally charged cations is fragmentary. Calorimetric measurements have shown that heat is absorbed in the exchange of magnesium,³ calcium,⁴ and barium³ with K^+ ions and in the exchange of Mg^{2+} with H^+ ions,³ whereas heat is evolved in the Sr^{2+} - H^+ reaction.⁵ Measurements of the temperature dependence of the equilibrium constants for the exchange of Mg^{2+} and Cu^{2+} ions with hydrogen ion^{6,7} have indicated that heat is absorbed, while in the exchange of Ba^{2+} with H^+ ions heat is evolved.⁸

No studies have been reported on the dependence of the heats and entropies of exchange of unequally charged cations on the cross-linking or on the ionic composition of the exchanger. Accordingly, measurements were undertaken to determine values for these thermodynamic quantities for the Zn^{2+} - Na^+ reaction in an attempt to improve the current limited understanding of divalent-univalent ion-exchange reactions. The equilibrium distribution of Zn^{2+} and Na^+ ions between dilute aqueous solutions and a series of cross-linked polystyrenesulfonic acid type cation exchangers was measured and calorimetric determinations of heats

(1) Research sponsored by the U. S. Atomic Energy Commission under contract with the Union Carbide Corp.

(2) A discussion of this factor, termed "electroselectivity" by K. F. Bonhoeffer, has been given by F. Helfferich, "Ion Exchange," McGraw-Hill Book Co., Inc., New York, N. Y., 1962, pp 157, 158.

(3) D. S. Flett and P. Meares, *Trans. Faraday Soc.*, **61**, 1469 (1965).

(4) N. T. Coleman, *Soil Sci.*, **44**, 115 (1952).

(5) E. H. Cruickshank and P. Meares, *Trans. Faraday Soc.*, **53**, 1289 (1957).

(6) O. D. Bonner and L. L. Smith, *J. Phys. Chem.*, **61**, 1614 (1957).

(7) O. D. Bonner and R. R. Pruett, *ibid.*, **63**, 1420 (1959).

(8) J. F. Duncan and B. A. J. Lister, *Discussions Faraday Soc.*, **7**, 104 (1949).

of partial exchange were made at 25° with the same preparations. Standard free energy and enthalpy changes were estimated and standard entropy changes were derived.

Experimental Section

Materials. The polystyrenesulfonic acid cation exchangers nominally cross-linked with 2, 4, 8, and 12 mole % divinylbenzene (DVB) were reagent grade (J. T. Baker) Dowex-50W preparations. The 16 and 24% DVB exchangers were laboratory products supplied by the Physical Research Laboratory of the Dow Chemical Co., Midland, Mich. Exchange capacities on a vacuum dry basis, determined by acidimetric titration, and water contents for the exchangers in vapor phase equilibrium with 0.1 *m* NaBr solution are presented in Table I. The dilute aqueous electrolyte solutions used in the selectivity coefficient and calorimeter measurements were prepared with AR grade Zn(NO₃)₂ and NaNO₃.

Equilibrium Measurements. Determinations of the distribution coefficients for the uptake of Zn²⁺ ion were performed with 0.1 *N* aqueous solutions with which equilibrium was rapidly achieved. The "progressive batch" method⁹ was employed in the majority of the measurements to avoid separating the equilibrium aqueous electrolyte mixture from the exchanger and washing the latter, an operation which may disturb the

Table I: Capacities and Equivalent Water Contents of Cross-Linked Polystyrenesulfonate Cation Exchangers

Nominal cross-linking, % DVB	Capacity, mequiv/g of dry HR	Equivalent water content, ^a g of H ₂ O/equiv	
		NaR	ZnR ₂
2	5.28	537	391
4	5.15	350	305
8	5.19	176	188
12	5.08	142	160
16	4.75	122	151
24	4.67	88.0	106.4

^a Exchangers in vapor pressure equilibrium with 0.1 *m* NaBr solutions.

ionic distribution seriously. Errors tended to accumulate in this procedure, however, and it ultimately became of limited value. Therefore, a column technique was applied in which electrolyte solution was filtered through a bed of 20–30 mequiv of exchanger until the effluent and influent concentrations were equal. The solution occluded in the bed was removed by suction and by a rapid rinse with ethanol. The sodium and zinc ions in the exchanger were eluted with 1 *M*

HCl solution, the exchanger was rinsed with pure water, and the rinse was combined with the eluate and made up to volume. The concentration of Zn²⁺ in the aqueous phases was found by complexometric titration with standardized solutions of the disodium salt of ethylenediaminetetraacetic acid (EDTA) using Eriochrome Black T or xylenol orange as indicators.¹⁰ Sodium ion concentrations were determined with 15-hr ²⁴Na or 2.60-year ²²Na tracers and 245-day ⁶⁵Zn activity was utilized in the experiments where the distribution of microconcentrations of Zn²⁺ ion was measured.

Heat of Exchange Measurements. The calorimetric methods were identical with those described in the report from this laboratory on the heat of exchange of silver with sodium ion.¹¹ Homoionic sodium or zinc form of exchanger in vapor equilibrium with 0.1 *N* NaNO₃ or Zn(NO₃)₂ solution was mixed with 0.1 *N* Zn(NO₃)₂ or 0.1 *N* NaNO₃ solution, respectively, or with 0.1 *N* aqueous mixed electrolyte. The electrolyte solution in the calorimeter after equilibrium had been reached was analyzed with the procedures described above. The equivalent fraction of Zn²⁺ ion in the exchanger was determined by analysis of the exchanger recovered from the calorimeter. The milliequivalents of reaction were estimated from the predetermined weight of the exchanger and its initial and final zinc content. Approximately 5–15 mequiv of exchanger was used and the amount of reaction was known to ±0.05 mequiv. The calorimeter possessed a sensitivity of ca. 0.005 cal.

Treatment of Experimental Data

Evaluation of the Standard Free Energy Change, ΔG°. The ion-exchange reaction of zinc with sodium ion will be formulated on a mole basis and the composition of the exchanger will be expressed in terms of mole fractions with the components being NaR and ZnR₂, respectively. The treatment of Argersinger, Davidson, and Bonner¹² will be followed, according to which the thermodynamic equilibrium constant, *K*_{th}, for the reaction is given by

$$K_{th} = \frac{(N_{ZnR_2} m_{NaNO_3})^2 / (N_{NaR} m_{Zn(NO_3)_2})}{(f_{ZnR_2} \gamma_{NaNO_3})^4 / (f_{NaR}^2 \gamma_{Zn(NO_3)_2})^3} \quad (1)$$

The quantities *f*_{ZnR₂} and *f*_{NaR} in eq 1 are the activity coefficients of the respective components in the ex-

(9) J. D. Cosgrove and J. D. H. Strickland, *J. Chem. Soc.*, 1845 (1950).

(10) H. Flaschka and H. Abdine, *Chemist Analyst*, 45, 58 (1956).

(11) F. Vaslow and G. E. Boyd, *J. Phys. Chem.*, 70, 2295 (1966).

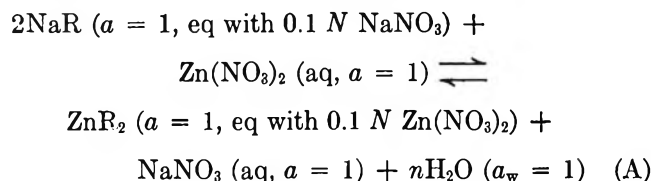
(12) W. J. Argersinger, Jr., A. W. Davidson, and O. D. Bonner, *Trans. Kansas Acad. Sci.*, 53, 404 (1950).

changer, m_{NaNO_3} and $m_{\text{Zn(NO}_3)_2}$ are the molalities of sodium and zinc nitrates in the mixed aqueous electrolyte solution, and γ_{NaNO_3} and $\gamma_{\text{Zn(NO}_3)_2}$ are the mean molal activity coefficients in the mixed electrolyte. The experimentally measured equilibrium distribution quotient, K_N , is defined by

$$K_N = N_{\text{ZnR}_2} m_{\text{NaNO}_3}^2 / N_{\text{NaR}}^2 m_{\text{Zn(NO}_3)_2} \quad (2)$$

and K_N° will be given by $K_N^\circ = K_N (\gamma_{\text{NaNO}_3}^4 / \gamma_{\text{Zn(NO}_3)_2}^3)$.

The standard free energy of exchange, ΔG° , per equivalent for reaction A when the products and re-



actants are in their standard states is then

$$\begin{aligned} -\Delta G^\circ (\text{kcal equiv}^{-1}) &= (2.3RT/2) \log K_{\text{th}} = \\ &(2.3RT/2) \int_0^1 \log K_N^\circ dx_{\text{Zn}^{2+}} \quad (3) \end{aligned}$$

where $x_{\text{Zn}^{2+}}$ is the equivalent fraction of zinc ion in the exchanger.¹³ The dependence of K_N on the exchanger cross-linking and composition is shown in Figure 1.

Ion-exchange reactions between like but unequally charged ions in aqueous solutions of necessity occur at *constant weight normality* rather than at constant ionic strength, μ , as when equally charged ions exchange assuming that water is not taken up or released by the exchanger. Thus, $\mu = 0.1$ in the uptake of microamounts of Zn^{2+} ion from 0.1 N NaNO_3 , while for the exchange reaction microamounts of Na^+ ion in 0.1 N $\text{Zn(NO}_3)_2$, $\mu = 0.15$. Consequently, the activity coefficient ratio, $[\gamma_{\pm}(\text{NaNO}_3)^4 / \gamma_{\pm}(\text{Zn(NO}_3)_2)^3]$, required to correct K_N before performing the integration indicated in eq 3 will vary with $x_{\text{Zn}^{2+}}$ as well as with the relative concentrations of NaNO_3 and $\text{Zn(NO}_3)_2$ in solution. The magnitude of this ratio is such that it may not be neglected. Its numerical value in principle may be determined by extrapolating K_N measured as a function of the ionic strength to infinite dilution under conditions in which the composition and degree of swelling of the exchanger remain unchanged, and attempts to do this have been made.¹⁴ However, practically, it is difficult, if not impossible, to prevent variations in the swelling so that this approach was not attempted. An alternative procedure, recently outlined by Robinson,¹⁵ based on the equation of Guggenheim¹⁶ and of Scatchard¹⁷ and on the Brønsted principle of specific interaction was employed and the

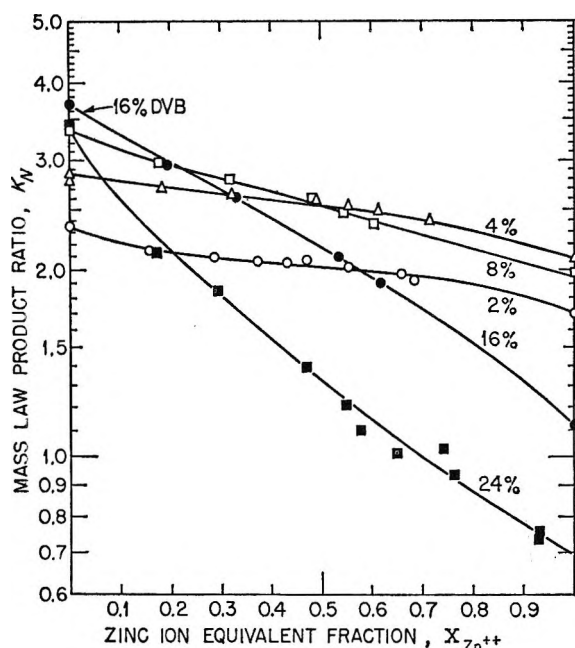


Figure 1. Zinc-sodium ion-exchange equilibrium with variously cross-linked polystyrenesulfonates (data for nominal 12% DVB cross-linked exchanger omitted).

equation for the logarithm of the activity coefficient ratio for the sodium-zinc nitrate aqueous mixture was derived.¹⁸

$$\begin{aligned} \log [\gamma_{\pm}(\text{NaNO}_3)^4 / \gamma_{\pm}(\text{Zn(NO}_3)_2)^3] = \\ 1.0214\sqrt{\mu} / (1 + 1.5\sqrt{\mu}) + \\ Bm_{\text{NaNO}_3} + 2Bm_{\text{Zn(NO}_3)_2} \quad (4) \end{aligned}$$

where $B = 2B_{\text{NaNO}_3} - B_{\text{Zn(NO}_3)_2} = -0.406$. The values $B_{\text{NaNO}_3} = -0.085$ and $B_{\text{Zn(NO}_3)_2} = 0.236$ were obtained with the equations

$$\begin{aligned} \log \gamma_{\pm}^\circ(\text{NaNO}_3) = \\ -0.5107\sqrt{\mu} / (1 + 1.5\sqrt{\mu}) + B_{\text{NaNO}_3} m_{\text{NaNO}_3} \quad (5) \end{aligned}$$

$$\begin{aligned} \log \gamma_{\pm}^\circ(\text{Zn(NO}_3)_2) = -1.0214\sqrt{\mu} / (1 + \\ 1.5\sqrt{\mu}) + (4/3)B_{\text{Zn(NO}_3)_2} m_{\text{Zn(NO}_3)_2} \quad (6) \end{aligned}$$

where $\gamma_{\pm}^\circ(\text{NaNO}_3)$ and $\gamma_{\pm}^\circ(\text{Zn(NO}_3)_2)$ are the activity

(13) It may be shown that eq 3 is identical with eq 17 of G. L. Gaines and H. C. Thomas, *J. Chem. Phys.*, **21**, 714 (1953), assuming that the contribution from the change in water activity accompanying the ion-exchange reaction may be neglected. The validity of this assumption has been discussed by E. Högfeltdt, *Arkiv Kemi*, **5**, 147 (1952).

(14) O. D. Bonner and L. L. Smith, *J. Phys. Chem.*, **61**, 326 (1957).

(15) R. A. Robinson and V. E. Bower, *J. Res. Natl. Bur. Std.*, **A70**, 313 (1966).

(16) E. A. Guggenheim, *Phil. Mag.*, **19**, 588 (1935).

(17) G. Scatchard, *Chem. Rev.*, **19**, 309 (1936).

(18) The authors are indebted to Dr. R. A. Robinson for his assistance in the derivation of eq 4.

coefficients for 0.1 *m* pure NaNO₃ and Zn(NO₃)₂ solutions, respectively. Values for $\gamma_{\pm}(\text{NaNO}_3)^4/\gamma_{\pm}(\text{Zn}(\text{NO}_3)_2)^3$ of 1.508 and 1.620 were computed for decinormal solutions in which the zinc ion fraction in solution was $x_{\text{Zn}^{2+}} = 0.0$ and $x_{\text{Zn}^{2+}} = 1.0$, respectively. The validity of this procedure was checked by activity coefficient measurements¹⁹ made on aqueous NaBr + ZnBr₂ mixtures. A good agreement between the measured and calculated values of $\gamma_{\pm}(\text{NaBr})^4/\gamma_{\pm}(\text{ZnBr}_2)^3$ at an ionic strength of 0.1 was realized.

The integration required by eq 3 was performed graphically after correcting the data in Figure 1 by the appropriate values of the activity coefficient ratio. Alternatively, the method of Freeman²⁰ was employed wherein $\log K_{\text{th}}$ was found by fitting $\log K_N^\circ$ to a polynomial in the equivalent fraction of Zn²⁺ ion in the exchanger

$$\log K_N^\circ = \log K_{\text{th}} + (A_0 - A_1)/2.3RT - [(2A_0 - 6A_1)/2.3RT]x_{\text{Zn}^{2+}} - (6A_1/2.3RT)x_{\text{Zn}^{2+}}^2 \quad (7)$$

Evaluation of the Standard Enthalpy Change, ΔH° . The dependence of the differential heat of exchange, $\Delta\bar{H}$, on $x_{\text{Zn}^{2+}}$ was derived by applying the chord-area technique²¹ to the experimental heats of partial exchange shown in Figure 2. The integral heat of exchange, ΔH , for the reaction in the calorimeter was obtained with the defining relation

$$\Delta H = \int_0^1 \Delta\bar{H} dx_{\text{Zn}^{2+}} \quad (8)$$

Values for the standard enthalpy change, ΔH° , for reaction A were obtained by correcting ΔH by the difference in the heats of dilution per equivalent for NaNO₃ and Zn(NO₃)₂, respectively, at a concentration of 0.1 *N*.

$$\Delta H^\circ = \Delta H + \Delta\phi_L \quad (9)$$

where

$$\Delta\phi_L = \frac{1}{2}\phi_L[\text{Zn}(\text{NO}_3)_2] - \phi_L[\text{NaNO}_3] \quad (10)$$

The value $\phi_L[\text{NaNO}_3] = 31 \text{ cal mole}^{-1}$ was taken from the literature; however, no determinations of the apparent molal heat content of Zn(NO₃)₂ solutions in the concentration range of interest appear to have been reported. Accordingly, heat of dilution measurements were made with 0.05 and 0.10 *m* Zn(NO₃)₂ solutions containing 10⁻³ *m* HNO₃ to repress hydrolysis. A value, $\phi_L[\text{Zn}(\text{NO}_3)_2] = 370 \pm 10 \text{ cal mole}^{-1}$, was measured for *m* = 0.05 from which $\Delta\phi_L = 154 \text{ cal equiv}^{-1}$ was obtained. Interestingly, the magnitude of $\phi_L[\text{Zn}(\text{NO}_3)_2]$ at 0.05 and 0.10 *m* was almost identical with the reported values²² for $\phi_L[\text{Mg}(\text{NO}_3)_2]$ at the same concentrations.

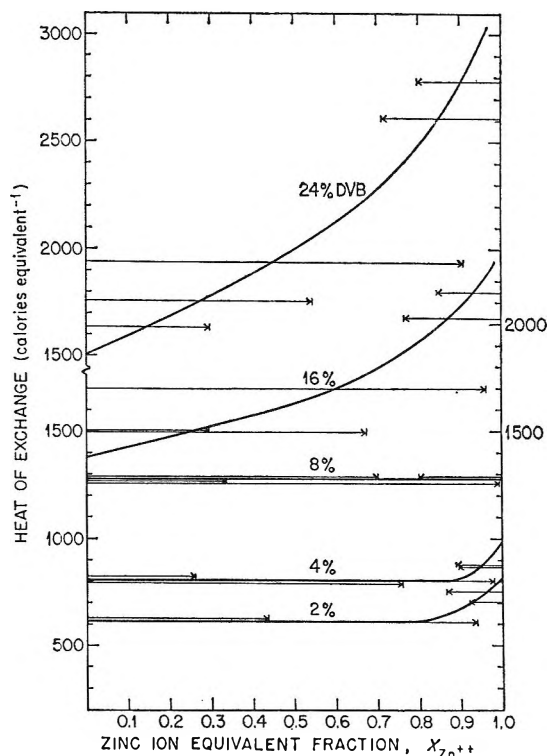


Figure 2. Heats of partial exchange of zinc with sodium ion in variously cross-linked polystyrenesulfonates (arrows indicate direction of ion-exchanger composition change from reaction in calorimeter).

Results and Discussion

The mass law product ratio, K_N , for the zinc-sodium ion-exchange reaction shows a complex dependence on the ionic composition, $x_{\text{Zn}^{2+}}$, and cross-linking of the exchanger (Figure 1). $\log K_N$ for all the exchangers decreased approximately linearly with increasing $x_{\text{Zn}^{2+}}$ and the higher the cross-linking, the larger this dependence became, so that the curves for the 8, 16, and 24% DVB preparations cross those for the 2 and 4% DVB cross-linked exchangers. In the case of the 24% DVB exchanger, K_N became less than unity when $x_{\text{Zn}^{2+}} > 0.7$ and was smaller than for any of the other exchangers when $x_{\text{Zn}^{2+}}$ exceeded 0.2. A maximum in K_N was observed with the 16% DVB preparation when microamounts of zinc ion were exchanged, whereas the 4% DVB exchanger was the most selective for zinc when microquantities of sodium ion were present. Interestingly, the values of K_N for the most highly

(19) S. Lindenbaum and G. E. Boyd, to be submitted for publication.

(20) D. H. Freeman, *J. Chem. Phys.*, **35**, 189 (1961).

(21) T. F. Young and O. G. Vogel, *J. Am. Chem. Soc.*, **54**, 3030 (1932).

(22) Cf. H. S. Harned and B. B. Owen, "The Physical Chemistry of Electrolytic Solutions," 2nd ed, Reinhold Publishing Corp., New York, N. Y., 1950, p 539.

cross-linked exchanger were smaller than those for the 16% DVB preparation over the entire composition range.

The results in Figure 1 differ from those taken in other studies on the $\text{Cu}^{2+}\text{-H}^+$, $\text{Mg}^{2+}\text{-H}^+$, and $\text{Zn}^{2+}\text{-H}^+$ ion-exchange equilibria,^{14,23,24} respectively, which showed a significant increase in K_N when the equivalent fraction of divalent ion in the exchanger exceeded *ca.* 0.85. This same behavior was noted initially in our investigations, but later this was shown to be the consequence of a shifting of the equilibrium caused by washing the exchanger with water after separation from its equilibrium electrolyte mixture and before its analysis. The importance of this effect was recognized by Bonner and Livingston²³ and by Meyer, Argersinger, and Davidson²⁴ but evidently was not avoided successfully in their work.

The heats of exchange of zinc with sodium ions (Figure 2), in contrast to the free energies, behaved more regularly. As the cross-linking increased the exchange reaction became progressively more endothermic. The reaction also became increasingly endothermic with the nominal 16 and 24% DVB exchangers as $x_{\text{Zn}^{2+}}$ increased, while with the 2, 4, and 8% DVB preparations the differential heat of exchange was virtually independent of composition except when $x_{\text{Zn}^{2+}} > 0.85$.

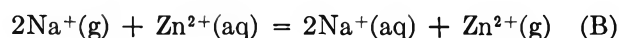
A summary of the estimated values for the standard thermodynamic quantities is given in Table II where it may be observed that $-\Delta G^\circ$ increases with cross-linking, passes through a broad maximum, and then decreases when the nominal DVB content of 8% is exceeded. Further, in all cases the selective uptake of Zn^{2+} ion was determined by the relatively large standard entropy increase accompanying its exchange with sodium ion. The value of ΔS° was surprisingly large for the most highly cross-linked exchanger (*i.e.*, +8.3 eu) and approached that typical of the increase in entropy on the release of water by crystalline hydrates²⁵ (*i.e.*, *ca.* 9.4 eu), suggesting that an extensive dehydration of zinc ion must occur when it enters the exchanger. It is to be remembered, however, that the observed ΔS° represents the net change in the standard entropy and that it also contains an important negative contribution from the increased hydration of Na^+ ion when the latter is displaced from the exchanger and enters the external aqueous phase. Smaller contributions to the net ΔS° arise as a consequence of the change in swelling when the exchanger is transformed from the sodium to the zinc form according to reaction A and because of the increased configurational entropy when two singly charged ions are replaced by one doubly charged ion. As Cruickshank and Meares have pointed out,⁵ if the $N/2$ doubly charged ions in one equivalent

of exchanger are randomly distributed over N sites, the increase in entropy per equivalent will be *ca.* 1.4 eu. The change in the configurational entropy in the cross-linked molecular network of the exchanger on swelling or deswelling will be much smaller. It therefore may be concluded that the ΔS° of exchange is largely determined by the difference in the entropies of hydration of the exchanging ions. Generally, the hydration en-

Table II: Standard Heats, Free Energies, and Entropies of Exchange at 298.2°K of Zinc with Sodium Ion in Various Cross-Linked Polystyrenesulfonates

Nominal cross-linking, % DVB	$-\Delta G^\circ$, cal equiv ⁻¹	ΔH° , cal equiv ⁻¹	ΔS° , cal deg ⁻¹ equiv ⁻¹
2	340	785	3.8
4	405	970	4.6
8	405	1430	6.2
12	400
16	365	1855	7.4
24	225	2255	8.3

tropies for divalent cations are much more negative than for univalent cations so that ΔS° usually will be positive. This generalization is supported by a comparison of the reaction between zinc and sodium ions in an ion exchanger with the hypothetical exchange reaction



for which $\Delta S^\circ = 29$ eu.²⁶ However, even in the most highly cross-linked exchanger employed in this research, sodium and zinc ions were far from being completely dehydrated (*cf.* Table I). Thus, while a positive ΔS° might be expected, its magnitude should be far less than for reaction B.

The endothermic character of the $\text{Zn}^{2+}\text{-Na}^+$ ion-exchange reaction appears to derive from the strongly exothermic heats of hydration of divalent cations relative to univalent cations. A large amount of heat must be absorbed to remove zinc ion from solution and this is only partially compensated by the heat evolved when two sodium ions enter the aqueous phase. The

(23) O. D. Bonner and F. L. Livingston, *J. Phys. Chem.*, **60**, 530 (1956).

(24) N. J. Meyer, W. J. Argersinger, and A. W. Davidson, *J. Am. Chem. Soc.*, **79**, 1024 (1957).

(25) W. M. Latimer, "Oxidation Potentials," Prentice-Hall, Englewood Cliffs, N. J., 1952, p 364.

(26) Entropy values at 298.2°K for anhydrous sodium and zinc polystyrenesulfonates do not appear to have been determined. Comparisons with the reaction between $\text{Na}^+(\text{aq})$ and $\text{Zn}^{2+}(\text{aq})$ and these salts would be more meaningful than with reaction B.

sign of the heat of exchange may be predicted from the thermal properties of aqueous uni-univalent and divalent electrolyte solutions. For example, the integral heat of exchange, ΔH (eq 8), may be approximated²⁷ by the difference in the apparent molal heat contents, $\phi_L(m_i)$ and $\phi_L(m_t)$, of the sodium and zinc salts, respectively, of *p*-ethylbenzenesulfonate, which is the "model compound" for polystyrenesulfonate cation exchangers

$$\Delta H = \phi_L(m_t) - \phi_L(m_i) \quad (11)$$

The concentrations m_i and m_t to be employed in eq 11 must be estimated from the equivalent water contents of the homoionic, cross-linked exchangers (Table I). Measurements of ϕ_L for divalent salts of *p*-ethylbenzenesulfonic acid have not been reported; therefore, heat of dilution data ($\phi_L \equiv -\Delta H_D$) for sodium²⁸ and zinc nitrate²⁹ were utilized. Heat is evolved on dilution of aqueous $\text{Zn}(\text{NO}_3)_2$ solutions to infinite dilution over the entire concentration range up to 30 *m*, while, in contrast, heat is absorbed on dilution of NaNO_3 solutions more concentrated than 0.2 *m*. Thus, ΔH must be positive (*cf.* eq 11) and will have the same sign as the observed heat of exchange of zinc for sodium ion. Comparisons of the ϕ_L values for magnesium, calcium, and barium nitrates with those for KNO_3 solutions indicate that the exchange of these divalent cations for K^+ ion also will be endothermic in agreement with experiment;^{3,4} comparisons of ϕ_L values for strontium and barium nitrates with those for HNO_3 indicate that the $\text{Sr}^{2+}-\text{H}^+$ and $\text{Ba}^{2+}-\text{H}^+$ exchange reactions will be exothermic in agreement with reports.^{5,8}

The relative magnitudes of the standard free energies of hydration of sodium and zinc ions³⁰ are such that a strongly positive ΔG° of ion exchange might be expected (*i.e.*, Na^+ preferred over Zn^{2+} ion) if these cations were completely dehydrated on entering the exchanger. However, the exchangers investigated in this research exhibited a small, negative ΔG° , so that a different

balance must have occurred between the net enthalpy change (to partially dehydrate Zn^{2+} ion and to fully hydrate two Na^+ ions) and the net gain in entropy for the same process. The water contents of the sodium and zinc forms of the exchangers were such (Table I) that these ions *on the average* retained their primary hydration shells. Accordingly, the magnitudes of the observed ΔH° and ΔS° must have been determined by enthalpy and entropy effects associated with their secondary hydration shells and it may be concluded that the gain in entropy on removing this water was sufficient to overcome the necessary enthalpy increase.

The maximum observed in the dependence of ΔG° (and K_N) on cross-linking appears to be novel, suggesting that the net enthalpy change increases more rapidly than the net entropy as the secondary hydration layer of Zn^{2+} ion is removed and that of Na^+ ion is completed. The trend of ΔG° with cross-linking is such that for very high DVB contents sodium would be preferred to zinc ion over the entire composition range. The dependence of the zinc ion selectivity on cross-linking also should be reflected in the concentration dependence of the mean molal activity coefficients for the zinc and sodium polystyrenesulfonates and possibly for other salts of these cations with anions similar to the sulfonate group. It therefore is relevant to note that γ_{\pm} for NaNO_3 solutions above 1 *M* is less than and becomes progressively smaller at higher concentrations than the activity coefficient for $\text{Zn}(\text{NO}_3)_2$. Hence, the ratio $f_{\text{Zn}^{2+}}/f_{\text{Na}^+}^2$ in eq 1 would be expected to increase with concentration (*i.e.*, cross-linking) thereby requiring K_N to decrease as is observed.

(27) G. E. Boyd, J. W. Chase, and F. Vaslow, *J. Phys. Chem.*, **71**, 573 (1967).

(28) V. B. Parker, "Thermal Properties of Aqueous Uni-univalent Electrolytes," National Standard Reference Data Series, National Bureau of Standards, NSRDS-NBS2, Washington, D. C., 1965.

(29) W. W. Ewing, J. D. Bradner, and W. R. F. Guyer, *J. Am. Chem. Soc.*, **61**, 260 (1939).

(30) W. M. Latimer, *J. Chem. Phys.*, **23**, 90 (1955).

Radiolysis of Liquid Hexafluoroethane

by A. Sokolowska and Larry Kevan

Department of Chemistry, University of Kansas, Lawrence, Kansas 66044 (Received December 20, 1966)

The γ radiolysis of liquid C_2F_6 at -78° was studied. The 100-ev product yields (G) are CF_4 (1.72), C_3F_8 (0.87), and $n-C_4F_{10}$ (0.45). With O_2 added as a radical scavenger, the yields are 0.97, 0.0, and 0.0, respectively. From these results $G(CF_3) = G(C_2F_5) = 2.5$. The CF_3/C_2F_5 ratio differs from that found by epr by which only CF_3 was observed.

A comparison of the radiation chemistry of perfluoroalkanes with alkanes is especially significant because of the large C-F bond strength. In alkane radiation chemistry in gas, liquid, and solid phases dimer is a major product. It is therefore clear that C-H bond breaks predominate over C-C bond breaks even though the C-H bond strength exceeds that of C-C by some 20 kcal. In gas phase perfluoroalkane radiolysis dimer is a minor product and the frequency of C-C bond break is equal to or greater than that of C-F bond break.^{1,2} The C-F bond strength is about 35 kcal greater than the C-C bond strength; this magnitude seems to be required to cause the shift in behavior described above.

Here we report results on the liquid phase radiolysis of C_2F_6 which allow us to extend the comparison with alkanes from the gas to liquid phase. From the final reaction products certain radical yields are deduced. These are of particular interest since a recent epr study of liquid C_2F_6 under steady-state radiolytic conditions showed that CF_3 was the only radical present at high dose.³

Experimental Section

C_2F_6 was from Air Products, Inc., and contained <0.02 mole % CF_3Cl as impurity; it was rigorously degassed before using. O_2 was also from Air Products and was used as received. Samples were prepared by condensing C_2F_6 or $C_2F_6 + O_2$ into 3.5-cm Pyrex capillary ampoules of 2-mm i.d. and 7-mm o.d. Irradiations were carried out with Co^{60} γ rays at -78° in a Dry Ice-acetone bath. The dose rate was 0.6 Mrad/hr to H_2O at 35° as measured by ferrous sulfate dosimetry. The dose to C_2F_6 was calculated from its total mass-energy absorption coefficient relative to that for H_2O . Analysis was by gas chromatography

with thermal conductivity detection on a 2-m silica gel column at 80° .

Results

The product yields were carefully examined as a function of dose from 1 to 7 Mrads both in the absence and in the presence of oxygen. Results are shown in Figure 1. In this dose range the yields are linear and show no evidence of secondary reactions. Table I gives the G values found with their average deviations for ten samples.

In addition to the products reported, a small gas chromatographic peak appears shortly after C_3F_8 . This peak is known from previous work² to be C_2F_5Cl which arises from <0.02 mole % CF_3Cl impurity in the original C_2F_6 . The area of this peak is about 5% of the C_3F_8 peak area and it represents less than 2% of the total products. This impurity product is ignored in the following discussion; its magnitude is sufficiently small not to affect our conclusions or calculations with respect to the liquid phase.

In the oxygen-containing samples the exact oxygen concentration in the liquid C_2F_6 is unknown. By using different nominal oxygen concentrations it was found that a nominal 10% O_2 gas phase concentration was sufficient to scavenge all scavengeable thermal radicals at doses up to 3 Mrads. Above this dose small scavengeable C_3F_8 yields were observed in the nominal 10% O_2 mixtures. The actual liquid phase O_2 concentration is estimated to be about 1%.

In the oxygen-scavenged systems several new gas chromatographic peaks were seen. These new peaks

(1) L. Kevan and P. Hamlet, *J. Chem. Phys.*, **42**, 2255 (1965).

(2) L. Kevan, *ibid.*, **44**, 683 (1966).

(3) R. W. Fessenden and R. H. Schuler, *ibid.*, **43**, 2704 (1965).

Table I: Product Yields per 100 ev (*G*) in C₂F₆ Radiolysis

Conditions	<i>G</i> (CF ₄)	<i>G</i> (C ₃ F ₈)	<i>G</i> (<i>n</i> -C ₄ F ₁₀)	F/C	<i>G</i> (-C ₂ F ₆)
C ₂ F ₆ liquid, -78°	1.72 ± 0.10	0.87 ± 0.05	0.45 ± 0.02	3.0	3.0
C ₂ F ₆ liquid, -78° + nominal 10% O ₂	0.97 ± 0.06	0.0	0.0	...	~3
C ₂ F ₆ gas, ^a 2 atm, 40°	2.5	0.45	0.20	3.3	2.4
C ₂ F ₆ gas, ^a 2 atm, 40°, + 1% O ₂	1.3	0.0	0.0

^a Reference 2, ±10%; these values supersede those in ref 1.

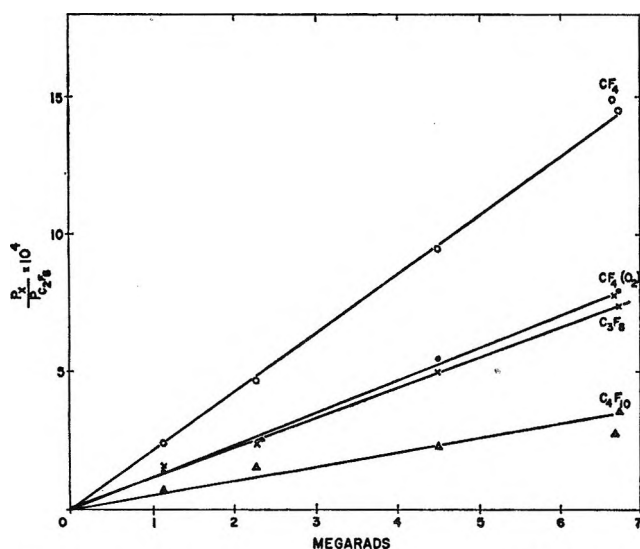


Figure 1. Yield-dose curves for liquid C₂F₆ γ radiolysis at -78°.

were not definitely identified, but on the basis of retention times they are thought to represent CO₂, CF₃OCF₃, C₂F₆OCF₃, and perhaps another oxygen-containing product. No analysis was made for O₃. The oxygen products were not analyzed quantitatively.

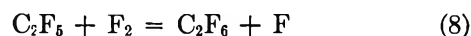
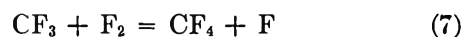
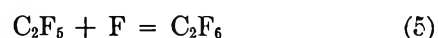
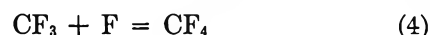
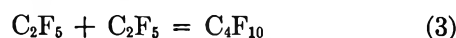
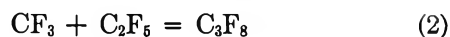
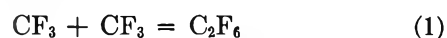
The F/C material balance calculated from liquid C₂F₆ radiolysis products is 3.00. This is excellent material balance and implies that no major products are unobserved. The good material balance and trace amounts of CO₂ observed show that wall reactions with Pyrex are unimportant in the liquid phase at -78°. This contrasts with gas phase studies in which Pyrex vessels were prohibited owing to wall reactions.

Discussion

Radical Reactions. Oxygen can react in the radiolysis system in at least three ways: as a thermal radical scavenger, as an electron trap, and as a charge-transfer receptor from the parent ion. Charge transfer could serve to protect C₂F₆ against decomposition, but at the oxygen concentrations used it would only be of minor importance. It is also roughly estimated from the

oxygen products that the total C₂F₆ decomposition in the O₂-scavenged system is about the same as in the absence of O₂. If O₂⁻ is formed it would probably provide the major neutralization reaction for positive ions. It would not necessarily interfere with any ion molecule reactions that may occur. The neutralized ions would be scavenged as radicals by O₂; if neutralization was by electrons rather than by O₂⁻ the same net effect would result. Therefore, we need only consider oxygen as a thermal free-radical scavenger. The oxygen-scavenging results then indicate that 100% of C₃F₈, 100% of C₄F₁₀, and 44% of CF₄ arise from thermal radical reactions.

The free-radical reactions are given by reactions 1-8.



Fluorocarbon radicals do not disproportionate⁴ and they readily react with F₂. No F₂ has been indicated or detected as a stable product in these or previous fluorocarbon radiolyses; it is presumably removed *via* reactions 7 and 8. F atoms do not abstract fluorine from fluorocarbons because of the high C-F and low F-F bond strengths. Reaction 1 has zero activation energy in the gas phase⁵ and seems to be diffusion controlled in the liquid phase at -95°.³ Reactions 2-6

(4) G. O. Pritchard, G. H. Miller, and J. R. Dacey, *Can. J. Chem.*, **39**, 1968 (1961).

(5) R. D. Gilles and E. Whittle, *Trans. Faraday Soc.*, **61**, 1425 (1965); earlier results of G. O. Pritchard and J. R. Dacey, *Can. J. Chem.*, **38**, 182 (1960), report a 2-kcal activation energy, but this now seems much too high.

should be similar to reaction 1. Reactions 7 and 8 may be expected to involve a small activation energy greater than the activation energy of diffusion, but the most recent results on reactions of CF_3 with halogens imply that reactions 7 and 8 may have zero activation energy in the gas phase.⁶

Perfluoro as well as alkyl radical pairs have combination-cross-combination ratios that are statistical.⁷

Thermal Radical Yields. If C_3F_8 and C_4F_{10} are formed entirely by reactions 2 and 3, one calculates on the basis of statistical combination that the $\text{CF}_3/\text{C}_2\text{F}_5$ ratio is 1.0. $G(\text{C}_2\text{F}_5)$ that contributes to C_3F_8 and C_4F_{10} equals 1.77 so $G(\text{CF}_3)$ that contributes to C_3F_8 and C_4F_{10} is likewise 1.77. In addition, one must consider reactions 4 and 5 as well as 7 and 8. We make the reasonable assumption that $k_4 = k_5$ and that $k_7 = k_8$. Then the scavengeable CF_4 yield (0.75) is a measure of the CF_3 radicals undergoing reaction 4 and/or 7. The total radical yields then become

$$G(\text{CF}_3) = 2.5$$

$$G(\text{C}_2\text{F}_5) = 2.5$$

From the yields of reactions 4 + 7 and 5 + 8 we calculate that $G(\text{F}) + G(\text{F}_2) = 1.5$. By material balance we find $G(\text{F}) = 0.5$ and $G(\text{F}_2) = 1.0$.

The radiation chemical result of $(\text{CF}_3)/(\text{C}_2\text{F}_5) = 1$ differs from the epr result³ of $(\text{CF}_3)/(\text{C}_2\text{F}_5) \gg 1$. The epr radiolysis conditions differ in that observation is made at a relatively high dose. Thus, a higher concentration of F_2 may exist; however, it is not now apparent how this fact can reconcile the epr and product analysis results.

Gas vs. Liquid Product Yields. Gas phase product

yields are also shown in Table I. From the C_3F_8 and C_4F_{10} yields one calculates that $(\text{CF}_3)/(\text{C}_2\text{F}_5) = 1$. The gas and liquid phase ratios are similar and show that C-C and C-F bond break are about equally probable in both phases. C-C bond break is much more likely in perfluoroalkanes than in alkanes in both phases. The scavengeable CF_4 yield is 65% larger in the gas than in the liquid (1.2 vs. 0.75) while the C_3F_8 and C_4F_{10} yields are smaller in the gas. This difference could be explained by a small activation energy for reactions 7 and 8 and/or by a lower rate for reaction 6 in the gas phase due to third-body stabilization requirements.

In alkanes the total radiation decomposition yield is greater in gas (30°) than in liquid (-78°) by 30-40%.⁸ In contrast, in C_2F_6 the total decomposition seems to be slightly larger in liquid than in gas. Since material balance is not too good in the gas and deviates so as to underestimate $G(-\text{C}_2\text{F}_6)$ we believe that $G(-\text{C}_2\text{F}_6)$ is the same in the 40° gas and the -78° liquid. More study at several temperatures is needed to verify this tentative conclusion.

Acknowledgment. This research was generously supported by the U. S. Atomic Energy Commission under Contract AT(11-1)1528 and by the Petroleum Research Fund administered by the American Chemical Society. This is AEC Document No. COO-1528-9.

(6) J. C. Amphlett and E. Whittle, *Trans. Faraday Soc.*, **62**, 1662 (1966).

(7) J. A. Kerr and A. F. Trotman-Dickenson, *Progr. Reaction Kinetics*, **1**, 100 (1961); later references quoted in W. G. Alcock and E. Whittle, *Trans. Faraday Soc.*, **62**, 128 (1966).

(8) For C_2H_6 , see H. A. Gillis, *J. Phys. Chem.*, **67**, 1399 (1963); K. Yang and P. L. Gant, *ibid.*, **65**, 1861 (1961).

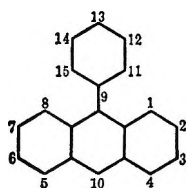
Electron Spin Resonance Spectra of 9-Phenylanthracene and 9,10-Diphenylanthracene Anion Radicals

by L. O. Wheeler, K. S. V. Santhanam, and Allen J. Bard¹

Department of Chemistry, The University of Texas, Austin, Texas 78712 (Received December 20, 1966)

The electron spin resonance (esr) spectra of 9-phenylanthracene and 9,10-diphenylanthracene anion radicals prepared by electroreduction in *N,N*-dimethylformamide and potassium metal reduction in dimethoxyethane are given. The assigned experimental coupling constants are shown to be in good agreement with those calculated using molecular orbital theory. A brief study of how different factors in radical ion preparation affect esr spectrum resolution is described.

In a previous paper² we reported a study of the esr spectrum of 9,10-diphenylanthracene (DPA) anion radical. An assignment for the coupling constants for this radical was presented and this assignment was shown to be consistent with a molecular orbital calculation for a certain angle between the phenyl rings and the anthracene nucleus. The study of the esr spectrum of 9-phenylanthracene (PA) anion radical reported here was undertaken to test whether the



calculated angle in DPA and its spectrum assignment was consistent with that for PA. The esr spectrum of PA is more difficult to interpret than that of DPA because exchange of the phenyl ring in the 10 position for a hydrogen makes the 1 and 4 and the 2 and 3 hydrogens no longer equivalent. This additional complexity required a more highly resolved spectrum to obtain a satisfactory interpretation. A study was therefore undertaken to examine how different methods of radical preparation affected the resolution in esr spectra. In the course of this study a more highly resolved spectrum of DPA anion radical was obtained and the improved assignment of coupling constants for this radical is also given.

Results and Discussion

Resolution of Spectra. Of the two principal methods of producing aromatic hydrocarbon anion radicals, alkali metal reduction and electrochemical reduction, the former method has been used in all but a few cases. There are two different techniques using electrochemical reduction: generation of the radical at an electrode inside the cavity (the *intra muros* technique)³ and external generation with some form of transfer to an esr cell.^{4,5} The advantages and disadvantages of both of these methods have been reviewed by Adams.⁶

A comparison of the alkali metal and electrochemical generation methods of anion radical production involves the use of different solvents and counterions. It has been shown that both solvent and counterion affect resolution and coupling constants in an esr spectrum.⁷⁻⁹

(1) To whom all correspondence and requests for reprints should be directed.

(2) L. O. Wheeler, K. S. V. Santhanam, and A. J. Bard, *J. Phys. Chem.*, **70**, 404 (1966).

(3) D. H. Geske and A. H. Maki, *J. Am. Chem. Soc.*, **82**, 2671 (1960).

(4) J. R. Bolton and G. K. Fraenkel, *J. Chem. Phys.*, **40**, 3307 (1964).

(5) K. S. V. Santhanam and A. J. Bard, *J. Am. Chem. Soc.*, **88**, 2669 (1966).

(6) R. N. Adams, *J. Electroanal. Chem.*, **8**, 151 (1964).

(7) J. Gendell, J. H. Freed, and G. K. Fraenkel, *J. Chem. Phys.*, **37**, 2832 (1962).

(8) P. Ludwig, T. Layloff, and R. N. Adams, *J. Am. Chem. Soc.*, **86**, 4568 (1964).

(9) A. H. Reddoch, *J. Chem. Phys.*, **43**, 225 (1965).

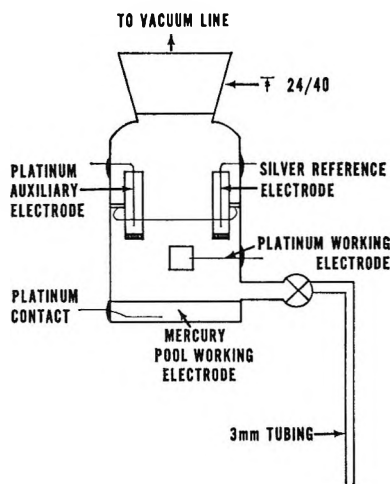


Figure 1. Vacuum cell for controlled-potential electrolysis.

In an attempt to determine the conditions which yield optimum resolution, experiments were performed varying solvent, counterion, and temperature. The solvents were dimethylformamide (DMF), acetonitrile (ACN), and dimethoxyethane (DME); the counterions were potassium and the tetra-*n*-butylammonium cation. The temperature was varied from -80° to room temperature.

A new electrolytic cell was designed in which oxidations and reductions could be carried out and solution transfer to 3-mm tubing made under an inert atmosphere (see Figure 1). This is very important because the anion radicals react with traces of oxygen and other substances. This cell is simpler and more convenient than the one previously described.⁵ We at first thought that the flat Varian aqueous solution sample cell would have to be employed in studies involving DMF as a solvent to avoid difficulties in tuning the esr spectrometer. The use of this cell is inconvenient because it is not vacuum tight and it does not fit into the variable-temperature apparatus dewar flask. We found, however, that the esr spectrometer could be tuned with some difficulty, using 3-mm tubing containing DMF.

The apparatus used for alkali metal reductions¹⁰ (Figure 2) differs from the one usually employed.¹¹ The five side arms make it possible to observe the resolution of the spectrum as a function of the concentration of the radical in a single experiment by allowing the reaction to proceed to different extents in the reaction bulb and transferring the solution to the esr side-arm tubes at various times. Actually two factors that affect resolution are changed simultaneously in this kind of experiment—the concentration of the radical and the rate of electron exchange between parent com-

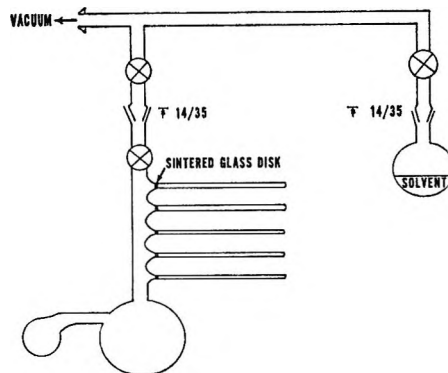


Figure 2. Vacuum apparatus for alkali metal reduction.

pound and radical. However, this latter effect is probably negligible at the temperatures employed, -60 to -80° . The frits filter the potassium metal from the solution and thus prevent the reaction from continuing in the esr sample tube.

The effect of different factors on resolution was examined by observing the spectrum of DPA anion radical prepared by different methods. The spectrum for DPA anion radical prepared by internal generation has been described by Sioda and Koski,¹² who observed a rather poorly resolved 13-line spectrum. We have found similar lack of resolution in several studies using a room-temperature *intra muros* technique. Somewhat better resolution is obtained when exhaustive external electrochemical reduction is used and the spectrum examined in a flat sample cell at room temperature.² Even higher resolution is obtained when the radical is prepared by exhaustive external controlled-potential electrolysis in DMF under vacuum and examined at -50° (Figure 3 (top)) and when it is obtained by potassium reduction in DME and examined at -80° (Figure 3 (bottom)).

In this study we found that the resolution improves according to the following sequence: the *intra muros* generation technique at room temperature yields the poorest resolution followed by exhaustive external controlled-potential electrolytic generation examined at room temperature and external electrolytic generation examined at -50° . Potassium metal reduction examined at -80° produces the most highly resolved spectrum. The reason external electrolytic generation gives a better spectrum than that obtained with internal generation at room temperature is probably

(10) This apparatus was designed with the cooperation of N. L. Bauld and co-workers.

(11) D. E. Paul, D. Lipkin, and S. I. Weissman, *J. Am. Chem. Soc.*, **78**, 116 (1956).

(12) R. E. Sioda and W. S. Koski, *ibid.*, **87**, 5573 (1965).

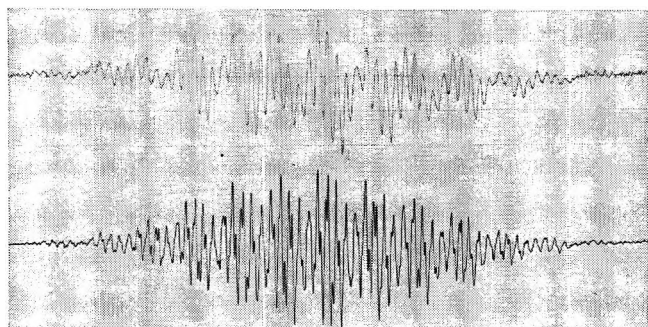


Figure 3. Top: derivative esr spectrum of DPA anion radical produced by electroreduction of $10^{-3} M$ DPA solution containing $0.1 M$ tetra-*n*-butylammonium iodide in DMF. Temperature, -50° . Bottom: derivative esr spectrum of DPA anion radical produced by potassium reduction in DME. Temperature, -80° .

because the exchange rate between parent compound and radical¹³ is much lower in the external case. It is very difficult to achieve quantitative conversion of parent to radical using the internal generation technique. The difference between electrolytic generation and potassium reduction at low temperatures is probably caused by differences in solvent and counterions. We conclude that in the case of hydrocarbon anion radicals optimum resolution is achieved by alkali metal reduction and observation of the spectra at low temperatures. The anion radicals of benzene, naphthalene, anthracene, and biphenyl produced by alkali metal reduction have been examined. The optimum resolution was achieved by examination of their esr spectra at -60° or lower, which would appear to further verify this conclusion, although we have not prepared these anion radicals by electrolytic methods. It is not possible from our data to state whether the increased resolution is caused by the change in solvent or counterion or both.

DPA Anion Radical. The improved resolution in the spectrum of DPA anion radical when prepared by potassium metal reduction (Figure 3 (bottom)) allows the following assignment of coupling constants (in gauss): $a_H(1, 4, 5, 8) = 2.60$, $a_H(2, 3, 6, 7) = 1.47$, $a_H(p) = 0.30$, and $a_H(o) = 0.24$. These values are slightly different from those previously reported² and separate coupling constants of the *o*- and *p*-hydrogens of the phenyl rings are observed. The calculated angle between the phenyl rings and the anthracene nucleus, θ (68°), is unaltered.

PA Anion Radical. The esr spectrum of PA has been reported by Fu, Sheng, and P'an.¹⁴ Their spectrum was very poorly resolved and consisted of 17 major lines with a very slight indication of further splitting. They postulated the following coupling con-

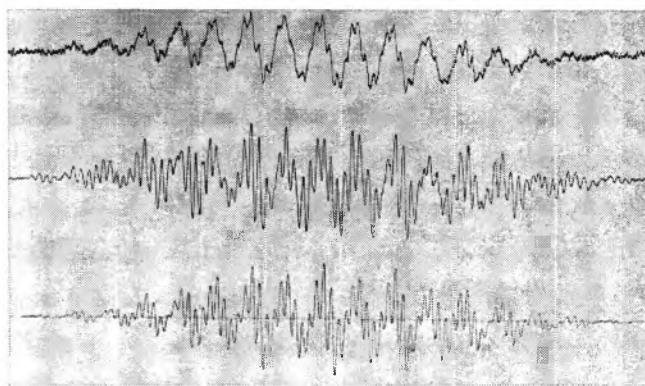


Figure 4. Top: derivative esr spectrum of PA anion radical produced by electroreduction of $10^{-3} M$ PA solution containing $0.1 M$ tetra-*n*-butylammonium iodide in DMF. Temperature, 25° . Middle: derivative esr spectrum of PA anion radical produced by potassium metal reduction in DME. Temperature, -80° . Bottom: calculated spectrum using constants in last column of Table I with a line width of 0.12 gauss.

stants (in gauss): $a_H(10) = 5.36$, $a_H(1, 4, 5, 8, 13) = 2.68$, $a_H(11, 15) = 1.34$, and $a_H(2, 3, 6, 7) = 0.27$.

The spectrum of PA anion radical obtained by exhaustive, external controlled-potential electrolysis and examined at room temperature is shown in Figure 4 (top), while that obtained by potassium metal reduction and examined at -80° is shown in Figure 4 (middle). A theoretically computed spectrum using the coupling constants in the last column of Table I

Table I: Experimental and Theoretical Coupling Constants for the Anion Radical of 9-Phenylanthracene

Carbon atom	Spin density		a_H , gauss		Experimental
	Hückel ^a	McLachlan ^b	Theory ^c	Theory ^d	
1	0.091	0.110	2.83	2.54	2.52 ^e
2	0.048	0.034	0.91	1.34	1.66 ^e
3	0.045	0.027	0.72	1.26	1.34 ^e
4	0.093	0.117	3.00	2.60	2.76 ^e
10	0.193	0.263	6.28	5.40	5.60
11	0.009	0.012	0.32	0.25	0.28
12	0.000	-0.004	0.11	0.00	
13	0.010	0.014	0.38	0.28	0.28

^a Calculated using $\theta = 68^{\circ}$. ^b Calculated using $\theta = 68^{\circ}$ and $\lambda = 1.2$. ^c Calculated using the Colpa-Bolton equation where $Q = 27$ and $K = 12$ and using the McLachlan spin density. ^d Calculated using the McConnell equation where $Q = 28$ and using the HMO spin density. ^e Assigned to this position on the basis of analogy with HMO theory.

(13) R. L. Ward and S. I. Weissman, *J. Am. Chem. Soc.*, **79**, 2086 (1957).

(14) K-H. Fu, H-Y. Sheng, and C-L. P'an, *K'o Hsueh T'ung Pao*, **540** (1956).

and assuming 100% Lorentzian line shape is shown in Figure 4 (bottom). Using the internal generation technique, a spectrum of PA anion radical in DMF was obtained which was comparable in resolution to that obtained by external controlled-potential electrolysis. When the internal generation technique was tried using ACN as a solvent, the esr spectrum of anthraquinone anion radical was obtained. This same type of reaction has been observed with anthracene anion radical. Studies are currently in progress to determine the mechanism of this reaction.

Molecular Orbital Calculations. It has been shown that the resonance integral, β , for the bond between the phenyl ring and the anthracene nucleus can be represented by $\beta = \beta_0 \cos \theta$ where β_0 is the resonance integral for a carbon-carbon bond in a planar system.¹⁵ β_0 is defined for a bond length of 1.397 Å. Streitwieser¹⁶ has described procedures that can be used to correct for deviations from this standard bond length, but they have a negligible effect on the calculated value of θ , if θ is greater than 60°. Simple Hückel molecular orbital¹⁶ and McLachlan¹⁷ calculations were made for PA assuming values of θ between 0 and 90°. A plot of the spin density, ρ , as a function of θ based on HMO calculation is given in Figure 5.

From an examination of the spectrum of PA anion radical, a quartet of splitting 0.28 gauss is evident in the extreme wing lines. This splitting can only be attributed to the *o*- and *p*-hydrogens on the phenyl substituent. From this fact and from Figure 5, a value of $\theta = 68^\circ$ is found. After complete determination of all the coupling constants, it is seen that the predicted values from simple HMO theory are in very good agreement with the experimental values. The value of θ is also in good agreement with those previously reported for this type of compound.^{2,18} It has not been possible despite repeated attempts to observe separate coupling constants for the *o*- and *p*-protons of PA anion radicals. It can be seen that our assignment differs from that given by Fu, *et al.*,¹⁴ which they made on the basis of a very poorly resolved spectrum. We have found that their coupling constants and the line widths found in this study give a poor reproduction of our spectra. This illustrates an important point seldom mentioned in esr literature. The ability of a given set of coupling constants to reproduce a spectrum does not guarantee that they are the correct assignment. This point becomes particularly important in the case of poor resolution.

Experimental Section

DPA and PA were obtained from Aldrich Chemical Co. DPA was used as received since its high purity

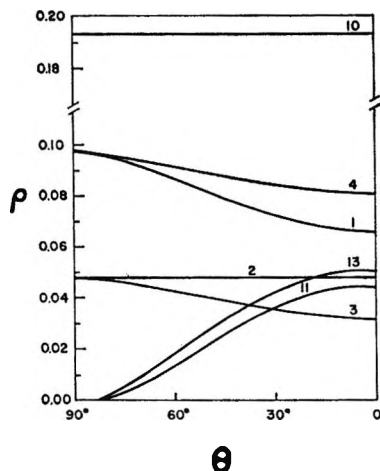


Figure 5. Variation of the spin density (ρ) as a function of the angle between the phenyl ring and the anthracene nucleus (θ) as calculated by HMO theory. The numbers represent the appropriate carbon atom.

was established by electrochemical studies⁵ and melting point. PA was purified by vacuum sublimation with the purest component being taken from the first sublimation and subjected to a second purification. Its purity was then established by polarography and melting point. DME obtained from Ansol Co. was dehydrated by the addition of calcium hydride and lithium aluminum hydride, refluxed for 16 hr over lithium aluminum hydride, and vacuum distilled. The method of purification of the DMF has been described previously.⁵

Preparation of the radical by reduction with potassium was as follows. The potassium was stored under mineral oil and prior to use it was washed with purified solvent before being cut and placed in the reaction vessel (Figure 2). The hydrocarbon was placed in a capillary tube and put in the reaction vessel along with a stirrer. The system was evacuated and the potassium metal was distilled from the side bulb into the main flask to form a mirror. The solvent was then distilled over by cooling the reaction flask with liquid nitrogen. By activating the stirrer the capillary tube was broken and the speed of the reaction between potassium and hydrocarbon was controlled by adjusting the temperature.

External electrolysis was carried out in the cell shown in Figure 1. This cell has the advantage of not requiring separate inlets for auxiliary and reference

(15) H. Preuss, *Z. Naturforsch.*, **12a**, 603 (1957).

(16) A. Streitwieser, Jr., "Molecular Orbital Theory for Organic Chemists," John Wiley and Sons, Inc., New York, N. Y., 1961.

(17) A. D. McLachlan, *Mol. Phys.*, **3**, 233 (1960).

(18) F. Tonnard and S. Odier, *J. Chim. Phys.*, **63**, 227 (1966).

electrode. The cell was attached to the vacuum line and the sample tube and vacuum stopcock were evacuated. The stopcock was then closed and the cell removed from the vacuum line. Mercury was added first and then a solution containing the hydrocarbon and the supporting electrolyte. The cell was reattached to the vacuum line and again evacuated. After electrolysis the cell was brought to atmospheric pressure by bleeding in helium. The stopcock was then opened only to the bulb portion of the vacuum stopcock and a few milliliters of solution was drained. Then the stopcock was opened to the sample cell. The solution was frozen in the tube while the tube was removed with a torch. Transfer was then made to the spectrometer.

A Varian Associates V-4502 spectrometer employing 100-kc field modulation was used. A Varian V-153c klystron (output 300 mw) was used.

The HMO and McLachlan calculations were done

on a Control Data Corp. 6600 computer. The theoretical simulated spectra were calculated on the CDC 1604 computer and were then plotted on the CDC 160 plotter.

The field sweep was calibrated by using Frey's salt in one side of a V-4532 dual sample cavity and the low-field splitting of this spectrum was taken to be 13.0 gauss. The spectra were recorded on a Moseley 7100B dual channel recorder.

Acknowledgment. The support of this research by the Robert A. Welch and the National Science Foundation (Grant No. GP-1921) is gratefully acknowledged. The esr instrument was purchased with funds provided by the National Science Foundation (Grant No. GP-2090). We are grateful to Tzeng-Ming Chen for translation of the paper by Kuei-Hsiang Fu, *et al.*, and to John Phelps for his assistance in the purification of DME.

Nuclear Magnetic Resonance Spectra of Alkylenebisamides and Alkylenebiscarbamates

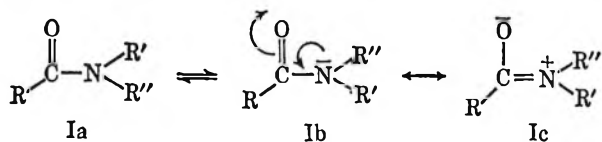
by Robert H. Barker, Sidney L. Vail, and Gordon J. Boudreaux

Southern Regional Research Laboratory,¹ New Orleans, Louisiana 70119 (Received December 22, 1966)

The nuclear magnetic resonance spectra of selected alkylenebisamides and biscarbamates have been studied as a function of solvent and temperature. Intramolecular hydrogen bonding was found to be important in determining the relative conformational stabilities of methylenebisformamide but was relatively unimportant in the other compounds studied. The rotational forms of the two amide groups have been shown to be interdependent in methylene- and ethylenebisformamides, but the magnitude of the interaction between the groups decreased with increasing size of the alkylene group. The amide moieties in the bisacetamides all existed predominantly in the *trans* form. Unexpected high multiplicities were encountered in several of the spectra. No evidence of hindered rotation was found in the spectra of the biscarbamates.

Introduction

The nuclear magnetic resonance (nmr) spectral properties of simple N-monosubstituted²⁻⁶ and N,N-disubstituted amides⁵⁻¹³ and carbamates^{8,14} have been the subject of many recent studies. Interest in these compounds has been primarily due to the fact that rotation about the carbonyl to nitrogen bond is hindered because of interaction of the nonbonding electrons on the nitrogen atom with the π system of the carbonyl function (I). Thus, in the only two stable conforma-



tions, a substituent on the nitrogen could be oriented either *cis* or *trans* to the carbonyl, and interconversions between these conformations would be slow. Since the magnetic environments in these two orientations are not the same, the nmr spectra become more complex in those cases where the mean lifetimes of the individual conformers are long in comparison to the reciprocal frequency separation of the resonances from the two conformers. Studies of N-monosubstituted amides have detected observable hindered rotation in a variety of formamides, acetamides, and isobutyramides.⁴ Both conformers were observed with the

formamides but with a large preponderance of the more stable form. The spectra of the higher homologs indicated that these all existed in only the more stable form at 36°; however, recent results² have indicated that N-methylacetamide contains *ca.* 3% of the less

- (1) One of the laboratories of the Southern Utilization Research and Development Division, Agricultural Research Service, U. S. Department of Agriculture. The mention of trade names and firms does not imply their endorsement by the Department of Agriculture over similar products or firms not mentioned.
- (2) R. H. Barker and G. J. Boudreaux, *Spectrochim. Acta*, **23A**, 727 (1967).
- (3) A. J. R. Bourn, D. G. Gillies, and E. W. Randall, *Tetrahedron*, **20**, 1811 (1964).
- (4) L. A. LaPlanche and M. T. Rogers, *J. Am. Chem. Soc.*, **86**, 337 (1964).
- (5) V. J. Kowalewski and D. G. deKowalewski, *J. Chem. Phys.*, **32**, 1272 (1960).
- (6) D. G. deKowalewski, *J. Phys. Radium*, **23**, 255 (1962).
- (7) H. S. Gutowsky and C. H. Holm, *J. Chem. Phys.*, **25**, 1228 (1956).
- (8) M. T. Rogers and J. C. Woodbrey, *J. Phys. Chem.*, **66**, 540 (1962).
- (9) L. A. LaPlanche and M. T. Rogers, *J. Am. Chem. Soc.*, **85**, 3728 (1963).
- (10) T. H. Siddall and C. A. Prohaska, *ibid.*, **88**, 1172 (1966).
- (11) A. G. Whittaker, D. W. Moore, and S. Siegal, *J. Phys. Chem.*, **68**, 3431 (1964).
- (12) J. V. Hatton and R. E. Richards, *Mol. Phys.*, **3**, 253 (1960); **5**, 139 (1962).
- (13) B. B. Wayland, R. S. Drago, and H. F. Henneke, *J. Am. Chem. Soc.*, **88**, 2455 (1966).
- (14) T. M. Valega, *J. Org. Chem.*, **31**, 1150 (1966).

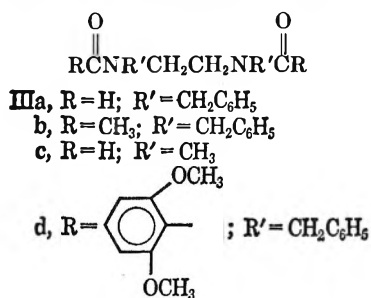
stable form at this temperature. It is generally accepted that the more stable conformer of N-alkyl amides is the *trans* form (Ia; R' = alkyl, R'' = H) in which the alkyl group and carbonyl oxygen are located *cis* to each other. Since the carbonyl tends to shield the alkyl group *cis* to it,^{4,13} the alkyl protons generally exhibit an intense set of resonance signals, each of which have a small satellite peak several cps downfield.⁴ The formyl protons of the simple formamides were found to be more highly shielded in the *cis* form than in the *trans*,⁴ whereas in N-methylacetamide the acetyl protons of the *cis* conformer were responsible for the lower field signal.²

The nmr spectra of the alkylenebisamides (II) would be expected to show an even greater complexity than those of the monoamides since the equilibrium mixtures

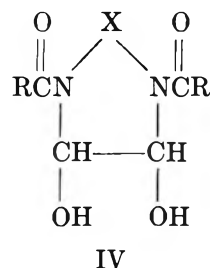


- IIa, R = H; X = CH₂
 b, R = H; X = CH₂CH₂
 c, R = H; X = CH₂CH₂CH₂
 d, R = H; X = CH₂C(CH₃)H-
 e, R = -CH₃; X = CH₂
 f, R = -CH₃; X = CH₂CH₂
 g, R = CH₃; X = CH₂CH₂CH₂
 h, R = CH₃; X = CH₂C(CH₃)H-
 i, R = OCH₃; X = CH₂
 j, R = OCH₃; X = CH₂CH₂
 k, R = OCH₂CH₃; X = CH₂
 l, R = OCH₂CH₃; X = CH₂CH₂
 m, R = OCH₂CH₃; X = CH₂CH₂CH₂

in these cases could contain the *cis-cis*, *cis-trans*, and *trans-trans* conformers. In a recent study¹⁵ of N,N'-dialkylethylenebisamides (III) a high multiplicity of signals in their nmr spectra has been observed and



interpreted in terms of this type of rotational isomerism. We have also noted previously a similar multiplicity of peaks in the spectra of a variety of bisamide-glyoxal adducts of type IV.¹⁶ In order to provide a more sound basis for the interpretation of the spectra of these



and related compounds, the present study of the spectra of a series of simple linear alkylenebisamides in various solvents was undertaken.

Experimental Section

All measurements were made on a Varian A60-A spectrometer equipped with a V-6040 variable-temperature probe and a V-6058A spin decoupler. Chemical shifts were measured relative to tetramethylsilane as an internal standard in DMSO solutions and relative to sodium 3-trimethylsilyl-1-propane sulfonate as an internal standard in D₂O and H₂O solutions. Normal probe temperature was 35°.

The bisamides and carbamates were prepared as described previously^{17,18} and were recrystallized from water or ethanol solution and dried *in vacuo* prior to use. Compounds which showed no evidence of spin coupling of the NH moieties with adjacent C-H were washed with cld, dilute, ethanolic HCl to remove traces of diamine before recrystallization. Deuterated solvents were obtained from NMR Specialties, Inc.

Results and Discussion

The spectrum of methylenebisformamide (IIa) in D₂O showed a singlet at τ 5.32 due to the methylene protons. Interference with the HOD peak made it impossible to detect any definitive evidence of either coupling between the methylene and formyl protons or nonequivalence due to rotational isomerism. In H₂O solution the methylene signal was completely obliterated by the intense water signal. However, the spectrum in dimethylsulfoxide (DMSO) solution

(15) T. H. Siddall, *J. Mol. Spectry.*, **20**, 183 (1966).

(16) S. L. Vail, R. H. Barker, and C. M. Moran, *J. Org. Chem.*, **31**, 1642 (1966).

(17) S. L. Vail, C. M. Moran, and H. B. Moore, *ibid.*, **27**, 2067 (1962).

(18) S. L. Vail and C. M. Moran, *Am. Dyestuff Repr.*, **53**, 282 (1964).



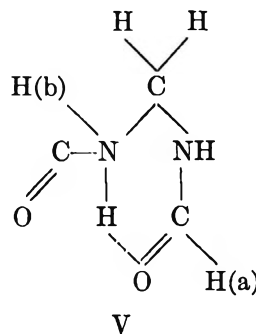
Figure 1. Methylenebisformamide: A, methylene protons in DMSO solution; B, formyl protons in D_2O solution; C, formyl protons in DMSO solution.

(Figure 1A) appeared as a weak doublet superimposed on a rather intense triplet ($J = 6.4$ cps). Addition of D_2O to the solution caused the collapse of the triplet to a singlet because of exchange of the N-H with D_2O . Thus, the triplet was unambiguously assigned as the upper-field half of the A_2X_2 pattern expected for the methylene with two adjacent NH groups. The further splitting of this signal was rather poorly resolved and was probably due to weak coupling with the formyl protons as shown by double irradiation experiments using a difference frequency of 213 cps. The methylene portion of the spectrum provided no evidence for the presence of one or more of the less stable rotational isomers.

The signal due to the formyl protons was found to be the only reliable indicator of hindered rotation. In DMSO solution, the formyl signal of methylenebisformamide (Figure 1C) showed peaks at τ 1.96, 1.93, and 1.89 with relative intensities of *ca.* 1:2:1. These coalesced to a single peak upon heating to 80° as would be expected if the triplet were due to the existence of the bisamide in different conformational forms.

It is not clear why the signal due to the formyl protons existed as a triplet in DMSO. When water was added to this solution, the τ 1.96 signal shifted downfield to τ 1.80. Thus, it would seem that the peaks should be attributable to the presence of the bisamide in *trans-trans*, *cis-trans*, and *cis-cis* forms. There are, however, several factors which would tend to eliminate such an interpretation. Previous reports have shown that very little of the *cis* form is present in simple N-substituted monoamides⁹ except in those cases where the N-substituent is a bulky group.³ The statistical probability of both amide moieties existing in the *cis* conformation at the same time should be very low unless there is some interaction which would force the molecule into this conformation.

Formamide functions are known to be quite susceptible to hydrogen-bond formation. However, with a molecule such as methylenebisformamide, hydrogen bonding may occur in either an intermolecular or an intramolecular fashion. Intramolecular bonding would necessitate a conformation such as V. This postulate is attractive since it would involve a stable six-membered ring. From Dreiding models it was easily



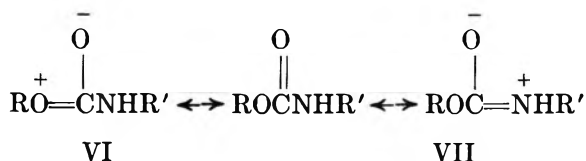
seen that in order for such a conformation to exist, at least one of the amide groups would have to assume a *trans* conformation. The cyclic, hydrogen-bonded portion of the molecule could provide the bulky substituent which might allow the amide portion containing H(b) to exist partially in a *cis* conformation. Taking all these factors into consideration, it would be more plausible to assume that the vast majority of the amide moieties are present in the *trans* form.

Multiple nmr peaks for *trans*-formyl protons are obtained from methylenebisformamide since various hydrogen-bonded species are possible. Nonequivalence would be expected for H(a) and H(b) when both amide moieties are in the *trans* conformation. Therefore, they would not be expected to resonate at the same frequency. In the O-bonded group, H(a) would be deshielded by the depletion in electron density at the carbonyl in a manner analogous to the deshielding which occurs upon protonation of formamides. On the other hand, in the N-bonded form hydrogen bonding causes a polarization of the N-H bond toward the N atom and a resulting increase in electron density in the amido function. This would be expected to lead to increased shielding of H(b) relative to the intermolecularly bonded species. The further assignment of these formyl peaks to specific hydrogen-bonded structures could not be accomplished based on the present information.

Such solvent effects and high peak multiplicities due to the presence of these different rotational forms were expected to be limited mainly to the bisformamide series. The simple N-alkylformamides were known to exist in both *cis* and *trans* forms at *ca.* 35° but the analogous amides of higher acids were found to exist almost solely in the *trans* conformation.⁴ Thus, the nmr spectrum of methylenebisacetamide (IIe) was found to be much less complex than that of methylenebisformamide. In H_2O solution the methylene protons of IIe were seen as the triplet expected for an A_2X_2 system ($J = 6.0$ cps) centered at τ 5.43 although this triplet was partially obscured by the H_2O signal. The spectrum in DMSO showed the same triplet free

of interference. As expected, D₂O caused the triplet to collapse to a sharp singlet. In all three solvents the acetyl protons were seen as a sharp singlet at τ 8.00. A small satellite peak occurred 8 cps downfield from the main peak which may have been due to *ca.* 1–2% of one of the less stable rotational forms. This interpretation was strengthened by the disappearance of the satellite peak upon heating to 80°. Since the acetyl protons in the spectrum of N-methylacetamide in the *cis* conformation absorbed at lower field than those in the *trans*,² it seemed reasonable to assign the conformations of the amide groups of IIe as *ca.* 99% *trans* and *ca.* 1% *cis*. The observation that the relative conformational stabilities were essentially solvent independent was not unexpected.

Whereas the spectra of the bisacetamides were simplified by the existence of essentially a single isomer due to a high-energy barrier to rotation about the C–N bond and a large difference in conformational stabilities, the spectra of the bis-carbamates were expected to show the effects of exactly the opposite situation. Here, contribution of the canonical form VII should



decrease the importance of form VII resulting in a lower C–N bond order and a much lower energy barrier to rotation. The spectra of the simple carbamates showed no evidence of hindered rotation when R was small.¹⁴ The spectrum of methylenebis(methyl carbamate) (III) contained only a singlet at τ 6.42 for the methoxyl protons and the triplet ($J = 6.1$ cps) of the A₂X₂ system centered at τ 5.65 for the methylene protons in DMSO solution. Insolubility of the compound precluded measurement of the spectrum in H₂O or D₂O at 35°, but the spectra at 60° showed the expected signals. The spectrum in CDCl₃ at 35° was essentially the same as that in DMSO.

Methylenebis(ethyl carbamate) (IIk) also showed no evidence of hindered rotation in CDCl₃ or DMSO at 35°. The compound was not sufficiently soluble to allow measurement of the spectra in H₂O or D₂O at 35°. In CDCl₃, the A₂X₃ pattern of the ethoxy group was easily seen as a triplet centered at τ 8.76 and a quartet centered at τ 5.82 with $J = 7.0$ cps. The A₂X₂ pattern of the NHCH₂NH moiety was seen as a triplet centered at τ 5.46 and an ill-defined, but nevertheless recognizable, triplet centered at τ 3.50 and with $J = 6.1$ cps.

The spectra of the ethylenebiscarbamates and bis-amides also showed unexpected high multiplicities. The greatest difficulty in interpretation arose from the odd shape of the ethylene signal when the NH protons were not exchanged. In both H₂O and DMSO at 35° the ethylene signal of ethylenebisformamide (IIb) occurred as a triplet with a spacing between peaks of 3 cps. However, the shape of the triplet (Figure 2A) was not compatible with any simple coupling pattern. Instead, this signal seemed to be composed of a doublet with $J = 6.0$ cps superimposed on either a singlet or a poorly resolved doublet with a small coupling constant. The large doublet was, of course, exactly what would be expected for the AX₂ system of equivalent methylenes, each adjacent to an NH.

That the appearance of this unusual pattern was indeed due to coupling with the NH moiety was demonstrated unambiguously since this signal appeared as a sharp singlet in D₂O solution. The occurrence of this singlet also allowed the elimination of the explanation that the conformation of the molecule caused the two methylenes to become nonequivalent and that the different methylenes coupled differently with their adjacent NH groups. Siddall¹⁵ has recently postulated a similar nonequivalence between the methylenes of some N,N'-disubstituted ethylenebisformamides (III) but this resulted in a chemical shift difference between the methylenes. This chemical shift difference should result in the appearance of a doublet for the ethylene signal in D₂O rather than the observed singlet. There was also the possibility that slow rotation about the CH₂NH bond could result in the presence of conformations with different H–C–N–H dihedral angles which would give rise to different spin-spin interactions. Such a possibility could not be eliminated unequivocally, but intuitively it seemed highly unlikely. Rotation about such bonds is rarely slow enough to permit observation of the separate conformations at 35°. In addition, this unusual coupling seemed to be characteristic of the ethylene compounds and was not observed in the methylene, 1,3-propylene, or 1,2-propylene analogs. This specificity for the ethylene compound

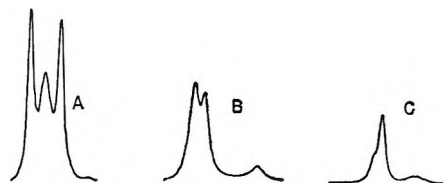


Figure 2. Ethylenebisformamide: A, ethylene protons in H₂O solution; B, formyl protons in H₂O solution; C, formyl protons in D₂O solution.

would be difficult to reconcile with an explanation based on slow rotation about the CH_2NH bond. Any dependence of this phenomenon on hindered rotation about the amide C-N bond could be eliminated by consideration of the spectra of ethylenebisacetamide (II f) and the ethylenebiscarbamates (II j) and (III). These spectra in H_2O or DMSO all contained an ethylene signal very similar to that of the formamide. The ethylenebisacetamide seemed to exist almost completely as a single rotational isomer with respect to the amide bonds so that the presence of more than one amide conformation could not be necessary to observe this coupling pattern. In fact, the same ethylene signal was observed with the biscarbamates where rotation about the amide bond seemed to be quite unhindered.

With the exception of the anomalous ethylene signal, the H_2O , D_2O , DMSO, and CDCl_3 spectra of the ethylenebiscarbamates and the ethylenebisacetamide were found to be essentially identical with the spectra of the analogous methylene compounds. On the other hand, the shape of the formyl signal of ethylenebisformamide was distinctly different from that of the methylene analog. In H_2O solution, the formyl signal (Figure 2B) was seen as three fairly well-resolved peaks which were quite misleading, as shown by the spectrum in D_2O (Figure 2C). Apparently, the NH signal was sufficiently sharp in this case to cause noticeable interference with the formyl signal. In all of the compounds studied, the NH and formyl signals appeared together, but the NH was usually broadened to such an extent that it was seen only as a bulge in the base line. But in the case of the ethylene compound, only the spectrum in D_2O offered a reliable indication of the rotational isomerism about the amide C-N bond.

In D_2O the three formyl peaks could be rationalized by assigning the two downfield peaks to *trans* conformations and the small upfield peak, which represents about 15% of the total amide concentration, to a *cis* conformation. The separation between the *trans* peaks was small compared to the signals obtained from the formyl protons in methylenebisformamide. This comparatively simple spectrum for the formyl protons appeared to result from the insertion of the additional methylene group between the amide moieties. As a result, formyl protons acted more as they would in a simple *N*-alkyl monoamide. If this interpretation were correct, the formyl protons of the 1,3-propylenebisformamide (II c) would be expected to act even more like the formyl protons of *N*-methylformamide. In other words, as we proceeded through the homologous series methylene to ethylene to 1,3-propylene, it would

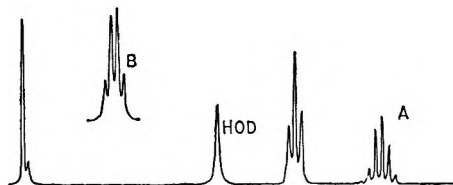


Figure 3. 1,3-Propylenebisformamide: A, in D_2O solution; B, methylene protons adjacent to nitrogen in DMSO solution.

be expected that the molecule would become less rigid and less apt to assume an internally bonded conformation such as V.

In actuality, the spectrum of II c in D_2O (Figure 3) showed a formyl proton signal very similar to that found in simple monoformamides, indicating that each formamide group could assume either a *cis* or a *trans* conformation completely independently of the other. The formyl spectra in DMSO and H_2O were similar except that the resolution was not quite as good, perhaps owing to line broadening from weak coupling with the NH. On heating, the formyl signal became a singlet, as expected. The remainder of the spectrum in D_2O was perfectly normal for the propylene A_4X_2 system with $J = 6.5$ cps. In DMSO and H_2O solution the triplet at $\tau 6.70$ was split to a symmetrical quartet (Figure 3B) which might seem to be part of an AX_3 pattern ($J = 6.5$ cps) and thus incompatible with the previous interpretation. However, double resonance experiments showed that this was not the case as irradiation of the quintet due to the central methylene caused the quartet to collapse to a doublet ($J = 6.5$ cps) while irradiation of the NH peak produced a triplet ($J = 6.5$ cps) in place of the quartet. The same phenomenon was observed with the 1,3-propylenebisacetamide (II g) and bis(ethyl carbamate) II m (Figure 4).

As might be expected, branching of the alkylene por-

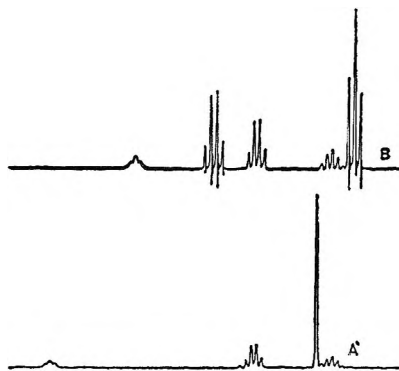


Figure 4. A, 1,3-Propylenebisacetamide in CDCl_3 solution; B, 1,3-propylenebis(ethyl carbamate) in CDCl_3 solution.

tion of the bisamide molecule not only complicated the spectrum but also seemed to decrease the interaction of the two amide groups. Thus, the formyl signal in the spectrum of 1,2-propylenebisformamide (Figure 5b) showed two strong peaks at τ 1.89 and 1.94 with a much weaker, very poorly resolved doublet at τ 1.98–2.04. This pattern seemed to be interpreted best in terms of the presence of two different and independent formamide groups, each of which was capable of existing in either a *cis* or *trans* form. Confirmation was obtained by heating the sample to 80° and coalescence of the signals to a pair of sharp peaks. There was no apparent difference in the shape of this signal in D₂O and DMSO solutions, a further indication that there was little or no interaction between the amide functions.

The interpretation of the remainder of the spectrum (Figure 5) was quite straightforward. In D₂O solution the methine proton at τ 5.92 was coupled to both the methyl and methylene protons causing it to be split into a multiplet with an apparent coupling constant of 6 cps. The methylene protons, being adjacent to an asymmetric center, were nonequivalent and were seen as the upfield portion of an ABC pattern centered at τ ca. 6.7. Irradiation of the methine proton caused the methylene signal to collapse to a broad singlet which was probably a poorly resolved AB quartet.

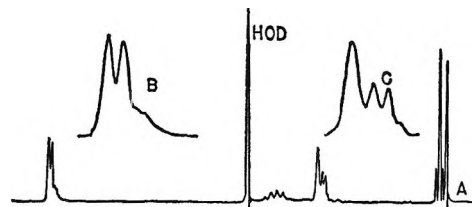


Figure 5. 1,2-Propylenebisformamide: A, in D₂O solution; B, formyl protons in D₂O solution; C, methylene protons in D₂O solution.

A similar coupling pattern was observed with the parent 1,2-propylenediamine and there was no evidence of the conformational nonequivalence of the alkylene group such as that observed by Siddall.¹⁵ However, it was of some interest to note that the methyl signal of II_d appeared as two doublets ($J = 7.0$ cps). Heating to 80° caused coalescence to one doublet indicating that the nonequivalence of methyl protons was caused by rotational isomerism about the amide C–N bond. Presumably, the pendant methyl groups are in significantly different magnetic environments, whereas the alkylene bridges are not.

Studies presently underway are aimed at an evaluation of the effects of various substituents on the alkylene bridge on the steric and electronic interactions between portions of alkylenebisamide molecules.

Melting of Polymer-Diluent Mixtures under Pressure. I.

Polyethylene- α -Chloronaphthalene

by F. E. Karasz and L. D. Jones

General Electric Research and Development Center, Schenectady, New York 12301 (Received December 22, 1966)

A theory for the effect of pressure on the melting point of polymers with added diluents is developed, using the Flory-Huggins lattice model as a basis. It is shown that the principal additional parameter that can be obtained from measurements of this type is ΔV_f , the volume of fusion of the hypothetical completely crystalline polymer. The concept has been tested on the polyethylene- α -chloronaphthalene system with satisfactory results. The polymer-diluent interaction parameter and its dependence on temperature and pressure may also be derived.

Introduction

The effect of pressure on the melting point of crystalline polymers has been reasonably well explored in the past in the determinations of heats and entropies of fusion and the variation in these parameters with pressure. Together with the measurement of melting-point depressions of polymer-diluent mixtures and direct calorimetric determination using samples of known crystallinity, the pressure method constitutes one of the major techniques for acquiring these thermodynamic quantities. In contrast, the effect of pressure on the melting point of polymer-diluent mixtures appears not to have been studied at all,¹ though theoretically the results are readily amenable to interpretation, for example, in terms of the Flory-Huggins lattice model, while experimentally the measurements can be carried out with only minor modifications of well-known techniques.

The principal additional parameter that can be obtained from such measurements is the change of volume on fusion, ΔV_f , where this refers to the hypothetical, completely crystalline polymer. As will be demonstrated below, a number of other quantities also emerge from a detailed treatment, and in addition a set of measurements of T_m as a function both of pressure and of diluent concentration provides data from which the polymer-diluent interaction energy may in principle be calculated with some accuracy.

The relation of all these types of measurements to each other may be seen from the set of equations

$$\left(\frac{\partial T_m}{\partial P_m}\right)_{N \rightarrow 1} = \frac{\Delta V_f}{\Delta S_f} \quad (1a)$$

$$\left(\frac{\partial \ln N}{\partial T_m}\right)_{P_m, N \rightarrow 1} = \frac{\Delta S_f}{RT_m} \quad (1b)$$

$$\left(\frac{\partial \ln N}{\partial P_m}\right)_{T_m, N \rightarrow 1} = \frac{-\Delta V_f}{RT_m} \quad (1c)$$

In these equations, N is the mole fraction of polymer in a polymer-diluent mixture, whose melting point is T_m at a pressure P_m . ΔS_f is the entropy of fusion of the pure polymer and, as ΔV_f , refers to the completely crystalline material. Equation 1a is the familiar Clapeyron equation, written in this instance, for illustration, as referring to the limiting case of pure polymer, though it may be noted that it is also valid at finite diluent concentrations, provided that ΔV_f and ΔS_f are appropriately redefined. Equation 1b is the ideal or dilute solution limit of the equation commonly used to evaluate ΔS_f (or the corresponding enthalpy, ΔH_f) from melting point depression experiments. In integrated form, (1b) can (necessarily) also be obtained as a limiting form of the equation obtained in the Flory-Huggins treatment,² namely

(1) J. S. Ham, M. C. Bolen, and J. K. Hughes, *J. Polymer Sci.*, **57**, 25 (1932), have investigated noncrystalline polymer-diluent mixtures under pressure.

(2) P. J. Flory, "Principles of Polymer Chemistry," Cornell University Press, Ithaca, N. Y., 1953, p 568 ff.

$$\frac{1}{T_m} - \frac{1}{T_m^0} = \frac{R V_u}{\Delta H_f V_1} (v_1 - \chi v_1^2) \quad (2)$$

in which T_m^0 refers to the pure polymer, V_u and V_1 are the molar volumes of the polymer repeating unit and of the diluent, respectively, v_1 is the volume fraction of diluent present, and χ is the Flory-Huggins polymer-solvent interaction parameter. Finally, eq 1c is the ideal solution limit of the equation which we propose to employ in this paper; it is set forth in this form merely to illustrate its relation to ΔV_f and, of course, to indicate that eq 1a can be obtained by combination of (1b) and (1c).

The system chosen for the initial study of this concept has been polyethylene (Marlex 50)- α -chloronaphthalene. Reasons for this choice are first, the system has been carefully studied in terms of the melting-point elevation (of the pure polymer) with pressure³ and of the melting-point depression with diluent (at 1 atm),^{4,5} and thus a reliable comparison with the limiting cases of our measurements is available. Secondly, the system lends itself to convenient analysis of the diluent concentration by virtue of the chlorine content of the latter.

Experimental Section

A relatively simple pressure-generating apparatus, described elsewhere,⁶ was employed for these measurements. Marlex 50 (Type 15), $M_w \sim 87,000$,⁷ was powdered and intimately mixed with the required quantity of α -chloronaphthalene (Fisher reagent grade). About 1 g of this mixture was used in the determination of the melting point. For each such constant composition mixture, the melting point was determined from volume-temperature plots at a number of fixed pressures up to about 2500 atm. Diluent concentrations up to 79 wt % were used. The heating rate in the melting range was about 5° hr^{-1} ; the extremely slow heating schedules that have been adopted in some cases⁵ were not employed, and consequently we expected our observed melting points to be slightly lower than those found in such experiments. However, each melting point determination was repeated a number of times under the same conditions until reproducibility to about $\pm 0.5^\circ$ was obtained; apparently, after two or three successive fusions the sample achieved complete homogeneity.

After the completion of a set of measurements with a particular diluent concentration, the plug of polymer-diluent was removed from the pressure cell and analyzed for α -chloronaphthalene content by standard techniques.

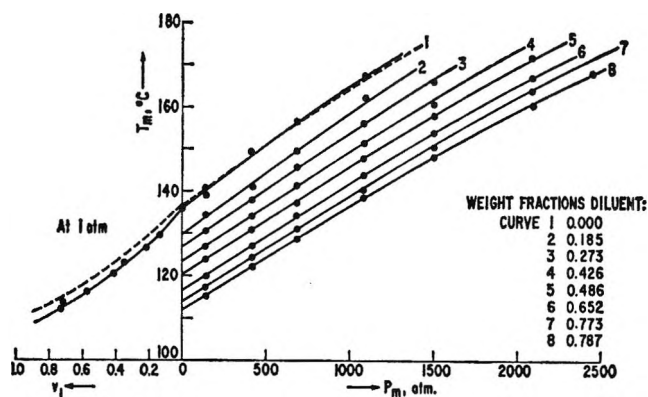


Figure 1. Melting temperature as a function of pressure for a series of polyethylene- α -chloronaphthalene mixtures, and (at left) melting temperature as a function of diluent volume fraction at constant pressure (1 atm). Dashed lines show results of Matsuoka³ (right) and of Quinn and Mandelkern⁴ (left), respectively.

Results

The primary data in terms of the melting points of constant composition mixtures as a function of pressure are shown in Figure 1. The results of Matsuoka³ and of Quinn and Mandelkern⁴ for pure polyethylene (also Marlex 50) and for the polymer-diluent mixtures at 1 atm, respectively, are also shown for comparison. It is seen that our data are in excellent agreement with the former, while relative to the latter, the melting points found in this study are 1-2° lower. As a reference for subsequent calculations, we have taken the melting point of the pure polymer at atmospheric pressure to be 136°. In the following discussion, we shall use the symbols ΔV_f° , ΔH_f° , etc., to distinguish the fusion parameters under these conditions.

To develop a useful analysis of the data, we start from the usual basis that the chemical potential of the crystalline polymer per segment, μ_u^c , at the equilibrium melting temperature and pressure, must equal that of the liquid polymer, μ_u , in the polymer-diluent mixture, *i.e.*

$$\mu_u^c - \mu_u^0 = \mu_u - \mu_u^0 \quad (3)$$

where μ_u^0 represents the potential of the pure liquid polymer, taken as a reference state. The change in $\mu_u^c - \mu_u^0$ with pressure is given by

(3) S. Matsuoka, *J. Polymer Sci.*, **57**, 569 (1962).

(4) F. A. Quinn, Jr., and L. Mandelkern, *J. Am. Chem. Soc.*, **80**, 3178 (1958); **81**, 6533 (1959).

(5) R. Chiang and F. J. Flory, *ibid.*, **83**, 2857 (1961).

(6) L. D. Jones and F. E. Karasz, *J. Polymer Sci.*, **B4**, 803 (1966).

(7) A. Ram and M. Narkis, *J. Appl. Polymer Sci.*, **10**, 481 (1966).

$$\left[\frac{\partial(\mu_u^c - \mu_u^0)}{\partial F} \right]_T = -\Delta V(P, T) \quad (4)$$

where $\Delta V(P, T)$ represents the difference in molar volumes of the liquid and crystalline polymer at P and T .

At the equilibrium melting point, $T = T_m$, $P = P_m$, and $\Delta V(P_m, T_m) \equiv \Delta V_f$, we can use eq 3 and insert the appropriate expression for $\mu_u - \mu_u^0$ into eq 4. Thus in the ideal solution case, the latter term is equal to $RT_m \ln N$, and we recover eq 1c. For practical consideration, over a wider range of diluent concentrations, we may employ the Flory-Huggins expression for $\mu_u - \mu_u^0$, namely²

$$\mu_u - \mu_u^0 = -RT_m \frac{V_u}{V_1} (v_1 - \chi v_1^2) \quad (5)$$

Combining eq 3, 4, and 5 and integrating, we find

$$P_m - P_m^0 = \frac{RT_m}{\Delta V_f} \frac{V_u}{V_1} (v_1 - \chi v_1^2) \quad (6)$$

where the integration constant P_m^0 refers to the equilibrium melting pressure of undiluted polymer at T_m ($\equiv T_m^0$). In obtaining eq 6, it should be noted that we have neglected the pressure dependence of ΔV_f . For most polymers, this is probably not as good an assumption, numerically, as the neglect of the temperature dependence of ΔH_f in deriving eq 2; if desirable, eq 6 can be appropriately modified.

Equation 6 bears an obvious similarity to eq 2 and, in further analogy, the parameters ΔV_f and χ may be obtained by plotting $(P_m - P_m^0)/v_1$ against v_1 . However, we can proceed further by expressing the interaction parameter in the usual approximation,² $\chi = BV_1/RT$, where B is a temperature-independent energy density parameter, and then, assuming that B is pressure dependent, we write, empirically, $B = B_0(1 + aP_m)$, obtaining [at constant P_m ($\equiv P_m^0$)]

$$\frac{1}{T_m} - \frac{1}{T_m^0} = \frac{R}{\Delta H_f} \frac{V_u}{V_1} \left[1 - \frac{B_0 V_1 (1 + aP_m)}{RT_m} v_1 \right] \quad (7a)$$

and (at constant T_m)

$$\frac{P_m - P_m^0}{v_1} = \frac{RT_m}{\Delta V_f} \frac{V_u}{V_1} \left[1 - \frac{B_0 V_1 (1 + aP_m)}{RT_m} v_1 \right] \quad (7b)$$

The parameters ΔH_f , B_0 and a can thus be obtained from isobaric plots of $(1/T_m - 1/T_m^0)/v_1$ vs. v_1/T_m at a number of pressures.

Using the results shown in Figure 1, we first plotted T_m as a function of the diluent weight fraction, w_1 , at 400-atm intervals (Figure 2). This process smoothed

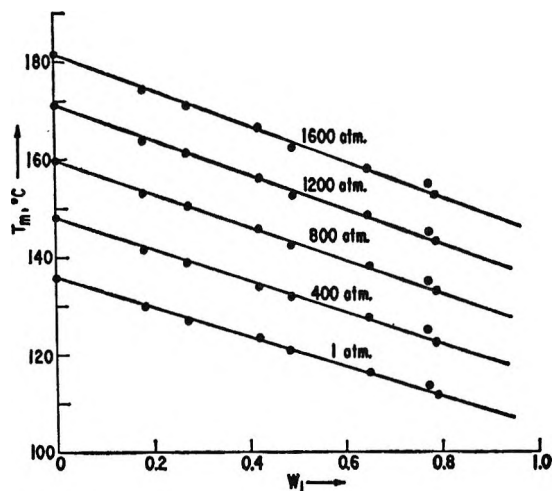


Figure 2. Melting temperature as a function of weight fraction diluent, w_1 , at a series of constant pressures.

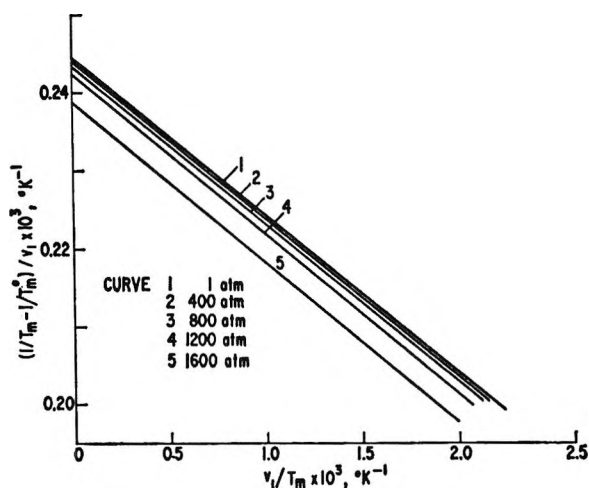


Figure 3. Left-hand side of eq 7a vs. v_1/T_m at constant pressure. Values calculated using smoothed data from Figure 2.

the data for the subsequent plot of $(1/T_m - 1/T_m^0)/v_1$ against v_1/T_m , shown in Figure 3. In the calculation of v_1 , we took into account the variation of the specific volumes of the polymer and of α -chloronaphthalene with both temperature and pressure. The relevant data for polyethylene (linearly extrapolated below the melting curve of the pure polymer where necessary) was taken from the comprehensive studies of Hellwege, Knappe, and Lehmann.⁸ The thermal expansion of the diluent at atmospheric pressure has been given by Chiang and Flory;⁵ additional P - V - T data at elevated pressures was obtained with sufficient accuracy in the

(8) K.-H. Hellwege, W. Knappe, and P. Lehmann, *Kolloid-Z.*, **183**, 110 (1962).

pressure cell referred to above. The results show that the ratio V_u/V_1 is essentially temperature independent at all relevant pressures, but decreases by about 3% from 1 to 2000 atm.

From the intercepts and slopes in Figure 3, ΔH_f and B were calculated. We postpone discussion of the former to a later section, but note at this point that the variation in B with pressure is rather small over the range studied (Table I). We can, at least formally, express this variation as follows: $B = 1.09(1 + 5 \times 10^{-5}P_m)$ cal ml $^{-1}$.

Table I: Summary of Thermodynamic Data for Polyethylene

A. Heats and Entropies of Fusion along Melting Curve of Pure Polymer, and Polymer-Diluent Interaction Parameter from Eq 7a

T_m° , °C	P_m° , atm	ΔH_f , cal mole $^{-1}$	ΔS_f , eu mole $^{-1}$	$B_0(1 + aP_m)$ (eq 7a), cal ml $^{-1}$
136.0	1	982	2.40	1.09
148.0	400	970	2.30	1.11
160.0	800	965	2.23	1.14
171.5	1200	962	2.16	1.165
181.5	1600	975	2.14	1.21

B. Volume of Fusion along Melting Curve of Pure Polymer, and Polymer-Diluent Interaction Parameter from Eq 7b

T_m° , °C	P_m° , atm	ΔV_f , ml mole $^{-1}$	B_0 , (eq 7b), cal ml $^{-1}$
136.0	1	2.73	1.59
140.0	140	2.665	1.58
150.0	460	2.435	1.52
160.0	800	2.25	1.45
170.0	1170	2.00	1.31

The data from Figure 1 were then replotted in terms of P_m vs. w_1 curves at 10° intervals (Figure 4). Then, in accordance with eq 7b, plots were constructed of $(P_m - P_m^\circ)/v_1$ vs. $(1 + aP_m)v_1$, using the value of a obtained above. From the intercepts and slopes in Figure 5, ΔV_f and B_0 were calculated.

Table I summarizes the results for the heats and volumes of fusion of the pure polymer along the melting curve, together with values of B and B_0 calculated from the isobaric and isothermal plots, Figures 3 and 5, respectively.

Discussion

(a) *Volume of Fusion.* The volume of fusion, ΔV_f , of completely crystalline polyethylene as calculated by this method is shown as a function of T_m and

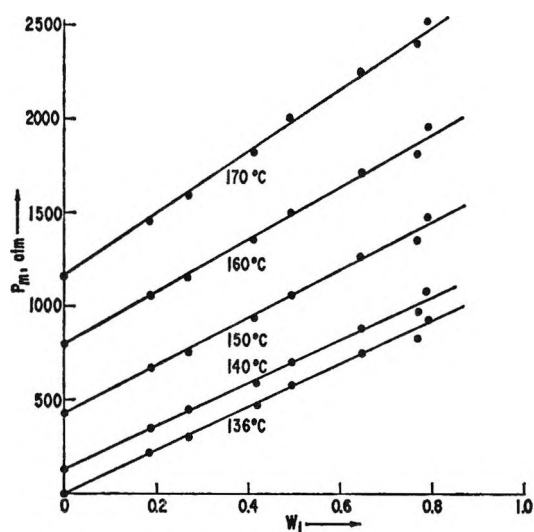


Figure 4. Melting pressure as a function of weight fraction diluent, w_1 , at a series of constant temperatures.

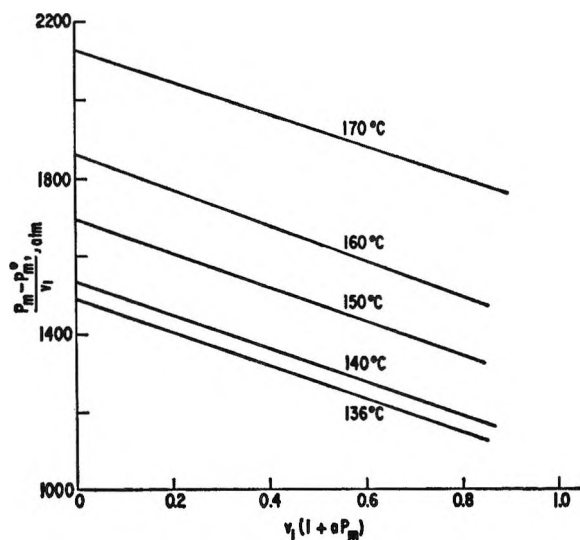


Figure 5. Left-hand side of eq 7b vs. $v_1(1 + aP_m)$ at constant temperature. Values calculated using smoothed data from Figure 4.

P_m in Figure 6. For comparison, we have included Matsuoka's results,³ in which ΔV_f° was obtained from unit cell data and liquid densities, and then ΔV_f calculated along the melting curve using known thermal expansion coefficients and compressibilities. Our result for ΔV_f° of 2.72 ml mole $^{-1}$ (of CH $_2$ units) is in very good agreement with Matsuoka's value of 2.80 ml mole $^{-1}$. At elevated pressures, the agreement deteriorates somewhat; there is, for example, about 13% difference at 1200 atm. It seems probable that the present method is inherently more reliable for obtaining ΔV_f at high pressure, because the uncer-

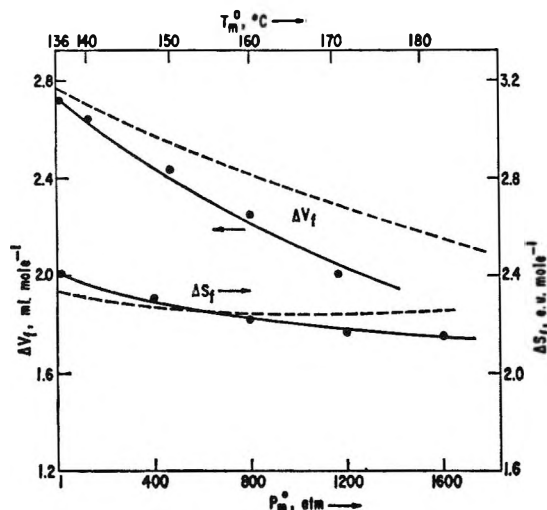


Figure 6. Volume and entropy of fusion of pure polyethylene (per mole of CH_2 units) along melting curve. Dashed lines show data of Matsuoka³ for comparison. Points correspond to values calculated at arbitrarily chosen temperatures and pressures (*i.e.*, those used in Figures 2-5).

tainty in published values of expansivity and, especially, compressibility (both of which are themselves functions of P and T) precludes an accurate computation. It should be pointed out that in the literature values there is somewhat surprisingly about $\pm 10\%$ uncertainty in ΔV_f° for polyethylene. The specific volume based on unit cell dimensions at 136° has been reported as 1.033,⁹ 1.040,¹⁰ and 1.058 ml g^{-1} ¹¹ (the last for polymethylene), while Matsuoka³ apparently adopted a value of 1.060 ml g^{-1} (shown in Figure 10 of ref 3) in arriving at 0.20 ml g^{-1} or 2.80 ml mole^{-1} for ΔV_f° . Slightly lower, but for this calculation still significant, uncertainty exists with regard to the specific volume of liquid polyethylene at 136° and 1 atm. Richardson, Flory, and Jackson¹² report 1.272 ml g^{-1} , Quinn and Mandelkern⁴ (as analyzed by Swan¹⁰) report 1.256 ml g^{-1} , and Matsuoka³ finds 1.260 ml g^{-1} . All of the above results (except where otherwise stated) refer to a high density linear polymer essentially of the same type as used in the present work. Using the above data, one may compute values of ΔV_f° ranging from 2.75 to 3.35 ml mole^{-1} , and our own result, therefore, lies at the lower limit of this range. Finally, in comparing the results of Baer and Kardos,¹³ we find that their values of ΔV_f are uniformly higher than either Matsuoka's or our own throughout the pressure range studied in this work. This divergence may be a result of an underestimation of the crystallinity of the sample. This would be consistent, also, with the fact that their decrease in ΔV_f with pressure agrees well with our own results.

(b) *Heat and Entropy of Fusion.* In contrast to ΔV_f° , the agreement with regard to ΔH_f° and ΔS_f° for polyethylene is good. Diluent depression results in a heat of fusion ranging from 930 to 990 cal mole^{-1} according to diluent⁴ (970 cal mole^{-1} using α -chloronaphthalene), and from calorimetric data using samples of known crystallinity, a ΔH_f° of 928 cal mole^{-1} was derived.¹⁴ In a careful analysis based on thermodynamic data for linear hydrocarbons, Broadhurst¹⁵ concluded that ΔH_f° for polymethylene was close to 1000 cal mole^{-1} . In light of these results, our own value of 982 cal mole^{-1} is in excellent agreement. At higher pressures, there is also reasonable agreement with Matsuoka's data;³ nearly all of the divergence indicated in Figure 6 stems from his use of slightly different values of ΔV_f , already discussed above, in conjunction with eq 1a.

Finally, our directly determined fusion parameters may be used to calculate dT_m/dP_m along the melting curve of undiluted polyethylene. The result, of course, is not independent and serves merely to verify the preceding calculations. However, in practice, it may serve a useful purpose in obviating the need to construct tangents to the T_m vs. P_m curve. We find that at 136° and 1 atm, dT_m/dP_m is 2.84×10^{-2} deg atm^{-1} .

(c) *Polymer-Solvent Interaction.* The value of B_0 derived from eq 7a has already been discussed in connection with the pressure dependence of B . For convenience, we shall adopt the symbol $B_{0,T}$ for this value, and $B_{0,P}$ for the same parameter obtained from eq 7b. The interaction parameter for the polyethylene- α -chloronaphthalene system from melting point depression studies at atmospheric pressure (*i.e.*, $B_{0,T}$ in our nomenclature) found by Quinn and Mandelkern⁴ was 1.5 cal ml^{-1} . This compares with our own value of 1.1 cal ml^{-1} . Formally, the divergence can be ascribed to a slightly differing curvature in the T_m vs. v_1 plots. Expressed in terms of a difference in melting points, this amounts to $\sim 1.5^\circ$ at $v_1 = 0.8$, *i.e.*, at a melting point depression of about 35° .

The apparent temperature dependence in the "constant" $B_{0,P}$ (Table I) could obviously be used to calculate directly the hitherto neglected entropic contributions to χ . However, the observed variation may also

- (9) E. A. Cole and D. R. Holmes, *J. Polymer Sci.*, **46**, 245 (1960).
- (10) P. R. Swan, *ibid.*, **42**, 525 (1960).
- (11) M. G. Gubler and A. J. Kovacs, *ibid.*, **34**, 551 (1959).
- (12) M. J. Richardson, P. J. Flory, and J. B. Jackson, *Polymer*, **4**, 221 (1963).
- (13) E. Baer and J. L. Kardos, *J. Polymer Sci.*, **A3**, 2827 (1965).
- (14) B. Wunderlich and M. Dole, *ibid.*, **24**, 201 (1957).
- (15) M. G. Broadhurst, *J. Res. Natl. Bur. Std.*, **67A**, 233 (1963).

originate from other approximations introduced in the derivation of eq 7b, especially in the neglect of the (isothermal) pressure dependence of ΔV_f . Since χ itself is obviously highly sensitive to experimental error,¹⁶ it seems inappropriate to proceed further with a detailed analysis in the present study. (We note in passing that with some experimental elaboration, it should be possible to increase accuracy in this type of measurement by about an order of magnitude relative to the present investigation, and thus provide a powerful means of studying these effects.) The above remarks also apply to the inequality of $B_{0,T}$ and $B_{0,P}$ demonstrated in Table I. Formally, it may be readily shown that by limiting the expression for $\mu_u - \mu_u^0$ to terms no higher than the second power in v_1 (eq 5), the consequences of imposing equality on $B_{0,T}$ and $B_{0,P}$ (*i.e.*, or the respective χ 's) are too restrictive relative to the experimental observations.

It should be noted, however, that none of the approximations involved in the evaluation of the polymer-solvent interaction constant can result in errors in the fusion parameters.

Conclusions

We wish, finally, to draw attention to some of the applications and implications of this technique. The method described represents, primarily, a new technique for measuring ΔV_f for polymers. It is independent of a knowledge of the crystallinity of the sample, or of the crystal structure and unit cell dimen-

sions. In fact, where the latter are unavailable, one may wish to reverse the normal procedure and use this technique to calculate theoretical crystal densities at room temperature (or elsewhere), and thus this method may have applications in initiating routine crystallinity measurements from density determinations. In many circumstances, also, the method may yield values of ΔV_f of greater precision than are normally available. This is especially the case when ΔV_f is required at elevated pressure, or where samples of only low crystallinity are available. The fact that ΔH_f as a function of pressure can be obtained directly may also be useful in certain instances.

A further area in which this method may be of use is in obtaining ΔV_f for samples which decompose below the melting point of the pure polymer. This case is analogous to techniques already described for obtaining ΔH_f (and T_m) for cellulose esters.¹⁷ Obviously, the density of the amorphous polymer may also be calculated. Finally, the method at least has the potential for evaluating B (or rather χ) more accurately than is achieved with normal diluent-depression measurements, in addition to the possibility of finding pressure-dependent effects. In principle, the self-consistency of the data and the applicability of the Flory-Huggins treatment may be verified.

(16) See, for example, A. Nakajima and F. Hamada, *Kolloid-Z.*, **205**, 55 (1965).

(17) L. Mandelkern and P. J. Flory, *J. Am. Chem. Soc.*, **73**, 3206 (1951).

Electronic Structure of Nitrogen Dioxide, Its Ions, and Its Dimer¹

by L. Burnelle, P. Beaudouin, and L. J. Schaad

Department of Chemistry, New York University, New York, New York 10003 (Received December 27, 1966)

The extended Hückel method has been applied to nitrogen dioxide for a series of bond angles extending from 90 to 180° and for three values (1.50, 1.75, and 2.00) of the parameter K appearing in the Wolfsberg-Helmholtz formula. For $K = 2.00$, very good agreement with experiment is obtained for the bond angle of NO_2^- , NO_2 , and NO_2^+ , while the experimental bending force constants are reproduced in a satisfactory fashion. Comparison is made between Walsh's diagram for AB_2 molecules and the curves obtained for the orbital energies. The adiabatic ionization potential of NO_2 is found equal to 10.98 eV, which coincides with a recent experimental determination by photoelectron spectroscopy.² The first excited state of NO_2^+ is predicted to be bent. It is found that upon dimerization all the occupied b_2 orbitals of NO_2 give rise to some destabilization; this is suggested to be the reason for the low dissociation energy of the dimer. The loss of color associated with the dimerization appears to be linked with the stabilization incurred by the $4a_1$ orbital of NO_2 .

Introduction

The electronic structure of nitrogen dioxide has been the object of several theoretical works for the last few years.^{3,4} Among the questions which have been debated, that of the position of the excited states of the molecule is of primary importance, because accurate information on this point would be very helpful in disentangling the long-wavelength absorption spectrum of the compound. The spectrum, which extends from 10,000 to 3200 Å,⁵⁻⁷ is of such a complexity that it has so far resisted attempts at detailed analysis. Another question of importance concerns the nature of the molecular orbital containing the unpaired electron, because this orbital is most probably used in the formation of the NN bond connecting the two NO_2 groups in the most stable dimer. It is known that NO_2 dimerizes readily and that it forms several distinct dimers.^{8,9} The most stable of these, which has the planar O_2NNO_2 structure, is characterized by a low dissociation energy of 12.9 kcal/mole.¹⁰ Correspondingly, the central NN bond has an anomalous length of 1.75 Å.¹¹ The reasons for these peculiar features are not yet well understood. The various models which have been proposed for the bond¹²⁻¹⁵ do not, in our opinion, provide a convincing explanation for its unusual properties.

In the present work, we have attacked the problem by using the three-dimensional Hückel method in its plainest form, as devised by Hoffmann.¹⁶ Since this

(1) Work sponsored by the Air Force Cambridge Research Laboratories, Office of Aerospace Research, under Contract No. AF 19(628)-5729 and by the U. S. Army Research Office (Durham), under Grant No. DA-ARO-D-31-124-G718.

(2) M. I. Al-Jaboury and D. W. Turner, *J. Chem. Soc.*, 4434 (1964).

(3) (a) K. L. McEwen, *J. Chem. Phys.*, **32**, 1801 (1961); (b) M. Green and J. W. Linnett, *Trans. Faraday Soc.*, **57**, 1 (1961); (c) J. Serre, *Mol. Phys.*, **4**, 269 (1961).

(4) H. Kato, T. Yonezawa, K. Morokuma, and K. Fukui, *Bull. Chem. Soc. Japan*, **37**, 1710 (1964).

(5) R. W. B. Pearse and A. G. Gaydon, "The Identification of Molecular Spectra," 3rd ed, Chapman and Hall, London, 1963.

(6) G. W. Robinson, M. McCarthy, and M. C. Keilty, *J. Chem. Phys.*, **27**, 972 (1957).

(7) A. E. Douglas and K. P. Huber, *Can. J. Phys.*, **43**, 74 (1965).

(8) W. G. Fateley, H. A. Bent, and B. Crawford, Jr., *J. Chem. Phys.*, **31**, 204 (1959).

(9) I. C. Hisatsune, J. P. Devlin, and Y. Wada, *ibid.*, **33**, 714 (1960).

(10) W. F. Giauque and J. D. Kemp, *ibid.*, **6**, 40 (1938).

(11) D. W. Smith and K. Hedberg, *ibid.*, **25**, 1282 (1956).

(12) C. A. Coulson and J. Duchesne, *Bull. Acad. Roy. Med. Belg.*, **43**, 522 (1957).

(13) M. Green and J. W. Linnett, *Trans. Faraday Soc.*, **57**, 10 (1961).

(14) H. A. Bent, *Inorg. Chem.*, **2**, 747 (1963).

(15) (a) R. D. Brown and R. D. Harcourt, *Australian J. Chem.*, **16**, 737 (1963); (b) R. D. Brown and R. D. Harcourt, *ibid.*, **18**, 1115 (1964); (c) R. D. Brown and R. D. Harcourt, *ibid.*, **18**, 1885 (1965).

method deals with excited states with a limited success only, it could not be hoped to treat the problem of the electronic spectrum of NO_2 in its entirety. Our main concern has been the ground state, but it was also hoped that the method might be appropriate for the study of the few first low-lying excited states of NO_2 . In particular, it was of interest to investigate whether the method could provide an explanation for the disappearance of the intense brown color when one goes from the compound to its dimer.

NO_2 , NO_2^+ , and NO_2^-

In his famous series of papers concerned with the electronic structure and spectra of polyatomic molecules,¹⁷ Walsh discussed the electronic structure of these three species in the framework of the correlation diagram he suggested for AB_2 molecules. Walsh interpreted the change in bond angle in the series NO_2^+ (180°), NO_2 (134°), NO_2^- (114°) in terms of the slopes of the orbital energies. One of our main objectives was to determine whether extended Hückel calculations would substantiate Walsh's diagram. The nature of the orbital containing the unpaired electron in NO_2 is of course related to this question. In 1957, in order to explain the peculiarities of the NN bond in N_2O_4 , Coulson and Duchesne¹² proposed for the electronic structure of NO_2 a model different from that of Walsh;¹⁷ the unpaired electron was placed in the $1a_2$ orbital, whereas Walsh (as well as Mulliken¹⁸) places it in the $4a_1$ orbital. Then Green and Linnett^{3b} carried out a quantitative treatment, essentially based on the extended Hückel method but different from the Hoffmann procedure in the construction of the elements of the Hamiltonian matrix. A feature of Green and Linnett's treatment was also the neglect of all overlap integrals when solving the secular determinant. Their calculations indicated that the $1a_2$ orbital lies lower than the $4a_1$ orbital; in the ground state of the molecule the latter orbital is singly occupied in agreement with Walsh's scheme.

Recently, Kato, Yonezawa, Morokuma, and Fukui⁴ used the Hoffmann procedure to obtain the molecular orbitals in the three species considered here; they agree with Linnett on the symmetry of the orbital containing the unpaired electron, although some differences appear in the ordering of the levels. Kato, *et al.*, made their calculations for the experimental geometrical configurations of the molecules and they used a value of 1.75 for the constant K which appears in the Wolfsberg-Helmholtz formula¹⁹ for the nondiagonal elements of the Hamiltonian matrix

$$H_{ij} = 1/2KS_{ij}(H_{ii} + H_{jj})$$

We decided to extend the treatment by varying the bond angle in order to be able to make a comparison with Walsh's diagram; furthermore, we have investigated the effect of the variation of the parameter K on the results.

The ONO angle has been varied from 90 to 180° , keeping the NO bond length equal to the value of 1.20 Å it has in nitrogen dioxide. The variations in bond length when going from the molecule²⁰ to its positive²¹ or negative²² ion are so small (0.05 Å at most) that for our purposes it is unnecessary to take them into account. For the diagonal elements of the Hamiltonian matrix we have adopted the same values as Kato, *et al.*,⁴ namely, the ionization potentials associated with the valence states sp^2pp and sp^2p^2p of nitrogen and oxygen, respectively; the figures used for the ionization potentials were those calculated by Skinner and Pritchard²³

$$\begin{aligned} H_{ii}(\text{N}, 2s) &= -27.5 \text{ ev} & H_{ii}(\text{N}, 2p) &= -14.5 \text{ ev} \\ H_{ii}(\text{O}, 2s) &= -35.3 \text{ ev} & H_{ii}(\text{O}, 2p) &= -17.8 \text{ ev} \end{aligned}$$

The more recent values computed by Hinze and Jaffé²⁴ are close to those given by Skinner and Pritchard and their utilization would certainly not modify the results significantly. In the calculation of the overlap integrals the atomic orbitals were given Slater orbital exponents.

Figures 1 and 2 give a plot of the orbital energies vs. the bond angle for $K = 1.75$ and $K = 2.00$, respectively. For comparison, Walsh's diagram for AB_2 molecules¹⁷ is reproduced in Figure 3. If one considers the linear case first, one notices that, except for the inversion of the $2\sigma_u$ and $1\pi_u$ orbitals, the ordering of the levels resulting from the extended Hückel treatment is the same as that predicted by Walsh. *Ab initio* calculations,²⁵ in agreement with ours, also indicate that the $2\sigma_u$ orbital is actually above the $1\pi_u$ orbital. If one now considers the changes in the orbital energies taking place when the molecule bends, there is a general agree-

(16) R. Hoffmann, *J. Chem. Phys.*, **39**, 1397 (1963).

(17) A. D. Walsh, *J. Chem. Soc.*, 2260 (1953), and following papers.

(18) R. S. Mulliken, *Can. J. Phys.*, **36**, 10 (1958).

(19) M. Wolfsberg and L. Helmholz, *J. Chem. Phys.*, **20**, 837 (1952).

(20) G. R. Bird, J. C. Baird, A. W. Jache, J. A. Hodgeson, R. F. Curl, Jr., A. C. Kunkle, J. W. Bransford, J. Rastrup-Andersen, and J. Rosenthal, *ibid.*, **40**, 3378 (1964).

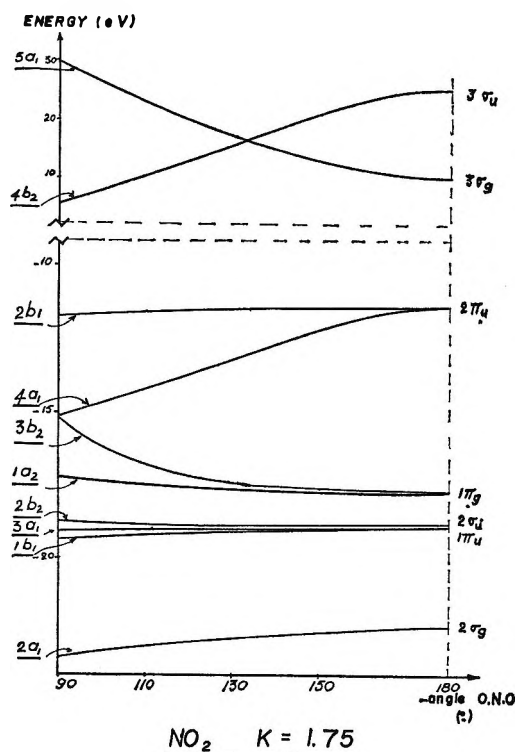
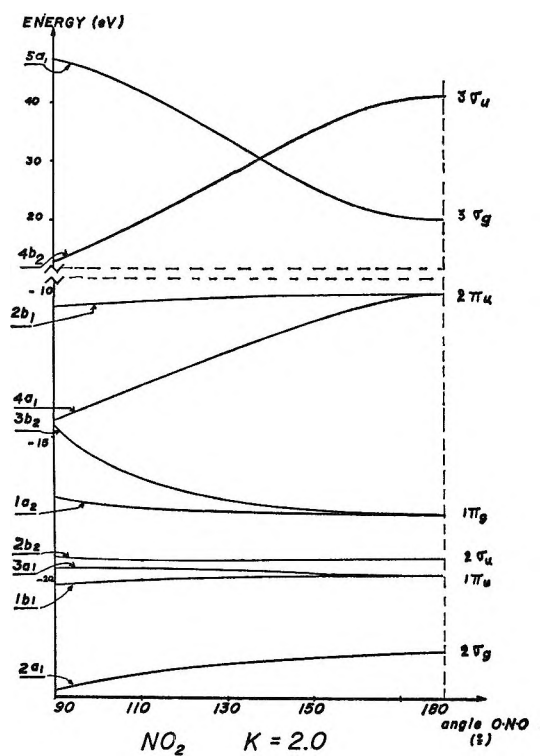
(21) E. Grison, K. Eriks, and J. L. de Vries, *Acta Cryst.*, **3**, 290 (1950).

(22) (a) G. B. Carpenter, *ibid.*, **5**, 132 (1952); (b) M. R. Truter, *ibid.*, **7**, 73 (1954).

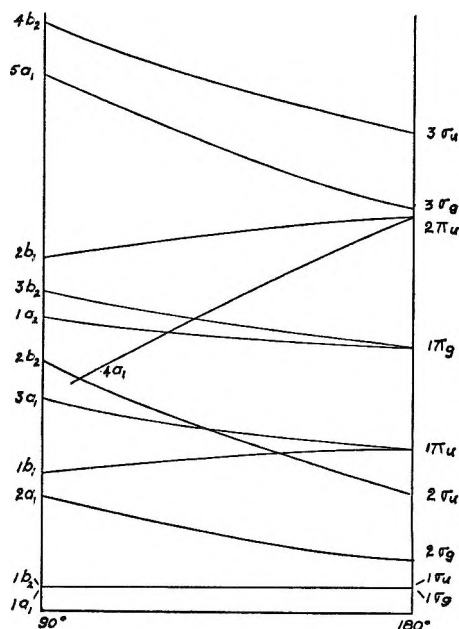
(23) H. A. Skinner and H. O. Pritchard, *Chem. Rev.*, **55**, 745 (1955).

(24) J. Hinze and H. H. Jaffé, *J. Am. Chem. Soc.*, **84**, 540 (1962).

(25) E. Clementi and A. D. McLean, *J. Chem. Phys.*, **39**, 323 (1963).

Figure 1. Orbital energies vs. bond angle; $K = 1.75$.Figure 2. Orbital energies vs. bond angle; $K = 2.00$.

ment between the two sets of curves, although a few differences show up. First, it is seen that the $2\sigma_g$

Figure 3. Walsh diagram for AB_2 molecules.

($2a_1$) orbital is stabilized when the bond angle changes to 90° , while Walsh predicts the opposite effect. The same discrepancy has been reported for this orbital in molecules of the AH_2 type by Peyerimhoff, Buenker, and Allen.²⁶ These authors point out that Walsh made a crude oversimplification when he postulated that the larger amount of s character an orbital contains the more binding it is: the effect of p_z mixing is to polarize the charge more into the triangle formed by the bonds, which makes $2a_1$ more bonding than $2\sigma_g$. They also show, on the basis of the SCF molecular orbitals they computed, that there is no justification for Walsh's assumption that the $2a_1$ orbital does not contain any contribution from the $2s$ atomic orbital of the apex atom when the bond angle is equal to 90° . Their argument, which accounts for the behavior of the $2a_1$ orbital as a function of the bending in AH_2 molecules, applies equally well to the orbitals we obtain for NO_2 .

Another discrepancy is noticed in the behavior of the $3\sigma_u$ ($4b_2$) orbital, which Walsh predicted to be more binding in the linear configuration; we find the opposite effect. Walsh's argument was based on the fact that this orbital is both $\text{N} \leftrightarrow \text{O}$ and $\text{O} \leftrightarrow \text{O}$ antibonding, since it is built from the out-of-phase overlap of orbitals centered on the exterior atoms which are themselves overlapping out of phase with a $2p_y$ orbital on the central atom. Walsh reasoned that since no

(26) S. D. Peyerimhoff, R. J. Buenker, and L. C. Allen, *J. Chem. Phys.*, **45**, 734 (1966).

Table I: Bond Angles in NO_2 and NO_2^-

NO_2			$\alpha_{\text{exptl}}^{20}$	NO_2^-			$\alpha_{\text{exptl}}^{21}$
α_{calcd}				α_{calcd}			
$K = 1.50$	$K = 1.75$	$K = 2.00$		$K = 1.50$	$K = 1.75$	$K = 2.00$	
116.0°	125.5°	131.8°	134.25°	104.9°	111.6°	115.6°	116°

change of hybridization is involved when the angle changes, the $\text{O} \leftrightarrow \text{O}$ antibonding nature of the orbital should be the major factor to be considered. This then would make the orbital more stable when the two outer atoms are as far apart as possible. However, by using an argument somewhat similar to that of Peyerimhoff, Buenker, and Allen,²⁶ it can easily be seen that when the angle is decreased there is at the same time a decrease in the overlap between the nitrogen p_y orbital and the oxygen orbitals, which reduced the $\text{N} \leftrightarrow \text{O}$ antibonding effect. This factor is actually larger than the one due to the $\text{O} \leftrightarrow \text{O}$ antibonding nature of the orbital, as our calculations indicate. This is not too surprising, since the $\text{O} \leftrightarrow \text{O}$ antibonding character concerns nonbonded atoms, while the effect we are considering involves the overlap between orbitals on adjacent atoms.

A further discrepancy lies in the behavior of the $2\pi_u$ ($4a_1$) orbital, whose energy curve is much steeper in the Walsh diagram than in ours. The energy of the corresponding orbital in the AH_2 molecules,²⁷ as computed by Peyerimhoff, Buenker, and Allen,²⁶ is also found to decrease less sharply than predicted by Walsh. Peyerimhoff, *et al.*, by using essentially the argument we have briefly summarized above, provide a pertinent explanation for the observed situation.

It is of interest to note that Walsh's original idea of utilizing the correlation diagrams to predict the shapes of molecules can be applied successfully to the curves we have computed to study the changes in geometry when one goes along the series NO_2^+ , NO_2 , NO_2^- .

NO_2^+ is correctly predicted to be linear in its ground state,²⁸ for which the electronic configuration is

$$(1\sigma_g)^2(1\sigma_u)^2(2\sigma_g)^2(1\pi_u)^4(2\sigma_u)^2(1\pi_g)^4$$

In the first excited state of the ion an electron is excited from the $1\pi_g$ to the $2\pi_u$ orbital. Due to the steep slope of the $4a_1$ component of the latter, the ion is predicted to adopt a bent form, with a bond angle in the vicinity of 120° .²⁹

In the ground state of NO_2 the unpaired electron is located in the $4a_1$ ($2\pi_u$) orbital, which again causes the system to become angular; the electronic configuration of NO_2 is thus

$$(1a_1)^2(1b_2)^2(2a_1)^2(1b_1)^2(3a_1)^2(2b_2)^2(1a_2)^2(3b_2)^2(4a_1)$$

The bond angle is larger than in the first excited state of NO_2^+ due to the double occupancy of the $3b_2$ ($1\pi_g$) orbital. In NO_2^- the extra electron is allotted to the $4a_1$ orbital which now becomes doubly occupied and this decreases the bond angle. Quantitatively, there is a good agreement with the experimental values for the bond angle, as appears from Table I. One sees that an increase of the parameter K moves the angle toward the experimental values; for $K = 2.00$, the agreement is quite good for both species. Since the position of the energy minimum is predicted with a good accuracy, an interesting question was whether this would also apply to the curvature of the potential curve. It has been observed that the bending force constant increases steadily in the series NO_2^+ , NO_2 , NO_2^- .³⁰⁻³³ It was of interest to see if our treatment would at least account for this trend. Table II summarizes the results for $K = 2.00$. In view of the fact that the calculations are based on very small variations of a large quantity, we feel that the agreement we obtain must be considered gratifying.

Table II: Bending Force Constants in NO_2^+ , NO_2 , and NO_2^-

	F_α/d^2 , 10^5 dynes/cm	
	Calcd	Obsd
NO_2^+	0.26	0.42 ³⁰
NO_2	0.92	1.10 ³¹
NO_2^-	1.78	1.64-1.75, ³² 2.5 ³³

(27) In the AH_2 systems this orbital is $1\pi_u$ ($2a_1$).(28) See R. J. Gillespie and D. J. Allen, *Quart. Rev. (London)*, **2**, 277 (1948).(29) The existence of a bent excited state of NO_2^+ has been suggested in order to explain the high value obtained for the ionization potential of NO_2 by the electron impact method. See J. Collin and F. P. Lossing, *J. Chem. Phys.*, **28**, 900 (1958); J. Collin, *ibid.*, **30**, 1621 (1959).(30) R. Teranishi and J. C. Decius, *J. Chem. Phys.*, **22**, 896 (1954).(31) R. E. Weston, *ibid.*, **26**, 1248 (1957); E. Arakawa and H. Nielsen, *J. Mol. Spectry.*, **2**, 413 (1958).(32) R. E. Weston and T. F. Brodasky, *J. Chem. Phys.*, **27**, 683 (1957).(33) J. W. Sidman, *J. Am. Chem. Soc.*, **79**, 2675 (1957).

Table III: Orbital Energies and Lcao Expressions for the Molecular Orbitals^a

Label	Orbital energy, ev	The lcao expression
$K = 1.75$		
1a ₁	-39.89	$0.4136s_N + 0.0224z_N + 0.5128(s_O + s_{O'}) - 0.007(z_O + z_{O'}) - 0.0016(y_O - y_{O'})$
1b ₂	-35.50	$0.1833y_N + 0.6407(s_O - s_{O'}) + 0.0137(z_O - z_{O'}) + 0.0323(y_O + y_{O'})$
2a ₁	-22.72	$0.4607s_N - 0.1961z_N - 0.3428(s_O + s_{O'}) - 0.2278(z_O + z_{O'}) - 0.4099(y_O - y_{O'})$
1b ₁	-19.13	$0.4154x_N + 0.5691(x_O + x_{O'})$
3a ₁	-19.00	$0.0564s_N - 0.3719z_N + 0.0604(s_O + s_{O'}) - 0.4676(z_O + z_{O'}) + 0.3539(y_O - y_{O'})$
2b ₂	-18.87	$0.2257y_N - 0.1300(s_O - s_{O'}) - 0.4055(z_O - z_{O'}) - 0.4594(y_O + y_{O'})$
1a ₂	-17.70	$0.7099(x_O - x_{O'})$
3b ₂	-17.49	$0.0564y_N - 0.0043(s_O - s_{O'}) + 0.5488(z_O - z_{O'}) - 0.4562(y_O + y_{O'})$
4a ₁	-13.05	$0.3118s_N - 0.8115z_N - 0.0228(s_O + s_{O'}) + 0.4866(z_O + z_{O'}) + 0.0366(y_O - y_{O'})$
2b ₁	-11.52	$0.9488x_N - 0.4564(x_O + x_{O'})$
$K = 2.00$		
1a ₁	-42.34	$0.4472s_N + 0.0375z_N + 0.4858(s_O + s_{O'}) - 0.0085(z_O + z_{O'}) - 0.0204(y_O + y_{O'})$
1b ₂	-36.56	$0.2627y_N + 0.6032(s_O - s_{O'}) + 0.0109(z_O - z_{O'}) + 0.0329(y_O + y_{O'})$
2a ₁	-22.82	$0.3840s_N - 0.2246z_N - 0.3377(s_O + s_{O'}) - 0.2694(z_O + z_{O'}) - 0.4177(y_O - y_{O'})$
1b ₁	-19.88	$0.4644x_N + 0.5444(x_O + x_{O'})$
3a ₁	-19.64	$0.0559s_N - 0.4061z_N + 0.0890(s_O + s_{O'}) - 0.4282(z_O + z_{O'}) + 0.3744(y_O - y_{O'})$
2b ₂	-19.29	$0.2702y_N - 0.1631(s_O - s_{O'}) - 0.3974(z_O - z_{O'}) - 0.4655(y_O + y_{O'})$
1a ₂	-17.66	$0.7099(x_O - x_{O'})$
3b ₂	-18.39	$0.0541y_N - 0.0046(s_O - s_{O'}) + 0.5547(z_O - z_{O'}) - 0.4492(y_O + y_{O'})$
4a ₁	-11.94	$0.2976s_N - 0.8089z_N - 0.0156(s_O + s_{O'}) + 0.5015(z_O + z_{O'}) - 0.0074(y_O - y_{O'})$
2b ₁	-10.22	$0.9257x_N - 0.4856(x_O + x_{O'})$

^a The system of axes used is the following one: z along the binary axis, y perpendicular to z in the molecular plane and pointing in the direction of oxygen O, x perpendicular to the molecular plane.

The increase of the force constant associated with the progressive allotment of electrons in the 4a₁ orbital is certainly accounted for in a satisfactory manner.

The simple extended Hückel scheme can thus deal reasonably well with the changes in energy associated with angular distortions in the systems considered in spite of the fairly large number of electrons they contain. We can take advantage of this situation to compute the adiabatic ionization potential of NO₂. In the method used in this work, the vertical ionization potential is merely equal to minus the orbital energy of the highest occupied molecular orbital. This provides a value of 11.94 eV for $K = 2.00$. In order to obtain the adiabatic ionization potential, one has to subtract from this quantity the difference in energy between the bent ion and the linear equilibrium configuration of NO₂⁺. This difference amounts to 0.96 eV, which provides the value of 10.98 eV for the adiabatic potential. The experimental determinations of the ionization potential of NO₂ have yielded various discordant values, ranging from 9.78 to 13.98 eV. One of the most reliable values seems to be that recently determined by Al-Jaboury and Turner,² which was obtained by photoelectron spectroscopy. They give an adiabatic

potential of 10.97 eV, which coincides with our calculations. It is to be noted that utilization of $K = 1.75$ in building the nondiagonal matrix elements leads to a vertical potential of 13.05 and an adiabatic potential of 12.54. As in the calculation of the bond angle and of the bending force constant, an increase of K to the value of 2.00 brings a considerable improvement of the result. This value for K thus seems to lead to a sound picture of the electronic structure of the species in their ground state. The positions of the occupied molecular orbitals, as well as their variation with bending, appear to be described with good accuracy.

It can be noticed from Figures 1 and 2 that the increase of K , while not affecting significantly the energies of the orbitals from 2a₁ to 3b₂, raises 4a₁ and 2b₁. The two highest orbitals, 5a₁ and 4b₂, are raised considerably but they already lie too high for $K = 1.75$ and are valueless anyway for spectral predictions. The electronic transitions involving 4a₁ and 2b₁ will be discussed in the next section dealing with the dimer.

The expressions for the mo's up to 2b₁ are given in Table III for a bond angle of 134°. With regard to the 4a₁ orbital, which contains the unpaired electron in NO₂, the lcao coefficients of the nitrogen atomic or-

bitals appear to be relatively too large. The method thus gives a large pile-up of odd electron density around the nitrogen atom, which is not in agreement with recent estimates based on electron paramagnetic measurements.^{34,35}

N₂O₄

We will be concerned here with the most stable form of the dimer, whose peculiar feature is a long, weak, central NN bond. The structure of this molecule poses a few intriguing questions. If oxygen-oxygen repulsions are the primary cause of bond weakening, then one might expect the molecule to adopt a skew configuration. It does not, but the energy advantage of the planar over the twisted form is small (the barrier to internal rotation has been estimated by Snyder and Hisatsune³⁶ to be 2.9 kcal/mole), which perhaps does indicate a delicate compromise between π bonding and oxygen-oxygen repulsions. The exact nature of the antibonding factors causing the bond to be so weak is not known. Several models have been proposed for this anomalous bond, which we will merely list briefly: " π -only" bond, involving no σ bond at all;¹² splayed single bond;¹⁴ and delocalization of the electrons of the $2p\pi$ orbitals of the oxygens into the antibonding NN σ orbital;¹⁵ Green and Linnett¹³ have also carried out a semiempirical treatment of N₂O₄ based on the same approach as their treatment of nitrogen dioxide.^{3b} Their calculations indicate that the NN bond is essentially σ in nature, although the $4a_1$ orbital of NO₂ is found practically not to contribute to the bonding. Some π bonding is also found, not only above and below the plane, but also in it.

Since in the Hückel method the total energy is obtained by merely adding the orbital energies of the occupied levels, a simple picture of the binding in a molecule can be arrived at by breaking down the energy among the various molecular orbitals. This is precisely what we have done with the dimerization energy in order to analyze the bonding and antibonding effects produced by each orbital of NO₂ upon dimerization. In a similar fashion, we have computed the contribution of each occupied orbital in N₂O₄ to the overlap population for the NN bond. This was done with the purpose of verifying whether the picture of the NN bond emerging from energy considerations would be consistent with that one based on the electron density distribution.

Calculations have been carried out for the three values of K used in the study of NO₂. Qualitatively, the three sets of results are essentially the same. As for the geometry of the molecule, we have adopted for the NO bond length and for the ONO angle the values

determined by Smith and Hedberg in the gas phase,¹¹ namely $r_{NO} = 1.18$ Å and $ONO = 133.7^\circ$. The NN distance has been varied so as to minimize the energy. The bond length calculated this way is fairly insensitive to the value of the parameter K . The values of 1.50, 1.75, and 2.00 for K give bond lengths equal to 1.504, 1.491, and 1.488 Å, respectively. That those values are sensibly different from the observed bond length of 1.75 Å¹¹ is not too surprising since it is known that the extended Hückel method in general does not describe properly the variation of the molecular energy with bond stretching. Consequently, we have decided to study the binding by considering the orbitals obtained at the experimental internuclear distance. Figure 4 gives the position of the one-electron energies of N₂O₄ and NO₂ for $K = 1.75$ and $K = 2.00$. The labeling of the irreducible representations of the D_{2h} group is based on the following choice of coordinate axes: z axis along the NN bond, y axis perpendicular to the NN bond in the molecular plane, and x axis perpendicular to the molecular plane. The binding

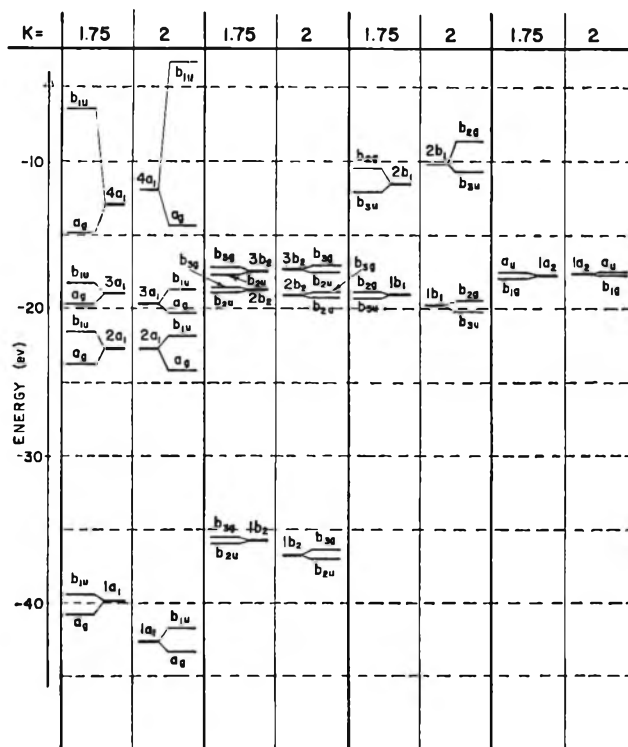


Figure 4. Splitting of orbital energies of NO₂ upon dimerization.

(34) P. W. Atkins, N. Keen, and M. C. R. Symons, *J. Chem. Soc.*, 2873 (1962).

(35) P. W. Atkins and M. C. R. Symons, *ibid.*, 4794 (1962).

(36) R. G. Snyder and I. D. Hisatsune, *J. Mol. Spectry.*, 1, 139 (1957).

appears to be largely due to the $4a_1$ orbital of NO_2 . The other a_1 orbitals (except $3a_1$) also contribute to the σ -type bonding, but to a smaller extent. In addition, there is some π bonding, originating from the $1b_1$ orbital of NO_2 . It is definitely weaker than the one associated with the σ bond, which is in agreement with the fairly low barrier of 3 kcal/mole hindering internal rotation. On the other hand, the b_2 orbitals give rise to a destabilization, which appears to be the main negative factor. It seems plausible to us to consider this effect as the reason for the weakness of the NN bond. All three b_2 orbitals of NO_2 act in the same direction. The $3a_1$ orbital also gives some destabilization; this is the effect which has been proposed by Brown and Harcourt¹⁵ to play a major part in the small stability of the system. According to this calculation, the antibonding effect due to the b_2 orbitals appears to be larger. Table IV summarizes the contributions

Table IV: Contributions (in eV) from the Various Groups of Orbitals of NO_2 to the Energy of Dimerization

	$K = 1.75$	$K = 2.00$
a_1	4.44	5.96
b_2	-0.35	-0.32
b_1	0.33	0.48
a_2	-0.05	-0.07
Total	4.37	6.05

from the various groups of orbitals to the energy of dimerization. Obviously the results obtained must be accepted on a qualitative basis only. The computed energy of dimerization is much too large; one of the reasons for this discrepancy is that the charge distribution in the odd-electron orbital $4a_1$ is too much concentrated around the nitrogen atom, which gives too large a contribution to the NN binding from this orbital.³⁷ Although the absolute values in Table IV cannot be trusted, the relative importance of the various factors seems to be reasonable and meaningful. The results of the electron population analysis for the NN bond, indicated in Table V, certainly support this point. Here again, the σ bonding seems to be exaggerated, but there emerges a picture involving a weak π bond superimposed on a σ bond, while the $2p_v$ orbitals of the nitrogens give some destabilization.

Let us now consider the spectral changes accompanying the formation of the dimer. For this question also, quantitative predictions cannot be made in view of the general inadequacy of the extended Hückel method

Table V: Contributions from the Various Groups of Orbitals of NO_2 to the Overlap Population of NN

	$K = 1.75$	$K = 2.00$
a_1	0.437	0.440
b_2	-0.001	-0.001
b_1	0.004	0.005
a_2	0	0
Total	0.440	0.444

for spectral calculations. The first spectral transitions in NO_2 are computed as

	$K = 1.75$	$K = 2.00$
$4a_1 \rightarrow 2b_1$	1.53 eV	1.72 eV
$3b_2 \rightarrow 4a_1$	4.44 eV	5.45 eV
$1a_2 \rightarrow 4a_1$ (forbidden)	4.64 eV	5.72 eV
$2b_2 \rightarrow 4a_1$	5.82 eV	7.34 eV
$3a_1 \rightarrow 4a_1$	5.95 eV	7.70 eV
$3b_2 \rightarrow 2b_1$ (forbidden)	5.97 eV	7.17 eV
$1b_1 \rightarrow 4a_1$	6.07 eV	7.94 eV
$1a_2 \rightarrow 2b_1$	6.17 eV	7.44 eV

The first two transitions contribute probably to the visible spectrum of the molecule.^{17,18} Walsh¹⁷ suggests that the fourth transition also contributes to the long-wavelength spectrum.

As can be seen from Figure 4, a consequence of the stabilization associated the $4a_1$ orbital is to shift the first transition toward the ultraviolet region. Taking into account the double occupancy of the $4a_g$ orbital in N_2O_4 , one sees immediately that the next four transitions will exhibit an even larger shift. The observed loss of color accompanying the dimerization is thus easily explained on the basis of this simple model. As we have indicated above, the stabilization of the $4a_1$ orbital is probably exaggerated and for this reason the discussion can only be limited to qualitative arguments.

The energy of the 90° -twisted system has also been computed, keeping the NN bond length equal to 1.75 Å and using a value of $K = 1.75$. The barrier to internal rotation was found this way equal to 1.76 kcal/mole, which is to be compared with the estimate of 2.9 kcal/mole made by Snyder and Hisatsune.³⁶

Conclusions

The present work shows that the simple Hückel method properly describes most, but not all, of the features of the systems studied. A series of properties

(37) On the other hand, Green and Linnett's treatment indicated no bonding at all associated with this orbital,¹³ which seems to be another extreme.

of the ground states of NO_2^+ , NO_2 , and NO_2^- are properly accounted for. As for the planar dimer, some insight into the nature of the central bond and into the reason for the low stability of the molecule has been obtained. An obvious shortcoming of the method lies in the poor quality of the charge distribution, which is particularly exemplified in the $4a_1$ orbital of NO_2 . A refinement which would probably improve this situation would consist in modifying the Hamiltonian matrix elements according to the charges on the atoms and in applying an iterative procedure until self-consistency is reached between the atomic charges and the matrix elements.³⁵

Although the predictions of this work, like those of all semiempirical calculations, must not be trusted too far, it is worth pointing out that the approach

followed here may be helpful in future *a priori* calculations. Such calculations on systems of the size considered here are necessarily laborious and expensive; any guidelines are worthwhile.

Acknowledgments. The calculations have been carried out on the CDC 6600 computer of the Courant Institute of New York University. A grant of computer time from the NYU AEC Computing Center is gratefully acknowledged. We are also thankful to Mr. J. R. Hamann who has written the extended Hückel program.

(38) See, for instance, D. G. Carroll, A. T. Armstrong, and S. P. McGlynn, *J. Chem. Phys.*, **44**, 1865 (1966); H. Basch, A. Viste, and H. B. Gray, *ibid.*, **44**, 10 (1966); R. Rein, N. Fukuda, and G. A. Clarke, *ibid.*, **45**, 4743 (1966).

Inhibited Autoxidation of Squalane

by James C. W. Chien

Research Center, Hercules Incorporated, Wilmington, Delaware 19899 (Received December 27, 1966)

The induction period observed in inhibited autoxidation of cumene corresponds to the scavenging of two radicals by the inhibitor (hindered phenols). The induction periods are several times longer when the substrate is squalane, cyclohexene, dicyclohexyl, or 2,4,6-trimethylnonane. This increase is larger at high concentrations of the initiator and the inhibitor. Addition of chlorobenzene, methyl benzoate, or diphenyl ether reduces the induction period to the normal values. The results are interpreted to mean that the inhibition stoichiometry is not invariant and is dependent upon these experimental variables.

Introduction

Several investigators have demonstrated that, in inhibited autoxidations, each inhibitor molecule reacts with two chain-carrying radicals. Thus, the inhibition stoichiometric factor, n , was found to be equal to 2 in the hydroquinone-inhibited autoxidation of benzaldehyde¹ and of ethyl linoleate.² Similar results were obtained³ in cumene oxidation inhibited by 2,6-di-*t*-butyl-4-*m*-ethylphenol.

A value of $n = 2$ implies that all radicals terminate by reacting with the inhibitor. Under these circumstances, the efficiency of an initiator can be determined

(1) T. A. Ingles and H. W. Melville, *Proc. Roy. Soc. (London)*, **A218**, 163, 175 (1953).

(2) J. L. Bolland and P. ten Have, *Trans. Faraday Soc.*, **43**, 20 (1947).

(3) C. E. Boozer, G. S. Hammond, C. E. Hamilton, and J. N. Sen, *J. Am. Chem. Soc.*, **77**, 3233, 3238 (1955).

by measuring the induction period. In order to establish the general validity of this stoichiometry, we have investigated the inhibited autoxidations of several aliphatic substrates. This paper describes those conditions where apparent departures from $n = 2$ stoichiometry were observed.

Results

Many cumene oxidations initiated by di-*t*-butyl peroxide (DTBP) or α, α' -bis(isobutyronitrile) (AIBN) were carried out at 62–110° with chlorobenzene as the solvent. The rates of oxidation and the rate constant ratio obtained are in complete agreement with literature values.³ In the presence of inhibitor such as 2,6-di-*t*-butyl-4-methylphenol, the observed induction periods correspond to $n = 2$, regardless of the initiator used. The value of n is calculated from the equation

$$n = 2\alpha[\text{initiator}]_0[1 - \exp(-k_d t_{\text{ind}})]/[\text{IH}]_0 \quad (1)$$

where k_d is the rate constant of decomposition of the initiator and α is the fraction of radical in the decomposition which escapes primary cage recombinations.

The rate of decomposition of AIBN and the value of n were measured by the rate of nitrogen evolution and the disappearance of iodine added as scavenger. The results obtained from 52.5 to 82.5° are in excellent agreement with the literature values.⁴

The rate of decomposition of DTBP in squalane was measured from 100 to 145°. The disappearance of DTBP and the formation of products were followed by gas chromatography. The reaction is first order in DTBP concentration to better than 95% completion. The results (Figure 1) are in good agreement with those reported⁵ in other solvents. The gas-phase decomposition rates, also shown in the figure, are about 30% slower than the others. It is assumed that there is no appreciable cage recombination of *t*-butoxy radicals and that $\alpha = 1$ in eq 1.

In the gas phase, the decomposition product is predominantly acetone;⁴ the products in aromatic solvents are mixtures of *t*-butyl alcohol and acetone. In squalane, the only product detected is *t*-butyl alcohol; acetone was not formed in measurable quantities at the experimental temperatures.

The induction periods in squalane oxidation inhibited by either 2,6-di-*t*-butyl-4-methylphenol (I), 2,6-di-*t*-butylphenol (II), or 2,4,6-tri-*t*-butylphenol (III) are appreciably longer than the corresponding reaction in cumene-chlorobenzene (Table I). The calculated values of n increase with the increase of inhibitor concentration (runs 7–13) and of initiator concentration (runs 2–4).

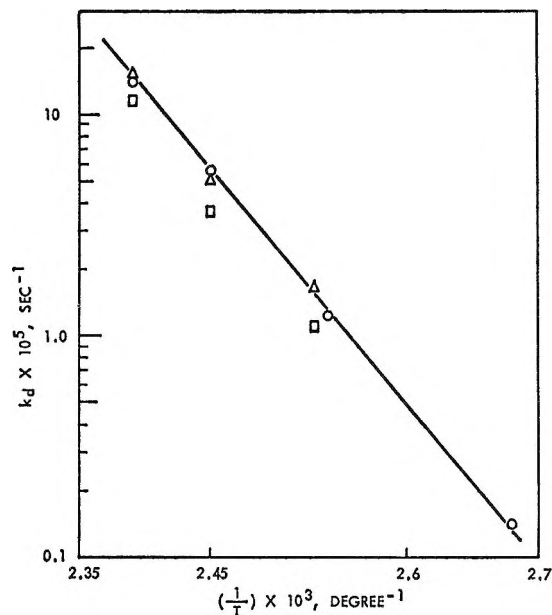


Figure 1. Rate constants for the decomposition of DTBP: O, in squalane; Δ , in cumene;⁵ \square , in the gas phase.⁵

The changes in the rate of oxygen uptake at the end of the induction period in all the experiments are abrupt; the maximum rates⁶ are given in column 7 of Table I. From this rate and with the known rates of initiation, the rate constant ratio $k_p/k_t^{1/2}$ is calculated by

$$\frac{k_p}{k_t^{1/2}} = \left(\frac{2}{R_i}\right)^{1/2} \left[\left(-\frac{dO_2}{dt}\right)_m - \frac{R_i}{2} \right] / [\text{RH}] \quad (2)$$

where k_p is the rate constant for hydrogen abstraction, k_t is the rate constant for termination, and R_i is the rate of initiation. The variation of the density of squalane with temperature was measured and introduced in this calculation (see the Experimental Section). Figure 2 is the Arrhenius plot of the results, from which we find $E_p - 1/2E_t = 16 \text{ kcal mole}^{-1}$.

During the induction period, the rates of oxidation are slow but measurable. These rates were found to be approximately equivalent to the rates of decomposition of the initiator (compare columns 6 and 7 of Table I).

Addition of chlorobenzene markedly reduces the induction period. A stoichiometric factor of $n = 2$ was obtained in mixtures of squalane containing 50% or more of chlorobenzene. Table II and Figure 3 give these results, where phenol I was the inhibitor. Chloro-

(4) G. S. Hammond, J. N. Sen, and C. E. Boozer, *J. Am. Chem. Soc.*, **77**, 3244 (1955).

(5) J. H. Raley, F. F. Rust, and W. E. Vaughan, *ibid.*, **70**, 1336 (1948).

(6) A. V. Tobolsky, D. J. Metz, and R. B. Mesrobian, *ibid.*, **72**, 1942 (1950).

Table I: Autoxidation of Squalane

Run no.	[DTBP], <i>M</i>	Inhibitor		Temp., °C	$\left(\frac{dO_2}{dt}\right)_i^a$ $\times 10^6$, <i>M sec</i> ⁻¹	R_i^b $\times 10^6$, <i>M sec</i> ⁻¹	t_{ind} $\times 10^{-1}$, sec	<i>n</i>	$\left(\frac{dO_2}{dt}\right)_m^c$ $\times 10^6$, <i>M sec</i> ⁻¹	$(k_p/k_t^{1/2})$ $\times 10^2$, <i>l.</i> ^{1/2} mole ^{-1/2} sec ^{-1/2}
		Phenol	Concn $\times 10^3$, <i>M</i>							
1	0.015	None	...	140			...	61	2.2	
2	0.01	I	3.0	140	1.2	1.8	5.2	2.5	69	3.6
3	0.024	I	1.2	140	4.8	4.3	1.1	3.8	91	2.7
4	0.06	I	3.0	140			2.0	6.6		
5	0.1	I	3.0	140			0.86	4.7		
6	0.01	None	...	125			19	1.0
7	0.2	I	0.2	125			0.13	3.6		
8	0.2	I	0.8	125			0.56	4.6	43	0.93
9	0.2	I	2.7	125			2.4	5.2	39	0.87
10	0.2	I	6.0	125			10.5	10.8		
11	0.2	I	9.0	125			12.5	9.0		
12	0.2	I	15.0	125			27.0	11.0		
13	0.2	I	30.0	125			88.0	10.0		
14	0.5	None	...	115			5.0	1.2
15	0.02	I	1.0	110	0.21	0.11	34.0	3.6		
16	1.0	None	...	95			4.0	0.24
17	0.5	I	1.0	95	0.21	0.38	14.0	5.5	3.9	0.37
18	1.0	None	...	85			1.9	0.22
19	1.0	I	0.5	85			13.0	5.7	1.9	0.22
20	0.46	II	1.0	95	0.35	0.35	21.6	8.2	3.5	0.34
21	0.19	II	5.9	125			3.4	3.5	33	0.80
22	0.47	III	1.0	95			13.6	4.9	24	0.24
23	0.2	III	6.4	125	3.2	6.4	2.6	2.7		
24	0.2	III	6.3	125	3.3	6.4	2.5	2.6		

^a Rate of oxidation during induction period. ^b Rate of initiation. ^c Maximum rate of oxidation.

benzene also increases the value of $k_p/k_t^{1/2}$. Similar effects were observed when the inhibitor was phenol II or III (Table III).

Table II: Oxidation of Squalane in Chlorobenzene^a

Squalane, vol %	t_{ind} $\times 10^{-1}$, sec	<i>n</i>	$(-dO_2/dt)_m$ $\times 10^6$, sec ⁻¹	$(k_p/k_t^{1/2})$ $\times 10^2$, <i>l.</i> ^{1/2} mole ^{-1/2} sec ^{-1/2}
100	17.4	6.4	3.2	3.0
91	14.2	5.2	3.8	3.9
75	6.7	2.5	4.0	4.8
50	5.7	2.1	3.0	5.8
25	5.0	1.9	1.7	6.2

^a [DTBP] = 0.5 *M*; [phenol I] = 10⁻³ *M*; temperature = 95°.

Several other solvents were also found to reduce t_{ind} . When squalane was diluted with 25 vol % of diphenyl ether, *t*-butylbenzene, or methyl benzoate, the corresponding values of *n* were 2.6, 2.6, and 2.9, respectively. These experiments were carried out at

Table III: Effect of Chlorobenzene on Squalane Oxidation

[DTBP], <i>M</i>	Squalane, vol %	Inhibitor		Temp., °C	t_{ind} $\times 10^{-1}$, sec	<i>n</i>
		Phenol	Concn $\times 10^3$, <i>M</i>			
0.45	25	II	0.97	95	6.86	2.4
0.46	20	II	0.94	95	6.15	2.3
0.19	20	III	6.3	125	2.2	2.2
0.47	25	III	0.93	95	5.0	2.2

125° in the presence of 0.2 *M* DTBP and 3 $\times 10^{-3}$ *M* phenol I. Nitrobenzene, under the same conditions, gave an even shorter induction period, corresponding to a value of 0.9 for *n*.

Figure 3 shows an apparent dependence of *n* and of $k_p/k_t^{1/2}$ upon viscosity. This correlation is, however, found to be not a very important factor. Long induction periods were observed for three low-viscosity substrates—cyclohexene, dicyclohexyl, and 2,4,6-trimethylnonane. The viscosity of cyclohexene is nearly the same as that of chlorobenzene, being 0.797 and 0.707 cp at 30°, respectively. The autoxidation of cyclohexene–chlorobenzene mixture (1:2 volume ratio)

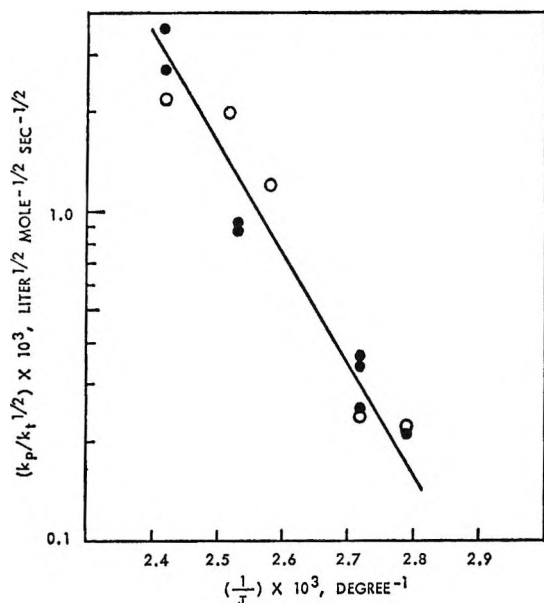


Figure 2. Variation of $k_p/k_t^{1/2}$ with temperature for squalane oxidation: O, uninhibited; ●, inhibited.

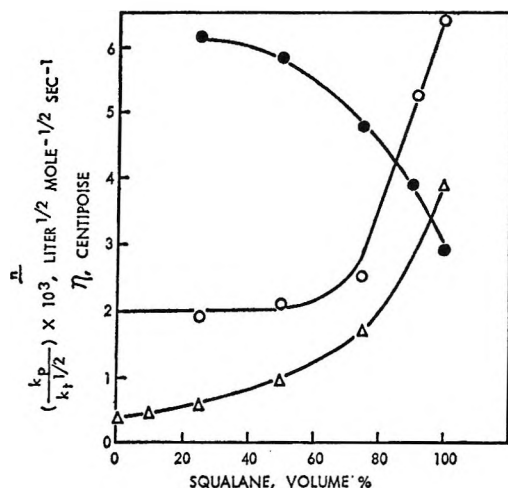


Figure 3. Variation of $k_p/k_t^{1/2}$ (●), viscosity (Δ), and n (○) with squalane concentration.

initiated by $1.07 \times 10^{-2} M$ AIBN in the presence of $5 \times 10^{-3} M$ phenol **I** has an induction period of 5.14×10^3 sec. The value of n is 1.8. The induction periods and values of n in neat cyclohexene under otherwise identical conditions are 18.4×10^3 sec and 6.0, respectively.

Similarly, in phenol **I**-inhibited autoxidations of neat dicyclohexyl and of 2,4,6-trimethylnonane, the observed induction periods correspond to values of $n = 3.2$ and 5.2, respectively. The initiator used here was DTBP. Dilution by 30% of chlorobenzene re-

duced the values of n to 2.1 and 2.0 for dicyclohexyl and 2,4,6-trimethylnonane, respectively.

Discussion of Results

The most significant observation made here is that the inhibited autoxidations of aliphatic substrates have unusually long induction periods. Various experimental artifacts which could increase the induction period have been examined.

Anomalously long induction periods could result from cage recombination of the initiator radicals in a viscous environment. This possibility was mitigated by the direct determinations of the rates of decomposition of the initiators and the attendant cage recombination efficiencies of the initiator radicals in the actual experimental systems. The stoichiometric factors were calculated using these measured quantities.

Since only *t*-butyl alcohol was found in the decomposition of DTBP in squalane, every *t*-butoxy radical must abstract hydrogen from the substrate. From the known reactivities⁷ of *t*-butoxy radical toward aliphatic hydrogens, secondary and tertiary alkyl radicals are produced in approximately the same ratio (9:7) leading to nearly equal amounts of secondary and tertiary peroxy radicals. It is unlikely that the peroxy radicals would be found in the same solvent cage because during the time it takes for hydrogen abstraction and reaction with oxygen to take place, the radical pair must have diffused out of the solvent cage and become separated. To the extent that these peroxy radicals are still in close vicinity and that a finite probability exists for their rapid termination, the value of n would be increased and the increase is larger in environment of higher viscosity. To resolve this uncertainty, three aliphatic substrates of low viscosities were studied. Those results indicate that geminal recombinations are generally unimportant.

If the initiator was appreciably depleted during the induction period, then the oxidation products could assume control of the initiation process and significantly alter the induction period and the apparent inhibition stoichiometry. In all the experiments reported here, t_{ind} is much shorter than the half-life of the initiator. Even in run 13 of Table I, t_{ind} is about one-half of the half-life of DTBP at this temperature. We have furthermore prepared squalane hydroperoxide and studied its thermal decomposition.⁸ Squalane hydroperoxide decomposes at the same rate as DTBP at 100°; the rate is about one-half that of DTBP at 135°. It appears that the oxidation product could

(7) A. L. Williams, E. A. Oberright, and J. W. Brooks, *J. Am. Chem. Soc.*, **78**, 1190 (1956).

(8) J. C. W. Chien and H. Jabloner, *ibid.*, in press.

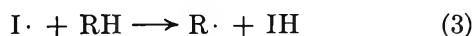
not significantly alter the rate of initiation. Non-hydroperoxidic oxidation products could conceivably affect the rates of propagation and of termination. The products cannot be present in amounts exceeding the amount of oxygen consumed during the induction period. This amount corresponds to 10^{-4} of the substrate concentration. The values of $k_p/k_t^{1/2}$ were found to be the same with or without added inhibitor (Figure 1). It is concluded that oxidation products are also not altering the courses of propagation and termination.

The possibility that the oxidation products of phenols are also scavengers of radicals was considered. Stilbenequinones derived from phenol **I** have been shown to inhibit autoxidations.⁹ This possibility can be rejected for the following reasons. Known oxidation chemistry of hindered phenols could not account for values of n larger than 3, yet values as high as 10 have been observed. It is difficult to rationalize the effect of aromatic solvents. Finally, phenol **III** which oxidizes quantitatively to 2,4,6-tri-*t*-butyl-4-peroxy-cyclohexadienone¹⁰ also gives $n > 2$.

Based upon these considerations, we conclude that the long induction periods are real and that the inhibition stoichiometric factors are apparently larger than those reported for other systems. Furthermore, this stoichiometry is sensitive to experimental variables such as initiator concentration, inhibitor concentration, temperature, and solvent. Therefore, inhibited autoxidation cannot be employed indiscriminately to determine rates of initiation.

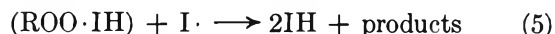
The mechanism responsible for the observed stoichiometry is not immediately evident. The dependence of n on inhibitor concentration implicates the inhibitor in higher than first-order reactions. The dependence on initiator concentration suggests the involvement of the chain-propagating radicals. The effect of chlorobenzene and other aromatic solvents can be interpreted to mean that the species responsible are stabilized thus preventing those reactions which lead to long induction periods.

An explanation which appears to be capable of explaining the above data is suggested by the proposal^{11,12} that phenol-inhibited autoxidation involves the reaction



where IH is the inhibitor. This reaction as written could not affect the inhibition stoichiometry. However, if a radical such as $I \cdot$ abstracts a neighboring hydrogen or the activated α hydrogen of the peroxy radical, the product of this reaction could be carboxylic acid or a stable cyclic peroxide. The value of

n would be effectively increased. This speculative mechanism may be represented by



where the species in the bracket is the complex postulated by Boozer, *et al.*³ Accordingly, the induction period should vary with the square of the inhibitor concentration. By assuming a reaction similar to eq 5 for the peroxy radical with recovery of the inhibitor, the dependence of n on the initiator concentration may be rationalized. Chlorobenzene and other aromatic solvents probably stabilize the radicals to prevent the postulated hydrogen abstraction reactions.¹³

There are at least two objections to the reactions postulated here to rationalize the results. First, hydrogen abstraction by phenoxy radical is known for unhindered phenols; it has not yet been established for hindered phenols. Second, if eq 5 is to be consequential, the α hydrogen of the peroxy radical must be sufficiently activated so that its abstraction can compete with the statistical reaction 3. Because of these difficulties, other experiments are underway to seek a better understanding of the processes involved in the inhibited autoxidations of aliphatic substrates.

Experimental Section

Materials. Squalane, chlorobenzene, cumene, cyclohexene, dicyclohexyl, α, α' -azobis(isobutyronitrile) (AIBN), 2,6-di-*t*-butyl-4-methylphenol, 2,6-di-*t*-butylphenol, and 2,4,6-tri-*t*-butylphenol were purchased from Eastman Organic Chemical Co. Di-*t*-butyl peroxide (DTBP) was obtained from Lucidol Co.

All the liquid compounds were fractionated at 100 theoretical plates. The middle constant-boiling ($\pm 0.1^\circ$) fraction was collected and stored at 0° in the dark. Dicyclohexyl and di-*t*-butyl peroxide were fractionated at reduced pressure.

Squalane was purified by stirring with concentrated sulfuric acid; the colored acid was replaced by fresh acid. This procedure was repeated until the acid remained colorless after 24 hr of stirring. After separation from the acid, the squalane was neutralized, washed, dried over anhydrous $MgSO_4$, and fractionated as above at reduced pressure. Infrared analysis detected no olefinic impurities.

(9) R. F. Moore and W. A. Waters, *J. Chem. Soc.*, 243 (1954).

(10) A. L. Bickel and E. C. Kooyman, *ibid.*, 3211 (1953).

(11) L. R. Mahoney and F. C. Ferris, *J. Am. Chem. Soc.*, **85**, 2345 (1963).

(12) W. G. Lloyd and C. E. Lange, *ibid.*, **86**, 1491 (1964).

(13) C. Walling and P. Wagner, *ibid.*, **85**, 2333 (1963).

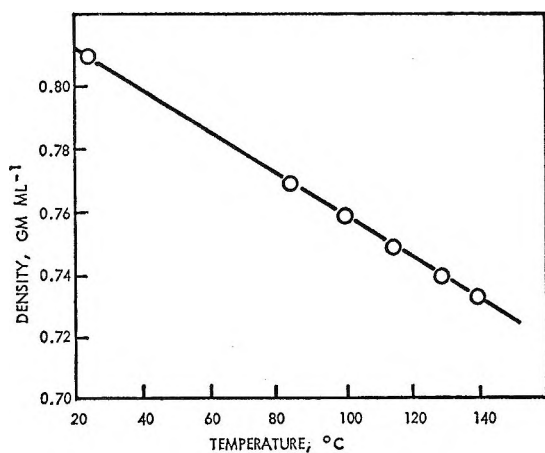


Figure 4. Density of squalane as a function of temperature.

Density of Squalane. The density of squalane from 25 to 140° was determined volumetrically. The results are shown in Figure 4.

Viscosity of Squalane. The viscosity of squalane as a function of temperature is given in Figure 5. The activation energy for diffusion is 4.6 kcal mole⁻¹.

The viscosities of squalane-chlorobenzene mixtures at 95° have been given in Figure 3. Squalane containing up to 1 *M* DTBP and 3×10^{-2} *M* phenol I

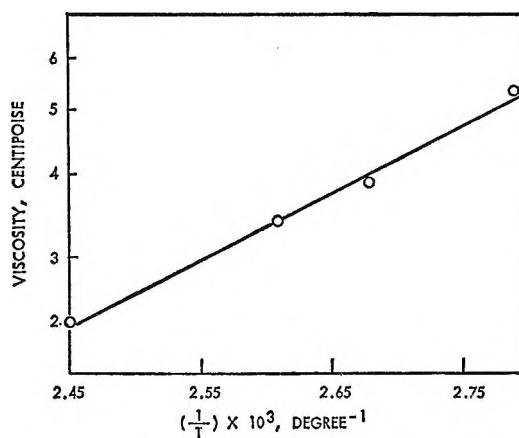


Figure 5. Viscosity of squalane as a function of temperature.

was found to have the same viscosity as neat squalane at a given temperature.

Autoxidation. The procedure and equipment used in these experiments have been described elsewhere.

Decomposition of DTBP. DTBP was decomposed in capsules sealed under 1 atm of nitrogen. The amounts of undecomposed DTBP and of products were determined by quantitative gas chromatography eluted at 75°. A 12-ft column of Carbowax was used in this work.

The Significant Structure and Properties of Liquid Hydrazine and Liquid Diborane

by Mu Shik Jhon,

*Department of Chemistry and the Center for Advanced Studies in the Sciences,
University of Virginia, Charlottesville, Virginia*

Joe Grosh, and Henry Eyring

Department of Chemistry, University of Utah, Salt Lake City, Utah (Received December 27, 1966)

The significant structure theory of the liquid is shown to be applicable also to rocket fuels such as liquid hydrazine and liquid diborane over the entire liquid range. The following properties were calculated and compared with experiment with good agreement: vapor pressure, molar volume, entropy, the critical constants, heat capacity at constant volume and constant pressure, thermal coefficient of expansion, and compressibility. The surface tensions of the liquids were computed in the generalized manner developed by Chang, *et al.* Also, the dielectric constant of the liquid hydrazine was calculated in a manner similar to that developed by Hobbs, Jhon, and Eyring. The results show good agreement with experimental observations.

Introduction

The significant structure theory of liquids¹ is based on the assumption that the following three significant structures make the most important contributions to the partition function of a liquid: (1) molecules with solidlike degrees of freedom arising from lattice vibrations in the liquids, (2) the positional degeneracy of these solidlike molecules, and (3) molecules with translational degrees of freedom. This means that at one instant a molecule of the liquid behaves like a gas and a moment later it has solidlike properties.

The mole fractions of gaslike and solidlike structures are $(V - V_s)/V$ and V_s/V , respectively, where V is the molar volume of the liquid and V_s is the molar volume of the solid at the melting point. This theory has been successfully applied to a number of liquids² ranging from liquefied gases, hydrocarbons, molten metals, and fused salts to water and liquid mixtures.

Our purpose here is to apply this theory to calculate and predict the properties of simple rocket fuels such as liquid hydrazine and liquid diborane. A partition function is developed and all the properties of these compounds are calculated successfully.

The Partition Function. Based upon the above considerations, the partition function of a liquid is written as a product of the partition functions for each significant structure weighed by the fraction of molecules in each structure.

$$f = (f_{\text{solid}} f_{\text{deg}})^{NV_0/V} (f_{\text{gas}})^{N(V-V_0)/V} \left/ \left(\frac{N(V-V_0)}{V} \right) ! \right.$$

Here f_{solid} , f_{deg} , and f_{gas} are the partition function of the solid, positional degeneracy, and the gas, respec-

(1) (a) H. Eyring and T. Ree, *Proc. Natl. Acad. Sci. U. S.*, **47**, 526 (1961); (b) H. Eyring and R. P. Marchi, *J. Chem. Educ.*, **40**, 562 (1963); (c) M. E. Zandler and M. S. Jhon, *Ann. Rev. Phys. Chem.*, **17**, 373 (1966).

(2) D. Henderson, H. Eyring, and D. Felix, *J. Phys. Chem.*, **66**, 1128 (1962); T. R. Thomson, H. Eyring, and T. Ree, *ibid.*, **67**, 2701 (1963); T. S. Ree, T. Ree, and H. Eyring, *ibid.*, **68**, 1163 (1964); **68**, 3262 (1964); T. S. Ree, T. Ree, and H. Eyring, *J. Chem. Phys.*, **41**, 524 (1964); R. P. Marchi and H. Eyring, *J. Phys. Chem.*, **68**, 221 (1964); S. H. Lin, H. Eyring, and W. Davis, *ibid.*, **68**, 3617 (1964); Y. L. Wang, T. Ree, T. S. Ree, and H. Eyring, *J. Chem. Phys.*, **42**, 1926 (1965); S. M. Ma and H. Eyring, *ibid.*, **42**, 1920 (1965); M. S. Jhon, J. Grosh, T. Ree, and H. Eyring, *ibid.*, **44**, 1465 (1966); M. S. Jhon, J. Grosh, T. Ree, and H. Eyring, *J. Phys. Chem.*, **70**, 1591 (1966); W. C. Lu, M. S. Jhon, T. Ree, and H. Eyring, *J. Chem. Phys.*, in press. (See also the series of papers appearing in *Proc. Natl. Acad. Sci. U. S.* from 1958 to the present.)

tively, V is the molar volume of the liquid, V_0 is the molar volume of the solidlike structure in the molten state, N is Avogadro's number, and the factorial term is due to the indistinguishability of the gaslike molecules.

Liquid hydrazine and diborane have an abnormally high entropy of fusion³ (11.01 eu for liquid hydrazine and 9.859 eu for liquid diborane). No solid-state transitions³ have been observed and the increase in volume upon melting is not sufficient to permit the rotation of solidlike molecules in the liquid. The hindrance to rotation is sufficient to justify treating this motion as a simple vibration. The justification of this will be considered later. Accordingly, the rotation term only appears in the gas partition function and a 6-degree Einstein oscillator term appears in the solid.

Using standard expressions for f_{solid} and f_{gas} and using Eyring's expression for f_{deg} and applying Stirling's approximation for the factorial term, the partition functions for hydrazine and diborane take the form

$$j = \left\{ \frac{e^{E_s/RT}}{(1 - e^{-\theta/T})^6} \prod_{i=1}^m \frac{1}{1 - e^{-h\nu_i/RT}} \times [1 + n(x-1)e^{-aE_s/n(x-1)RT}] \right\}^{N(V_0/V)} \times \left\{ \frac{(2\pi mkT)^{3/2} eV}{h^3} \frac{8\pi^2 (8\pi^3 ABC)^{1/2} (kT)^{3/2}}{N \sigma h^3} \prod_{i=1}^m \frac{1}{1 - e^{-h\nu_i/kT}} \right\}^{N[(V-V_0)/V]} \quad (1)$$

Here, E_s , θ , and V_0 are, respectively, the heat of sublimation, the Einstein characteristic temperature, and the molar volume of the solid upon melting; a is a proportionality constant; A , B , and C are the moments of inertia; σ is the symmetry number; ν_i the internal molecular vibration frequency; m molecular mass; $x = V/V_0$; N is Avogadro's number; and n is another proportionality constant which is approximately equal to the number of nearest neighbors around a molecule at the melting point. This is given by $n = 12V_0/V_m$ for a close-packed structure, V_m being the liquid molar volume at the melting point; the rest of the notation has the usual significance. The parametric values a , E_s , θ , and V_0 are calculated in a manner similar to that described by Chang, *et al.*⁴

Knowing these values and the molecular constants, all the thermodynamic and dielectric properties are calculated using the IBM 7044 and the Burroughs B-5500 computers.

The input data⁵ were as follows. For N_2H_4 , molecular weight = 32.048; $A = 6.18 \times 10^{-40}$ g cm²; $B =$

35.30×10^{-40} g cm²; $C = 36.98 \times 10^{-40}$ g cm²; $\sigma = 2$; the vibrational energies in units of cm⁻¹ are 3325, 3160, 1493, 1098, 833, 780, 725, 3350, 3297, 1607, 1275, and 950. The parametric values obtained are $V_0 = 31.141$ cc/mole; $\theta = 103.53$; $a = 0.24897 \times 10^{-3}$; $E_s = 11721$ cal/mole. For B_2H_6 , molecular weight = 27.69; $A = 1.051 \times 10^{-39}$ g cm²; $B = 4.575 \times 10^{-39}$ g cm²; $C = 4.959 \times 10^{-39}$ g cm², $\sigma = 4$; the vibrational energies in units of cm⁻¹ are 2526, 2615, 1763, 922, 369, 1012, 2522, 798, 2105, 1177, 1037, 1916, 2594, 830, 1604, 950, 1181, and 974. The parametric values obtained are $V_0 = 56.81$; $\theta = 51.77$; $a = 0.1626 \times 10^{-3}$; $E_s = 4344.9$.

Results

Volume and Pressure. The Helmholtz free energy is given by

$$A = -kT \ln f$$

If A is plotted as a function of V for a constant T and a common tangent to the points corresponding to the liquid and vapor phases is drawn, the vapor pressure is given by the slope of the common tangent. The abscissas at the two points of tangency indicate the volumes of the liquid and vapor.

The results obtained are shown in Figure 1 and are

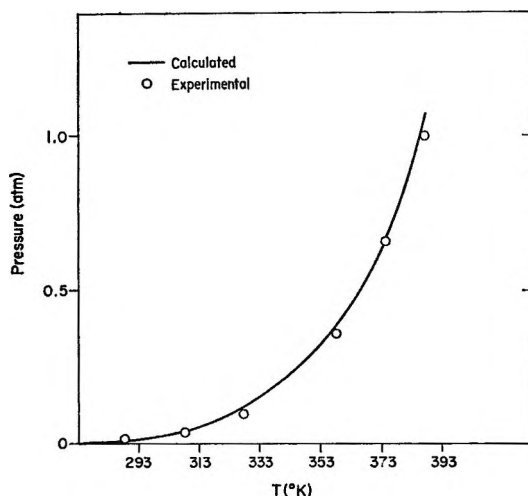


Figure 1. Vapor pressure of liquid N_2H_4 vs. temperature. The experimental data are obtained from ref 8.

(3) H. H. Landolt and R. Börnstein, "Zahlenwerte und Function aus Physik, Chemie, Astronomie, Geophysik und Technik," 3 Teil, II Band, Springer-Verlag, Berlin, 1956.

(4) S. Chang, H. Pak, W. K. Paik, S. H. Park, M. S. Jhon, and W. S. Ahn, *J. Korean Chem. Soc.*, **8**, 33 (1964); M. S. Jhon and S. Chang, *ibid.*, **8**, 85 (1964); W. Park and S. Chang, *ibid.*, **8**, 29 (1964); H. Pak and S. Chang, *ibid.*, **8**, 68 (1964); W. S. Ahn and S. Chang, *ibid.*, **8**, 125 (1964). (See also the appendix appearing in *J. Chem. Phys.*, **44**, 1465 (1966).)

(5) "JANAF Thermochemical Tables," The Dow Chemical Co., Midland, Mich.

given in Table I and Table II. There is good agreement between theory and experiment.^{3,6-9}

Table I: Calculated and Observed Molar Volumes

Temp, °K	$V_{\text{calcd.}}$ cc/mole	$V_{\text{obsd.}}^a$ cc/mole	$\Delta\%$
N₂H₄			
274.69 (mp)	31.327	31.327	0.00
288.15	31.582	31.593	0.03
308.15	31.984	32.190	0.06
328.15	32.425
358.15	33.172
387.3 (bp)	34.016
B₂H₆			
108.3 (mp)	57.09	(57.09)	0.00
130.12	58.96
145.03	60.49
155.40	61.70
165.14	62.95	60.99	-3.21
175.04	64.36	62.50	-2.97
180.66 (bp)	65.22	63.36	-2.93

^a For N₂H₄ see ref 6; for B₂H₆ see ref 3, except for the value in parentheses estimated from Cailletet-Mathias plot.

Table II: Calculated and Observed Vapor Pressure of Liquid Diborane

Temp, °K	$P_{\text{calcd.}}$ atm	$P_{\text{obsd.}}^a$	$\Delta\%$
108.3 (mp)	0.708×10^{-3}	0.710×10^{-3}	-0.28
130.12	0.01706	0.01690	0.95
145.03	0.08082	0.07982	1.25
155.40	0.1947	0.1910	1.94
165.14	0.3953	0.3910	1.10
175.04	0.7387	0.7280	1.47
180.66 (bp)	1.0163	1.0000	1.63
195.70	2.1475
203.90	3.0576

^a Reference 7.

Entropy of Vaporization. The entropy of vaporization is calculated from eq 1 by the relation

$$S = -\left(\frac{\partial A}{\partial T}\right)_v = \left(\frac{\partial}{\partial T}(kT \ln f)\right)_v$$

The entropy of vaporization is equal to $S_g - S_l$, where S_g and S_l are the entropies of the vapor and liquid, respectively. In Figure 2, the calculated entropies of vaporization of liquid N₂H₄ and B₂H₆ are compared with the observed values.⁶⁻⁸ One again sees good agreement between theory and experiment.

Heat Capacity, Compressibility, and Coefficient of

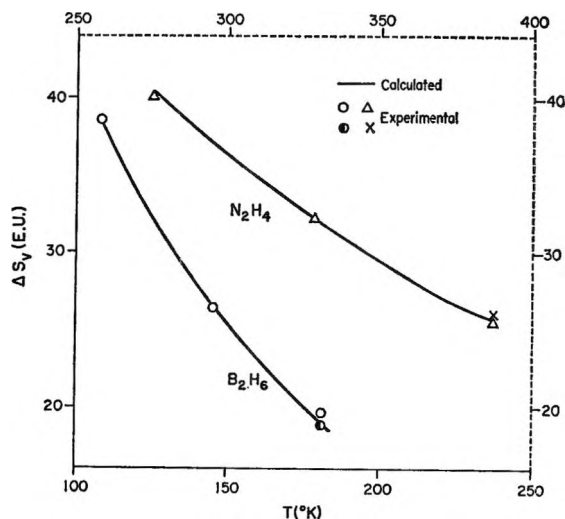


Figure 2. Entropies of vaporization of liquid N₂H₄ and B₂H₆ vs. temperature. The experimental data (O, Δ) were obtained from the vapor pressure equation in ref 7 and 8, respectively, by using an ideal gas approximation. The experimental data (O, X) were obtained from ref 7 and 6, respectively.

Thermal Expansion. The heat capacity at constant volume may be calculated from eq 1 by the relation

$$C_v = \frac{\partial}{\partial T} \left(kT^2 \frac{\partial \ln f}{\partial T} \right)_v$$

This can be converted to C_p by the use of the term involving compressibility, β , and the coefficient of expansion, α , both of which can be calculated from the partition function

$$C_p = C_v + TV \frac{\alpha^2}{\beta}$$

$$\alpha = \frac{1}{V} \left(\frac{\partial V}{\partial T} \right)_p = -\frac{1}{V} \left(\frac{\partial p}{\partial T} \right)_v / \left(\frac{\partial p}{\partial v} \right)_T =$$

$$-\frac{1}{V} \left(\frac{\partial^2 A}{\partial V \partial T} \right)_{TV} / \left(\frac{\partial^2 A}{\partial V^2} \right)_T$$

$$\beta = -\frac{1}{V} \left(\frac{\partial V}{\partial p} \right)_T = \frac{-1}{V \left(\frac{\partial p}{\partial V} \right)_T} = \frac{1}{V \left(\frac{\partial^2 A}{\partial V^2} \right)_T}$$

The calculated results are summarized in Table III and compared with experiment^{6,9} with good agreement.

(6) C. C. Clarke, "Hydrazine," Matheson Chemical Corp., Baltimore, Md., 1953.

(7) H. E. Wirth and E. D. Palmer, *J. Phys. Chem.*, **60**, 911 (1956).

(8) D. W. Scott, G. D. Oliver, M. E. Gross, W. N. Hubbard, and H. M. Huffman, *J. Am. Chem. Soc.*, **71**, 2293 (1949).

(9) E. B. Rifkin, E. C. Kerr, and H. L. Johnston, *ibid.*, **75**, 785 (1953).

Table III: Calculated Values for α , β , C_v , and C_p for Liquid N_2H_4 and B_2H_6

Temp, °K	$\alpha \times 10^3$, deg ⁻¹	$\beta \times 10^5$, atm ⁻¹	C_v , cal/g mole deg	C_p , cal/g mole deg	C_p (obsd), cal/g mole deg	$\Delta\%$
N_2H_4						
274.69 (mp)	0.6232	0.1225	14.23	20.84	23.29 ^a	10.52
288.15	0.6083	0.1287	14.53	20.87
308.15	0.6569	0.1541	14.97	21.66	23.62 ^a	8.29
328.15	0.7135	0.1853	15.41	22.49	24.00 ^a	6.29
338.15	0.8090	0.2441	16.04	23.77
387.3 (bp)	0.9180	0.3202	16.62	25.03
B_2H_6						
108.3	1.425	0.5381	12.12	17.69	18.23 ^b	2.96
130.12	1.613	0.8071	12.28	18.19	18.03 ^b	-0.89
145.03	1.823	1.0944	12.38	18.76	18.09 ^b	3.70
155.40	1.984	1.3494	12.27	19.17	18.16 ^b	5.56
165.14	2.150	1.6424	12.56	19.56	18.26 ^b	7.11
175.04	2.336	2.0079	12.66	19.99	18.37 ^b	8.82
180.66	2.449	2.2530	12.72	20.23

^a See ref 6. ^b The experimental data were obtained by interpolating the values given in ref 9.

Critical Constants. The critical temperature T_c , the critical pressure P_c , and the critical volume V_c are calculated from 1 using the usual iteration technique, *i.e.*, by using the conditions

$$\left(\frac{\partial p}{\partial V}\right)_T = 0 \quad \left(\frac{\partial^2 p}{\partial V^2}\right)_T = 0$$

in conjunction with the relation, $p = -(\partial A/\partial V)_T$.

The calculated and observed^{6,10} results are shown in Table IV. One can see that our model gives reasonable results even for the calculation of such thermodynamic properties as the specific heat and the critical constants which depend upon the second derivatives of the partition function. These constitute a severe test of the theory.

Table IV: Critical Point Properties

	N_2H_4	B_2H_6
	T_c , °K	
Calcd	692.7	317.6
Obsd	653.15 ^a	289.9 ^b
$\Delta\%$	6.05	9.55
	P_c , atm	
Calcd	199	50.25
Obsd	145 ^a	40.85 ^c
$\Delta\%$	37.2	23.01
	V_c , cc mole ⁻¹	
Calcd	102.8	187.8
Obsd	...	173.1 ^b
$\Delta\%$...	8.49

^a Reference 6. ^b Reference 3. ^c Reference 10.

Surface Tension. For the calculation of surface tension, the generalized method of Chang, *et al.*,¹¹ was used. According to our generalized scheme to improve Chang's method, we assumed that the partition function for the surface layers of a nonpolar liquid is as proposed by Chang, *et al.*, but also for the number of nearest neighbors around molecules and the Einstein characteristic temperature on the basis that the partition function for the surface layers has the same form as for the bulk liquid. The above scheme was used for the surface tension of liquid diborane and an iteration technique similar to that of Chang, *et al.*, was adopted.

For a polar liquid, in which the molecules in the first layer are in an asymmetric field owing to their dipole moment which tends to orient them in the direction of the field, the partition function for the top surface layer was used

$$f = \left[\frac{e^{E_s/RT}}{(1 - e^{-\theta/T})^5} \frac{2\pi(2\pi IkT)^{1/2} kT}{\sigma h} \frac{kT}{\mu X} + \sin h \frac{\mu X}{kT} (1 + n(x-1)e^{-\alpha E_s/n(x-1)RT}) f_0 \right]^{(V_s/V)N} \times \left[\frac{(2\pi mkT)^{3/2} eV}{h^3} \frac{8\pi^2(8\pi^3 ABC)^{1/2} (kT)^{1/2} kT}{\sigma h^3} \frac{kT}{\mu X} + \sin h \frac{\mu X}{kT} f_s \right]^{[(V-V_s)/V]N}$$

(10) A. E. Newkirk, *J. Am. Chem. Soc.*, **70**, 1978 (1948).

(11) S. Chang, T. Ree, H. Eyring, and I. Matzner, *Progress in International Research on Thermodynamic and Transport Properties*, The American Society of Mechanical Engineers, New York, N. Y., 1962.

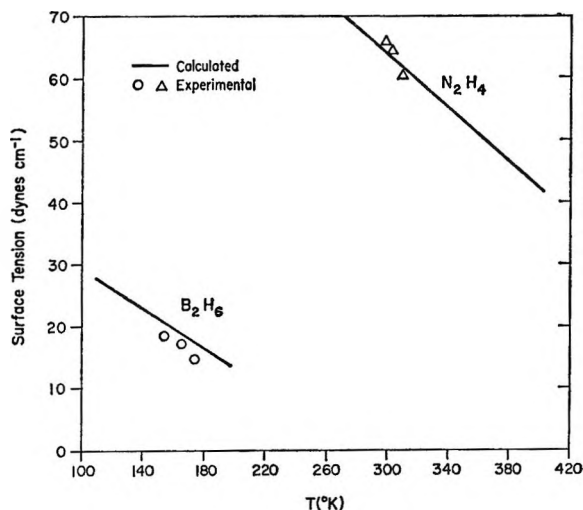


Figure 3. Surface tension of liquid N_2H_4 and B_2H_6 vs. temperature. The experimental data (O, Δ) are taken from ref 13 and 6, respectively.

where $x = V_1/V_s$, V_1 is the molar volume of the top surface layer, μ is the dipole moment, and X is the field strength.

Besides the usual iteration techniques of Chang, *et al.*, the above consideration of the orientation effect¹² was involved in the calculation of the surface tension of liquid hydrazine. The value of $\mu X = 8.97 \times 10^{-14} \approx 2kT$ in ergs was used. The calculated and observed results are shown in Figure 3.¹³ The results show reasonable agreement with experiment.

Direct Constant. The introduction of the concept of solidlike and gaslike molecules as previously shown by Hobbs, Jhon, and Eyring¹⁴ leads to an explanation of the observed temperature coefficient of the dielectric constant in polar liquids expressed by

$$\frac{(\epsilon - n_1^2)(2\epsilon + n_1^2)}{3\epsilon} = 4\pi \frac{N(n_1^2 + 2)}{V} \left[\frac{V_s \mu^2 G}{V kT} + \frac{V - V_s}{V} \frac{\mu^2}{3kT} \right] \quad (2)$$

Here ϵ and n_1 are the dielectric constant and index of refraction, respectively, and μ is the dipole moment. For hydrazine $\mu = 1.87 \times 10^{-18}$ and $n_1 = 1.464$. The single parameter G can be determined by evaluating eq 2 at one temperature from experimental data.² The calculated results show excellent agreement with experimental values available in Figure 4. In addition, the G value of 0.900 is nearly equal to that of ice and water, which was to be expected. A value of G slightly less than unity indicates slightly less than parallel orientation of the dipoles in the molecular domains.

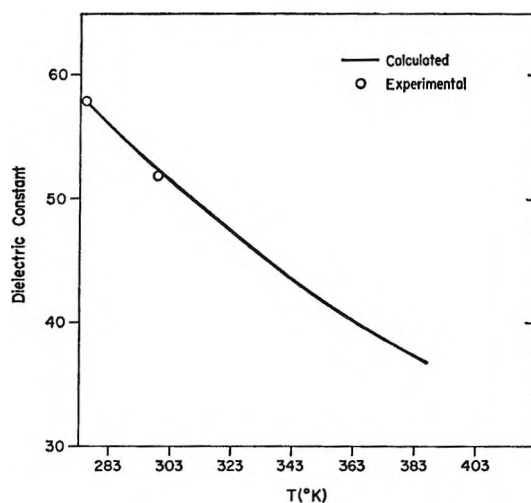


Figure 4. Dielectric constant of liquid N_2H_4 vs. temperature. The experimental data are taken from ref 6.

Discussion

The agreement between calculated and observed properties of liquid diborane and liquid hydrazine are highly satisfactory. The only notable deviations occur in the critical pressure calculations. In another paper we will report the results of replacing the perfect gas partition function f_{gas} in the model with an imperfect one¹⁵ for simple liquids as a means of improving the critical properties.

In our present calculations, we used a single value of θ assuming that three lattice vibrations and three librations have an average characteristic temperature. This is a simplification. In accord with the facts discussed previously, we tested whether the solidlike molecules should be treated as rotating or as hindered rotators. The following partition function for hindered rotation was tried in the solidlike partition function

$$\frac{e^{E_s/RT}}{(1 - e^{-\theta/T})^3} \left[\frac{1}{(1 - e^{-\theta/T})^3} (1 - e^{-u/RT}) + e^{-u/RT} f_R \right]$$

Here, u indicates the hindering potential.

Our calculations show that this procedure did not improve the results. We therefore conclude that these degrees of freedom are well represented as oscillators.

Acknowledgment. We wish to thank the National

(12) H. Lee, M. S. Jhon, and S. Chang, *J. Korean Chem. Soc.*, **8**, 179 (1964).

(13) A. W. Laubengaya, R. P. Ferguson, and A. E. Newkirk, *J. Am. Chem. Soc.*, **63**, 559 (1941).

(14) M. E. Hobbs, M. S. Jhon, and H. Eyring, *Proc. Natl. Acad. Sci. U. S.*, **56**, 31 (1966).

(15) J. Grosh, M. S. Jhon, T. Ree, and H. Eyring, submitted for publication.

Science Foundation (Grant GP-3698) for support of this work. M. S. J. also expresses his appreciation to

the Center for Advanced Studies in the Sciences of the University of Virginia for support of this work.

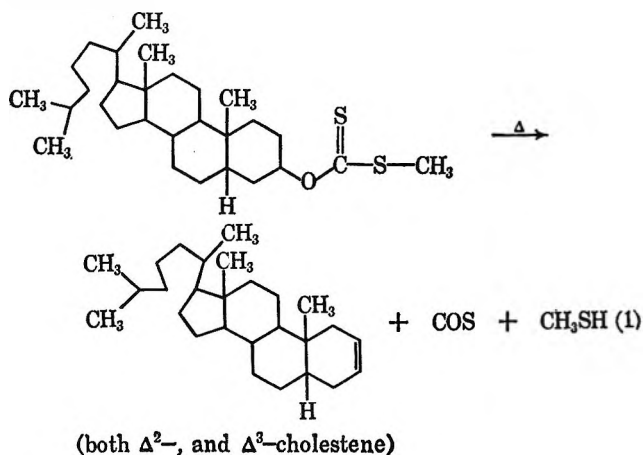
Pressure Effects on the Thermal Decomposition of β -Cholestanyl S-Methyl Xanthate

by Lin-sen Pan, Terrell N. Andersen, and Henry Eyring

Rate Processes Institute, University of Utah, Salt Lake City, Utah (Received January 3, 1967)

A study of the thermal decomposition of β -cholestanyl S-methyl xanthate has been made at temperatures of 176–236° and pressures of 1–12,000 atm. The unimolecular decomposition is continuously retarded as the pressure increases and the back reaction is unimportant under the experimental conditions. With increasing pressure the heat of activation increases, the (positive) volume of activation decreases, and the entropy of activation becomes less negative. These effects are discussed on the basis of the reaction occurring by several barriers in parallel, some of which pressure favors more than others.

Various mechanisms have been suggested concerning the Chugaev reaction.^{1–7} The kinetics of the thermal decomposition of β -cholestanyl S-methyl xanthate at atmospheric pressure have been extensively studied by O'Connor and Nace.¹ They showed that the above reaction follows the elimination mechanism of the Chugaev reaction exhibiting first-order kinetics. This reaction is homogeneous and proceeds at a readily measurable rate (between 146 and 236°) according to the equation



with almost complete absence of any complicating simultaneous reactions.¹

In the present work a study has been made of the influence of pressure on this decomposition reaction. The rates of the several unimolecular decomposition reactions which have been studied decrease with increasing pressure.^{8–11} The study of decompositions of pure liquids is perhaps one of the best cases for comparing the volume of the activated state to that of the

(1) G. L. O'Connor and H. R. Nace, *J. Am. Chem. Soc.*, **74**, 5454 (1952).

(2) D. S. Tarbell and D. P. Harnish, *Chem. Rev.*, **49**, 60 (1951).

(3) D. J. Cram, *J. Am. Chem. Soc.*, **71**, 3883 (1949).

(4) W. Hückel, W. Tapp, and G. Legutke, *Ann. Chem.*, **543**, 191 (1940).

(5) E. R. Alexander and A. Mudrak, *J. Am. Chem. Soc.*, **72**, 1810 (1950).

(6) E. R. Alexander and A. Mudrak, *ibid.*, **72**, 3194 (1950).

(7) E. R. Alexander and A. Mudrak, *ibid.*, **73**, 59 (1951).

(8) S. D. Hamann, "High Pressure Physics and Chemistry," Vol. II, R. S. Bradley, Ed., Academic Press Inc., New York, N. Y., 1963, p 163.

(9) P. W. Bridgman, *Proc. Am. Acad. Arts Sci.*, **72**, 233 (1938).

(10) K. R. Brower, *J. Am. Chem. Soc.*, **82**, 4535 (1960).

(11) B. Raistrick, R. H. Sapiro, and D. M. Newitt, *J. Chem. Soc.*, 1761 (1939).

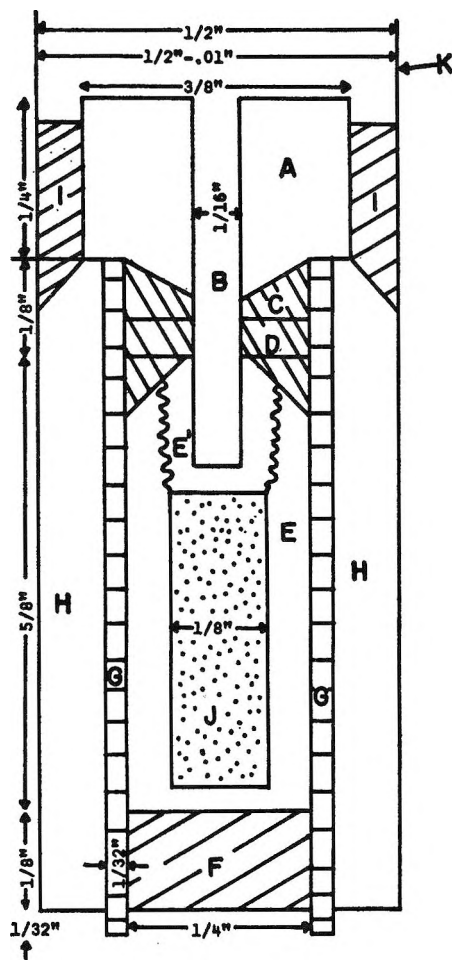


Figure 1. Cross section of cylindrical sample cell and furnace: A, stainless steel power lead; B, thermocouple hole; C, D, and F, pyrophyllite washers; E, Teflon sample cell; E', Teflon screw plug; G, carbon furnace; H, talc insulator and pressure-transmitting medium; I, pyrophyllite sleeve for sealing talc into cylinder; J, sample; K, 0.005-in. lead foil for lubricating purposes.

initial state without introducing the complications of a solvent.

Experimental Section

The sample, which was contained in a Teflon holder, was heated and pressed in a piston-cylinder-type press. Details of the press are given elsewhere.¹² The contents of the pressure chamber including the sample cell and the carbon resistance furnace are given in Figure 1. At the top end of the Teflon sample holder pyrophyllite plugs were used for the purpose of preventing leakage of the sample and extrusion of the thermocouple. The pyrophyllite plugs at the top and bottom also served to prevent a large temperature gradient along the axis of the furnace.

The temperature was controlled to within $\pm 1.5^\circ$ by two Variacs and a step-down high-current transformer in series. All pressures used here were calibrated by the fixed-point method developed by Tamayama.¹³

The β -cholestanyl S-methyl xanthate was prepared by the same method as that of O'Connor and Nace¹ and was identified by the melting point and infrared spectroscopy. Each sample was carefully weighed and packed into the high-pressure sample cell shown in Figure 1. Pressure was then applied very slowly in order to prevent the formation of local hot spots due to friction and to prevent extrusion of the sample. When the desired pressure was reached, electric current was passed through the furnace (carbon heating element) and the reaction temperature was reached within 3 min. When the reaction had run for the desired length of time, the current was shut off and the temperature dropped to 40° within 2 min.¹⁴

Both the β -cholestanyl S-methyl xanthate (reactant) and the cholestene (product) were liquids under the reaction conditions as evidenced by the plateau or inflection in the heating curves, one of which is shown in Figure 2. The cooling curves did not show any evidence of solidification (*cf.* Figure 2) and the resulting mixtures of xanthate ester and cholestene, upon opening the cell following each experiment, were observed to be viscous liquids. In order to prevent extrusion of these liquid products, the whole system was cooled to -30° with a Dry Ice-acetone cooling agent to solidify the products.

The failure of the cell to seal was detected by the strong odor of the mercaptan which was given off, a sudden drop of pressure, and the appearance of the liquid mixture around the cell lid and in the furnace. Successful sealing was evidenced by the lack of odor and of reaction mixture around the cell and also by the positive pressure of gas within the cell when it was cut open following an experiment. When the liquids extruded, analyses (expressed as per cent decomposition) were found to be erroneously high owing to mechanical loss of reactant. At reaction pressures lower than 5 kbars, extrusion of the thermocouple and reaction cell easily occurred unless the pressure was first raised to 8 kbars and then decreased back to the desired pressure.

(12) L. S. Pan, Ph.D. Thesis, University of Utah, Salt Lake City, Utah, 1967.

(13) M. Tamayama, Ph.D. Thesis, University of Utah, Salt Lake City, Utah, 1966.

(14) At 1 atm pressure there was no perceptible reaction below the melting point of the xanthate ester. Therefore, the lengths of time taken to increase and decrease the temperature were of no significance compared to the reaction times (see Figure 3) at all pressures.

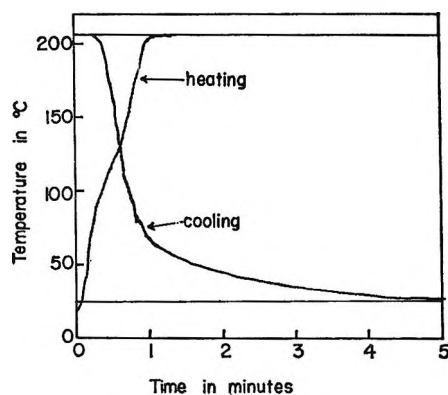


Figure 2. Heating and cooling curve for sample.

In order to determine the per cent decomposition of the xanthate ester, the amount of reactant left following the reaction was determined by using ultraviolet absorption spectra as measured with a Cary 14 spectrophotometer. A known weight of the reaction mixture was dissolved in *n*-hexane and diluted to standard volume; the peak height corresponding to the ester group¹⁵ (270- μ band) was compared with a calibration curve. This analysis agreed with weight-loss studies.

Results

The effect of varying pressures on the rate of the thermal decomposition of β -cholestanyl S-methyl xanthate was determined. All the plots of log (per cent decomposition of xanthate) *vs.* time were linear and passed through the origin as shown in Figure 3 for 176°. At 205 and 236° reactions were carried out to over 90% decomposition. From the slopes of the plots (*cf.* Figure 3) first-order rate constants were calculated and are tabulated in Table I. It is seen that pressure

Table I: Rate Constants ($k' \times 10^4 \text{ min}^{-1}$) for the Decomposition of β -Cholestanyl S-Methyl Xanthate at Various Temperatures and Pressures

Pressure	Temperature, °C		
	176	206	236
1 atm	50.7 (44.4) ^a	545 (492) ^a	
3 kbars	27.0		
6 kbars	12.85		
8 kbars	9.83		
12 kbars	7.73	154	989

^a By O'Connor and Nace.¹

retards the rate of the reaction. From reaction-rate theory the rate constant, k' , may be written as¹⁶

$$k' = \frac{\kappa k T}{h} \exp(-\Delta G^\ddagger/RT) = \frac{\kappa k T}{h} \exp\left(-\frac{\Delta H^\ddagger}{RT}\right) \exp(\Delta S^\ddagger/R) \quad (2)$$

Here κ is the transmission coefficient (taken as 1 in this work) and ΔG^\ddagger , ΔH^\ddagger , and ΔS^\ddagger , are the average free energy, enthalpy, and entropy of activation for the over-all reaction. Averages are taken here for the

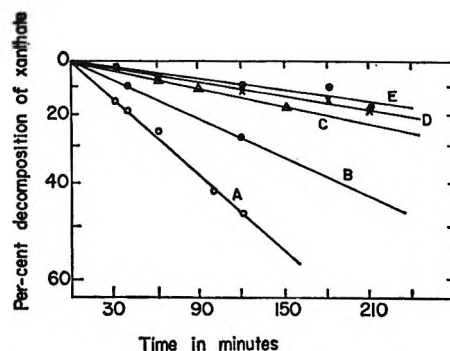


Figure 3. Plot of log per cent decomposition of xanthate against time at 176° and various pressures: A, 1 atm; B, 3000 atm; C, 6000 atm; D, 8000 atm; E, 12,000 atm.

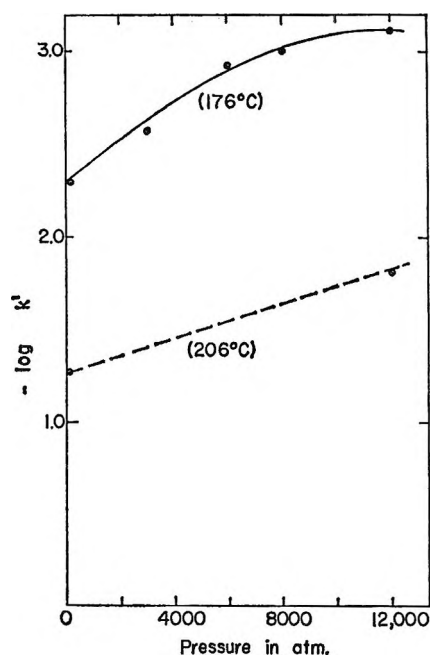


Figure 4. Plot of $(-\log k')$ against pressure.

(15) A. I. Scott, "Interpretation of the Ultraviolet Spectra of Natural Compounds," Pergamon Press Inc., New York, N. Y., 1964, p 374.

(16) S. Glasstone, K. J. Laidler, and H. Eyring, "The Theory of Rate Processes," McGraw-Hill Book Co. Inc., New York, N. Y., 1941.

purpose of evaluating experimental data and represent the appropriate activation free energy, etc., for all reaction paths. ΔH^\ddagger and ΔS^\ddagger were calculated from the slope and intercept of the plot of $\log k'/kT$ vs. $1/T$ and are tabulated in Table II. The least-squares method was used to obtain ΔH^\ddagger (for 12 kbars) as well as all the rate constants. At 1 atm studies were made in an open test tube as well as in a sealed Teflon tube in order to compare our values with those of O'Connor and Nace¹ and to see if Teflon affected the reaction rate. The present rate constants obtained in a test tube were essentially identical with those of O'Connor and Nace (obtained in the identical manner) and yielded an Arrhenius activation energy ($2.3R$ d $\log k'/d(1/T)$) of 33.8 kcal/mole. In Teflon the Arrhenius activation energy was 32.8 kcal/mole and the rate constants were slightly different (*cf.* Table I). The agreement between the two is within probable experimental error and we hence conclude that neither Teflon nor glass influences the kinetics.

Table II: Rate Data (Obtained at 1 atm and 12 kbars)

	1 atm	12 kbars
ΔH^\ddagger	+32.6 kcal mole ⁻¹	+35.3 kcal mole ⁻¹
ΔS^\ddagger	-5.38 cal deg ⁻¹ mole ⁻¹	-2.18 cal deg ⁻¹ mole ⁻¹
ΔG^\ddagger (176°)	+35.0 kcal mole ⁻¹	+36.3 kcal mole ⁻¹
ΔV^\ddagger (176°)	+12.3 cm ³ mole ⁻¹	+0.35 cm ³ mole ⁻¹

The volume of activation, ΔV^\ddagger , was obtained from the relationship

$$\partial \ln k' / \partial P = -\Delta V^\ddagger / RT \quad (3)$$

and is shown in Figure 4 and tabulated for 1 and 12,000 atm (at 176°) in Table II. The volume of activation is seen to be positive and decreases with increasing pressure as shown by the 176° experiments. At 206° only two points (at 1 atm and 12 kbars) were taken and hence the shape of the variation of ΔV^\ddagger with pressures could not be obtained.

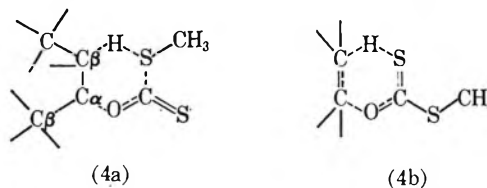
Discussion

That the decomposition of the xanthate ester at all temperatures and pressures and for all times of study in this work obeys first-order kinetics has been shown in the last section.

An increase of the activation energy and a decrease in reaction rate with increasing pressure is to be explained by Le Chatelier's principle extended to include the activated complex. The first-order kinetics observed for all times and conditions studied disproves

the idea of the existence of equilibrium of reactants with products and supports the idea that the reaction takes place irreversibly. Therefore, the rate data reflect the dependence of the forward rate constant on pressure and temperature and the effect of pressure is determined by the molar volume differences between the appropriate average activated and the appropriate average initial states.

A cyclic intermediate (six-membered ring) as shown in structures 4a or 4b is commonly accepted as the tran-



sition state in the decomposition of the presently studied and other xanthate esters.^{1,3,4,17,18} This is based on the homogeneous nature of the reaction, the products, and the kinetics of the studied reactions. Kinetic isotope effect studies of the thermal decomposition of S-methyl-*trans*-2-methyl-1-indanyl xanthate yield results which are not consistent with intermediate 4a but support the reaction path in which the decomposition of compound 4b to the alkene and an unstable xanthic acid is rate determining.¹⁸ From the few stereochemical studies made on the Chugaev reaction, it is concluded that the elimination goes predominantly *cis*, although both *cis* and *trans* elimination do occur.⁵⁻⁷ It has also been shown that H elimination occurs from both β -C atoms¹ (*cf.* eq 4). Unfortunately, stereochemical studies cannot be made on the β -cholestanyl S-methyl xanthate elimination, so the present discussion can be no more specific than to include the present results and the general characteristics of other Chugaev studies (*i.e.*, to include *cis* and *trans* elimination, with probable preference for the former).

In the initial state at 1 atm for the liquid reactant there is partial rotation about the C ^{α} -O, the O-C, and the C-S bonds as evidenced from model studies and from the variety of isomers produced in other studied Chugaev reactions. In rotation about these bonds, there are certain positions or "conformations" for which the potential energy is lower than others and the molecule will be in these conformations. Only certain of these conformations (*e.g.*, those in structure 4 in which a sulfur atom (probably the thion S)¹⁸ is close to a H atom) are pathways leading to the activated

(17) P. G. Stevens and J. H. Richmond, *J. Am. Chem. Soc.*, **63**, 3132 (1941).

(18) R. F. W. Bader and A. N. Bourns, *Can. J. Chem.*, **39**, 348 (1961).

states and hence can lead to reaction. The net rate of formation of these activated states (more than one of which may or may not lead to the same product) is the measured reaction rate. Since the measured activation free energy is 35.0–36.3 kcal mole⁻¹, we may suppose that molecules in the initial liquid state can transform from one conformation (state) to another more easily than they can achieve activation. Thus, all initial states may feed each activated state (such that a common ground state exists) and we may thus write the reaction rate as the sum of rates over each activation barrier. Assuming $\kappa = 1$ in each case we have

$$k' = \frac{kT}{h} \sum_j \exp[-(G_j^\ddagger - G_i)/RT] = \frac{kT}{h} \sum_j \exp(-\Delta G_j^\ddagger/RT) = \frac{kT}{h} \sum_j \exp\{-[\Delta H_{j,1}^\ddagger - T\Delta S_{j,1}^\ddagger + (P-1)\overline{\Delta V}_{j,1}^\ddagger]\}/RT \quad (5)$$

Here j represents the j th barrier, i represents the initial state which is common to all barriers, and the subscript 1 represents 1 atm pressure. $\overline{\Delta V}^\ddagger$ represents the average volume of activation; although ΔV^\ddagger may vary with pressure such that $(P-1)\overline{\Delta V}_{j,1}^\ddagger$ should be replaced by

$$\int_{P=1}^P \Delta V^\ddagger dP$$

the above approximation will serve sufficiently for the present argument.

The relative change in H , S , and V for the over-all activated (\ddagger) and initial (i) states can be qualitatively represented as shown in Figure 5. The changes in ΔH^\ddagger , ΔS^\ddagger , and ΔV^\ddagger with pressure can be understood from eq 5 if $\overline{\Delta V}_{j,1}^\ddagger$ for the j th term is sufficiently smaller than $\overline{\Delta V}_{j,1}^\ddagger$ for other terms such that the reaction takes place predominantly *via* the j th barrier at high pressures but by other barriers at low pressures. As illustration let us consider just two barriers at atmospheric pressure and at 12 kbars. For barrier "1" let us assume that $\Delta H_{1,1}^\ddagger = 32.6$ kcal/mole, $\Delta S_{1,1}^\ddagger = -5.4$ cal deg⁻¹ mole⁻¹, and $\overline{\Delta V}_{1,1}^\ddagger = +12.8$ cm³ mole⁻¹ and for barrier "2" assume that $\Delta H_{2,1}^\ddagger = 35.3$ kcal mole⁻¹, $\Delta S_{2,1}^\ddagger = -2.2$ cal deg⁻¹ mole⁻¹, and $\Delta V_{2,1}^\ddagger = 0.35$ cm³ mole⁻¹. Then at 176°

$$k'_{1(1)} = \frac{kT}{h} (8.8 \times 10^{-18}) \text{ sec}^{-1} \quad (6a)$$

$$k'_{1(12,000)} = \frac{kT}{h} (1.3 \times 10^{-19}) \text{ sec}^{-1} \quad (6b)$$

$$k'_{2(1)} = \frac{kT}{h} (2.2 \times 10^{-18}) \text{ sec}^{-1} \quad (6c)$$

$$k'_{2(12,000)} = \frac{kT}{h} (2.0 \times 10^{-18}) \text{ sec}^{-1} \quad (6d)$$

From eq 6 it is thus seen that $k_2' = 4k_1'$ at 1 atm such that path "1" is predominant, while at 12,000 atm $k_2' = 15.4k_1'$ so path "2" is predominant. Although more than two barriers may be significant, the model developed (according to which the reaction path changes with pressure) is in accordance with the above calculation.

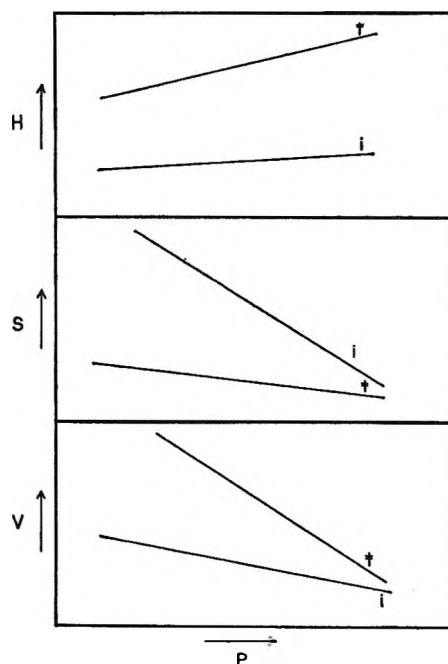


Figure 5. Schematic representation of enthalpy, entropy, and volume as a function of pressure for the average activated (\ddagger) and average initial states.

Our calculation suffices to show that with a proper choice of ΔG_j^\ddagger a sum of two or more rates could easily be made to fit the observed data. It would be interesting to make stereochemical studies of suitable Chugaev reactions under pressure to see if any correlation can be made between various barriers and the products obtained.

Acknowledgment. The authors gratefully acknowledge the Army Research Office (Durham) for financial support of this work under contract No. DA-ARO-D-31-124-G-618. They also express their appreciation to Mr. C. M. Roestenburg for machining the sample cells.

Pyrrole: Chemical Thermodynamic Properties¹

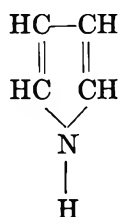
by D. W. Scott, W. T. Berg, I. A. Hossenlopp, W. N. Hubbard, J. F. Messerly,
S. S. Todd, D. R. Douslin, J. P. McCullough, and G. Waddington

Contributor. No. 148 from the Thermodynamics Laboratory of the Bartlesville Petroleum Research Center, Bureau of Mines, U. S. Department of the Interior, Bartlesville, Oklahoma 74003 (Received December 27, 1966)

Experimental studies of pyrrole provided the following information: values of heat capacity for the solid (11–249.74°K, the triple point), for the liquid (249.74–365°K), and for the vapor (338–500°K); the temperature of a λ -type transition of the solid; the enthalpy of fusion; thermodynamic properties for the solid and liquid (0–400°K); the enthalpy of vaporization (362–403°K); equation-of-state constants; vapor pressure (339–439°K); and standard enthalpies of combustion and formation at 298.15°K. Association of pyrrole was revealed by an unusual linear variation of the heat capacity of the liquid with temperature and by other properties. The chemical thermodynamic properties in the ideal gas state (0–1500°K) were calculated by methods of statistical mechanics.

Introduction

A comprehensive thermodynamic investigation of pyrrole



was made as part of a continuing program of studies of organic nitrogen compounds. The experimental part of this investigation included measurements of thermodynamic properties by methods of low-temperature calorimetry, comparative ebulliometry, vapor flow calorimetry, and combustion calorimetry. One of the significant features of the experimental part of this research was the elaborate precautions necessary to protect pyrrole samples from even minute traces of atmospheric oxygen. The accurate experimental values of vapor heat capacity and entropy were used to aid in interpreting the molecular spectra and to arrive at a vibrational assignment, which, in turn, was used in statistical thermodynamic calculations of the vapor-state chemical thermodynamic properties for the entire temperature range of likely interest.

Experimental Section and Results

Physical Constants and Techniques. The reported

values are based on a molecular weight of 67.091 (1961 atomic weights²) and the relations: 0°C = 273.15°K and 1 cal = 4.184 joules (exactly). The 1963 values of the fundamental physical constants³ were used.⁴ Measurements of temperature were made with platinum resistance thermometers calibrated in terms of the international temperature scale⁵ between 90 and 500°K and the provisional scale⁶ of the National Bureau of Standards below 90°K. All electrical and mass measurements were referred to standard devices calibrated at the National Bureau of Standards. The energy equivalent of the combustion calorimetric system, ϵ (calor.), was determined by combustion of benzoic acid (NBS sample 39 g).

The basic experimental techniques used for pyrrole are as described in published descriptions of apparatus

(1) This investigation was performed as part of American Petroleum Institute Research Project 52, "Nitrogen Constituents of Petroleum," which was conducted at the University of Kansas, Lawrence, Kan., and at the Bureau of Mines Research Centers in Laramie, Wyo., and Bartlesville, Okla.

(2) A. E. Cameron and E. Wichers, *J. Am. Chem. Soc.*, **84**, 4175 (1962).

(3) F. D. Rossini, *J. Pure Appl. Chem.*, **9**, 453 (1964).

(4) Some of the results originally were computed with previously accepted atomic weights and physical constants and the relation: 0°C = 273.16°K. Only results affected significantly were recalculated. Any remaining inconsistencies are much smaller than the accuracy uncertainty of the reported data.

(5) H. F. Stimson, *J. Res. Natl. Bur. Std.*, **42**, 209 (1949).

(6) H. J. Hoge and F. G. Brickwedde, *ibid.*, **22**, 351 (1939).

and methods for low-temperature calorimetry,⁷ vapor-flow calorimetry,⁸ comparative ebulliometry,⁹ and combustion calorimetry.¹⁰

The Material. The sample of pyrrole used for low-temperature calorimetry, comparative ebulliometry, and combustion calorimetry was part of the Standard Sample of Organic Nitrogen Compound, API-USBM 52-2, prepared at the Bureau of Mines Research Center in Laramie, Wyo. The purity, as determined by a calorimetric study of melting point as a function of fraction melted, was 99.994 mole %. For vapor flow calorimetry, which required a larger volume of material, a sample of slightly lower purity was used.

Scrupulous care was taken to avoid exposure of the samples to atmospheric oxygen. The material was always transferred in a vacuum system and stored *in vacuo* in ampoules with break-off tips. In the vapor-flow calorimetry and comparative ebulliometry, the material was blanketed with dry helium in which the concentration of oxygen had been reduced to the parts-per-million range by passage over activated charcoal at liquid air temperature. The sample used for vapor-flow calorimetry eventually did darken slightly in spite of the precautions to exclude oxygen, but heat-of-vaporization determinations with the darkened sample checked ones made earlier when the material was still "water white." The pyrrole was dried when necessary with calcium hydride.

Heat Capacity in the Solid and Liquid States. The observed values of heat capacity, C_s , are listed in Table I. Above 30°K, the accuracy uncertainty is estimated to be no greater than 0.2%. The heat capacity curve for the solid (C_s vs. T) shows a small λ -type transition with peak near 65.5°K; the excess enthalpy relative to the "normal" curve is only about 3 cal mole⁻¹. No hysteresis was observed in two series of measurements through this region. The heat capacity curve for the liquid is unusual in being linear over the experimental range of more than 100° with no trace of the positive curvature observed for nearly all liquids. The following equation represents the observed values with a maximum deviation of 0.03 cal deg⁻¹ mole⁻¹.

$$C_s(\text{liq}) = 12.699 + 0.059825T \\ \text{cal deg}^{-1} \text{mole}^{-1} \quad (250\text{--}365^\circ\text{K}) \quad (1)$$

The unusual heat capacity of the liquid is probably a manifestation of association.

Enthalpy of Fusion, Triple Point Temperature, Cryoscopic Constants, and Purity of Sample. Values of the enthalpy of fusion, ΔH_m , from three determinations were 1889.7, 1890.1, and 1890.1 cal mole⁻¹.

Table I: Molal Heat Capacity (cal deg⁻¹)

T_s^a °K	C_s^b	T_s^a °K	C_s^b	T_s^a °K	C_s^b
Crystals					
11.48	0.587	46.89	7.109	102.16	10.995
12.10	0.670	49.82	7.522	108.53	11.250
12.41	0.708	51.68	7.766	114.74	11.501
13.33	0.859	52.88	7.924	120.80	11.752
13.46	0.875	53.81	8.039	126.73	11.996
14.60	1.076	55.93	8.306	132.54	12.248
14.62	1.083	56.48	8.364	138.69	12.519
16.16	1.365	58.36	8.599 ^c	145.18	12.820
16.23	1.377	60.21	8.801 ^c	149.28	13.014
17.77	1.679	61.88	9.027 ^c	155.12	13.319
18.30	1.786	62.74	9.158 ^c	161.40	13.651
19.68	2.067	63.27	9.209 ^c	168.12	14.032
20.56	2.242	64.38	9.377 ^c	174.68	14.419
21.90	2.525	65.33	10.031 ^c	181.09	14.821
22.72	2.699	66.28	9.378 ^c	187.35	15.231
24.26	3.033	67.25	9.472 ^c	193.47	15.674
25.03	3.199	67.56	9.546 ^c	199.47	16.104
26.82	3.567	68.44	9.470 ^c	205.34	16.541 ^d
27.62	3.736	69.87	9.501 ^c	208.10	16.756 ^d
29.47	4.107	71.83	9.570 ^c	213.16	17.168 ^d
30.45	4.301	72.73	9.616	215.32	17.348 ^d
33.48	4.896	74.99	9.728	219.25	17.685 ^d
35.12	5.205	78.19	9.902	222.33	17.963 ^d
37.00	5.551	83.88	10.207	225.67	18.263 ^d
38.64	5.826	84.81	10.254	229.16	18.582 ^d
41.09	6.238	89.53	10.476	231.93	18.860 ^d
42.54	6.456	89.80	10.507	235.80	19.223 ^d
45.60	6.929	95.70	10.733	238.03	19.439 ^d
Liquid					
256.15	28.05	281.35	29.518	310.32	31.280
256.79	28.08	284.49	29.710	320.12	31.865
264.17	28.504	290.95	30.086	329.78	32.434
264.88	28.549	295.13	30.351	339.67	33.032
271.96	28.961	300.77	30.679	349.79	33.623
273.56	29.050	301.19	30.729	359.74	34.210
274.03	29.080	305.20	30.957		

^a T is the mean temperature of each heat capacity measurement. ^b C_s is the heat capacity of the condensed phase at saturation pressure. ^c The temperature increments and series number of measurements in the λ region are given in order of increasing temperature (°K): 1.877, II; 1.826, II; 1.526, II; 4.879, I; 1.244, II; 0.977, II; 0.930, II; 0.971, II; 0.960, II; 4.762, I; 1.435, II; 1.420, II; 2.501, II. ^d The temperature increment of each measurement for which premelting corrections were made is given in order of increasing temperature (°K): 5.301, 7.318, 5.683, 7.116, 6.498, 6.920, 6.338, 6.735, 6.186, 6.551, 6.017.

(7) H. M. Huffman, *Chem. Rev.*, **40**, 1 (1947); H. M. Huffman, S. S. Todd, and G. D. Oliver, *J. Am. Chem. Soc.*, **71**, 584 (1949); D. W. Scott, D. R. Douslin, M. E. Gross, G. D. Oliver, and H. M. Huffman, *ibid.*, **74**, 883 (1952).

(8) G. Waddington, S. S. Todd, and H. M. Huffman, *ibid.*, **69**, 22 (1947); J. P. McCullough, D. W. Scott, R. E. Pennington, I. A. Hossenlopp, and G. Waddington, *ibid.*, **76**, 4791 (1954).

The accepted value is 1890.0 ± 0.3 cal mole⁻¹. The results of a study of the melting temperature, T_F , as a function of the fraction of total sample melted, F , are listed in Table II. Also listed in Table II are

Table II: Melting Point Summary^a

F	$1/F$	$T_F, ^\circ\text{K}$	$T_{\text{calcd.}}^b, ^\circ\text{K}$
0.1084	9.225	249.6975	249.6992
0.2559	3.908	249.7201	249.7201
0.4921	2.032	249.7277	249.7274
0.6989	1.431	249.7298	249.7298
0.9057	1.104	249.7297	249.7311
1.0000	1.000		249.7315
		(Pure)	249.7354

^a $T_{tp} = 249.74 \pm 0.05^\circ\text{K}$; $N_2^* = \Lambda F(T_{tp} - T_F) = 0.00006 \pm 0.00005$; $\Lambda = 0.01525 \text{ deg}^{-1}$; $B = 0.00208 \text{ deg}^{-1}$. ^b Temperatures read from a straight line through a plot of T_F vs. $1/F$.

the values obtained for the triple point temperature, T_{tp} , the mole fraction of impurity in the sample, N_2^* , and the cryoscopic constants,¹¹ $A = \Delta Hm/RT_{tp}^2$ and $B = (1/T_{tp}) - (\Delta Cm/2\Delta Hm)$, calculated from the observed values of T_{tp} , ΔHm , and ΔCm (the heat capacity of the liquid minus that of the solid, $7.26 \text{ cal deg}^{-1} \text{ mole}^{-1}$).

Thermodynamic Properties in the Solid and Liquid States. Values of the thermodynamic properties for the condensed phases were computed from the calorimetric data for selected temperatures between 10 and 400°K . The results are given in Table III. The values at 10°K were computed from a Debye function for 3.5 degrees of freedom with $\theta = 111.6^\circ$; these constants were evaluated from the heat capacity data between 12 and 21°K . Extrapolation above the temperature range of the experimental measurements was done with eq 1. Corrections for the premelting effects of 0.00005 mole fraction of impurity have been applied to the "smoothed" data recorded in Table III.

Vapor Pressure. Observed values of vapor pressure are listed in Table IV. The condensation temperature of the sample was 0.002° lower than the ebullition temperature at 1 atm. The Antoine and Cox equations selected to represent the results are

$$\log p = 7.30296 - [1507.015/(t + 211.010)] \quad (2)$$

and

$$\log (p/760) = A[1 - (402.914/T)] \quad (3)$$

$$\log A = 0.870073 -$$

$$(5.43768 \times 10^{-4})T + (4.16086 \times 10^{-7})T^2$$

In these equations, p is in millimeters, t is in degrees Celsius, and T is in degrees Kelvin. The observed and calculated vapor pressures for both the Antoine and Cox equations are compared in Table IV. The comparison demonstrates clearly the superiority of the Cox equation in representing accurate vapor pressure data over a wide temperature range—a superiority that derives from the functional form as well as the extra constant. The normal boiling point, evaluated from the experimental measurements, is 129.76°C (402.91°K).

Enthalpy of Vaporization, Vapor Heat Capacity, and Effects of Gas Imperfection. The experimental values of enthalpy of vaporization and vapor heat capacity are given in Tables V and VI. The estimated accuracy uncertainty of the values of ΔHv and C_p° are 0.1 and 0.2%, respectively. The enthalpy of vaporization may be represented by the empirical equation

$$\Delta Hv = 12,734 - 0.97662T - (1.8971 \times 10^{-2})T^2 \text{ cal mole}^{-1} \quad (362\text{--}403^\circ\text{K}) \quad (4)$$

The effects of gas imperfection were correlated by the procedure described in an earlier paper.¹² The empirical equation obtained for B , the second virial coefficient in the equation of state, $PV = RT[1 + (B/V)]$, is

$$B = -536 - 2.160 \exp(2300/T) \text{ cc mole}^{-1} \quad (334\text{--}500^\circ\text{K}) \quad (5)$$

"Observed" values of B and $-T(d^2B/dT^2) = \lim_{P \rightarrow 0} (\partial C_p/\partial P)_T$ and those calculated from eq 5 are compared in Tables V and VI. The enthalpy of vaporization and gas imperfection are both somewhat greater than for a normal unassociated substance of the same molecular weight and therefore indicate some association of pyrrole by hydrogen bonding in both liquid and vapor states.

(9) (a) A. G. Osborn and D. R. Douslin, *J. Chem. Eng. Data*, **11**, 502 (1966); (b) G. Waddington, J. W. Knowlton, D. W. Scott, G. D. Oliver, S. S. Todd, W. N. Hubbard, J. C. Smith, and H. M. Huffman, *J. Am. Chem. Soc.*, **71**, 797 (1949).

(10) W. N. Hubbard, F. R. Frow, and G. Waddington, *J. Phys. Chem.*, **65**, 1326 (1961).

(11) A. R. Glasgow, A. J. Streiff, and F. D. Rossini, *J. Res. Natl. Bur. Std.*, **35**, 355 (1945).

(12) J. P. McCullough, H. L. Finke, J. F. Messerly, R. E. Pennington, I. A. Hossenlopp, and G. Waddington, *J. Am. Chem. Soc.*, **77**, 6119 (1955).

Table III: Molal Thermodynamic Properties for Condensed Phases^a

T , °K	$-(G_s - H_s^\circ)/T$, cal deg ⁻¹	$(H_s - H_s^\circ)/T$, cal deg ⁻¹	$H_s - H_s^\circ$, cal	S_s , cal deg ⁻¹	C_s , cal deg ⁻¹
Crystals					
10	0.033	0.097	0.970	0.130	0.385
15	0.109	0.310	4.655	0.419	1.145
20	0.241	0.639	12.785	0.880	2.124
25	0.425	1.042	26.047	1.467	3.189
30	0.654	1.486	44.56	2.140	4.208
35	0.917	1.945	68.06	2.862	5.178
40	1.207	2.405	96.19	3.612	6.057
45	1.517	2.854	128.44	4.371	6.832
50	1.840	3.288	164.41	5.128	7.543
60	2.513	4.103	246.19	6.616	8.787
64	2.787	4.412	282.36	7.199	9.314
65.5	2.891	4.532	296.86	7.423	10.023
66	2.925	4.572	301.7	7.497	9.426
70	3.203	4.851	339.5	8.054	9.508
80	3.891	5.462	436.9	9.353	9.999
90	4.566	5.995	539.5	10.561	10.496
100	5.223	6.465	646.5	11.688	10.906
110	5.859	6.887	757.5	12.746	11.308
120	6.475	7.272	872.6	13.747	11.713
130	7.071	7.630	991.8	14.701	12.134
140	7.650	7.967	1115.4	15.617	12.577
150	8.210	8.290	1243.5	16.500	13.048
160	8.755	8.604	1376.5	17.359	13.572
170	9.286	8.912	1515.0	18.198	14.136
180	9.805	9.219	1659.4	19.024	14.748
190	10.311	9.528	1810.2	19.839	15.418
200	10.808	9.840	1968.0	20.648	16.140
210	11.295	10.158	2133.1	21.453	16.902
220	11.776	10.483	2306.3	22.259	17.745
230	12.248	10.819	2488.3	23.067	18.653
240	12.717	11.164	2679.4	23.881	19.562
249.74	13.168	11.509	2874.4	24.677	20.447
Liquid					
249.74	13.168	19.077	4764.4	32.245	27.707
250	13.18	19.086	4771	32.27	27.720
260	13.94	19.428	5051	33.37	28.265
270	14.68	19.766	5336	34.44	28.853
273.15	14.91	19.872	5428	34.78	29.042
280	15.40	20.101	5628	35.50	29.451
290	16.11	20.434	5925	36.55	30.04
298.15	16.68	20.704	6173	37.39	30.53
300	16.81	20.765	6229	37.58	30.64
310	17.50	21.093	6538	38.59	31.24
320	18.17	21.420	6854	39.59	31.84
330	18.84	21.745	7175	40.58	32.44
340	19.49	22.068	7503	41.56	33.04
350	20.14	22.390	7836	42.53	33.63
360	20.77	22.711	8175	43.48	34.23
370	21.40	23.030	8521	44.43	34.83
380	22.02	23.349	8872	45.36	35.43
390	22.63	23.666	9229	46.29	36.03
400	23.23	23.983	9593	47.21	36.63

^a The properties tabulated are the Gibbs energy function, enthalpy function, enthalpy content, entropy, and heat capacity of the condensed phases at saturation pressure.

Table IV: Vapor Pressure

Ref compd ^a	Bp, °C	$p(\text{obsd})$, ^b mm	$-p(\text{obsd}) - p(\text{calcd})$, mm	
			Antoine eq 2	Cox eq 3
	Pyrrole			
19.061	65.671	71.87	+0.06	+0.01
21.720	68.522	81.64	+0.03	0.00
24.388	71.374	92.52	+0.01	0.00
27.068	74.233	104.63	-0.01	+0.01
29.757	77.098	118.06	-0.03	0.00
32.460	79.970	132.95	-0.05	+0.01
60.000	82.847	149.41	-0.06	+0.02
65	88.622	187.57	-0.11	-0.01
70	94.422	233.72	-0.12	-0.01
75	100.244	289.13	-0.08	+0.01
80	106.096	355.22	-0.05	0.00
85	111.972	433.56	+0.03	+0.01
90	117.875	525.86	+0.13	+0.01
95	123.806	633.99	+0.22	0.00
100	129.764	760.00	+0.32	0.00
105	135.753	906.06	+0.31	-0.09
110	141.768	1074.6	+0.3	-0.1
115	147.812	1268.0	+0.1	-0.2
120	153.884	1489.1	-0.1	-0.2
125	159.984	1740.8	-0.4	-0.1
130	166.109	2026.0	-0.9	0.0

^a The reference compound from 71.87 to 132.95 mm was pure benzene and that from 149.41 to 2026.0 mm was pure water.

^b From vapor pressure data for benzene [F. D. Rossini, K. S. Pitzer, R. L. Arnett, R. M. Braun, and G. C. Pimentel, "Selected Values of Physical and Thermodynamic Properties of Hydrocarbons and Related Compounds," Carnegie Press, Pittsburgh, Pa., 1953, Table 21k] and for water [N. S. Osborne, H. F. Stimson, and D. C. Ginnings, *J. Res. Natl. Bur. Std.*, **23**, 261 (1939)].

Table V: Molal Enthalpy of Vaporization and Second Virial Coefficient

T , °K	P , atm	ΔH_v , cal	B , cc	
			Obsd	Calcd ^b
362.11	0.250	9893 ± 9 ^a	-1759	-1775
381.21	0.500	9605 ± 5 ^a	-1456	-1437
402.91	1.000	9261 ± 3 ^a	-1185	-1187

^a Maximum deviation from the mean of five or more determinations. ^b Calculated from eq 5.

The enthalpy of vaporization at 298.15°K was calculated by extrapolation with eq 4 (10.76 kcal mole⁻¹), by use of the Clapeyron equation with eq 3 and 5 (10.78 kcal mole⁻¹), and by use of a thermodynamic network with the thermodynamic properties of Tables III and XIII (10.79 kcal mole⁻¹). The value from the thermodynamic network was selected as the most reliable. From this value and eq 5, the standard

Table VI: Molal Vapor Heat Capacity (cal deg⁻¹)

	Temp, °K				
	388.20	415.20	442.20	471.20	500.20
C_p (1.000 atm)		25.418	26.228	27.350	28.504
C_p (0.500 atm)	23.671				
C_p (0.250 atm)	23.036	24.305	25.614	26.955	28.257
C_p°	22.43	23.96	25.42	26.83	28.18
$-T(d^2B/dT^2)^a$ obsd	2.38	1.36	0.76	0.50	0.32
$-T(d^2B/dT^2)^b$ calcd	2.38	1.34	0.80	0.49	0.32

^a Units: cal deg⁻¹ mole⁻¹ atm⁻¹. ^b Calculated from eq 5.

enthalpy of vaporization was calculated, $\Delta H_v^\circ_{298.15} = 10.80$ kcal mole⁻¹.

Entropy in the Ideal Gaseous State. The entropy in the ideal gaseous state at 1 atm was calculated as shown in Table VII.

Table VII: Molal Entropy in the Ideal Gas State (cal deg⁻¹)

	Temp, °K		
	362.11	381.21	402.91
$S_s(\text{liq})$	43.69 ^d	45.48 ^d	47.49 ^d
$\Delta H_v/T$	27.32	25.20	22.98
$S(\text{ideal}) - S(\text{real})^a$	0.13	0.18	0.23
$R \ln P^b$	-2.76	-1.38	0.00
$S^\circ(\text{obsd}) = 0.15^c$	68.38	69.48	70.70

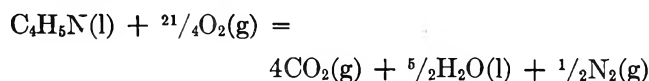
^a The entropy in the ideal gas state minus that in the real gas state. ^b Entropy of compression, calculated from eq 3. ^c Estimated accuracy uncertainty. ^d By interpolation in Table III.

Table VIII: Summary of a Typical Combustion Calorimetric Experiment^a

m' (pyrrole), g	0.93869
$\Delta t_c = t_f - t_i - \Delta t_{cor}$, deg	2.16973
$\varepsilon(\text{calor})(-\Delta t_c)$, cal	-8445.91
$\varepsilon(\text{cont})(-\Delta t_c)$, cal ^b	-10.90
ΔE_{ign} , cal	1.35
$\Delta E_{dec}(\text{HNO}_3 + \text{HNO}_2)$, cal	17.94
ΔE , cor to std states, cal ^c	4.11
$-m''\Delta Ec^\circ/M$ (auxiliary oil), cal	560.22
$-m'''\Delta Ec^\circ/M$ (fuse), cal	15.34
$m'\Delta Ec^\circ/M$ (pyrrole), cal	-7857.85
$\Delta Ec^\circ/M$ (pyrrole), cal g ⁻¹	-8371.08

^a Auxiliary data: $\varepsilon(\text{calor}) = 3892.61 \pm 0.15$ cal deg⁻¹; $V(\text{bomb}) = 0.344$ l.; $\Delta Ec/M$ (auxiliary oil) = -10,984.8 cal g⁻¹; $\Delta Ec^\circ/M$ (fuse) = -3923 cal g⁻¹; physical properties at 25°: $\rho = 0.96565$ g ml⁻¹, $(\partial E/\partial P)_T = -0.0074$ cal g⁻¹ atm⁻¹, $C_p = 0.455$ cal deg⁻¹ g⁻¹. ^b $\varepsilon^i(\text{cont})(t_i - 25^\circ) + \varepsilon^f(\text{cont})(25^\circ - t_f + \Delta t_{cor})$. ^c Items 81-85, inclusive, 87-90, inclusive, 93, and 94 of the computation form of ref 13.

Enthalpy of Combustion and Formation. A typical determination of the enthalpy of combustion of pyrrole is summarized in Table VIII. The symbols and abbreviations are those of Hubbard, Scott, and Waddington,¹³ except as noted. Eleven determinations gave the following values of $\Delta Ec^\circ/M$: -8369.13, -8371.08, -8370.54, -8370.98, -8371.97, -8372.22, -8370.66, -8372.50, -8371.39, -8370.24, and -8371.30 cal g⁻¹. The average value with the standard deviation of the mean is -8371.10 ± 0.29 cal g⁻¹. The calorimetric apparatus and procedures were the same as used in earlier studies of pyridine.¹⁰ In seven experiments, the final contents of the bomb were analyzed for carbon dioxide to check the amount of reaction measured by the mass of sample. On the average, the amount of carbon dioxide was 99.98% of that predicted. The values of $\Delta Ec^\circ/M$ apply to the idealized combustion reaction at 298.15°K



For this reaction, the experimental value of $\Delta Ec^\circ_{298.15}$ is -561.63 ± 0.08 kcal mole⁻¹ and of $\Delta Hc^\circ_{298.15}$ is -562.07 ± 0.08 kcal mole⁻¹. The uncertainties listed are uncertainty intervals equal to twice the final "over-all" standard deviation.¹⁴

The older value of Berthelot and Andre¹⁵ for the "heat of combustion at constant pressure," 567.7 kcal mole⁻¹, has been used heretofore to calculate the resonance energy of pyrrole. The values of the resonance energy must be revised by about 6 kcal mole⁻¹ to accord with the accurate thermochemical data of this research.

(13) W. N. Hubbard, D. W. Scott, and G. Waddington, "Experimental Thermochemistry," F. D. Rossini, Ed., Interscience Publishers, Inc., New York, N. Y., 1956, Chapter 5, pp 75-128.

(14) F. D. Rossini, ref 13, Chapter 14, pp 297-320.

(15) Quoted by M. S. Kharasch, *J. Res. Natl. Bur. Std.*, **2**, 359 (1929).

The derived results in Table IX were computed by use of the values of ΔH_c° , ΔH_v° , S_s , and S° for pyrrole and the literature values of the standard enthalpy of formation of $\text{CO}_2(\text{g})$ and $\text{H}_2\text{O}(\text{l})$ ¹⁶ and of the standard entropy of graphite, hydrogen gas, and nitrogen gas,¹⁷ all at 298.15°K.

Table IX: Derived Results for the Molal Chemical Thermodynamic Properties at 298.15°K^a

State	ΔH_f° , kcal	ΔS_f° , cal deg ⁻¹	ΔG_f° , kcal	Log Kf
Liquid	15.08 ± 0.10	-68.95	35.64	-26.14
Gas	25.88 ± 0.12	-41.68	38.31	-28.08

^a For the reaction: $4\text{C}(\text{c, graphite}) + {}^5/2\text{H}_2(\text{g}) + {}^1/2\text{N}_2(\text{g}) = \text{C}_4\text{H}_5\text{N}(\text{l or g})$.

Table X: Observed Wavenumbers (cm⁻¹)

Liquid	Vapor	Appearance ^a	Interpretation
560	474	R(d), IR(C)	Fundamental b ₂
618		R?	Fundamental a ₂
649	601	R(d), IR(C)	Fundamental b ₂
710		R(d)	Fundamental a ₂
733	721	IR(C)	Fundamental b ₂
840	826	R(d), IR(C)	Fundamental b ₂
867	864	R(d), IR	Fundamental b ₁
880	881	R(-), IR	Fundamental a ₁
	963	IR	2 × 474 = 948A ₁ (vap)
1013	1016	R(-), IR	Fundamental b ₁
1048	1048	R(d), IR	Fundamental b ₁
1073	1074	R(p), IR	Fundamental a ₁
1144	~1144	R(p), IR	Fundamental a ₁
1220		IR	560 + 649 = 1209A ₁ (liq)
1235	1235?	R(p), IR?	Fundamental a ₁
1286	1287	IR	Fundamental b ₁
1382	1386?	R(p), IR	Fundamental a ₁
1418	1422	IR	Fundamental b ₁
1467	1460?	R(p), IR	Fundamental a ₁
	1480	IR	3 × 474 = 1422B ₂ (vap)?
1530		R(-), IR	Fundamental b ₁
1569	1545	R(-), IR	{ 733 + 840 = 1573A ₁ (liq) { 721 + 826 = 1547A ₁ (vap)
1705	1693	IR	{ 840 + [869a ₂] = 1709B ₁ (liq) { 826 + [869a ₂] = 1695B ₁ (vap)
1735	1742	IR	2 × [869a ₂] = 1738A ₁
(Region 1800-3000 cm ⁻¹ omitted)			
3056	3058	R(-), IR	2 × 1530 = 3060A ₁
	3115	IR	? ^b
3104	3129	R(p), IR	Fundamental a ₁ (and b ₁)
3133	3145	R(p), IR	Fundamental a ₁ (and b ₁)
3410	3531	R(p), IR	Fundamental a ₁
(Region of higher wavenumbers omitted)			

^a Abbreviations: R, Raman; p, polarized; d, depolarized; IR, infrared; C, C-type band contour in vapor-state infrared spectrum indicative of b₂ species. ^b Possibly fundamental b₁.

Table XI: Vibrational Assignment (cm⁻¹)

a ₁	b ₁	a ₂
881	864	618
1074	1016	710
1144	1048	869
1235	1287	
1382	1422	b ₂
1467	1530	474
3129	(3129)	601
3145	(3145)	721
3531		826

Chemical Thermodynamic Properties

Thermodynamic functions for pyrrole were calculated by standard formulas of statistical thermodynamics. The vibrational assignment needed for that purpose was made by interpreting the available molecular spectral data with the aid of the calorimetric values of vapor heat capacity and entropy. The molecular spectra and vibrational assignment of pyrrole have been studied repeatedly.¹⁸ The observed wavenumbers in the regions of interest are summarized in Table X, which also includes the interpretation based on the proposed assignment in Table XI. The selection rules, discussed in detail in several of the publications of ref 18, were used in making the assignment. Because of hydrogen bonding in liquid pyrrole, wavenumbers of some modes are significantly different in the liquid and vapor spectra, notably the modes of the b₂ species

(16) D. D. Wagman, W. H. Evans, I. Halow, V. B. Parker, S. M. Bailey, and R. H. Schumm, "Selected Values of Chemical Thermodynamic Properties," National Bureau of Standards Technical Note 270-1, U. S. Government Printing Office, Washington, D. C., 1965.

(17) "JANAF Thermochemical Tables," The Dow Chemical Co., Midland, Mich.

(18) W. W. Coblenz, "Investigation of Infra-red Spectra," Part I, Carnegie Institution of Washington, Washington, D. C., 1905; S. Venkateswaren, *Indian J. Phys.*, **5**, 145 (1930); G. B. Bonino, R. Manzoni-Ansidei, and P. Pratesi, *Z. Physik. Chem.*, **B22**, 21 (1933); G. B. Bonino and R. Manzoni-Ansidei, *Ric. Sci.*, **7**, 510 (1936); A. Stern and K. Thalmayer, *Z. Physik. Chem.*, **B31**, 403 (1936); A. W. Reitz, *ibid.*, **B33**, 179 (1936); **B38**, 275 (1937); O. Redlich and W. Stricks, *Monatsh.*, **68**, 47 (1936); R. Manzoni-Ansidei and M. Rolla, *Atti. Accad. Nazl. Lincei, Rend., Classe Sci. Fis. Mat. Nat.*, **27**, 410 (1938); R. Manzoni-Ansidei, *Ric. Sci.*, **10**, 328 (1939); R. C. Lord, Jr., and F. A. Miller, *J. Chem. Phys.*, **10**, 328 (1942); J. Lecomte, *Bull. Soc. Chim. France*, 415 (1946); H. M. Randall, R. G. Fowler, N. Fuson, and J. R. Dangle, "Infrared Determination of Organic Structures," D. Van Nostrand Co., Inc., New York, N. Y., 1949, p 221; P. Mirone and C. Bonino, Jr., *Atti. Accad. Nazl. Lincei, Rend., Classe Sci. Fis. Mat. Nat.*, **17**, 250 (1954); P. Mirone, *Gazz. Chim. Ital.*, **86**, 165 (1956); American Petroleum Institute Research Project 44 at Texas A & M University, Catalog of Infrared Spectral Data, Serial No. 2014 and 2015; P. Mirone and G. Fabbri, *Gazz. Chim. Ital.*, **86**, 1079 (1956); J. Morcillo and J. M. Orza, *Anales Real Soc. Espan. Fis. Quim.* (Madrid), **B56**, 231, 253 (1960); A. Kreuzberger and P. A. Kalter, *J. Phys. Chem.*, **65**, 624 (1961).

Table XII: Observed and Calculated Molal Properties in the Ideal Gas State

T, °K	Entropy, S° , cal deg ⁻¹		T, °K	Heat capacity, C_p° , cal deg ⁻¹	
	Obsd	Calcd		Obsd	Calcd
362.11	68.38	68.34	388.20	22.43	22.46
381.21	69.48	69.45	415.20	23.96	23.96
402.91	70.70	70.70	442.20	25.42	25.38
			471.20	26.83	26.82
			500.20	28.18	28.18

band in the neighborhood of 1144 cm⁻¹ remain unexplained by the present assignment. (c) Some observed wavenumbers attributed to fundamentals have alternative explanations as sum combinations; for instance, 1235 cm⁻¹ could be the overtone of 618 cm⁻¹. However, the present assignment is consistent with the calorimetric data, and it is unlikely that any revision of the assignment in the light of further spectroscopic studies or interpretations will have any very significant effect on the calculated thermody-

Table XIII: Molal Thermodynamic Properties in the Ideal Gas State^a

T, °K	$(G^\circ - H^\circ_0)/T$, cal deg ⁻¹	$(H^\circ - H^\circ_0)/T$, cal deg ⁻¹	$H^\circ - H^\circ_0$, kcal	S° , cal deg ⁻¹	C_p° , cal deg ⁻¹	ΔH_f° , ^b kcal	ΔG_f° , ^b kcal	Log K_f^b
0	0	0	0	0	0	29.87	29.87	-∞
273.15	-53.33	9.906	2.706	63.24	15.49	26.18	37.27	-29.82
298.15	-54.22	10.44	3.112	64.66	17.05	25.88	38.31	-28.08
300	-54.28	10.48	3.144	64.76	17.16	25.86	38.38	-27.96
400	-57.62	12.91	5.164	70.53	23.12	24.81	42.73	-23.34
500	-60.78	15.48	7.738	76.26	28.17	24.01	47.30	-20.68
600	-63.82	17.94	10.77	81.76	32.26	23.42	52.02	-18.95
700	-66.76	20.24	14.17	87.00	35.60	23.00	56.82	-17.74
800	-69.60	22.34	17.87	91.94	38.38	22.73	61.67	-16.85
900	-72.35	24.25	21.83	96.60	40.74	22.58	66.55	-16.16
1000	-75.00	26.00	26.00	101.00	42.77	22.55	71.44	-15.61
1100	-77.55	27.61	30.37	105.16	44.53	22.62	76.32	-15.16
1200	-80.01	29.09	34.90	109.10	46.07	22.77	81.20	-14.79
1300	-82.40	30.45	39.58	112.85	47.44	22.99	86.06	-14.47
1400	-84.70	31.70	44.39	116.40	48.64	23.27	90.91	-14.19
1500	-86.93	32.87	49.30	119.80	49.71	23.61	95.73	-13.95

^a To retain internal consistency, some values are given to one more decimal place than is justified by the absolute accuracy. ^b The standard enthalpy, Gibbs energy, and common logarithm of the equilibrium constant of formation by the reaction: $4C(c, \text{graphite}) + {}^{5/2}H_2(g) + {}^{1/2}N_2(g) = C_4H_5N(g)$.

and the N-H stretching mode. Vapor-state values, characteristic of the unassociated molecule, are given in Table XI except for a few modes for which accurate vapor-state values are not available and for which the effect of hydrogen bonding on the wavenumber is probably insignificant. The difference in the liquid- and vapor-state fundamentals was useful in identifying sum-combinations appearing for both states, including one used in obtaining the value of 869 cm⁻¹ for the unobserved highest a_2 fundamental.

Despite the wealth of molecular spectral data that has accumulated for pyrrole during the past 60 years, the vibrational assignment still cannot be made with complete certainty. Examples of remaining uncertainties are as follows. (a) The value of 618 cm⁻¹ for the lowest a_2 fundamental comes from a very weak band reported in only one of the several investigations of the Raman spectrum. (b) Indications in the solution- and vapor-state infrared spectra of a second

dynamic functions, which are the primary concern of this research.

To obtain improved agreement with the observed values of heat capacity at the higher end of the temperature range studied, an empirical anharmonicity function¹⁹ with $\nu = 1300$ cm⁻¹ and $Z = 1.6$ cal deg⁻¹ mole⁻¹ was used. The contributions of this function to S° and C_p° , in cal deg⁻¹ mole⁻¹, are only 0.0004 and 0.005 at 298.15°K and 0.03 and 0.16 at 500°K but increase to 1.14 and 2.27 at 1500°K. In actuality, there must be compensation between "positive" anharmonicity of the higher stretching modes and "negative" anharmonicity of the lower bending modes. Evidence for extraordinary "negative" anharmonicity of the predominantly out-of-plane NH bending mode, 474 cm⁻¹, is seen not only in the value of its first over-

(19) R. E. Pennington and K. A. Kobe, *J. Chem. Phys.*, 22, 1442 (1954).

tone, which is 15 cm^{-1} higher than if the mode were harmonic, but also in the intensity of the overtone, which exceeds that of most of the fundamentals. Possibly the second overtone also has observable intensity; at least it is a plausible interpretation for the medium-intensity 1480-cm^{-1} band observed only for the vapor. Similar effects are observed for the deuterium derivatives studied by Morcillo and Orza.¹⁸ In $\text{C}_4\text{D}_4\text{NH}$, the N-H out-of-plane bending is more mixed among the b_2 modes, and not only the overtone $2 \times 461 = 922\text{ cm}^{-1}$ (observed 936) but also the combinations $461 + 516 = 977\text{ cm}^{-1}$ (observed 979) and $461 + 598 = 1059\text{ cm}^{-1}$ (observed 1054 cm^{-1}) appear. For $\text{C}_4\text{H}_4\text{ND}$, the overtone of the N-D out-of-plane bending mode is masked by an intense fundamental, but for $\text{C}_4\text{D}_4\text{ND}$ it appears as a moderately intense band at 740 cm^{-1} . The empirical anharmonicity function, of course, is intended to include the smaller contributions from the other 23 modes in addition to the particularly large contributions from the N-H out-of-plane bending mode.

Values of moments of inertia for calculating the contributions of rotation to the thermodynamic functions were taken from the work of Bak and co-workers.²⁰

The calculated values of entropy and heat capacity are compared with the experimental values in Table XII. The calculated values of the thermodynamic functions for selected temperatures up to 1500°K are listed in columns 2-6 of Table XIII. The experimental value of $\Delta Hf^\circ_{298.15}$ (Table IX) and values of the thermodynamic functions of C(c, graphite), $\text{H}_2(\text{g})$, and $\text{N}_2(\text{g})$ ¹⁷ were used in computing values of ΔHf° , ΔGf° , and $\log Kf$; they are listed in columns 7-9 of Table XIII.

Acknowledgment. The authors gratefully acknowledge the assistance of Thelma C. Kincheloe, Frankie R. Frow, and James P. Dawson in some of the experiments reported.

(20) B. Bak, D. Christensen, L. Hansen, and J. Rastrup-Andersen, *J. Chem. Phys.*, **24**, 720 (1956).

Low-Frequency Raman Spectra and Molecular Association in

Liquid Formic and Acetic Acids¹

by Peter Waldstein and L. A. Blatz

University of California, Los Alamos Scientific Laboratory, Los Alamos, New Mexico 87544
(Received December 27, 1966)

The low-frequency Raman spectra of normal and perdeuterated liquid formic and acetic acids and their solutions in water and hydrocarbons are reported. All the lines seen can be attributed to out-of-plane vibrations of various hydrogen-bonded associated species of the acids. Only lines assignable to cyclic dimers were observed in the hydrocarbon solutions. Glacial acetic acid also consists primarily of cyclic dimers. In anhydrous formic acid and in aqueous solutions of both acids, the predominant species is either an open dimer or a chain polymer.

Introduction

Molecular association of formic and acetic acids in the liquid and in solution has been studied by a wide variety of physical methods.²⁻¹⁷ Several infrared and Raman studies have been made,¹⁸⁻²² but in most cases interpretation has been complicated by the difficulty in assigning particular bands to particular vibrations of particular associated species (monomer, cyclic dimer, open dimer, chain polymer) of the acid. Spectra below 300 cm^{-1} are partially free from this difficulty. The monomers have no fundamentals below 500 cm^{-1} ^{23,24} except for the internal rotation of the methyl group in acetic acid, which is probably very weak and which, if observed, can easily be identified by its frequency shift on deuteration. Furthermore, some of the bands can be assigned to the cyclic dimer on the basis of the work of Miyazawa and Pitzer.²⁵ The low-frequency infrared spectra of these acids in the gas,²⁶ in the pure liquid,^{27,28} and in CCl_4 solution²⁸ have been reported and low-frequency Raman lines have been observed in the pure liquids.^{29,30} No low-frequency Raman spectra of these acids in solution or isotopic effects on the Raman spectra of the pure liquids have been reported. Here we report the low-frequency Raman spectra of normal and perdeuterated formic acid in benzene, acetic acid in *n*-pentane, and both acids in the pure liquid and in aqueous solution.

Experimental Section

The method of observing low-frequency Raman lines has been described elsewhere.^{30,31} No essential changes in method were made during this study.

- (1) Work performed under the auspices of the U. S. Atomic Energy Commission.
- (2) G. C. Pimentel and A. L. McClellan, "The Hydrogen Bond," W. H. Freeman and Co., San Francisco, Calif., 1960.
- (3) G. A. Allen and M. A. Caldin, *Quart. Rev. (London)*, **7**, 255 (1953).
- (4) N. I. Gulivets, A. E. Lutskii, and I. V. Radchenko, *Zh. Strukt. Khim.*, **6**, 27 (1965).
- (5) H. Giesenfelder and H. Zimmermann, *Ber. Bunsenges. Physik. Chem.*, **67**, 480 (1963).
- (6) A. E. Lutskii and V. N. Solon'ko, *Zh. Fiz. Khim.*, **39**, 783 (1965).
- (7) A. E. Lutskii and S. A. Mikhaïlenko, *Zh. Strukt. Khim.*, **4**, 14 (1963).
- (8) D. Tabuchi, *Z. Electrochem.*, **64**, 141 (1960).
- (9) (a) D. L. Martin and F. J. C. Rossotti, *Proc. Chem. Soc.*, 73 (1961); (b) D. L. Martin and F. J. C. Rossotti, *ibid.*, 60 (1959); (c) E. E. Schrier, M. Pottle, and H. A. Scheraga, *J. Am. Chem. Soc.*, **86**, 3444 (1964).
- (10) M. Pancholy and S. P. Singal, *Nuovo Cimento*, **32**, 847 (1964).
- (11) F. B. Stumpf and L. A. Crum, *J. Acoust. Soc. Am.*, **39**, 170 (1966).
- (12) (a) A. N. Campbell and J. M. T. M. Gieskes, *Can. J. Chem.*, **43**, 1004 (1965); (b) J. M. T. M. Gieskes, *ibid.*, **43**, 2448 (1965).
- (13) G. E. Maciel and D. D. Traficante, *J. Am. Chem. Soc.*, **88**, 220 (1966).
- (14) J. C. Davis and K. S. Pitzer, *J. Phys. Chem.*, **64**, 886 (1960).
- (15) (a) A. Parmigiani, A. Perotti, and V. Riganti, *Gazz. Chim. Ital.*, **91**, 1148 (1961); (b) A. Perotti and M. Cola, *ibid.*, **91**, 1153 (1961).

The Steinheil (three-glass prism, $f/10$ optics) spectrograph was used with an entrance slit width of 0.300 mm and 15-mm height. The linear dispersion for the region 0–100 cm^{-1} from the Hg 4358 Å exciting line was 16.4 cm^{-1}/mm . The exit slit had a radius of curvature of 100.0 mm. It was moved in the focal plane of the spectrograph at rates of 19.68 and 9.84 $\text{cm}^{-1}/\text{min}$ with time constants of 20 and 40 sec, respectively.

In all cases the Raman line frequencies and relative areas were determined after the lines were reconstructed on flat, straight base lines. The lines were always separated from the backgrounds by the use of straight lines. In some cases subjectively estimated curved background lines were drawn. This was found to make essentially no difference in the values obtained for the frequencies as long as the ratio of Raman line to background height was large. However, for such cases as water, where the background is larger than the Raman line, the nominal value of $190 \pm 5 \text{ cm}^{-1}$ for the frequency of this line pertains only to the method of drawing background lines and for baffle settings (10.0 mm) such as were used for the acids. In all cases the lines were reconstructed by working from the high-frequency toward the low-frequency side assuming the lines to be symmetric.

The uncertainty in the absolute values of the frequencies is estimated to be $\pm 3 \text{ cm}^{-1}$ for the formic acid upper line (larger frequency) and $\pm 5 \text{ cm}^{-1}$ for the acetic acid upper line or the lower formic acid line. This uncertainty for a weak, broad line such as the acetic acid 47- cm^{-1} line may be somewhat larger than $\pm 5 \text{ cm}^{-1}$. The reproducibility from one scan to another scan nearby in time was usually $\pm 1 \text{ cm}^{-1}$ for the formic acid upper line and $\pm 2 \text{ cm}^{-1}$ for the acetic acid upper line at room temperature. At temperatures of 8 and 56°, the reproducibility of these lines was somewhat poorer.

When precise relative frequencies were needed as in comparing the normal acids and deuterated acids, the lines were scanned (a) with the slower scanning rate and longer time constant, (b) as near to each other in time as possible, (c) repeatedly, that is, five times each for the pure acids and solutions in *n*-pentane (two scans of each were used for the water solutions and somewhat poorer precision was obtained), and (d) in addition to determining the frequencies from line peaks, corresponding points of each spectrum were compared. In this way average frequencies of the formic acid upper line relative to the upper line from perdeuterioformic acid reliable to $\pm 1 \text{ cm}^{-1}$ were obtained and $\pm 2 \text{ cm}^{-1}$ for the acetic acid upper line relative to the upper line from perdeuterioacetic acid.

The half-widths of the lines refer to the values obtained by doubling the high-frequency half of the half-widths. The line intensities are approximate values obtained by comparing the heights of the lines relative to the formic acid upper line (at 23°).

The precision with which the relative areas of the acid Raman lines were determined in the water solution was less than $\pm 5\%$ for the pure acid and about $\pm 30\%$ for the most dilute acid solutions.

The formic acid was 97+ % superior grade acid. In one case a bottle of acid which had been opened about 9 months previously was distilled at about 10-cm pressure from anhydrous copper sulfate. The background decreased fourfold at 375 cm^{-1} following this distillation. Formic acid newly received from supply houses sometimes had only a slightly larger background than the distilled acid.

The perdeuterio acids, both DCOOD (Nuclear Research Chemicals, Inc.) and CD₃COOD (Merck Sharp and Dohme of Canada) had a minimum of 99% isotopic purity.

The glacial acetic acid was reagent grade, minimum 99.7% acetic acid. Freshly opened bottles had backgrounds that were only slightly improved by filtration through 0.2- μ pore size Gelman filters. Several bottles of acid which had been on the shelves for 2 years or more were found to give intolerably high backgrounds.

The Eastman practical grade *n*-pentane was filtered through 0.1- μ pore size Millipore filters. The conductivity water used was found to give only a negligibly different background after filtration through 0.01- μ

- (16) E. Constant and A. Lebrun, *J. Chim. Phys.*, **61**, 163 (1964).
- (17) G. Werner, *J. Prakt. Chem.*, **29**, 26 (1965).
- (18) H. Dunken and P. Fink, *Z. Chem.*, **2**, 117 (1962).
- (19) (a) N. G. Zarakhani and M. I. Vinnik, *Zh. Fiz. Khim.*, **37**, 2550 (1963); (b) N. G. Zarakhani and M. I. Vinnik, *ibid.*, **38**, 632 (1964).
- (20) A. A. Glagoleva and A. A. Ferkhmin, *Zh. Obshch. Khim.*, **28**, 289 (1958).
- (21) L. J. Bellamy, R. F. Lake, and R. J. Pace, *Spectrochim. Acta*, **19**, 443 (1963).
- (22) Y. Nagai and O. Simamura, *Bull. Chem. Soc. Japan*, **35**, 132 (1962).
- (23) K. Nakamoto and S. Kishida, *J. Chem. Phys.*, **41**, 1554 (1964).
- (24) M. Haurie and A. Novak, *J. Chim. Phys.*, **62**, 137 (1965).
- (25) T. Miyazawa and K. S. Pitzer, *J. Am. Chem. Soc.*, **81**, 74 (1959).
- (26) G. L. Carlson, R. E. Witkowski, and W. G. Fately, *Spectrochim. Acta*, **22**, 1117 (1966).
- (27) A. E. Stanevich, *Opt. i Spektroskopiya*, **16**, 446 (1964).
- (28) V. Lorenzelli, *Ann. Chim. (Rome)*, **53**, 1018 (1963).
- (29) U. A. Zirnit and M. M. Sushchinskii, *Opt. i Spektroskopiya*, **16**, 903 (1964).
- (30) L. A. Blatz, *Spectrochim. Acta*, **21**, 1973 (1965).
- (31) Low-frequency "liquid structure" lines of benzene, *n*-pentane, and a large number of other liquids are being reported elsewhere. L. A. Blatz, submitted for publication.

pore size Millipore filters. The benzene was reagent grade and was used as received.

Results

All spectra reported below were obtained with unpolarized exciting light. Insertion of crossed or axial polarizers around the sample tube did not change the spectra of pure HCOOH and glacial CH₃COOH except to reduce the relative intensity of the residual Rayleigh line (at the extreme left of the spectra shown here) and to reduce the total intensity of the entire spectrum because of the attenuation of the polaroid. The relative intensities of the Raman lines remained the same, as would be expected from depolarized Raman spectra.

Acetic Acid. Spectra were obtained of 49, 34, and 20% (by volume) solutions of acetic acid in *n*-pentane and of glacial acetic acid and pure *n*-pentane,³¹ all at 23°. When the background and the appropriate fraction of the pentane spectrum are subtracted, the resultant spectra of all three solutions are essentially the same. The integrated intensity of the solution spectrum relative to the intensity of the glacial acetic acid spectrum is proportional to the volume fraction of acetic acid in the solution within the experimental error (± 5 –10% for the more concentrated solutions; ± 20 % for the most dilute, where the pentane contri-

bution to the spectrum is relatively large). Figure 1 shows the spectrum of a 34% solution of CH₃COOH in *n*-pentane. The line at 124 ± 5 cm⁻¹ can be identified with the B_g fundamental of the cyclic dimer, for which Miyazawa and Pitzer²⁵ predict a frequency of 128 cm⁻¹. The isotopic shift confirms this assignment; in a pentane solution of CD₃COOD, the line appears at 115 ± 5 cm⁻¹. The shifts predicted for the A_g fundamentals are about 3.5%; for the B_g they are 8%. The line at 47 ± 7 cm⁻¹ is probably a "liquid structure" line.^{31,32}

Figure 2 shows the spectrum of glacial acetic acid at 23°. Spectra taken at 8 and 56° were the same except for small changes in background. The spectrum is similar to that of the pentane solutions, but the two lines are not as well resolved and their maxima are somewhat closer together. This might suggest the presence of a weak third line around 95 cm⁻¹ perhaps owing to an open dimer or to a polymer. If there is such a third line, its specific intensity must be about equal to the sum of the specific intensities of the 124- and 47-cm⁻¹ lines, since the total intensity of the glacial acetic acid spectrum is twice that of the spectrum of the 49% solution in *n*-pentane. The frequency of the upper maximum in glacial CH₃COOH is 116 ± 5 cm⁻¹; in glacial CD₃COOD it is 106 ± 5 cm⁻¹, consistent with

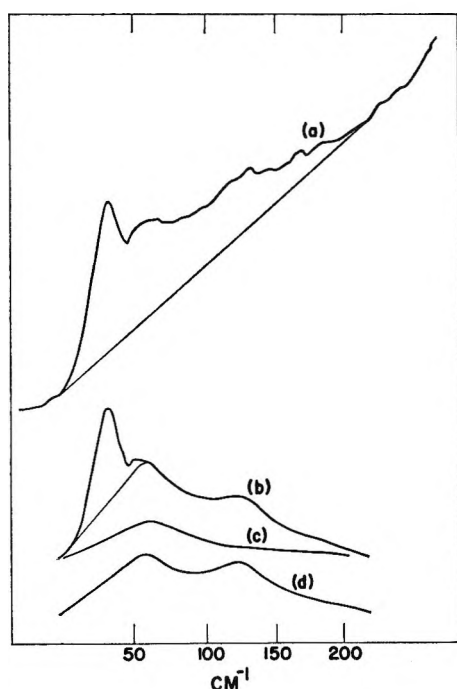


Figure 1. A 34% (by volume) solution of CH₃COOH in *n*-pentane, 23°: (a) observed spectrum with linear background; (b) spectrum with linear background and residual line removed; (c) two-thirds of the *n*-pentane spectrum; (d) spectrum b minus spectrum c.

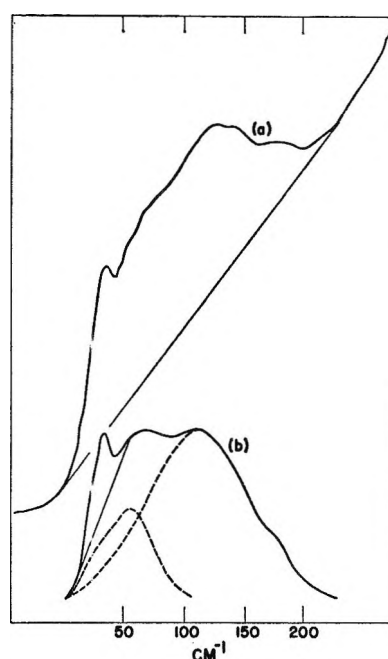


Figure 2. Glacial acetic acid, 23°: (a) observed spectrum with linear background; (b) spectrum with linear background removed.

(32) V. S. Starunov, *Opt. i. Spektroskopiya*, 18, 300 (1965).

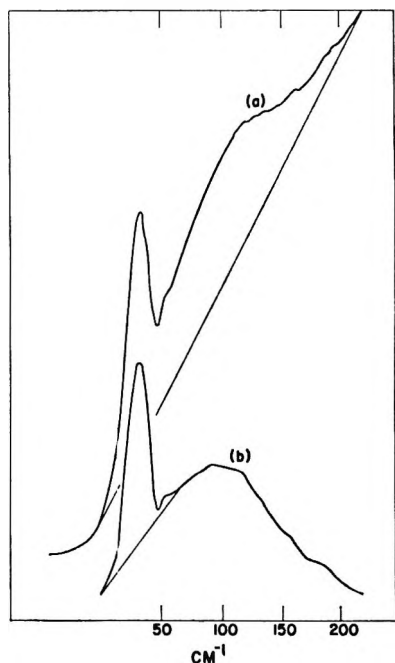


Figure 3. Aqueous solution, 32 mole % H_2O , 68 mole % CH_3COOH , 23° : (a) observed spectrum with linear background; (b) spectrum with linear background removed.

the isotopic shift expected for the B_g vibration of the cyclic dimer.

Figure 3 shows the spectrum of an aqueous solution (32 mole % H_2O) of acetic acid at 23° . Only one broad line can be distinguished; its maximum is located at $95 \pm 5 \text{ cm}^{-1}$. The spectrum is the same, except for intensity, in all aqueous acetic acid solutions below 80 mole % acid. The isotopic shift of this maximum is $9 \pm 2 \text{ cm}^{-1}$ ($9.5 \pm 2\%$). A plot of specific intensity of the aqueous solution spectrum against concentration of acetic acid is shown in Figure 4.

Formic Acid. The only solvent available for this work in which substantial amounts of formic acid could be dissolved without the formation of solute-solvent hydrogen bonds was benzene. Unfortunately, the benzene spectrum has a very strong, very broad "liquid structure" line^{31,32} which completely obscures the formic acid spectrum below about 200 cm^{-1} . One line could be observed in a saturated solution of HCOOH in benzene at 23° ; it was located at $245 \pm 5 \text{ cm}^{-1}$. In a saturated solution of DCOOD in benzene at 23° , a line could be detected with poor precision at $210 \pm 10 \text{ cm}^{-1}$. The isotopic shift ($14 \pm 4\%$) and the frequency permit assignment of this line to the B_g fundamental of the cyclic dimer, for which a frequency of 243 cm^{-1} and an isotopic shift of 19% are predicted.²⁵

The spectrum of anhydrous HCOOH at 23° is shown

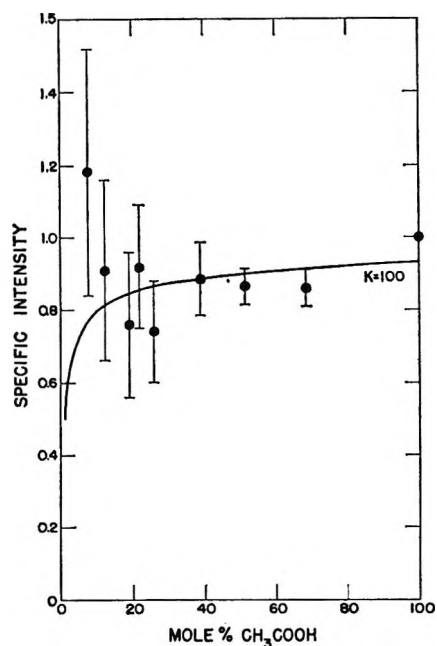


Figure 4. Specific intensity of the aqueous solution spectrum of CH_3COOH at 23° relative to the spectrum of glacial acetic acid. The solid curve is the curve to be expected for $K = 100$ if the 95-cm^{-1} line is due to a dimer and has a specific intensity equal to the sum of the specific intensities of the 47- and 124-cm^{-1} lines.

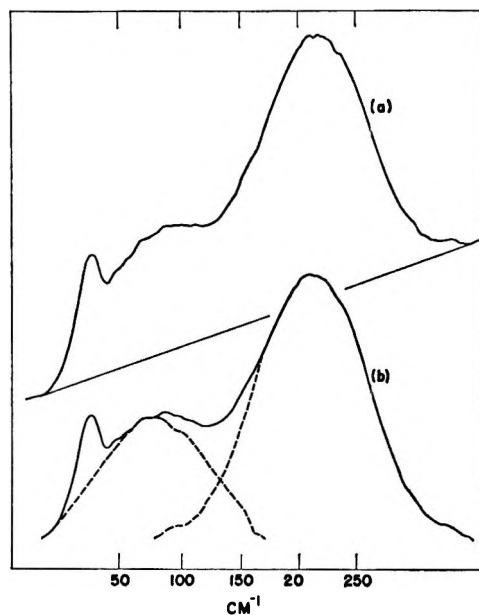


Figure 5. Anhydrous formic acid, 23° : (a) observed spectrum with linear background; (b) spectrum with linear background removed.

in Figure 5.³⁰ Two lines can be distinguished. The lower line, at $71 \pm 5 \text{ cm}^{-1}$, is probably a "liquid structure" line. The upper line is about 4.5 times as intense as the upper line of the glacial CH_3COOH spec-

trum and about 1.3 times as broad (*i.e.*, about 100 cm^{-1}). Its frequency is temperature dependent. The frequency is $209 \pm 3\text{ cm}^{-1}$ at 23° , $215 \pm 5\text{ cm}^{-1}$ at 8° , and $205 \pm 5\text{ cm}^{-1}$ at 56° . The frequency of the upper line of the anhydrous DCOOD spectrum at 23° is $176 \pm 3\text{ cm}^{-1}$. The 16% isotopic shift is about what is expected for an out-of-plane bend of an associated species of formic acid. However, the frequency is much lower than the 245 cm^{-1} observed for the B_g vibration of the cyclic dimer in benzene solution.

The spectra of aqueous solutions of HCOOH at 23° look about the same as the spectrum of the pure acid. The location of the upper maximum is concentration dependent, dropping from 209 cm^{-1} in pure HCOOH to $196 \pm 5\text{ cm}^{-1}$ in a 19 mole % aqueous solution. The isotopic shift in these solutions is the same as that in the pure acid, 16%. Figure 6 shows the spectrum of a 19 mole % aqueous solution of HCOOH. Water has a broad, weak line around 190 cm^{-1} ,³³ which can contribute an appreciable fraction of the observed intensity in the 180–200- cm^{-1} region of the spectra of the more dilute formic acid solutions. This fraction has been subtracted from the intensities shown in Figure 7, a plot of the specific intensity of the upper formic acid line as a function of the acid concentration in water.

Discussion

Acetic Acid. The spectrum of glacial acetic acid can be interpreted as the superposition of a weak line around 95 cm^{-1} on the spectrum of acetic acid in pentane solution. The dimerization equilibrium constants for acetic acid in alkanes³⁴ predict almost complete dimerization of the acid at the concentrations used in this work. Since no lines attributable to any species except the cyclic dimer have been found in the pentane solutions, it is assumed here that all the dimers at these concentrations in pentane are cyclic. The 95-cm^{-1} component can have no more than 15% of the total intensity of the spectrum without destroying the resolution between the 124- and 47-cm^{-1} lines. This puts a lower limit of 85% to the fraction of acid present as cyclic dimers in glacial acetic acid. X-Ray diffraction results⁴ and low-frequency infrared spectra^{27,28} are consistent with this conclusion.

As water is added to the acid, the 95-cm^{-1} component of the spectrum becomes more prominent and in solutions with less than 50 mole % acid it probably accounts for most of the observed intensity. The isotopic shift identifies this component as an out-of-plane bend (or possibly more than one out-of-plane bend) but gives no information as to whether the species responsible is an open dimer or a polymer. The specific intensity

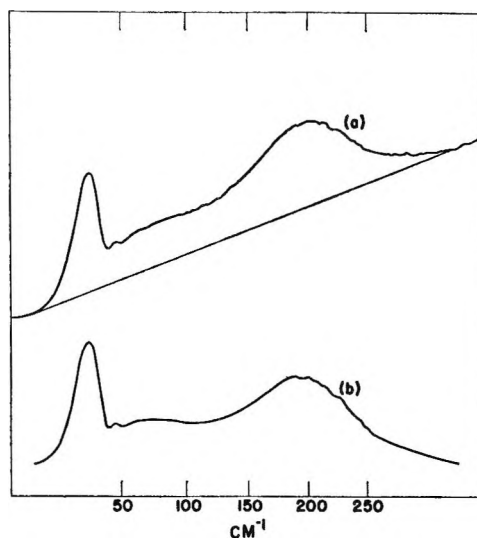


Figure 6. Aqueous solution, 19 mole % HCOOH, 81 mole % H_2O , 23° : (a) observed spectrum with linear background; (b) spectrum with linear background removed.

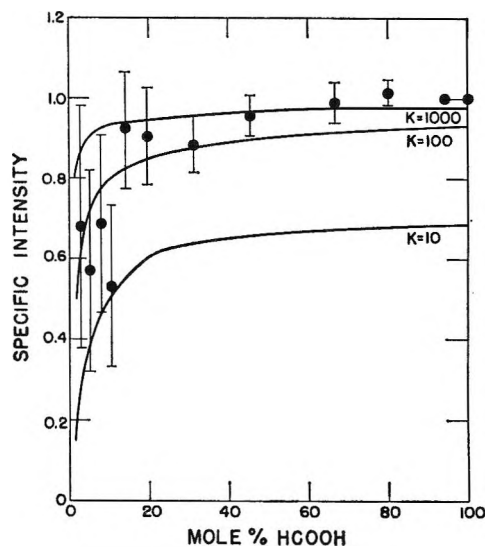


Figure 7. Specific intensity of the upper line in the spectrum of aqueous solutions of HCOOH at 23° , relative to the upper line of anhydrous HCOOH. The solid curves represent the intensity *vs.* concentration relationships expected for various values of K if the line is due to a dimer at all concentrations and if its specific intensity is independent of hydration effects.

is constant within the experimental error for solutions between 7.3 and 50 mole % acid, so that not much information can be obtained on equilibria involving the

(33) G. E. Walrafen, *J. Chem. Phys.*, **44**, 1546 (1966). Walrafen reports this line at 175 cm^{-1} . On our instrument, at the baffle settings used in this work and with the background drawn as shown in Figures 5 and 6, the maximum is located at $190 \pm 5\text{ cm}^{-1}$.

(34) (a) H. A. Pohl, M. E. Hobbs, and P. M. Gross, *ibid.*, **9**, 403 (1941); (b) M. Davies, P. Jones, D. Patnaik, and E. A. Moelwyn-Hughes, *J. Chem. Soc.*, 1249 (1951).

species responsible for the spectrum. If the species is indeed a dimer, then the dimerization equilibrium constant, $K = (\text{dimer})/(\text{monomer})^2$ in mole fraction units, must be greater than about 100 in the 10–20 mole % concentration region. In much more dilute solutions (<1 mole %), values of this constant have been reported as 2.8⁵⁵ and 10.^{9b}

Formic Acid. The temperature dependence of the frequency of the 209-cm⁻¹ line in anhydrous formic acid suggests that this line may be a composite of lines due to different associated species. The line is wide enough to include a 245-cm⁻¹ component (from the cyclic dimer), a 195-cm⁻¹ component (from species similar to those in dilute aqueous solution), and possibly others. The concentration dependence of the frequency in aqueous solutions (greater than 20 mole % in acid) may reflect changes in degree of association, degree of hydration, or both. If, in fact, the predominant species in the region between 2.5 and 20 mole % acid is an open dimer, then the break in the specific intensity vs. concentration curve can be fit by a dimerization equilibrium constant, $K = (\text{dimer})/(\text{monomer})^2$, of around 100 (in mole fraction units). In dilute solutions (<<1 mole %), a value of $K = 5$ has been reported.^{9c}

Dimerization Constants. Past attempts to determine the dimerization constants of these acids in water by high-frequency Raman spectra¹⁹ have been based on the assumption that all the associated acid is associated in the form of cyclic dimer. This assumption is clearly erroneous; the predominant associated species changes with concentration and below 20 mole % is probably the open dimer. The values of K reported here are based on intensities in the low-con-

centration region. The spectra are weak and these values are good only to an order of magnitude. These K values are, of course, quotients of concentrations, not of activities; they would not be expected to be the same as those measured in dilute (<1 mole %) solutions.

In-Plane Vibrations. In hydrocarbon solvents, only the B_g (out-of-plane bending) fundamentals of the cyclic dimers have been observed. The A_g vibrations, *i.e.*, the symmetric stretches calculated at 221 cm⁻¹ for (HCOOH)₂ and 193 cm⁻¹ for (CH₃COOH)₂ and the in-plane twist calculated at 95 cm⁻¹ for (CH₃COOH)₂,²⁵ are too weak to see. The weakness of the in-plane fundamentals can be understood on the assumption that the major contribution to the polarizability comes from the π electrons in the carbonyl bonds. A stretch or an in-plane bend of a hydrogen bond to a carbonyl oxygen may distort the in-plane lone pairs on the oxygen without disturbing the π electrons much. An out-of-plane bend of the hydrogen bond, however, will mix σ character into the π electrons and hence produce a change in their polarizability. The same argument can be applied to the lines in anhydrous formic acid and in the aqueous solutions, whether they are attributed to open dimers or to polymers. The isotopic shifts identify these vibrations as hydrogen bond bends and the intensities specify that the bends are out of the plane of the carbonyl groups.

Acknowledgments. The authors wish to thank C. E. Holley, Jr., under whose general direction most of this work was done, and especially Professor Henry Taube, who first suggested this problem and has furnished much valuable advice and criticism since.

(35) G. R. Nash and C. B. Monk, *J. Chem. Soc.*, 4274 (1957).

Electron Affinities of Polynuclear Acceptors.

Dinitro- and Trinitrophenanthrenequinones¹

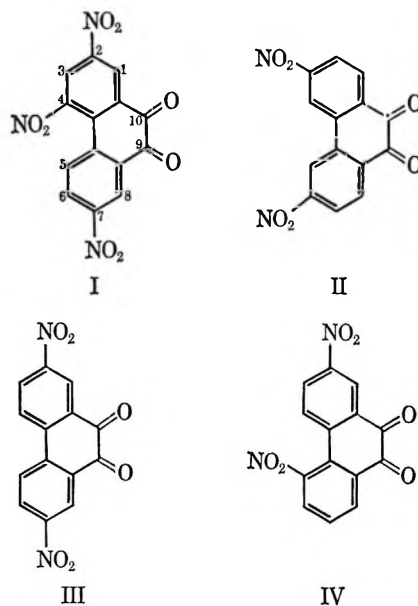
by Tapan K. Mukherjee

*Energetics Branch, Air Force Cambridge Research Laboratories, Bedford, Massachusetts
(Received January 5, 1967)*

Electron-acceptor strengths of 2,4,7-trinitrophenanthrenequinone (I), 3,6-dinitrophenanthrenequinone (II), 2,7-dinitrophenanthrenequinone (III), and 2,5-dinitrophenanthrenequinone (IV) have been determined from charge-transfer spectra and from half-wave reduction potentials. The order of electron affinities is found to be 2,4,7- > 3,6- > 2,7- > 2,5-. The energies of the absorption bands of the semiquinone radical ions are linearly related to the electron affinities and half-wave potentials of the quinones. Stable salts of 2,4,7-trinitrosemiquinone (I) radical ions with N-methylquinolinium and lithium cations, respectively, have been isolated. The acceptor property of the 2,5-dinitro isomer is decreased owing to the steric interference of the nitro group at position 5. From the reported data of the spin densities of phenanthrenequinone radical ion, it is suggested that the 3,6-dinitro isomer will be the strongest acceptor in the dinitro series and 1,3,6,8-tetra-nitrophenanthrenequinone will be a very powerful acceptor.

Introduction

This study was designed to investigate the complexing properties of organic charge-transfer acceptors of relatively large molecular radii. It is hoped that this work will lead to the discovery of powerful acceptors which will form solid complexes of sandwich configuration and maximum π -orbital overlap with polynuclear donor molecules. Such complexes are needed for better understanding of the mechanism of solid-state electrical conduction in donor-acceptor complexes. Most of the known strong acceptors like chloranil, tetracyanoethylene, etc., are relatively small molecules, their acceptor strengths depending on the number and electronegativity of the functional groups which are suitably placed around restricted conjugated systems. Lepley and Thelman² have set up qualitative criteria of acceptor strengths on the basis of the above-mentioned characteristics. The structural features of electron acceptors have been reviewed by Briegleb³ and Andrews.⁴ We have studied the properties of several acceptors derived from nitrofluorenes.⁵ Electron-acceptor characteristics of the following nitro derivatives of phenanthrenequinone are reported in this paper.



(1) A part of this work was presented at the 4th Caribbean Chemical Symposium held at Kingston, Jamaica, Jan 3-7, 1967.

(2) A. R. Lepley and J. P. Thelman, *Tetrahedron*, **22**, 101 (1966).

(3) G. Briegleb, *Angew. Chem.*, **76**, 326 (1964).

(4) L. J. Andrews and R. M. Keifer, "Molecular Complexes in Organic Chemistry," Holden-Day, Inc., San Francisco, Calif., 1964.

Experimental Section

Synthesis of 2,7-Dinitrophenanthrenequinone and 2,5-Dinitrophenanthrenequinone. Nitration of phenanthrenequinone (purified by crystallization and sublimation) with nitric acid (*d* 1.51) by the method outlined by Schmidt and Kamf⁶ afforded a mixture of dinitrophenanthrenequinones in 82% yield. Separation of the isomers was effected by fractional crystallization from glacial acetic acid, in which 2,5-dinitro isomer was more soluble. Repeated crystallizations from glacial acetic acid, followed by chromatography over silica gel using benzene as eluent, gave 2,7-dinitrophenanthrenequinone, mp 301–303°, and 2,5-dinitrophenanthrenequinone, mp 230–232° (lit.⁷ 228–230°). The purity of the isomers was checked by thin layer chromatography. Since pure materials were needed in this work, no attention was given to the yields of the separated isomers.

3,6-Dinitrophenanthrenequinone was synthesized via a multistep reaction sequence described by Schenck and Schmidt-Thombeé,⁸ which involved the preparation of the photoadduct of phenanthrenequinone with sulfur dioxide, its nitration, and the pyrolytic elimination of sulfur dioxide; mp 293–295° (from Ac₂O).

2,4,7-Trinitrophenanthrenequinone was synthesized by drastic nitration of 2,7-dinitrophenanthrenequinone.⁹ The crude product was crystallized three times from benzene when shiny yellow crystals of the benzene complex were obtained, mp 203–205°. Recrystallization from glacial acetic acid afforded pure 2,4,7-trinitrophenanthrenequinone, mp 212–213° dec.¹⁰

Spectra. The charge-transfer absorption spectra were taken in a Cary Model 14 recording spectrophotometer. The measurements were made at room temperature, using methylene dichloride as a solvent, in stoppered quartz cells of 1-cm path lengths. Solutions of the complexes were prepared by adding a solution of the acceptor to the solution of large excess of the donor. The reference cell contained the solution of the donor. In several cases, mixing of the solution of I with a donor resulted in the separation of solid complexes which were removed by filtration and the filtrate was used for spectral measurement. Analyses of the solids corresponded with 1:1 composition for complexes with 1,2-benzanthracene, 3,4-benzopyrene, and anthracene, respectively. Charge-transfer spectra of a few of the powdered solid complexes in Nujol film were recorded. There was no significant difference between the peaks of the long wavelength absorption maxima of the solids and solutions. The donor hydrocarbons were used in the form obtained from Rutgerswerke-Aktiengesellschaft, Frankfurt-am-Main, West Germany.

Polarography. Both a Sargent Model XV and a Sargent Model XXI polarograph were employed in this research. Spectral grade acetonitrile as solvent and tetra-*n*-butylammonium perchlorate (TBA) and lithium perchlorate as supporting electrolytes were used. Polarographic data were obtained at room temperature, using a three-electrode Arthur and Vanderkam¹¹ cell. The *IR* drop in the cell was compensated by a Sargent Model A compensator. Two identical calomel electrodes were used as the electrolysis reference electrode (ERE) and the stable reference electrode (SRE). The electrolyses were carried out under nitrogen atmosphere and the measurements were recorded under conditions of "long immersion."¹² The dropping mercury electrode was used at 71-cm pressure and had a drop time of 3.6 sec (open circuit) in acetonitrile; concentration was 1 mmole/l.

Results and Discussion

Charge-Transfer Spectra. Molecules capable of donating an electron react with molecules which can accept the electron and during this process often give rise to new absorption bands at lower frequencies than those of the donors or acceptors. The extent of the reaction ranges from weak orbital interaction to complete transfer of an electron from the highest filled orbital of the donor to the lowest unfilled orbital of the acceptor, and the energy of the resultant charge-transfer band, derived from simple molecular orbital treatment,¹³ is given by the relationship

$$E_{\pi} = B_j - (\alpha + \chi_i\beta) \quad (1)$$

where B_j is the energy of the acceptor orbital involved in the interaction, α is the coulomb integral for carbon, β is the carbon-carbon resonance integral, and χ_i is the energy coefficient of the highest filled orbital of the

(5) (a) T. K. Mukherjee and L. Levasseur, *J. Org. Chem.*, **30**, 644 (1965); (b) T. K. Mukherjee, *J. Phys. Chem.*, **70**, 12, 3848 (1966); (c) T. K. Mukherjee and A. Golubovic, Abstracts, 149th National Meeting of the American Chemical Society, Detroit, 1965, p 108.

(6) J. Schmidt and A. Kamf, *Chem. Ber.*, **35**, 3117 (1902).

(7) Schmidt and Kamf⁶ thought that they obtained the 4,5-dinitro isomer; however, Christie and Kenner (*J. Chem. Soc.*, 671 (1926)) later showed that this was, in fact, the 2,5-dinitro isomer.

(8) G. O. Schenck and G. A. Schmidt-Thombeé, *Ann. Chem.*, **584**, 199 (1953).

(9) G. H. Christie and J. Kenner, *J. Chem. Soc.*, **123**, 779 (1926).

(10) The apparent discrepancy of the melting point with literature prompted us to confirm the structure of the 2,4,7-trinitrophenanthrenequinone by potassium dichromate oxidation leading to the known 4,4',6-trinitrodiphenic acid, mp 290–291.

(11) P. Arthur and R. H. Vanderkam, *Anal. Chem.*, **33**, 765 (1961). This cell is supplied by E. H. Sargent and Co.

(12) J. F. Coetzee and G. R. Padmanabhan, *J. Phys. Chem.*, **66**, 1709 (1962).

(13) (a) M. J. S. Dewar and A. R. Lepley, *J. Am. Chem. Soc.*, **83**, 4560 (1961); (b) M. J. S. Dewar and H. Rogers, *ibid.*, **84**, 395 (1962).

Table I: The Charge-Transfer Absorption Maxima for Hydrocarbon Complexes with the Nitro Derivatives of Phenanthrenequinones and Their Relative Electron Affinities

No.	Donor	$\chi_i(\beta)^a$	Acceptor (Nitrophenanthrenequinone)							
			—2,4,7-Trinitro (I)—		—3,6-Dinitro (II)—		—2,7-Dinitro (III)—		—2,5-Dinitro (IV)—	
			$E_\pi, m\mu$	EA^b	$E_\pi, m\mu$	EA^b	$E_\pi, m\mu$	EA^b	$E_\pi, m\mu$	EA^b
	None		367, 322		410, 317		385, 295		375, 278	
1.	Anthracene	0.414	635 ± 5	1.26	595 ± 5	1.15	570 ± 10	1.06	560 ± 8	1.02
2.	Perylene	0.347	735 ± 2	1.26	705	1.19	660	1.07	650 ± 3	1.04
3.	3,4-Benzopyrene	0.371	680 ± 3	1.22	645 ± 3	1.12	615	1.03	605 ± 5	1.00
4.	1,2-Benzopyrene	0.497	580 ± 5	1.24	540 ± 5	1.08	523 ± 10	1.00	507 ± 10	0.93
5.	1,2-Benzanthracene	0.452	610 ± 2	1.26	572 ± 5	1.13	550	1.04	537 ± 5	0.99
6.	3,4-Benzotetraphene	0.405	650 ± 3	1.24	600 ± 5	1.08	585 ± 2	1.03	575 ± 5	0.99
7.	Pyrene	0.445	610 ± 2	1.29	575 ± 5	1.17	555 ± 12	1.09	545 ± 10	1.05
8.	1,2,5,6-Dibenzanthracene	0.473	600	1.24	555 ± 5	1.07	537 ± 10	1.00	525	0.94
9.	1,2,3,4-Dibenzanthracene	0.499	585	1.28	535	1.08	517	0.99	505	0.94
10.	Decacyclene	0.470	600 ± 2	1.27	560 ± 10	1.11	560 ± 5	1.12	525 ± 5	0.07

^a Energy of highest occupied MO; C. A. Coulson and R. Daudel, "Dictionary of Values of Molecular Constants." ^b From $(E_\pi)_i - (E_\pi)_k = EA_k - EA_i$.

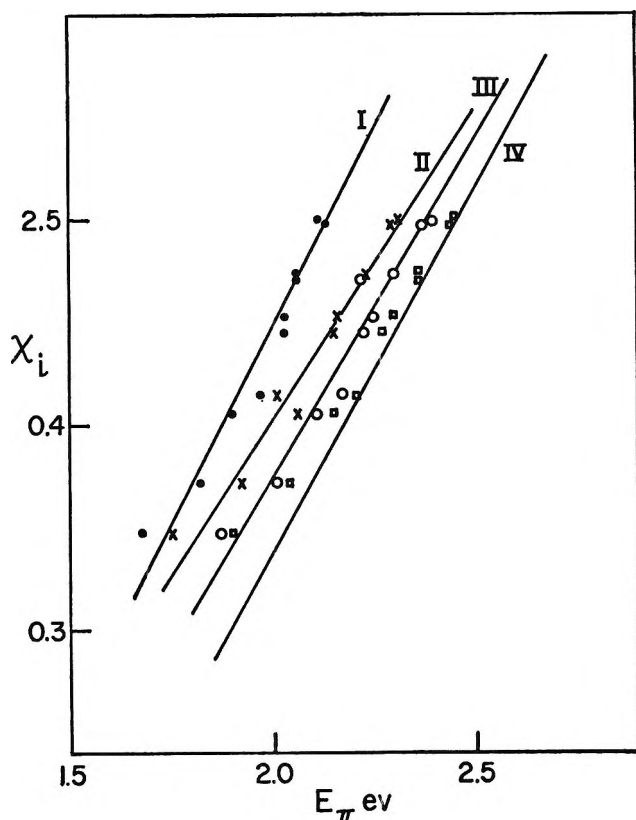


Figure 1. Plots of the transition energies of the charge-transfer bands of polynitrophenanthrenequinones against the energies of the highest occupied molecular orbitals of donor hydrocarbons (Table I): ●, 2,4,7-trinitrophenanthrenequinone (I); ×, 3,6-dinitrophenanthrenequinone (II); ○, 2,7-dinitrophenanthrenequinone, (III); □, 2,5-dinitrophenanthrenequinone (IV).

donor. This relationship holds reasonably well for large sets of $\pi-\pi$ interactions between a given acceptor

and a series of aromatic hydrocarbon donors for which $\chi_i\beta$ values are available.¹⁴ The weakness in the binding of the π complexes is shown by the fact that the principle bands of the donors and acceptors are not perturbed. Table I lists the wavelengths (E_π) of the charge-transfer absorption bands found for ten donors. The wavelength maxima of the acceptors are recorded in the first row. Since the charge-transfer bands are sufficiently separated from the first singlet transitions of the donors, the latter are not included in the table.¹⁵ Plots between E_π and $\chi_i\beta$ for the four acceptors are shown in Figure 1 and, as expected from eq 1, close linear relationships are observed. The straight lines are those derived from the method of least squares.¹⁶

The slope from eq 1 gives the value of β which has been found by other workers to be constant and is close to -3.01 , the β value for benzene. The intercept of the straight line ($E_\pi = 0$) gives the value of $(B_j - \alpha)$, a measure of acceptor strength. Inspection of Table I reveals that, for a given donor, the absorption maxima for the first C-T transition shifts regularly from lower to higher energy, indicating the following order of the acceptor strengths of the nitro derivatives of phenanthrenequinone; 2,4,7-trinitro (I) > 3,6-dinitro (II) > 2,7-dinitro (III) > 2,5-dinitro (IV). However, this order is not retained in the intercepts of the straight lines of I-IV ($\beta = -2.65, -3.02, -3.29, -3.38$ and $(B_j - \alpha) = 0.81, 0.87, 0.67, 0.76$ for ac-

(14) C. A. Coulson and R. Daudel, "Dictionary of Values of Molecular Constants," Mathematical Institute, Oxford, England. A handy compilation is available in ref 13.

(15) For convenient tabulation, see A. R. Lepley, *J. Am. Chem. Soc.*, **84**, 3577 (1962), Tables I and II.

(16) We wish to thank Miss N. Dimond for her assistance with the computation work carried out at the AFCRL Computation Center.

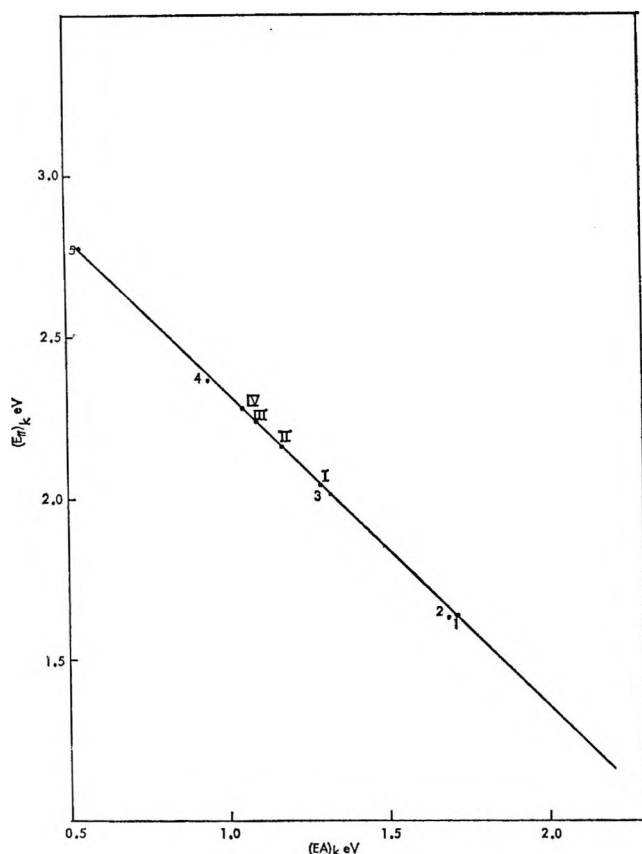


Figure 2. Charge-transfer energy $(E_{\pi})_k$ as a function of electron affinities, $(EA)_k$, of acceptors according to eq 2: donor, pyrene; acceptors, (I) 2,4,7-trinitrophenanthrenequinone, (II) 3,6-dinitrophenanthrenequinone, (III) 2,7-dinitrophenanthrenequinone, (IV) 2,5-dinitrophenanthrenequinone. (1) Tetracyanoethylene, (2) tetracyanoquinodimethene, (3) chloranil, (4) 2,4,7-trinitrofluorenone, (5) 1,3,5-trinitrobenzene.

ceptors I, II, III, and IV, respectively). The reason for this discrepancy is mainly owing to the scatter of the points and limited number of the complexes studied. A small deviation in the slope induces a large deviation in the intercept. Further, the linear relationship itself is predicted by an oversimplified use of the Hückel theory.^{15,17}

Alternatively, the electron affinities of two acceptors can be compared from their charge-transfer transitions with a common donor. Thus, if $(E_{\pi})_i$ and EA_i stand for the charge-transfer energy and electron affinity of the standard acceptor, respectively, then EA_k , the electron affinity of a second acceptor, is obtained from

$$(E_{\pi})_i - (E_{\pi})_k = EA_k - EA_i \quad (2)$$

where $(E_{\pi})_k$ is the charge-transfer energy of the complex with the same donor. This relationship is re-

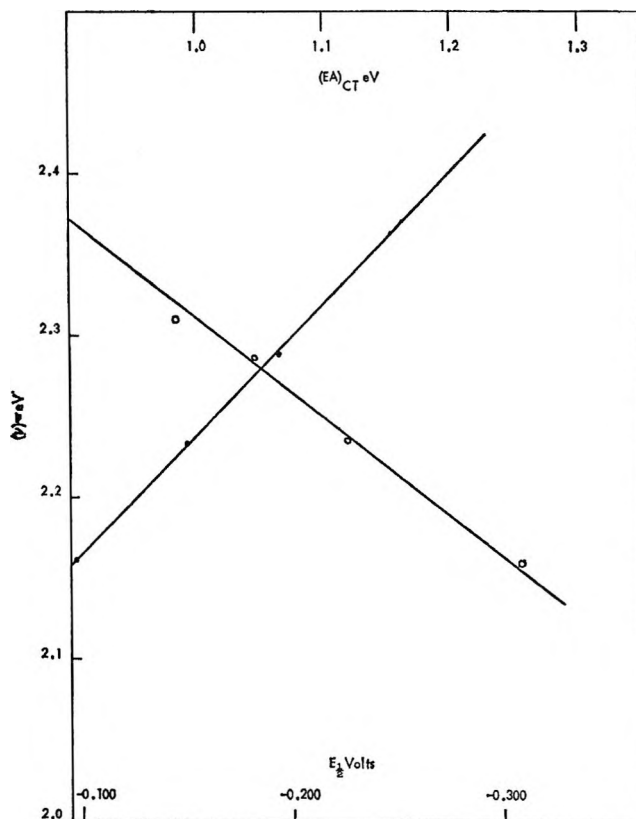


Figure 3. Correlation between the energy of the semiquinone anion radical and (a) half-wave potential, ●, and (b) average electron affinities, ○, of polynitrophenanthrenequinones.

stricted to the complexes of same bond type and configuration.³ In the present case, we have used 2,4,7-trinitrofluorenone (TNF) as the standard. This preference has no special significance except that the molecular dimension of TNF is comparable with the acceptors used here and it has been used as a standard in the determination of electron affinities of polynitro derivatives of fluorene- $\Delta^{9\alpha}$ -malononitrile.¹⁸

The average electron affinity of 2,4,7-trinitrofluorenone, as determined from charge-transfer spectra, is 1 eV (compared to chloranil).³ From polarographic half-wave potential the value is 0.94 eV; since the one-electron reversible reduction potential is more accurate than the C-T bands, $EA_i = 0.94$ eV has been used as standard. The electron affinities of the dinitro- and trinitrophenanthrenequinones as calculated from eq 2 are shown in Table I. An approximately linear relationship exists between the C-T energy and electron affinities of these acceptors with one and the same

(17) R. S. Mulliken and W. B. Person, *Ann. Rev. Phys. Chem.*, **13**, 107 (1962).

(18) T. K. Mukherjee, submitted.

Table II: Polarography of Quinones in Acetonitrile

Compound	Supporting electrolyte, N-t-butyl perchlorate					Supporting electrolyte LiClO ₄	
	$E_{1/2}'$ vs. sce	$E_{1/4}'' - E_{1/4}'$	I^a	EA^b	EA^c	$E_{1/2}'$ vs. sce	$E_{1/4}'' - E_{1/4}'$
Phenanthrenequinone	-0.660	72	3.68	0.69	0.70 ^d	-0.235	30
2,4,7-Trinitrophenanthrenequinone (I)	-0.098	75	3.63	1.29	1.256	0.085	30
3,6-Dinitrophenanthrenequinone (II)	-0.150	90	4.07	1.23	1.118	0.062	30
2,7-Dinitrophenanthrenequinone (III)	-0.195	70	4.01	1.19	1.043	0.045	30
2,5-Dinitrophenanthrenequinone (IV)	-0.265	110	3.16	1.11	0.982	0.012	30

^a Limiting current constant $I = i_d/Cm^{3/2}t^{1/2}$, where i_d is the limiting current in microamperes, C is concentration in millimoles per liter, m is the mass of mercury flowing in milligrams per second, and t is drop time in seconds. ^b From eq 3, positive values of $E_{1/2}'$ taken. ^c Average values from charge-transfer spectra, Table I. ^d See ref 3, Table VI.

donor, which is illustrated in Figure 2 using pyrene as the donor. A relative comparison of the acceptor strengths of these quinones with other well-known acceptor molecules can be obtained from the additional data included in Figure 2.

Polarography. The one-electron reversible half-wave reduction potential, measured in aprotic solvents, against a calomel electrode is related linearly to the electron affinity of an acceptor according to eq 3^{3,19}

$$EA = 1.04E_{1/2}^{\text{red}} + 1.39 \quad (3)$$

In these solvents, quinones are reduced by two one-electron steps to the semiquinone anions and hydroquinone dianions, respectively. In alkali metal perchlorate as supporting electrolyte, the reduction can proceed either by two consecutive one-electron transfers or a one-step two-electron transfer. Lithium cation markedly shifts $E_{1/2}$ to more positive potential.²⁰ The first half-wave potentials for 2,4,7-trinitrophenanthrenequinone and the three dinitro isomers are shown in Table II. The number of electrons involved in each step are deduced from Tomés' relationship,²¹ $E_{1/4}'' - E_{1/4}' = 59$ mv for a one-electron reversible electrode process at 25°. Excepting the large deviation of 2,5-dinitro isomer (IV) in TBA, this criterion is approximately fulfilled in both the electrolytes; in the latter, reductions proceed by two-electron single steps. The reversibility of the reduction in TBA is not as good as in lithium perchlorate. However, electron affinities calculated from $E_{1/2}$ values²² in TBA fit in the same order as those obtained from charge-transfer spectra. Since aromatic nitro groups are reduced at more negative potentials,²³ it is reasonable to assume that the first electron addition takes place to the lowest unoccupied orbital of the α -diketone function.

Neglecting the questionable constancy of the reduction mechanism and of the transfer coefficient, the large negative displacement of the half-wave poten-

tial of the 2,5-dinitro compound (IV) can be attributed to the decoupling of the 5-nitro group from the ring due to steric hindrance. A space-filling model, together with a simple calculation involving normal bond lengths and angles with allowable distortions, indicates that the nitro group at position 5 is twisted out of the plane of the ring by 75–90°. Geske and co-workers²³ found that in substituted nitrobenzenes, the half-wave potentials shift linearly with the angle of twist of the nitro group. In 2,4,7-trinitro derivative (I) the inductive effect of the third nitro group supersedes the inhibitory influence of the sterically hindered nitro group at position 4.

In the absence of any steric factor, the difference in the resonance energies of II and III is probably responsible for the differences in electron affinities.

Anion Radical. Watson and Matsen²⁴ showed that the half-wave reduction potentials of aromatic hydrocarbons are related to the frequencies of the long wavelength absorption maxima according to

$$\nu = 2E_{1/2} + \text{constant} \quad (4)$$

Apparently, this relationship has not been extensively examined for π acceptors. In the first place, the task of assignment of energy levels in polysubstituted quinones is difficult owing to the absence of suitable parameters in molecular orbital calculation.²⁵ Berg,

(19) R. M. Hedges and F. A. Matsen, *J. Chem. Phys.*, **28**, 950 (1958).

(20) M. E. Peover and J. D. Davis, *J. Electroanal. Chem.*, **6**, 46 (1963).

(21) J. Tomés, *Collection Czech. Chem. Commun.*, **9**, 12 (1937).

(22) M. E. Peover, *Trans. Faraday Soc.*, **58**, 1656 (1962), see footnote, p 1657.

(23) D. H. Geske, J. L. Ragle, M. A. Bambenek, and A. L. Blach, *J. Am. Chem. Soc.*, **86**, 987 (1964).

(24) (a) A. T. Watson and F. A. Matsen, *J. Chem. Phys.*, **18**, 1305 (1950); (b) I. Bergman, *Trans. Faraday Soc.*, **50**, 829 (1954).

(25) M. E. Peover, *J. Chem. Soc.*, 4540 (1962).

however, found that the first half-wave reduction potentials of quinones (measured in 40% isopropyl alcohol and 60% aqueous buffer at pH 7) show linear dependencies on the excitation energies of the $n-\pi^*$ transitions.²⁶

As some uncertainty remains in the identification of $\pi-\pi^*$ and $n-\alpha^*$ transitions in the acceptors studied here, the spectra of their anion radicals were correlated with the electron affinities and half-wave potentials. In order to avoid the formation of diamagnetic ion pairs (commonly encountered when alkali metals are used), the semiquinone radical ions were generated by adding acetonitrile solution of N-methyl-N-triethylammonium iodide to the solutions of the quinones.²⁷ Fairly stable semiquinone radical ions^{28,29} with absorption in 500–600-m μ range were obtained. The 2,5-dinitro compound (IV) gave two peaks at 537 and 508 m μ , respectively. Absorption maxima for other radical ions were (I) 572 m μ , (II) 555 m μ , and (III) 543 m μ . In Figure 3, it will be observed that a linear relationship exists between the energy of the semiquinone radical ion and the average electron affinities of the acceptors (from Table I). Similarly, the energy of the radical ion is approximately related to the reduction potential by $(\nu) \cdot^- = 0.88E_{1/2} + \text{constant}$.

Dehl and Fraenkel³⁰ found that the odd electron densities in phenanthrenequinone ion radical are larger in positions 1 (0.057) and 3 (0.071) than those at 2 (0.008) and 4 (0.018). Their experimental results

were in accord with the Hückel and McLachlan calculations. Highly polar nitro groups at 1,3 and their equivalent 6 and 8 positions will cause enhanced depletion of electrons from the ring; consequently, 1,3-dinitrophenanthrenequinone is expected to be the strongest acceptor in the dinitro series. On the same basis, one can predict that 1,3,6,8-tetranitrophenanthrenequinone will be an extremely powerful acceptor.

Acknowledgment. The author is grateful to Dr. R. Payne for helping with the polarographic measurements. Thanks are also due to Dr. Jerry Silverman for helpful discussions.

(26) H. Berg and K. Kramarczyk, *Ber. Bunsenges. Physik. Chem.*, **68**, 296 (1964).

(27) (a) Potassium is known to produce even a trianion radical from phenanthrenequinone. N. A. Bauld, *J. Am. Chem. Soc.*, **86**, 3894 (1964). (b) Iodide ion functions as an electron donor, in turn being oxidized to iodine which is scavenged as I_3 by excess of iodide present in the solution. Iodine in acetonitrile absorbs at 465 and 380 m μ , respectively. For peaks in other solvents, see H. A. Benesi and J. H. Hildebrand, *J. Am. Chem. Soc.*, **71**, 2703 (1949). The cation does not absorb in the visible range.

(28) Corresponding absorption for mononegative sodium ketyl from unsubstituted phenanthrenequinone absorbs at 475 m μ . K. Maruyama, *Bull. Chem. Soc. Japan*, **37**, 553 (1964).

(29) Strongly paramagnetic semiquinone radical salts of I have been isolated as black crystals; e.g., (a) N-methylquinolinium salt, mp 237° dec, *Anal.* Calcd for $C_{24}H_{15}N_4O_8$: C, 59.13; H, 3.10; N, 11.49. Found: C, 59.09; H, 3.43; N, 13.2; (b) lithium salt, mp 308° (explodes), *Anal.* Calcd for $C_{14}H_5LiN_3O_8$: C, 48.02; H, 1.43; N, 12; Li, 1.98. Found: C, 47.84; H, 1.70; N, 12.24; Li, 1.77. Although the free-radical contents of these salts have not been determined, it is almost certain that the lithium salt is contaminated with some diamagnetic dianion.

(30) R. Dehl and G. K. Fraenkel, *J. Chem. Phys.*, **39**, 1793 (1963).

The Hydration of Amines in Organic Solvents

by M. Duane Gregory, Sherril D. Christian, and Harold E. Affsprung

Department of Chemistry, University of Oklahoma, Norman, Oklahoma 73069 (Received January 9, 1967)

The hydration of a number of amines has been studied using partition and water solubility data at various water activities. Solutions of cyclohexylamine and its N-methyl derivatives in benzene at 25 and 35° and of triethylamine in benzene, cyclohexane, and toluene at 25° have been investigated. Equilibrium constants for the 1:1 complexes have been determined. Enthalpies of hydration for the cyclohexylamines have been calculated.

Introduction

Numerous studies have been reported of the hydrogen bonding of amines with alcohols, acids, water, and other proton donors.¹⁻⁸ However, little quantitative information relating to the formation of amine hydrates in organic solvents is available. Mohr, Wilk, and Barrow⁷ have reported an infrared spectral investigation of the hydration of various organic bases in CCl₄; they suggest that the water spectra are consistent with the existence of 1:1 hydrates at low base concentration and also bridged hydrates, involving two base molecules and one water molecule, at higher base concentrations. Thompson⁵ has reported that pyridine and water form a 1:1 complex in CCl₄; Sidorov⁶ reports both the 1:1 and 2:1 hydrates for this system.

Previous reports from this laboratory have described studies of the hydration of various proton donors and acceptors in organic solvents.⁹⁻¹² Techniques were presented for inferring hydration constants from measurements of water solubility at known water activity and of distribution ratios.⁹⁻¹³ We report here a similar study of the hydration of several aliphatic amines in benzene and of triethylamine in benzene, toluene, and cyclohexane.

Experimental Section and Results

Reagent grade benzene, toluene, and cyclohexane were fractionally distilled using a 30-plate Oldershaw column. The cyclohexylamines were obtained from Eastman Organic Chemicals; the triethylamine was a product of Matheson Coleman and Bell. The amines were purified by distillation with no special effort to remove the water present since the amines were to be

hydrated. The temperature of the thermostated bath was controlled at 25.0 ± 0.1 and $35.0 \pm 0.05^\circ$.

Partition experiments were performed using the method described by Christian, Affsprung, and Taylor.⁵ Water solubilities were obtained using solute isopiestic equilibrators described previously.¹³ The various water activity solutions were prepared with reagent grade calcium chloride.

All amine concentrations were determined by titration with 0.1 N HCl, which was standardized with Na₂CO₃. The end points were determined with a Beckman Zeromatic pH meter. Water concentrations were determined with a Beckman KF-3 aquameter.

- (1) C. S. Marvel, M. J. Copley, and E. Ginsberg, *J. Am. Chem. Soc.*, **62**, 3109 (1940).
- (2) T. J. V. Findlay and A. D. Kidman, *Australian J. Chem.*, **18**, 521 (1965).
- (3) E. A. Yerger and G. M. Barrow, *J. Am. Chem. Soc.*, **77**, 4474 (1955).
- (4) T. Zeegers-Huyskens, *Bull. Soc. Chim. Belges*, **69**, 282 (1960).
- (5) W. K. Thompson, *J. Chem. Soc.*, 4028 (1964).
- (6) A. N. Sidorov, *Opt. Spectry. (USSR)*, **7**, 24 (1960).
- (7) S. C. Mohr, W. D. Wilk, and G. M. Barrow, *J. Am. Chem. Soc.*, **87**, 3048 (1965).
- (8) R. L. Denyer, A. Gilchrist, J. A. Pegg, J. Smith, T. E. Tomlinson, and L. E. Sutton, *J. Chem. Soc.*, 3889 (1955).
- (9) S. D. Christian, H. E. Affsprung, and S. A. Taylor, *J. Phys. Chem.*, **67**, 187 (1963).
- (10) J. R. Johnson, S. D. Christian, and H. E. Affsprung, *J. Chem. Soc.*, 1 (1965).
- (11) T. F. Lin, S. D. Christian, and H. E. Affsprung, *J. Phys. Chem.*, **69**, 2980 (1965).
- (12) G. O. Wood, D. D. Mueller, S. D. Christian, and H. E. Affsprung, *ibid.*, **70**, 2691 (1966).
- (13) S. D. Christian, H. E. Affsprung, J. R. Johnson, and J. D. Worley, *J. Chem. Educ.*, **40**, 419 (1963).

Table I: Distribution Constants for Amines

Amine	Solvent	Temp, °C	Concn range, M	K_D^f
Cyclohexylamine	Benzene	25	0.067-0.149	4.18 ± 0.15
Cyclohexylamine	Benzene	35	0.039-0.187	5.50 ± 0.16
N-Methylcyclohexylamine	Benzene	25	0.040-0.131	11.35 ± 0.82
N,N-Dimethylcyclohexylamine	Benzene	25	0.040-0.138	42.48 ± 0.76
Triethylamine	Benzene	25	0.044-0.467	14.20 ± 0.38
Triethylamine	Toluene	25	0.048-0.484	11.64 ± 0.25

The Karl Fischer reagent used in these titrations was standardized by two methods. The first method involved titrating weighed amounts of sodium tartrate dihydrate and the second method employed a solution of pure benzene saturated with water at 25°. The solubility of water in benzene at this temperature was assumed to be 0.035 M.¹⁴ The solubility of water in benzene at 35° was determined to be 0.0465 M and for toluene and cyclohexane the solubility at 25° was found, by the isopiestic method, to be 0.0268 and 0.00297 M, respectively.

Distribution ratios for the amines at constant temperature were found to be independent of concentration within experimental error. Values of the formal distribution constant, K_D^f , defined as the ratio of the formal concentration of the amine in the organic solvent (f_A^O) to its formal concentration in water (f_A^W), are given in Table I. Based on the constancy of the values of K_D^f for each system, it has been concluded that the amine monomer and monomer hydrates are the principal amine species present in the organic phases.

Table II includes values of Δf_w , the increase in the formal solubility of water in the organic phase which occurs at a given water activity, a_w , owing to the presence of amine at the measured formal concentration, f_A^O . The increase in water solubility is attributed entirely to the formation of amine hydrates.

Figure 1 shows a plot of Δf_w as a function of f_A^O at various fixed values of a_w for one of the systems, triethylamine-water-benzene at 25°.

Discussion

Figure 1, which is typical of the amine-water-organic solvent systems, reveals the principal features of the water solubility data. Increases in Δf_w at constant a_w appear to be proportional to f_A^O and Δf_w varies nearly linearly with a_w at constant f_A^O . This immediately suggests that the amine monohydrate is the primary hydrated species present in the organic media. A nonlinear least-squares method¹⁵ was used

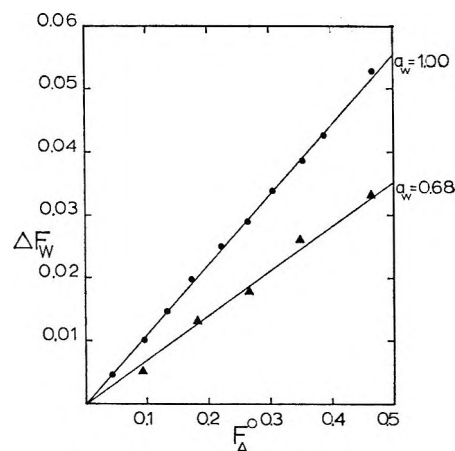


Figure 1. Triethylamine-water-benzene.

to obtain the best values of K_{AW} , the formation constant for the 1:1 hydrate, consistent with the equations

$$\Delta f_w = K_{AW} C_A C_W \quad (1)$$

$$f_A^O = C_A + K_{AW} C_A C_W \quad (2)$$

$$C_W = a_w C_W^O \quad (3)$$

where K_{AW} is the equilibrium constant for formation of the amine monohydrate, C_W and C_A are monomer concentrations of water and amine, respectively, and C_W^O is the solubility of water at unit water activity in the given solvent at the given temperature. It was assumed that all the experimental error resides in the Δf_w values. Equations 1-3 will be valid if the 1:1 hydrate is the only solute complex present and if Henry's law is obeyed by each solute species individually.

The calculated values of the increase in water solubility, Δf_w (calcd), appearing in Table II were obtained from the least-squares treatment as were the solid curves appearing in Figure 1. It is observed that the

(14) J. R. Johnson, S. D. Christian, and H. E. Affsprung, *J. Chem. Soc., Sect. A*, 77 (1966).

(15) T. F. Lin, Ph.D. Dissertation, University of Oklahoma, 1966.

Table II: Change in Water Solubility with Changes in Water Activity and Concentration of Amine

Solute	Solvent	Temp, °C	f_A^0 , M	a_w	Δf_w , M	Δf_w (calcd), M	
CHA	Benzene	25	0.0847	0.327	0.0038	0.0062	
				0.440	0.0066	0.0081	
				0.559	0.0087	0.0100	
				0.712	0.0117	0.0122	
			0.1102	0.851	0.0133	0.0143	
				0.327	0.0062	0.0080	
				0.440	0.0094	0.0103	
				0.559	0.0136	0.0127	
			0.1491	0.712	0.0163	0.0157	
				0.327	0.0082	0.0094	
				0.440	0.0114	0.0142	
				0.559	0.0152	0.0175	
			0.0670	0.712	0.0187	0.0218	
				0.851	0.0233	0.0252	
				0.327	0.0059	0.0047	
				0.440	0.0046	0.0058	
			0.0469	0.712	0.0086	0.0079	
				0.851	0.0114	0.0087	
				1.00	0.0085	0.0090	
				0.0668	0.0133	0.0140	
				0.0872	0.0169	0.0165	
				0.1351	0.0265	0.0256	
				0.1752	0.0349	0.0331	
				0.0535	0.0102	0.0102	
0.0792	0.0154	0.0150					
0.1077	0.0210	0.0204					
0.1590	0.0314	0.0300					
0.1961	0.0402	0.0367					
CHA	Benzene	35	0.0390	1.00	0.0072	0.0076	
					0.0501	0.0086	0.0099
					0.0565	0.0117	0.0107
					0.0640	0.0126	0.0123
			0.0843	0.0729	0.0146	0.0139	
				0.0837	0.0167	0.0160	
				0.0944	0.0179	0.0183	
				0.1076	0.0194	0.0211	
			0.1087	0.1086	0.0230	0.0204	
				0.0540	0.0071	0.0076	
				0.0843	0.0122	0.0117	
				0.1087	0.0146	0.0153	
0.1867	0.1351	0.0183	0.0190				
	0.1867	0.0258	0.0261				
	0.0405	0.0056	0.0064				
	0.0581	0.0086	0.0091				
NMCHA	Benzene	25	0.0405	1.00	0.0125	0.0128	
					0.0820	0.0157	
					0.1009	0.0160	
					0.1147	0.0181	
			0.0383	0.1315	0.0209	0.0178	
				0.0383	0.0035	0.0204	
				0.0694	0.0064	0.0037	
				0.0946	0.0087	0.0067	
			0.0694	0.1406	0.0127	0.0092	
				0.1554	0.0143	0.0137	
				0.0383	0.0043	0.0151	
				0.0694	0.0078	0.0047	
0.1554	0.0946	0.0111	0.0086				
	0.1406	0.0172	0.0116				
	0.1554	0.0189	0.0172				
	0.1554	0.0189	0.0190				

Table II (Continued)

Solute	Solvent	Temp, °C	f_A^0 , M	a_w	Δf_w , M	Δf_w (calcd), M
NMCHA	Benzene	25	0.0383	0.909	0.0055	0.0055
			0.0694		0.0100	0.0100
			0.0946		0.0142	0.0142
			0.1406	1.00	0.0213	0.0200
			0.1554		0.0233	0.0222
			0.0405		0.0056	0.0064
			0.0581		0.0086	0.0091
			0.0820		0.0125	0.0128
			0.1009		0.0160	0.0157
			0.1147	0.0181	0.0178	
			0.1315	0.0209	0.0204	
			NMCHA	Benzene	35	0.0418
0.0597	0.0066	0.0072				
0.0809	0.0089	0.0097				
0.0988	1.00	0.0111				0.0119
0.1150		0.0131				0.0138
0.1405		0.0167				0.0168
0.0420		0.0067				0.0070
0.0612		0.0097				0.0102
0.0782		0.0128				0.0130
0.1016	0.0175	0.0167				
0.1237	0.0208	0.0205				
NNDMCHA	Benzene	25				0.1334
			0.0421	0.0026	0.0031	
			0.0711	0.0042	0.0052	
			0.1012	0.680	0.0064	0.0074
			0.1327		0.0086	0.0097
			0.1580		0.0101	0.0115
			0.0416		0.0032	0.0035
			0.0711		0.0055	0.0060
			0.1040		0.0074	0.0088
			0.1373	0.0108	0.0116	
			0.1646	0.0194	0.0196	
			0.0421	0.702	0.0028	0.0037
			0.0711		0.0054	0.0062
			0.1012		0.0076	0.0088
			0.1327	0.830	0.0106	0.0115
			0.1580		0.0126	0.0137
			0.0416		0.0040	0.0042
			0.0711		0.0077	0.0071
			0.1040		0.0095	0.0106
			0.1373		0.0137	0.0138
			0.0421	0.929	0.0043	0.0047
			0.0711		0.0073	0.0081
			0.1012		0.0106	0.0113
			0.1327	0.935	0.0147	0.0148
0.1580	0.0180	0.0176				
0.0416	0.0051	0.0046				
0.0711	0.0082	0.0079				
0.1040	0.0115	0.0117				
0.1373	0.0155	0.0153				
0.0379	1.00	0.0051	0.0048			
0.0400		0.0055	0.0046			
0.0405		0.0055	0.0044			
0.0594		0.0074	0.0071			
0.0600		0.0082	0.0069			
0.0790		0.0102	0.0093			
0.0967		0.0126	0.0117			

Table II (Continued)

Solute	Solvent	Temp, °C	f_A^0 , M	a_w	Δf_w , M	Δf_w (calcd), M
NNDMCHA	Benzene	25	0.0996		0.0133	0.0112
			0.1098		0.0151	0.0128
			0.1176		0.0153	0.0138
			0.1381		0.0175	0.0162
NNDMCHA	Benzene	35	0.0396	0.680	0.0030	0.0033
			0.0682		0.0048	0.0057
			0.0814		0.0067	0.0076
			0.1028		0.0088	0.0084
			0.1216		0.0102	0.0102
			0.1413		0.0112	0.0117
			0.0451	1.00	0.0049	0.0053
			0.0688		0.0082	0.0080
			0.0836		0.0099	0.0097
			0.1068		0.0126	0.0124
			0.1283		0.0156	0.0149
Et ₂ N	Benzene	25	0.0442	1.00	0.0046	0.0048
			0.0966		0.0100	0.0105
			0.1343		0.0147	0.0145
			0.1736		0.0198	0.0198
			0.2256		0.0250	0.0240
			0.2656		0.0290	0.0287
			0.3064		0.0339	0.0330
			0.3545		0.0386	0.03834
			0.3898		0.0426	0.04335
			0.4655		0.0528	0.05009
			0.0922	0.680	0.0051	0.00719
			0.1838		0.0132	0.01407
			0.2563		0.0179	0.01934
			0.3493		0.0261	0.02667
0.4670		0.0330	0.03581			
Et ₂ N	Toluene	25	0.0479	1.00	0.0044	0.00432
			0.0922		0.0077	0.00840
			0.1854		0.0168	0.01676
			0.1835		0.0164	0.01661
			0.2202		0.0200	0.01991
			0.2808		0.0257	0.02537
			0.3193		0.0290	0.02877
			0.3547		0.0323	0.03206
			0.3980		0.0365	0.03595
			0.4429		0.0417	0.03990
			0.0908	0.680	0.0056	0.00576
			0.1748		0.0104	0.01111
			0.2762		0.0168	0.01754
			0.3606		0.0210	0.02296
0.4841		0.02950	0.03074			
Et ₂ N	Cyclohexane	25	0.0426	1.00	0.00087	0.00087
			0.0937		0.00188	0.00191
			0.1335		0.00263	0.00272
			0.1738		0.00321	0.00355
			0.2207		0.00398	0.00451
			0.2616		0.00492	0.00536
			0.3069		0.00587	0.00626
			0.3507		0.00685	0.00715
			0.3801		0.00791	0.00774
			0.4152		0.00850	0.00846
			0.1880	0.830	0.00304	0.00319
			0.2828		0.00503	0.00480
			0.3637		0.00657	0.00621
			0.5385		0.00987	0.00913

Table III: Hydration Constant of Amines

Amine	Temp. °C	K_{AW} (assuming only 1:1 species)	K_{AW} (assuming 1:1 and 2:1 species)	K_{A_2W}
Cyclohexylamine-C ₆ H ₆	25	6.74 ± 0.15	6.58 ± 0.84	0.99 ± 9.33
Cyclohexylamine-C ₆ H ₆	35	5.14 ± 0.13	5.38 ± 0.30	Negative
N-Methylcyclohexylamine-C ₆ H ₆	25	5.28 ± 0.08	5.12 ± 0.185	1.88 ± 1.98
N-Methylcyclohexylamine-C ₆ H ₆	35	4.29 ± 0.08	3.95 ± 0.25	3.97 ± 3.18
N,N-Dimethylcyclohexylamine-C ₆ H ₆	25	3.85 ± 0.09	3.81 ± 0.48	1.31 ± 4.89
N,N-Dimethylcyclohexylamine-C ₆ H ₆	35	2.82 ± 0.07	2.74 ± 0.22	1.21 ± 2.52
Triethylamine-C ₆ H ₆	25	3.47 ± 0.05	3.41 ± 0.07	0.21 ± 0.27
Triethylamine-C ₆ H ₁₂	25	7.01 ± 0.16	5.90 ± 0.22	3.15 ± 0.61
Triethylamine-C ₆ H ₅ CH ₃	25	3.72 ± 0.05	3.16 ± 0.52	2.43 ± 1.76

single parameter K_{AW} provides an adequate fit of the data for each system. However, in view of the conclusions of Mohr, Wilk, and Barrow⁷ and of previous investigators in this laboratory¹⁶ that organic bases tend to form the dimer monohydrate at higher base concentrations, the data were also fitted assuming the presence of both the monomer monohydrate AW and the dimer monohydrate A₂W. This necessitated incorporation of the additional terms $K_{A_2W}C_A^2C_W$ in eq 1 and $2K_{A_2W}C_A^2C_W$ in eq 2. Table III lists values of equilibrium constants and standard errors obtained using both the one-parameter and the two-parameter nonlinear least-squares fitting methods. In most of the systems, the uncertainty in K_{A_2W} is at least as large as the best value of the constant and K_{AW} is not much affected by the inclusion of a second hydration constant. The magnitude of the root-mean-square deviation in Δf_W changes only slightly for each of the systems as the second constant is added. Hence, while the 2:1 hydrate is probably present at the greater amine concentrations, the results presented here do not justify reporting values of K_{A_2W} .

Based on the one-parameter fitting method, approximate values of ΔH and ΔS were calculated for the formation of the 1:1 hydrates of the three cyclohexylamines in benzene. These values and their estimated uncertainties are given in Table IV. The standard state used in calculating ΔS is 1 mole/l. for each solute species. The ΔH values show no important trend, although ΔH for the tertiary amine is larger in magnitude than that for the other two cyclohexylamines. Similarly, ΔS is most negative for the tertiary amine. K_{AW} decreases from primary to secondary to tertiary amine, indicating that the entropy effect predominates over that of the enthalpy in limiting the formation of the monomer monohydrate.

Whetsel and Lady¹⁷ have reported that the ΔH of formation of amine-substituted aniline complexes is

Table IV

Amine	$-\Delta H$, kcal	$-\Delta S$, eu
Cyclohexylamine	4.94 ± 0.86	12.8 ± 2.8
N-Methylcyclohexylamine	3.82 ± 0.63	9.5 ± 2.1
N,N-Dimethylcyclohexyl- Amine	5.6 ± 0.65	16.1 ± 2.1

large for tertiary amines. They also note that ΔS becomes quite negative for the complexes involving tertiary amines, indicating that there is a significant steric effect attributable to the N-methyl groups.

The values of the 1:1 hydration constants reported in Table III lie in the same range as the equilibrium constants reported by Zeegers-Huyskens⁴ for the formation of 1:1 complexes between aliphatic alcohols and amines in CCl₄ at 25°. Since the solvents used here (except for cyclohexane) are more reactive than CCl₄, it may be concluded that water forms somewhat stronger complexes with aliphatic amines than do the aliphatic alcohols. The value obtained here for K_{AW} for Et₃N in cyclohexane is more than twice that reported by Zeegers-Huyskens for the formation constant for the 1:1 complex of 1-butanol with Et₃N in CCl₄ (3.17 l./mole).

One reason for the apparent unimportance of the 2:1 hydrate in the systems reported here may be that the strong hydrogen bond formed in the 1:1 complex significantly reduces the acidity of the water molecule hydrogen which is not bonded. Frank and Wen¹⁸ have proposed that the water oxygen becomes more

(16) D. D. Mueller, Ph.D. Dissertation, University of Oklahoma, 1966.

(17) K. B. Whetsel and J. H. Lady, *J. Phys. Chem.*, **69**, 1596 (1965).

(18) H. S. Frank and W. Y. Wen, *Discussions Faraday Soc.*, **24**, 133 (1957).

basic when one of the water hydrogens interacts with an electron donor, whereas the nonbonded hydrogen loses acidity. This effect would be less important in the case of solutions of weaker bases, such as ketones or pyridine, in which apparently both the 1:1 and 2:1 hydrates are present in significant concentrations.¹⁹ These observations have all had some confirmation from studies of the infrared spectrum of water with triethylamine and dioxane in carbon tetrachloride and of water as a solute in triethylamine and dioxane. Also, dielectric constant measurements by Kohler, *et al.*,²⁰ of water + triethylamine and water + dioxane

in carbon tetrachloride and benzene as solvents have indicated that the water-amine hydrogen bond is much more polar than that between water and dioxane.

Acknowledgment. This investigation was supported in part by a Public Health Service Fellowship (5-F1-GM-30,419-02) from the National Institute of General Medical Sciences.

(19) R. L. Lynch, M.S. Thesis, University of Oklahoma, 1966.

(20) H. E. Affsprung, J. Derkosch, and F. Kohler, *Discussions Faraday Soc.*, **40**, 224 (1965); F. Kohler, private communication.

Substituent Effects on the Properties of Stable Aromatic Free Radicals.

Oxidation-Reduction Potentials of Triarylamine-Triarylaminium Ion Systems¹

by Lily Hagopian, Günter Köhler, and Robert I. Walter²

Department of Chemistry, Haverford College, Haverford, Pennsylvania 19041 (Received January 16, 1967)

The oxidation-reduction potentials of a series of tri-*para*-substituted triphenylamine-aminium ion systems have been determined by oxidative titrations with Pb(IV) in acetonitrile-trifluoroacetic acid solution. Potentials of some less stable partially substituted systems have been measured only at 50% oxidation. The data show that donor substitution increases and acceptor substitution decreases the ease of oxidation of triphenylamine, even though the free radicals which participate in these oxidation-reduction systems display class S substituent effects. These results are attributed to larger effects of substitution on electron pair delocalization (and free energy) in the amines than those due to unpaired electron delocalization in the radicals. They are consistent with the appearance of class O effects of substitution on the properties of free radicals alone when competitive electron pair-unpaired electron delocalization is structurally possible in these systems. They are not inconsistent with the class S effects of substitution observed on properties dependent upon structural effects in the aminium salt radicals alone. Stepwise substitution of methoxy or carbomethoxy groups in the three equivalent *para* positions of triphenylamine appears to give diminishing increments in the oxidation-reduction potentials but no general regularities in the optical spectra. The oxidation of methoxy-substituted triphenylamines proceeds in two steps through the aminium salts to quinone analogs.

Most of the published data on the potentials of organic oxidation-reduction systems (the field has been reviewed by Clark³) apply to hydroquinone-quinone pairs or to their nitrogen analogs, in which the overall oxidation or reduction process involves two electrons. The classic work of Michaelis⁴ established that these two-electron systems react by successive one-electron steps which overlap to a greater or lesser extent and involve an intermediate free radical. Very few organic oxidation-reduction systems (other than metal chelates) are known in which the over-all observed process involves only one electron and consequently includes a stable free radical as one participant in the reaction. Even in these cases, it should in principle be possible to carry the reactions one step further to give a total process which involves two electrons, although both steps may not be readily accessible experimentally. One case of this type is the reduction of triarylcarbonium ions to triarylmethyl free radicals, studied by Conant and co-workers.^{5a}

Michaelis and Granick reported a second case—the one-electron oxidation of tri-*p*-tolylamine to the aminium ion with lead tetraacetate in aqueous acetic acid solution.^{5b} Neither of these earlier studies was concerned with the effects of substituents on the properties of the systems investigated, but a recent paper reports the potentiometric study of a series of 4-substituted-2,6-diphenylphenols, which are oxidized to the phenoxy radicals.^{5c}

Most recent work of this type has been carried out by

(1) We are pleased to acknowledge support of this work by U. S. Public Health Service Grant GM-10605 to Haverford College.

(2) Correspondence should be addressed to this author.

(3) W. M. Clark, "Oxidation-Reduction Potentials of Organic Systems," The Williams and Wilkins Co., Baltimore, Md., 1960.

(4) L. Michaelis, *Chem. Rev.*, **16**, 243 (1935); L. Michaelis and M. P. Schubert, *ibid.*, **22**, 437 (1938).

(5) (a) J. B. Conant and B. F. Chow, *J. Am. Chem. Soc.*, **55**, 3752 (1933), and references given there; (b) S. Granick and L. Michaelis, *ibid.*, **62**, 2241 (1940); (c) K. Dimroth and K. J. Kraft, *Chem. Ber.*, **99**, 264 (1966).

polarographic techniques rather than by potentiometry. The first such investigation was reported by Maki and Geske^{6a} on the reduction of substituted nitrobenzenes to the corresponding ion radicals. All of these studies of systems which include radicals as one species in an oxidation-reduction equilibrium happen to involve free radicals which are assigned to class O in a recently reported scheme for classification of substituent effects.⁷ Our interest in these effects has led us to study the oxidation-reduction potentials of a series of triarylamine-triarylaminiium ion systems with various sets of three identical substituents in the three *para* positions of the benzene rings. The aminium salts display class S substituent effects⁷ and we wished to determine whether these are reflected in the potentials of these systems. A very recent report by Seo and co-workers^{6b} is concerned with the polarographic study of aromatic amine-aminium salt systems. It covers some of the compounds reported in this study, but the range of substituents studied is insufficient to afford conclusions on the nature of substituent effects in these systems.

The partially substituted compounds of this series offer an opportunity to examine the effects on their properties (potentials and optical spectra) of stepwise introduction of a given substituent into three identical *para* sites on these molecules. The results of these investigations also are reported in this paper.

Experimental Section

The preparation of the triarylaminines used in this study has been described elsewhere.⁸ Potentials for most of the systems studied were determined by oxidative or reductive titrations carried out on 0.00200 *F* solutions of the amines in 25 ml of solvent. Those systems which proved too unstable for study by this method were oxidized to the 50% point, their potentials determined as a function of time, and the data extrapolated graphically back to zero time.

Our choice of solvent was dictated by considerations of the solubility of the variously substituted amines and aminium ions and of silver perchlorate, by the requirement that the medium contain a Lewis acid in order for the oxidizing agents to function, and by the necessity for a supporting electrolyte to stabilize the potentials. These requirements were met reasonably well by acetonitrile containing 0.500 *F* trifluoroacetic acid and 0.200 *F* lithium perchlorate. Our initial studies showed that titrations performed in untreated chromatography quality acetonitrile⁹ still showed significant reductive potential drifts, particularly in the case of those amines which are more difficult to oxidize. These drifts were largely eliminated by purification of the ace-

tonitrile. Chromatography quality solvent (4.5 l.) was stirred and refluxed for 90 hr with 50 g of anhydrous chromium trioxide and then distilled. (Preliminary tests showed that this time interval is adequate for the removal of oxidizable impurities. Further slow reduction of Cr(VI) is due to reaction with the acetonitrile.) Lithium perchlorate (85.2 g) was stirred for 20 hr with 1 l. of this treated acetonitrile at room temperature and the solution was then filtered to remove a small amount of undissolved solid (believed to be sodium perchlorate). The filtrate was then diluted to 3.7 l. with additional acetonitrile and 222 g of trifluoroacetic acid (Baker reagent grade) added. Aliquots of this solution were diluted with water and the acid concentration was determined by titration with base; the solution was then diluted with additional acetonitrile to adjust the concentration of acid to 0.500 *F*.

The apparatus used in this study is similar to that described earlier by one of us,¹⁰ with modifications in some details. Potentials were read on a Leeds and Northrup Type K-2 potentiometer which was standardized by comparison with a reference cell made by Epply Laboratories. Platinum working electrodes and silver-silver perchlorate reference electrodes were installed in duplicate, with switches to permit them to be read in any combination. Each reference electrode consisted of pure silver sheet welded to a platinum lead, immersed in the solvent mixture already described made up to 0.0100 *F* in silver perchlorate. The electrodes and salt bridges were connected through a Y stopcock, with the third arm of the Y leading to a reservoir of electrode solution. By this means, electrode solution could be flushed through the salt bridge to establish a fresh junction for each titration; the junction was formed through a 10-mm medium fritted disk.

Potentials measured by titration of stable systems against freshly prepared electrodes made up in this way are reproducible within the precision of our data. Unfortunately, these potentials drift slowly and the two reference electrodes generally did not agree for more than 1-2 weeks after they were assembled. (Both platinum electrodes gave the same readings against a given reference electrode.) After 6 months, the

(6) (a) A. H. Maki and D. H. Geske, *J. Am. Chem. Soc.*, **83**, 1852 (1961); (b) E. T. Seo, R. F. Nelson, J. M. Fritsch, L. S. Marcoux, D. W. Leedy, and R. N. Adams, *ibid.*, **88**, 3498 (1966).

(7) R. I. Walter, *ibid.*, **88**, 1923 (1966).

(8) R. I. Walter, *ibid.*, **77**, 5999 (1955); T. N. Baker, W. P. Doherty, Jr., W. S. Kelley, W. Newmeyer, J. E. Rogers, Jr., R. E. Spalding, and R. I. Walter, *J. Org. Chem.*, **30**, 3714 (1965).

(9) Sold by Matheson Coleman and Bell, East Rutherford, N. J.

(10) R. I. Walter, *J. Biol. Chem.*, **196**, 151 (1952).

potentials differed by as much as 6 mv. Under these circumstances, it is necessary to check cell potentials by repeating the titration of a stable system from time to time. Fortunately, we were able to make our measurements within the interval during which at least one reference electrode was stable by this criterion. Other investigators have not observed drifts in silver-silver ion reference electrodes in pure acetonitrile;¹¹ we are not aware of the prior use of this electrode in our particular solvent mixture.

We have been unable to find reagents for these titrations which fully meet the desirable criteria of stability, potentials adequate to oxidize or reduce the entire series of compounds studied, and complete absence of interfering reactions. Of those metal ions known to be strong reductants, Ti(III), V(II), V(III), Cr(II), Mo(III), and Ru(III) react with perchlorate ion in aqueous solution¹² and this reaction appears qualitatively to be still faster in our solvent system. Titrations with Sn(II) prepared as the trifluoroacetate approached equilibrium slowly (as evidenced by the potential drifts observed), particularly with the less easily reduced systems. A reductant with limited usefulness was prepared from 2-methyl-3-hydroxy-1,4-naphthoquinone (phthiocol)¹³ by reduction of 0.0200 *F* solutions in the titration solvent with hydrogen gas in the presence of palladium on charcoal catalyst. These solutions were filtered into a protected buret¹⁰ and stored under nitrogen gas, and they were stable for several years except for slight (photochemical?) darkening. Reductive titrations with this solution duplicated the potentials obtained by oxidative titrations for those aminium salts which are least easily reduced. The more easily reduced compounds did not react stoichiometrically with reduced phthiocol and the potentials obtained were not the same as those obtained by oxidative titrations. Essentially identical results were obtained in reductive titrations with ferrocene. We conclude that the oxidation products of these reagents are unstable in solutions which contain an excess of a strong oxidizing agent; possibly there is a secondary reaction with aromatic hydrogen atoms under these conditions.

Very strong oxidants are required to convert those amines substituted by strong electron-withdrawing groups to the radicals. Of these, potassium peroxydisulfonate is insufficiently soluble in the solvent mixture, permanganate in some cases gives products other than the blue aminium salts, and Ce(IV) solutions (prepared as the trifluoroacetate) failed to give stable potentials. Chromium trioxide is not a sufficiently strong oxidant and its solutions in the acidic solvent mixture decompose slowly at room temperature, but

they can be stored in the freezer. It was used in spite of these drawbacks to obtain an independent check on data obtained with other reagents. (It was ill suited to this use due to complex formation, for which evidence will be presented later.) Potentials were unstable in titrations with lead tetraacetate. Pb(IV) as the trifluoroacetate proved far the best reagent; it was prepared as a brown solution in the solvent mixture by electrolytic oxidation of the Pb(II) solution.¹⁴ Solutions of this reagent showed a decrease in titer for an initial period of up to 2 weeks; after this, they were reasonably stable for periods up to 2 months when stored in the freezer. Occasionally they deposited a brown solid which was assumed to be PbO₂ formed by reaction with atmospheric moisture; such solutions were unsuitable for titrations because potentials drifted badly. These oxidizing agents need not be protected from air; titrations were conveniently carried out with an RGI micrometer buret.¹⁵ Optical absorption spectra were recorded on a Cary Model 14 spectrophotometer.¹⁶

Results

We use the IUPAC sign convention (more positive potential means oxidation is more difficult) in reporting potentials. All potentials are given relative to our silver-0.01 *F* silver perchlorate reference electrode system. The problem of converting these to potentials relative to the standard hydrogen electrode is considered in the Discussion section. Data for all titrations have been analyzed by the procedure of Reed and Berkson,¹⁷ which transforms the sigmoid titration curve relating potential and titration volume to a new function ϕ , which is linear in the titration volume *V*. A program written for the Haverford College IBM 1620 computer makes this transformation, makes a least-squares fit to the data, and computes from the slope and *V* intercept of this line the concentration ratio and midpoint potential which correspond to each data point of the titration.¹⁸ The data in Table I for the oxidative titration of tris(*p*-fluorophenyl)amine with

(11) P. C. Larson, R. T. Iwamoto, and R. N. Adams, *Anal. Chim. Acta*, **25**, 371 (1961).

(12) W. R. King and C. S. Garner, *J. Phys. Chem.*, **58**, 29 (1954), and references reviewed there.

(13) L. F. Fieser, "Experiments in Organic Chemistry," 3rd ed, D. C. Heath and Co., New York, N. Y., 1955, p 211.

(14) Details of the preparation of this reagent will be published elsewhere.

(15) Sold by Kontes Glass Co., Vineland, N. J.

(16) We are indebted to Professor J. Varimbi and the Chemistry Department at Bryn Mawr College for use of this instrument.

(17) L. J. Reed and J. Berkson, *J. Phys. Chem.*, **33**, 760 (1929).

(18) Mr. Griffith Smith, a Haverford College senior, wrote the first version of this program.

Pb(IV) are typical of the systems which are reasonably stable. Data within a titration are more precise by an order of magnitude than the agreement between separate titrations of the same system; these values fall within a range which averages 1 mv. These variations may be due to fluctuations in the junction potentials at the fritted disks which terminated the salt bridges to the reference electrodes; significant diffusion of the colored radical solutions occurred past these disks. The averaged potentials for the systems studied by titration are listed in part A of Table II.

Table I: Oxidative Titration of Tris(*p*-fluorophenyl)amine with Pb(IV)

Titrant volume, ml	Observed potential, ^a v	Concentration ratio, O/R	Computed midpoint potential, ^a v	Deviation from average, v
0.200	-0.56508	0.0412	(+0.64700)	(-0.00280)
0.650	0.59645	0.1271	0.64945	-0.00035
0.900	0.60586	0.1813	0.64974	-0.00006
1.200	0.61464	0.2536	0.64990	+0.00010
1.600	0.62391	0.3649	0.64982	+0.00002
2.000	0.63190	0.4979	0.64982	+0.00002
2.500	0.64094	0.7057	0.64989	+0.00009
3.000	0.64925	0.9804	0.64975	-0.00005
3.500	0.65772	1.3607	0.64980	0.00000
4.025	0.66720	1.9567	0.64994	+0.00014
4.500	0.67650	2.8321	0.64974	-0.00006
5.000	0.68887	4.5671	0.64982	+0.00002
5.500	0.70686	9.1730	0.64989	+0.00009
5.700	0.71740	14.2048	(0.64919)	(-0.00061)
		Av ^b	+0.64980	0.00008

^a Potentials are given relative to the silver-silver perchlorate reference electrode used. ^b Data in parentheses (outside the range 10-90% reaction) are excluded from the averages.

A number of systems were too unstable to yield reasonable data by titration; solutions of these amines were oxidized to the 50% point at time zero by Pb(IV) solutions which were standardized by titration of one of the stable systems. The potentials were then read as a function of time for 10 min and the data extrapolated graphically back to time zero. These potentials are collected in part B of Table II; the estimated precision of the results is given as a range which exceeds four times the spread of the set of individual values. The values are reasonably reproducible in spite of the fact that the clear blue color of the freshly oxidized solutions changes within a few minutes to gray-blue and finally to brown. These changes are particularly striking in the carbomethoxy-substituted series. Although the partially substituted radicals

Table II: Potentials of Triarylamine-Triarylamini-um Ion Systems

<i>para</i> substituents in compounds studied	Observed potential, ^a v	Range of observed potentials, mv	Estimated precision, mv
Part A. Potentials Determined by Titration			
(OCH ₃) ₃	+0.2224	0.5	±1
(CH ₃) ₃	0.4415	1.0	±1
(COOCH ₃) ₃	0.9774 ^b	3.0	±6 ^c
(F) ₃	0.6494	0.3	±1
(Cl) ₃	0.7481	0.5	±1
(Br) ₃	0.7615	0.5	±1
(C ₆ H ₅) ₃	0.534 ^d		±10 ^c
(OCH ₃) ₂	0.3363	0.2	±1
Part B. Potentials Determined by Extrapolation of Potential-Time Curves of Half-Oxidized Solutions			
(COCH ₃) ₃	+0.958	1.0	±3 ^c
(OCH ₃) ₂	0.447	4.0	±10 ^c
(COOCH ₃) ₂	0.737	3.0	±10 ^c
(COOCH ₃) ₁	0.638	1.0	±10 ^c

^a Potentials are given relative to the silver-silver perchlorate reference electrode used at 25.0°. ^b The ϕ - V plots for all titrations of this system were nonlinear beyond 50% oxidation. Data from only the linear first part of each titration were analyzed to obtain this potential. ^c Estimated precision of these data is very uncertain. ^d Titrations were carried out on 0.0002 *F* solutions; the amine is not soluble throughout even at this low concentration.

are too unstable to study by titration, more reliable data for them should be obtained by ac polarography. This has recently been done for some of them by Seo, *et al.*^{6b}

All of the potentiometric data in Tables I and II were obtained at 25.0°. The effect of temperature change was investigated for the trimethoxy-substituted system only. Here, lowering the temperature to 1.5° raised the potential 4.3 mv. Since the total temperature range which was both accessible to our thermostat and maintained reasonable radical stability is only about 50°, no further investigation was undertaken of these small effects.

One might expect a second oxidation stage for the triarylamines, from the aminium salts Ar₃N^{•+} to the quinone analogs Ar₃N²⁺. Presumably this reaction would usually require a stronger oxidant than any which we have available and the products would be quite unstable. In the particular case of the methoxy-substituted compounds, excess Pb(IV) converts the deep blue aminium salt solutions first to purple and finally to deep red. These red solutions no longer give the esr signals of the blue radicals. The second oxidation step occurs rather slowly, in contrast to the rapid first

step. This second oxidation stage can be carried out as a titration in the case of the trianisylaminium ion; the system is not very stable, but the potential so determined is 0.448 ± 0.002 v. The compounds substituted by one or two methoxy groups are insufficiently stable for titration, but we were able to record their optical spectra in acetonitrile solution containing 0.500 *F* trifluoroacetic acid. (This was made up in the same manner as the titration solvent, with the omission of the lithium perchlorate.) These data are collected in Table III, together with the spectra of the accessible oxidation states for the series of carbomethoxy-substituted compounds.

Table III: Absorption Maxima in the Optical Spectra of Various Oxidation States of Stepwise-Substituted Triarylamines^a

Para substituents	—Ar ₃ N:—		—Ar ₃ N ⁺ —		—Ar ₃ N ²⁺ —	
	λ _{max.} A	OD × 10 ⁻⁴	λ _{max.} A	λ _{max.} A	λ _{max.} A	λ _{max.} A
(OCH ₃) ₃	2947 ^b	2.66	3730 ^b	7164 ^b	2802	5188
(OCH ₃) ₂	2918	2.00	3692 ^c	7375	2748 ^d	5134
(OCH ₃)	2930	2.83	3550 ^e	6956	2742	4220
None	2956	3.20	...	6550 ^f
(COOCH ₃)	3295	2.08	3275 ^g	6728
(COOCH ₃) ₂	3486	3.08	3447 ^h	6680
(COOCH ₃) ₃	3453	4.60	<i>i, j</i>	6865

^a Spectra recorded in acetonitrile containing 0.500 *F* trifluoroacetic acid. Extinction coefficients are given only for species which are reasonably stable in solution. ^b These spectra (in acetonitrile solution) have been published in ref 7. ^c Shoulder at 5688 Å. ^d Shoulder at 3731 Å. ^e This is a broad peak, with some structure. ^f Absorption in EPA glass, from G. N. Lewis and D. Lipkin, *J. Am. Chem. Soc.*, **64**, 2801 (1942). ^g As this solution decomposes, a new peak grows in at 4900 Å. ^h As this solution decomposes, a new peak grows in at 4830 Å. ⁱ Two peaks at 3734 and 3532 Å change in relative intensity as the radical decomposes. ^j Shoulder at 5814 Å.

It was impossible to obtain satisfactory potentiometric data for the reagents used in this study. One of the Pb(IV) solutions used for oxidations was titrated reductively with phthiocol. This system was so unstable that the result can be regarded only as an order of magnitude, but analysis of the data indicates that the electrolytic oxidation of Pb(II) to Pb(IV) is far from complete. A number of Fe(II) chelates with known potentials in aqueous solution have been titrated with Pb(IV); the data in these cases are good and afford some basis for relating the potentials determined in our solvent and electrode system to those in aqueous solution referred to the standard hydrogen electrode. All of these results are collected in Table IV.

Table IV: Potentials of Reagents and Reference Compounds

Substance titrated	Titrated with	Observed potential, ^a v	Reported potential, ^b v
Ferrocene	Pb(IV)	+0.0610	+0.400 ^c
Ferrous 2,2'-bipyridine	Pb(IV)	0.7325	1.096
Ferrous 1,10-phenanthroline	Pb(IV)	0.7492	1.120
Pb(IV)	Phthiocol	1.18	...

^a Potentials reported for our solvent system, against the silver-0.01 *F* silver perchlorate electrode at 25°. ^b Potentials reported by Clark (ref 7) for aqueous solutions, referred to the standard hydrogen electrode. ^c This value is taken from ref 20; it seems more consistent with the potential changes observed between water and acetonitrile solution for the other metal-complex ion systems than do other reported values.

Discussion

Attempts to obtain potentiometric data on some triarylamines in addition to those listed in Table II were unsuccessful. This appears not to be due to any breakdown in the theoretically expected reaction scheme, since other reasons can be assigned for the failure of the measurements in each case. The basic substituents in tris(*p*-aminophenyl)amine are partially protonated in our acidic solvent system (evidenced by a color shift from green to blue). In pure acetonitrile solution, the colorless amine is oxidized to the green free radical by the blue trianisylaminium radical, so the potential for the nonprotonated system is less positive by at least 50–100 mv than that for the trianisyl system. The tripotassium salt of triphenylamine-4,4',4''-trisulfonic acid is insoluble in the titration solvent. The marginal solubility of tri-*p*-biphenylamine has already been noted. Tris(*p*-nitrophenyl)amine also is not sufficiently soluble, nor is it oxidized significantly by any reagent which we have investigated. Triphenylamine cannot be studied by this method: the appreciable carbon free-radical character which results from delocalization of the unpaired electron to the ring positions *para* to the nitrogen atom produces high reactivity of the types observed in the triaryl-methyl series. This might take the form either of reaction with residual oxygen in the titration cell or of acid-catalyzed disproportionations. Reactions of this type probably account also for the instability of the systems with partially substituted *para* positions listed in part B of Table II.

We should point out some pitfalls in the use of the Reed and Berkson titration analysis procedure.¹⁹

(19) These matters have already received some attention in ref 3, Chapter 5.

The least-squares procedure for fitting the ϕ - V line assigns equal weight to all data points. In fact, they are not equally precise; small volumetric errors or drifts in the middle of a titration (which is an oxidation-reduction buffer region) introduce negligible error in the potentials, but the same errors or drifts at the titration extremes produce large errors. Consequently, we have established the convention that only data points between 10 and 90% reaction are retained in the final analysis of the data. The analysis procedure is quite sensitive to small errors in the arbitrarily chosen data point (called the pivot point) to which all other data are referred during the calculation. We have found it best to plot the ϕ - V function (which is much more sensitive than the raw titration curve to small deviations from the theoretical relationship defined by the Nernst equation) for each titration in order to check for these pitfalls. On the ϕ - V plot, an error in the pivot point produces deviations from the theoretical linear relationship which are positive on one side and negative on the other side of the pivot point coordinates, and which increase uniformly from the extremes of the plot toward the pivot point. When this is observed, a new pivot point is selected and the calculation repeated. Large curvature in the ϕ - V plot may indicate complex formation, secondary reactions, or inability of the reagent to complete the reaction because it is not a sufficiently strong oxidant or reductant. In view of these facts, we have applied several criteria to the selection of valid titration data (and the exclusion of others). The ϕ - V plot must be linear over the range of data points for which computed midpoint potentials are averaged. (A linear section of the plot can be used to compute the potential for a system which reacts incompletely or undergoes a secondary reaction.) The change in averaged midpoint potential as data points are excluded from the titration analysis should be less than 0.5 mv. Finally, the correlation coefficient for the values of the potential computed within one titration should exceed 0.998.

It is usual to take the identity of potentials determined by oxidative and by reductive titrations as evidence that an oxidation-reduction system is thermodynamically reversible. We have found no reducing agent which is generally useful for the study of these systems. Our best evidence for reversibility is the quantitative fit of individual titrations to the theoretical relationship specified by the Nernst equation typified by the data in Table I. Data for the tricarbomethoxy-substituted system do not fit and the systems in part B of Table II cannot be tested in this way.

Oxidative titrations of tri-*p*-tolylamine with chromium trioxide solutions gave exactly the same potential

as the Pb(IV) oxidations. Oxidations of tri-*p*-anisylamine with chromium trioxide gave midpoint potentials which average 0.2263 v, while the Pb(IV) oxidations gave 0.2224 v. The difference could indicate a weak complex formation between the amine and metal ion—probably Cr(III). This possibility is supported by the optical spectra of these substances; the absorption of solutions which contain tri-*p*-anisylamine and Cr(III) is greater than the sum of the absorptions of the separate solutions at the wavelength of the amine peak. Unfortunately, the chromium trioxide solutions are not sufficiently strong oxidants to permit a search for complexes with other oxygen-containing amines in our series by investigation of the potentials of these systems.

Problems in relating potentials determined in non-aqueous solution against arbitrary reference electrodes to those in aqueous solution against the hydrogen electrode remain largely unsolved. One approach has been discussed by Koepp, Wendt, and Strehlow.²⁰ They propose that some acid-insensitive oxidation-reduction systems which cannot complex with solvents should display reasonably constant potentials relative to the hydrogen electrode in all solvents. We have determined the potential of one of these systems, ferrocene, together with some other complexed iron systems (Table IV). The results indicate that potentials in our system are roughly 0.35 v less positive than those in water against the standard hydrogen electrode.

These potentiometric data on systems which involve class S free radicals show the same trends as earlier data reported^{5c,6a} for systems which involve class O radicals. We turn now to consideration of their significance for the theory of substituent effects in stable aromatic free radicals.⁷ The oxidation-reduction potentials are a measure of the free energy differences between the amines and corresponding radicals and reflect the effects of substitution on the free energies of both compounds. The evidence is that all observed properties of the aminium salts which depend upon the distribution of the unpaired electron in the π system display class S effects of introduction of substituents; that is, both donor and acceptor substituents shift these properties in the *same* direction.⁷ In particular, both types of substituents should stabilize the radicals and lower their free energies, relative to the unsubstituted triphenylaminium ion. In the amines, the unshared electron pair is in the highest energy occupied MO (from simple LCAO-MO calculations) and is

(20) H. M. Koepp, W. Wendt, and H. Strehlow, *Z. Elektrochem.*, **64**, 483 (1960).

delocalized (and the amine stabilized) with increasing effectiveness as the *para* substituents become better electron acceptors. Donor substituents possibly inhibit delocalization of the unshared pair on nitrogen to the rings by a competitive donation of their own electrons. As a result, donor substituents may raise and acceptor substituents should lower the free energies of the substituted triarylamines, relative to triphenylamine. Thus, the potentiometric measurements compare the effects of substituents on free energy changes owing to delocalization of the unpaired electron in the radicals with the different effects owing to delocalization of the unshared electron pairs in the amines, and they indicate that the latter are larger when the substituents are electron acceptors. These competing effects in *different* molecules are analogous to the proposed competitive effects of unpaired electron and unshared electron pair within the *same* molecule in the class O free radicals, where it is postulated that electron pair delocalization is the more important. Thus, the potentiometric data support the postulate that effects of substitution on electron pair delocalization will exceed those due to unpaired electron delocalization when both are possible.⁷

The partially substituted compounds listed in the last line of part A and in part B of Table II were studied in the hope that they would indicate whether stepwise introduction of substituents into equivalent positions in a system affects its properties in roughly equal or in diminishing increments. The instability of these sys-

tems and our inability to obtain data for triphenylamine itself leave the situation in doubt. The potentials reported for some of the same compounds by Seo, *et al.*,^{6b} from polarographic studies undoubtedly are more precise, since the oxidized species need only be stable for one cycle at the frequency used for the ac polarography. Their potentials are 0.30 ± 0.01 v more positive than our values and thus seem comparable to potentials in our system after subtraction of this increment from their data. This correction gives the value $+0.62$ v for the potential of the triphenylamine-aminium ion system; this fits well with the values listed in Table II. Their data give the potential increments -0.16 , -0.13 , and -0.11 v on successive substitution of one, two, or three methoxy groups in triphenylamine and 0.23 and 0.19 v for successive substitution of one and two nitro groups. Thus, the effects of substitution on potentials diminish with the successive introduction of like groups into structurally equivalent positions. These regularities are not observed in the optical spectra; the data in Table III show that introduction of the third substituent into the amines or the radicals produces a shift in the longest wavelength absorption in the opposite direction to that produced by introduction of the first or the second substituents. The potential increments of course represent differences between the effects in the amines and the radicals, while the optical spectra reflect substituent effects in only one of these species, in two different electronic states.

The Absorption Spectra of Simple Amides and Peptides¹

by Eigil B. Nielsen and John A. Schellman

Department of Chemistry, University of Oregon, Eugene, Oregon (Received January 17, 1967)

Absorption curves have been obtained for a number of substituted amides and diamides. The effect of substitution and solvent on the position and intensity of the strong π, π^* absorption band near 200 m μ was studied. Solvent shifts were utilized to locate the n, π^* transition and estimate its oscillator strength.

Introduction

In the course of investigations of the optical rotatory properties of small molecules containing one or two peptide groups, we developed a need for more complete information concerning the absorption properties of the amide group than was available in the literature. For example, it is known that the position and intensity of the main π, π^* band of the amide group vary under changes in the nature of the solvent and with the degree and nature of substitution on the nitrogen and carbon atoms. These factors also affect the properties of the n, π^* transition relative to the main absorption band^{2a,b} and can produce profound effects on optical rotatory properties. Moreover, it is unknown at what stage of complexity polypeptide effects such as hypochromicity or band splitting become perceptible in the absorption spectra, though exploratory investigations of the absorption spectra of di- and polypeptides were begun by Ham and Platt,³ Goldfarb,⁴ and Saidel,⁵ and have been continued in recent times by Gratzler, *et al.*⁶ The status of the field is discussed in two excellent reviews by Wetlaufer⁷ and by Gratzler.⁸ The latter covers the literature up to 1966.

Since both the empirical analysis of rotatory dispersion curves and optical rotation theory are greatly aided by knowledge of the position and intensities of absorption bands, we have undertaken a systematic study of a number of variously substituted amides and diamides in a highly polar solvent (water) and in a nonpolar solvent (cyclohexane) together with a number of results at longer wavelengths in dioxane, acetonitrile, and other solvents. The results of these investigations are briefly presented in this paper.

Experimental Section

See the tables for the formulas of the compounds

used. N-Acetylpyrrolidine (XV), bp 107–108° (13 mm) (lit.⁹ bp 108° (15 mm)), was prepared by acetylation of pyrrolidine by means of acetyl chloride in the presence of pyridine. N-Methylformamide (IV) (chromatoquality), N,N-dimethylformamide (IX), and N,N-dimethylacetamide (X) (both spectroquality) were supplied by Matheson Coleman and Bell, and 2-pyrrolidinone (XVI) by Aldrich Chemical Co. The rest of the moncamides were from Eastman Organic Chemicals. Acetamide was purified following the procedure described by Vogel.¹⁰ Several of the amides were distilled through a small column, and the fraction obtained after a forerun was used in the experiments. However, between such fractions and the undistilled compounds no significant difference in the ultraviolet absorption spectra was apparent.

L-Pyroglutamic acid (XVII) was prepared from L-pyroglutamic acid (California Biochemical Corp., Grade A) by esterification at room temperature with ethanol saturated with hydrogen chloride, evapora-

(1) This research was supported by grants from the National Science Foundation and the National Institutes of Health (Cancer Institute Ca-4216).

(2) (a) A. N. Glazer and K. Rosenheck, *J. Biol. Chem.*, **237**, 3674 (1962); (b) B. J. Litman and J. A. Schellman, *J. Phys. Chem.*, **69**, 978 (1965).

(3) J. S. Ham and J. R. Platt, *J. Chem. Phys.*, **20**, 335 (1953).

(4) A. R. Goldfarb, *J. Biol. Chem.*, **201**, 319 (1953).

(5) L. J. Saidel, *Arch. Biochem.*, **56**, 45 (1955).

(6) W. R. Gratzler, W. Rhodes, and G. D. Fasman, *Bipolymers*, **1**, 319 (1963).

(7) D. B. Wetlaufer, *Advan. Protein Chem.*, **17**, 303 (1962).

(8) W. B. Gratzler in "Poly- α -Amino Acids," G. Fasman, Ed., in press.

(9) S. Komori, N. Okahara, and E. Shinsugi, *Technol. Rept. Osaka Univ.*, **8**, 497 (1958); *Chem. Abstr.*, **53**, 18874d (1958).

(10) A. I. Vogel, "Practical Organic Chemistry," Longmans, Green and Co., London, 1962, p 402.

tion *in vacuo* to dryness, and subsequent treatment with alcoholic ammonia at room temperature. After several recrystallizations from 99% ethanol, the product had mp 166–168° and $[\alpha]^{25D} -43.3^\circ$ (H₂O, *c* 0.15) (lit.¹¹ mp 166–168° and $[\alpha]^{25D} -42.25^\circ$ (H₂O, *c* 2)). The preparation of L-3-acetamidopyrrolidin-2-one (X-VIII) was described by Wilkinson,¹² to whom we are indebted for a sample. The compound had mp 190–192° and $[\alpha]^{25D} -97.3^\circ$ (H₂O, *c* 0.038) (Wilkinson reported mp 191° and $[\alpha]^{21D} -96.5^\circ$ (H₂O, *c* 0.8)). N-Acetyl-L-proline amide (XIX) was supplied by Cyclo Chemical Corp. (purity class CCP). Repeated crystallization from benzene gave the pure compound, mp 146–147°, $[\alpha]^{25_{578}} -110.5^\circ$ (H₂O, *c* 0.1). Glycine anhydride (XX) was supplied by California Biochemical Corp. (Grade A). L-Alanine anhydride (XXI) was prepared by S. Zimmerman in this laboratory following the procedure given by Fischer.¹³ All the above diamides gave satisfactory results for elemental analysis.

Measurements in organic solvents were performed using Matheson Coleman and Bell Spectrograde solvents, with no further purification. Dioxane was stored under nitrogen to prevent oxidation, and all solvents were kept at 4°.

The absorption spectra were determined by means of a Cary Model 15 recording spectrophotometer with fused silica cells, 0.1 and 1 cm in path length. The concentration range studied was from 0.5 to 1.5 × 10⁻³ M for the π, π^* region and from 1 to 30 × 10⁻³ M for the n, π^* region. For all measurements below 200 m μ the spectrophotometer was flushed with nitrogen. This procedure enabled us to penetrate down to 174 m μ with an empty instrument. With 1-mm cells filled with pure solvent, the slit width at 180 m μ could be kept <1 mm in the case of water and <0.5 mm in the case of cyclohexane. For practically all the solutions, measurements could be extended down to 180 m μ , maintaining the slit width <0.5 mm at 181 m μ in most cases.

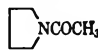
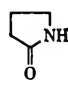
Results

The work can be divided into the following categories: the position of the π, π^* band, the intensity of the π, π^* band, the n, π^* band, and the spectra of molecules containing two amide groups.

The Effect of Solvent and Substitution on the Absorption Maxima of Simple Amides. Table I shows the values of λ_{\max} obtained for a number of variously substituted amides in cyclohexane and in water. This maximum has been assigned in related compounds to an NV transition in the π system of the amide group¹⁴ and will be referred to hereafter as the π, π^*

transition. The maxima of the primary amides could not be observed in cyclohexane because they are below the cut-off limit of the solvent. The form of the absorption curves indicates the maximum is near 178 m μ . The following trends are to be noted.

Table I: Absorption Maxima of Amides

	R ¹ CON< R ²			$\lambda_{\max}, m\mu$	
	R ¹	R ²	R ¹	H ₂ O	Cyclohexane
I	CH ₃	H	H	182	<180
II	C ₂ H ₅	H	H	183	<180
III	C ₃ H ₇	H	H	184	<180
IV	H	CH ₃	H		190
V	H	C ₂ H ₅	H		192
VI	CH ₃	CH ₃	H	186 ^a	184
VII	CH ₃	C ₂ H ₅	H		186
VIII	CH ₃	C ₄ H ₉	H	188.5	186
IX	H	CH ₃	CH ₃		199
X	CH ₃	CH ₃	CH ₃	196 ^b	196
XI	CH ₃	C ₂ H ₅	C ₂ H ₅	199	202
XII	CH ₃	C ₂ H ₇	C ₃ H ₇	200	202
XIII	C ₂ H ₅	C ₂ H ₇	C ₃ H ₇	202	202.5
XIV	C ₃ H ₇	C ₂ H ₅	C ₂ H ₅		203
XV				197.5	200
XVI				190 ^c	185

^a Rosenheck, unpublished data, *cf.* ref 6, found 187 m μ and ϵ_{\max} 8800. ^b Gratzler, Rhodes, and Fasman⁶ reported 195 m μ and ϵ_{\max} 9360. ^c K. Stich and H. Leeman (*Helv. Chim. Acta*, 46, 1151 (1963)) reported 190 m μ and ϵ_{\max} 7070.

There is a general red shift in going from cyclohexane to water. This is in accord with the proposals of Kasha,¹⁵ McConnell,¹⁶ and Bayliss and McRae¹⁷ for the effect of solvent on transitions of this kind. In the terms of the latter reference, the red shift in water results from the favorable interaction of the highly polar excited state with the solvent cage of water. The data of the table demonstrate that we can be more specific than this. Evidently, it is solvent interaction

(11) R. B. Angier, C. W. Waller, B. L. Hutchings, J. H. Boothe, J. W. Mowat, J. Semb, and Y. Subburow, *J. Am. Chem. Soc.*, 72, 74 (1950).

(12) S. Wilkinson, *J. Chem. Soc.*, 107 (1951).

(13) E. Fischer, *Ber.*, 39, 453 (1906).

(14) H. D. Hunt and W. T. Simpson, *J. Am. Chem. Soc.*, 75, 4540 (1953).

(15) M. Kasha, *Discussions Faraday Soc.*, 9, 14 (1950).

(16) H. McConnell, *J. Chem. Phys.*, 20, 700 (1952).

(17) N. S. Bayliss and E. G. McRae, *J. Phys. Chem.*, 58, 1002 (1954).

with the nitrogen atom, *via* its attached hydrogens, which produces the most profound solvent effect. We conclude this because the expected red shift is large in the primary amide series, small in the secondary amide series, and negligible or reversed with tertiary amides. Once again, this is not opposed to expectation, since this transition has been described as essentially an intramolecular charge transfer from the N atom to the O atom or carbonyl group (see Nagakura,¹⁸ Simpson and Rosa,¹⁹ and Schellman and Nielsen²⁰). The resulting positively charged nitrogen interacts strongly with a polar solvent *via* hydrogen bonds when hydrogen substituents are present, but is insulated from solvent when they are absent. The irregular solvent shifts with the tertiary amides show that hydrogen bonding with the oxygen atom of the amide has no uniform effect on the π, π^* spectra. We shall see that the entire situation is reversed for the n, π^* transition.

Substitution on the nitrogen atoms causes strong red shifts for λ_{\max} in the series tertiary > secondary > primary. This has been previously noted.^{6,21} In addition, for comparable situations, we have the series $C_4H_9 \sim C_3H_7 \sim C_2H_5 > CH_3 > H$. It will be shown in a subsequent paper²⁰ that all of these results correlate with the ionization potential of the substituent amine.

In the two cases for which the table permits comparison (both in cyclohexane), the substitution of a methyl for a hydrogen on the C atom of the amide produces a substantial blue shift (compare IV and VI, IX and X).

Ring formation does not appear to have a very noticeable effect on the absorption maxima of amides. Acetylpyrrolidine shows spectral properties intermediate between those of amides formed from dimethyl- and diethylamines. The pyrrolidone compound shows spectral properties typical of a secondary amide even though the amide has the *cis* conformation.

The Intensity of Absorption of the π, π^ Transition of Amides.* Values of the molecular extinction coefficient at the absorption maxima, oscillator strengths, and transition moments are recorded in Table II. The dipole strength D is related to the area under the absorption curve by the relation

$$D = \mu^2 = \frac{(2303)3hc}{8\pi^3N} \int \frac{\epsilon d\lambda}{\lambda} \cong 9.183 \times 10^{-39} / \lambda_{\max} \int \epsilon d\lambda = \frac{9.183 \times 10^{-3}}{\lambda_{\max}} \int \epsilon d\lambda \quad (D.^2)$$

from which the oscillator strength can be obtained by means of the formula

$$f = \frac{8\pi^2mc}{3he^2\lambda_{\max}} D = 4.702 \times 10^{29} D / \lambda_{\max}$$

μ is the electric transition moment. We give explicit formulas because of the existence of several conventions in the field. In particular, the statistical factor G of Mulliken²² has not been introduced. The quantities defined above are those which are useful in dipole coupling calculations. In addition, no internal field correction for solvent has been introduced.

Since isolated absorption bands could not be obtained for these compounds, the procedure was adopted of taking the area under the curves on the long wavelength side of the maximum and multiplying by 2. Accordingly, any lack of symmetry in the bands introduces an error in the results.

Two clear-cut trends are perceivable in the table: (1) oscillator strengths fall in the sequence: primary < secondary \simeq tertiary; (2) oscillator strengths are greater in water than in cyclohexane for all substances where comparisons are possible (except for pyrrolidone). This is opposite to the direction predicted by a Lorentz correction for solvent which introduces a factor $(1/n_0)[(n_0^2 + 2)^2/3]$, where n_0 is the refractive index of pure solvent. The use of the Sellmeier formula to extrapolate the data of Foss and Schellman²³ on the near-ultraviolet refractive index of cyclohexane, together with the observed values for water, leads to a prediction of a decrease in extinction in water of the order of 10%. Evidently, the standard internal field effect is being overridden by a strong specific solvent effect, presumably the solvent cage in aqueous solution. It is noteworthy that the effect of solvent on absorption intensity is very large for the tertiary amides even though there are no pronounced shifts in the position of the absorption maximum. Observe also that the effect of increasing the size of the N substituents is reversed for the secondary and tertiary amides in cyclohexane and that the effect is greatly diminished in aqueous solution. If nothing else, the table demonstrates that the influence of solvent and substitution on absorption intensities is both complex and subtle.

(18) S. Nagakura, *Mol. Phys.*, **3**, 105 (1960).

(19) W. T. Simpson and E. Rosa in "Physical Processes in Radiation Biology," Academic Press, Inc., New York, N. Y., 1964, pp 43-49.

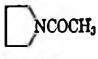
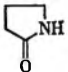
(20) J. A. Schellman and E. B. Nielsen, in press.

(21) E. E. Barnes and W. T. Simpson, *J. Chem. Phys.*, **39**, 670 (1963).

(22) R. S. Mulliken, *ibid.*, **7**, 14 (1939).

(23) J. G. Foss and J. A. Schellman, *J. Chem. Eng. Data*, **9**, 551 (1964).

Table II: Absorption Intensities of Amides

	$R^1\text{CON}\begin{matrix} R^2 \\ R^1 \end{matrix}$			Water				Cyclohexane			
	R^1	R^2	R^1	ϵ^d	D	f	Δ	ϵ	D	f	Δ
I	CH ₃	H	H	7600	8.2	0.21	12.5				
II	C ₂ H ₅	H	H	8000	8.3	0.21	12				
III	C ₃ H ₇	H	H	7700	8.3	0.21	12.5				
IV	H	CH ₃	H					3700	3.7	0.09	12
V	H	C ₂ H ₅	H					5200	5.5	0.13	12
VI	CH ₃	CH ₃	H	8800 ^a	11.8	0.30	15	5400	6.8	0.17	15
VII	CH ₃	C ₂ H ₅	H					6250	8.2	0.21	15.5
VIII	CH ₃	C ₄ H ₉	H	8750	11.3	0.28	15	7650	9.4	0.24	15.5
IX	H	CH ₃	CH ₃					6950	9.6	0.23	16
X	CH ₃	CH ₃	CH ₃	9350 ^b	14.0	0.33	17.5	6850	9.6	0.23	18
XI	CH ₃	C ₂ H ₅	C ₂ H ₅	8650	11.7	0.28	17	7200	9.1	0.21	14.5
XII	CH ₃	C ₃ H ₇	C ₃ H ₇	9300	12.6	0.30	17	7200	8.6	0.20	14.5
XIII	C ₂ H ₅	C ₃ H ₇	C ₃ H ₇	8750	11.9	0.28	17	6500	8.1	0.19	14.5
XIV	C ₃ H ₇	C ₂ H ₅	C ₂ H ₅					6900	7.7	0.18	14
XV				9100	13.9	0.33	18	7100	9.8	0.23	16.5
XVI				7400 ^c	8.9	0.22	14.5	6250	9.4	0.24	17

^a See footnote a in Table I. ^b See footnote b in Table I. ^c See footnote c in Table I. ^d In this and subsequent tables, units are ϵ , l./mole cm²; D , (Debye units)²; and Δ , m μ .

Table III: Absorption Data of Acetamides and Higher Amides (Average Values)

	λ_{max}		Δ		D		f	
	H ₂ O	Cyclohexane	H ₂ O	Cyclohexane	H ₂ O	Cyclohexane	H ₂ O	Cyclohexane
Primary	183	<180	12.5		8		0.21	
Secondary	186-188	184-186	15	15.5	11	8	0.29	0.21
Tertiary	196-202	202-203	17	14.5 ^a	12	9	0.30	0.20

^a N,N-Dimethylacetamide: 18.

Apparent band widths, obtained from the nearest half of the absorption curves, are also recorded. Δ is the value of $\lambda - \lambda_{\text{max}}$ at which the extinction coefficient drops to $1/e$ of its maximal value on the long wavelength side.

The results of the first two sections are shown in averaged form in Table III. Several representative curves are shown in Figure 1.

The n, π^ Band.* When amides are placed in non-polar solvents such as cyclohexane or dioxane, the n, π^* band appears as a shoulder in the neighborhood of 225-235 m μ (see Glazer and Rosenheck^{2a} and Litman and Schellman^{2b}). The fact that this band is not perceivable in aqueous solution results from the red shift of the very intense π, π^* band coupled with the strong blue shift of the n, π^* band when the amide group is transferred to this solvent. (An analysis of a number

of amide Cotton effects in aqueous solution indicates that the n, π^* band is at about 212 m μ for most amides in aqueous solution.²⁴)

It is not easy to get a reliable estimate of the position and intensity of the n, π^* band. Solvent difference spectra can be obtained either directly or by subtraction, but as is well known, the shift of the strong π, π^* band would give a difference spectrum irrespective of the presence of an n, π^* band. One might negate this shift by translating the water spectrum on the wavelength scale to give the best match of the π, π^* spectra and then taking the difference. This leads to error because the principal absorption band changes in absolute intensity when the solvent is varied, as was shown in the previous section. A third method is to

(24) E. B. Nielsen and J. A. Schellman, unpublished results.

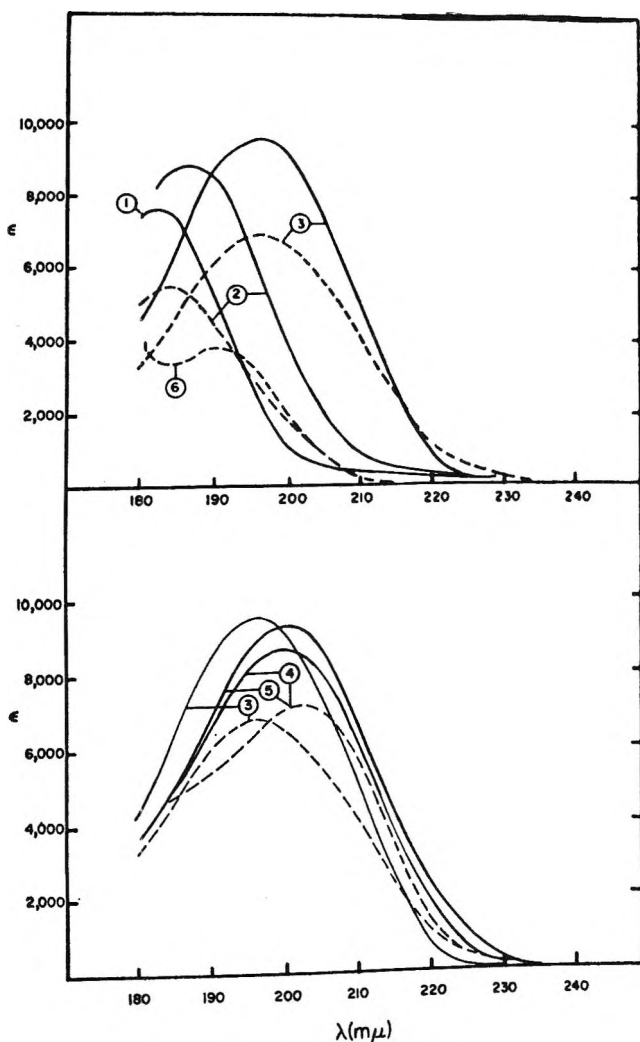


Figure 1. Ultraviolet spectra in water (—) and in cyclohexane (---) of: 1, acetamide; 2, N-methylacetamide; 3, N,N-dimethylacetamide; 4, N,N-diethylacetamide; 5, N,N-dipropylacetamide; 6, N-methylformamide.

treat the principal band as a gaussian function and to find the difference by subtraction. Unfortunately, the assumption of a gaussian function is likely to be least reliable far from the maximum where the absorption has fallen to about 1% of its maximal value.

We have employed all three methods to analyze the data, as well as another which shifts the background aqueous spectrum to a position which gives a symmetrical curve for the n, π^* difference spectrum (Figure 2). The results are summarized in Table IV, where we have included some of the results of Glazer and Rosenheck for comparison. In general, the methods agree within 1 or 2 $m\mu$ with one another for λ_{max} , which gives us confidence that the bands are locatable with some precision. On the other hand, the method of straight difference spectra tends to give

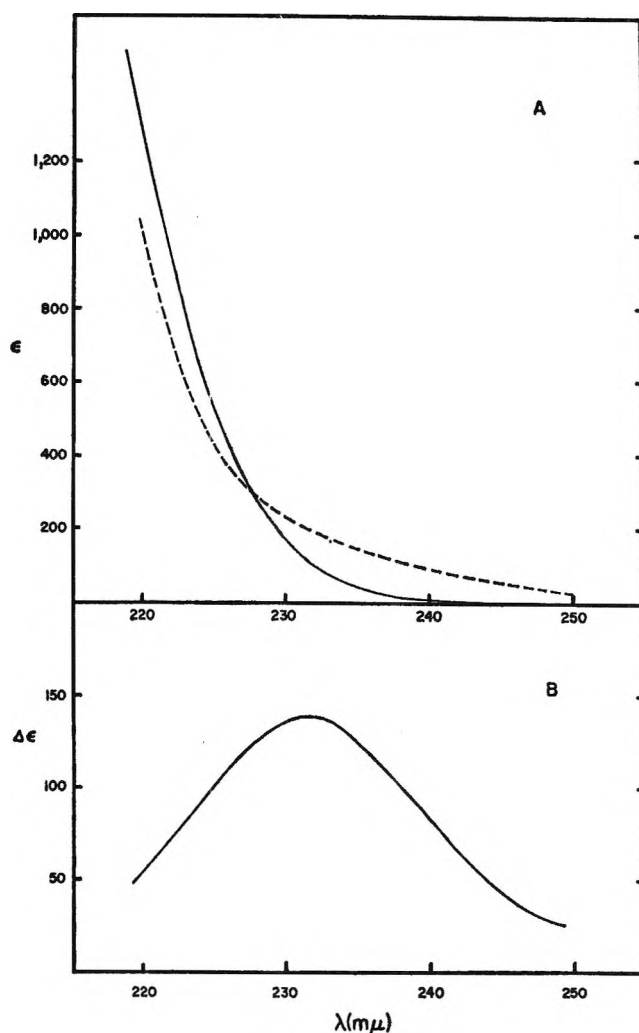
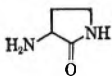


Figure 2. A, ultraviolet spectrum of N,N-dimethylacetamide in water (—) and in cyclohexane (---); B, difference spectrum: cyclohexane vs. water. The water curve is shifted $-2 m\mu$ prior to subtraction.

somewhat lower values for the absorption maxima and the integrated absorption. Since it is very likely that this difference stems from the shift in π, π^* spectra which moves the absorption from high wavelengths to low wavelengths in nonpolar solvents, we have used the other procedures to calculate the oscillator strength and magnitude of the transition moment. The oscillator strength of n, π^* transition of the amides is of the order of 0.0025 and the transition dipole of the order of 0.12 D. This may be compared with the value for the oscillator strength of 0.004 obtained by Gratzer, *et al.*, from the difference spectra of helices and random chains.

The data are too scanty to permit extensive comparisons. In cyclohexane and dioxane, λ_{max} is in the region 223–227 $m\mu$ for ordinary secondary amides. It is

Table IV: Difference Spectra of Amides, Relative to Aqueous Solution

	H ₂ O—curve not shifted			H ₂ O—curve shifted ^a	
	λ_{\max}	$\Delta\epsilon_{\max}$	$\lambda_{\Delta\epsilon=0}$	λ_{\max}	$\Delta\epsilon_{\max}$
Acetamide in dioxane	228	50	<215		
N-Methylacetamide in dioxane	224	90	215	223	100
in dioxane	224 ^b	73 ^b	216 ^b		
in cyclohexane	227 ^b	44 ^b	219 ^b		
N-Ethylacetamide in dioxane	227	90	218	223	110
N,N-Dimethylacetamide in dioxane	232 ^b	129 ^b	224 ^b		
in cyclohexane	233	110	227	232	140
 in dioxane ^c	235	65	224	231	110

^a For explanation, see text. ^b Taken from Glazer and Rosenheck.^{2a} ^c Data, taken from Litman and Schellman,^{2b} relative to aqueous solution at pH 9.2.

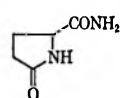
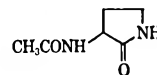
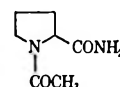
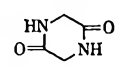
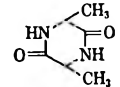
noteworthy that this is also the location of this band in the α helix as revealed by circular dichroism and optical rotation studies. Evidently, the α helix provides an essentially nonpolar environment for the n electrons of the amide group which are nestled in the densely packed cylindrical core of atoms. For tertiary amides and amide groups in rings, λ_{\max} is between 231 and 233 m μ even when the ring compounds are secondary amides. This contrasts with the π, π^* spectra where the *cis*-ring structure appears to make very little difference in the position of the band.

The Spectra of Diamides. These experiments were performed to test the additivity of amide spectra in dimers. In principle, molecules containing two amide groups could possess most of the specialized optical properties of a helical polymer. If the amide levels are degenerate, the splitting of bands is predictable from theory if strong coupling is assumed.²⁵ If they are not degenerate, a shifting of position and a transfer of intensity between the bands (hypochromicity or hyperchromicity) should result.^{26,27} Since the degeneracy of the levels depends principally upon the nature and number of substituents on the amide nitrogen atom, models can be studied which illustrate either case.

Spectral phenomena which result from the coupling of absorption bands in adjacent amide groups can best be revealed by comparing the absorption curves of the diamide with the sum of the absorption curves

of monoamides selected to be appropriate moieties of the diamide. Figure 3 and Table V show the results for a number of diamides which have been investigated in aqueous solution. These substances, except for diketopiperazine, were originally prepared as models for optical rotation studies. We note the following. (1) All the diamides show some hypochromicity, though only in the case of acetamidopyrrolidinone is it appreciable. (2) There is little evidence of broadening of the π, π^* band except perhaps in alanine diketopiperazine. (3) The absorption maximum is shifted to the red except for alanine diketopiperazine, where it is shifted to the blue.

Table V: Absorption Data of Diamides in Water

	λ_{\max}	ϵ	<i>D</i>	<i>f</i>	Δ
XVII 	186	14,000	18	0.44	13
XVIII 	190	14,500	18	0.45	14
XIX 	188	13,400	26	0.65	22
XX 	189	13,500	19	0.47 ^a	16
XXI 	188	16,500	22	0.55	16

^a Ham and Platt³ reported $f = (0.19 \pm 0.05) \times 2$.

In some instances the absence of substantial shifts or intensity transfer is attributable to the degree of internal freedom available to the diamide molecules. Apart from the diketopiperazines, the conformational space of these molecules consists of line segments on the Ramachandran diagram. Since both the coupling energy and the intensity transfer terms can assume positive or negative values and are strongly dependent on geometry, it is conceivable that a great deal of cancellation occurs. Because of electrostatic interactions, the internal freedom of these molecules is greatly reduced in nonpolar solvents. Here, however, experi-

(25) W. T. Simpson and D. L. Peterson, *J. Chem. Phys.*, **26**, 588 (1957).

(26) I. Tinoco, *Advan. Chem. Phys.*, **4**, 113 (1962).

(27) W. Rhodes and M. Chase, Bulletin No. 31, Division of Biology and Medicine, U. S. Atomic Energy Commission, Florida State University, Tallahassee, Fla., Oct 1966.

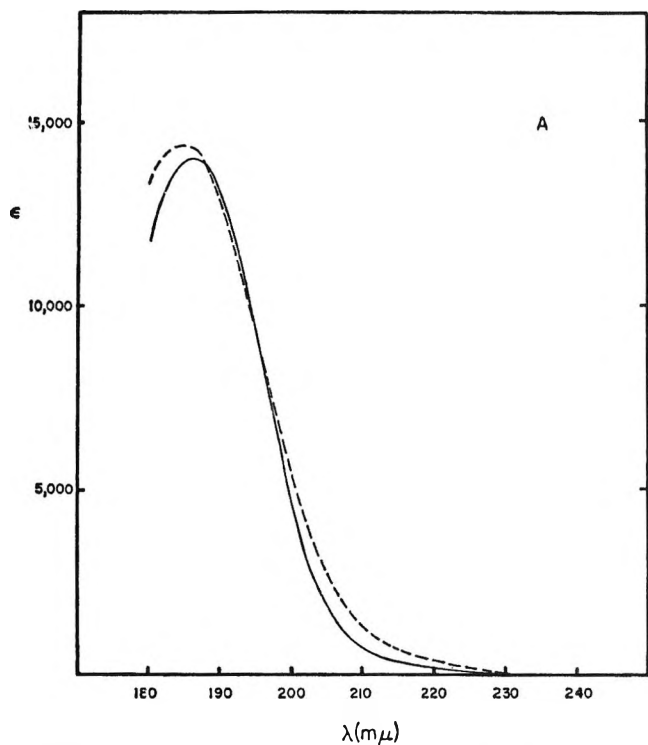


Figure 3A. Ultraviolet spectra in water of diamides (—) and the sum of the appropriate monoamides (---). L-Pyrroglutamide and the sum of 2-pyrrolidinone and propionamide.

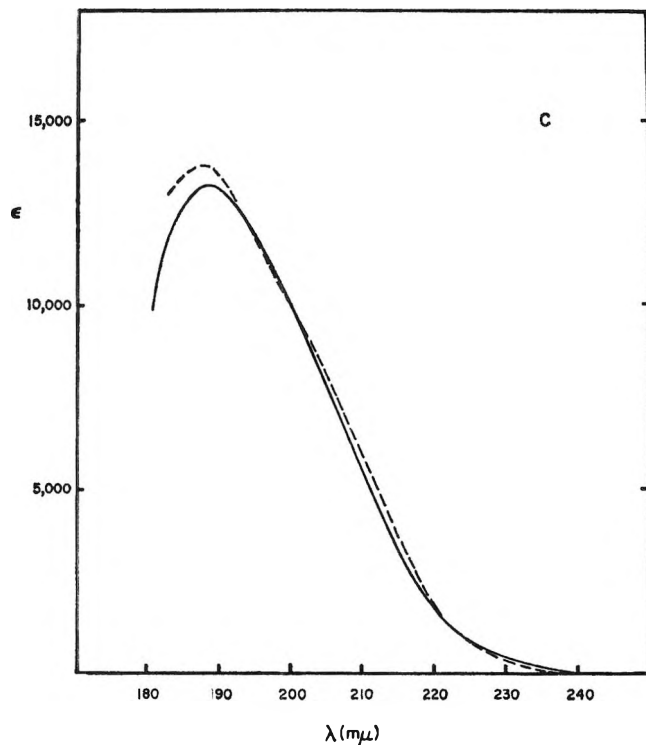


Figure 3C. N-Acetyl-L-proline amide and the sum of N-acetylpyrrolidine and propionamide.

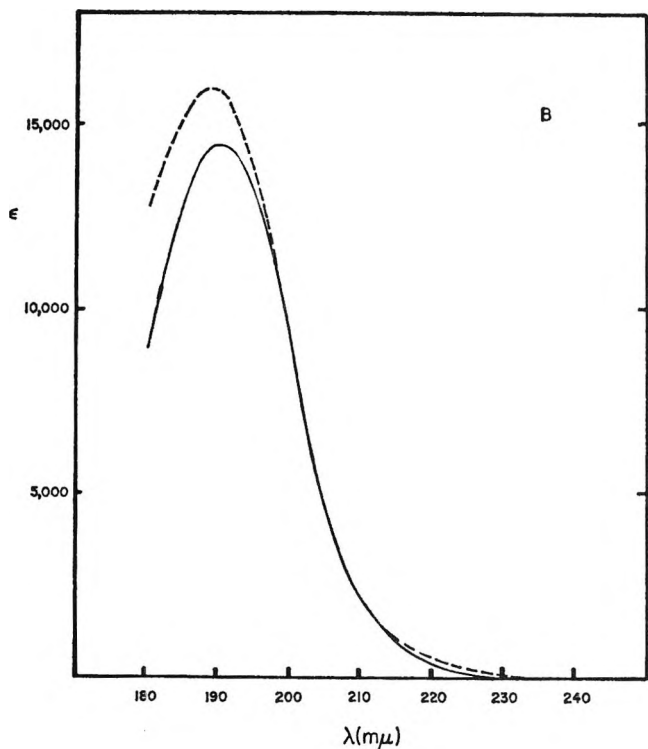


Figure 3B. L-3-Acetamidopyrrolidin-2-one and the sum of 2-pyrrolidinone and N-n-butylacetamide.

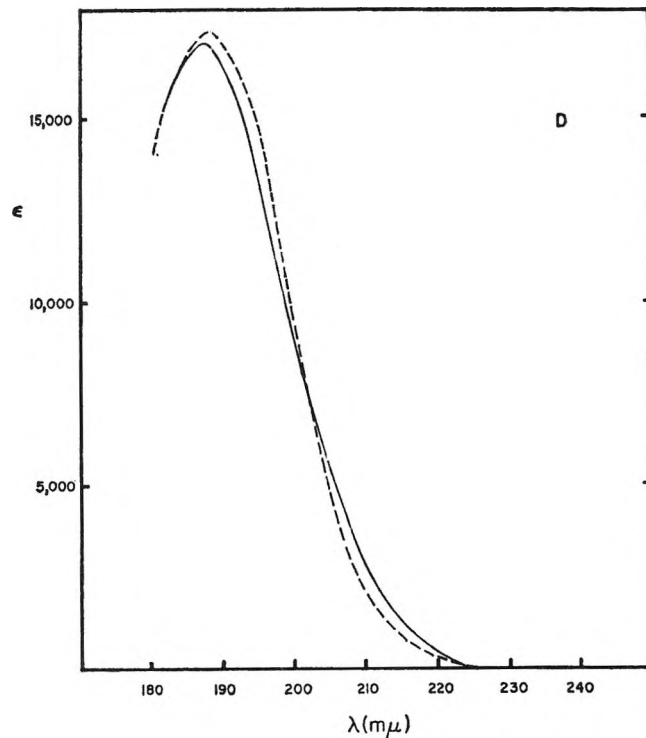


Figure 3D. L-Alanine anhydride and N-n-butylacetamide, the latter multiplied by 2.

mental difficulties are encountered. Dioxane is opaque in the region of interest, and the diamides have extremely small solubilities in solvents like cyclohexane.

These remarks do not apply to the diketopiperazines, where the conformational angles are fixed aside from torsional oscillations. Glycine diketopiperazine has been shown to be planar in the crystalline state.²⁸ We assume that alanine diketopiperazine is not planar because both methyl groups are on one side of the diketopiperazine ring. Further, the amide Cotton effects observed for this substance are not consistent with a planar conformation. Strong coupling theory predicts splittings of the order of 7 $m\mu$ for ringed dimers with all (diketopiperazine) or nearly all (alanine diketopiperazine) of the absorption intensity in the transition at short wavelength. This should show up as a marked blue shift and a slight broadening. These phenomena are observed, but the shift is much smaller than predicted.

This may indicate a failure of standard coupling theory for such molecules,²⁹ or it may result from the fortuitous cancellation of the coupling effects by other perturbations which accompany dimer formation. These would include, for example, the static interactions between amides. Moreover, the bond lengths and angles in diketopiperazine deviate somewhat from those which are standard for the peptide group. This could lead to energy shifts in the π -electron system in both the ground and excited states.

By contrast, interactions between the π, π^* transitions in all the models show up clearly in studies of rotatory dispersion in the amide Cotton effect region.

The Problem of Association in Nonaqueous Solvents.

It is known from many investigations that amides associate by hydrogen-bond formation in nonaqueous solvents. The investigations of Franzen and Stephens³⁰ and Luck³¹ are especially pertinent, the former with extensive variation of solvent, the latter with extensive variation of amides. Their results indicate that amides of the lactam type have an association constant of the order of 10^2 in carbon tetrachloride and that simple amides have lower association constants. Association should be stronger in cyclohexane, weaker in dioxane, and negligible in water. This means that our solutions for the investigation of the π, π^* band in cyclohexane probably possessed very small fractions of associated molecules. On the other hand, the curves for the n, π^* transition had to be obtained under conditions of concentration such that some of the amides, particularly the cyclic amides, were probably highly dimerized in cyclohexane. No substantial effects of concentration were observed. This either means that H bonding has a small effect on the ultraviolet spectra or that the association is so strong that it is not perturbed by dilution to $10^{-3} M$. We consider the latter possibility unlikely.

(28) R. B. Corey, *Chem. Rev.*, **26**, 227 (1940).

(29) Examination of the criteria of Simpson and Peterson²⁶ indicates that these molecules fall into the category of intermediate coupling.

(30) J. S. Franzen and R. E. Stephens, *Biochemistry*, **2**, 1321 (1963).

(31) V. W. Luck, *Naturwissenschaften*, **52**, 25, 49 (1965).

Equations for the Calculation of Activity Coefficients of Solutions from the Intensity of Brillouin Scattering

by George A. Miller

School of Chemistry, Georgia Institute of Technology, Atlanta, Georgia (Received January 18, 1967)

The thermodynamic theory of Brillouin scattering is extended to binary solutions. Formulas are developed for the absolute intensity of the unshifted scattering in the form of a Rayleigh ratio and for the intensity ratio of the unshifted to the Doppler-shifted scattering. A determination of either quantity can serve as a method of obtaining activity coefficients of binary solutions, which requires less subsidiary data than the corresponding method based on total isotropic Rayleigh scattering.

In the classical thermodynamic theory of Rayleigh scattering by solutions¹ a portion of the total light scattering is attributed to concentration fluctuations. Since the chemical potential plays an important part in these fluctuations, the measurement of the Rayleigh ratio can, under favorable conditions, lead to a determination of activity coefficients. Recent experiments of this nature have been performed by Coumou and Mackor² on binary solutions of nonelectrolytes and by Pethica and Smart³ on aqueous electrolytes.

At the same time the availability of intense and highly monochromatic light from lasers has resulted in renewed interest in the fine structure of Rayleigh scattering, often called the Brillouin spectrum, which consists of an unshifted *Rayleigh* peak and two Doppler-shifted *Brillouin* satellites.⁴ A new approach suggests itself for the determination of activity coefficients, in which one would measure the intensity of the Rayleigh peak only. Since concentration fluctuations contribute to only the Rayleigh peak, whereas fluctuations in the other variables contribute to the Brillouin peaks as well, one would, in effect, subtract at least a share of the contribution from uninteresting fluctuations by this procedure. Alternately, one could measure the ratio of intensities of Rayleigh and Brillouin peaks and thereby eliminate the need to measure the ratio of scattered to incident light.

In this paper the thermodynamic approach is used to develop expressions for the intensity of the fine-structure components of Brillouin scattering. Fluctuation averages are derived by the method of Landau

and Lifshitz.⁵ The treatment necessarily differs somewhat from that of total isotropic light scattering,^{1,6,7} especially in the choice of thermodynamic variables. In particular, the introduction of density fluctuations is avoided, because they mix statistically with concentration fluctuations. The notion that the dielectric constant varies only with density at constant composition is then introduced at a later stage as an approximation that may easily be withdrawn.

Fluctuation Theory

Imagine a small volume element, V , of a binary solution at constant temperature and pressure, which contains a constant number of moles, n_1 , of one component, arbitrarily called the solvent. From the standpoint of small, rapid fluctuations, the solution may be treated as a thermally isolated system. According to Landau and Lifshitz, fluctuations in the total entropy of the system arise from fluctuations inside element V of the absolute temperature, T , the entropy,

(1) See, for example, the review by G. Oster, *Chem. Rev.*, **43**, 319 (1948).

(2) D. J. Coumou and E. L. Mackor, *Trans. Faraday Soc.*, **60**, 1726 (1964).

(3) B. A. Pethica and C. Smart, *ibid.*, **62**, 1890 (1966).

(4) For an excellent example of the kind of measurements to be considered here, see H. Z. Cummins and R. W. Gammon, *J. Chem. Phys.*, **44**, 2785 (1966).

(5) L. D. Landau and E. M. Lifshitz, "Statistical Physics," Pergamon Press Ltd., London, 1958.

(6) J. G. Kirkwood and R. J. Goldberg, *J. Chem. Phys.*, **18**, 54 (1950).

(7) W. H. Stockmayer, *ibid.*, **18**, 58 (1950).

S , the pressure, P , the chemical potential of the solute, μ_2 , and the number of moles of solute, n_2 , as well as V itself, through the relation

$$\Delta S_t = -\frac{1}{2T}(\Delta T \Delta S - \Delta P \Delta V + \Delta \mu_2 \Delta n_2) \quad (1)$$

If the fluctuations of the various variables are expressed as linear functions of three chosen variables of state, the result is the general quadratic form

$$\Delta S_t = -\frac{1}{2} \sum_i \sum_j B_{ij} x_i x_j \quad (2)$$

where the x_i are fluctuations in the three variables of choice. The B_{ij} form a matrix for which $B_{ij} = B_{ji}$ from simple physical considerations. Average values of products are given by $\langle x_i x_j \rangle = k B_{ij}^{-1}$, where B_{ij}^{-1} is an element of the inverse matrix and k is the Boltzmann constant. The situation of particular interest here is the one in which $B_{13} = B_{23} = 0$, *i.e.*, one in which x_3 is said to be statistically independent of x_1 and x_2 . The inverse matrix then has the elements

$$B_{11}^{-1} = -B_{22}/(B_{12}^2 - B_{11}B_{22})$$

$$B_{12}^{-1} = B_{12}/(B_{12}^2 - B_{11}B_{22})$$

$$B_{22}^{-1} = -B_{11}/(B_{12}^2 - B_{11}B_{22})$$

$$B_{33}^{-1} = 1/B_{33}$$

Consider first the state of the volume element, V , to be a function of the variables T , P , and n_2 . For small fluctuations one can write the linear relation

$$\Delta S = \left(\frac{\partial S}{\partial T}\right)_{P,n_2} \Delta T + \left(\frac{\partial S}{\partial P}\right)_{T,n_2} \Delta P + \left(\frac{\partial S}{\partial n_2}\right)_{T,P} \Delta n_2$$

Similar expressions may be written for ΔV and $\Delta \mu_2$, it being understood that n_1 is always held constant. Putting these expressions into eq 1 with suitable, elementary thermodynamic transformations yields the result

$$\Delta S_t = -\frac{1}{2} \left(\frac{C_p}{T^2} (\Delta T)^2 - \frac{2V\alpha}{T} \Delta T \Delta P + \frac{V\beta_T}{T} (\Delta P)^2 + \frac{1}{T} \left(\frac{\partial \mu_2}{\partial n_2} \right)_{T,P} (\Delta n_2)^2 \right)$$

where α is the isothermal coefficient of expansion, β_T is the isothermal compressibility, and C_p is the heat capacity at constant pressure. Comparing with eq 2 and setting $x_1 = \Delta T$, $x_2 = \Delta P$, and $x_3 = \Delta n_2$, one obtains

$$B_{11} = C_p/T^2$$

$$B_{12} = -V\alpha/T$$

$$B_{22} = V\beta_T/T$$

$$B_{13} = B_{23} = 0$$

$$B_{33} = \frac{1}{T} \left(\frac{\partial \mu_2}{\partial n_2} \right)_{T,P}$$

which leads to the following fluctuation averages

$$\langle (\Delta T)^2 \rangle = kT^2/C_p$$

$$\langle \Delta T \Delta P \rangle = kT^2 \alpha / \beta_T C_p$$

$$\langle (\Delta P)^2 \rangle = kT/V\beta_s$$

$$\langle (\Delta n_2)^2 \rangle = \frac{kT}{(\partial \mu_2 / \partial n_2)_{T,P}}$$

$$\langle \Delta T \Delta n_2 \rangle = \langle \Delta P \Delta n_2 \rangle = 0$$

where β_s is the adiabatic compressibility and C_v is the heat capacity at constant volume.

Consider now the variables S , n_2 , and P . Setting $x_1 = \Delta S$, $x_2 = \Delta n_2$, $x_3 = \Delta P$, one obtains a similar set of coefficients, of which the important ones for Brillouin scattering are

$$B_{13} = B_{23} = 0$$

$$B_{33} = V\beta_s/T$$

which yields $\langle (\Delta P)^2 \rangle = kT/V\beta_s$ as before, and $\langle (\Delta S \Delta P) \rangle = \langle (\Delta n_2 \Delta P) \rangle = 0$.

A similar analysis would show that the variables V and n_2 are not statistically independent. It follows that density fluctuations mix with fluctuations in n_2 . However, since the dielectric constant is to a good approximation only a function of density at constant composition, an alternate approach is to consider density as a function of T and P , at constant composition. The latter approach has been used often but is not advantageous for the present discussion.

Application to Brillouin Spectra

According to classical scattering theory, a beam of light of intensity I_0 , polarized with the electrical vector perpendicular to the plane of scattering, will be scattered as it passes through volume element V by fluctuations in the dielectric constant, ϵ , such that the intensity of the scattered light at a distance r from the volume element is given by

$$i/I_0 = (\pi^2/r^2\lambda^4) V^2 \langle (\Delta \epsilon)^2 \rangle$$

where λ is the wavelength of the incident light. The scattered light consists of a central, Rayleigh peak at $\omega = 1/\lambda$ and two Brillouin peaks at $\omega \pm \Delta\omega$, where

$$\Delta\omega = 2\omega(v_s/c) \sin(\theta/2) \quad (3)$$

v_s and c are the velocities of sound and light in the solution, and θ is the scattering angle.

In the thermodynamic approach to Brillouin scattering of pure fluids,^{4,8} fluctuations in ϵ are separated into two kinds. Pressure fluctuations at constant entropy propagate as sound waves, giving rise to Doppler-shifted scattering. Fluctuations in entropy at constant pressure relax by thermal processes and do not propagate, thus giving rise to unshifted scattering. In solutions there are concentration fluctuations as well. Since they relax by diffusion processes and do not propagate, they also contribute to the unshifted scattering.

It has been shown above that adiabatic pressure fluctuations do not mix with entropy and composition fluctuations. Thus, the term needed in the intensity formula for the Brillouin peaks is

$$\langle(\Delta\epsilon)_{\text{adiab}}^2\rangle = \left(\frac{\partial\epsilon}{\partial P}\right)_{S,n_2}^2 \langle(\Delta P)^2\rangle$$

This may be expressed in terms of measurable quantities using the relation

$$\left(\frac{\partial\epsilon}{\partial P}\right)_{S,n_2} = \left(\frac{\partial\epsilon}{\partial T}\right)_{P,n_2} \frac{TV\alpha}{C_p} + \left(\frac{\partial\epsilon}{\partial P}\right)_{T,n_2}$$

The final result is

$$\langle(\Delta\epsilon)_{\text{adiab}}^2\rangle = \frac{kT^2}{C_v} \left(1 - \frac{1}{\gamma}\right) \left(\frac{\partial\epsilon}{\partial T}\right)_{P,n_2}^2 + \frac{2kT^2\alpha}{\beta_T C_v} \left(\frac{\partial\epsilon}{\partial T}\right)_{P,n_2} \left(\frac{\partial\epsilon}{\partial P}\right)_{T,n_2} + \frac{kT}{V\beta_S} \left(\frac{\partial\epsilon}{\partial P}\right)_{T,n_2}^2 \quad (4)$$

where $\gamma = C_p/C_v$. The intensity formula for the two Brillouin peaks combined is obtained by substituting eq 4 into

$$2i_B/I_0 = (\pi^2/r^2\lambda^4)V^2\langle(\Delta\epsilon)_{\text{adiab}}^2\rangle$$

The sum of the intensities of the Brillouin and Rayleigh peaks is now calculated using the variables T , P , and n_2

$$\begin{aligned} \langle(\Delta\epsilon)^2\rangle &= \left(\frac{\partial\epsilon}{\partial T}\right)_{P,n_2}^2 \langle(\Delta T)^2\rangle + \\ &2\left(\frac{\partial\epsilon}{\partial T}\right)_{P,n_2} \left(\frac{\partial\epsilon}{\partial P}\right)_{T,n_2} \langle\Delta T\Delta P\rangle + \left(\frac{\partial\epsilon}{\partial P}\right)_{T,n_2}^2 \langle(\Delta P)^2\rangle + \\ &\left(\frac{\partial\epsilon}{\partial n_2}\right)_{T,P}^2 \langle(\Delta n_2)^2\rangle = \frac{kT^2}{C_v} \left(\frac{\partial\epsilon}{\partial T}\right)_{P,n_2}^2 + \\ &\frac{2kT^2\alpha}{\beta_T C_v} \left(\frac{\partial\epsilon}{\partial T}\right)_{P,n_2} \left(\frac{\partial\epsilon}{\partial P}\right)_{T,n_2} + \frac{kT}{V\beta_S} \left(\frac{\partial\epsilon}{\partial P}\right)_{T,n_2}^2 + \\ &\frac{kT(\partial\epsilon/\partial n_2)_{T,P}^2}{(\partial\mu_2/\partial n_2)_{T,P}} \quad (5) \end{aligned}$$

Since concentration fluctuations are statistically independent of adiabatic pressure fluctuations, the last term contributes only to the central, Rayleigh peak. The first three terms contribute to the central and Brillouin peaks as well. The total contribution to the central peak is obtained by subtracting eq 4 from eq 5 to give

$$\begin{aligned} \langle(\Delta\epsilon)_C^2\rangle &= \frac{kT^2}{C_p} \left(\frac{\partial\epsilon}{\partial T}\right)_{P,n_2}^2 + \frac{kT(\partial\epsilon/\partial n_2)_{T,P}^2}{(\partial\mu_2/\partial n_2)_{T,P}} \\ i_C/I_C &= (\pi^2/r^2\lambda^4)V^2\langle(\Delta\epsilon)_C^2\rangle \end{aligned}$$

The ratio of the intensity of the central peak to that of the two Brillouin peaks is

$$J = i_C/2i_B = \langle(\Delta\epsilon)_C^2\rangle/\langle(\Delta\epsilon)_{\text{adiab}}^2\rangle$$

One may introduce at this point the usual approximation that the dielectric constant of a given solution is intrinsically only a function of the density, ρ , that is, at constant composition

$$\begin{aligned} (\partial\epsilon/\partial T) &= -(\rho d\epsilon/d\rho)\alpha \\ (\partial\epsilon/\partial P) &= (\rho d\epsilon/d\rho)\beta_T \end{aligned} \quad (6)$$

The subscripts for partial differentiation are omitted, since the variables from here on will be exclusively T , P , and composition. Equation 4 may now be expressed in terms of, say, $(\partial\epsilon/\partial T)$ with great simplification

$$\langle(\Delta\epsilon)_{\text{adiab}}^2\rangle = \frac{kT\beta_S}{V\alpha^2} \left(\frac{\partial\epsilon}{\partial T}\right)^2 = \frac{kT^2}{C_p} \left(\frac{1}{\gamma - 1}\right) \left(\frac{\partial\epsilon}{\partial T}\right)^2 \quad (7)$$

For a pure liquid, where the concentration fluctuation term is absent, this leads to the well known Landau-Placzek formula

$$J = \gamma - 1 = (\beta_T/\beta_S) - 1$$

One may equally well introduce some specific relation between ϵ and ρ like the Clausius-Mosotti equation. Then, the appropriate function is $(\rho d\epsilon/d\rho)$. In particular, the familiar Einstein-Smoluchowski formula for total isotropic light scattering is obtained by rewriting eq 5 in this way.

Deviations from the Landau-Placzek formula can arise from other causes than the failure of eq 6. For example, large deviations are shown by viscous liquids⁹ and liquids near the critical point (critical opalescence). Similar complications can be expected for solutions. Also, it has been recognized only recently that fluctua-

(8) L. Landau and G. Placzek, *Physik. Z. Sowjetunion*, **5**, 172 (1934).

(9) D. H. Rank, E. M. Kiess, and U. Fink, *J. Opt. Soc. Am.*, **56**, 163 (1966).

tions can couple with internal modes in a way that enhances the central peak.¹⁰ This has been detected experimentally for carbon tetrachloride.¹¹

Final Formulas

With these reservations in mind the intensity formulas may be written down in terms of the mole fraction of solute, x_2 , for nonelectrolytes, or the molality, m , for electrolytes, using the simplified form represented by eq 7. Letting M_1 be the molecular weight of the solvent and remembering that n_1 is held constant, one gets the conversion formulas

$$dx_2 = dn_2x_1/(n_1 + n_2)$$

$$dm = dn_2(1000/M_1n_1)$$

The intensity of scattered light may be conveniently expressed as the Rayleigh ratio at a scattering angle of 90°

$$R_{90} = r^2i/VI_0 = (\pi^2/\lambda^4)V\langle(\Delta\epsilon)^2\rangle$$

The factor, $1/V$, in the Rayleigh ratio may be considered to be the inverse total scattering volume by the usual arguments. The remaining factor V is absorbed by converting extensive properties of the volume element into intensive ones. Also, the index of refraction is introduced at this point by the relation $d\epsilon = 2ndn$. For nonelectrolytes, the result is

$$(R_{90})_C = \frac{4\pi^2n^2}{\lambda^4} \left[\frac{kT^2v}{c_p} \left(\frac{\partial n}{\partial T} \right)^2 + kTv x_1 \frac{(\partial n/\partial x_2)^2}{\partial \mu_2/\partial x_2} \right]$$

$$J = (\gamma - 1) + \frac{c_p}{T}(\gamma - 1)x_1 \frac{(\partial n/\partial x_2)^2}{(\partial n/\partial T)^2} \frac{1}{\partial \mu_2/\partial x_2}$$

where v and c_p are the volume and heat capacity at constant pressure per mole of solution, respectively. For electrolytes, the result is

$$(R_{90})_C = \frac{4\pi^2n^2}{\lambda^4} \left[\frac{kT^2v'}{c_p'} \left(\frac{\partial n}{\partial T} \right)^2 + kTv' \frac{(\partial n/\partial m)^2}{\partial \mu_2/\partial m} \right]$$

$$J = (\gamma - 1) + \frac{c_p'}{T}(\gamma - 1) \frac{(\partial n/\partial m)^2}{(\partial n/\partial T)^2} \frac{1}{\partial \mu_2/\partial m}$$

where c_p' and v' are now values for that amount of solution containing 1 kg of solvent.

These formulas form a basis for the determination of the composition derivative of μ_2 , from which activity coefficients of solute and solvent may be evaluated with the aid of the Gibbs–Duhem relation. If $(R_{90})_C$ is

the quantity being measured, the additional data needed are the temperature and composition dependence of the index of refraction at the wavelength of the incident light, the heat capacity, and the molar (or molal) volume. If the ratio J is being measured, the value of the isothermal coefficient of expansion is also needed. Then, the heat capacity terms are calculated through the relations

$$(\gamma - 1) = Tv\alpha^2/c_p\beta_s$$

$$\beta_s = 1/\rho v_s^2$$

Here, v_s is obtained through eq 3 by measuring the frequency shift of the Brillouin doublet.

The full expression for $(R_{90})_{iso}$, the Rayleigh ratio for total isotropic scattering, which may be derived from eq 5, involves a good deal of additional data. Usually, however, $(R_{90})_{iso}$ is written in simplified form by means of eq 6. In either case, one virtue of the present approach is to avoid the quantities $\partial n/\partial P$ and β_T , at least one of which always appears in the expression for $(R_{90})_{iso}$.

With the measurement of J the difficulties associated with the refraction and volume corrections¹² are avoided. They may also be avoided in the measurement of $(R_{90})_C$ if a scanning Fabry–Perot interferometer is used without a collecting lens, since only collimated light is passed. Present sensitive techniques of photo-detection coupled with the use of higher power lasers makes this feasible.

The shape of the central peak is of special interest. Neglecting the cross term $\langle\Delta S\Delta n_2\rangle$, one can consider the central peak to be a sum of two Lorentzians, each characterized by a different decay process, hence, each having a different width. Therefore, it may be possible to separate the concentration component experimentally. Since these widths are generally very narrow, however, they cannot be studied by ordinary, interferometric techniques.¹³

Acknowledgment.—This research was supported by a grant from the National Science Foundation (GP-4027).

(10) R. Mountain, *J. Res. Natl. Bur. Std.*, **A70**, 207 (1966).

(11) W. S. Gornall, G. I. A. Stegeman, B. P. Stoicheff, R. H. Stolen, and V. Volterra, *Phys. Rev. Letters*, **17**, 297 (1966).

(12) C. I. Carr, Jr., and B. H. Zimm, *J. Chem. Phys.*, **18**, 111 (1950).

(13) H. Z. Cummins, N. Knable, and Y. Yeh, *Phys. Rev. Letters*, **14**, 486 (1965).

Nuclear Magnetic Resonance Fluorine-Fluorine Coupling

Constants in Fluorotitanate Complexes

by Daniel S. Dyer and Ronald O. Ragsdale

Department of Chemistry, University of Utah, Salt Lake City, Utah 84112 (Received January 23, 1967)

The factors which determine the F^{19} spin-spin coupling constants in the $TiF_4 \cdot 2(\text{donor})$ complexes ($TiF_4 \cdot 2D$ and $TiF_4 \cdot D, D'$) have been studied. The coupling constants for several complexes are reported. The data are discussed in terms of through-space F-F nuclear interaction.

Introduction

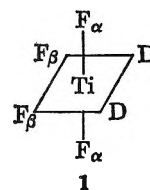
In a fluorine-19 nmr study¹ of a series of titanium tetrafluoride adducts, $TiF_4 \cdot (CH_3)_2NC(O)CH_3, 4-ZC_5H_4NO$, the chemical shifts were shown to be sensitive to the nature of the *para* substituent (*Z*) on pyridine 1-oxide. On the other hand, the spin-spin coupling constants of these complexes are only very slightly affected by electron-density changes produced by the different *Z* substituents. Since relatively little was known about the factors which determine the couplings between fluorine-19 nuclei in complex ions, a study of spin-spin interaction in the *cis*- $TiF_4 \cdot 2D$ (*D* = donor) complexes was conducted. The results of this research are reported, and the data are examined in view of related studies of fluorine-substituted organic compounds.

Experimental Section

The spectra were obtained at 56.4 Mc/sec with a Varian A-56/60A spectrometer equipped with the V-6057 variable-temperature system. The studies were conducted on samples cooled to temperatures at which the spin-spin multiplets are completely resolved. The mixed adduct ($TiF_4 \cdot D, D'$) solutions were prepared by the method reported previously.¹ The $TiF_4 \cdot 2D$ samples were prepared either by dissolving titanium tetrafluoride (Allied Chemical Corp.) in an excess of organic donor or, when possible, by isolating the TiF_4 diadduct and dissolving it in an appropriate solvent. The solvents chloroform, dichloromethane, acetonitrile, and chloroacetonitrile were purified by standard procedures. The nmr samples were of sufficient purity that no extraneous F^{19} peaks were observed.

Results

The identical donor molecules in the *cis*- $TiF_4 \cdot 2D$ octahedron (1) create two electronic environments each containing two F^{19} nuclei.^{2,3} At sufficiently low



temperatures, depending upon the nature of the donor molecules, the nmr spectra of these complexes consist of two triplets of equal intensity (first-order A_2X_2). The spin-spin coupling constants (*J*) for several $TiF_4 \cdot 2D$ complexes were determined and are listed in Table I. Whenever possible the *J* value of a complex was determined in more than one solvent (chloroform, dichloromethane, acetonitrile, chloroacetonitrile, or excess organic donor). Within experimental error the different solvents did not appear to affect the magnitude of the coupling constants.

In the *cis*- $TiF_4 \cdot D, D'$ complexes¹ there are two equivalent and two nonequivalent fluorine atoms. The spectra of the mixed adducts considered here are of the A_2MX type, consisting of a doublet of doublets and two doublets of triplets. The doublet of doublets has twice the intensity of either of the doublets of triplets. The coupling constants of the $TiF_4 \cdot DMA, 4-ZC_5H_4NO$

(1) D. S. Dyer and R. O. Ragsdale, *Inorg. Chem.*, **6**, 8 (1967).

(2) E. L. Muetterties, *J. Am. Chem. Soc.*, **82**, 1082 (1960).

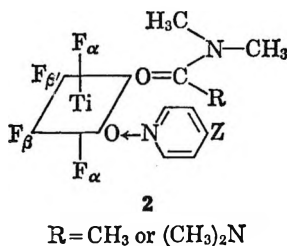
(3) R. O. Ragsdale and B. B. Stewart, *Inorg. Chem.*, **2**, 1002 (1963).

Table I: F^{19} Spin-Spin Coupling Constants^a (Magnitudes) for the $TiF_4 \cdot 2D$ Complexes

Donor	<i>J</i>	Donor	<i>J</i>
4-CH ₃ O ₂ CC ₅ H ₄ NO	34	<i>i</i> -C ₃ H ₇ OH	36
4-ClC ₅ H ₄ NO	34	CH ₃ S(O)CH ₃	37
4-HC ₅ H ₄ NO	35	HC(O)N(CH ₃) ₂	38
4-CH ₃ C ₅ H ₄ NO	35	HC(O)N(C ₂ H ₅) ₂	38
4-CH ₃ OC ₅ H ₄ NO	35	CH ₃ C(O)N(CH ₃) ₂	39
2-CH ₃ C ₅ H ₄ NO	36	C ₂ H ₅ C(O)N(CH ₃) ₂	40
CH ₃ OH	36	(CH ₃) ₂ NC(O)N(CH ₃) ₂	41
C ₂ H ₅ OH	36		

^a ±1 cps.

complexes (**2**, DMA = N,N-dimethylacetamide) are listed in Table II for reference. The *J* values for three new $TiF_4 \cdot D, D'$ complexes, $TiF_4 \cdot TMU, 4-ZC_5H_4NO$ (TMU = tetramethylurea and Z = CH₃O, H, and NO₂), are also given in Table II. The peaks in the spectra of these complexes were assigned on the same basis



as in the study of $TiF_4 \cdot DMA, 4-ZC_5H_4NO$,¹ where it was shown that the chemical shift of the fluorine *trans* to 4- ZC_5H_4NO is influenced most by Z.

Table II: F^{19} Spin-Spin Coupling Constants^a (Magnitudes) for the $TiF_4 \cdot D, D'$ Complexes

D	D'	<i>J</i> _{αβ}	<i>J</i> _{αβ'}	<i>J</i> _{ββ'}
4-CH ₃ O ₂ CC ₅ H ₄ NO	N,N-Dimethylacetamide	39	34	48
4-ClC ₅ H ₄ NO	N,N-Dimethylacetamide	39	34	48
4-HC ₅ H ₄ NO	N,N-Dimethylacetamide	39	35	48
4-CH ₃ C ₅ H ₄ NO	N,N-Dimethylacetamide	39	35	48
4-CH ₃ OC ₅ H ₄ NO	N,N-Dimethylacetamide	39	35	48
4-O ₂ NC ₅ H ₄ NO	Tetramethylurea	41	34	49
4-HC ₅ H ₄ NO	Tetramethylurea	41	35	49
4-CH ₃ OC ₅ H ₄ NO	Tetramethylurea	41	35	49

^a ±1 cps.

Two results of this study are especially noteworthy: (1) comparison of the F-F coupling constants of the $TiF_4 \cdot D, D'$ complexes shows that the spin-spin interactions are insensitive to the nature of Z, and (2) the

three coupling constants of each $TiF_4 \cdot D, D'$ complex are quite different from each other.

Discussion

It has been shown that H-H spin coupling constants can be calculated semiquantitatively by a consideration of the valence-bond theory of the Fermi contact term in the Hamiltonian.⁴⁻¹⁰ The deviations from perfect pairing of the binding electrons provide the dominant contributions to the interactions between protons separated by two or more bonds. Physically the magnitude of the coupling constant depends in part on the number of covalent bonds through which the protons interact and also on the geometrical orientation of the interacting nuclei.

The theory of coupling between nuclei of atoms other than hydrogen is complicated by the larger contributions of the electron-spin and the electron-orbital terms in the Hamiltonian. Qualitatively, the problem of F^{19} spin-spin coupling is made more difficult by the presence of occupied p orbitals in the vicinity of the fluorine nuclei. It might be expected, therefore, that F^{19} nuclear coupling could occur *via* more than one mechanism.

Convincing evidence for the existence of "through-space" coupling between fluorine nuclei has been presented.^{11,12} This type of nuclear interaction is thought to come about as a result of overlap between the electronic clouds of the coupled fluorine atoms. Through-space interaction can be expected when the distance between the fluorine nuclei becomes less than twice the van der Waals radius for a fluorine atom (~2.72 Å). However, an exact expression of through-space coupling as a function of the F-F internuclear distance has not as yet been reported.¹³ Isolation of a through-space contribution to a fluorine-19 coupling constant is complicated by the possibility of contributions of the same or opposite sign from other pathways for the transmission of spin information.

(4) M. Karplus, D. H. Anderson, T. C. Farrar, and H. S. Gutowsky, *J. Chem. Phys.*, **27**, 597 (1957).

(5) M. Karplus and D. H. Anderson, *ibid.*, **30**, 6 (1959).

(6) M. Karplus, *ibid.*, **30**, 11 (1959).

(7) H. S. Gutowsky, M. Karplus, and D. M. Grant, *ibid.*, **31**, 1278 (1959).

(8) M. Karplus and D. M. Grant, *Proc. Natl. Acad. Sci. U. S.*, **45**, 1269 (1959).

(9) M. Karplus, *J. Chem. Phys.*, **33**, 1842 (1960).

(10) M. Barfield and D. M. Grant, *ibid.*, **36**, 2054 (1962); *J. Am. Chem. Soc.*, **83**, 4726 (1961); **85**, 1899 (1963).

(11) L. Petrakis and C. H. Sederholm, *J. Chem. Phys.*, **35**, 1243 (1961).

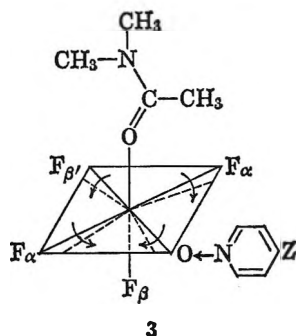
(12) S. Ng and C. H. Sederholm, *ibid.*, **40**, 2090 (1964).

(13) N. Boden, J. Feeney, and L. H. Sutcliffe, *J. Chem. Soc.*, 3482 (1965).

All of the F-F couplings in the $\text{TiF}_4 \cdot 2\text{D}$ and $\text{TiF}_4 \cdot \text{D}, \text{D}'$ complexes are of the geminal type (interaction between nuclei separated by two bonds). The geminal fluorine coupling constants of the fluoroethanes extend over a wide range and in one series, $\text{QF}_2\text{C}-\text{CClHF}$, were found to be dependent on the electronegativity of the substituent Q.¹⁴ An nmr study of a variety of trifluorovinyl derivatives¹⁵ ($\text{YCF}=\text{CF}_2$) showed that the chemical shifts and the coupling constants of the vinyl fluorines are very sensitive to the mesomeric and inductive nature of the species to which the trifluorovinyl group is bonded. In another study of the trifluorovinyl derivatives, a linear relationship between the geminal coupling constant and the mean of the two chemical shifts of the terminal fluorines was pointed out.¹⁶ It was recently suggested¹⁵ that through-space coupling in the trifluorovinyl compounds does not seem plausible.

In contrast to the coupling behavior of geminal fluorines bonded to carbon, the F-F coupling constants in the $\text{TiF}_4 \cdot \text{DMA}, 4\text{-ZC}_5\text{H}_4\text{NO}$ and $\text{TiF}_4 \cdot \text{TMU}, 4\text{-ZC}_5\text{H}_4\text{NO}$ complexes were not sensitive to the mesomeric or inductive characteristics of the substituents. In spite of the considerable influence which the *para* substituent exerts upon the σ - and π -bonding ability of the $\text{N} \rightarrow \text{O}$ oxygen,^{1,17} the largest range observed for any of the three couplings was 1 cps. (This can be compared with the range of J_{gem} in the trifluorovinyl derivatives (5 to 101 cps).)

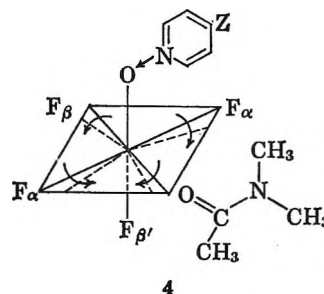
The insensitivity of the F^{19} coupling constants of the $\text{TiF}_4 \cdot \text{D}, \text{D}'$ complexes to the electron density about titanium can be explained if the F-F nuclear interaction is assumed to occur primarily through space rather than through the bonds. In through-space interaction a decrease in the F-F internuclear distance is expected to cause an increase in the magnitude of the coupling constant. Consider model 3 for the $\text{TiF}_4 \cdot \text{DMA}, 4\text{-ZC}_5\text{H}_4\text{NO}$ complexes. Steric in-



3

teraction between DMA and the adjacent (*cis*) fluorines should shorten the internuclear distances $\text{F}_\alpha\text{-F}_\beta$ and $\text{F}_\beta\text{-F}_{\beta'}$ by decreasing the angles $\text{F}_\alpha\text{TiF}_\beta$ and $\text{F}_\beta\text{TiF}_{\beta'}$,

and increasing the magnitudes of $J_{\alpha\beta}$ and $J_{\beta\beta'}$. To a first approximation the angle $\text{F}_\alpha\text{TiF}_{\beta'}$ and $J_{\alpha\beta'}$ would not be affected by the presence of the DMA molecule. By the same reasoning and as seen from model 4, repulsion between $4\text{-ZC}_5\text{H}_4\text{NO}$ and the adjacent fluorines should affect $J_{\alpha\beta'}$ and $J_{\beta\beta'}$, but not $J_{\alpha\beta}$. The angle $\text{F}_\beta\text{TiF}_{\beta'}$ is therefore decreased by both donor-fluorine interactions and would be expected to be the smallest FTiF angle in the complex. Experimentally, $J_{\beta\beta'}$ is found to be the largest of the three coupling constants. In addition $J_{\alpha\beta}$, the coupling constant determined by fluorine-DMA repulsion, is equal to J for $\text{TiF}_4 \cdot 2\text{DMA}$, and $J_{\alpha\beta'}$, the coupling constant determined by fluorine-pyridine 1-oxide repulsion, is equal to J for the corresponding $\text{TiF}_4 \cdot 2(4\text{-ZC}_5\text{H}_4\text{NO})$ complex.



4

The same reasoning explains the relative values of the three coupling constants for each $\text{TiF}_4 \cdot \text{TMU}, 4\text{-ZC}_5\text{H}_4\text{NO}$ complex. The largest coupling is again between F_β and $\text{F}_{\beta'}$. The coupling constants determined by the fluorine-TMU repulsion and the fluorine-pyridine 1-oxide repulsion are equal respectively to the coupling constants for $\text{TiF}_4 \cdot 2\text{TMU}$ and $\text{TiF}_4 \cdot 2(4\text{-ZC}_5\text{H}_4\text{NO})$. It appears, therefore, that spin-spin interaction in the $\text{TiF}_4 \cdot \text{D}, \text{D}'$ complexes can be qualitatively explained on the basis of a through-space coupling mechanism, although other mechanisms might exhibit a similar dependence on F-F internuclear separation.

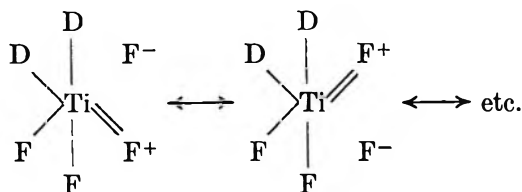
This model may be used to elucidate some of the finer structural features of the $\text{TiF}_4 \cdot 2\text{D}$ complexes. The relative magnitudes of the J values of $\text{TiF}_4 \cdot 2(\text{N}, \text{N-dimethylformamide})$ (I), $\text{TiF}_4 \cdot 2(\text{N}, \text{N-diethylformamide})$ (II), $\text{TiF}_4 \cdot 2(\text{N}, \text{N-dimethylacetamide})$ (III), and $\text{TiF}_4 \cdot 2(\text{N}, \text{N-dimethylpropionamide})$ (IV) decrease in the order $J_{\text{IV}} > J_{\text{III}} > J_{\text{II}} = J_{\text{I}}$. This indicates that the alkyl group attached to the carbonyl

(14) J. Dyer, *Proc. Chem. Soc.*, 275 (1963).(15) C. G. Moreland and W. S. Brey, Jr., *J. Chem. Phys.*, **45**, 803 (1966).(16) J. Reuben, Y. Shoo, and A. Demiel, *J. Am. Chem. Soc.*, **87**, 3995 (1965).(17) H. H. Jaffé, *J. Org. Chem.*, **23**, 1790 (1958).

rather than the dialkylamino group has the greater steric interaction with the fluorines. The coupling constants for the $\text{TiF}_4 \cdot 2\text{ROH}$ complexes ($\text{R} = \text{CH}_3$, C_2H_5 , and $i\text{-C}_3\text{H}_7$) are experimentally the same, suggesting that the donor molecules are oriented such that there is no difference within the series in steric interaction with the fluorines.

The F-F coupling constants of the $\text{TiF}_4 \cdot 2\text{D}$ and $\text{TiF}_4 \cdot \text{D}, \text{D}'$ complexes are small when compared with the geminal coupling constants of other inorganic fluorides. (For examples see Table I in ref 13.) The small values could result either from mutual cancellation by couplings of opposite sign or, as was suggested earlier, the through-bond contribution to spin coupling in the TiF_4 complexes may be relatively small. Since ionic bonds would be unable to transmit through-bond nuclear interaction, and since the Ti-F bonds in the $\text{TiF}_4 \cdot 2\text{D}$ complexes might be expected to be appreciably ionic,¹⁸ the latter explanation seems to be more plausible.

A previous study¹ indicated that there is some fluorine-titanium $p\pi\text{-}d\pi$ interaction in the TiF_4 complexes. The existence of both high ionic character in the σ bonds and π donation by the fluorines is compatible with contributions from valence bond structures such as



Conclusions

Fluorine-19 spin-spin interaction in the $\text{TiF}_4 \cdot 2\text{D}$ and $\text{TiF}_4 \cdot \text{D}, \text{D}'$ complexes appears to occur *via* a through-space mechanism. In contrast to the geminal F-F couplings in fluorinated organic compounds the coupling constants of these complexes are insensitive to electron-density changes produced by electron-withdrawing or -donating substituents. The apparent lack of through-bond nuclear interaction is suggested to be a result of high ionic character in the F-Ti σ bonds.

Acknowledgment. Support of this work by the Air Force Materials Laboratory, Research and Technology Division, Wright-Patterson Air Force Base, Ohio, is gratefully acknowledged.

(18) R. F. Fenske, *Inorg. Chem.*, **4**, 33 (1965).

Hexamethylenetetramine Aqueous Solutions. Isopiestic Data at

25° and Density and Viscosity Data in the Range 3–34°

by V. Crescenzi, F. Quadrifoglio, and V. Vitagliano

Centro Nazionale di Chimica delle Macromolecole, (CNR) Sez. III, Istituto Chimico, Università di Napoli, Naples, Italy

Accepted and Transmitted by The Faraday Society (November 28, 1966)

The results of isopiestic measurements at 25° and of density and viscosity measurements performed in the range 3–34° on hexamethylenetetramine (HMT) aqueous solutions are reported. The isopiestic data show that deviation from ideal behavior exhibited by HMT aqueous solutions is strong and suggest that solute-solvent interactions should play a dominant role. It is proposed that in HMT aqueous solution immobilization of water molecules in solvation cages around the hydrophobic solute takes place, and an evaluation of HMT average hydration number is attempted in terms of a simplified treatment of the isopiestic data. Increasing the temperature, an extensive breakdown of HMT hydration structure occurs as indicated by our viscosity and density data.

Recently, a number of indications have been discussed according to which hexamethylenetetramine (HMT) in water would noticeably perturb the structural organization of the solvent.¹ Indirect evidence in favor of this hypothesis was provided by the marked influence exerted by HMT on the occurrence, in aqueous solution, of a few phenomena in which hydrophobic interactions are of critical importance. These interesting features have prompted an investigation directed toward a more detailed description of some basic physicochemical properties of HMT aqueous solutions. Knowledge of these properties is, in fact, poor at present.

We wish to report here the results of isopiestic measurements carried out at 25° and of density and viscosity measurements, performed in the range 3–34° on HMT aqueous solutions. Our data confirm the hypothesis that HMT noticeably influences water structural organization and behaves in aqueous solution in a way typical of "structure-forming" substances.

Experimental Section

Materials. Hexamethylenetetramine was obtained from Carlo Erba (Milan) and the reagent grade product recrystallized from absolute ethanol.

Potassium chloride was a Merck product, analytical

grade. Solutions of the carefully dried hexamine and KCl samples were prepared gravimetrically using doubly distilled demineralized water.

Apparatus. (a) *Isopiestic Measurements.* About 3 ml of the solution whose solvent activity we wished to determine was placed in each of two or three weighing bottles. A similar amount of the reference solution was placed in another set of weighing bottles. All bottles were placed on a flat aluminum block contained in a stainless steel vacuum desiccator and evacuated to a pressure of approximately 10 mm. The evacuation was carried out very slowly in order to avoid splattering of the solutions. The solutions were then allowed to equilibrate under vacuum for 3 or 4 days in a large thermostat bath at 25°, controlled to approximately $\pm 0.01^\circ$, before being reweighed. Each weighing bottle contained a few glass beads to assist equilibration while the desiccator was being rocked in the thermostat bath. The concentrations of unknown and reference solutions were prepared initially so as to be fairly close to the anticipated equilibrium value. The solutions were accepted as being at equilibrium if the molalities of a particular set differed by not more

(1) G. Barone, V. Crescenzi, A. M. Liquori, and F. Quadrifoglio, *J. Phys. Chem.*, **71**, 934 (1967).

than 0.1%. Osmotic coefficients, φ , and water activity, a_w , at 25° of HMT solutions were obtained by the equations $\varphi = (2m_{\text{KCl}}/m)\varphi_{\text{KCl}}$ and $\ln a_w = -(\varphi m/55.51)$. The φ_{KCl} values were obtained by interpolation of data reported by Robinson and Stokes.² The very small degree of protonation³ of HMT was not taken into consideration. Molecular weights of 74.553 and 140.19 for potassium chloride and hexamethylenetetramine, respectively, were used.

(b) *Density Measurements.* Densities were measured with pycnometers, the total volume of which was approximately 25 ml. The volumes were computed at each working temperature from measurements on doubly distilled deionized water and density data from the literature.⁴ The temperature of the constant-temperature water bath was controlled to $\pm 0.01^\circ$. Solutions in the pycnometers were allowed to equilibrate in the water bath at the highest temperature considered (33.46°) for a few hours. After temperature equilibrium had been achieved, a few drops of liquid were carefully added in the pycnometers until the meniscus reached the calibration mark on the capillary tube of the pycnometers. The pycnometers were then dried with a lint-free cloth and weighed on a Mettler balance. After weighing, the pycnometers were returned to the water bath for reequilibration at the next-lowest temperature. Apparent molal volumes of HMT were calculated from the experimental data by the equation $\phi_v = (M/d) - [1000(d - d_{\text{H}_2\text{O}})/md \cdot d_{\text{H}_2\text{O}}]$ where m is the molality of HMT and d and $d_{\text{H}_2\text{O}}$ are the density of the solution and of pure water, respectively. Replicate determinations of the density reproduced within 5×10^{-5} , corresponding to a precision for the apparent molal volume of ± 0.1 ml.

(c) *Viscosity Measurements.* All solutions for the viscosity measurements were prepared on a weight basis. Ubbelohde-type suspended-level viscometers with flow times for water at 25° of about 300 sec were employed. In no case was a kinetic energy correction found to be required. Runs were repeated until determinations within 0.2 sec were obtained.

Results

(a) *Isopiestic Data.* Osmotic coefficient (φ) data, at 25°, of HMT aqueous solutions are reported in Table I. From these data the linear correlation $\varphi = 1 + 0.220m$ where m is HMT molality is derived (standard deviation ± 0.0052).

Although our isopiestic measurements have not been extended to solutions less concentrated than 0.4 m (owing to experimental difficulties), it appears reasonable to assume that the linear φ - m relationship is

Table I: Isopiestic Solutions of Hexamethylenetetramine and Potassium Chloride

m	φ	m_{KCl}
0.4368	1.095	0.2641
1.028	1.228	0.704
1.399	1.302	1.015
1.864	1.410	1.436
2.323	1.504	1.919
2.330	1.518	1.941
2.991	1.663	2.679
3.363	1.746	3.125
3.810	1.844	3.678
4.586	2.017	4.689
4.683	2.027	Saturated

also valid at higher dilutions. On the basis of the general relationship

$$\ln \gamma = (\varphi - 1) + \int_0^m (\varphi - 1) d \ln m$$

the equation for the activity coefficient of HMT in aqueous solution would then be $\ln \gamma = 0.440m$. These results indicate that deviation from ideal behavior exhibited by HMT aqueous solutions is noticeable indeed. The type of deviation suggests that solute-solvent interactions should play a dominant role.

(b) *Density and Viscosity Data.* Density and viscosity of HMT aqueous solutions have been determined for a range of HMT concentrations and at different temperatures in the interval 3–34°. Density data are reported in Table II in which, for each temperature considered, the parameters of the d - m relations, as obtained by a least-square analysis of the experimental values, are also reported.

In Figure 1 the apparent molal volume, ϕ_v , of HMT is plotted as a function of molality, m . It is interesting to point out that the ϕ_v values decrease with increasing m . The effect, however, is smoothed out with increasing temperature. For each given molality, ϕ_v is larger the higher the temperature. Of course the same features are found for the partial molal volume, \bar{V}_2 , of HMT (dotted curves of Figure 1). The \bar{V}_2° value is seen to increase from 108.9 to 3.66° to 110.9 at 33.46°.

The results of the viscosity measurements are reported in Figure 2 and in Table III.

The parameters B and Q of the equation⁵ $\ln \eta/\eta_0 =$

(2) R. A. Robinson and R. H. Stokes, "Electrolyte Solutions," Butterworth and Co. Ltd., London, 1959, p 476.

(3) H. Tada, *J. Am. Chem. Soc.*, **82**, 255 (1960).

(4) "International Critical Tables," Vol. 3, p 24.

(5) Reference 2, p 305.

Table II: Relative Densities of HMT Solutions at Various Temperatures $d/d_0 = 1 + am + bm^2 + cm^3 + dm^4$ ^a

3.66°			16.07°			28.73°			33.46°		
<i>m</i>	<i>d/d</i> ₀	$\Delta^b \times 10^5$	<i>m</i>	<i>d/d</i> ₀	$\Delta \times 10^5$	<i>m</i>	<i>d/d</i> ₀	$\Delta \times 10^5$	<i>m</i>	<i>d/d</i> ₀	$\Delta \times 10^5$
0.2405	1.00733	+3	0.477	1.01380	0	0.615	1.01703	+1	0.2405	1.00701	0
0.3956	1.01199	-7	0.998	1.02742	+1	1.178	1.03132	-5	0.3956	1.01138	-1
1.2367	1.03427	+16	1.950	1.04934	-2	1.516	1.03920	-7	1.2367	1.03274	+1
1.7354	1.04643	-17	2.720	1.06466	+4	1.950	1.04834	+14	1.7354	1.04376	-2
2.6955	1.06665	+4	3.687	1.08098	-1	2.720	1.06340	-10	2.6955	1.06246	0
						3.687	1.08006	+3			

Parameters of equation

<i>t</i> , °C	<i>a</i> × 10 ⁵	<i>b</i> × 10 ⁴	<i>c</i> × 10 ⁴	<i>d</i> × 10 ⁵
3.66	+3.1342	-3.153	+2.612	...
16.07	+3.0481	-3.480	+5.357	-5.93
28.73	+2.8788	-1.557	-3.862	+7.83
33.46	+2.9789	-2.577	-1.872	+8.62

^a See lower part of table for parameters of equation. ^b Difference between the calculated and experimental value.

Table III: Relative Viscosities of HMT at Various Temperatures;^a $\ln(\eta/\eta_0) = BC/(1 - QC)$ ^b

3.66°		16.07°		28.73°		33.46°	
<i>C</i> , moles/l.	η/η_0	<i>C</i> , moles/l.	η/η_0	<i>C</i> , moles/l.	η/η_0	<i>C</i> , moles/l.	η/η_0
0.2344	1.107	0.0513	1.021	0.0511	1.020	0.2330	1.093
0.3793	1.182	0.1984	1.082	0.1977	1.077	0.3770	1.156
0.5764	1.291	0.4102	1.186	0.4088	1.174	0.5728	1.250
1.0903	1.671	1.4273	1.918	1.4222	1.838	1.0826	1.553
1.4604	2.049	1.6678	2.182	1.6616	2.072	1.4490	1.840
2.0867	2.987	2.0441	2.689	2.0356	2.509	2.0672	2.504
				2.6149	3.483		

Parameters of equation

<i>t</i> , °C	<i>B</i>	<i>Q</i>
3.66	0.423	0.093
16.07	0.398	0.088
28.73	0.379	0.080
33.46	0.374	0.076

^a Results reported in Figure 3. All solutions were prepared by weight and the concentrations, *C*, in moles of HMT/l. were calculated using the equations for the density reported in Table II. ^b See lower part of table for parameters of equation.

$BC/(1 - QC)$ according to which our viscosity data may be reproduced, at each temperature considered, within the limits of the experimental accuracy ($\pm 0.1\%$) are also listed in Table III. The values of both parameters are seen to increase with decreasing temperature.

Discussion

Considering the osmotic coefficient data it may be argued that deviation from ideality exhibited by HMT aqueous solutions is to be attributed in large part to solute-solvent interactions. Of course other important factors such as difference in dimensions between solute

and solvent molecules and the structured nature of water contribute to the observed effects. An even qualitative evaluation of such factors, however, does not appear feasible at present. It is nevertheless of some interest to consider the conclusions to which a very simplified theoretical approach to nonionic compound aqueous solutions as applied to the HMT-H₂O system may lead.

The HMT-H₂O system is here considered to belong to the class of "semiideal" mixtures. The semi-ideality approximation, introduced by Scatchard,⁶

(6) G. Scatchard, *J. Am. Chem. Soc.*, **43**, 2387 (1921).

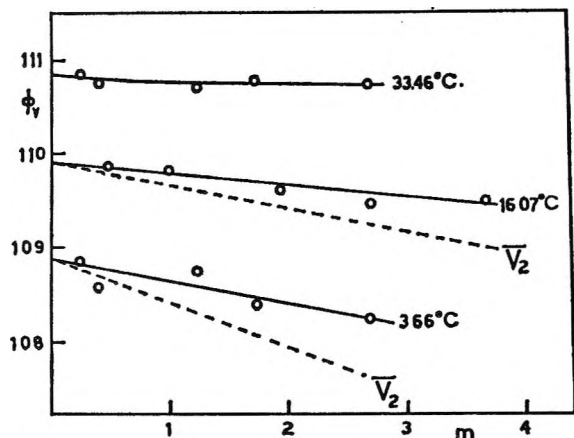


Figure 1. Apparent molal volume, ϕ_v , and partial molal volume, \bar{V}_2 , at different temperatures, as functions of molality of HMT aqueous solutions, m . ϕ_v values are calculated from experimental density data. The \bar{V}_2 - m lines were drawn considering the ϕ_v - m relations to be linear and with the aid of the equation $\bar{V}_2 = \phi_v + m(\partial\phi_v/\partial m)$.

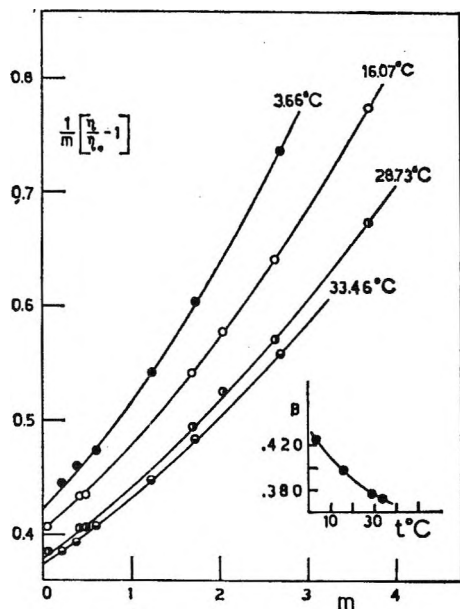


Figure 2. Reduced viscosity at different temperatures as a function of molality of HMT aqueous solutions, m . In the insert the coefficient B (see text) is plotted against the temperature.

has been recently utilized by Stokes and Robinson⁷ to interpret osmotic coefficient data of sucrose, glucose, and glycerol aqueous solutions. The approximation consists in considering that solute molecules interact with the solvent in a succession of solvation equilibrium steps to yield species which mix conforming to ideal laws. Deviations from ideality as experimentally observed would thus be entirely ascribed to hydration

of the solute. The latter is conceivably an important phenomenon for HMT in water. As an application of the Stokes and Robinson⁷ treatment let us suppose that each HMT molecule binds n water molecules in n successive steps characterized by a common value of the equilibrium constant K .

Average hydration number, \bar{h} , of HMT is accordingly defined as

$$\bar{h} = \frac{\sigma}{\Sigma} \quad (1)$$

where

$$\Sigma = 1 + Ka_w + \dots + (Ka_w)^n \quad (2)$$

and

$$\sigma = \frac{d\Sigma}{d \ln a_w} = Ka_w + 2K^2a_w^2 + \dots + n(Ka_w)^n \quad (3)$$

For an aqueous semiideal solution it is

$$\frac{55.51}{m} - \frac{a_w}{1 - a_w} = \bar{h} \quad (4)$$

Then from eq 1 and 4 is obtained

$$\frac{55.51}{m} - \frac{a_w}{1 - a_w} = \frac{\sigma}{\Sigma} \quad (5)$$

Manipulations carried out according to relation 5 on osmotic coefficient data of the HMT-H₂O system indicate that a very good agreement with the experimental data (pairs of a_w - m values for a_w values ranging from 0.84 to 0.96) has been obtained putting $n = 18$. The corresponding value of the hydration equilibrium constant is $K = 1.06 \pm 0.01$ in the indicated range of a_w values. The value of \bar{h} increases from 6.5 to 8.8 in the dilution range 4.7 to 0.96 m HMT. For n values greater or less than 18, eq 5 does not correctly fit the experimental m - a_w data with a constant value for K . For $n = 9$, furthermore, no acceptable K value was found to reproduce the data.

Quite naturally the n and \bar{h} values reported above are merely indicative. In the case of sucrose the value $n = 11$ used by Stokes and Robinson,⁷ besides giving a best fit of the experimental data ($K = 0.994$), was a reasonable guess of the possible number of water-binding sites on a sucrose molecule. In the case of HMT there is not, of course, such a high number of sites per molecule to which water molecules may be directly bound. Relying entirely on the validity of the treatment outlined above, it might be argued that the high hydration number obtained for HMT would

(7) R. H. Stokes and R. A. Robinson, *J. Phys. Chem.*, **70**, 2126 (1966).

actually reflect the immobilization of water molecules in a solvation cage around the hydrophobic solute.

Considering the structure of the clathrate hydrate of HMT⁸ (easily formed upon cooling an HMT solution toward 0°) in which three nitrogen atoms out of four of an HMT molecule are hydrogen bonded with three water molecules, it is logical to assume that also in solution and at $t > 0^\circ$, hydrogen-bond formation of water with HMT nitrogens takes place. Water molecules engaged in direct interaction with HMT may be also linked with other water molecules to give rise to a kind of flickering clusters of which HMT molecules constitute the cores. A justification of this hypothesis may be also found in the negative temperature coefficient of HMT solubility in water, a phenomenon which is common to other nonpolar structure-forming solutes.

Qualitative indications about the nature and extent of solute-solvent interactions in HMT aqueous solutions are also provided by the viscosity and density data reported in Figures 1 and 2 (Tables II and III).

The parameters B and Q of the viscosity equation $\ln \eta/\eta_0 = B[C/(1 - QC)]$, which gives a very good representation of the viscosity of HMT solutions at each temperature considered (see Table III), may be related to the so-called "effective rigid molar volume," V_2 , of the solute.⁵

According to theory it is $B = 2.5V_2$, while Q is a function of V_2 and of the interactions between solute particles. The value of V_2 may be assumed to represent the molar volume of the solute including the hydration shell which is held too firmly to participate in the viscous shearing process.

If the value 104 cc mole⁻¹ is taken for the molar volume of HMT ($d = 1.34$ g/cc³ of solid HMT and $M = 140.19$) then the B values reported in Table III suggest that an average of three water molecules is firmly attached per HMT molecule in solution.

According to the interpretation of our isopiestic data presented above, an "equilibrium" hydration of HMT is derived which is about twice the hydration evaluated from the viscosity data. In our opinion, however, a critical comparison of these hydration numbers would be highly questionable.

For what concerns the dependence of HMT solvation upon temperature, the negative temperature coefficient of parameter B suggests that hydration of HMT in dilute solution decreases with increasing temperature.¹⁰

Knowledge of B values at different temperatures also permits evaluation of activation energy for the viscous flow of the HMT solution. It is easily shown in fact

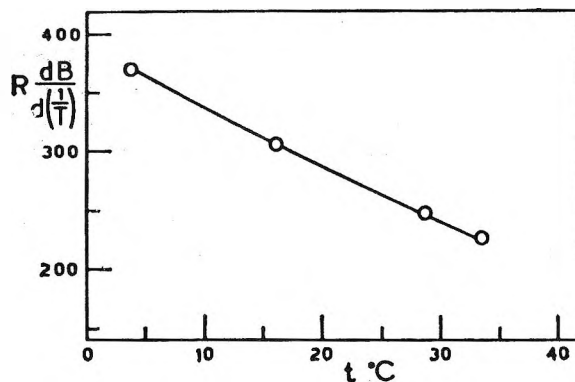


Figure 3. Difference between activation energy (cal mole⁻²) for the viscous flow of HMT aqueous solution (in the limit for $m \rightarrow 0$) and water as a function of the temperature.

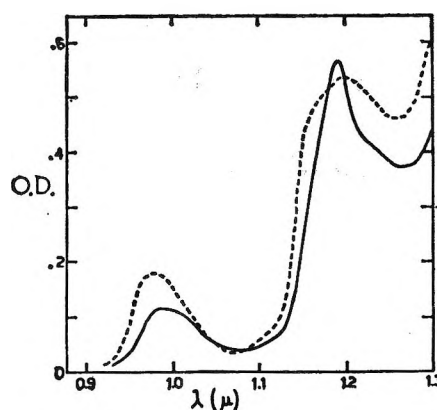


Figure 4. Near-infrared spectra at 25° of water (---) and of water in 2.5 M HMT aqueous solution (—). Spectra were recorded with a Beckman DK-2 spectrophotometer equipped with thermostated cell holders. Matched 1.000-cm cells were used.

that $RdB/d(1/T) = \lim_{m \rightarrow 0} [(E^* - E_0^*)/m]$, where E^* and E_0^* are the activation energies for the viscous flow of an infinitely dilute HMT solution and water, respectively. Values of $RdB/d(1/T)$, plotted in Figure 3 against T , are seen to steadily increase with decreasing temperature. This may be interpreted to reflect a buildup of structure in the solutions promoted by the hydrophobic solute, which is obviously facilitated by decreasing the temperature.

The density data (Table II and Figure 1) show that at all temperatures the limiting ($m \rightarrow 0$) partial molal volume of HMT (see Figure 1) is at least 5% higher than the molar volume of HMT ($V_2^\circ = 104$ cc).

(8) T. C. W. Mak, *J. Chem. Phys.*, **43**, 2799 (1965).

(9) G. W. Smith, *ibid.*, **36**, 3081 (1962).

(10) R. L. Kay, T. Vituccio, C. Zawoyski, and D. F. Evans, *J. Phys. Chem.*, **70**, 2336 (1966).

Calculation of the latter is based on the density of solid HMT and although the comparison is in this case a qualitative one, it appears plausible to assume that an "excess" increase in volume takes place when 1 mole of HMT is dissolved in a large amount of liquid water. The negative slopes of the approximate V_2 - m relations (Figure 2) lead us to think that an increased ice-likeness of water in the HMT solutions is promoted by the solute.

This view appears to be in agreement also with some features exhibited by the near-infrared spectrum of water in HMT solution (see Figure 4) which suggest

that HMT affects water structure in a way formally equivalent to a decrease in temperature.¹¹ The attempted description of the HMT-H₂O system is of course still highly speculative, but one according to which the results reported here find a consistent though qualitative interpretation.

Acknowledgments. The authors wish to thank Professor Alfonso M. Liquori for his helpful advices during the course of this work and Dr. Donald G. Miller for critically reading the manuscript.

(11) K. Buijs and G. R. Choppin, *J. Chem. Phys.*, **39**, 2035 (1963)

Barriers to Internal Rotation in Thioamides. Experimental

Results and Molecular Orbital Calculations

by Jan Sandström

Department of Chemistry, University of Lund, Lund, Sweden

Accepted and Transmitted by The Faraday Society (November 30, 1966)

The influence of the substituent R in RCSN(CH₃)₂ on the barrier to the rotation of the dimethylamino group has been studied by nuclear magnetic resonance. The Arrhenius parameters have been determined together with the ΔF^\ddagger , ΔH^\ddagger , and ΔS^\ddagger values and the effects of solvent and concentration on these have been studied. The ΔF^\ddagger values show a very qualitative correlation with C-N π -bond orders calculated by a modified ω method and a better correlation with the loss in π -electron energy, ΔE_π , which occurs when the dimethylamino group is rotated out of conjugation. This quantity also gives correct relations between the barriers of thioamides, amides, and amidinium ions, and it allows a crude prediction of the barriers in amidines and enamines.

Introduction

It has been observed by Lüttringhaus, *et al.*,¹ that the carbonyl group interacts more strongly than the thiocarbonyl group with weakly electron-donating groups, whereas the reverse is true with strongly electron-donating groups. This is in agreement with the opinion expressed by several authors² that thioamides are more strongly polarized than the corresponding amides. As has been shown by Loewenstein, *et al.*,³

one consequence of this is a considerably higher barrier to internal rotation in N,N-dialkylthioformamides

(1) (a) A. Lüttringhaus and J. Grohmann, *Z. Naturforsch.*, **10b**, 365 (1955); (b) A. Lüttringhaus, R. Mecke, R. Mecke, and J. Grohmann in "Elektronentheorie den Homöpolaren Bindung," Akademie-Verlag, Berlin, 1956, p 152.

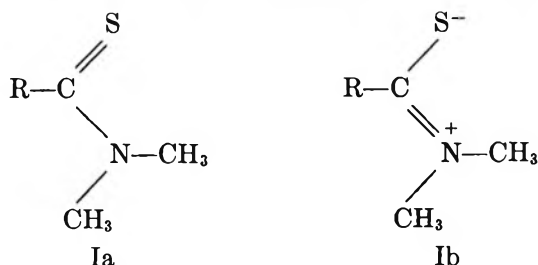
(2) (a) C. M. Lee and W. D. Kumler, *J. Org. Chem.*, **27**, 2052 (1962); (b) K. A. Jensen, *Acta Chem. Scand.*, **17**, 551 (1963).

(3) A. Loewenstein, A. Melera, P. Rigny, and W. Walter, *J. Phys. Chem.*, **68**, 1597 (1964).

than in dimethylformamide, as measured by standard nmr technique. This observation is supported by the data for N,N-dimethylthioacetamide and N,N-dimethylacetamide obtained in the same way by Neuman and Young.⁴ However, the Arrhenius activation energies reported by these authors are considerably higher than earlier values, probably because of the very polar solvent used (formamide). Quite recently, Walter, *et al.*,⁵ have obtained in a very elegant way the barrier in N-methyl-N-benzylthioformamide by studying the temperature dependence of the rate of *cis-trans* interconversion, as obtained from precise integration of the spectra of the two rotamers. Their data are in good agreement with those reported by Loewenstein, *et al.*³

It is apparent from the barriers for N,N-dimethylamides reported by Rogers and Woodbrey⁶ that the substituent on the carbon atom has a strong influence on the height of the barrier. This was interpreted as an effect on the bond order of the carbon-nitrogen bond.

It has been found that the ultraviolet spectra⁷ and also the polarities⁸ of a wide range of thiocarbonyl compounds can be satisfactorily described by an LCAO-MO method of modified ω type and it was considered as a matter of interest to test this method on the barriers to internal rotation of a series of substituted N,N-dimethylthioamides (I), where the groups R have electron-attracting or electron-donating properties.



Experimental Methods

Materials. The thioamides were prepared by literature methods. The solid compounds were purified by distillation, followed by recrystallization and, in some cases, by vacuum sublimation. The only non-crystalline compound (I, R = CH₃O) was purified by fractional vacuum distillation. The question of finding a suitable solvent is rather difficult, since it should remain liquid and have good dissolving properties in the temperature range -60 to +200° and there should be little interaction between solvent and solute molecules. Finally, *o*-dichlorobenzene was chosen (molar fraction of solute 0.333) following the example of Loewenstein, *et al.*³ This solvent is not as inert as should have been desired, but it fulfills the other re-

quirements and it has an AA'BB' spectrum with sharp lines, which is convenient for checking the resolution of the spectrometer.

Recording of the Nmr Spectra. The spectra were obtained at 60 Mc/sec with a Varian A-60 spectrometer equipped with a Varian V-6031 variable-temperature probe and temperature controller. The spectra were recorded with a sweep width of 1 or 2 cps/cm, depending on the peak separation, and at a sweep rate of 0.1 or 0.2 cps/sec. The amplitude of the radiofrequency field was kept well below the level where saturation effects could be observed. At each temperature five to ten spectra were recorded with both upfield and downfield direction of the recorder. Where a reference was required, the chemical shifts were measured against hexamethyldisiloxane as an internal standard. Its resonance falls 0.055 ppm downfield from tetramethylsilane.

Temperature Measurement. For determining the temperature of the sample a narrow concentric capillary, containing ethylene glycol or acidified methanol, was inserted into the sample tube and the shift between the OH and CH signals was recorded simultaneously with the spectrum of the sample. The shifts were calibrated using the ordinary Varian ethylene glycol and methanol samples. In this way an accuracy of about $\pm 0.4^\circ$ could be obtained. In each run the spectra were recorded at 10-12 different temperatures. This method failed for N,N-dimethyl-N'-acetylthiourea (I, R = CH₃CONH) and ethyl N,N-dimethylthiooxamate (I, R = EtOCO) because of overlap of sample and temperature standard signals. In these cases the conventional method had to be used.

Calculation of Thermodynamic Parameters

The calculation of the rate constants for the rotation around the carbon-nitrogen bond was performed according to the ratio method described in detail by Rogers and Woodbrey.⁶ Quite recently, Allerhand, *et al.*,⁹ have critically examined the different methods for obtaining chemical-exchange rates from nmr data. From their results it is possible to estimate the magnitude of the systematic errors which are introduced by use of the ratio approximation. It appears

(4) R. C. Neuman, Jr., and L. B. Young, *J. Phys. Chem.*, **69**, 2570 (1965).

(5) W. Walter, G. Maerten, and H. Rose, *Ann. Chem.*, **691**, 25 (1966).

(6) M. T. Rogers and J. C. Woodbrey, *J. Phys. Chem.*, **66**, 540 (1962).

(7) (a) M. J. Janssen, *Rec. Trav. Chim.*, **79**, 1066 (1960); (b) J. Sandström, *Acta Chem. Scand.*, **20**, 689 (1966), and earlier papers.

(8) M. J. Janssen and J. Sandström, *Tetrahedron*, **20**, 2339 (1964).

(9) A. Allerhand, H. S. Gutowsky, J. Jonas, and R. A. Meinzer, *J. Am. Chem. Soc.*, **88**, 3185 (1966).

that in most cases the error in τ is less than 5%, but in one case, *viz.*, I, R = C, the peak separation in the absence of exchange is only 4.0 cps and the parameters obtained for this compound must be regarded as somewhat less reliable. In all cases the error works in the same direction, *i.e.*, it will tend to decrease the slope of the $\log k$ vs. $1/T$ plot and therefore it is not expected to affect the correlation in a very serious way. Wittaker and Siegel¹⁰ have observed that the methyl doublet separation in N,N-dimethylformamide in a variety of solvents is considerably sensitive to the temperature even at temperatures where the internal rotation must be quite slow. In some cases a variation of about 12% over a temperature range of 40° was observed. This was ascribed to a temperature-dependent dipole-dipole association which affects the anisotropy of the carbonyl group. With one exception, this effect is rather small in the systems investigated here. From the temperature where exchange effects could first be observed and 10–20° or more downward, the doublet separation varied by less than 2%. One reason for this may be that solvent-solute interactions are more important and less temperature sensitive than solute-solute interactions. The only exception is ethyl N,N-dimethylthiooxamate (I, R = EtOCO), for which an increase in peak separation is observed with increasing temperature up to a ratio of about 5. This may be due to a temperature-dependent change in the ratio between *cis* and *trans* conformers. For this compound the largest observed peak separation was used for $\delta\nu_0$, but it is obvious that this complication renders the thermodynamic parameters for this compound somewhat uncertain.

The rate constants and temperatures were fitted by the method of least squares to a straight line according to eq 1 and the other activation parameters were obtained by use of eq 2–4.¹¹ The transmission coefficient

$$\log k = -\frac{E_a}{2.303RT} + \log A \quad (1)$$

$$\Delta F^\ddagger = -2.303RT \log \frac{hk}{kT\kappa} \quad (2)$$

$$\Delta H^\ddagger = E_a - RT \quad (3)$$

$$\Delta S^\ddagger = \frac{\Delta H^\ddagger - \Delta F^\ddagger}{T} \quad (4)$$

κ is as usual assumed to be unity. The results are shown in Table I. The errors in E_a and $\log A$ are standard deviations from the least-squares plot and the errors in ΔH^\ddagger and ΔF^\ddagger are assumed to be the same. Thus, the errors in ΔS^\ddagger are obtained by doubling the deviations in E_a and dividing by the temperature. The

activation parameters show a slight temperature dependence and the values in Table I refer to the coalescence temperature.

In the spectrum of N,N-dimethylthioacetamide (I, R = CH₃) a coupling with $J = 0.6$ cps is observed between the C methyl group and one of the N methyl groups.¹² This introduces an extra systematic error when the simple ratio method is used for calculation of rate constants, but an examination of the analysis in ref 9 shows that this error is only of the order of 1–2% in the present case.

For tetramethylthiourea only one sharp signal was observed down to –60°. This can be due to an accidental overlap of the two methyl signals, as is observed for dimethylthioformamide in *o*-dichlorobenzene in the molar ratio 1:2, but it seems less likely since the same result is obtained in different solvents and at different concentrations. A low barrier is an explanation which is more in line with the general result of this investigation.

Molecular Orbital Calculations

The calculations have been performed by a modified ω method, in which Coulomb integrals are corrected according to π -electron charges and resonance integrals according to bond orders in an iterative procedure. It was found⁸ that in order to reproduce with this method the interaction of electron-donating substituents with carbonyl and thiocarbonyl groups, as manifested in dipole moments, a low-resonance integral for the thiocarbonyl group and an element of electronegativity for the sulfur atom were necessary. As parameters for substituent atoms and bonds, standard values were tried, but they were mostly found to give too large dipole moments. When the resonance integrals were scaled down to 0.67–0.75 of the original values, reasonable figures for the dipole moment differences between corresponding carbonyl and thiocarbonyl compounds were found. The parameters thus obtained (set 4 in ref 8) are shown in Table II and the calculated π -bond orders and π -electron energies in Table III.

Other parameter sets with $\omega = 1.0$ or 1.4 and with larger k_{CX} or smaller h_X values have also been tried and found to give qualitatively similar results in the barrier calculations, as long as the relation between the parameters for the carbonyl and thiocarbonyl group is the same as here.

(10) A. G. Wittaker and S. Siegel, *J. Chem. Phys.*, **42**, 3320 (1965); **43**, 1575 (1965).

(11) A. A. Frost and R. G. Pearson in "Kinetics and Mechanism," 2nd ed, John Wiley and Sons, Inc., New York, N. Y., 1961, p 98.

(12) R. C. Neuman, Jr., and L. B. Young, *J. Phys. Chem.*, **69**, 1777 (1965).

Table I

R	Solvent	Molar fraction of thioamide	ν_A , cps	ν_B , cps	E_a , kcal/mole	log A	ΔF^\ddagger , kcal/mole	ΔH^\ddagger , kcal/mole	ΔS^\ddagger , eu	T_0 , °K
CH ₃	ODC ^a	0.333	196.5	182.0	21.0 ± 0.3	12.6 ± 0.2	21.6 ± 0.3	20.2 ± 0.3	-3.5 ± 1.5	414.1
CH ₃ O	Neat	1	195.5	183.6	16.4 ± 0.2	12.0 ± 0.2	17.9 ± 0.2	15.8 ± 0.2	-6.2 ± 1.2	340.9
CH ₃ O	ODC	0.82	194.0	180.8	16.0 ± 0.5	11.7 ± 0.3	17.8 ± 0.5	15.3 ± 0.5	-7.3 ± 2.7	341.0
CH ₃ O	ODC	0.64	192.7	177.6	16.7 ± 0.3	12.2 ± 0.2	17.8 ± 0.3	16.0 ± 0.3	-5.2 ± 1.8	342.6
CH ₃ O	ODC	0.50	191.6	175.3	17.0 ± 0.3	12.4 ± 0.2	17.7 ± 0.3	16.3 ± 0.3	-4.1 ± 1.8	342.7
CH ₃ O	ODC	0.333	190.1	172.0	17.3 ± 0.2	12.6 ± 0.2	17.7 ± 0.2	16.6 ± 0.2	-3.2 ± 1.2	343.4
CH ₃ O	ODC	0.20	187.8	168.8	17.6 ± 0.4	12.8 ± 0.3	17.7 ± 0.4	16.9 ± 0.4	-2.5 ± 2.3	345.0
CH ₃ S	ODC	0.333	203.2	189.4	14.0 ± 0.4	11.6 ± 0.3	15.6 ± 0.4	13.4 ± 0.4	-7.4 ± 2.7	302.2
CH ₃ S	CCl ₄	0.333	207.0	200.0	11.7 ± 0.4	9.9 ± 0.3	15.6 ± 0.4	11.1 ± 0.4	-15.2 ± 2.7	294.3
CH ₃ S	CHCl ₃	0.333	208.8	199.2	11.5 ± 0.5	9.6 ± 0.4	15.9 ± 0.5	10.9 ± 0.5	-16.4 ± 3.3	302.4
CH ₃ S	(CH ₃) ₂ CHOH	0.20	201.4	188.9	11.2 ± 0.6	9.6 ± 0.4	15.7 ± 0.6	10.6 ± 0.6	-16.7 ± 4.0	303.0
Cl	ODC	0.333	195.6	191.6	13.7 ± 0.4	9.4 ± 0.2	19.1 ± 0.4	13.0 ± 0.4	-17.5 ± 2.3	350.2
Ph	ODC	0.333	199.5	167.6	19.1 ± 0.5	13.3 ± 0.4	18.4 ± 0.5	18.4 ± 0.5	-0.1 ± 2.7	365.0
N≡C	ODC	0.333	201.6	189.6	23.2 ± 0.5	12.8 ± 0.2	23.4 ± 0.5	22.3 ± 0.5	-2.6 ± 2.3	443.9
EtOCO	ODC	0.333	193.1	186.7	20.8 ± 0.8	11.7 ± 0.5	23.4 ± 0.8	19.9 ± 0.8	-7.9 ± 3.7	432.6
AcNH	ODC	0.333	195.6	182.5	17.1 ± 1.0	13.5 ± 0.8	16.1 ± 1.0	16.4 ± 1.0	+1.2 ± 6.5	309.7

^a ODC, *o*-dichlorobenzene.Table II^c

Atom (X)	h_X^b	Bond (C—X)	k_{CX}^c
C	0	C—C	0.75
N	0.5	C=N	0.9
N	1.5	C—N	0.8
O	1.0	C—O	0.8
O	2.5	C—S	0.4
S	0.5	C—Cl	0.4
S	1.0		
Cl	3.0		

^a $\omega = 1.4$. ^b $\alpha_X = \alpha_C + h_X\beta_{CC}$. ^c $\beta_{CX} = k_{CX}\beta_{CC}$.Table III: Bond Orders and π -Electron Energies (in Units of β)

R	X	ρ_{CN}	$E_{\pi, R, CXNMe_2}$	$E_{\pi, R, CX} + 2\alpha_N$	ΔE_{π}
H	O	0.422	6.962	6.430	0.532
H	S	0.455	5.342	4.706	0.636
RO	O	0.402	12.248	11.778	0.470
RO	S	0.436	10.656	10.106	0.550
RS	O	0.408	9.100	8.616	0.484
RS	S	0.438	7.511	6.956	0.555
Cl	O	0.419	13.017	12.498	0.519
Cl	S	0.452	11.402	10.784	0.618
CH ₂ =CH	O	0.393	9.408	8.911	0.497
CH ₂ =CH	S	0.412	7.868	7.302	0.566
Ph	O	0.395	15.156	14.659	0.497
Ph	S	0.415	13.614	13.046	0.568
N≡C	O	0.408	11.717	11.193	0.524
N≡C	S	0.434	10.176	9.551	0.625
EtOCO	O	0.404	15.933	15.419	0.514
EtOCO	S	0.428	14.390	13.786	0.604
AcNH	O	0.392	14.255	13.804	0.451
AcNH	S	0.421	12.695	12.181	0.514
NR ₂	O	0.387	10.390	9.962	0.428
NR ₂	S	0.417	8.830	8.342	0.488

Hatton and Richards¹³ to account for the shifts of the N-methyl signals in the nmr spectra of N,N-dimethylamides on dilution with benzene and other aromatic solvents. Similar solvent shifts have previously been reported for N,N-dialkylthioformamides^{3,5} and, in connection with the present work, have also been ob-

(13) J. V. Hatton and R. E. Richards, *Mol. Phys.*, **3**, 253 (1960).

Discussion

Effect of Solvent and Concentration. The influence of the solvent on the thermodynamic parameters was studied only with methyl N,N-dimethyldithiocarbamate (I, R = CH₃S). It was expected that hydrogen bonding should increase the barrier by stabilizing the polar structure Ib more than Ia. However, no such effect was observed within the limits of experimental accuracy. The ΔF^\ddagger and ΔS^\ddagger values are almost the same in carbon tetrachloride, chloroform, and 2-propanol. On the other hand, in *o*-dichlorobenzene, ΔF^\ddagger has almost the same value, whereas ΔS^\ddagger is about 8 eu higher. This corresponds to a greater loss of order on rotation in the latter case and the effect can be rationalized in terms of complex formation between the aromatic solvent molecules and the thioamide molecules. Such complexes have been proposed by

served for a number of other thioamides. The results indicate, in agreement with the observations of Neuman and Young,¹² that the magnetic anisotropy in dimethylthioformamide is the same as in dialkylamides, whereas it is inverted in the other thioamides.

The effect of concentration has been studied with methyl N,N-dimethylthiocarbamate (I, R = CH₃O), the only liquid compound in the series, in *o*-dichlorobenzene with the molar fraction of the solute varying from 1.0 to 0.200. The ΔF^\ddagger values are almost independent of the concentration (Table I), whereas the ΔS^\ddagger values show a gradual increase over a 5-eu range. The variation is not very much larger than the standard deviation and not too much weight can be attached to the trend. However, it is in the same direction as should be expected on the basis of the theory of Hatton and Richards,¹³ with an increasing proportion of the thioamide molecules forming complexes with the solvent.

Correlation of Barriers with Calculated Bond Orders and π -Electron Energy Differences. It is naturally of considerable interest to select as the barrier for correlation with the molecular orbital quantities the thermodynamic parameter which is the best measure of the bonding energy in the molecule. According to Streitwieser,¹⁴ ΔF^\ddagger is better in this respect than ΔH^\ddagger . Hepler¹⁵ has shown that under certain conditions ΔF^\ddagger measures rather well the internal enthalpy of activation. It is not possible to check if the conditions are fulfilled in the present systems, but the rather constant values of ΔF^\ddagger in different solvents and concentrations show that this quantity is fairly independent of external influences and therefore it is chosen to represent the barriers. However, the differences between ΔF^\ddagger and E_a (ΔH^\ddagger) are not very large and correlation with one of the latter parameters gives essentially the same result. As a consequence of the insensitivity of ΔF^\ddagger , the well-known compensation of changes in ΔH^\ddagger and ΔS^\ddagger ¹⁶ is observed.

For the amides, the $\Delta F^\ddagger_{298.2}$ values of Rogers and Woodbrey⁶ are taken to represent the barriers. They are, with one exception, measured without solvent, but it is probable that they at least fall in the same order as they would have done in *o*-dichlorobenzene.

It is somewhat distressing that the barriers for dimethylformamide and dimethylacetamide differ by 3.6 kcal/mole, whereas the simple calculations predict the same barrier for them. However, as will be discussed later, the inductive effect of the methyl group is predicted to lower the barrier and hyperconjugation will work in the same direction. Therefore, dimethylformamide and dimethylthioformamide are chosen to represent the simple systems. From the data given

in ref 3, ΔF^\ddagger values of 26.6 kcal/mole (neat) and 24.0 kcal/mole (40% in *o*-dichlorobenzene) can be calculated for dimethylthioformamide and the latter value can be used for correlation, even if the thioamide concentration is higher than in the present work.

As a crude first approximation, a correlation was attempted with the π -bond orders, as an increased C-N bond order should lead to a stiffening of the bond and an increase in the barrier. However, the correlation is not very good (Figure 1), even if the bond order in all cases is higher in a thioamide than in the corresponding amide, which is also the case with the barriers. In particular, too low barriers are predicted for the compounds in which R contains double or triple bonds compared to those in which R conjugates with lone pairs.

π -Electron Energy Effect. In the transition state, the dimethylamino group is rotated 90° out of the molecular plane around the C-N bond and therefore no π -electron interaction between the two parts of the molecule can take place. If this were the only effect on the energy of the molecule, the barrier should be measured by the loss in π -electron energy, ΔE_π , following a 90° rotation.

$$\Delta E_\pi = E_{\pi, \text{RCXNM}_{e_2}} - (E_{\pi, \text{RCX}} + 2\alpha_N) \quad (\text{X} = \text{O}, \text{S})$$

In this case, the effect of the substituent R on the barrier can be represented as the difference between

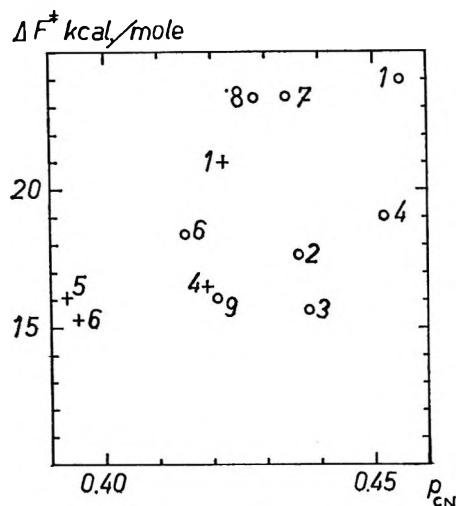


Figure 1. Correlation between ΔF^\ddagger and ρ_{CN} : O, thioamide; +, amide; 1, R = H; 2, CH₃O; 3, CH₃S; 4, Cl; 5, CH₂=CH; 6, Ph; 7, N≡C; 8, EtOCO; 9, AcNH.

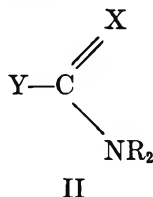
(14) A. Streitwieser, Jr., "Molecular Orbital Theory for Organic Chemists," John Wiley and Sons, Inc., New York, N. Y., 1961, p 311

(15) L. G. Hepler, *J. Am. Chem. Soc.*, **85**, 3089 (1963).

(16) J. E. Leffler, *J. Org. Chem.*, **20**, 1202 (1955); cf. also O. Exner, *Collection Czech. Chem. Commun.*, **29**, 1094 (1964), and J. E. Leffler, *J. Org. Chem.*, **31**, 533 (1966).

its energies of interaction with the thiocarbonyl group and with the thioamide group. Since the interaction with the thioamide group involves cross-conjugation with the strongly conjugating amino group, this term can be expected to be less affected by R than the energy of interaction with the thiocarbonyl group. The result is that the barrier will be lowered more, the more strongly R can interact with the thiocarbonyl group. Thus, whereas tetramethylthiourea shows no line broadening due to exchange down to -60° , diminishing the electron-donating capacity of one amino group by substitution with an acetyl group leads to a barrier of 16.1 kcal/mole. For N,N-dimethyl-N'-phenylthiourea (I, R = PhNH) a preliminary barrier of 11.5 kcal/mole ($T_c = 230^\circ\text{K}$) has been obtained. In general, a rather good correlation between ΔE_π and ΔF^\ddagger was found (Figure 2). For the thioamides a least-squares calculation gave regression line $\Delta F^\ddagger = 67.9\Delta E_\pi - 19.9$ with a correlation coefficient of 0.859.

Model with Conjugating Heteroatom. The effect on p_{CN} and ΔE_π of increasing electron-donating capacity of a heteroatom substituent (Y in II) can be clearly demonstrated by increasing k_{CY} with constant h_Y (Figure 3) or by decreasing h_Y with constant k_{CY} (Figure 4). In both cases X = S.



In this connection it is of interest to compare the barriers for the thioamides with R = CH_3O and R = CH_3S . With the present parameters, both bond orders and ΔE_π values predict the same barrier, whereas in fact for I, R = CH_3S ΔF^\ddagger is about 2 kcal/mole lower than for I, R = CH_3O . This shows that alkylthio groups interact more strongly with the thiocarbonyl group than do alkoxy groups. The same order is valid for the carbonyl group, as is shown by the more qualitative observations reported by Valega.¹⁷ This difference can be ascribed to the greater polarizability of the substituent sulfur atom, which responds more strongly to the electron demand of the carbonyl and thiocarbonyl group, probably by contraction of the 3p orbitals. This points out a serious shortcoming of the simple HMO method and also of the ω method. When the same parameters as have been employed here are used to calculate the interaction of RS and RO with phenyl, thiophene, and thiazole rings, the results predict stronger effects, *e.g.*, electron displacements, with RS than with RO, whereas, as is well known, the reverse is

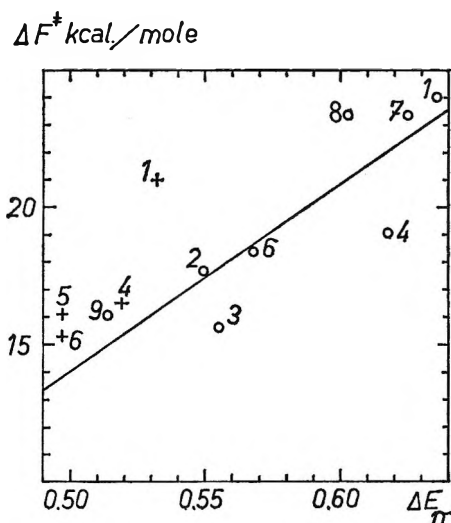


Figure 2. Correlation between ΔF^\ddagger and ΔE_π . The regression line is calculated for the thioamides only. ΔE_π is in units of β ; for other symbols see Figure 1.

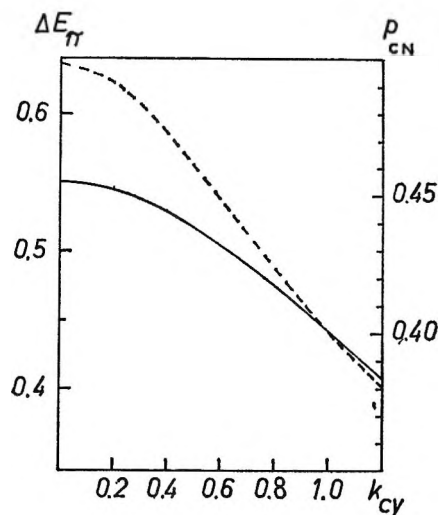


Figure 3. Plot of p_{CN} (—) and ΔE_π (---) vs. k_{CY} when $h_Y = 1.5$.

true, as is shown by the Hammett σ_p values of -0.047 for CH_3S and -0.268 for CH_3O .¹⁸ Obviously, the characteristics of the sulfur atom cannot even approximately be universally represented by only two parameters. The HMO method can only be expected to give reasonable agreement with observables within series of structurally rather closely related compounds. Thus, Kramer¹⁹ has shown that the barriers previously determined by himself and Gompper²⁰ for a series of

(17) T. M. Valega, *J. Org. Chem.*, **31**, 1150 (1966).

(18) H. H. Jaffé, *Chem. Rev.*, **53**, 191 (1953).

(19) H. E. A. Kramer, *Ann. Chem.*, **696**, 28 (1966).

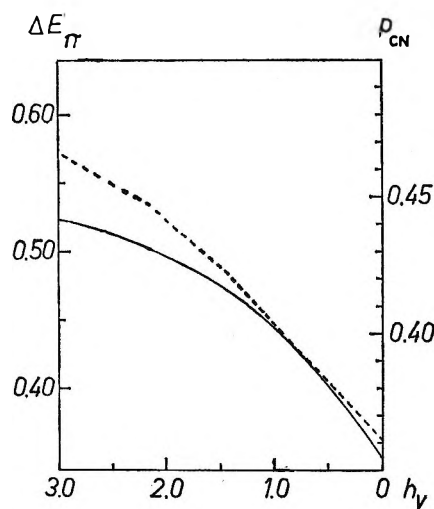


Figure 4. Plot of p_{CN} (—) and ΔE_{π} (---) vs. h_Y when $k_{CY} = 0.8$.

N,N-dimethyl- β -acylenamines show a reasonable correlation with ΔE_{π} values from HMO calculations.

The Inductive Effect. The influence of a purely inductive effect of Y has been studied by varying hc in II, X = S. The ΔE_{π} values (Table IV) show that a sub-

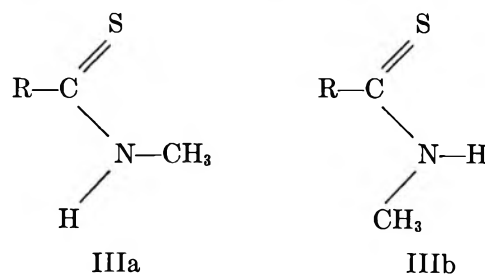
Table IV

hc	p_{CN}	ΔE_{π}
+0.2	0.452	0.651
0	0.455	0.636
-0.2	0.459	0.622

stituent with $-I$ effect should increase the barrier and one with $+I$ effect lower it. The former effect could, at least partly, explain the relation between the barriers of dimethylformamide (21.0 kcal/mole), dimethylacetamide (17.4 kcal/mole), and dimethylpropionamide (16.7 kcal/mole), and the latter effect the relation between the barriers of dimethylacetamide and dimethyltrifluoroacetamide (17.6 kcal/mole). For the latter molecule, models indicate a small steric hindrance to the planar state, which, as discussed later, should lower the barrier, and this effect should be still greater in dimethyltrichloroacetamide (14.9 kcal/mole). All barriers are from ref 6.

Steric Effects. It is obvious that the barriers to internal rotation must be considerably sensitive to steric effects. Crowding in the planar state will raise its energy and thus lower the barrier, and Mannschreck²¹ and Staab²² have shown that crowding in the transition state can raise its energy to such an extent that

individual rotamers can be isolated. Dahlqvist and Forsén²³ have shown that the ΔF^{\ddagger} values for benzaldehyde, *p*-methoxybenzaldehyde, and *p*-dimethylaminobenzaldehyde increase in the same order as the ΔE_{π} values obtained by the HMO method, but that the ratio between the highest and the lowest ΔE_{π} value is only 1.05 whereas the ratio between the corresponding barriers is 1.37. When 2-furaldehyde was compared with the benzaldehydes, no good correlation was obtained. The authors ascribe this shortcoming to important contributions to the barriers from nonbonding interaction. In the thioamide series the ratio between the highest and the lowest ΔE_{π} value is 1.24 and between the corresponding ΔF^{\ddagger} values 1.49. Thus, the relation is somewhat better than for the benzaldehydes, though the calculations still underestimate the differences between the barriers of the different compounds. On the other hand, insertion in ΔE_{π} of acceptable β values of the order of 30 kcal/mole gives ΔF^{\ddagger} values ranging from 15 to 19 kcal/mole, which means that π -electron effects can account for the larger part of the barriers. There are also good reasons to believe that the dimethylamino group is comparatively free from interactions with neighboring groups in most of the cases investigated here. It has been found²⁴ in a series of N-methylthioamides (III, R = H, CH₃, C₂H₅, *i*-C₃H₇, and *t*-C₄H₉) that the rotamer (IIIa) predominates strongly in solution. This ob-



servation shows that no repulsion of importance can exist between the sulfur atom and the methyl group. A similar observation has been made for some oxygen analogs.²⁵ Molecular models and known van der Waals radii show that no interaction needs to take place between the other methyl group and R when R is H, CH₃, CH₃O, CH₃S, and Cl. On the other hand, it has been shown that when R = (CH₃)₂N,²⁶ Ph,²⁷

(20) H. E. A. Kramer and R. Gompper, *Z. Physik. Chem.* (Frankfurt), **43**, 292 (1964).

(21) A. Mannschreck, *Tetrahedron Letters*, 1341 (1965).

(22) H. A. Staab and D. Lauer, *ibid.*, 4593 (1966).

(23) K.-I. Dahlqvist and S. Forsén, *J. Phys. Chem.*, **69**, 4062 (1965).

(24) J. Sandström and B. Uppström, submitted for publication.

(25) L. A. LaPlanche and M. T. Rogers, *J. Am. Chem. Soc.*, **86**, 371 (1964).

or EtOCO,²⁸ considerable steric effects are at work, which in the two latter molecules probably lead to rotation of the planar or nearly planar thioamide group out of the molecular plane. It is still possible, by a simultaneous rotation around C-N and C-C bonds, to transfer a methyl group between the two nonequivalent sites without having to press it past the obstructing atom. However, in this case the shape of the potential surface will probably be different from that when the dimethylamino group is unhindered, but the moderate agreement between calculated and experimental barriers indicates that this effect is not of overwhelming importance.

Calculation of Barriers in Amidinium Salts, Amidines, and Enamines. An extrapolation from the relation between amides and thioamides leads to the assumption that mesomeric interaction between an amino group and a C=X group will decrease with decreasing electronegativity of X and with increasing tendency of C and X to form a double bond. The effect of the nature of X can be demonstrated with the same model as before (II). With Y = alkyl, calculations have been performed with parameters for X corresponding to NR₂⁺ (amidinium ion, $h_N = 1.5$), NR (amidine), and CH₂ (enamine). The results (Table V) show a crude correlation between experimental and calculated quantities. For aniline the same parameters predict almost the same barrier ($p_{CN} = 0.314$, $\Delta E_\pi = 0.396\beta$) as for enamines. Evans²⁹ has found the barrier in aniline to be 3.54 kcal/mole and a value of the same

Table V

X	p_{CN}	ΔE_π	$-\Delta F^\ddagger$
S	0.455	0.636	24.5 ^a
O	0.422	0.532	19.2 ^a
⁺ NR ₂	0.484	0.632	19.8 ^a
NR	0.363	0.449	<i>b</i>
CH ₂	0.316	0.394	<i>c</i>

^a Calculated from data in ref 4. ^b No exchange broadening above -40°. ^c No value known.

order of magnitude should be expected for the enamines. It is true that the nonplanarity of the aniline³⁰ and probably also of the enamine molecule should require a higher h_N and a lower k_{CN} value, but the resultant lowerings of the barriers are parallel for the two systems and the above arguments are still approximately valid.

Acknowledgments. The author is grateful to The Swedish Natural Sciences Research Council for financial support and to Fil. Mag. Kerstin Malmqvist for programming the nmr calculations.

(26) M. J. Janssen, *Rec. Trav. Chem.*, **79**, 454 (1960).

(27) J. Sandström, *Acta Chem. Scand.*, **16**, 1616 (1962); J. Sandström and B. Uppström, *ibid.*, **19**, 2432 (1965).

(28) B. Persson and J. Sandström, *ibid.*, **18**, 1059 (1964).

(29) J. C. Evans, *Spectrochim. Acta*, **16**, 428 (1960).

(30) D. G. Lister and J. K. Tyler, *Chem. Commun.*, **3**, 152 (1966).

The Kinetics of the Thermal Decomposition of 3,3-Dimethyloxetane¹

by George F. Cohoe² and W. D. Walters

Department of Chemistry, University of Rochester, Rochester, New York (Received February 15, 1967)

The kinetics of the pyrolysis of 3,3-dimethyloxetane have been investigated over the temperature range 400–450° for pressures near 10 mm. The kinetic and analytical data indicate that the main reaction in a seasoned unpacked vessel is a homogeneous decomposition yielding isobutene and formaldehyde. Experiments with initial pressures from 7 to 74 mm at 420° have provided the major evidence for the first-order character of the reaction. The rate constant for the decomposition into isobutene and formaldehyde can be expressed as $(3.8 \pm 0.1) \times 10^{15} \exp(-60,700/RT) \text{ sec}^{-1}$. From experiments with added nitric oxide or propylene, it appears that free-radical chain processes do not contribute to the decomposition to an extent greater than a few per cent, if at all.

Studies concerning the homogeneous, vapor-phase pyrolyses of cyclic compounds, particularly hydrocarbons containing small rings, have been carried out in a number of laboratories and have provided much information of interest to kineticists. Among the compounds with small heterocyclic rings, ethylene oxide³ has received considerable attention, but less work has been done on the kinetics of the thermal decomposition of molecules having a four-membered ring containing an oxygen atom. Oxetane (trimethylene oxide) has been found to undergo a first-order, homogeneous decomposition at 420–460° in the presence of a free-radical inhibitor.⁴ Earlier Barbot⁵ had observed that oxetane pyrolyzes at 450° and that its 2,2-diethyl derivative decomposes to give two sets of products: (a) formaldehyde and 2-ethyl-1-butene and (b) diethyl ketone and ethylene. Later studies⁶ of the pyrolysis of substituted oxetanes over quartz packing and in the vapor phase have also been concerned with the kinds of products and their relative importance. Searles and his co-workers^{6c,d} have reported that 2,2-diethyloxetane decomposes more slowly and a 3,3-dialkyloxetane more rapidly than the parent compound. It was of interest to investigate the kinetics and mechanism of the decomposition of 3,3-dimethyloxetane and to compare the results with those obtained for unsubstituted oxetane and other cyclic molecules.

Experimental Section

Materials and Apparatus. 3,3-Dimethyloxetane was

synthesized⁷ from neopentyl glycol according to the method of Schmoyer and Case.⁸ From this synthesis a fraction IV with a boiling point of 79° (742 mm) and $n_{D}^{24.8} 1.3948$ [lit.⁸ bp 79.2–80.3° (756 mm) and $n_{D}^{25.1} 1.3956$] was purified in the present study on a gas chromatographic column (with diisodecyl phthalate as the liquid phase). This sample designated as IVa was found to be about 99.9% pure on two different columns, namely, a Golay Type R (UCON LB-550-X) in a Perkin-Elmer Model 154D chromatograph with flame ionization detector and a column with Carbowax 20M on Chromosorb P. A second sample (IVb) was

(1) This work was supported by a grant from the National Science Foundation. Abstracted from the Ph.D. thesis of G. F. Cohoe, University of Rochester, 1964.

(2) Sherman Clarke Fellow, 1962.

(3) M. L. Neufeld and A. T. Blades, *Can. J. Chem.*, **41**, 2956 (1963); S. W. Benson, *J. Chem. Phys.*, **40**, 105 (1964). These articles refer to the earlier work.

(4) D. A. Bittker and W. D. Walters, *J. Am. Chem. Soc.*, **77**, 1429 (1955).

(5) A. Barbot, *Bull. Soc. Chim. France*, [5] **2**, 1438 (1935); *Ann. Chim. (Paris)*, [11] **11**, 519 (1939).

(6) (a) E. Kovacs, N. I. Shuikin, M. Bartok, and I. F. Bel'skii, *Bull. Acad. Sci. USSR, Div. Chem. Sci.*, **111** (1962); (b) E. A. S. Cavell, R. E. Parker, and A. W. Scaplehorn, *J. Chem. Soc., Sect. C*, **389** (1966); (c) S. Searles, Jr., in "Heterocyclic Compounds with Three- and Four-membered Rings," Part 2, A. Weissberger, Ed., John Wiley and Sons, Ltd., London, 1964, p 991; (d) P. E. Throckmorton and S. Searles, Jr., 152nd National Meeting of the American Chemical Society, New York, N. Y., Sept 11–16, 1966.

(7) The synthesis and several exploratory pyrolyses were performed in this laboratory by Roger W. Nelson as part of his senior research for the B.S. degree, 1960.

(8) L. F. Schmoyer and L. C. Case, *Nature*, **183**, 389 (1959).

obtained by the purification of IV on the Carbowax 20M column. Sample IVa was used in most of the kinetic experiments. To test whether undetected impurities in IVa might be influencing the rate, 10-mm experiments were also carried out with each of the following: (1) sample IVa after thorough contact with a doubly distilled sodium surface, (2) sample IVb, and (3) a prepyrolyzed sample of IVa. The ratio of the rate of the special sample to the mean rate of sample IVa under similar conditions was (1) 0.99 ± 0.03 , (2) 1.025 ± 0.003 , and (3) 0.99. Thus the rates for the various samples showed no significant differences. The propylene and isobutene used in this study were found to be 99.9 and 99.6% pure, respectively. Nitric oxide (99%, Matheson) was distilled under vacuum two times between traps at -159 and -196° . Prior to use it was degassed and passed as a gas through a spiral at -78° .

Experiments below 40 mm involved the use of two cylindrical reaction vessels of Pyrex glass. The unpacked vessel had a volume of 313 ml, and the vessel packed with thin-walled glass tubes had a volume of 290 ml with a 27-fold greater surface-to-volume (S/V) ratio. The electrically heated furnace and vacuum system were similar to those used in earlier work.⁹

The temperature was determined with a platinum-platinum-13% rhodium thermocouple standardized at the melting point of zinc (419.5°). Pressures in the reaction vessel were measured with a wide-bore mercury manometer and a Gaertner M930-303 cathetometer. Experiments above 70 mm were carried out in a 350-ml glass vessel contained in a second furnace, and pressures were read on a capillary mercury manometer. In two experiments a vessel packed with copper wire was used. In all experiments the tubing adjacent to the reaction vessel was heated sufficiently to prevent condensation. Before each experiment isobutene was kept in the reaction vessel for at least 1 hr (in some cases, overnight) to season the surface, and then the vessel was evacuated to 10^{-4} mm or lower. More intensive seasoning was used for the packed vessel. In experiments with added nitric oxide the reaction vessel was flushed with a preliminary sample of nitric oxide. In most cases any added substance was introduced into the vessel before 3,3-dimethyloxetane, but when the order was reversed for propylene, no change in rate was observed.

Products. In a number of experiments with the unpacked vessel in the region 410 – 450° , the reaction mixture was removed for analysis when the decomposition had reached about 30% (indicated by the pressure-time curve). The procedures which are described below gave evidence that the main products of

the decomposition are isobutene and formaldehyde. Gas chromatography involving the use of four different columns was employed for identification (by retention time) and separation of isobutene from the entire reaction mixture or from the fraction volatile at -78° , which had been treated with water or an aqueous solution of hydroxylamine hydrochloride and sodium acetate to remove formaldehyde. This material which was collected from several experiments gave an infrared spectrum on a Perkin-Elmer 421 instrument in good agreement with that of pure isobutene. Likewise in other experiments similar fractions separated from the reaction mixtures in two ways gave mass spectra which agreed satisfactorily with the fragmentation pattern for isobutene measured on the same Consolidated Model 21-620 mass spectrometer.

The water-soluble portion of the reaction mixture was mixed with lithium hydroxide-lithium chloride solution. The half-wave potential (*vs.* pool) obtained with a Fisher Electrode and a Sargent Model XV polarograph was the same (within 0.01 v) as that for a solution of Mallinckrodt formaldehyde and agreed with the value of Whitnack and Moshier.¹⁰ The formaldehyde in the reaction products was identified and determined quantitatively by the use of a colorimetric method.¹¹ Tests showed that under the conditions used isobutene and 3,3-dimethyloxetane did not interfere. Precautions were taken to minimize the polymerization of formaldehyde after removal of the mixture from the reaction vessel.

The size of the gas fraction noncondensable at -196° (P_{NC}) from the 11-mm experiments averaged only 0.005 times the pressure increase (ΔP). In two 75–80-mm experiments at 420° with and without 1.5 mm of added NO, the values of P_{NC} were $0.007\Delta P$ and $0.016\Delta P$, respectively. Since noncondensable gases were not significant products in the unpacked vessel, they were not analyzed quantitatively, but a mass spectrum for $m/e > 11$ indicated the presence of CO.

The third major component of the reaction mixture was found in fraction 3, not volatile at -78° , and was established as undecomposed 3,3-dimethyloxetane by comparing its retention time with that of the starting material on two packed chromatographic columns (dimethylsulfolane and Carbowax 20-M) and a capillary column (Perkin-Elmer R). A combined sample of fraction 3 from several 20-mm experiments also showed a trace of isobutene. Fraction 3 had an infrared spec-

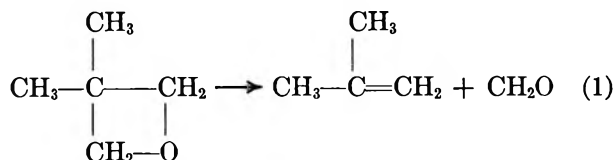
(9) B. C. Roquette and W. D. Walters, *J. Am. Chem. Soc.*, **84**, 4049 (1962).

(10) G. C. Whitnack and R. W. Moshier, *Ind. Eng. Chem., Anal. Ed.*, **16**, 496 (1944).

(11) C. E. Bricker and H. K. Johnson, *ibid.*, **17**, 400 (1945).

trum corresponding to 3,3-dimethyloxetane and gave rates of pressure increase at 410 and 450° which agreed with those of pure 3,3-dimethyloxetane. When the entire reaction mixture after about 30% reaction was analyzed gas chromatographically, the only peaks of significance were those attributable to the compounds mentioned above. In this study definite evidence was not obtained for any isomerization of 3,3-dimethyloxetane.¹² If an isomerization were about 0.01 as fast as the decomposition, the isomer in the early stages of the pyrolysis would have a very small concentration compared to that of the undecomposed oxetane and might have escaped detection. However, such an amount of isomerization, which produces no pressure increase, should not have an appreciable effect on the rate constants calculated for the decomposition under the present conditions.

Stoichiometry. The data indicated that the decomposition in the unpacked vessel proceeds mainly by



reaction 1. Table I shows the results of the analyses of the products (millimeters) in the heated vessel at reaction conditions.

For the experiments in which the pressure of isobutene P_{IB} was compared with the pressure increase (corrected for dead space), the ratio $P_{\text{IB}}/\Delta P$ had a

Table I: Major Products from the Decomposition of 3,3-Dimethyloxetane in an Unpacked Reaction Vessel

Temp, °C	P_0 , mm	ΔP , mm	P_{IB} , mm	$P_{\text{CH}_2\text{O}}$, mm
440	10.0	3.64	3.67	
440	10.6	3.89		3.78
430	11.0	3.88	3.93	
430	10.3	3.60		3.45
420 ^a	9.5	3.20	3.14 ^b	
420	11.2	3.78	3.78	
420	28.5	9.81	9.94	
420	73 ^c	26.1	26.0	
420	10.8	3.66		3.58
420	28.5	9.45		9.07
410	10.6	3.50	3.47	
410	10.9	3.64		3.48
400 ^a	10.2	3.06		2.92

^a Intensively seasoned reaction vessel. ^b Determined on the same chromatogram as 3,3-dimethyloxetane. The latter amounted to $1.02(P_0 - \Delta P)$. ^c In the presence of 40 mm of added propylene.

mean value and average deviation of 1.00 ± 0.01 . Moreover, several experiments with isobutene¹³ indicated that the correction to ΔP for any subsequent reaction of isobutene during the first quarter of the decomposition of 11 mm of 3,3-dimethyloxetane at 440° probably would not exceed the error in the pressure measurement (~ 0.01 mm). From the formaldehyde analyses a value of 0.96 ± 0.01 was obtained for $P_{\text{CH}_2\text{O}}/\Delta P$. This slightly lower value compared to that for isobutene may result from some loss of formaldehyde (*e.g.*, polymerization) after removal from the reaction vessel. In view of the analytical results, particularly those for isobutene, it was concluded that the decomposition proceeds mainly according to eq 1 and that the pressure increase can be used to determine the amount of decomposition (up to at least 30% reaction).

Some analyses were also made on reaction mixtures from experiments performed in the packed bulb after only a few preliminary decompositions. The pressure of the fraction volatile at -78° after removal of formaldehyde was $1.11(\Delta P)$. Gas chromatograms of the reaction mixtures had two additional peaks of moderate size, one lying between and one after the peaks of isobutene and 3,3-dimethyloxetane. Since processes other than (1) were occurring, the packed vessel was given a strong seasoning by allowing 1 atm of isobutene to remain in the vessel for 2 days at 460°. After this treatment the two extraneous chromatographic peaks disappeared. After $\sim 30\%$ of the oxetane had reacted in the packed vessel, the formaldehyde was $0.80\text{--}0.89(\Delta P)$, and the pressure of non-condensable gases was $0.002(\Delta P)$. It appears that even with a 27-fold larger S/V , the reaction shown in eq 1 predominates if the packed vessel is well seasoned.

Results

Order and Homogeneity. The first-order character of the decomposition was indicated by the observation that the quarter-times from the pressure-time curves at 420° were not altered significantly by an 11-fold change in the initial pressure. The values for the first-order rate constants at 420° are shown in Table II. Also consistent with first-order behavior is the fact that a plot of $\log [P_0/(2P_0 - P_t)]$ vs. time was linear as far as the decomposition was carried in the kinetic study ($\sim 33\%$ reaction). The slope of the line yielded a rate constant in agreement with that calculated from the quarter-time. For 42 experiments without added gas, the ratio $t_{1/4}/t_{1/8}$ averaged $2.12 \pm$

(12) Likewise in the work cited in ref 6d, the decompositions of 3,3-dialkyloxetanes were observed, but not the isomerization into 2,2-dialkylpropanals.

(13) Work of P. C. Rotoli in this laboratory.

Table II: First-Order Rate Constant for the Decomposition of 3,3-Dimethyloxetane for Various Pressures at 420°^a

P_0 , mm	$10^4 k$, sec ⁻¹	P_0 , mm	$10^4 k$, sec ⁻¹
6.63	2.74	10.76	2.76
9.48	2.79	11.23	2.76
10.09	2.77	28.46	2.72
10.49	2.80	28.68	2.71
10.64	2.76	73.5 ^b	2.94 ^b
10.62	2.72		

^a Temperatures are within $\pm 0.2^\circ$ of this, and small corrections were applied when appropriate. ^b Experiment in the second apparatus.

0.02 in comparison with the value 2.15 for a first-order rate law.

For the purpose of obtaining kinetic data about the homogeneous decomposition, the experiments were performed in a seasoned unpacked vessel, but, to investigate the importance of surface processes in the rate studies, experiments were carried out also in packed vessels (Table III). With only moderate seasoning of the packed vessel (S/V increased 27-fold), the rate of pressure rise was severalfold greater than that observed for the unpacked vessel. After strong seasoning, the quarter-times in the packed bulb were close to those for the unpacked vessel at a corresponding temperature. In the unpacked vessel, an intensification of the seasoning treatment above that normally used did not alter the rate significantly. From the results in Table III one can conclude that the decomposition in the seasoned unpacked vessel was essentially free from any surface catalysis on the walls. An experiment at a higher pressure in a vessel packed with copper wire had a quarter-time in accord with that for an unpacked vessel under similar conditions. The presence of the copper packing provides a large surface area and tends to eliminate any temperature gradient in the vessel.¹⁴

Effect of Added Gases. Since free-radical chain processes have often been detected by the addition of inhibitors, rate experiments in the presence of propylene or nitric oxide were performed between experiments without added gas. Comparisons are given in Table IV in terms of the ratio of the rate constants in the presence and absence of the inhibitor. The ratio is quite close to unity in most cases. No evidence for an appreciable amount of chain decomposition has been found, but in view of the experimental error an inhibition of about 1–3% cannot be established or ruled out by the present rate data.

Activation Energy. The temperature dependence

Table III: Comparison of Apparent Quarter-Times for Various Reaction Vessels

Temp., °C	P_0 , mm	Unpacked vessels Seasoning		Packed vessels Seasoning	
		Strong	Normal	Strong	Moderate
430	9.8	9.4	9.3 \pm 0.1 ^a		
	7.5			9.2 ^c	
420	7.9				2.6 ^o
	10.1 ^b	17.4 ^b	17.4 \pm 0.1 ^a		
	10.8			16.7 ^c	
	74		16.1 ^d		
400	78				16.2 ^{d,e}
	10.3 ^b	63.6 ^b	64.1 ^a		
	10.4			60.7 ^c	

^a Average of quarter-times (in min) for experiments under usual conditions for the unpacked vessel. ^b Average of two experiments. ^c Packed with glass tubes. S/V was 27-fold greater than unpacked bulb. ^d Experiment performed in the second apparatus. ^e Packed with copper wire. S/V was 4.5-fold greater than unpacked bulb.

Table IV: Effect of Added Gases upon the Rate of Decomposition

Temp., °C	P_0 , ^a mm	Added gas, mm	k_a/k_n ^b
400	10.0	C ₃ H ₆ , 7.3	0.97
	10.6	NO, 0.13	0.98
	10.6	NO, 0.01	0.99
410	10.2	C ₃ H ₆ , 6.8	1.00
	420	10.3	C ₃ H ₆ , 7.0
74		NO, 1.4	0.98
74		C ₃ H ₆ , 39	1.00 ^c
79 ^d		C ₃ H ₆ , 33	0.99 ^d
430	13.1	C ₃ H ₆ , 7.6	0.96
	9.4	C ₃ H ₆ , 5.3	0.98
440	9.7	C ₃ H ₆ , 7.9	0.95
450	10.7	C ₃ H ₆ , 6.0	0.96
	10.7	NO, 0.07	0.98
	9.2	NO, 0.03	0.99

^a P_0 denotes the initial pressure of 3,3-dimethyloxetane. ^b k_a/k_n represents the ratio of the rate constant with added gas to the rate constant without added gas. ^c Average of two experiments. ^d Experiments with and without added propylene (C₃H₆) in the vessel packed with copper wire. In other cases, unpacked vessels.

of the rate was found from a series of 33 experiments at 400–450° in an unpacked vessel with initial pressures kept in the pressure range from 9.1 to 11.8 mm.

(14) The question of thermal gradients in various gaseous reactions has been discussed by S. W. Benson, "The Foundations of Chemical Kinetics," McGraw-Hill Book Co., Inc., New York, N. Y., 1960, pp 426–431, and by D. J. Wilson, *J. Phys. Chem.*, **62**, 653 (1958).

The rate constant was determined by the use of the integrated first-order rate equation and the measured quarter-time (and eighth-time) corrected for dead space. The two values for each experiment were in good agreement. The values of $\log k$ (from quarter-times) were plotted against $(1/T)$, and the slope of the line (visual fit) gave an activation energy of 60.8 kcal/mole. By a least-squares analysis of the same rate constant data (see Figure 1), the activation energy was found to be 60.7 ± 0.2 kcal/mole. With $E = 60.7$, a value of the Arrhenius factor was calculated from each experiment. The rate expression for the decomposition in the unpacked vessel without added gas is $k = (3.8 \pm 0.1) \times 10^{15} \exp(-60,700/RT)$ sec⁻¹. From a series of 11 experiments with 9.2–13.1 mm of 3,3-dimethyloxetane at 400–450° in the presence of propylene or nitric oxide, the activation energy was evaluated as 60.7 ± 0.4 kcal/mole by least-squares analysis and as 60.6 kcal/mole from the slope of a $\log k$ vs. $(1/T)$ plot. The rate constants for the experiments with added propylene or nitric oxide could be represented by the expression $k = (3.7 \pm 0.1) \times 10^{15} \exp(-60,700/RT)$ sec⁻¹, which is almost the same as that for the experiments with 3,3-dimethyloxetane alone.

Discussion

From the results of the analyses and rate measurements, the decomposition of 3,3-dimethyloxetane into formaldehyde and isobutene appears to occur in an unpacked vessel as a homogeneous reaction which obeys a first-order rate law. With respect to the mechanism, it is significant that the amount of formaldehyde is close to the quantity expected from eq 1, and the amount of noncondensable gas is very minor. According to previous work,¹⁵ formaldehyde in the presence of free methyl radicals or H atoms would undergo a chain decomposition forming chiefly H₂ and CO, but formaldehyde alone reacts only slowly near 400°.

In an earlier study⁴ the decomposition of 100 mm of oxetane (trimethylene oxide) without added inhibitor at 440° occurred to the extent of about 10% by free-radical chain processes which produced some H₂, CO, and C₂H₆ in addition to H₂CO and C₂H₄. In the absence of inhibitor the time for 25% pressure increase depended somewhat upon the pressure and for 100 mm of oxetane was about 20% shorter than that observed when nitric oxide (1.9 mm) was added.⁴ For an experiment in the present system with a lower pressure of unsubstituted oxetane (11 mm) purified by gas chromatography, the time for 25% pressure increase was about 10% smaller than that for a similar

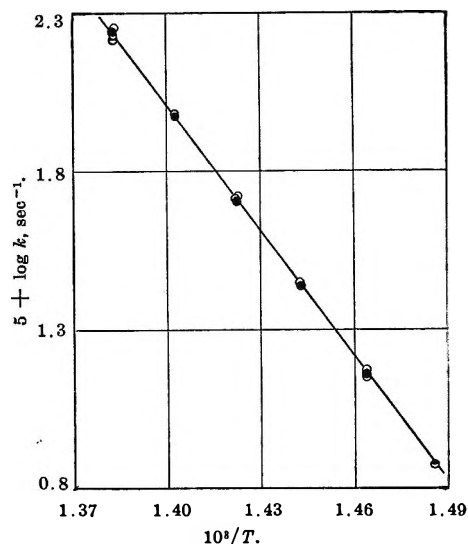


Figure 1. Temperature dependence of the first-order rate constant for the decomposition of 3,3-dimethyloxetane: O, single experiment; ◐, two experiments; ●, three or more experiments with values too close to be shown separately.

sample in the presence of 0.14 mm of NO. Thus, in the decomposition of oxetane free-radical processes apparently are not as close to being insignificant as in the case of 3,3-dimethyloxetane.

To ascertain the influence of methyl substitution upon the nonchain decomposition, comparison has been made between the rate constant for 3,3-dimethyloxetane (11 mm) and the earlier result for oxetane (100 mm)¹⁶ in the presence of inhibitor. The rate constant for 3,3-dimethyloxetane at 420° is about $3^{2/3}$ times that of the parent molecule. It is interesting that the increase in rate constant due to the dimethylation of oxetane in the 3 position is near to that observed for the dimethylation of cyclobutane.¹³

The Arrhenius factor for the decomposition of 3,3-dimethyloxetane into isobutene and formaldehyde has a magnitude comparable to the preexponential factor measured in this laboratory for various alkyl derivatives of cyclobutane.¹⁷ The value of the Arrhenius factor for $(\text{CH}_3)_2\text{C}_3\text{H}_4\text{O}$ is larger than $(ek_B T/h)$, and the main factor in producing this result is probably the positive entropy of activation associated with a ring-

(15) J. E. Longfield and W. D. Walters, *J. Am. Chem. Soc.*, **77**, 6098 (1955).

(16) The rate constant for each compound at the pressure used is essentially independent of the initial pressure. The rate constant for 11 mm of oxetane with added NO in the present apparatus was about 14% smaller than the rate constant obtained for 100 mm in ref 4. This difference may be the result of a slight falloff with pressure or a discrepancy in the temperature.

(17) M. Zupan and W. D. Walters, *J. Phys. Chem.*, **67**, 1845 (1963).

cleavage process. If the over-all decomposition were a one-step reaction, an entropy of activation (~ 9 eu) could be estimated from the present results, but, if the decomposition involves more than one step, more information is needed.

The activation energy for the oxetane decomposition with or without inhibitor was found earlier to be 60 ± 1 kcal/mole, but, on account of the size of the combined experimental error for the decompositions of the two oxetanes, the amount of the difference in the activation energy resulting from 3,3-dimethyl substitution cannot be determined from the existing data.

In a consideration of the details of the ring cleavage one can envision the breaking of two of the original bonds in the ring either (a) in succession or (b) simultaneously. These same alternatives have been considered for the cleavage of the cyclobutane ring, with preference being given to mechanism a in the majority of the recent publications.¹⁸ If mechanism a applies to 3,3-dimethyloxetane, the results indicate that the intermediate biradical decomposes before it can react with formaldehyde or isobutene under the experimental conditions used. With mechanism b there arises the question of whether a C-O or a C-C bond breaks first, and the results of an experiment in which a biradical was detected or identified experimentally

would be of considerable interest. Various data have indicated that the C-O distance in the oxetane ring is slightly longer than the normal value for an unstrained molecule, whereas the C-C distance is nearly normal,¹⁹ but an exact relationship between these data and the dissociation energies of the bonds in the oxetane ring has not been established. Moreover, bond distances for 3,3-dimethyloxetane do not seem to have been reported. If a biradical intermediate exists, the over-all rate of pyrolysis will be dependent upon the rates of formation, decomposition, recyclization, and isomerization of the biradical. In such a case a detailed interpretation of the differences observed for related compounds will involve a consideration of the effect of substitution upon the rate of formation of the biradical and upon the rates of the various reactions by which the biradical may disappear.

Acknowledgment. The authors are grateful to Mr. Carl Whiteman and Mr. Roger Nelson for their assistance. They also wish to thank the General Railway Signal Co. for the use of an IBM computer.

(18) S. W. Benson and W. B. DeMore, *Ann. Rev. Phys. Chem.*, **16**, 421 (1965).

(19) S. I. Chan, J. Zinn, and W. D. Gwinn, *J. Chem. Phys.*, **34**, 1319 (1961); E. J. Goldish, *J. Chem. Educ.*, **36**, 408 (1959).

Relaxation Mechanisms in Polymeric Sulfur^{1a}

by A. Eisenberg^{1b} and L. A. Teter

Contribution No. 1957 from the Department of Chemistry, University of California, Los Angeles, California 90024 (Received December 9, 1966)

The observation is made that polymeric sulfur above the glass transition temperature is subject to two relaxation mechanisms, a "simple" molecular flow and bond interchange. The effects of these mechanisms on the viscoelastic properties are separated quantitatively, and their relative contributions to the shear viscosity are computed. The activation energies of each of the mechanisms are also determined, and it is shown that the molecular flow is subject to a WLF type temperature dependence, while that of the interchange mechanism is of the Arrhenius type. It is tentatively suggested that the chemical relaxation mechanism is of a radical nature, with homolytic chain scission predominating.

I. Introduction

It has been known for a long time that elemental sulfur can exist in a metastable "plastic" modification at room temperature, and many of the properties, including viscoelastic properties, of that modification have been studied;² but practically no attention seems to have been paid to the relaxation and flow mechanisms in that material. The elucidation of the flow mechanisms for this polymer is, however, of great interest, because, as we shall show below, both simple diffusional motion and bond interchange are to be expected as relaxation mechanisms, and both are indeed encountered.

The two relaxation mechanisms mentioned above can be expected for the following reasons. Polymeric sulfur, owing to its high molecular weight, can be expected to have a high viscosity³ assuming simple molecular flow to be the only mechanism. A high viscosity is indeed encountered,⁴ indicating that this might be the relaxation mechanism. On the other hand, it is known that above 160°, a dynamic equilibrium exists between rings and chains,^{5,6} indicating that some type of chemical bond breakage and reformation goes on in the liquid. Furthermore, Tobolsky and co-workers have shown² that bond interchange is the only relaxation mechanism in cross-linked polysulfide rubbers at temperatures as low as 70° or even lower in the presence of a catalyst. Thus, since elemental polymeric sulfur has a very high molecular weight and since the activation energy for the bond interchange process encountered in the polysulfide

rubbers is relatively low (24–36 kcal), both processes could be expected in the glass transition region and above.

As has been demonstrated in a number of preceding publications from this laboratory and from the work by Tobolsky,^{2,7,8} the differentiation between bond interchange or molecular flow as mechanisms of stress relaxation is relatively straightforward. If polymers of various molecular weights are synthesized and the stress relaxation of the resulting materials studied, one would expect, on the basis of previous experience, to find the following situation. If the materials relax by simple molecular flow, then the maximum relaxation time (reflecting the equivalent "ultimate Maxwell element") will vary with the molecular weight in accordance with the relation⁹

(1) (a) Paper no. 7 in a series on the viscoelastic relaxation mechanism in inorganic polymers; based, in part, on a Ph.D. dissertation submitted by L. A. Teter to the Department of Chemistry. (b) McGill University, Montreal, Canada.

(2) A. V. Tobolsky and W. J. MacKnight, "Polymeric Sulfur and Related Polymers," Interscience Publishers, Inc., New York, N. Y., 1965.

(3) R. E. Powell and H. Eyring, *J. Am. Chem. Soc.*, **65**, 648 (1943).

(4) R. F. Bacon and R. Fanelli, *ibid.*, **65**, 639 (1943).

(5) (a) G. Gee, *Trans. Faraday Soc.*, **48**, 515 (1952); (b) F. Fairbrother, G. Gee, and G. T. Merrall, *J. Polymer Sci.*, **16**, 459 (1955).

(6) A. V. Tobolsky and A. Eisenberg, *J. Am. Chem. Soc.*, **81**, 780 (1959).

(7) A. Eisenberg and L. Teter, *ibid.*, **87**, 2108 (1965).

(8) A. Eisenberg and L. Teter, *Trans. Soc. Rheol.*, **9**, 229 (1965).

(9) A. V. Tobolsky and K. Murakami, *J. Colloid Sci.*, **15**, 282 (1960).

$$\log \tau_m = \log A + C_1 \frac{T - T_g}{C_2 + T - T_g} + B \log \bar{M}_w$$

where τ_m is the maximum relaxation time, A is a constant, C_1 and C_2 are the constants of the WLF equation,¹⁰ \bar{M}_w is the weight-average molecular weight, and B is another constant which ranges from 1 to 2 for polymers below the critical entanglement molecular weight and assumes the universal value of *ca.* 3.4 above the critical entanglement length (the constant A would also change accordingly). If, on the other hand, the polymer relaxes by bond interchange in the terminal flow region, then, to a very good approximation, the maximum relaxation time should be independent of the molecular weight but should reflect only the rate of the interchange reaction.

If both bond interchange and molecular flow are occurring simultaneously with comparable relaxation times, then the situation is far more complicated;¹¹ however, one can still resolve the mechanisms to some extent and evaluate their relative contributions, for instance, to the shear viscosity. This can be done by converting stress relaxation data into compliance data and shifting the compliance curves to obtain a master curve by optimizing the overlap at the shortest times. Following Ferry's lead^{12,13} it is postulated that the lower envelope of points corresponds to the molecular flow (or α) mechanism, while any deviation therefrom corresponds to the bond interchange (or χ) mechanism. This will be described much more fully below and has been previously reported in a preliminary fashion.¹¹

In order to elucidate the relaxation mechanisms in polymeric sulfur, we resorted to the technique of stress relaxation and utilized, in addition to pure sulfur, a cross-linked polymer, *i.e.*, sulfur cross-linked with As atoms allowing us to vary the molecular weight between cross-links. The reason for this choice will emerge later.

Before concluding this introduction, it should be pointed out that the book by Tobolsky and MacKnight² summarizes the pertinent preceding studies on sulfur and related polymers. Since that review is very recent, for the sake of brevity no summary of previous work is presented here. Occasional pertinent comparisons will be made in the text of the paper itself.

II. Experimental Techniques

Since most of the techniques used here have not been described before, they will be presented in some detail.

A. Preparation of Samples. 1. Polymeric Sulfur. The crystalline sulfur (Gallard, Schlesinger) of 99.9999% purity was introduced into small Pyrex tubes

(*ca.* 0.35-cm inside diameter) and boiled under vacuum (prior to seal-off) to free it from adsorbed gases. The tubes were then heated to 300° in the furnace (subsequent to seal-off) and were maintained at that temperature for at least 1 day. Thereupon, the samples were quickly quenched in cold alcohol (temperature *ca.* -25 to -28°) and then brought to *ca.* -80° by the slow addition of crushed Dry Ice to the bath. Next, an excess of Dry Ice was added and the tops of the tubes were broken off. The tubes were then allowed to remain completely submerged in the bath for several minutes during which time the alcohol, saturated with CO₂, would seep between the wall of the glass tube and the sample. The tubes, one at a time, were withdrawn from the bath and allowed to warm slightly. The pressure of the escaping CO₂ then usually caused the sample either to be extruded completely or to be forced out of the tube sufficiently so that it could be pulled out the remainder of the way with a pair of tweezers. Care had to be taken in the course of this procedure that the temperature did not rise above T_g ; otherwise, extensive deformation of the sample could take place.

Once prepared and liberated, the samples were stored at Dry Ice temperature until actually placed in the stress relaxation machine.

2. Arsenic-Cross-Linked Polymers. In general, the arsenic trisulfide-sulfur copolymers were synthesized by the simple expedient of heating together glassy As₂S₃ obtained by the procedure to be described below and the amount of sulfur necessary to achieve the desired mole ratio of arsenic to sulfur. After seal-off under vacuum, the Pyrex glass ampoules were heated at 450° for 1-2 days with frequent agitation of the contents. The tubes were then removed from the furnace and allowed to cool. After liberation from the tube, the samples were pulverized and sieved through a 10-mesh screen.

The stress relaxation samples were prepared by filling the fragmented polymer into Pyrex glass tubes *ca.* 0.5 cm in diameter followed by vacuum seal-off and heating at 450° for at least 1 day. The tubes were then withdrawn from the furnace and allowed to cool, and the intact sample was liberated from its tube. The sample was subsequently pressed between smoothed pieces of aluminum foil in the Carver press, the tem-

(10) M. L. Williams, R. F. Landel, and J. D. Ferry, *J. Am. Chem. Soc.*, **77**, 3701 (1955).

(11) A. Eisenberg, S. Saito, and L. A. Teter, *J. Polymer Sci.*, **C14**, 323 (1966).

(12) J. D. Ferry, W. C. Child, Jr., R. Z. Stern, D. M. Stern, M. L. Williams, and R. F. Landel, *J. Colloid Sci.*, **12**, 53 (1957).

(13) W. C. Child, Jr., and J. D. Ferry, *ibid.*, **12**, 327, 389 (1957).

perature being above T_g . When the sample had been pressed to a thickness of *ca.* 0.2 cm, it was removed from the press and ground to constant dimensions by the use of sandpaper. The final result was a bar that varied somewhat in its exact dimensions from one sample to the next. They were all cut to a suitable length with a hot razor blade. Following fabrication, the samples were all stored at temperatures well below their T_g until use.

Polymers with the composition of As_2S_{12} and higher sulfur content showed an increasing tendency toward crystallization at elevated temperatures (above T_g but not much higher than *ca.* 100°) as the sulfur content increased. Above *ca.* 100°, the crystals in a crystallized sample would melt.

B. Glass Transitions. The T_g 's were all measured dilatometrically using some liquid, usually a higher alcohol, of a uniform coefficient of expansion in the temperature range being measured. The T_g 's for the sulfur-arsenic system are listed in Table I.

Table I

Material	T_g , °C	Activation energy, kcal
As_2S_3	69	28.3
As_2S_{12}	46	37.6
As_2S_{15}	32	40.3
As_2S_{25}	4	35.4
S_z	-27	33.6
		36.7 ± 2.1^a

^a Mean \pm average deviation.

*C. Preparation of As_2S_3 .*¹⁴ A 0.3-mole sample of reagent grade As_2O_3 was dissolved in 3 l. of 3 N HCl and heated on the steam bath with stirring while H_2S gas was slowly passed into the solution. Following complete precipitation, the mixture was filtered and washed on the funnel and afterward sucked as dry as possible. The precipitate was then dissolved in *ca.* 0.5 l. of concentrated NH_4OH and kept on the steam bath for *ca.* 24 hr during which time a red gritty material precipitated from the original deep yellow solution. This precipitate was subsequently filtered off and dried by allowing a stream of clean dry air to pass over its surface for *ca.* 24 hr. Following this treatment, a reddish orange powder was obtained.

When heated in a test tube, the initial heating caused the material to both melt and sublime at the same time; however, once the melting had become well advanced, little material was lost *via* sublimation.

During the melting procedure, additional powdery As_2S_3 was added until the final volume of molten As_2S_3 amounted to *ca.* two-thirds of the volume of the test tube. At this point, the mixture was heated to the boiling point and then poured into molds for stress-relaxation samples or else the molten material was allowed to cool in the tube for subsequent removal and pulverization; this pulverized material was then used to prepare other arsenic-containing samples of higher sulfur content than As_2S_3 .

It must be mentioned at this point that the final composition of the cooled As_2S_3 melt could very well deviate slightly from the stoichiometric arsenic to sulfur ratio 2:3, the most probable composition being slightly on the low sulfur side; however, since a great deal of sulfur was added to form other sulfur-arsenic samples, this possible deviation was not considered significant.

III. Results and Interpretations

A. Multiple-Mechanism Relaxation and Separation of the Mechanisms. Although the criteria for the occurrence of simultaneous multiple-mechanism relaxation have been discussed before,¹¹ they will be reviewed here briefly because of their importance. These criteria are given in following paragraphs.

(1) The time-temperature superposition principle^{15,16} is not applicable, for instance, to stress-relaxation data obtained on a sample of the material at different temperatures. In some regions of temperature or modulus, time-temperature superposition may very well apply, but its inapplicability in others demonstrates the presence of additional mechanisms besides simple molecular flow (the α mechanism); the material must, of course, be in the region of linear viscoelasticity. The failure of time-temperature superposition manifests itself also in a change in the distribution of relaxation times. In the case of sulfur this is particularly evident in the rubbery modulus region, where a dip appears in the distribution and deepens with increasing temperature, indicating that the rubbery plateau lengthens and that the relaxation times associated with the two mechanisms move farther and farther apart. This was discussed briefly elsewhere.¹¹

(2) A log-log plot of the maximum relaxation time τ_m against the shift factors a_t is nonlinear. It should be recalled that the shift factor is the horizontal shift

(14) J. W. Mellor, "A Comprehensive Treatise on Inorganic Theoretical Chemistry," Vol. IX, Longmans, Green, and Co., London, 1929, p 273.

(15) A. V. Tobolsky, "Properties and Structure of Polymers," John Wiley and Sons, Inc., New York, N. Y., 1960.

(16) J. D. Ferry, "Viscoelastic Properties of Polymers," John Wiley and Sons, Inc., New York, N. Y., 1961.

needed to bring into coincidence the stress-relaxation curves obtained at various temperatures^{15,16} with the curve obtained at $T = T_g$ used as the reference, while the maximum relaxation time⁹ refers to the "equivalent ultimate Maxwell Element" and is obtained from a plot of $\log E_r(t)$ (the time-dependent Young's modulus in stress relaxation) against time on a linear scale. If only one mechanism were observed, then the kinetic factors governing both of these values should be identical. If, on the other hand, two mechanisms of unequal activation energy are encountered, then the short-time relaxation behavior (reflected in a_T) should be governed by one set of kinetic parameters, while the maximum relaxation time is governed by another set, leading to a nonlinear relationship. The slope of the log-log plot should be related to the ratio of the activation energies of the two processes. An example of such a plot is shown in Figure 1 for As_2S_{12} ; the points are experimental while the line is calculated from the ratio of the activation energies, the method of computation of which will be described in a subsequent section.

As was mentioned in the Introduction, the relative contributions to the relaxation behavior by each of the mechanisms can be determined by the following procedure.¹¹ First, the stress-relaxation data are converted to creep compliance data [$J(t)$] by the method suggested by Tobolsky and Aklonis.¹⁷ The curves are then subjected to the usual shifting procedure, so as to maximize the overlap in the short-time region of any one curve with the master curve. Since the creep compliance for multiple mechanism relaxations is in some ways analogous to the reciprocal resistance of a system of resistors connected in parallel [for which $1/R = (1/R_1) + (1/R_2)$, quite analogous to $J(t) = J_1(t) + J_2(t)$], the lower envelope of points (obtained from the short-time segments by simple shifting) is subtracted from the individual curves obtained at various temperatures and the difference is ascribed to the second mechanism, the lower envelope of points being representative of the first mechanism. An example of this procedure is shown in Figure 2 for As_2S_{16} .

B. The Activation Energy of the Two Processes. Since the identification of the mechanisms is based to a very large extent on the activation energies, the estimation of these will now be described in detail. As was pointed out before, time-temperature superposition has been found to be valid above a certain modulus region (10^7 – 10^8 dynes/cm² depending on the cross-link density). The shift factors in the region of applicability for all of the materials are of the WLF form,¹⁰ as shown in Figure 3, the constants of the WLF equation

$$\log a_T = C_1 \frac{T - T_g}{C_2 + T - T_g}$$

being $C_1 = 14.1$ and $C_2 = 47.4$. From these, by the usual differentiation of $\log a_T$ with respect to $1/T$, the activation energies for the first mechanism can be calculated.

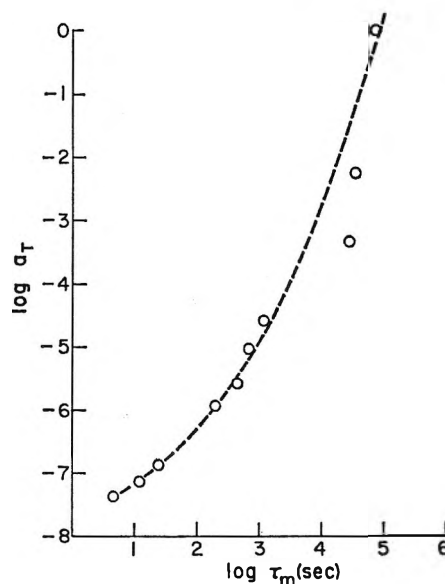


Figure 1. The maximum relaxation time (τ_m) vs. the shift factor (a_T) for As_2S_{12} : points, experimental (46–110°); line, calculated.

The determination of the activation energy for the second mechanism is based on the following factors. It is clear from Figure 2 that the deviations from superposition are pronounced, the deviations appearing even larger on a stress-relaxation plot. This has been taken to mean that at long times, the second mechanism becomes predominant, in those temperature regions in which it is not obscured by the first mechanism, *i.e.*, at low temperatures (see Figures 6 and 7). Thus, if we determine the maximum relaxation time in the usual manner, the value should reflect within experimental error only the kinetic factors due to the second mechanism. Therefore, if one plots $\log \tau_m$ vs. $1/T$, the slope should reflect the activation energy of the second mechanism. Plots for all the samples of $\log \tau_m$ vs. $1000/T$ are shown in Figure 4, and the activation energies calculated from them are listed in Table I, indicating that the activation energies for the second mechanism for all the samples are close.

(17) A. V. Tobolsky and J. J. Aklonis, O.N.R. Technical Report RLT 88, Princeton, N. J., 1965.

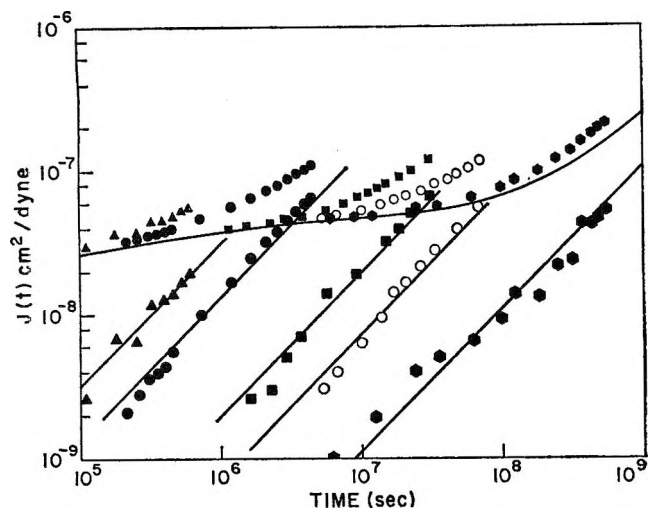


Figure 2. Separation of the α and χ mechanisms in As_2S_{15} . The smooth curved line is the lower envelope of points (points omitted for the sake of clarity). Temperatures are indicated near the experimental points. Reference temperature is T_g , 32° . Plot of $\log J(t)$ vs. $\log t$: \blacktriangle , 35.8° ; \bullet , 40.0° ; \blacksquare , 46.6° ; \circ , 50.0° ; \odot , 55.4° . Lower lines represent contribution of J_χ .

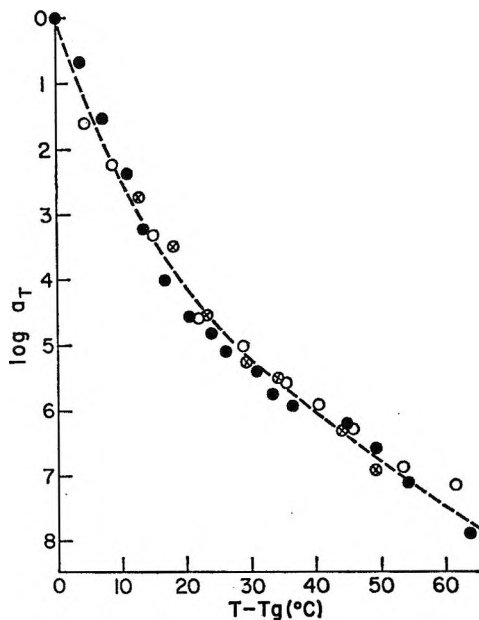


Figure 3. Shift factors ($\log a_T$) vs. $T - T_g$ for arsenic-sulfur copolymers: points, experimental: \circ , As_2S_{12} ; \otimes , As_2S_{16} ; \bullet , As_2S_{26} ; line, calculated from WLF equation and $C_1 = 14.1$ and $C_2 = 47.4$.

There is one other method of determining the activation energy for the second mechanism. From the compliance plots due to the second mechanism, the viscosity due to that mechanism can be computed. As can be seen in Figure 2, the plots are linear with a

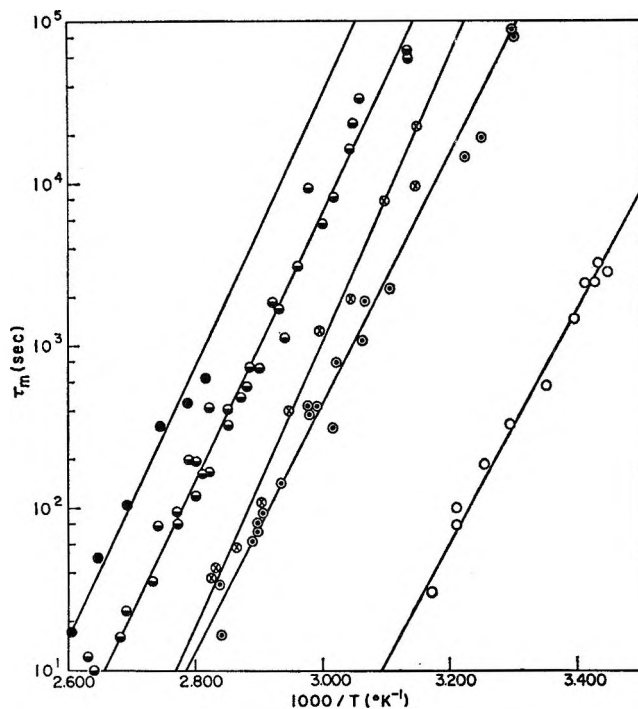


Figure 4. $\log \tau_m$ vs. $1000/T$ for all samples: points, experimental: \bullet , As_2S_9 ; \ominus , As_2S_{12} ; \otimes , As_2S_{16} ; \circ , As_2S_{26} ; \circ , S_2 . The lines are the "best" straight lines through the points, the activation energies being given in Table I.

slope of 1, indicating that only irrecoverable compliance is involved here, *i.e.*, a pure viscosity. The viscosity is obtained from the simple relation $\eta = t/J(t)$. If the master curve has been plotted for $T = T_g$ as the reference temperature, then the viscosities thus calculated have to be divided by the shift factors due to the first mechanism; *i.e.*, the logarithmic shift factor has to be subtracted from the logarithm of the viscosity.¹¹⁻¹³ It should be recalled that $\eta = \tau_m G$ so here again a plot of $\log \tau_m$ vs. $1/T$ would give the activation energy. However, since G does not vary appreciably with temperature over the narrow temperature range accessible, a plot of $\log \eta$ vs. $1/T$ yields the correct value of the activation energy. This plot is presented for As_2S_{15} in Figure 5. For this material, a value of 39.3 kcal/mole was obtained which, within experimental error, is identical with the value calculated from τ_m .

τ_m is known as a function of temperature from the plot in Figure 4 (the expression for the smooth line was used here), and $\log a_T$ is known from the WLF expression. A simple plot of one variable against the other yields Figure 1, the slope of which, incidentally, yields the ratio of the activation energies of the various processes; the curvature indicates the variation of the activation energy for one of the processes.

C. Identification of the Mechanisms. The identi-

fication of the mechanism is based on the following factors.

(1) The shift factors corresponding to the first mechanism are of the WLF form.

(2) The shift factors for the first mechanism are very much in line with those obtained for polymeric selenium,⁷ which has been shown to relax by simple molecular flow (the α mechanism).

(3) The activation energy for the second mechanism does not vary with temperature; *i.e.*, it is of the Arrhenius type.

(4) The compliance resulting from the second mechanism is strictly irreversible, as shown by linearity of the difference plots and the slope of 1.

For these reasons, the first mechanism is identified as the α mechanism, while the second is assigned to bond interchange and is called the χ mechanism owing to its chemical nature. The linearity of the $\log \tau_m$ vs. $1000/T$ plot is believed to be particularly significant and to indicate that the size of the reacting group does not change with temperature, in contrast to molecular motion of the type responsible for the α mechanism, which is governed by the WLF relation.

D. Relative Contributions to the Viscosity by Each of the Mechanisms. The method of determining the viscosity due to the χ mechanism (η_χ) was described in section B. The calculation of the viscosity due to the α mechanism now remains to be described. It should be recalled, however, that even the highest temperature experiments may still contain a contribution of the χ mechanism and that therefore the lowest envelope of points at the longest times may not be a true reflection of the complete α mechanism; *i.e.*, we might have to go to still higher temperatures.

In order to obtain the α viscosity by one method, the lowest envelope of points on the compliance curve is recalculated back into a modulus curve, and the distribution of relaxation times is computed. The viscosity is then calculated from the equations: $\eta^{(t)} = \int H(\tau)d(\tau)$, where $\eta^{(t)}$ is the tensile viscosity and $H(\tau)d(\tau)$ is the distribution of relaxation times, and $\eta = \eta^{(t)}/3$. To obtain the *total* viscosity for any one temperature, the above procedure is followed except that here the real relaxation master curve for the particular temperature is utilized rather than the master curve corresponding to the lowest envelope on the compliance plot. It should be stressed that in this procedure, the α -viscosity curve is a result of a recalculation of modulus into compliance, subsequent shifting to obtain a master curve, a recalculation back to modulus, computation of the distribution of relaxation times, and, finally, graphic integration. The results, therefore are not expected to be highly accurate. Figures

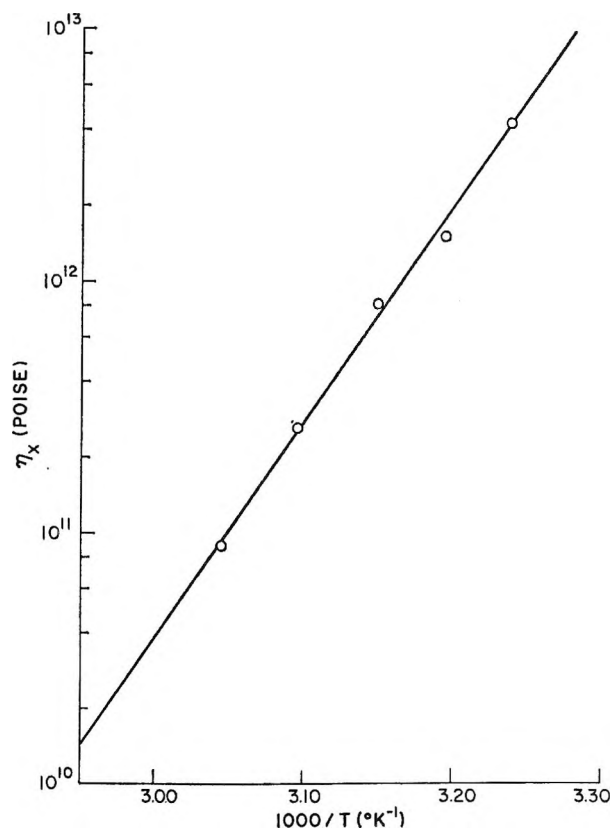


Figure 5. $\log \eta_\chi$ vs. $1000/T$ for As_2S_{16} : points, experimental; line indicates activation energy of 39.3 kcal.

6 and 7 show these results for both pure sulfur and the As_2S_{16} sample. In both of these cases the η_α curve crosses the η_χ curve above T_g , the α viscosity predominating at higher temperatures. The total viscosity, as might be expected, is lower than that due to either of the two mechanisms alone, quite analogous to the case of the two resistors connected in parallel.

It should be noted that in these two materials at the highest accessible temperatures (*ca.* 50° above T_g for $\text{As}_{12}\text{S}_{16}$ and 70° above T_g for pure sulfur) the extrapolated chemical viscosity is at least an order of magnitude greater than the total observed viscosity. Thus, the observed viscosity in those temperature regions is almost entirely a reflection of the α process. The total viscosity and the α viscosity in those temperature regions are identical, and the α viscosity as a function of temperature can be obtained simply by an application of the WLF equation to the observed viscosity at the highest temperatures. The viscosity-temperature plots for the α mechanism obtained by these two procedures agree within experimental error.

If, however, at the highest accessible temperatures η_{obsd} and η_χ do not diverge appreciably (which is the case for As_2S_{12}), then the viscosity data obtained

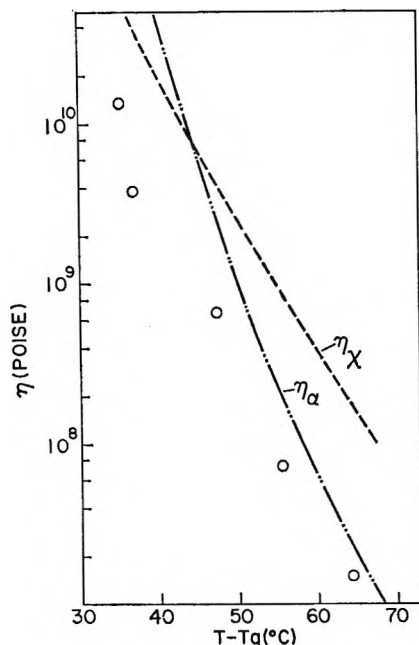


Figure 6. The total viscosity (O) and the calculated viscosities due to the α (- · - ·) and χ (- - -) mechanisms for pure sulfur.

at the highest temperature cannot be ascribed to η_α only.

As might be expected, the relation

$$\frac{1}{\eta} = \frac{1}{\eta_\alpha} + \frac{1}{\eta_\chi}$$

has been found applicable to all these systems; the total viscosity value for As_2S_{16} calculated in this manner is also shown in Figure 7.

In spite of the fact that the χ viscosity is usually the lower one at T_g , the mechanism of the glass transition is undoubtedly short-range motion of chain segments rather than bond interchange. It should be recalled that the extrapolated α viscosity represents a cooperative movement of the entire chain (as evidenced, for instance, by the molecular weight dependence of the viscosity of normal polymers) rather than that of small segments, but that the latter are of critical importance to the glass transition.

E. Speculations on the Detailed Interchange Mechanism. Three items need to be considered in this section. The first concerns itself with the problem of the identity of the species subject to bond interchange in pure sulfur on the one hand and in the As cross-polymers on the other, the second inquires into whether the interchange reaction proceeds by a free-radical or an ionic mechanism, while the third describes a mechanistic scheme for the interchange reaction.

The first problem is easy to settle. Owing to the

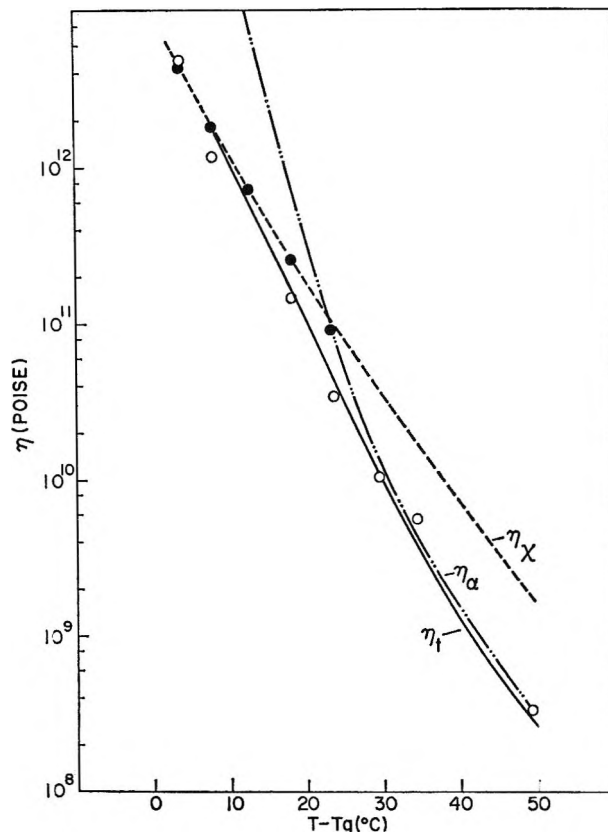


Figure 7. The total viscosity (O) and the calculated viscosities due to the α (- · - ·) and χ (- - -) mechanisms. The solid line is obtained from the relation $1/\eta = (1/\eta_\chi) + (1/\eta_\alpha)$.

similarity of the activation energies for all of the materials from pure sulfur to As_2S_9 , it seems highly probable that S-S bonds are interchanging in all cases. In pure sulfur nothing else is possible, while the probability that an S-As bond interchange reaction should have the same activation energy as an S-S interchange is exceedingly small.

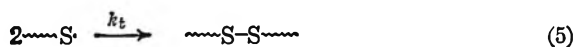
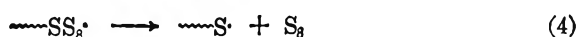
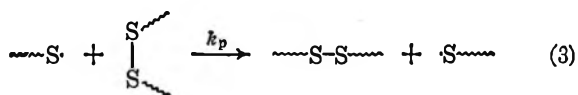
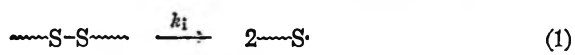
The distinction between an ionic and free-radical mechanism is somewhat more difficult. In view of two lines of evidence to be described below, it is highly probable that a free-radical reaction is involved. The evidence follows.

(1) Tobolsky, *et al.*,¹⁵ investigated the stress relaxation of cross-linked polysulfide rubbers cured with various recipes, some of which most certainly introduced ionic groups onto the end of some sulfur terminated chains, while one (2,4-toluene diisocyanate plus N-methyl-2-pyrrolidone) did not. It was found that all of the cures which introduced ionic groups yielded relatively low activation energies, ranging around 25 kcal, but the one that introduced no ionic groups yielded an activation energy of 36.6 kcal. While originally this was ascribed to a possible cleavage of

the isourethane linkage, it seems probable now that a free-radical S-S interchange predominated in that sample. Additional confirmation comes from the work described below.

(2) Recently, Kende, Pickering, and Tobolsky¹⁸ investigated the thermal decomposition of dimethyl tetrasulfide by following the disappearance of previously incorporated Banfield free radical. The rate constant for the disappearance reaction yielded an activation energy of 36.6 kcal. Since it is extremely difficult, if not impossible, to postulate an ionic mechanism for the splitting of the dimethyl tetrasulfide and the subsequent reaction with the stable organic free radical, the authors postulated that the decomposition of dimethyl tetrasulfide is a free-radical reaction. It seems to us that, most probably, this is also the case in the bond interchange of pure polymeric sulfur and of sulfur cross-linked with arsenic, since the activation energies are closer to 36 than 25 kcal.

With regard to the detailed mechanistic steps, the following sequence of reactions seems reasonable



In this scheme, reaction 4 is an exact reversal of reaction 2, involving a chain end reacting with a ring to prolong the chain or a chain end "biting off" an eight-membered ring and regenerating a free radical. It is clear that rings of various sizes may be present in the sulfur, but this is of little consequence to the present argument since neither reaction 2 nor reaction 4 nor reactions involving small rings of other sizes contribute to stress relaxation. Only reaction 1, which presumably has an activation energy of 36.6 kcal, and reaction 3 are active in stress relaxation, reaction 5 being merely a recombination reaction, which, while possibly introducing stress at a microscopic level, does not do so macroscopically since the microscopic stresses are introduced in all directions with equal probability. Finally, it should be clear that, in a strict sense, reaction 1 represents the initiation of a kinetic chain and reaction 3 is one of the possibly many identical propagation steps, reaction (5) being the chain termination reaction, both in the sense of the "kinetic chain" and the polymeric chain.

If the rate of reaction 3 is significant with regard to reaction 1, *i.e.*, if sulfur relaxes by a true free-radical chain reaction, then the activation energy should be lower than the observed value of 36.6 kcal which applies to the initiation reaction only, the actual value depending on the values of the activation energies for the propagation and termination steps.

In a parallel study of hydrogen- or bromine-terminated sulfur polymers¹⁹ we have observed that the activation energy of the interchange process decreases with increasing concentration of H or Br, reaching values of *ca.* 24 and 19 kcal for the hydrogen- and bromine-terminated systems, respectively. It is interesting to note that the values for the activation energy for the interchange reaction in polysulfide rubbers range from 19.4 to 36.6 kcal, the highest value having been obtained for a diisocyanate cure (36.6 kcal), the others ranging around 25 kcal; the low values of the activation energy in the polysulfides were ascribed to the presence of an ionic mechanism, whereas the high value of 36 kcal found in our work seems to be due to a free-radical mechanism, since it is exceedingly similar to the value found by Kende, Pickering, and Tobolsky for the activation energy for the decomposition of dimethyl tetrasulfide and also for the diisocyanate-cured polysulfide rubber. It seems reasonable to suppose that the decrease of the activation energy due to the addition of hydrogen and bromine is most probably due to increasing importance of an anionic mechanism. Similarly the wide variations encountered in the activation energies for the polysulfide rubbers might also be explained on the basis of changes of the relative importance of a free-radical and an ionic mechanism.

In summary, we can only say that the bond interchange in sulfur and sulfur-arsenic polymers proceeds most probably by a free-radical mechanism in which the initiation reaction seems to be most important; *i.e.*, the kinetic chain length is very low. This, however, is only a very preliminary conclusion, and much further work remains to be done.

F. Arsenic as a Cross-Link for Sulfur. There are two possible approaches to the evaluation of the cross-linking efficiency of arsenic in polymeric sulfur; one is based on the assumption that each arsenic atom forms a trifunctional cross-link; the rubbery modulus of the material should thus be a simple function of the arsenic concentration. The second approach starts with the statistical theory of rubber elasticity²⁰ and

(18) I. Kende, T. L. Pickering, and A. V. Tobolsky, *J. Am. Chem. Soc.*, **87**, 5582 (1965).

(19) A. Eisenberg and L. Teter, to be published.

Table II

Composi- tion	S atoms between cross-links calcd from stoichiometry	$M_c(\text{calcd})$ (from column 2)	ρ	T_g , °K	$E_{\text{calcd.}}^a$ (from column 3)	E_{exptl}	$M_c(\text{exptl})^b$	$M_c(\text{calcd})/M_c(\text{exptl})$
As ₂ S ₁₂	4	128	2.2	319	1.4×10^8	1×10^8	1800	14
As ₂ S ₁₅	5	160	2.2	305	1.0×10^9	7×10^7	2400	15
As ₂ S ₂₅	8	256	2.1	277	8.7×10^8	3×10^7	5100	20

^a $E = 3\rho RT/M_c$; ρ = density, weighted average of densities of S and As₂S₃; M_c = molecular weight between cross-links. ^b From equation footnote a using E_{exptl} .

attempts to predict the concentration of effective cross-links in the polymer.

Utilizing the first method, the average molecular weight between cross-links can be calculated (assuming only simple stoichiometry), and thus also the modulus. The results are shown in Table II, the *resulting* values being labeled with the subscript calcd.

The second method allows the calculation of some type of effective chain length between cross-links, and these values are also listed in Table II being labeled with the subscript exptl. It is seen that the effective M_c is 14–20 times larger than that calculated on the basis of simple stoichiometry, indicating that a substantial fraction of the As atoms is not effective as cross-links. There are several possible reasons for this, the most probable being the formation of some types of rings or loops along the chain in which case the As would not act as a cross-link but would merely tend to change the structure of the chain.

G. *The Rate Constant for the Interchange Reaction.* In a study of the viscoelastic properties of cross-linked polyethylene tetrasulfide polymers²¹ Tobolsky, Beevers, and Owen suggest the expression for the rate constant as a function of temperature

$$k = 5.86 \times 10^{12} \exp(-25,900/RT)$$

the rate constant being related to the relaxation time by the relation $\tau_m = 1/km$, where m is the number of interchangeable bonds between cross-links. Since we are not sure of the structure of the As-cross-linked polymers, we applied the same reasoning to the pure sulfur sample, the value of m being simply the number of S–S bonds between entanglements tabulated as $M_c(\text{exptl})$ in Table II as calculated from the theory of rubber elasticity. The results are

$$k = 1.74 \times 10^{17} \exp(-33,400/RT)$$

It is interesting to note that at 17° the lines intersect, but owing to the different nature of the material and possibly also of the mechanism, the intersection is probably accidental.

Acknowledgment. The financial assistance of the Office of Naval Research is gratefully acknowledged.

(20) L. R. G. Treloar, "The Physics of Rubber Elasticity," 2nd ed, Clarendon Press, Oxford, 1958.

(21) A. V. Tobolsky, R. B. Beevers, and G. D. T. Owen, *J. Colloid Sci.*, **18**, 359 (1963).

Solubilization of Polycyclic Aromatic Hydrocarbons in Poly(methacrylic acid) Aqueous Solutions

by G. Barone, V. Crescenzi, A. M. Liquori, and F. Quadrifoglio

Centro Nazionale di Chimica delle Macromolecole (CNR), Istituto Chimico, Università di Napoli, Naples, Italy

Accepted and Transmitted by The Faraday Society (July 18, 1966)

An investigation on the solubility of some aromatic polycyclic hydrocarbons (phenanthrene, anthracene, pyrene, 3,4-benzpyrene, 1,2-benzpyrene) in aqueous solutions of conventional poly(methacrylic acid) (PMA) and poly(acrylic acid) (PAA) has been carried out. PMA aqueous solutions at low degrees of neutralization (α) exhibit a solubilizing power toward these hydrocarbons, which, at $\alpha \simeq 0.1$, is lost in a rather abrupt way. In the case of PAA similar phenomena are absent. The influence of the concentration and molecular weight of PMA together with that of ionic strength on the solubility of hydrocarbons in PMA aqueous solutions has been investigated. The solubilization phenomenon is related to the peculiar conformational state of unneutralized PMA in aqueous solution and briefly discussed, in qualitative terms, assuming that a partition of the hydrocarbon molecules between bulk water and PMA globular coils takes place.

In a preceding paper¹ it has been shown that unneutralized poly(methacrylic acid) (PMA) aqueous solutions display the ability to increase the solubility of some C₃-C₆ alkanes. This effect has been correlated with the numerous evidences according to which unneutralized PMA chains assume in dilute aqueous solution tightly coiled conformations,²⁻⁶ and it has been attributed to the presence in the interior of each tightly coiled PMA chain of hydrophobic domains where the alkane molecules are preferentially located.

In this paper data are reported regarding the solubility, at 25°, in unneutralized PMA solutions of some large polycyclic aromatic hydrocarbons, namely, phenanthrene, anthracene, pyrene, 3,4-benzpyrene, and 1,2-benzpyrene. The results indicate that in unneutralized PMA aqueous solutions the solubility of the polycyclic hydrocarbons is noticeably increased with respect to that in water, the effect being simply proportional to the concentration of the polyelectrolyte. Increasing the molecular weight of the latter initially increases the solubility of the hydrocarbons up to an asymptotic value. The solubility of the polycyclic hydrocarbons has furthermore been found to be markedly dependent on the degree of neutralization,

α , of PMA and to be strongly influenced by the addition of simple salts in a characteristic way, depending on hydrocarbon size. The results to be illustrated here are discussed, similarly to those previously reported on the C₃-C₆ alkanes,¹ by considering that in the unneutralized PMA solutions a partition of the hydrocarbon molecules between bulk water and hydrophobic PMA coiled chains takes place.

The above-mentioned effects have not been found with solutions of poly(acrylic acid) whose monomer units are completely polar. A comparison between the solubilization of aromatic hydrocarbons in DNA water solution^{7,8} and the present results is also made,

(1) G. Barone, V. Crescenzi, B. Pispisa, and F. Quadrifoglio, submitted.

(2) G. Barone, V. Crescenzi, and F. Quadrifoglio, *Ric. Sci. Suppl.*, **35**, 243 (1965).

(3) A. M. Liquori, G. Barone, V. Crescenzi, F. Quadrifoglio, and V. Vitagliano, *J. Macromol. Chem.*, **1**, 291 (1966).

(4) T. M. Birshtein, E. V. Anufrieva, T. N. Nekrasova, O. B. Ptitsyn, and T. V. Sheveleva, *Vysokomolekul. Soyedin.*, **2**, 372 (1965).

(5) J. C. Leyte and M. Mandel, *J. Polymer Sci.*, **A2**, 1879 (1964).

(6) G. Barone, V. Crescenzi, and F. Quadrifoglio, *Ric. Sci. Suppl.*, **35**, 1069 (1965).

(7) E. Boyland and B. Green, *Brit. J. Cancer*, **16**, 507 (1962).

and the higher specificity of the former effect is emphasized.

Experimental Section

Poly(methacrylic acid) (PMA) and poly(acrylic acid) (PAA) samples were those described in a previous paper.² Three fractions of PMA (viscosity-average molecular weights, \bar{M}_v , are 1.4×10^4 , 25×10^4 and 85×10^4 , respectively) and a single fraction of PAA ($\bar{M}_v = 30 \times 10^4$) have been used. The concentration of the polyacid solutions was determined potentiometrically, and solutions at various degrees of neutralization were prepared by adding appropriate amounts of 0.1 N NaOH and finally by diluting to volume.

Pyrene (P) (mp 155°), anthracene (A) (mp 217°), and 1,2-benzpyrene (1,2-BP) (mp 179.5°) were purified according to Sangster and Irvine.⁹

3,4-Benzpyrene (3,4-BP) (mp 176°) and phenanthrene (Ph) (mp 100°) were purified by repeated crystallization from benzene-ethanol (1:9) mixtures. Thin layer chromatographic analyses of the hydrocarbons confirmed their final purity.

Urea and methylurea were purified by repeated crystallization from ethanol, at temperatures below 60°.

NaCl was a reagent grade product.

Lauric acid was a BDH product used without further purification.

The solutions of potassium laurate were prepared by adding appropriate amounts of KOH to lauric acid solutions up to pH 9 and then diluting to volume.

Cyclohexane was a spectrophotometric grade product.

The solubilization experiments were carried out as follows. Finely powdered crystals of the hydrocarbons were suspended in the polyelectrolyte and in the potassium laurate solutions, respectively. The flasks containing the solutions were gently shaken in a thermostat at $25 \pm 0.1^\circ$. In order to avoid photo-oxidation of the hydrocarbons, the polyelectrolyte solutions were degassed with a flux of nitrogen and the flasks, tightly stoppered, were protected from radiation by painting their outer surface black. The time to reach the equilibrium varied from hydrocarbon to hydrocarbon and depended on the viscosity of the solution and on the amount of salts. In all cases this time did not exceed 1 month, the solubility of most hydrocarbons being already $\sim 80\%$ of the saturation value after 10 days, on the average.

Once the equilibrium was reached, the solutions were filtered through sintered-glass (G-4) filters. Solutions were examined for the presence of microcrystals

by fluorescence spectroscopy and refiltered if necessary.¹⁰

The amount of hydrocarbon solubilized in the aqueous phases was determined in all cases by carrying out ultraviolet spectral measurements on cyclohexane extracts of the hydrocarbons. In the case of PMA solutions the pH was brought to ~ 10 with NaOH immediately before treatment with cyclohexane, to facilitate extraction of the hydrocarbons.

Examination of the original aqueous solutions, after extraction, by fluorescence spectroscopy indicated that removal of the hydrocarbons was complete. The reproducibility of the results was found to be satisfactory in all cases.

The maximum difference between the results of independent sets of measurements never exceeded 10%.

Calculations of the amount of hydrocarbon solubilized were based on the following molar extinction coefficient values in cyclohexane: $\epsilon_{383}^{3,4-BP}$ 30,000, ϵ_{334}^P 52,000, ϵ_{375}^A 8700, $\epsilon_{331}^{1,2-BP}$ 36,800, ϵ_{293}^{Ph} 13,750. These values are in good agreement with data reported in the literature.¹¹

The same experimental procedure applied to determine the solubility of three (A, P, Ph) polycyclic hydrocarbons in water has led to values close to those reported in the literature.^{12,13} However, in the case of the much less soluble hydrocarbons (1,2-BP and 3,4-BP), the uncertainty of our data is larger.

Quantitative fluorescence measurements on cyclohexane extracts from aqueous solutions of these latter two hydrocarbons have led to values more reproducible and in the case of 3,4-BP our value ($1.9 \times 10^{-8} M$) is in satisfactory agreement with those reported in the literature.^{7,13,14} In the following, therefore, comparison between hydrocarbon solubilities in the various solutions studied and water will be made using the more precise figures for water taken from the literature in the case of anthracene, phenanthrene, and pyrene. In the case of 3,4-BP a mean value obtained from our data and literature data will be used. In the case of 1,2-BP our data will be used, lacking any data in the literature.

The ultraviolet and fluorescence measurements were

(8) A. M. Liquori, B. De Lerma, F. Ascoli, C. Botrè, and M. Trasciatti, *J. Mol. Biol.*, **5**, 521 (1962).

(9) R. C. Sangster and J. W. Irvine, *J. Chem. Phys.*, **24**, 670 (1956).

(10) E. Boyland and B. Green, *Br. J. Cancer*, **16**, 347 (1962).

(11) E. Clar in "Polycyclic Hydrocarbons," Academic Press Inc., London, 1964.

(12) H. B. Klevens, *J. Phys. Chem.*, **54**, 283 (1950).

(13) W. W. Davis, M. E. Krahl, and G. H. A. Clowes, *J. Am. Chem. Soc.*, **64**, 108 (1942).

(14) H. Weil-Malherbe, *Biochem. J.*, **40**, 351 (1964).

carried out with a Beckman DK-2 spectrophotometer and an Aminco-Bowman spectrofluorometer, respectively.

Quartz cells from 0.1 to 1 cm of optical path were used in absorption experiments.

Potentiometric titrations were made using a Beckman Model 76 expanded-scale pH meter, with adapted miniature glass and calomel Leeds and Northrup electrodes.

Results

Data on the solubility of P and 3,4-BP in aqueous solutions of unneutralized PMA as a function of polyelectrolyte concentration are reported in Figure 1. The results are given as ratios between the concentration of hydrocarbon (C_H , moles per liter) and PMA concentration (C_{PMA} , equivalents per liter). It appears from Figure 1 that the solubility of P and 3,4-BP increases linearly with unneutralized PMA concentration and increases with PMA molecular weight. The influence of PMA molecular weight, however, appears to level off already for $\bar{M}_v = 10^5$. On the contrary, experiments carried out with PAA have shown that P and 3,4-BP, as well as other polycyclic hydrocarbons, have solubilities, in dilute PAA aqueous solutions, close to those in water. Ultraviolet spectra of P and 3,4-BP in an unneutralized PMA solution have shown that the absorption bands of the two hydrocarbons in the PMA solution are only slightly red-shifted with respect to those in cyclohexane solution. Spectra of P and 3,4-BP in the PMA solution are furthermore nearly identical with those characteristic of the two hydrocarbons solubilized in potassium laurate or sodium lauryl sulfate micellar solutions. On the contrary, a more marked red shift has been reported for the spectra of P and 3,4-BP solubilized in DNA solutions^{7,8,15} (see Table I).

Similar results have been obtained with other polycyclic hydrocarbons studied (*i.e.*, phenanthrene, anthracene, and 1,2-benzpyrene) with regard to their ultra-

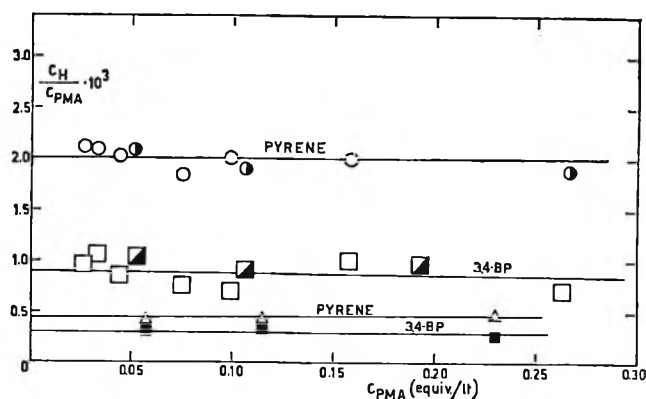


Figure 1. Solubility of pyrene (\circ , \bullet , Δ) and 3,4-benzpyrene (\square , \blacksquare , \blacksquare) (expressed as ratio between the concentration of hydrocarbon (moles per liter) and PMA concentration (equivalents per liter)) in PMA solutions as a function of polyelectrolyte concentration. PMA molecular weight: (\bullet , \blacksquare) $\bar{M}_v = 856,000$; (\circ , \square) $\bar{M}_v = 250,000$; (Δ , \blacksquare) $\bar{M}_v = 14,000$.

violet spectra in PMA solution and in particular the trend of their solubility with PMA concentration and molecular weight. In view of the linear dependence of hydrocarbon solubilities upon PMA concentration, and of the almost invariant solubilities in all cases for PMA molecular weight exceeding 10^5 , our data may be simply reported as moles of hydrocarbon/(moles of PMA \times hydrocarbon solubility in water) = K . This feature lends strong support to the occurrence of real "solubilization" of the various hydrocarbons in PMA solutions, as opposed to the possibility of even partial "colloidal suspension" (which is also ruled out by the fluorescence spectra).

For PMA molecular weight above 10^5 the K values thus acquire the meaning of a characteristic parameter for each hydrocarbon-aqueous PMA system. In Table II a summary of solubilities and K values for the various hydrocarbons in unneutralized PMA solution and in potassium laurate solution is given. Some of the K values (P, Ph, A) were calculated with the data on the solubility of the above-mentioned hydrocarbons in potassium laurate solutions reported by Kleven.¹² For 1,2-BP and 3,4-BP our solubilization data were used. In computing the K values only the micellar potassium laurate concentration was taken into account, excluding the free soap concentration.¹²

The influence of the degree of neutralization, α , of PMA upon the solubility of the hydrocarbons is shown in Figure 2. The K values for P and 3,4-BP reported in Figure 2 as a function of α clearly indicate that solubilizing power of PMA aqueous solutions is

Table I: Wavelengths (m μ) of Characteristic Ultraviolet Absorption Bands of Pyrene (P) and 3,4-Benzpyrene (3,4-BP), in Different Media

	Cyclohexane	Aqueous solutions		
		PMA ($\alpha = 0$) ^a	NaLS ^b	DNA ^{7,8,15}
P	334	338	337	345
3,4-BP	383	387	386	394

^a Spectra of the hydrocarbons are independent of unneutralized ($\alpha = 0$) PMA concentration in the range investigated.

^b Spectra recorded in a 0.05 N sodium lauryl sulfate solution.

(15) E. Boyland, B. Green, and S. L. Liu, *Biochim. Biophys. Acta*, **87**, 653 (1964).

Table II

Hydrocarbon	Solubility in H ₂ O (mole/l.) at 25°	Solubility (mole/l.) in PMA solution at 25° ($\alpha = 0, C = 0.1 N,$ $\bar{M}_v = 85 \times 10^4$)	K (l./equiv) ^a at 25°	
			Potassium laurate	PMA ($\alpha = 0$)
Phenanthrene	9.0×10^{-6} ^{12,13}	2.70×10^{-4}	1.6×10^4 ^b	3.0×10^2 ^c
Anthracene	4.47×10^{-7} ^{12,13}	0.31×10^{-4}	4.0×10^4 ^b	7.0×10^2 ^c
Pyrene	7.7×10^{-8} ^{12,13}	2.08×10^{-4}	6.4×10^4 ^b	2.7×10^3 ^c
1,2-Benzpyrene	2.9×10^{-8} ^e	0.67×10^{-4}	13.5×10^4 ^c	2.3×10^4 ^c
3,4-Benzpyrene	1.6×10^{-8} ¹³	1.25×10^{-4}	40.0×10^4 ^{c,d}	7.8×10^4 ^{c,d}
	2.4×10^{-8} ¹⁴			
	0.9×10^{-8} ⁷			
	1.9×10^{-8} ^e			

^a K = moles of hydrocarbon/(moles of solubilizing agent \times hydrocarbon solubility in water). ^b Values based on data reported by Kleven.¹² For an explanation see text. ^c Values based on our data of solubilization. For the explanation see text. ^d Based on the value 1.6×10^{-8} mole/l. for the solubility in water. ^e This work.

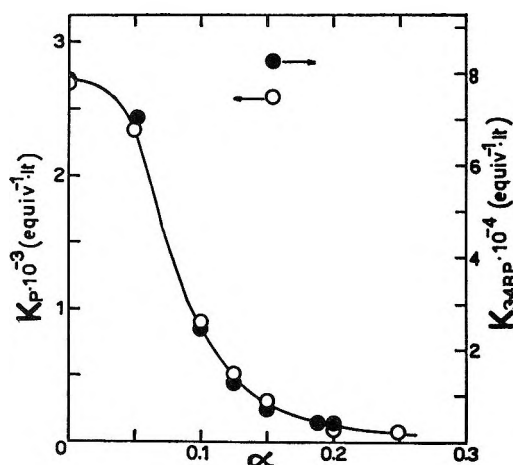


Figure 2. K values for pyrene (\circ) and 3,4-benzopyrene (\bullet) as a function of the degree of neutralization α of PMA.

abruptly and almost completely lost at the early stages of polyelectrolyte neutralization. A similar effect has been observed studying the solubility of *n*-pentane and *n*-hexane in PMA aqueous solutions.¹

In Figure 3 hydrocarbon solubilities in a 0.10 *N* unneutralized PMA solution for different ionic strengths (*NaCl*) are reported against *NaCl* molarity. It is seen that for P, A, and Ph the solubility in the PMA solution increases with increasing ionic strength, while for 1,2-BP a maximum is observed at around 1.0 *M* *NaCl*. In the case of 3,4-BP, on the contrary, the solubility steadily decreases with increasing *NaCl* concentration.

Discussion

The results reported here may be interpreted, in our opinion, in a way similar to that which has been found to correlate satisfactorily, even though qualita-

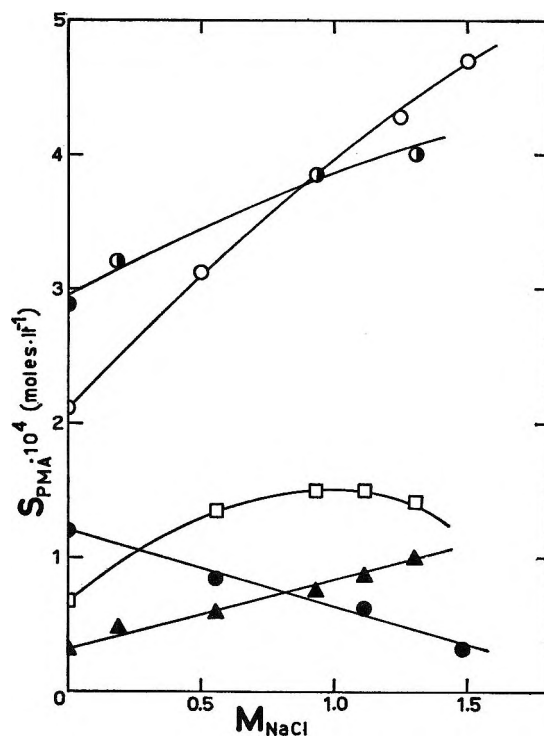


Figure 3. Solubility of (\bullet) phenanthrene, (\circ) pyrene, (\blacktriangle) anthracene, (\square) 1,2-benzopyrene, and (\bullet) 3,4-benzopyrene in 0.1 *N* (unneutralized) PMA solution as a function of *NaCl* molarity.

tively, a previously reported set of data regarding the solubility of some C_3 - C_6 alkanes in PMA aqueous solutions.¹ Unneutralized high molecular weight PMA solutions are formally visualized as a two-phase system: water and globular coils of PMA chains.

Within the latter a number of polycyclic aromatic molecules may be located, in equilibrium with those dissolved in bulk water. The K values reported in Table II would thus be treated as partition coefficients

for the various hydrocarbons between PMA globular chains and water.

The lack of solubilizing power of PAA toward both simple alkanes¹ and polycyclic hydrocarbons is a consequence of the less hydrophobic character of the nonpolar moiety of the repeating units.³ As clearly evidenced by a number of experiments, neutralization of PMA with NaOH promotes a conformational transition of PMA chains from tight, sparingly solvated coils to open, more solvated coils,³⁻⁷ which are unable to uptake an appreciable number of apolar molecules. The trend of K values against PMA degree of neutralization, for P and 3,4-BP reported in Figure 2, therefore, sensitively monitors the PMA conformational transition. In this connection it is also interesting to report that addition of urea to unneutralized PMA solutions saturated with P and 3,4-BP, respectively (final concentration of urea = 8 M), brings about precipitation of both hydrocarbons. Determination of the amounts of hydrocarbon left in the urea-poly-methacrylic acid aqueous solution has led to values nearly identical with those found for the solubility of P and 3,4-BP, respectively, in 8 M urea (6.56×10^{-6} mole/l. for P and 1.76×10^{-7} mole/l. for 3,4-BP). Studies carried out on PMA aqueous solutions containing urea indicate that the conformational transition of PMA is no longer detectable (upon titration with NaOH) in 4 M urea.¹⁶ These results may be consistently attributed to a change in the conformational state of unneutralized PMA promoted by urea, which would render PMA unable to uptake hydrocarbon molecules.

The mechanism of action of urea onto PMA is being investigated. The effect exerted by NaCl on the solubilizing power of unneutralized PMA solution (Figure 3) may be interpreted in our opinion considering that, in general, addition of neutral salts to a polyelectrolyte solution induces a marked reduction on the average chain dimensions of the polymeric solute. In the case of unneutralized PMA this would also be accompanied by an increase in hydrophobicity of the cores of PMA coils.¹

The two effects would oppositely influence the solubilization of the polycyclic hydrocarbons, depending mainly on the size of hydrocarbon molecules, as shown in Figure 3. The hydrocarbons with larger sized molecules are in fact seen to exhibit either a con-

tinuous decrease or a flat maximum in the solubility in the PMA solution with increasing the ionic strength. The solubility of the relatively smaller polycyclic hydrocarbons would, on the contrary, be positively affected, in the NaCl concentration range studied, by the increased hydrophobicity of solution domains occupied by PMA coils. Probably a maximum solubility could be observed in these systems also, at higher NaCl concentrations, were it not for PMA coacervation.

Focusing attention once more on the data of Table II it is seen, however, that in the case of unneutralized PMA solutions in the absence of salts, no simple quantitative correlation of the observed trend of K values with hydrocarbon size and/or water solubility appears feasible.

It is interesting to point out that qualitatively the same trend in K values has been found in the case of potassium laurate solution, on the basis of Klevens'¹² and our data. In the case of PMA, however, the K values exhibit a more marked increase going from phenanthrene to 3,4-benzpyrene.

The solubilizing power of unneutralized PMA solutions toward 3,4-BP happens to be very close to that of native DNA on the basis of the repeating unit of each strand.⁸ For this macromolecule, also, polycyclic aromatic hydrocarbon solubilization has been attributed to the presence of "hydrophobic cavities" in defective regions of the molecule.

In the case of DNA, however, a higher selectivity is displayed in the solubilization process, as a result of geometric restrictions in the insertion of the aromatic molecules in the disordered double-stranded helix cavities. Another consequence of such geometric restrictions is the significant red shift (see Table I) in the absorption spectrum of the hydrocarbon due to the perturbing influence of the uneven charge distribution of the bases between which the aromatic hydrocarbon is sandwiched. Obviously such specific features are absent in the solubilization process in PMA aqueous solutions, as well as in potassium laurate solution.

Acknowledgments. The authors wish to thank Miss Bianca Sorrentino, who carried out some measurements. This work was conducted with CNR aid.

(16) G. Barone, V. Crescenzi, and F. Quadrioglio, *Ric. Sci. Suppl.*, 36, 482 (1966).

The Photochemical Decomposition of Hydrogen Sulfide. The Reactions of Hydrogen Atoms and HS Radicals¹

by B. deB. Darwent, R. L. Wadlinger, and Sr. Mary John Allard

The Martin Maloney Chemistry Laboratory,
The Catholic University of America, Washington, D. C. 20017
(Received October 24, 1966)

The photochemical decomposition of hydrogen sulfide in the gaseous state has been investigated by conventional photochemical techniques^{2,3} and by flash photolysis.^{4,5} There is good evidence that H and HS are formed in the initial act, *e.g.*, the detection of HS in the flash photolysis experiments,^{4,5} and the photolysis of H₂S has been used to study the reactions of H atoms with a variety of hydrocarbons⁶ and oxygen.⁷ The validity of using the photolysis of H₂S as a means of studying the reactions of H atoms hinges on the assumptions (a) that the H atoms produced by the photolysis do not contain a significant amount of excess energy and (b) that the HS radicals disappear without producing H or H₂.

The above assumptions have been examined (a) by observing the effect of a large excess of inert gas (CO₂) on the rates of formation of H₂ in the photolysis of H₂S mixed with I₂ and Br₂ and (b) by photolyzing acetone in the presence of H₂S and analyzing the products for H₂.

The effect of inert gas on the rate of formation of H₂ in the photolysis of H₂S mixed with I₂ or Br₂ was investigated in a conventional system, which included a quartz reaction vessel and optics and a gas circulating pump. The unfiltered, collimated light from a medium-pressure Hg lamp, principally at 2537 Å, completely filled the cell. The absorbed intensity was taken to be equal to the rate of formation of H₂ in the photolysis of H₂S alone. The halogen (I₂ or Br₂) was stored in a tube, which could be surrounded by a constant-temperature bath, from which it was admitted to the reaction system. The concentration of the halogen in the reaction system was controlled by the temperature of the bath surrounding the storage tube and was checked spectrophotometrically before and after the experiment.

The results of experiments with I₂ and Br₂ (Table I) show that the halogens are much more effective in

reducing Φ_{H_2} when CO₂ is present. This strongly suggests that the photochemically produced H is "hot" and therefore does not discriminate greatly between its reactions with H₂S and the halogens. When CO₂ is present, the "hot" H atoms are deactivated and thus show a much higher reactivity toward the halogen than to H₂S.

Table I: Effect of Inert Gas on the Photolysis of H₂S in the Presence of Halogens^a

Halogen	$p_{\text{H}_2\text{S}}$	p_{hal}	p_{CO_2}	ϕ
I ₂	9.5	0.2	...	0.67
I ₂	9.5	0.2	689	0.22
Br ₂	9.0	1.0	...	0.66
Br ₂	9.0	1.0	600	0.43

^a All pressures in torr; temperature 50°; reaction cell volume 200 cm³; reaction system volume 2.0 l.

If all the H were deactivated by collision with excess CO₂, the data in the table give values of the ratios $k_{\text{X}_2}/k_{\text{H}_2\text{S}}$ of 166 for I₂ and 11.7 for Br₂, where the k 's are the rate constants for the reaction of H with the halogen and H₂S, respectively.

Values⁸ of 1.365, 4.708, 6.16, and 6.92 Å for kinetic theory diameters of H, H₂S, Br₂, and I₂, respectively, lead to $Z_{\text{H,Br}_2}/Z_{\text{H,H}_2\text{S}} = 1.5$ and $Z_{\text{H,I}_2}/Z_{\text{H,H}_2\text{S}} = 1.8$. By assuming equal probability factors, we find $\Delta E = E_{\text{H,H}_2\text{S}} - E_{\text{H,hal}} = 2.9$ and 1.2 kcal mole⁻¹ for I₂ and Br₂, respectively. Since $E_{\text{H,I}_2}$ and $E_{\text{H,Br}_2}$ are known to be 0.0 and 1.5 kcal mole⁻¹, respectively, the values of $E_{\text{H,H}_2\text{S}}$ turn out to be 2.9 and 2.7 kcal mole⁻¹. The agreement is satisfactory and the average value of 2.8 kcal mole⁻¹ is very close to the value of 2.6 kcal mole⁻¹ found⁹ for the analogous reaction of CH₃ with H₂S.

(1) This work was supported in part by Project SQUID, which is supported by the U. S. Office of Naval Research, Department of the Navy, under Contract N6 ori-105-Task 3.

(2) (a) N. O. Stein, *Trans. Faraday Soc.*, **29**, 583 (1933); (b) W. H. Avery and G. S. Forbes, *J. Am. Chem. Soc.*, **60**, 1005 (1938).

(3) B. deB. Darwent and R. Roberts, *Proc. Roy. Soc. (London)*, **A216**, 344 (1953).

(4) D. A. Ramsay, *J. Chem. Phys.*, **20**, 1920 (1952).

(5) G. Porter, *Discussions Faraday Soc.*, **9**, 60 (1951).

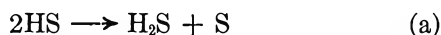
(6) B. deB. Darwent and R. Roberts, *ibid.*, **14**, 55 (1953).

(7) B. deB. Darwent and V. J. Krasnansky, *Symp. Combust., 7th, London*, 1958, 3 (1959).

(8) E. A. Moelwyn-Hughes, "Physical Chemistry," 2nd ed, Pergamon Press Ltd., London, 1961, p 610.

(9) N. Imai and O. Toyama, *Bull. Chem. Soc. Japan*, **33**, 652 (1960).

The second assumption involves the manner in which HS radicals disappear in the photolysis of H₂S.



Reactions a and b are the only plausible reactions and we therefore seek to distinguish between them.

Acetone was photolyzed in the presence of H₂S and a careful search made for H₂ in the products. No hydrogen was detected whereas we could have found it if it amounted to even less than 1% of the CH₄. The reaction



is known to be very fast. We used, typically, 5–10 torr of acetone and 5–45 torr of H₂S at temperatures between 140 and 220°. Under those conditions it is safe to conclude that virtually all the CH₃ radicals disappeared by reaction c. No CH₃SH was found. We have obtained good evidence¹⁰ that CH₃CO either decomposed or reacted with H₂S to form CH₃CHO and HS. Accordingly, reactions a and b are the only paths by which HS could disappear. The absence of detectable amounts of H₂ shows conclusively that $R_a \gg R_b$ so that the second assumption has been verified.

These results show that the photolysis of H₂S is an acceptable method for producing H atoms for kinetic studies, provided that an inert gas is present in large excess. The data in ref 6 may be erroneous owing to "hot" H atom effects.

(10) M. J. Allard, Ph.D. Dissertation, The Catholic University of America, 1965.

Ion-Solvent Interactions in Aqueous Lanthanide Solutions

by J. Padova

Radiochemistry Department, Soreq Nuclear Research Center, Israel Atomic Energy Commission, Yavne, Israel
(Received November 7, 1966)

Spedding and co-workers^{1,2} have recently determined the B coefficients of the Jones-Dole³ equation and partial molal volumes, \bar{V}_2° , at infinite dilution from viscosity and density measurements, respectively, of rare earth salts in aqueous solutions. For spherical hydrated ions it has been shown⁴⁻⁶ that

$$B = 2.5\bar{V}_h \quad (1)$$

where \bar{V}_h is the molar volume of the hydrated ion. Since⁷

$$\bar{V}_h = \bar{V}_2^\circ + n^\circ\bar{V}^\circ \quad (2)$$

where n° and \bar{V}° are the electrolyte solvation number deduced with respect to partial ionic volumes and partial molal volume of water at infinite dilution, it is possible to calculate the solvation number for each of the lanthanides concerned. The values of the ionic solvation numbers are obtained by taking for the chlo-

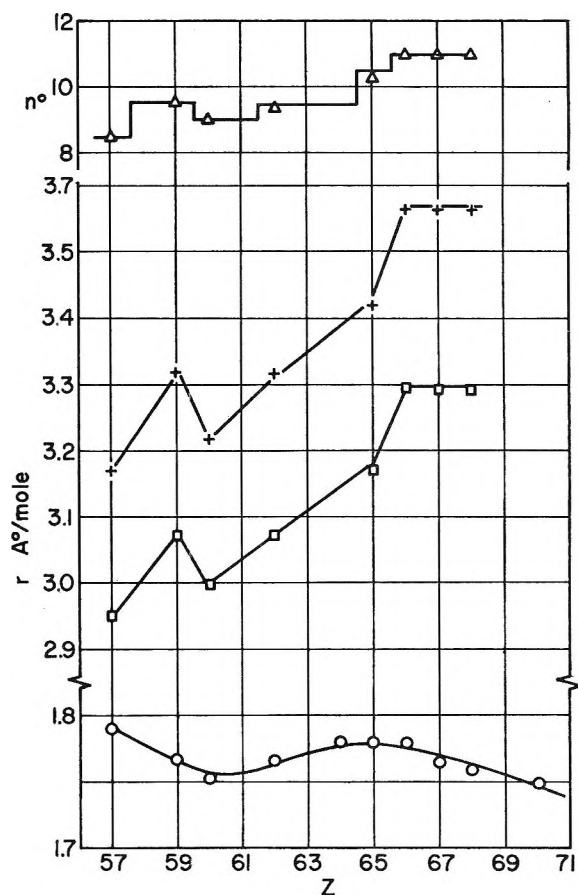


Figure 1. The solvation numbers and ionic radii of lanthanides in solution at infinite dilution: ○, r_e intrinsic radii; □, r_a (ref 9) + r_c (ref 10); Δ, n° .

- (1) F. H. Spedding and M. J. Pikal, *J. Phys. Chem.*, **70**, 2430 (1966).
- (2) F. H. Spedding, M. J. Pikal, and B. O. Ayers, *ibid.*, **70**, 2440 (1966).
- (3) G. Jones and M. Dole, *J. Am. Chem. Soc.*, **51**, 2959 (1929).
- (4) R. A. Robinson and R. H. Stokes, "Electrolyte Solutions," 2nd ed, Butterworth and Co. Ltd., London, 1959, p 305.
- (5) J. Padova, *J. Chem. Phys.*, **38**, 2635 (1963).
- (6) R. H. Stokes and R. Mills, "Viscosity of Electrolytes and Related Properties," 1st ed, Pergamon Press Ltd., London, 1965, p 49.
- (7) J. Padova, *Bull. Res. Council Israel*, **A10**, 63 (1961).

ride ion⁸ $n^\circ = 1$ and $\bar{V}_2^\circ = 18.60$ and may be seen in Figure 1 where they have been plotted *vs.* the atomic number Z , since the use of crystalline ionic radii is not a very good criterion for the interpretation of properties of species in solution. The solvation number increases somewhat irregularly from 8.5 for La^{3+} to 11 for Dy^{3+} , Ho^{3+} , and Er^{3+} , agreeing with the coordination number 9 for the rare earth ions from La^{3+} to Nd^{3+} but not with the coordination number 8 given² for Gd^{3+} to Er^{3+} . It is interesting to note that both sets are obtained from the same partial molar volume data.

However, since the ionic partial molal volume at infinite dilution does decrease smoothly with the intrinsic ionic radii,⁸ r_e , in solution, these have been calculated and are shown in Figure 1. The ionic radii of the hydrated volumes were computed by either Stokes and Robinson's expression⁹

$$\bar{V}_H = 4.35r_s^3$$

or from the relation of Conway, Verrall, and Desnoyers¹⁰

$$\bar{V}_H = 2.51r_e^3 + 3.15r_e^2$$

and are plotted on the same graph.

The trend is similar for r_s , r_e , and n° and slightly different for r_e , and clearly shows the variations observed in other properties.^{11,12}

(8) J. Padova, *J. Chem. Phys.*, **39**, 1552 (1963).

(9) R. H. Stokes and R. A. Robinson, *Trans. Faraday Soc.*, **53**, 301 (1957).

(10) B. E. Conway, R. E. Verrall, and J. E. Desnoyers, *Z. Physik. Chem. (Leipzig)*, **230**, 157 (1965).

(11) Y. Marcus, M. Givon, and G. R. Choppin, *J. Inorg. Nucl. Chem.*, **25**, 1457 (1963).

(12) I. Abrahamer, Ph.D. Thesis, Jerusalem, 1966.

The Relative Dissociation Constants of Hydrochloric, Hydrobromic, Hydriodic, Nitric, and Perchloric Acid in Pyridine. A Hydrogen Electrode Study

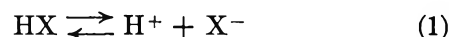
by L. M. Mukherjee and John J. Kelly

Chemistry Department, Polytechnic Institute of Brooklyn, Brooklyn, New York 11201 (Received December 27, 1966)

Previously reported potentiometric investigations of the acid-base equilibria in pyridine are extremely inadequate.¹ It has been shown, however, from previous conductance measurements^{2,3} that pyridine acts

as a differentiating solvent toward acids. The purpose of the present work is to elucidate the behavior of HCl, HBr, HI, HNO₃, and HClO₄ in pyridine through potentiometric measurements using a Pt|H₂(g) electrode (*vs.* a Zn(Hg)|ZnCl₂(s) reference electrode) and to establish the relative order of their dissociation constants.

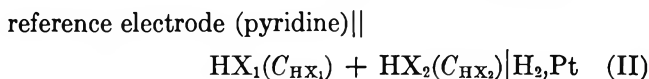
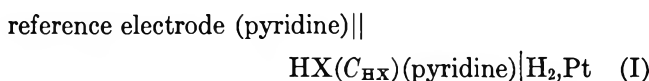
Assuming that an acid dissociates in pyridine according to



the over-all dissociation constant, K_{HX} , is given by

$$K_{\text{HX}} = \frac{a_{\text{H}^+} a_{\text{X}^-}}{a_{\text{HX}}} \quad (1a)$$

Accordingly, using the notations used previously,⁴ the emf values of cells I and II



at 25° can be represented by eq 2 and 3, respectively, provided the activity coefficients of all ionic species

$$\begin{aligned} E_{\text{HX}} &= E_{\text{ref}} + E_{\text{ij}} + \\ &0.02956 \log K_{\text{HX}} + 0.02956 \log [\text{HX}] \quad (2) \end{aligned}$$

$$\begin{aligned} E_{\text{HX}_1, \text{HX}_2} &= E_{\text{ref}} + E_{\text{ij}} + \\ &0.02956 \log (K_{\text{HX}_1} [\text{HX}_1] + K_{\text{HX}_2} [\text{HX}_2]) \quad (3) \end{aligned}$$

are considered equal and those of the uncharged molecules set equal to one. Furthermore, if the over-all dissociation constants are small, the equilibrium concentrations of the undissociated species can be replaced by the corresponding total analytical concentrations. Thus, eq 2 and 3, under such a situation, reduce to

$$\begin{aligned} E_{\text{HX}} &= E_{\text{ref}} + E_{\text{ij}} + \\ &0.02956 \log K_{\text{HX}} + 0.02956 \log C_{\text{HX}} \quad (4) \end{aligned}$$

and

$$\begin{aligned} E_{\text{HX}_1, \text{HX}_2} &= E_{\text{ref}} + E_{\text{ij}} + \\ &0.02956 \log (K_{\text{HX}_1} C_{\text{HX}_1} + K_{\text{HX}_2} C_{\text{HX}_2}) \quad (5) \end{aligned}$$

(1) (a) H. Angerstein, *Rocznik. Chem.*, **30**, 855 (1956); (b) J. S. Fritz and F. E. Gainer, *Talanta*, **13**, 939 (1966).

(2) A. Hantzsch and K. S. Caldwell, *Z. Physik. Chem. (Frankfurt)*, **61**, 227 (1908).

(3) (a) M. M. Davies, *Trans. Faraday Soc.*, **31**, 1561 (1935); (b) D. S. Burgess and C. A. Kraus, *J. Am. Chem. Soc.*, **70**, 706 (1948).

(4) (a) S. Bruckenstein and L. M. Mukherjee, *J. Phys. Chem.*, **66**, 2228 (1962); (b) L. M. Mukherjee, S. Bruckenstein, and F. A. K. Badawi, *ibid.*, **69**, 2537 (1965).

Table I: Potentiometric Study of Acid Mixtures (cf. eq 6)

	C_{HX_1}, M		C_{HX_2}, M	$\Delta E, v$	$\frac{pK_{HX_1} - pK_{HX_2}}$
HCl	1.52×10^{-2}	HNO ₃	2.87×10^{-2}	0.051	1.44
	1.52×10^{-2}		4.32×10^{-2}	0.056	1.43
	1.52×10^{-2}		6.64×10^{-2}	0.063	1.49
	1.98×10^{-2}		1.48×10^{-2}	0.041	1.495
	1.98×10^{-2}		3.95×10^{-2}	0.053	1.48
					Av 1.47 ± 0.02
HBr	7.83×10^{-3}	HNO ₃	1.43×10^{-2}	0.020	0.31
	7.83×10^{-3}		3.67×10^{-2}	0.031	0.34
	7.83×10^{-3}		5.58×10^{-2}	0.038	0.41
					Av 0.35 ± 0.04
HNO ₃	1.41×10^{-2}	HI	2.01×10^{-2}	0.022	0.50
	1.41×10^{-2}		3.12×10^{-2}	0.031	0.66
	1.41×10^{-2}		4.07×10^{-2}	0.036	0.73
					Av 0.63 ± 0.09
HNO ₃	2.12×10^{-2}	HClO ₄	2.79×10^{-2}	0.027	0.74
	2.12×10^{-2}		5.84×10^{-2}	0.035	0.72
	2.12×10^{-2}		7.04×10^{-2}	0.037	0.71
					Av 0.72 ± 0.01

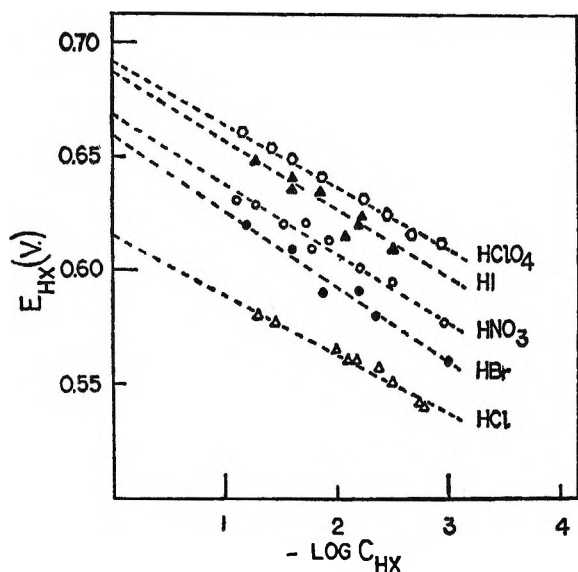


Figure 1. Plot of eq 4. Data fitted to $E_{HX} = A + B \log C_{HX}$. Least-squares constants given in the format HX, A, B are: HCl, 0.616, 0.0263; HBr, 0.660, 0.0337; HI, 0.687, 0.0305; HNO₃, 0.668, 0.0301; HClO₄, 0.692, 0.0277. Least-squares lines are shown in the figure.

where the C_{HX} terms denote analytical concentrations.

After substitution of HX by HX₁ in eq 4 and assuming that E_{ij} remains constant, one obtains eq 6 from the difference between the emf values of cell I and cell II

Table II: Summary of the Relative pK Values of Acids

HX	$\frac{pK_{HNO_3} - pK_{HX}}$
HCl	-1.74 ^a
	-1.47 ^b
Av -1.60 ± 0.13	
HBr	-0.24 ^a
	-0.35 ^b
Av -0.30 ± 0.05	
HI	+0.66 ^a
	+0.63 ^b
Av +0.64 ± 0.01	
HClO ₄	+0.84 ^a
	+0.72 ^b
Av +0.78 ± 0.06	

^a Cell I (using eq 4). ^b Cell I and cell II (using eq 6).

where both cells contain the same concentration C_{HX_1} of HX₁.

$$E_{HX_1, HX_2} - E_{HX_1} = \Delta E =$$

$$0.02956 \log \left(1 + \frac{K_{HX_2} C_{HX_2}}{K_{HX_1} C_{HX_1}} \right) \quad (6)$$

In the present case, eq 4 appears valid for each of the five acids studied, as shown by the linearity of the plot of E_{HX} vs. $\log C_{\text{HX}}$ (Figure 1) having slopes in good agreement with the expected value of 0.02956 v at 25°. In Table I the results of the mixture experiments together with the calculated ΔpK values for various acid pairs (*cf.* eq 6) are given. Table II presents a summary of the relative pK values (*vs.* HNO_3) calculated from the least-squares constants of the plot of eq 4 and those obtained from the experiments on acid mixtures using eq 6. The order of acid strengths $\text{HClO}_4 > \text{HI} > \text{HNO}_3 > \text{HBr} > \text{HCl}$, as shown by the present hydrogen electrode study, is the same as that found in earlier conductance studies^{2,3} and it further corroborates the "differentiating" effect of pyridine toward acids. However, our measurements with the pure acids (eq 4) and with the HNO_3 -HI and HNO_3 - HClO_4 mixtures (eq 6) yield (Table II) 0.64 and 0.78 for the average value of $pK_{\text{HNO}_3} - pK_{\text{HI}}$ and $pK_{\text{HNO}_3} - pK_{\text{HClO}_4}$, respectively, as compared to the available conductometric value³ of 1.07 and 1.18.

Acknowledgment. Acknowledgment is made to the donors of the Petroleum Research Fund, administered by the American Chemical Society, for partial support of this research.

Adiabatic Heating of Hydrazine by Flash

Photolysis. Nitrogen Formation with

Integrity of the N-N Bond

by L. J. Stief and V. J. DeCarlo

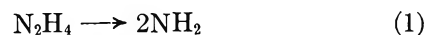
Research Division, Melpar, Inc., Falls Church, Virginia
(Received January 6, 1967)

The recent demonstration¹ that approximately 80% of the nitrogen formed in the direct photolysis of hydrazine results from reactions which do not involve the fission of the N-N bond has prompted us to examine the thermal decomposition of hydrazine for a similar effect. The photochemical experiments employed mixtures of hydrazine and hydrazine-¹⁵N and showed that the isotopic nitrogens formed in the photochemical decomposition were only 13% randomized.

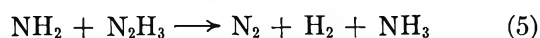
The thermal nature of the reaction in the flash photolysis of hydrazine has been reported by Ramsay² and verified by Husain and Norrish.³ The temperature attained in these systems was estimated to be in the range 1200–2000°K based on measurement of the rota-

tional² and vibrational³ temperature of the NH radical observed by kinetic spectroscopy. The utilization of the thermal effect in flash photolysis has been discussed.^{4,5}

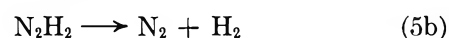
The adiabatic flash heating of hydrazine has been considered^{2,3} in terms of the reactions



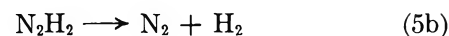
with reaction 3 taking place at high temperatures to explain the observation of NH under these conditions. The final products were considered³ in terms of the reactions



Reaction 4 represents the combination of N_2H_3 radicals and probably proceeds *via* the intermediate formation of tetrazane (N_4H_6). Based on the results of the oxidation in solution of hydrazine enriched with hydrazine-¹⁵N, combination of N_2H_3 radicals results in 50–100% randomization^{6,7} in the isotopic nitrogen produced depending on the mechanism of N_2 elimination from tetrazane. Cross-disproportionation of NH_2 and N_2H_3 (reaction 5) probably proceeds *via* intermediate formation of diimide (N_2H_2)



This would not lead to isotopic mixing in the nitrogen since the N_2 formed comes from a single molecule of hydrazine by successive dehydrogenation. Disproportionation^{1,7} of N_2H_3



would be an equally plausible source of N_2 and would also lead to a lack of mixing of isotopic nitrogen. Thus, an examination of the distribution of the isotopic ni-

(1) L. J. Stief and V. J. DeCarlo, *J. Chem. Phys.*, **44**, 4638 (1966).

(2) D. A. Ramsay, *J. Phys. Chem.*, **57**, 415 (1953).

(3) D. Husain and R. G. W. Norrish, *Proc. Roy. Soc. (London)*, **A273**, 145 (1963).

(4) G. Porter in "Techniques of Organic Chemistry," Vol. VIII, Part II, 2nd ed, John Wiley and Sons, Inc., New York, N. Y., 1963, p 1055, Chapter 19.

(5) R. G. W. Norrish, *Chem. Brit.*, **1**, 289 (1965).

(6) W. C. E. Higginson and D. Sutton, *J. Chem. Soc.*, 1402 (1953).

(7) J. W. Cahn and R. E. Powell, *J. Am. Chem. Soc.*, **76**, 2568 (1954).

Table I: Formation of Isotopic Nitrogens in Adiabatic Flash Heating of Mixtures of Hydrazine and Hydrazine-¹⁵N

Sample pressure, torr		Relative amount of product			$\frac{(^{29}\text{N}_2)^2 / (^{28}\text{N}_2)(^{30}\text{N}_2)^d}{\text{Orig data}}$		H ₂ /N ₂
²⁸ N ₂ H ₄	³⁰ N ₂ H ₄	²⁸ N ₂	²⁹ N ₂	³⁰ N ₂	Cor ^e data		
...	1.0 ^a	17.2	12.0	100	0.7
0.3	0.7 ^b	100	40.3	154	0.11	0.03	1.1
0.3	0.7 ^b	100	33.3	140	0.08	0.03	0.9
0.5	0.5 ^b	100	11.6	20.8	0.06	0.04	1.1
0.5	0.5 ^c	100	9.7	19.8	0.05	0.03	0.7
1.0	...	100	1.7	1.0	1.0

^a The hydrazine-¹⁵N was prepared by photolysis (1849 Å) of ammonia-¹⁵N (97.3% ¹⁵N, Merck Sharp and Dohme Ltd. of Canada) and is 82% ¹⁵N based on the isotopic nitrogen formed. ^b ³⁰N₂H₄ introduced into the cell first. ^c ²⁸N₂H₄ introduced into the cell first. ^d Measure of randomization independent of relative concentration of labeled and unlabeled species; value of 4 = 100% randomization. ^e Corrected for ²⁹N₂ and ²⁸N₂ formed from decomposition of incompletely labeled ³⁰N₂H₄.

trogen formed in the adiabatic flash heating of mixtures of hydrazine and hydrazine-¹⁵N should enable an evaluation to be made of the relative importance in this system of radical-radical combination to radical-radical disproportionation.

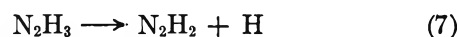
The results of such experiments are shown in Table I. The total pressure in the 75-cc cylindrical quartz reaction vessel was 1 torr and a single 720J flash (160 μf, 3 kv) was sufficient to decompose about 10% of the hydrazine. Separate experiments indicated no detectable decomposition (<0.1%) in the absence of the flash. The relatively low yields of ²⁹N₂ suggest that radical-radical disproportionation is considerably more important than radical-radical combination in the adiabatic flash heating of hydrazine.

The average value of the ratio $(^{29}\text{N}_2)^2 / (^{28}\text{N}_2)(^{30}\text{N}_2)$, when corrected for incomplete labeling in the ³⁰N₂H₄, is 0.033. From this value, the nitrogen isotopes are estimated to be 17% randomized. Thus, by identifying nonrandomization in N₂ formation with disproportionation and randomization in N₂ with combination, we conclude that the ratio of the nitrogen formed by disproportionation (reactions 5 and 6) to those formed by combination (reaction 4) is about 5:1. This assumes that N₂H₃ combination leads to 100% randomization and that there are no other reactions resulting in nitrogen formation.

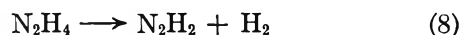
The excess ²⁸N₂ formed in the decomposition of 1:1 mixtures of hydrazine-¹⁵N is unexpected but reproducible; a unique explanation for this result cannot be given at the present time.

It may be noted that the ratio of H₂ to N₂ is approximately unity in all the experiments reported here. Thus the decomposition of N₂H₂ (reaction 5b) as the immediate source of both N₂ and H₂ is consistent not only with the lack of mixing in the isotopic nitrogen, but also with the ratio of H₂ to N₂ in the products.

These results could also be explained by decomposition of N₂H₃ to diimide



or by direct formation of N₂H₂ from hydrazine



followed by decomposition of N₂H₂ (reaction 5b). However, these reactions would not explain the production of NH₂ and NH observed by kinetic spectroscopy.^{2,3}

The present observation that disproportionation reactions are considerably more important than combination reactions in this system is an unexpected result in view of the fact that little prominence has been given to disproportionation reactions in the thermal decomposition of hydrazine. Indeed, disproportionation of N₂H₃ has not, to our knowledge, previously been considered in mechanisms for the thermal decomposition of hydrazine.

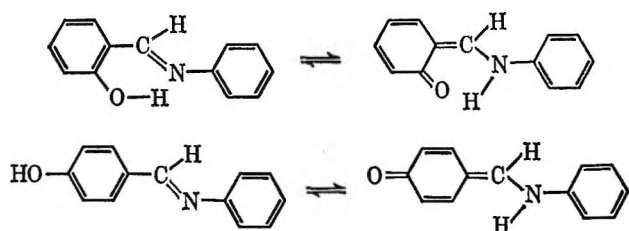
Acknowledgment. We wish to thank Walter Payne for his assistance in conducting the experiments.

Tautomerism of *N*-*o*-Hydroxybenzylidene Anils in Nonacidic Solvents

by John W. Ledbetter, Jr.

*Department of Chemistry, University of Kentucky,¹
Lexington, Kentucky (Received May 16, 1966)*

In a previous paper² evidence was cited for the enol imine-keto enamine tautomerism of *N*-*o*- and *N*-*p*-hydroxybenzylidene anils in solvents having an acidic hydrogen.



It was concluded that the tautomerism occurred as a result of hydrogen bonding between the solvent acidic hydrogen and the imine nitrogen of the anil. This tautomerism was discussed and references were cited in a previous paper.² There was still concern, however, whether the intramolecular hydrogen bond of *N*-*o*-hydroxybenzylidene anils would give rise to the tautomerism in solvents not having an acidic hydrogen.

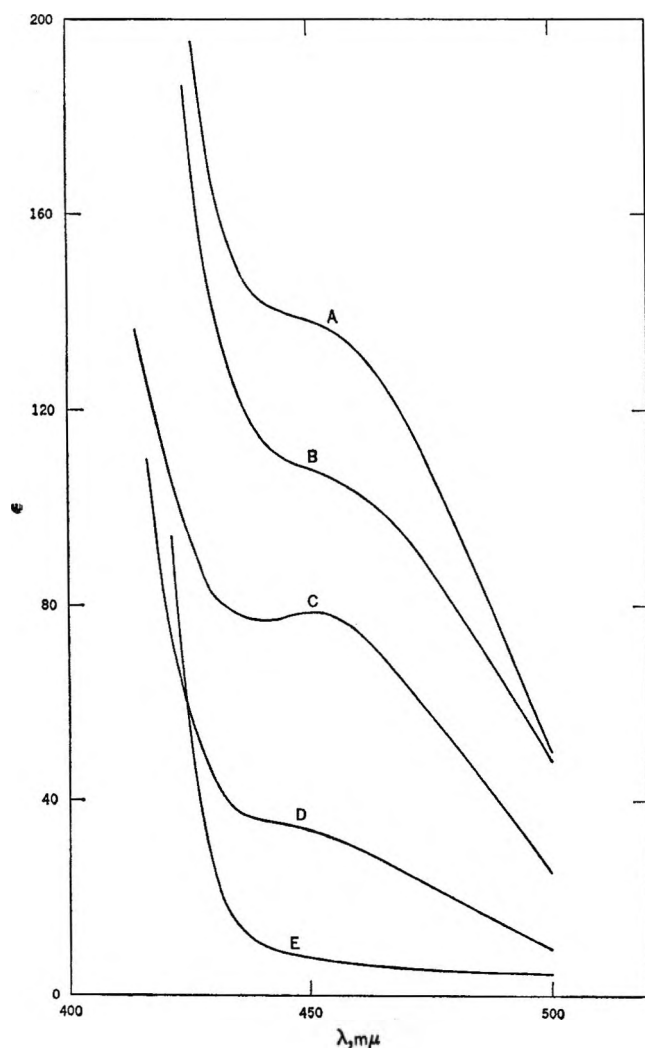


Figure 1. Spectra of *N*-*o*-hydroxybenzylidene-*o*-hydroxyaniline in: A, *N,N'*-dimethylformamide; B, pyridine; C, methyl formate; D, methyl acetate; E, cyclohexane.

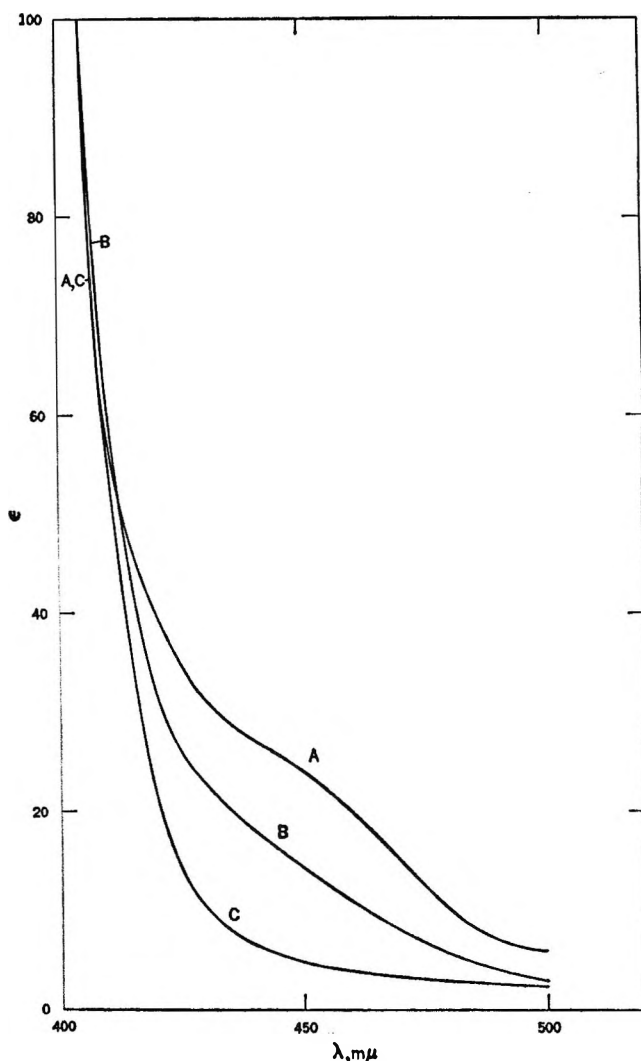


Figure 2. Spectra of *N*-*o*-hydroxybenzylideneaniline in: A, methyl formate; B, acetone; C, cyclohexane.

It has now been found that these *o*-hydroxy anils exhibit the tautomerism in nonprotonic solvents, but significantly less than in the proton-donating solvents. *N*-*p*-Hydroxybenzylidene anils were found to give no response in nonprotonic solvents, demonstrating that the tautomerism does occur *via* the intramolecular hydrogen-bond bridge in these solvents. Recently, Dudek³ has shown by pmr measurements and ultraviolet spectra that *N*-*o*-hydroxybenzylidene anils exhibit the tautomerism in alcoholic solution.

The compounds prepared in the laboratory for the investigation were *N*-*o*-hydroxybenzylidene-*o*-hydroxy-

(1) Visiting Appointment. New address: Department of Chemistry, Medical College of South Carolina, Charleston, S. C.

(2) J. W. Ledbetter, *J. Phys. Chem.*, **70**, 2245 (1966).

(3) G. O. Dudek and E. P. Dudek, *J. Am. Chem. Soc.*, **88**, 2407 (1966).

aniline, *N-p*-hydroxybenzylidene-*p*-hydroxyaniline, *N-o*-hydroxybenzylideneaniline, and *N-p*-hydroxybenzylideneaniline. The melting points and the elemental analyses were in agreement with the literature and theory, respectively.

Most of the solvents for recording the spectra were of spectral quality. Anhydrous ethyl ether, ethyl acetate, methyl ethyl ketone, cyclohexanone, and acetonitrile were of reagent quality and the methyl acetate was chromatographic quality.

The spectra were recorded at 10^{-3} *M* concentration in 1.00-cm quartz cells with a Cary Model 15 recording spectrophotometer. The instrument was calibrated in the wavelength of interest with a holmium oxide filter.

In the earlier work, the tautomerism in acidic sol-

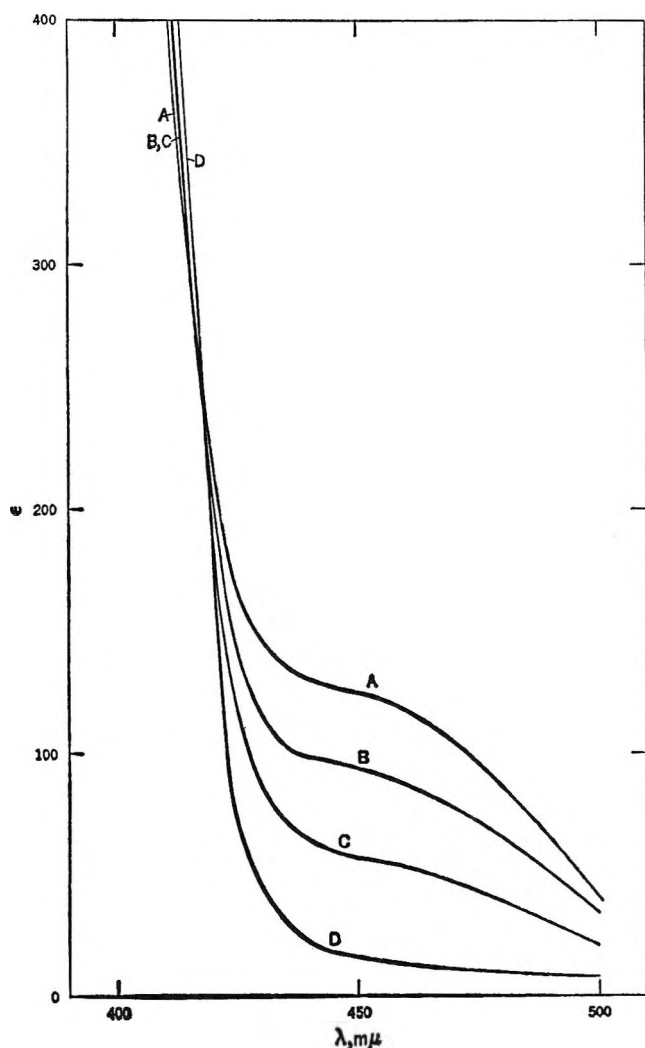


Figure 3. Spectra of *N-o*-hydroxybenzylidene-*o*-hydroxyaniline in carbon tetrachloride-*N,N'*-dimethylformamide: A, DMF; B, 60% CCl_4 -40% DMF; C, 90% CCl_4 -10% DMF; D, CCl_4 .

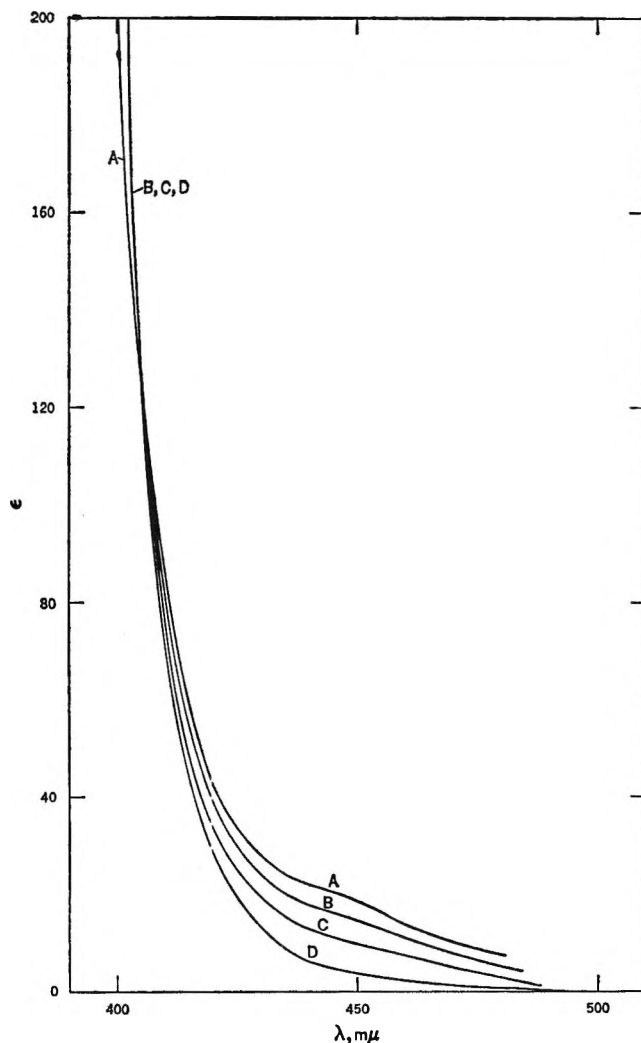


Figure 4. Spectra of *N-o*-hydroxybenzylideneaniline in carbon tetrachloride-*N,N'*-dimethylformamide: A, DMF; B, 60% CCl_4 -40% DMF; C, 80% CCl_4 -20% DMF; D, CCl_4 .

vents was observed by the formation of an additional electronic absorption band. This band, which was solvent dependent, occurred at about $440 \text{ m}\mu$ for the less acidic solvents and shifted to $390 \text{ m}\mu$ for sulfuric acid. The determination of electronic absorption spectra of the above *o*-hydroxy anils at high concentration in a variety of nonprotonic solvents shows a very weak band appearing as a shoulder or tail at about $451 \text{ m}\mu$. This is shown in Figures 1 and 2. The corresponding *p*-hydroxy anils do not show a band formation in this region. The molar extinction coefficients at $451 \text{ m}\mu$ for the compounds in the various solvents are tabulated in Table I. Rather than trying to estimate any wavelength shift with solvent, $451 \text{ m}\mu$ was chosen since Figure 1 shows a defined peak at $451 \text{ m}\mu$ for methyl formate.

Isobestic points were found for the *o*-hydroxy anils in the carbon tetrachloride-*N,N'*-dimethylformamide solvent system. Figures 3 and 4 show these occurring at 414 $m\mu$ for *N-o*-hydroxybenzylidene-*o*-hydroxyaniline and at 404 $m\mu$ for *N-o*-hydroxybenzylideneaniline. This definitely points out the existence of two molecular absorbing species in each system.

Table I: Solvent Effects on the Absorbance of Anils at 451 $m\mu$

Solvent	Molar extinction coefficient ^a			
	I	II	III	IV
Cyclohexane	8	...	5	...
Carbon tetrachloride	15	...	5	...
Ethyl ether	19	...	8	...
Ethyl acetate	24	7	8	Zero
Methyl acetate	33	...	13	...
<i>p</i> -Dioxane	36	7	13	Zero
Methyl ethyl ketone	45	...	15	...
Acetone	54	7	15	Zero
Cyclohexanone	55	...	15	...
Methyl formate	79	7	22	Zero
Pyridine	107	...	18	...
<i>N,N'</i> -Dimethylformamide	125	7	18	Zero
Acetonitrile	124	...	24	...
<i>N,N'</i> -Dimethylacetamide	138	8	21	Zero

^a I, *N-o*-hydroxybenzylidene-*o*-hydroxyaniline; II, *N-p*-hydroxybenzylidene-*p*-hydroxyaniline; III, *N-o*-hydroxybenzylideneaniline; IV, *N-p*-hydroxybenzylideneaniline.

The additional band occurring only with the *o*-hydroxy anils implies the necessity of the intramolecular hydrogen-bond bridge in nonprotonic solvents. From the low intensity of the band, the extent of the tautomerism must be very small. In cyclohexane it might be said that the tautomerism does not even occur. It is further evident that the tautomerism increases generally with the dielectric constant. This was realized earlier with the protonic solvents. In Table I it is evident that anil I tautomerizes to a greater degree than anil III. This was observed in the protonic solvents and was explained in the previous paper.

It appears, therefore, that the tautomerism of *N-o*-hydroxybenzylidene anils occurs in a variety of solvents. In nonprotonic solvents the tautomerism occurs only weakly and as a result of intramolecular hydrogen bonding. In protonic solvents the process is greatly enhanced owing to strong intermolecular hydrogen bonding and also occurs in the *p*-hydroxy derivatives. The essential theme of the tautomerism is hydrogen bonding with the imine nitrogen of the anil.

Correlation of Spectra of the Monosubstituted Benzenes and Their Hydroxy Radical Adducts

by B. Cercek

Paterson Laboratories, Christie Hospital and Holt Radium Institute, Manchester 20, England

Accepted and Transmitted by The Faraday Society (December 30, 1966)

In monosubstituted benzenes there is a regularity in the bathochromic shifts of the primary benzene absorption band.¹ The amount of shift is correlated to the magnitude of the resonance and inductive interactions of the substituents with the benzene ring.²

Optical spectra of the transients produced by the reaction of OH radicals with monosubstituted benzenes were obtained by pulse radiolysis.³ The positions of the absorption maxima of these transients are recorded in Table I. These and other reported spectra of OH adducts^{4,5} show the absorption band of the hydroxycyclohexadienyl radical at 313 nm to be displaced in an analogous way to that of the benzene at 203.5 nm in the monosubstituted derivatives. In Figure 1 are plotted

Table I: Maxima of the $\cdot\text{HO}\text{C}_6\text{H}_5\text{-X}$ Absorption Spectra

-X	λ_{max} , nm, and estimated uncertainty	References
1. $-\text{NO}_2$	410 \pm 3	This work
2. $-\text{SO}_2\text{NH}_2$	330 \pm 4	
3. $-\text{I}$	318 \pm 3	
4. $-\text{SO}_3\text{H}$	320 \pm 3	
5. $-\text{Cl}$	322 \pm 5	Mean value of this work and ref 4
6. $-\text{COOH}$	350 \pm 4	
7. $-\text{CO}_2^-$	332 \pm 5	Mean value of this work and ref 5
8. $-\text{NH}_2$	350 \pm 5	E. J. Land
9. $-\text{OCH}_3$	330 \pm 5	
10. $-\text{COC}_6\text{H}_5$	380 \pm 5	
11. $-\text{CHO}$	370 \pm 5	B. Chutny
12. $-\text{COCH}_3$	370 \pm 5	
13. $-\text{CN}$	340 \pm 5	

(1) H. H. Jaffé and M. Orchin, "Theory and Applications of Ultraviolet Spectroscopy," John Wiley and Sons, Inc., London, 1962, p 256.

(2) F. A. Matsen, *J. Am. Chem. Soc.*, **72**, 5243 (1950).

(3) J. P. Keene, *J. Sci. Instr.*, **41**, 493 (1964).

(4) L. M. Dorfman, I. A. Taub, and R. E. Bühler, *J. Chem. Phys.* **36**, 305 (1962).

(5) D. F. Sangster, *J. Phys. Chem.*, **70**, 1712 (1966).

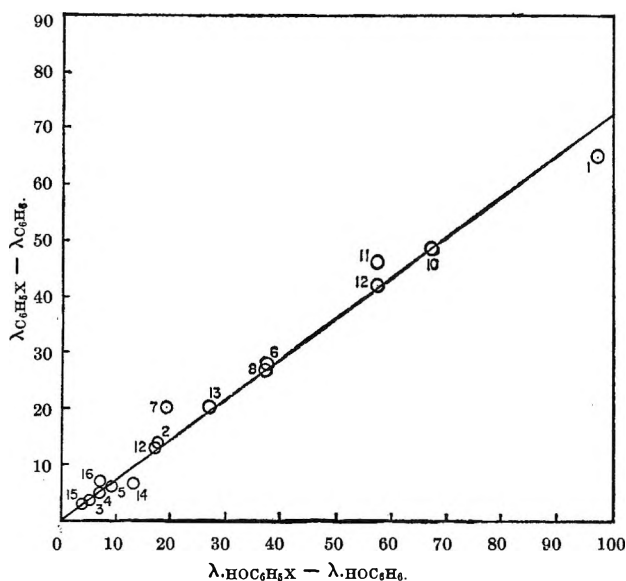


Figure 1. Correlation of the bathochromic shifts in the monosubstituted benzenes and hydroxycyclohexadienyl radicals. Numbers refer to substituents 1–13 as given in Table I, including 14 (Br); 15 (CH₃), and 16 (OH) from ref 4.

the amounts of bathochromic shift of the monosubstituted benzene derivatives *vs.* those of the corresponding hydroxycyclohexadienyl radical. The correlation coefficient, a measure of the tightness of the correlation, is 0.92. The average bathochromic shift of the primary absorption band is 0.73 times smaller for the benzene ring than for the hydroxycyclohexadienyl structure. However, if the relative shifts $(\lambda_{C_6H_5X} - \lambda_{C_6H_6})/\lambda_{C_6H_5X}$ and $(\lambda_{HOC_6H_5X} - \lambda_{HOC_6H_6})/\lambda_{HOC_6H_5X}$ are calculated these are 13% greater for the parent aromatic compound.

Acknowledgments. The author wishes to thank Dr. M. Ebert for his helpful discussions of this note and Drs. E. J. Land and B. Chutny for allowing him to use some of their unpublished spectra of the monosubstituted benzene OH radical adducts.

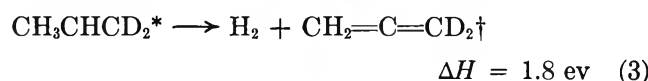
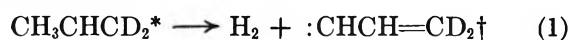
Photolysis of Propene at 1470 Å

by E. Tschuikow-Roux¹

National Bureau of Standards, Washington, D. C. 20234
(Received September 21, 1966)

The vacuum ultraviolet photolysis of propene has recently been reported by Becker, Okabe, and McNesby,² and primary processes for the decomposition of the excited propene molecule have been delineated.

Based on the finding that nearly two-thirds of the hydrogen in the photolysis of CH₃CHCD₂ is H₂, two possible mechanisms for the production of allene were suggested: (a) carbene elimination of H₂ from the methyl group, reaction 1, followed by isomerization of the allylidene, reaction 2, and (b) direct olefin elimination of H₂, reaction 3.



Propyne is also formed in an amount comparable to allene. Thus isomerization of the excited allene, formed in reactions 2 or 3 with a maximum possible excess energy of 6.6 eV, occurs. Propyne may also result directly from a rearrangement of the allylidene



Whether structural isomerization of the excited allylidene to form cyclopropene also occurs was not discussed. Recently, it has been shown that isobutylidene produced in the gas-phase photolysis of isobutane at 1470 Å undergoes intramolecular insertion to form methylcyclopropane (MCP) in competition with the isomerization to isobutene.³ It was therefore of interest to explore the possibility of allylidene formed in the photolysis of propene undergoing an analogous intramolecular cyclization, in this case to form cyclopropene. As may be seen from Table I, this expectation was not borne out. The present results, however, do show some novel features and confirm an earlier surmise in the photolysis of propene. They also differ to some degree in the observed product distribution from those previously reported. Since this is relevant in the assessment of the importance of the various primary processes, they are reported here.

Experimental Section

The light source was a sealed, electrodeless xenon discharge lamp operated from a 10 to 100-w microwave power generator at 2450 MHz (Raytheon Model PGM-10). With liquid oxygen as refrigerant, the monochromatic purity of the 1470-Å resonance line of Xe was demonstrated by means of a vacuum

(1) National Academy of Sciences-National Research Council Postdoctoral Research Associate, 1965–1966. Address correspondence to Department of Chemistry, University of Calgary, Calgary, Alberta, Canada.

(2) D. A. Becker, H. Okabe, and J. R. McNesby, *J. Phys. Chem.*, **69**, 538 (1965).

(3) E. Tschuikow-Roux and J. R. McNesby, *Trans. Faraday Soc.*, **62**, 2158 (1966).

Table I: Product Distribution in the Photolysis of Propene at 1470 Å and 25°

	% product	
	This work; 0.6% con- version; $P_{\text{C}_3\text{H}_6} =$ 40 torr	Ref 2; ^a 0.2% con- version; $P_{\text{C}_3\text{H}_6} =$ 10 torr
H ₂	12.6	6.6
CH ₄	4.8	3.0
C ₂ H ₂	24.7	33.1
C ₂ H ₄	6.7	10.6
C ₂ H ₆	4.5	6.4
C ₃ H ₈	...	~6.4
Propyne	...	~6.4
C ₃ H ₈ + propyne	11.7	...
Allene	15.6	6.4
Cyclopropene	0.0	...
<i>i</i> -C ₄ H ₁₀	14.7	10.0
(C ₄ H ₉ -1) + (<i>i</i> -C ₄ H ₈)	2.6	3.1
<i>n</i> -C ₄ H ₁₀	1.5	...
<i>trans</i> -Butene-2	0.16	6.3
Methylcyclopropane	0.14	...
<i>cis</i> -Butene-2	0.12	1.7
<i>i</i> -C ₅ H ₁₂	0.16	...
H ₂ /CH ₄	2.6	2.2
Mass balance	C ₃ H _{5.7}	C ₃ H _{6.4}

^a Data recalculated to include propyne and propane.

ultraviolet monochromator in the wavelength region 1050–2100 Å. Radiation of $\lambda > 2100$ Å is of no consequence since propene does not absorb at these longer wavelengths.⁴ Epoxy cement was used to seal the lithium fluoride window to the lamp body. The lamp was then connected to the reaction vessel by means of a ground-glass joint with Apiezon W wax. The design of the lamp–reaction vessel assembly was such that neither the epoxy nor the W wax was exposed to the ultraviolet radiation; however, as a precautionary measure, photolyses with pure helium (as carrier gas) were carried out in the usual way and analyzed for decomposition products. None was found.

Research grade propene with no detectable impurities was used without further purification. The system was mercury free. During photolysis, the contents of the reaction vessel were continuously circulated by means of a Watson pump to assure complete mixing and to minimize secondary processes. The maximum conversion was kept below 1%.

The progress of the photolysis was followed by expanding the gases into a small sampling volume (less than 1% of the reaction vessel volume) and withdrawing samples for analysis through a septum by means of a

1-cc Hamilton gas syringe which had been flushed with helium. The hydrocarbon products were analyzed using two gas chromatographs with flame ionization detectors. One of these was equipped with a 6-m long column of 20% Squalane on Chromosorb-P (column I); in the second, a column of 20% Squalene (5.2 m) in series with 1.2 m of silver nitrate saturated triethylene glycol, both on Chromosorb-P (column II), was used. With two exceptions, the resulting chromatograms gave a complete resolution of all hydrocarbon products. Calibrations were carried out with a standard gas mixture prepared from commercially available gases, cyclopropene excepted. The latter was synthesized according to the simple method of Closs and Krantz.⁵ The hydrogen–methane ratio was determined mass spectrometrically.

Results

The results of product analysis are listed in Table I. Also included are the results of Becker, *et al.*,² recalculated to include propyne and propane. While there is reasonable agreement for the lighter hydrocarbon products, the relative hydrogen yield in the present work is 1.9 times higher. A possible reason for this discrepancy may lie in the fact that, unlike the rest of their photolysis products, Becker, *et al.*, determined the hydrogen–methane distribution from separate experiments in a static, noncirculating system which is suspect to secondary reactions in the vicinity of the cell window. In order to establish if secondary reactions were involved in the present work, ratios of product/propene were plotted as a function of photolysis time and found to be linear, thus indicating that secondary reactions were absent or negligible. Propyne and propane could not be effectively separated using the Squalane column I, while on column II propyne was irreversibly absorbed and propane could not be isolated from the large parent C₃H₈ peak. However, detailed calibrations (column I) showed that the value reported in Table I as (propyne + C₃H₈) was mostly C₃H₄. Becker, *et al.*, using a column of an unspecified nature but different from Squalane (used throughout their work), indicated that propyne and propane were present, each approximately equal to allene (Table I). Unfortunately, this question cannot be resolved for lack of further information.

The analysis of methylcyclopropane in the presence of the butenes was carried out with column II, excellent separation being obtained. In contrast, the Squalane

(4) J. A. R. Samson, F. F. Marmo, and K. Watanabe, *J. Chem. Phys.*, **36**, 783 (1962).

(5) G. L. Closs and K. D. Krantz, *J. Org. Chem.*, **31**, 638 (1966).

column was found to be inadequate for the separation of the C_4H_8 species. In view of this, the large amount of *trans*-butene-2 reported by Becker, *et al.*, appears to be an error in analysis.

Discussion

If all the hydrogen produced resulted from reactions 1 and 3, the H_2 yield should be equal to the total C_3H_4 yield. There is, however, another H_2 contribution from reactions of H atoms. Thus Becker, *et al.*, have shown that of the total hydrogen produced in the photolysis of an equimolar mixture of $C_3H_6 + C_3D_6$, 11% is in the form of HD. Addition of 15% of NO had the effect of lowering this HD yield to 3%. In order to account for the observed HD, it was proposed that H abstraction from propene, reaction 5,



is competitive with H-atom scavenging, reaction 6



The net effect of reaction 5 is that it provides an additional source of H_2 and leads to the prediction that $C_3H_4/H_2 < 1$. As may be seen from Table I, while there is no evidence for cyclopropene, the sum of allene plus propyne is considerably greater than H_2 ; *i.e.*, $C_3H_4/H_2 = 2.2$, in marked disagreement with the above prediction. Therefore, it is suggested that in addition to reactions 1 and 3, C_3H_4 may also be formed by the simultaneous expulsion of two hydrogen atoms



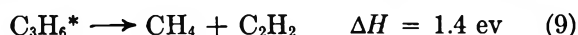
An analogous mechanism has been shown to be operative in the case of ethylene photolysis at 1470 Å.⁶

Aside from reaction 7, the principal source of H atoms is derived from the formation of acetylene, the major hydrocarbon product. For its principal mode of formation, Becker, *et al.*, suggested the consecutive rupture of C-C and C-H bonds, the over-all process being

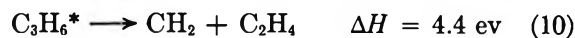


It is clear that only a small fraction of the hydrogen atoms produced in reactions 7 and 8 ultimately result in H_2 from either H-abstraction or association reactions, and it is necessary to conclude that the bulk of H atoms is scavenged in reaction 6.

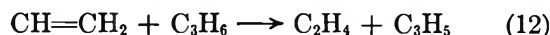
The fact that the ratio $C_2H_2/CH_4 = 5.1$ is less than half the ratio previously reported² indicates that the molecular elimination of methane, reaction 9, may have a greater relative importance than had been suggested.



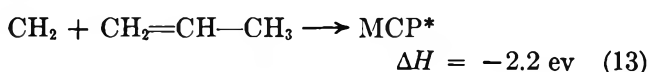
The ethylene is formed by molecular elimination



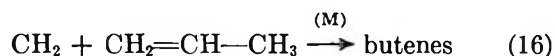
as well as by way of vinyl radicals²



It was also suggested that methylene produced in reaction 10 reacts with propene leading to butene formation. The existence of excited methylcyclopropane (MCP*) as an intermediate was invoked, although because of analytical difficulties, no MCP was observed. This suggestion is confirmed in the present work where MCP has been identified, together with the four butenes, as small but definite reaction products



The four butene isomers are also formed, to some extent, from the direct insertion reaction of methylene in propene⁷



Butler and Kistiakowsky⁷ have shown that the relative rates of attack of methylene on the C=C bond and the three types of C-H bonds in C_3H_6 depend on the source of methylene, and that differentiation in the rate of attack decreases with increasing energy of CH_2 . In systems where methylene resulted from the photolysis of ketene at 3100 and 2600 Å, and diazomethane using polychromatic radiation, Butler and Kistiakowsky's data give, in the high pressure limit, the relative rates of addition (13) to the insertion processes (16) as $k_{13}/k_{16} = 8.4, 4.6,$ and 3.5 , respectively. Further, the sum of *i*- C_4H_8 plus C_4H_8-1 arising from the isomerization of excited MCP is approximately equal to the sum of *cis*- plus *trans*- C_4H_8-2 independent of pressure, and butene-1 is 2 or 3 times larger than *i*- C_4H_8 .⁷ Therefore, from Table I it is clear that CH_2 plus C_3H_6 reactions account for only a small fraction of the total butenes, and that the value reported as ($C_4H_8-1 + i$ - C_4H_8) is more than 96% butene-1. The large amount of *trans*- and *cis*-butene-2 reported by Becker, *et al.*, appears to be in error.

Butene-1 results most likely from an association

(6) H. Okabe and J. R. McNesby, *J. Chem. Phys.*, **36**, 601 (1962).

(7) J. N. Butler and G. B. Kistiakowsky, *J. Am. Chem. Soc.*, **82**, 759 (1960).

reaction of CH_3 plus $\text{CH}_2=\text{CH}-\text{CH}_2$ radicals. The methyl radicals are formed in reaction 8 and are the



precursors of ethane, while allyl radicals results from H-atom abstraction from propene, reaction 5.²

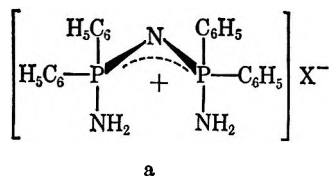
The relatively large yield of isobutane provides evidence that scavenging of H atoms by propene to form isopropyl radicals followed by their association with methyl radicals is an important reaction. The preferential addition of H atoms to the terminal carbon is demonstrated by the relative yield of isobutane to n-butane, this ratio being 10:1.

Conductance Studies of Ammonium and Phosphonitrimium Salts in Acetonitrile at 25°¹

by Ismail Y. Ahmed and C. D. Schmulbach²

Department of Chemistry, The Pennsylvania State University,
University Park, Pennsylvania (Received November 28, 1966)

The nature of solute species in acetonitrile is of increasing interest because of expanded use of acetonitrile as a reaction solvent.³ Conductance measurements were made on a series of typical 1:1 electrolyte ammonium salts as well as phosphonitrimium salts of type a where X is Cl^- ⁴ and SbCl_6^- .⁵ The principal



objectives were to establish the extent of association of ions (ion-pair formation) in acetonitrile and to elucidate the nature of the solute phosphonitrimium salts.

Experimental Section

Purification of Acetonitrile and Conductance Measurements. Acetonitrile (Fisher Certified reagent) was purified by the method described by Coetzee.⁶ The distillation apparatus together with the conductance cells and bridge are described elsewhere.⁷ The specific conductance of the purified solvent was in the range of $0.8-1.7 \times 10^{-7} \text{ ohm}^{-1} \text{ cm}^{-1}$ at 25°. This compares

well with previously reported values of $0.7-1.5 \times 10^{-7}$ and $1-2 \times 10^{-7} \text{ ohm}^{-1} \text{ cm}^{-1}$.⁹ Values of $2-5 \times 10^{-8} \text{ ohm}^{-1} \text{ cm}^{-1}$ have recently been reported.¹⁰

Purification of Salts. Compound I, $[(\text{C}_6\text{H}_5)_4\text{P}_2\text{N}_3\text{H}_4]\text{Cl}$, was prepared by a method previously described.¹¹ It was recrystallized from acetonitrile and dried for 2 hr under vacuum at 110°, mp 244–246°.

Compound II, $[(\text{C}_6\text{H}_5)_4\text{P}_2\text{N}_3\text{H}_4]\text{SbCl}_6$, was provided by Dr. C. Derderian. This compound was recrystallized from carbon tetrachloride and petroleum ether and dried at 25° *in vacuo* for several hours. The pale yellow crystals melted sharply at 143–144°.

A suspension of 6.30 g (0.038 mole) of tetraethylammonium chloride (Eastman White Label) in 200 ml of anhydrous dichloroethane was cooled in a Dry Ice-acetone bath. An excess of boron trichloride (Matheson) was added from a syringe. The solution was allowed to warm to room temperature to give a homogeneous solution. White needlelike crystals of tetraethylammonium tetrachloroborate precipitated upon cooling and were filtered from the chilled solution. The crystals were washed several times with chilled dichloroethane and dried under vacuum overnight at room temperature. The solid melted with decomposition to a brown liquid at 165–170° in a sealed ampoule. *Anal.* Calcd for $\text{C}_8\text{H}_{20}\text{NBCL}_4$: C, 33.95; H, 7.07; N, 4.49; Cl, 50.20. Found: C, 33.73; H, 7.09; N, 4.89; Cl, 49.80. Elemental analyses were performed by Galbraith Laboratories, Knoxville, Tenn.

Tetraethylammonium chloride and tetraethylammonium perchlorate were Eastman White Label and were used without further purification.

Results

The results of conductance measurements are summarized in Table I. The limiting molar conductance was calculated by means of the Onsager equation. A

- (1) Supported in part by the National Science Foundation.
- (2) To whom all correspondence should be addressed at the Department of Chemistry, Southern Illinois University, Carbonale, Ill.
- (3) See R. A. Walton, *Quart. Rev.* (London), **19**, 126 (1965).
- (4) I. I. Bezman and J. H. Smalley, *Chem. Ind.* (London), 839 (1960).
- (5) C. Derderian, Doctoral Thesis, The Pennsylvania State University, 1966.
- (6) J. F. Coetzee, G. P. Cunningham, D. C. McGuire, and G. R. Padmanaphan, *Anal. Chem.*, **34**, 1139 (1962).
- (7) I. Ahmed, Master's Thesis, The Pennsylvania State University, 1965.
- (8) I. M. Kolthoff, S. Bruckenstein, and M. K. Chantooni, *J. Am. Chem. Soc.*, **83**, 3927 (1961).
- (9) I. M. Kolthoff, M. K. Chantooni, and J. W. Wallis, *ibid.*, **85**, 426 (1963).
- (10) J. F. Coetzee and G. P. Cunningham, *ibid.*, **87**, 2529 (1965).
- (11) C. D. Schmulbach and C. Derderian, *J. Inorg. Nucl. Chem.*, **25**, 1395 (1963).

Table I: Conductance of Typical 1:1 Electrolytes in Acetonitrile

Et ₄ NCl		Et ₄ NClO ₄		Et ₄ NBCl ₄		[(C ₆ H ₅) ₄ P ₂ N ₃ H ₄] ⁺ Cl ⁻		[(C ₆ H ₅) ₄ P ₂ N ₃ H ₄] ⁺ SbCl ₆ ⁻	
C × 10 ⁴ , mole/l.	Λ	C × 10 ⁴ , mole/l.	Λ	C × 10 ⁴ , mole/l.	Λ	C × 10 ⁴ , mole/l.	Λ	C × 10 ⁴ , mole/l.	Λ
1.035	170.0	1.687	185.5	1.629	176.2	2.170	104.6	0.496	160.1
2.030	166.0	3.290	173.8	3.330	172.9	2.172	104.8	1.364	151.4
2.988	163.9	4.830	170.8	4.658	170.0	2.654	100.5	2.601	147.9
4.800	163.5	7.688	168.7	6.070	172.6	2.760	97.8	4.033	145.4
5.657	161.0	10.29	169.1	11.13	171.5	3.480	91.7	5.561	140.3
7.280	160.7	13.84	155.8	13.45	170.9	4.550	87.3	6.885	138.9
10.22	158.3	18.87	152.7	18.21	167.9	4.956	82.7	8.033	137.2
12.18	157.4	23.06	150.8	22.26	164.9	5.820	80.4	9.037	137.7
15.08	149.7	29.65	148.6	25.68	163.5	7.440	76.3	9.923	134.5
19.80	148.0	34.75	147.5	29.68	162.5	9.740	68.8	10.89	134.2
21.74	147.3	38.44	143.7	33.38	162.0	12.94	58.1	11.89	132.4

least-squares treatment of the data was applied. For compound I, the Fuoss method¹² for associated electrolytes was used to obtain the value for Λ_0 , 148.9 $\text{ohm}^{-1} \text{cm}^2 \text{mole}^{-1}$, and the dissociation constant for the ion pair, K_D , $3.2 \times 10^{-4} \text{mole l.}^{-1}$. The other four electrolytes do not show any association in the range of concentration studied. Acetonitrile is, therefore, a leveling solvent for ionization of four of the five compounds studied. Additional evidence for ion-pair formation for compound I was obtained from molecular weight measurements. The apparent molecular weight of compound I is $305 \pm 8 \text{mole}^{-1}$ in the concentration range 5.5×10^{-3} to $1.2 \times 10^{-2} M$.¹³ The error is expressed as a standard deviation. The formula weight for compound I is 452. The existence of ion pairs in equilibrium with univalent ions would account for this observation. For comparison, the apparent molecular weight of compound I is 444 when measured by vapor pressure osmometry in chloroform, a solvent of low dielectric constant (ϵ^{30} 4.8). The solute concentration was 1.02×10^{-3} and $1.77 \times 10^{-2} M$. In this case the solute species is predominantly ion pairs or molecules. Furthermore, compound I is a nonconductor in chloroform.

The limiting molar conductances for the remaining salts are Et₄NCl (176.6 ± 0.5), Et₄NClO₄ (188.9 ± 0.9), Et₄NBCl₄ (180.2 ± 0.4), and (C₆H₅)₄P₂N₃H₄⁺SbCl₆⁻ ($162.5 \pm 0.3 \text{ohm}^{-1} \text{cm}^2 \text{mole}^{-1}$). In a recent study, Coetzee and Cunningham adopted the reference electrolyte tetraisoamylammonium tetraisoamylborate to evaluate ionic conductances in acetonitrile.¹⁰ Transference studies of the reference electrolyte in nitromethane gave equal values for the transference number of the cation and anion and provide experimental support for their claim that the ionic conductance may be equally divided between the reference cation and anion in other solvents such as acetonitrile.

A value of $85.05 \text{ohm}^{-1} \text{cm}^2 \text{mole}^{-1}$ was given for the limiting ionic conductance of tetraethylammonium ion in acetonitrile.¹⁰ We have accepted this as the most reliable value for $\lambda_0(\text{Et}_4\text{N}^+)$ and have computed limiting ionic conductances by the application of Kohrausch's law of independent migration of ions to our conductance data. The results are summarized in Table II.

Table II: Single Ion Conductances, λ_0 , in Acetonitrile at 25°

Cation	λ_0 , $\text{ohm}^{-1} \text{cm}^2$ mole^{-1}	Anion	λ_0 , $\text{ohm}^{-1} \text{cm}^2$ mole^{-1}
Et ₄ N ⁺	85.05 ^a	Cl ⁻	91.6
(C ₆ H ₅) ₄ P ₂ N ₃ H ₄ ⁺	57.3	ClO ₄ ⁻	103.8
		BCl ₄ ⁻	95.2
		SbCl ₆ ⁻	105.2

^a Reported in ref 10. This value referred to $\lambda_0(\text{tetraisoamylammonium ion}) = 57.24$.

The limiting ionic conductances of the ClO₄⁻ and BCl₄⁻ anions are larger than the value for the chloride ion. Such a relationship is expected because the smaller, more polarizable chloride ion would interact more strongly with the polar solvent than the larger ions. The small ionic conductance of the phosphonium cation, (C₆H₅)₄P₂N₃H₄⁺, suggests substantial solute-solvent interaction.

(12) R. M. Fuoss and F. Accascina, "Electrolytic Conductance," Interscience Publishers, Inc., New York, N. Y., 1959, pp 225-230; R. M. Fuoss, *J. Am. Chem. Soc.*, **57**, 488 (1935).

(13) Molecular weights were determined on a Mechrolab vapor pressure osmometer, Model 301A. The data in chloroform were obtained by Dr. F. G. Sherif.

Acknowledgment. The generous support in the form of a fellowship to Ismail Y. Ahmed from the National Science Foundation administered by the American Friends of the Middle East is gratefully acknowledged.

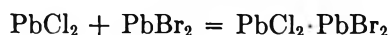
The Formation of Lead(II) Chloride Bromide (PbClBr) in the Vapor Phase

by H. Bloom and J. W. Hastie

Chemistry Department, The University of Tasmania, Hobart, Australia (Received October 28, 1966)

From the measurement, by transpiration, of partial vapor pressures of PbCl₂ and PbBr₂ above molten mixtures of the two salts at 770°, Greiner and Jellinek¹ found that the apparent activities of PbBr₂ were slightly lower than Raoult's law values over the whole composition range, but that those of PbCl₂ were higher than the Raoult's law values from 0 to 0.7 mole fraction of PbCl₂. These observations were contrary to the Gibbs-Duhem relation and also to the results of Salstrom and Hildebrand,² whose activity values of PbBr₂ from measurement of the emf's of formation cells were considerably lower than those reported by Greiner and Jellinek.

To account for the discrepancies, Greiner and Jellinek suggested a vapor phase equilibrium



This equilibrium would cause the apparent vapor pressures of both components and therefore the derived activities to be higher than the real values, but only in the case of PbCl₂ would apparent activities exceed the Raoult's law values.

The present investigation relates to a mass spectrometric study to identify the vapor phase species.

Experimental Section

Using a quadrupole mass spectrometer, details of which will be published separately, the mass spectra and ionization characteristics of vapors above an equimolar PbCl₂ + PbBr₂ mixture were investigated between 421 and 495°. The melt was contained in a silica crucible within a silver Knudsen cell and heated in a furnace in the chamber of the mass spectrometer. A shutter was used to eliminate background ions. Temperature was measured by a Pt vs. Pt + 13% Rh thermocouple and a Leeds and Northrup millivolt potentiometer.

Results and Discussion

The vapor was found to contain only the species PbCl₂, PbBr₂, and PbClBr (identified as positively charged ions); hence the discrepancy in vapor pressure measurements is explicable not by the formation of PbCl₂·PbBr₂ but by the equilibrium



Table I gives a summary of the mass spectral data (listed in order of measurement) using 20-ev electron energy and photomultiplier amplification. The formation constant of PbClBr is given in terms of the partial pressures by

$$K_P = \frac{P_{\text{PbClBr}}^2}{P_{\text{PbCl}_2} P_{\text{PbBr}_2}}$$

Its heat of formation (per 2 moles) is

$$\Delta H = 2\Delta H_{(\nu, \text{PbClBr})} - \Delta H_{(\nu, \text{PbBr}_2)} - \Delta H_{(\nu, \text{PbCl}_2)}$$

where $\Delta H_{(\nu, \text{PbClBr})}$, etc., are the heats of vaporization of PbClBr, etc., and are obtainable from the slopes of the graphs of $\log P$ vs. $1/T$ for each species or, in the present investigation, from the graphs of $\log I+T$ vs. $1/T$.

Table I: Ion Current vs. Temperature Data

Temp. °C	$I+T$ for the vapor species ^a			
	PbCl ⁺	PbBr ⁺	PbClBr ⁺	PbBr ₂ ⁺
495	200	720	55.6	175
486	133	460	42.5	118
480	143	450	39.6	131
450	37	150	14	37
454	59	210	19	55
461	90.5	310	29.4	83.4
475	129	500	39.8	121
466	72.2	300	26.3	71.2
441	34.3	...	13.1	37.2
421	19.3	...	5.1	26.9

^a Ion current in arbitrary units; T in °K.

Ion currents for PbCl₂⁺ could not be determined accurately owing to interference by an intense PbBr⁺ ion close in mass number to PbCl₂; hence $\Delta H_{(\nu, \text{PbCl}_2)}$ was assumed to be equal to $\Delta H_{(\nu, \text{PbBr}_2)}$ and equal to the heats of vaporization for the two pure salts, which have been found by direct measurement³ to be the same within experimental error (32 ± 2 kcal mole⁻¹). These assumptions are reasonable in view of the lack

(1) B. Greiner and K. Jellinek, *Z. Physik. Chem. (Leipzig)*, **165**, 97 (1933).

(2) E. J. Salstrom and J. H. Hildebrand, *J. Am. Chem. Soc.*, **52**, 4641 (1930).

(3) H. Bloom and J. W. Hastie, unpublished results.

of strong interactions in the liquid mixtures, as evidenced by the not too far from ideal activity values determined by Salstrom and Hildebrand and by the simple phase diagram for the system.⁴ The equality of slopes of $\log I^+T$ against $1/T$ for PbCl^+ and PbBr^+ supports the assumption.

From the mass spectral data, $\Delta H_{(v, \text{PbClBr})} = 31 \pm 2$ kcal, hence $\Delta H = 1 \pm 3$ kcal/mole for PbClBr . The ratio $P_{\text{PbBr}_2}/P_{\text{PbClBr}} = I^+_{\text{PbBr}_2}/I^+_{\text{PbClBr}}$ was found to be 3.15 ± 0.4 from our ion current results. This may be compared with a value of 3.43 from the vapor pressure results of Greiner and Jellinek, corrected for the partial pressure of PbClBr by using Salstrom and Hildebrand's results for the activity of PbBr_2 at 450° . (The temperature difference has only a minor effect on activity.)

The partial pressures of PbBr_2 , PbCl_2 , and PbClBr of the equimolar mixture for use in the equilibrium constant expression were calculated as follows. P_{PbBr_2} was obtained from the activity measurements of Salstrom and Hildebrand together with the measured value³ of vapor pressure of pure PbBr_2 at the same temperature. P_{PbCl_2} was obtained likewise by using the Gibbs-Duhem calculation of the activity of PbCl_2 and the vapor pressure³ of pure PbCl_2 . The partial pressure of PbClBr was then obtained by combining these "true" partial pressure results with the apparent pressures of Greiner and Jellinek. The value of K_P is 0.38 at 700° (neglecting change of activity with change of temperature) and the corresponding ΔG for the reaction is 1 kcal/mole of PbClBr .

Acknowledgment. We wish to thank Dr. A. L. G. Rees and Dr. J. D. Morrison of the Division of Chemical Physics, C.S.I.R.O., Melbourne, for use of the mass spectrometer and the Australian Research Grants Committee for financial support.

(4) K. Monkemeyer, *Neues Jahrb. Mineral.*, **22**, 1 (1906).

Pressure and Viscosity Effects on the Recombination of *t*-Butoxy Radicals from Di-*t*-butyl Peroxide¹

by Cheves Walling and Harold P. Waits

Department of Chemistry, Columbia University,
New York, New York 10027 (Received January 30, 1967)

The cage effect (recombination of radicals produced in pairs in close proximity to one another) often deter-

mines the efficiency of radical production in homolytic scission reactions, as counted by scavengers or by the initiation of chain processes. When recombination regenerates the original radical source, the cage effect may also affect its measured rate of dissociation leading to a decrease in rate with increasing solvent viscosity.

In 1959, Walling and Metzger² reported a study of the effect of pressure on the rate of decomposition of di-*t*-butyl peroxide and noted that ΔV^\ddagger varied significantly with solvent and since the larger values were observed in toluene and cyclohexene which are readily attacked by *t*-butoxy radicals, they suggested that the differences arose from competition between *t*-butoxy radical recombination and attack on solvent, both within the solvent cage. This proposal can now be reevaluated in the light of new data on cage effects and alkoxy radical chemistry.

Significant cage recombination of acetoxy radicals from acetyl peroxide was deduced by Braun, Rajbenbach, and Eirich³ from the dependence of both decomposition rate and products on solvent viscosity and has been confirmed by Taylor and Martin⁴ by O¹⁸ labeling experiments. More pertinent here, extensive recombination of *t*-butoxy radicals from di-*t*-butyl peroxalate in viscous solvents has been detected by Hiatt and Traylor.⁵ Finally, concentration levels at which scavenger reactions can compete with cage recombination of radicals from azo-1-cyanocyclohexane have been determined by Waits and Hammond,⁶ with results indicating directly that cage reactions must occur within a very small number of diffusive displacements.

Cage recombination of *t*-butoxy radicals from di-*t*-butyl peroxide itself is best examined by kinetic measurements, since isotopic scrambling is inapplicable and scavengers suitable for use at high levels at the necessary temperatures are not known. Early work has shown that the decomposition rate is remarkably solvent independent (except in systems in which induced decomposition gives high rates).⁷ Very recently, a detailed study by Huyser⁸ has shown that, while

(1) Support of this work by a grant from the National Science Foundation is gratefully acknowledged.

(2) C. Walling and G. Metzger, *J. Am. Chem. Soc.*, **81**, 5365 (1959).

(3) W. Braun, L. Rajbenbach, and F. R. Eirich, *J. Phys. Chem.*, **66**, 1591 (1962).

(4) J. W. Taylor and J. C. Martin, *J. Am. Chem. Soc.*, **88**, 3650 (1966).

(5) R. Hiatt and T. G. Traylor, *ibid.*, **87**, 3766 (1965).

(6) H. P. Waits and G. S. Hammond, *ibid.*, **86**, 1911 (1964).

(7) C. Walling, "Free Radicals in Solution," John Wiley and Sons, Inc., New York, N. Y., 1957, p 469.

(8) E. S. Huyser, private communication.

there are small differences in Arrhenius parameters, unimolecular rate constants in some 13 solvents at 125° all lie between 1.22 and $3.47 \times 10^{-5} \text{ sec}^{-1}$. Although the lowest value was in decalin, a relatively viscous medium, no solvent of really high viscosity was included. We have now compared decomposition rates in CCl_4 , *t*-butyl benzene, and Nujol, Table I. Experiments were run in sealed ampoules, sampled periodically, and peroxide decomposition was followed by disappearance of the 875-cm^{-1} O-O stretching peak in the infrared region. Insensitivity to oxygen or I_2 indicates that induced decomposition is unimportant and the low rate in Nujol suggests that significant cage recombination is now taking place, in spite of the fact that bulk viscosity is considerably lower at 125° than at room temperature (approximately 80 cp).

Table I: Decomposition Rates of Di-*t*-Butyl Peroxide at 125°

Solvent	Conditions	k , $\text{sec}^{-1} \times 10^6$
<i>t</i> -Butylbenzene (η_{125} 0.358 cp)	Vacuum	2.12, 2.07
	Air	2.49
	Air, 0.05 <i>M</i> I_2	2.03
Carbon tetrachloride (η_{75} 0.486 cp)	Vacuum, 0.05 <i>M</i> I_2	1.40
	Vacuum, 0.10 <i>M</i> I_2	1.65
Nujol (η_{125} 2.58 cp)	Vacuum	0.78
	Air	0.73, 0.60

Applying this result to the earlier pressure measurements, pertinent data are summarized in Table II.⁹ In the original data, gathered at 1–5000 atm, variation of $\log k$ with P was almost linear so that ΔV^\ddagger values apply over the entire range. We see that, in all solvents for which there are data, pressure increases solvent viscosity to the range of our Nujol experiments.¹⁰ Since simple theory and what data are available indicate that diffusion and viscosity vary inversely to each other with changes in pressure¹¹ and since Hiatt and Traylor's work shows a good correlation between solvent viscosity and cage recombination of *t*-butoxy radicals,^{5,12} the earlier assumption that cage recombination becomes important at high pressures seems justified, particularly since pressure should also increase the rate of radical recombination within the solvent cage.

The second proposal, that *t*-butoxy radical reaction with solvent can compete with cage recombination, however, now seems less tenable. The rate of the *t*-butoxy radical reaction with toluene

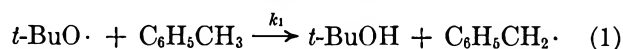


Table II: Pressure Effects on Di-*t*-Butyl Peroxide Decomposition² and Solvent Viscosity⁹

Solvent	k_{120} , $\text{sec}^{-1} \times 10^6$	ΔV , cc/mole	η , cp
Toluene	1.34	5.4 ± 0.6	0.327 (1 atm)
			2.06 (4000 atm)
Cyclohexene	0.83	6.7 ± 0.3	...
Benzene	1.39	12.6 ± 1.3	0.330 (1 atm)
			1.78 (3000 atm)
Carbon tetra- chloride	0.9	13.3 ± 3	0.486 (1 atm)
			2.94 (4000 atm)

has recently been estimated here¹³ as 7.2×10^4 l./mole sec at 30° and by Ingold¹⁴ as 3×10^3 l./mole sec at 24°. Taking the mean of the two values and Ingold's activation energy of 5.6 kcal, the value at 120° becomes 1.2×10^5 . Since ΔV^\ddagger for eq 1 is -5 cc/mole² the rate will be increased further with pressure to 2.6×10^5 at 5000 atm, giving a half-life for the *t*-butoxy radical in 10 *M* toluene of 2.7×10^{-7} sec, a number which may be uncertain by a factor of 10.

In fluid solvents diffusion theory indicates that cage processes are essentially complete in 10^{-9} sec,¹⁵ or even less in light of Waits' and Hammond's results on the high levels of scavenger required to compete with them.⁶ Diffusion theory also indicates that their time scale will increase linearly with viscosity, but the moderate viscosity changes which occur with pressure (less than tenfold) make the probability of reaction 1 competing with cage recombination doubtful, at best.

Unfortunately, if this part of the Metzger and Walling hypothesis is discarded, some parallel between ΔV^\ddagger and solvent viscosity changes with pressure (rather than solvent reactivity) would be expected, but are not evident in Table II. However, it may be significant that the largest value of ΔV^\ddagger is observed in CCl_4 , a solvent in which cage effects are unexpectedly large.¹⁶

(9) P. W. Bridgman, "The Physics of High Pressure," The Macmillan Co., New York, N. Y., 1952, pp 341–344.

(10) Viscosities are given at the highest temperatures reported, but they vary little with temperature for these liquids (unlike Nujol).

(11) W. A. Steele and W. Webb in "High Pressure Physics and Chemistry," R. S. Bradley, Ed., Academic Press Inc., New York, N. Y., 1963, Chapter 4.

(12) The relation seems best for molecules of somewhat similar size but breaks down for polymer solutions: F. R. Mayo, private communication.

(13) C. Walling and V. Kurkov, *J. Am. Chem. Soc.*, **88**, 4727 (1966).

(14) D. J. Carlsson, J. A. Howard, and K. U. Ingold, *ibid.*, **88**, 4725 (1966).

(15) R. M. Noyes, *ibid.*, **77**, 2042 (1955).

(16) F. W. Lampe and R. M. Noyes, *ibid.*, **76**, 2140 (1954).

COMMUNICATIONS TO THE EDITOR

On the Radiation Chemistry of Aqueous Nitrous Oxide Solutions

Sir: In their paper on the radiolysis of nitrous oxide solutions, Dainton and Walker¹ commented on differences between their results and our earlier paper² on the radiation-induced chain reaction between dissolved nitrous oxide and hydrogen. These differences, their comments, and some other aspects of their paper are considered here.

Dainton and Walker's values of $G(N_2)$ for the chain reaction were obtained from single-point determinations at one fixed dose. Simple computations will show that the strikingly abrupt transition of their results into a "pH-independent" range above pH 13 and the seemingly linear dependence on (H_2) actually were due to serious overexposure, so that the extent of reaction was limited by complete consumption of the hydrogen initially in the aqueous phase plus an additional amount that diffused into the depleted solution from the gas space.

In regard to other pH effects, we have confirmed our earlier statement² that the depression in our yields at

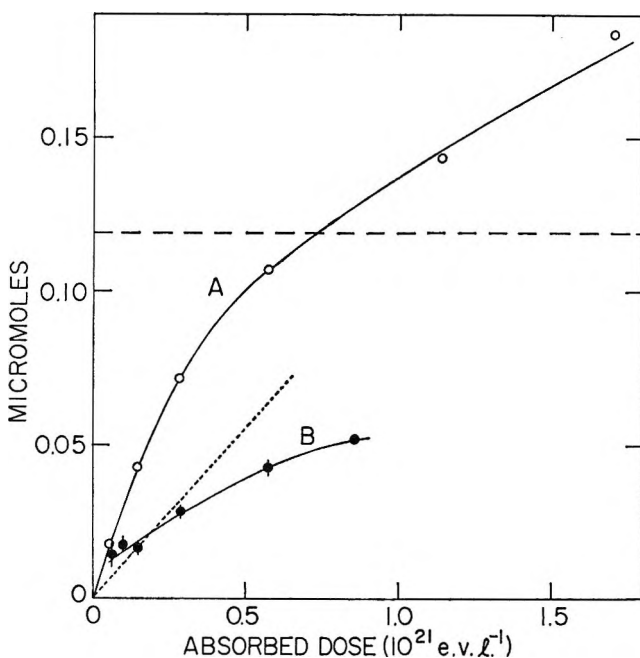


Figure 1. Curve A: Dependence of N_2 yield on absorbed dose for $7.9 \times 10^{-6} M$ aqueous solutions of N_2O ; data from ref 1; dashed horizontal line indicates initial quantity of N_2O in 15-cc sample. Curve B: Dependence of H_2 yield on absorbed dose for pure water; data from ref 1; dashed line through origin indicates $G(H_2) = 0.45$.

pH 8-12 could be removed by the use of carbonate-free base, and we stand by our result indicating that no chain reaction occurs in $HClO_4$ at pH 0.4, *not* pH 1.

Contrary to Dainton and Walker's assertion, the yield in our Figure 1 (ref 2) is independent of (H_2) to nearly 50% decomposition. Similar graphs for neutral and carbonate-free alkaline solutions were linear to over 80% depletion of H_2 , indicating that the yield is essentially independent of (H_2) .

The chain-terminating process in our mechanism for alkaline solutions² is revised to $H + M \rightarrow$ term, which is in better accord with the verbal argument. The chain length depends upon competition of the termination step with $H + N_2O \rightarrow OH + N_2$ in neutral solution and with $H + OH^- \rightarrow e_{aq}^-$ above pH 12. Then $G(N_2)$ and $G(-H_2)$ should be independent of (H_2) at any pH, as observed. The dependence on (N_2O) should be unity in neutral solution, as found by Dainton and Walker,¹ and zero at pH >12, for which neither paper presents evidence (discounting their fortuitous zero value obtained by overexposure).

Dainton and Walker's expression describing our mechanism in neutral solution should not contain $k_9 \cdot (H_2O_2)$ in the denominator of the last term, and their indicated method of converting to an expression for alkaline solutions is inapplicable.

Dainton and Walker attribute differences in the results to our use of much higher doses than theirs. The fact is that our dosages were substantially *lower*. For example, the G value in our Figure 1 (ref 2) was obtained in the linear range up to 8.25×10^{19} ev l^{-1} , less than one-tenth of the fixed dosage used in their chain-reaction studies. At the sensitivity of $70 \text{ cm}^2/\mu\text{mole}$ of hydrogen,³ our analytical method will detect the lower limit of 3×10^{-9} mole reported for their method; yet no hydrogen could be detected in our N_2O solutions at pH >3 after irradiation without gas space.

The data from which Dainton and Walker obtained single-point, "integral" G values for the nitrogen yield in very dilute N_2O solutions and for the H_2 yield in pure water at very low doses are re-presented in Figure 1 as the quantity of gas formed as a function of absorbed dose.

Curve A shows the nonlinearity of N_2 formation. The amounts of N_2 formed at the higher doses consider-

(1) F. S. Dainton and D. C. Walker, *Proc. Roy. Soc. (London)*, **A285**, 339 (1965).

(2) C. H. Cheek and J. W. Swinnerton, *J. Phys. Chem.*, **68**, 1429 (1964).

(3) C. H. Cheek, V. J. Linnenbom, and J. W. Swinnerton, *Radiation Res.*, **19**, 636 (1963).

ably exceed the initial amount of N_2O in solution, so that once again the overexposure and the effect of the gas space are manifest. These results provide a highly questionable basis for their novel arguments concerning the dependence of $G(N_2)$ on dose, dose rate, and (N_2O).

Curve B shows that $G(H_2)$ in irradiated pure water does not exceed 0.45 between any two data points. Furthermore, the data strongly suggest that their high values of $G(H_2)$ at very low doses may be due to neglect of a substantial blank correction.

U. S. NAVAL RESEARCH LABORATORY CONRAD H. CHEEK
WASHINGTON, D. C. 20390

RECEIVED FEBRUARY 13, 1967

Circular Dichroism of Some Polypeptides in Solvent Mixtures Containing Strong Organic Acids

Sir: Increasing concentrations of strong organic acids such as dichloroacetic acid (DCA) and trifluoroacetic acid (TFA) have been utilized to elicit transitions of polypeptides in organic solvents. These transitions have been studied using various physical methods, *e.g.*, optical rotatory dispersion, flow birefringence, viscometry, and Kerr effect, and generally have been interpreted as α -helix-random coil transformations.¹⁻⁸ However, the mechanism and the type of forces involved in the disruption of ordered structures of polypeptides are not yet clear. A strong solvation of the polypeptide chain by DCA and TFA³⁻⁵ and/or the large ability of these acids to form hydrogen bonds with the peptide groups⁷ have been suggested to be the main causes of the phenomenon.

Recently, a number of investigators,⁹⁻¹² on the basis of near-infrared spectra in the overtone region of the amide group and on the basis of conductivity measurements, have concluded that some polypeptides, namely poly- γ -benzyl-L-glutamate (PBLG), poly-L-alanine (PLA), and poly-L-leucine (PLL), dissolved in chloroform or ethylene dichloride (EDC) are protonated at the amide group in presence of DCA and TFA. On the basis of their results, these authors concluded that the transitions observed in b_0 could not reflect disruption of intramolecular peptide hydrogen bonds.¹⁰

On the other hand, Stewart, *et al.*,¹³ on the basis of nmr spectral data, concluded that in the case of PLA and PLL dissolved in $CHCl_3$ -TFA there is no evidence for the protonation of the peptide group, but rather their data suggest that TFA is hydrogen-bonded to the polypeptide chain. In their view, the inter-

molecular hydrogen bonding is the driving force converting the polypeptide from the helical to the random coil form.

In order to clarify the effect of strong organic acids, we are carrying out systematic circular dichroism (CD) measurements in the region of the peptide chromophore on PBLG, PLA, PLL, poly- γ -methyl-L-glutamate (PMLG), and poly-L-methionine (PLM) dissolved in various solvents in the presence of increasing amounts of DCA and TFA.

We wish to communicate some preliminary results which, for the polyglutamate systems herein reported, rule out the protonation mechanism prior to the order-disorder transition. The basis of our argument is the assignment of an $n-\pi^*$ transition (a transition from a nonbonding orbital on the oxygen atom to a π^* orbital delocalized over the entire peptide chromophore) to the 222-m μ CD extremum¹⁴ and the position that protonation at the acyl oxygen cannot occur without markedly altering this CD extremum.

PBLG (Lot G-79, MW 350,000) and PMLG (Lot 6612, MW 290,000) were Pilot samples. All the solvents were purified by distillation over desiccants prior to use. The solutions were prepared in a drybox and run immediately to avoid possible hydrolysis.¹⁵ The CD measurements were carried out on a Cary 60 spectropolarimeter with a prototype CD attachment, built by Cary Instruments. A 0.064-mm cell was used throughout.

In Figure 1, circular dichroism spectra of PBLG dissolved in EDC and $CHCl_3$, and of PMLG dissolved in trifluoroethanol (TFE) are reported. In the case of

- (1) P. Doty, *Proc. Intern. Symp. Macromol. Chem.*, 5 (1957); *Tetrahedron Suppl.*, 2, 1951 (1957).
- (2) W. Moffitt and J. T. Yang, *Proc. Natl. Acad. Sci., U. S.*, 42, 596 (1956).
- (3) J. T. Yang and P. Doty, *J. Am. Chem. Soc.*, 79, 761 (1957).
- (4) P. Doty and J. T. Yang, *ibid.*, 78, 498 (1956).
- (5) P. Doty, A. M. Holtzer, J. H. Bradbury, and E. R. Blout, *ibid.*, 76, 4493 (1956).
- (6) G. E. Perlmann and E. Katchalski, *ibid.*, 84, 452 (1962).
- (7) G. D. Fasman, *Proceedings of the International Symposium on Polyamino Acids, Polypeptides, and Proteins, Madison, Wis., 1961*, pp 222-226.
- (8) H. Watanabe, K. Yoshioka, and A. Wada, *Biopolymers*, 2, 91 (1964).
- (9) S. Hanlon, S. F. Russo, and I. M. Klotz, *J. Am. Chem. Soc.*, 85, 2024 (1963).
- (10) S. Hanlon and I. M. Klotz, *Biochemistry*, 6, 37 (1965).
- (11) M. A. Stake and I. M. Klotz, *ibid.*, 5, 1726 (1966).
- (12) S. Hanlon, *ibid.*, 5, 2049 (1966).
- (13) W. E. Stewart, L. Mandelkern, and R. E. Glick, *ibid.*, 6, 143 (1967).
- (14) G. Holzwarth and P. Doty, *J. Am. Chem. Soc.*, 87, 218 (1965).
- (15) M. V. Vol'kenshtein, A. T. Kol'tsov, and Zh. Marshal, *Vysokomol. Soedin.*, 4, 944 (1962).

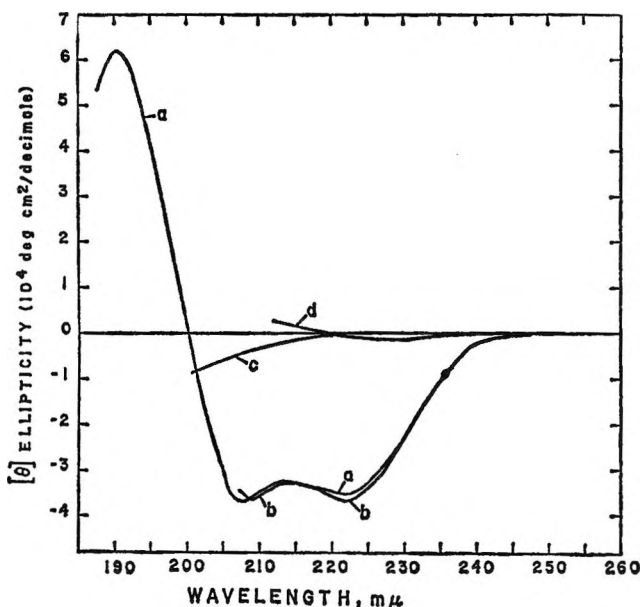


Figure 1. Circular dichroism spectra of (a) PMLG in TFE; (b) PBLG in EDC (down to 207 $m\mu$) and in $CHCl_3$ (down to 214 $m\mu$); (c) PMLG in TFE-TFA (30:70 w/w); (d) PBLG in $CHCl_3$ -TFA (80:20 w/w).

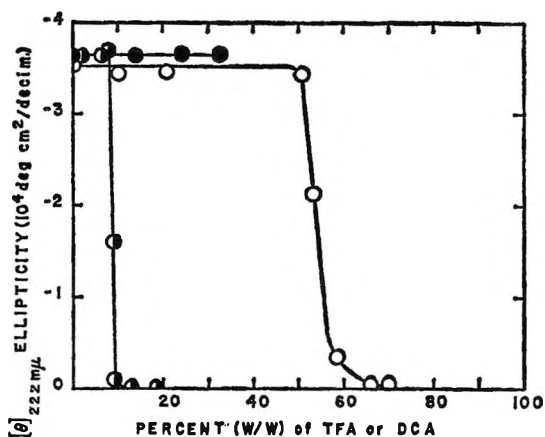


Figure 2. Ellipticity at 222 $m\mu$ as a function of percent of added strong organic acid: \bullet , PBLG in $CHCl_3$ -TFA; \circ , PMLG in TFE-TFA; \bullet , PBLG in EDC-DCA.

EDC and $CHCl_3$, owing to the strong absorption of these solvents at short wavelengths, it was not possible to obtain CD curves down to 185 $m\mu$ as in the case of TFE. All of these spectra exhibit the characteristic features (*i.e.*, location and amplitude of extrema) attributed to a right-handed α -helix.¹⁴

Addition of TFA to the solutions of PMLG in TFE brings about a sharp transition at about 55% (w/w) TFA, as monitored by plotting the ellipticity of the $n-\pi^*$ band centered at 222 $m\mu$ as a function of per cent

TFA in the solvent mixture. Before this transition, the amplitude of the 222- $m\mu$ minimum is constant, ruling out any protonation mechanism in this region (Figure 2). However, the solution with 51% TFA showed a blue shift in the position of the $n-\pi^*$ CD extremum from 222 to 220 $m\mu$. The same conclusions may be drawn in the PBLG- $CHCl_3$ -TFA system. In this case, the transition is located at about 9% of TFA in the solvent mixture (Figure 2). For PBLG dissolved in EDC-DCA, the transition could not be reached because of the stronger absorption of DCA at low wavelengths; *i.e.*, solutions with concentrations of DCA greater than 33% could not be studied. No variation in the magnitude of the $n-\pi^*$ transition band was observed in this concentration range. The CD curves for the PBLG- $CHCl_3$ -TFA and PMLG-TFE-TFA systems after the transition are also reported in Figure 1.

To determine if the transitions observed in the PBLG- $CHCl_3$ -TFA and PMLG-TFE-TFA systems were order-disorder transitions, viscosity measurements were carried out. In both systems intrinsic viscosity exhibited transitions corresponding to the loss of the $n-\pi^*$ CD band.¹⁶

The systems of poly-L-alanine and of poly-L-leucine in $CHCl_3$ -TFA show qualitative agreement, independent of interpretation, in the variation of the nmr,¹³ infrared,^{9,10} and CD parameters as a function of TFA concentration. Studies on a monomeric peptide system are in progress in order to facilitate the interpretation of the CD data.

In our view, the following conclusions may be drawn concerning the poly-L-glutamate systems.

(a) The polypeptides show cooperative transitions when a critical concentration of DCA or TFA in the solvent mixture has been reached. On the basis of cd data, these transitions may be considered as α -helix-random coil transformations, in accord with the early interpretations.¹⁻⁷ The nature of the polymer after the transition cannot be determined until solvent effects on the random coil have been studied.

(b) Before these transitions, there is no evidence of protonation. The protonation of chain ends suggested by Watanabe, *et al.*,⁸ represents less than 1% of the total number of peptide chromophores, and, therefore, could not be detected.

(c) The mechanism of intermolecular hydrogen bonding between TFA or DCA and the polypeptide, suggested by Stewart, *et al.*,¹³ cannot be ruled out by our

(16) F. Quadrifoglio, unpublished results.

experiments. However, should hydrogen bonding to solvent exist, it does not greatly alter the coordinates of the helical polypeptide.

AMERICAN MEDICAL ASSOCIATION FRANCO QUADRIFOGLIO
INSTITUTE FOR BIOMEDICAL RESEARCH DAN W. URRY
CHICAGO, ILLINOIS 60610

RECEIVED FEBRUARY 23, 1967

On the Scaled-Particle Theory of

Dilute Aqueous Solutions

Sir: Recently, Ben-Naim and Friedman¹ discussed the application of the scaled-particle theory of fluids to dilute aqueous solutions of nonpolar gases.^{2,3} Their argument is that the scaled-particle theory does not give the correct temperature dependence for the surface tension of water and hence the entropy of cavity formation, \bar{S}_c , calculated using this theory cannot be correct. They base their argument upon the work of Mayer^{4,5} in which it was found that in order to obtain the correct temperature dependence of the surface tension using the scaled-particle theory it was necessary to assume that the hard-sphere parameter, a_1 , was temperature dependent. In fact, Pierotti examined the temperature dependence of a_1 and found it to be very small and hence unimportant in the calculation of the free energy and entropy of cavity formation.³ The question appears to be whether or not the scaled particle theory can adequately account for the entropy of cavity formation if it does not adequately account for the temperature dependence of the bulk surface tension of a fluid.

The first point to be made is that the scaled-particle theory strictly applies only to rigid wall cavities, a situation met well when the cavity is filled by a molecule but not so well when the cavity is filled with a dilute gas. As pointed out by Ben-Naim and Friedman in footnote 7 of their note, the surface tension given by the theory is for the interface between the liquid and a rigid wall. Ordinary surface tension measurements involve an interface between the liquid and a dilute gas. Although it is often assumed for lack of anything better that these two surface tensions are not very different, no evidence is available to indicate the magnitude of their difference. Of even more importance to the argument of Ben-Naim and Friedman is the effect of temperature on the nature of the gas-liquid interface and to what extent this effect is being ascribed to the term da_1/dT . This is a serious difficulty and hence one should perhaps look to other

physical properties to determine the temperature dependence of a_1 .

Compressibility seems to be a less questionable property to use for this purpose than is surface tension. The greatest problem with compressibilities is that reliable data are difficult to obtain. Nevertheless, if one examines position number 2 of the figure in ref 1, it is found that while the actual values of \bar{S}_c are altered as a result of the temperature dependence of a_1 obtained from compressibilities, the relative differences between solvents are pretty much preserved. It is this difference that distinguishes water as a solvent different from say ether or benzene. The problem still remains, however, that if one accepts the values of \bar{S}_c obtained from their assumption number 2, then at least the fair numerical agreement found^{2,3} is lost unless as they suggest the entropy of interaction, \bar{S}_i , is important. It is interesting to note that if the \bar{S}_c 's under their assumption 2 are correct, then a larger contribution from \bar{S}_i will be required for the non-aqueous solvents than for water.

Now it is this writer's belief that the temperature dependence of the a_1 's given by Mayer are unreasonably large because of the interface problem mentioned above. There is no question that a_1 should have some temperature dependence especially for nonspherical molecules, but the very nature of a collision diameter implies that there exists a large energy gradient with respect to distance and hence a small change in kinetic energy should not appreciably change the collision diameter.

A more consistent approach to the temperature dependence of a_1 is to use the extrapolation method described in ref 2 and 3. This method is equivalent to determining the solubility of a nonpolarizable hard sphere and is therefore a direct and proper test of the adequacy of the scaled-particle theory. If data for the solubility of the rare gases in a given solvent are available at several temperatures, then it is possible to compute a_1 for the solvent at each temperature from the intercept of a plot of $\ln K_H$ vs. α , where K_H is the Henry law constant and α is the polarizability. This has been done for water and benzene and the results are shown in Table I along with values of a_1 calculated from surface tension and compressibility. Examination of this table indicates that at least insofar as the solubility of a hard sphere is concerned, a_1 for these

(1) A. Ben-Naim and H. L. Friedman, *J. Phys. Chem.*, **71**, 448 (1967).

(2) R. A. Pierotti, *ibid.*, **67**, 1840 (1963).

(3) R. A. Pierotti, *ibid.*, **69**, 281 (1965).

(4) S. W. Mayer, *J. Chem. Phys.*, **38**, 1803 (1963).

(5) S. W. Mayer, *J. Phys. Chem.*, **67**, 2160 (1963).

Table I: The Variation of a_1 with Temperature

Temp. °K	a_1 (A), surface tension ^a	a_1 (A), compress- ibility ^a	a_1 (A), solubility ^b
Benzene			
288	5.05	5.02	5.24 ^c
298	5.02	5.00	5.24
315	4.94	4.96	5.24
Water			
277	(2.94)	2.71	2.75 ^d
298	2.88	2.72	2.75
323	2.83	2.71	2.75
343	2.77	2.70	2.74

^a From ref 5. ^b From extrapolation method described in the text. ^c This number is in excellent agreement with values determined from other sources (see Table III of ref 2). ^d The bulk of data for a_1 in the literature fall very close to 2.7 A (see references in ref 3).

solvents is at most only very slightly temperature dependent.

The fact pointed out by Ben-Naim and Friedman that S_c is a fairly strong function of a_1 is not surprising. The most remarkable thing about positions 3, 4, and 5 on their figure is that even with the wide choice of a_1 's used for the various solvents, the essential differences between aqueous and nonaqueous solvents are maintained in every case.

At first the fact that the scaled-particle theory seems to work for both aqueous and nonaqueous solution appears disturbing especially since no explicit mention of the structure of the solvent is brought into the theory. It should be pointed out, however, that the scaled-particle theory requires the volume of the system to be experimentally determined; that is, the volume and all of its derivatives are external to the theory. It is the inclusion of the volume as experimentally determined that implicitly carries with it the structure of the solvent.

SCHOOL OF CHEMISTRY
GEORGIA INSTITUTE OF TECHNOLOGY
ATLANTA, GEORGIA 30332

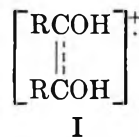
ROBERT A. PIEROTTI

RECEIVED FEBRUARY 24, 1967

Electron Spin Resonance Spectra of Radicals Produced by the Acetaldehyde-Hydrogen Peroxide-Titanous System

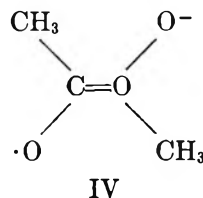
Sir: When acetaldehyde reacts with mixed aqueous solutions of titanous ion and hydrogen peroxide, the

esr spectrum of the transient radicals produced is predominantly a septet¹ (A). Evidence presented previously¹ led to this being assigned to the radical cation I (R = Me). If the acetaldehyde is mixed with the



peroxide before contact is made with the titanous solution, the spectrum obtained^{1,2} is more complex and consists mainly of a doublet of quartets (B) and a quartet (C) as well as the (weaker) septet A. Spectrum B has been assigned to the radical $\text{CH}_3\dot{\text{C}}\text{HOH}^{1,2}$ (II), and C to $\text{CH}_3\dot{\text{C}}\text{O}^2$, but it was pointed out¹ that the hyperfine splitting and g value of C were indistinguishable from those of the radical $\text{CH}_3\cdot$ (III). Different assignments have recently been proposed for spectra A and B and it has been asserted *de novo* that spectrum C is due to $\text{CH}_3\dot{\text{C}}\text{O}$; the purpose of this note is, therefore, to present further evidence in support of the assignments B = II, C = III, and to revise our earlier interpretation of the septet A.

Russell, *et al.*,^{3,4} disagree with the assignment of septet A ($a_{\text{H}} = 8.5$ oersteds) to I on the grounds that they observe another septet ($a_{\text{H}} = 2.17$ oersteds) when biacetyl is added to 98% sulfuric acid containing a small amount of sodium dithionite, and they assign *this* spectrum to I. They suggest that the septet A might be the same as that obtained from a stable radical produced by the reaction of acetoin with potassium *t*-butoxide in dimethylsulfoxide solution. This radical they identify with



We have repeated this experiment and are satisfied that the septet obtained ($a_{\text{H}} = 5.6$ oersteds, $g = 2.0050$) is distinct from A ($a_{\text{H}} = 8.5$ oersteds, $g = 2.0043$). (Septet A is also distinct from the weak septet ($a_{\text{H}} = 7.0$ oersteds) accompanying the 5.6-oersted septet assigned by Russell, *et al.*, to the *cis* isomer of IV.) In any case, one would not expect a species such as IV

- (1) J. R. Steven and J. C. Ward, *Chem. Commun.*, (13), 273 (1965).
- (2) A. L. Buley and R. O. C. Norman, *Proc. Chem. Soc.*, 225 (1964).
- (3) G. A. Russell and R. D. Stephens, *J. Phys. Chem.*, **70**, 1320 (1966).
- (4) G. A. Russell, E. R. Talaty, and M. C. Young, *ibid.*, **70**, 1321 (1966).

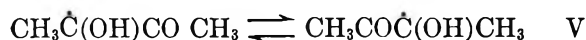
Table I: Comparison of Spectra B and C with Those Obtained from $\text{CH}_3\dot{\text{C}}\text{HOH}$ and $\text{CH}_3\cdot$

Spectrum	Source	Hyperfine splitting, oersteds	g value
B	$(\text{CH}_3\text{CHO}-\text{H}_2\text{O}_2) + \text{TiCl}_3$	a_1 15.1 ± 0.3^a a_2 22.6 ± 0.3	2.0033
$\text{CH}_3\dot{\text{C}}\text{HOH}$	$\text{CH}_3\text{CH}_2\text{OH} + \text{TiCl}_3 + \text{H}_2\text{O}_2$	a_{H}^{CH} 15.0 ± 0.1 a_{H}^{Me} 22.5 ± 0.3	2.0033
C	$(\text{CH}_3\text{CHO}-\text{H}_2\text{O}_2) + \text{TiCl}_3$	22.5 ± 0.2	2.0028
$\text{CH}_3\cdot$	$t\text{-BuO}_2\text{H} + \text{TiCl}_3$	22.3 ± 0.2	2.0028

^a Standard deviation of splitting over the whole spectrum, after correction for nonlinearity of field sweep rate.

to be present at pH 0.7, the usual condition in the aqueous flow system.

Alternatively, Russell⁵ has pointed out that the septet A may arise from the uncharged species V if one assumes that the proton transfer is acid catalyzed,



and fast enough at pH 0.7 to give equivalent methyl groups. Also, our observation¹ that the septet A shows an alternating line-width effect, with incipient collapse to a quartet ($a_{\text{H}} = 17$ oersteds) as the pH is raised from 0.7 to 2.0 could be explained by assuming a decrease in proton transfer rate in V with increase in pH. We agree that all the facts now known can be more simply explained by assigning septet A to a structure such as V with rapid proton exchange taking place.

Turkevich, *et al.*,⁶ have recently published a spectrum, obtained by injecting acetaldehyde into the titanous-peroxide flow system, which consists mainly of a doublet of quartets and a quartet, assigned by them to $[\text{CH}_3\text{CH}-\text{O}]^+$ and $\text{CH}_3\dot{\text{C}}\text{O}$, respectively. We have attempted to reproduce their spectrum, but succeeded only when the acetaldehyde and peroxide were premixed. The hyperfine splittings and g values were identical with those attributed previously¹ to spectra B and C. Moreover, careful measurements showed them to be indistinguishable from those of the spectra given by ethanol-titanous-peroxide and *t*-butylhydroperoxide-titanous, respectively, and these systems are generally accepted⁷ as giving uncomplicated spectra of the $\text{CH}_3\dot{\text{C}}\text{HOH}$ and $\text{CH}_3\cdot$ radicals. The various spectra were run consecutively, with repetition to check the constancy of the field sweep rate, Frémy's salt being used as a standard ($a_{\text{H}} = 13.07$ oersteds, $g = 2.0055$). The results are given in Table I. The correspondence of the splittings and g values may be taken, in the absence of positive evidence to the contrary, to imply the identity of the radicals.

Reasonably straightforward mechanisms are available¹ for the production of both $\text{CH}_3\dot{\text{C}}\text{HOH}$ and $\text{CH}_3\cdot$ in the acetaldehyde-titanous-peroxide system.

Further evidence of the production of $\text{R}\dot{\text{C}}\text{HOH}$ radicals from aldehydes was obtained by Dixon, *et al.*,⁸ who reported $\dot{\text{C}}\text{H}_2\text{OH}$ from formaldehyde, and even detected a splitting of 1.0 oersted from the hydroxyl proton (which is not present in CH_2O^+). The assignment of spectrum C to $\text{CH}_3\cdot$ rather than $\text{CH}_3\dot{\text{C}}\text{O}$ is supported by the spectra obtained from the reaction of other aldehydes RCHO with the titanous-peroxide system: spectra corresponding to $\text{R}\cdot$ have also been found for $\text{R} = \text{C}_2\text{H}_5$,¹ and for $\text{R} = n\text{-C}_3\text{H}_7$, $i\text{-C}_3\text{H}_7$; and $t\text{-C}_4\text{H}_9$.⁹ It is improbable that in all five cases $\text{RCO}\cdot$ would give rise to the same spectrum as $\text{R}\cdot$.

(5) G. A. Russell, private communication.

(6) Y. S. Chiang, J. Craddock, D. Mickewich, and J. Turkevich, *J. Phys. Chem.*, **70**, 3509 (1966).

(7) H. Fischer, "Landolt-Börnstein Numerical Data and Functional Relationships in Science and Technology," New Series, Group II, Vol. I, Springer-Verlag, Berlin, 1965.

(8) W. T. Dixon, R. O. C. Norman, and A. L. Buley, *J. Chem. Soc.*, 3625 (1964).

(9) J. R. Steven and J. C. Ward, *Australian J. Chem.*, in press.

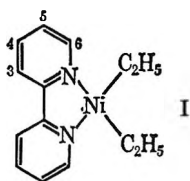
DIVISION OF COAL RESEARCH
CSIRO
CHATSWOOD
NEW SOUTH WALES, AUSTRALIA

J. R. STEVEN
J. C. WARD

RECEIVED MARCH 2, 1967

Comments on the Nuclear Magnetic Resonance Spectrum of Diethyldipyridylnickel

Sir: In a recent paper Saito, *et al.*,¹ have described the preparation and characterization of diethyldipyridylnickel (I).



As nmr evidence in support of structure I, the authors have reported: (a) the ratio (10:8) between the areas of the signals corresponding to the aliphatic and aromatic protons of the complex; (b) the high-field part of the proton spectrum of I, consisting of a triplet and a quartet centered at τ 8.85 and 9.18, respectively; (c) the low-field part of the same spectrum, whose pattern is formed by two doublets and a quartet centered, in order, at τ 0.93, 1.95, and 2.45; the areas of these multiplets were reported to be in the ratio 1:2:1. Evidences (a) and (b) are self-explanatory, and the deductions by Saito, *et al.*, from these data are reasonable. The interpretation of the low-field part of the spectrum (c) may, however, be questioned.

Saito, *et al.*, have assigned the chemical shifts of the aromatic protons by a direct comparison of the pattern of the spectrum of I with those of the spectrum of the complex $[\text{Fe}^{\text{II}}(\text{C}_{10}\text{H}_8\text{N}_2)_3]\text{Cl}_2$ (II), which has been completely analyzed and published earlier.² In the latter, the chemical shifts of protons 3, 4, 5, and 6 occur at τ 1.15, 1.74, 2.41, and 2.42 in that order, and the whole spectrum may be very roughly described,³ as done by Saito, *et al.*, as the sequence of a doublet, a quintet, and a doublet with intensity ratio 1:1:2. It must be pointed out that the high-field shift of proton 6 in II has been explained, in our paper,² in terms of the magnetic anisotropy of the aromatic ring of an adjacent ligand in the octahedral complex and the low-field shift of proton 3 in terms of the dispersion forces arising because of the *cis* coplanar conformation of each ligand in II. By matching the pattern of the two spectra, Saito, *et al.*, assigned the low-field doublet of the spectrum of I to the resonance of proton 3, the next doublet to the resonances of protons 5 and 6, and the high-field multiplet to the resonance of proton 4. According to these assignments, the resonance of proton 6 in diethyl-dipyridylnickel would still occur at a higher field than in the free 2,2'-bipyridyl molecule; since I contains only one bipyridyl ligand, Saito, *et al.*, concluded that our interpretation of the high-field shift of proton 6 in II was wrong, and attributed the observed effect to the proximity of the metal atom.

We believe, however, that another interpretation of the nmr spectrum of I is more consistent with the experimental data and that the assignments made by Saito, *et al.*, are very likely incorrect. By inspection of the spectrum published in Figure 3 of their paper, it is

evident that the splitting of the low-field doublet falls in the range 4.5–5.5 cps, which is the correct order of magnitude for the coupling constants between α and β protons in pyridine^{4,5} and in α - and β -monosubstituted pyridines.^{2,6–10} This doublet must be assigned, therefore, to the resonance of proton 6 and not to the resonance of proton 3. In the latter case, the splitting of the doublet should have been of the order of 8.0 cps, as found in the spectrum of II as well as in the spectrum of any α -monosubstituted pyridine so far analyzed.^{6–10} The assignment of the resonances of the other protons then follows naturally. The intense doublet at τ 1.95 is assigned to protons 3 and 4 which are very strongly coupled and interact, to the first approximation, with the other protons as a particle of spin 1. They will split each component of the low-field doublet in triplets which are not seen in the spectrum because of the poor resolution and the smallness of the splitting [$(J_{46} + J_{36})/2 \simeq 1.18$ cps]; the same splitting should also be present in each component of the intense doublet. The high-field quartet is then assigned to the resonance of proton 5; its multiplicity arises from the overlapping of a doublet ($J_{56} \simeq 4$ –5 cps) further split into triplets [$(J_{35} + J_{45})/2 \simeq 4.3$ cps] by interaction with protons 3 and 4; the latter spacing represents also the separation between the components of the main doublet at τ 1.95.

According to these assignments, the experimental data of Saito, *et al.*, fully support our conclusions about the strong shielding effect exerted by the other ligand groups on the resonance of proton 6 in II. On the basis of the results obtained from the analysis of the nmr spectrum of the latter molecule, one would anticipate that the resonance of proton 3 should occur in I at a τ value lower than 1.95; a small deviation from a coplanar arrangement of the two aromatic nuclei

(1) T. Saito, Y. Uchida, A. Misono, A. Yamamoto, K. Morifuji, and S. Ikeda, *J. Am. Chem. Soc.*, **88**, 5198 (1966).

(2) S. Castellano, H. Günther, and S. Ebersole, *J. Phys. Chem.*, **69**, 4166 (1965).

(3) Actually, in the spectrum of II, much more fine structure is present. Both the experimental and calculated spectra of II are reported in ref 2.

(4) J. A. Pople, W. G. Schneider, and H. J. Bernstein, "High-Resolution Nuclear Magnetic Resonance," McGraw-Hill Book Co. Inc., New York, N. Y., 1959, p 266.

(5) S. Castellano, C. Sun, and R. Kostelnik, *J. Chem. Phys.*, **46**, 327 (1967).

(6) W. Brügel, *Z. Elektrochem.*, **66**, 159 (1961).

(7) V. J. Kowalewski and D. G. de Kowalewski, *J. Chem. Phys.*, **36**, 266 (1962).

(8) V. J. Kowalewski and D. G. de Kowalewski, *ibid.*, **37**, 2603 (1962).

(9) S. Castellano and A. A. Bothner-By, *ibid.*, **41**, 3863 (1964).

(10) H. Günther and S. Castellano, *Ber. Bunsenges. Physik. Chem.* **70**, 913 (1966).

would, however, account for this discrepancy.¹¹ Furthermore, the high-field shift of τ 0.2 observed for the chemical shift of proton 4 in I seems to indicate that, for the outermost protons in the molecule, solvent and concentration effects may also be very effective in altering the position of the resonance.

(11) In II, the main contribution to the low-field shift of proton 3 (and 3') is due to the van der Waals interaction between the two protons. This effect decreases with the 6th power of the distance, and a small deviation from the coplanar arrangement of the two aromatic rings may, therefore, cause very large effects.

MELLON INSTITUTE
PITTSBURGH, PENNSYLVANIA

S. CASTELLANO

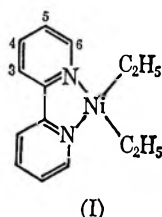
INSTITUT FÜR ORGANISCHE CHEMIE
DER UNIVERSITÄT KÖLN
KÖLN, GERMANY

H. GÜNTHER

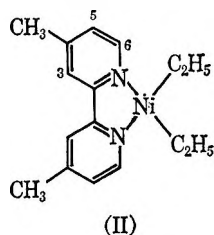
RECEIVED MARCH 16, 1967

The Nuclear Magnetic Resonance Interpretation of Diethylnickel Complexes of Substituted Dipyriddy

Sir: In the previous paper,¹ we reported the preparation and characterization of diethyldipyridylnickel (I).



During the course of our study of the analogous nickel complexes of 4,4'-disubstituted 2,2'-dipyridyl, we found that our previous nmr assignments of the ring protons were incorrect. We wish to report in this communication the synthesis and the nmr interpretation of diethyl-(4,4'-dimethyl 2,2'-dipyridyl)nickel (II), and to correct the nmr assignments of the ring protons of I.



The complex (II) was prepared by the reaction of nickel acetylacetonate, 4,4'-dimethyldipyridyl, and diethylaluminum monoethoxide in ether. *Anal.* Calcd for C₁₆H₂₂N₂Ni: C, 63.8; H, 7.4; N, 9.3; Ni, 19.5.

Found: C, 63.3; H, 7.4; N, 8.3; Ni, 19.3. The crystalline complex is dark green and is very air-sensitive. It decomposes at 125° *in vacuo*, evolving ethane and ethylene.

The nmr spectra were recorded in dimethoxyethane solutions by use of a 60 Mc/sec spectrometer. As tetramethylsilane could not be used, the chemical shifts were measured by using a methyl signal of the solvent as an internal reference and then were converted into a τ scale.

Table I: Chemical Shifts of the Ring Protons of the Ligands and Their Complexes in Dimethoxyethane Solutions. (The Figures in Brackets Are the Intensity Ratios.)

	Chemical shifts, τ			
	H ₃	H ₄	H ₅	H ₆
	1.62 (1)	2.29 (1)	2.80 (1)	1.46 (1)
	doublet	triplet	quartet	doublet
		1.95 (2)	2.45 (1)	0.93 (1)
	doublet	quartet	doublet	
	1.64 (1)	...	2.80 (1)	1.45 (1)
	singlet		doublet	doublet
	2.16 (1)	...	2.66 (1)	1.17 (1)
	singlet		doublet	doublet
	1.97 (1)	...	3.03 (1)	1.53 (1)
	doublet		quartet	doublet
	2.33 (1)	...	2.84 (1)	1.30 (1)
	doublet		quartet	doublet

In Figure 1, the signal at τ 2.16, which is a singlet due presumably to the small J_{35} and J_{36} and/or to the poor resolution of the spectrum, is assigned to H₃, because the adjacent carbon has no proton. It is most reasonable to assign the doublet at τ 1.17 to H₆ and the doublet at τ 2.66 to H₅, because it is very improbable that the coordination of the ligand to nickel exerts such an effect to deshield the H₅ to shift the signal to the field as low as τ 1.17, and because the J_{56} estimated from the splitting of the H₆ signal is *ca.* 6.0 cps.

(1) T. Saito, Y. Uchida, A. Misono, Y. Yamamoto, K. Morifuji, and S. Ikeda, *J. Am. Chem. Soc.*, **88**, 5198 (1966).

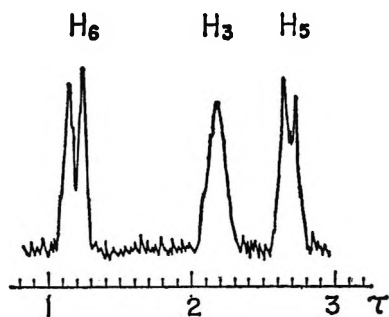


Figure 1. The nmr spectrum of the ring protons of diethyl(4,4'-dimethyl 2,2'-dipyridyl)nickel in a dimethoxyethane solution at 60 mc/sec.

In the same way, we synthesized diethyl(4,4'-dimethoxy 2,2'-dipyridyl)nickel and carried out the nmr measurements of it. The data in Table I support the assignments described above of II.

From the comparison of the spectrum of I with that of II, the assignments of the ring protons of I follows naturally. The chemical shifts of H_6 and H_5 of I are probably near those of II because of the similarity of the structures of I and II, and hence the doublet at τ 0.93 is assigned to H_6 and the quartet at τ 2.45 to H_5 . Consequently, the doublet at τ 1.95 is assigned to H_3 and H_4 . As was pointed out by Castellano and Günther,² the high-field shift of H_6 signal observed in the spectra of $[\text{Fe}(\text{dipy})_3]\text{Cl}_2$ ³ is lacking in the spectrum of I due to the absence of the shielding effect of the adjacent ligand. We conclude, therefore, contrary to our previous presumption,¹ that the shielding effect of the nickel atom upon H_6 is not predominant. The high-field shift of H_3 of I might be due to a deviation from a complete *cis* coplanar structure of the two aromatic rings. This is also suggested by Castellano and Günther.²

(2) S. M. Castellano and H. Günther, *J. Phys. Chem.*, **71**, 2368 (1967).

(3) S. Castellano, H. Günther, and S. Ebersole, *ibid.*, **69**, 4166 (1965).

DEPARTMENT OF INDUSTRIAL CHEMISTRY
UNIVERSITY OF TOKYO
HONGO, TOKYO, JAPAN

T. SAITO
M. ARAKI
Y. UCHIDA
A. MISONO

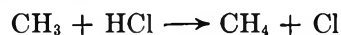
RECEIVED APRIL 3, 1967

Abstraction of Halogen Atoms by Methyl Radicals

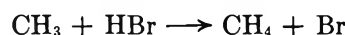
Sir: Recent reports on the abstraction of halogen atoms by methyl radicals in the gas phase^{1,2} refer to

abstraction from fully halogenated compounds, in particular halogenated methanes, as well as $\text{C}_6\text{H}_6\text{CCl}_3$, $\text{C}_6\text{H}_5\text{I}$, *n*- $\text{C}_3\text{H}_7\text{I}$, and *sec*- $\text{C}_3\text{H}_7\text{I}$. Di-*t*-butyl peroxide was used as thermal source of methyl radicals.

Attempts by us³ to obtain similar quantitative results for ethyl chloride, neopentyl chloride, ethyl bromide, *n*-propyl bromide, and *sec*-propyl bromide were largely unsuccessful owing to complicating reactions resulting from hydrogen abstraction. The presence of hydrogen halide among the products also led us to suspect that because of facile reactions of the types



and



halogen atoms were largely replacing methyl radicals as the attacking species.

We believe it important also to report that in experiments with di-*t*-butyl peroxide and ethyl iodide, explosions occurred when mixtures were frozen under vacuum to liquid nitrogen temperature.

The reactions were carried out in a conventional static system at 120–200°, and in most cases there was an excess of alkyl halide over di-*t*-butyl peroxide. With alkyl chlorides, methyl chloride was only formed in trace amounts, although with the corresponding bromides methyl bromide was formed somewhat more readily. In both instances, however, the nature of the products indicated that hydrogen abstraction was the dominant process, as noted by Tomkinson and Pritchard,² and also by Alcock and Whittle⁴ for the reaction of trifluoromethyl radicals with methyl chloride.

Typical product analyses for the reaction of ethyl chloride with di-*t*-butyl peroxide are shown in Table I.⁵

It may be observed that methane and ethylene are the major products. Tomkinson and Pritchard² noted that ethylene is a by-product (*ca.* 0.5–1% yield) of the thermal decomposition of di-*t*-butyl peroxide, and that when the peroxide is decomposed in the presence of large amounts of carbon tetrachloride, the amount of ethylene formed is comparable to the ethane. We also observed a similar increase in the ethylene:ethane ratio as the initial concentration ratio of ethyl chloride to

(1) D. M. Tomkinson, J. P. Galvin, and H. O. Pritchard, *J. Phys. Chem.*, **68**, 541 (1964).

(2) D. M. Tomkinson and H. O. Pritchard, *ibid.*, **70**, 1579 (1966).

(3) A preliminary report was given in *Australian J. Chem.*, **18**, 121 (1965).

(4) W. G. Alcock and E. Whittle, *Trans. Faraday Soc.*, **61**, 244 (1965).

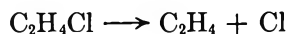
(5) A. M. Hogg and P. Kebarle, *J. Am. Chem. Soc.*, **86**, 4558 (1964)

Table I: Product Distribution from the Reaction of Di-*t*-butyl Peroxide with Ethyl Chloride

	Run no. 1	Run no. 2
Temperature	189°C	163°C
Reaction time	8 min	25 min
C ₂ H ₅ Cl, initial pressure	45.4 mm	38.3 mm
Di- <i>t</i> -BP, initial pressure	23.6 mm	15.7 mm
Products		
CH ₄	20.2 mm	11.7 mm
C ₂ H ₆	1.0 mm	0.5 mm
C ₂ H ₄	2.9 mm	2.1 mm
C ₃ H ₈	1.0 mm	0.5 mm
CH ₃ Cl	Trace	Trace
HCl	<i>a</i>	<i>a</i>

^a Not measured quantitatively. Its presence was tested for by a procedure similar to that used by Hogg and Kebarle.⁶

di-*t*-butyl peroxide was increased (see Table II). However, we feel that in our experiments the ethylene is also produced from decomposing chloroethyl radicals



Correspondingly, propene was formed, probably *via* bromopropyl radicals with similar experiments using *n*-propyl bromide.

Table II: Effect of Ethyl Chloride Concentration upon the Relative Production of Ethylene and Ethane at 163°

$\frac{[(\text{C}_2\text{H}_5\text{Cl})]}{[\text{Di-}t\text{-BP}]_{\text{initial}}}$	$\frac{[(\text{C}_2\text{H}_4)]}{[(\text{C}_2\text{H}_6)]_{\text{products}}}$
0.4	1.2
1.6	3.3
2.4	4.5

Isobutylene oxide is one of the major products resulting from chlorine atom attack on di-*t*-butyl peroxide,⁵ but was not detected among our products. Conditions in our experiments probably favored chlorine atom attack upon the hydrogen atoms in the alkyl halides in preference to those on the di-*t*-butyl peroxide. The fully halogenated compounds used in the experiments of Tomkinson and Pritchard² would be inert to chlorine atom attack.

Likely reactions resulting from methyl radical attack on ethyl chloride are



The nature of the products with other alkyl chlorides and bromides indicated complicated reaction systems of a similar nature. These studies have therefore been discontinued because of the difficulty in obtaining useful quantitative information from such complicated systems.

SCHOOL OF CHEMISTRY

THE UNIVERSITY OF NEW SOUTH WALES
SYDNEY, AUSTRALIA

K. D. KING

E. S. SWINBOURNE

RECEIVED MARCH 27, 1967

Comment on "Electron Spin Resonance of O¹⁶-O¹⁷, O¹⁷-O¹⁸, and O¹⁸-O¹⁶" by L. K. Keys

Sir: We wish to call in question a number of statements in a recent communication by Keys¹ on the electron resonance spectrum of gaseous O₂.

First, it is not the case that lines below 5500 gauss (at X-band frequency) have not previously been reported. Tinkham and Strandberg,² in their classic papers on O₂, list no fewer than 35 lines between 1400 and 5500 gauss and interpret all of them with high accuracy in terms of O¹⁶-O¹⁶ alone.

Second, the formula $E = g_J\beta HM_J$ is quite inapplicable to the O₂ molecule, for a number of reasons. Even if there were no zero-field splitting of the spin triplet, this formula would be inadequate because of off-diagonal magnetic field matrix elements which give rise to a nonlinear Zeeman effect. However, as shown originally by Kramers,³ and in more detail by Van Vleck⁴ and by Tinkham and Strandberg, the spin-spin and spin-orbit interactions are extremely important. They split the triplet components of each rotational level, the $J = N \pm 1$ components being separated from the $J = N$ component by about 2 cm⁻¹. The $J = N \pm 1$ components are themselves not degenerate and the splitting between them (10⁻² to 1 cm⁻¹ for different rotational levels) is sufficient for the

(1) L. K. Keys, *J. Phys. Chem.*, **70**, 3760 (1966).

(2) M. Tinkham and M. W. P. Strandberg, *Phys. Rev.*, **97**, 937, 951 (1955).

(3) H. A. Kramers, *Z. Physik*, **53**, 422, 429 (1929).

(4) J. H. Van Vleck, *Phys. Rev.*, **71**, 413 (1947).

$\Delta J = \pm 2$ transitions, which are allowed in a magnetic field, to occur at considerably less than 5500 gauss at X-band frequencies. These are the lines observed by Keys.

The suggestion by Keys that some of the lines below 5500 gauss arise from the isotopic species $O^{16}-O^{17}$ and $O^{17}-O^{18}$ deserves comment on other grounds. The natural abundance of $O^{17}-O^{18}$ is approximately 0.016%. Taking into account the sixfold hyperfine splitting from O^{17} (*i.e.*, $2I + 1$, not $2S(S + 1)$ as given by Keys), observation of $O^{17}-O^{18}$ lines implies a signal-to-noise ratio of approximately 10^6 to 1 for some of the $O^{16}-O^{18}$ lines. On the basis of our experience with a Varian 100-kc epr spectrometer, Keys' hopes of $O^{17}-O^{18}$ resonances, even at 77°K, are about three orders of magnitude too optimistic.

DEPARTMENT OF THEORETICAL CHEMISTRY
UNIVERSITY OF CAMBRIDGE
CAMBRIDGE, ENGLAND

A. CARRINGTON
D. H. LEVY
T. A. MILLER

ACCEPTED AND TRANSMITTED BY THE FARADAY SOCIETY

DECEMBER 22, 1966

Reply to "Comment on Electron Spin

Resonance of $O^{16}-O^{17}$, $O^{17}-O^{18}$, and $O^{18}-O^{16}$ "

by Carrington, Levy, and Miller

Sir: Recently we reported the observation of several low-field electron spin resonance peaks in gaseous O_2 .¹ Based upon simple considerations of the vector model of the atom,² we have interpreted these as possible $O^{16}-O^{17}$, $O^{17}-O^{18}$, and $O^{16}-O^{18}$ absorption peaks. More quantitative studies of these peaks have been carried by Tinkham and Strandberg,³ who observed a large number (also subsequently observed by the author) in this same field region. These esr peaks have been interpreted as $O^{16}-O^{16}$ transitions from considerations of detailed calculations correcting for the various effects as mentioned in the previous communication.⁴

While these results seem to weaken the previous interpretation¹ of these lines, the disagreement between the various investigators apparently indicates, however, that the more quantitative treatment cannot be rigorously applied. Hendrie and Kusch⁵ have obtained results from independent measurements at low-field strengths by a molecular-beam method. These results are not in accord with those of Tinkham and Strandberg. More recent studies by Bowers, *et al.*,⁶ a repeat of the work of Tinkham and Strandberg, produced results in disagreement with both of the previous investigations. According to these results,

there are still discrepancies in the various theories to explain the absorption peaks.

In view of the recent observation of the hfs of O^{17} in SiO ,⁷ and the high spin molecular density of oxygen, it is believed that O^{17} can contribute to the observed esr spectra of oxygen. The reported possible $O^{18}-O^{17}$ transitions would be naturally very weak and are believed only to contribute possibly to the background esr of oxygen.

- (1) L. K. Keys, *J. Phys. Chem.*, **70**, 3760 (1966).
- (2) A. F. Henry, *Phys. Rev.*, **80**, 396 (1950).
- (3) M. Tinkham and M. W. P. Strandberg, *ibid.*, **97**, 937, 951 (1955).
- (4) A. Carrington, D. H. Levy, and T. A. Miller, *J. Phys. Chem.*, **71**, 2372 (1967).
- (5) J. M. Hendrie and P. Kusch, *Phys. Rev.*, **107**, 716 (1957).
- (6) K. D. Bowers, R. A. Kamper, and C. D. Lustig, *Proc. Roy. Soc. (London)*, **A251**, 565 (1959).
- (7) P. Cornaz, H. Choffat, M. Parot, and J.-P. Borel, "Physics of Non-Crystalline Solids," J. A. Prins, Ed., Interscience Publishers, Inc., New York, N. Y., 1965, p 207.

MATERIALS RESEARCH LABORATORY
PENNSYLVANIA STATE UNIVERSITY
UNIVERSITY PARK, PENNSYLVANIA 16802

L. K. KEYS

RECEIVED APRIL 7, 1967

A Comment on the Steric Factor Approach to Translational-Vibrational Energy Transfer¹

Sir: In many theoretical treatments² of vibrational excitation of a diatomic molecule B-C colliding with atom A (or one end of diatomic molecule A-D), the initial relative A,B-C velocity vector \mathbf{v}_A , or an effective \mathbf{v}_A ,³ is considered directed toward the B-C center of mass. Approximations² are introduced so that the vibrational energy transfer to B-C averaged over θ ,⁴ the angle between the B-C axis and \mathbf{v}_A , is obtained by multiplying the collinear ($\theta = 0$) energy transfer value by a steric factor σ less than unity.² We show that this steric factor approach cannot be generally correct.

We have obtained exact numerical solutions to the classical equations of motion, with A,B,C restricted to

(1) Research performed under the auspices of the U. S. Atomic Energy Commission.

(2) See, for instance: (a) K. Takanayagi, *Progr. Theoret. Phys. Suppl.*, **25**, 1 (1963); (b) K. F. Herzfeld and T. A. Litovitz, "Absorption and Dispersion of Ultrasonic Waves," Academic Press Inc., New York, N. Y., 1959, Chapter 7; (c) K. F. Herzfeld and V. Griffing, *J. Phys. Chem.*, **61**, 884 (1957); (d) C. B. Moore, *J. Chem. Phys.*, **43**, 2979 (1965).

(3) Takanayagi (ref 2a) employs the quantum analog of an "effective \mathbf{v}_A " in his MWN approximation.

(4) Or the appropriate quantum mechanical operation.

Table I: Angle-Averaged Energy Transfer Values. Initial $E_{\text{rot}}, E_{\text{vib}} = 0$; Collision Energy $E_{\text{coll}} = 1.0$ ev

System no.	A	B-C	k , mdynes/A	$\overline{\Delta E_{\text{rot}}}$, ^b ev	$\overline{\Delta E_{\text{vib}}}$, ^b ev	ΔE_{lin} , ev
1	2	12-12	10.57	9.2×10^{-2}	2.7×10^{-2}	6.4×10^{-2}
2	2	1-1	10.57	0.27	1.2×10^{-3}	1.3×10^{-3}
3	12	1-1	10.57	0.19	1.8×10^{-4}	6.1×10^{-6}
4	13	1-12	5.312	0.11	8.4×10^{-3}	$\sim 5 \times 10^{-6}$ ^a

^a Average of two collinear values: $\Delta E_{\text{lin}}(13 + 12-1) = 9.0 \times 10^{-6}$ ev, $\Delta E_{\text{lin}}(13 + 1-12) = 1.2 \times 10^{-6}$ ev. ^b A simple average over θ_0 , appropriate for two-dimensional calculations.

motion in a plane^{5,6} and \mathbf{v}_A directed toward the B-C center of mass, for a harmonic oscillator BC [$V_{\text{BC}} = \frac{1}{2}k(r_{\text{BC}} - r_{\text{BC}}^0)^2$] interacting with A through repulsive pair potentials $V_{\text{ABC}} = A[\exp(-r_{\text{AB}}/L) + \exp(-r_{\text{AC}}/L)]$; the r 's are interparticle distances.⁷ Initial A,B-C relative translational energy E_{coll} ($=\frac{1}{2}\mu_{\text{ABC}}\mathbf{v}_A^2$) is 1.0 ev, and initial B-C vibrational-rotational energy E_{BC} is zero.⁸

Separate definitions of B-C rotational and vibrational energy are somewhat arbitrary because of coupling. We define rotational energy

$$E_{\text{rot}} = \frac{\mathbf{M}^2}{2\mu_{\text{BC}}r'_{\text{BC}}{}^2} + \frac{1}{2}k(r'_{\text{BC}} - r_{\text{BC}}^0)^2$$

where \mathbf{M} is B-C angular momentum, μ_{BC} the reduced mass, and $r'_{\text{BC}} - r_{\text{BC}}^0$ the change in equilibrium value of r_{BC} for given \mathbf{M} if the only B-C motion were rotation; vibrational energy E_{vib} equals $E_{\text{BC}} - E_{\text{rot}}$.⁹

ΔE_{rot} and ΔE_{vib} , the differences between initial and final B-C rotational and vibrational energies, were calculated as functions of θ_0 (initial θ). These quantities averaged over θ_0 appear in the table as $\overline{\Delta E_{\text{rot}}}$, $\overline{\Delta E_{\text{vib}}}$. For θ_0 zero, the systems remain collinear

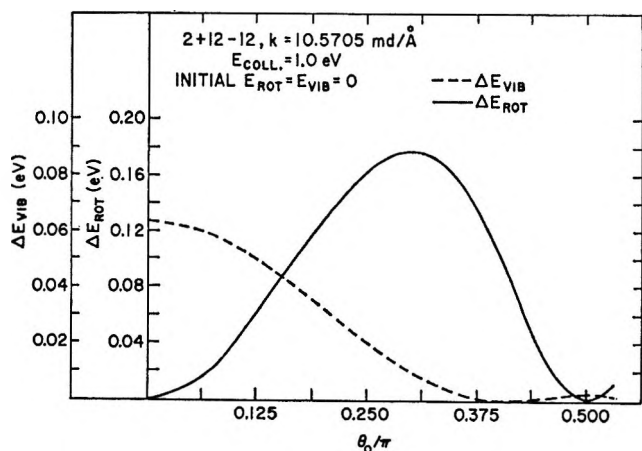


Figure 1. Variation of ΔE_{vib} and ΔE_{rot} with initial A,B-C relative orientation angle θ_0 .

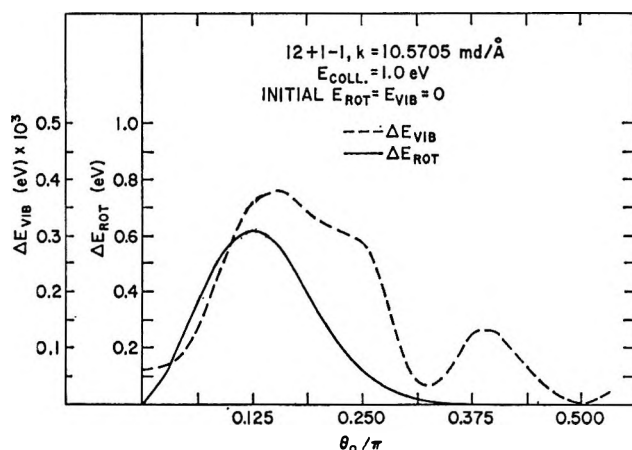


Figure 2. Variation of ΔE_{vib} and ΔE_{rot} with initial A,B-C relative orientation angle θ_0 .

throughout collision, and corresponding energy transfers ΔE_{lin} are listed to test the steric factor concept.

In system¹⁰ 2 + 12-12 (Figure 1, no. 1 in table), ΔE_{vib} decreases smoothly with θ_0 ($\overline{\Delta E_{\text{vib}}}/\Delta E_{\text{lin}} = 0.42$), so that a steric factor approach seems plausible. System 12 + 1-1 (Figure 2, no. 3 in table) shows that such an approach cannot be generally valid; ΔE_{vib} is strongly influenced by rotation-vibration coupling and $\overline{\Delta E_{\text{vib}}}/\Delta E_{\text{lin}} = 3.0$. A more dramatic effect occurs in system no. 4; $\overline{\Delta E_{\text{vib}}}/\Delta E_{\text{lin}} \cong 10^3$, and the θ_0 variation of ΔE_{vib} and ΔE_{rot} is extremely complex. In system 2 + 1-1, perhaps representing collision between identical homonuclear molecules, $\overline{\Delta E_{\text{vib}}}/$

(5) J. D. Kelley and M. Wolfsberg, *J. Chem. Phys.*, **44**, 324 (1966). Discussion of technique for collinear collisions.

(6) S. W. Benson and G. C. Berend, *ibid.*, **44**, 4247 (1966). Two-dimensional calculations with different emphasis for a specific chemical system.

(7) Potential parameters: $A = 1.040 \times 10^8$ ev; $L = 0.2214$ Å; $r_{\text{BC}}^0 = 1.21$ Å.

(8) More extensive calculations will be reported later.

(9) Reference 6 also uses this definition.

(10) Notation: an atom A, mass 2 amu, colliding with a B-C molecule, mass B = mass C = 12 amu.

$\Delta E_{\text{lin}} = 0.92$; the θ_0 variation of ΔE_{vib} is intermediate between those illustrated, and rotational effects are definitely non-negligible.

We conclude that, in general, the steric factor approach has limited validity, and adequate treatment of vibrational excitation of diatomic molecules free to rotate requires explicit consideration of dynamic rotation-vibration interaction.

DEPARTMENT OF CHEMISTRY
BROOKHAVEN NATIONAL LABORATORY
UPTON, NEW YORK 11973

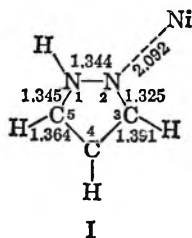
J. DANIEL KELLEY
MAX WOLFSBERG

RECEIVED APRIL 10, 1967

On the Structure of Pyrazole

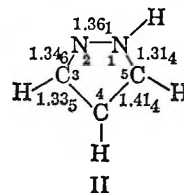
Sir: The purpose of this communication is to present evidence for a revised structural formulation of pyrazole. Recently, we determined the crystal and molecular structure of the coordination complex dichlorotetrapyrazolenickel(II), $\text{Ni}(\text{C}_3\text{H}_4\text{N}_2)_4\text{Cl}_2$.¹ The structural model was refined by full-matrix least-squares analysis to an R value of 5.4% based upon 2072 observed reflections. The structure of molecular pyrazole had previously been published² and this made possible a comparison between coordinated and molecular pyrazole. As expected, the ring-bond distances observed in coordinated pyrazole were found to be similar to those in hydrogen-bonded molecular pyrazole. However, the two structures differed in one very significant detail—the assignment of the pyridine-type ($-\text{N}=\text{}$) and the pyrrole-type ($>\text{NH}$) nitrogen atoms. The location of all hydrogen atoms and the observed stereochemistry about the coordinating nitrogen atoms both require that coordination occur through the pyridine-type nitrogen atoms. This provides an unambiguous distinction between ($-\text{N}=\text{}$) and $>\text{NH}$. As a consequence of our assignment, a relocation of a hydrogen atom in molecular pyrazole is required. This leads to a reassessment of the resonance description of pyrazole.

The structure of coordinated pyrazole in $\text{Ni}(\text{C}_3\text{H}_4\text{N}_2)_4\text{Cl}_2$ and the average ring-bond distances (av $\sigma = 0.005$ Å) are shown in I. Included in I are the position



of the nickel ion relative to a pyrazole ring and the average nickel-nitrogen coordinate bond distance. The pyrazole rings in the structure of $\text{Ni}(\text{C}_3\text{H}_4\text{N}_2)_4\text{Cl}_2$ were found to be planar to within experimental error.

The principal details in the structure of molecular pyrazole are indicated in II. As in our structure de-



termination, the ring-bond distances given in II (av $\sigma = 0.018$ Å) are averages obtained from the two crystallographically independent molecules in the unit cell.

A comparison between I and II shows either that there is a large dissimilarity in corresponding ring-bond distances or that these distances are quite similar but a different assignment of pyrrole ($>\text{NH}$) and pyridine types ($-\text{N}=\text{}$) of nitrogen atoms has been made. As coordination and hydrogen bonding represent relatively small and qualitatively similar interactions, these would not be expected to introduce grossly dissimilar distributions of ring-bond distances. Hence the two structures differ in the location of a hydrogen atom.

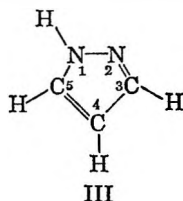
The relocation of the hydrogen atom in molecular pyrazole would not be unreasonable in view of the fact that this structure was determined from projection data and that the choice between pyrrole and pyridine types of nitrogen atoms was a crystallographically difficult one. The relocation of a hydrogen atom in coordinated pyrazole would not only contradict the observed hydrogen atom positions but also would require that pyrazole be coordinated to the nickel ion through the $>\text{NH}$ group rather than through the ($-\text{N}=\text{}$) group. Coordination through the $>\text{NH}$ group would result in the formation of a quaternary nitrogen atom with a tetrahedral configuration. As the Ni-N coordinate bond makes an average angle of 2° with the plane of the pyrazole rings compared with the required half tetrahedral angle of about 54° , coordination through $>\text{NH}$ is excluded. Thus, based upon the consideration of the foregoing crystallographic evidence, we conclude that in molecular pyrazole the assignment of pyrrole and pyridine types of nitrogen atoms should be interchanged.

The identification of the nitrogen atom to which the

(1) C. W. Reimann, A. D. Mighell, and F. A. Mauer, *Acta Cryst.*, in press.

(2) H. W. W. Ehrlich, *ibid.*, **13**, 946 (1960).

hydrogen atom is attached is essential to a correct assessment of the composition of the resonance hybrid. This can be understood from the structural formula for pyrazole, III. The transfer of a hydrogen



atom from one nitrogen atom to the other in III is, in effect, an alteration of the ring-atom labeling ($N_1 \leftrightarrow N_2$ and $C_3 \leftrightarrow C_5$ where the nitrogen in the N-H group is assigned as N_1) with respect to the crystallographically determined set of bond distances. This relabeling interchanges double and single bonds and forces a reversal of the estimates of the amount of double- and single-bond character. As there is extensive need for accurate bond distances for theoretical calculations on small planar molecules, a complete redetermination of the structure of molecular pyrazole using three-dimensional X-ray data is planned.

INSTITUTE FOR MATERIALS RESEARCH
NATIONAL BUREAU OF STANDARDS
GAITHERSBURG, MARYLAND

ALAN D. MIGHELL
CURT W. REIMANN

RECEIVED APRIL 12, 1967

Infrared Spectra of Carbon Monoxide Adsorbed on Palladium

Sir: This is a preliminary report of a study of the infrared spectrum of carbon monoxide adsorbed on silica-supported palladium. Earlier workers¹⁻⁴ have found the spectrum of carbon monoxide adsorbed on palladium, or on related metals such as platinum or nickel, often shows two regions of absorption, one near 4.8 and the other near 5.2 μ . These bands are usually assigned to the CO stretching mode of, respectively, linear or bridged carbonyl-like species formed by the adsorbed carbon monoxide and surface metal atoms. The present work shows (Figure 1) that the relative intensities of these absorptions strongly depend on the details of sample preparation (see below) which may affect average particle size of the dispersed metal. The spectra show clearly that the absorption near 4.8 μ increases with respect to that at 5.2 μ as the metal concentration of the impregnating solution decreases. For a given concentration, increasing the number of

impregnations favors formation of the species absorbing at the shorter wavelength as exemplified by cases b and c. We attribute these intensity variations to differences in metal particle size: when the metal is deposited in a manner which leads to small particle size, the 4.8- μ band increases, and, conversely, when large particle sizes are expected, the 5.2- μ band predominates. The present results are consistent with those of Yates, *et al.*,³ who obtained a similar variation

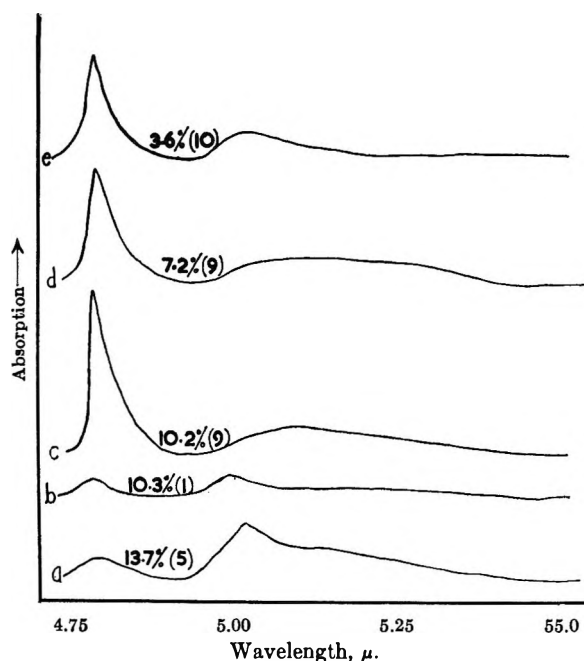


Figure 1. Spectra of CO adsorbed on SiO_2 -supported Pd. The weight per cent of dispersed Pd is given for each spectrum. The number in parentheses is the number of impregnations used in preparing the given sample.

in relative band intensities for carbon monoxide adsorbed on alumina-supported nickel. Nash and DeSieno⁴ found only 5.2- μ carbon monoxide absorption on palladium crystallites formed under conditions which gave relatively large particles in the 200-Å size range.

In these systems, as for those reported earlier,¹⁻³ the band near 5.2 μ appears at lower carbon monoxide pressures than does the 4.8- μ band, and it persists longer on desorption than does the short-wavelength band, indicating that the species which absorbs at 5.2

(1) R. P. Eischens, S. A. Francis, and W. A. Pliskin, *J. Phys. Chem.*, **60**, 194 (1956).

(2) R. P. Eischens and W. A. Pliskin, *Advan. Catalysis*, **10**, 1 (1958).

(3) J. T. Yates and C. W. Garland, *J. Phys. Chem.*, **65**, 617 (1961).

(4) C. P. Nash and R. P. DeSieno, *ibid.*, **69**, 2139 (1965).

μ is more tightly bound to the surface than the species which absorbs at 4.8μ .

These observations are consistent with the hypothesis that absorption at 4.8μ is due to linear carbonyl-like species, and absorption at 5.2μ is due to a bridged species. It is not unreasonable to expect that relatively more high Miller-index faces are exposed on small particles than on large particles and that the average distance between adjacent pairs of metal atoms is greater on high-index faces than on low-index faces. The relative stabilities and numbers of bridged and linear species on a given crystal face will depend, *inter alia*, on the distribution of distances between neighboring metal atoms on that face. It is obvious that for sufficiently large distances between metal atoms, bridged species will not form. Thus we suggest that the variation in the relative intensities of the bands at 4.8 and 5.2μ arises because at lower metal concentrations the average particle sizes tend to be smaller, and the crystal faces with interatomic spacings unfavorable for the bridged species become more numerous. Further, our results do not support Blyholder's⁵ contention that on large crystals (of these metals) with well-developed planes there will be a relative increase in the high-frequency band.

Samples were prepared by making a slurry from 1 g of Cabosil and 20 ml of aqueous ammonium chloropalladate, drying the mixture while stirring, and heating the residue to decompose the palladium salt. This impregnation sequence was repeated until the required metal concentration was obtained, and the number of impregnations used was chosen to vary the metal particle dispersion as desired. One-inch diameter circular disks weighing approximately 85 mg were compressed from the impregnated silica at about 40 tons in.⁻² pressure. These were dried, oxidized, and reduced in an *in situ* cell.⁶ Typically, the transmission of the dried disks was about 40% at 4.75μ .

Spectra were obtained with a Grubb Parsons "Spectromaster." Work continues on this system in this laboratory.

(5) G. Blyholder, *J. Phys. Chem.*, **68**, 2772 (1964); see also J. T. Yates' communicated comments on ref 5, *ibid.*, **68**, 2777 (1964).

(6) This cell and other relevant material will be described in a subsequent paper.

(7) Communications regarding this note should be sent to this author.

DEPARTMENT OF CHEMISTRY
UNIVERSITY COLLEGE
DUBLIN, IRELAND

J. K. A. CLARKE
G. FARREN
H. E. RUBALCAVA⁷

ACCEPTED AND TRANSMITTED BY THE FARADAY SOCIETY

FEBRUARY 22, 1967

Calorimetric Measurement of Transition Enthalpies in the Polynucleotide System Poly A-Poly U

Sir: The synthetic polynucleotides polyriboadenylic acid (poly A) and polyribouridylic acid (poly U) are able to associate in aqueous solution to a double-stranded helical complex poly(A + U) and a three-stranded poly(A + 2U) complex.¹ In heating the solutions, these highly ordered systems convert to partially ordered structures or to randomly coiled forms. For an equimolar mixture of the two polymers, the regions of temperature over which the different conformations exist (within a limited pH range) depend on the concentration of cations in the solution.²

The transition enthalpies ΔH of thermal structural conversions of this cooperative type can be determined by accurate measurements of the temperature course of the heat capacity using an adiabatic calorimeter.^{3,4} The characteristic behavior of the transition curves obtained by ultraviolet absorption measurements is reflected in the corresponding temperature course of the heat capacity data (Figures 1 and 2). According to the phase diagram given by Stevens and Felsenfeld, the first peak of the heat capacity *vs.* T curve in Figure 2 refers to the conversion of poly(A + U) to poly(A + 2U), and poly A,⁵ the second one, is caused by the dissociation of the poly(A + 2U) complex. Since poly A is forming an intramolecular secondary structure in the course of these reactions, the measured transition enthalpies are reduced ΔH values because of heat released in the partial helix formation of poly A. Therefore, an extrapolation to about 95° is necessary, where poly A is assumed to exist completely in the randomly coiled conformation.⁶

The combination of the results obtained from the calorimetric measurements carried out for different cation concentrations (in order to vary the conversion temperature T_c) and at neutral pH yields the extrapolated ΔH° values for the transitions of both the complexes into the completely randomly coiled polymers

$$\Delta H^\circ(A + U) = 8.5 \pm$$

0.5 kcal/mole of base pair (Figure 3)⁷

(1) R. F. Steiner and R. F. Beers, Jr. "Polynucleotides," Elsevier Publishing Co., Amsterdam, 1961.

(2) C. L. Stevens and G. Felsenfeld, *Biopolymers*, **2**, 293 (1964).

(3) Th. Ackermann in "Experimental Thermodynamics," Vol. I, Butterworth and Co. Ltd., London, in press, Chapter 12.

(4) Th. Ackermann, *Z. Elektrochem.*, **62**, 411 (1958).

(5) H. T. Miles and J. Frazier, *Biochem. Biophys. Res. Commun.*, **14**, 129 (1964).

(6) M. Leng and G. Felsenfeld, *J. Mol. Biol.*, **15**, 455 (1966).

$$\Delta H^\circ(A + 2U) = 12.5 \pm$$

0.5 kcal/mole of (A + 2U) residue

The heat of conversion of the double-stranded poly(A + U) into the three-stranded complex was found to be

$$\Delta H_e^\circ = 4.5 \pm 0.5 \text{ kcal/mole of (A + 2U) formed}$$

and the enthalpy change for the addition reaction $\text{poly(A + U) + poly U} = \text{poly(A + 2U)}$ is

$$\Delta H(\text{addition}) = -4.0 \pm$$

0.1 kcal/mole of (A + 2U) formed⁸

We are trying to reduce the margin of error for the extrapolated values in further measurements. The influence of polymer concentration on the ΔH values is about to be investigated.

The results of the calorimetric measurements will

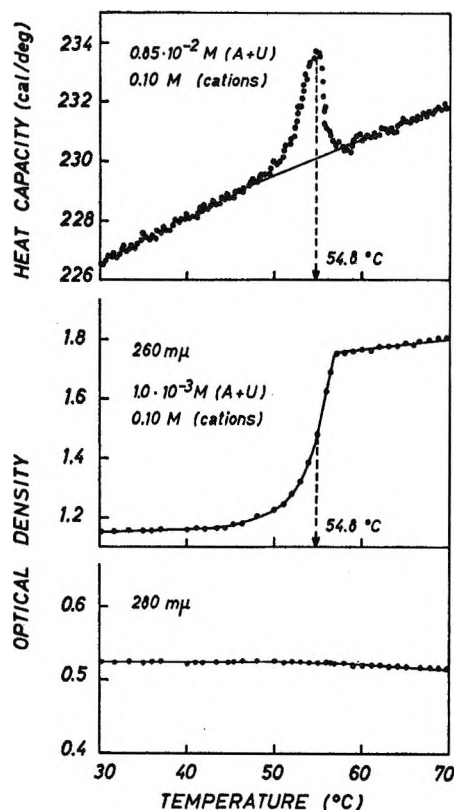


Figure 1. The conversion of an equimolar mixture of poly A and poly U in aqueous salt solution. The total concentration of cations is 0.10 M; 0.01 M citrate buffer, pH 6.8. (The change in optical density at 260 mμ refers to the transition reaction $\text{poly(A + U)} = \text{poly A} + \text{poly U}$, and $\text{poly(A + 2U)} = \text{poly A} + 2 \text{ poly U}$. The change in optical density at 280 mμ refers to the formation and dissociation of the three-stranded poly(A + 2U) complex. See ref 2.)

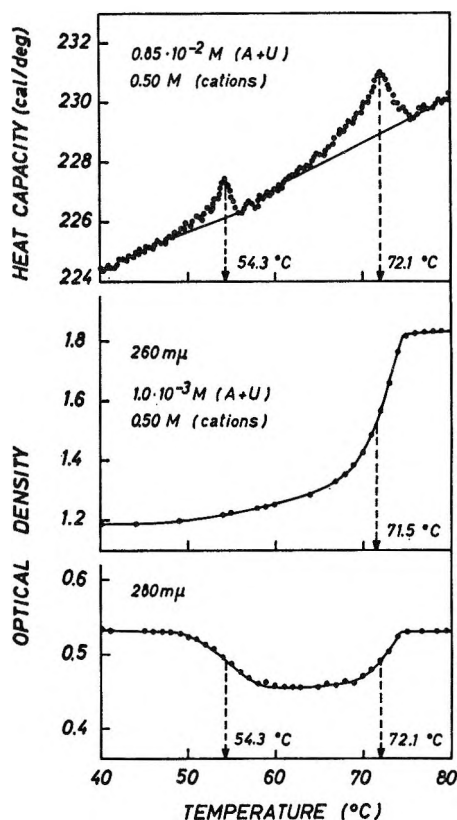


Figure 2. The conversions of an equimolar mixture of poly A and poly U in aqueous salt solution. The total concentration of cations is 0.50 M; 0.01 M citrate buffer, pH 6.8. (See Figure 1.)

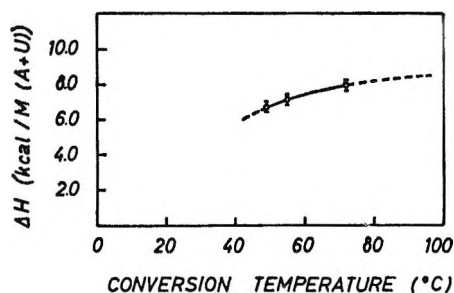


Figure 3. The enthalpy change ΔH for the helix-coil transition of poly(A + U) at pH 6.8 for different conversion temperatures, *i.e.*, different concentrations of cations.

provide us with information about the energetic interactions (stacking energy) in the ordered polynucleotide structures. The polymers were purchased from Miles Laboratories. The dried products were mixed 1:1 in aqueous salt solutions containing 0.01 M citrate buffer,

(7) See M. A. Rawitscher, P. D. Ross, and J. M. Sturtevant, *J. Am. Chem. Soc.*, **85**, 1915 (1963).

(8) See P. D. Ross and R. L. Scruggs, *Biopolymers*, **3**, 491 (1965).

pH 6.8. All concentrations are given in moles per kilogram of the pure solvent. The weight of every solution prepared for the calorimetric measurements was about 200 g. The heating rate was $0.06^\circ/\text{min}$.

INSTITUT FÜR PHYSIKALISCHE CHEMIE EBERHARD NEUMANN
UNIVERSITÄT MÜNSTER, GERMANY THEODOR ACKERMANN

ACCEPTED AND TRANSMITTED BY THE FARADAY SOCIETY

(FEBRUARY 2, 1967)

Hybridization, Conjugation, and Bond

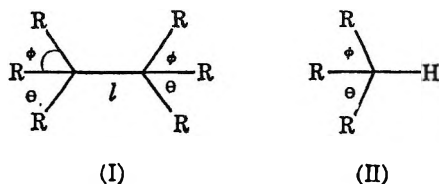
Lengths. An Experimental Test¹

Sir: The reasons for decreased lengths and increased strengths of single carbon-carbon bonds in "conjugated" molecules such as butadiene and diacetylene are the subjects of a longstanding controversy.² The shortening of these bonds has been attributed to: (1) the introduction of double-bond character by conjugation^{3a-b} as in $\text{CH}_2=\text{CHCH}=\text{CH}_2 \leftrightarrow \dot{\text{C}}\text{H}_2\text{CH}=\text{CH}\dot{\text{C}}\text{H}_2$; (2) decreased repulsions in unsaturated molecules;^{4a,b} (3) changes in hybridization,⁵ and to various combinations of all three effects.^{3c} Dewar and Schmeising^{5b,c} have plotted single-bond lengths against the mean per cent *s* character in the orbitals composing the bond, and have obtained a straight line which can be expressed as⁶

$$l = 1.692 - 0.0062 \times s \quad (1)$$

(*l* is the bond length; *s* is the mean per cent *s* character). Equation 1 fits available data within experimental error ($\pm 0.004 \text{ \AA}$).⁷

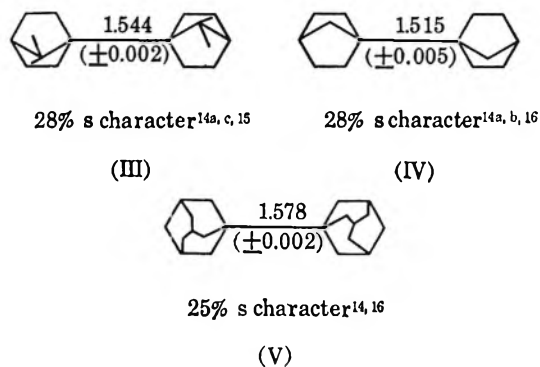
To separate the effect of hybridization⁸ from that of conjugation, an experiment was designed in which the bond lengths of a series of single bonds with varying per cent *s* character would be measured precisely by X-ray diffraction crystallography. In order to exclude conjugation and keep the bond environment constant, a series of *bis*-bridgehead hydrocarbons was chosen.



Theoretical considerations,⁹ $J_{13\text{CH}}$ measurements,¹⁰⁻¹² and several chemical properties,^{10,13} show that decreasing the angles θ and ϕ increases the *s* character in the central bond of I, and in the C-H bond of II.

In fact, a rather accurate estimate of this per cent *s* character may be obtained from the carbon-13 to hydrogen coupling constant in the nmr of II ($J_{13\text{CH}} = 5 \times \%s$). By a suitable selection of compounds, it is theoretically possible to synthesize a series of dimers with hybridization at the central bond covering the range 25% to 42%*s*.^{11,13b}

Thus far, three structures of this type have been investigated by X-ray methods: 1-biapocamphane (III), 1-binorbornane (IV), and 1-biadamantane (V).⁷



(1) This work was supported by the Army Research Office (Durham) under Grant No. DA-ARO-D-31-124-G-602.

(2) (a) D. R. Lide, Jr., *Tetrahedron*, **17**, 125 (1962); (b) R. S. Mulliken, *ibid.*, **17**, 247 (1962); (c) B. P. Stoicheff, *ibid.*, **17**, 135 (1962); (d) O. Bastiensen and M. Traeteberg, *ibid.*, **17**, 147 (1962); (e) L. S. Bartell, *ibid.*, **17**, 177 (1962); (f) I. Fisher-Hjalmars, *ibid.*, **17**, 235 (1962). See also the discussion section, pp 247-266.

(3) (a) L. Pauling, "The Nature of the Chemical Bond," 3rd ed, Cornell University Press, Ithaca, N. Y., 1960, p 299; (b) G. Wheland, "Resonance in Organic Chemistry," John Wiley and Sons, Inc., New York, N. Y., 1955, pp 174-185; (c) A. Streitwieser, Jr., "Molecular Orbital Theory for Organic Chemists," John Wiley and Sons, Inc., New York, N. Y., 1961, p 247; (d) J. D. Roberts and M. C. Caserio, "Basic Principles of Organic Chemistry," W. A. Benjamin, Inc., New York, N. Y., 1964, p 247; (e) currently, Mulliken,^{3f} Wilson^{3g} and others^{2,3b} attribute bond shortening to a combination of conjugation and hybridization; (f) R. S. Mulliken, *Tetrahedron*, **6**, 68 (1959); (g) E. B. Wilson, Jr., *ibid.*, **17**, 191 (1962); (h) B. Bak and L. Hansen-Nygaard, *J. Chem. Phys.*, **33**, 418 (1960).

(4) (a) L. S. Bartell, *ibid.*, **32**, 827 (1960); (b) J. B. Conn, G. B. Kistiakowsky, and E. A. Smith, *J. Am. Chem. Soc.*, **61**, 1868 (1939).

(5) (a) M. J. S. Dewar and H. N. Schmeising, *Tetrahedron*, **5**, 166 (1959); (b) *ibid.*, **11**, 96 (1960); (c) M. J. S. Dewar, "Hyperconjugation," The Ronald Press Co., New York, N. Y., 1962, p 53.

(6) Equation 1 is our expression of the Dewar and Schmeising plot.

(7) See ref 2a for discussions of accuracy of bond length measurements. Our bond lengths were determined with a precision of $\pm 0.005 \text{ \AA}$ or less, as computed by standard least-squares techniques, and as confirmed by the internal consistency of other C-C bond lengths. This is somewhat better than usual, probably because of centrosymmetry, the absence of atoms heavier than carbon, low *R* factors (4-6%) and low and almost spherical temperature factors ($2.2-4.6 \text{ \AA}^2$). While absolute errors are difficult to evaluate, and are probably appreciable, our arguments are based solely upon comparisons of bonds situated in similar environments and measured in the same way.

(8) We do not attempt to distinguish between the hybridization postulate (3) and the bond repulsion proposal (2). Indeed, they are not entirely independent.

(9) C. A. Coulson, "Valence," Clarendon Press, Oxford, 1962, p 255.

(10) W. Muller and O. E. Pritchard, *J. Chem. Phys.*, **31**, 768 (1959).

The results provide a tentative resolution of the subject controversy in two ways. Consider first comparison of III with V. Our X-ray data reveal that III and V each have six H---H repulsions across the central bond. Fortunately, these H---H distances are the same in both compounds, resulting in the same degree of repulsion between monomer units in III and V.¹⁷ Thus the central bond lengths are directly comparable. According to the conjugation concept, they should therefore be identical, whereas the Dewar and Schmeising hybridization theory predicts that the bond in III should be $0.0062 \times (28 - 25) = 0.019$ Å shorter than that in V. A shortening of 0.034 Å is actually observed, even larger than required by the latter postulate. Secondly, eq 1 predicts a bond length of 1.518 Å in IV, to be compared with the observed value of 1.515 Å. It should be noted that even this bond is probably somewhat stretched by two H---H interactions. These two sets of observations suggest that changes in hybridization rather than conjugation or hyperconjugation

bring about bond length shortening in molecules such as propylene and butadiene.^{18,19}

Details of the methods and of the crystal structures will be described shortly in a full publication.

(14) (a) We have measured J_{13CH} at the bridgehead in norbornane to be 139 ± 1 Hz. (b) Professor Christopher Foote has also measured the coupling constant and found it to be 140 ± 2 Hz. We wish to thank Professor Foote for the information. (c) K. Tori, R. Muneyuki, and H. Tanida, *Can. J. Chem.*, **41**, 3142 (1963), report 142 ± 2 Hz. (d) We assume that J_{13CH} for apocamphane is the same as for norbornane.

(15) R. Fort, Jr., and P. von R. Schleyer, *J. Org. Chem.*, **30**, 789 (1965), have measured an average J_{13CH} for all hydrogens in adamantane (120 Hz). We assume 25%*s* at the bridgehead.¹²

(16) As an alternative to J_{13CH} we have used our measured internal angles (ϕ and θ) and the relationship of Mislow¹² to calculate the *s* character in the central bonds of III and V to be 28 and 25.5%, respectively.

(17) The steric equivalence of III and V across the central bonds may be seen with molecular models. Both III and V are in the staggered configuration across the central bond.

(18) Additional *bis*-bridgehead compounds are being investigated to confirm this result.

(19) We do not imply that conjugation is not important in carbonium ions or excited states.

(11) C. Foote, *Tetrahedron Letters*, No. 9, 579 (1963).

(12) K. Mislow, *ibid.*, No. 22, 1415 (1964).

(13) (a) D. F. Applequist and L. Kaplan, *J. Am. Chem. Soc.*, **87**, 2194 (1965); (b) G. L. Closs and L. E. Closs, *ibid.*, **85**, 2023 (1963); (c) see D. J. Cram, "Fundamentals of Carbanion Chemistry," Academic Press, New York, N. Y., 1965, p 49.

DEPARTMENT OF CHEMISTRY
REVELLE COLLEGE
UNIVERSITY OF CALIFORNIA, SAN DIEGO
LA JOLLA, CALIFORNIA

RICHARD ALDEN
J. KRAUT
T. G. TRAYLOR

RECEIVED APRIL 20, 1967